

ENANTIOSELECTIVE SYNTHESSES OF  
TETRAHYDROISOQUINOLINES (THIQS)  
VIA IRIIDIUM-CATALYZED ASYMMETRIC HYDROGENATION  
AND PROGRESS TOWARD THE TOTAL SYNTHESIS OF (+)-CYANOCYCLINE A

Thesis by

Alexia Nahyun Kim

In Partial Fulfillment of the Requirements

for the Degree of

Doctor of Philosophy

CALIFORNIA INSTITUTE OF TECHNOLOGY

Pasadena, California

2023

(Defended: May 22, 2023)

© 2023

Alexia Kim

ORCID: 0000-0002-4060-8892

All Rights Reserved

To *엄마* and *아빠*

## ACKNOWLEDGEMENTS

Words truly can't express the gratitude and appreciation that I have for everyone that has helped me throughout my graduate career. First, I would like to thank my advisor, Professor Brian Stoltz, for being an incredible mentor throughout the past five years. I still distinctly remember the first mechanism bootcamp class I took with Brian in my first year, quickly realizing how supportive and encouraging he is as a teacher. He kindly took me in as a summer student the month before I started graduate school, and my time interacting with him as well as the rest of the group made me feel incredibly welcomed during a time when I felt major imposter syndrome. His mentorship style of providing us the freedom to explore our own chemistry while giving direction and feedback when we need it is quite amazing—and I believe it has truly made me a stronger, more independent scientist. I am deeply grateful for his unwavering support over the past five years.

I would also like to especially thank Professor Sarah Reisman for her expertise and support as another advisor on the 3<sup>rd</sup> floor of Schlinger, and contributing advice to my talks in our joint group meetings and committee meetings. Sarah is also a leader I look up to, and I am constantly in awe of her creativity and highly intellectual ideas that she brings to every single meeting.

I would like to thank the chair of my committee Professor Max Robb, and committee member Professor Linda Hsieh-Wilson for their continuous support and valuable feedback during my committee meetings and exams. Even throughout the pandemic they have handled all my committee meetings with class and a level of professionalism that I can only hope to aspire to.



I would also like to thank my previous teachers before graduate school that truly instilled in me a passion for chemistry. First, I'd like to thank Mr. Hadan Kauffman, an excellent chemistry teacher in my high school who was one of the first people who introduced me to chemistry. If not for him and the summer chemistry bootcamp class I took my freshman year, perhaps I would not have been as fascinated with chemistry in the same way. Dr. Brian Kennedy was also a fantastic teacher who introduced me to organic chemistry in my senior year of high school. Both of their teachings has built in me a foundational passion for chemistry that led me to pursue chemistry as a major at Princeton. In college, I was incredibly fortunate to have worked with Professor Rob Knowles, who like Brian was also a very supportive and encouraging advisor. It was ultimately his mentorship and his group that made me consider applying to graduate school for chemistry. I would also like to thank Professor Tim Warren for having me in his group for a year at Georgetown, learning about organometallic chemistry and getting very comfortable with glovebox chemistry before I started graduate school at Caltech.

I'd like to express my deepest gratitude to the Caltech staff that kept our research going in such a high-paced environment. First and foremost, I would like to thank Dr. Scott Virgil for all of his help running the 3<sup>rd</sup> floor catalysis center and helping me at any time whenever I had trouble using an instrument or the Parr bomb reactor. I truly enjoy the chances I get to converse with him due to his endless knowledge and expertise on instrumentation, spectroscopy, and synthesis. I would like to thank Scott and Silva as well for hosting the annual holiday party each year, and getting to hear Scott play the piano and talk about classical music is always a treat.

I'd like to thank Dr. David VanderVelde for his expertise in NMR spectroscopy, and his unrelenting support in maintaining the NMR facility. I'm grateful for Dr. Mike Takase and Larry Henling for their expertise in X-ray crystallography and obtaining publishable crystal structures. I would also like to thank Dr. Mona Shahgoli for her expertise in mass spectrometry. It was a pleasure to work for her as a GLA for a year, as I truly learned a lot about high-resolution mass spectrometry techniques. I'd like to thank Nate Siladke and Joe Drew for maintaining Caltech facilities and EH&S, especially during my time as the safety officer of the lab. I definitely appreciated the support especially during the pandemic as we had to create documentation and figure out shift schedules. Finally, I'd like to thank Greg and Armando, Alison Ross, Leslie, and Beth Marshall for keeping everything running smoothly in the CCE department.

I have been so lucky to work with so many amazing and talented scientists up on the 3<sup>rd</sup> floor of Schlinger. I'd like to thank Dr. Eric Alexy who was my very first mentor when I joined in the summer, and taught me all the basic lab skills and techniques to get started in the Stoltz lab. I'd also like to thank Dr. Fa Ngamnithiporn who brought me on to her project, and for being an amazing mentor, project partner, and friend. Not only is she an excellent chemist with an incredible work ethic, but she is also a great friend that I could rely on for anything. I really enjoyed our times grabbing coffee, going to hip-hop dance classes, and playing video games outside of the lab. I distinctly remember her being the first person to invite me out to group lunch, where she randomly threw a french fry coated in ketchup on Eric Alexy's shirt. That was the moment I knew I wanted to join the Stoltz group. Jokes aside, I've been incredibly fortunate to work with her and Dr. Eric Welin on

THIQ alkaloids, and learned a lot in a short amount of time about working with these molecules and developing a methods project.

I'd also like to thank Dr. Chris Reimann, Dr. Carina Jette, and Dr. Sean Feng for being wonderful scientists and friends of the same cohort. Hearing drunk Chris spit out words of wisdom was always a treat, and he was also a friend that I looked up to as a first and second year graduate student. Dr. Sean Feng and Dr. Skyler Mendoza were also close friends especially during my first few years of graduate school, and I truly enjoyed the random outings we had to get soufflé pancakes or go out to LA. Dr. Nick Fastuca was also a good friend who helped me navigate graduate school, and I enjoyed our random trips watching artsy movies at the Laemmle Pasadena.

I'd like to thank Dr. Nick Hafeman and Dr. Tyler Fulton for being incredible scientists and great friends as well. I enjoyed the times we went to Ernie's to grab lunch before the pandemic, when I could barely finish three tacos and they ate a huge Jaws sandwich in its entirety. Their sarcastic humor, Twin Peaks references, and the random print-outs of collaged photos and memes never failed to make me laugh no matter the circumstances. It was tough on everyone during the pandemic, but they have gone above and beyond to ensure our lab was running smoothly and that everyone was on the same page. Thank you for the ping-pong sessions, the random Zoom hangout sessions, the insightful advice and ideas about chemistry, and all the guidance you have given me throughout the years.

I'm thankful for my cohort, including Zack Sercel, Tyler Casselman, and Alex Cusumano, for keeping me sane and for all their help going through this PhD journey

together. I especially would like to thank Alex for being the best hoodmate, and “partner in crime” that I could ask for. He has supported me since day one with his insight and humor, and truly has helped me through the darkest times of graduate school. It’s been a blast navigating through graduate school together, especially in recruiting the younger graduate students to our group, revamping the group website, and stress-relieving by “dancing” in the bay. I’m so proud of how far we’ve come over these 5 years, and am so grateful to have had you there each step of the way.

I’d like to thank Melinda Chan, Dr. Stephen Sardini, Joel Monroy, and Dr. Veronica Hubble who have been especially supportive during the pandemic. Without them I definitely would have gone insane from social isolation, and I appreciate all their support as I was struggling through graduate school. I enjoyed all the food adventures, mahjong sessions, and random memes that have helped me relieve stress during such stressful times.

I’d also like to thank the younger graduate students that I’ve had the pleasure of getting to know over the last couple of years. The current third and fourth years—Ally, Melinda, Adrian, Farbod, Kevin, Elliot, Jay, Kali, and Samir—are some of the brightest and most humble people I’ve ever met. All of you are incredible chemists, and I can’t wait to see how the group flourishes as you all become fifth years. I’d like to thank Kali for being my gym buddy with Veronica and Vaishnavi over the past year—it has truly helped me grow stronger (literally). I’d also like to thank Jay for taking over almost all of my group jobs and going above and beyond with them—and going to fun concerts with me.

To the second and first years—Ruby, Ben, Kim, Christian, Cami, Marva, Hao, Adrian, Sydney, Chloe, and Jonathan—you all are incredibly talented and thank you for

making the lab such a fun place to be. I wish I had gotten to know each of you more before I turned into a reclusive senior graduate student, but I'm excited to see where you will take the group moving forward. I'd especially like to thank Cami for joining the cyanocycline A project and allowing me to mentor her the past two years. It's been exciting to watch her grow as a skilled and independent chemist, and I am confident that she'll continue to flourish and succeed during the rest of her PhD.

Outside of my academic career, I would like to thank the Caltech community for being so supportive over the years. First, I'd like to thank Denise Lin and Dr. Maria Oh for being indispensable therapists during my five years at Caltech. They have truly helped me during the hardest times, and due to their guidance I've grown a lot as a person that has definitely contributed to my development as a scientist as well. I'd also like to thank the Caltech music community, including the Caltech orchestra, Dr. Glenn Price, and Dr. Hyesung Park for allowing me to continue playing music.

Outside of Caltech, I am deeply grateful for my close friends who have kept me grounded throughout all these years. I'm thankful to my friends from high school— Ben, Esther, Hans, Jackie, Ji Soo, Jiyoung, Justin, Kevin, Michelle, and Yujin—who I rarely get to see because they mostly all live in Virginia, but no matter how long time has passed, the conversation always picks up so naturally when we do hang out. It's been such a joy watching everyone go through major milestones over the past 15 years, and I'm so grateful to have you guys in my life for so many years.

I'd also like to thank my college friends—Rachel Klebanov and Monica Magalhaes—for being so supportive despite being on the opposite coast. Both have visited me several

times in the LA area when I was too busy with school to travel and visit them, for which I'm extremely grateful, and at the same time regretful for not being able to do the same. Thank you for keeping it fun and grounded whenever we do get the chance to hang out, and for staying connected despite the distance and our chaotic schedules.

I am deeply grateful for my partner Matthew Chen and the Chen and Tan family for their incredible support over the last three years. Being a graduate student is often extremely isolating, but they truly made me feel at home with their hospitality and kindness when I started to join Sunday family dinners and holiday festivities. I'd like to thank Audrey Chen for all her support and generosity especially over the last year. Moreover, I'd like to thank Matthew for being the best support system, partner, and best friend I could ask for. Even when I come home from lab in a sour mood, he never fails to cheer me up and make me laugh with his infectious humor, compassion, and patience. I am so lucky to have his overwhelming love and support, and am looking forward to the next chapter of our lives.

Finally, I would like to thank my family for their unconditional support and sacrifice to make this possible. My mom (엄마) and dad (아빠) immigrated to the U.S. in 1992 so that my dad could complete his PhD studies, so in a way it feels like my PhD journey is coming full circle. Despite the challenges of being an immigrant, they decided to stay in the U.S. so that my brothers and I could continue our education, and I am eternally grateful and indebted to them for that. I am deeply thankful for my parents, Branden, Caelan, and my dog Daisy for their continued support and love to make this journey even possible. 감사하고 사랑합니다!

## ABSTRACT

Described herein are two reviews and three projects related to the asymmetric syntheses of tetrahydroisoquinoline (THIQs) alkaloids, and the progress toward the total synthesis of (+)-cyanocycline A. In Chapter 1, a review of the development of asymmetric methodologies for the preparation of enantioenriched *N*-heteroarenes is detailed. In Chapter 2, the development of an iridium-catalyzed enantio- and diastereoselective hydrogenation of 1,3-disubstituted isoquinolines to achieve *cis*-THIQs is reported. Chapter 3 describes the iridium-catalyzed asymmetric hydrogenation of 1,3-disubstituted isoquinolines that can afford *trans*-THIQs in a single transformation. Preliminary mechanistic insights to the iridium-catalyzed asymmetric hydrogenation method using deuterium experiments are detailed.

Chapter 4 details a comprehensive review of the advances in the total syntheses of complex THIQ alkaloids from 2000 – 2020, ranging from simple benzyl THIQ natural products to complex THIQ alkaloids such as Ecteinasclidin-743. In Chapter 5, efforts toward the total synthesis of (+)-cyanocycline A are described, harnessing a non-biomimetic synthetic route through a convergent cross-coupling of two heterocyclic fragments followed by a global hydrogenation event.

**PUBLISHED CONTENT AND CONTRIBUTIONS**

1. Kim, A. N.;<sup>‡</sup> Ngamnithiporn, A.;<sup>‡</sup> Welin, E. R.; Daiger, M. T.; Grünanger, C. U.; Bartberger, M. D.; Virgil, S. C.; Stoltz, B. M. “Iridium-Catalyzed Enantioselective and Diastereoselective Hydrogenation of 1,3-Disubstituted Isoquinolines.” *ACS Catal.* **2020**, *10*, 3241–3248. DOI: 10.1021/acscatal.0c00211

A.N.K. participated in reaction optimization, experimental work, data analysis, and manuscript preparation.

2. Kim, A. N.; Stoltz, B. M. “Recent Advances in Homogeneous Catalysts for the Asymmetric Hydrogenation of Heteroarenes.” *ACS Catal.* **2020**, *10*, 13834–13851. DOI: 10.1021/acscatal.0c03958

A.N.K. participated in collecting references and manuscript preparation.

3. Kim, K. E.; Kim, A. N.; McCormick, C. J.; Stoltz, B. M. “Late-Stage Diversification: A Motivating Force in Organic Synthesis.” *J. Am. Chem. Soc.* **2021**, *143*, 16890–16901. DOI: 10.1021/jacs.1c08920

A.N.K. participated in collecting references and manuscript preparation.

4. Kim, A. N.; Ngamnithiporn, A.; Bartberger, M. D.; Stoltz, B. M. “Iridium-Catalyzed Asymmetric *trans*-Selective Hydrogenation of 1,3-Disubstituted Isoquinolines.” *Chem. Sci.* **2022**, *13*, 3227–3232. DOI: 10.1039/D1SC06729J



A.N.K. participated in reaction optimization, experimental work, data analysis, and manuscript preparation.

5. Kim, A. N.; Ngamnithiporn, A.; Du, E.; Stoltz, B. M. "Recent Advances in the Total Synthesis of the Tetrahydroisoquinoline Alkaloids (2002–2020)." *Chem. Rev.* Manuscript Submitted.

A.N.K. participated in collecting references and manuscript preparation.

## TABLE OF CONTENTS

Dedication.....	iii
Acknowledgements .....	iv
Abstract .....	xi
Published Content and Contributions.....	xii
Table of Contents .....	xiv
List of Figures .....	xx
List of Schemes.....	xlvi
List of Tables.....	lvi
List of Abbreviations .....	lviii
<b>CHAPTER 1</b>	<b>1</b>
<i>Advances in Homogeneous Catalysts for the Asymmetric Hydrogenation of Heteroarenes (2002–2020)</i>	
1.1 Introduction .....	1
1.2 General Mechanistic Considerations .....	2
1.3 Ruthenium-Catalyzed Asymmetric Hydrogenation .....	6
1.4 Iridium-Catalyzed Asymmetric Hydrogenation .....	14
1.5 Rhodium-Catalyzed Asymmetric Hydrogenation .....	23
1.6 Palladium-Catalyzed Asymmetric Hydrogenation .....	25
1.7 Iron-Catalyzed Asymmetric Hydrogenation .....	29
1.8 Borane-Catalyzed Asymmetric Hydrogenation .....	31
1.9 Chiral Phosphoric Acid-Catalyzed Asymmetric Hydrogenation.....	34

1.10	Conclusion .....	38
1.11	References and Notes .....	41

## **CHAPTER 2** **51**

### *Iridium-Catalyzed Enantioselective and Diastereoselective Hydrogenation of 1,3-Disubstituted Isoquinolines*

2.1	Introduction .....	51
2.2	Substrate Syntheses .....	55
2.3	Reaction Optimization .....	56
2.4	Substrate Scope .....	58
2.5	Synthetic Utility .....	65
2.6	Conclusion .....	67
2.7	Experimental Section .....	67
2.7.1	Materials and Methods .....	67
2.7.2	Experimental Procedures and Spectroscopic Data .....	69
2.7.2.1	Syntheses of Hydroxymethyl 1,3-Disubstituted Isoquinolines ....	69
2.7.2.2	Syntheses of Isoquinolines with Different Directing Groups .....	108
2.7.2.3	Hydrogenation Reactions .....	112
2.7.2.4	Product Transformations .....	139
2.7.3	Additional Optimization Results .....	144
2.7.4	Determination of Enantiomeric Excess .....	145
2.7.5	Determination of Relative and Absolute Stereochemistry .....	151
2.8	References and Notes .....	156

## **APPENDIX 1** **161**

### *Spectra Relevant to Chapter 2*

<b>APPENDIX 2</b>	<b>377</b>
<i>X-Ray Crystallography Reports Relevant to Chapter 2</i>	
<b>CHAPTER 3</b>	<b>385</b>
<i>Iridium-Catalyzed Asymmetric Trans-Selective Hydrogenation of 1,3-Disubstituted Isoquinolines</i>	
3.1 Introduction .....	385
3.2 Reaction Optimization .....	387
3.3 Substrate Scope .....	390
3.4 Synthetic Utility .....	392
3.5 Preliminary Mechanistic Insights.....	393
3.6 Conclusions .....	395
3.7 Experimental Section .....	396
3.7.1 Materials and Methods .....	396
3.7.2 Experimental Procedures and Spectroscopic Data .....	397
3.7.2.1 Syntheses of Hydroxymethyl 1,3-Disubstituted Isoquinolines ..	397
3.7.2.2 Syntheses of Isoquinolines with Different Directing Groups .....	415
3.7.2.3 Hydrogenation Reactions.....	419
3.7.2.4 Product Transformations .....	435
3.7.3 Additional Optimization Results.....	438
3.7.4 Deuterium Incorporation Experiments.....	439
3.7.5 Proposed Catalytic Cycle .....	440
3.7.6 Determination of Enantiomeric Excess .....	441
3.7.7 Determination of Relative and Absolute Stereochemistry .....	444
3.8 References and Notes .....	446
<b>APPENDIX 3</b>	<b>451</b>
<i>Spectra Relevant to Chapter 3</i>	

**APPENDIX 4** **501**  
*X-Ray Crystallography Reports Relevant to Chapter 3*

**CHAPTER 4** **512**  
*Advances in the Total Synthesis of the  
 Tetrahydroisoquinoline Alkaloids (2002–2020)*

4.1	Introduction .....	512
4.2	Tetrahydroisoquinoline Alkaloids .....	513
4.2.1	General Structure and Biosynthesis .....	513
4.3	Spirocyclic Tetrahydroisoquinoline Alkaloids .....	514
4.3.1	General Structure and Biosynthesis .....	514
4.3.2	Total Synthesis of Erythrina Alkaloids .....	515
4.4	Benzyltetrahydroisoquinoline Alkaloids .....	523
4.4.1	Aporphine Alkaloids .....	525
4.4.1.1	General Structure and Biosynthesis .....	525
4.4.1.2	Total Synthesis of Aporphine Alkaloids.....	526
4.4.2	Bisbenzyltetrahydroisoquinoline Alkaloids .....	534
4.4.2.1	General Structure and Biosynthesis .....	534
4.4.2.2	Total Synthesis of Bisbenzyl THIQ Alkaloids .....	536
4.4.3	Protoberberine Alkaloids .....	541
4.4.3.1	General Structure and Biosynthesis .....	541
4.4.3.2	Total Synthesis of Protoberberine Alkaloids.....	542
4.4.4	Morphinan Alkaloids .....	553
4.4.4.1	General Structure and Biosynthesis .....	553
4.4.4.2	Total Synthesis of Morphinan Alkaloids.....	555
4.4.5	Pavine and Isopavine Alkaloids .....	570
4.4.5.1	General Structure and Biosynthesis .....	570
4.4.5.2	Total Synthesis of Pavine and Isopavine Alkaloids.....	571
4.5	THIQ Alkaloids from the Saframycin Family .....	575

4.5.1	Saframycin Alkaloids .....	576
4.5.1.1	General Structure and Biosynthesis .....	576
4.5.1.2	Total Synthesis of Saframycin Alkaloids .....	579
4.5.2	Safracin Alkaloids .....	581
4.5.2.1	General Structure and Biosynthesis .....	582
4.5.2.2	Total Synthesis of Safracin Alkaloids.....	582
4.5.3	Renieramycin Alkaloids .....	583
4.5.3.1	General Structure and Biosynthesis .....	583
4.5.3.2	Total Synthesis of Renieramycin Alkaloids.....	585
4.5.4	Ecteinasidin Alkaloids .....	602
4.5.4.1	General Structure and Biosynthesis .....	602
4.5.4.2	Total Synthesis of Ecteinasidin Alkaloids.....	604
4.6	THIQ Alkaloids from the Naphthyridinomycin Family .....	612
4.6.1	General Structure and Biosynthesis .....	612
4.6.2	Total Synthesis of Naphthyridinomycin Alkaloids.....	615
4.7	THIQ Alkaloids from the Quinocarcin Family .....	616
4.7.1	General Structure and Biosynthesis .....	617
4.7.2	Total Synthesis of Quinocarcin Alkaloids .....	618
4.7.3	Total Synthesis of Tetrazomine.....	623
4.7.4	Total Synthesis of Lemonomycin.....	626
4.8	Conclusions .....	629
4.9	References and Notes .....	629

## **CHAPTER 5** **645**

### *Progress Toward the Total Synthesis Of (+)-Cyanocycline A*

5.1	Introduction.....	645
5.2	Retrosynthetic Analysis .....	648

5.3	First Generation Approach .....	649
5.4	Second Generation Approach .....	661
5.5	Third Generation Approach .....	665
5.6	Conclusion and Future Directions .....	669
5.7	Experimental Section .....	671
5.7.1	Materials and Methods .....	671
5.7.2	Experimental Procedures and Spectroscopic Data .....	672
5.8	References and Notes .....	711
<b>APPENDIX 5</b>		<b>715</b>
<i>Synthetic Summary of Chapter 5</i>		
<b>APPENDIX 6</b>		<b>721</b>
<i>Spectra Relevant to Chapter 5</i>		
Comprehensive Bibliography.....		778
About the Author.....		808

## LIST OF FIGURES

### CHAPTER 1

#### *Advances in Homogeneous Catalysts for the Asymmetric Hydrogenation of Heteroarenes (2002–2020)*

<b>Figure 1.1</b>	Overview of the total number of published reports on the asymmetric hydrogenation of common heteroarenes .....	3
<b>Figure 1.2</b>	Common Ru-based catalyst systems for the asymmetric hydrogenation of heteroarenes .....	7
<b>Figure 1.3</b>	Proposed catalytic cycle for the asymmetric hydrogenation of quinolines with a Ru/TsDPEN catalyst.....	11
<b>Figure 1.4</b>	Common Ir-based catalyst systems for the asymmetric hydrogenation of heteroarenes .....	15
<b>Figure 1.5</b>	Proposed catalytic cycle for the Ir-catalyzed asymmetric hydrogenation of quinolines.....	17
<b>Figure 1.6</b>	Common Rh-based catalyst systems for the asymmetric hydrogenation of heteroarenes .....	24
<b>Figure 1.7</b>	Proposed catalytic cycle for the Rh-catalyzed asymmetric hydrogenation of indoles .....	26
<b>Figure 1.8</b>	Common Pd-based catalyst systems for the asymmetric hydrogenation of heteroarenes .....	27
<b>Figure 1.9</b>	Proposed catalytic cycle for the Pd-catalyzed asymmetric hydrogenation of indoles .....	28
<b>Figure 1.10</b>	Proposed cooperative catalytic cycle for the Fe-catalyzed asymmetric hydrogenation of benzoxazines .....	31
<b>Figure 1.11</b>	Common chiral phosphoric acid catalyst systems for the asymmetric hydrogenation of heteroarenes .....	35
<b>Figure 1.12</b>	Proposed catalytic cycle for the asymmetric transfer hydrogenation of quinolines using a chiral phosphoric acid and Hantzsch ester .....	37



**CHAPTER 2***Iridium-Catalyzed Enantioselective and Diastereoselective Hydrogenation of 1,3-Disubstituted Isoquinolines*

<b>Figure 2.1</b>	Limitations in enantioselective hydrogenation of <i>N</i> -heterocycles and previous examples of Ir-catalyzed asymmetric hydrogenation .....	53
<b>Figure 2.2</b>	Our research on Ir-catalyzed enantioselective and diastereoselective hydrogenation of 1,3-disubstituted isoquinolines .....	54
<b>Figure 2.3</b>	Experimental and computed IR and VCD spectra for the cis isomers of <b>167e</b> .....	153
<b>Figure 2.4</b>	Experimental and computed IR and VCD spectra for the trans isomers of <b>167e</b> .....	153

**APPENDIX 1***Spectra Relevant to Chapter 2*

<b>Figure A1.1</b>	<sup>1</sup> H NMR (400 MHz, CDCl <sub>3</sub> ) of compound <b>159a</b> .....	162
<b>Figure A1.2</b>	Infrared spectrum (Thin Film, NaCl) of compound <b>159a</b> .....	163
<b>Figure A1.3</b>	<sup>13</sup> C NMR (100 MHz, CDCl <sub>3</sub> ) of compound <b>159a</b> .....	163
<b>Figure A1.4</b>	<sup>1</sup> H NMR (400 MHz, CDCl <sub>3</sub> ) of compound <b>159b</b> .....	164
<b>Figure A1.5</b>	Infrared spectrum (Thin Film, NaCl) of compound <b>159b</b> .....	165
<b>Figure A1.6</b>	<sup>13</sup> C NMR (100 MHz, CDCl <sub>3</sub> ) of compound <b>159b</b> .....	165
<b>Figure A1.7</b>	<sup>19</sup> F NMR (282 MHz, CDCl <sub>3</sub> ) of compound <b>159b</b> .....	166
<b>Figure A1.8</b>	<sup>1</sup> H NMR (400 MHz, CDCl <sub>3</sub> ) of compound <b>159c</b> .....	167
<b>Figure A1.9</b>	Infrared spectrum (Thin Film, NaCl) of compound <b>159c</b> .....	168
<b>Figure A1.10</b>	<sup>13</sup> C NMR (100 MHz, CDCl <sub>3</sub> ) of compound <b>159c</b> .....	168
<b>Figure A1.11</b>	<sup>1</sup> H NMR (400 MHz, CDCl <sub>3</sub> ) of compound <b>159d</b> .....	169

<b>Figure A1.12</b>	Infrared spectrum (Thin Film, NaCl) of compound <b>159d</b> .....	170
<b>Figure A1.13</b>	$^{13}\text{C}$ NMR (100 MHz, $\text{CDCl}_3$ ) of compound <b>159d</b> .....	170
<b>Figure A1.14</b>	$^1\text{H}$ NMR (400 MHz, $\text{CDCl}_3$ ) of compound <b>160a</b> .....	171
<b>Figure A1.15</b>	Infrared spectrum (Thin Film, NaCl) of compound <b>160a</b> .....	172
<b>Figure A1.16</b>	$^{13}\text{C}$ NMR (100 MHz, $\text{CDCl}_3$ ) of compound <b>160a</b> .....	172
<b>Figure A1.17</b>	$^{19}\text{F}$ NMR (282 MHz, $\text{CDCl}_3$ ) of compound <b>160a</b> .....	173
<b>Figure A1.18</b>	$^1\text{H}$ NMR (400 MHz, $\text{CDCl}_3$ ) of compound <b>160b</b> .....	174
<b>Figure A1.19</b>	Infrared spectrum (Thin Film, NaCl) of compound <b>160b</b> .....	175
<b>Figure A1.20</b>	$^{13}\text{C}$ NMR (100 MHz, $\text{CDCl}_3$ ) of compound <b>160b</b> .....	175
<b>Figure A1.21</b>	$^{19}\text{F}$ NMR (282 MHz, $\text{CDCl}_3$ ) of compound <b>160b</b> .....	176
<b>Figure A1.22</b>	$^1\text{H}$ NMR (400 MHz, $\text{CDCl}_3$ ) of compound <b>160c</b> .....	177
<b>Figure A1.23</b>	Infrared spectrum (Thin Film, NaCl) of compound <b>160c</b> .....	178
<b>Figure A1.24</b>	$^{13}\text{C}$ NMR (100 MHz, $\text{CDCl}_3$ ) of compound <b>160c</b> .....	178
<b>Figure A1.25</b>	$^{19}\text{F}$ NMR (282 MHz, $\text{CDCl}_3$ ) of compound <b>160c</b> .....	179
<b>Figure A1.26</b>	$^1\text{H}$ NMR (400 MHz, $\text{CDCl}_3$ ) of compound <b>160d</b> .....	180
<b>Figure A1.27</b>	Infrared spectrum (Thin Film, NaCl) of compound <b>160d</b> .....	181
<b>Figure A1.28</b>	$^{13}\text{C}$ NMR (100 MHz, $\text{CDCl}_3$ ) of compound <b>160d</b> .....	181
<b>Figure A1.29</b>	$^{19}\text{F}$ NMR (282 MHz, $\text{CDCl}_3$ ) of compound <b>160d</b> .....	182
<b>Figure A1.30</b>	$^1\text{H}$ NMR (400 MHz, $\text{CDCl}_3$ ) of compound <b>161a</b> .....	183
<b>Figure A1.31</b>	Infrared spectrum (Thin Film, NaCl) of compound <b>161a</b> .....	184
<b>Figure A1.32</b>	$^{13}\text{C}$ NMR (100 MHz, $\text{CDCl}_3$ ) of compound <b>161a</b> .....	184
<b>Figure A1.33</b>	$^1\text{H}$ NMR (400 MHz, $\text{CDCl}_3$ ) of compound <b>161b</b> .....	185

<b>Figure A1.34</b>	Infrared spectrum (Thin Film, NaCl) of compound <b>161b</b> .....	186
<b>Figure A1.35</b>	$^{13}\text{C}$ NMR (100 MHz, $\text{CDCl}_3$ ) of compound <b>161b</b> .....	186
<b>Figure A1.36</b>	$^1\text{H}$ NMR (400 MHz, $\text{CDCl}_3$ ) of compound <b>161c</b> .....	187
<b>Figure A1.37</b>	Infrared spectrum (Thin Film, NaCl) of compound <b>161c</b> .....	188
<b>Figure A1.38</b>	$^{13}\text{C}$ NMR (100 MHz, $\text{CDCl}_3$ ) of compound <b>161c</b> .....	188
<b>Figure A1.39</b>	$^1\text{H}$ NMR (400 MHz, $\text{CDCl}_3$ ) of compound <b>161d</b> .....	189
<b>Figure A1.40</b>	Infrared spectrum (Thin Film, NaCl) of compound <b>161d</b> .....	190
<b>Figure A1.41</b>	$^{13}\text{C}$ NMR (100 MHz, $\text{CDCl}_3$ ) of compound <b>161d</b> .....	190
<b>Figure A1.42</b>	$^1\text{H}$ NMR (400 MHz, $\text{CDCl}_3$ ) of compound <b>161e</b> .....	191
<b>Figure A1.43</b>	Infrared spectrum (Thin Film, NaCl) of compound <b>161e</b> .....	192
<b>Figure A1.44</b>	$^{13}\text{C}$ NMR (100 MHz, $\text{CDCl}_3$ ) of compound <b>161e</b> .....	192
<b>Figure A1.45</b>	$^{19}\text{F}$ NMR (282 MHz, $\text{CDCl}_3$ ) of compound <b>161e</b> .....	193
<b>Figure A1.46</b>	$^1\text{H}$ NMR (400 MHz, $\text{CDCl}_3$ ) of compound <b>161f</b> .....	194
<b>Figure A1.47</b>	Infrared spectrum (Thin Film, NaCl) of compound <b>161f</b> .....	195
<b>Figure A1.48</b>	$^{13}\text{C}$ NMR (100 MHz, $\text{CDCl}_3$ ) of compound <b>161f</b> .....	195
<b>Figure A1.49</b>	$^{19}\text{F}$ NMR (282 MHz, $\text{CDCl}_3$ ) of compound <b>161f</b> .....	196
<b>Figure A1.50</b>	$^1\text{H}$ NMR (400 MHz, $\text{CDCl}_3$ ) of compound <b>161g</b> .....	197
<b>Figure A1.51</b>	Infrared spectrum (Thin Film, NaCl) of compound <b>161g</b> .....	198
<b>Figure A1.52</b>	$^{13}\text{C}$ NMR (100 MHz, $\text{CDCl}_3$ ) of compound <b>161g</b> .....	198
<b>Figure A1.53</b>	$^1\text{H}$ NMR (400 MHz, $\text{CDCl}_3$ ) of compound <b>161h</b> .....	199
<b>Figure A1.54</b>	Infrared spectrum (Thin Film, NaCl) of compound <b>161h</b> .....	200
<b>Figure A1.55</b>	$^{13}\text{C}$ NMR (100 MHz, $\text{CDCl}_3$ ) of compound <b>161h</b> .....	200

<b>Figure A1.56</b>	$^1\text{H}$ NMR (400 MHz, $\text{CDCl}_3$ ) of compound <b>161i</b> .....	201
<b>Figure A1.57</b>	Infrared spectrum (Thin Film, NaCl) of compound <b>161i</b> .....	202
<b>Figure A1.58</b>	$^{13}\text{C}$ NMR (100 MHz, $\text{CDCl}_3$ ) of compound <b>161i</b> .....	202
<b>Figure A1.59</b>	$^{19}\text{F}$ NMR (282 MHz, $\text{CDCl}_3$ ) of compound <b>161i</b> .....	203
<b>Figure A1.60</b>	$^1\text{H}$ NMR (400 MHz, $\text{CDCl}_3$ ) of compound <b>161j</b> .....	204
<b>Figure A1.61</b>	Infrared spectrum (Thin Film, NaCl) of compound <b>161j</b> .....	205
<b>Figure A1.62</b>	$^{13}\text{C}$ NMR (100 MHz, $\text{CDCl}_3$ ) of compound <b>161j</b> .....	205
<b>Figure A1.63</b>	$^1\text{H}$ NMR (400 MHz, $\text{CDCl}_3$ ) of compound <b>161k</b> .....	206
<b>Figure A1.64</b>	Infrared spectrum (Thin Film, NaCl) of compound <b>161k</b> .....	207
<b>Figure A1.65</b>	$^{13}\text{C}$ NMR (100 MHz, $\text{CDCl}_3$ ) of compound <b>161k</b> .....	207
<b>Figure A1.66</b>	$^1\text{H}$ NMR (400 MHz, $\text{CDCl}_3$ ) of compound <b>161l</b> .....	208
<b>Figure A1.67</b>	Infrared spectrum (Thin Film, NaCl) of compound <b>161l</b> .....	209
<b>Figure A1.68</b>	$^{13}\text{C}$ NMR (100 MHz, $\text{CDCl}_3$ ) of compound <b>161l</b> .....	209
<b>Figure A1.69</b>	$^1\text{H}$ NMR (400 MHz, $\text{CDCl}_3$ ) of compound <b>161m</b> .....	210
<b>Figure A1.70</b>	Infrared spectrum (Thin Film, NaCl) of compound <b>161m</b> .....	211
<b>Figure A1.71</b>	$^{13}\text{C}$ NMR (100 MHz, $\text{CDCl}_3$ ) of compound <b>161m</b> .....	211
<b>Figure A1.72</b>	$^1\text{H}$ NMR (400 MHz, $\text{CDCl}_3$ ) of compound <b>161n</b> .....	212
<b>Figure A1.73</b>	Infrared spectrum (Thin Film, NaCl) of compound <b>161n</b> .....	213
<b>Figure A1.74</b>	$^{13}\text{C}$ NMR (100 MHz, $\text{CDCl}_3$ ) of compound <b>161n</b> .....	213
<b>Figure A1.75</b>	$^1\text{H}$ NMR (400 MHz, $\text{CDCl}_3$ ) of compound <b>161o</b> .....	214
<b>Figure A1.76</b>	Infrared spectrum (Thin Film, NaCl) of compound <b>161o</b> .....	215
<b>Figure A1.77</b>	$^{13}\text{C}$ NMR (100 MHz, $\text{CDCl}_3$ ) of compound <b>161o</b> .....	215

<b>Figure A1.78</b>	$^1\text{H}$ NMR (400 MHz, $\text{CDCl}_3$ ) of compound <b>161p</b> .....	216
<b>Figure A1.79</b>	Infrared spectrum (Thin Film, NaCl) of compound <b>161p</b> .....	217
<b>Figure A1.80</b>	$^{13}\text{C}$ NMR (100 MHz, $\text{CDCl}_3$ ) of compound <b>161p</b> .....	217
<b>Figure A1.81</b>	$^1\text{H}$ NMR (400 MHz, $\text{CDCl}_3$ ) of compound <b>161q</b> .....	218
<b>Figure A1.82</b>	Infrared spectrum (Thin Film, NaCl) of compound <b>161q</b> .....	219
<b>Figure A1.83</b>	$^{13}\text{C}$ NMR (100 MHz, $\text{CDCl}_3$ ) of compound <b>161q</b> .....	219
<b>Figure A1.84</b>	$^1\text{H}$ NMR (400 MHz, $\text{CDCl}_3$ ) of compound <b>161r</b> .....	220
<b>Figure A1.85</b>	Infrared spectrum (Thin Film, NaCl) of compound <b>161r</b> .....	221
<b>Figure A1.86</b>	$^{13}\text{C}$ NMR (100 MHz, $\text{CDCl}_3$ ) of compound <b>161r</b> .....	221
<b>Figure A1.87</b>	$^1\text{H}$ NMR (400 MHz, $\text{CDCl}_3$ ) of compound <b>172a</b> .....	222
<b>Figure A1.88</b>	Infrared spectrum (Thin Film, NaCl) of compound <b>172a</b> .....	223
<b>Figure A1.89</b>	$^{13}\text{C}$ NMR (100 MHz, $\text{CDCl}_3$ ) of compound <b>172a</b> .....	223
<b>Figure A1.90</b>	$^{19}\text{F}$ NMR (282 MHz, $\text{CDCl}_3$ ) of compound <b>172a</b> .....	224
<b>Figure A1.91</b>	$^1\text{H}$ NMR (400 MHz, $\text{CDCl}_3$ ) of compound <b>172b</b> .....	225
<b>Figure A1.92</b>	Infrared spectrum (Thin Film, NaCl) of compound <b>172b</b> .....	226
<b>Figure A1.93</b>	$^{13}\text{C}$ NMR (100 MHz, $\text{CDCl}_3$ ) of compound <b>172b</b> .....	226
<b>Figure A1.94</b>	$^{19}\text{F}$ NMR (282 MHz, $\text{CDCl}_3$ ) of compound <b>172b</b> .....	227
<b>Figure A1.95</b>	$^1\text{H}$ NMR (400 MHz, $\text{CDCl}_3$ ) of compound <b>172c</b> .....	228
<b>Figure A1.96</b>	Infrared spectrum (Thin Film, NaCl) of compound <b>172c</b> .....	229
<b>Figure A1.97</b>	$^{13}\text{C}$ NMR (100 MHz, $\text{CDCl}_3$ ) of compound <b>172c</b> .....	229
<b>Figure A1.98</b>	$^{19}\text{F}$ NMR (282 MHz, $\text{CDCl}_3$ ) of compound <b>172c</b> .....	230
<b>Figure A1.99</b>	$^1\text{H}$ NMR (400 MHz, $\text{CDCl}_3$ ) of compound <b>172d</b> .....	231

<b>Figure A1.100</b>	Infrared spectrum (Thin Film, NaCl) of compound <b>172d</b> .....	232
<b>Figure A1.101</b>	$^{13}\text{C}$ NMR (100 MHz, $\text{CDCl}_3$ ) of compound <b>172d</b> .....	232
<b>Figure A1.102</b>	$^1\text{H}$ NMR (400 MHz, $\text{CDCl}_3$ ) of compound <b>172e</b> .....	233
<b>Figure A1.103</b>	Infrared spectrum (Thin Film, NaCl) of compound <b>172e</b> .....	234
<b>Figure A1.104</b>	$^{13}\text{C}$ NMR (100 MHz, $\text{CDCl}_3$ ) of compound <b>172e</b> .....	234
<b>Figure A1.105</b>	$^1\text{H}$ NMR (400 MHz, $\text{CDCl}_3$ ) of compound <b>172f</b> .....	235
<b>Figure A1.106</b>	Infrared spectrum (Thin Film, NaCl) of compound <b>172f</b> .....	236
<b>Figure A1.107</b>	$^{13}\text{C}$ NMR (100 MHz, $\text{CDCl}_3$ ) of compound <b>172f</b> .....	236
<b>Figure A1.108</b>	$^1\text{H}$ NMR (400 MHz, $\text{CDCl}_3$ ) of compound <b>162a</b> .....	237
<b>Figure A1.109</b>	Infrared spectrum (Thin Film, NaCl) of compound <b>162a</b> .....	238
<b>Figure A1.110</b>	$^{13}\text{C}$ NMR (100 MHz, $\text{CDCl}_3$ ) of compound <b>162a</b> .....	238
<b>Figure A1.111</b>	$^1\text{H}$ NMR (400 MHz, $\text{CDCl}_3$ ) of compound <b>162b</b> .....	239
<b>Figure A1.112</b>	Infrared spectrum (Thin Film, NaCl) of compound <b>162b</b> .....	240
<b>Figure A1.113</b>	$^{13}\text{C}$ NMR (100 MHz, $\text{CDCl}_3$ ) of compound <b>162b</b> .....	240
<b>Figure A1.114</b>	$^1\text{H}$ NMR (400 MHz, $\text{CDCl}_3$ ) of compound <b>162c</b> .....	241
<b>Figure A1.115</b>	Infrared spectrum (Thin Film, NaCl) of compound <b>162c</b> .....	242
<b>Figure A1.116</b>	$^{13}\text{C}$ NMR (100 MHz, $\text{CDCl}_3$ ) of compound <b>162c</b> .....	242
<b>Figure A1.117</b>	$^1\text{H}$ NMR (400 MHz, $\text{CDCl}_3$ ) of compound <b>162d</b> .....	243
<b>Figure A1.118</b>	Infrared spectrum (Thin Film, NaCl) of compound <b>162d</b> .....	244
<b>Figure A1.119</b>	$^{13}\text{C}$ NMR (100 MHz, $\text{CDCl}_3$ ) of compound <b>162d</b> .....	244
<b>Figure A1.120</b>	$^1\text{H}$ NMR (400 MHz, $\text{CDCl}_3$ ) of compound <b>162e</b> .....	245
<b>Figure A1.121</b>	Infrared spectrum (Thin Film, NaCl) of compound <b>162e</b> .....	246

<b>Figure A1.122</b>	$^{13}\text{C}$ NMR (100 MHz, $\text{CDCl}_3$ ) of compound <b>162e</b> .....	246
<b>Figure A1.123</b>	$^{19}\text{F}$ NMR (282 MHz, $\text{CDCl}_3$ ) of compound <b>162e</b> .....	247
<b>Figure A1.124</b>	$^1\text{H}$ NMR (400 MHz, $\text{CDCl}_3$ ) of compound <b>162f</b> .....	248
<b>Figure A1.125</b>	Infrared spectrum (Thin Film, NaCl) of compound <b>162f</b> .....	249
<b>Figure A1.126</b>	$^{13}\text{C}$ NMR (100 MHz, $\text{CDCl}_3$ ) of compound <b>162f</b> .....	249
<b>Figure A1.127</b>	$^{19}\text{F}$ NMR (282 MHz, $\text{CDCl}_3$ ) of compound <b>162f</b> .....	250
<b>Figure A1.128</b>	$^1\text{H}$ NMR (400 MHz, $\text{CDCl}_3$ ) of compound <b>162g</b> .....	251
<b>Figure A1.129</b>	Infrared spectrum (Thin Film, NaCl) of compound <b>162g</b> .....	252
<b>Figure A1.130</b>	$^{13}\text{C}$ NMR (100 MHz, $\text{CDCl}_3$ ) of compound <b>162g</b> .....	252
<b>Figure A1.131</b>	$^1\text{H}$ NMR (400 MHz, $\text{CDCl}_3$ ) of compound <b>162h</b> .....	253
<b>Figure A1.132</b>	Infrared spectrum (Thin Film, NaCl) of compound <b>162h</b> .....	254
<b>Figure A1.133</b>	$^{13}\text{C}$ NMR (100 MHz, $\text{CDCl}_3$ ) of compound <b>162h</b> .....	254
<b>Figure A1.134</b>	$^1\text{H}$ NMR (400 MHz, $\text{CDCl}_3$ ) of compound <b>162i</b> .....	255
<b>Figure A1.135</b>	Infrared spectrum (Thin Film, NaCl) of compound <b>162i</b> .....	256
<b>Figure A1.136</b>	$^{13}\text{C}$ NMR (100 MHz, $\text{CDCl}_3$ ) of compound <b>162i</b> .....	256
<b>Figure A1.137</b>	$^{19}\text{F}$ NMR (282 MHz, $\text{CDCl}_3$ ) of compound <b>162i</b> .....	257
<b>Figure A1.138</b>	$^1\text{H}$ NMR (400 MHz, $\text{CDCl}_3$ ) of compound <b>162j</b> .....	258
<b>Figure A1.139</b>	Infrared spectrum (Thin Film, NaCl) of compound <b>162j</b> .....	259
<b>Figure A1.140</b>	$^{13}\text{C}$ NMR (100 MHz, $\text{CDCl}_3$ ) of compound <b>162j</b> .....	259
<b>Figure A1.141</b>	$^1\text{H}$ NMR (400 MHz, $\text{CDCl}_3$ ) of compound <b>162k</b> .....	260
<b>Figure A1.142</b>	Infrared spectrum (Thin Film, NaCl) of compound <b>162k</b> .....	261
<b>Figure A1.143</b>	$^{13}\text{C}$ NMR (100 MHz, $\text{CDCl}_3$ ) of compound <b>162k</b> .....	261

<b>Figure A1.144</b>	$^1\text{H}$ NMR (400 MHz, $\text{CDCl}_3$ ) of compound <b>162l</b> .....	262
<b>Figure A1.145</b>	Infrared spectrum (Thin Film, NaCl) of compound <b>162l</b> .....	263
<b>Figure A1.146</b>	$^{13}\text{C}$ NMR (100 MHz, $\text{CDCl}_3$ ) of compound <b>162l</b> .....	263
<b>Figure A1.147</b>	$^1\text{H}$ NMR (400 MHz, $\text{CDCl}_3$ ) of compound <b>162m</b> .....	264
<b>Figure A1.148</b>	Infrared spectrum (Thin Film, NaCl) of compound <b>162m</b> .....	265
<b>Figure A1.149</b>	$^{13}\text{C}$ NMR (100 MHz, $\text{CDCl}_3$ ) of compound <b>162m</b> .....	265
<b>Figure A1.150</b>	$^1\text{H}$ NMR (400 MHz, $\text{CDCl}_3$ ) of compound <b>162n</b> .....	266
<b>Figure A1.151</b>	Infrared spectrum (Thin Film, NaCl) of compound <b>162n</b> .....	267
<b>Figure A1.152</b>	$^{13}\text{C}$ NMR (100 MHz, $\text{CDCl}_3$ ) of compound <b>162n</b> .....	267
<b>Figure A1.153</b>	$^1\text{H}$ NMR (400 MHz, $\text{CDCl}_3$ ) of compound <b>162o</b> .....	268
<b>Figure A1.154</b>	Infrared spectrum (Thin Film, NaCl) of compound <b>162o</b> .....	269
<b>Figure A1.155</b>	$^{13}\text{C}$ NMR (100 MHz, $\text{CDCl}_3$ ) of compound <b>162o</b> .....	269
<b>Figure A1.156</b>	$^1\text{H}$ NMR (400 MHz, $\text{CDCl}_3$ ) of compound <b>162p</b> .....	270
<b>Figure A1.157</b>	Infrared spectrum (Thin Film, NaCl) of compound <b>162p</b> .....	271
<b>Figure A1.158</b>	$^{13}\text{C}$ NMR (100 MHz, $\text{CDCl}_3$ ) of compound <b>162p</b> .....	271
<b>Figure A1.159</b>	$^1\text{H}$ NMR (400 MHz, $\text{CDCl}_3$ ) of compound <b>162q</b> .....	272
<b>Figure A1.160</b>	Infrared spectrum (Thin Film, NaCl) of compound <b>162q</b> .....	273
<b>Figure A1.161</b>	$^{13}\text{C}$ NMR (100 MHz, $\text{CDCl}_3$ ) of compound <b>162q</b> .....	273
<b>Figure A1.162</b>	$^1\text{H}$ NMR (400 MHz, $\text{CDCl}_3$ ) of compound <b>162r</b> .....	274
<b>Figure A1.163</b>	Infrared spectrum (Thin Film, NaCl) of compound <b>162r</b> .....	275
<b>Figure A1.164</b>	$^{13}\text{C}$ NMR (100 MHz, $\text{CDCl}_3$ ) of compound <b>162r</b> .....	275
<b>Figure A1.165</b>	$^1\text{H}$ NMR (400 MHz, $\text{CDCl}_3$ ) of compound <b>164a</b> .....	276



<b>Figure A1.166</b>	Infrared spectrum (Thin Film, NaCl) of compound <b>164a</b> .....	277
<b>Figure A1.167</b>	$^{13}\text{C}$ NMR (100 MHz, $\text{CDCl}_3$ ) of compound <b>164a</b> .....	277
<b>Figure A1.168</b>	$^{19}\text{F}$ NMR (282 MHz, $\text{CDCl}_3$ ) of compound <b>164a</b> .....	278
<b>Figure A1.169</b>	$^1\text{H}$ NMR (400 MHz, $\text{CDCl}_3$ ) of compound <b>164b</b> .....	279
<b>Figure A1.170</b>	Infrared spectrum (Thin Film, NaCl) of compound <b>164b</b> .....	280
<b>Figure A1.171</b>	$^{13}\text{C}$ NMR (100 MHz, $\text{CDCl}_3$ ) of compound <b>164b</b> .....	280
<b>Figure A1.172</b>	$^{19}\text{F}$ NMR (282 MHz, $\text{CDCl}_3$ ) of compound <b>164b</b> .....	281
<b>Figure A1.173</b>	$^1\text{H}$ NMR (400 MHz, $\text{CDCl}_3$ ) of compound <b>164c</b> .....	282
<b>Figure A1.174</b>	Infrared spectrum (Thin Film, NaCl) of compound <b>164c</b> .....	283
<b>Figure A1.175</b>	$^{13}\text{C}$ NMR (100 MHz, $\text{CDCl}_3$ ) of compound <b>164c</b> .....	283
<b>Figure A1.176</b>	$^{19}\text{F}$ NMR (282 MHz, $\text{CDCl}_3$ ) of compound <b>164c</b> .....	284
<b>Figure A1.177</b>	$^1\text{H}$ NMR (400 MHz, $\text{CDCl}_3$ ) of compound <b>164d</b> .....	285
<b>Figure A1.178</b>	Infrared spectrum (Thin Film, NaCl) of compound <b>164d</b> .....	286
<b>Figure A1.179</b>	$^{13}\text{C}$ NMR (100 MHz, $\text{CDCl}_3$ ) of compound <b>164d</b> .....	286
<b>Figure A1.180</b>	$^1\text{H}$ NMR (400 MHz, $\text{CDCl}_3$ ) of compound <b>164e</b> .....	287
<b>Figure A1.181</b>	Infrared spectrum (Thin Film, NaCl) of compound <b>164e</b> .....	288
<b>Figure A1.182</b>	$^{13}\text{C}$ NMR (100 MHz, $\text{CDCl}_3$ ) of compound <b>164e</b> .....	288
<b>Figure A1.183</b>	$^1\text{H}$ NMR (400 MHz, $\text{CDCl}_3$ ) of compound <b>164f</b> .....	289
<b>Figure A1.184</b>	Infrared spectrum (Thin Film, NaCl) of compound <b>164f</b> .....	290
<b>Figure A1.185</b>	$^{13}\text{C}$ NMR (100 MHz, $\text{CDCl}_3$ ) of compound <b>164f</b> .....	290
<b>Figure A1.186</b>	$^1\text{H}$ NMR (400 MHz, $\text{CDCl}_3$ ) of compound <b>166a</b> .....	291
<b>Figure A1.187</b>	Infrared spectrum (Thin Film, NaCl) of compound <b>166a</b> .....	292

<b>Figure A1.188</b>	$^{13}\text{C}$ NMR (100 MHz, $\text{CDCl}_3$ ) of compound <b>166a</b> .....	292
<b>Figure A1.189</b>	$^1\text{H}$ NMR (400 MHz, $\text{CDCl}_3$ ) of compound <b>166b</b> .....	293
<b>Figure A1.190</b>	Infrared spectrum (Thin Film, NaCl) of compound <b>166b</b> .....	294
<b>Figure A1.191</b>	$^{13}\text{C}$ NMR (100 MHz, $\text{CDCl}_3$ ) of compound <b>166b</b> .....	294
<b>Figure A1.192</b>	$^1\text{H}$ NMR (400 MHz, $\text{CDCl}_3$ ) of compound <b>166c</b> .....	295
<b>Figure A1.193</b>	Infrared spectrum (Thin Film, NaCl) of compound <b>166c</b> .....	296
<b>Figure A1.194</b>	$^{13}\text{C}$ NMR (100 MHz, $\text{CDCl}_3$ ) of compound <b>166c</b> .....	296
<b>Figure A1.195</b>	$^1\text{H}$ NMR (400 MHz, $\text{CDCl}_3$ ) of compound <b>166d</b> .....	297
<b>Figure A1.196</b>	Infrared spectrum (Thin Film, NaCl) of compound <b>166d</b> .....	298
<b>Figure A1.197</b>	$^{13}\text{C}$ NMR (100 MHz, $\text{CDCl}_3$ ) of compound <b>166d</b> .....	298
<b>Figure A1.198</b>	$^1\text{H}$ NMR (400 MHz, $\text{CDCl}_3$ ) of compound <b>166f</b> .....	299
<b>Figure A1.199</b>	Infrared spectrum (Thin Film, NaCl) of compound <b>166f</b> .....	300
<b>Figure A1.200</b>	$^{13}\text{C}$ NMR (100 MHz, $\text{CDCl}_3$ ) of compound <b>166f</b> .....	300
<b>Figure A1.201</b>	$^1\text{H}$ NMR (400 MHz, $\text{CDCl}_3$ ) of compound <b>cis•163a</b> .....	301
<b>Figure A1.202</b>	Infrared spectrum (Thin Film, NaCl) of compound <b>163a</b> .....	302
<b>Figure A1.203</b>	$^{13}\text{C}$ NMR (100 MHz, $\text{CDCl}_3$ ) of compound <b>cis•163a</b> .....	302
<b>Figure A1.204</b>	$^1\text{H}$ NMR (400 MHz, $\text{CDCl}_3$ ) of compound <b>trans•163a</b> .....	303
<b>Figure A1.205</b>	$^{13}\text{C}$ NMR (100 MHz, $\text{CDCl}_3$ ) of compound <b>trans•163a</b> .....	304
<b>Figure A1.206</b>	$^1\text{H}$ NMR (400 MHz, $\text{CDCl}_3$ ) of compound <b>163b</b> .....	305
<b>Figure A1.207</b>	Infrared spectrum (Thin Film, NaCl) of compound <b>163b</b> .....	306
<b>Figure A1.208</b>	$^{13}\text{C}$ NMR (100 MHz, $\text{CDCl}_3$ ) of compound <b>163b</b> .....	306
<b>Figure A1.209</b>	$^1\text{H}$ NMR (400 MHz, $\text{CDCl}_3$ ) of compound <b>163c</b> .....	307

<b>Figure A1.210</b>	Infrared spectrum (Thin Film, NaCl) of compound <b>163c</b> .....	308
<b>Figure A1.211</b>	$^{13}\text{C}$ NMR (100 MHz, $\text{CDCl}_3$ ) of compound <b>163c</b> .....	308
<b>Figure A1.212</b>	$^1\text{H}$ NMR (400 MHz, $\text{CDCl}_3$ ) of compound <b>163d</b> .....	309
<b>Figure A1.213</b>	Infrared spectrum (Thin Film, NaCl) of compound <b>163d</b> .....	310
<b>Figure A1.214</b>	$^{13}\text{C}$ NMR (100 MHz, $\text{CDCl}_3$ ) of compound <b>163d</b> .....	310
<b>Figure A1.215</b>	$^1\text{H}$ NMR (400 MHz, $\text{CDCl}_3$ ) of compound <b>163e</b> .....	311
<b>Figure A1.216</b>	Infrared spectrum (Thin Film, NaCl) of compound <b>163e</b> .....	312
<b>Figure A1.217</b>	$^{13}\text{C}$ NMR (100 MHz, $\text{CDCl}_3$ ) of compound <b>163e</b> .....	312
<b>Figure A1.218</b>	$^{19}\text{F}$ NMR (282 MHz, $\text{CDCl}_3$ ) of compound <b>163e</b> .....	313
<b>Figure A1.219</b>	$^1\text{H}$ NMR (400 MHz, $\text{CDCl}_3$ ) of compound <b>163f</b> .....	314
<b>Figure A1.220</b>	Infrared spectrum (Thin Film, NaCl) of compound <b>163f</b> .....	315
<b>Figure A1.221</b>	$^{13}\text{C}$ NMR (100 MHz, $\text{CDCl}_3$ ) of compound <b>163f</b> .....	315
<b>Figure A1.222</b>	$^{19}\text{F}$ NMR (282 MHz, $\text{CDCl}_3$ ) of compound <b>163f</b> .....	316
<b>Figure A1.223</b>	$^1\text{H}$ NMR (400 MHz, $\text{CDCl}_3$ ) of compound <b>163g</b> .....	317
<b>Figure A1.224</b>	Infrared spectrum (Thin Film, NaCl) of compound <b>163g</b> .....	318
<b>Figure A1.225</b>	$^{13}\text{C}$ NMR (100 MHz, $\text{CDCl}_3$ ) of compound <b>163g</b> .....	318
<b>Figure A1.226</b>	$^1\text{H}$ NMR (400 MHz, $\text{CDCl}_3$ ) of compound <b>163h</b> .....	319
<b>Figure A1.227</b>	Infrared spectrum (Thin Film, NaCl) of compound <b>163h</b> .....	320
<b>Figure A1.228</b>	$^{13}\text{C}$ NMR (100 MHz, $\text{CDCl}_3$ ) of compound <b>163h</b> .....	320
<b>Figure A1.229</b>	$^1\text{H}$ NMR (400 MHz, $\text{CDCl}_3$ ) of compound <b>163i</b> .....	321
<b>Figure A1.230</b>	Infrared spectrum (Thin Film, NaCl) of compound <b>163i</b> .....	322
<b>Figure A1.231</b>	$^{13}\text{C}$ NMR (100 MHz, $\text{CDCl}_3$ ) of compound <b>163i</b> .....	322

<b>Figure A1.232</b>	$^{19}\text{F}$ NMR (282 MHz, $\text{CDCl}_3$ ) of compound <b>163i</b> .....	323
<b>Figure A1.233</b>	$^1\text{H}$ NMR (400 MHz, $\text{CDCl}_3$ ) of compound <b>163j</b> .....	324
<b>Figure A1.234</b>	Infrared spectrum (Thin Film, NaCl) of compound <b>163j</b> .....	325
<b>Figure A1.235</b>	$^{13}\text{C}$ NMR (100 MHz, $\text{CDCl}_3$ ) of compound <b>163j</b> .....	325
<b>Figure A1.236</b>	$^1\text{H}$ NMR (400 MHz, $\text{CDCl}_3$ ) of compound <b>163k</b> .....	326
<b>Figure A1.237</b>	Infrared spectrum (Thin Film, NaCl) of compound <b>163k</b> .....	327
<b>Figure A1.238</b>	$^{13}\text{C}$ NMR (100 MHz, $\text{CDCl}_3$ ) of compound <b>163k</b> .....	327
<b>Figure A1.239</b>	$^1\text{H}$ NMR (400 MHz, $\text{CDCl}_3$ ) of compound <b>163l</b> .....	328
<b>Figure A1.240</b>	Infrared spectrum (Thin Film, NaCl) of compound <b>163l</b> .....	329
<b>Figure A1.241</b>	$^{13}\text{C}$ NMR (100 MHz, $\text{CDCl}_3$ ) of compound <b>163l</b> .....	329
<b>Figure A1.242</b>	$^1\text{H}$ NMR (400 MHz, $\text{CDCl}_3$ ) of compound <b>163m</b> .....	330
<b>Figure A1.243</b>	Infrared spectrum (Thin Film, NaCl) of compound <b>163m</b> .....	331
<b>Figure A1.244</b>	$^{13}\text{C}$ NMR (100 MHz, $\text{CDCl}_3$ ) of compound <b>163m</b> .....	331
<b>Figure A1.245</b>	$^1\text{H}$ NMR (400 MHz, $\text{CDCl}_3$ ) of compound <b>163n</b> .....	332
<b>Figure A1.246</b>	Infrared spectrum (Thin Film, NaCl) of compound <b>163n</b> .....	333
<b>Figure A1.247</b>	$^{13}\text{C}$ NMR (100 MHz, $\text{CDCl}_3$ ) of compound <b>163n</b> .....	333
<b>Figure A1.248</b>	$^1\text{H}$ NMR (400 MHz, $\text{CDCl}_3$ ) of compound <b>163o</b> .....	334
<b>Figure A1.249</b>	Infrared spectrum (Thin Film, NaCl) of compound <b>163o</b> .....	335
<b>Figure A1.250</b>	$^{13}\text{C}$ NMR (100 MHz, $\text{CDCl}_3$ ) of compound <b>163o</b> .....	335
<b>Figure A1.251</b>	$^1\text{H}$ NMR (400 MHz, $\text{CDCl}_3$ ) of compound <b>163p</b> .....	336
<b>Figure A1.252</b>	Infrared spectrum (Thin Film, NaCl) of compound <b>163p</b> .....	337
<b>Figure A1.253</b>	$^{13}\text{C}$ NMR (100 MHz, $\text{CDCl}_3$ ) of compound <b>163p</b> .....	337

<b>Figure A1.254</b>	$^1\text{H}$ NMR (400 MHz, $\text{CDCl}_3$ ) of compound <b>163q</b> .....	338
<b>Figure A1.255</b>	Infrared spectrum (Thin Film, NaCl) of compound <b>163q</b> .....	339
<b>Figure A1.256</b>	$^{13}\text{C}$ NMR (100 MHz, $\text{CDCl}_3$ ) of compound <b>163q</b> .....	339
<b>Figure A1.257</b>	$^1\text{H}$ NMR (400 MHz, $\text{CDCl}_3$ ) of compound <b>163r</b> .....	340
<b>Figure A1.258</b>	Infrared spectrum (Thin Film, NaCl) of compound <b>163r</b> .....	341
<b>Figure A1.259</b>	$^{13}\text{C}$ NMR (100 MHz, $\text{CDCl}_3$ ) of compound <b>163r</b> .....	341
<b>Figure A1.260</b>	$^1\text{H}$ NMR (400 MHz, $\text{CDCl}_3$ ) of compound <b>165a</b> .....	342
<b>Figure A1.261</b>	Infrared spectrum (Thin Film, NaCl) of compound <b>165a</b> .....	343
<b>Figure A1.262</b>	$^{13}\text{C}$ NMR (100 MHz, $\text{CDCl}_3$ ) of compound <b>165a</b> .....	343
<b>Figure A1.263</b>	$^{19}\text{F}$ NMR (282 MHz, $\text{CDCl}_3$ ) of compound <b>165a</b> .....	344
<b>Figure A1.264</b>	$^1\text{H}$ NMR (400 MHz, $\text{CDCl}_3$ ) of compound <b>165b</b> .....	345
<b>Figure A1.265</b>	Infrared spectrum (Thin Film, NaCl) of compound <b>165b</b> .....	346
<b>Figure A1.266</b>	$^{13}\text{C}$ NMR (100 MHz, $\text{CDCl}_3$ ) of compound <b>165b</b> .....	346
<b>Figure A1.267</b>	$^{19}\text{F}$ NMR (282 MHz, $\text{CDCl}_3$ ) of compound <b>165b</b> .....	347
<b>Figure A1.268</b>	$^1\text{H}$ NMR (400 MHz, $\text{CDCl}_3$ ) of compound <b>165c</b> .....	348
<b>Figure A1.269</b>	Infrared spectrum (Thin Film, NaCl) of compound <b>165c</b> .....	349
<b>Figure A1.270</b>	$^{13}\text{C}$ NMR (100 MHz, $\text{CDCl}_3$ ) of compound <b>165c</b> .....	349
<b>Figure A1.271</b>	$^{19}\text{F}$ NMR (282 MHz, $\text{CDCl}_3$ ) of compound <b>165c</b> .....	350
<b>Figure A1.272</b>	$^1\text{H}$ NMR (400 MHz, $\text{CDCl}_3$ ) of compound <b>165d</b> .....	351
<b>Figure A1.273</b>	Infrared spectrum (Thin Film, NaCl) of compound <b>165d</b> .....	352
<b>Figure A1.274</b>	$^{13}\text{C}$ NMR (100 MHz, $\text{CDCl}_3$ ) of compound <b>165d</b> .....	352
<b>Figure A1.275</b>	$^1\text{H}$ NMR (400 MHz, $\text{CDCl}_3$ ) of compound <b>165e</b> .....	353

<b>Figure A1.276</b>	Infrared spectrum (Thin Film, NaCl) of compound <b>165e</b> .....	354
<b>Figure A1.277</b>	$^{13}\text{C}$ NMR (100 MHz, $\text{CDCl}_3$ ) of compound <b>165e</b> .....	354
<b>Figure A1.278</b>	$^1\text{H}$ NMR (400 MHz, $\text{CDCl}_3$ ) of compound <b>165f</b> .....	355
<b>Figure A1.279</b>	Infrared spectrum (Thin Film, NaCl) of compound <b>165f</b> .....	356
<b>Figure A1.280</b>	$^{13}\text{C}$ NMR (100 MHz, $\text{CDCl}_3$ ) of compound <b>165f</b> .....	356
<b>Figure A1.281</b>	$^1\text{H}$ NMR (400 MHz, $\text{CDCl}_3$ ) of compound <b>167a</b> .....	357
<b>Figure A1.282</b>	Infrared spectrum (Thin Film, NaCl) of compound <b>167a</b> .....	358
<b>Figure A1.283</b>	$^{13}\text{C}$ NMR (100 MHz, $\text{CDCl}_3$ ) of compound <b>167a</b> .....	358
<b>Figure A1.284</b>	$^1\text{H}$ NMR (400 MHz, $\text{CDCl}_3$ ) of compound <b>167b</b> .....	359
<b>Figure A1.285</b>	Infrared spectrum (Thin Film, NaCl) of compound <b>167b</b> .....	360
<b>Figure A1.286</b>	$^{13}\text{C}$ NMR (100 MHz, $\text{CDCl}_3$ ) of compound <b>167b</b> .....	360
<b>Figure A1.287</b>	$^1\text{H}$ NMR (400 MHz, $\text{CDCl}_3$ ) of compound <b>167c</b> .....	361
<b>Figure A1.288</b>	Infrared spectrum (Thin Film, NaCl) of compound <b>167c</b> .....	362
<b>Figure A1.289</b>	$^{13}\text{C}$ NMR (100 MHz, $\text{CDCl}_3$ ) of compound <b>167c</b> .....	362
<b>Figure A1.290</b>	$^1\text{H}$ NMR (400 MHz, $\text{CDCl}_3$ ) of compound <b>167d</b> .....	363
<b>Figure A1.291</b>	Infrared spectrum (Thin Film, NaCl) of compound <b>167d</b> .....	364
<b>Figure A1.292</b>	$^{13}\text{C}$ NMR (100 MHz, $\text{CDCl}_3$ ) of compound <b>167d</b> .....	364
<b>Figure A1.293</b>	$^1\text{H}$ NMR (400 MHz, $\text{CDCl}_3$ ) of compound <b>167e</b> .....	365
<b>Figure A1.294</b>	Infrared spectrum (Thin Film, NaCl) of compound <b>167e</b> .....	366
<b>Figure A1.295</b>	$^{13}\text{C}$ NMR (100 MHz, $\text{CDCl}_3$ ) of compound <b>167e</b> .....	366
<b>Figure A1.296</b>	$^1\text{H}$ NMR (400 MHz, $\text{CDCl}_3$ ) of compound <b>168</b> .....	367
<b>Figure A1.297</b>	Infrared spectrum (Thin Film, NaCl) of compound <b>168</b> .....	368

<b>Figure A1.298</b>	$^{13}\text{C}$ NMR (100 MHz, $\text{CDCl}_3$ ) of compound <b>168</b> .....	368
<b>Figure A1.299</b>	$^1\text{H}$ NMR (400 MHz, $\text{CDCl}_3$ ) of compound <b>169</b> .....	369
<b>Figure A1.300</b>	Infrared spectrum (Thin Film, NaCl) of compound <b>169</b> .....	370
<b>Figure A1.301</b>	$^{13}\text{C}$ NMR (100 MHz, $\text{CDCl}_3$ ) of compound <b>169</b> .....	370
<b>Figure A1.302</b>	$^1\text{H}$ NMR (400 MHz, $\text{CDCl}_3$ ) of compound <b>170</b> .....	371
<b>Figure A1.303</b>	Infrared spectrum (Thin Film, NaCl) of compound <b>170</b> .....	372
<b>Figure A1.304</b>	$^{13}\text{C}$ NMR (100 MHz, $\text{CDCl}_3$ ) of compound <b>170</b> .....	372
<b>Figure A1.305</b>	$^1\text{H}$ NMR (400 MHz, $\text{CDCl}_3$ ) of compound <b>171</b> .....	373
<b>Figure A1.306</b>	Infrared spectrum (Thin Film, NaCl) of compound <b>171</b> .....	374
<b>Figure A1.307</b>	$^{13}\text{C}$ NMR (100 MHz, $\text{CDCl}_3$ ) of compound <b>171</b> .....	374

## **APPENDIX 2**

### *X-Ray Crystallography Reports Relevant to Chapter 2*

<b>Figure A2.1</b>	X-Ray crystal structure of THIQ <b>163p</b> .....	377
--------------------	---	-----

## **CHAPTER 3**

### *Iridium-Catalyzed Asymmetric Trans-Selective Hydrogenation of 1,3-Disubstituted Isoquinolines*

<b>Figure 3.1</b>	Challenges in diastereoselectivity of trans-selective arene hydrogenation .....	386
<b>Figure 3.2</b>	Proposed catalytic cycle .....	440
<b>Figure 3.3</b>	Experimental and theoretical IR and VCD spectra of <b>174</b> .....	446

## **APPENDIX 3**

### *Spectra Relevant to Chapter 3*

<b>Figure A3.1</b>	$^1\text{H}$ NMR (400 MHz, $\text{CDCl}_3$ ) of compound <b>161s</b> .....	452
<b>Figure A3.2</b>	Infrared spectrum (Thin Film, NaCl) of compound <b>161s</b> .....	453
<b>Figure A3.3</b>	$^{13}\text{C}$ NMR (100 MHz, $\text{CDCl}_3$ ) of compound <b>161s</b> .....	453
<b>Figure A3.4</b>	$^1\text{H}$ NMR (400 MHz, $\text{CDCl}_3$ ) of compound <b>173l</b> .....	454
<b>Figure A3.5</b>	Infrared spectrum (Thin Film, NaCl) of compound <b>173l</b> .....	455
<b>Figure A3.6</b>	$^{13}\text{C}$ NMR (100 MHz, $\text{CDCl}_3$ ) of compound <b>173l</b> .....	455
<b>Figure A3.7</b>	$^1\text{H}$ NMR (400 MHz, $\text{CDCl}_3$ ) of compound <b>166g</b> .....	456
<b>Figure A3.8</b>	Infrared spectrum (Thin Film, NaCl) of compound <b>166g</b> .....	457
<b>Figure A3.9</b>	$^{13}\text{C}$ NMR (100 MHz, $\text{CDCl}_3$ ) of compound <b>166g</b> .....	457
<b>Figure A3.10</b>	$^1\text{H}$ NMR (400 MHz, $\text{CDCl}_3$ ) of compound <b>167d</b> .....	458
<b>Figure A3.11</b>	Infrared spectrum (Thin Film, NaCl) of compound <b>167d</b> .....	459
<b>Figure A3.12</b>	$^{13}\text{C}$ NMR (100 MHz, $\text{CDCl}_3$ ) of compound <b>167d</b> .....	459
<b>Figure A3.13</b>	$^1\text{H}$ NMR (400 MHz, $\text{CDCl}_3$ ) of compound <b>175a</b> .....	460
<b>Figure A3.14</b>	Infrared spectrum (Thin Film, NaCl) of compound <b>175a</b> .....	461
<b>Figure A3.15</b>	$^{13}\text{C}$ NMR (100 MHz, $\text{CDCl}_3$ ) of compound <b>175a</b> .....	461
<b>Figure A3.16</b>	$^1\text{H}$ NMR (400 MHz, $\text{CDCl}_3$ ) of compound <b>175b</b> .....	462
<b>Figure A3.17</b>	Infrared spectrum (Thin Film, NaCl) of compound <b>175b</b> .....	463
<b>Figure A3.18</b>	$^{13}\text{C}$ NMR (100 MHz, $\text{CDCl}_3$ ) of compound <b>175b</b> .....	463
<b>Figure A3.19</b>	$^1\text{H}$ NMR (400 MHz, $\text{CDCl}_3$ ) of compound <b>175c</b> .....	464
<b>Figure A3.20</b>	Infrared spectrum (Thin Film, NaCl) of compound <b>175c</b> .....	465
<b>Figure A3.21</b>	$^{13}\text{C}$ NMR (100 MHz, $\text{CDCl}_3$ ) of compound <b>175c</b> .....	465
<b>Figure A3.22</b>	$^1\text{H}$ NMR (400 MHz, $\text{CDCl}_3$ ) of compound <b>175d</b> .....	466



<b>Figure A3.23</b>	Infrared spectrum (Thin Film, NaCl) of compound <b>175d</b> .....	467
<b>Figure A3.24</b>	$^{13}\text{C}$ NMR (100 MHz, $\text{CDCl}_3$ ) of compound <b>175d</b> .....	467
<b>Figure A3.25</b>	$^{19}\text{F}$ NMR (282 MHz, $\text{CDCl}_3$ ) of compound <b>175d</b> .....	468
<b>Figure A3.26</b>	$^1\text{H}$ NMR (400 MHz, $\text{CDCl}_3$ ) of compound <b>175e</b> .....	469
<b>Figure A3.27</b>	Infrared spectrum (Thin Film, NaCl) of compound <b>175e</b> .....	470
<b>Figure A3.28</b>	$^{13}\text{C}$ NMR (100 MHz, $\text{CDCl}_3$ ) of compound <b>175e</b> .....	470
<b>Figure A3.29</b>	$^{19}\text{F}$ NMR (282 MHz, $\text{CDCl}_3$ ) of compound <b>175e</b> .....	471
<b>Figure A3.30</b>	$^1\text{H}$ NMR (400 MHz, $\text{CDCl}_3$ ) of compound <b>175f</b> .....	472
<b>Figure A3.31</b>	Infrared spectrum (Thin Film, NaCl) of compound <b>175f</b> .....	473
<b>Figure A3.32</b>	$^{13}\text{C}$ NMR (100 MHz, $\text{CDCl}_3$ ) of compound <b>175f</b> .....	473
<b>Figure A3.33</b>	$^1\text{H}$ NMR (400 MHz, $\text{CDCl}_3$ ) of compound <b>175g</b> .....	474
<b>Figure A3.34</b>	Infrared spectrum (Thin Film, NaCl) of compound <b>175g</b> .....	475
<b>Figure A3.35</b>	$^{13}\text{C}$ NMR (100 MHz, $\text{CDCl}_3$ ) of compound <b>175g</b> .....	475
<b>Figure A3.36</b>	$^1\text{H}$ NMR (400 MHz, $\text{CDCl}_3$ ) of compound <b>175h</b> .....	476
<b>Figure A3.37</b>	Infrared spectrum (Thin Film, NaCl) of compound <b>175h</b> .....	477
<b>Figure A3.38</b>	$^{13}\text{C}$ NMR (100 MHz, $\text{CDCl}_3$ ) of compound <b>175h</b> .....	477
<b>Figure A3.39</b>	$^1\text{H}$ NMR (400 MHz, $\text{CDCl}_3$ ) of compound <b>175i</b> .....	478
<b>Figure A3.40</b>	Infrared spectrum (Thin Film, NaCl) of compound <b>175i</b> .....	479
<b>Figure A3.41</b>	$^{13}\text{C}$ NMR (100 MHz, $\text{CDCl}_3$ ) of compound <b>175i</b> .....	479
<b>Figure A3.42</b>	$^1\text{H}$ NMR (400 MHz, $\text{CDCl}_3$ ) of compound <b>175j</b> .....	480
<b>Figure A3.43</b>	Infrared spectrum (Thin Film, NaCl) of compound <b>175j</b> .....	481
<b>Figure A3.44</b>	$^{13}\text{C}$ NMR (100 MHz, $\text{CDCl}_3$ ) of compound <b>175j</b> .....	481

<b>Figure A3.45</b>	$^1\text{H}$ NMR (400 MHz, $\text{CDCl}_3$ ) of compound <b>175k</b> .....	482
<b>Figure A3.46</b>	Infrared spectrum (Thin Film, NaCl) of compound <b>175k</b> .....	483
<b>Figure A3.47</b>	$^{13}\text{C}$ NMR (100 MHz, $\text{CDCl}_3$ ) of compound <b>175k</b> .....	483
<b>Figure A3.48</b>	$^1\text{H}$ NMR (400 MHz, $\text{CDCl}_3$ ) of compound <b>175l</b> .....	484
<b>Figure A3.49</b>	Infrared spectrum (Thin Film, NaCl) of compound <b>175l</b> .....	485
<b>Figure A3.50</b>	$^{13}\text{C}$ NMR (100 MHz, $\text{CDCl}_3$ ) of compound <b>175l</b> .....	485
<b>Figure A3.51</b>	$^1\text{H}$ NMR (400 MHz, $\text{CDCl}_3$ ) of compound <b>175m</b> .....	486
<b>Figure A3.52</b>	Infrared spectrum (Thin Film, NaCl) of compound <b>175m</b> .....	487
<b>Figure A3.53</b>	$^{13}\text{C}$ NMR (100 MHz, $\text{CDCl}_3$ ) of compound <b>175m</b> .....	487
<b>Figure A3.54</b>	$^{19}\text{F}$ NMR (282 MHz, $\text{CDCl}_3$ ) of compound <b>175m</b> .....	488
<b>Figure A3.55</b>	$^1\text{H}$ NMR (400 MHz, $\text{CDCl}_3$ ) of compound <b>175n</b> .....	489
<b>Figure A3.56</b>	Infrared spectrum (Thin Film, NaCl) of compound <b>175n</b> .....	490
<b>Figure A3.57</b>	$^{13}\text{C}$ NMR (100 MHz, $\text{CDCl}_3$ ) of compound <b>175n</b> .....	490
<b>Figure A3.58</b>	$^{19}\text{F}$ NMR (282 MHz, $\text{CDCl}_3$ ) of compound <b>175n</b> .....	491
<b>Figure A3.59</b>	$^1\text{H}$ NMR (400 MHz, $\text{CDCl}_3$ ) of compound <b>174</b> .....	492
<b>Figure A3.60</b>	Infrared spectrum (Thin Film, NaCl) of compound <b>174</b> .....	493
<b>Figure A3.61</b>	$^{13}\text{C}$ NMR (100 MHz, $\text{CDCl}_3$ ) of compound <b>174</b> .....	493
<b>Figure A3.62</b>	$^1\text{H}$ NMR (400 MHz, $\text{CDCl}_3$ ) of compound <b>176</b> .....	494
<b>Figure A3.63</b>	Infrared spectrum (Thin Film, NaCl) of compound <b>176</b> .....	495
<b>Figure A3.64</b>	$^{13}\text{C}$ NMR (100 MHz, $\text{CDCl}_3$ ) of compound <b>176</b> .....	495
<b>Figure A3.65</b>	$^1\text{H}$ NMR (400 MHz, $\text{CDCl}_3$ ) of compound <b><i>d</i><sub>5</sub>-174</b> .....	496
<b>Figure A3.66</b>	$^2\text{H}$ NMR (61 MHz, $\text{CDCl}_3$ ) of compound <b><i>d</i><sub>5</sub>-174</b> .....	497

<b>Figure A3.67</b>	$^1\text{H}$ NMR (400 MHz, $\text{CDCl}_3$ ) of compound <b><i>d<sub>n</sub>-cis-174</i></b> .....	498
<b>Figure A3.68</b>	$^1\text{H}$ NMR (400 MHz, $\text{CDCl}_3$ ) of compound <b><i>d<sub>n</sub>-174</i></b> .....	499
<b>Figure A3.69</b>	$^1\text{H}$ NMR (400 MHz, $\text{CDCl}_3$ ) of compound <b><i>d<sub>n</sub>-174</i></b> .....	500

## **APPENDIX 4**

### *X-Ray Crystallography Reports Relevant to Chapter 3*

<b>Figure A4.1</b>	X-Ray crystal structure of THIQ <b>175a</b> .....	503
--------------------	---	-----

## **CHAPTER 4**

### *Advances in the Total Synthesis of the Tetrahydroisoquinoline Alkaloids (2002–2020)*

<b>Figure 4.1</b>	Tetrahydroisoquinoline alkaloids (–)-salsolidine <b>183</b> and ecteinascidin 743 <b>184</b> .....	513
<b>Figure 4.2</b>	General structures of THIQ alkaloid families .....	514
<b>Figure 4.3</b>	General structure of simple THIQ alkaloids .....	514
<b>Figure 4.4</b>	General structure of the Erythrina alkaloids .....	515
<b>Figure 4.5</b>	Proposed biosynthesis of the Erythrina alkaloids .....	516
<b>Figure 4.6</b>	Synthetic approaches to Erythrina alkaloids .....	517
<b>Figure 4.7</b>	Early biosynthetic pathways to yield ( <i>S</i> )-reticuline <b>247</b> .....	524
<b>Figure 4.8</b>	Diverging biosynthetic pathways from ( <i>S</i> )-reticuline <b>247</b> that access a wide variety of structural classes of THIQ alkaloids .....	525
<b>Figure 4.9</b>	General structure of the aporphine alkaloids .....	526
<b>Figure 4.10</b>	Proposed biosynthesis of aporphine alkaloid ( <i>S</i> )-magnoflorine <b>249</b> .....	526
<b>Figure 4.11</b>	General structure of bisbenzyl THIQ alkaloids .....	535

<b>Figure 4.12</b>	Proposed biosynthesis of bisbenzyl THIQ alkaloids <b>303</b> and <b>304</b> .	536
<b>Figure 4.13</b>	General structure of the protoberberine THIQ alkaloids .....	542
<b>Figure 4.14</b>	Proposed biosynthesis of protoberberine alkaloids <b>345</b> and <b>351</b> ..	543
<b>Figure 4.15</b>	General structure of the morphinan THIQ alkaloids .....	554
<b>Figure 4.16</b>	Proposed biosynthesis of morphine <b>423</b> and related morphinan alkaloids .....	555
<b>Figure 4.17</b>	General structure of the pavine and isopavine THIQ alkaloids .....	571
<b>Figure 4.18</b>	Core skeleton of THIQ alkaloids in the saframycin family .....	576
<b>Figure 4.19</b>	General structure and representative examples of saframycin alkaloids .....	577
<b>Figure 4.20</b>	General structure of safracin alkaloids.....	582
<b>Figure 4.21</b>	General structure and representative examples of renieramycin alkaloids .....	584
<b>Figure 4.22</b>	Ecteinasidin natural products.....	603
<b>Figure 4.23</b>	Fukuyama's synthetic strategy toward Et-743 <b>184</b> .....	605
<b>Figure 4.24</b>	Core skeleton of THIQ alkaloids in the naphthyridinomycin family and examples.....	614
<b>Figure 4.25</b>	General skeleton of THIQ alkaloids in the quinocarcin family .....	617

## **CHAPTER 5**

### *Progress Toward the Total Synthesis*

#### *Of (+)-Cyanocycline A*

<b>Figure 5.1</b>	General skeleton of THIQ alkaloids in the naphthyridinomycin family and examples.....	646
<b>Figure 5.2</b>	Structure of (+)-cyanocycline A ( <b>771</b> ).....	646

<b>Figure 5.3</b>	Initial retrosynthetic analysis of (+)-cyanocycline A ( <b>771</b> ).....	649
<b>Figure 5.4</b>	2 <sup>nd</sup> generation retrosynthetic analysis of (+)-cyanocycline A ( <b>771</b> )	662
<b>Figure 5.5</b>	3 <sup>rd</sup> generation retrosynthetic analysis of (+)-cyanocycline A ( <b>771</b> )	666

## **APPENDIX 6**

### *Spectra Relevant to Chapter 5*

<b>Figure A6.1</b>	<sup>1</sup> H NMR (400 MHz, CDCl <sub>3</sub> ) of compound <b>896</b> .....	722
<b>Figure A6.2</b>	Infrared spectrum (Thin Film, NaCl) of compound <b>896</b> .....	723
<b>Figure A6.3</b>	<sup>13</sup> C NMR (100 MHz, CDCl <sub>3</sub> ) of compound <b>896</b> .....	723
<b>Figure A6.4</b>	<sup>1</sup> H NMR (400 MHz, CDCl <sub>3</sub> ) of compound <b>897</b> .....	724
<b>Figure A6.5</b>	Infrared spectrum (Thin Film, NaCl) of compound <b>897</b> .....	725
<b>Figure A6.6</b>	<sup>13</sup> C NMR (100 MHz, CDCl <sub>3</sub> ) of compound <b>897</b> .....	725
<b>Figure A6.7</b>	<sup>1</sup> H NMR (400 MHz, CDCl <sub>3</sub> ) of compound <b>898</b> .....	726
<b>Figure A6.8</b>	Infrared spectrum (Thin Film, NaCl) of compound <b>898</b> .....	727
<b>Figure A6.9</b>	<sup>13</sup> C NMR (100 MHz, CDCl <sub>3</sub> ) of compound <b>898</b> .....	727
<b>Figure A6.10</b>	<sup>1</sup> H NMR (400 MHz, CDCl <sub>3</sub> ) of compound <b>899</b> .....	728
<b>Figure A6.11</b>	Infrared spectrum (Thin Film, NaCl) of compound <b>899</b> .....	729
<b>Figure A6.12</b>	<sup>13</sup> C NMR (100 MHz, CDCl <sub>3</sub> ) of compound <b>899</b> .....	729
<b>Figure A6.13</b>	<sup>1</sup> H NMR (400 MHz, CDCl <sub>3</sub> ) of compound <b>900</b> .....	730
<b>Figure A6.14</b>	Infrared spectrum (Thin Film, NaCl) of compound <b>900</b> .....	731
<b>Figure A6.15</b>	<sup>13</sup> C NMR (100 MHz, CDCl <sub>3</sub> ) of compound <b>900</b> .....	731
<b>Figure A6.16</b>	<sup>1</sup> H NMR (400 MHz, CDCl <sub>3</sub> ) of compound <b>901</b> .....	732
<b>Figure A6.17</b>	Infrared spectrum (Thin Film, NaCl) of compound <b>901</b> .....	733

<b>Figure A6.18</b>	$^{13}\text{C}$ NMR (100 MHz, $\text{CDCl}_3$ ) of compound <b>901</b> .....	733
<b>Figure A6.19</b>	$^1\text{H}$ NMR (400 MHz, $\text{CDCl}_3$ ) of compound <b>902</b> .....	734
<b>Figure A6.20</b>	Infrared spectrum (Thin Film, NaCl) of compound <b>902</b> .....	735
<b>Figure A6.21</b>	$^{13}\text{C}$ NMR (100 MHz, $\text{CDCl}_3$ ) of compound <b>902</b> .....	735
<b>Figure A6.22</b>	$^1\text{H}$ NMR (400 MHz, $\text{CDCl}_3$ ) of compound <b>903</b> .....	736
<b>Figure A6.23</b>	Infrared spectrum (Thin Film, NaCl) of compound <b>903</b> .....	737
<b>Figure A6.24</b>	$^{13}\text{C}$ NMR (100 MHz, $\text{CDCl}_3$ ) of compound <b>903</b> .....	737
<b>Figure A6.25</b>	$^1\text{H}$ NMR (400 MHz, $\text{CDCl}_3$ ) of compound <b>904</b> .....	738
<b>Figure A6.26</b>	Infrared spectrum (Thin Film, NaCl) of compound <b>904</b> .....	739
<b>Figure A6.27</b>	$^{13}\text{C}$ NMR (100 MHz, $\text{CDCl}_3$ ) of compound <b>904</b> .....	739
<b>Figure A6.28</b>	$^1\text{H}$ NMR (400 MHz, $\text{CDCl}_3$ ) of compound <b>907</b> .....	740
<b>Figure A6.29</b>	Infrared spectrum (Thin Film, NaCl) of compound <b>907</b> .....	741
<b>Figure A6.30</b>	$^{13}\text{C}$ NMR (100 MHz, $\text{CDCl}_3$ ) of compound <b>907</b> .....	741
<b>Figure A6.31</b>	$^1\text{H}$ NMR (400 MHz, $\text{CDCl}_3$ ) of compound <b>908</b> .....	742
<b>Figure A6.32</b>	Infrared spectrum (Thin Film, NaCl) of compound <b>908</b> .....	743
<b>Figure A6.33</b>	$^{13}\text{C}$ NMR (100 MHz, $\text{CDCl}_3$ ) of compound <b>908</b> .....	743
<b>Figure A6.34</b>	$^1\text{H}$ NMR (400 MHz, $\text{CDCl}_3$ ) of compound <b>909</b> .....	744
<b>Figure A6.35</b>	Infrared spectrum (Thin Film, NaCl) of compound <b>909</b> .....	745
<b>Figure A6.36</b>	$^{13}\text{C}$ NMR (100 MHz, $\text{CDCl}_3$ ) of compound <b>909</b> .....	745
<b>Figure A6.37</b>	$^1\text{H}$ NMR (400 MHz, $\text{CDCl}_3$ ) of compound <b>910</b> .....	746
<b>Figure A6.38</b>	Infrared spectrum (Thin Film, NaCl) of compound <b>910</b> .....	747
<b>Figure A6.39</b>	$^{13}\text{C}$ NMR (100 MHz, $\text{CDCl}_3$ ) of compound <b>910</b> .....	747

<b>Figure A6.40</b>	$^1\text{H}$ NMR (400 MHz, $\text{CDCl}_3$ ) of compound <b>911</b> .....	748
<b>Figure A6.41</b>	Infrared spectrum (Thin Film, NaCl) of compound <b>911</b> .....	749
<b>Figure A6.42</b>	$^1\text{H}$ NMR (400 MHz, $\text{CDCl}_3$ ) of compound <b>912</b> .....	750
<b>Figure A6.43</b>	Infrared spectrum (Thin Film, NaCl) of compound <b>912</b> .....	751
<b>Figure A6.44</b>	$^{13}\text{C}$ NMR (100 MHz, $\text{CDCl}_3$ ) of compound <b>912</b> .....	751
<b>Figure A6.45</b>	$^1\text{H}$ NMR (400 MHz, $\text{CDCl}_3$ ) of compound <b>914</b> .....	752
<b>Figure A6.46</b>	Infrared spectrum (Thin Film, NaCl) of compound <b>914</b> .....	753
<b>Figure A6.47</b>	$^{13}\text{C}$ NMR (100 MHz, $\text{CDCl}_3$ ) of compound <b>914</b> .....	753
<b>Figure A6.48</b>	$^1\text{H}$ NMR (400 MHz, $\text{CDCl}_3$ ) of compound <b>915</b> .....	754
<b>Figure A6.49</b>	Infrared spectrum (Thin Film, NaCl) of compound <b>915</b> .....	755
<b>Figure A6.50</b>	$^{13}\text{C}$ NMR (100 MHz, $\text{CDCl}_3$ ) of compound <b>915</b> .....	755
<b>Figure A6.51</b>	$^1\text{H}$ NMR (400 MHz, $\text{CDCl}_3$ ) of compounds <b>916 + 917</b> .....	756
<b>Figure A6.52</b>	$^1\text{H}$ NMR (400 MHz, $\text{CDCl}_3$ ) of compound <b>924</b> .....	757
<b>Figure A6.53</b>	Infrared spectrum (Thin Film, NaCl) of compound <b>924</b> .....	758
<b>Figure A6.54</b>	$^{13}\text{C}$ NMR (100 MHz, $\text{CDCl}_3$ ) of compound <b>924</b> .....	758
<b>Figure A6.55</b>	$^1\text{H}$ NMR (400 MHz, $\text{CDCl}_3$ ) of compound <b>921</b> .....	759
<b>Figure A6.56</b>	Infrared spectrum (Thin Film, NaCl) of compound <b>921</b> .....	760
<b>Figure A6.57</b>	$^{13}\text{C}$ NMR (100 MHz, $\text{CDCl}_3$ ) of compound <b>921</b> .....	760
<b>Figure A6.58</b>	$^{19}\text{F}$ NMR (282 MHz, $\text{CDCl}_3$ ) of compound <b>921</b> .....	761
<b>Figure A6.59</b>	$^1\text{H}$ NMR (400 MHz, $\text{CDCl}_3$ ) of compound <b>927</b> .....	762
<b>Figure A6.60</b>	Infrared spectrum (Thin Film, NaCl) of compound <b>927</b> .....	763
<b>Figure A6.61</b>	$^{13}\text{C}$ NMR (100 MHz, $\text{CDCl}_3$ ) of compound <b>927</b> .....	763

<b>Figure A6.62</b> $^1\text{H}$ NMR (400 MHz, $\text{CDCl}_3$ ) of compound <b>928</b> .....	764
<b>Figure A6.63</b> Infrared spectrum (Thin Film, NaCl) of compound <b>928</b> .....	765
<b>Figure A6.64</b> $^{13}\text{C}$ NMR (100 MHz, $\text{CDCl}_3$ ) of compound <b>928</b> .....	765
<b>Figure A6.65</b> $^1\text{H}$ NMR (400 MHz, $\text{CDCl}_3$ ) of compound <b>929</b> .....	766
<b>Figure A6.66</b> Infrared spectrum (Thin Film, NaCl) of compound <b>929</b> .....	767
<b>Figure A6.67</b> $^{13}\text{C}$ NMR (100 MHz, $\text{CDCl}_3$ ) of compound <b>929</b> .....	767
<b>Figure A6.68</b> $^1\text{H}$ NMR (400 MHz, $\text{CDCl}_3$ ) of compound <b>935</b> .....	768
<b>Figure A6.69</b> Infrared spectrum (Thin Film, NaCl) of compound <b>935</b> .....	769
<b>Figure A6.70</b> $^{13}\text{C}$ NMR (100 MHz, $\text{CDCl}_3$ ) of compound <b>935</b> .....	769
<b>Figure A6.71</b> $^1\text{H}$ NMR (400 MHz, $\text{CDCl}_3$ ) of compound <b>936</b> .....	770
<b>Figure A6.72</b> Infrared spectrum (Thin Film, NaCl) of compound <b>936</b> .....	771
<b>Figure A6.73</b> $^{13}\text{C}$ NMR (100 MHz, $\text{CDCl}_3$ ) of compound <b>936</b> .....	771
<b>Figure A6.74</b> $^1\text{H}$ NMR (400 MHz, $\text{CDCl}_3$ ) of compound <b>932</b> .....	772
<b>Figure A6.75</b> Infrared spectrum (Thin Film, NaCl) of compound <b>932</b> .....	773
<b>Figure A6.76</b> $^{13}\text{C}$ NMR (100 MHz, $\text{CDCl}_3$ ) of compound <b>932</b> .....	773
<b>Figure A6.77</b> $^1\text{H}$ NMR (400 MHz, $\text{CDCl}_3$ ) of compound <b>938</b> .....	774
<b>Figure A6.78</b> Infrared spectrum (Thin Film, NaCl) of compound <b>938</b> .....	775
<b>Figure A6.79</b> $^{13}\text{C}$ NMR (100 MHz, $\text{CDCl}_3$ ) of compound <b>938</b> .....	775
<b>Figure A6.80</b> $^1\text{H}$ NMR (400 MHz, $\text{CDCl}_3$ ) of compound <b>939</b> .....	776
<b>Figure A6.81</b> Infrared spectrum (Thin Film, NaCl) of compound <b>939</b> .....	777
<b>Figure A6.82</b> $^{13}\text{C}$ NMR (100 MHz, $\text{CDCl}_3$ ) of compound <b>939</b> .....	777



## LIST OF SCHEMES

### CHAPTER 1

#### *Advances in Homogeneous Catalysts for the Asymmetric Hydrogenation of Heteroarenes (2002–2020)*

<b>Scheme 1.1</b>	Examples for the asymmetric hydrogenation of heteroarenes.....	4
<b>Scheme 1.2</b>	Possible mechanistic pathways for the hydrogenation of 2-methylquinoline <b>11</b> .....	5
<b>Scheme 1.3</b>	Ru-catalyzed asymmetric hydrogenation of quinolines and applications of hydrogenated products.....	9
<b>Scheme 1.4</b>	Ru-catalyzed asymmetric hydrogenation with PhTRAP ligand <b>L1</b> ...	12
<b>Scheme 1.5</b>	Ru-catalyzed asymmetric hydrogenation of furans and benzofurans with NHC ligand <b>L2</b> .....	13
<b>Scheme 1.6</b>	First reported Ir-catalyzed asymmetric hydrogenation of quinolines.....	14
<b>Scheme 1.7</b>	Ir-catalyzed asymmetric hydrogenation of isoquinolines and pyridines using TCCA as the activator.....	18
<b>Scheme 1.8</b>	Ir-catalyzed asymmetric hydrogenation of quinolines, quinoxalines, and benzoxazines.....	19
<b>Scheme 1.9</b>	Key Ir-catalyzed enantioselective hydrogenation step in the total synthesis of jorumycin.....	19
<b>Scheme 1.10</b>	Ir-catalyzed asymmetric hydrogenation of 1,3-disubstituted isoquinolines.....	20
<b>Scheme 1.11</b>	Ir-catalyzed asymmetric hydrogenation with P–OP ligand <b>L8</b> .....	21

<b>Scheme 1.12</b> Ir-catalyzed asymmetric hydrogenation with SpinPHOX ligand <b>L9</b> .....	22
<b>Scheme 1.13</b> Ir-catalyzed asymmetric hydrogenation of quinolines with Ir/TsDPEN catalyst <b>78</b> .....	23
<b>Scheme 1.14</b> Rh-catalyzed asymmetric hydrogenation of <i>N</i> -heteroarenes using ZhaoPhos ligand <b>L10</b> .....	25
<b>Scheme 1.15</b> Pd-catalyzed asymmetric hydrogenation of <i>N</i> -H indoles.....	28
<b>Scheme 1.16</b> Fe-catalyzed asymmetric hydrogenation of quinoxalines and benzoxazines with chiral phosphoric acid <b>105</b> .....	30
<b>Scheme 1.17</b> In situ formation of chiral borane catalyst <b>115</b> from chiral dienes...	32
<b>Scheme 1.18</b> Metal-free asymmetric hydrogenation of heteroarenes through in situ formation of a chiral borane catalyst from ligand <b>117</b> .....	33
<b>Scheme 1.19</b> Asymmetric hydrogenation of quinolines using spiro-bicyclic bisborane catalyst <b>122</b> .....	33
<b>Scheme 1.20</b> First reported chiral phosphoric acid-catalyzed asymmetric hydrogenation of quinolines.....	34
<b>Scheme 1.21</b> Asymmetric transfer hydrogenation with SPINOL-derived phosphoric acid <b>135</b> .....	36
<b>Scheme 1.22</b> Biomimetic asymmetric transfer hydrogenation of heteroarenes .....	39

## **CHAPTER 2**

### *Iridium-Catalyzed Enantioselective and Diastereoselective Hydrogenation of 1,3-Disubstituted Isoquinolines*

<b>Scheme 2.1</b>	Syntheses of 1-(hydroxymethyl)-3-aryl isoquinoline substrates .....	56
<b>Scheme 2.2</b>	Substrate scope of different aryl substituents.....	60
<b>Scheme 2.3</b>	Substrate scope of heteroaryl substituents.....	61
<b>Scheme 2.4</b>	Substrate scope of IQ backbone substituents.....	62
<b>Scheme 2.5</b>	Substrate scope of different directing groups .....	64
<b>Scheme 2.6</b>	Derivatization of hydrogenated product <b>163I</b> .....	66

### **CHAPTER 3**

#### *Iridium-Catalyzed Asymmetric Trans-Selective Hydrogenation of 1,3-Disubstituted Isoquinolines*

<b>Scheme 3.1</b>	Substrate scope of the <i>trans</i> -selective hydrogenation of 1,3-disubstituted isoquinolines.....	391
<b>Scheme 3.2</b>	Substrate scope of heteroaryl and fluorinated isoquinolines .....	392
<b>Scheme 3.3</b>	Synthetic derivatizations of product <b>175a</b> .....	393
<b>Scheme 3.4</b>	Control experiments of the asymmetric <i>trans</i> -selective hydrogenation.....	394
<b>Scheme 3.5</b>	Deuterium experiments of substrate <b>173a</b> .....	395

### **CHAPTER 4**

#### *Advances in the Total Synthesis of the Tetrahydroisoquinoline Alkaloids (2002–2020)*

<b>Scheme 4.1</b>	Matsumoto's total synthesis of <i>O</i> -methylerysodienone <b>199</b> .....	517
<b>Scheme 4.2</b>	Matsumoto's enantioselective synthesis of <i>O</i> -methylerysodienone <b>199</b> .....	518
<b>Scheme 4.3</b>	Padwa's synthetic strategy toward the Erythrinan alkaloids.....	518
<b>Scheme 4.4</b>	Padwa's total synthesis of erysotramidine <b>208</b> .....	519
<b>Scheme 4.5</b>	Padwa's total synthesis of demethoxyerythratidinone <b>213</b> .....	520

<b>Scheme 4.6</b>	Simpkin's enantioselective synthesis of (+)-demethoxyerythratidinone <b>213</b> .....	520
<b>Scheme 4.7</b>	Reisman's enantioselective synthesis of (–)-demethoxyerythratidinone <b>213</b> .....	521
<b>Scheme 4.8</b>	Ciufolini's enantioselective synthesis of (+)-demethoxyerythratidinone <b>213</b> .....	522
<b>Scheme 4.9</b>	Ciufolini's enantioselective synthesis of (+)-erysotramidine <b>208</b> ...	523
<b>Scheme 4.10</b>	Kaluza's enantioselective synthesis of (–)-erysotramidine <b>208</b> .....	524
<b>Scheme 4.11</b>	Cuny's synthesis of aporphine <b>255</b> .....	527
<b>Scheme 4.12</b>	Vicario's synthesis of (+)-glaucine <b>260</b> .....	528
<b>Scheme 4.13</b>	Fürstner's synthesis of O-methyl-dehydroisopiline <b>264</b> .....	529
<b>Scheme 4.14</b>	Raminelli's synthesis of (–)-aporphine <b>255</b> .....	529
<b>Scheme 4.15</b>	Nimgirawath's synthesis of telisatin A <b>272</b> .....	530
<b>Scheme 4.16</b>	Cuny's synthesis of (–)-artabonatin A <b>276</b> .....	531
<b>Scheme 4.17</b>	A. Honda's synthesis of stepharine <b>280</b> and pronuciferine <b>281</b> B. Magnus' synthesis of stepharine <b>280</b> .....	532
<b>Scheme 4.18</b>	Takao's synthesis of (–)-misramine <b>290</b> .....	533
<b>Scheme 4.19</b>	Fagnou's synthesis of aporphine alkaloids .....	534
<b>Scheme 4.20</b>	Opatz's synthesis of (+)-tetramethylmagnolamine <b>313</b> and (+)-O-methylthalibrine <b>312</b> .....	537
<b>Scheme 4.21</b>	Bracher's synthesis of tetrandine <b>321</b> and isotetrandine <b>322</b> .....	538
<b>Scheme 4.22</b>	Georghiou's synthesis of (–)-tejedine <b>334</b> .....	539

<b>Scheme 4.23</b> Nishiyama's electrochemical synthesis of (+)- <i>O</i> -methylthalibrine <b>312</b> .....	540
<b>Scheme 4.24</b> Lumb's synthesis of tetramethylmagnolamine <b>313</b> .....	541
<b>Scheme 4.25</b> Davis' synthesis of (–)-xylopinine <b>356</b> .....	544
<b>Scheme 4.26</b> Ruano's synthesis of (–)-xylopinine <b>356</b> .....	544
<b>Scheme 4.27</b> Cho's synthesis of oxypalmatine <b>364</b> .....	545
<b>Scheme 4.28</b> Chrzanowska's synthesis of A. oxoberberine <b>367</b> and B. (–)-oxoxylopinine <b>370</b> .....	546
<b>Scheme 4.29</b> Ender's synthesis of (–)-tetrahydropalmatine <b>346</b> .....	546
<b>Scheme 4.30</b> Yang's synthesis of (–)-stepholidine <b>379</b> .....	547
<b>Scheme 4.31</b> Harding's synthesis of isocorypalmine <b>382</b> .....	547
<b>Scheme 4.32</b> Georghiou's synthesis of (–)-corytenchine <b>385</b> .....	548
<b>Scheme 4.33</b> Hiemstra's synthesis of (+)-javaberine A <b>392</b> and (+)-javaberine B <b>393</b> .....	549
<b>Scheme 4.34</b> van Maarseveen's synthesis of (–)-govaniadine <b>397</b> .....	549
<b>Scheme 4.35</b> Opatz's synthesis of A. xylopinine <b>356</b> B. Pseudopalmatine <b>401</b> ..	550
<b>Scheme 4.36</b> Donohoe's synthesis of palmatine <b>405</b> .....	551
<b>Scheme 4.37</b> Mhaske's synthesis of oxotetrahydropalmitine <b>408</b> .....	551
<b>Scheme 4.38</b> Cheng's synthesis of corysamine <b>411</b> .....	551
<b>Scheme 4.39</b> Glorius' general synthesis of protoberberine alkaloids.....	552
<b>Scheme 4.40</b> Tong's synthesis of thalictricavine <b>419</b> and dehydrothalictricavine <b>420</b> .....	553

<b>Scheme 4.41</b> Ward's chemoenzymatic synthesis of tetrahydroprotoberberine alkaloid <b>422</b> .....	553
<b>Scheme 4.42</b> Fukuyama's synthesis of (–)-morphine <b>423</b> .....	557
<b>Scheme 4.43</b> Chida's formal synthesis of (–)-morphine <b>423</b> .....	558
<b>Scheme 4.44</b> Smith's total synthesis of morphine <b>423</b> .....	559
<b>Scheme 4.45</b> Tu's total synthesis of (–)-morphine <b>423</b> .....	560
<b>Scheme 4.46</b> Fukuyama's total synthesis of (–)-oxycodone <b>474</b> .....	561
<b>Scheme 4.47</b> Chen's total synthesis of (+)-oxycodone <b>474</b> .....	562
<b>Scheme 4.48</b> Chen's total synthesis of (+)-dihydrocodeinone <b>489</b> .....	563
<b>Scheme 4.49</b> Opatz's total synthesis of (–)-dihydrocodeine <b>497</b> .....	564
<b>Scheme 4.50</b> A. Opatz's electrochemical oxidative coupling. B. Application toward the total synthesis of (–)-thebaine <b>428</b> .....	565
<b>Scheme 4.51</b> Hudlicky's total synthesis of (+)-oxycodone <b>474</b> .....	566
<b>Scheme 4.52</b> Zhang's total synthesis of codeine <b>430</b> .....	568
<b>Scheme 4.53</b> Ellman's total synthesis of (–)-naltrexone <b>424</b> .....	569
<b>Scheme 4.54</b> Metz's total synthesis of thebainone A <b>536</b> .....	570
<b>Scheme 4.55</b> Marazano's enantioselective synthesis of (–)-argemonine <b>542</b> .....	572
<b>Scheme 4.56</b> Nishigaichi's synthesis of argemonine <b>542</b> and eschsoltzidine <b>550</b> .....	572
<b>Scheme 4.57</b> Jiang's enantioselective synthesis of (–)-amurensinine <b>556</b> .....	573
<b>Scheme 4.58</b> Stoltz's enantioselective synthesis of (+)-amurensinine <b>556</b> .....	574
<b>Scheme 4.59</b> Martin's synthesis of roelactamine <b>568</b> .....	575

<b>Scheme 4.60</b> Nakagawa-Goto's synthesis of neocaryachine <b>574</b> .....	575
<b>Scheme 4.61</b> A. Domain organization of saframycin A NRPS. B. Proposed biosynthetic mechanism for the construction of saframycin A's pentacyclic skeleton.....	578
<b>Scheme 4.62</b> Liu's total synthesis of (–)-saframycin A <b>575</b> .....	579
<b>Scheme 4.63</b> Saito's total synthesis of saframycin A <b>575</b> .....	581
<b>Scheme 4.64</b> A. Domain organization of renieramycins NRPS. B. Proposed biosynthetic mechanism for the construction of renieramycin E's pentacyclic skeleton.....	585
<b>Scheme 4.65</b> Danishefsky's total synthesis of (–)-cribrostatin 4 <b>602</b> .....	587
<b>Scheme 4.66</b> William's total synthesis of (–)-cribrostatin 4 <b>602</b> .....	588
<b>Scheme 4.67</b> Zhu's strategy to prepare the pentacyclic skeleton of (–)-cribrostatin 4 <b>602</b> .....	590
<b>Scheme 4.68</b> William's total synthesis of (–)-renieramycin G <b>597</b> and (–)-jorumycin <b>613</b> .....	591
<b>Scheme 4.69</b> William's unexpected C3-epimerization toward the synthesis of 3-epi-renieramycin G, and 3-epi-jorumycin .....	592
<b>Scheme 4.70</b> Magnus' total synthesis of renieramycin G <b>597</b> .....	593
<b>Scheme 4.71</b> Zhu's total synthesis of (–)-renieramycins G <b>597</b> , M <b>599</b> , (–)-jorunnamycin A <b>608</b> , and (–)-jorumycin <b>613</b> .....	595
<b>Scheme 4.72</b> Saito's total synthesis of renieramycin G <b>597</b> .....	596

<b>Scheme 4.73</b> Yang's strategy to assemble the pentacyclic core of renieramycin alkaloids .....	597
<b>Scheme 4.74</b> Yokoya's and Williams' total synthesis of (-)-renieramycin T <b>606</b> .	599
<b>Scheme 4.75</b> Chen's total synthesis of (-)-renieramycin T <b>606</b> .....	600
<b>Scheme 4.76</b> Stoltz's total synthesis of (-)-jorunnamycin A <b>608</b> and (-)-jorumycin <b>613</b> .....	601
<b>Scheme 4.77</b> A. Domain organization of Et-743 NRPS. B. Proposed biosynthetic mechanism for the construction of Et-743's pentacyclic skeleton .	604
<b>Scheme 4.78</b> Fukuyama's total synthesis of Et-743 <b>184</b> .....	606
<b>Scheme 4.79</b> Fukuyama's revised total synthesis of Et-743 <b>184</b> .....	608
<b>Scheme 4.80</b> Danishefsky's formal total synthesis of Et-743 <b>184</b> .....	609
<b>Scheme 4.81</b> Zhu's total synthesis of ecteinascidin 770 <b>699</b> and ecteinascidin 743 <b>184</b> .....	610
<b>Scheme 4.82</b> Zhu's total synthesis of ecteinascidin 597 <b>705</b> and ecteinascidin 583 <b>704</b> .....	611
<b>Scheme 4.83</b> Ma's total synthesis of ecteinascidin 743 <b>184</b> and lurbinectedin <b>769</b> .....	613
<b>Scheme 4.84</b> Garner's formal synthesis of cyanocycline A <b>771</b> and bioxalomycin $\beta$ 2 <b>788</b> .....	616
<b>Scheme 4.85</b> Proposed biosynthetic mechanism for the construction of the quinocarcin core.....	618
<b>Scheme 4.86</b> Myers' total synthesis of (-)-quinocarcin <b>789</b> .....	619



<b>Scheme 4.87</b> Zhu's total synthesis of (–)-quinocarcin <b>789</b> .....	620
<b>Scheme 4.88</b> Stoltz's total synthesis of (–)-quinocarcin <b>789</b> .....	622
<b>Scheme 4.89</b> Ohno's total synthesis of (–)-quinocarcin <b>789</b> .....	623
<b>Scheme 4.90</b> Williams' total synthesis of (–)-tetrazomine <b>791</b> .....	624
<b>Scheme 4.91</b> Williams' synthesis of tetrazomine analogues.....	625
<b>Scheme 4.92</b> Stoltz's total synthesis of (–)-lemonomycin <b>792</b> .....	627
<b>Scheme 4.93</b> Fukuyama and Kan's total synthesis of (–)-lemonomycin <b>792</b> .....	619

## **CHAPTER 5**

### *Progress Toward the Total Synthesis*

#### *Of (+)-Cyanocycline A*

<b>Scheme 5.1</b> Synthesis of the western isoquinoline fragment <b>887</b> .....	650
<b>Scheme 5.2</b> Synthesis of the eastern pyrrole fragment <b>898</b> .....	651
<b>Scheme 5.3</b> One-pot Pd-catalyzed borylation/Suzuki cross-coupling reaction of heterocycles <b>887</b> and <b>898</b> .....	651
<b>Scheme 5.4</b> 2 <sup>nd</sup> generation synthesis of pyrrole fragment <b>902</b> .....	652
<b>Scheme 5.5</b> Stille cross-coupling of heterocycles <b>887</b> and <b>902</b> .....	653
<b>Scheme 5.6</b> Key asymmetric hydrogenation of pyrrole-substituted isoquinoline <b>904</b> .....	654
<b>Scheme 5.7</b> 3 <sup>rd</sup> generation synthesis of pyrrole fragment <b>908</b> .....	654
<b>Scheme 5.8</b> Stille cross-coupling and synthesis of hydrogenation precursor <b>910</b> .....	655
<b>Scheme 5.9</b> Key asymmetric hydrogenation attempts of isoquinoline <b>910</b> .....	656
<b>Scheme 5.10</b> Heterogeneous hydrogenation investigation of isoquinoline <b>910</b> ..	658

<b>Scheme 5.11</b> Investigation of solvent in heterogeneous hydrogenation of isoquinoline <b>910</b> .....	659
<b>Scheme 5.12</b> Investigation of solvent in heterogeneous hydrogenation of isoquinoline <b>910</b> at ambient temperature .....	660
<b>Scheme 5.13</b> Competitive cyclization of secondary amine on to esters at C3- and C5-positions of the pyrrolidine ring .....	661
<b>Scheme 5.14</b> Synthesis of dihydropyrrole coupling partner <b>921</b> .....	662
<b>Scheme 5.15</b> Conversion of isoquinoline triflate <b>887</b> to a nucleophilic coupling partner .....	663
<b>Scheme 5.16</b> Cross-coupling of heterocycles <b>921</b> and <b>927</b> and synthesis of hydrogenation precursor .....	664
<b>Scheme 5.17</b> Synthesis of oxazoline dihydropyrrole coupling partner <b>932</b> .....	666
<b>Scheme 5.18</b> Initial Pd-catalyzed CMD cross-coupling reaction of triflate <b>887</b> and dihydropyrrole <b>932</b> .....	667
<b>Scheme 5.19</b> Optimization of Pd-catalyzed CMD cross-coupling reaction of triflate <b>887</b> and dihydropyrrole <b>938</b> .....	668
<b>Scheme 5.20</b> Proposed completion of (+)-cyanocycline A ( <b>771</b> ) .....	670

## **APPENDIX 5**

### *Synthetic Summary of Chapter 5*

<b>Scheme A5.1</b> Synthesis of the western isoquinoline fragment <b>887</b> .....	716
<b>Scheme A5.2</b> Synthesis of the eastern pyrrole fragment <b>898</b> .....	716
<b>Scheme A5.3</b> 2 <sup>nd</sup> generation synthesis of pyrrole fragment <b>902</b> .....	716

<b>Scheme A5.4</b> Cross-coupling of heterocycles <b>887</b> and <b>902</b> , and synthesis of hydrogenation precursor <b>904</b> .....	717
<b>Scheme A5.5</b> 3 <sup>rd</sup> generation synthesis of pyrrole fragment <b>908</b> .....	717
<b>Scheme A5.6</b> Stille cross-coupling and synthesis of hydrogenation precursor <b>910</b> .....	717
<b>Scheme A5.7</b> Hydrogenation attempts of isoquinoline <b>910</b> .....	718
<b>Scheme A5.8</b> Synthesis of dihydropyrrole coupling partner <b>921</b> .....	718
<b>Scheme A5.9</b> Stannylation of isoquinoline triflate <b>887</b> and synthesis of dihydropyrrole hydrogenation precursor <b>929</b> .....	719
<b>Scheme A5.10</b> Synthesis of oxazoline dihydropyrrole coupling partner <b>932</b> .....	719
<b>Scheme A5.11</b> Reduction of oxazoline <b>932</b> and Pd-catalyzed CMD cross-coupling of heterocycles <b>887</b> and <b>938</b> .....	720

## LIST OF TABLES

### CHAPTER 2

#### *Iridium-Catalyzed Enantioselective and Diastereoselective Hydrogenation of 1,3-Disubstituted Isoquinolines*

<b>Table 2.1</b>	Optimization of the enantioselective hydrogenation of isoquinolines to afford <i>cis</i> -THIQs.....	57
<b>Table 2.2</b>	Additional ligand screen .....	144
<b>Table 2.3</b>	Additive effects in Ir-catalyzed enantio- and diastereoselective hydrogenation.....	145
<b>Table 2.4</b>	Determination of enantiomeric excess .....	145

### APPENDIX 2

#### *X-Ray Crystallography Reports Relevant to Chapter 2*

<b>Table A2.1</b>	Crystal data and structure refinement for product <b>163p</b> .....	377
<b>Table A2.2</b>	Atomic coordinates ( $\times 10^5$ ) and equivalent isotropic displacement parameters ( $\text{\AA}^2 \times 10^4$ ) and population for <b>163p</b> . $U(\text{eq})$ is defined as one third of the trace of the orthogonalized $U^{ij}$ tensor .....	378
<b>Table A2.3</b>	Bond lengths [ $\text{\AA}$ ] and angles [ $^\circ$ ] for <b>163p</b> .....	377
<b>Table A2.4</b>	Anisotropic displacement parameters ( $\text{\AA}^2 \times 10^4$ ) for <b>163p</b> . The anisotropic displacement factor exponent takes the form: $-2\pi^2[h^2a^{*2}U^{11} + \dots + 2hka^*b^*U^{12}]$ .....	382
<b>Table A2.5</b>	Hydrogen coordinates ( $\times 10^4$ ) and isotropic displacement parameters ( $\text{\AA}^2 \times 10^3$ ) for <b>163p</b> .....	382
<b>Table A2.6</b>	Torsion angles [ $^\circ$ ] for <b>163p</b> .....	383
<b>Table A2.7</b>	Hydrogen bonds for <b>163p</b> [ $\text{\AA}$ and $^\circ$ ] .....	384

**CHAPTER 3***Iridium-Catalyzed Asymmetric Trans-Selective Hydrogenation of 1,3-Disubstituted Isoquinolines*

<b>Table 3.1</b>	Optimization of the asymmetric <i>trans</i> -selective hydrogenation.....	388
<b>Table 3.2</b>	Investigation of different directing groups to optimize the asymmetric <i>trans</i> -selective hydrogenation.....	389
<b>Table 3.3</b>	Additional additive, acid, and pressure studies.....	438
<b>Table 3.4</b>	Additional ligand screen .....	438
<b>Table 3.5</b>	Determination of enantiomeric excess .....	441

**APPENDIX 4***X-Ray Crystallography Reports Relevant to Chapter 3*

<b>Table A4.1</b>	Crystal data and structure refinement for product <b>175a</b> .....	503
<b>Table A4.2</b>	Atomic coordinates ( $\times 10^4$ ) and equivalent isotropic displacement parameters ( $\text{\AA}^2 \times 10^3$ ) and population for <b>175a</b> . $U(\text{eq})$ is defined as one third of the trace of the orthogonalized $U^{ij}$ tensor .....	504
<b>Table A4.3</b>	Bond lengths [ $\text{\AA}$ ] and angles [ $^\circ$ ] for <b>175a</b> .....	505
<b>Table A4.4</b>	Anisotropic displacement parameters ( $\text{\AA}^2 \times 10^3$ ) for <b>175a</b> . The anisotropic displacement factor exponent takes the form: $-2\pi^2[h^2a^{*2}U^{11} + \dots + 2hka^*b^*U^{12}]$ .....	508
<b>Table A4.5</b>	Hydrogen coordinates ( $\times 10^4$ ) and isotropic displacement parameters ( $\text{\AA}^2 \times 10^3$ ) for <b>175a</b> .....	509
<b>Table A4.6</b>	Torsion angles [ $^\circ$ ] for <b>175a</b> .....	509

## LIST OF ABBREVIATIONS

$[\alpha]_D$	specific rotation at wavelength of sodium D line
$^{\circ}\text{C}$	degrees Celsius
Å	Ångstrom
Ac	acetyl
AcOH	acetic acid
APCI	atmospheric pressure chemical ionization app apparent
aq	aqueous
Ar	aryl
atm	atmosphere
Bn	benzyl
Boc	<i>tert</i> -butyloxycarbonyl
bp	boiling point
br	broad
Bu	butyl
Bz	benzoyl
<i>c</i>	concentration for specific rotation measurements (g/100 mL)
ca.	about (Latin <i>circa</i> )
calc'd	calculated
cat	catalytic
CDI	1,1'-carbonyldiimidazole
$\text{cm}^{-1}$	wavenumber(s)
cod	1,5-cyclooctadiene

CPME	cyclopentyl methyl ether
DBU	1,8-diazabicyclo[5.4.0]undec-7-ene
DCE	1,2-dichloroethane
DDQ	2,3-dichloro-5,6-dicyano- <i>p</i> -benzoquinone
DIAD	diisopropyl azodicarboxylate
DIBAL	diisobutylaluminum hydride
DIPEA	<i>N,N</i> -diisopropylethylamine
DMA	<i>N,N</i> -dimethylacetamide
DMAP	4-dimethylaminopyridine
DME	1,2-dimethoxyethane
DMF	<i>N,N</i> -dimethylformamide
DMP	Dess–Martin periodinane
DMS	dimethyl sulfide
DMSO	dimethyl sulfoxide
dr	diastereomeric ratio
e.g.	for example (Latin <i>exempli gratia</i> )
<i>ee</i>	enantiomeric excess
EI+	electron impact
equiv	equivalent(s)
ESI	electrospray ionization
Et	ethyl
EtOAc	ethyl acetate
EWG	electron withdrawing group

FAB	fast atom bombardment
g	gram(s)
GC	gas chromatography
gCOSY	gradient-selected correlation spectroscopy
h	hour(s)
HFIP	hexafluoroisopropanol
HMBC	heteronuclear multiple bond correlation
HMDS	1,1,1,3,3,3-hexamethyldisilazane
HPLC	high-performance liquid chromatography
HRMS	high-resolution mass spectroscopy
HSQC	heteronuclear single quantum correlation
Hz	hertz
$h\nu$	light
<i>i</i> -Pr	isopropyl
i.e.	that is (Latin id est)
IPA	isopropanol, 2-propanol
IQ	isoquinoline
IR	infrared (spectroscopy)
<i>J</i>	coupling constant
K	Kelvin(s) (absolute temperature)
kcal	kilocalorie
KHMDS	potassium hexamethyldisilazide
L	liter; ligand



LAH	Lithium aluminium hydride
L*	chiral ligand
LCMS	liquid chromatography-mass spectrometry
LDA	lithium diisopropylamide
LG	leaving group
lit.	literature value
m	multiplet; milli
<i>m</i>	meta
M	metal; molar; molecular ion
<i>m</i> -CPBA	<i>meta</i> -chloroperoxybenzoic acid
<i>m/z</i>	mass to charge ratio
Me	methyl
mg	milligram(s)
MHz	megahertz
min	minute(s)
MM	mixed method
mol	mole(s)
mp	melting point
MS	molecular sieves
n	nano
N	normal
<i>n</i> -Bu	butyl
NBS	<i>N</i> -bromosuccinimide

NHSI	<i>N</i> -hydroxysuccinimide
NMR	nuclear magnetic resonance
Nu	nucleophile
<i>o</i>	ortho
<i>p</i>	para
Pd/C	palladium on carbon
Ph	phenyl
pH	hydrogen ion concentration in aqueous solution
Phth	phthalimide
PHOX	phosphinooxazoline ligand
PIDA	Phenyliodine(III) diacetate
Pin	2,3-dimethylbutane-2,3-diol (pinacol)
Piv	trimethylacetyl, pivaloyl
<i>pKa</i>	<i>pK</i> for association of an acid
pMBz	4-methoxy-benzoyl
ppm	parts per million
Pr	propyl
Py	pyridine
q	quartet
R	generic for any atom or functional group
RCM	ring-closing metathesis
Ref.	reference
<i>R<sub>f</sub></i>	retention factor

rr	rotameric ratio
s	singlet or strong or selectivity factor
sat.	saturated
SFC	supercritical fluid chromatography
STAB	Sodium triacetoxyborohydride
t	triplet
<i>t</i> -Bu	<i>tert</i> -butyl
TBABr	tetrabutylammonium bromide
TBAF	tetrabutylammonium fluoride
TBAI	tetrabutylammonium iodide
TBME/MTBE	<i>tert</i> -butyl methyl ether
TBS	<i>tert</i> -butyldimethylsilyl
TES	triethylsilyl
Tf	trifluoromethanesulfonyl (triflyl)
TFA	trifluoroacetic acid
TFAA	trifluoroacetic anhydride
TFE	2,2,2-trifluoroethanol
THF	tetrahydrofuran
THIQ	tetrahydroisoquinoline
TIPS	triisopropylsilyl
TLC	thin-layer chromatography
TMEDA	<i>N,N,N',N'</i> -tetramethylethylenediamine
TMS	trimethylsilyl

TOF	time-of-flight
Tol	tolyl
$t_R$	retention time
Ts	<i>p</i> -toluenesulfonyl (tosyl)
UV	ultraviolet
$v/v$	volume to volume
w	weak
$w/v$	weight to volume
X	anionic ligand or halide
$\lambda$	wavelength
$\mu$	micro

## CHAPTER 1

### *Advances in Homogeneous Catalysts for the Asymmetric Hydrogenation of Heteroarenes (2000 – 2020)<sup>†</sup>*

#### 1.1 INTRODUCTION

Heterocycles are important structural motifs found frequently in natural products<sup>1</sup> and industrial products, such as pharmaceuticals<sup>2</sup> and agrochemicals.<sup>3</sup> Nitrogen heterocycles constitute approximately 59% of recent FDA-approved small-molecule drugs, with an average of two to three nitrogen atoms per drug.<sup>2a</sup> In the context of pharmaceutical development, a significant positive correlation exists between key structural elements of drug candidates, such as degree of saturation and number of stereogenic centers, with observed clinical success.<sup>2c,d</sup> Thus, the ability to access stereochemically complex heterocyclic scaffolds has been of great interest in recent years. Considering the ubiquity of both aromatic and saturated heterocycles in pharmaceuticals, the direct access to enantiopure heterocycles via heteroarene hydrogenation continues to be an important research area in both academia and industry.<sup>2</sup>

---

<sup>†</sup>Portions of this chapter have been reproduced with permission from Kim, A. N.; Stoltz, B. M. *ACS Catal.* **2020**, *10*, 13834–13851. © 2020 American Chemical Society.

## *Chapter 1 – Recent Advances in Homogeneous Catalysts for the Asymmetric Hydrogenation of Heteroarenes*

While significant progress has been made in the area of asymmetric heteroarene hydrogenation, these transformations continue to pose a challenge for catalytic processes, ostensibly due to the high energetic cost of breaking aromaticity, and the presence of heteroatoms that may poison and deactivate the catalyst.<sup>4</sup> Nevertheless, the asymmetric hydrogenation of heteroarenes, including quinolines, isoquinolines, quinoxalines, pyridines, indoles, furans, and benzoxazines has been extensively explored, and several comprehensive reviews have been published on this subject (Figure 1.1).<sup>4</sup> The hydrogenation of many common heteroarenes can be achieved using a variety of catalyst systems, including homogeneous and heterogeneous catalysts, such as metal nanoparticles.<sup>4d</sup> Among these, homogeneous catalyst systems have found widespread application for the asymmetric hydrogenation of heteroarenes, often providing access to different enantioenriched motifs with a simple adjustment of the chiral ligand.<sup>4,5</sup> This Perspective is focused on highlighting homogeneous catalyst systems that have recently been developed for the asymmetric hydrogenation of heteroarenes, evaluating the general relationships between different catalyst complexes and their reactivity for various heterocycles. The following sections will feature reports that have been published since 2011, as previous reports have already been discussed comprehensively in prior review articles.<sup>4</sup>

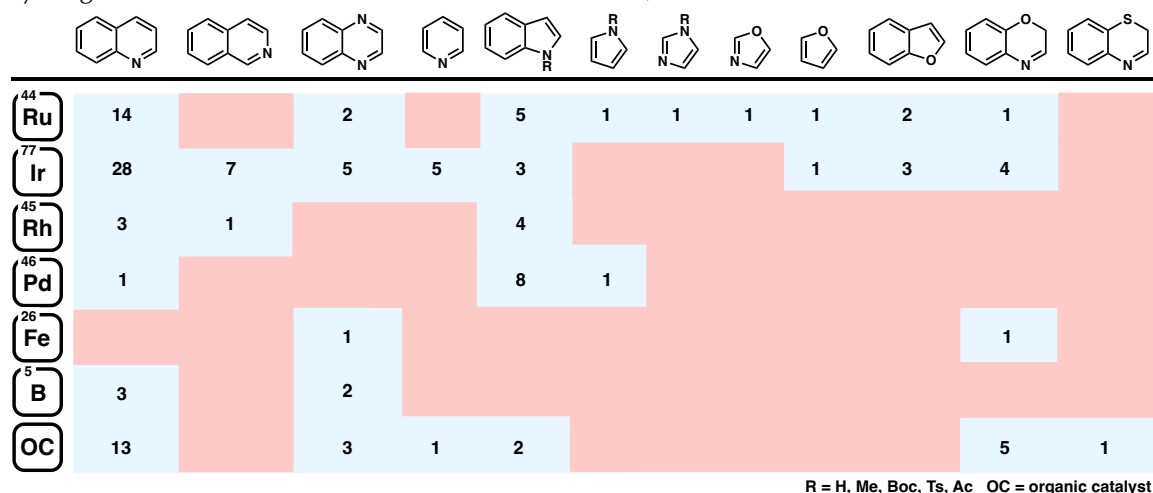
### **1.2 GENERAL MECHANISTIC CONSIDERATIONS**

Heteroarenes pose a significant challenge for asymmetric catalysis due to their inherent thermodynamic stability and the tendency of both reactants and products to

Chapter 1 – Recent Advances in Homogeneous Catalysts for the Asymmetric Hydrogenation of Heteroarenes

deactivate catalysts. Three general strategies have been employed to overcome these difficulties: catalyst activation, substrate activation, and relay catalysis.<sup>4a</sup>

**Figure 1.1** Overview of the total number of published reports on the asymmetric hydrogenation of common heteroarenes ( $\geq 90\%$  ee, minimum of three substrates).

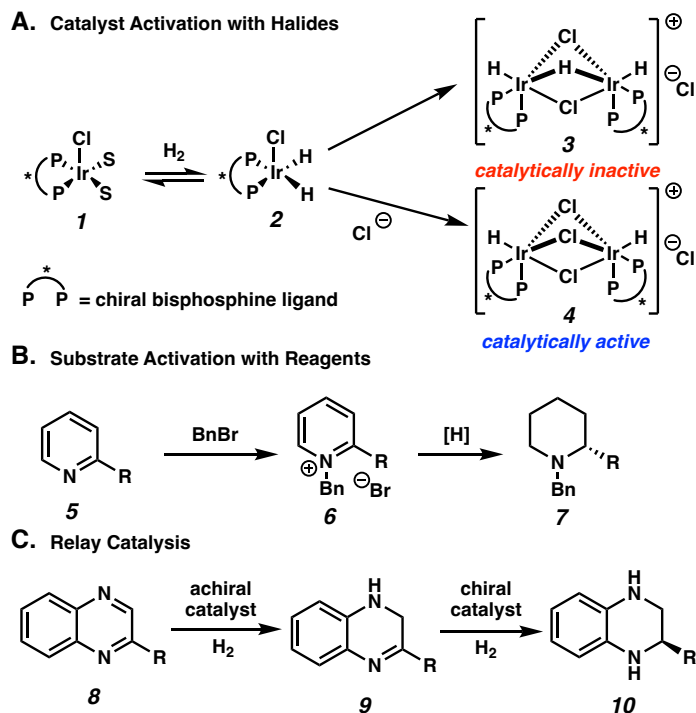


Catalyst activation involves either the preformation of the active catalyst or the addition of reagents to form a more active catalyst species in situ. For instance, the addition of halide sources to an iridium precatalyst was reported by Mashima and coworkers to prevent the irreversible formation of catalytically inactive dimeric iridium hydride species **3** (Scheme 1.1A).<sup>6</sup> The substrate activation approach introduces reagents to overcome the inherent aromatic stability of heteroarenes through in situ generation or pre-formation of activated substrates, such as quinolinium or pyridinium salts (e.g., **6**, Scheme 1.1B).<sup>7</sup> Finally, relay catalysis involves the use of two or more catalysts for the asymmetric hydrogenation of heteroarenes. For example, an achiral transition metal catalyst is often employed to induce initial partial hydrogenation of the substrate **8**, followed by an enantioselective hydrogenation of an intermediate such as imine **9** aided by a chiral Brønsted acid catalyst

Chapter 1 – Recent Advances in Homogeneous Catalysts for the Asymmetric Hydrogenation of Heteroarenes

(Scheme 1.1C).<sup>8</sup> Overall, these distinct strategies enable high stereoselectivity and functional group tolerance in the asymmetric hydrogenation of heteroarenes.

**Scheme 1.1.** Examples for the asymmetric hydrogenation of heteroarenes.



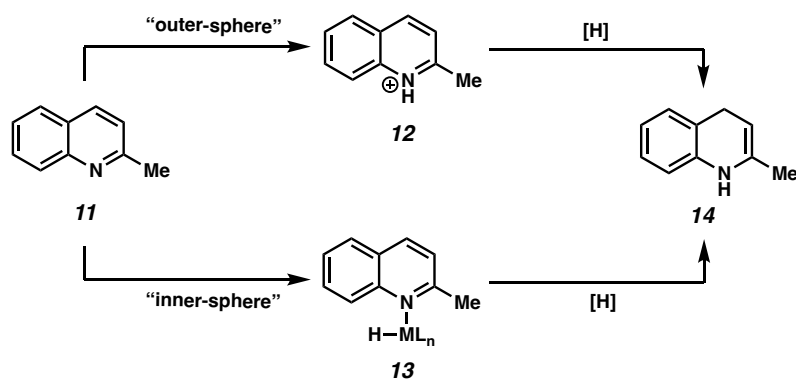
The general mechanism of the asymmetric hydrogenation of heteroarenes can be thought of to involve the following steps (depending on the degree of unsaturation): formation of the active catalyst species, hydride addition from the catalyst to the substrate, and regeneration of the catalyst from a hydrogen source.<sup>9</sup> However, several questions regarding the mechanism of asymmetric hydrogenation that could be addressed include the order of hydride addition (1,2- vs. 1,4-addition), substrate coordination to the catalyst (inner- vs. outer-sphere), the rate-determining step, and the enantio-determining step.<sup>4a-d,9c</sup> For instance, both inner-sphere and outer-sphere processes have been



Chapter 1 – Recent Advances in Homogeneous Catalysts for the Asymmetric Hydrogenation of Heteroarenes

proposed to explain the mechanism for the iridium-catalyzed hydrogenation of 2-methylquinoline **11** (Scheme 1.2).<sup>9b</sup> In an outer-sphere pathway, protonation of the substrate occurs to form iminium intermediate **12**, followed by external hydride delivery to the activated substrate from the transition metal center. In contrast, an inner-sphere process involves a substrate that is bound to the metal hydride species (**13**) that undergoes a hydride transfer step. While other catalyst systems have been proposed to undergo an outer-sphere mechanism for the hydrogenation of various heterocycles (vide infra), other studies also support an inner-sphere coordination of the substrate to the catalyst.<sup>10</sup> Thus, the coordinating ability of different heteroatom-containing substrates to the catalyst complex is not explicitly defined, and therefore difficult to predict how it would behave under different hydrogenation systems.

**Scheme 1.2.** Possible mechanistic pathways for the hydrogenation of 2-methylquinoline **11**.



Although the asymmetric hydrogenation of heteroarenes is often difficult to monitor due to the use of high-pressure reactors, several mechanistic studies have been conducted using empirical data and computational modeling to elucidate the mechanisms of transition metal-catalyzed and organic-catalyzed heteroarene hydrogenation reactions.

*Chapter 1 – Recent Advances in Homogeneous Catalysts for the Asymmetric Hydrogenation of Heteroarenes*

The proposed catalytic cycles of these studies will be addressed in the following sections of this Perspective for each transition metal and organic catalyst system.

### 1.3 RUTHENIUM-CATALYZED ASYMMETRIC HYDROGENATION

With regards to homogeneous catalysis, ruthenium was among the first transition metals explored in asymmetric hydrogenation reactions. In 1995, Noyori and coworkers introduced a Ru(II) catalyst with a chiral diamine ligand that promotes the highly stereoselective reduction of aromatic ketones through an asymmetric transfer hydrogenation process.<sup>11</sup> Shortly after, this catalyst system was applied to the asymmetric hydrogenation of imines with a formic acid–triethylamine mixture as the hydrogen source.<sup>12</sup> Since then, several established ruthenium catalyst systems with common ligand scaffolds were developed for the asymmetric hydrogenation of heteroarenes (Figure 1.2), as well as the hydrogenation of carbocyclic aromatic compounds.<sup>13</sup>

The air-stable Ru/TsDPEN catalyst (TsDPEN = *N*-(*p*-toluenesulfonyl)-1,2-diphenylethylenediamine), initially developed by Fan and Chan for the hydrogenation of quinolines, has found widespread applications in the asymmetric hydrogenation of *N*-heterocycles (Figure 1.2).<sup>14–19</sup> In these reports, hydrogen gas is activated by the catalyst to reduce quinolines at ambient temperatures in ionic liquids and even under solvent-free conditions. Subsequent studies also utilize this system for sequential reductive amination and asymmetric hydrogenation cascade reactions of quinoline derivatives to access structurally diverse scaffolds.<sup>15</sup> Since 2011, the Ru/TsDPEN catalyst

Chapter 1 – Recent Advances in Homogeneous Catalysts for the Asymmetric Hydrogenation of Heteroarenes

system has evolved with important applications toward the development of novel chiral ligands. Fan and coworkers demonstrated that chiral Ru/TsDPEN catalysts can reduce 2,2'-bisquinoline and bisquinoxaline derivatives with high stereoselectivity.<sup>16</sup>

**Figure 1.2.** Common Ru-based catalyst systems for the asymmetric hydrogenation of heteroarenes ( $\geq 90\%$  ee, minimum three substrates). Only one enantiomer of ligand shown for simplicity.

Catalyst System	Heteroarenes	References
<p>Ru/DPEN</p> <p>R<sup>1</sup> = Ts, Ms R<sup>2</sup> = H, Me R<sup>3</sup> = <i>p</i>-cymene, hexamethylbenzene X = OTf, PF<sub>6</sub>, BF<sub>4</sub>, OPOPh<sub>2</sub></p>		<p>14–17</p> <p>14c</p> <p>15d</p> <p>15c, 18</p> <p>19</p>
<p>Ru/PhTRAP, base</p> <p>(<i>S,S</i>)-(<i>R,R</i>)-PhTRAP (L1)</p>		<p>23a</p> <p>23b</p> <p>23c</p> <p>23d</p>
<p>Ru/NHC, KO<sup>t</sup>-Bu</p> <p>NHC·BF<sub>4</sub> (L2)</p>		<p>25a</p> <p>25b–c</p>

*Chapter 1 – Recent Advances in Homogeneous Catalysts for the Asymmetric Hydrogenation of Heteroarenes*

More recently, the system was applied to hydrogenate 2-(pyridine-2-yl)quinoline derivatives for the synthesis of novel *N,P*-ligands (Scheme 1.3).<sup>17</sup> Using chiral catalyst complex **16** (Scheme 1.3A), selective hydrogenation of the quinoline ring was observed in a range of substrates **15** with high enantioselectivities. Although *ortho*-substituents on the pyridine ring are necessary to prevent catalyst deactivation, this requirement further enables the tuning of the steric effect of the chiral ligand generated.

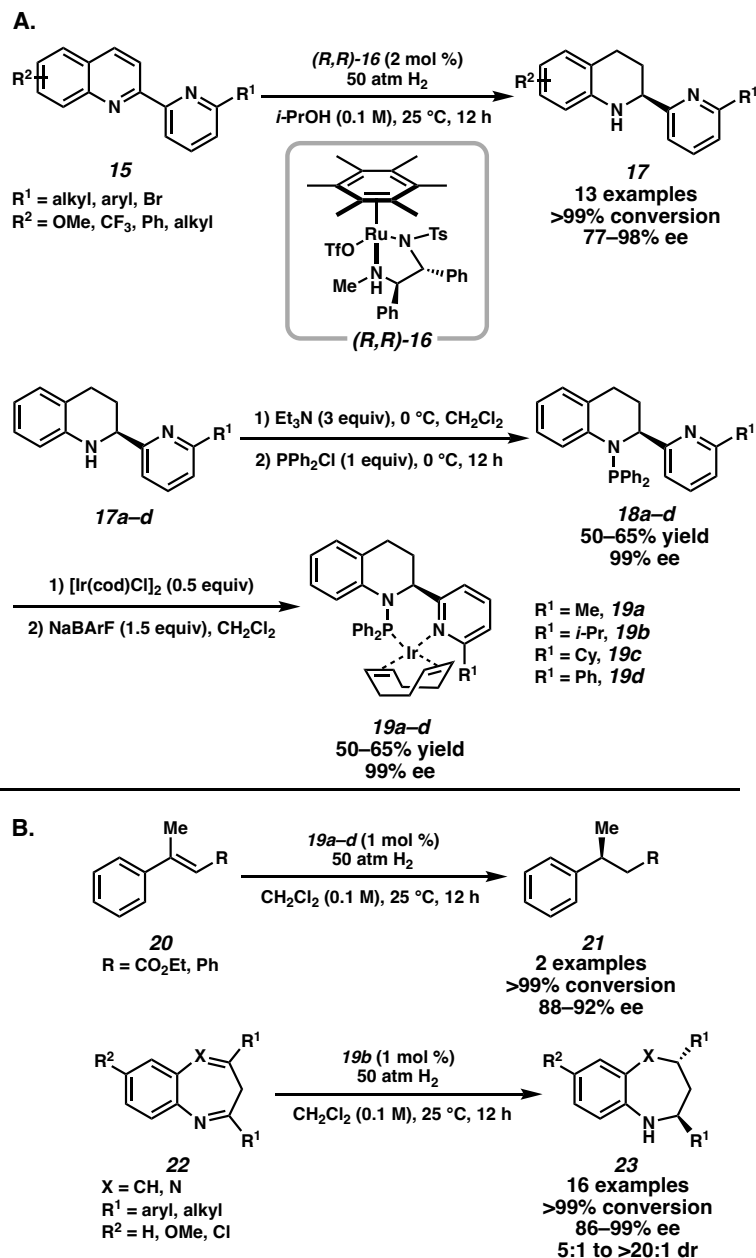
The hydrogenated products **17a–d** can then be transformed into a novel class of chiral *N,P*-ligands by treatment with  $\text{PPh}_2\text{Cl}$  in  $\text{NEt}_3$ . After recrystallization, these ligands are then treated with  $[\text{Ir}(\text{COD})\text{Cl}]_2$ , followed by anion metathesis to yield chiral iridium complexes **19a–d**.<sup>17</sup> These catalysts are then successfully used for the asymmetric hydrogenation of olefins and seven-membered cyclic imines (Scheme 1.3B). Notably, replacement of the phenyl substituent on the pyridine ring of **19d** with an alkyl group (**19a–c**) improves the enantioselectivity of the hydrogenation of trisubstituted olefin **20** to **21** in 88–92% ee. Catalyst **19b** is further utilized in the asymmetric hydrogenation of benzazepines and benzodiazepines, providing products **23** in up to 99% ee and 20:1 dr. The efficient synthesis of a novel class of chiral ligands through the asymmetric hydrogenation of heteroarenes is a promising application of this hydrogenation technology. The Ru/TsDPEN catalyst system is also effective for the asymmetric hydrogenation of unprotected indoles, which traditionally require protection of the indole nitrogen to prevent catalyst deactivation,<sup>18</sup> C(3)-substituted benzoxazines,<sup>19</sup> and a variety of polycyclic heteroarenes.<sup>20</sup>

*Chapter 1 – Recent Advances in Homogeneous Catalysts for the Asymmetric Hydrogenation of Heteroarenes*

Based on experimental results and theoretical calculations, Fan and coworkers propose a catalytic cycle for the asymmetric hydrogenation of quinolines with Ru/TsDPEN catalysts (Figure 1.3). The Ru(II) catalyst activates molecular H<sub>2</sub> to form dihydrogen complex **24**. After heterolytic cleavage of H<sub>2</sub> to generate complex **27** and the activated substrate **26**, subsequent 1,4-hydride addition affords an enamine intermediate **29**.<sup>4e,15a</sup>

**Scheme 1.3.** *Ru-catalyzed asymmetric hydrogenation of quinolines and applications of hydrogenated products.*

Chapter 1 – Recent Advances in Homogeneous Catalysts for the Asymmetric Hydrogenation of Heteroarenes



Tautomerization then occurs to form imine **30**, which is protonated by complex **24** to produce iminium **31**. Intermediate **31** undergoes an asymmetric 1,2-hydride transfer from complex **27** to deliver product **32** via **TS1**. The enantioselectivity is proposed to originate from the attractive  $\text{CH}/\pi$  interaction between the  $\eta^6$ -arene ligand and the

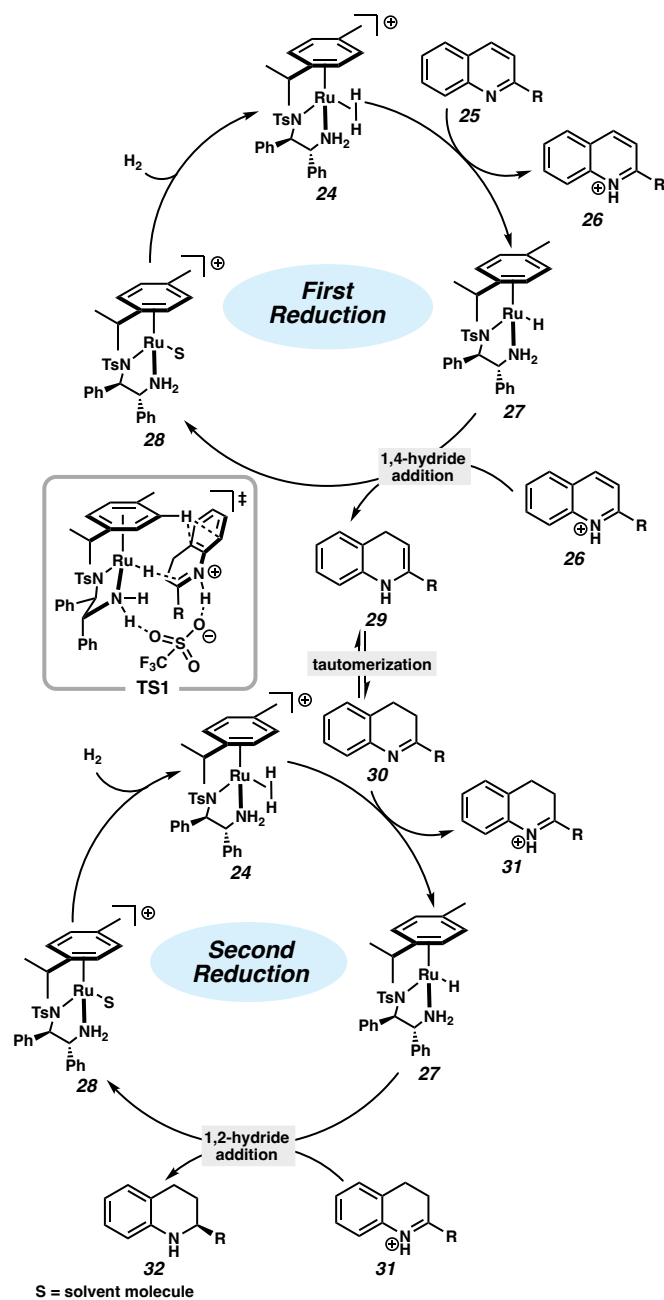
*Chapter 1 – Recent Advances in Homogeneous Catalysts for the Asymmetric Hydrogenation of Heteroarenes*

carbocyclic ring of the dihydroquinoline via a 10- membered transition state with participation of the triflate anion, as shown in **TS1**.<sup>15a,21</sup>

Although Ru/TsDPEN systems are efficient catalysts for the hydrogenation of bicyclic aromatic compounds, preformation of the active catalyst is required. Alternatively, other common chiral bisphosphine ligands that are explored in ruthenium-catalyzed asymmetric hydrogenations include PhTRAP (2,2''-bis[1-(diphenylphosphino)-ethyl]-1,1''-biferrocene), a  $C_2$  symmetric biferrocene framework.<sup>22</sup> Kuwano and coworkers demonstrate that ruthenium catalysts bearing PhTRAP ligand (**L1**) are productive in the hydrogenation of *N*-Boc-protected indoles (Scheme 1.4A), as well as substituted *N*-Boc-protected pyrroles and imidazoles (Scheme 1.4B, C).<sup>23</sup> Considering the high aromatic stability of single-ring aromatic compounds, the exhaustive hydrogenation of trisubstituted pyrroles to yield chiral pyrrolidines under this catalyst manifold is a significant advancement.<sup>4a,23c</sup> The Ru/PhTRAP catalyst can also be applied to the hydrogenation of other 5-membered heterocycles such as disubstituted imidazoles and oxazoles, however, only partial hydrogenation is observed in these cases.<sup>23d</sup>

**Figure 1.3.** *Proposed catalytic cycle for the asymmetric hydrogenation of quinolines with a Ru/TsDPEN catalyst.*

Chapter 1 – Recent Advances in Homogeneous Catalysts for the Asymmetric Hydrogenation of Heteroarenes

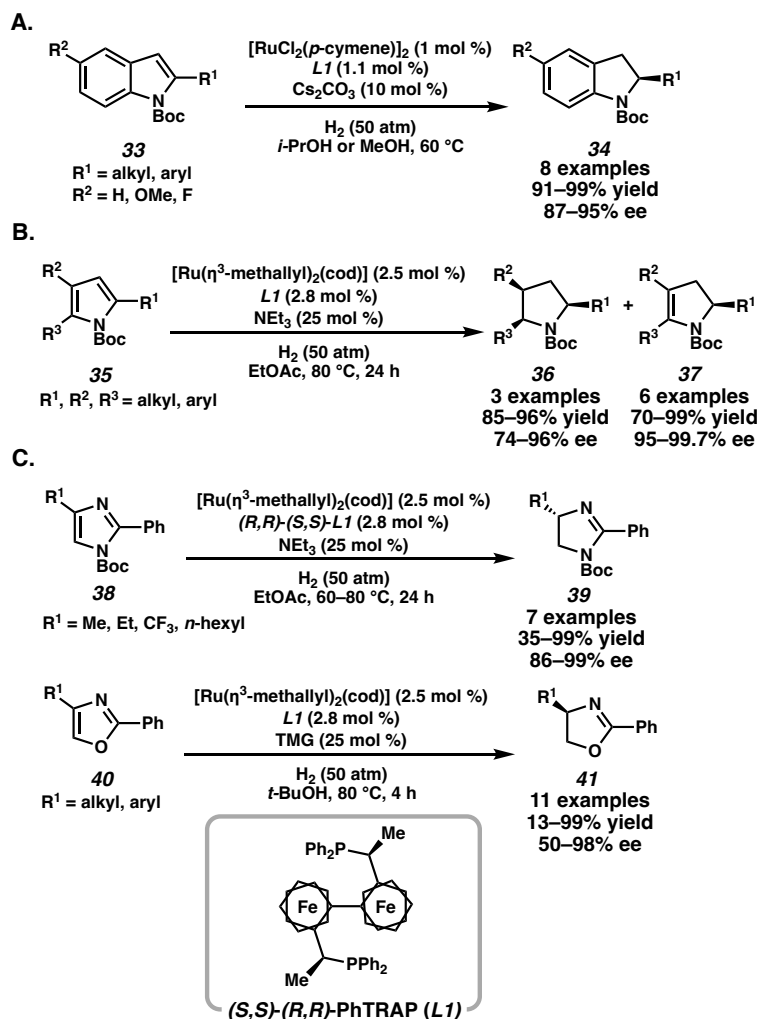


Finally, ruthenium *N*-heterocyclic carbene (NHC) complexes have found many applications in the transfer hydrogenation of ketones, nitriles, as well as the regioselective hydrogenation of heterocycles.<sup>24</sup>

**Scheme 1.4.** Ru-catalyzed asymmetric hydrogenation with PhTRAP ligand **L1**.



Chapter 1 – Recent Advances in Homogeneous Catalysts for the Asymmetric Hydrogenation of Heteroarenes

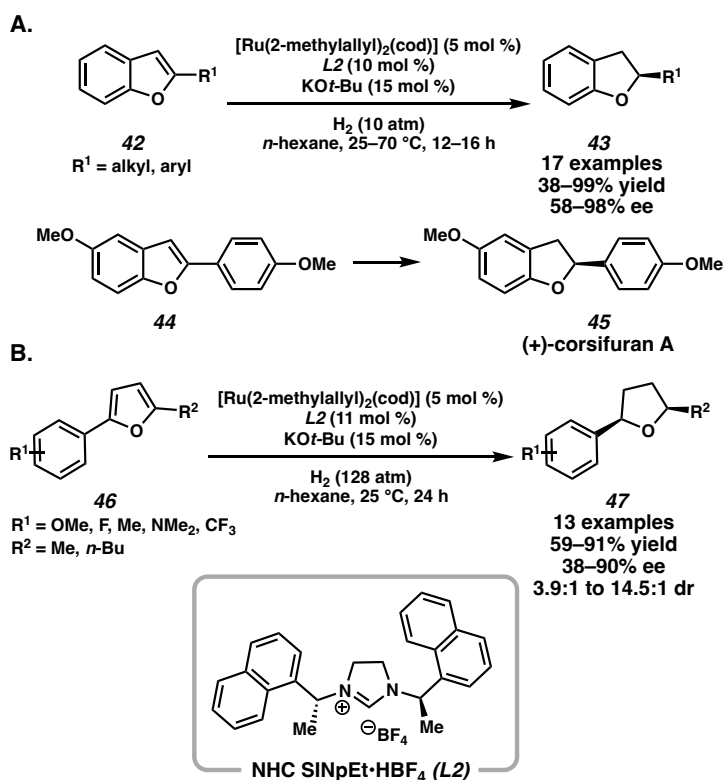


Glorius and coworkers first demonstrated the regioselective hydrogenation of the aromatic carbocyclic ring of quinoxalines, albeit with moderate enantioselectivity. They observed that the identity of NHC ligand was critical in determining the regioselectivity of hydrogenation, and found that these catalytic systems can also be applied toward the asymmetric hydrogenation of furans and benzofurans.<sup>25</sup> Using chiral NHC ligand SINpEt•HBF<sub>4</sub> (**L2**), the asymmetric hydrogenation of disubstituted furans and 2-substituted benzofurans proceeded in high yields and enantioselectivities (Scheme 1.5). A wide range of substituted furans were hydrogenated with this catalyst system,

Chapter 1 – Recent Advances in Homogeneous Catalysts for the Asymmetric Hydrogenation of Heteroarenes

demonstrating a significant correlation between strongly electron-withdrawing groups on the substrate and diminished enantioselectivity.<sup>25a</sup> Overall, the Ru/NHC complex demonstrated its capability to hydrogenate a range of heteroarenes, particularly oxygen-containing heterocycles, allowing direct access to natural metabolites such as (+)-corsifuran A (Scheme 1.5A). Further studies of the Ru/L2 catalyst system by Glorius and coworkers revealed that hydrogenation of the naphthyl substituents of the NHC ligand was a key step in accessing the active catalyst.<sup>26</sup>

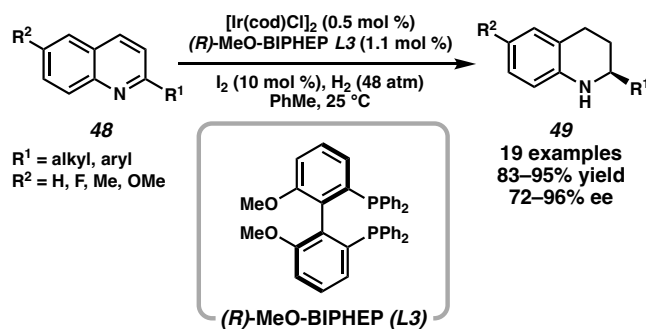
**Scheme 1.5.** Ru-catalyzed asymmetric hydrogenation of furans and benzofurans with NHC ligand L2.



Chapter 1 – Recent Advances in Homogeneous Catalysts for the Asymmetric Hydrogenation of Heteroarenes

Following the initial disclosure of the enantioselective hydrogenation of quinolines using  $[\text{Ir}(\text{cod})\text{Cl}]_2$  and bisphosphine ligand MeO-BIPHEP (**L3**) in 2003 (Scheme 1.6),<sup>27</sup> much attention has been devoted toward the development of the iridium-catalyzed hydrogenation of heteroarenes. Most studies have focused on the exploration of different types of activating agents to reduce substrate aromaticity, as well as to prevent the irreversible formation of catalytically inactive dimeric iridium hydride species **3**.<sup>6,27</sup> Common ligand scaffolds utilized in this transformation include atropisomeric biaryl bisphosphine ligands, as well as phosphine-phosphite ligands, *N,P*-ligands, and chiral diamine ligands that have been explored for the asymmetric hydrogenation of a range of heterocycles (Figure 1.4).


**Scheme 1.6.** First reported Ir-catalyzed asymmetric hydrogenation of quinolines.

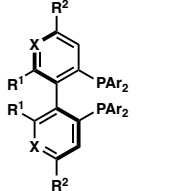
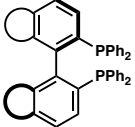
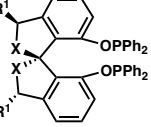
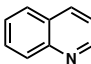
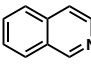
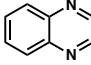
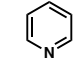
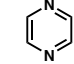
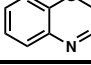
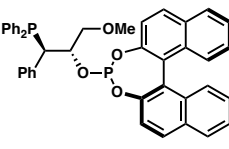
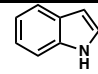
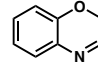
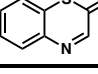
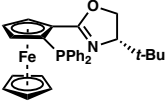
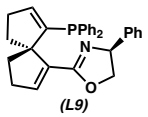
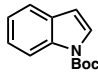
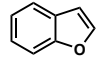
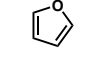
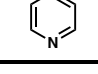
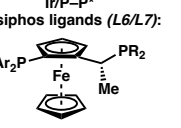
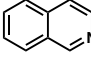
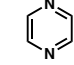
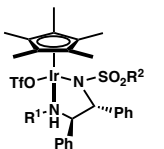
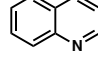


The biaryl bisphosphine ligand scaffold is most common in iridium-catalyzed asymmetric hydrogenation due to its excellent steric and electronic tunability. Structural variations of the ligand include alteration of *P*-substitution and modifications of the phenyl backbone, including the synthesis of supramolecular chiral ligands appended with crown ethers that induce strong complexation between the ligand and alkali cations.<sup>28</sup>

Chapter 1 – Recent Advances in Homogeneous Catalysts for the Asymmetric Hydrogenation of Heteroarenes

**Figure 1.4.** Common Ir-based catalyst systems for the asymmetric hydrogenation of heteroarenes ( $\geq 90\%$  ee, minimum three substrates). Only one enantiomer of ligand shown for simplicity.



Catalyst System	Heteroarenes	References	Catalyst System	Heteroarenes	References
<p>Ir/P-P* biaryl bisphosphine ligands:</p>  <p>Ar = Ph, xylyl X = CH, N R<sup>1</sup> = OMe, OCF<sub>3</sub>, OTf, OC<sub>12</sub>H<sub>25</sub>, OPEG, O<sub>2</sub>(C<sub>5</sub>H<sub>10</sub>) (TunePhos) R<sup>2</sup> = H, OMe, OPEG</p>  <p>SEGPHOS (L4), DIFLUORPHOS = SYNPHOS, BINAP, H<sub>8</sub>-BINAP</p>  <p>X = CH<sub>2</sub>, O R<sup>1</sup> = H, Et</p>	     	27–29, 35  6, 30  29e, 31  30e  32  33	<p>Ir/P-OP* P-OP* ligand (L8):</p> 	  	38b  38c  38c
			<p>Ir/N-P* N-P* ligands:</p> <p>Select Examples:</p>  	   	39a  39a,b  39b  39d
<p>Ir/P-P* Josiphos ligands (L6/L7):</p>  <p>Ar = Ph, DMM (4-methoxy-3,5-dimethylphenyl) R = xylyl, t-Bu</p>	 	37  32a	<p>Ir/N-N* TsDPEN ligands:</p>  <p>R<sup>1</sup> = H, Me R<sup>2</sup> = 4-CH<sub>3</sub>C<sub>6</sub>H<sub>4</sub>, 4-CF<sub>3</sub>C<sub>6</sub>H<sub>4</sub></p>		16c, 40

Since 2011, the combination of iridium and biaryl bisphosphine ligands has been extensively studied by Zhou, Agbossou-Niedercorn, and Mashima in the asymmetric hydrogenation of heteroarenes, including quinolines,<sup>29</sup> isoquinolines,<sup>6,30</sup> quinoxalines,<sup>29e,31</sup> pyridines,<sup>30e</sup> pyrazines,<sup>32</sup> and benzoxazines.<sup>33</sup> Iodine, chloroformates, amines, and Brønsted acids are common activating reagents for enhancing catalytic activity of these heterocyclic substrates.

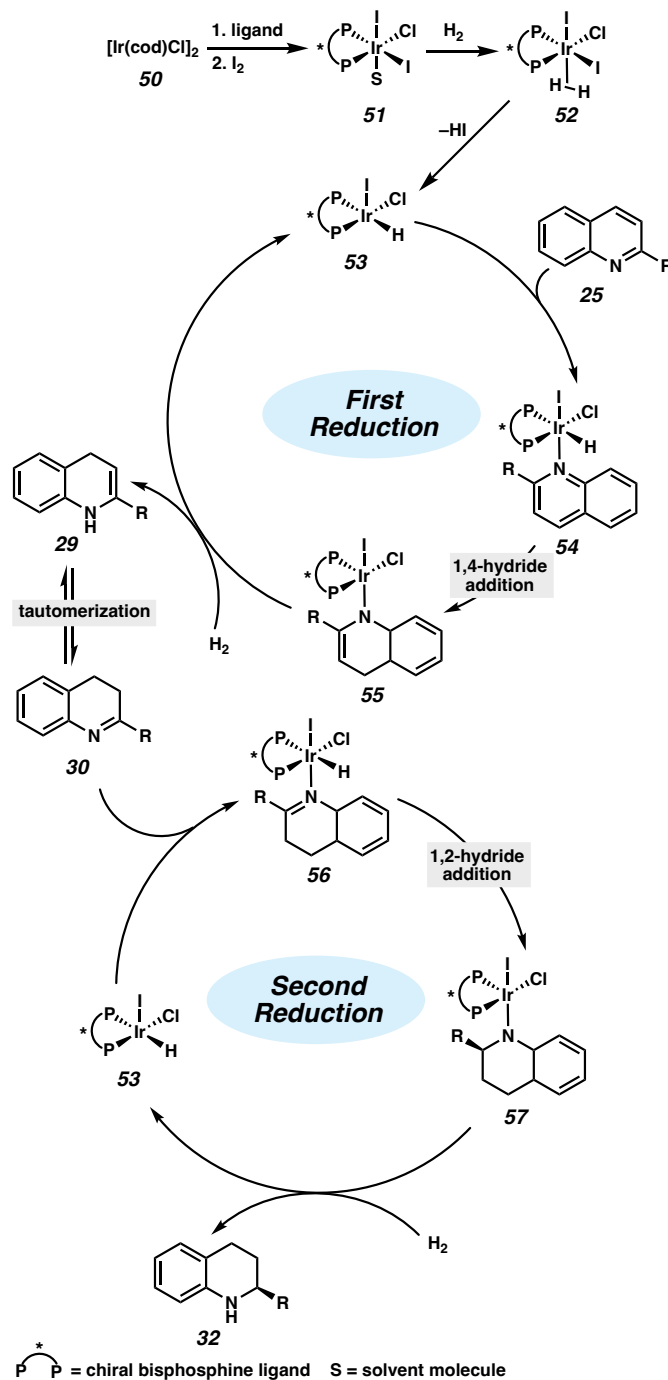
*Chapter 1 – Recent Advances in Homogeneous Catalysts for the Asymmetric Hydrogenation of Heteroarenes*

The mechanism and the role of iodine as an activator was initially proposed by Zhou and Li (Figure 1.5).<sup>27b</sup> Starting from  $[\text{Ir}(\text{cod})\text{Cl}]_2$ , the addition of  $\text{I}_2$  oxidizes the Ir(I) precursor to an Ir(III) species **51**. Subsequent heterolytic cleavage of  $\text{H}_2$  with release of HI forms catalytically active Ir(III) complex **53**. The heteroarene then coordinates to generate octahedral complex **54**, followed by a 1,4-hydride transfer to form intermediate **55**. An additional molecule of  $\text{H}_2$  regenerates the iridium hydride species **53** and protonates the enamine, which can isomerize to imine **30** and undergo a second reduction. The enantiodetermining step is proposed to be a 1,2-hydride addition that establishes the stereogenic center, with the addition of  $\text{H}_2$  releasing the product and regenerating Ir(III) species **53**. It is unclear, however, whether substrate coordination to the metal center occurs, as other studies have proposed an outer-sphere pathway for the homogeneous iridium-catalyzed hydrogenation of quinolines and isoquinolines (*vide supra*).<sup>6,9b</sup>

Recently, Zhou and coworkers employed trichloroisocyanuric acid (TCCA) as a traceless activating reagent for the iridium-catalyzed hydrogenation of isoquinolines and pyridines (Scheme 1.7). This method circumvents the additional steps of installing and removing the *N*-acyl group to activate the substrates. Pairing  $[\text{Ir}(\text{cod})\text{Cl}]_2$  and bisphosphine ligand (*R*)-SEGPHOS (**L4**), a range of disubstituted isoquinolines and pyridines were hydrogenated in high yield and excellent enantioselectivity.<sup>30e</sup> The use of TCCA as a halogen-bond activator gave the highest enantioselectivity compared to *N*-chlorosuccinimide or *N*-iodosuccinimide. Notably, 2,3,6-trisubstituted pyridines **60** were also converted to chiral piperidines **61** with higher enantioselectivity than previous methods, which often require more activated pyridinium salts as substrates.<sup>7</sup>

Chapter 1 – Recent Advances in Homogeneous Catalysts for the Asymmetric Hydrogenation of Heteroarenes

**Figure 1.5.** Proposed catalytic cycle for the Ir-catalyzed asymmetric hydrogenation of quinolines with  $I_2$  as additive.

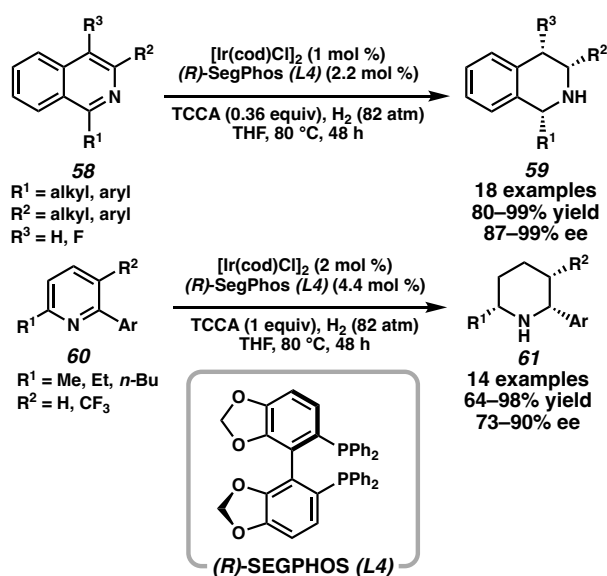


Extending BINAP-derived ligand scaffolds, biaryl spirocyclic ligands have emerged as powerful tools for asymmetric catalysis due to their higher rigidity.<sup>34</sup> Nagorny and

Chapter 1 – Recent Advances in Homogeneous Catalysts for the Asymmetric Hydrogenation of Heteroarenes

coworkers reported that chiral spiroketal-based bisphosphinite ligand (SPIRAPO) (**L5**) is effective in the asymmetric hydrogenation of quinolines, quinoxalines, and benzoxazinones (Scheme 1.8).<sup>35</sup> Using 10 mol % I<sub>2</sub> and low catalyst loadings, the synthesis of a range of enantioenriched saturated heterocycles was achieved at 24 atm H<sub>2</sub> and room temperature.

**Scheme 1.7.** Ir-catalyzed asymmetric hydrogenation of isoquinolines and pyridines using TCCA as the activator.

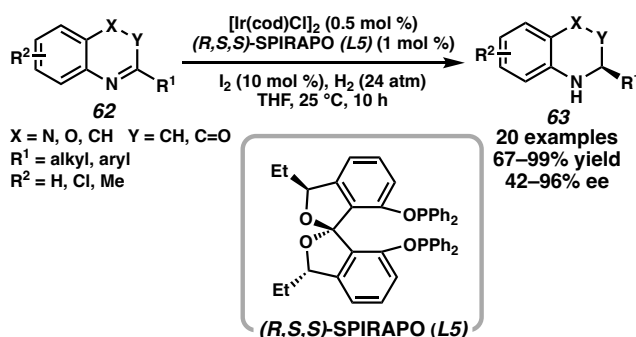


While there has been extensive development of biaryl bisphosphine (vide supra) and phosphoramidite<sup>36</sup> ligands for iridium-catalyzed hydrogenation, ferrocenyl-based Josiphos ligands are also efficacious ligand scaffolds for *N*-heterocycles, imparting excellent enantioselectivity and diastereoselectivity.<sup>37</sup> Inspired by the iridium catalyst system employed in the ether-directed asymmetric imine reduction en route to the herbicide metolachlor,<sup>10</sup> Stoltz and coworkers explored the potential of directing groups as iridium catalyst chelating agents for the directed hydrogenation to a specific face of the substrate. Toward the total synthesis of the complex bis-tetrahydroisoquinoline alkaloid jorumycin, the hydroxymethyl functionality was utilized as a directing group for the iridium-catalyzed

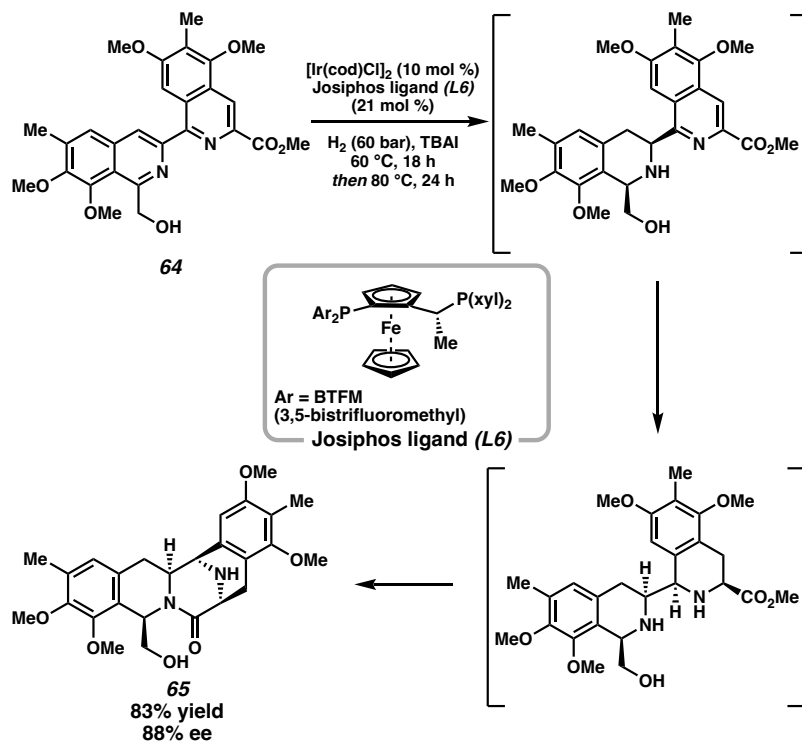
Chapter 1 – Recent Advances in Homogeneous Catalysts for the Asymmetric Hydrogenation of Heteroarenes

asymmetric hydrogenation of bis-isoquinoline **64** to generate pentacyclic intermediate **65** in one step as a single diastereomer in 88% ee (1.9).<sup>37</sup>

**Scheme 1.8.** Ir-catalyzed asymmetric hydrogenation of quinolines, quinoxalines, and benzoxazinones.



**Scheme 1.9.** Key Ir-catalyzed enantioselective hydrogenation step in the total synthesis of jorumycin.



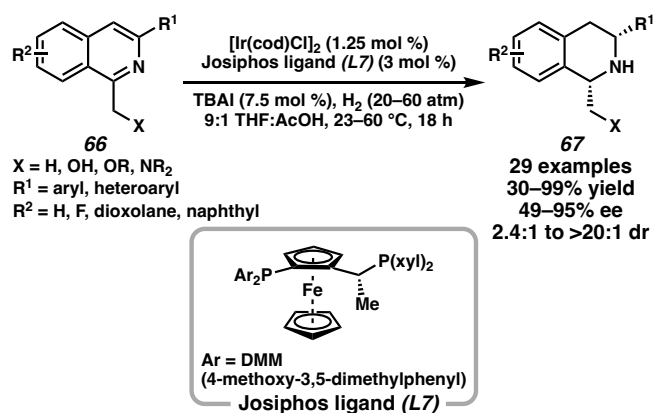
Utilizing directing groups is an underdeveloped activation strategy for the asymmetric hydrogenation of *N*-heterocycles, as Lewis basic functional groups are not as



Chapter 1 – Recent Advances in Homogeneous Catalysts for the Asymmetric Hydrogenation of Heteroarenes

well tolerated with previous hydrogenation methods.<sup>30</sup> However, Stoltz and coworkers have extended this application of using a hydroxymethyl directing group toward the asymmetric hydrogenation of a range of 1,3-disubstituted isoquinolines. Using 1.25 mol % of  $[\text{Ir}(\text{cod})\text{Cl}]_2$  and 3 mol % of chiral Josiphos ligand (**L7**), a range of differentially substituted isoquinolines were hydrogenated in high yields and enantio- and diastereoselectivity (Scheme 1.10, see Chapter 2).<sup>37b</sup> Heterocyclic substituents, such as furan and thiophene, at the C(3) position were also tolerated in this transformation. Interestingly, altering the directing groups at the C(1) position of the isoquinoline lowered the levels of conversion but maintained similar levels of stereoselectivity. Stoltz and coworkers later reported the first *trans*-selective asymmetric hydrogenation of 1,3-disubstituted isoquinolines as well with a similar catalyst system, wherein non-coordinating chlorinated solvents and halide additives were necessary to enable *trans*-selectivity (see Chapter 3).<sup>37c</sup>

**Scheme 1.10.** Ir-catalyzed asymmetric hydrogenation of 1,3-disubstituted isoquinolines.

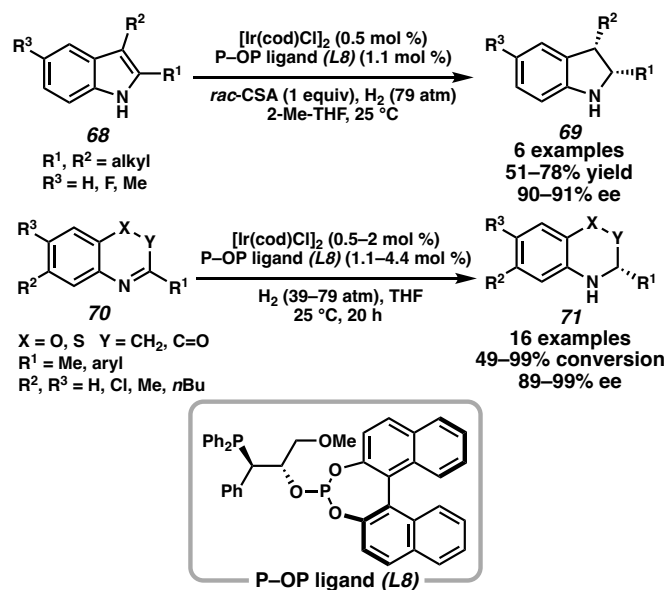


Phosphine-phosphite (P–OP) ligands, an emerging class of chiral bisphosphine ligands, have been developed by Vidal-Ferran and coworkers for the iridium-catalyzed asymmetric hydrogenation of heterocycles.<sup>38</sup> This catalyst system is particularly reactive in

Chapter 1 – Recent Advances in Homogeneous Catalysts for the Asymmetric Hydrogenation of Heteroarenes

the enantioselective synthesis of indolines from unprotected indoles,<sup>38b</sup> as well as the asymmetric hydrogenation of benzoxazines and benzothiazinones.<sup>38c</sup> Although stoichiometric amounts of sulfonic acids are needed to promote isomerization to the iminium intermediate, the transformation can be carried out using only 0.5 mol % of  $[\text{Ir}(\text{cod})\text{Cl}]_2$  (Scheme 1.11).<sup>38</sup>

**Scheme 1.11.** Ir-catalyzed asymmetric hydrogenation with P–OP ligand **L8**.

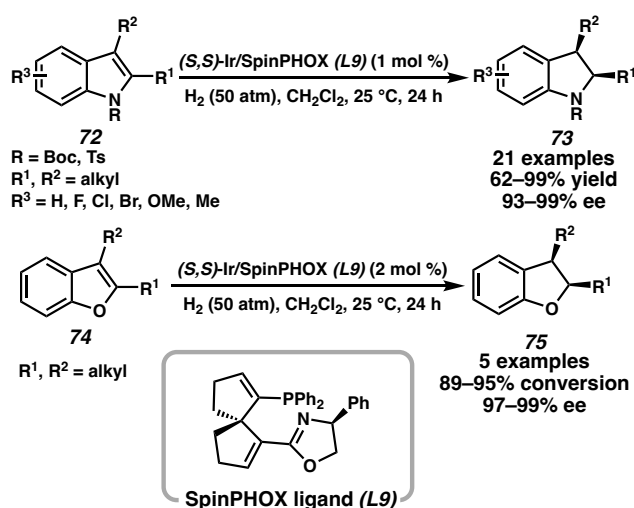


Although chiral bisphosphine ligands are most commonly employed for iridium-catalyzed asymmetric hydrogenation, chiral PHOX ligands with nitrogen and phosphorous chelating groups (*N,P*) have also been used to reduce a range of heteroarenes.<sup>39</sup> Most recently, Ding and coworkers reported the use of a SpinPHOX (spiro[4,4]-1,6-nonadiene-based phosphinooxazoline) ligand (**L9**) for the enantioselective hydrogenation of indole and benzofuran derivatives (Scheme 1.12). This iridium catalyst system is effective for the asymmetric hydrogenation of a diverse range of indoles with high functional group

Chapter 1 – Recent Advances in Homogeneous Catalysts for the Asymmetric Hydrogenation of Heteroarenes

tolerance, using 1 mol % of catalyst loading and mild reaction conditions.<sup>39a</sup> Although preformation of the Ir/SpinPHOX catalyst complex is necessary, up to 99% isolated yield and 99% enantiomeric excess are observed across differentially substituted indole and benzofuran substrates.

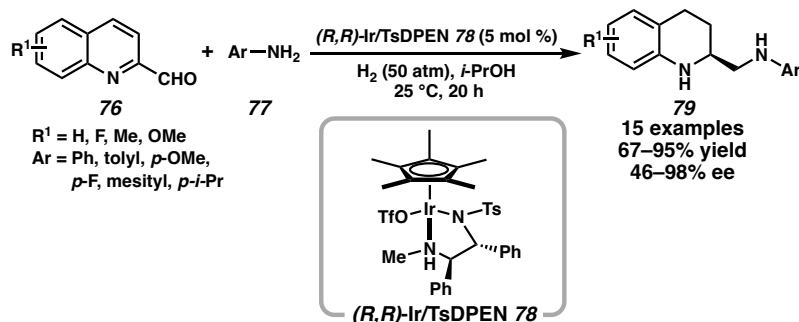
**Scheme 1.12.** Ir-catalyzed asymmetric hydrogenation with SpinPHOX ligand **L9**.



Unlike the ruthenium catalyst system, only a few reports employ the TsDPEN ligand for iridium-catalyzed asymmetric heteroarene hydrogenation.<sup>16c,40</sup> In 2019, Fan and coworkers developed Ir/TsDPEN catalyst complex **78** for the enantioselective synthesis of vicinal chiral diamines. These products are synthesized through a relay sequence of intermolecular reductive amination followed by asymmetric hydrogenation of a range of 2-quinoline aldehydes and aromatic amines (Scheme 1.13).<sup>16c</sup> For more sterically encumbered substrates, an addition of 10 mol % TfOH is required to generate chiral diamines with high levels of selectivity.

Chapter 1 – Recent Advances in Homogeneous Catalysts for the Asymmetric Hydrogenation of Heteroarenes

**Scheme 1.13.** Ir-catalyzed asymmetric hydrogenation of quinolines with Ir/TsDPEN catalyst 78.

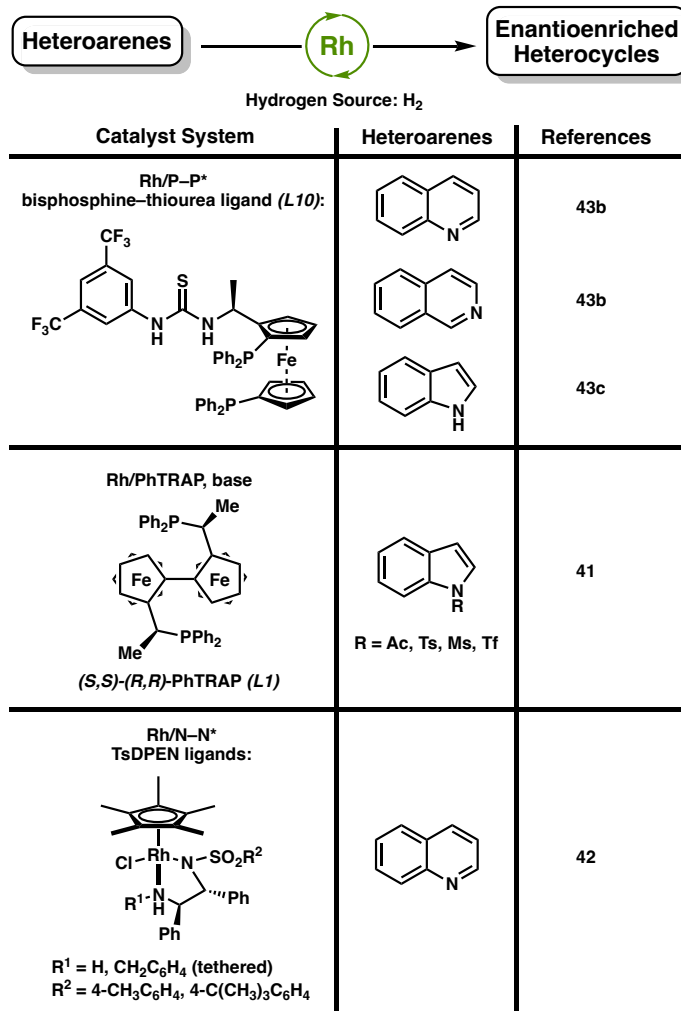


## 1.5 RHODIUM-CATALYZED ASYMMETRIC HYDROGENATION

Apart from iridium and ruthenium catalyst systems in the asymmetric hydrogenation of heteroarenes, rhodium catalysts have also been effective for the reduction of quinolines, isoquinolines, and indoles (Figure 1.6). The combination of a rhodium(I) source and either a PhTRAP<sup>41</sup> or TsDPEN<sup>42</sup> ligand have been explored for the enantioselective hydrogenation of indoles and quinolines, respectively. More recently, Zhang and coworkers have developed a novel ferrocene-based bisphosphine-thiourea ligand, ZhaoPhos (**L10**), for the cooperative catalysis of a transition metal center for hydrogenation and anion binding of the thiourea derivative.<sup>43</sup> This strategy allows a broader range of Brønsted acids to be tolerated through hydrogen bonding interactions with the thiourea moiety, and simple tunability with the phosphine substituents to improve selectivity. Using ligand **L10** with 0.5 mol % rhodium catalyst loading, differentially substituted quinolines, isoquinolines, and unprotected indoles are hydrogenated with excellent yield and enantioselectivity (Scheme 1.14). The addition of HCl as a strong acid is well tolerated under this catalyst system due to the stabilizing interaction with the thiourea derivative.

Chapter 1 – Recent Advances in Homogeneous Catalysts for the Asymmetric Hydrogenation of Heteroarenes

**Figure 1.6.** Common Rh-based catalyst systems for the asymmetric hydrogenation of heteroarenes ( $\geq 90\%$  ee, minimum three substrates). Only one enantiomer of ligand shown for simplicity.

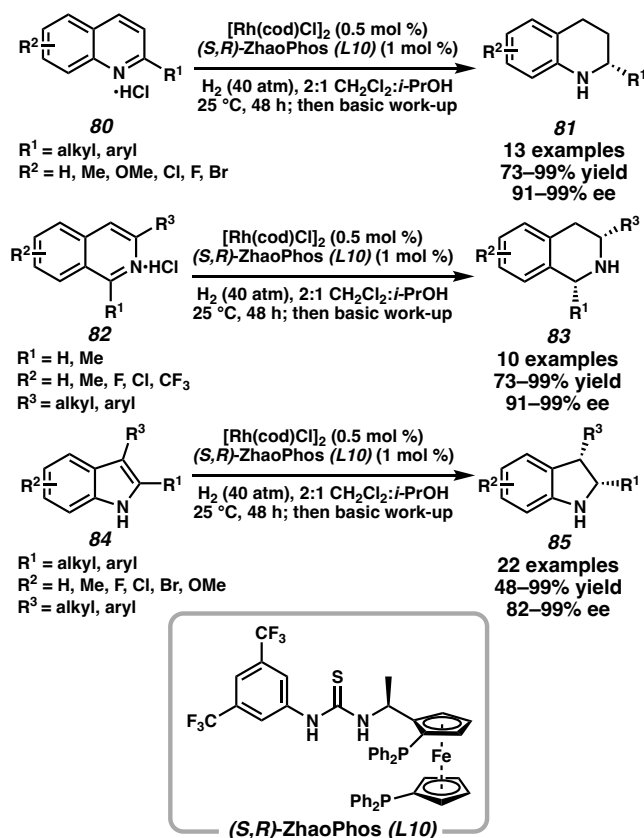


Zhang and coworkers performed DFT calculations to gain insight into the mechanism of the Rh-catalyzed transformation (Figure 1.7).<sup>43c</sup> Rh(I) catalyst **86** undergoes oxidative addition with H<sub>2</sub> to generate the active Rh(III) species **88**. Protonation of the indole substrate with HCl allows anion binding with the thiourea moiety to form intermediate **90**, allowing hydrogen bonding interactions between the chloride ion and the indole N–H group. Hydride transfer then proceeds through an outer-sphere pathway to release the chiral indoline product

Chapter 1 – Recent Advances in Homogeneous Catalysts for the Asymmetric Hydrogenation of Heteroarenes

**91** and complex **92**. Addition of another molecule of H<sub>2</sub> facilitates heterolytic cleavage of dihydrogen in complex **93** to generate Rh(III) catalyst **94** and HCl, in what was computed to be the rate-determining step. Overall, the thiourea–chloride anion binding proved to be crucial for inducing high enantioselectivity and reactivity in this system.<sup>43c</sup>

**Scheme 1.14.** Rh-catalyzed asymmetric hydrogenation of N-heteroarenes using ZhaoPhos ligand **L10**.



## 1.6

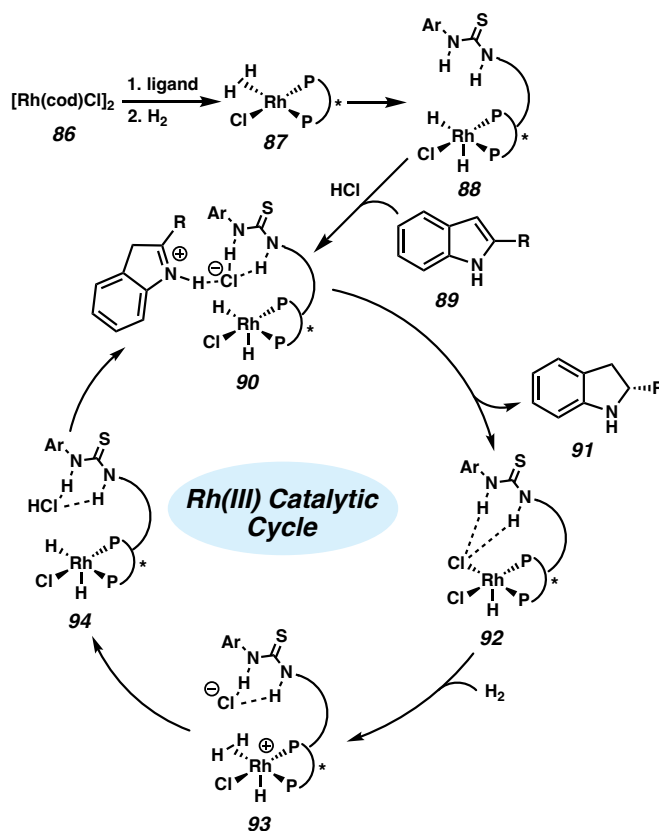
## PALLADIUM-CATALYZED ASYMMETRIC HYDROGENATION

Compared to ruthenium, iridium, and rhodium catalysts, homogeneous palladium catalysts for the asymmetric hydrogenation of heteroarenes remain relatively unexplored.<sup>4</sup>In

Chapter 1 – Recent Advances in Homogeneous Catalysts for the Asymmetric Hydrogenation of Heteroarenes

2010, Zhou and Zhang reported the first Pd-catalyzed asymmetric hydrogenation of *N*-H indoles using Pd(OCOCF<sub>3</sub>)<sub>2</sub>, a chiral H<sub>8</sub>-BINAP ligand, and (–)-camphorsulfonic acid.<sup>44</sup>

**Figure 1.7.** Proposed catalytic cycle for the Rh-catalyzed asymmetric hydrogenation of indoles with ZhaoPhos ligand **L10**.



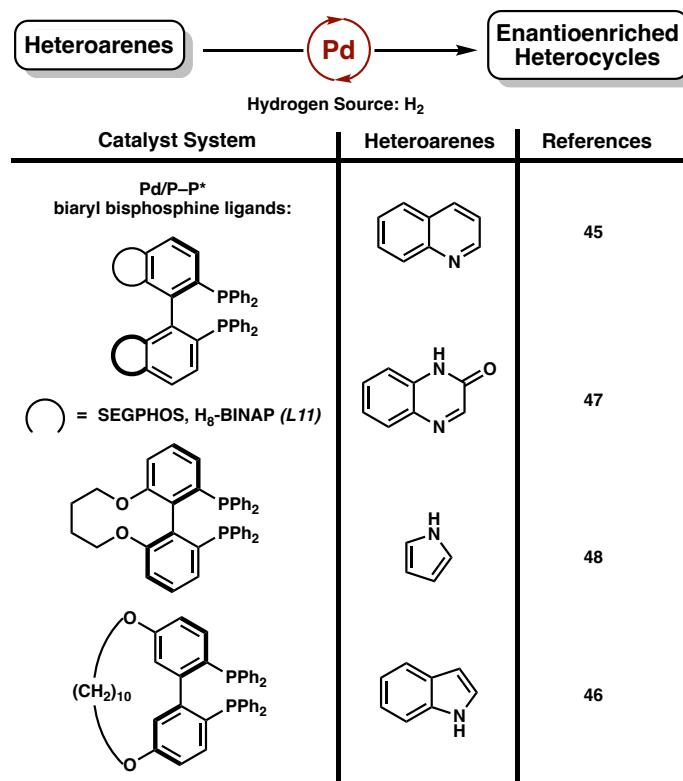
Since their seminal report, the homogeneous palladium catalyst system has been extended to accommodate a range of *N*-heteroarenes, including quinolines,<sup>45</sup> indoles,<sup>46</sup> quinoxalinones,<sup>47</sup> and the partial hydrogenation of pyrroles (Figure 1.8).<sup>48</sup> Common amongst all these catalytic systems is the use of chiral biaryl bisphosphine ligands with different steric environments of the naphthyl ring.

Zhou and coworkers have extensively developed palladium catalyst systems for the hydrogenation of *N*-heteroarenes, as palladium complexes demonstrate a higher tolerance for

Chapter 1 – Recent Advances in Homogeneous Catalysts for the Asymmetric Hydrogenation of Heteroarenes

strong Brønsted acids. Using chiral ligand (*R*)-H<sub>8</sub>-BINAP (**L11**), palladium(II) trifluoroacetate, and 1 equivalent of (–)-camphorsulfonic acid or TsOH•H<sub>2</sub>O, the asymmetric hydrogenation of 2-substituted and 2,3-disubstituted indoles is achieved to synthesize enantioenriched indolines in up to 99% yield and 98% ee (Scheme 1.15).<sup>46c</sup> Isotope-labeling studies demonstrate that the acid is necessary for formation of the iminium salt, which then undergoes hydrogenation by a Pd–H species.

**Figure 1.8.** Common Pd-based catalyst systems for the asymmetric hydrogenation of heteroarenes (≥90% ee, minimum three substrates). Only one enantiomer of ligand shown for simplicity.



Using both experimental and theoretical methods, Zhou and coworkers analyzed several possible mechanisms and propose a stepwise outer-sphere pathway (Figure 1.9).<sup>46c</sup> The indole is initially protonated by TsOH to give iminium **97**, which subsequently induced



Chapter 1 – Recent Advances in Homogeneous Catalysts for the Asymmetric Hydrogenation of Heteroarenes

hydrogen-bonding interactions with the trifluoroacetate ligand to generate intermediate **99**.

A hydride transfer from the Pd(II) center to the hydrogen-bound iminium of complex **100** is proposed to be the enantiodetermining step.

**Scheme 1.15.** Pd-catalyzed asymmetric hydrogenation of *N*-H indoles.

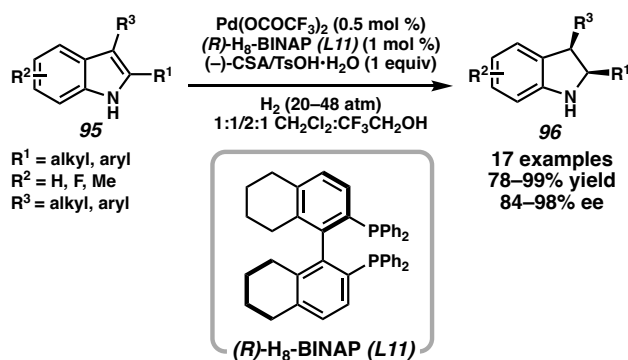
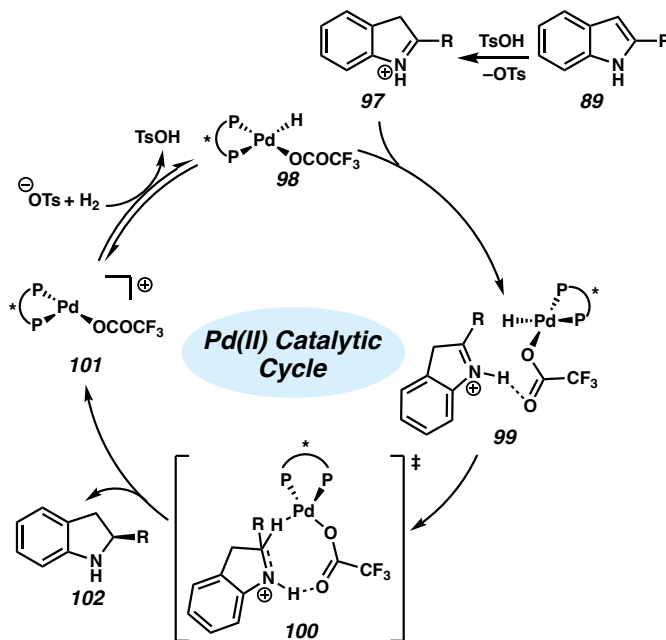


**Figure 1.9.** Proposed catalytic cycle for the Pd-catalyzed asymmetric hydrogenation of indoles.



The addition is postulated to occur through an eight-membered transition state, in which differentiation of the enantiotopic face is achieved through steric interactions with the

*Chapter 1 – Recent Advances in Homogeneous Catalysts for the Asymmetric Hydrogenation of Heteroarenes*

chiral bisphosphine ligand. After dissociation of the chiral indoline product **102**, palladium hydride species **98** is regenerated with the release of TsOH from activation of H<sub>2</sub>. Additional mechanistic studies of palladium-catalyzed asymmetric hydrogenation of *N*-heteroarenes may provide key insights for further chiral catalyst design to improve the substrate scope of this transformation.

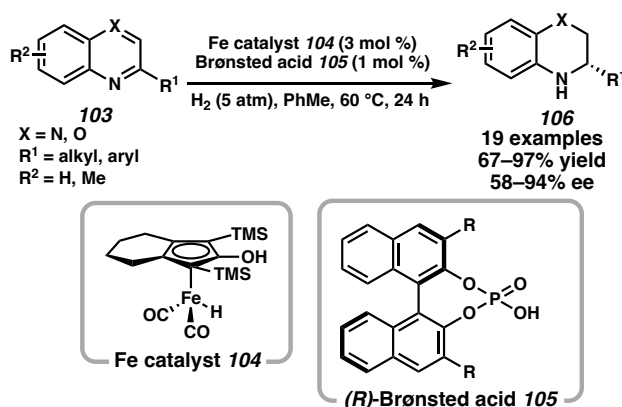
## 1.7 IRON-CATALYZED ASYMMETRIC HYDROGENATION

Despite the development of many efficient transition metal catalysts for the asymmetric hydrogenation of heteroarenes, the application of earth-abundant metals such as iron as hydrogenation catalysts are a promising avenue of further development. The first report of the homogeneous asymmetric hydrogenation of imines using first-row transition metals has only recently been published in 2011.<sup>49</sup> Beller and coworkers developed a novel cooperative catalytic system combining an achiral iron hydrogenation catalyst with a chiral Brønsted acid that facilitates the enantioselective reduction of quinoxalines and benzoxazines.<sup>50</sup> Using chiral phosphoric acid **105** to activate the substrate and control the enantioselectivity, an iron complex (**104**) reacts with the activated intermediate to deliver enantioenriched tetrahydroquinoxalines and dihydrobenzoxazines in high yields and selectivity (Scheme 1.16).<sup>50a</sup> Notably, both electron-donating and electron-withdrawing substituents on the C2-substituted phenyl ring, as well as *meta*- and *para*-substituted substrates, had little impact on the reactivity and enantioselectivity of the hydrogenation reaction. The levels of selectivity observed with

Chapter 1 – Recent Advances in Homogeneous Catalysts for the Asymmetric Hydrogenation of Heteroarenes

the iron catalyst system rival those of late transition metal-based catalysts for the hydrogenation of the same heteroarenes.

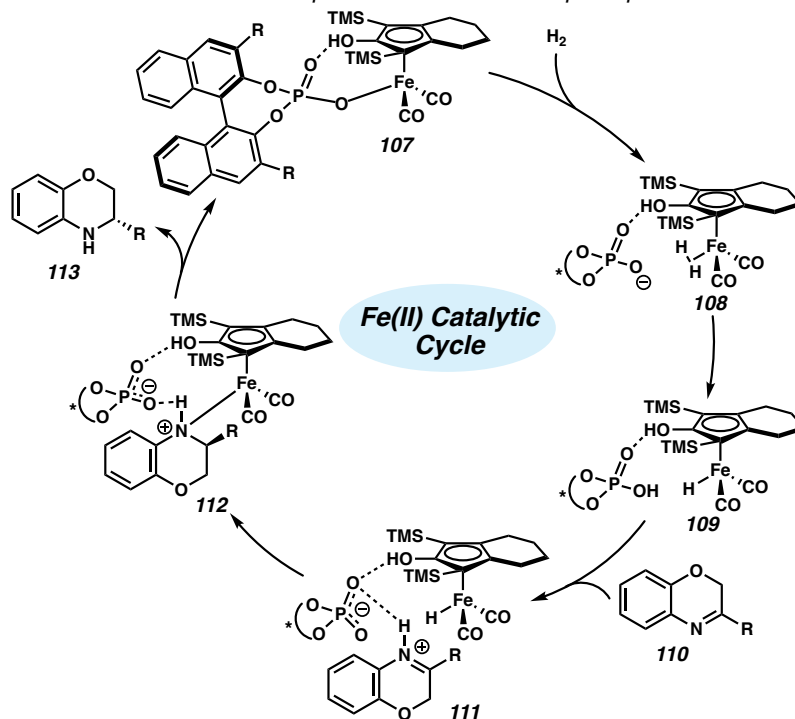
**Scheme 1.16.** Fe-catalyzed asymmetric hydrogenation of quinoxalines and benzoxazines with chiral phosphoric acid **105**.



Although the mechanism for this transformation has been previously investigated computationally using acyclic imines,<sup>51</sup> Hopmann has proposed an alternative mechanism with benzoxazine as the substrate (Figure 1.10).<sup>52</sup> Calculations indicate that hydrogenation may likely occur through a stepwise mechanism, in which initially the resting state **107** involves an adduct between the deprotonated acid and the iron complex. A molecule of H<sub>2</sub> generates dihydrogen complex **108**, subsequently splitting H<sub>2</sub> through proton abstraction by the phosphate to yield iron hydride species **109**. Benzoxazine **110** then coordinates to the chiral acid through hydrogen bonding interactions, allowing hydride transfer to occur to form catalyst species **112**. Finally, product **113** is released with regeneration of the catalyst complex **107**.<sup>52</sup> Computationally predicted enantioselectivities are in excellent agreement with experimental values, and the proposed mechanism is consistent with experimental observations by Beller and coworkers on possible reaction intermediates.<sup>50</sup>

Chapter 1 – Recent Advances in Homogeneous Catalysts for the Asymmetric Hydrogenation of Heteroarenes

**Figure 1.10.** Proposed cooperative catalytic cycle for the Fe-catalyzed asymmetric hydrogenation of benzoxazines in the presence of a chiral phosphoric acid.



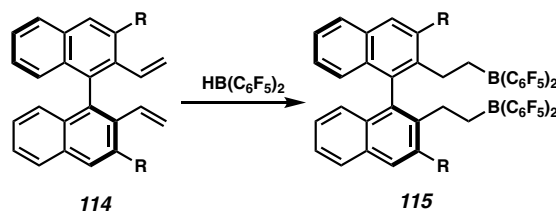
## 1.8 BORANE-CATALYZED ASYMMETRIC HYDROGENATION

Avoiding the use of transition metals for catalysis, the metal-free asymmetric hydrogenation of heteroarenes is an emerging research field for further development. Recently, frustrated Lewis pair (FLP) catalysis has been explored for the hydrogenation of heteroarenes with hydrogen gas or  $\text{NH}_3 \cdot \text{BH}_3$  as the hydrogen source.<sup>53</sup> Du and coworkers reported a novel FLP catalyst system using a chiral borane catalyst (**115**), generated in situ from the direct hydroboration of chiral dienes **114** with  $\text{HB}(\text{C}_6\text{F}_5)_2$  (Scheme 1.17).<sup>54</sup> The binaphthyl substituent presumably serves to control the stereoselectivity of the transformation, often requiring bulky aryl groups to achieve high selectivity. Although the mechanism for the asymmetric hydrogenation of heteroarenes using chiral borane catalysts

Chapter 1 – Recent Advances in Homogeneous Catalysts for the Asymmetric Hydrogenation of Heteroarenes

has not been investigated thoroughly, FLP catalysts are well known to activate  $H_2$  splitting and undergo hydride transfer.<sup>55</sup>

**Scheme 1.17.** *In situ* formation of chiral borane catalyst **115** from chiral dienes.



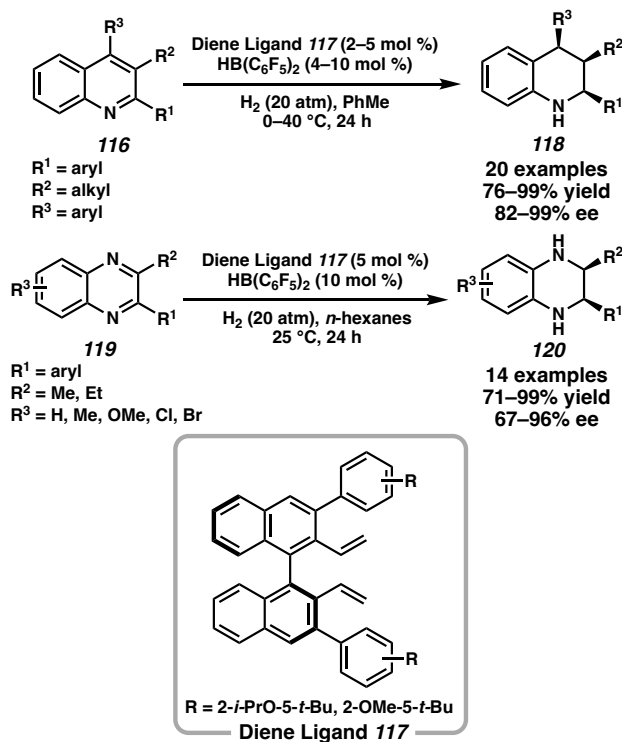
Chiral borane catalysts such as **115** are effective for the asymmetric hydrogenation of trisubstituted quinolines and disubstituted quinoxalines.<sup>53</sup> Du optimized the catalyst system to generate the borane catalyst in situ with 2 to 5 mol % of the chiral diene ligand **117** and  $HB(C_6F_5)_2$  in the presence of molecular  $H_2$  gas (Scheme 1.18). Under mild reaction conditions, a range of chiral tetrahydroquinolines and tetrahydroquinoxalines were synthesized in high yield and enantioselectivity.<sup>53a-d</sup> Overall, this catalyst system is a promising step toward the in situ generation of a library of chiral borane catalysts, and their application to the asymmetric hydrogenation of other heteroarenes could be explored.

In 2019, Wang and coworkers developed a similar catalytic system, employing chiral spiro-bicyclic bisborane catalysts for the asymmetric hydrogenation of C(2)-substituted quinolines.<sup>53e</sup> The novel spiro-bicyclic bisborane catalyst **122** exhibited excellent activity and selectivity for alkyl-substituted quinolines at the C(2)-position, which previously have not been well tolerated (Scheme 1.19). A range of quinolines bearing alkenes, alkynes, and heterocycles were hydrogenated in excellent yield,

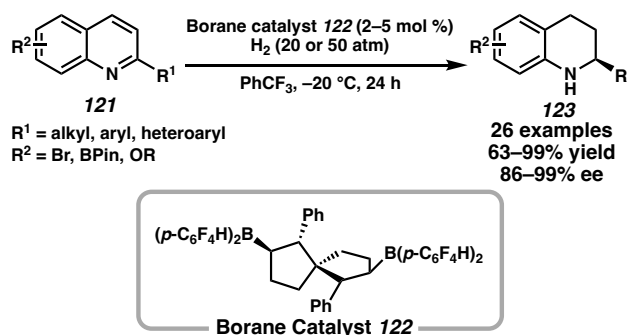
Chapter 1 – Recent Advances in Homogeneous Catalysts for the Asymmetric Hydrogenation of Heteroarenes

enantioselectivity, and chemoselectivity, demonstrating the catalyst's broad functional group tolerance.

**Scheme 1.18.** Metal-free asymmetric hydrogenation of heteroarenes through in situ formation of a chiral borane catalyst from ligand **117**.



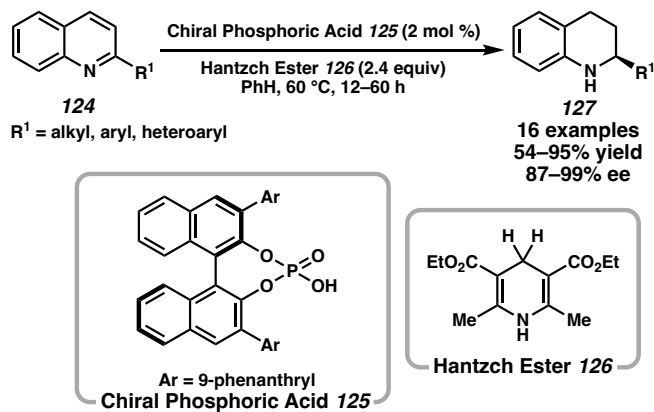
**Scheme 1.19.** Asymmetric hydrogenation of quinolines using spiro-bicyclic bisborane catalyst **122**.



## 1.9 CHIRAL PHOSPHORIC ACID-CATALYZED ASYMMETRIC HYDROGENATION

Since Rueping's first report of an organic-catalyzed asymmetric reduction of heteroarenes in 2006, various chiral Brønsted acid catalysts have emerged as powerful agents for asymmetric arene hydrogenation (Scheme 1.20).<sup>4,56</sup> Asymmetric transfer hydrogenation (ATH) reactions are promising alternatives to the use of transition metals or high pressure reactors, instead employing hydrogen sources like Hantzsch esters (HEH), dihydrophenanthridine (DHPD), and 4,5-dihydropyrrolo[1,2-*a*]quinoxalines.<sup>57</sup> In most cases, however, an unrecyclable excess of reductant is required for hydrogenation.

**Scheme 1.20.** First reported chiral phosphoric acid-catalyzed asymmetric hydrogenation of quinolines.

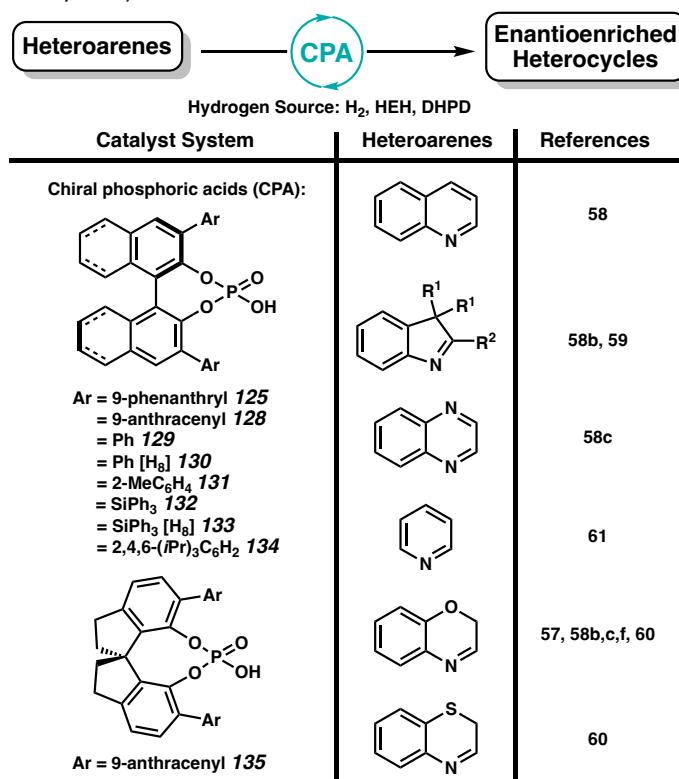


Over the past decade, several effective organic catalyst systems have been developed with chiral phosphoric acids (CPA) for the asymmetric reduction of quinolines,<sup>58</sup> indoles,<sup>58b, 59</sup> quinoxalines,<sup>58c</sup> benzoxazines,<sup>57,58b,c,f, 60</sup> benzothiazines,<sup>60</sup> and the partial hydrogenation of pyridines (Figure 1.11).<sup>61</sup> Rueping, Zhou, Gong, and Bhanage have reported the use of BINOL-based phosphoric acid catalysts for the asymmetric hydrogenation of heteroarenes, with similar catalyst systems as shown in Scheme 1.20.<sup>56</sup>

Chapter 1 – Recent Advances in Homogeneous Catalysts for the Asymmetric Hydrogenation of Heteroarenes

More recently, Shi and coworkers have developed a new class of CPA catalysts with a 1,1'-spirobiindane-7,7'-diol (SPINOL) backbone for the enantioselective hydrogenation of a range of quinolines and benzoxazines.<sup>58f</sup> Using 1 mol % of CPA **135** and 1.25 to 2.5 equivalents of HEH (**126**), electron-withdrawing and electron-donating substituents at the C(2)-position are all well tolerated and afforded excellent enantioselectivities (Scheme 1.21).<sup>58f</sup> The metal-free and mild reaction conditions of this transformation is an appealing alternative to transition metal catalyst systems.

**Figure 1.11.** Common chiral phosphoric acid catalyst systems for the asymmetric hydrogenation of heteroarenes ( $\geq 90\%$  ee, minimum three substrates). Only one enantiomer of ligand shown for simplicity.



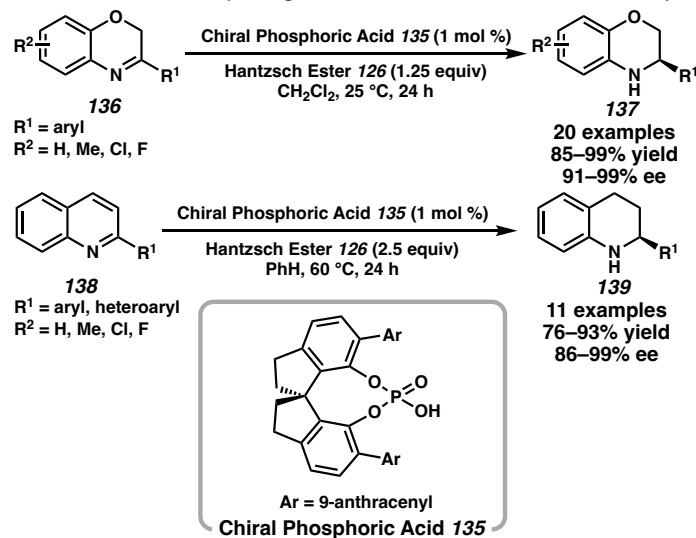
The general mechanism of the asymmetric transfer hydrogenation of quinolines by Hantzsch esters has been explored computationally by Frison and coworkers.<sup>62</sup> It is well-



Chapter 1 – Recent Advances in Homogeneous Catalysts for the Asymmetric Hydrogenation of Heteroarenes

precedented that two subsequent reduction cycles occur, each with one equivalent of the hydride source and a chiral phosphoric acid.

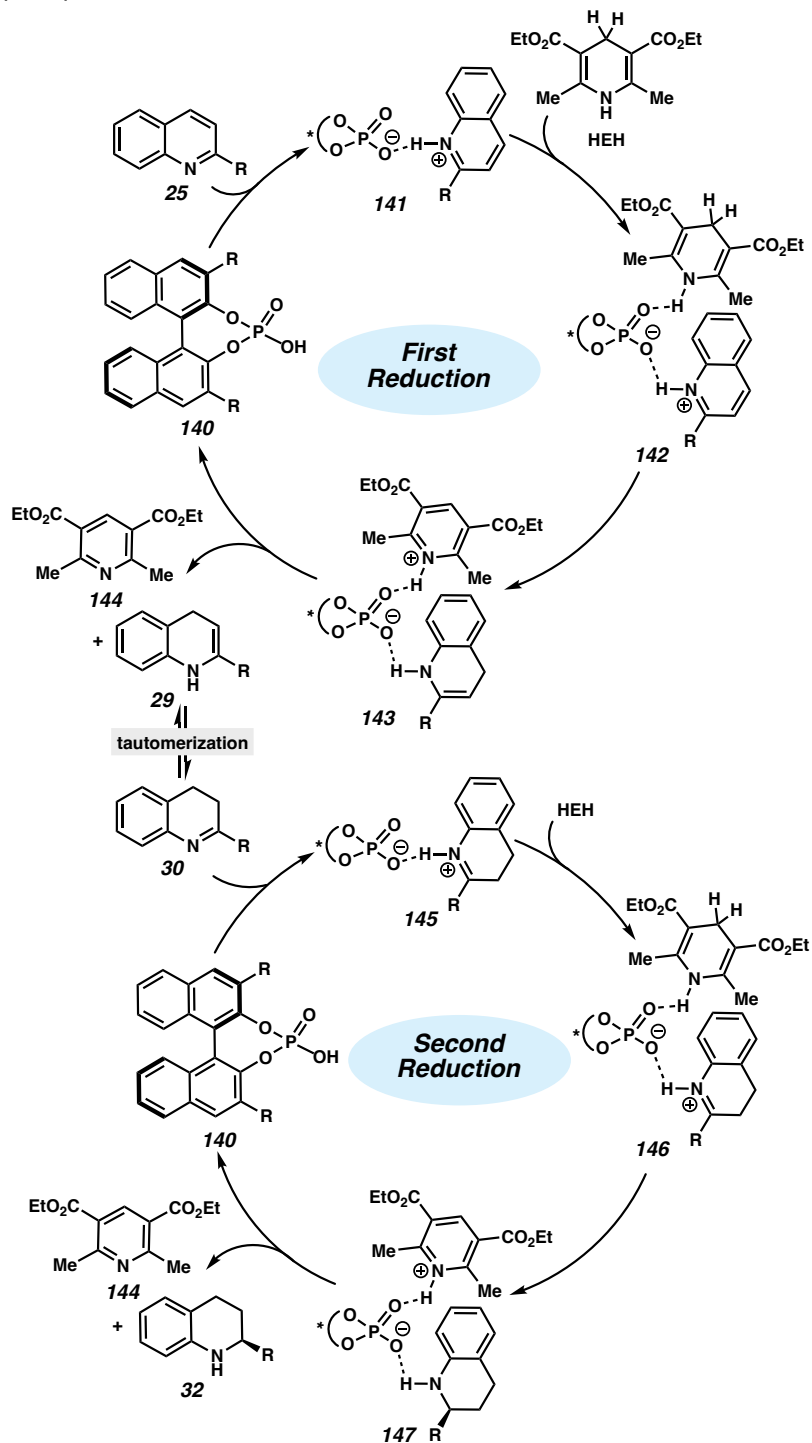
**Scheme 1.21.** Asymmetric transfer hydrogenation with SPINOL-derived phosphoric acid **135**.



Quinoline **25** is first activated through a proton transfer from the phosphoric acid to the substrate, followed by a 1,4-hydride addition using HEH. The resulting dihydroquinoline can then isomerize to the imine, entering a second reduction cycle involving a similar stepwise process (Figure 1.12). Although previous studies have proposed the hydride transfer from **146** to **147** to be the rate- and enantiodetermining step,<sup>63</sup> Frison revisited these calculations and proposed that the stereocontrol is determined from the steric constraints by the aryl substituent of the CPA with HEH instead. Thus, the enantiodetermining step would not be the hydride transfer, but rather the coordination of HEH to complex **145** to generate intermediate **146**, hindering access of the HEH to the catalytic site and controlling the facial approach of the hydride addition.<sup>62</sup>

Chapter 1 – Recent Advances in Homogeneous Catalysts for the Asymmetric Hydrogenation of Heteroarenes

**Figure 1.12.** Proposed catalytic cycle for the asymmetric transfer hydrogenation of quinolines using a chiral phosphoric acid and Hantzsch ester.



*Chapter 1 – Recent Advances in Homogeneous Catalysts for the Asymmetric Hydrogenation of Heteroarenes*

Using relay catalysis, Zhou and coworkers took inspiration from NAD(P)H models that enable the biomimetic asymmetric hydrogenation of heteroarenes, harnessing the in situ generation of dihydrophenanthridine (DHPD) from catalytic amounts of ruthenium, phenanthridine, and H<sub>2</sub> as the terminal reductant.<sup>58c, 64</sup> Using 0.5 mol % of [Ru(*p*-cymene)I<sub>2</sub>]<sub>2</sub>, 10 mol % of DHPD, and 1 mol % of CPA **130** or **131**, the asymmetric hydrogenation of 2-substituted quinolines, quinoxalines, and benzoxazines proceeded in up to 99% yield and 97% ee (Scheme 1.22A).

The mechanism of the biomimetic asymmetric hydrogenation reaction is proposed to involve two catalytic cycles, initially with Ru-catalyzed hydrogenation of phenanthridine **149** to generate DHPD **153**. DHPD then coordinates to the chiral phosphoric acid to enantioselectively reduce the substrate **154**, which is then regenerated to DHPD by the ruthenium hydride species (Scheme 1.22B). Interestingly, using a Hantzsch ester as the hydride source reverses the stereoselectivity due to the different steric demands of the coordination of the substrate and CPA, favoring the *Re*-face reduction instead.<sup>58c</sup> Although a transition metal is employed to recycle the hydride source, the biomimetic cascade hydrogenation can be performed under mild conditions with excellent activities and enantioselectivities.

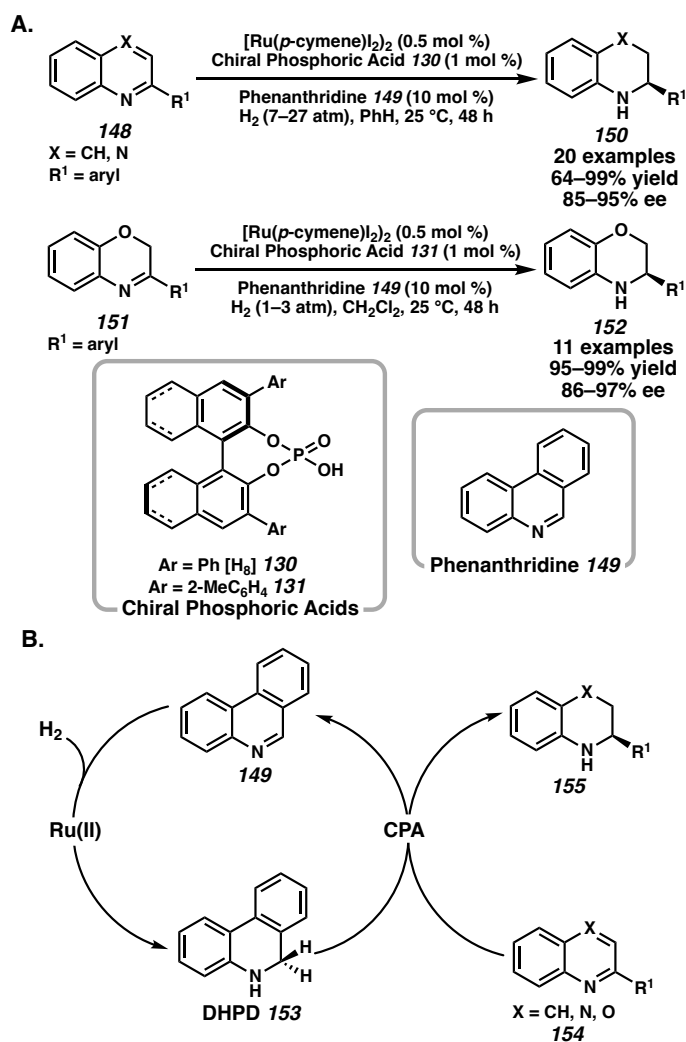
## 1.10 CONCLUSION

Over the past decade, many effective catalyst systems have been developed for the asymmetric hydrogenation or asymmetric transfer hydrogenation of heteroarenes. Although transition metal catalysts are most commonly employed for stereoselective

Chapter 1 – Recent Advances in Homogeneous Catalysts for the Asymmetric Hydrogenation of Heteroarenes

hydrogenation with molecular hydrogen gas, a number of organic catalysts and dual catalytic systems have also been successfully applied for the synthesis of enantioenriched saturated heterocycles.

**Scheme 1.22.** Biomimetic asymmetric transfer hydrogenation of heteroarenes.



Despite the recent advances made in the field of asymmetric hydrogenation, as well as reports that have been discussed in prior reviews,<sup>4</sup> significant challenges in this field remain. The discovery of a catalyst system with a broad substrate scope of more than four

*Chapter 1 – Recent Advances in Homogeneous Catalysts for the Asymmetric Hydrogenation of Heteroarenes*

different heteroarenes has still not been achieved. Moreover, many asymmetric hydrogenation systems rely on acid activation of the substrates, which can be a limitation for more basic products. Development of novel ligand scaffolds and homogeneous catalyst systems will continue to be explored to design hydrogenation catalysts with improved selectivity. Creative activation strategies for these transformations should also be considered to extend the substrate scope, whether it be through pendant directing groups or recyclable activating reagents. Exploring these strategies will also provide insight into the challenge of developing a technology for the exhaustive asymmetric hydrogenation of simple 5- or 6-membered heteroarenes and benzene derivatives. Finally, a thorough mechanistic understanding of these asymmetric transformations is necessary to advance this field. Although experimental mechanistic studies are often limited by high pressure reactors and catalyst deactivation pathways, further investigation is needed to guide the development of the next generation of hydrogenation catalyst systems.

The asymmetric hydrogenation of heteroarenes using homogeneous catalysts continues to be a valuable technology for the direct synthesis of enantioenriched, saturated heterocycles. These small molecules are critical structural motifs in natural products,<sup>1</sup> as well as pharmaceuticals,<sup>2</sup> and other molecules of industrial importance.<sup>3</sup> Thus, the development of efficient catalyst systems for the enantioselective hydrogenation of a broad range of heteroarenes in good yields, stereoselectivity, and chemoselectivity remains highly desirable. We anticipate further advances in asymmetric hydrogenation technology that will revolutionize this field of research.

## 1.11 REFERENCES AND NOTES

- (1) a) *Heterocycles in Natural Product Synthesis*; Majumdar, K. C.; Chattopadhyay, S. K., Eds.; John Wiley & Sons: New York, 1991; pp 1–611. b) Walsh, C. T. *Tetrahedron Lett.* **2015**, *56*, 3075–3081.
- (2) a) Vitaku, E.; Smith, D. T.; Njardarson, J. T. *J. Med. Chem.* **2014**, *57*, 10257–10274; b) Taylor, R. D.; MacCoss, M.; Lawson, A. D. G. *J. Med. Chem.* **2014**, *57*, 5845–5859; c) Lovering, F.; Bikker, J.; Humblet, C. *J. Med. Chem.* **2009**, *52*, 6752–6756; d) Lovering, F. *MedChemComm* **2013**, *4*, 515–519; e) Roughley, S. D.; Jordan, A. M. *J. Med. Chem.* **2011**, *54*, 3451–3479; f) Meanwell, N. A. *Adv. Heterocycl. Chem.* **2017**, *123*, 245–361.
- (3) a) Sanemitsu, Y.; Kawamura, S. *J. Pestic. Sci.* **2008**, *33*, 175–177; b) Katritzky, A. R. *Chem. Heterocycl. Compd.* **1992**, *28*, 241–259.
- (4) For selected reviews of asymmetric hydrogenation of heteroarenes, see: a) Wang, D.-S.; Chen, Q.-A.; Lu, S.-M.; Zhou, Y.-G. *Chem. Rev.* **2012**, *112*, 2557–2590; b) Zhou, Y.-G. *Acc. Chem. Res.* **2007**, *40*, 1357–1366; c) Zhao, D.; Glorius, F. *Angew. Chem. Int. Ed.* **2013**, *52*, 9616–9618; d) Wiesenfeldt, M. P.; Nairoukh, Z.; Dalton, T.; Glorius, F. *Angew. Chem. Int. Ed.* **2019**, *58*, 10460–10476; e) Luo, Y.-E.; He, Y.-M.; Fan, Q.-H. *Chem. Rec.* **2016**, *16*, 2697–2711; f) Fleury-Bregeot, N.; delaFuente, V.; Castilloñ, S.; Claver, C. *ChemCatChem* **2010**, *2*, 1346–1371.
- (5) Fadhel, A. Z.; Pollet, P.; Liotta, C. L.; Eckert, C. A. *Molecules* **2010**, *15*, 8400–8424.

Chapter 1 – Recent Advances in Homogeneous Catalysts for the Asymmetric Hydrogenation of Heteroarenes

- (6) Kita, Y.; Yamaji, K.; Higashida, K.; Sathaiah, K.; Iimuro, A.; Mashima, K. *Chem. Eur. J.* **2015**, *21*, 1915–1927.
- (7) Huang, W.-X.; Wu, B.; Gao, X.; Chen, M.-W.; Wang, B.; Zhou, Y.-G. *Org. Lett.* **2015**, *17*, 1640–1643.
- (8) Chen, Q.-A.; Wang, D.-S.; Zhou, Y.-G.; Duan, Y.; Fan, H.-J.; Yang, Y.; Zhang, Z. *J. Am. Chem. Soc.* **2011**, *133*, 6126–6129.
- (9) a) Cui, C.-X.; Chen, H.; Li, S.-J.; Zhang, T.; Qu, L.-B.; Lan, Y. *Coord. Chem. Rev.* **2020**, *412*, 213251–213272; b) Dobereiner, G. E.; Nova, A.; Schley, N. D.; Hazari, N.; Miller, S. J.; Eisenstein, O.; Crabtree, R. H. *J. Am. Chem. Soc.* **2011**, *133*, 7547–7562; c) Bianchini, C.; Meli, A.; Vizza, F. *Eur. J. Inorg. Chem.* **2001**, *2001*, 43–68.
- (10) Dorta, R.; Broggin, D.; Stoop, R.; Rügger, H.; Spindler, F.; Togni, A. *Chem. Eur. J.* **2004**, *10*, 267–278.
- (11) a) Hashiguchi, S.; Fujii, A.; Takehara, J.; Ikariya, T.; Noyori, R. *J. Am. Chem. Soc.* **1995**, *117*, 7562–7563; b) Fujii, A.; Hashiguchi, S.; Uematsu, N.; Ikariya, T.; Noyori, R. *J. Am. Chem. Soc.* **1996**, *118*, 2521–2522.
- (12) Uematsu, N.; Fujii, A.; Hashiguchi, S.; Ikariya, T.; Noyori, R. *J. Am. Chem. Soc.* **1996**, *118*, 4916–4917.
- (13) For selected examples of the asymmetric hydrogenation of carbocyclic aromatic compounds, see: a) Kuwano, R.; Morioka, R.; Kashiwabara, M.; Kameyama, N. *Angew. Chem. Int. Ed.* **2012**, *51*, 4136–4139; b) Kuwano, R.; Ikeda, R.; Hirasada, K. *Chem. Commun.* **2015**, *51*, 7558–7561; c) Yan, Z.; Xie, H.-P.; Shen, H.-Q.;

Chapter 1 – Recent Advances in Homogeneous Catalysts for the Asymmetric Hydrogenation of Heteroarenes

- Zhou, Y.-G. *Org. Lett.* **2018**, *20*, 1094–1097.
- (14) a) Zhou, H.; Li, Z.; Wang, Z.; Wang, T.; Xu, L.; He, Y.; Fan, Q.-H.; Pan, J.; Gu, L.; Chan, A. S. C. *Angew. Chem. Int. Ed.* **2008**, *47*, 8464–8467; b) Wang, Z.-J.; Zhou, H.-F.; Wang, T.-L.; He, Y.-M.; Fan, Q.-H. *Green Chem.* **2009**, *11*, 767–769; c) Ding, Z.-Y.; Wang, T.; He, Y.-M.; Chen, F.; Zhou, H.-F.; Fan, Q.-H.; Guo, Q.; Chan, A. S. C. *Adv. Synth. Catal.* **2013**, *355*, 3727–3735. For recent reports on the asymmetric hydrogenation of quinolines and isoquinolines using a Ru/TsDPEN catalyst, see: d) Wang, T.; Chen, Y.; Ouyang, G.; He, Y.-M.; Li, Z.; Fan, Q.-H. *Chem. Asian. J.* **2016**, *11*, 2773–2777; e) Yang, Z.; Chen, F.; He, Y.-M.; Yang, N.; Fan, Q.-H. *Catal. Sci. Technol.* **2014**, *4*, 2887–2890.
- (15) a) Wang, T.; Zhuo, L.-G.; Li, Z.; Chen, F.; Ding, Z.; He, Y.; Fan, Q.-H.; Xiang, J.; Yu, Z.-X.; Chan, A. S. C. *J. Am. Chem. Soc.* **2011**, *133*, 9878–9891; b) Wang, T.; Ouyang, G.; He, Y.-M.; Fan, Q.-H. *Synlett* **2011**, *2011*, 939–942; c) Xu, C.; Feng, Y.; Li, F.; Han, J.; He, Y.-M.; Fan, Q.-H. *Organometallics* **2019**, *38*, 3979–3990; d) Chen, Y.; He, Y.-M.; Zhang, S.; Miao, T.; Fan, Q.-H. *Angew. Chem. Int. Ed.* **2019**, *58*, 3809–3813. (e) Wang, L.-R.; Chang, D.; Feng, Y.; He, Y.-M.; Deng, G. J.; Fan, Q.-H. *Org. Lett.* **2020**, *22*, 2251–2255.
- (16) a) Ma, W.; Zhang, J.; Xu, C.; Chen, F.; He, Y.-M.; Fan, Q.-H. *Angew. Chem. Int. Ed.* **2016**, *55*, 12891–12894; b) Li, B.; Xu, C.; He, Y.-M.; Deng, G.-J.; Fan, Q.-H. *Chin. J. Chem.* **2018**, *36*, 1169–1173; c) Chen, Y.; Pan, Y.; He, Y.-M.; Fan, Q.-H. *Angew. Chem. Int. Ed.* **2019**, *58*, 16831–16834.



Chapter 1 – Recent Advances in Homogeneous Catalysts for the Asymmetric Hydrogenation of Heteroarenes

- (17) Liu, Y.; Chen, F.; He, Y.-M.; Li, C.; Fan, Q.-H. *Org. Biomol. Chem.* **2019**, *17*, 5099–5105.
- (18) a) Touge, T.; Arai, T. *J. Am. Chem. Soc.* **2016**, *138*, 11299–11305; b) Yang, Z.; Chen, F.; He, Y.; Yang, N.; Fan, Q.-H. *Angew. Chem. Int. Ed.* **2016**, *55*, 13863–13866.
- (19) Qin, J.; Chen, F.; He, Y.-M.; Fan, Q.-H. *Org. Chem. Front.* **2014**, *1*, 952–955.
- (20) For select examples of polycyclic heteroarene hydrogenation using Ru/TsDPEN catalyst systems, see: a) Zhang, J.; Chen, F.; He, Y.-M.; Fan, Q.-H. *Angew. Chem. Int. Ed.* **2015**, *54*, 4622–4625; b) Wang, T.; Chen, F.; Qin, J.; He, Y.-M.; Fan, Q.-H. *Angew. Chem. Int. Ed.* **2013**, *52*, 7172–7176; c) Ma, W.; Chen, F.; Liu, Y.; He, Y.-M.; Fan, Q.-H. *Org. Lett.* **2016**, *18*, 2730–2733; d) Yang, Z.; Chen, F.; Zhang, S.; He, Y.; Yang, N.; Fan, Q.-H. *Org. Lett.* **2017**, *19*, 1458–1461.
- (21) a) Yamakawa, M.; Ito, H.; Noyori, R. *J. Am. Chem. Soc.* **2000**, *122*, 1466–1478; b) Yamakawa, M.; Yamada, I.; Noyori, R. *Angew. Chem. Int. Ed.* **2001**, *40*, 2818–2821.
- (22) Sawamura, M.; Hamashima, H.; Ito, Y. *Tetrahedron: Asymmetry* **1991**, *2*, 593–596.
- (23) a) Kuwano, R.; Kashiwabara, M. *Org. Lett.* **2006**, *8*, 2653–2655; b) Makida, Y.; Saita, M.; Kuramoto, T.; Ishizuka, K.; Kuwano, R. *Angew. Chem. Int. Ed.* **2016**, *55*, 11859–11862; c) Kuwano, R.; Kashiwabara, M.; Ohsumi, M.; Kusano, H. *J. Am. Chem. Soc.* **2008**, *130*, 808–809; d) Kuwano, R.; Kameyama, N.; Ikeda, R. *J. Am. Chem. Soc.* **2011**, *133*, 7312–7315.

Chapter 1 – Recent Advances in Homogeneous Catalysts for the Asymmetric Hydrogenation of Heteroarenes

- (24) Urban, S.; Ortega, N.; Glorius, F. *Angew. Chem. Int. Ed.* **2011**, *50*, 3803–3806.
- (25) a) Wysocki, J.; Ortega, N.; Glorius, F. *Angew. Chem. Int. Ed.* **2014**, *53*, 8751–8755; b) Ortega, N.; Urban, S.; Beiring, B.; Glorius, F. *Angew. Chem. Int. Ed.* **2012**, *51*, 1710–1713; c) Ortega, N.; Beiring, B.; Urban, S.; Glorius, F. *Tetrahedron* **2012**, *68*, 5185–5192.
- (26) Paul, D.; Beiring, B.; Plois, M.; Ortega, N.; Kock, S.; Schlüns, D.; Neugebauer, J.; Wolf, R.; Glorius, F. *Organometallics* **2016**, *35*, 3641–3646.
- (27) a) Wang, W.-B.; Lu, S.-M.; Yang, P.-Y.; Han, X.-W.; Zhou, Y.-G. *J. Am. Chem. Soc.* **2003**, *125*, 10536–10537; b) Wang, D.-W.; Wang, X.-B.; Wang, D.-S.; Lu, S.-M.; Zhou, Y.-G.; Li, Y.-X. *J. Org. Chem.* **2009**, *74*, 2780–2787.
- (28) Zhang, X.-C.; Hu, Y.-H.; Chen, C.-F.; Fang, Q.; Yang, L.-Y.; Lu, Y.-B.; Xie, L. J.; Wu, J.; Li, S.; Fang, W. *Chem. Sci.* **2016**, *7*, 4594–4599.
- (29) a) Zhang, D.-Y.; Wang, D.-S.; Wang, M.-C.; Yu, C.-B.; Gao, K.; Zhou, Y.-G. *Synthesis* **2011**, *2011*, 2796–2802; b) Zhang, D.-Y.; Yu, C.-B.; Wang, M.-C.; Gao, K.; Zhou, Y.-G. *Tetrahedron Lett.* **2012**, *53*, 2556–2559; c) Cai, X.-F.; Guo, R.-N.; Chen, M.-W.; Shi, L.; Zhou, Y.-G. *Chem. Eur. J.* **2014**, *20*, 7245–7248; d) Maj, A. M.; Suisse, I.; Hardouin, C.; Agbossou-Niedercorn, F. *Tetrahedron* **2013**, *69*, 9322–9328; e) Hu, S.-B.; Zhai, X.-Y.; Shen, H.-Q.; Zhou, Y.-G. *Adv. Synth. Catal.* **2018**, *360*, 1334–1339.
- (30) a) Guo, R.-N.; Cai, X.-F.; Shi, L.; Ye, Z.-S.; Chen, M.-W.; Zhou, Y.-G. *Chem. Commun.* **2013**, *49*, 8537–8539; b) Iimuro, A.; Yamaji, K.; Kandula, S.; Nagano, T.; Kita, Y.; Mashima, K. *Angew. Chem. Int. Ed.* **2013**, *52*, 2046–2050; c) Shi, L.;

Chapter 1 – Recent Advances in Homogeneous Catalysts for the Asymmetric Hydrogenation of Heteroarenes

- Ye, Z.-S.; Cao, L.-L.; Guo, R.-N.; Hu, Y.; Zhou, Y.-G. *Angew. Chem. Int. Ed.* **2012**, *51*, 8286–8289; d) Ye, Z.-S.; Guo, R.-N.; Cai, X.-F.; Chen, M.-W.; Shi, L.; Zhou, Y.-G. *Angew. Chem. Int. Ed.* **2013**, *52*, 3685–3689; e) Chen, M.-W.; Ji, Y.; Wang, J.; Chen, Q.-A.; Shi, L.; Zhou, Y.-G. *Org. Lett.* **2017**, *19*, 4988–4991.
- (31) a) Nagano, T.; Iimuro, A.; Schwenk, R.; Ohshima, T.; Kita, Y.; Togni, A.; Mashima, K. *Chem. Eur. J.* **2012**, *18*, 11578–11592; b) Cartigny, D.; Berhal, F.; Nagano, T.; Phansavath, P.; Ayad, T.; Genêt, J.-P.; Ohshima, T.; Mashima, K.; Ratovelomanana-Vidal, V. *J. Org. Chem.* **2012**, *77*, 4544–4556.
- (32) a) Huang, W.-X.; Liu, L.-J.; Wu, B.; Feng, G.-S.; Wang, B.; Zhou, Y.-G. *Org. Lett.* **2016**, *18*, 3082–3085; b) Huang, W.-X.; Yu, C.-B.; Shi, L.; Zhou, Y.-G. *Org. Lett.* **2014**, *16*, 3324–3327.
- (33) Gao, K.; Yu, C.-B.; Wang, D.-S.; Zhou, Y.-G. *Adv. Synth. Catal.* **2012**, *354*, 483–488.
- (34) a) Rahman, A.; Lin, X. *Org. Biomol. Chem.* **2018**, *16*, 4753–4777; b) Ding, K.; Han, Z.; Wang, Z. *Chem. Asian J.* **2009**, *4*, 32–41.
- (35) Sun, S.; Nagorny, P. *Chem. Commun.* **2020**, *56*, 8432–8435.
- (36) Hu, X.-H.; Hu, X.-P. *Org. Lett.* **2019**, *21*, 10003–10006.
- (37) a) Welin, E. R.; Ngamnithiporn, A.; Klatte, M.; Lapointe, G.; Pototschnig, G. M.; McDermott, M. S.; Conklin, D.; Gilmore, C. D.; Tadross, P. M.; Haley, C. K.; Negoro, K.; Glibstrup, E.; Grünanger, C. U.; Allan, K. M.; Virgil, S. C.; Slamon, D. J.; Stoltz, B. M. *Science* **2019**, *363*, 270–275; b) Kim, A. N.; Ngamnithiporn, A.; Welin, E. R.; Daiger, M. T.; Grünanger, C. U.; Bartberger, M. D.; Virgil, S.

Chapter 1 – Recent Advances in Homogeneous Catalysts for the Asymmetric Hydrogenation of Heteroarenes

- C.; Stoltz, B. M. *ACS Catal.* **2020**, *10*, 3241–3248. c) Kim, A. N.; Ngamnithiporn, A.; Bartberger, M. D.; Stoltz, B. M. *Chem. Sci.* **2022**, *13*, 3227–3232.
- (38) a) Núñez-Rico, J. L.; Fernández-Pérez, H.; Benet-Buchholz, J.; Vidal-Ferran, A. *Organometallics* **2010**, *29*, 6627–6631; b) Núñez-Rico, J. L.; Fernández-Pérez, H.; Vidal-Ferran, A. *Green Chem.* **2014**, *16*, 1153–1157; c) Núñez-Rico, J. L.; Vidal Ferran, A. *Org. Lett.* **2013**, *15*, 2066–2069.
- (39) a) Ge, Y.; Wang, Z.; Han, Z.; Ding, K. *Chem. Eur. J.* **2020**, *26*, 15482–15486; b) Pauli, L.; Tannert, R.; Scheil, R.; Pfaltz, A. *Chem. Eur. J.* **2015**, *21*, 1482–1487; c) Meng, K.; Xia, J.; Wang, Y.; Zhang, X.; Yang, G.; Zhang, W. *Org. Chem. Front.* **2017**, *4*, 1601–1605; d) Qu, B.; Mangunuru, H. P. R.; Teyrulnikov, S.; Rivalenti, D.; Zatolochnaya, O. V.; Kurouski, D.; Radomkit, S.; Biswas, S.; Karyakarte, S.; Fandrick, K. R.; Sieber, J. D.; Rodriguez, S.; Desrosiers, J.-N.; Haddad, N.; McKellop, K.; Pennino, S.; Lee, H.; Yee, N. K.; Song, J. J.; Kozlowski, M. C.; Senanayake, C. H. *Org. Lett.* **2018**, *20*, 1333–1337.
- (40) Li, Z.-W.; Wang, T.-L.; He, Y.-M.; Wang, Z.-J.; Fan, Q.-H.; Pan, J.; Xu, L.-J. *Org. Lett.* **2008**, *10*, 5265–5268.
- (41) a) Kuwano, R.; Sato, K.; Kurokawa, T.; Karube, D.; Ito, Y. *J. Am. Chem. Soc.* **2000**, *122*, 7614–7615; b) Kuwano, R.; Kaneda, K.; Ito, T.; Sato, K.; Kurokawa, T.; Ito, Y. *Org. Lett.* **2004**, *6*, 2213–2215; c) Kuwano, R.; Kashiwabara, M.; Sato, K.; Ito, T.; Kaneda, K.; Ito, Y. *Tetrahedron: Asymmetry* **2006**, *17*, 521–535.
- (42) a) Wang, C.; Li, C.; Wu, X.; Pettman, A.; Xiao, J. *Angew. Chem. Int. Ed.* **2009**, *48*,

Chapter 1 – Recent Advances in Homogeneous Catalysts for the Asymmetric Hydrogenation of Heteroarenes

- 6524–6528; b) Parekh, V.; Ramsden, J. A.; Wills, M. *Tetrahedron: Asymmetry* **2010**, *21*, 1549–1556.
- (43) a) Zhao, Q.; Li, S.; Huang, K.; Wang, R.; Zhang, X. *Org. Lett.* **2013**, *15*, 4014–4017; b) Wen, J.; Tan, R.; Liu, S.; Zhao, Q.; Zhang, X. *Chem. Sci.* **2016**, *7*, 3047–3051; c) Wen, J.; Fan, X.; Tan, R.; Chien, H.-C.; Zhou, Q.; Chung, L. W.; Zhang, X. *Org. Lett.* **2018**, *20*, 2143–2147.
- (44) Wang, D.-S.; Chen, Q.-A.; Li, W.; Yu, C.-B.; Zhou, Y.-G.; Zhang, X. *J. Am. Chem. Soc.* **2010**, *132*, 8909–8911.
- (45) Cai, X.-F.; Huang, W.-X.; Chen, Z.-P.; Zhou, Y.-G. *Chem. Commun.* **2014**, *50*, 9588–9590.
- (46) a) Duan, Y.; Chen, M.-W.; Chen, Q.-A.; Yu, C.-B.; Zhou, Y.-G. *Org. Biomol. Chem.* **2012**, *10*, 1235–1238; b) Li, C.; Chen, J.; Fu, G.; Liu, D.; Liu, Y.; Zhang, W. *Tetrahedron* **2013**, *69*, 6839–6844; c) Duan, Y.; Li, L.; Chen, M.-W.; Yu, C. B.; Fan, H.-J.; Zhou, Y.-G. *J. Am. Chem. Soc.* **2014**, *136*, 7688–7700; d) Yu, C. B.; Wang, J.; Zhou, Y.-G. *Org. Chem. Front.* **2018**, *5*, 2805–2809; e) Yu, C.-B.; Li, X.; Zhou, Y.-G. *Asian J. Org. Chem.* **2019**, *8*, 1118–1121.
- (47) Chen, M.-W.; Deng, Z.; Yang, Q.; Huang, J.; Peng, Y. *Org. Chem. Front.* **2019**, *6*, 746–750.
- (48) Wang, D.-S.; Ye, Z.-S.; Chen, Q.-A.; Zhou, Y.-G.; Yu, C.-B.; Fan, H.-J.; Duan, Y. *J. Am. Chem. Soc.* **2011**, *133*, 8866–8869.
- (49) Zhou, S.; Fleischer, S.; Junge, K.; Beller, M. *Angew. Chem. Int. Ed.* **2011**, *50*, 5120–5124.

Chapter 1 – Recent Advances in Homogeneous Catalysts for the Asymmetric Hydrogenation of Heteroarenes

- (50) a) Fleischer, S.; Zhou, S.; Werkmeister, S.; Junge, K.; Beller, M. *Chem. Eur. J.* **2013**, *19*, 4997–5003; b) Lu, L.-Q.; Li, Y.; Junge, K.; Beller, M. *J. Am. Chem. Soc.* **2015**, *137*, 2763–2768.
- (51) a) von der Höh, A.; Berkessel, A. *ChemCatChem* **2011**, *3*, 861–867; b) Moulin, S.; Dentel, H.; Pagnoux-Ozherelyeva, A.; Gaillard, S.; Poater, A.; Cavallo, L.; Lohier, J.-F.; Renaud, J.-L. *Chem. Eur. J.* **2013**, *19*, 17881–17890.
- (52) Hopmann, K. H. *Chem. Eur. J.* **2015**, *21*, 10020–10030.
- (53) a) Zhang, Z.; Du, H. *Org. Lett.* **2015**, *17*, 6266–6269; b) Zhang, Z.; Du, H. *Org. Lett.* **2015**, *17*, 2816–2819; c) Li, S.; Meng, W.; Du, H. *Org. Lett.* **2017**, *19*, 2604–2606; d) Zhang, Z.; Du, H. *Angew. Chem. Int. Ed.* **2014**, *54*, 623–626; e) Li, X.; Tian, J.-J.; Liu, N.; Tu, X.-S.; Zeng, N.-N.; Wang, X.-C. *Angew. Chem. Int. Ed.* **2019**, *58*, 4664–4668.
- (54) Liu, Y.; Du, H. *J. Am. Chem. Soc.* **2013**, *135*, 6810–6813.
- (55) a) Feng, X.; Du, H. *Tetrahedron Lett.* **2014**, *55*, 6959–6964; b) Gao, B.; Feng, X.; Meng, W.; Du, H. *Angew. Chem. Int. Ed.* **2020**, *59*, 4498–4504.
- (56) Rueping, M.; Antonchick, A. P.; Theissmann, T. *Angew. Chem. Int. Ed.* **2006**, *45*, 3683–3686.
- (57) Chen, Z.-P.; Chen, M.-W.; Guo, R.-N.; Zhou, Y.-G. *Org. Lett.* **2014**, *16*, 1406–1409.
- (58) a) Rueping, M.; Theissmann, T.; Stoeckel, M.; Antonchick, A. P. *Org. Biomol. Chem.* **2011**, *9*, 6844–6850; b) Rueping, M.; Bootwicha, T.; Sugiono, E. *Beilstein J. Org. Chem.* **2012**, *8*, 300–307; c) Chen, Q.-A.; Gao, K.; Duan, Y.; Ye, Z.-S.;

Chapter 1 – Recent Advances in Homogeneous Catalysts for the Asymmetric Hydrogenation of Heteroarenes

- Shi, L.; Yang, Y.; Zhou, Y.-G. *J. Am. Chem. Soc.* **2012**, *134*, 2442–2448; d) Tu, X.-F.; Gong, L.-Z. *Angew. Chem. Int. Ed.* **2012**, *51*, 11346–11349; e) More, G. V.; Bhanage, B. M. *Tetrahedron: Asymmetry* **2015**, *26*, 1174–1179; f) Zhang, Y.; Zhao, R.; Bao, R. L.; Shi, L. *Eur. J. Org. Chem.* **2015**, *2015*, 3344–3351; g) Wang, J.; Chen, M.-W.; Ji, Y.; Hu, S.-B.; Zhou, Y.-G. *J. Am. Chem. Soc.* **2016**, *138*, 10413–10416.
- (59) Rueping, M.; Brinkmann, C.; Antonchick, A. P.; Atodiresei, I. *Org. Lett.* **2010**, *12*, 4604–4607.
- (60) Rueping, M.; Antonchick, A. P.; Theissmann, T. *Angew. Chem. Int. Ed.* **2006**, *45*, 6751–6755.
- (61) Rueping, M.; Antonchick, A. P. *Angew. Chem. Int. Ed.* **2007**, *46*, 4562–4565.
- (62) Pastor, J.; Rezabal, E.; Voituriez, A.; Betzer, J.-F.; Marinetti, A.; Frison, G. *J. Org. Chem.* **2018**, *83*, 2779–2787.
- (63) a) Marcelli, T.; Hammar, P.; Himo, F. *Chem. Eur. J.* **2008**, *14*, 8562–8571; b) Simón, L.; Goodman, J. M. *J. Am. Chem. Soc.* **2008**, *130*, 8741–8747.
- (64) a) Wang, J.; Zhu, Z.-H.; Chen, M.-W.; Chen, Q.-A.; Zhou, Y.-G. *Angew. Chem. Int. Ed.* **2019**, *58*, 1813–1817; b) Wang, J.; Zhao, Z.-B.; Zhao, Y.; Luo, G.; Zhu, Z.-H.; Luo, Y.; Zhou, Y.-G. *J. Org. Chem.* **2020**, *85*, 2355–2368; c) Zhu, Z.-H.; Ding, Y.-X.; Wu, B.; Zhou, Y.-G. *Chem. Sci.* **2020**, *11*, 10220–10224.

## CHAPTER 2

### *Iridium-Catalyzed Enantioselective and Diastereoselective Hydrogenation of 1,3-Disubstituted Isoquinolines<sup>†</sup>*

#### 2.1 INTRODUCTION

The stereocontrolled synthesis of nitrogen-containing heterocycles remains a challenge of great importance, as it provides direct access to chiral compounds that are prevalent structural motifs in many biologically active molecules.<sup>1</sup> As a result, the asymmetric hydrogenation of various hetero-aromatic compounds has been extensively explored as a direct, efficient synthesis of enantiopure cyclic amines.<sup>2</sup> Despite recent progress made toward the asymmetric hydrogenation of *N*-heterocycles such as quinolines, quinoxalines, and pyridines, the synthesis of 1,2,3,4-tetrahydroisoquinolines (THIQs) from isoquinolines remains significantly under-developed (Figure 2.1A).<sup>2</sup> This is due in part to the stronger basicity and coordinating ability of the THIQ products compared to those of other

---

<sup>†</sup>This research was performed in collaboration with Dr. Ngamnithiporn, Dr. Eric Welin, Martin T. Daiger, Christian U. Grünanger, Dr. Michael D. Bartberger, and Dr. Scott C. Virgil. Portions of this chapter have been reproduced with permission from Kim, A. N.; Ngamnithiporn, A.; Welin, E. R.; Daiger, M. T.; Grünanger, C. U.; Bartberger, M. D.; Virgil, S. C.; Stoltz, B. M. *ACS Catal.* **2020**, *10*, 3241–3248. © 2020 American Chemical Society.



heterocycles (e.g., quinolines), leading to catalyst deactivation, as well as the overall lower reactivity of isoquinoline substrates.<sup>3</sup> Although a few effective strategies toward the asymmetric hydrogenation of substituted isoquinolines have been reported, these typically require preparation of the isoquinolinium salt, substrate activation with halogenides, and harsher hydrogenation reaction conditions (Figure 2.1B).<sup>4</sup>

Furthermore, previous to our research, there were only 2 catalytic systems describing efficient methods to access chiral 1,3-disubstituted tetrahydroisoquinolines,<sup>4c,e,g</sup> a more complex and sterically challenging system that generates two stereogenic centers. In addition, the limited substrate scope from these reports demonstrates the low tolerance of additional Lewis basic functionalities, such as alcohols or heteroaryl-substituted isoquinolines, which limit the applicability of these methodologies in synthesis. Since 1,3-disubstituted tetrahydroisoquinolines with Lewis basic moieties are ubiquitous motifs present in a wide range of natural products, such as the saframycin, naphthyridinomycin, and quinocarcin families,<sup>5</sup> a general method for highly enantioselective and diastereoselective hydrogenation of neutral disubstituted isoquinolines under mild reaction conditions would be a significant advancement toward the preparation of chiral amine-containing cyclic molecules.

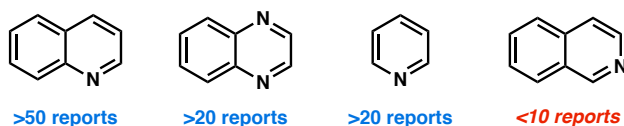
Recently, our group has successfully completed the total synthesis of jorumycin (**156**) and jorunnamycin A (**157**), two bis-tetrahydroisoquinoline natural products that exhibit potent antiproliferative activity, as well as strong Gram-positive and Gram-negative antibiotic character.<sup>6</sup> Through an unprecedented, nonbiomimetic synthetic route, we were successful in harnessing catalysis to allow expedient access to these natural products, as well

as a diverse range of non-natural analogs that are otherwise inaccessible using prior biomimetic synthetic approaches.

**Figure 2.1** A) Limitations in enantioselective hydrogenation of *N*-heterocycles. B) Previous examples of iridium-catalyzed enantioselective and diastereoselective hydrogenation of mono- and di-substituted isoquinolines.

**A. Asymmetric Hydrogenation of *N*-Heterocycles:**

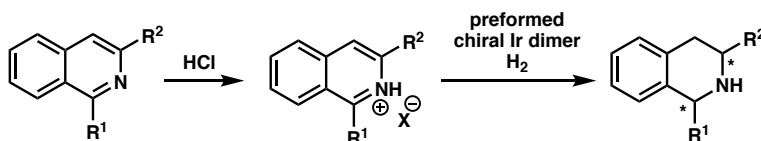
Substrates:



**B. Prior Art in Ir-Catalyzed Asymmetric Hydrogenation of Isoquinolines:**

a) Substrate Activation via Isoquinolinium Salts

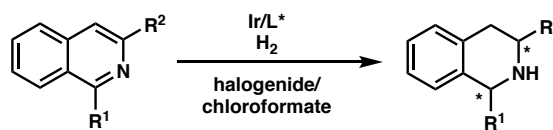
- 4 reports with only 1 report describing 1,3-disubstituted isoquinolines
- Requires prior formation of the salt for activation
- No example of substrate with additional Lewis basic functionalities



R<sup>1</sup>, R<sup>2</sup> = alkyl, aryl

b) in situ and Transient Activation

- 3 reports with only 1 report describing 1,3-disubstituted isoquinolines
- Requires high temperature & pressure
- No example of substrate with additional Lewis basic functionalities



R<sup>1</sup>, R<sup>2</sup> = alkyl, aryl

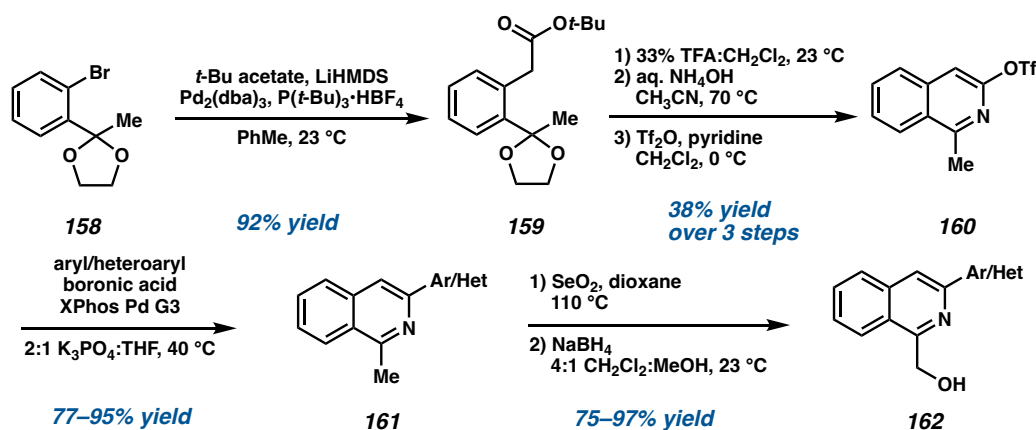
One of the key steps of this synthesis involves a catalytic enantioselective hydrogenation of bis-isoquinoline **64** to afford the THIQ motif, a crucial intermediate that forms the pentacyclic carbon skeleton **65** in one step by further hydrogenation of the second isoquinoline and eventual amide ring closure (Figure 2.2).



hydrogenation technology for bis-isoquinolines, herein we disclose a mild, general method for the enantioselective and diastereoselective hydrogenation of 1,3-disubstituted isoquinolines.

## 2.2 SUBSTRATE SYNTHESSES

Due to a limited number of methods for the syntheses of 1,3-disubstituted isoquinolines,<sup>7</sup> we first established a simple and divergent sequence to access a wide variety of 1-(hydroxymethyl)-3-arylisoquinoline substrates (i.e., **162**, Scheme 2.1). Utilizing Pd-catalyzed arylation of ester enolates reported by Donohoe and coworkers,<sup>8</sup> monoarylated *tert*-butyl acetate **158** was isolated in an excellent 92% yield. Cyclization to isoquinoline triflate **160** was then achieved via hydrolysis of the ketal, followed by isoquinoline annulation with aqueous ammonium hydroxide, and alcohol triflation.<sup>9</sup> At this stage, different aryl or heteroaryl groups could be coupled with intermediate **160** using Suzuki coupling conditions to deliver a wide range of 1,3-disubstituted isoquinolines (i.e., **161**), highlighting the divergent synthesis of our synthetic route. Finally, SeO<sub>2</sub> oxidation to the aldehyde and subsequent NaBH<sub>4</sub> reduction provided our desired isoquinoline starting materials **162a–r**. It is worth noting that this sequence allows for an introduction of various aryl and heteroaryl groups at the C3-position of isoquinolines, as well as different substituents with varied electronics on the isoquinoline carbocycle (e.g., **164a–f**, *vide infra*, Scheme 4). Currently in the literature, the 1,3-disubstituted isoquinoline motif is typically accessed via transition-metal-catalyzed tandem C–H activation/annulation of arenes with alkynes.<sup>10</sup> These methods have shown limited success in producing C3-heteroaryl isoquinolines.<sup>11</sup>

**Scheme 2.1.** Syntheses of 1-(hydroxymethyl)-3-aryl isoquinoline substrates.

### 2.3 REACTION OPTIMIZATION

With a divergent sequence to access 1,3-disubstituted isoquinolines, we began our hydrogenation studies with 1-(hydroxymethyl)-3-phenylisoquinoline (**162a**) as our model substrate, using slightly modified conditions from our previously reported hydrogenation on the bis-isoquinoline system (Table 1). An initial experiment, employing 1.25 mol %  $[\text{Ir}(\text{cod})\text{Cl}]_2$  and 3 mol % of the BTFM-xylyphos ligand (**L6**), gave high conversion of the substrate but surprisingly modest enantioselectivity (49% ee, entry 1). Seeking to improve the ee, we surveyed a wide variety of chiral ligand scaffolds (see Supporting Information) and found the xylyphos ligand framework to be optimal. By exploring different electronics of this ligand scaffold, we observed that replacing the 3,5-bistrifluoromethylphenyl (BTFM) with more electron-rich aryl groups provided the product with both excellent conversion and higher enantioselectivity (entries 1–5). Ligand **L7**, which features 4-methoxy-3,5-dimethylphenyl (DMM) substituted phosphine delivers the product with the highest ee of 89%, albeit with a low 2:1 diastereoselectivity (entry 5). Interestingly, a background reaction was observed in the absence of the chiral ligand,

providing the product in excellent conversion and diastereoselectivity (entry 6). From this finding, we obtained all racemic hydrogenated products by simply performing the hydrogenation in the absence of ligand, affording the *cis*-product as a single diastereomer.

**Table 2.1.** Optimization of the enantioselective hydrogenation of isoquinolines to afford *cis*-THIQs.<sup>a</sup>

entry	ligand	Solvent	% conversion <sup>b</sup>	cis:trans <sup>b</sup>	% ee of cis <sup>c</sup>
1	L6	PhMe:AcOH	>95	>20:1	-49 <sup>d</sup>
2	L12	PhMe:AcOH	>95	3.2:1	84
3	L13	PhMe:AcOH	66	4.5:1	63
4	L14	PhMe:AcOH	92	4.9:1	3
5	L7	PhMe:AcOH	>95	2.0:1	89
6	–	PhMe:AcOH	>95	>20:1	0
7	L7	CH <sub>2</sub> Cl <sub>2</sub> :AcOH	>95	1.5:1	84
8	L7	dioxane:AcOH	66	5.5:1	87
9	L7	THF:AcOH	>95	9.7:1	90
10	L7	CPME:AcOH	38	>20:1	88
11	L7	2-MeTHF:AcOH	>95	9.5:1	90
12 <sup>e</sup>	L7	THF:AcOH	>95	15.7:1	92

L6: Ar = BTFM<sup>d</sup>

L12: Ar = Ph

L13: Ar = 2-naphthyl

L14: Ar = furyl

L7: Ar = DMM

[a] Reaction conditions: 0.04 mmol of **162a**, 1.25 mol % [Ir(cod)Cl]<sub>2</sub>, 3 mol % ligand, 7.5 mol % TBAI, 60 bar H<sub>2</sub> in 2.0 mL 9:1 solvent:AcOH. [b] Determined from crude <sup>1</sup>H NMR using 1,3,5-trimethoxybenzene as standard. [c] Determined by chiral SFC analysis of Cbz-protected product. [d] Opposite enantiomer of ligand used. [e] Reaction performed on a 0.2 mmol scale at 23 °C, 20 bar H<sub>2</sub>, and 0.1 M concentration of **162a**. BTFM = 3,5-bis(trifluoromethyl)phenyl; DMM = 4-methoxy-3,5-dimethylphenyl.

Investigation of different solvents with **L7** as the optimal ligand reveals that while the use of CH<sub>2</sub>Cl<sub>2</sub> provided similar results to toluene (entry 7), the diastereoselectivity could be improved with the use of ethereal solvents (entries 8–11).

Although bulkier ethereal solvents proved to worsen conversion (entries 8 and 10), we were delighted to find that THF and the more sustainable solvent 2-MeTHF delivered the product in excellent conversion with high levels of diastereoselectivity and enantioselectivity (entries 9 and 11). The absence of AcOH resulted in low conversion,<sup>12</sup> while further exploration of different additives (e.g., LiI, NaI, KI, etc.) demonstrated that TBAI is the optimal additive (see Table 2.3, Section 2.7.3). Finally, we were excited to observe that lowering the temperature to 23 °C and H<sub>2</sub> pressure to 20 bar maintained excellent levels of conversion, diastereo-selectivity, and enantioselectivity (entry 12). To the best of our knowledge, these are the mildest reaction conditions reported for isoquinoline hydrogenation to afford chiral THIQs to date.<sup>4</sup>

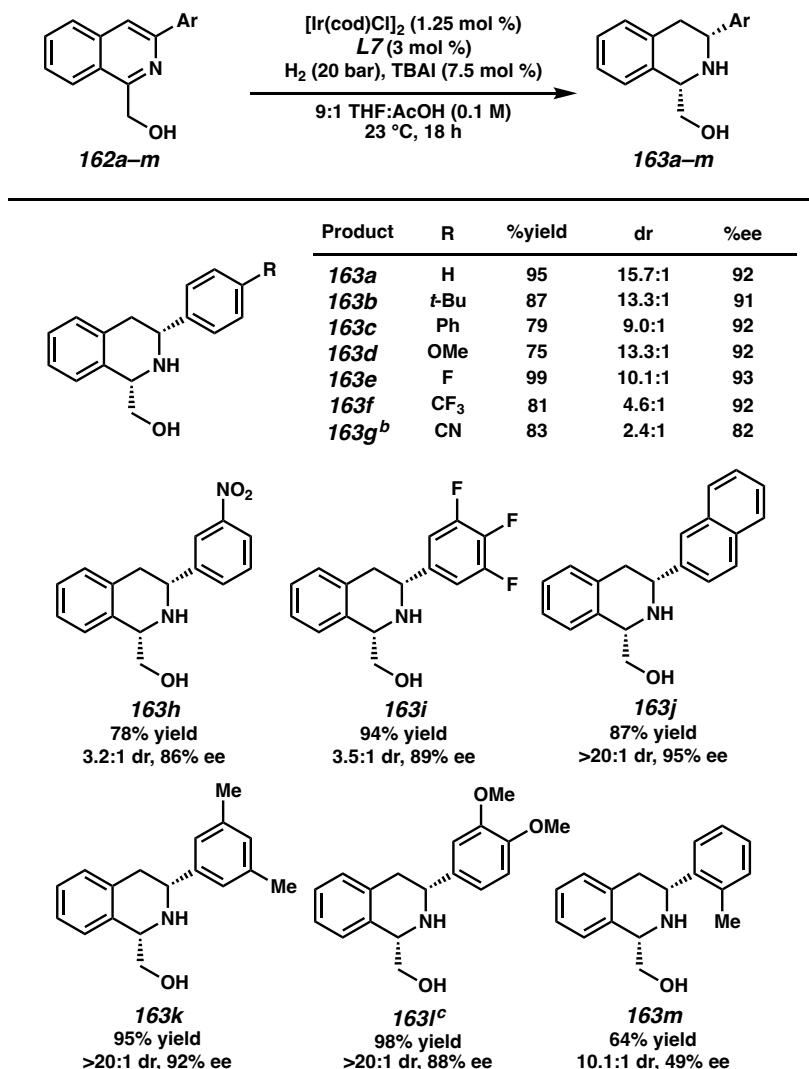
## 2.4 SUBSTRATE SCOPE

With optimized reaction conditions identified, we explored the general substrate scope for this transformation (Scheme 2.2). Gratifyingly, a wide variety of aryl substituents at the 3-position of the isoquinoline are well tolerated under the mild reaction conditions of 20 bar H<sub>2</sub> at ambient temperature. Substitution at the *para*-position of the 3-aryl ring delivered the hydrogenated products **163a–g** in consistently high yields and enantioselectivity. Electron-rich substrates such as the 3-(*p*-*tert*-butylphenyl)isoquinoline (**162b**) and the *p*-methoxyphenyl (**162d**) afforded chiral THIQs with excellent yields, diastereoselectivity, and enantioselectivity, similar to **162a**. Interestingly, however, a general trend of lower diastereoselectivity was observed with electron-withdrawing substituents both at the *para*- and *meta*- positions (**163f–i**). We envision that the observed lower diastereoselectivity arises from the weaker coordinating ability of the nitrogen to the

iridium catalyst in electron-poor substrates, discouraging coordination to the catalyst in a bidentate fashion,<sup>13</sup> and thus resulting in poorer facial selectivity in the second hydride addition step. However, at this time, we still cannot rule out the possibility that epimerization in situ also influences the trend seen in diastereoselectivity.<sup>14</sup> Investigation of steric effects revealed that more sterically encumbered isoquinolines such as the 3-naphthyl and 3-xylyl substrates furnished the products (**163j–k**) in excellent isolated yields with similarly high enantioselectivity (95% and 92% ee, respectively) as a single diastereomer. The most sterically demanding substrate **162m**, bearing an *ortho*-tolyl substituent, provided product **163m** in a modest 64% yield with lower enantioselectivity (49% ee), albeit still with a high 10.1:1 diastereoselectivity. Additionally, we were pleased to find that the nitrile and nitro functional groups as well as the naphthyl substituent were not reduced (**163g**, **163h**, and **163j**), highlighting the chemoselectivity of this catalytic process.

Pleased to find the reaction tolerable to a range of 3-aryl substituted isoquinolines, we sought to further extend the scope of the transformation by exploring heteroaryl-substituted isoquinolines (Scheme 2.3). Although performing the hydrogenation at 23 °C and 20 bar H<sub>2</sub> resulted in lower conversion, partially due to solubility issues, we found that heterocyclic substituents including furan, thiophene, pyrazole, and pyridine were well tolerated at 60 °C and under higher pressure of 60 bar H<sub>2</sub>, producing THIQs **163n–r**. We also observed that the substitution pattern on the heteroaryl groups strongly affects the reaction conversion. For instance, an isoquinoline with a 3-substituted thiophene proceeded with a significantly lower conversion than the 2-thiophene substrate (**163o** and **163p**).



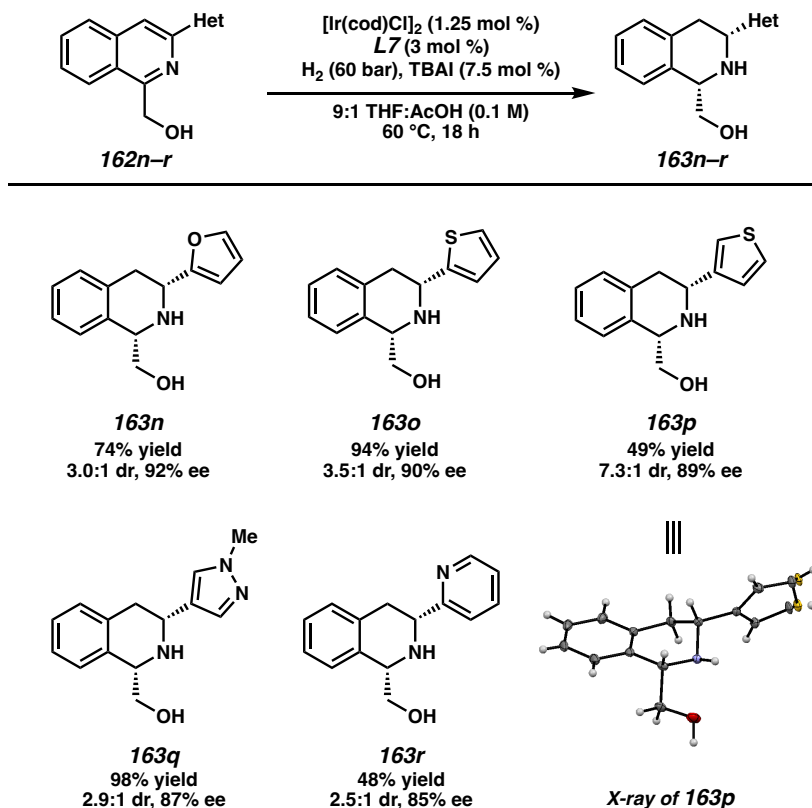
**Scheme 2.2.** Substrate scope of different aryl substituents.<sup>a</sup>

[a] Reactions performed on a 0.2 mmol scale. [b] Reaction performed at 60 °C and 60 bar H<sub>2</sub>. [c] CH<sub>2</sub>Cl<sub>2</sub> cosolvent used to improve substrate solubility.

Similarly, no conversion was observed with 3- and 4-pyridyl substrates, whereas 2-pyridyl THIQ **163r** was isolated in 48% yield under the same reaction conditions. We speculate that this may be due to the competitive binding of the catalyst by the more distal heteroatom of 3- and 4-substituted heterocycles that inhibits directed hydrogenation of the isoquinoline ring. From product **163p** we were successful in obtaining an X-ray crystal

structure to confirm the relative and absolute stereochemistry of our hydrogenation product.

**Scheme 2.3.** Substrate scope of heteroaryl substituents.<sup>a</sup>

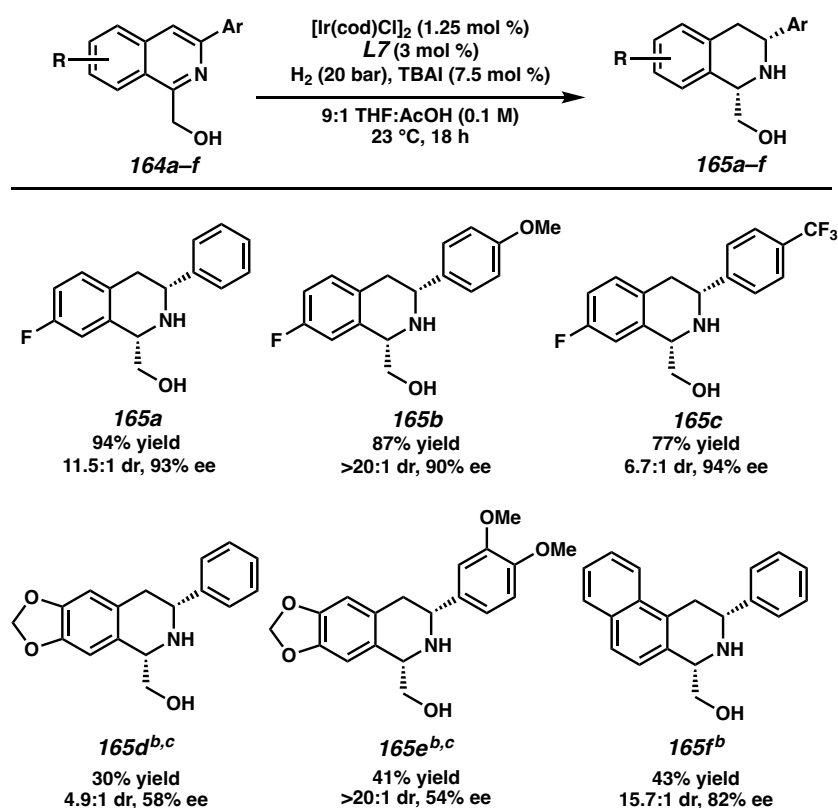


[a] Reactions performed on a 0.2 mmol scale.

Furthermore, we were interested in exploring the substrate scope of isoquinolines with different electronics and substitution patterns on the isoquinoline carbocycle (Scheme 2.4). Electron-poor fluorinated isoquinolines with varied electronics at the 3-position provided THIQs in high yields (77–94%) with high diastereoselectivity and enantioselectivity under our standard conditions (**165a–c**). It should be noted that these electron-poor THIQs would be difficult to access utilizing electrophilic aromatic substitution strategies, a classical method for the syntheses of THIQs. On the other hand,

the electron-rich dioxolane-appended isoquinolines (**164d–e**) afforded lowered conversion under the same reaction conditions, due in part to the poor solubility of the substrates in THF. Nevertheless, executing the reaction at 60 °C and 60 bar H<sub>2</sub> with CH<sub>2</sub>Cl<sub>2</sub> as cosolvent improved the solubility and conversion to yield products **165d–e** with high diastereoselectivity.<sup>15</sup>

**Scheme 2.4.** Substrate scope of IQ backbone substituents.<sup>a</sup>



[a] Reactions performed on a 0.2 mmol scale. [b] Reaction performed at 60 °C and 60 bar H<sub>2</sub>. [c] CH<sub>2</sub>Cl<sub>2</sub> cosolvent used to improve substrate solubility.

Interestingly, we observed significantly lower enantioselectivity for the dioxolane THIQs, which is observed in other reports as well.<sup>4a,g</sup> Finally, the naphthyl-fused THIQ **165f** was obtained with high diastereoselectivity and enantio-selectivity, despite its extended

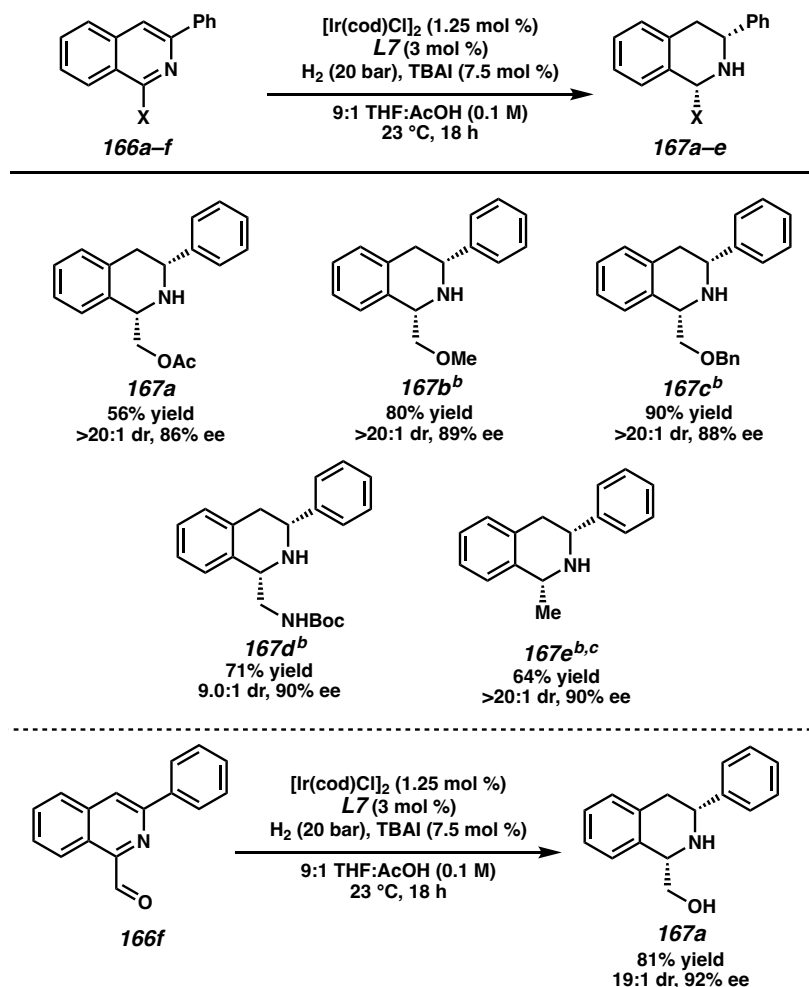
aromatic system and larger steric hindrance. Although we observed modest conversion for these highly decorated isoquinolines, we were pleased to see that we were able to isolate unreacted starting material after column chromatography to obtain 80%, 99%, and 79% yield, respectively, of **165d–f** based on recovered starting material. Consistent with our results for THIQs **163j** and **163r**, we observed that only the ring with the least degree of aromatic stabilization was reduced for **165f**.

Having demonstrated that this transformation is general for a wide variety of 1,3-disubstituted isoquinolines, we then turned our attention to investigate the effects of different “directing” groups at the C1-position (Scheme 2.5). Isoquinolines bearing other polar groups such as an ester (**167a**), ethers (**167b–c**), and a Boc-protected amine (**167d**) delivered the products in lower yields than the hydroxy-directed substrate at 23 °C and 20 bar H<sub>2</sub>. However, to our delight, by increasing the temperature and H<sub>2</sub> pressure, these yields could be improved with no erosion of enantioselectivity and diastereoselectivity.

Additionally, we found that aldehyde **166f** was reduced to the alcohol in situ, affording the hydroxymethyl THIQ **163a** in comparable yield, enantioselectivity, and diastereoselectivity to that of the hydroxy-directing substrate **162a** (*vide supra*). Interestingly, an isoquinoline lacking a potential directing group (**167e**) also afforded chiral THIQs with no erosion of enantioselectivity (90% ee),<sup>16</sup> although elevated temperature and pressure are needed to obtain a synthetically useful yield (64%). While the hydroxy-directing aspect is the enabling feature in the context of our total synthesis of jorumycin, we are pleased to find that we can obviate this requirement in our developed hydrogenation technology. Nevertheless, surveying a variety of different directing groups demonstrates the importance of a functional group for directed hydrogenation, with the hydroxy functionality

acting as the best directing group for mild and efficient asymmetric hydrogenation. Notably, this is the first asymmetric hydrogenation method of isoquinolines in which additional Lewis basic functionalities are tolerated. It is also the first report investigating the effects of different directing groups in enantioselective hydrogenation of isoquinolines.

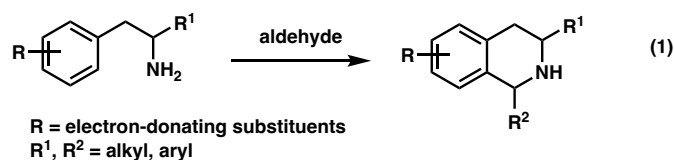
**Scheme 2.5.** Substrate scope of different directing groups.<sup>a</sup>



[a] Reactions performed on a 0.2 mmol scale. [b] Reaction performed at 60 °C and 60 bar  $\text{H}_2$ . [c] Relative and absolute stereochemistry determined by experimental and computed VCD and optical rotation, see Section 2.7.4.

## 2.5 SYNTHETIC UTILITY

Overall, the broad application of our hydrogenation technology to afford chiral THIQs provides access to a range of decorated analogs that are difficult to synthesize via biomimetic approaches (e.g., Pictet-Spengler, Bischler-Napieralski). These often require electron-rich substrates to undergo cyclization (eq 1).<sup>17</sup>



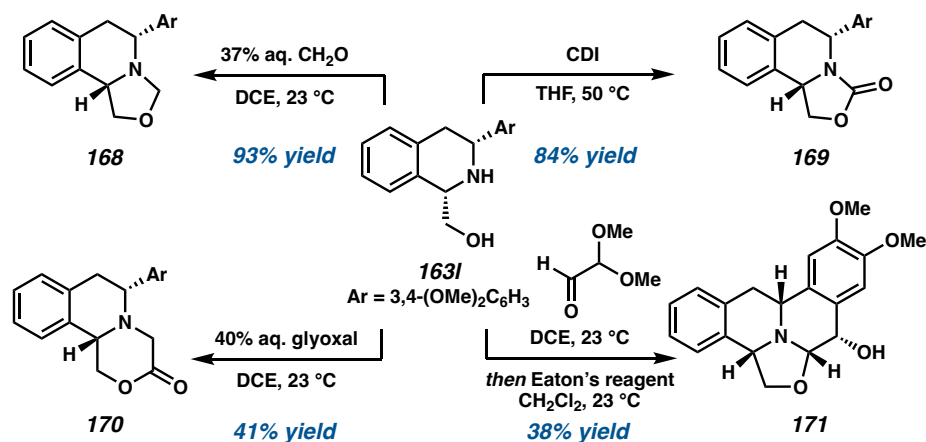
With the scope of the transformation established, we sought to demonstrate the synthetic utility of the produced chiral THIQs toward more complex scaffolds that could be applicable to natural products. Additionally, we envisioned taking advantage of the chiral  $\beta$ -amino alcohol that is generated in our product as a building block to forge more complex enantioenriched heterocyclic scaffolds (Scheme 2.6).<sup>18</sup>

Prior to our investigation into the synthetic utility of THIQ products, we performed the hydrogenation of isoquinoline **162I** on a larger scale (1 mmol). We were pleased to find that the hydrogenated product **163I** was still obtained in good yield (91% isolated yield) with excellent selectivity (>20:1 dr, 88% ee). With an ample amount of **163I** in hand, we subjected THIQ **163I** to aqueous formaldehyde solution and found that the tricyclic 1,2-fused oxazolidine THIQ **168** was formed rapidly via the cyclization of the alcohol onto the iminium generated in situ. Furthermore, the reaction of amino alcohol **163I** with carbonyldiimidazole (CDI) afforded oxazolidinone-fused THIQ **169** in 84% yield.<sup>19</sup> To our delight, we found that these 6,6,5-tricyclic systems are conserved structural motifs in a number of natural products such as quinocarcin, tetrazomine, and bioxalomycin.<sup>5</sup> Lastly, a

different tricyclic scaffold containing fused morpholinone (**170**) can be isolated in 41% yield by the addition of excess glyoxal to **163I** at room temperature.<sup>20</sup> Being able to access a variety of complex heterocyclic scaffolds in one step from our hydrogenated THIQs further highlights the advantages of the hydroxymethyl functionality at the C1 position, beyond directing hydrogenation.

In addition to the tricyclic scaffold, we were pleased to find that an analog of tetrahydroprotoberberine alkaloids, a family of natural products with a tetracyclic bis-THIQ core,<sup>21</sup> can be synthesized via a 2-step sequence. First, reaction of **163I** with glyoxal dimethyl acetal delivered the oxazolidine-fused intermediate with a dimethoxy acetal substituent at the carbinol-amine carbon. Subsequently, exploration of both Brønsted and Lewis acid-mediated Pomeranz-Fritsch reaction revealed that the use of Eaton's reagent<sup>22</sup> delivered pentacyclic THIQ **171** in 38% yield as a single diastereomer. This complex scaffold could be of medicinal interest, as previous studies have shown that tetrahydroprotoberberine derivatives possess a wide array of interesting biological activities.<sup>17,23</sup>

**Scheme 2.6.** Derivatization of hydrogenated product **163I**.



## 2.6 CONCLUSION

We have developed a general, efficient enantioselective hydrogenation reaction of 1,3-disubstituted isoquinolines toward the syntheses of chiral THIQs. Key to the success of this reaction is the installation of a directing group at the C1-position that facilitates hydrogenation to reduce a variety of isoquinolines under mild reaction conditions. The developed method affords chiral THIQs in good yields, with high levels of diastereoselectivity and enantioselectivity. The reaction conditions tolerate a wide range of substitution on the 1-, 3-, 6-, 7-, and 8-position of the isoquinoline core. To date, this report represents the broadest scope and highest tolerance of Lewis-basic functionality of any asymmetric isoquinoline reduction technology currently known. Furthermore, this method is amenable to the production of electron-deficient THIQs that are difficult to obtain through the classical Pictet–Spengler approach. To demonstrate the synthetic utility of the hydrogenated products, we utilize the hydroxyl directing group as a functional handle for further synthetic manipulations. As a result, we have completed the syntheses of various tricyclic and pentacyclic skeletons that are of potential medicinal interest. Further exploration of the mechanism, and other applications of this technology are currently underway.

## 2.7 EXPERIMENTAL SECTION

### 2.7.1 MATERIALS AND METHODS

Unless otherwise stated, reactions were performed in flame-dried glassware under an argon or nitrogen atmosphere using dry, deoxygenated solvents. Solvents were dried by

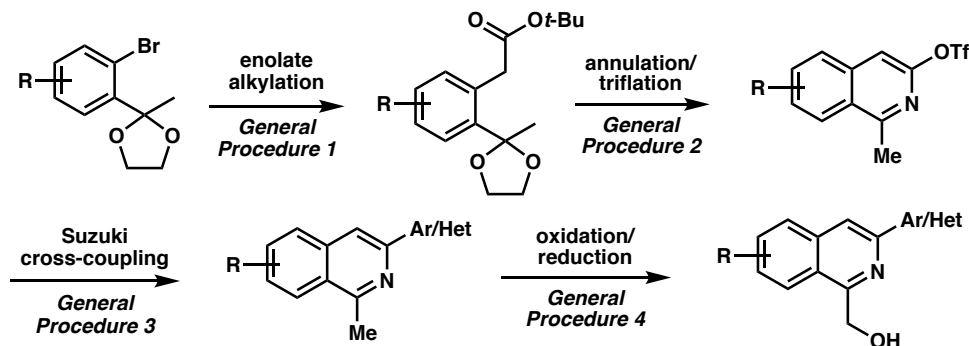


passage through an activated alumina column under argon.<sup>24</sup> Reaction progress was monitored by thin-layer chromatography (TLC) or Agilent 1290 UHPLC-MS. TLC was performed using E. Merck silica gel 60 F254 precoated glass plates (0.25 mm) and visualized by UV fluorescence quenching, *p*-anisaldehyde, or KMnO<sub>4</sub> staining. Silicycle SiliaFlash® P60 Academic Silica gel (particle size 40–63 μm) was used for flash chromatography. <sup>1</sup>H NMR spectra were recorded on Varian Inova 500 MHz and Oxford 600 MHz spectrometers and are reported relative to residual CHCl<sub>3</sub> (δ = 7.26 ppm) or TMS (δ = 0.00 ppm). <sup>13</sup>C NMR spectra were recorded on a Bruker 400 MHz spectrometer (100 MHz) and are reported relative to CHCl<sub>3</sub> (δ = 77.16 ppm), C<sub>6</sub>D<sub>6</sub> (δ = 128.06 ppm). Data for <sup>1</sup>H NMR are reported as follows: chemical shift (δ ppm) (multiplicity, coupling constant (Hz), integration). Multiplicities are reported as follows: s = singlet, d = doublet, t = triplet, q = quartet, p = pentet, sept = septuplet, m = multiplet, br s = broad singlet, br d = broad doublet. Data for <sup>13</sup>C NMR are reported in terms of chemical shifts (δ ppm). IR spectra were obtained by use of a Perkin Elmer Spectrum BXII spectrometer or Nicolet 6700 FTIR spectrometer using thin films deposited on NaCl plates and reported in frequency of absorption (cm<sup>-1</sup>). Optical rotations were measured with a Jasco P-2000 polarimeter operating on the sodium D-line (589 nm), using a 100 mm path-length cell. High resolution mass spectra (HRMS) were obtained from Agilent 6200 Series TOF with an Agilent G1978A Multimode source in electrospray ionization (ESI+), atmospheric pressure chemical ionization (APCI+), or mixed ionization mode (MM: ESI-APCI+). Reagents were purchased from commercial sources and used as received unless otherwise stated.

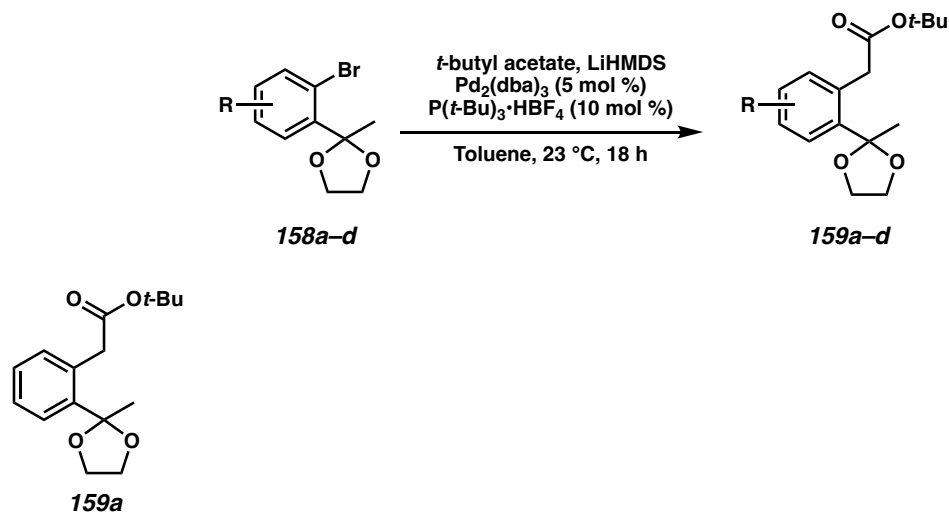
## 2.7.2 EXPERIMENTAL PROCEDURES AND SPECTROSCOPIC DATA

### 2.7.2.1 Syntheses of hydroxymethyl 1,3-disubstituted isoquinolines

#### General Sequence:

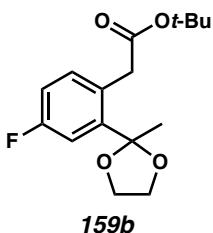


#### General Procedure 1: Enolate Alkylation of Aryl Bromide



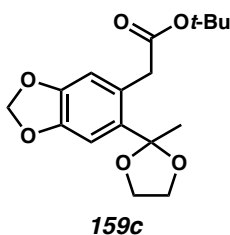
***tert*-butyl 2-(2-(2-(2-methyl-1,3-dioxolan-2-yl)phenyl)acetate (159a):** This procedure has been adapted from a previous report.<sup>8</sup> In a Schlenk flask was added P(*t*-Bu)<sub>3</sub>·HBF<sub>4</sub> (119 mg, 0.41 mmol), Pd<sub>2</sub>(dba)<sub>3</sub> (188 mg, 0.21 mmol), a solution of 2-(2-bromophenyl)-2-methyl-1,3-dioxolane (**158a**) (1.0 g, 4.1 mmol, 0.42 M), and *tert*-butyl acetate (0.95 g, 8.2 mmol), respectively. The reaction mixture was cooled to −78 °C and sparged with nitrogen for 15 minutes. A degassed solution of LiHMDS (1.72 g, 10.25 mmol, 1 M in toluene) was

then added via syringe. The reaction mixture was degassed for an additional 15 minutes at  $-78\text{ }^{\circ}\text{C}$ , and allowed to slowly warm to room temperature. The reaction was stirred at room temperature for 18 hours, and then quenched with saturated aqueous  $\text{NaHCO}_3$ . The aqueous layer was extracted with  $\text{Et}_2\text{O}$  twice. The combined organic phases were dried over  $\text{MgSO}_4$ , filtered, and the solvent was removed in vacuo. The crude product was purified by silica gel flash chromatography (5%  $\text{EtOAc}$  in hexanes) to afford **159a** as a yellow oil (1.05 g, 92% yield):  $^1\text{H NMR}$  (400 MHz,  $\text{CDCl}_3$ )  $\delta$  7.53 – 7.45 (m, 1H), 7.20 – 7.06 (m, 3H), 3.96 – 3.83 (m, 2H), 3.71 (s, 2H), 3.68 – 3.55 (m, 2H), 1.60 (s, 3H), 1.39 (s, 9H);  $^{13}\text{C NMR}$  (100 MHz,  $\text{CDCl}_3$ )  $\delta$  171.6, 141.1, 132.6, 132.3, 128.2, 127.1, 126.4, 109.2, 80.4, 64.3, 40.4, 28.2, 28.2, 27.6; IR (Neat Film, NaCl) 3454, 3062, 2977, 2936, 2893, 1731, 1484, 1455, 1392, 1368, 1218, 1196, 1168, 1037, 952, 869, 763, 706  $\text{cm}^{-1}$ ; HRMS (MM:ESI-APCI+)  $m/z$  calc'd for  $\text{C}_{16}\text{H}_{23}\text{O}_4$   $[\text{M}+\text{H}]^+$ : 279.1591, found 279.1589.



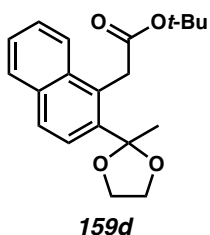
**tert-butyl 2-(4-fluoro-2-(2-methyl-1,3-dioxolan-2-yl)phenyl)acetate (159b):** Compound **159b** was prepared from aryl bromide (2-(2-bromo-5-fluorophenyl)-2-methyl-1,3-dioxolane) (**158b**) using general procedure 1, and purified by column chromatography (10%  $\text{EtOAc}$  in hexanes) to afford **159b** with impurities. The compound was then subjected to the second column chromatography (15%  $\text{Et}_2\text{O}$  in hexanes) to obtain **159b** as a colorless solid (74 mg, 61% yield);  $^1\text{H NMR}$  (400 MHz,  $\text{CDCl}_3$ )  $\delta$  7.28 (dd,  $J = 10.3, 2.8$  Hz, 1H), 7.15 (dd,  $J = 8.4, 5.7$  Hz, 1H), 6.94 (td,  $J = 8.2, 2.9$  Hz, 1H), 4.06 – 3.90 (m, 2H), 3.74 (s,

2H), 3.72 – 3.69 (m, 2H), 1.65 (s, 3H), 1.45 (s, 9H);  $^{13}\text{C}$  NMR (100 MHz,  $\text{CDCl}_3$ )  $\delta$  171.5, 161.9 (d,  $J = 245.1$  Hz), 143.9 (d,  $J = 6.2$  Hz), 134.2 (d,  $J = 7.8$  Hz), 127.9 (d,  $J = 3.3$  Hz), 114.9 (d,  $J = 21.1$  Hz), 113.5 (d,  $J = 23.0$  Hz), 108.6, 80.6, 64.4, 39.6, 28.2, 27.3;  $^{19}\text{F}$  NMR (282 MHz,  $\text{CDCl}_3$ )  $\delta$  -115.6 (ddd,  $J = 10.3, 8.0, 5.8$  Hz); IR (Neat Film, NaCl) 2980, 1732, 1613, 1493, 1412, 1392, 1368, 1340, 1256, 1200, 1179, 1147, 1037, 947, 878  $\text{cm}^{-1}$ ; HRMS (MM:ESI-APCI+)  $m/z$  calc'd for  $\text{C}_{16}\text{H}_{22}\text{FO}_4$   $[\text{M}+\text{H}]^+$ : 297.1497, found 297.1494.



***tert*-butyl 2-(6-(2-methyl-1,3-dioxolan-2-yl)benzo[*d*][1,3]dioxol-5-yl)acetate (159c):**

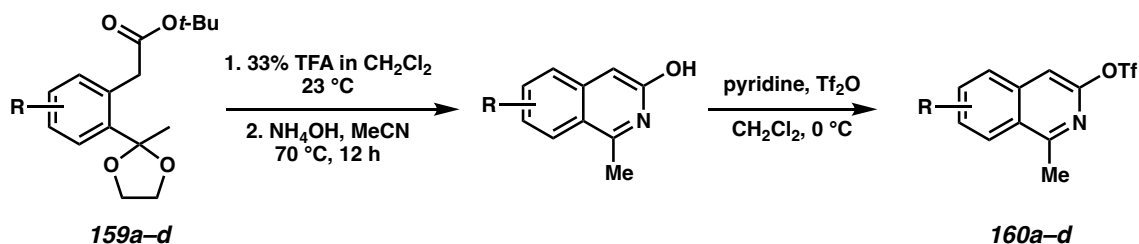
Compound **159c** was prepared from aryl bromide (5-bromo-6-(2-methyl-1,3-dioxolan-2-yl)benzo[*d*][1,3]dioxole) (**158c**) using general procedure 1, and purified by column chromatography (5% to 15% EtOAc in hexanes) to afford **159c** as a pale yellow oil (83.4 mg, 63% yield):  $^1\text{H}$  NMR (400 MHz,  $\text{CDCl}_3$ )  $\delta$  7.07 (s, 1H), 6.66 (s, 1H), 5.93 (s, 2H), 3.95 – 3.93 (m, 2H), 3.72 – 3.69 (m, 2H), 3.62 (s, 2H), 1.64 (s, 3H), 1.46 (s, 9H);  $^{13}\text{C}$  NMR (100 MHz,  $\text{CDCl}_3$ )  $\delta$  171.7, 147.2, 146.7, 135.2, 125.9, 112.3, 109.1, 107.0, 101.3, 80.6, 64.3, 40.0, 28.3, 27.6; IR (Neat Film, NaCl) 2978, 2897, 1732, 1504, 1486, 1369, 1332, 1259, 1197, 1166, 1142, 1041, 929, 869, 935  $\text{cm}^{-1}$ ; HRMS (MM:ESI-APCI+)  $m/z$  calc'd for  $\text{C}_{17}\text{H}_{23}\text{O}_6$   $[\text{M}+\text{H}]^+$ : 323.1489, found 323.1501.

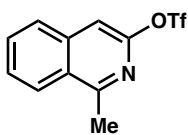


**tert-butyl 2-(2-(2-methyl-1,3-dioxolan-2-yl)naphthalen-1-yl)acetate (159d):**

Compound **159d** was prepared from aryl bromide (2-(1-bromonaphthalen-2-yl)-2-methyl-1,3-dioxolane) (**158d**) using general procedure 1, and purified by column chromatography (0% to 5% EtOAc in hexanes) to afford **159d** as a pale yellow oil (2.15 g, 98% yield): <sup>1</sup>H NMR (400 MHz, CDCl<sub>3</sub>) δ 7.93 (d, *J* = 8.0 Hz, 1H), 7.82 (d, *J* = 8.0 Hz, 1H), 7.76 (s, 2H), 7.48 (ddd, *J* = 7.9, 6.7, 1.4 Hz, 2H), 4.38 (s, 2H), 4.04 – 4.00 (m, 2H), 3.79 – 3.73 (m, 2H), 1.78 (s, 3H), 1.45 (s, 9H); <sup>13</sup>C NMR (100 MHz, CDCl<sub>3</sub>) δ 171.4, 139.3, 133.6, 128.7, 128.6, 127.8, 126.5, 125.8, 124.3, 124.1, 109.7, 80.7, 64.4, 36.2, 28.2, 27.8. IR (Neat Film, NaCl) 2980, 2890, 1732, 1454, 1368, 1336, 1142, 1100, 1037, 951, 884, 870, 822, 750 cm<sup>-1</sup>; HRMS (MM:ESI-APCI+) *m/z* calc'd for C<sub>20</sub>H<sub>25</sub>O<sub>4</sub> [M+H]<sup>+</sup>: 329.1747, found 329.1739.

**General Procedure 2: Isoquinoline Annulation and Triflation**



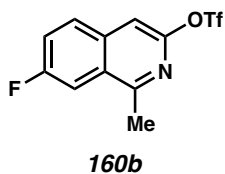


**160a**

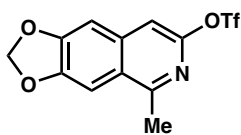
**1-methylisoquinolin-3-yl trifluoromethanesulfonate (160a):** This procedure has been adapted from a previous report.<sup>9</sup> In a RBF were added ester **159a** (2.78 g, 10.0 mmol), anhydrous CH<sub>2</sub>Cl<sub>2</sub> (75 mL, 0.13 M), and TFA (25 mL, 33% volume of CH<sub>2</sub>Cl<sub>2</sub>), respectively. The reaction was stirred at room temperature for 2 hours, and then concentrated in vacuo. The crude was transferred to a Schlenk tube, dissolved in MeCN (10 mL, 1 M), and aqueous NH<sub>4</sub>OH (28–30%, 20 mL, 200% volume of MeCN). The tube was sealed with Kontes valve to prevent loss of gaseous ammonia and stirred at 70 °C. Within 1 hour, the yellow solid of the 3-hydroxyisoquinoline began to precipitate from the reaction solution. After stirring for 18 hours at 70 °C, the reaction was cooled to room temperature, then placed in a –20 °C freezer, and the yellow solid was collected via vacuum filtration. This yellow powder was then washed with cold MeCN and dried at high vacuum to provide 3-hydroxyisoquinoline intermediate (0.70 g, 4.39 mmol). If any starting material remains, the filtrate could be transferred to a flask and concentrated in vacuo to undergo a second condensation reaction.

To a separate flame-dried RBF containing CH<sub>2</sub>Cl<sub>2</sub> (22 mL, 0.2 M) and distilled pyridine (3.6 mL, 44 mmol), the collected yellow powder (0.70 g, 4.39 mmol) was added, and the resulting mixture was cooled to 0 °C. Trifluoromethanesulfonic anhydride (1.5 mL, 8.8 mmol) was then added dropwise at 0 °C, and the reaction was stirred at 0 °C for 1 hour. The reaction was then quenched with saturated aqueous NaHCO<sub>3</sub> at 0 °C, and then slowly warmed to room temperature. The reaction was extracted with CH<sub>2</sub>Cl<sub>2</sub>, dried over Na<sub>2</sub>SO<sub>4</sub>,

and concentrated in vacuo. The crude product was purified by column chromatography (10% EtOAc in hexanes) to afford **160a** as a pale yellow oil (1.11 g, 38% yield over 3 steps):  $^1\text{H}$  NMR (400 MHz,  $\text{CDCl}_3$ )  $\delta$  8.17 (dd,  $J = 8.5, 1.0$  Hz, 1H), 7.88 (dt,  $J = 8.3, 1.0$  Hz, 1H), 7.76 (ddd,  $J = 8.2, 6.9, 1.2$  Hz, 1H), 7.67 (ddd,  $J = 8.3, 6.9, 1.3$  Hz, 1H), 7.42 (s, 1H), 2.97 (s, 3H);  $^{13}\text{C}$  NMR (100 MHz,  $\text{CDCl}_3$ )  $\delta$  160.3, 151.3, 138.6, 131.5, 128.1, 127.8, 127.6, 126.1, 118.9 (q,  $J = 320.5$  Hz), 109.0, 22.1;  $^{19}\text{F}$  NMR (282 MHz,  $\text{CDCl}_3$ )  $\delta$  -73.0; IR (Neat Film, NaCl) 1624, 1600, 1563, 1422, 1327, 1213, 1138, 1116, 987, 958, 891, 832, 742, 616  $\text{cm}^{-1}$ ; HRMS (MM:ESI-APCI+)  $m/z$  calc'd for  $\text{C}_{11}\text{H}_9\text{F}_3\text{NO}_3\text{S}$   $[\text{M}+\text{H}]^+$ : 292.0250, found 292.0253.



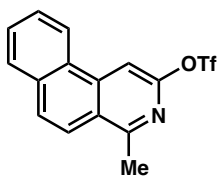
**7-fluoro-1-methylisoquinolin-3-yl trifluoromethanesulfonate (160b):** Compound **160b** was prepared from ester **159b** using general procedure 2 and purified by column chromatography (10% EtOAc in hexanes) to provide a pale brown oil (384 mg, 31% yield over 3 steps):  $^1\text{H}$  NMR (400 MHz,  $\text{CDCl}_3$ )  $\delta$  7.90 (dd,  $J = 9.0, 5.3$  Hz, 1H), 7.76 (dd,  $J = 9.6, 2.5$  Hz, 1H), 7.56 (ddd,  $J = 8.9, 8.0, 2.5$  Hz, 1H), 7.43 (s, 1H), 2.92 (s, 3H);  $^{13}\text{C}$  NMR (100 MHz,  $\text{CDCl}_3$ )  $\delta$  161.4 (d,  $J = 251.1$  Hz), 159.4 (d,  $J = 6.1$  Hz), 151.1 (d,  $J = 3.3$  Hz), 135.5, 130.3 (d,  $J = 8.7$  Hz), 128.5 (d,  $J = 8.3$  Hz), 122.2 (d,  $J = 25.6$  Hz), 118.9 (q,  $J = 320.5$  Hz), 109.8 (d,  $J = 21.8$  Hz), 108.9, 22.1;  $^{19}\text{F}$  NMR (282 MHz,  $\text{CDCl}_3$ )  $\delta$  -73.0, -109.0 (ddd,  $J = 9.5, 8.0, 5.4$  Hz); IR (Neat Film, NaCl) 1598, 1573, 1516, 1416, 1209, 1136, 1114, 986, 960, 933, 875, 805, 764  $\text{cm}^{-1}$ ; HRMS (MM:ESI-APCI+)  $m/z$  calc'd for  $\text{C}_{11}\text{H}_8\text{F}_4\text{NO}_3\text{S}$   $[\text{M}+\text{H}]^+$ : 310.0156, found 310.0149.



**160c**

**5-methyl-[1,3]dioxolo[4,5-g]isoquinolin-7-yl trifluoromethanesulfonate (160c):**

Compound **160c** was prepared from ester **159c** using general procedure 2 and purified by column chromatography (10 to 20% EtOAc in hexanes) to provide a white solid (608 mg, 58% yield over 3 steps):  $^1\text{H}$  NMR (400 MHz,  $\text{CDCl}_3$ )  $\delta$  7.35 (s, 1H), 7.23 (s, 1H), 7.10 (s, 1H), 6.15 (s, 2H), 2.82 (s, 3H);  $^{13}\text{C}$  NMR (100 MHz,  $\text{CDCl}_3$ )  $\delta$  156.9, 151.9, 150.9, 149.2, 137.3, 124.8, 118.8 (q,  $J = 321.2$  Hz), 108.4, 103.3, 102.2, 101.8, 22.2;  $^{19}\text{F}$  NMR (282 MHz,  $\text{CDCl}_3$ )  $\delta$  -73.0; IR (Neat Film, NaCl) 2918, 1584, 1504, 1464, 1416, 1223, 1134, 1038, 964, 940, 873, 840  $\text{cm}^{-1}$ ; HRMS (MM:ESI-APCI+)  $m/z$  calc'd for  $\text{C}_{12}\text{H}_9\text{F}_3\text{NO}_5\text{S}$   $[\text{M}+\text{H}]^+$ : 336.0148, found 336.0146.



**160d**

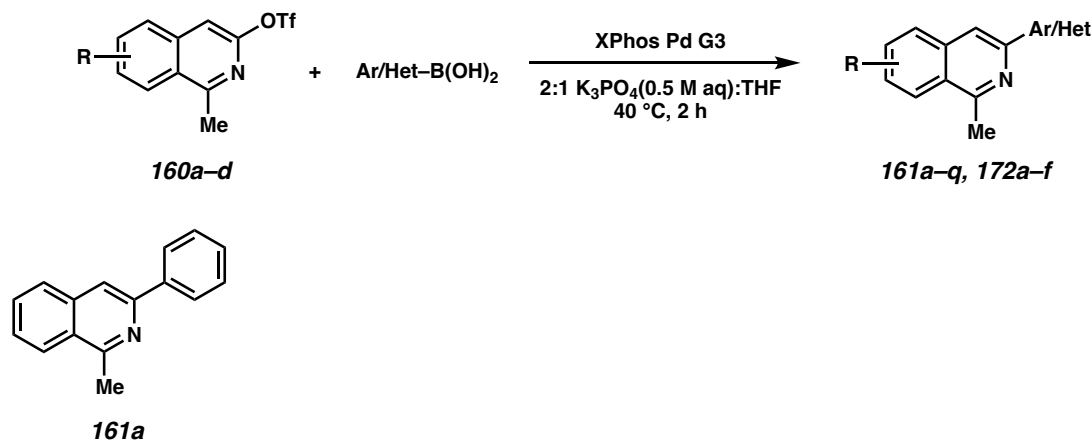
**4-methylbenzo[f]isoquinolin-2-yl trifluoromethanesulfonate (160d):**

Compound **160d** was prepared from ester **159d** using general procedure 2 and purified by column chromatography (5 to 10% EtOAc in hexanes) to provide a white solid (497 mg, 65% yield over 3 steps):  $^1\text{H}$  NMR (400 MHz,  $\text{CDCl}_3$ )  $\delta$  8.63 – 8.57 (m, 1H), 8.15 (s, 1H), 8.01 – 7.95 (m, 2H), 7.90 (d,  $J = 9.2$  Hz, 1H), 7.81 – 7.73 (m, 2H), 3.01 (s, 3H);  $^{13}\text{C}$  NMR (100 MHz,  $\text{CDCl}_3$ )  $\delta$  158.8, 152.5, 138.6, 133.3, 129.6, 129.1, 128.9, 128.6, 127.8, 125.8, 123.6, 122.2, 118.8 (q,  $J = 321.2$  Hz), 105.1, 22.4;  $^{19}\text{F}$  NMR (282 MHz,  $\text{CDCl}_3$ )  $\delta$  -78.3; IR (Neat Film,



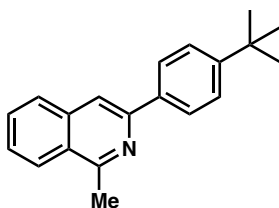
NaCl) 1588, 1416, 1377, 1207, 1180, 1138, 972, 878, 846, 817, 754  $\text{cm}^{-1}$ ; HRMS (MM:ESI-APCI+)  $m/z$  calc'd for  $\text{C}_{15}\text{H}_{11}\text{F}_3\text{NO}_3\text{S}$   $[\text{M}+\text{H}]^+$ : 342.0406, found 342.0399.

### General Procedure 3: Suzuki Cross-Coupling



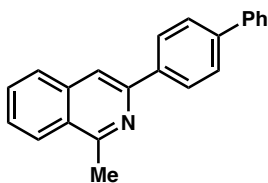
**1-methyl-3-phenylisoquinoline (161a):** This procedure has been adapted from a previous report.<sup>25</sup> To a flame-dried 20-mL scintillation vial capped with a PTFE-lined septum was added XPhos Pd G3 (11.63 mg, 0.014 mmol) and phenyl boronic acid (126 mg, 1.03 mmol). The reaction vial was then evacuated and backfilled with  $\text{N}_2$  three times. The isoquinoline triflate **160a** (200 mg, 0.687 mmol) in degassed THF (2 mL, 0.3 M) was then added to the vial, followed by degassed 0.5 M  $\text{K}_3\text{PO}_4$  solution (4 mL, 0.2 M). The reaction was then stirred at 40  $^\circ\text{C}$  for 2 hours. Afterwards, the reaction was diluted with water and the aqueous layer was extracted with  $\text{Et}_2\text{O}$ . The combined organic phases were dried over  $\text{Na}_2\text{SO}_4$ , concentrated in vacuo, and purified by column chromatography (5% EtOAc in hexanes) to afford **161a** as a white solid (138 mg, 92% yield):  $^1\text{H}$  NMR (400 MHz,  $\text{CDCl}_3$ )  $\delta$  8.15 – 8.13 (m, 3H), 7.93 (s, 1H), 7.86 (dt,  $J = 8.3, 1.0$  Hz, 1H), 7.67 (ddd,  $J = 8.2, 6.9, 1.2$  Hz, 1H), 7.57 (ddd,  $J = 8.2, 6.8, 1.3$  Hz, 1H), 7.52 – 7.48 (m, 2H), 7.42 – 7.38 (m, 1H), 3.05 (s, 3H);  $^{13}\text{C}$  NMR (100 MHz,  $\text{CDCl}_3$ )  $\delta$  158.7, 150.2, 140.0, 136.9, 130.2, 128.9,

128.4, 127.8, 127.1, 126.9, 126.7, 125.8, 115.4, 22.9; IR (Neat Film, NaCl) 3060, 1621, 1589, 1571, 1501, 1440, 1390, 1332, 1030, 902, 880, 786, 765, 692  $\text{cm}^{-1}$ ; HRMS (MM:ESI-APCI+)  $m/z$  calc'd for  $\text{C}_{16}\text{H}_{14}\text{N}$   $[\text{M}+\text{H}]^+$ : 220.1121, found 220.1129.



**161b**

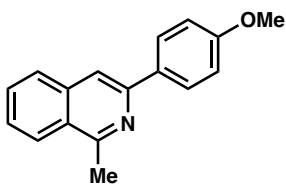
**3-(4-(*tert*-butyl)phenyl)-1-methylisoquinoline (161b):** Compound **161b** was prepared from triflate **160a** using general procedure 3 and purified by column chromatography (5% EtOAc in hexanes) to provide a pale yellow oil (177 mg, 93% yield);  $^1\text{H}$  NMR (400 MHz,  $\text{CDCl}_3$ )  $\delta$  8.12 (d,  $J = 8.4$  Hz, 1H) 8.06 (d,  $J = 8.5$  Hz, 2H), 7.90 (s, 1H), 7.85 (d,  $J = 8.2$  Hz, 1H), 7.66 (ddd,  $J = 8.1, 6.8, 1.2$  Hz, 1H), 7.57 – 7.52 (m, 3H), 3.04 (s, 3H), 1.38 (s, 9H);  $^{13}\text{C}$  NMR (100 MHz,  $\text{CDCl}_3$ )  $\delta$  158.6, 151.5, 150.3, 137.3, 136.9, 130.1, 127.7, 126.8, 126.7, 126.6, 125.8, 125.8, 115.0, 34.8, 31.5, 22.8; IR (Neat Film, NaCl) 2961, 1622, 1591, 1568, 1515, 1442, 1390, 1362, 1333, 1268, 1112, 1017, 837, 754, 743, 685  $\text{cm}^{-1}$ ; HRMS (MM:ESI-APCI+)  $m/z$  calc'd for  $\text{C}_{20}\text{H}_{22}\text{N}$   $[\text{M}+\text{H}]^+$ : 276.1747, found 276.1749.



**161c**

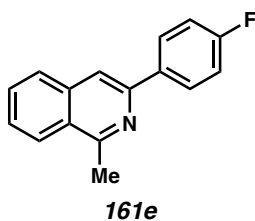
**3-([1,1'-biphenyl]-4-yl)-1-methylisoquinoline (161c):** Compound **161c** was prepared from triflate **160a** using general procedure 3 and purified by column chromatography (5% EtOAc in hexanes) to provide a colorless solid (191 mg, 94% yield);  $^1\text{H}$  NMR (400 MHz,

CDCl<sub>3</sub>) δ 8.24 – 8.22 (m, 2H), 8.14 (d, *J* = 8.4 Hz, 1H), 7.98 (s, 1H), 7.88 (d, *J* = 8.1 Hz, 1H), 7.75 – 7.73 (m, 2H), 7.70 – 7.67 (m, 3H), 7.58 (ddd, *J* = 8.3, 6.9, 1.3 Hz, 1H), 7.50 – 7.46 (m, 2H), 7.39 – 7.37 (m, 1H), 3.06 (s, 3H); <sup>13</sup>C NMR (100 MHz, CDCl<sub>3</sub>) δ 158.8, 149.7, 141.2, 141.0, 138.9, 136.9, 130.2, 128.9, 127.8, 127.6, 127.5, 127.5, 127.2, 126.9, 126.8, 125.8, 115.2, 22.9; IR (Neat Film, NaCl) 3028, 1621, 1568, 1488, 1440, 1389, 1334, 842, 766, 730, 696 cm<sup>-1</sup>; HRMS (MM:ESI-APCI+) *m/z* calc'd for C<sub>22</sub>H<sub>18</sub>N [M+H]<sup>+</sup>: 296.1434, found 296.1426.

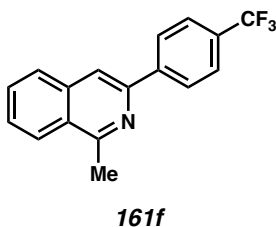


**161d**

**3-(4-methoxyphenyl)-1-methylisoquinoline (161d):** Compound **161d** was prepared from triflate **160a** using general procedure 3 and purified by column chromatography (5% EtOAc in hexanes) to afford a white solid (79 mg, 93% yield): <sup>1</sup>H NMR (400 MHz, CDCl<sub>3</sub>) δ 8.14 – 8.07 (m, 3H), 7.84 (s, 1H), 7.81 (d, *J* = 8.5, 1H), 7.64 (ddd, *J* = 8.2, 6.8, 1.2 Hz, 1H), 7.53 (ddd, *J* = 8.2, 6.8, 1.3 Hz, 1H), 7.06 – 7.01 (m, 2H), 3.88 (s, 3H), 3.03 (s, 3H); <sup>13</sup>C NMR (100 MHz, CDCl<sub>3</sub>) δ 160.0, 158.4, 149.8, 136.9, 132.6, 130.0, 128.2, 127.5, 126.4, 126.3, 125.7, 114.1, 114.1, 55.4, 22.7; IR (Neat Film, NaCl) 3060, 2955, 2835, 1608, 1568, 1514, 1439, 1390, 1290, 1249, 1174, 1034, 833, 751, 730 cm<sup>-1</sup>; HRMS (MM:ESI-APCI+) *m/z* calc'd for C<sub>17</sub>H<sub>16</sub>NO [M+H]<sup>+</sup>: 250.1226, found 250.1220.

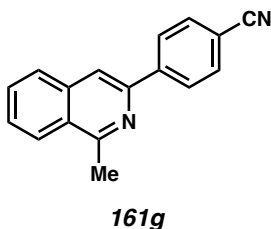


**3-(4-fluorophenyl)-1-methylisoquinoline (161e):** Compound **161e** was prepared from triflate **160a** using general procedure 3 and purified by column chromatography (10% EtOAc in hexanes) to provide a white solid (155 mg, 95% yield);  $^1\text{H}$  NMR (400 MHz,  $\text{CDCl}_3$ )  $\delta$  8.17 – 8.07 (m, 3H), 7.89 – 7.81 (m, 2H), 7.68 (ddd,  $J = 8.2, 6.9, 1.2$  Hz, 1H), 7.58 (ddd,  $J = 8.2, 6.8, 1.3$  Hz, 1H), 7.20 – 7.16 (m, 2H), 3.04 (s, 3H);  $^{13}\text{C}$  NMR (100 MHz,  $\text{CDCl}_3$ )  $\delta$  163.3 (d,  $J = 247.3$  Hz), 162.1, 158.8, 149.1, 136.9, 136.0 (d,  $J = 3.3$  Hz), 130.3, 128.8 (d,  $J = 8.2$  Hz), 127.7, 127.0, 126.6, 125.8, 115.8, 115.6, 115.1, 22.8;  $^{19}\text{F}$  NMR (282 MHz,  $\text{CDCl}_3$ )  $\delta$  -114.2; IR (Neat Film, NaCl) 1605, 1570, 1510, 1440, 1390, 1332, 1231, 1156, 836, 749, 723  $\text{cm}^{-1}$ ; HRMS (MM:ESI-APCI+)  $m/z$  calc'd for  $\text{C}_{16}\text{H}_{13}\text{FN}$   $[\text{M}+\text{H}]^+$ : 238.1027, found 238.1030.

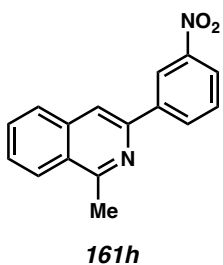


**1-methyl-3-(4-(trifluoromethyl)phenyl)isoquinoline (161f):** Compound **161f** was prepared from triflate **160a** using general procedure 3 and purified by column chromatography (2% to 3% EtOAc in hexanes) to afford a white solid (89 mg, 91% yield):  $^1\text{H}$  NMR (400 MHz,  $\text{CDCl}_3$ )  $\delta$  8.26 (d,  $J = 8.1$  Hz, 2H), 8.15 (d,  $J = 8.4$ , 1H), 7.96 (s, 1H), 7.88 (d,  $J = 8.2$  Hz, 1H), 7.78 – 7.73 (m, 2H), 7.73 – 7.67 (m, 1H), 7.63 – 7.59 (m, 1H), 3.05 (s, 3H);  $^{13}\text{C}$  NMR (100 MHz,  $\text{CDCl}_3$ )  $\delta$  159.1, 148.5, 143.3, 136.7, 130.4, 130.2 (q,  $J$

= 32.5 Hz), 127.9, 127.5, 127.3, 127.1, 125.8, 125.7 (q,  $J = 3.8$  Hz), 124.4 (q,  $J = 271.9$  Hz), 116.1, 22.8;  $^{19}\text{F}$  NMR (282 MHz,  $\text{CDCl}_3$ )  $\delta$  -62.4; IR (Neat Film, NaCl) 3070, 2357, 1622, 1573, 1418, 1390, 1324, 1162, 1122, 1066, 1015, 842, 754, 742, 682  $\text{cm}^{-1}$ ; HRMS (MM:ESI-APCI+)  $m/z$  calc'd for  $\text{C}_{17}\text{H}_{13}\text{F}_3\text{N}$   $[\text{M}+\text{H}]^+$ : 288.0995, found 288.0988.

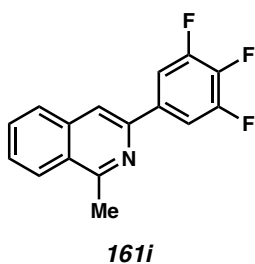


**4-(1-methylisoquinolin-3-yl)benzonitrile (161g):** Compound **161g** was prepared from triflate **160a** using general procedure 3 and purified by column chromatography (10% to 20% EtOAc in hexanes) to provide a white solid (144 mg, 86% yield);  $^1\text{H}$  NMR (400 MHz,  $\text{CDCl}_3$ )  $\delta$  8.38 – 8.22 (m, 2H), 8.16 (d,  $J = 8.3$  Hz, 1H), 7.99 (s, 1H), 7.89 (d,  $J = 8.3$ , 1H), 7.82 – 7.75 (m, 2H), 7.73 (ddd,  $J = 8.1, 6.9, 1.2$  Hz, 1H), 7.64 (ddd,  $J = 8.2, 6.9, 1.3$  Hz, 1H), 3.05 (s, 3H);  $^{13}\text{C}$  NMR (100 MHz,  $\text{CDCl}_3$ )  $\delta$  159.3, 147.6, 144.0, 136.6, 132.7, 130.7, 128.0, 127.9, 127.6, 127.3, 125.9, 119.3, 116.6, 111.8, 22.8; IR (Neat Film, NaCl) 2224, 1618, 1570, 1508, 1441, 1390, 1334, 878, 844, 748, 731  $\text{cm}^{-1}$ ; HRMS (MM:ESI-APCI+)  $m/z$  calc'd for  $\text{C}_{17}\text{H}_{13}\text{N}_2$   $[\text{M}+\text{H}]^+$ : 245.1073, found 245.1070.

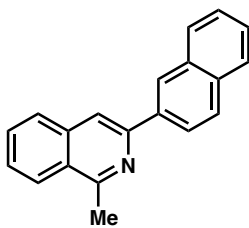


**1-methyl-3-(3-nitrophenyl)isoquinoline (161h):** Compound **161h** was prepared from triflate **160a** using general procedure 3 and purified by column chromatography (10%

EtOAc in hexanes) to provide a white solid (139 mg, 77% yield);  $^1\text{H}$  NMR (400 MHz,  $\text{CDCl}_3$ )  $\delta$  9.01 (t,  $J = 2.0$  Hz, 1H), 8.51 (ddd,  $J = 7.8, 1.8, 1.1$  Hz, 1H), 8.24 (ddd,  $J = 8.2, 2.3, 1.1$  Hz, 1H), 8.16 (dd,  $J = 8.3, 1.0$  Hz, 1H), 8.01 (s, 1H), 7.90 (dd,  $J = 8.1, 0.7$  Hz, 1H), 7.72 (ddd,  $J = 8.1, 6.9, 1.2$  Hz, 1H), 7.72 – 7.59 (m, 2H), 3.05 (s, 3H);  $^{13}\text{C}$  NMR (100 MHz,  $\text{CDCl}_3$ )  $\delta$  159.3, 149.0, 147.3, 141.7, 136.6, 132.8, 130.6, 129.7, 127.9, 127.8, 127.2, 125.9, 123.0, 121.9, 116.0, 22.8; IR (Neat Film, NaCl) 1619, 1568, 1524, 1442, 1390, 1350, 880, 806, 749, 692  $\text{cm}^{-1}$ ; HRMS (MM:ESI-APCI+)  $m/z$  calc'd for  $\text{C}_{16}\text{H}_{13}\text{N}_2\text{O}_2$   $[\text{M}+\text{H}]^+$ : 265.0972, found 265.0974.

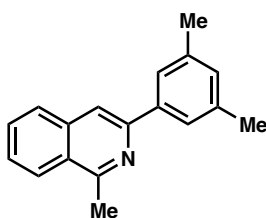


**1-methyl-3-(3,4,5-trifluorophenyl)isoquinoline (161i):** Compound **161i** was prepared from triflate **160a** using general procedure 3 and purified by column chromatography (5% EtOAc in hexanes) to afford a white solid (103 mg, 87% yield):  $^1\text{H}$  NMR (400 MHz,  $\text{CDCl}_3$ )  $\delta$  8.13 (d,  $J = 8.4$ , 1H), 7.86 – 7.78 (m, 4H), 7.72 – 7.68 (m, 1H), 7.65 – 7.58 (m, 1H), 3.02 (s, 3H);  $^{13}\text{C}$  NMR (100 MHz,  $\text{CDCl}_3$ )  $\delta$  159.1, 151.6 (ddd,  $J = 248.4, 10.1, 4.1$  Hz), 146.5, 140.0 (dt,  $J = 252.6, 15.7$  Hz), 136.6, 136.0 (td,  $J = 7.5, 4.5$  Hz), 130.6, 127.8, 127.7, 127.1, 125.8, 115.4, 110.9 – 110.7 (m), 22.7;  $^{19}\text{F}$  NMR (282 MHz,  $\text{CDCl}_3$ )  $\delta$  –134.4 (dd,  $J = 20.5, 9.2$  Hz), –161.1 – –161.3 (m); IR (Neat Film, NaCl) 1619, 1570, 1526, 1446, 1392, 1352, 1237, 1034, 879, 847, 753  $\text{cm}^{-1}$ ; HRMS (MM:ESI-APCI+)  $m/z$  calc'd for  $\text{C}_{16}\text{H}_{11}\text{F}_3\text{N}$   $[\text{M}+\text{H}]^+$ : 274.0838, found 274.0841.



**161j**

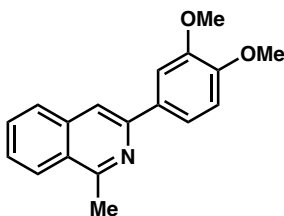
**1-methyl-3-(naphthalen-2-yl)isoquinoline (161j):** Compound **161j** was prepared from triflate **160a** using general procedure 3 and purified by column chromatography (5% EtOAc in hexanes) to provide a white solid (159 mg, 86% yield);  $^1\text{H}$  NMR (400 MHz,  $\text{CDCl}_3$ )  $\delta$  8.68 (s, 1H), 8.27 (dd,  $J = 8.6, 1.8$  Hz, 1H), 8.16 (dq,  $J = 8.3, 1.0$  Hz, 1H), 8.07 (s, 1H), 8.00 – 7.96 (m, 2H), 7.91 – 7.86 (m, 2H), 7.70 (ddd,  $J = 8.2, 6.8, 1.2$  Hz, 1H), 7.59 (ddd,  $J = 8.2, 6.8, 1.3$  Hz, 1H), 7.56 – 7.46 (m, 2H), 3.09 (s, 3H);  $^{13}\text{C}$  NMR (100 MHz,  $\text{CDCl}_3$ )  $\delta$  158.9, 149.9, 137.2, 137.0, 133.9, 133.5, 130.2, 128.9, 128.5, 127.8, 127.8, 127.0, 126.8, 126.3, 126.3, 125.8, 124.9, 115.7, 22.9; IR (Neat Film, NaCl) 3059, 1621, 1585, 1567, 1508, 1439, 1390, 879, 848, 816, 744  $\text{cm}^{-1}$ ; HRMS (MM:ESI-APCI+)  $m/z$  calc'd for  $\text{C}_{20}\text{H}_{16}\text{N}$   $[\text{M}+\text{H}]^+$ : 270.1277, found 270.1270.



**161k**

**3-(3,5-dimethylphenyl)-1-methylisoquinoline (161k):** Compound **161k** was prepared from triflate **160a** using general procedure 3 and purified by column chromatography to provide a white solid (156 mg, 92% yield);  $^1\text{H}$  NMR (400 MHz,  $\text{CDCl}_3$ )  $\delta$  8.13 (dd,  $J = 8.4, 1.1$  Hz, 1H), 7.90 (s, 1H), 7.85 (dd,  $J = 8.2, 0.7$  Hz, 1H), 7.75 (s, 2H), 7.66 (ddd,  $J =$

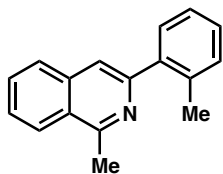
8.2, 6.8, 1.2 Hz, 1H), 7.56 (ddd,  $J = 8.2, 6.9, 1.3$  Hz, 1H), 7.05 (s, 1H), 3.05 (s, 3H), 2.43 (s, 6H);  $^{13}\text{C}$  NMR (100 MHz,  $\text{CDCl}_3$ )  $\delta$  158.6, 150.5, 139.9, 138.3, 136.9, 130.2, 130.1, 127.7, 126.8, 126.7, 125.8, 125.0, 115.4, 22.8, 21.7; IR (Neat Film, NaCl) 2919, 2358, 1622, 1582, 1568, 1443, 1391, 1335, 874, 846, 786, 750, 711  $\text{cm}^{-1}$ ; HRMS (MM:ESI-APCI+)  $m/z$  calc'd for  $\text{C}_{18}\text{H}_{18}\text{N}$   $[\text{M}+\text{H}]^+$ : 248.1434, found 248.1434.



**161I**

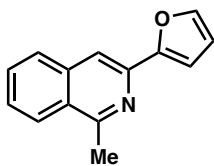
**3-(3,4-dimethoxyphenyl)-1-methylisoquinoline (161I):** Compound **161I** was prepared from triflate **160a** using general procedure 3 and purified by column chromatography (20% EtOAc in hexanes) to provide a white solid (195 mg, 99% yield);  $^1\text{H}$  NMR (400 MHz,  $\text{CDCl}_3$ )  $\delta$  8.11 (d,  $J = 8.4$ , 1H), 7.89 – 7.81 (m, 2H), 7.77 (d,  $J = 2.1$  Hz, 1H), 7.71 – 7.61 (m, 2H), 7.55 (ddd,  $J = 8.3, 6.9, 1.3$  Hz, 1H), 6.99 (d,  $J = 8.4$  Hz, 1H), 4.04 (s, 3H), 3.95 (s, 3H), 3.04 (s, 3H);  $^{13}\text{C}$  NMR (100 MHz,  $\text{CDCl}_3$ )  $\delta$  158.6, 149.8, 149.6, 149.3, 137.0, 132.9, 130.2, 127.6, 126.7, 126.5, 125.8, 119.5, 114.5, 111.4, 110.3, 56.1, 22.8; IR (Neat Film, NaCl) 2936, 2833, 1568, 1516, 1454, 1436, 1317, 1259, 1236, 1170, 1026, 874, 817, 751  $\text{cm}^{-1}$ ; HRMS (MM:ESI-APCI+)  $m/z$  calc'd for  $\text{C}_{18}\text{H}_{18}\text{NO}_2$   $[\text{M}+\text{H}]^+$ : 280.1332, found 280.1337.





**161m**

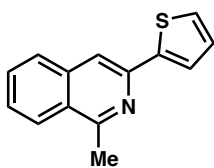
**1-methyl-3-(*o*-tolyl)isoquinoline (161m):** Compound **161m** was prepared from triflate **160a** using general procedure 3 and purified by column chromatography (10% EtOAc in hexanes) to provide a white solid (153 mg, 96% yield);  $^1\text{H}$  NMR (400 MHz,  $\text{CDCl}_3$ )  $\delta$  8.17 (d,  $J = 8.4$ , 1H), 7.84 (d,  $J = 8.3$ , 1H), 7.70 (ddd,  $J = 8.2$ , 6.8, 1.3 Hz, 1H), 7.65 – 7.57 (m, 2H), 7.53 – 7.45 (m, 1H), 7.32 – 7.30 (m, 3H), 3.04 (s, 3H), 2.43 (s, 3H);  $^{13}\text{C}$  NMR (100 MHz,  $\text{CDCl}_3$ )  $\delta$  158.1, 152.7, 140.9, 136.5, 136.3, 130.9, 130.1, 130.1, 128.1, 127.5, 127.0, 126.2, 126.0, 125.7, 118.9, 22.6, 20.6; IR (Neat Film, NaCl) 3053, 2950, 2920, 2355, 1622, 1584, 1567, 1498, 1446, 1392, 1360, 1330, 1144, 1033, 969, 906, 884, 763, 752, 726  $\text{cm}^{-1}$ ; HRMS (MM:ESI-APCI+)  $m/z$  calc'd for  $\text{C}_{17}\text{H}_{16}\text{N}$   $[\text{M}+\text{H}]^+$ : 234.1277, found 234.1286.



**161n**

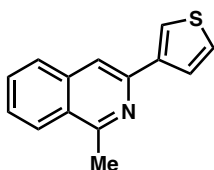
**3-(furan-2-yl)-1-methylisoquinoline (161n):** Compound **161n** was prepared from triflate **160a** using general procedure 3 and purified by column chromatography (5% EtOAc in hexanes) to provide a white solid (106 mg, 99% yield):  $^1\text{H}$  NMR (400 MHz,  $\text{CDCl}_3$ )  $\delta$  8.06 (d,  $J = 8.4$  Hz, 1H), 7.86 (s, 1H), 7.80 (dd,  $J = 8.4$  Hz, 1H), 7.67 – 7.59 (m, 1H), 7.57 – 7.49 (m, 2H), 7.13 (dd,  $J = 3.4$ , 0.8 Hz, 1H), 6.56 (dd,  $J = 3.4$ , 1.8 Hz, 1H), 2.99 (s, 3H);  $^{13}\text{C}$  NMR (100 MHz,  $\text{CDCl}_3$ )  $\delta$  159.0, 154.4, 142.9, 142.3, 136.5, 130.2, 127.6, 126.7, 126.6, 125.8, 113.0, 112.0, 108.1, 22.6; IR (Neat Film, NaCl) 3067, 1622, 1568, 1488,

1447, 1390, 1325, 1288, 1216, 1157, 1007, 970, 883, 814, 736  $\text{cm}^{-1}$ ; HRMS (MM:ESI-APCI+)  $m/z$  calc'd for  $\text{C}_{14}\text{H}_{12}\text{NO}$   $[\text{M}+\text{H}]^+$ : 210.0913, found 210.0910.



**161o**

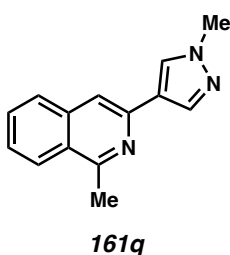
**1-methyl-3-(thiophen-2-yl)isoquinoline (161o):** Compound **161o** was prepared from triflate **160a** using general procedure 3 and purified by column chromatography (3% EtOAc in hexanes) to provide a white solid (103 mg, 92% yield):  $^1\text{H}$  NMR (400 MHz,  $\text{CDCl}_3$ )  $\delta$  8.07 (dt,  $J = 8.4$  Hz, 1H), 7.82 (s, 1H), 7.79 (dd,  $J = 8.2$  Hz, 1H), 7.69 (dd,  $J = 3.6, 1.1$  Hz, 1H), 7.64 (ddd,  $J = 8.1, 6.8, 1.2$  Hz, 1H), 7.52 (ddd,  $J = 8.2, 6.8, 1.2$  Hz, 1H), 7.38 (dd,  $J = 5.1, 1.1$  Hz, 1H), 7.14 (dd,  $J = 5.0, 3.6$  Hz, 1H), 2.99 (s, 3H);  $^{13}\text{C}$  NMR (100 MHz,  $\text{CDCl}_3$ )  $\delta$  158.8, 145.5, 145.4, 136.6, 130.2, 128.1, 127.4, 126.7, 126.6, 125.8, 123.8, 113.1, 22.5; IR (Neat Film, NaCl) 3068, 1620, 1586, 1568, 1446, 1387, 1330, 1238, 1194, 1036, 876, 820, 748, 704  $\text{cm}^{-1}$ ; HRMS (MM:ESI-APCI+)  $m/z$  calc'd for  $\text{C}_{14}\text{H}_{12}\text{NS}$   $[\text{M}+\text{H}]^+$ : 226.0685, found 226.0680.



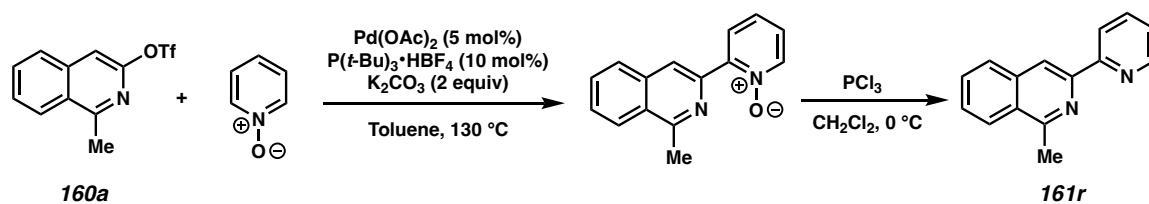
**161p**

**1-methyl-3-(thiophen-3-yl)isoquinoline (161p):** Compound **161p** was prepared from triflate **160a** using general procedure 3 and purified by column chromatography (5% EtOAc in hexanes) to provide a white solid (148 mg, 95% yield);  $^1\text{H}$  NMR (400 MHz,  $\text{CDCl}_3$ )  $\delta$  8.10 (dd,  $J = 8.4, 1.0$  Hz, 1H), 8.04 (dd,  $J = 3.1, 1.3$  Hz, 1H), 7.81 (dt,  $J = 8.2,$

0.9 Hz, 1H), 7.79 (s, 1H), 7.73 (dd,  $J = 5.0, 1.3$  Hz, 1H), 7.65 (ddd,  $J = 8.2, 6.8, 1.2$  Hz, 1H), 7.54 (ddd,  $J = 8.3, 6.9, 1.3$  Hz, 1H), 7.42 (dd,  $J = 5.0, 3.1$  Hz, 1H), 3.01 (s, 3H);  $^{13}\text{C}$  NMR (100 MHz,  $\text{CDCl}_3$ )  $\delta$  158.8, 146.4, 142.7, 136.9, 130.2, 127.6, 126.7, 126.6, 126.3, 126.2, 125.8, 123.2, 114.7, 22.8; IR (Neat Film, NaCl) 3056, 2920, 1622, 1591, 1568, 1496, 1446, 1388, 1317, 874, 842, 795, 749, 696  $\text{cm}^{-1}$ ; HRMS (MM:ESI-APCI+)  $m/z$  calc'd for  $\text{C}_{14}\text{H}_{12}\text{NS}$   $[\text{M}+\text{H}]^+$ : 226.0685, found 226.0687.

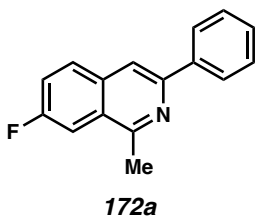


**1-methyl-3-(1-methyl-1H-pyrazol-4-yl)isoquinoline (161q):** Compound **161q** was prepared from triflate **160a** using general procedure 3 and purified by column chromatography (50% to 60% EtOAc in hexanes) to provide a white solid (112 mg, 99% yield):  $^1\text{H}$  NMR (400 MHz,  $\text{CDCl}_3$ )  $\delta$  8.07 (d,  $J = 8.4$  Hz, 1H), 8.04 – 8.00 (m, 2H), 7.77 (dd,  $J = 8.2, 1.1$  Hz, 1H), 7.67 – 7.60 (m, 2H), 7.54 – 7.47 (m, 1H), 3.98 (s, 3H), 2.97 (s, 3H);  $^{13}\text{C}$  NMR (100 MHz,  $\text{CDCl}_3$ )  $\delta$  158.8, 137.4, 136.8, 130.1, 128.9, 127.1, 126.2, 126.1, 125.7, 113.3, 39.1, 22.6; IR (Neat Film, NaCl) 2940, 2351, 1620, 1601, 1568, 1556, 1493, 1416, 1182, 983, 840, 750, 702  $\text{cm}^{-1}$ ; HRMS (MM:ESI-APCI+)  $m/z$  calc'd for  $\text{C}_{14}\text{H}_{14}\text{N}_3$   $[\text{M}+\text{H}]^+$ : 224.1182, found 224.1176.

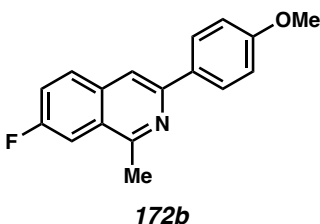


**1-methyl-3-(pyridin-2-yl)isoquinoline (161r):** Compound **161r** was prepared from triflate **160a** using a procedure adapted from a previous report.<sup>6</sup> To a microwave vial was added flame-dried  $\text{K}_2\text{CO}_3$  (142 mg, 1.03 mmol),  $\text{Pd}(\text{OAc})_2$  (5.8 mg, 0.026 mmol),  $\text{P}(t\text{-Bu})_3 \cdot \text{HBF}_4$  (15 mg, 0.052 mmol), and the *N*-oxide (147 mg, 1.55 mmol). The vial was then evacuated and backfilled with argon three times. A solution of **160a** (150 mg, 0.52 mmol) in toluene (2 mL, 0.3 M) was then added, and the reaction was stirred at 130 °C overnight. The reaction was then cooled to room temperature, filtered through celite, and dissolved in  $\text{CH}_2\text{Cl}_2$  (10 mL, 0.05 M). The reaction flask was then cooled to 0 °C and  $\text{PCl}_3$  (0.27 mL, 3.1 mmol) was added dropwise, then the reaction stirred for 30 minutes at 0 °C. The reaction was then quenched with saturated aqueous  $\text{K}_2\text{CO}_3$ , extracted with EtOAc, and dried over  $\text{Na}_2\text{SO}_4$ . The crude product was purified by column chromatography (30% EtOAc in hexanes + 1%  $\text{NEt}_3$ ) to provide a pale yellow solid (56 mg, 50% yield over 2 steps);  $^1\text{H NMR}$  (400 MHz,  $\text{CDCl}_3$ )  $\delta$  8.72 (dd,  $J = 4.8, 1.9$  Hz, 1H), 8.62 (s, 1H), 8.56 (dd,  $J = 8.0, 1.1$  Hz, 1H), 8.14 (dd,  $J = 8.3, 1.0$  Hz, 1H), 7.95 (dt,  $J = 8.2, 1.0$  Hz, 1H), 7.84 (td,  $J = 7.7, 1.8$  Hz, 1H), 7.68 (ddd,  $J = 8.1, 6.8, 1.2$  Hz, 1H), 7.60 (ddd,  $J = 8.2, 6.9, 1.4$  Hz, 1H), 7.29 (ddd,  $J = 7.5, 4.8, 1.2$  Hz, 1H), 3.05 (s, 3H);  $^{13}\text{C NMR}$  (100 MHz,  $\text{CDCl}_3$ )  $\delta$  158.5, 156.9, 149.4, 148.7, 137.1, 136.9, 130.2, 128.6, 127.7, 127.5, 125.8, 123.3, 121.4, 116.5, 22.9; IR (Neat Film, NaCl) 3053, 3004, 2916, 1621, 1580, 1568, 1474, 1443, 1426,

1391, 1335, 1142, 891, 796, 742, 681, 624  $\text{cm}^{-1}$ ; HRMS (MM:ESI-APCI+)  $m/z$  calc'd for  $\text{C}_{15}\text{H}_{13}\text{N}_2$   $[\text{M}+\text{H}]^+$ : 221.1073, found 221.1076.

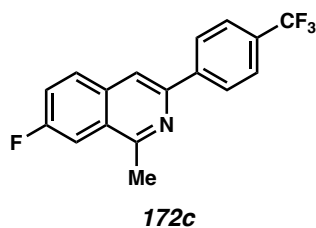


**7-fluoro-1-methyl-3-phenylisoquinoline (172a):** Compound **172a** was prepared from triflate **160b** using general procedure 3 and purified by column chromatography (5% EtOAc in hexanes) to provide a white solid (110 mg, 93% yield):  $^1\text{H}$  NMR (400 MHz,  $\text{CDCl}_3$ )  $\delta$  8.14 – 8.11 (m, 2H), 7.90 (s, 1H), 7.85 (dd,  $J = 9.2, 5.7$  Hz, 1H), 7.73 – 7.68 (m, 1H), 7.54 – 7.48 (m, 2H), 7.48 – 7.38 (m, 2H), 2.99 (s, 3H);  $^{13}\text{C}$  NMR (100 MHz,  $\text{CDCl}_3$ )  $\delta$  160.7 (d,  $J = 248.3$  Hz), 158.0 (d,  $J = 5.8$  Hz), 149.8 (d,  $J = 2.8$  Hz), 139.7, 133.9, 130.3 (d,  $J = 8.5$  Hz), 128.9, 128.5, 127.3 (d,  $J = 7.8$  Hz), 127.0, 120.6 (d,  $J = 25.3$  Hz), 114.9 (d,  $J = 1.7$  Hz), 109.4 (d,  $J = 21.0$  Hz), 22.8;  $^{19}\text{F}$  NMR (282 MHz,  $\text{CDCl}_3$ )  $\delta$  -109.7 – -111.8 (m); IR (Neat Film, NaCl) 3031, 2358, 1576, 1506, 1446, 1393, 1372, 1313, 1230, 1183, 1028, 972, 922, 904, 881, 822, 777, 764, 704  $\text{cm}^{-1}$ ; HRMS (MM:ESI-APCI+)  $m/z$  calc'd for  $\text{C}_{16}\text{H}_{13}\text{FN}$   $[\text{M}+\text{H}]^+$ : 238.1027, found 238.1027.

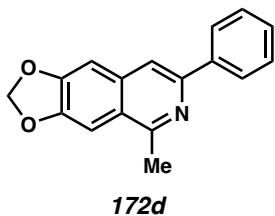


**7-fluoro-3-(4-methoxyphenyl)-1-methylisoquinoline (172b):** Compound **172b** was prepared from triflate **160b** using general procedure 3 and purified by column chromatography (5% EtOAc in hexanes) to provide a white solid (110 mg, 99% yield):  $^1\text{H}$

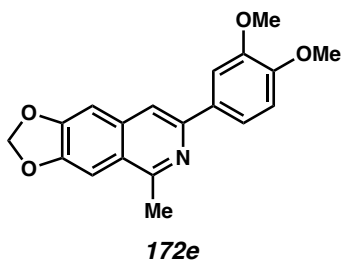
NMR (400 MHz, CDCl<sub>3</sub>)  $\delta$  8.10 – 8.04 (m, 2H), 7.87 – 7.81 (m, 2H), 7.70 (dd,  $J = 9.9, 2.6$  Hz, 1H), 7.44 (ddd,  $J = 9.0, 8.3, 2.5$  Hz, 1H), 7.06 – 6.99 (m, 2H), 3.88 (s, 3H), 2.98 (s, 3H); <sup>13</sup>C NMR (100 MHz, CDCl<sub>3</sub>)  $\delta$  160.4 (d,  $J = 248.5$  Hz), 160.1, 157.7 (d,  $J = 5.7$  Hz), 149.4 (d,  $J = 2.8$  Hz), 133.9, 132.2, 130.0 (d,  $J = 8.5$  Hz), 128.1, 126.7 (d,  $J = 7.7$  Hz), 120.5 (d,  $J = 25.3$  Hz), 114.2, 113.7 (d,  $J = 1.8$  Hz), 109.3 (d,  $J = 20.9$  Hz), 55.4, 22.7; <sup>19</sup>F NMR (282 MHz, CDCl<sub>3</sub>)  $\delta$  –111.9 (ddd,  $J = 9.3, 9.1, 5.7$  Hz); IR (Neat Film, NaCl) 1608, 1514, 1443, 1393, 1288, 1252, 1186, 1029, 878, 863, 836, 821 cm<sup>-1</sup>; HRMS (MM:ESI-APCI+)  $m/z$  calc'd for C<sub>17</sub>H<sub>15</sub>FNO [M+H]<sup>+</sup>: 268.1132, found 268.1133.



**7-fluoro-1-methyl-3-(4-(trifluoromethyl)phenyl)isoquinoline (172c):** Compound **172c** was prepared from triflate **160b** using general procedure 3 and purified by column chromatography (5% EtOAc in hexanes) to provide a white solid (150 mg, 98% yield): <sup>1</sup>H NMR (400 MHz, CDCl<sub>3</sub>)  $\delta$  8.22 (d,  $J = 8.0$  Hz, 2H), 7.94 (s, 1H), 7.90 – 7.85 (m, 1H), 7.74 (d,  $J = 8.0$  Hz, 2H), 7.71 – 7.69 (m, 1H), 7.53 – 7.43 (m, 1H), 2.99 (s, 3H); <sup>13</sup>C NMR (100 MHz, CDCl<sub>3</sub>)  $\delta$  161.1 (d,  $J = 249.4$  Hz), 158.4 (d,  $J = 6.2$  Hz), 148.1, 143.0, 133.7, 130.4 (d,  $J = 8.5$  Hz), 130.2 (q,  $J = 32.4$  Hz), 127.8 (d,  $J = 8.1$  Hz), 127.2, 125.8 (q,  $J = 3.8$  Hz), 124.5 (q,  $J = 272.7$  Hz), 120.9 (d,  $J = 24.9$  Hz), 115.6, 109.5 (d,  $J = 21.4$  Hz), 22.8; <sup>19</sup>F NMR (282 MHz, CDCl<sub>3</sub>)  $\delta$  –62.5, –110.2 (ddd,  $J = 9.9, 8.2, 5.5$  Hz); IR (Neat Film, NaCl) 1592, 1418, 1393, 1330, 1157, 1126, 1107, 1067, 880, 868, 847, 816 cm<sup>-1</sup>; HRMS (MM:ESI-APCI+)  $m/z$  calc'd for C<sub>17</sub>H<sub>12</sub>NF<sub>4</sub> [M+H]<sup>+</sup>: 306.0900, found 306.0895.

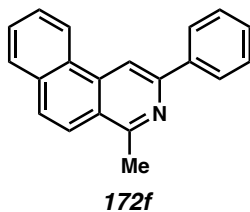


**5-methyl-7-phenyl-[1,3]dioxolo[4,5-g]isoquinoline (172d):** Compound **172d** was prepared from triflate **160c** using general procedure 3 and purified by column chromatography (10% EtOAc in hexanes) to provide a white solid (153 mg, 97% yield):  $^1\text{H}$  NMR (400 MHz,  $\text{CDCl}_3$ )  $\delta$  8.08 (d,  $J = 7.2$  Hz, 2H), 7.77 (s, 1H), 7.52 – 7.44 (m, 2H), 7.41 – 7.32 (m, 2H), 7.11 (s, 1H), 6.10 (s, 2H), 2.92 (s, 3H);  $^{13}\text{C}$  NMR (100 MHz,  $\text{CDCl}_3$ )  $\delta$  156.4, 150.5, 149.5, 148.1, 140.0, 135.1, 128.7, 128.1, 126.8, 123.5, 115.1, 103.4, 101.9, 101.6, 23.0; IR (Neat Film, NaCl) 2914, 1591, 1486, 1462, 1232, 1189, 1039, 945, 878, 846, 695, 684  $\text{cm}^{-1}$ ; HRMS (MM:ESI-APCI+)  $m/z$  calc'd for  $\text{C}_{17}\text{H}_{14}\text{NO}_2$   $[\text{M}+\text{H}]^+$ : 264.1019, found 264.1021.



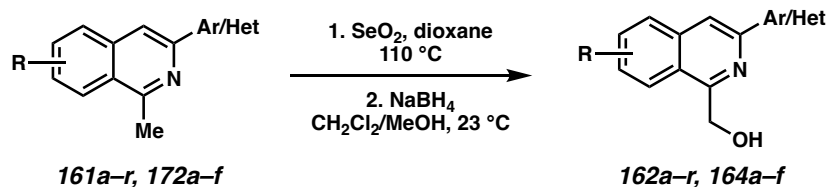
**7-(3,4-dimethoxyphenyl)-5-methyl-[1,3]dioxolo[4,5-g]isoquinoline (172e):** Compound **172e** was prepared from triflate **160c** using general procedure 3 at 65 °C and purified by column chromatography via dry loading (40% EtOAc in hexanes) to provide a white solid (202 mg, 82% yield);  $^1\text{H}$  NMR (400 MHz,  $\text{CDCl}_3$ )  $\delta$  7.72 (d,  $J = 2.1$  Hz, 1H), 7.69 (s, 1H), 7.60 (dd,  $J = 8.3, 2.0$  Hz, 1H), 7.34 (s, 1H), 7.09 (s, 1H), 6.96 (d,  $J = 8.4$  Hz, 1H), 6.09 (s, 2H), 4.02 (s, 3H), 3.94 (s, 3H), 2.91 (s, 3H);  $^{13}\text{C}$  NMR (100 MHz,  $\text{CDCl}_3$ )  $\delta$  156.2, 150.5,

149.3, 149.2, 147.9, 135.2, 134.3, 133.0, 123.2, 119.1, 114.3, 111.2, 110.0, 103.3, 101.8, 101.5, 56.0, 56.0, 23.0; IR (Neat Film, NaCl) 2935, 1591, 1517, 1462, 1267, 1230, 1165, 1143, 1024, 872, 731  $\text{cm}^{-1}$ ; HRMS (MM:ESI-APCI+)  $m/z$  calc'd for  $\text{C}_{19}\text{H}_{18}\text{NO}_4$   $[\text{M}+\text{H}]^+$ : 324.1230, found 324.1229.

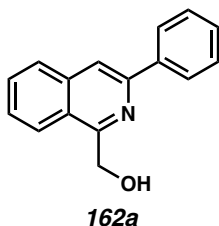


**4-methyl-2-phenylbenzo[f]isoquinoline (172f):** Compound **172f** was prepared from triflate **160d** using general procedure 3 and the product was collected via vacuum filtration to provide a white solid (246 mg, 63% yield);  $^1\text{H}$  NMR (400 MHz,  $\text{CDCl}_3$ )  $\delta$  8.55 – 8.40 (m, 2H), 7.96 – 7.88 (m, 2H), 7.73 (t,  $J = 8.7$  Hz, 1H), 7.69 – 7.61 (m, 1H), 7.54 (t,  $J = 8.3$  Hz, 1H), 7.45 – 7.42 (m, 2H), 7.26 (td,  $J = 7.6, 1.7$  Hz, 2H), 7.16 (td,  $J = 7.3, 1.7$  Hz, 1H), 2.81 (s, 3H);  $^{13}\text{C}$  NMR (100 MHz,  $\text{CDCl}_3$ )  $\delta$  157.9, 152.0, 140.3, 135.6, 133.4, 129.3, 128.8, 128.7, 128.5, 128.4, 127.7, 127.2, 127.1, 124.4, 123.4, 122.9, 111.0, 23.1; IR (Neat Film, NaCl) 2342, 1574, 1506, 1483, 1444, 1386, 1242, 1028, 876, 824, 760, 725, 692  $\text{cm}^{-1}$ ; HRMS (MM:ESI-APCI+)  $m/z$  calc'd for  $\text{C}_{20}\text{H}_{16}\text{N}$   $[\text{M}+\text{H}]^+$ : 270.1277, found 270.1289.

#### General Procedure 4: Oxidation and Reduction to Hydroxymethyl Isoquinoline



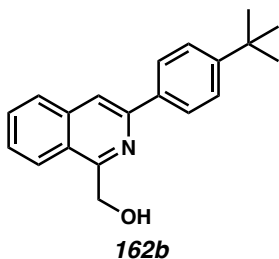




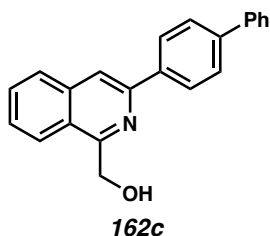
**(3-phenylisoquinolin-1-yl)methanol (162a):** This procedure has been adapted from a previous report.<sup>6</sup> To a 20-mL microwave vial containing a stir bar was added SeO<sub>2</sub> (140 mg, 1.26 mmol), isoquinoline **161a** (138 mg, 0.63 mmol), and 1,4-dioxane (13 mL, 0.05 M). The reaction vial was then sealed and heated to 110 °C while stirring for 2 hours. The reaction was then cooled to room temperature, filtered through celite, and rinsed with EtOAc. The filtrate was then concentrated in vacuo to afford the aldehyde intermediate, which was used in the next step without further purification.

A scintillation vial containing the crude in 4:1 DCM:MeOH (0.1 M) was added sodium borohydride (24 mg, 0.63 mmol) at room temperature. The reaction was stirred until no starting material remained by TLC, and then quenched by the addition of citric acid monohydrate (132 mg, 0.63 mmol). The reaction was stirred for an additional 10 minutes then basified by the addition of saturated aqueous NaHCO<sub>3</sub>. The layers were separated and the aqueous phase was extracted with CH<sub>2</sub>Cl<sub>2</sub>. The combined organic phases were dried over Na<sub>2</sub>SO<sub>4</sub> and concentrated in vacuo. The crude product was purified by column chromatography (20% acetone in hexanes) to afford **162a** as a white solid (100 mg, 68% yield over 2 steps): <sup>1</sup>H NMR (400 MHz, CDCl<sub>3</sub>) δ 8.18 – 8.15 (d, *J* = 7.0 Hz, 2H), 8.03 (s, 1H), 7.94 – 7.92 (m, 2H), 7.73 (ddd, *J* = 8.3, 6.9, 1.1 Hz, 1H), 7.61 (ddd, *J* = 8.1, 6.9, 1.2 Hz, 1H), 7.53 (t, *J* = 7.6 Hz, 2H), 7.46 – 7.42 (m, 1H), 5.31 (s, 2H), 5.26 (br s, 1H, OH);

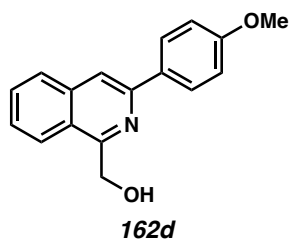
$^{13}\text{C}$  NMR (100 MHz,  $\text{CDCl}_3$ )  $\delta$  157.4, 148.7, 138.9, 137.1, 130.9, 129.0, 128.9, 128.0, 127.5, 127.0, 124.2, 123.3, 116.3, 61.6; IR (Neat Film, NaCl) 3378, 3060, 2867, 1624, 1574, 1502, 1461, 1443, 1370, 1331, 1304, 1088, 1072, 1024, 1009, 882, 782, 766, 693  $\text{cm}^{-1}$ ; HRMS (MM:ESI-APCI+)  $m/z$  calc'd for  $\text{C}_{16}\text{H}_{14}\text{NO}$   $[\text{M}+\text{H}]^+$ : 236.1070, found 236.1078.



**((3-(4-(tert-butyl)phenyl)isoquinolin-1-yl)methanol (162b):** Compound **162b** was prepared from isoquinoline **161b** using general procedure 4 and purified by column chromatography (20% EtOAc in hexanes) to provide a white solid (162 mg, 95% yield);  $^1\text{H}$  NMR (400 MHz,  $\text{CDCl}_3$ )  $\delta$  8.20 – 8.06 (m, 2H), 8.00 (s, 1H), 7.97 – 7.85 (m, 2H), 7.72 (ddd,  $J = 8.4, 6.9, 1.2$  Hz, 1H), 7.62 – 7.58 (m, 1H), 7.58 – 7.52 (m, 2H), 5.30 (s, 3H), 1.40 (s, 9H);  $^{13}\text{C}$  NMR (100 MHz,  $\text{CDCl}_3$ )  $\delta$  157.2, 152.1, 148.7, 137.1, 136.2, 130.8, 127.9, 127.3, 126.7, 125.9, 124.1, 123.3, 115.9, 61.5, 34.9, 31.5; IR (Neat Film, NaCl) 3385, 2958, 1626, 1574, 1514, 1446, 1416, 1360, 1333, 1265, 1088, 1014, 841, 744, 680  $\text{cm}^{-1}$ ; HRMS (MM:ESI-APCI+)  $m/z$  calc'd for  $\text{C}_{20}\text{H}_{22}\text{NO}$   $[\text{M}+\text{H}]^+$ : 292.1696, found 292.1696.

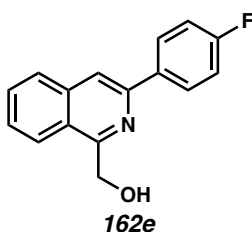


**(3-([1,1'-biphenyl]-4-yl)isoquinolin-1-yl)methanol (162c):** Compound **162c** was prepared from isoquinoline **161c** using general procedure 4 and purified by column chromatography (20% EtOAc in hexanes) to provide a colorless solid (181 mg, 92% yield);  $^1\text{H}$  NMR (400 MHz,  $\text{CDCl}_3$ )  $\delta$  8.30 – 8.20 (m, 2H), 8.07 (s, 1H), 7.98 – 7.88 (m, 2H), 7.81 – 7.66 (m, 5H), 7.62 (ddd,  $J = 8.4, 6.9, 1.2$  Hz, 1H), 7.49 (dd,  $J = 8.2, 6.8$  Hz, 2H), 7.43 – 7.34 (m, 1H), 5.32 (s, 3H);  $^{13}\text{C}$  NMR (100 MHz,  $\text{CDCl}_3$ )  $\delta$  157.4, 148.3, 141.7, 140.7, 137.8, 137.1, 130.9, 129.0, 128.0, 127.7, 127.7, 127.6, 127.3, 127.2, 124.2, 123.3, 116.2, 61.6; IR (Neat Film, NaCl) 3382, 3060, 2359, 1623, 1574, 1488, 1445, 1412, 1374, 1334, 1088, 1006, 840, 766, 729, 697  $\text{cm}^{-1}$ ; HRMS (MM:ESI-APCI+)  $m/z$  calc'd for  $\text{C}_{22}\text{H}_{18}\text{NO}$   $[\text{M}+\text{H}]^+$ : 312.1382, found 312.1383.

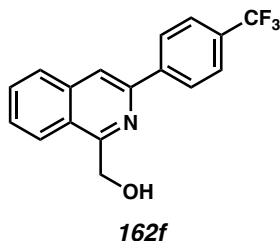


**(3-(4-methoxyphenyl)isoquinolin-1-yl)methanol (162d):** Compound **162d** was prepared from isoquinoline **161d** using general procedure 4 and purified by column chromatography (20% EtOAc in hexanes) to provide a white solid (48 mg, 73% yield):  $^1\text{H}$  NMR (400 MHz,  $\text{CDCl}_3$ )  $\delta$  8.14 – 8.07 (m, 2H), 7.93 (s, 1H), 7.91 – 7.85 (m, 2H), 7.69 (ddd,  $J = 8.2, 6.9, 1.1$  Hz, 1H), 7.56 (ddd,  $J = 8.2, 6.9, 1.2$  Hz, 1H), 7.06 – 7.03 (m, 2H), 5.28 (s, 3H), 3.89

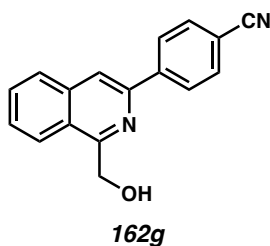
(s, 3H);  $^{13}\text{C}$  NMR (100 MHz,  $\text{CDCl}_3$ )  $\delta$  160.3, 157.0, 148.3, 137.1, 131.4, 130.7, 128.1, 127.7, 127.0, 123.7, 123.1, 115.0, 114.2, 61.4, 55.4; IR (Neat Film, NaCl) 3376, 2928, 2836, 1608, 1573, 1515, 1442, 1372, 1334, 1287, 1250, 1175, 1087, 1032, 1010, 832, 750, 730  $\text{cm}^{-1}$ ; HRMS (MM:ESI-APCI+)  $m/z$  calc'd for  $\text{C}_{17}\text{H}_{16}\text{NO}_2$   $[\text{M}+\text{H}]^+$ : 266.1176, found 266.1185.



**(3-(4-fluorophenyl)isoquinolin-1-yl)methanol (162e):** Compound **162e** was prepared from isoquinoline **161e** using general procedure 4 and purified by column chromatography (20% EtOAc in hexanes) to provide a colorless solid (149 mg, 95% yield);  $^1\text{H}$  NMR (400 MHz,  $\text{CDCl}_3$ )  $\delta$  8.13 (dd,  $J = 8.9, 5.4$  Hz, 2H), 7.96 (s, 1H), 7.95 – 7.89 (m, 2H), 7.73 (ddd,  $J = 8.3, 6.9, 1.1$  Hz, 1H), 7.61 (ddd,  $J = 8.1, 6.9, 1.2$  Hz, 1H), 7.21 (dd,  $J = 8.9, 8.5$  Hz, 2H), 5.30 (s, 2H), 5.17 (br s, 1H, OH);  $^{13}\text{C}$  NMR (100 MHz,  $\text{CDCl}_3$ )  $\delta$  163.5 (d,  $J = 248.3$  Hz), 157.5, 147.8, 137.0, 135.1 (d,  $J = 3.2$  Hz), 131.0, 128.7 (d,  $J = 8.2$  Hz), 127.9, 127.6, 124.1, 123.3, 116.0, 115.8, 61.6;  $^{19}\text{F}$  NMR (282 MHz,  $\text{CDCl}_3$ )  $\delta$  -113.3 – -113.4 (m); IR (Neat Film, NaCl) 3382, 3059, 2354, 1622, 1604, 1574, 1512, 1446, 1331, 1230, 1157, 1087, 1011, 837, 750, 725  $\text{cm}^{-1}$ ; HRMS (MM:ESI-APCI+)  $m/z$  calc'd for  $\text{C}_{16}\text{H}_{13}\text{FNO}$   $[\text{M}+\text{H}]^+$ : 254.0974, found 254.0976.

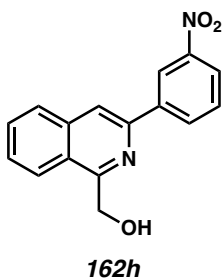


**(3-(4-(trifluoromethyl)phenyl)isoquinolin-1-yl)methanol (162f):** Compound **162f** was prepared from isoquinoline **161f** using general procedure 4 and purified by column chromatography (10% to 20% EtOAc in hexanes) to provide a white solid (23 mg, 25% yield);  $^1\text{H}$  NMR (400 MHz,  $\text{CDCl}_3$ )  $\delta$  8.26 (d,  $J = 7.8$  Hz, 2H), 8.07 (s, 1H), 8.00 – 7.92 (m, 2H), 7.82 – 7.73 (m, 3H), 7.70 – 7.61 (m, 1H), 5.32 (s, 2H), 5.10 (br s, 1H, OH);  $^{13}\text{C}$  NMR (100 MHz,  $\text{CDCl}_3$ )  $\delta$  157.9, 147.1, 142.3, 136.8, 131.2, 130.7 (q,  $J = 32.5$  Hz), 128.2, 128.1, 127.2, 125.9 (q,  $J = 3.8$  Hz), 124.6, 124.4 (q,  $J = 273.7$  Hz), 123.4, 117.2, 61.6;  $^{19}\text{F}$  NMR (282 MHz,  $\text{CDCl}_3$ )  $\delta$  -62.5; IR (Neat Film, NaCl) 3408, 1623, 1574, 1418, 1324, 1166, 1111, 1075, 1014, 842, 753, 682  $\text{cm}^{-1}$ ; HRMS (MM:ESI-APCI+)  $m/z$  calc'd for  $\text{C}_{17}\text{H}_{13}\text{F}_3\text{NO}$   $[\text{M}+\text{H}]^+$ : 304.0944, found 304.0934.

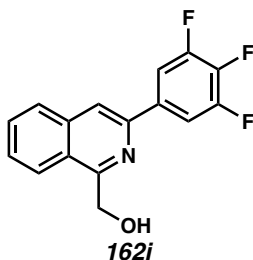


**4-(1-(hydroxymethyl)isoquinolin-3-yl)benzonitrile (162g):** Compound **162g** was prepared from isoquinoline **161g** using general procedure 4 and purified by column chromatography (30% EtOAc in hexanes) to provide a white solid (138 mg, 92% yield);  $^1\text{H}$  NMR (400 MHz,  $\text{CDCl}_3$ )  $\delta$  8.31 – 8.18 (m, 2H), 8.09 (s, 1H), 7.97 (m, 2H), 7.86 – 7.74 (m, 3H), 7.68 (ddd,  $J = 8.2, 6.9, 1.2$  Hz, 1H), 5.32 (s, 2H), 4.99 (s, 1H);  $^{13}\text{C}$  NMR (100

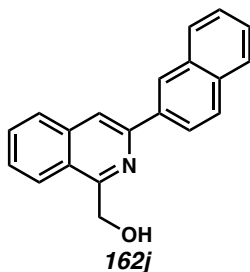
MHz, CDCl<sub>3</sub>)  $\delta$  158.2, 146.5, 143.2, 136.7, 132.8, 131.4, 128.5, 128.2, 127.4, 124.7, 123.5, 119.0, 117.7, 112.3, 61.7; IR (Neat Film, NaCl) 3404, 2895, 2358, 2224, 1416, 1332, 1303, 1085, 1006, 840, 764, 682 cm<sup>-1</sup>; HRMS (MM:ESI-APCI+)  $m/z$  calc'd for C<sub>17</sub>H<sub>13</sub>N<sub>2</sub>O [M+H]<sup>+</sup>: 261.1022, found 261.1032.



**(3-(3-nitrophenyl)isoquinolin-1-yl)methanol (162h):** Compound **162h** was prepared from isoquinoline **161h** using general procedure 4 and purified by column chromatography (20% EtOAc in CH<sub>2</sub>Cl<sub>2</sub>) to provide a white solid (67 mg, 38% yield); <sup>1</sup>H NMR (400 MHz, CDCl<sub>3</sub>)  $\delta$  8.95 (t,  $J$  = 2.0 Hz, 1H), 8.52 (dt,  $J$  = 7.9, 1.3 Hz, 1H), 8.27 (ddd,  $J$  = 8.2, 2.3, 1.1 Hz, 1H), 8.11 (s, 1H), 8.04 – 7.90 (m, 2H), 7.78 (ddd,  $J$  = 8.0, 6.9, 1.2 Hz, 1H), 7.73 – 7.60 (m, 2H), 5.33 (s, 2H), 4.96 (br s, 1H, OH); <sup>13</sup>C NMR (100 MHz, CDCl<sub>3</sub>)  $\delta$  158.2, 149.0, 146.1, 140.7, 136.8, 132.7, 131.4, 129.9, 128.4, 128.2, 124.7, 123.5, 123.4, 121.6, 117.2, 61.7; IR (Neat Film, NaCl) 3389, 2614, 1538, 1520, 1505, 1353, 1333, 1088, 1007, 892, 751, 690 cm<sup>-1</sup>; HRMS (MM:ESI-APCI+)  $m/z$  calc'd for C<sub>16</sub>H<sub>13</sub>N<sub>2</sub>O<sub>3</sub> [M+H]<sup>+</sup>: 281.0921, found 281.0930.

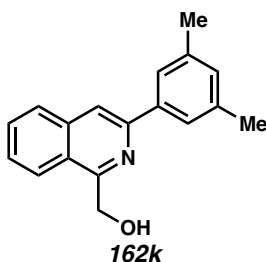


**(3-(3,4,5-trifluorophenyl)isoquinolin-1-yl)methanol (162i):** Compound **162i** was prepared from isoquinoline **161i** using general procedure 4 and purified by column chromatography (20% EtOAc in hexanes) to provide a white solid (90 mg, 82% yield);  $^1\text{H}$  NMR (400 MHz,  $\text{CDCl}_3$ )  $\delta$  7.99 – 7.89 (m, 3H), 7.84 – 7.71 (m, 3H), 7.65 (ddd,  $J = 8.2, 6.9, 1.3$  Hz, 1H), 5.30 (s, 2H), 4.89 (br s, 1H, OH);  $^{13}\text{C}$  NMR (100 MHz,  $\text{CDCl}_3$ )  $\delta$  158.0, 151.7 (ddd,  $J = 249.3, 10.2, 4.1$  Hz), 145.4 (d,  $J = 2.5$  Hz), 140.2 (dt,  $J = 253.9, 15.7$  Hz), 136.7, 135.1 (td,  $J = 7.6, 4.5$  Hz), 131.4, 128.3, 128.0, 124.5, 123.4, 116.6 (d,  $J = 1.4$  Hz), 110.9 – 110.7 (m), 61.7;  $^{19}\text{F}$  NMR (282 MHz,  $\text{CDCl}_3$ )  $\delta$  -133.8 – -133.9 (m), -160.1 – -160.3 (m); IR (Neat Film, NaCl) 3351, 2882, 1557, 1531, 1451, 1350, 1326, 1080, 1039, 1008, 864, 848, 778, 747, 706  $\text{cm}^{-1}$ ; HRMS (MM:ESI-APCI+)  $m/z$  calc'd for  $\text{C}_{16}\text{H}_{11}\text{F}_3\text{NO}$   $[\text{M}+\text{H}]^+$ : 290.0787, found 290.0795.



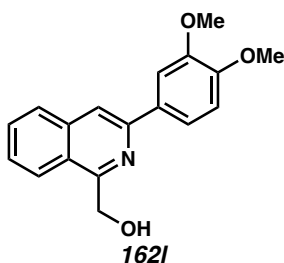
**(3-(naphthalen-2-yl)isoquinolin-1-yl)methanol (162j):** Compound **162j** was prepared from isoquinoline **161j** using general procedure 4 and purified by column chromatography (20% EtOAc in hexanes) to provide a white solid (158 mg, 97% yield);  $^1\text{H}$  NMR (400

MHz, CDCl<sub>3</sub>) δ 8.67 (s, 1H), 8.27 (dd, *J* = 8.6, 1.8 Hz, 1H), 8.16 (s, 1H), 8.05 – 7.93 (m, 4H), 7.91 – 7.89 (m, 1H), 7.75 (ddd, *J* = 8.2, 6.9, 1.1 Hz, 1H), 7.62 (ddd, *J* = 8.2, 6.9, 1.2 Hz, 1H), 7.58 – 7.47 (m, 2H), 5.34 (s, 3H); <sup>13</sup>C NMR (100 MHz, CDCl<sub>3</sub>) δ 157.5, 148.5, 137.1, 136.2, 133.7, 133.7, 130.9, 128.8, 128.6, 128.0, 127.8, 127.6, 126.7, 126.6, 126.3, 124.6, 124.2, 123.3, 116.6, 61.6; IR (Neat Film, NaCl) 3393, 3056, 1622, 1573, 1506, 1445, 1410, 1375, 1344, 1314, 1086, 1008, 856, 817, 744 cm<sup>-1</sup>; HRMS (MM:ESI-APCI+) *m/z* calc'd for C<sub>20</sub>H<sub>16</sub>NO [M+H]<sup>+</sup>: 286.1231, found 286.1226.

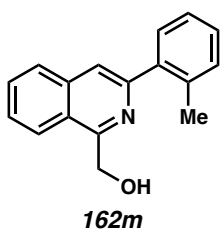


**(3-(3,5-dimethylphenyl)isoquinolin-1-yl)methanol (162k):** Compound **162k** was prepared from isoquinoline **161k** using general procedure 4 and purified by column chromatography (20% EtOAc in hexanes) to provide a white solid (155 mg, 95% yield); <sup>1</sup>H NMR (400 MHz, CDCl<sub>3</sub>) δ 8.00 (s, 1H), 7.94 – 7.91 (m, 2H), 7.78 – 7.76 (m, 2H), 7.72 (ddd, *J* = 8.3, 6.9, 1.2 Hz, 1H), 7.60 (ddd, *J* = 8.2, 6.9, 1.2 Hz, 1H), 7.09 (s, 1H), 5.30 (s, 3H), 2.44 (s, 6H); <sup>13</sup>C NMR (100 MHz, CDCl<sub>3</sub>) δ 157.2, 149.0, 138.9, 138.5, 137.1, 130.8, 130.6, 127.9, 127.4, 124.8, 124.1, 123.3, 116.3, 61.6, 21.7; IR (Neat Film, NaCl) 3382, 2913, 2338, 1622, 1574, 1503, 1444, 1379, 1332, 1084, 1011, 882, 849, 824, 750, 709 cm<sup>-1</sup>; HRMS (MM:ESI-APCI+) *m/z* calc'd for C<sub>18</sub>H<sub>18</sub>NO [M+H]<sup>+</sup>: 264.1382, found 264.1383.



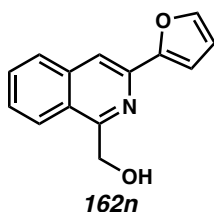


**(3-(3,4-dimethoxyphenyl)isoquinolin-1-yl)methanol (162l):** Compound **162l** was prepared from isoquinoline **161l** using general procedure 4 and purified by column chromatography (40% EtOAc in hexanes) to provide a white solid (180 mg, 91% yield);  $^1\text{H}$  NMR (400 MHz,  $\text{CDCl}_3$ )  $\delta$  7.95 (s, 1H), 7.93 – 7.90 (m, 2H), 7.77 – 7.67 (m, 3H), 7.58 (ddd,  $J = 8.2, 6.9, 1.2$  Hz, 1H), 7.03 – 7.01 (m, 1H), 5.30 (s, 2H), 5.26 (br s, 1H, OH), 4.03 (s, 3H), 3.97 (s, 3H);  $^{13}\text{C}$  NMR (100 MHz,  $\text{CDCl}_3$ )  $\delta$  157.0, 149.8, 149.3, 148.3, 137.0, 131.8, 130.7, 127.7, 127.1, 123.8, 123.2, 119.5, 115.3, 111.3, 110.0, 61.4, 56.1, 56.0; IR (Neat Film, NaCl) 3372, 2936, 2838, 1623, 1604, 1573, 1518, 1456, 1438, 1314, 1260, 1237, 1134, 1027, 1008  $\text{cm}^{-1}$ ; HRMS (MM:ESI-APCI+)  $m/z$  calc'd for  $\text{C}_{18}\text{H}_{18}\text{NO}_3$   $[\text{M}+\text{H}]^+$ : 296.1284, found 296.1283.

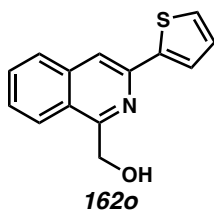


**(3-(*o*-tolyl)isoquinolin-1-yl)methanol (162m):** Compound **162m** was prepared from isoquinoline **161m** using general procedure 4 and purified by column chromatography (15% EtOAc in hexanes) to provide a white solid (130 mg, 79% yield);  $^1\text{H}$  NMR (400 MHz,  $\text{CDCl}_3$ )  $\delta$  7.96 (dd,  $J = 8.4, 1.1$  Hz, 1H), 7.91 (dd,  $J = 8.2, 1.2$  Hz, 1H), 7.75 (ddd,  $J = 8.3, 6.9, 1.2$  Hz, 1H), 7.71 (s, 1H), 7.64 (ddd,  $J = 8.3, 6.8, 1.3$  Hz, 1H), 7.53 (d,  $J = 6.6$

Hz, 1H), 7.39 – 7.29 (m, 3H), 5.30 (s, 2H), 5.14 (s, 1H), 2.45 (s, 3H);  $^{13}\text{C}$  NMR (100 MHz,  $\text{CDCl}_3$ )  $\delta$  156.8, 151.4, 140.1, 136.7, 136.5, 131.0, 130.8, 130.2, 128.4, 127.8, 127.6, 126.1, 123.7, 123.3, 120.0, 61.6, 20.9; IR (Neat Film, NaCl) 3389, 3057, 2932, 1626, 1573, 1502, 1455, 1402, 1377, 1330, 1087, 1069, 1008, 884, 786, 757, 727  $\text{cm}^{-1}$ ; HRMS (MM:ESI-APCI+)  $m/z$  calc'd for  $\text{C}_{17}\text{H}_{16}\text{NO}$   $[\text{M}+\text{H}]^+$ : 250.1226, found 250.1232.

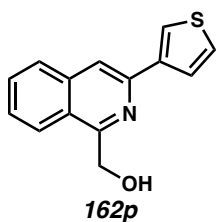


**(3-(furan-2-yl)isoquinolin-1-yl)methanol (162n):** Compound **162n** was prepared from isoquinoline **161n** using general procedure 4 and purified by column chromatography (20% EtOAc in hexanes) to provide a white solid (56 mg, 52% yield):  $^1\text{H}$  NMR (400 MHz,  $\text{CDCl}_3$ )  $\delta$  7.94 – 7.92 (m, 1H), 7.90 – 7.82 (m, 2H), 7.70 – 7.66 (m, 1H), 7.60 – 7.50 (m, 2H), 7.16 – 7.14 (m, 1H), 6.58 – 6.56 (m, 1H), 5.23 (s, 2H), 5.05 (br s, 1H, OH);  $^{13}\text{C}$  NMR (100 MHz,  $\text{CDCl}_3$ )  $\delta$  157.5, 153.7, 143.1, 140.9, 136.6, 130.9, 127.8, 127.2, 124.0, 123.3, 113.6, 112.1, 108.6, 61.3; IR (Neat Film, NaCl) 3390, 3118, 2886, 1624, 1574, 1492, 1372, 1323, 1306, 1157, 1092, 1079, 1006, 884, 836, 743  $\text{cm}^{-1}$ ; HRMS (MM:ESI-APCI+)  $m/z$  calc'd for  $\text{C}_{14}\text{H}_{12}\text{NO}_2$   $[\text{M}+\text{H}]^+$ : 226.0863, found 226.0871.

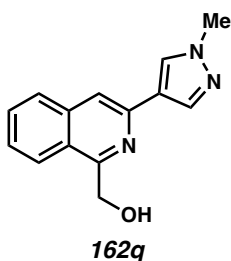


**(3-(thiophen-2-yl)isoquinolin-1-yl)methanol (162o):** Compound **162o** was prepared from isoquinoline **161o** (0.5 mmol) using general procedure 4 and purified by column

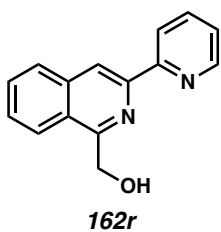
chromatography (10% to 20% EtOAc in hexanes) to provide a white solid (46 mg, 38% yield):  $^1\text{H}$  NMR (400 MHz,  $\text{CDCl}_3$ )  $\delta$  7.89 (s, 1H), 7.88 – 7.83 (m, 2H), 7.75 – 7.65 (m, 2H), 7.55 (ddd,  $J = 8.2, 6.9, 1.2$  Hz, 1H), 7.41 (dd,  $J = 5.0, 1.2$  Hz, 1H), 7.16 (dd,  $J = 5.0, 3.6$  Hz, 1H), 5.25 (s, 2H), 5.02 (br s, 1H, OH);  $^{13}\text{C}$  NMR (100 MHz,  $\text{CDCl}_3$ )  $\delta$  157.4, 144.4, 144.1, 136.8, 131.0, 128.2, 127.6, 127.2, 127.0, 124.1, 124.0, 123.3, 114.0, 61.3; IR (Neat Film, NaCl) 3382, 3066, 2868, 1621, 1589, 1573, 1501, 1452, 1402, 1329, 1084, 1006, 878, 822, 748, 701  $\text{cm}^{-1}$ ; HRMS (MM:ESI-APCI+)  $m/z$  calc'd for  $\text{C}_{14}\text{H}_{12}\text{NOS}$   $[\text{M}+\text{H}]^+$ : 242.0634, found 242.0637.



**(3-(thiophen-3-yl)isoquinolin-1-yl)methanol (162p):** Compound **162p** was prepared from isoquinoline **161p** (0.58 mmol) using general procedure 4 and purified by column chromatography (20% EtOAc in hexanes) to provide a white solid (127 mg, 91% yield);  $^1\text{H}$  NMR (400 MHz,  $\text{CDCl}_3$ )  $\delta$  8.06 (dd,  $J = 3.1, 1.3$  Hz, 1H), 7.94 – 7.84 (m, 3H), 7.76 (dd,  $J = 5.1, 1.3$  Hz, 1H), 7.71 (ddd,  $J = 8.2, 6.9, 1.1$  Hz, 1H), 7.58 (ddd,  $J = 8.2, 6.9, 1.1$  Hz, 1H), 7.45 (dd,  $J = 5.1, 3.0$  Hz, 1H), 5.27 (s, 2H), 5.19 (br s, 1H);  $^{13}\text{C}$  NMR (100 MHz,  $\text{CDCl}_3$ )  $\delta$  157.4, 145.0, 141.7, 137.0, 130.9, 127.8, 127.3, 126.6, 126.0, 124.1, 123.4, 123.4, 115.6, 61.5; IR (Neat Film, NaCl) 3372, 3098, 2888, 2363, 1622, 1594, 1573, 1456, 1350, 1318, 1299, 1086, 1008, 880, 842, 793, 748, 697  $\text{cm}^{-1}$ ; HRMS (MM:ESI-APCI+)  $m/z$  calc'd for  $\text{C}_{14}\text{H}_{12}\text{NOS}$   $[\text{M}+\text{H}]^+$ : 242.0634, found 242.0631.

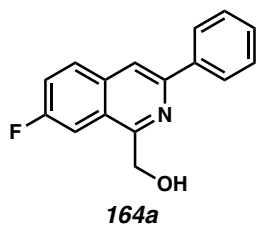


**(3-(1-methyl-1H-pyrazol-4-yl)isoquinolin-1-yl)methanol (162q):** Compound **162q** was prepared from isoquinoline **161q** using general procedure 4 and purified by column chromatography (70% to 80% EtOAc in hexanes + 1% NEt<sub>3</sub>) to provide a pale beige solid (72 mg, 62% yield): <sup>1</sup>H NMR (400 MHz, CDCl<sub>3</sub>) δ 8.08 – 7.95 (m, 2H), 7.85 – 7.79 (m, 2H), 7.71 – 7.59 (m, 2H), 7.53 – 7.49 (m, 1H), 5.21 (s, 2H), 3.98 (s, 3H); <sup>13</sup>C NMR (100 MHz, CDCl<sub>3</sub>) δ 157.3, 143.2, 137.3, 136.9, 130.8, 128.8, 127.2, 126.7, 123.5, 123.2, 114.1, 61.2, 39.2; IR (Neat Film, NaCl) 3370, 3068, 2937, 1626, 1603, 1573, 1503, 1416, 1321, 1278, 1186, 1092, 1011, 845, 753, 702 cm<sup>-1</sup>; HRMS (MM:ESI-APCI+) *m/z* calc'd for C<sub>14</sub>H<sub>14</sub>N<sub>3</sub>O [M+H]<sup>+</sup>: 240.1131, found 240.1123.

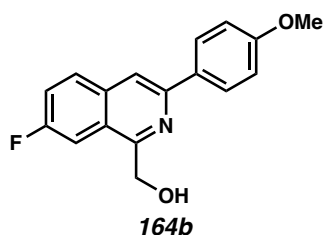


**(3-(pyridin-2-yl)isoquinolin-1-yl)methanol (162r):** Compound **162r** was prepared from isoquinoline **161r** using general procedure 4 and purified by column chromatography (10% to 20% acetone in CH<sub>2</sub>Cl<sub>2</sub> + 1% NEt<sub>3</sub>) to provide a pale cream solid (52 mg, 86% yield); <sup>1</sup>H NMR (400 MHz, CDCl<sub>3</sub>) δ 8.74 – 8.72 (m, 2H), 8.52 (d, *J* = 8.2 Hz, 1H), 8.00 (d, *J* = 8.3 Hz, 1H), 7.94 (d, *J* = 8.3 Hz, 1H), 7.86 (td, *J* = 7.8, 1.8 Hz, 1H), 7.78 – 7.69 (m, 1H), 7.63 (ddd, *J* = 8.1, 6.8, 1.2 Hz, 1H), 7.33 (ddd, *J* = 7.5, 4.8, 1.2 Hz, 1H), 5.31 (s, 2H), 5.13

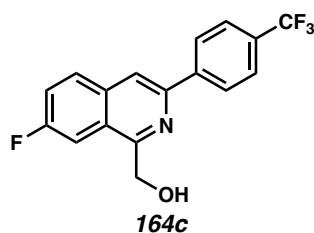
(br s, 1H, OH);  $^{13}\text{C}$  NMR (100 MHz,  $\text{CDCl}_3$ )  $\delta$  157.2, 155.8, 149.5, 147.3, 137.2, 137.0, 130.9, 128.7, 128.1, 125.1, 123.6, 123.3, 121.1, 117.6, 61.6; IR (Neat Film, NaCl) 3390, 3048, 2359, 1622, 1583, 1474, 1428, 1333, 1309, 1166, 1087, 1009, 897, 793, 747, 681  $\text{cm}^{-1}$ ; HRMS (MM:ESI-APCI+)  $m/z$  calc'd for  $\text{C}_{15}\text{H}_{13}\text{N}_2\text{O}$   $[\text{M}+\text{H}]^+$ : 237.1022, found 237.1020.



**(7-fluoro-3-phenylisoquinolin-1-yl)methanol (164a):** Compound **164a** was prepared from isoquinoline **172a** using general procedure 4 and purified by column chromatography (10% EtOAc in hexanes) to provide a white solid (94 mg, 81% yield):  $^1\text{H}$  NMR (400 MHz,  $\text{CDCl}_3$ )  $\delta$  8.13 (d,  $J = 8.0$  Hz, 2H), 8.00 (s, 1H), 7.96 – 7.87 (m, 1H), 7.57 – 7.47 (m, 4H), 7.44 (td,  $J = 6.9, 6.4, 1.4$  Hz, 1H), 5.21 (s, 2H), 5.11 (br s, 1H, OH);  $^{13}\text{C}$  NMR (100 MHz,  $\text{CDCl}_3$ )  $\delta$  161.0 (d,  $J = 250.3$  Hz), 156.8 (d,  $J = 5.9$  Hz), 148.4, 138.6, 134.1, 130.5 (d,  $J = 8.6$  Hz), 129.0, 126.8, 124.7 (d,  $J = 8.5$  Hz), 121.4 (d,  $J = 25.2$  Hz), 115.9 (d,  $J = 2.0$  Hz), 107.2 (d,  $J = 21.3$  Hz), 61.6;  $^{19}\text{F}$  NMR (282 MHz,  $\text{CDCl}_3$ )  $\delta$  -109.5 – -109.6 (m); IR (Neat Film, NaCl) 3393, 3063, 2878, 1594, 1579, 1506, 1417, 1392, 1321, 1232, 1185, 1085, 1015, 930, 777, 694  $\text{cm}^{-1}$ ; HRMS (MM:ESI-APCI+)  $m/z$  calc'd for  $\text{C}_{16}\text{H}_{13}\text{FNO}$   $[\text{M}+\text{H}]^+$ : 254.0976, found 254.0968.

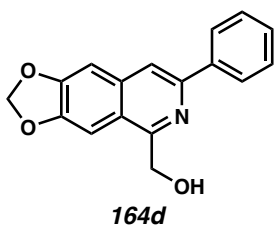


**(7-fluoro-3-(4-methoxyphenyl)isoquinolin-1-yl)methanol (164b):** Compound **164b** was prepared from isoquinoline **172b** using general procedure 4 and purified by column chromatography (20% EtOAc in hexanes) to provide a white solid (116 mg, 99% yield):  $^1\text{H}$  NMR (400 MHz,  $\text{CDCl}_3$ )  $\delta$  8.10 – 8.08 (m, 2H), 7.93 (s, 1H), 7.92 – 7.88 (m, 1H), 7.52 – 7.45 (m, 2H), 7.07 – 7.02 (m, 2H), 5.21 (s, 2H), 5.14 (s, 1H), 3.90 (s, 3H);  $^{13}\text{C}$  NMR (100 MHz,  $\text{CDCl}_3$ )  $\delta$  160.8 (d,  $J = 249.0$  Hz), 160.5, 156.6 (d,  $J = 5.9$  Hz), 148.3 (d,  $J = 2.9$  Hz), 134.3, 131.3, 130.4 (d,  $J = 8.6$  Hz), 128.1, 124.3 (d,  $J = 8.2$  Hz), 121.4 (d,  $J = 25.3$  Hz), 114.8 (d,  $J = 1.7$  Hz), 114.4, 107.2 (d,  $J = 21.3$  Hz), 61.6, 55.6;  $^{19}\text{F}$  NMR (282 MHz,  $\text{CDCl}_3$ )  $\delta$  –110.2 (ddd,  $J = 8.9, 8.8, 5.5$  Hz); IR (Neat Film, NaCl) 3388, 2936, 1608, 1593, 1516, 1389, 1289, 1251, 1180, 1069, 1032, 1015, 929, 835  $\text{cm}^{-1}$ ; HRMS (MM:ESI-APCI+)  $m/z$  calc'd for  $\text{C}_{17}\text{H}_{15}\text{FNO}_2$   $[\text{M}+\text{H}]^+$ : 284.1081, found 284.1074.

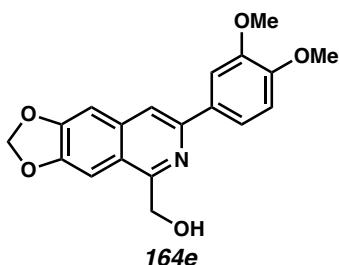


**(7-fluoro-3-(4-(trifluoromethyl)phenyl)isoquinolin-1-yl)methanol (164c):** Compound **164c** was prepared from isoquinoline **172c** using general procedure 4 and purified by column chromatography (10% EtOAc in hexanes) to provide a white solid (80 mg, 60% yield):  $^1\text{H}$  NMR (400 MHz,  $\text{CDCl}_3$ )  $\delta$  8.20 (d,  $J = 8.1$  Hz, 2H), 8.02 (s, 1H), 7.95 (dd,  $J =$

9.8, 5.4 Hz, 1H), 7.74 (d,  $J = 8.3$  Hz, 2H), 7.58 – 7.47 (m, 2H), 5.21 (s, 2H), 4.94 (br s, 1H, OH);  $^{13}\text{C}$  NMR (100 MHz,  $\text{CDCl}_3$ )  $\delta$  161.3 (d,  $J = 251.5$  Hz), 157.3 (d,  $J = 5.9$  Hz), 146.8 (d,  $J = 2.9$  Hz), 141.8 (d,  $J = 1.5$  Hz), 133.8, 130.7 (d,  $J = 8.7$  Hz), 130.7 (q,  $J = 33.3$  Hz), 127.0, 125.9 (q,  $J = 3.8$  Hz), 125.2 (d,  $J = 8.4$  Hz), 124.3 (q,  $J = 272.7$  Hz), 121.7 (d,  $J = 25.3$  Hz), 116.8 (d,  $J = 1.7$  Hz), 107.4 (d,  $J = 21.5$  Hz), 61.7;  $^{19}\text{F}$  NMR (282 MHz,  $\text{CDCl}_3$ )  $\delta$  -62.5, -108.4 (ddd,  $J = 8.7, 8.7, 5.4$  Hz); IR (Neat Film, NaCl) 3410, 2886, 1619, 1597, 1504, 1416, 1391, 1328, 1233, 1165, 1124, 1111, 1074, 1016, 931, 847, 680  $\text{cm}^{-1}$ ; HRMS (MM:ESI-APCI+)  $m/z$  calc'd for  $\text{C}_{17}\text{H}_{12}\text{F}_4\text{NO}$   $[\text{M}+\text{H}]^+$ : 322.0850, found 322.0839.

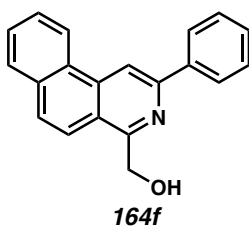


**(7-phenyl-[1,3]dioxolo[4,5-g]isoquinolin-5-yl)methanol (164d):** Compound **164d** was prepared from isoquinoline **172d** using general procedure 4 and purified by column chromatography (30% to 40% EtOAc in hexanes) to provide a white solid (135 mg, 83% yield):  $^1\text{H}$  NMR (400 MHz,  $\text{CDCl}_3$ )  $\delta$  8.13 – 8.05 (m, 2H), 7.82 (s, 1H), 7.50 (m, 2H), 7.44 – 7.37 (m, 1H), 7.15 – 7.06 (m, 2H), 6.10 (s, 2H), 5.28 (br s, 1H, OH), 5.10 (s, 2H);  $^{13}\text{C}$  NMR (100 MHz,  $\text{CDCl}_3$ )  $\delta$  154.9, 151.1, 148.6, 147.8, 138.9, 135.4, 128.8, 128.5, 126.6, 120.9, 115.9, 103.6, 101.9, 99.3, 61.4; IR (Neat Film, NaCl) 3324, 2914, 2355, 1597, 1497, 1463, 1436, 1422, 1236, 1066, 1036, 995, 940, 877, 775, 692  $\text{cm}^{-1}$ ; HRMS (MM:ESI-APCI+)  $m/z$  calc'd for  $\text{C}_{17}\text{H}_{14}\text{NO}_3$   $[\text{M}+\text{H}]^+$ : 280.0968, found 280.0975.



**(7-(3,4-dimethoxyphenyl)-[1,3]dioxolo[4,5-g]isoquinolin-5-yl)methanol (164e):**

Compound **164e** was prepared from isoquinoline **172e** using general procedure 4 and purified by column chromatography (40% EtOAc in hexanes) via dry-loading to provide a pale pink solid (126 mg, 65% yield):  $^1\text{H NMR}$  (400 MHz,  $\text{CDCl}_3$ )  $\delta$  7.77 (s, 1H), 7.69 – 7.60 (m, 2H), 7.16 – 7.07 (m, 2H), 6.99 (d,  $J = 8.2$  Hz, 1H), 6.11 (s, 2H), 5.26 (br s, 1H, OH), 5.11 (s, 2H), 4.01 (s, 3H), 3.96 (s, 3H);  $^{13}\text{C NMR}$  (100 MHz,  $\text{CDCl}_3$ )  $\delta$  154.7, 151.1, 149.7, 149.2, 148.4, 147.7, 135.5, 131.9, 120.6, 119.2, 115.1, 111.3, 109.7, 103.5, 101.8, 99.3, 61.4, 56.0, 56.0; IR (Neat Film, NaCl) 3378, 2912, 2353, 1595, 1519, 1496, 1463, 1456, 1435, 1258, 1234, 1034, 862, 730  $\text{cm}^{-1}$ ; HRMS (MM:ESI-APCI+)  $m/z$  calc'd for  $\text{C}_{19}\text{H}_{18}\text{NO}_5$   $[\text{M}+\text{H}]^+$ : 340.1179, found 340.1172.



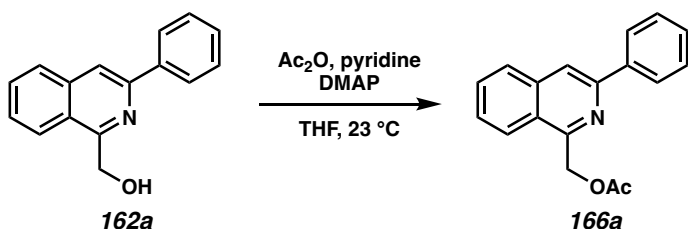
**(2-phenylbenzo[fl]isoquinolin-4-yl)methanol (164f):**

Compound **164f** was prepared from isoquinoline **172f** using general procedure 4 and purified by column chromatography (20% EtOAc in hexanes) to provide a white solid (51 mg, 62% yield):  $^1\text{H NMR}$  (400 MHz,  $\text{CDCl}_3$ )  $\delta$  8.78 – 8.76 (m, 2H), 8.23 – 8.20 (m, 2H), 7.94 – 7.92 (m, 1H), 7.88 – 7.78 (m, 1H), 7.78 – 7.62 (m, 3H), 7.57 (t,  $J = 7.5$  Hz, 2H), 7.48 (t,  $J = 7.3$  Hz, 1H), 5.46 – 5.19 (m,

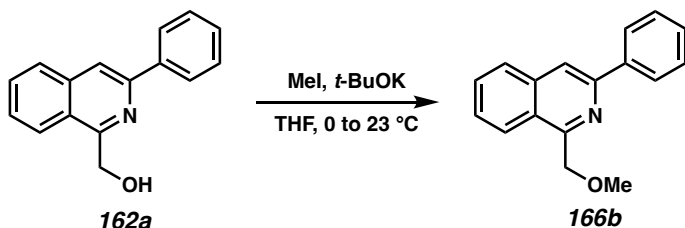


3H);  $^{13}\text{C}$  NMR (100 MHz,  $\text{CDCl}_3$ )  $\delta$  156.3, 150.4, 139.2, 135.9, 133.5, 129.0, 129.0, 129.0, 128.8, 128.6, 127.5, 127.1, 123.5, 122.1, 120.0, 120.0, 111.7, 61.7; IR (Neat Film, NaCl) 3322, 3064, 2890, 1589, 1494, 1428, 1386, 1304, 1242, 1081, 1050, 814, 747  $\text{cm}^{-1}$ ; HRMS (MM:ESI-APCI+)  $m/z$  calc'd for  $\text{C}_{20}\text{H}_{16}\text{NO}$   $[\text{M}+\text{H}]^+$ : 286.1226, found 286.1235.

### 2.7.2.2 Syntheses of isoquinolines with different directing groups



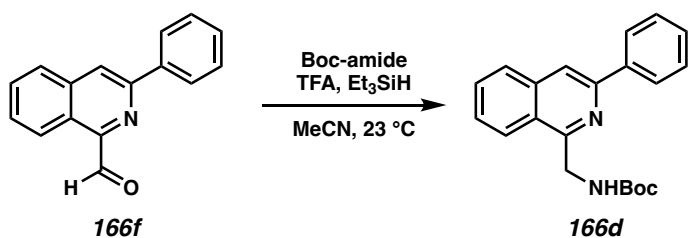
**(3-phenylisoquinolin-1-yl)methyl acetate (166a):** To a scintillation vial containing a stir bar and isoquinoline **162a** (165 mg, 0.70 mmol) in THF (7 mL, 0.1 M) was added DMAP (8.6 mg, 0.07 mmol) and pyridine (0.14 mL, 1.75 mmol). Acetic anhydride (0.1 mL, 1.05 mmol) was then added dropwise. The reaction was stirred overnight at room temperature then diluted with  $\text{Et}_2\text{O}$  and washed with saturated aqueous  $\text{NH}_4\text{Cl}$ . The organic phase was collected, dried over  $\text{Na}_2\text{SO}_4$  and concentrated in vacuo. The crude product was purified by column chromatography (10%  $\text{EtOAc}$  in hexanes) to afford **166a** as a colorless viscous oil (194 mg, >99% yield):  $^1\text{H}$  NMR (400 MHz,  $\text{CDCl}_3$ )  $\delta$  8.19 – 8.13 (m, 2H), 8.11 (dd,  $J$  = 8.4, 1.0 Hz, 1H), 8.07 (s, 1H), 7.92 (dt,  $J$  = 8.3, 0.9 Hz, 1H), 7.71 (ddd,  $J$  = 8.2, 6.8, 1.2 Hz, 1H), 7.61 (ddd,  $J$  = 8.2, 6.8, 1.3 Hz, 1H), 7.54 – 7.47 (m, 2H), 7.45 – 7.38 (m, 1H), 5.79 (s, 2H), 2.20 (s, 3H);  $^{13}\text{C}$  NMR (100 MHz,  $\text{CDCl}_3$ )  $\delta$  170.9, 154.4, 150.2, 139.3, 137.5, 130.5, 128.9, 128.7, 128.0, 127.6, 127.1, 126.0, 124.8, 117.2, 66.1, 21.1; IR (Neat Film, NaCl) 2826, 2364, 1704, 1574, 1455, 1333, 1054, 904, 783, 764, 748, 719, 678  $\text{cm}^{-1}$ ; HRMS (MM:ESI-APCI+)  $m/z$  calc'd for  $\text{C}_{18}\text{H}_{16}\text{NO}_2$   $[\text{M}+\text{H}]^+$ : 278.1176, found 278.1178.



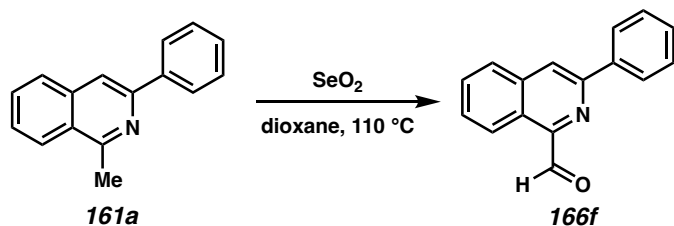
**1-(methoxymethyl)-3-phenylisoquinoline (166b):** To a scintillation vial containing a stir bar and isoquinoline **162a** (165 mg, 0.70 mmol) in THF (7 mL, 0.1 M) was added KO*t*-Bu (86 mg, 0.77 mmol) at room temperature. The resulting mixture was stirred for 5 minutes, then cooled to 0 °C, and MeI (0.05 mL, 0.77 mmol) was added. The reaction was allowed to slowly warm to room temperature overnight and then was quenched with saturated aqueous NH<sub>4</sub>Cl. The organic phase was collected and the aqueous phase was extracted with EtOAc. The organic phases were combined, dried over MgSO<sub>4</sub>, and concentrated in vacuo. The crude product was purified by column chromatography (5% EtOAc in hexanes) to afford **166b** as a white solid (79 mg, 45% yield): <sup>1</sup>H NMR (400 MHz, CDCl<sub>3</sub>) δ 8.36 (dd, *J* = 8.4, 1.1 Hz, 1H), 8.20 – 8.13 (m, 2H), 8.04 (s, 1H), 7.89 (d, *J* = 8.3 Hz, 1H), 7.69 (ddd, *J* = 8.2, 6.8, 1.2 Hz, 1H), 7.60 (ddd, *J* = 8.2, 6.8, 1.3 Hz, 1H), 7.51 (td, *J* = 7.3, 6.5, 1.2 Hz, 2H), 7.45 – 7.37 (m, 1H), 5.14 (s, 2H), 3.51 (s, 3H); <sup>13</sup>C NMR (100 MHz, CDCl<sub>3</sub>) δ 157.1, 149.9, 139.7, 137.5, 130.4, 128.9, 128.6, 127.7, 127.3, 127.1, 126.5, 125.9, 117.1, 75.8, 58.7; IR (Neat Film, NaCl) 3058, 2918, 2817, 1622, 1590, 1500, 1455, 1338, 1188, 1104, 885, 770, 752, 695, 668 cm<sup>-1</sup>; HRMS (MM:ESI-APCI+) *m/z* calc'd for C<sub>17</sub>H<sub>16</sub>NO [M+H]<sup>+</sup>: 250.1226, found 250.1236.



**1-((benzyloxy)methyl)-3-phenylisoquinoline (166c):** This procedure has been adapted from a previous report.<sup>26</sup> To a flame-dried RBF equipped with a stir bar was added NaH (36.4 mg, 60% w/w in oil, 0.91 mmol) and THF (7 mL, 0.1 M). To this suspension, isoquinoline **162a** (165 mg, 0.70 mmol) was added. After 5 minutes of stirring at room temperature, the reaction mixture was cooled to 0 °C and BnBr (0.91 mL, 0.91 mmol) was added. The reaction was allowed to slowly warm to room temperature overnight. Silica (1 g) was then added and the solvent was evaporated under vacuum. The crude product was purified by column chromatography (5% EtOAc in hexanes) to afford **166c** as a colorless viscous oil (153 mg, 67% yield): <sup>1</sup>H NMR (400 MHz, CDCl<sub>3</sub>) δ 8.39 (dd, *J* = 8.4, 1.1 Hz, 1H), 8.21 – 8.14 (m, 2H), 8.04 (s, 1H), 7.89 (d, *J* = 8.3 Hz, 1H), 7.69 (ddd, *J* = 8.2, 6.8, 1.2 Hz, 1H), 7.58 (ddd, *J* = 8.3, 6.8, 1.2 Hz, 1H), 7.51 (dd, *J* = 8.4, 6.9 Hz, 2H), 7.45 – 7.27 (m, 6H), 5.24 (s, 2H), 4.67 (s, 2H); <sup>13</sup>C NMR (100 MHz, CDCl<sub>3</sub>) δ 157.2, 149.9, 139.7, 138.2, 137.6, 130.4, 128.9, 128.6, 128.5, 128.3, 127.9, 127.7, 127.3, 127.1, 126.6, 126.1, 117.1, 73.6, 72.8; IR (Neat Film, NaCl) 3062, 2858, 1622, 1574, 1496, 1454, 1384, 1337, 1207, 1094, 1030, 885, 796, 768, 737, 696 cm<sup>-1</sup>; HRMS (MM:ESI-APCI+) *m/z* calc'd for C<sub>23</sub>H<sub>20</sub>NO [M+H]<sup>+</sup>: 326.1539, found 326.1544.



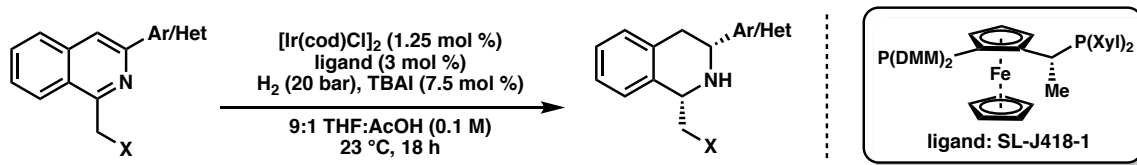
**tert-butyl ((3-phenylisoquinolin-1-yl)methyl)carbamate (166d):** This procedure has been adapted from a previous report.<sup>27</sup> To a solution of aldehyde **166f** (150 mg, 0.64 mmol) and *t*-butyl carbamate (150 mg, 1.28 mmol) in MeCN (6.5 mL, 0.1 M) were added trifluoroacetic acid (0.15 mL, 1.92 mmol) and triethylsilane (1.0 mL, 6.4 mmol). The reaction was stirred at room temperature overnight and then quenched with saturated aqueous Na<sub>2</sub>CO<sub>3</sub> and extracted with EtOAc. The combined organic phases were washed with brine, dried over Na<sub>2</sub>SO<sub>4</sub> and concentrated in vacuo. The crude product was purified by column chromatography (15% EtOAc in hexanes) to afford **166d** as a white solid (160 mg, 75% yield): <sup>1</sup>H NMR (400 MHz, CDCl<sub>3</sub>) δ 8.16 (d, *J* = 7.7 Hz, 2H), 8.10 (d, *J* = 8.4 Hz, 1H), 8.00 (s, 1H), 7.90 (d, *J* = 8.2 Hz, 1H), 7.70 (ddd, *J* = 8.1, 6.9, 1.1 Hz, 1H), 7.61 (ddd, *J* = 8.2, 6.9, 1.2 Hz, 1H), 7.53 (t, *J* = 7.6 Hz, 2H), 7.48 – 7.40 (m, 1H), 6.43 (br s, 1H), 5.03 (d, *J* = 4.4 Hz, 2H), 1.54 (s, 9H); <sup>13</sup>C NMR (100 MHz, CDCl<sub>3</sub>) δ 156.3, 155.0, 149.3, 139.4, 137.1, 130.6, 128.9, 128.8, 127.9, 127.6, 127.0, 125.1, 124.0, 116.3, 79.6, 43.5, 28.7; IR (Neat Film, NaCl) 3418, 2976, 1713, 1622, 1574, 1487, 1367, 1251, 1167, 1056, 882, 765, 695 cm<sup>-1</sup>; HRMS (MM:ESI-APCI+) *m/z* calc'd for C<sub>21</sub>H<sub>23</sub>N<sub>2</sub>O<sub>2</sub> [M+H]<sup>+</sup>: 335.1754, found 335.1760.



**3-phenylisoquinoline-1-carbaldehyde (166f):** To a Schlenk flask containing a stir bar was added SeO<sub>2</sub> (140 mg, 1.26 mmol) and isoquinoline **161a** (138 mg, 0.63 mmol) in 1,4-dioxane (13 mL, 0.05 M). The reaction vial was then sealed and heated to 110 °C while stirring for 2 hours. The reaction was then cooled to room temperature and filtered through celite rinsing with EtOAc. The crude product was then purified by column chromatography (5% EtOAc in hexanes) to afford **166f** as a pale yellow solid (1.32 g, 96% yield): <sup>1</sup>H NMR (400 MHz, CDCl<sub>3</sub>) δ 10.50 (s, 1H), 9.32 (d, *J* = 8.2 Hz, 1H), 8.31 (s, 1H), 8.24 (d, *J* = 8.1 Hz, 2H), 7.97 (d, *J* = 7.3 Hz, 1H), 7.84 – 7.67 (m, 2H), 7.56 (t, *J* = 7.5 Hz, 2H), 7.47 (t, *J* = 7.4 Hz, 1H); <sup>13</sup>C NMR (100 MHz, CDCl<sub>3</sub>) δ 196.2, 150.8, 149.7, 138.5, 138.1, 131.0, 129.9, 129.3, 129.1, 127.5, 127.1, 125.9, 125.5, 121.3; IR (Neat Film, NaCl) 2826, 2364, 1704, 1574, 1455, 1333, 1054, 904, 783, 764, 748, 719, 678 cm<sup>-1</sup>; HRMS (MM:ESI-APCI+) *m/z* calc'd for C<sub>16</sub>H<sub>12</sub>NO [M+H]<sup>+</sup>: 234.0913, found 234.0914.

### 2.7.2.3 Hydrogenation reactions

#### General Procedure 5: Hydrogenation Reactions

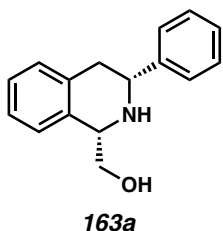


To an oven-dried 20-mL scintillation vial equipped with a stir bar and isoquinoline (0.2 mmol) was capped with a PTFE-lined septum and pierced with two 21 gauge green needles.

The vials were then placed in a Parr bomb and brought into the glovebox, with the exception of the pressure gauge. A layer of plastic wrap and a rubber band were also brought in to seal the top of the bomb. In a nitrogen-filled glovebox, a solution of the ligand (SL-J418-1) (4.53 mg, 0.006 mmol per reaction) and  $[\text{Ir}(\text{cod})\text{Cl}]_2$  (1.68 mg, 0.0025 mmol per reaction) in THF (1.8 mL per reaction) was prepared and allowed to stand for 10 minutes. Meanwhile, a solution of TBAI (5.54 mg, 0.015 mmol per reaction) in AcOH (0.2 mL per reaction) was prepared in a 1-dram vial, and 0.2 mL of the solution was added to each reaction vial via a syringe. Afterwards, 1.8 mL of the homogeneous iridium catalyst solution was added to each reaction vial via a syringe. After re-capping the vials with caps equipped with needles, the reactions were placed in the bomb and the top was covered tightly with plastic wrap secured by a rubber band. The bomb was then removed from the glovebox, and the pressure gauge was quickly screwed in place and tightened. The bomb was charged to 5-10 bar  $\text{H}_2$  and slowly released. This process was repeated two more times, before charging the bomb to 20 bar of  $\text{H}_2$  (or 60 bar  $\text{H}_2$ ). The bomb was then left stirring at 200 rpm at room temperature (or placed in an oil bath and heated to 60 °C) for 18 hours. Then, the bomb was removed from the stir plate and the hydrogen pressure was vented. The reaction vials were removed from the bomb and each solution was basified by the addition of saturated aqueous  $\text{K}_2\text{CO}_3$ . The layers were separated, and the aqueous layer was extracted with EtOAc. The combined organics layers were then dried over  $\text{Na}_2\text{SO}_4$ , and concentrated in vacuo. The product was then purified by column chromatography to furnish the product as an inseparable mixture of diastereomers.

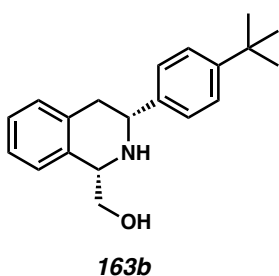
Please note that the NMR data listed is for the major diastereomer, and that the provided spectra for the following compounds reflect the inseparable mixture of *cis*- and

*trans*-products. The enantiomeric excess was determined by chiral SFC analysis of the Cbz-protected amine (see Table 2.4). The absolute configuration was determined for compound **163p** via x-ray crystallographic analysis. Absolute configuration of compound **167e** were determined using vibrational circular dichroism (VCD), *vide infra*. The absolute configuration for all other products has been inferred by analogy.



**((1S,3R)-3-phenyl-1,2,3,4-tetrahydroisoquinolin-1-yl)methanol (163a):** Compound **163a** was prepared from isoquinoline **162a** using general procedure 5 and purified by column chromatography (5% MeOH in CH<sub>2</sub>Cl<sub>2</sub>) to provide a tan solid as a mixture of diastereomers (47 mg, 98% yield) (dr = 15.7:1); 92% ee for major diastereomer;  $[\alpha]_D^{25} +110.2$  (*c* 1.02, CHCl<sub>3</sub>); *Cis*-diastereomer: <sup>1</sup>H NMR (400 MHz, CDCl<sub>3</sub>)  $\delta$  7.50 – 7.43 (m, 2H), 7.41 – 7.34 (m, 2H), 7.34 – 7.28 (m, 1H), 7.25 – 7.17 (m, 3H), 7.15 – 7.10 (m, 1H), 4.43 – 4.41 (m, 1H), 4.10 (dd, *J* = 11.1, 3.5 Hz, 1H), 4.02 (dd, *J* = 10.8, 3.3 Hz, 1H), 3.90 (dd, *J* = 10.9, 5.4 Hz, 1H), 3.02 (ddt, *J* = 15.9, 11.1, 1.4 Hz, 1H), 2.90 (dd, *J* = 15.7, 3.5 Hz, 1H); <sup>13</sup>C NMR (100 MHz, CDCl<sub>3</sub>)  $\delta$  144.3, 136.7, 134.9, 129.3, 128.8, 127.7, 126.8, 126.7, 126.5, 125.5, 66.7, 58.7, 57.7, 39.0; IR (Neat Film, NaCl) 3296, 3060, 2910, 2360, 1494, 1455, 1314, 1116, 1036, 909, 742, 700 cm<sup>-1</sup>; HRMS (MM:ESI-APCI+) *m/z* calc'd for C<sub>16</sub>H<sub>18</sub>NO [M+H]<sup>+</sup>: 240.1383, found 240.1385; SFC Conditions: 45% IPA, 3.5 mL/min, Chiralpak AD-H column,  $\lambda$  = 210 nm, *t<sub>R</sub>* (min): major = 2.34, minor = 4.02.

*Trans*-diastereomer:  $^1\text{H}$  NMR (400 MHz,  $\text{CDCl}_3$ )  $\delta$  7.49 – 7.43 (m, 2H), 7.42 – 7.38 (m, 2H), 7.36 – 7.27 (m, 1H), 7.26 – 7.10 (m, 4H), 4.23 (dd,  $J = 10.5, 4.8$  Hz, 1H), 4.16 (dd,  $J = 11.2, 3.9$  Hz, 1H), 3.80 (dd,  $J = 10.8, 4.8$  Hz, 1H), 3.71 (t,  $J = 10.7$  Hz, 1H), 3.07 (dd,  $J = 16.4, 3.9$  Hz, 1H), 2.95 (dd,  $J = 15.9, 11.2$  Hz, 1H);  $^{13}\text{C}$  NMR (100 MHz,  $\text{CDCl}_3$ )  $\delta$  143.5, 135.5, 134.7, 129.5, 128.8, 127.5, 127.0, 126.7, 126.6, 126.4, 63.8, 57.4, 50.7, 36.8.

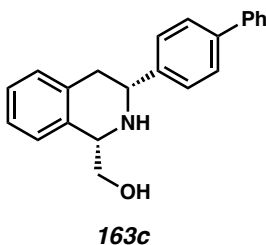


**((1*S*,3*R*)-3-(4-(*tert*-butyl)phenyl)-1,2,3,4-tetrahydroisoquinolin-1-yl)methanol (163b):**

Compound **163b** was prepared from isoquinoline **162b** using general procedure 5 and purified by column chromatography (50% EtOAc in hexanes) to provide a tan solid as a mixture of diastereomers (51 mg, 87% yield) (dr = 13.3:1); 91% ee for major diastereomer;  $[\alpha]_{\text{D}}^{25} +78.8$  ( $c$  1.03,  $\text{CHCl}_3$ ); Major diastereomer:  $^1\text{H}$  NMR (400 MHz,  $\text{CDCl}_3$ )  $\delta$  7.42 – 7.38 (m, 4H), 7.26 – 7.21 (m, 2H), 7.21 – 7.17 (m, 1H), 7.12 (d,  $J = 7.7$  Hz, 1H), 4.42 – 4.40 (m, 1H), 4.08 (dd,  $J = 11.2, 3.4$  Hz, 1H), 4.01 (dd,  $J = 10.8, 3.3$  Hz, 1H), 3.89 (dd,  $J = 10.8, 5.4$  Hz, 1H), 3.03 (dd,  $J = 15.8, 11.2$  Hz, 1H), 2.89 (dd,  $J = 15.7, 3.4$  Hz, 1H), 1.34 (s, 9H);  $^{13}\text{C}$  NMR (100 MHz,  $\text{CDCl}_3$ )  $\delta$  150.7, 141.2, 136.7, 135.0, 129.3, 126.7, 126.5, 126.5, 125.7, 125.5, 66.6, 58.7, 57.3, 38.8, 34.7, 31.5; IR (Neat Film, NaCl) 3318, 2961, 2868, 1494, 1454, 1362, 1312, 1270, 1116, 1038, 820, 743  $\text{cm}^{-1}$ ; HRMS (MM:ESI-APCI+)

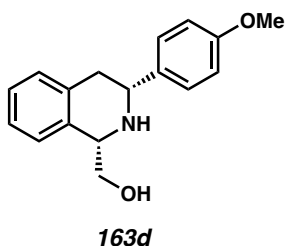


$m/z$  calc'd for  $C_{20}H_{26}NO$   $[M+H]^+$ : 296.2009, found 296.2005; SFC Conditions: 45% IPA, 3.5 mL/min, Chiralpak AD-H column,  $\lambda = 210$  nm,  $t_R$  (min): major = 1.81, minor = 2.73.



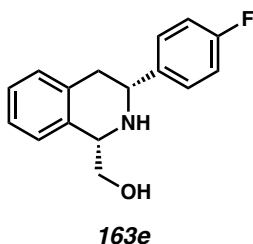
**((1S,3R)-3-((1,1'-biphenyl)-4-yl)-1,2,3,4-tetrahydroisoquinolin-1-yl)methanol (163c):**

Compound **163c** was prepared from isoquinoline **162c** using general procedure 5 and purified by column chromatography (50% EtOAc in hexanes) to provide a tan solid as a mixture of diastereomers (50 mg, 79% yield) (dr = 9.0:1); 92% ee for major diastereomer;  $[\alpha]_D^{25} +73.2$  ( $c$  1.03,  $CHCl_3$ ); Major diastereomer:  $^1H$  NMR (400 MHz,  $CDCl_3$ )  $\delta$  7.65 – 7.58 (m, 4H), 7.55 – 7.53 (m, 2H), 7.47 – 7.44 (m, 2H), 7.39 – 7.32 (m, 1H), 7.28 – 7.16 (m, 3H), 7.15 (d,  $J = 6.2$  Hz, 1H), 4.46 – 4.44 (m, 1H), 4.15 (dd,  $J = 11.2, 3.4$  Hz, 1H), 4.04 (dd,  $J = 10.9, 3.3$  Hz, 1H), 3.91 (dd,  $J = 10.9, 5.5$  Hz, 1H), 3.12 – 3.00 (m, 1H), 2.94 (dd,  $J = 15.6, 3.4$  Hz, 1H);  $^{13}C$  NMR (100 MHz,  $CDCl_3$ )  $\delta$  143.2, 141.0, 140.7, 136.5, 134.9, 129.3, 128.9, 127.5, 127.4, 127.3, 127.2, 126.8, 126.6, 125.5, 66.6, 58.7, 57.4, 38.9; IR (Neat Film, NaCl) 3318, 3029, 2924, 2365, 1487, 1455, 1312, 1218, 1112, 1038, 833, 763, 748, 699  $cm^{-1}$ ; HRMS (MM:ESI-APCI+)  $m/z$  calc'd for  $C_{22}H_{22}NO$   $[M+H]^+$ : 316.1696, found 316.1686; SFC Conditions: 45% IPA, 3.5 mL/min, Chiralpak AD-H column,  $\lambda = 210$  nm,  $t_R$  (min): major = 4.08, minor = 5.18.



**((1*S*,3*R*)-3-(4-methoxyphenyl)-1,2,3,4-tetrahydroisoquinolin-1-yl)methanol (163d):**

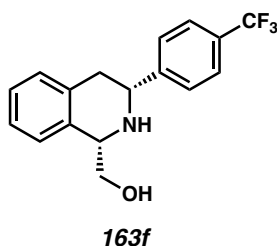
Compound **163d** was prepared from isoquinoline **162d** using general procedure 5 and purified by column chromatography (50% to 60% EtOAc in hexanes + 1% NEt<sub>3</sub>) to provide a pale yellow solid as a mixture of diastereomers (40 mg, 75% yield) (dr = 13.3:1); 92% ee for major diastereomer;  $[\alpha]_{\text{D}}^{25} +69.3$  (*c* 1.01, CHCl<sub>3</sub>); Major diastereomer: <sup>1</sup>H NMR (400 MHz, CDCl<sub>3</sub>)  $\delta$  7.39 – 7.36 (m, 2H), 7.24 – 7.15 (m, 3H), 7.12 (d, *J* = 7.6 Hz, 1H), 6.94 – 6.90 (m, 2H), 4.41 – 4.39 (m, 1H), 4.07 – 3.97 (m, 2H), 3.86 (dd, *J* = 10.9, 5.9 Hz, 1H), 3.83 (s, 3H), 3.06 – 2.95 (m, 1H), 2.86 (dd, *J* = 15.7, 3.4 Hz, 1H); <sup>13</sup>C NMR (100 MHz, CDCl<sub>3</sub>)  $\delta$  159.0, 136.6, 136.3, 134.8, 129.2, 127.8, 126.6, 126.3, 125.3, 114.0, 66.5, 58.6, 57.0, 55.4, 38.8; IR (Neat Film, NaCl) 3342, 2929, 2835, 1612, 1514, 1494, 1453, 1302, 1250, 1176, 1108, 1036, 824, 801, 743 cm<sup>-1</sup>; HRMS (MM:ESI-APCI+) *m/z* calc'd for C<sub>17</sub>H<sub>20</sub>NO<sub>2</sub> [M+H]<sup>+</sup>: 270.1489, found 270.1486; SFC Conditions: 45% IPA, 2.5 mL/min, Chiralpak AD-H column,  $\lambda$  = 210 nm, *t*<sub>R</sub> (min): major = 2.59, minor = 3.61.



**((1*S*,3*R*)-3-(4-fluorophenyl)-1,2,3,4-tetrahydroisoquinolin-1-yl)methanol (163e):**

Compound **163e** was prepared from isoquinoline **162e** using general procedure 5 and

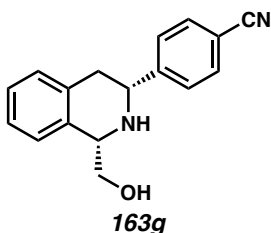
purified by column chromatography (40% EtOAc in hexanes + 1% NEt<sub>3</sub>) to provide a pale yellow solid as a mixture of diastereomers (51 mg, 99% yield) (dr = 10.1:1); 93% ee for major diastereomer;  $[\alpha]_D^{25} +79.2$  (*c* 1.00, CHCl<sub>3</sub>); Major diastereomer: <sup>1</sup>H NMR (400 MHz, CDCl<sub>3</sub>)  $\delta$  7.45 – 7.41 (m, 2H), 7.24 – 7.18 (m, 3H), 7.12 (d, *J* = 6.9 Hz, 1H), 7.08 – 7.04 (m, 2H), 4.42 – 4.40 (m, 1H), 4.08 (dd, *J* = 11.0, 3.5 Hz, 1H), 4.02 (dd, *J* = 10.8, 3.3 Hz, 1H), 3.88 (dd, *J* = 10.9, 5.5 Hz, 1H), 3.03 – 2.91 (m, 1H), 2.87 (dd, *J* = 15.7, 3.5 Hz, 1H); <sup>13</sup>C NMR (100 MHz, CDCl<sub>3</sub>)  $\delta$  162.3 (d, *J* = 245.5 Hz), 140.0 (d, *J* = 3.0 Hz), 136.4, 134.8, 129.3, 128.4 (d, *J* = 7.9 Hz), 126.6 (d, *J* = 19.9 Hz), 125.5, 115.5 (d, *J* = 21.2 Hz), 66.7, 58.6, 57.1, 39.1; <sup>19</sup>F NMR (282 MHz, CDCl<sub>3</sub>)  $\delta$  –115.0 – –115.1 (m); IR (Neat Film, NaCl) 3310, 3069, 2924, 2828, 1605, 1511, 1494, 1454, 1225, 1158, 1063, 1040, 844, 826, 744 cm<sup>-1</sup>; HRMS (MM:ESI-APCI+) *m/z* calc'd for C<sub>16</sub>H<sub>17</sub>FNO [M+H]<sup>+</sup>: 258.1289, found 258.1286; SFC Conditions: 45% IPA, 2.5 mL/min, Chiralpak AD-H column,  $\lambda$  = 210 nm, *t*<sub>R</sub> (min): major = 1.93, minor = 2.87.



**((1*S*,3*R*)-3-(4-(trifluoromethyl)phenyl)-1,2,3,4-tetrahydroisoquinolin-1-yl)methanol**

**(163f):** Compound **163f** was prepared from isoquinoline **162f** using general procedure 5 and purified by column chromatography (30% EtOAc in hexanes + 1% NEt<sub>3</sub>) to provide a yellow solid as a mixture of diastereomers (49 mg, 80% yield) (dr = 4.6:1); 92% ee for major diastereomer;  $[\alpha]_D^{25} +35.5$  (*c* 1.01, CHCl<sub>3</sub>); Major diastereomer: <sup>1</sup>H NMR (400 MHz, CDCl<sub>3</sub>)  $\delta$  7.57 – 7.55 (m, 2H, integration overlapped with minor diastereomer), 7.51

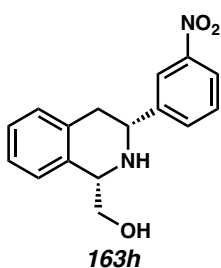
(d,  $J = 8.3$  Hz, 2H), 7.18 – 7.10 (m, 3H), 7.10 – 7.03 (m, 1H), 4.36 – 4.34 (m, 1H), 4.08 (dd,  $J = 10.6, 4.0$  Hz, 1H), 3.97 (dd,  $J = 10.8, 3.3$  Hz, 1H), 3.81 (dd,  $J = 10.9, 5.8$  Hz, 1H), 2.95 – 2.78 (m, 2H);  $^{13}\text{C}$  NMR (100 MHz,  $\text{CDCl}_3$ )  $\delta$  148.1, 135.9, 134.6, 129.1, 127.1, 127.0, 126.9, 126.7, 126.7, 126.6, 126.5, 125.7 – 125.5 (m), 125.4, 66.6, 58.4, 57.3, 38.8;  $^{19}\text{F}$  NMR (282 MHz,  $\text{CDCl}_3$ )  $\delta$  –115.1 (qd,  $J = 8.7, 5.6$  Hz); IR (Neat Film, NaCl) 3304, 2917, 1621, 1418, 1325, 1166, 1123, 1068, 1018, 844, 745  $\text{cm}^{-1}$ ; HRMS (MM:ESI-APCI+)  $m/z$  calc'd for  $\text{C}_{17}\text{H}_{17}\text{F}_3\text{NO}$   $[\text{M}+\text{H}]^+$ : 308.1257, found 308.1265; SFC Conditions: 25% IPA, 2.5 mL/min, Chiralpak AD-H column,  $\lambda = 210$  nm,  $t_{\text{R}}$  (min): major = 3.11 minor = 5.54.



**4-((1S,3R)-1-(hydroxymethyl)-1,2,3,4-tetrahydroisoquinolin-3-yl)benzonitrile (163g):**

Compound **163g** was prepared from isoquinoline **162g** using general procedure 5 and purified by column chromatography (30% EtOAc in  $\text{CH}_2\text{Cl}_2$  + 1%  $\text{NEt}_3$ ) to provide a pale tan solid as a mixture of diastereomers (44 mg, 83% yield) (dr = 2.4:1); 82% ee for major diastereomer;  $[\alpha]_{\text{D}}^{25} +57.4$  ( $c$  1.00,  $\text{CHCl}_3$ ); Major diastereomer:  $^1\text{H}$  NMR (400 MHz,  $\text{CDCl}_3$ )  $\delta$  7.69 – 7.66 (m, 2H), 7.60 – 7.57 (m, 2H), 7.26 – 7.17 (m, 3H, integration overlapped with minor diastereomer), 7.16 – 7.12 (m, 1H), 4.43 – 4.41 (m, 1H), 4.16 (dd,  $J = 10.0, 4.6$  Hz, 1H), 4.06 (dd,  $J = 10.9, 3.3$  Hz, 1H), 3.89 (dd,  $J = 10.9, 5.8$  Hz, 1H), 2.99 – 2.84 (m, 2H);  $^{13}\text{C}$  NMR (100 MHz,  $\text{CDCl}_3$ )  $\delta$  149.6, 135.7, 134.5, 132.6, 129.2, 127.6,

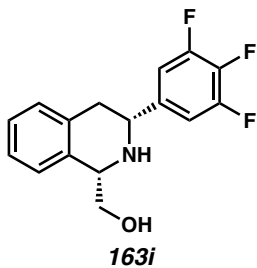
126.9, 126.8, 125.5, 118.9, 111.5, 66.7, 58.5, 57.4, 38.8; IR (Neat Film, NaCl) 3314, 3060, 2925, 2227, 1608, 1494, 1454, 1311, 1115, 1040, 910, 846, 826, 780, 740  $\text{cm}^{-1}$ ; HRMS (MM:ESI-APCI+)  $m/z$  calc'd for  $\text{C}_{17}\text{H}_{17}\text{N}_2\text{O}$   $[\text{M}+\text{H}]^+$ : 265.1335, found 265.1336; SFC Conditions: 45% IPA, 3.5 mL/min, Chiralpak AD-H column,  $\lambda = 210$  nm,  $t_{\text{R}}$  (min): major = 2.03, minor = 3.33.



**((1S,3R)-3-(3-nitrophenyl)-1,2,3,4-tetrahydroisoquinolin-1-yl)methanol (163h):**

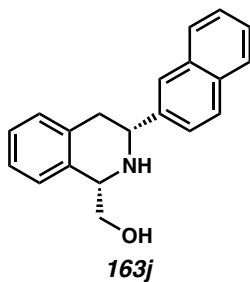
Compound **163h** was prepared from isoquinoline **162h** using general procedure 5 and purified by column chromatography (0% to 2% MeOH in  $\text{CH}_2\text{Cl}_2$ ) to provide a pale yellow solid as a mixture of diastereomers (44 mg, 78% yield) (dr = 3.2:1); 86% ee for major diastereomer;  $[\alpha]_{\text{D}}^{25} +54.4$  ( $c$  1.02,  $\text{CHCl}_3$ ); Major diastereomer:  $^1\text{H}$  NMR (400 MHz,  $\text{CDCl}_3$ )  $\delta$  8.34 (s, 1H), 8.15 (d,  $J = 8.2$  Hz, 1H), 7.81 (d,  $J = 8.1$  Hz, 1H), 7.62 – 7.47 (m, 1H), 7.25 – 7.07 (m, 4H, integration overlapped with minor diastereomer), 4.43 – 4.41 (m, 1H), 4.20 (dd,  $J = 9.2, 5.4$  Hz, 1H), 4.07 (dd,  $J = 10.9, 3.2$  Hz, 1H), 3.91 – 3.83 (m, 1H), 3.15 – 3.02 (m, 1H), 2.98 – 2.91 (m, 2H);  $^{13}\text{C}$  NMR (100 MHz,  $\text{CDCl}_3$ )  $\delta$  148.7, 146.5, 135.7, 134.6, 133.2, 129.8, 129.4, 127.0, 126.9, 125.6, 122.9, 122.0, 66.8, 58.7, 57.2, 38.9; IR (Neat Film, NaCl) 3388, 2924, 1635, 1531, 1495, 1454, 1350, 1220, 1117, 1038, 802, 781, 748, 738, 682  $\text{cm}^{-1}$ ; HRMS (MM:ESI-APCI+)  $m/z$  calc'd for  $\text{C}_{16}\text{H}_{17}\text{N}_2\text{O}_3$   $[\text{M}+\text{H}]^+$ :

285.1234, found 285.1234; SFC Conditions: 45% IPA, 3.5 mL/min, Chiralpak AD-H column,  $\lambda = 210$  nm,  $t_R$  (min): major = 2.45, minor = 3.23.



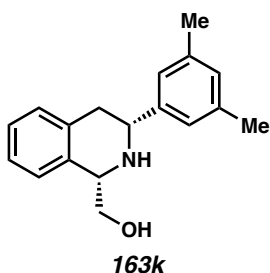
**((1*S*,3*R*)-3-(3,4,5-trifluorophenyl)-1,2,3,4-tetrahydroisoquinolin-1-yl)methanol**

**(163i):** Compound **163i** was prepared from isoquinoline **162i** using general procedure 5 and purified by column chromatography (5% to 10% EtOAc in CH<sub>2</sub>Cl<sub>2</sub> + 1% NEt<sub>3</sub>) to provide a pale yellow solid as a mixture of diastereomers (55 mg, 94% yield) (dr = 3.5:1); 89% ee for major diastereomer;  $[\alpha]_D^{25} +61.6$  (*c* 1.02, CHCl<sub>3</sub>); Major diastereomer: <sup>1</sup>H NMR (400 MHz, CDCl<sub>3</sub>)  $\delta$  7.25 – 7.18 (m, 2H, integration overlapped with minor diastereomer), 7.16 – 7.08 (m, 4H), 4.40 – 4.38 (m, 1H), 4.09 – 4.00 (m, 2H), 3.87 (dd, *J* = 10.9, 5.9 Hz, 1H), 2.88 (d, *J* = 8.4 Hz, 2H); <sup>13</sup>C NMR (100 MHz, CDCl<sub>3</sub>)  $\delta$  157.0, 151.4 (ddd, *J* = 250.1, 9.8, 3.6 Hz), 139.0 (dt, *J* = 250.9, 15.6 Hz), 135.5, 134.4, 129.2, 127.0, 126.8, 125.5, 110.9 – 110.6 (m), 66.7, 58.5, 56.2, 38.8; <sup>19</sup>F NMR (282 MHz, CDCl<sub>3</sub>)  $\delta$  –133.6 – –134.4 (m), –161.8 – –162.0 (m); IR (Neat Film, NaCl) 3307, 2928, 1621, 1532, 1454, 1372, 1340, 1235, 1043, 866, 804, 748, 698 cm<sup>-1</sup>; HRMS (MM:ESI-APCI+) *m/z* calc'd for C<sub>16</sub>H<sub>15</sub>F<sub>3</sub>NO [M+H]<sup>+</sup>: 294.1100, found 294.1095; SFC Conditions: 40% IPA, 2.5 mL/min, Chiralpak AD-H column,  $\lambda = 210$  nm,  $t_R$  (min): major = 1.67, minor = 2.20.



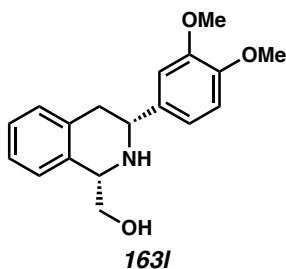
**((1S,3R)-3-(naphthalen-2-yl)-1,2,3,4-tetrahydroisoquinolin-1-yl)methanol (163j):**

Compound **163j** was prepared from isoquinoline **162j** using general procedure 5 and purified by column chromatography (30% EtOAc in hexanes + 1% NEt<sub>3</sub>) to provide a pale yellow solid as a single diastereomer (49 mg, 80% yield); 95% ee; [ $\alpha$ ]<sub>D</sub><sup>25</sup> +90.7 (*c* 1.00, CHCl<sub>3</sub>); <sup>1</sup>H NMR (400 MHz, CDCl<sub>3</sub>)  $\delta$  7.90 (s, 1H), 7.88 – 7.84 (m, 3H), 7.60 (dd, *J* = 8.5, 1.8 Hz, 1H), 7.53 – 7.45 (m, 2H), 7.28 – 7.20 (m, 3H), 7.15 (d, *J* = 6.8 Hz, 1H), 4.48 – 4.46 (m, 1H), 4.27 (dd, *J* = 11.1, 3.5 Hz, 1H), 4.06 (dd, *J* = 10.9, 3.3 Hz, 1H), 3.94 (dd, *J* = 10.8, 5.4 Hz, 1H), 3.14 – 3.07 (m, 1H), 2.98 (dd, *J* = 15.7, 3.5 Hz, 1H); <sup>13</sup>C NMR (100 MHz, CDCl<sub>3</sub>)  $\delta$  141.8, 136.7, 135.1, 133.7, 133.2, 129.4, 128.6, 128.1, 127.9, 126.9, 126.7, 126.4, 126.1, 125.6, 125.3, 66.8, 58.8, 57.9, 39.1; IR (Neat Film, NaCl) 3056, 2917, 2356, 1602, 1494, 1454, 1425, 1366, 1314, 1276, 1112, 1047, 862, 820, 743 cm<sup>-1</sup>; HRMS (MM:ESI-APCI+) *m/z* calc'd for C<sub>20</sub>H<sub>20</sub>NO [M+H]<sup>+</sup>: 290.1539, found 290.1540; SFC Conditions: 45% IPA, 3.5 mL/min, Chiralpak AD-H column,  $\lambda$  = 210 nm, t<sub>R</sub> (min): major = 3.61, minor = 5.81.



**((1*S*,3*R*)-3-(3,5-dimethylphenyl)-1,2,3,4-tetrahydroisoquinolin-1-yl)methanol (163k):**

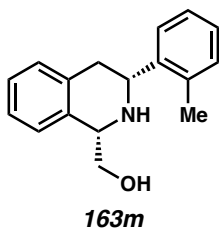
Compound **163k** was prepared from isoquinoline **162k** using general procedure 5 and purified by column chromatography (30% EtOAc in hexanes + 1% NEt<sub>3</sub>) to provide a pale yellow solid as a single diastereomer (49 mg, 80% yield); 92% ee; [α]<sub>D</sub><sup>25</sup> +93.5 (*c* 0.98, CHCl<sub>3</sub>): <sup>1</sup>H NMR (400 MHz, CDCl<sub>3</sub>) δ 7.25 – 7.16 (m, 3H), 7.12 (d, *J* = 6.5 Hz, 1H), 7.07 (s, 2H), 6.95 (s, 1H), 4.41 – 4.39 (m, 1H), 4.02 (dd, *J* = 10.9, 3.3 Hz, 2H), 3.90 (dd, *J* = 10.8, 5.4 Hz, 1H), 3.04 – 3.00 (m, 1H), 2.88 (dd, *J* = 15.8, 3.4 Hz, 1H), 2.34 (s, 6H); <sup>13</sup>C NMR (100 MHz, CDCl<sub>3</sub>) δ 144.2, 138.3, 136.8, 135.0, 129.3, 126.7, 126.4, 125.4, 124.6, 66.6, 58.7, 57.6, 38.9, 21.5; IR (Neat Film, NaCl) 3318, 3014, 2916, 1607, 1494, 1454, 1313, 1117, 1038, 854, 782, 746, 725 cm<sup>-1</sup>; HRMS (MM:ESI-APCI+) *m/z* calc'd for C<sub>18</sub>H<sub>22</sub>NO [M+H]<sup>+</sup>: 268.1696, found 268.1702; SFC Conditions: 45% IPA, 3.5 mL/min, Chiralpak AD-H column, λ = 210 nm, t<sub>R</sub> (min): major = 1.95, minor = 3.02.



**((1*S*,3*R*)-3-(3,4-dimethoxyphenyl)-1,2,3,4-tetrahydroisoquinolin-1-yl)methanol (163l):**

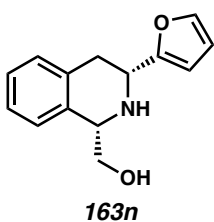


Compound **163l** was prepared from isoquinoline **162l** using general procedure 5 and purified by column chromatography (1% MeOH in CH<sub>2</sub>Cl<sub>2</sub> + 1% NEt<sub>3</sub>) to provide a pale yellow solid as a single diastereomer (49 mg, 80% yield); 88% ee; [ $\alpha$ ]<sub>D</sub><sup>25</sup> +62.4 (*c* 1.00, CHCl<sub>3</sub>); <sup>1</sup>H NMR (400 MHz, CDCl<sub>3</sub>)  $\delta$  7.22 – 7.16 (m, 3H), 7.12 (d, *J* = 6.7 Hz, 1H), 7.04 – 6.94 (m, 2H), 6.87 – 6.84 (m, 1H), 4.38 – 4.36 (m, 1H), 4.01 (dt, *J* = 11.2, 4.0 Hz, 2H), 3.90 (s, 3H), 3.88 (s, 3H), 3.84 (dd, *J* = 11.0, 6.0 Hz, 1H), 3.08 – 3.00 (m, 1H), 2.87 (dd, *J* = 15.8, 3.3 Hz, 1H); <sup>13</sup>C NMR (100 MHz, CDCl<sub>3</sub>)  $\delta$  149.2, 148.5, 136.5, 136.4, 134.6, 129.3, 126.7, 126.4, 125.3, 119.0, 111.2, 110.0, 66.3, 58.8, 57.6, 56.1, 38.7; IR (Neat Film, NaCl) 3332, 2934, 2832, 1593, 1518, 1494, 1454, 1264, 1238, 1141, 1028, 745, 720 cm<sup>-1</sup>; HRMS (MM:ESI-APCI+) *m/z* calc'd for C<sub>18</sub>H<sub>22</sub>NO<sub>3</sub> [M+H]<sup>+</sup>: 300.1594, found 300.1600; SFC Conditions: 45% IPA, 3.5 mL/min, Chiralpak AD-H column,  $\lambda$  = 210 nm, *t*<sub>R</sub> (min): major = 2.28, minor = 2.93.



**((1S,3R)-3-(*o*-tolyl)-1,2,3,4-tetrahydroisoquinolin-1-yl)methanol (163m):** Compound **163m** was prepared from isoquinoline **162m** using general procedure 5 and purified by column chromatography (30% EtOAc in hexanes + 1% NEt<sub>3</sub>) to provide a pale beige solid as a mixture of diastereomers (49 mg, 80% yield) (*dr* = 10.1:1); 49% ee from major diastereomer; [ $\alpha$ ]<sub>D</sub><sup>25</sup> +53.7 (*c* 1.01, CHCl<sub>3</sub>); <sup>1</sup>H NMR (400 MHz, CDCl<sub>3</sub>)  $\delta$  7.60 (d, *J* = 7.1 Hz, 1H), 7.29 – 7.26 (m, 1H), 7.26 – 7.17 (m, 5H), 7.14 (d, *J* = 7.3 Hz, 1H), 4.44 – 4.42 (m, 1H), 4.32 (dd, *J* = 10.9, 3.5 Hz, 1H), 4.04 (dd, *J* = 10.8, 3.2 Hz, 1H), 3.92 (dd, *J* = 10.8,

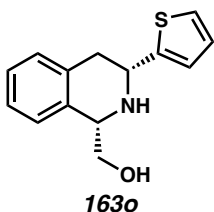
5.3 Hz, 1H), 3.03 – 2.92 (m, 1H), 2.88 (dd,  $J = 15.8, 3.5$  Hz, 1H), 2.39 (s, 3H);  $^{13}\text{C}$  NMR (100 MHz,  $\text{CDCl}_3$ )  $\delta$  142.2, 136.9, 135.2, 135.0, 130.6, 129.4, 127.3, 126.7, 126.5, 125.6, 125.5, 66.6, 58.9, 53.4, 37.7, 19.5; IR (Neat Film, NaCl) 3318, 3022, 2925, 2354, 1492, 1454, 1316, 1117, 1037, 864, 751, 743, 727  $\text{cm}^{-1}$ ; HRMS (MM:ESI-APCI+)  $m/z$  calc'd for  $\text{C}_{17}\text{H}_{20}\text{NO}$   $[\text{M}+\text{H}]^+$ : 254.1539, found 254.1539; SFC Conditions: 30% IPA, 2.5 mL/min, Chiralpak AD-H column,  $\lambda = 210$  nm,  $t_{\text{R}}$  (min): major = 5.91, minor = 6.39.



**((1S,3R)-3-(furan-2-yl)-1,2,3,4-tetrahydroisoquinolin-1-yl)methanol (163n):**

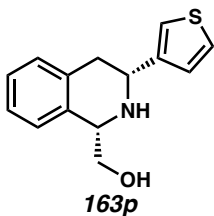
Compound **163n** was prepared from isoquinoline **162n** using general procedure 5 and purified by column chromatography (40% EtOAc in hexanes + 1%  $\text{NEt}_3$ ) to provide a pale yellow solid as a mixture of diastereomers (34 mg, 74% yield) (dr = 3.3:1); 92% ee for major diastereomer;  $[\alpha]_{\text{D}}^{25} +35.5$  ( $c$  1.00,  $\text{CHCl}_3$ ); Major diastereomer:  $^1\text{H}$  NMR (400 MHz,  $\text{CDCl}_3$ )  $\delta$  7.41 – 7.39 (m, 1H), 7.24 – 7.14 (m, 4H, integration overlapped with minor diastereomer), 6.37 (dd,  $J = 3.3, 1.9$  Hz, 1H), 6.28 (d,  $J = 3.2$  Hz, 1H), 4.37 – 4.35 (m, 1H), 4.20 (dd,  $J = 11.0, 3.7$  Hz, 1H), 4.03 (dd,  $J = 11.0, 3.3$  Hz, 1H), 3.86 – 3.75 (m, 1H), 3.18 – 3.05 (m, 1H), 3.05 – 2.95 (m, 1H);  $^{13}\text{C}$  NMR (100 MHz,  $\text{CDCl}_3$ )  $\delta$  141.8, 135.5, 134.7, 129.4, 126.9, 126.7, 126.5, 125.3, 110.2, 105.3, 66.2, 57.9, 50.7, 34.5; IR (Neat Film, NaCl) 3304, 2920, 1495, 1454, 1316, 1146, 1114, 1062, 1037, 1009, 883, 740  $\text{cm}^{-1}$ ; HRMS (MM:ESI-APCI+)  $m/z$  calc'd for  $\text{C}_{14}\text{H}_{16}\text{NO}_2$   $[\text{M}+\text{H}]^+$ : 230.1176, found 230.1181; SFC

Conditions: 35% IPA, 2.5 mL/min, Chiralpak OJ-H column,  $\lambda = 210$  nm,  $t_R$  (min): major = 1.52, minor = 1.82.



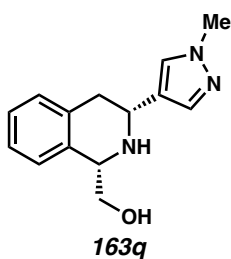
**((1*S*,3*R*)-3-(thiophen-2-yl)-1,2,3,4-tetrahydroisoquinolin-1-yl)methanol (163o):**

Compound **163o** was prepared from isoquinoline **162o** using general procedure 5 and purified by column chromatography (40% EtOAc in hexanes + 1% NEt<sub>3</sub>) to provide a pale beige solid as a mixture of diastereomers (46 mg, 94% yield) (dr = 3.6:1); 90% ee for major diastereomer;  $[\alpha]_D^{25} +57.4$  (*c* 1.04, CHCl<sub>3</sub>); Major diastereomer: <sup>1</sup>H NMR (400 MHz, CDCl<sub>3</sub>)  $\delta$  7.34 – 7.28 (m, 1H), 7.28 – 7.21 (m, 3H, integration overlapped with minor diastereomer), 7.19 – 7.15 (m, 1H), 7.11 – 7.09 (m, 1H), 7.07 – 7.04 (m, 1H), 4.47 – 4.42 (m, 2H), 4.06 (dd, *J* = 10.9, 3.4 Hz, 1H), 3.87 (dd, *J* = 11.0, 5.9 Hz, 1H), 3.19 – 2.98 (m, 2H); <sup>13</sup>C NMR (100 MHz, CDCl<sub>3</sub>)  $\delta$  148.1, 135.8, 134.7, 129.1, 126.7, 126.7, 126.6, 125.3, 124.2, 123.5, 66.4, 58.5, 53.1, 39.3; IR (Neat Film, NaCl) 3312, 2923, 2360, 1494, 1454, 1424, 1310, 1280, 1112, 1038, 850, 830, 744, 704 cm<sup>-1</sup>; HRMS (MM:ESI-APCI+) *m/z* calc'd for C<sub>14</sub>H<sub>16</sub>NOS [M+H]<sup>+</sup>: 246.0947, found 246.0941; SFC Conditions: 35% IPA, 2.5 mL/min, Chiralpak OJ-H column,  $\lambda = 210$  nm,  $t_R$  (min): major = 2.86, minor = 6.02.



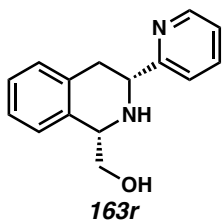
**((1S,3R)-3-(thiophen-3-yl)-1,2,3,4-tetrahydroisoquinolin-1-yl)methanol (163p):**

Compound **163p** was prepared from isoquinoline **162p** using general procedure 5 and purified by column chromatography (30% EtOAc in hexanes + 1% NEt<sub>3</sub>) to provide a pale beige solid as a mixture of diastereomers (25.5 mg, 52% yield) (dr = 7.3:1). The isolated product contained long-chain hydrocarbon impurities, so it was repurified by partitioning between acetonitrile and hexanes. The acetonitrile layer was collected and concentrated to afford **163p** as a pale yellow solid (24.0 mg, 49% yield); 89% ee for major diastereomer;  $[\alpha]_D^{25} +86.8$  (*c* 0.99, CHCl<sub>3</sub>): <sup>1</sup>H NMR (400 MHz, CDCl<sub>3</sub>) δ 7.24 (dd, *J* = 4.9, 3.0 Hz, 1H), 7.18 – 7.16 (m, 1H), 7.13 – 7.07 (m, 4H), 7.05 – 7.02 (m, 1H), 4.28 – 4.26 (m, 1H), 4.10 (dd, *J* = 10.8, 3.8 Hz, 1H), 3.93 (dd, *J* = 10.9, 3.4 Hz, 1H), 3.73 (dd, *J* = 11.0, 6.1 Hz, 1H), 2.99 – 2.90 (m, 1H), 2.86 (dd, *J* = 15.8, 3.8 Hz, 1H); <sup>13</sup>C NMR (100 MHz, CDCl<sub>3</sub>) δ 145.3, 136.2, 134.9, 129.3, 126.7, 126.5, 126.5, 126.2, 125.3, 120.9, 66.3, 58.5, 53.3, 38.1; IR (Neat Film, NaCl) 3318, 2924, 2366, 1494, 1454, 1424, 1313, 1279, 1218, 1116, 1038, 854, 782, 748 cm<sup>-1</sup>; HRMS (MM:ESI-APCI+) *m/z* calc'd for C<sub>14</sub>H<sub>16</sub>NOS [M+H]<sup>+</sup>: 246.0947, found 246.0952; SFC Conditions: 35% IPA, 2.5 mL/min, Chiralpak AD-H column, λ = 210 nm, t<sub>R</sub> (min): major = 3.19, minor = 4.05.



**((1S,3R)-3-(1-methyl-1H-pyrazol-4-yl)-1,2,3,4-tetrahydroisoquinolin-1-yl)methanol**

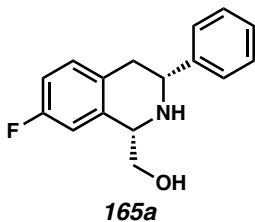
**(163q):** Compound **163q** was prepared from isoquinoline **162q** using general procedure 5 and purified by column chromatography (5% to 10% MeOH in EtOAc + 1% NEt<sub>3</sub>) to provide a pale yellow solid as a mixture of diastereomers (48 mg, 98% yield) (dr = 2.9:1); 87% ee for major diastereomer;  $[\alpha]_D^{25} +37.1$  (*c* 1.021, CHCl<sub>3</sub>); Major diastereomer: <sup>1</sup>H NMR (400 MHz, CDCl<sub>3</sub>) δ 7.63 – 7.61 (m, 2H), 7.26 – 7.16 (m, 2H, integration overlapped with minor diastereomer), 7.19 – 7.06 (m, 2H), 4.50 – 4.98 (m, 1H), 4.20 (dd, *J* = 11.8, 3.3 Hz, 1H), 4.02 (dd, *J* = 11.6, 3.3 Hz, 1H), 3.84 (s, 3H), 3.34 – 3.22 (m, 1H), 3.13 – 2.89 (m, 2H); <sup>13</sup>C NMR (100 MHz, CDCl<sub>3</sub>) δ 138.2, 134.7, 132.2, 129.3, 129.2, 127.2, 126.9, 125.4, 121.5, 64.6, 58.6, 49.1, 39.0, 36.1; IR (Neat Film, NaCl) 3315, 2931, 2371, 1560, 1494, 1455, 1408, 1295, 1169, 1031, 1008, 986, 748, 724 cm<sup>-1</sup>; HRMS (MM:ESI-APCI+) *m/z* calc'd for C<sub>14</sub>H<sub>18</sub>N<sub>3</sub>O [M+H]<sup>+</sup>: 244.1444, found 244.1448; SFC Conditions: 25% IPA, 2.5 mL/min, Chiralpak OJ-H column, λ = 210 nm, *t*<sub>R</sub> (min): minor = 1.84, major = 2.60.



**((1S,3R)-3-(pyridin-2-yl)-1,2,3,4-tetrahydroisoquinolin-1-yl)methanol** **(163r):**

Compound **163r** was prepared from isoquinoline **162r** using general procedure 5 and

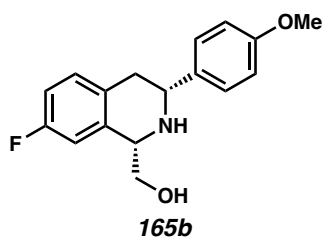
purified using reverse-phase (C<sub>18</sub>) preparative-HPLC (MeCN/0.4% acetic acid in water, 5.0 mL/min, monitor wavelength = 255 nm, 5–23% MeCN over 6 min, ramp to 95% MeCN over 0.5 min, and hold at 95% for 3.5 min) to provide a tan solid as a mixture of diastereomers (49 mg, 80% yield) (dr = 2.5:1). This compound appears to be unstable and significant decomposition was observed under prolonged storage; 85% ee for major diastereomer;  $[\alpha]_D^{25} +49.0$  (*c* 1.01, CHCl<sub>3</sub>); Major diastereomer: <sup>1</sup>H NMR (400 MHz, CDCl<sub>3</sub>) δ 8.60 – 8.57 (m, 1H), 7.72 – 7.67 (m, 2H), 7.43 (d, *J* = 7.8 Hz, 1H), 7.22 – 7.11 (m, 4H, integration overlapped with minor diastereomer), 4.41 – 4.39 (m, 1H), 4.23 – 4.20 (m, 1H, integration overlapped with minor diastereomer), 4.07 (dd, *J* = 11.1, 3.4 Hz, 1H), 3.85 (dd, *J* = 11.0, 6.4 Hz, 1H), 3.08 – 3.00 (m, 2H, integration overlapped with minor diastereomer); <sup>13</sup>C NMR (100 MHz, CDCl<sub>3</sub>) δ 162.2, 149.4, 137.0, 136.0, 135.3, 129.4, 126.7, 126.5, 125.4, 122.6, 121.1, 66.4, 58.6, 58.0, 36.5; IR (Neat Film, NaCl) 3300, 3056, 2934, 1592, 1574, 1473, 1454, 1435, 1316, 1142, 1060, 910, 744 cm<sup>-1</sup>; HRMS (MM:ESI-APCI+) *m/z* calc'd for C<sub>15</sub>H<sub>17</sub>N<sub>2</sub>O [M+H]<sup>+</sup>: 241.1335, found 241.1334; SFC Conditions: 30% IPA, 2.5 mL/min, Chiralpak OD-H column, λ = 210 nm, t<sub>R</sub> (min): minor = 2.52, major = 2.79.



**((1*S*,3*R*)-7-fluoro-3-phenyl-1,2,3,4-tetrahydroisoquinolin-1-yl)methanol (165a):**

Compound **165a** was prepared from isoquinoline **164a** using general procedure 5 and purified by column chromatography (30% EtOAc in hexanes + 1% NEt<sub>3</sub>) to provide a pale

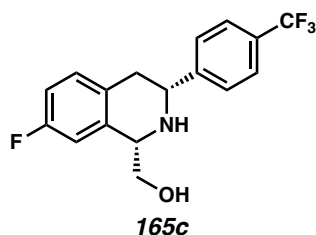
yellow solid as a mixture of diastereomers (49 mg, 94% yield) (dr = 11.5:1); 93% ee for major diastereomer;  $[\alpha]_D^{25} +76.9$  (*c* 1.04, CHCl<sub>3</sub>); Major diastereomer: <sup>1</sup>H NMR (400 MHz, CDCl<sub>3</sub>) δ 7.47 – 7.42 (m, 2H), 7.40 – 7.36 (m, 2H), 7.33 – 7.30 (m, 1H), 7.08 (dd, *J* = 8.4, 5.8 Hz, 1H), 6.97 – 6.87 (m, 2H), 4.38 – 4.36 (m, 1H), 4.06 (dd, *J* = 10.8, 3.7 Hz, 1H), 3.99 (dd, *J* = 10.9, 3.3 Hz, 1H), 3.86 (dd, *J* = 10.9, 5.2 Hz, 1H), 3.00 – 2.82 (m, 2H); <sup>13</sup>C NMR (100 MHz, CDCl<sub>3</sub>) δ 161.5 (d, *J* = 243.8 Hz), 144.0, 136.9 (d, *J* = 6.8 Hz), 132.2 (d, *J* = 3.0 Hz), 130.6 (d, *J* = 7.9 Hz), 128.8, 127.8, 126.8, 113.9 (d, *J* = 21.3 Hz), 112.1 (d, *J* = 21.8 Hz), 66.4, 58.6 (d, *J* = 2.1 Hz), 57.7, 38.2; <sup>19</sup>F NMR (282 MHz, CDCl<sub>3</sub>) δ –116.2 – –116.4 (m); IR (Neat Film, NaCl) 3309, 2918, 1614, 1498, 1455, 1428, 1255, 1221, 1031, 911, 868, 808, 758, 745, 700 cm<sup>-1</sup>; HRMS (MM:ESI-APCI+) *m/z* calc'd for C<sub>16</sub>H<sub>17</sub>FNO [M+H]<sup>+</sup>: 258.1289, found 258.1281; SFC Conditions: 40% IPA, 2.5 mL/min, Chiralpak AD-H column, λ = 210 nm, *t*<sub>R</sub> (min): major = 2.56, minor = 3.04.



**((1*S*,3*R*)-7-fluoro-3-(4-methoxyphenyl)-1,2,3,4-tetrahydroisoquinolin-1-yl)methanol**

**(165b):** Compound **165b** was prepared from isoquinoline **164b** using general procedure 5 and purified by column chromatography (30% to 40% EtOAc in hexanes + 1% NEt<sub>3</sub>) to provide a pale yellow solid as a single diastereomer (57 mg, 99% yield); 90% ee;  $[\alpha]_D^{25} +57.8$  (*c* 0.99, CHCl<sub>3</sub>); <sup>1</sup>H NMR (400 MHz, CDCl<sub>3</sub>) δ 7.38 – 7.34 (m, 2H), 7.07 (dd, *J* = 8.4, 5.8 Hz, 1H), 6.97 – 6.84 (m, 4H), 4.36 – 4.34 (m, 1H), 3.99 (ddd, *J* = 12.3, 10.9, 3.4 Hz, 2H), 3.86 – 3.84 (m, 1H), 3.82 (s, 3H), 2.99 – 2.87 (m, 1H), 2.83 (dd, *J* = 15.6, 3.5 Hz,

1H);  $^{13}\text{C}$  NMR (100 MHz,  $\text{CDCl}_3$ )  $\delta$  161.5 (d,  $J = 243.7$  Hz), 159.2, 136.9 (d,  $J = 6.7$  Hz), 136.2, 132.3, 130.6 (d,  $J = 7.9$  Hz), 127.9, 114.1, 113.8 (d,  $J = 21.3$  Hz), 112.1 (d,  $J = 21.8$  Hz), 66.4, 58.7 (d,  $J = 2.0$  Hz), 57.1, 55.5, 38.3;  $^{19}\text{F}$  NMR (282 MHz,  $\text{CDCl}_3$ )  $\delta$  -116.3 – -116.4 (m); IR (Neat Film, NaCl) 3305, 2930, 2838, 1614, 1591, 1514, 1498, 1304, 1249, 1178, 1111, 1034, 912, 868, 830, 816, 736  $\text{cm}^{-1}$ ; HRMS (MM:ESI-APCI+)  $m/z$  calc'd for  $\text{C}_{17}\text{H}_{19}\text{FNO}_2$   $[\text{M}+\text{H}]^+$ : 288.1394, found 288.1404; SFC Conditions: 30% IPA, 2.5 mL/min, Chiralpak OJ-H column,  $\lambda = 210$  nm,  $t_R$  (min): major = 1.93, minor = 2.42.

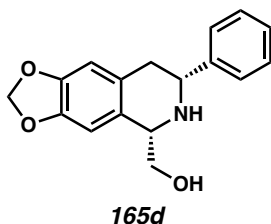


**((1S,3R)-7-fluoro-3-(4-(trifluoromethyl)phenyl)-1,2,3,4-tetrahydroisoquinolin-1-**

**yl)methanol (165c):** Compound **165c** was prepared from isoquinoline **164c** using general procedure 5 and purified by column chromatography (20% to 30% EtOAc in hexanes + 1%  $\text{NEt}_3$ ) to provide a pale yellow solid as a mixture of diastereomers (50 mg, 77% yield) (dr = 6.7:1); 94% ee for major diastereomer;  $[\alpha]_{\text{D}}^{25} +44.2$  ( $c$  1.002,  $\text{CHCl}_3$ ); Major diastereomer:  $^1\text{H}$  NMR (400 MHz,  $\text{CDCl}_3$ )  $\delta$  7.64 (d,  $J = 8.3$  Hz, 2H), 7.58 (d,  $J = 8.1$  Hz, 2H), 7.09 (dd,  $J = 8.4, 5.7$  Hz, 1H), 7.00 – 6.87 (m, 2H), 4.39 – 4.37 (m, 1H), 4.13 (dd,  $J = 8.9, 5.7$  Hz, 1H), 4.02 (dd,  $J = 10.9, 3.3$  Hz, 1H), 3.88 (dd,  $J = 10.9, 5.4$  Hz, 1H), 2.94 – 2.84 (m, 2H);  $^{13}\text{C}$  NMR (100 MHz,  $\text{CDCl}_3$ )  $\delta$  161.6 (d,  $J = 244.2$  Hz), 148.0, 136.7 (d,  $J = 6.7$  Hz), 131.5 (d,  $J = 3.1$  Hz), 130.6 (d,  $J = 7.9$  Hz), 130.1 (q,  $J = 32.5$  Hz), 127.2, 125.7 (q,  $J = 3.8$  Hz), 124.2 (q,  $J = 272.1$  Hz), 114.0 (d,  $J = 21.3$  Hz), 112.1 (d,  $J = 21.9$  Hz) 66.4, 58.5 (d,  $J = 2.0$  Hz), 57.4, 38.2;  $^{19}\text{F}$  NMR (282 MHz,  $\text{CDCl}_3$ )  $\delta$  -62.5, -115.8 – -115.9

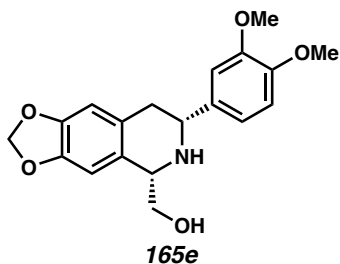


(m); IR (Neat Film, NaCl) 3304, 2922, 1620, 1593, 1500, 1428, 1326, 1255, 1222, 1165, 1125, 1068, 1018, 868, 836, 816  $\text{cm}^{-1}$ ; HRMS (MM:ESI-APCI+)  $m/z$  calc'd for  $\text{C}_{17}\text{H}_{16}\text{F}_4\text{NO}$   $[\text{M}+\text{H}]^+$ : 326.1163, found 326.1175; SFC Conditions: 20% IPA, 2.5 mL/min, Chiralpak AD-H column,  $\lambda = 210$  nm,  $t_R$  (min): major = 3.93, minor = 4.46.

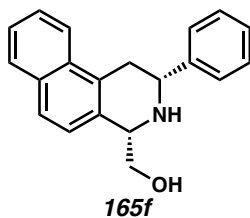


**((5*S*,7*R*)-7-phenyl-5,6,7,8-tetrahydro-[1,3]dioxolo[4,5-*g*]isoquinolin-5-yl)methanol**

**(165d):** Compound **165d** was prepared from isoquinoline **164d** using general procedure 5 and purified by column chromatography (75% EtOAc in hexanes + 1%  $\text{NEt}_3$ ) to provide a pale beige solid as a mixture of diastereomers (17 mg, 30% yield) (dr = 4.9:1); 58% ee for major diastereomer;  $[\alpha]_D^{25} +29.2$  ( $c$  0.940,  $\text{CHCl}_3$ ); Major diastereomer:  $^1\text{H}$  NMR (400 MHz,  $\text{CDCl}_3$ )  $\delta$  7.47 – 7.41 (m, 2H), 7.39 – 7.37 (m, 2H), 7.33 – 7.27 (m, 1H), 6.71 (s, 1H), 6.60 – 6.58 (m, 1H), 5.95 – 5.89 (m, 2H), 4.32 – 4.30 (m, 1H), 4.04 (dd,  $J = 11.1, 3.4$  Hz, 1H), 3.93 (dd,  $J = 10.9, 3.2$  Hz, 1H), 3.82 (dd,  $J = 10.9, 5.1$  Hz, 1H), 2.97 – 2.88 (m, 1H), 2.78 (dd,  $J = 15.5, 3.4$  Hz, 1H);  $^{13}\text{C}$  NMR (100 MHz,  $\text{CDCl}_3$ )  $\delta$  146.5, 146.4, 144.2, 130.0, 128.8, 127.9, 127.7, 126.8, 109.0, 105.5, 101.0, 66.7, 58.6, 57.7, 39.0; IR (Neat Film, NaCl) 3324, 3028, 2897, 1504, 1486, 1454, 1434, 1384, 1306, 1279, 1231, 1128, 1038, 936, 910, 858, 750, 733, 701  $\text{cm}^{-1}$ ; HRMS (MM:ESI-APCI+)  $m/z$  calc'd for  $\text{C}_{17}\text{H}_{18}\text{NO}_3$   $[\text{M}+\text{H}]^+$ : 284.1281, found 284.1276; SFC Conditions: 45% IPA, 2.5 mL/min, Chiralpak AD-H column,  $\lambda = 210$  nm,  $t_R$  (min): major = 5.00, minor = 7.22.

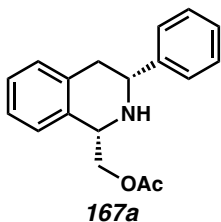


**((5*S*,7*R*)-7-(3,4-dimethoxyphenyl)-5,6,7,8-tetrahydro-[1,3]dioxolo[4,5-*g*]isoquinolin-5-yl)methanol (165e):** Compound **165e** was prepared from isoquinoline **164e** using general procedure 5 and purified by column chromatography (100% EtOAc to 10% MeOH in EtOAc + 1% NEt<sub>3</sub>) to provide a pale yellow solid as a single diastereomer (28 mg, 41% yield); 54% ee; [ $\alpha$ ]<sub>D</sub><sup>25</sup> +25.5 (*c* 0.197, CH<sub>3</sub>OH); <sup>1</sup>H NMR (400 MHz, CDCl<sub>3</sub>)  $\delta$  6.99 – 6.96 (m, 2H), 6.87 – 6.85 (m, 1H), 6.71 (s, 1H), 6.60 – 6.58 (m, 1H), 5.94 – 5.91 (m, 2H), 4.32 – 4.30 (m, 1H), 3.99 (dd, *J* = 11.1, 3.4 Hz, 1H), 3.94 (dd, *J* = 11.1, 3.4 Hz, 1H), 3.91 (s, 3H), 3.89 (s, 3H), 3.83 (dd, *J* = 11.0, 5.0 Hz, 1H), 2.97 – 2.85 (m, 1H), 2.76 (dd, *J* = 15.6, 3.4 Hz, 1H); <sup>13</sup>C NMR (100 MHz, CDCl<sub>3</sub>)  $\delta$  149.3, 148.7, 146.7, 146.5, 136.9, 130.1, 127.8, 119.0, 111.4, 110.0, 109.1, 105.6, 101.1, 66.7, 58.8, 57.7, 56.2, 39.1; IR (Neat Film, NaCl) 3374, 2890, 2360, 1505, 1487, 1268, 1260, 1237, 1140, 1076, 1024, 971, 932, 918, 730 cm<sup>-1</sup>; HRMS (MM:ESI-APCI+) *m/z* calc'd for C<sub>19</sub>H<sub>22</sub>NO<sub>5</sub> [M+H]<sup>+</sup>: 344.1492, found 344.1483; SFC Conditions: 45% IPA, 2.5 mL/min, Chiralpak AD-H column,  $\lambda$  = 210 nm, *t*<sub>R</sub> (min): major = 3.89, minor = 5.16.



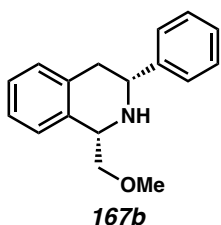
**((2*R*,4*S*)-2-phenyl-1,2,3,4-tetrahydrobenzo[*f*]isoquinolin-4-yl)methanol (165f):**

Compound **165f** was prepared from isoquinoline **164f** using general procedure 5 and purified by column chromatography (40% to 60% EtOAc in hexanes + 1% NEt<sub>3</sub>) to provide a pale yellow solid as a mixture of diastereomers (25 mg, 43% yield) (dr = 15.7:1); 82% ee for major diastereomer;  $[\alpha]_D^{25} +85.7$  (*c* 1.01, CHCl<sub>3</sub>); Major diastereomer: <sup>1</sup>H NMR (400 MHz, CDCl<sub>3</sub>) δ 7.93 – 7.91 (m, 1H), 7.85 – 7.82 (m, 1H), 7.75 (d, *J* = 8.6 Hz, 1H), 7.55 (d, *J* = 7.2 Hz, 2H), 7.50 – 7.47 (m, 2H), 7.45 – 7.34 (m, 4H), 4.61 – 4.59 (m, 1H), 4.20 (dd, *J* = 11.0, 3.4 Hz, 1H), 4.09 (dd, *J* = 10.9, 3.2 Hz, 1H), 4.01 (dd, *J* = 10.9, 4.8 Hz, 1H), 3.50 – 3.39 (m, 1H), 3.23 – 3.10 (m, 1H); <sup>13</sup>C NMR (100 MHz, CDCl<sub>3</sub>) δ 144.4, 132.2, 132.1, 132.0, 131.9, 128.8, 128.4, 127.7, 126.8, 126.7, 126.3, 125.5, 123.4, 122.9, 66.4, 59.1, 57.6, 35.4; IR (Neat Film, NaCl) 3306, 3056, 2918, 1417, 1308, 1034, 910, 884, 813, 762, 700, 736, 682 cm<sup>-1</sup>; HRMS (MM:ESI-APCI+) *m/z* calc'd for C<sub>20</sub>H<sub>20</sub>NO [M+H]<sup>+</sup>: 290.1539, found 290.1534; SFC Conditions: 45% IPA, 2.5 mL/min, Chiralpak AD-H column, λ = 210 nm, t<sub>R</sub> (min): major = 5.31, minor = 10.01.



**((1*S*,3*R*)-3-phenyl-1,2,3,4-tetrahydroisoquinolin-1-yl)methyl acetate (167a):**

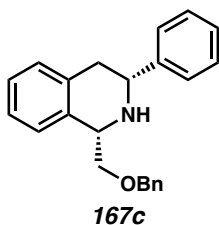
Compound **167a** was prepared from isoquinoline **166a** using general procedure 5 and purified by column chromatography (5% EtOAc in CH<sub>2</sub>Cl<sub>2</sub> + 1% NEt<sub>3</sub>) to provide a yellow oil as a single diastereomer (32 mg, 56% yield); 86% ee; [α]<sub>D</sub><sup>25</sup> +103.8 (*c* 1.01, CHCl<sub>3</sub>); <sup>1</sup>H NMR (400 MHz, CDCl<sub>3</sub>) δ 7.51 – 7.45 (m, 2H), 7.41 – 7.37 (m, 2H), 7.34 – 7.30 (m, 1H), 7.27 – 7.24 (m, 1H), 7.23 – 7.18 (m, 2H), 7.16 – 7.10 (m, 1H), 4.78 (dd, *J* = 10.8, 3.5 Hz, 1H), 4.54 – 4.51 (m, 1H), 4.14 (dd, *J* = 10.8, 8.7 Hz, 1H), 4.05 (dd, *J* = 11.1, 3.4 Hz, 1H), 3.08 – 3.01 (m, 1H), 2.90 (dd, *J* = 15.5, 3.6 Hz, 1H), 2.08 (s, 3H); <sup>13</sup>C NMR (100 MHz, CDCl<sub>3</sub>) δ 171.1, 144.4, 136.3, 134.1, 129.5, 128.8, 127.7, 126.9, 126.9, 126.3, 125.3, 69.1, 57.9, 56.4, 39.2, 21.2; IR (Neat Film, NaCl) 3024, 2926, 2802, 1741, 1494, 1454, 1386, 1366, 1314, 1229, 1118, 1034, 754, 701 cm<sup>-1</sup>; HRMS (MM:ESI-APCI+) *m/z* calc'd for C<sub>18</sub>H<sub>20</sub>NO<sub>2</sub> [M+H]<sup>+</sup>: 282.1489, found 282.1492; SFC Conditions: 20% IPA, 2.5 mL/min, Chiralpak OJ-H column, λ = 210 nm, *t*<sub>R</sub> (min): major = 3.32, major = 3.93.



**(1*S*,3*R*)-1-(methoxymethyl)-3-phenyl-1,2,3,4-tetrahydroisoquinoline (167b):**

Compound **167b** was prepared from isoquinoline **166b** using general procedure 5 and

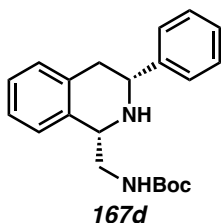
purified by column chromatography (10% EtOAc in CH<sub>2</sub>Cl<sub>2</sub>+ 1% NEt<sub>3</sub>) to provide a viscous yellow oil as a single diastereomer (40 mg, 80% yield); 89% ee; [ $\alpha$ ]<sub>D</sub><sup>25</sup> +94.3 (*c* 0.98, CHCl<sub>3</sub>); <sup>1</sup>H NMR (400 MHz, CDCl<sub>3</sub>)  $\delta$  7.48 – 7.46 (m, 2H), 7.39 – 7.35 (m, 2H), 7.32 – 7.27 (m, 1H), 7.25 – 7.20 (m, 1H), 7.20 – 7.15 (m, 2H), 7.16 – 7.10 (m, 1H), 4.45 – 4.42 (m, 1H), 4.07 – 3.94 (m, 2H), 3.59 (t, *J* = 8.7 Hz, 1H), 3.43 (s, 3H), 3.06 (dd, *J* = 16.0, 11.1 Hz, 1H), 2.92 (dd, *J* = 16.0, 3.6 Hz, 1H); <sup>13</sup>C NMR (100 MHz, CDCl<sub>3</sub>)  $\delta$  144.5, 136.3, 135.4, 129.5, 128.7, 127.5, 126.9, 126.6, 126.1, 124.8, 59.3, 58.1, 57.4, 39.0; IR (Neat Film, NaCl) 3028, 2895, 2812, 1604, 1494, 1454, 1313, 1194, 1112, 1072, 1030, 958, 923, 840, 744, 700 cm<sup>-1</sup>; HRMS (MM:ESI-APCI+) *m/z* calc'd for C<sub>17</sub>H<sub>20</sub>NO [M+H]<sup>+</sup>: 254.1539, found 254.1531; SFC Conditions: 20% IPA, 2.5 mL/min, Chiralpak OD-H column,  $\lambda$  = 210 nm, *t*<sub>R</sub> (min): major = 4.82, major = 5.25.



**(1*S*,3*R*)-1-((benzyloxy)methyl)-3-phenyl-1,2,3,4-tetrahydroisoquinoline (167c):**

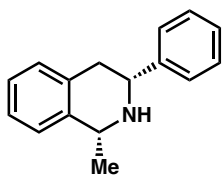
Compound **167c** was prepared from isoquinoline **166c** using general procedure 5 and purified by column chromatography (5% EtOAc in CH<sub>2</sub>Cl<sub>2</sub> + 1% NEt<sub>3</sub>) to provide a pale yellow oil as a single diastereomer (60 mg, 90% yield); 88% ee; [ $\alpha$ ]<sub>D</sub><sup>25</sup> +80.4 (*c* 1.02, CHCl<sub>3</sub>); <sup>1</sup>H NMR (400 MHz, CDCl<sub>3</sub>)  $\delta$  7.48 – 7.46 (m, 2H), 7.40 – 7.34 (m, 6H), 7.32 – 7.28 (m, 2H), 7.22 – 7.16 (m, 3H), 7.14 – 7.11 (m, 1H), 4.61 (s, 2H), 4.48 (dd, *J* = 8.7, 3.4 Hz, 1H), 4.12 (dd, *J* = 9.0, 3.6 Hz, 1H), 4.04 (dd, *J* = 11.1, 3.5 Hz, 1H), 3.67 (t, *J* = 8.7 Hz, 1H), 3.05 (dd, *J* = 15.9, 11.1 Hz, 1H), 2.91 (dd, *J* = 15.8, 3.5 Hz, 1H); <sup>13</sup>C NMR (100 MHz,

CDCl<sub>3</sub>)  $\delta$  144.6, 138.3, 136.3, 135.3, 129.5, 128.7, 128.6, 127.9, 127.8, 127.5, 126.9, 126.6, 126.1, 124.9, 74.8, 73.6, 58.1, 57.5, 39.2; IR (Neat Film, NaCl) 3060, 3028, 2862, 1494, 1454, 1366, 1312, 1098, 1028, 742, 698 cm<sup>-1</sup>; HRMS (MM:ESI-APCI+)  $m/z$  calc'd for C<sub>23</sub>H<sub>24</sub>NO [M+H]<sup>+</sup>: 330.1852, found 330.1857; SFC Conditions: 25% IPA, 2.5 mL/min, Chiralpak OD-H column,  $\lambda$  = 210 nm,  $t_R$  (min): major = 5.66, major = 6.38.



**tert-butyl (((1S,3R)-3-phenyl-1,2,3,4-tetrahydroisoquinolin-1-yl)methyl)carbamate**

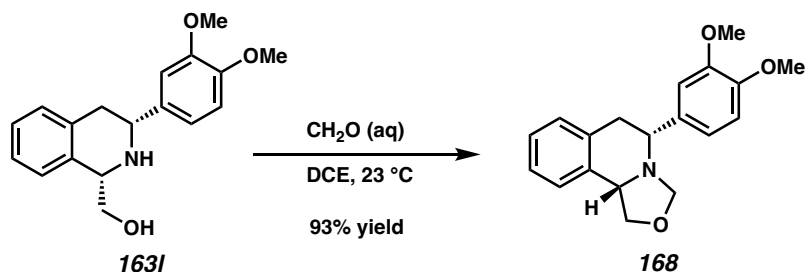
**(167d):** Compound **167d** was prepared from isoquinoline **166d** using general procedure 5 and purified by column chromatography (15% EtOAc in hexanes + 1% NEt<sub>3</sub>) to provide a white solid as a mixture of diastereomers (44 mg, 71% yield) (dr = 9.0:1); 90% ee for major diastereomer;  $[\alpha]_D^{25}$  +50.4 ( $c$  0.99, CHCl<sub>3</sub>); Major diastereomer: <sup>1</sup>H NMR (400 MHz, CDCl<sub>3</sub>)  $\delta$  7.46 (d,  $J$  = 7.1 Hz, 2H), 7.38 (t,  $J$  = 7.5 Hz, 2H), 7.36 – 7.26 (m, 2H), 7.26 – 7.14 (m, 2H), 7.11 (d,  $J$  = 6.7 Hz, 1H), 5.02 (s, 1H), 4.44 (s, 1H), 4.04 (dd,  $J$  = 11.0, 3.5 Hz, 1H), 3.77 – 3.72 (m, 1H), 3.49 (dt,  $J$  = 13.2, 6.3 Hz, 1H), 3.00 (dd,  $J$  = 15.8, 10.9 Hz, 1H), 2.89 (dd,  $J$  = 15.8, 3.5 Hz, 1H), 1.41 (s, 9H); <sup>13</sup>C NMR (100 MHz, CDCl<sub>3</sub>)  $\delta$  156.4, 144.4, 136.4, 135.2, 129.2, 128.7, 127.7, 126.8, 126.6, 126.4, 125.7, 79.4, 58.0, 57.1, 46.3, 39.1, 28.5; IR (Neat Film, NaCl) 3352, 2978, 2932, 1704, 1495, 1455, 1392, 1366, 1247, 1171, 752, 701 cm<sup>-1</sup>; HRMS (MM:ESI-APCI+)  $m/z$  calc'd for C<sub>21</sub>H<sub>27</sub>N<sub>2</sub>O<sub>2</sub> [M+H]<sup>+</sup>: 339.2067, found 339.2063; SFC Conditions: 40% IPA, 2.5 mL/min, Chiralpak AD-H column,  $\lambda$  = 210 nm,  $t_R$  (min): major = 1.41, major = 1.76.



**167e**

**(1*R*,3*R*)-1-methyl-3-phenyl-1,2,3,4-tetrahydroisoquinoline (167e):** Compound **167e** was prepared from 1-methyl-3-phenylisoquinoline **161a** using general procedure 5 and purified by column chromatography (10% to 20% EtOAc in hexanes + 1% NEt<sub>3</sub>) to provide a colorless oil as a single diastereomer (29 mg, 64% yield); 90% ee; [ $\alpha$ ]<sub>D</sub><sup>25</sup> +133.3 (*c* 0.79, CHCl<sub>3</sub>); <sup>1</sup>H NMR (400 MHz, CDCl<sub>3</sub>)  $\delta$  7.49 – 7.46 (m, 2H), 7.41 – 7.37 (m, 2H), 7.33 – 7.29 (m, 1H), 7.28 – 7.23 (m, 1H), 7.23 – 7.14 (m, 2H), 7.11 (d, *J* = 6.9 Hz, 1H), 4.34 (q, *J* = 6.6 Hz, 1H), 4.08 (dd, *J* = 11.1, 3.9 Hz, 1H), 3.12 – 3.01 (m, 1H), 2.96 (dd, *J* = 16.2, 4.1 Hz, 1H), 1.55 (d, *J* = 6.5 Hz, 3H); <sup>13</sup>C NMR (100 MHz, CDCl<sub>3</sub>)  $\delta$  144.5, 139.9, 135.2, 129.1, 128.7, 127.5, 126.7, 126.2, 126.2, 125.4, 58.8, 53.6, 38.9, 22.4; IR (Neat Film, NaCl) 3024, 2962, 2926, 2792, 1602, 1494, 1453, 1372, 1352, 1306, 1140, 1118, 1031, 790, 753, 733, 700 cm<sup>-1</sup>; HRMS (MM:ESI-APCI+) *m/z* calc'd for C<sub>16</sub>H<sub>18</sub>N [M+H]<sup>+</sup>: 224.1434, found 224.1426; SFC Conditions: 20% IPA, 3.5 mL/min, Chiralpak AS-H column,  $\lambda$  = 210 nm, *t*<sub>R</sub> (min): major = 2.16, minor = 2.62.

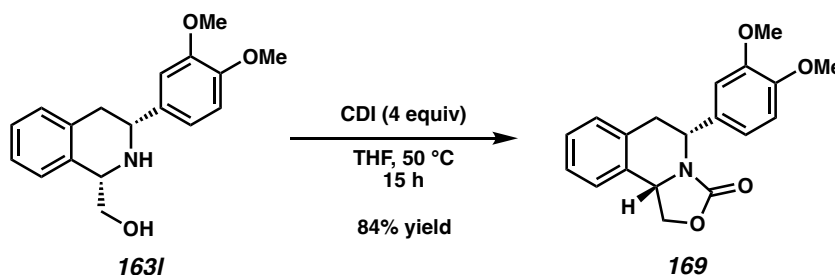
### 2.7.2.4 Product transformations



#### (5*R*,10*bS*)-5-(3,4-dimethoxyphenyl)-1,5,6,10*b*-tetrahydro-3*H*-oxazolo[4,3-*a*]isoquinoline (**168**):

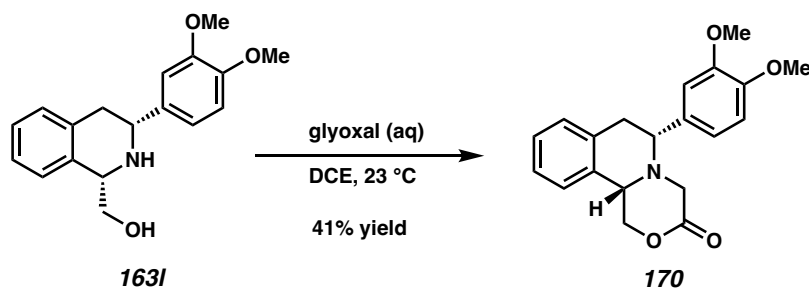
To a 1-dram vial equipped with a stir bar was added tetrahydroisoquinoline **163I** (20.0 mg, 0.067 mmol) in 1,2-dichloroethane (1.3 mL, 0.05 M). Formaldehyde solution (37 wt% in H<sub>2</sub>O, 9.2  $\mu$ L, 0.124 mmol) was then added and the reaction was stirred for 15 minutes at room temperature. The reaction was then basified with K<sub>2</sub>CO<sub>3</sub>, and extracted with CH<sub>2</sub>Cl<sub>2</sub>. The collected organic layers were dried over Na<sub>2</sub>SO<sub>4</sub>, and concentrated under vacuum. The crude product was purified by column chromatography (50% EtOAc in hexanes + 1% NEt<sub>3</sub>) to afford **168** as a white solid (19.3 mg, 93% yield):  $[\alpha]_{\text{D}}^{25} +134.8$  (*c* 1.03, CHCl<sub>3</sub>); <sup>1</sup>H NMR (400 MHz, CDCl<sub>3</sub>)  $\delta$  7.25 – 7.14 (m, 3H), 7.04 (d, *J* = 2.0 Hz, 1H), 7.02 – 6.90 (m, 2H), 6.83 (d, *J* = 8.2 Hz, 1H), 4.58 – 4.43 (m, 2H), 3.97 (t, *J* = 7.6 Hz, 1H), 3.94 – 3.87 (m, 2H), 3.89 (s, 6H), 3.83 (dd, *J* = 10.6, 4.8 Hz, 1H), 3.23 (dd, *J* = 16.8, 10.6 Hz, 1H), 3.11 (dd, *J* = 16.8, 4.8 Hz, 1H); <sup>13</sup>C NMR (100 MHz, CDCl<sub>3</sub>)  $\delta$  149.4, 148.7, 135.1, 134.7, 134.6, 128.6, 127.2, 126.3, 125.0, 119.6, 110.9, 110.2, 84.2, 71.5, 62.9, 61.3, 56.1, 56.0, 37.3; IR (Neat Film, NaCl) 2930, 1592, 1513, 1454, 1263, 1237, 1167, 1060, 1027, 918, 752, 680 cm<sup>-1</sup>; HRMS (MM:ESI-APCI+) *m/z* calc'd for C<sub>19</sub>H<sub>22</sub>NO<sub>3</sub> [M+H]<sup>+</sup>: 312.1594, found 312.1594.





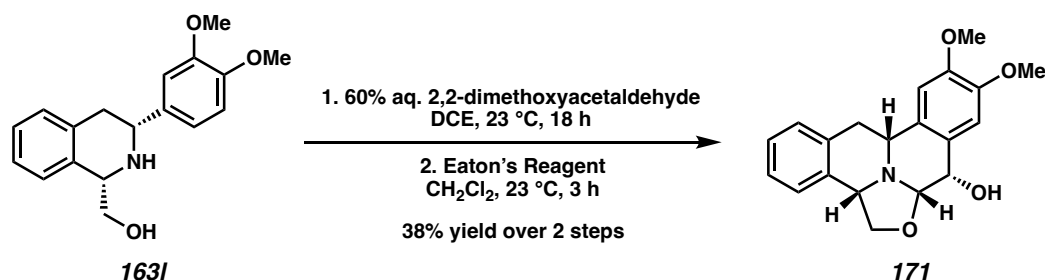
**(5R,10bS)-5-(3,4-dimethoxyphenyl)-1,5,6,10b-tetrahydro-3H-oxazolo[4,3-a]isoquinolin-3-one (169):**

To a 1-dram vial equipped with a stir bar was added tetrahydroisoquinoline **163I** (10.0 mg, 0.033 mmol), THF (0.7 mL, 0.05 M), and CDI (21.7 mg, 0.134 mmol). The solution was stirred at 50 °C for 15 h. After complete conversion of the starting material monitored by TLC, the reaction concentrated and the crude product was purified by preparative-TLC (100% EtOAc) to afford **169** as a white solid (9.2 mg, 84% yield):  $[\alpha]_{\text{D}}^{25} +71.4$  (*c* 0.76, CHCl<sub>3</sub>); <sup>1</sup>H NMR (400 MHz, CDCl<sub>3</sub>)  $\delta$  7.34 (dd, *J* = 8.3, 7.0 Hz, 1H), 7.30 – 7.23 (m, 1H), 7.08 (t, *J* = 6.6 Hz, 2H), 6.66 (d, *J* = 8.2 Hz, 1H), 6.52 (dd, *J* = 8.2, 2.1 Hz, 1H), 6.33 (d, *J* = 2.1 Hz, 1H), 5.14 – 5.02 (m, 2H), 4.92 (t, *J* = 7.9 Hz, 1H), 4.49 (dd, *J* = 10.1, 8.2 Hz, 1H), 3.78 (s, 3H), 3.60 (s, 3H), 3.36 (dd, *J* = 14.9, 6.4 Hz, 1H), 2.99 (dd, *J* = 14.9, 2.7 Hz, 1H); <sup>13</sup>C NMR (100 MHz, CDCl<sub>3</sub>)  $\delta$  156.1, 148.7, 148.3, 136.0, 134.2, 133.9, 129.4, 128.5, 127.5, 122.4, 118.5, 110.9, 109.3, 67.5, 55.9, 55.6, 54.6, 53.4, 36.8; IR (Neat Film, NaCl) 2933, 1756, 1515, 1464, 1396, 1260, 1234, 1139, 1025, 779, 762, 748 cm<sup>-1</sup>; HRMS (MM:ESI-APCI+) *m/z* calc'd for C<sub>19</sub>H<sub>20</sub>NO<sub>4</sub> [M+H]<sup>+</sup>: 326.1387, found 326.1386.



**(6*R*,11*bS*)-6-(3,4-dimethoxyphenyl)-1,6,7,11*b*-tetrahydro-[1,4]oxazino[3,4-*a*]isoquinolin-3(4*H*)-one (170):**

To a 1-dram vial equipped with a stir bar was added tetrahydroisoquinoline **163I** (20.0 mg, 0.067 mmol) in 1,2-dichloroethane (1.3 mL, 0.05 M). Glyoxal solution (40 wt% in H<sub>2</sub>O, 0.15 mL, 1.336 mmol) was then added, and the reaction was stirred at room temperature overnight. After complete conversion of the starting material monitored by TLC, the reaction was diluted with H<sub>2</sub>O, and extracted with CH<sub>2</sub>Cl<sub>2</sub>. The collected organic layers were dried over Na<sub>2</sub>SO<sub>4</sub>, and concentrated under vacuum. The crude product was purified by preparative-TLC (50% EtOAc in hexanes) to afford **170** as a white solid (9.2 mg, 41% yield):  $[\alpha]_{\text{D}}^{25} +187.8$  (*c* 0.61, CHCl<sub>3</sub>); <sup>1</sup>H NMR (400 MHz, CDCl<sub>3</sub>) δ 7.29 – 7.20 (m, 2H), 7.20 – 7.10 (m, 2H), 6.95 – 6.81 (m, 3H), 4.84 (dd, *J* = 10.5, 3.4 Hz, 1H), 4.33 (t, *J* = 10.7 Hz, 1H), 4.04 – 3.94 (m, 1H), 3.90 (s, 6H), 3.62 (d, *J* = 17.7 Hz, 1H), 3.43 (dd, *J* = 11.2, 3.2 Hz, 1H), 3.32 – 3.19 (m, 1H), 2.98 – 2.85 (m, 2H); <sup>13</sup>C NMR (100 MHz, CDCl<sub>3</sub>) δ 167.7, 149.8, 149.1, 135.0, 132.8, 130.6, 129.1, 127.7, 126.7, 124.7, 120.5, 111.4, 110.2, 73.3, 63.8, 59.5, 56.1, 56.1, 54.9, 38.9; IR (Neat Film, NaCl) 2932, 1745, 1511, 1463, 1421, 1263, 1242, 1137, 1028, 809, 746 cm<sup>-1</sup>; HRMS (MM:ESI-APCI+) *m/z* calc'd for C<sub>20</sub>H<sub>22</sub>NO<sub>4</sub> [M+H]<sup>+</sup>: 340.1543, found 340.1545.



(4*b**S*,6*a**S*,7*S*,11*b**R*)-9,10-dimethoxy-4*b*,5,6*a*,7,11*b*,12-

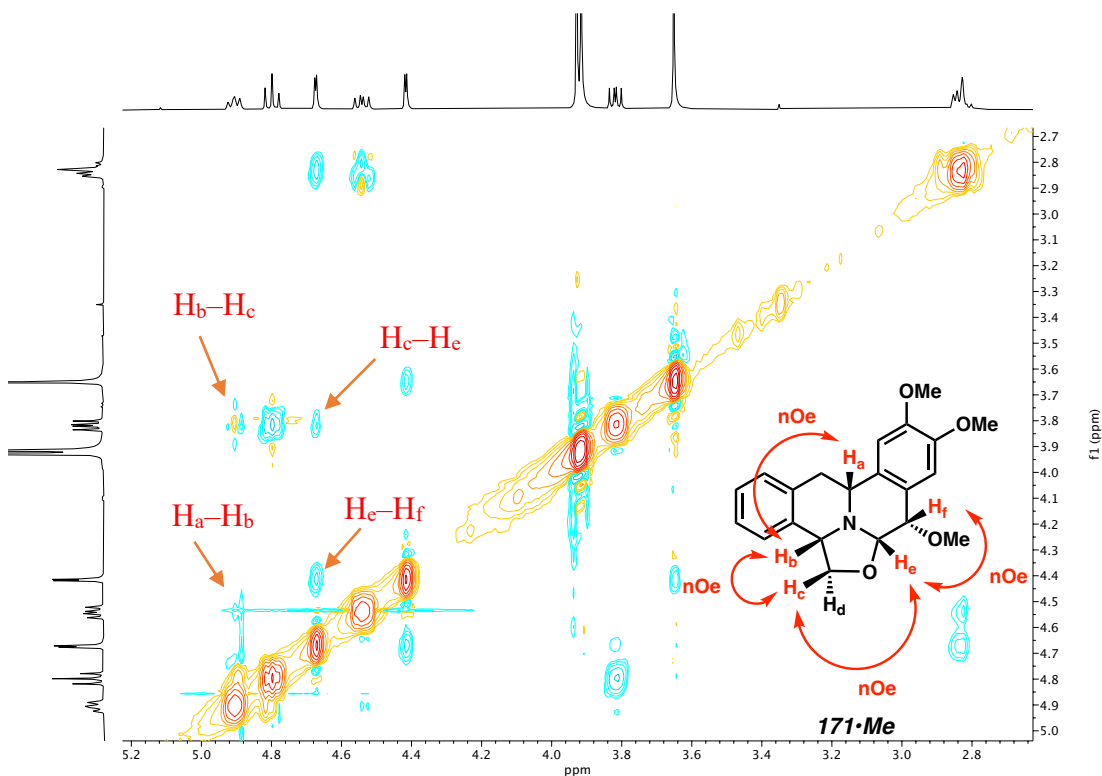
hexahydrodibenzo[*a,g*]oxazolo[2,3,4-*de*]quinolizin-7-ol (171):

To a 1-dram vial equipped with a stir bar was added tetrahydroisoquinoline **163I** (10.0 mg, 0.033 mmol) in 1,2-dichloroethane (0.5 mL, 0.07 M). 2,2-Dimethoxyacetaldehyde solution (60 wt% in H<sub>2</sub>O, 9.2 μL, 0.061 mmol) was then added and the reaction stirred at room temperature overnight. The reaction was then concentrated under vacuum to afford a yellow oil, which was then used in the next step without further purification.

To a 1-dram vial was added the crude product and CH<sub>2</sub>Cl<sub>2</sub> (0.5 mL, 0.07 M). Eaton's reagent (0.28 mL, 0.134 mmol) was then added dropwise, and the reaction was stirred for 3 hours. The reaction was then quenched by slow addition of saturated aqueous NaHCO<sub>3</sub>, diluted with H<sub>2</sub>O and extracted with CH<sub>2</sub>Cl<sub>2</sub>. The collected organic phases were dried over Na<sub>2</sub>SO<sub>4</sub>, and concentrated under vacuum. The crude product was purified by preparative-TLC (100% EtOAc) twice to afford **171** as a white solid as a single diastereomer (4.3 mg, 38% yield over 2 steps): [α]<sub>D</sub><sup>25</sup> +32.0 (*c* 0.29, CHCl<sub>3</sub>); <sup>1</sup>H NMR (400 MHz, CDCl<sub>3</sub>) δ 7.29 – 7.26 (m, 1H), 7.24 – 7.20 (m, 1H), 7.16 (d, *J* = 6.0 Hz, 1H), 7.08 (d, *J* = 6.8 Hz, 1H), 6.97 (s, 1H), 6.69 (s, 1H), 4.89 – 4.82 (m, 1H), 4.79 (t, *J* = 7.8 Hz, 1H), 4.71 (dd, *J* = 8.3, 2.1 Hz, 1H), 4.65 (d, *J* = 2.1 Hz, 1H), 4.47 (dd, *J* = 9.1, 7.0 Hz, 1H), 3.93

(s, 3H), 3.91 (s, 3H), 3.86 (dd,  $J = 7.9, 5.3$  Hz, 1H), 2.89 – 2.87 (m, 2H), 2.79 (d,  $J = 8.4$  Hz, 1H);  $^{13}\text{C}$  NMR (100 MHz,  $\text{CDCl}_3$ )  $\delta$  149.4, 148.6, 136.5, 133.1, 130.9, 129.3, 127.3, 127.3, 126.8, 126.6, 113.6, 109.2, 86.7, 74.4, 67.9, 57.3, 56.2, 56.1, 54.2, 31.1; IR (Neat Film, NaCl) 3442, 2918, 1610, 1515, 1464, 1380, 1353, 1270, 1242, 1160, 1117, 1074, 1010, 868, 762, 732, 642  $\text{cm}^{-1}$ ; HRMS (MM:ESI-APCI+)  $m/z$  calc'd for  $\text{C}_{20}\text{H}_{22}\text{NO}_4$   $[\text{M}+\text{H}]^+$ : 340.1543, found 340.1548.

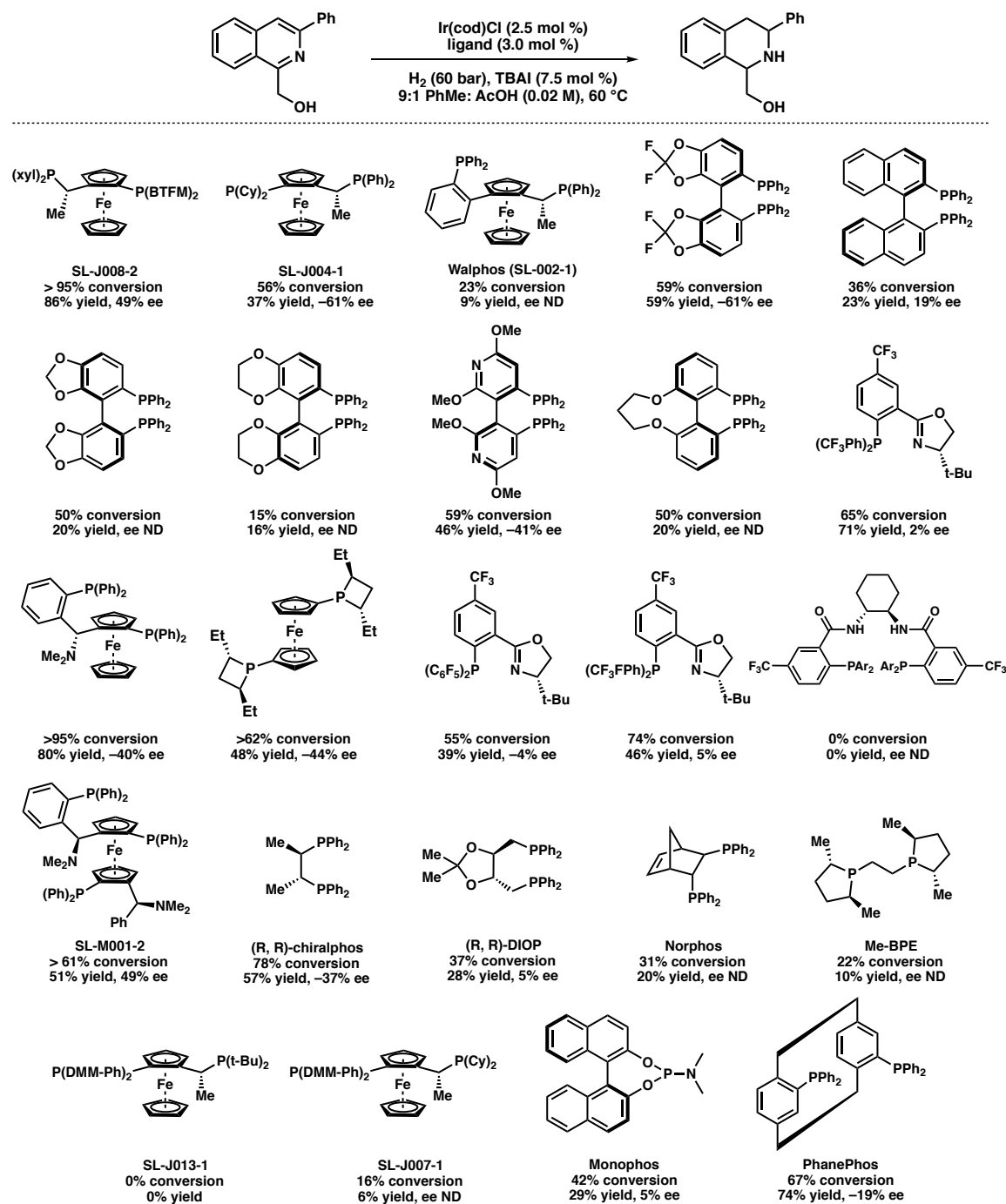
The stereochemistry of **171** was assigned using diagnostic nOe correlations (highlighted arrows, *vide infra*). Due to the ambiguous nOe correlations observed in **171**, the stereochemistry was determined by derivatizing the hydroxyl group of **171** to the methoxy group.

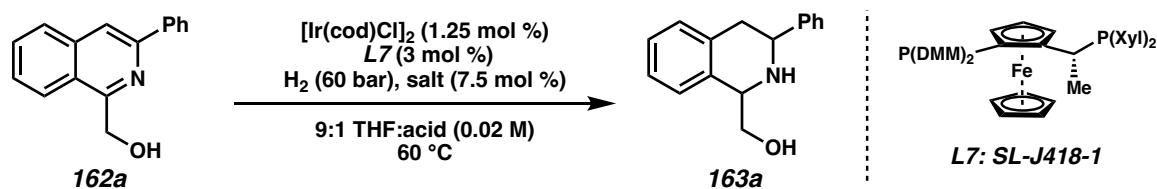


2D NOESY NMR of compound **171**•Me.

### 2.7.3 Additional optimization results

**Table 2.2.** Additional ligand screen.



**Table 2.3.** Additive effects in Ir-catalyzed enantio- and diastereoselective hydrogenation.<sup>a</sup>

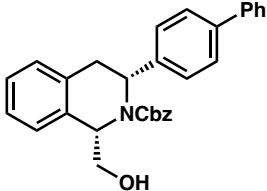
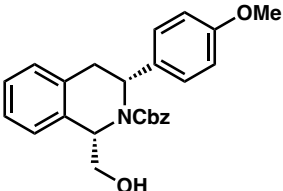
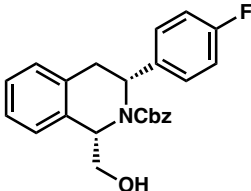
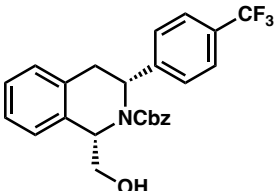
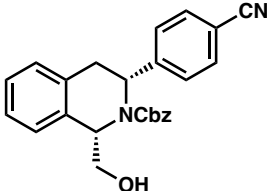
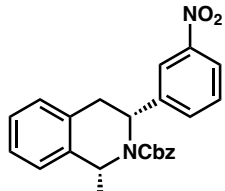
entry	salt additive	acid	% conversion <sup>b</sup>	cis:trans <sup>b</sup>	% ee of cis <sup>c</sup>
1	TBAI	AcOH	>95	10:1	89
2	Lil	AcOH	>95	10:1	89
3	NaI	AcOH	>95	10:1	90
4	KI	AcOH	92	10:1	87
5	TBACl	AcOH	>95	1:1.2	31
6	TBABr	AcOH	>95	1.2:1	63
7	none	AcOH	50	1:1	27
8	TBAI	none	31	ND	67
9	TBAI	TFA	>95	10:1	90
10	TBAI	(n-BuO) <sub>2</sub> PO <sub>2</sub> H	>95	7:1	84

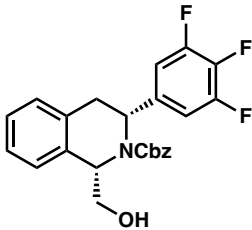
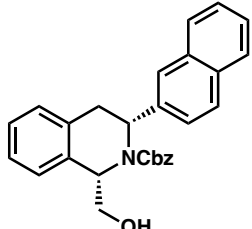
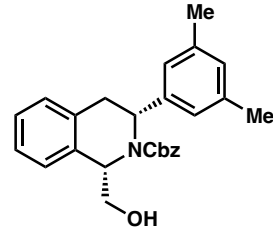
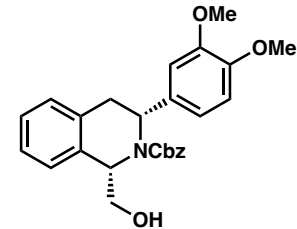
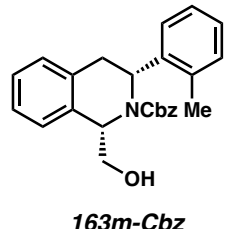
[a] Reaction conditions: 0.04 mmol of **162a**, 1.25 mol %  $[\text{Ir}(\text{cod})\text{Cl}]_2$ , 3 mol % ligand, 7.5 mol % TBAI, 60 bar  $\text{H}_2$  in 2.0 mL 9:1 solvent:AcOH. [b] Determined by crude  $^1\text{H}$  NMR using 1,3,5-trimethoxybenzene as a standard. [c] Determined by chiral SFC analysis of Cbz-protected product.

## 2.7.4 Determination of enantiomeric excess

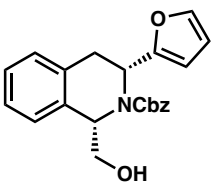
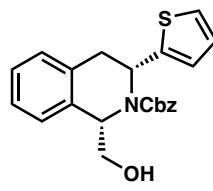
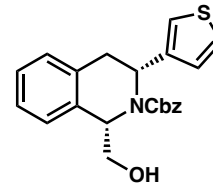
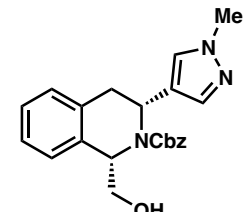
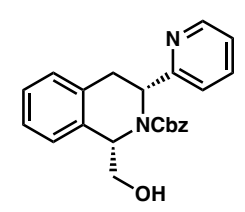
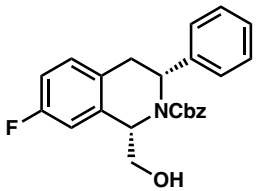
**Table 2.4.** Determination of enantiomeric excess.

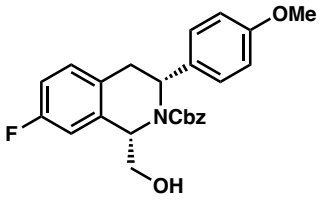
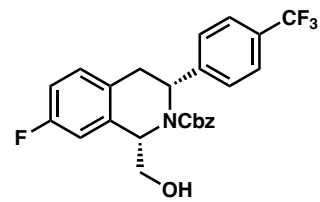
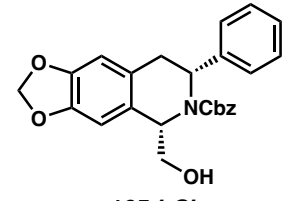
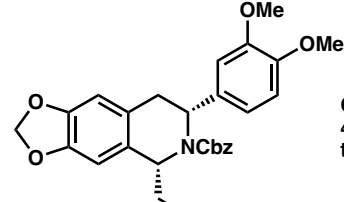
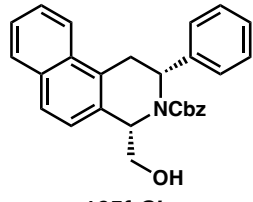
entry	compound	SFC analytic conditions	ee (%)
1	<p><b>163a-Cbz</b></p>	Chiralpak AD-H, $\lambda = 210$ nm 45% IPA/ $\text{CO}_2$ , 3.5 mL/min $t_R$ (min) major 2.34, minor 4.02	92
2	<p><b>163b-Cbz</b></p>	Chiralpak AD-H, $\lambda = 210$ nm 45% IPA/ $\text{CO}_2$ , 3.5 mL/min $t_R$ (min) major 1.81, minor 2.73	91

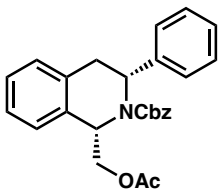
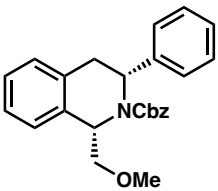
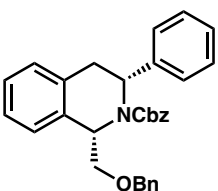
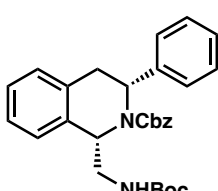
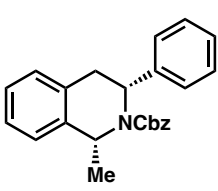
entry	compound	SFC analytic conditions	ee (%)
3	 <p><b>163c-Cbz</b></p>	Chiralcel AD-H, $\lambda = 210$ nm 45% IPA/CO <sub>2</sub> , 3.5 mL/min t <sub>R</sub> (min) major 4.08, minor 5.18	92
4	 <p><b>163d-Cbz</b></p>	Chiralpak AD-H, $\lambda = 210$ nm 45% IPA/CO <sub>2</sub> , 2.5 mL/min t <sub>R</sub> (min) major 2.59, minor 3.61	92
5	 <p><b>163e-Cbz</b></p>	Chiralpak AD-H, $\lambda = 210$ nm 45% IPA/CO <sub>2</sub> , 2.5 mL/min t <sub>R</sub> (min) major 1.93, minor 2.87	93
6	 <p><b>163f-Cbz</b></p>	Chiralpak AD-H, $\lambda = 210$ nm 25% IPA/CO <sub>2</sub> , 2.5 mL/min t <sub>R</sub> (min) major 3.11, minor 5.54	92
7	 <p><b>163g-Cbz</b></p>	Chiralpak AD-H, $\lambda = 210$ nm 45% IPA/CO <sub>2</sub> , 3.5 mL/min t <sub>R</sub> (min) major 2.03, minor 3.33	82
8	 <p><b>163h-Cbz</b></p>	Chiralpak AD-H, $\lambda = 210$ nm 45% IPA/CO <sub>2</sub> , 3.5 mL/min t <sub>R</sub> (min) major 2.45, minor 3.23	86

entry	compound	SFC analytic conditions	ee (%)
9	 <p><b>163i-Cbz</b></p>	Chiralcel AD-H, $\lambda = 210$ nm 40% IPA/CO <sub>2</sub> , 2.5 mL/min t <sub>R</sub> (min) major 1.67, minor 2.20	89
10	 <p><b>163j-Cbz</b></p>	Chiralpak AD-H, $\lambda = 210$ nm 45% IPA/CO <sub>2</sub> , 3.5 mL/min t <sub>R</sub> (min) major 3.61, minor 5.81	95
11	 <p><b>163k-Cbz</b></p>	Chiralpak AD-H, $\lambda = 210$ nm 45% IPA/CO <sub>2</sub> , 3.5 mL/min t <sub>R</sub> (min) major 1.95, minor 3.02	92
12	 <p><b>163l-Cbz</b></p>	Chiralpak AD-H, $\lambda = 210$ nm 45% IPA/CO <sub>2</sub> , 3.5 mL/min t <sub>R</sub> (min) major 2.28, minor 2.93	88
13	 <p><b>163m-Cbz</b></p>	Chiralpak AD-H, $\lambda = 210$ nm 30% IPA/CO <sub>2</sub> , 2.5 mL/min t <sub>R</sub> (min) major 5.91, minor 6.39	49



entry	compound	SFC analytic conditions	ee (%)
14	 <p><b>163n-Cbz</b></p>	Chiralpak OJ-H, $\lambda = 210$ nm 35% IPA/CO <sub>2</sub> , 2.5 mL/min t <sub>R</sub> (min) major 1.52, minor 1.82	92
15	 <p><b>163o-Cbz</b></p>	Chiralcel OJ-H, $\lambda = 210$ nm 35% IPA/CO <sub>2</sub> , 2.5 mL/min t <sub>R</sub> (min) major 2.86, minor 6.02	90
16	 <p><b>163p-Cbz</b></p>	Chiralpak AD-H, $\lambda = 210$ nm 45% IPA/CO <sub>2</sub> , 3.5 mL/min t <sub>R</sub> (min) major 3.19, minor 4.05	89
17	 <p><b>163q-Cbz</b></p>	Chiralpak OJ-H, $\lambda = 210$ nm 25% IPA/CO <sub>2</sub> , 2.5 mL/min t <sub>R</sub> (min) minor 1.84, major 2.60	87
18	 <p><b>163r-Cbz</b></p>	Chiralpak OD-H, $\lambda = 210$ nm 30% IPA/CO <sub>2</sub> , 2.5 mL/min t <sub>R</sub> (min) major 2.52, minor 2.79	85
19	 <p><b>165a-Cbz</b></p>	Chiralpak AD-H, $\lambda = 210$ nm 40% IPA/CO <sub>2</sub> , 2.5 mL/min t <sub>R</sub> (min) major 2.56, minor 3.04	93

entry	compound	SFC analytic conditions	ee (%)
20	 <p><b>165b-Cbz</b></p>	Chiralpak OJ-H, $\lambda = 210$ nm 30% IPA/CO <sub>2</sub> , 2.5 mL/min t <sub>R</sub> (min) major 1.93, minor 2.42	90
21	 <p><b>165c-Cbz</b></p>	Chiracel AD-H, $\lambda = 210$ nm 20% IPA/CO <sub>2</sub> , 2.5 mL/min t <sub>R</sub> (min) major 3.93, minor 4.46	94
22	 <p><b>165d-Cbz</b></p>	Chiralpak AD-H, $\lambda = 210$ nm 45% IPA/CO <sub>2</sub> , 2.5 mL/min t <sub>R</sub> (min) major 5.00, minor 7.22	58
23	 <p><b>165e-Cbz</b></p>	Chiralpak AD-H, $\lambda = 210$ nm 45% IPA/CO <sub>2</sub> , 2.5 mL/min t <sub>R</sub> (min) major 3.89, minor 5.16	54
24	 <p><b>165f-Cbz</b></p>	Chiralpak AD-H, $\lambda = 210$ nm 45% IPA/CO <sub>2</sub> , 2.5 mL/min t <sub>R</sub> (min) major 5.31, minor 10.01	82

entry	compound	SFC analytic conditions	ee (%)
25	 <p><b>167a-Cbz</b></p>	Chiralpak OJ-H, $\lambda = 210$ nm 20% IPA/CO <sub>2</sub> , 2.5 mL/min t <sub>R</sub> (min) major 3.32, minor 3.93	86
26	 <p><b>167b-Cbz</b></p>	Chiralcel OD-H, $\lambda = 210$ nm 20% IPA/CO <sub>2</sub> , 2.5 mL/min t <sub>R</sub> (min) major 4.82, minor 5.25	89
27	 <p><b>167c-Cbz</b></p>	Chiralpak OD-H, $\lambda = 210$ nm 25% IPA/CO <sub>2</sub> , 2.5 mL/min t <sub>R</sub> (min) major 5.66, minor 6.38	88
28	 <p><b>167d-Cbz</b></p>	Chiralpak AD-H, $\lambda = 210$ nm 40% IPA/CO <sub>2</sub> , 2.5 mL/min t <sub>R</sub> (min) major 1.41, minor 1.76	90
29	 <p><b>167e-Cbz</b></p>	Chiralpak AS-H, $\lambda = 210$ nm 20% IPA/CO <sub>2</sub> , 3.5 mL/min t <sub>R</sub> (min) major 2.16, minor 2.62	90

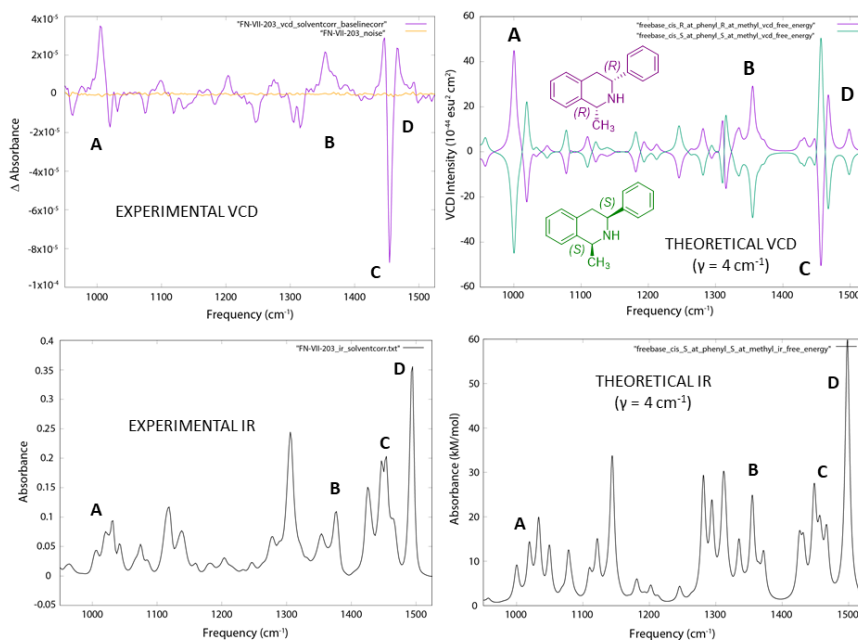
### 2.7.5 Determination of relative and absolute configuration

#### Method 1 – Vibrational Circular Dichroism (VCD)

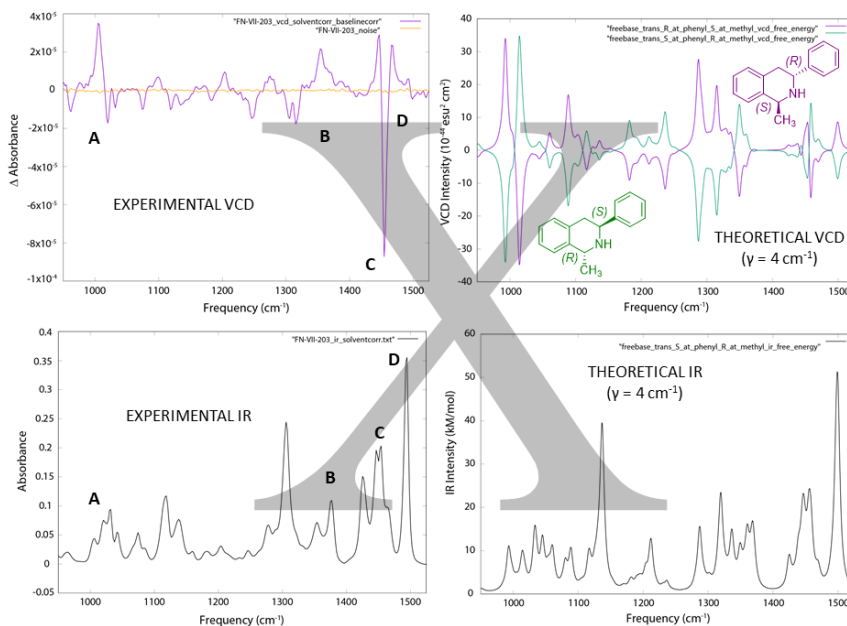
**Experimental Protocol.** A solution of **167e** (60 mg/mL) was prepared in CDCl<sub>3</sub> and loaded into a front-loading SL-4 cell (International Crystal Laboratories) possessing BaF<sub>2</sub> windows and 100 μm path length. Infrared (IR) and VCD spectra were acquired on a BioTools ChiralIR-2X VCD spectrometer as a set of set of 27 one-hour blocks (27 blocks, 3120 scans per block) in dual PEM mode. A 15-minute acquisition of neat (-)-α-pinene control (separate 75 μm BaF<sub>2</sub> cell) yielded a VCD spectrum in agreement with literature spectra. IR and VCD spectra were background-corrected using a 30-minute block IR acquisition of the empty instrument chamber under gentle N<sub>2</sub> purge, and were solvent corrected using an 8-hour (8 blocks, 3120 scans per block) IR/VCD acquisition of CDCl<sub>3</sub> in the same 100 μm BaF<sub>2</sub> cell as used for **167e**. The reported spectra represent the result of block averaging.

**Computational Protocol.** The arbitrarily chosen (*S,S*) stereoisomer of compound **167e** (*S* at methyl, *S* at phenyl; thus *cis*) was subjected to an exhaustive initial molecular mechanics-based conformational search (MMFF94 force field, 0.08 Å geometric RMSD cutoff, and 30 kcal/mol energy window) as implemented in MOE 2019.0102 (Chemical Computing Group, Montreal, CA). All conformers retained the (*S*) configuration at both centers. Separately, a study involving the *trans* stereoisomer possessing the (*R*) configuration at the methyl group and (*S*) configuration at phenyl was performed in identical fashion, with stereochemical integrity again retained throughout the stochastic conformational search. All MMFF94 conformers within a 10 kcal/mol energy window were then subjected to geometry optimization, harmonic frequency calculation, and VCD

rotational strength evaluation using density functional theory. All quantum mechanical calculations first utilized the B3LYP functional, small 6-31G\* basis, and IEFPCM model (chloroform solvent) as an initial filter, followed by subsequent optimization using B3PW91 functional, cc-pVTZ basis, and implicit IEFPCM chloroform solvation model on all IEFPCM-B3LYP/6-31G\* conformers below 5 kcal/mol. All calculations were performed with the *Gaussian 16* program system (Rev. C.01; Frisch *et al.*, Gaussian, Inc., Wallingford, CT). Resultant IEFPCM-B3PW91/cc-pVTZ harmonic frequencies were scaled by 0.98. All structurally unique conformers possessing all positive Hessian eigenvalues were Boltzmann weighted by relative free energy at 298.15 K. The predicted IR and VCD frequencies and intensities of the retained conformers were convolved using Lorentzian line shapes ( $\gamma = 4 \text{ cm}^{-1}$ ) and summed using the respective Boltzmann weights to yield the final predicted IR and VCD spectra of the species described above. The predicted VCD of the corresponding enantiomers were generated by inversion of sign. From a combination of (a) the best overall agreement of (*R,R*)-**167e** with experiment among all of the theoretical spectra in the useful range of the VCD ( $\sim 1000\text{-}1450 \text{ cm}^{-1}$ , regions **A-D**; see below) coupled with (b) support of this assignment by the agreement between predicted versus measured optical rotation (see Method 2) the absolute configuration of **167e** was established as *cis* and (*R,R*).

**Figure 2.3.** Experimental (left) and computed (right) IR and VCD spectra for the *cis* isomers of **167e**.

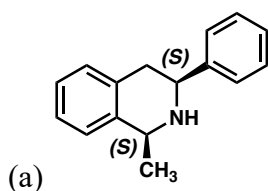
The better agreement with the *(R,R)* stereoisomer, upon alignment of the achiral IR spectra and correlation to VCD signals, is readily evident.

**Figure 2.4.** Experimental (left) and computed (right) IR and VCD spectra for the *trans* isomers of **167e**.

The worse agreement with experiment between either of the predicted *trans* stereoisomers, compared to the *cis*- and (*R,R*) stereoisomer above, can be seen. This assertion is further supported to an extent by the optical rotation data below.

### Method 2 – Optical Rotation (OR)

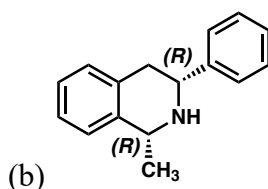
**Computational Protocol.** The ensemble of unique IEFPCM-B3PW91/cc-pVTZ conformers of **167e** generated in Method 1 above were subjected to optical rotation calculation at 589.0 nm using the B3LYP hybrid density functional, the large and diffuse 6-311++G(2df,2pd) basis set, and the IEFPCM implicit chloroform solvent model. The computed IEFPCM-B3LYP/6-311++G(2df,2pd) optical rotations (weighted by IEFPCM-B3PW91/cc-pVTZ free energies at 298.15 K) along with those resulting from alternatively weighting by either the IEFPCM-B3PW91/cc-pVTZ total energies or IEFPCM-B3LYP/6-311++G(2df,2pd)//IEFPCM-B3PW91/cc-pVTZ total energies are reported in (a)-(d) below.



Predicted OR, weighted by IEFPCM-B3PW91/cc-pVTZ free energies: **-144.5°**

Predicted OR, weighted by IEFPCM-B3PW91/cc-pVTZ total energies: **-144.6°**

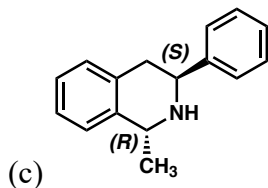
Predicted OR, weighted by IEFPCM-B3LYP/6-311++G(2df,2pd)//IEFPCM-B3PW91/cc-pVTZ total energies: **-147.0°**



Predicted OR, weighted by IEFPCM-B3PW91/cc-pVTZ free energies: **+144.5°**

Predicted OR, weighted by IEFPCM-B3PW91/cc-pVTZ total energies: **+144.6°**

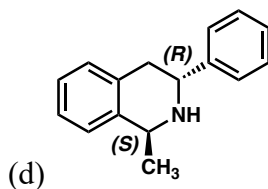
Predicted OR, weighted by IEFPCM-B3LYP/6-311++G(2df,2pd)//IEFPCM-B3PW91/cc-pVTZ total energies: **+147.0°**



Predicted OR, weighted by IEFPCM-B3PW91/cc-pVTZ free energies: **-94.5°**

Predicted OR, weighted by IEFPCM-B3PW91/cc-pVTZ total energies: **-101.0°**

Predicted OR, weighted by IEFPCM-B3LYP/6-311++G(2df,2pd)//IEFPCM-B3PW91/cc-pVTZ total energies: **-100.1°**



Predicted OR, weighted by IEFPCM-B3PW91/cc-pVTZ free energies: **+94.5°**

Predicted OR, weighted by IEFPCM-B3PW91/cc-pVTZ total energies: **+101.0°**

Predicted OR, weighted by IEFPCM-B3LYP/6-311++G(2df,2pd)//IEFPCM-B3PW91/cc-pVTZ total energies: **+100.1°**

Measured optical rotation:  $[\alpha]_D^{25} +133.3$  (c 0.79, CHCl<sub>3</sub>). Assuming only that the *sign* of the optical rotation is correctly predicted by theory, given the experimentally measured value of  $+133.3^\circ$ , the absolute configuration of **167e** must either be: (i) (*R*) at both chiral centers (and therefore *cis*); or (b) (*S*) at phenyl and (*R*) at methyl (*trans*). Scenario (b) is unlikely, given the wrong (opposite) directionality of the VCD signals in



regions **C** and **D** of the experimental spectrum. Scenario (a) also gives rise to the best agreement between the predicted and measured VCD spectra.

## 2.8 REFERENCES AND NOTES

- (1) a) Taylor, R. D.; MacCoss, M.; Lawson, A. D. G. *J. Med. Chem.* **2014**, *57*, 5845.  
b) Vitaku, E.; Smith, D. T.; Njardarson, J. T. *J. Med. Chem.* **2014**, *57*, 10257–10274. c) Lovering, F.; Bikker, J.; Humblet, C. *J. Med. Chem.* **2009**, *52*, 6752–6756. d) Lovering, F. *Med. Chem. Commun.* **2013**, *4*, 515–519. e) Roughley, S. D.; Jordan, A. M. *J. Med. Chem.* **2011**, *54*, 3451–3479.
- (2) a) Zhou, Y.-G. *Acc. Chem. Res.* **2007**, *40*, 1357–1366. b) Wang, D.-S.; Chen, Q.-A.; Lu, S.-M.; Zhou, Y.-G. *Chem. Rev.* **2012**, *112*, 2557–2590.
- (3) a) Zhao, D.; Glorius, F. *Angew. Chem. Int. Ed.* **2013**, *52*, 9616–9618. b) Wiedner, E. S.; Chambers, M. B.; Pitman, C. L.; Bullock, R. M.; Miller, A. J. M.; Appel, A. M. *Chem. Rev.* **2016**, *116*, 8655–8692.
- (4) For Ir-catalyzed asymmetric hydrogenation of isoquinolines, see a) Lu, S. M.; Wang, Y. Q.; Han, X. W.; Zhou, Y.-G. *Angew. Chem. Int. Ed.* **2006**, *45*, 2260–2263. b) Shi, L. Ye, Z.-S.; Cao, L. L.; Guo, R. N.; Hu, Y.; Zhou, Y.-G. *Angew. Chem. Int. Ed.* **2012**, *51*, 8286–8289. c) Iimuro, A.; Yamaji, K.; Kandula, S.; Nagano, T.; Kita, Y.; Mashima, K. *Angew. Chem. Int. Ed.* **2013**, *52*, 2046–2050. d) Ye, Z.-S.; Guo, R.-N.; Cai, X.-F.; Chen, M.-W.; Shi, L.; Zhou, Y.-G. *Angew. Chem. Int. Ed.* **2013**, *52*, 3685–3689. e) Kita, Y.; Yamaji, K.; Higashida, K.; Sathaiah, K.; Iimuro, A.; Mashima, K. *Chem. Eur. J.* **2015**, *21*, 1915–1927. f) Guo, R.-N.; Cai,

- X.-F.; Shi, L.; Ye, Z.-S.; Chen, M.-W.; Zhou, Y.-G. *Chem. Commun.* **2013**, *49*, 8537–8539. g) Chen, M.-W.; Ji, Y.; Wang, J.; Chen, Q.-A.; Shi, L.; Zhou, Y.-G. *Org. Lett.* **2017**, *19*, 4988–4991. For Ru-Catalyzed Enantioselective Hydrogenation of Isoquinolines, see h) Wen, J.; Tan, R.; Liu, S.; Zhao, Q.; Zhang, X. *Chem. Sci.* **2016**, *7*, 3047–3051.
- (5) a) Scott, J. D.; Williams, R. M. *Chem. Rev.* **2002**, *102*, 1669–1730. b) Siengalewicz, P.; Rinner, U.; Mulzer, J. *Chem. Soc. Rev.* **2008**, *37*, 2676–2690.
- (6) Welin, E. R.; Ngamnithiporn, A.; Klätte, M.; Lapointe, G.; Pototschnig, G. M.; McDermott, M. S. J.; Conklin, D.; Gilmore, C. D.; Tadross, P. M.; Haley, C. K.; Negoro, K.; Glibstrup, E.; Grünanger, C. U.; Allan, K. M.; Virgil, S. C.; Slamon, D. J.; Stoltz, B. M. *Science.* **2019**, *363*, 270–275.
- (7) For C–H activation/annulation strategy, see a) Zhang, Z.-W.; Lin, A.; Yang, J. *J. Org. Chem.* **2014**, *79*, 7041–7050. For ketone enolate-arylation/annulation, see b) Donohoe, T. J.; Pilgrim, B. S.; Jones, G. R.; Bassuto, J. A. *Proc. Natl. Acad. Sci. U.S.A.* **2012**, *109*, 11605–11608. For benzannulation of isocoumarins, see c) Manivel, P. Probakaran, K.; Khan, F. N.; Jin, J. S. *Res. Chem. Intermed.* **2012**, *38*, 347–357.
- (8) Pilgrim, B. S.; Gatland, A. E.; Esteves, C. H. A.; McTernan, C. T.; Jones, G. R.; Tatton, M. R. Procopiou, P. A.; Donohoe, T. J. *Org. Biomol. Chem.* **2016**, *14*, 1065–1090.
- (9) Allan, K. M.; Hong, B. D.; Stoltz, B. M. *Org. Biomol. Chem.* **2009**, *7*, 4960–4964.
- (10) For example of transition-metal-catalyzed tandem C–H activation/annulation of arenes and alkynes, see a) Zhu, Z.; Tang, X.; Li, X.; Wu, W.; Deng, G.; Jiang, H.

- J. Org. Chem.* **2016**, *81*, 1401–1409. b) Zhou, S.; Wang, M.; Wang, L.; Chen, K.; Wang, J.; Song, C.; Zhu, J. *Org. Lett.* **2016**, *18*, 5632–5635. c) Chinnagolla, R. K.; Pimparkar, S.; Jeganmohan, M. *Org. Lett.* **2012**, *14*, 3032–3035. d) Zhao, D.; Lied, F.; Glorius, F. *Chem. Sci.* **2014**, *5*, 2869–2873.
- (11) a) Chu, H.; Sun, S.; Yu, J.-T.; Cheng, J. *Chem. Commun.* **2015**, *51*, 13327. b) Arambasic, M.; Hooper, J. F.; Willis, M. C. *Org. Lett.* **2013**, *15*, 5162–5165.
- (12) See Table 2.3, Section 2.7.3 for additional results using other acids. Although further studies are required to fully understand the role of acid, we speculate that the acid helps promoting a) the tautomerization of enamine to imine prior to the second reduction and b) the dissociation of THIQ product from Ir-complex through protonation.
- (13) In a similar Ir-xylyphos system, it is reported that the alpha-alkoxy imine binds to the catalyst complex in a bidentate fashion, see a) Dorta, R.; Broggini, D.; Stoop, R.; Rügger, H. Spindler, F.; Togni, A. *Chem. Eur. J.* **2004**, *10*, 267–278. b) Dorta, R.; Broggini, D.; Kissner, R.; Togni, A. *Chem. Eur. J.* **2004**, *10*, 4546–4555.
- (14) Hopmann, K. H.; Bayer, A. *Organometallics.* **2011**, *30*, 2483–2497.
- (15) Increasing the catalyst loading to 2.5 mol % of [Ir(cod)Cl]<sub>2</sub> and 6 mol % of **L7** does not improve the conversion any further.
- (16) The absolute stereochemistry of product **167e** was determined via the combination of measured and computed vibrational circular dichroism (VCD) spectra and optical rotations. The configuration of **167e** (*R, R*) was found to be analogous to

that determined for hydroxymethyl product **163a** and also observed crystallographically for **163p**.

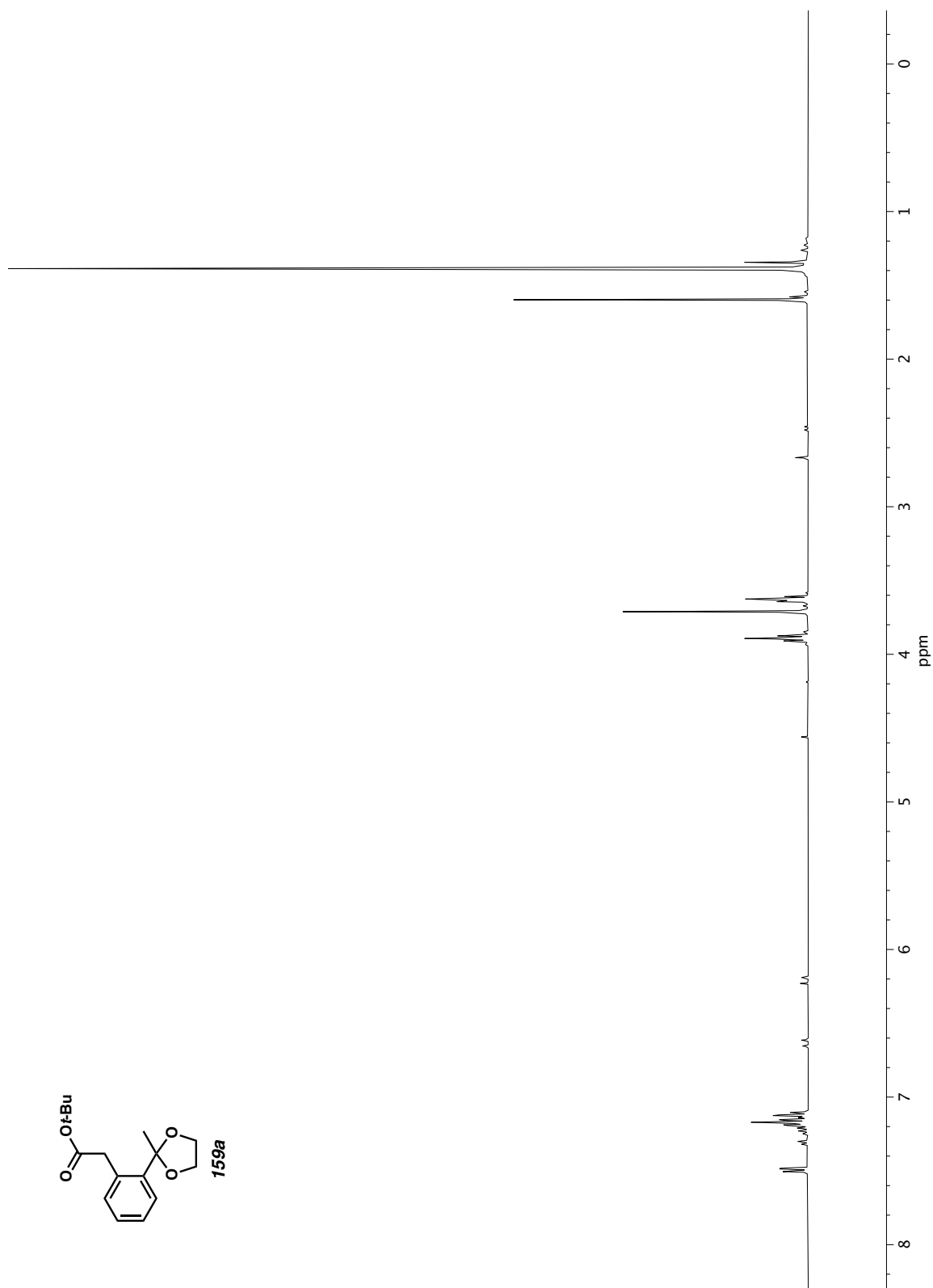
- (17) a) Chrzanowska, M. Grajewska, A.; Rozwadowska, M. D. *Chem. Rev.* **2016**, *116*, 12369–12465. b) Carrillo, L.; Badia, D.; Dominguez, E.; Anakabe, E.; Osante, I.; Tellitu, I.; Vicario, J. L. *J. Org. Chem.* **1999**, *64*, 115–1120.
- (18) Haftchenary, S.; Nelson, S. D.; Furst, L.; Dandapani, S.; Ferrara, S. J.; Bošković, Z. V.; Lazú, S. F.; Guerrero, A. M.; Serrano, J. C.; Crews, D. K.; Brackeen, C.; Mowat, J.; Brumby, T.; Bauser, M.; Schreiber, S. L.; Phillips, A. J. *ACS. Comb. Sci.* **2016**, *18*, 569–574.
- (19) Alternatively, the oxazolidinone-fused product **169** could be synthesized utilizing a 2-step sequence. First is the Boc-protection of the amine. The Boc-protected product was subsequently cyclized to afford oxazolidinone-fused THIQ **169** under the Appel reaction conditions.
- (20) Zhang, G.-L.; Chen, C.; Xiong, Y.; Zhang, L.-H.; Ye, J.; Ye, X.-S. *Carbohydrate Research.* **2010**, *345*, 780–786.
- (21) Gadhiya, S. V.; Giri, R.; Cordone, P.; Karki, A.; Harding, W. W. *Curr. Org. Chem.* **2018**, *22*, 1893–1905.
- (22) Thimmaiah, S.; Ningegowda, M.; Shivananju, N. S.; Ningegowda, R.; Siddaraj, R.; Priya, B. S. *Eur. J. Chem.* **2016**, *7*, 391–396.
- (23) Guo, D.; Li, J.; Lin, H.; Zhou, Y.; Chen, Y.; Sun, H.; Zhang, D.; Li, H.; Shoichet, B. K.; Shan, L.; Xie, X.; Jiang, H.; Liu, H. *J. Med. Chem.* **2016**, *59*, 9489–9502.
- (24) Pangborn, A. M.; Giardello, M. A.; Grubbs, R. H.; Rosen, R. K.; Timmers, F. J. *Organometallics* **1996**, *15*, 1518–1520.

- (25) Bruno, N. C.; Tudge, M. T.; Buchwald, S. L. *Chem. Sci.* **2013**, *4*, 916–920.
- (26) Legault, C. Y.; Charette, A. B. *J. Am. Chem. Soc.* **2005**, *127*, 8966–8967.
- (27) Xu, Z.; Xu, X.; O’Laoi, R.; Ma, H.; Zheng, J.; Chen, S.; Luo, L.; Hu, Z.; He, S.; Li, J.; Zhang, H.; Zhang, X. *Bioorg. Med. Chem.* **2016**, *24*, 5861–5872.

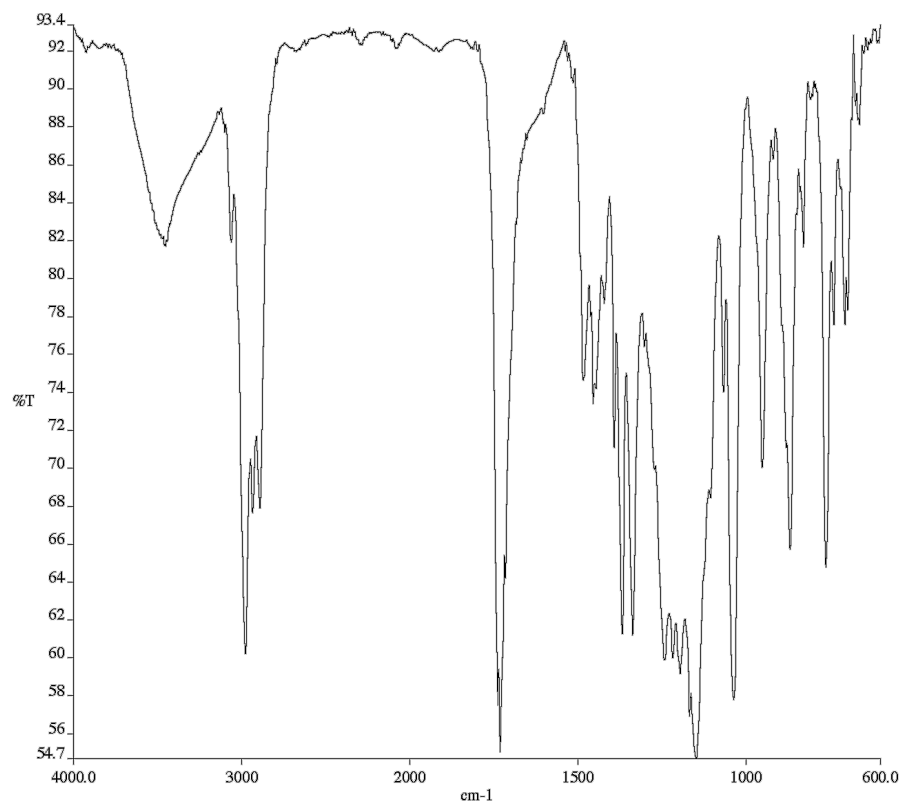
## **APPENDIX 1**

*Spectra Relevant to Chapter 2:*

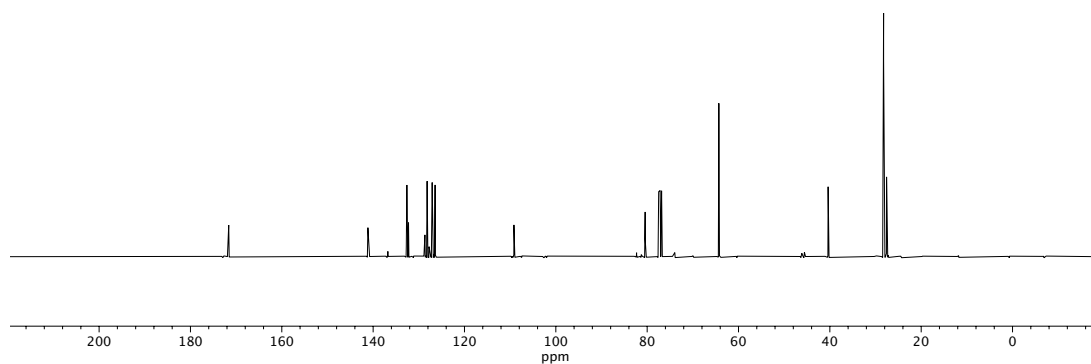
*Iridium-Catalyzed Enantioselective and Diastereoselective  
Hydrogenation of 1,3-Disubstituted Isoquinolines*



**Figure A1.1**  $^1\text{H}$  NMR (400 MHz,  $\text{CDCl}_3$ ) of compound **159a**.

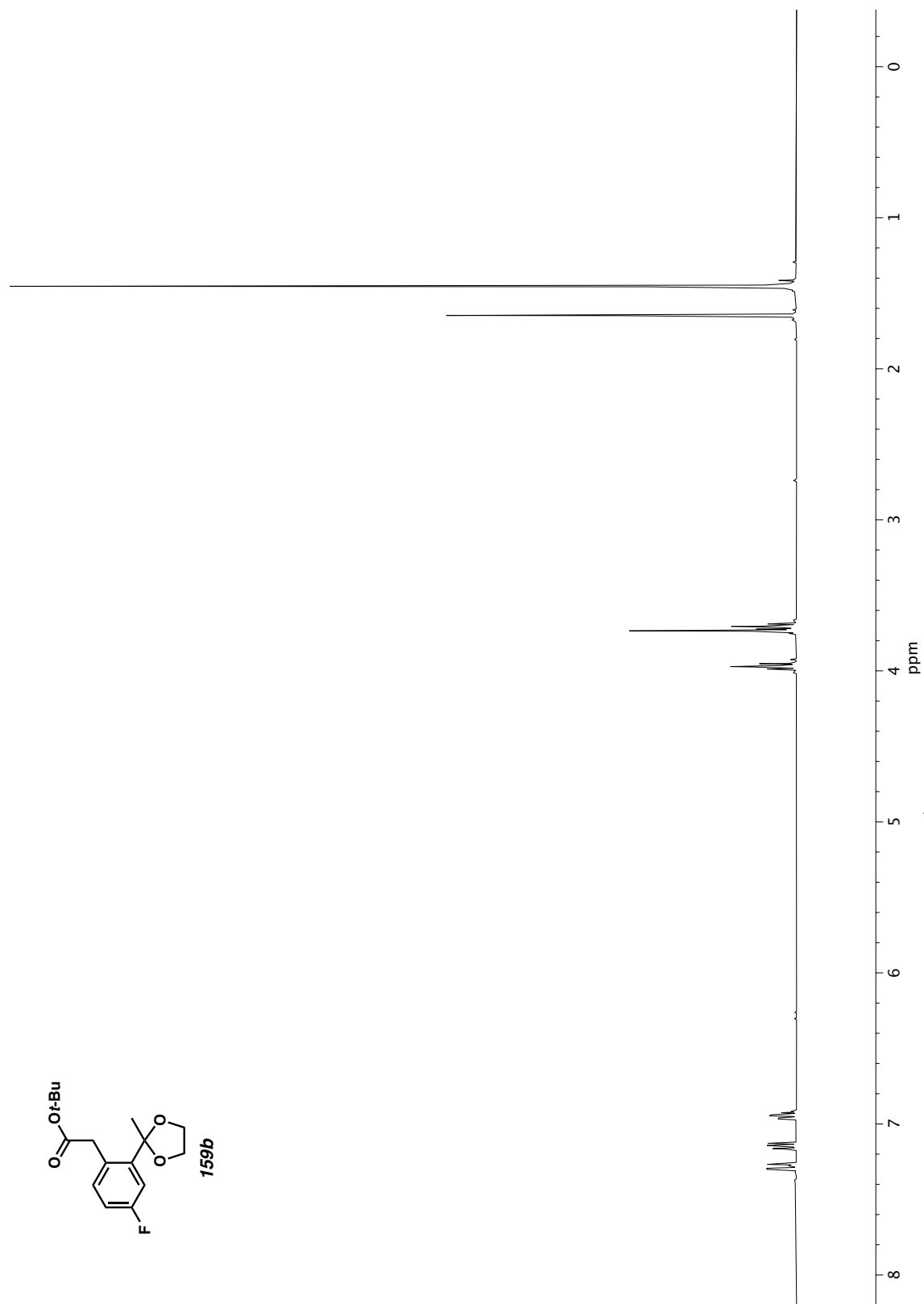


**Figure A1.2** Infrared spectrum (Thin Film, NaCl) of compound **159a**.

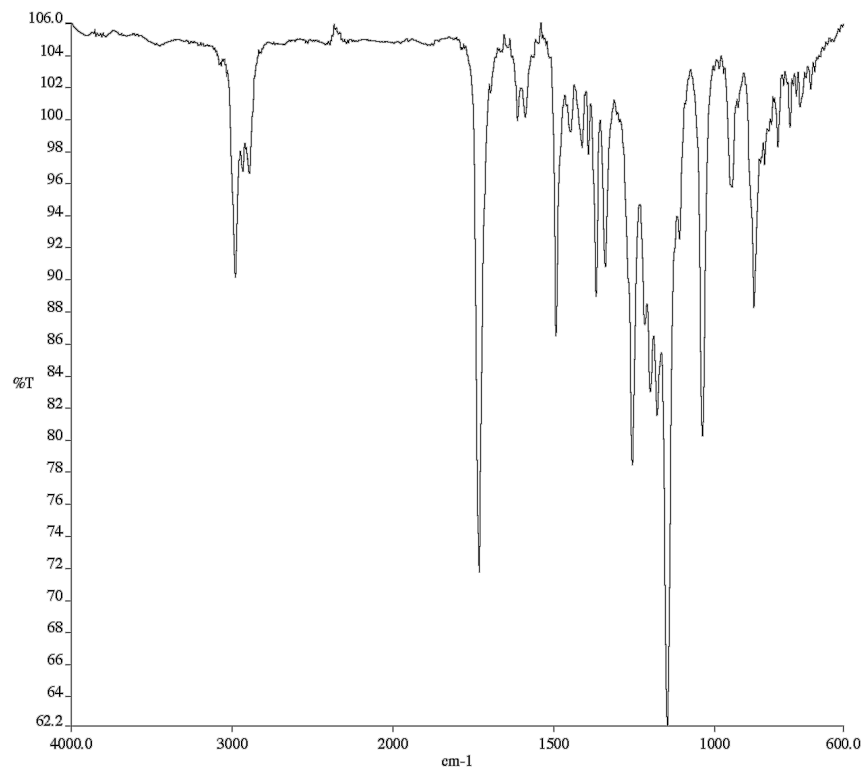


**Figure A1.3** <sup>13</sup>C NMR (100 MHz, CDCl<sub>3</sub>) of compound **159a**.

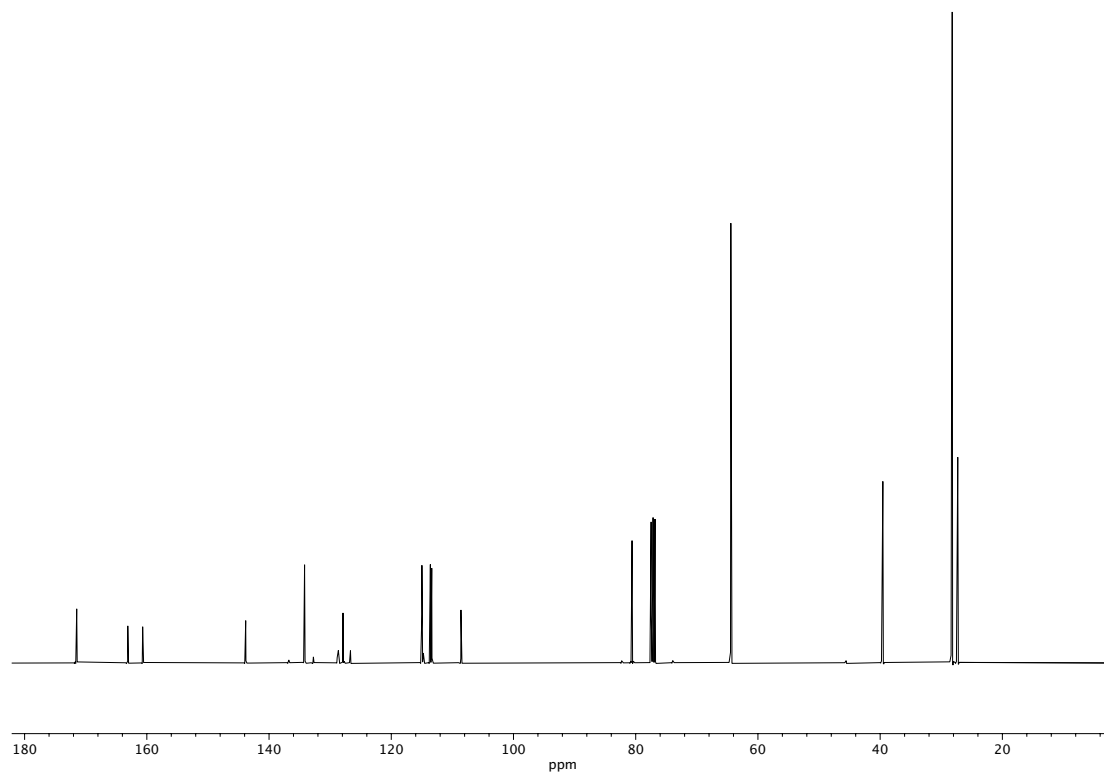




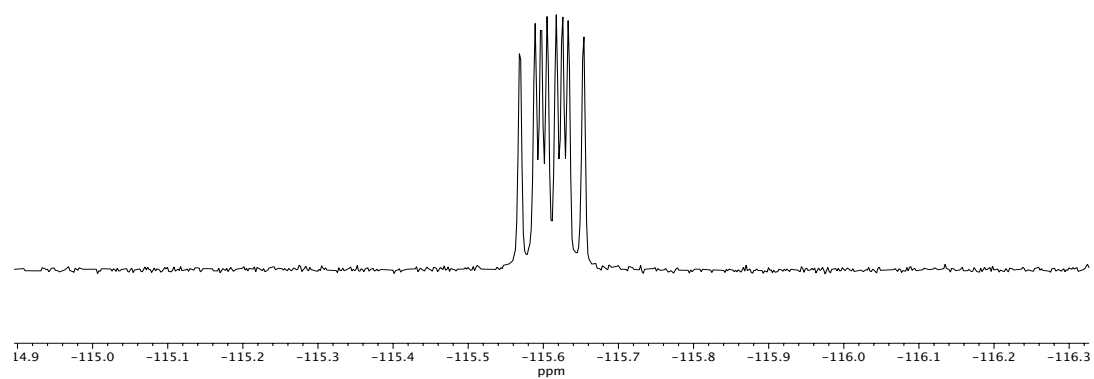
**Figure A1.4**  $^1\text{H}$  NMR (400 MHz,  $\text{CDCl}_3$ ) of compound **159b**.



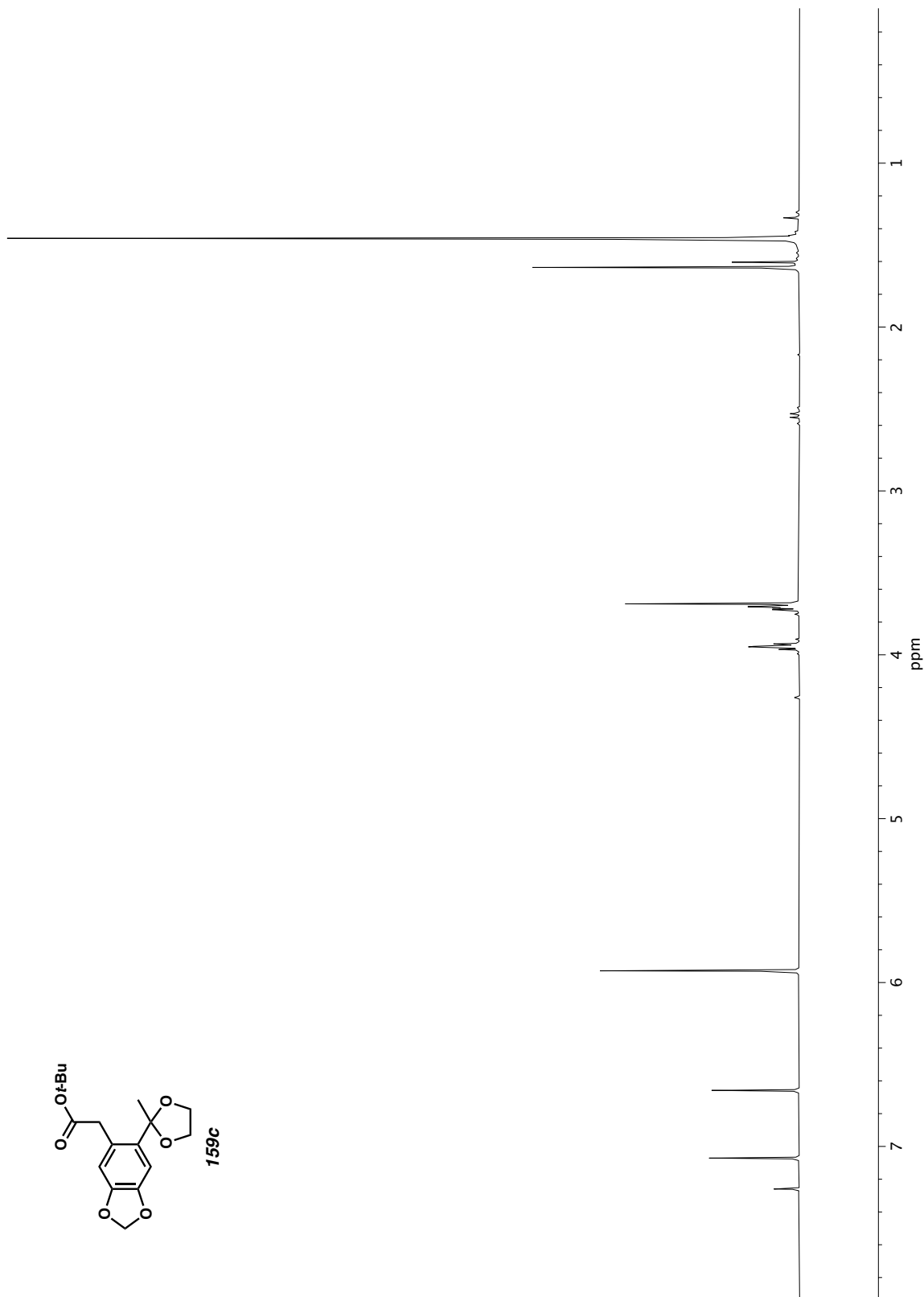
**Figure A1.5** Infrared spectrum (Thin Film, NaCl) of compound **159b**.



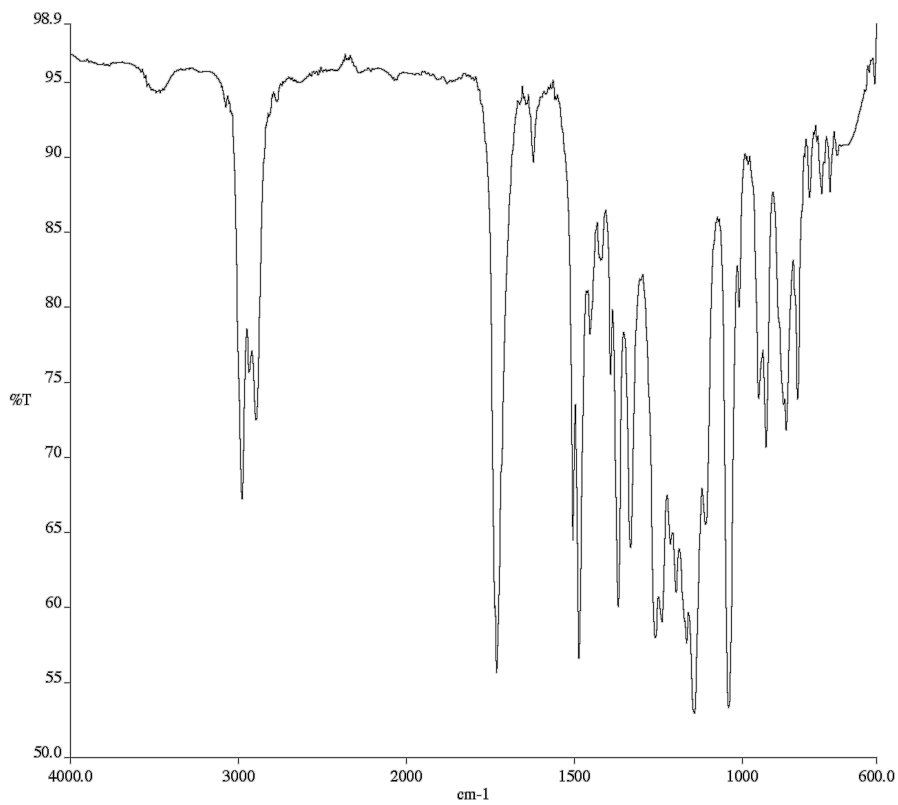
**Figure A1.6** <sup>13</sup>C NMR (100 MHz, CDCl<sub>3</sub>) of compound **159b**.



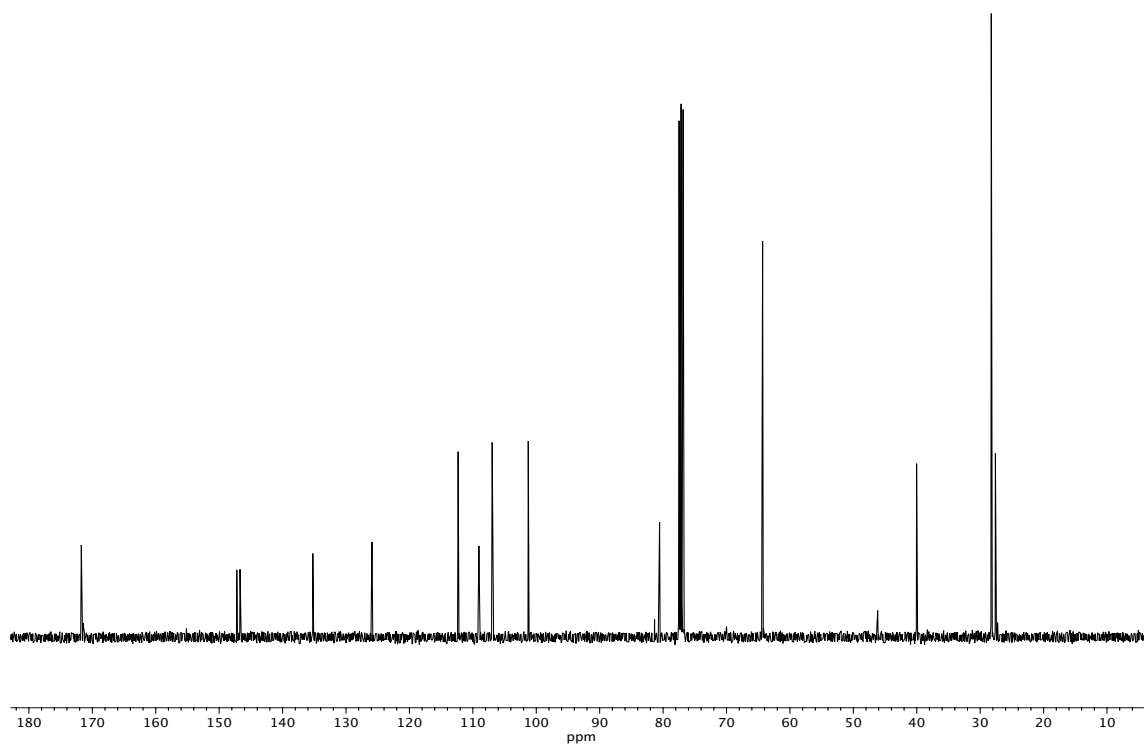
**Figure A1.7**  $^{19}\text{F}$  NMR (282 MHz,  $\text{CDCl}_3$ ) of compound **159b**.



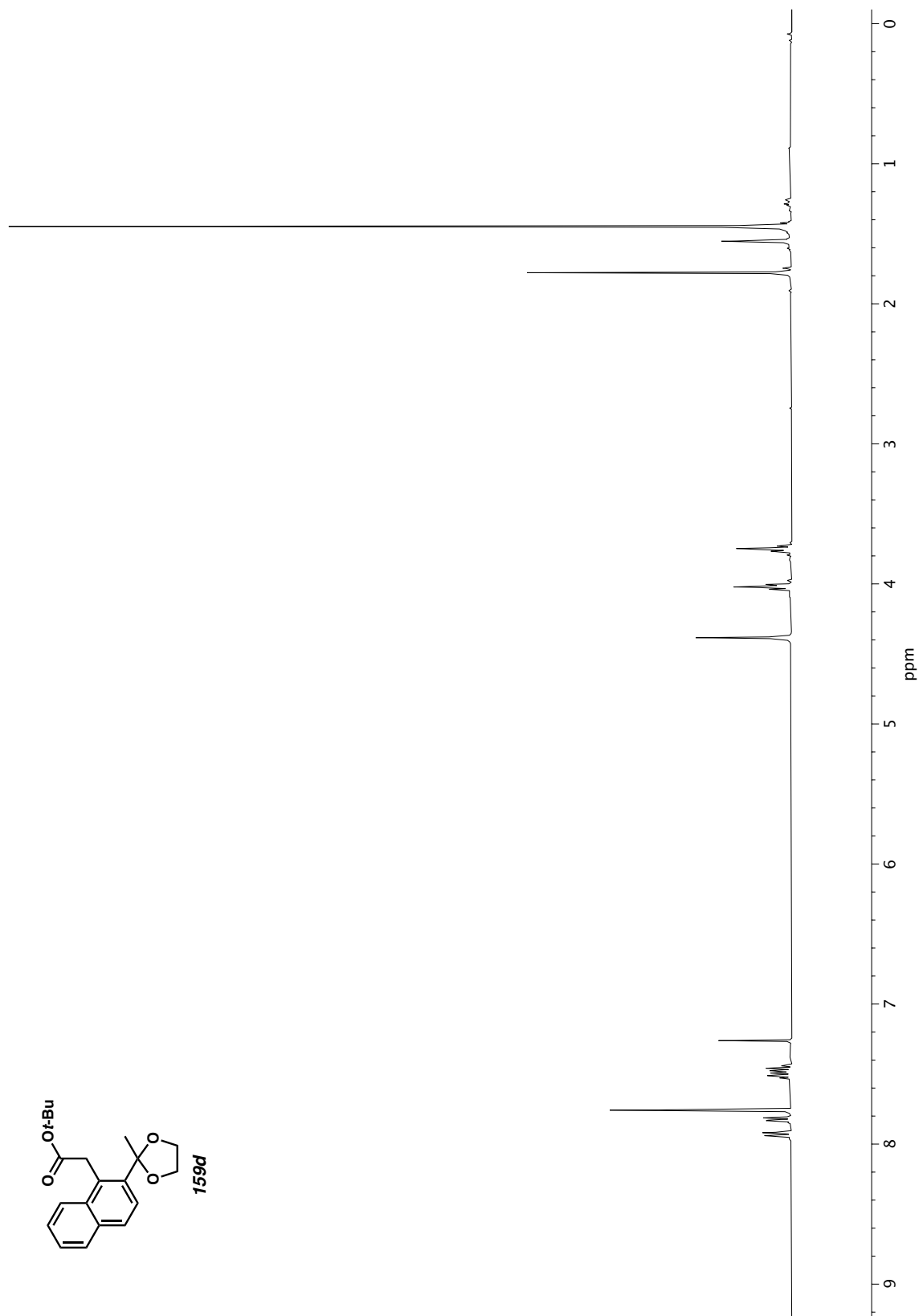
**Figure A1.8**  $^1\text{H}$  NMR (400 MHz,  $\text{CDCl}_3$ ) of compound **159c**.



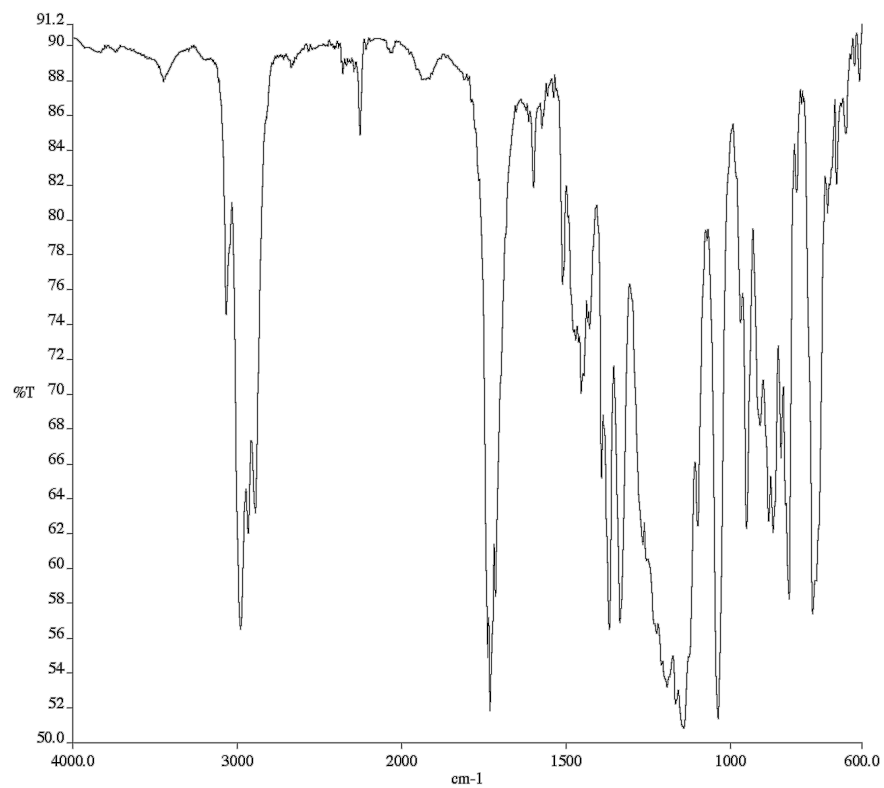
**Figure A1.9** Infrared spectrum (Thin Film, NaCl) of compound **159c**.



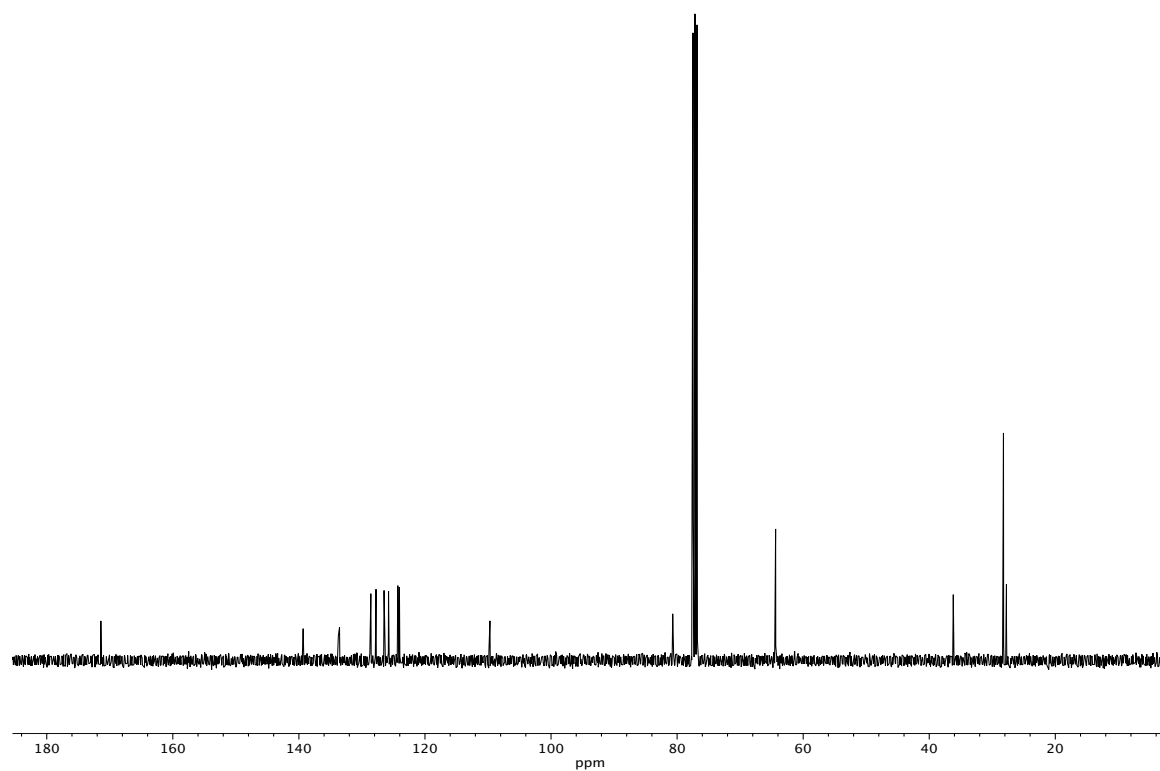
**Figure A1.10** <sup>13</sup>C NMR (100 MHz, CDCl<sub>3</sub>) of compound **159c**.



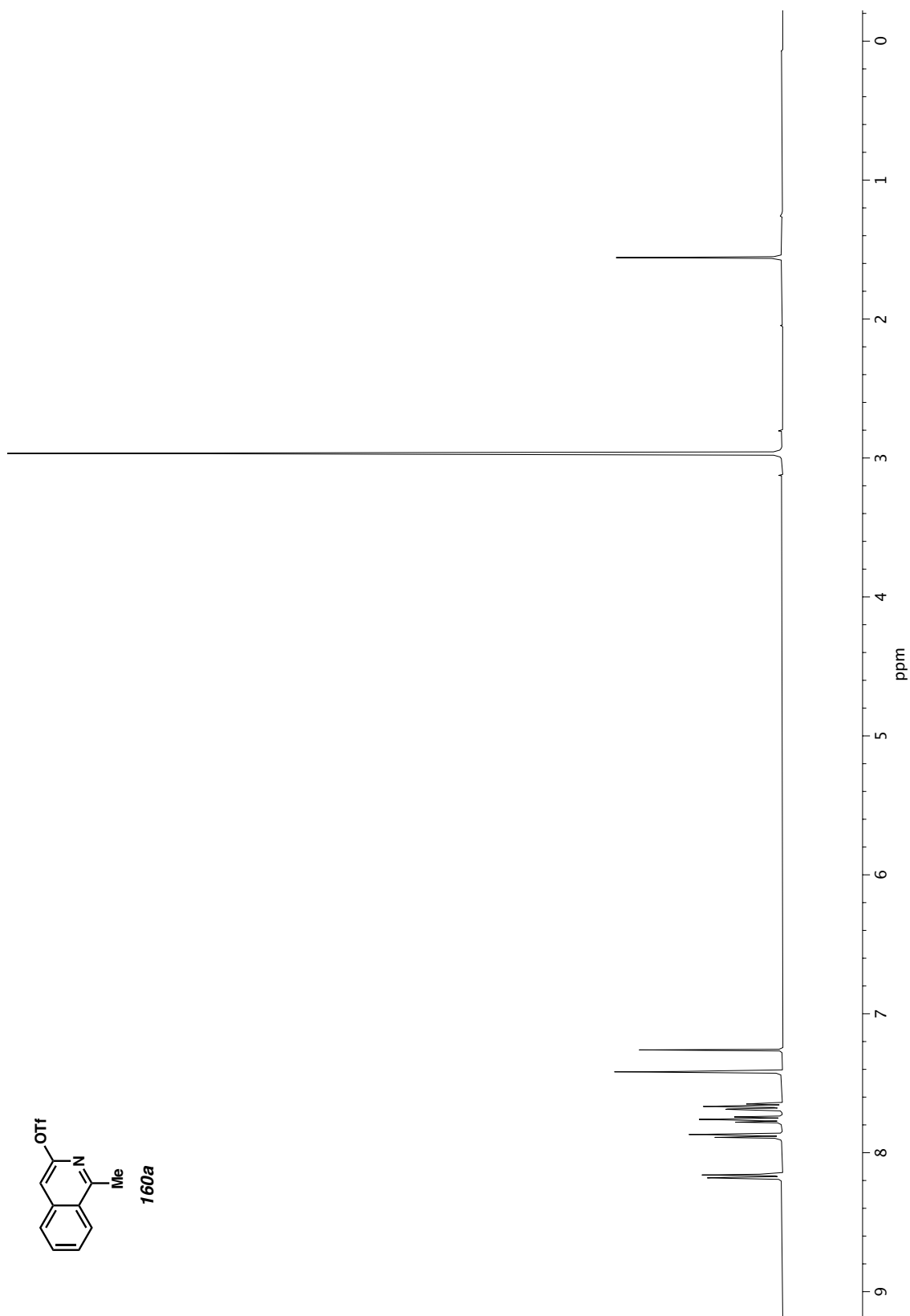
**Figure A1.11**  $^1\text{H}$  NMR (400 MHz,  $\text{CDCl}_3$ ) of compound **159d**.



**Figure A1.12** Infrared spectrum (Thin Film, NaCl) of compound **159d**.

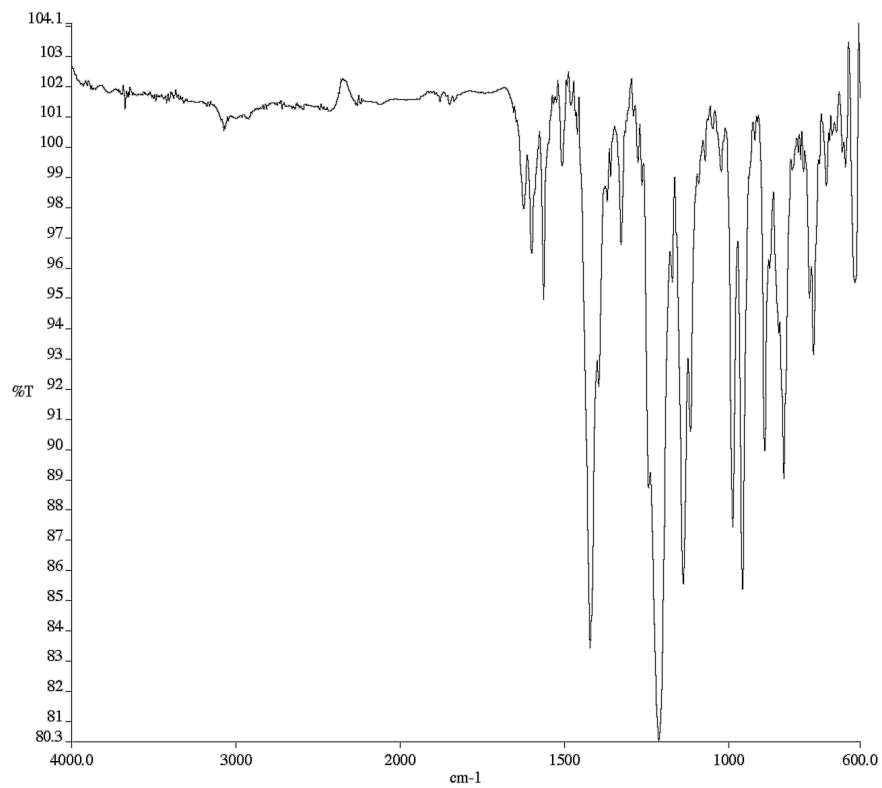


**Figure A1.13** <sup>13</sup>C NMR (100 MHz, CDCl<sub>3</sub>) of compound **159d**.

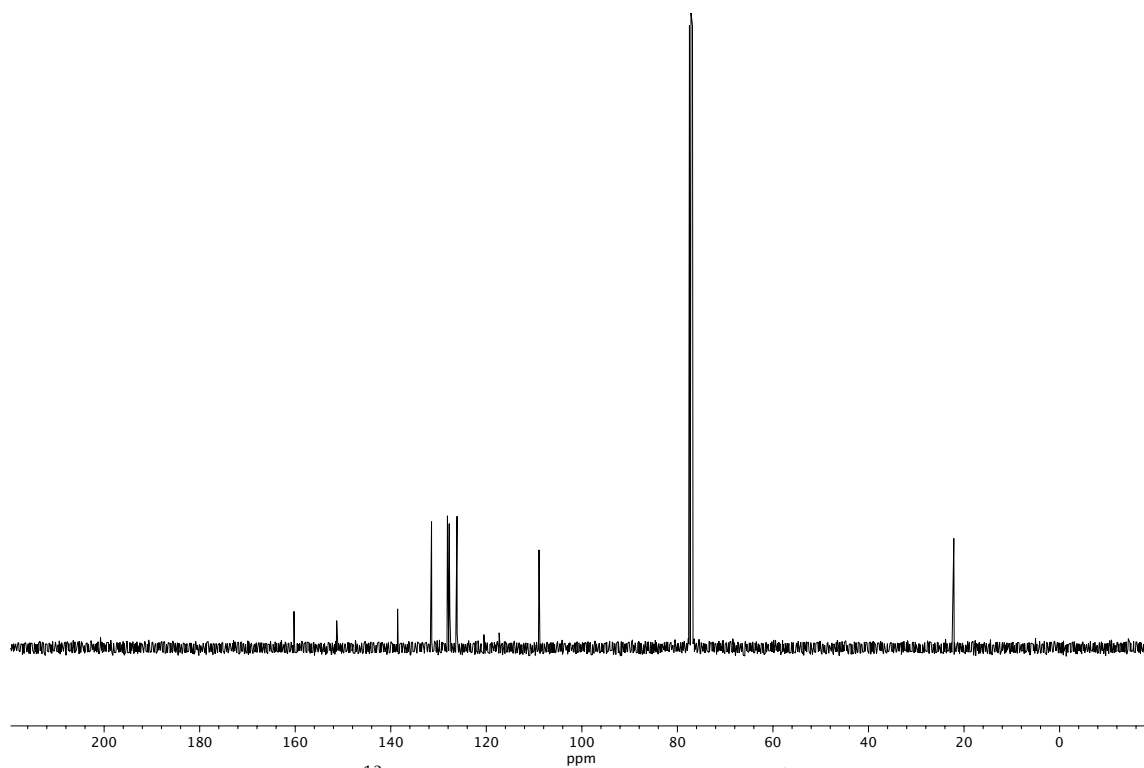


**Figure A1.14**  $^1\text{H}$  NMR (400 MHz,  $\text{CDCl}_3$ ) of compound **160a**.

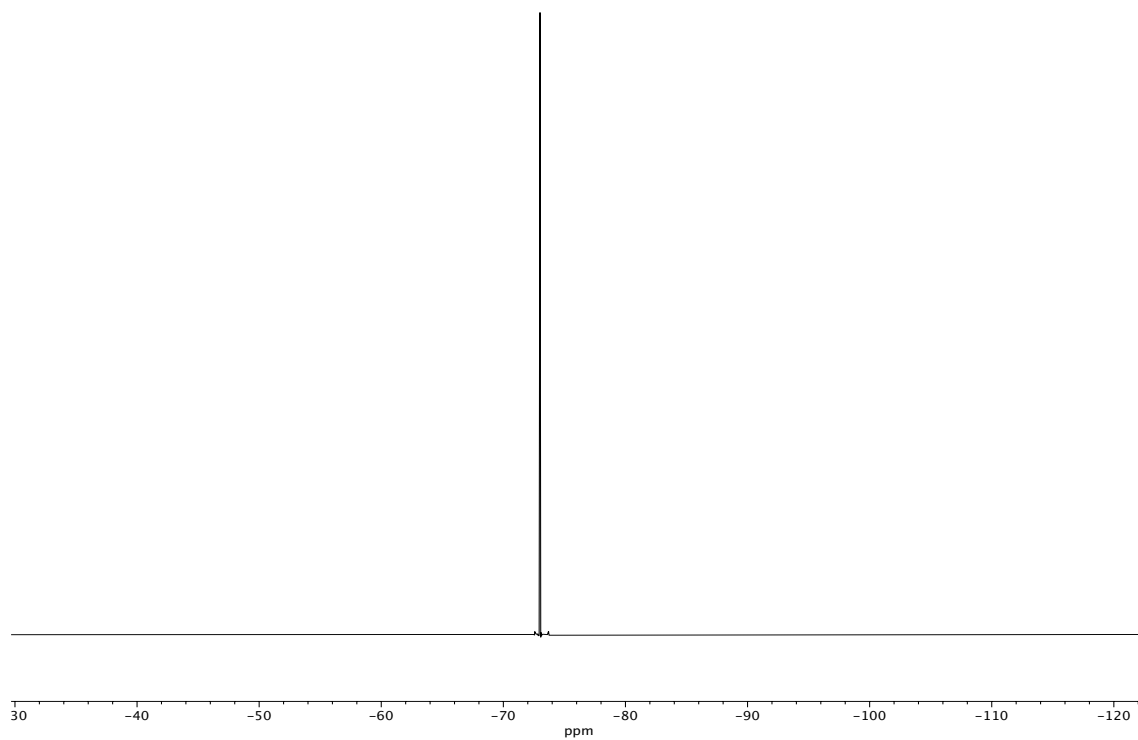




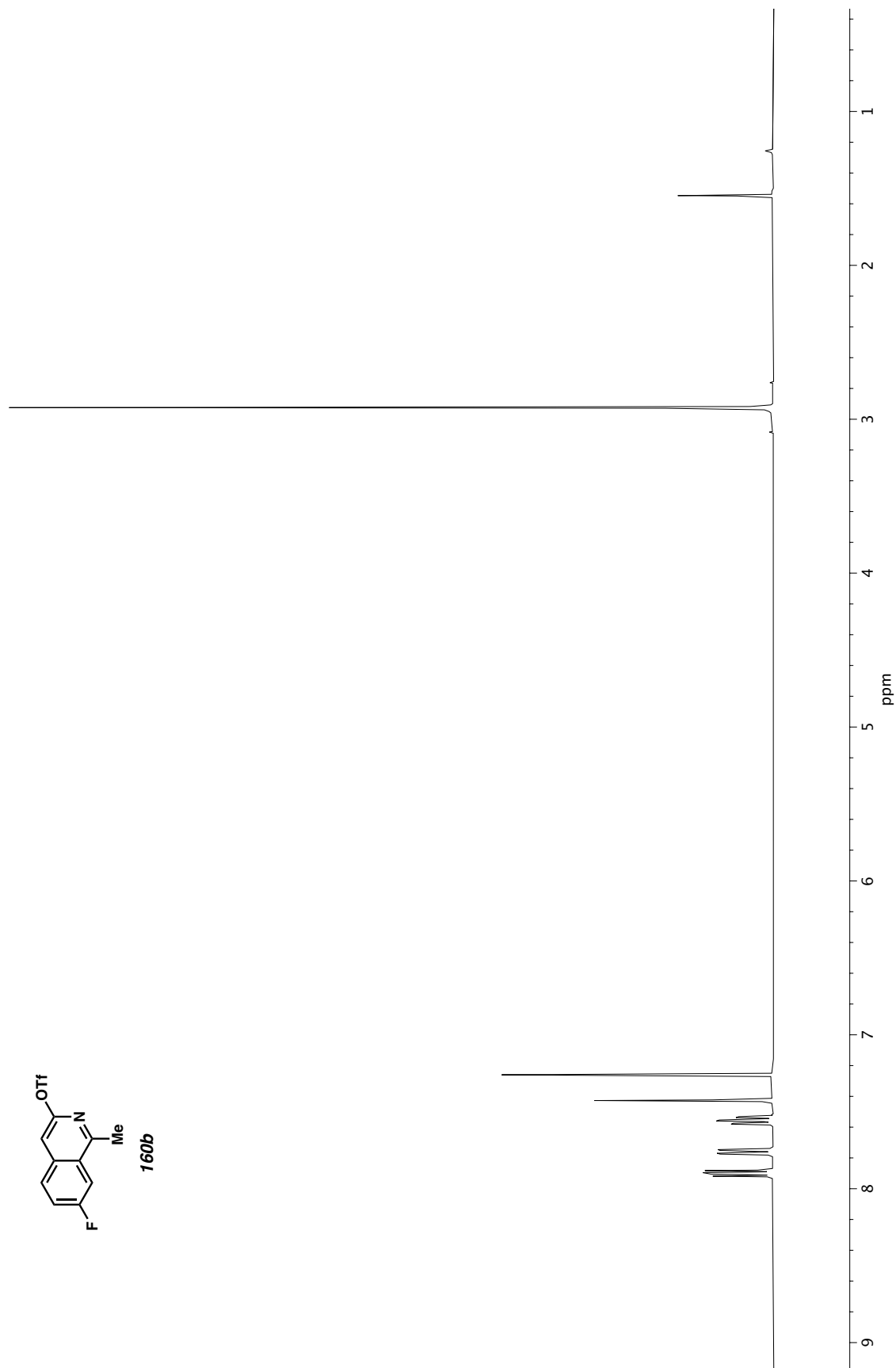
**Figure A1.15** Infrared spectrum (Thin Film, NaCl) of compound **160a**.



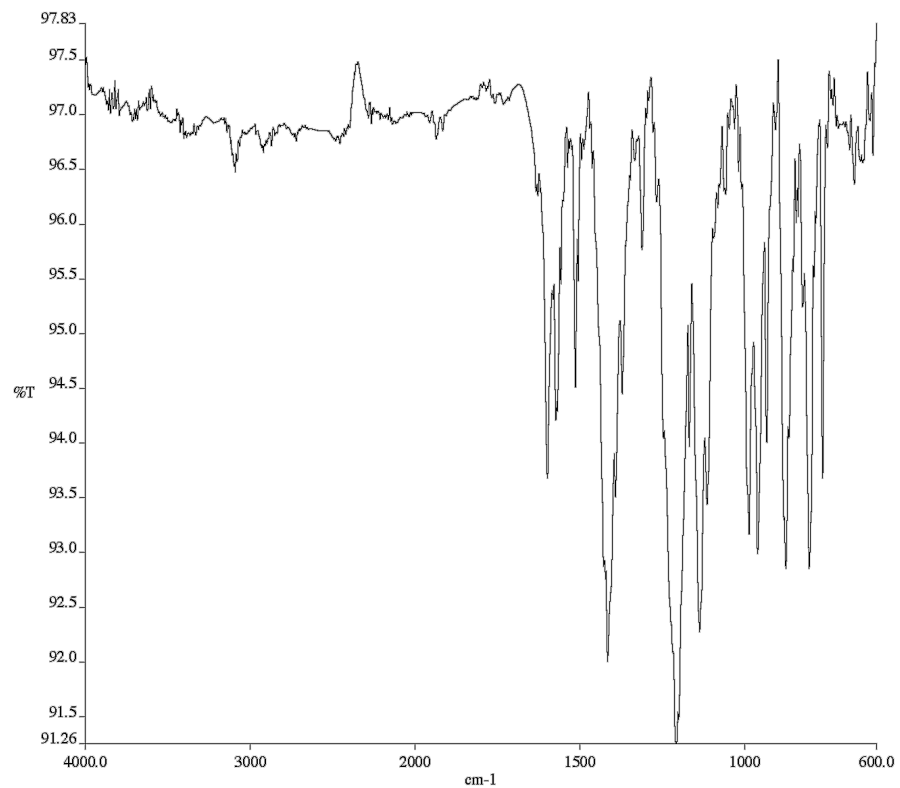
**Figure A1.16** <sup>13</sup>C NMR (100 MHz, CDCl<sub>3</sub>) of compound **160a**.



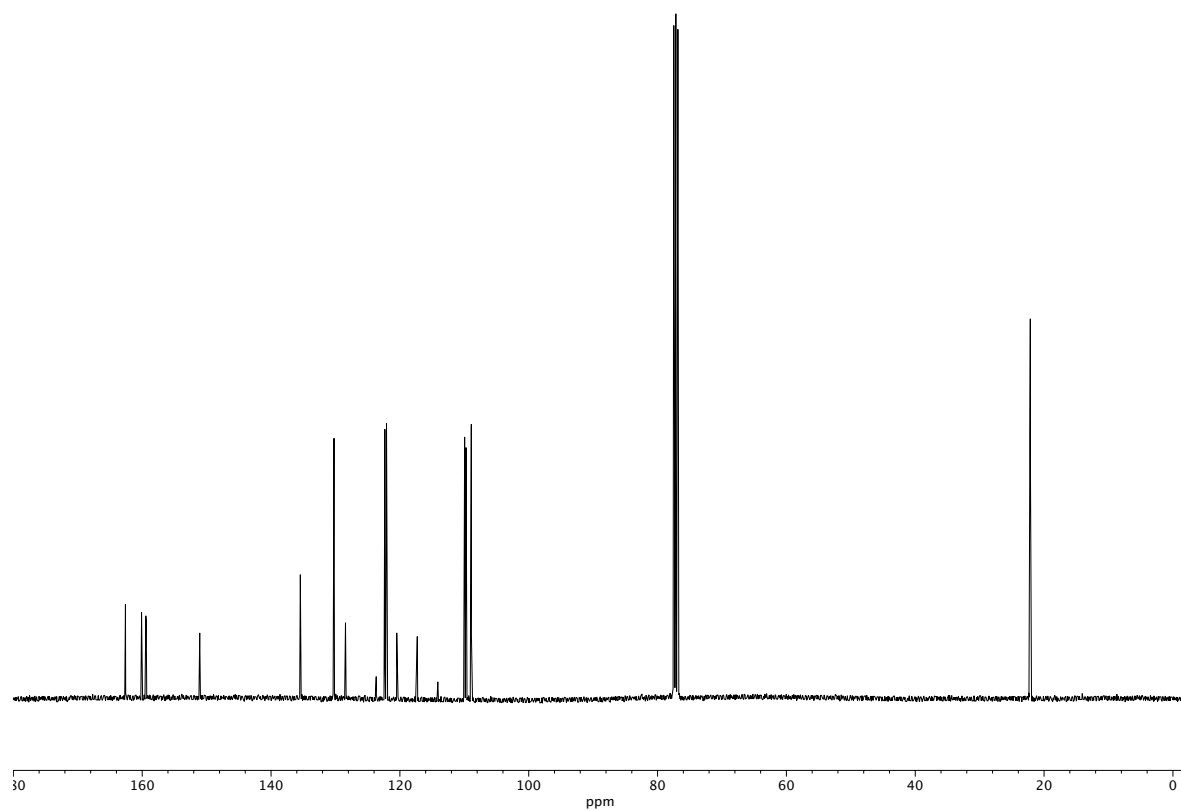
**Figure A1.17**  $^{19}\text{F}$  NMR (282 MHz,  $\text{CDCl}_3$ ) of compound **160a**.



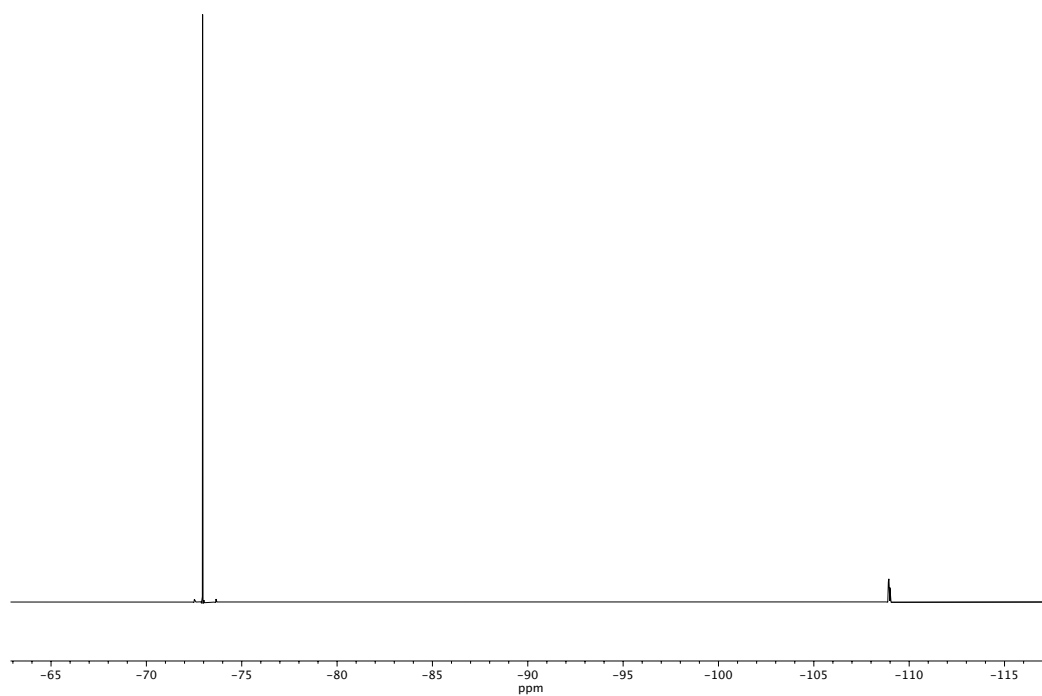
**Figure A1.18**  $^1\text{H}$  NMR (400 MHz,  $\text{CDCl}_3$ ) of compound **160b**.



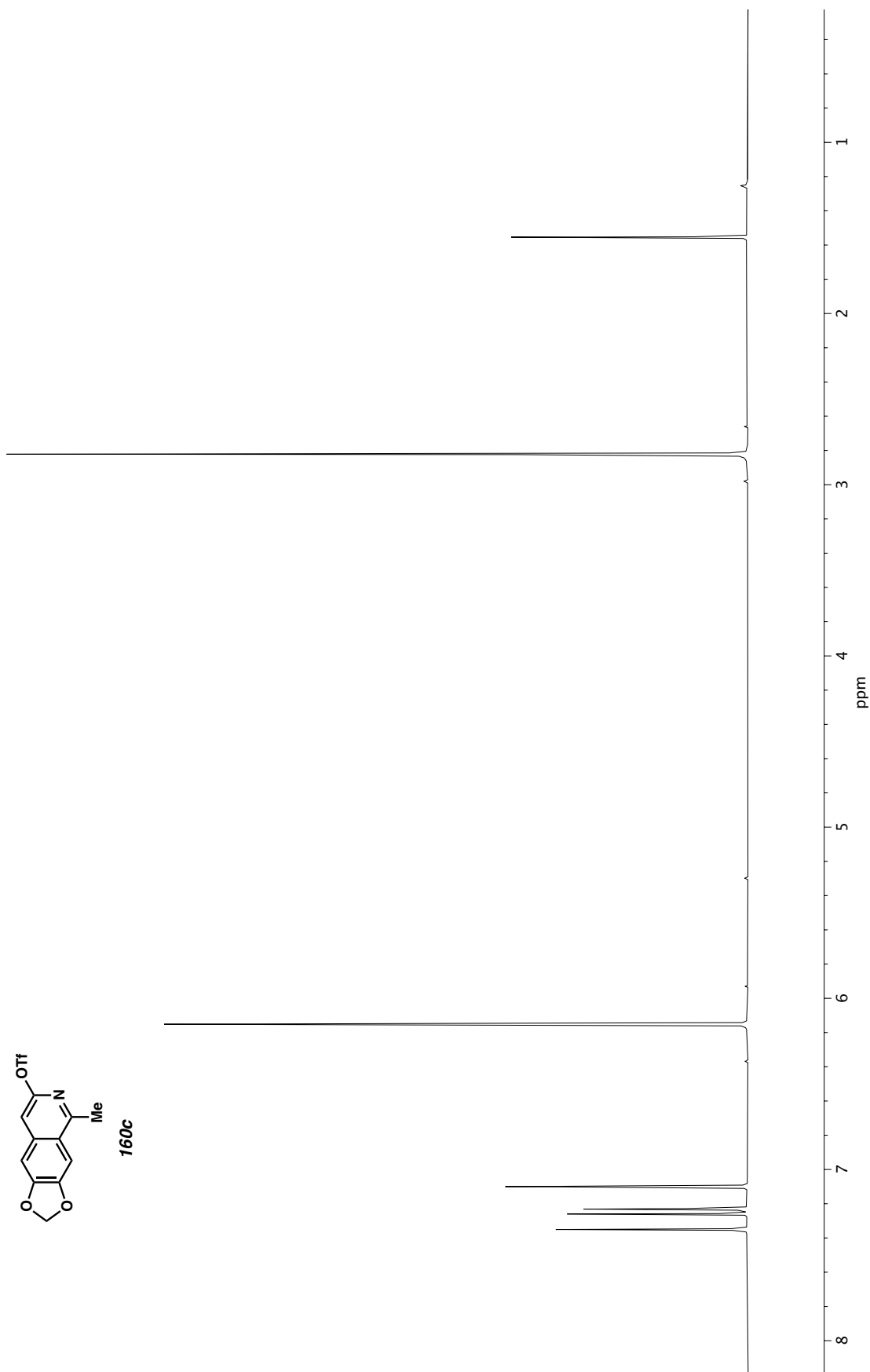
**Figure A1.19** Infrared spectrum (Thin Film, NaCl) of compound **160b**.



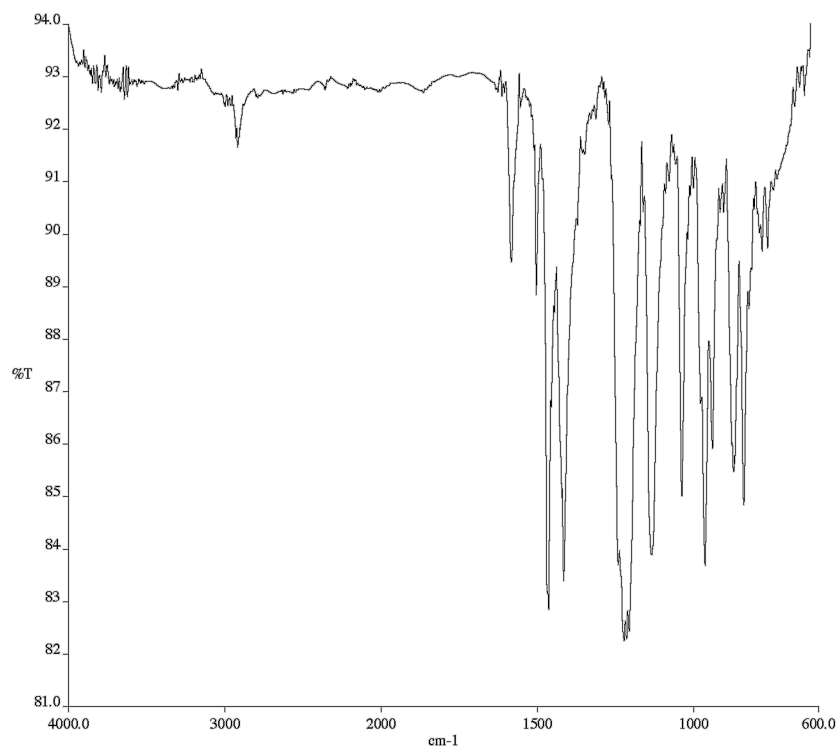
**Figure A1.20** <sup>13</sup>C NMR (100 MHz, CDCl<sub>3</sub>) of compound **160b**.



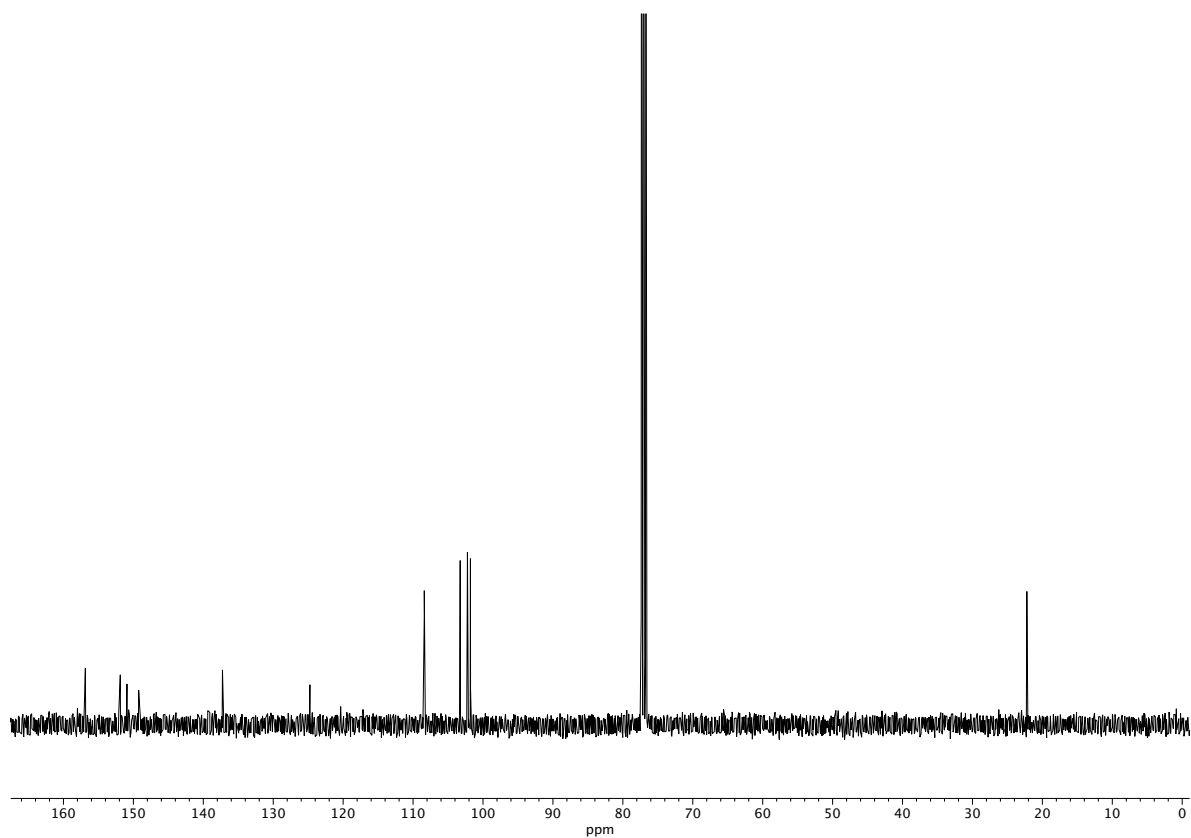
**Figure A1.21**  $^{19}\text{F}$  NMR (282 MHz,  $\text{CDCl}_3$ ) of compound **160b**.



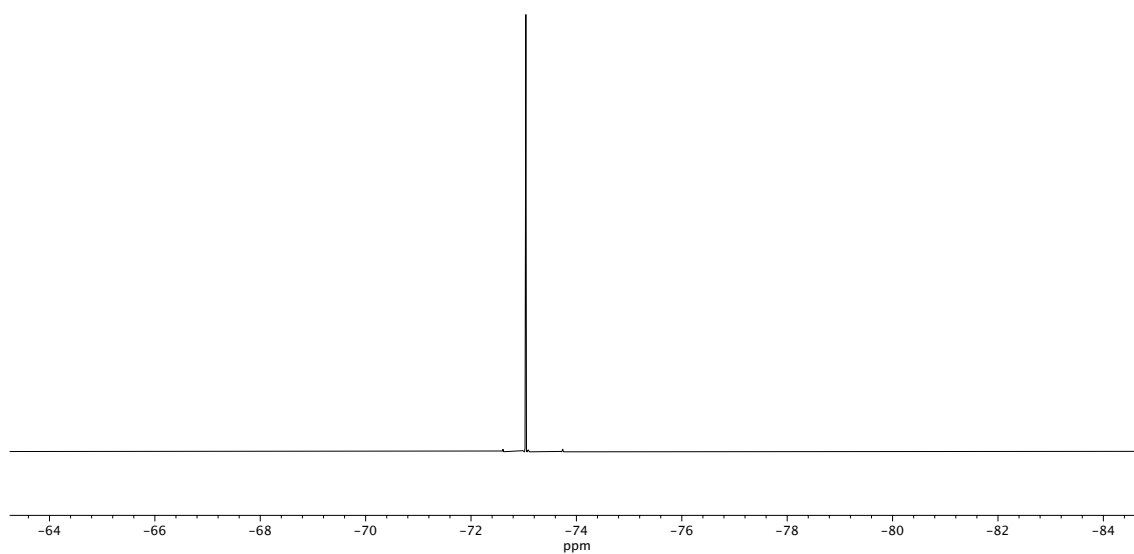
**Figure A1.122**  $^1\text{H}$  NMR (400 MHz,  $\text{CDCl}_3$ ) of compound **160c**.



**Figure A1.23** Infrared spectrum (Thin Film, NaCl) of compound **160c**.

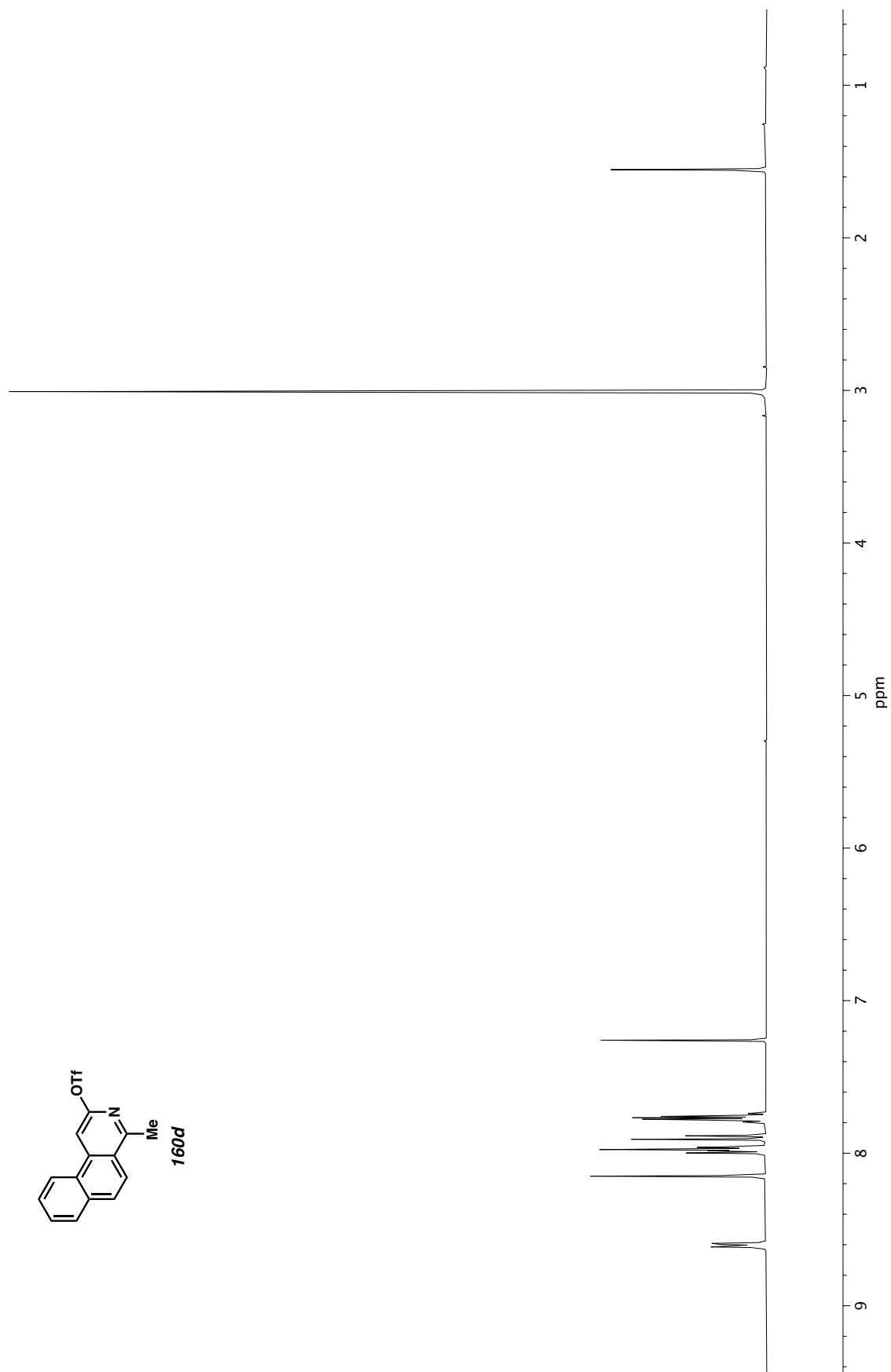


**Figure A1.24** <sup>13</sup>C NMR (100 MHz, CDCl<sub>3</sub>) of compound **160c**.

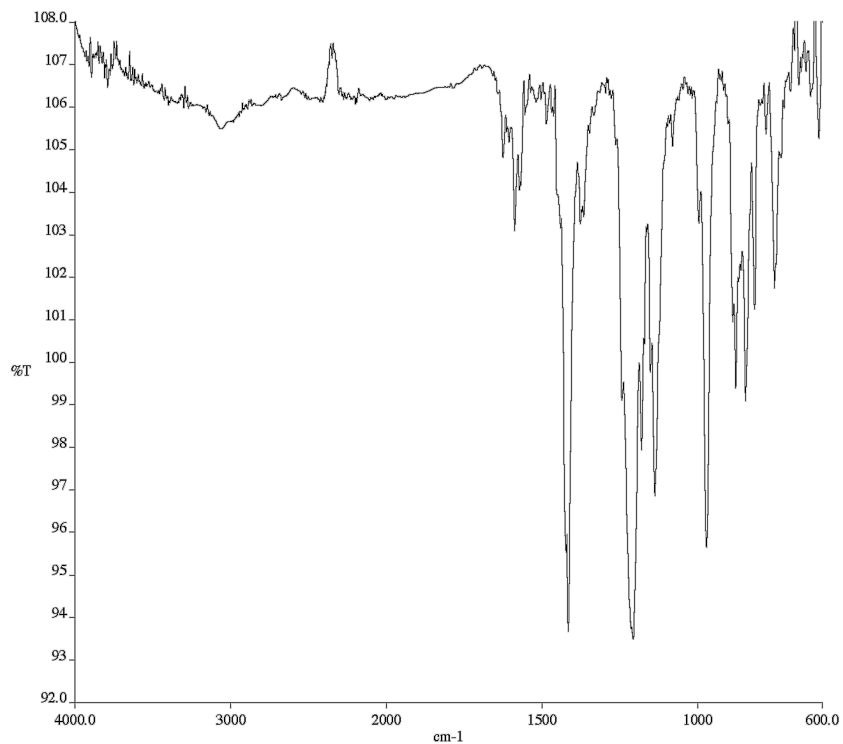


**Figure A1.25**  $^{19}\text{F}$  NMR (282 MHz,  $\text{CDCl}_3$ ) of compound **160c**.

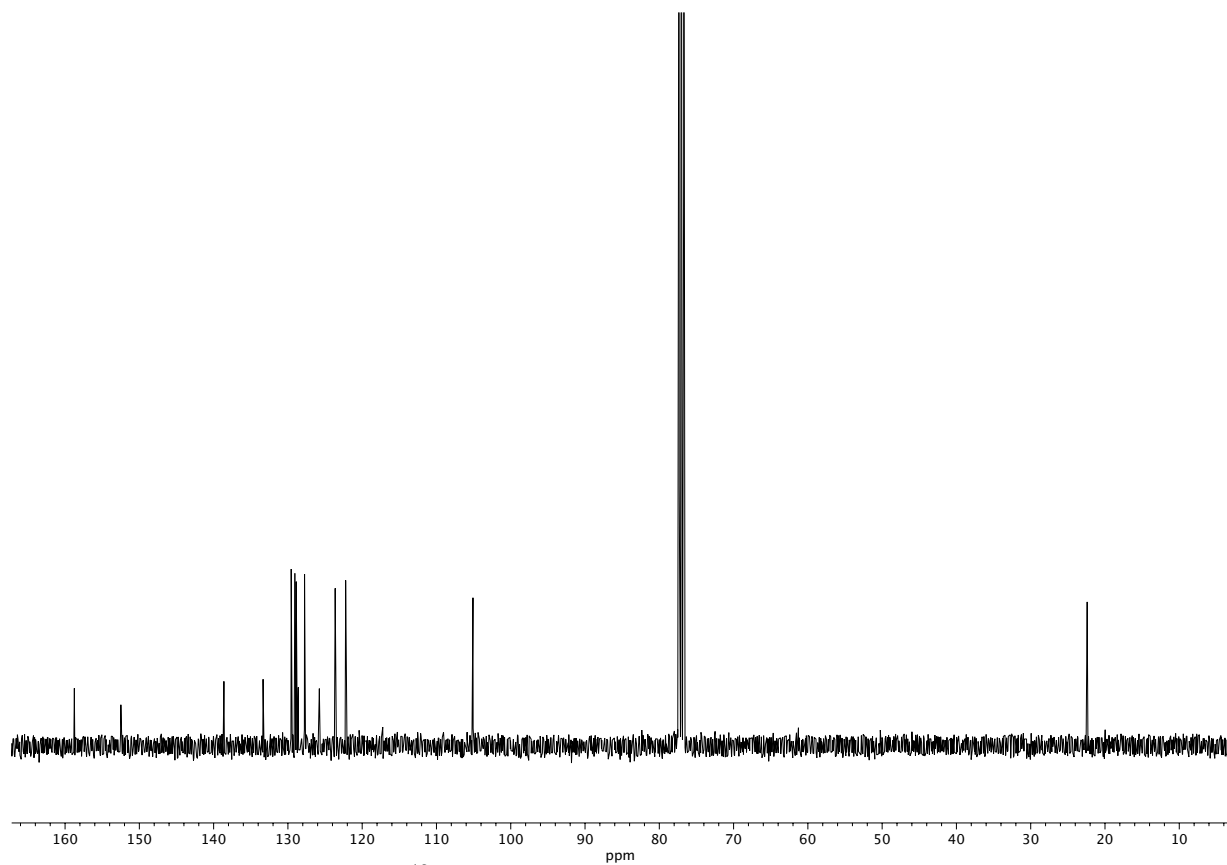




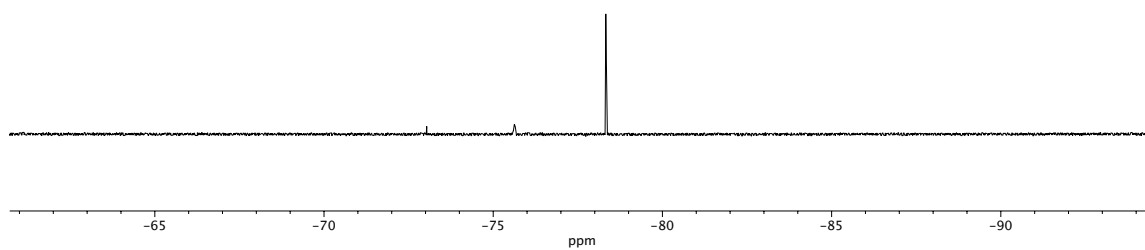
**Figure A1.26**  $^1\text{H}$  NMR (400 MHz,  $\text{CDCl}_3$ ) of compound **160d**.



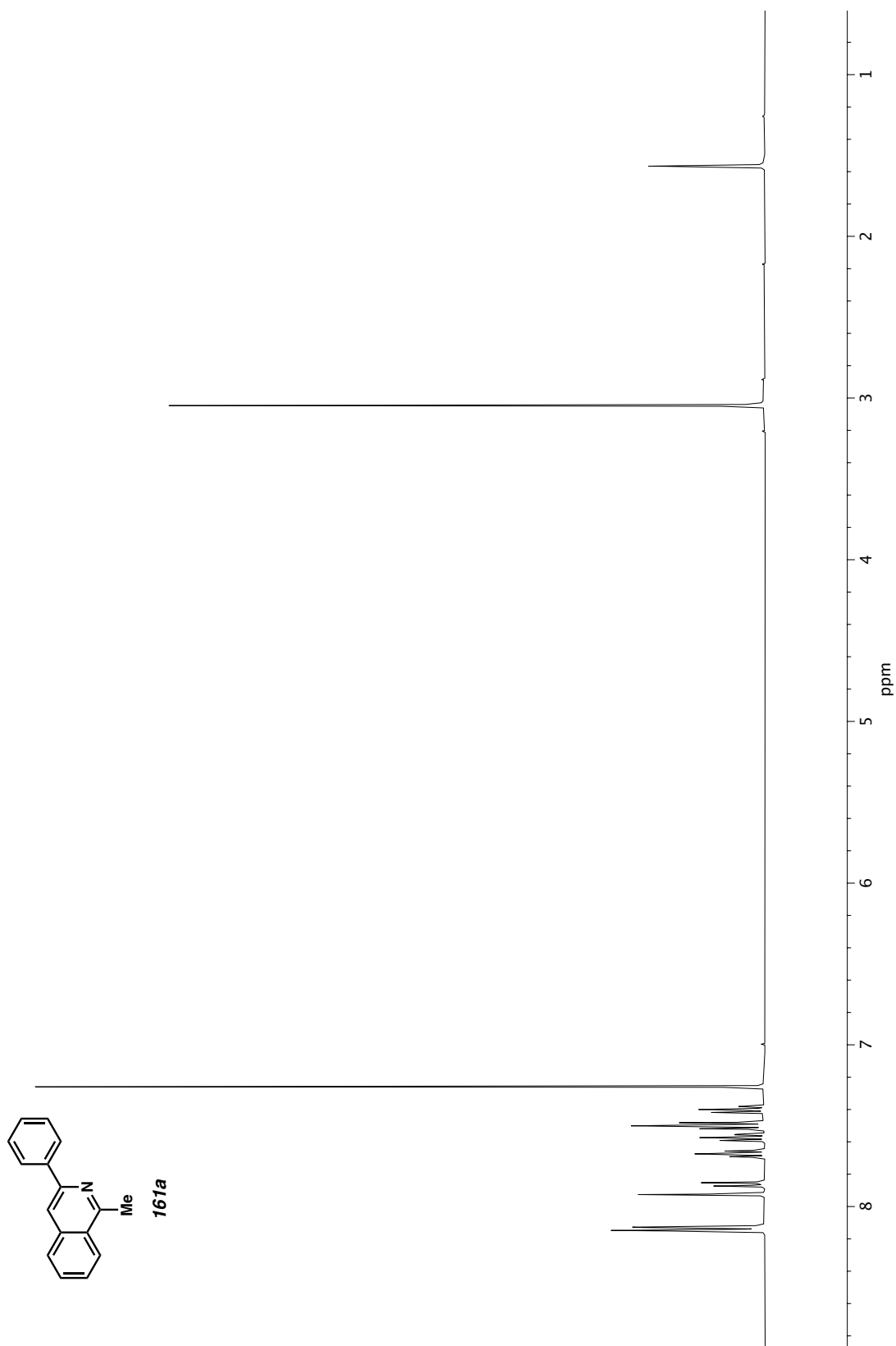
**Figure A1.27** Infrared spectrum (Thin Film, NaCl) of compound **160d**.



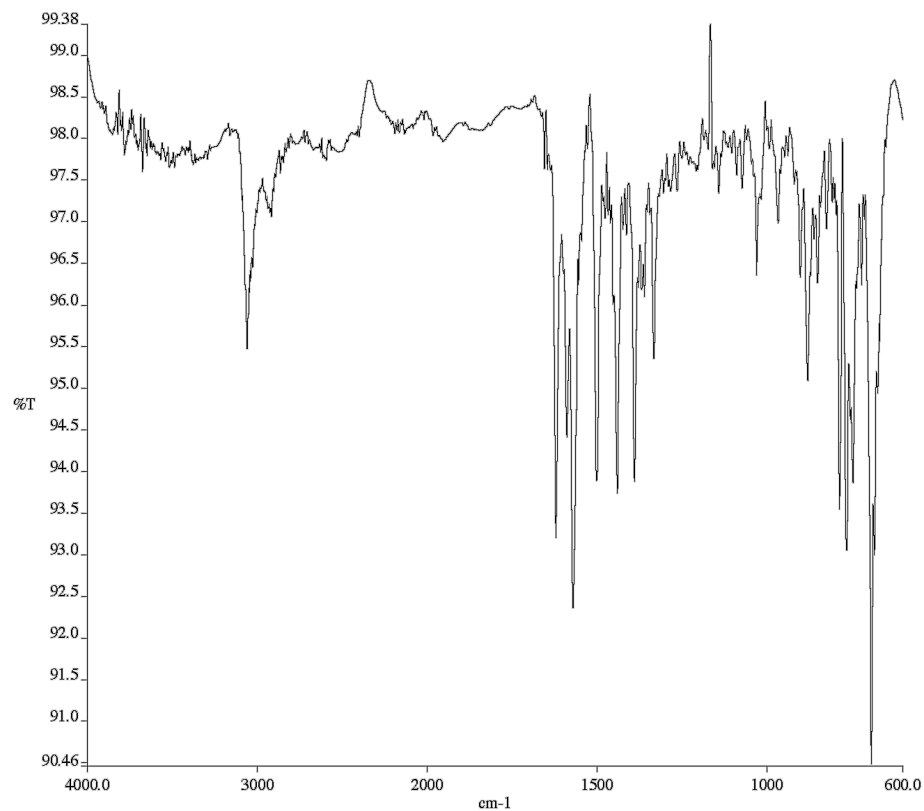
**Figure A1.28**  $^{13}\text{C}$  NMR (100 MHz,  $\text{CDCl}_3$ ) of compound **160d**.



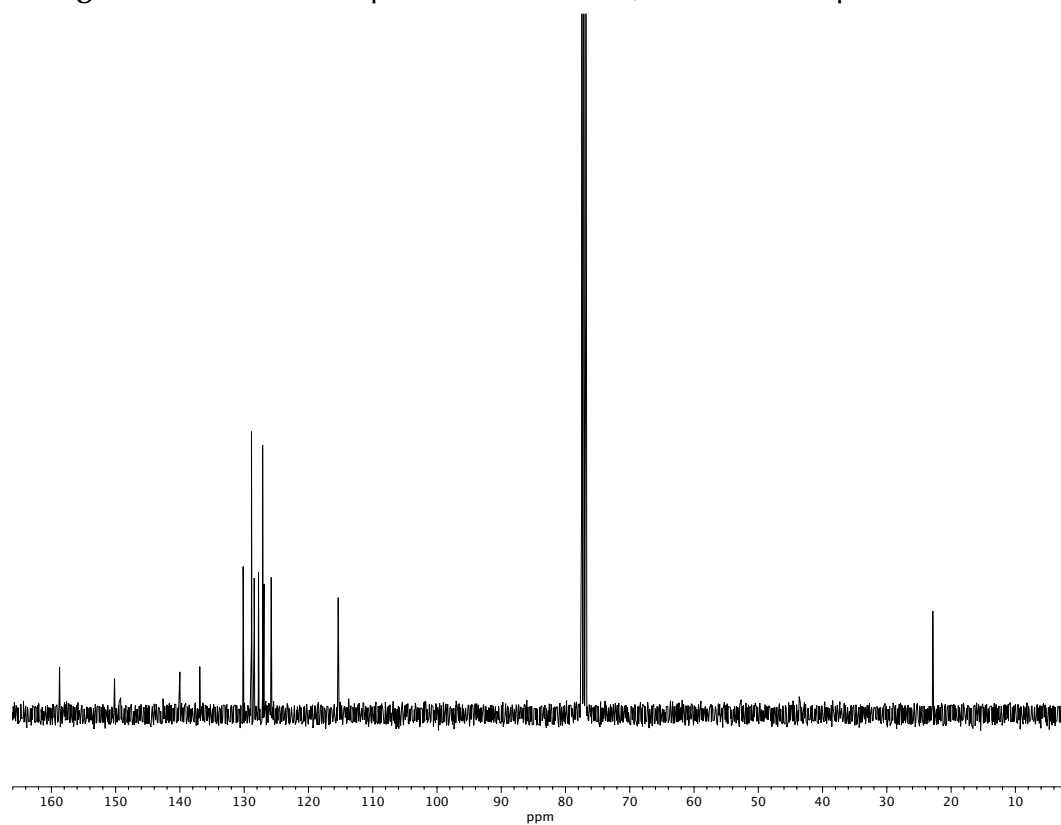
**Figure A1.29**  $^{19}\text{F}$  NMR (282 MHz,  $\text{CDCl}_3$ ) of compound **160d**.



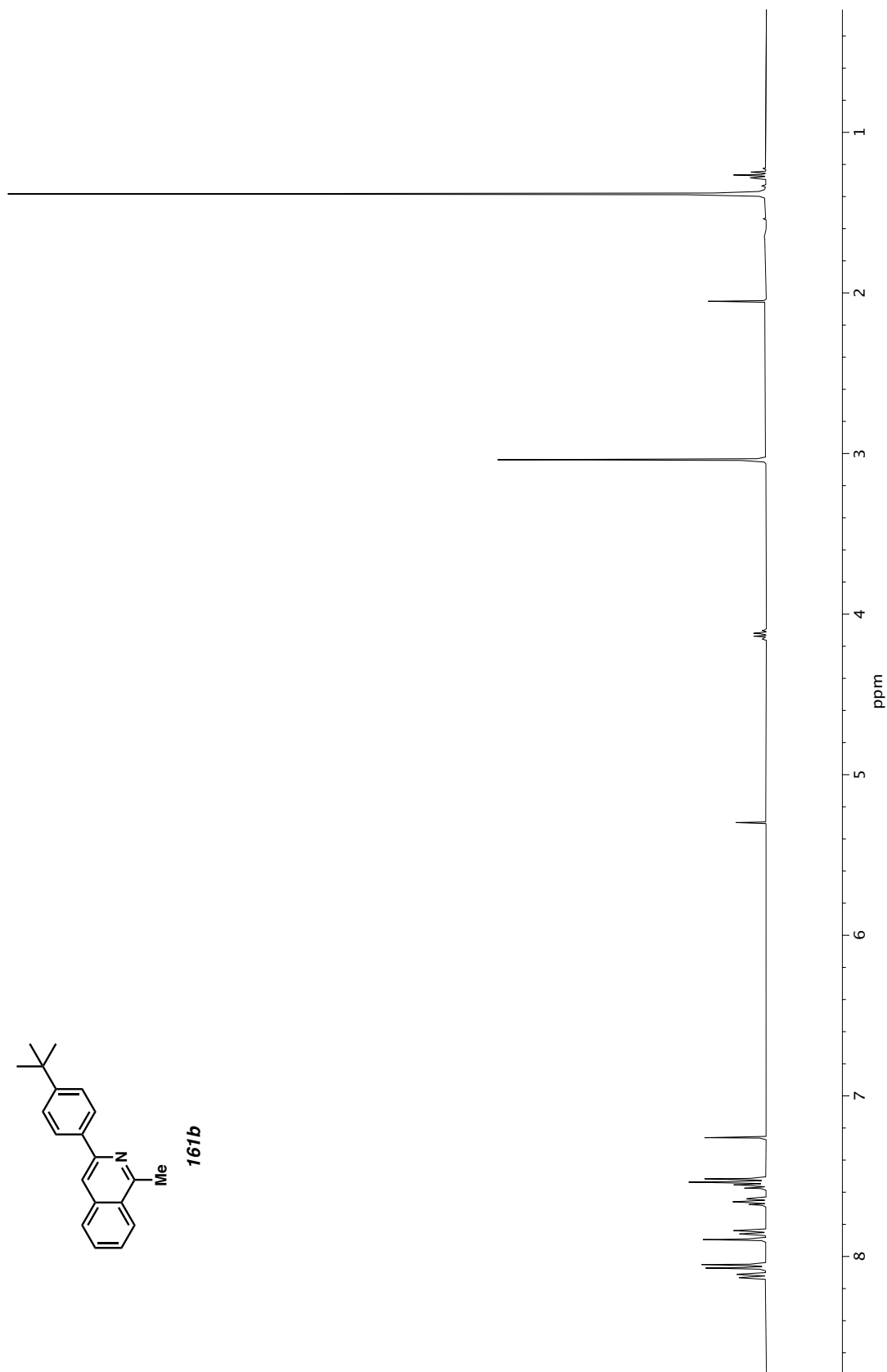
**Figure A1.30** <sup>1</sup>H NMR (400 MHz, CDCl<sub>3</sub>) of compound **161a**.



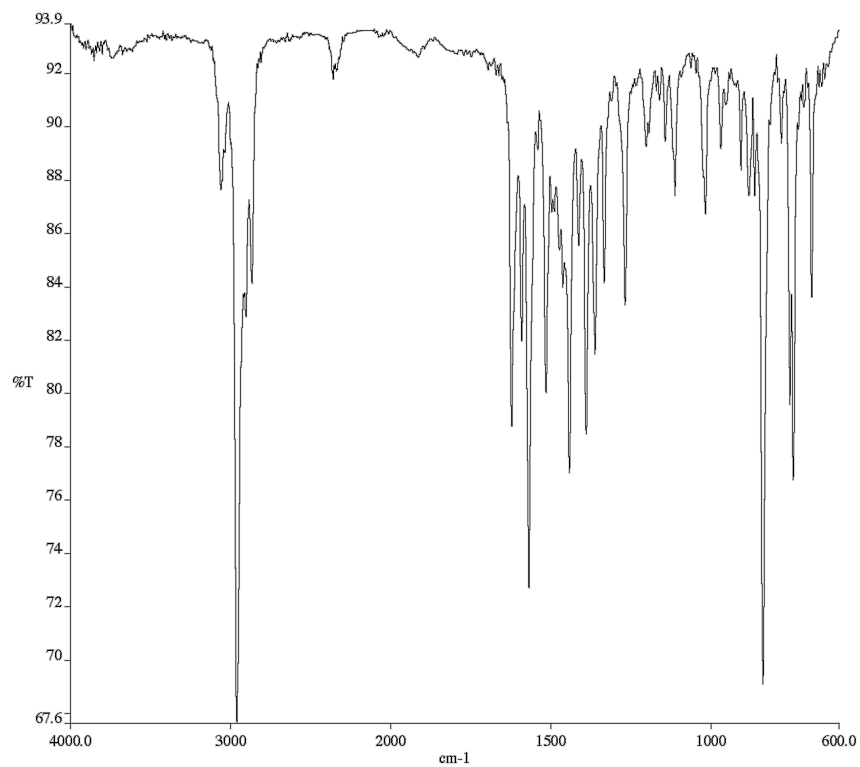
**Figure A1.31** Infrared spectrum (Thin Film, NaCl) of compound **161a**.



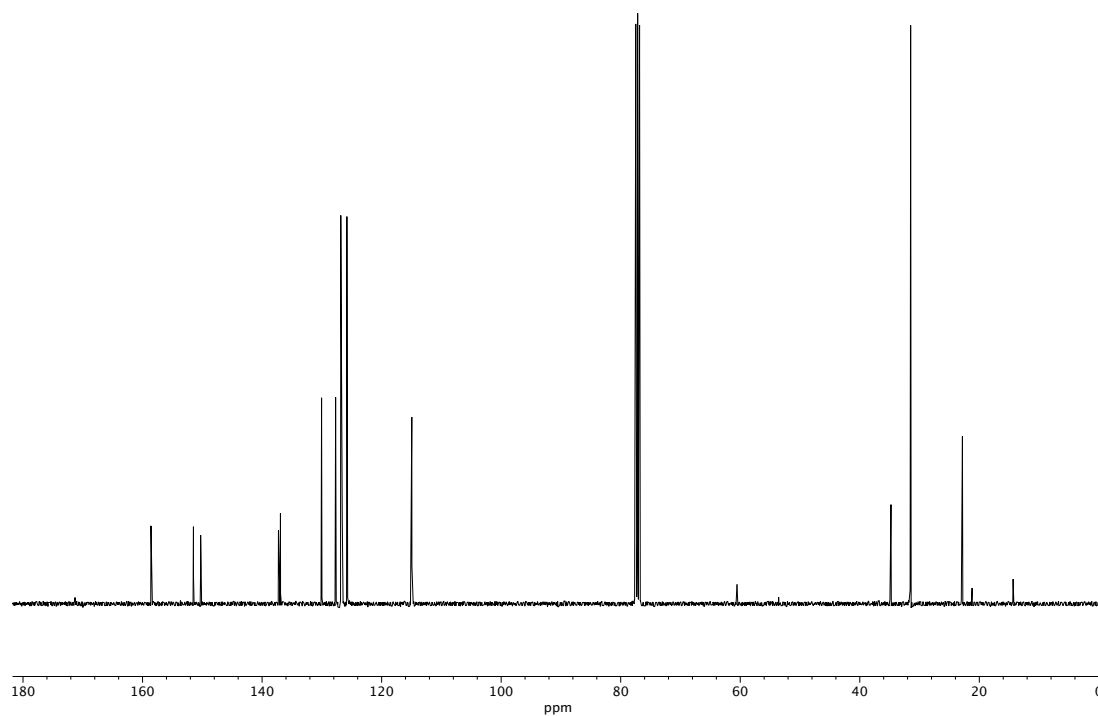
**Figure A1.32** <sup>13</sup>C NMR (100 MHz, CDCl<sub>3</sub>) of compound **161a**.



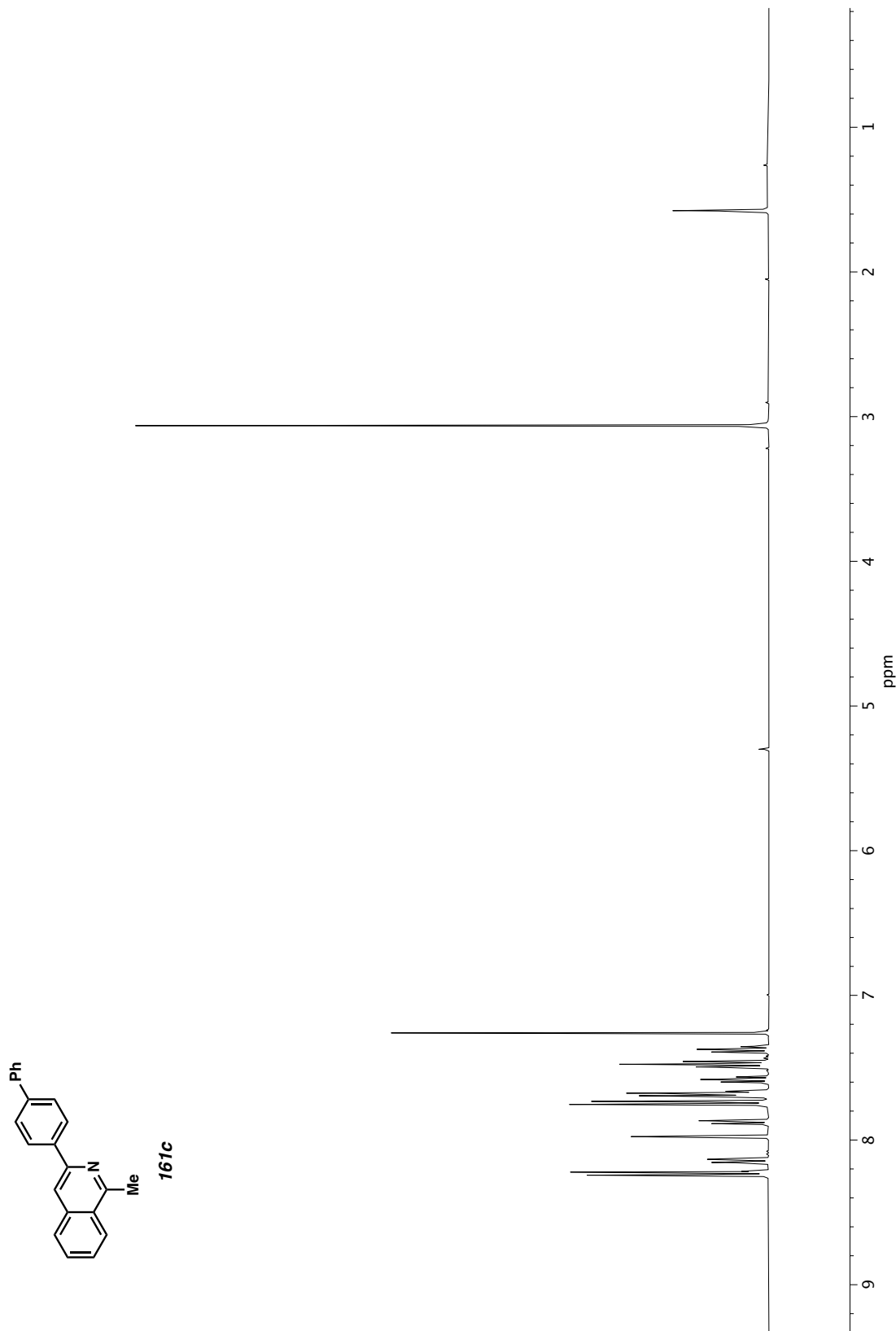
**Figure A1.33**  $^1\text{H NMR}$  (400 MHz,  $\text{CDCl}_3$ ) of compound **161b**.



**Figure A1.34** Infrared spectrum (Thin Film, NaCl) of compound **161b**.

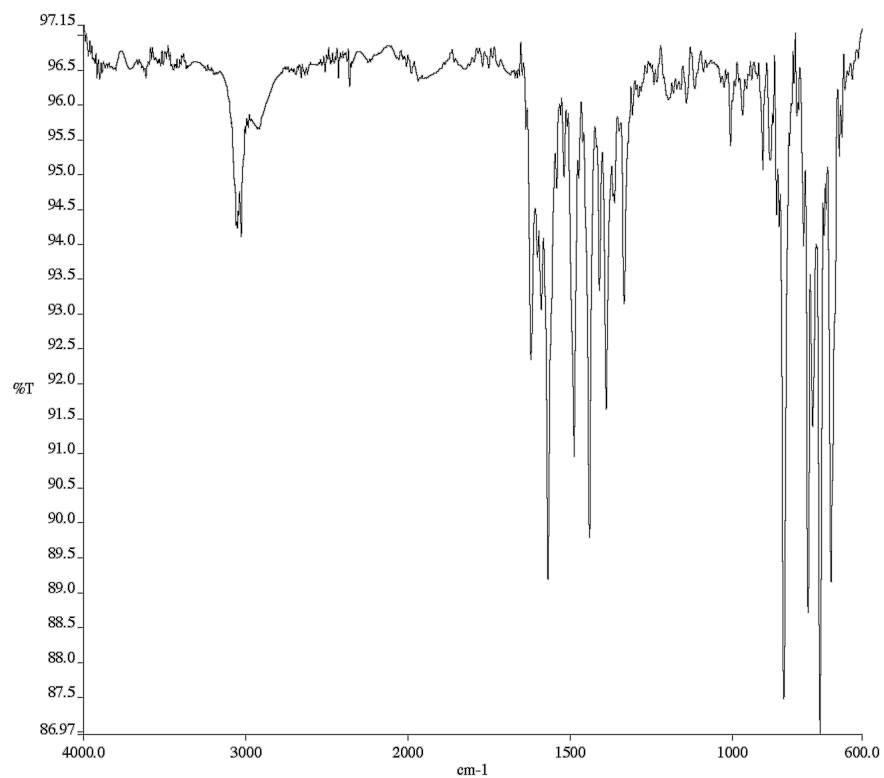


**Figure A1.35** <sup>13</sup>C NMR (100 MHz, CDCl<sub>3</sub>) of compound **161b**.

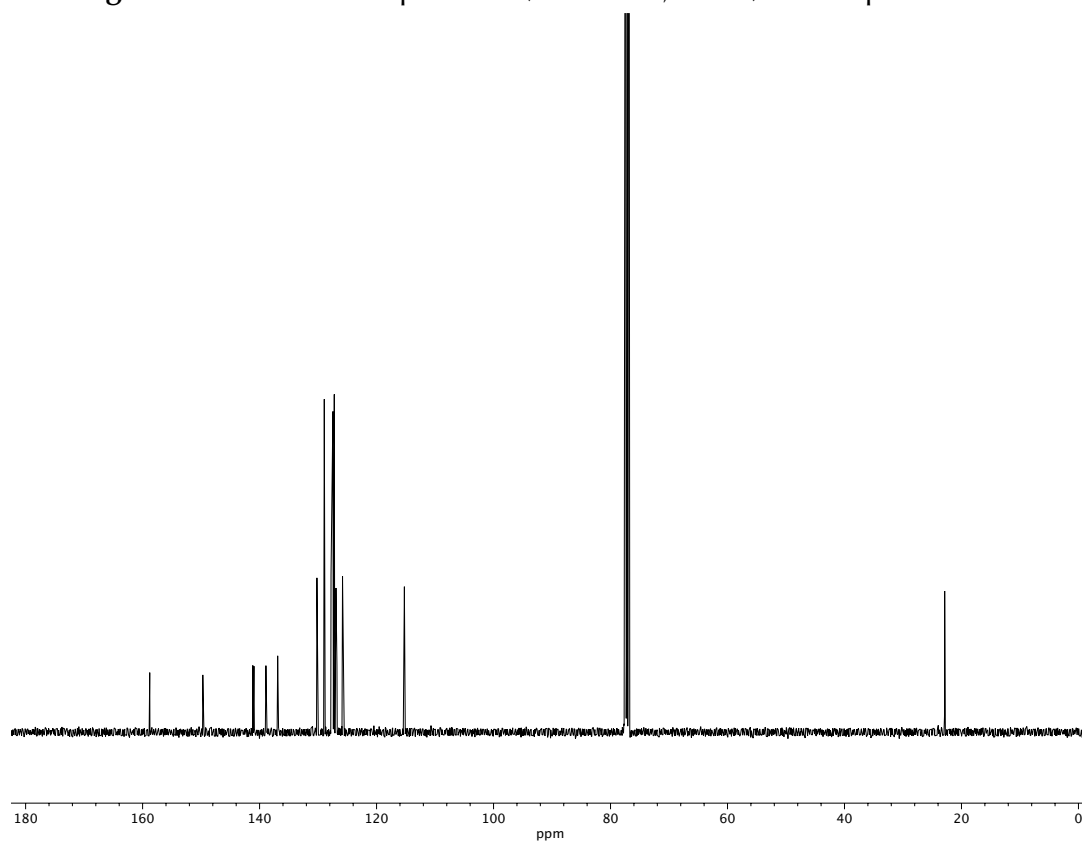


**Figure A1.36**  $^1\text{H}$  NMR (400 MHz,  $\text{CDCl}_3$ ) of compound **161c**.

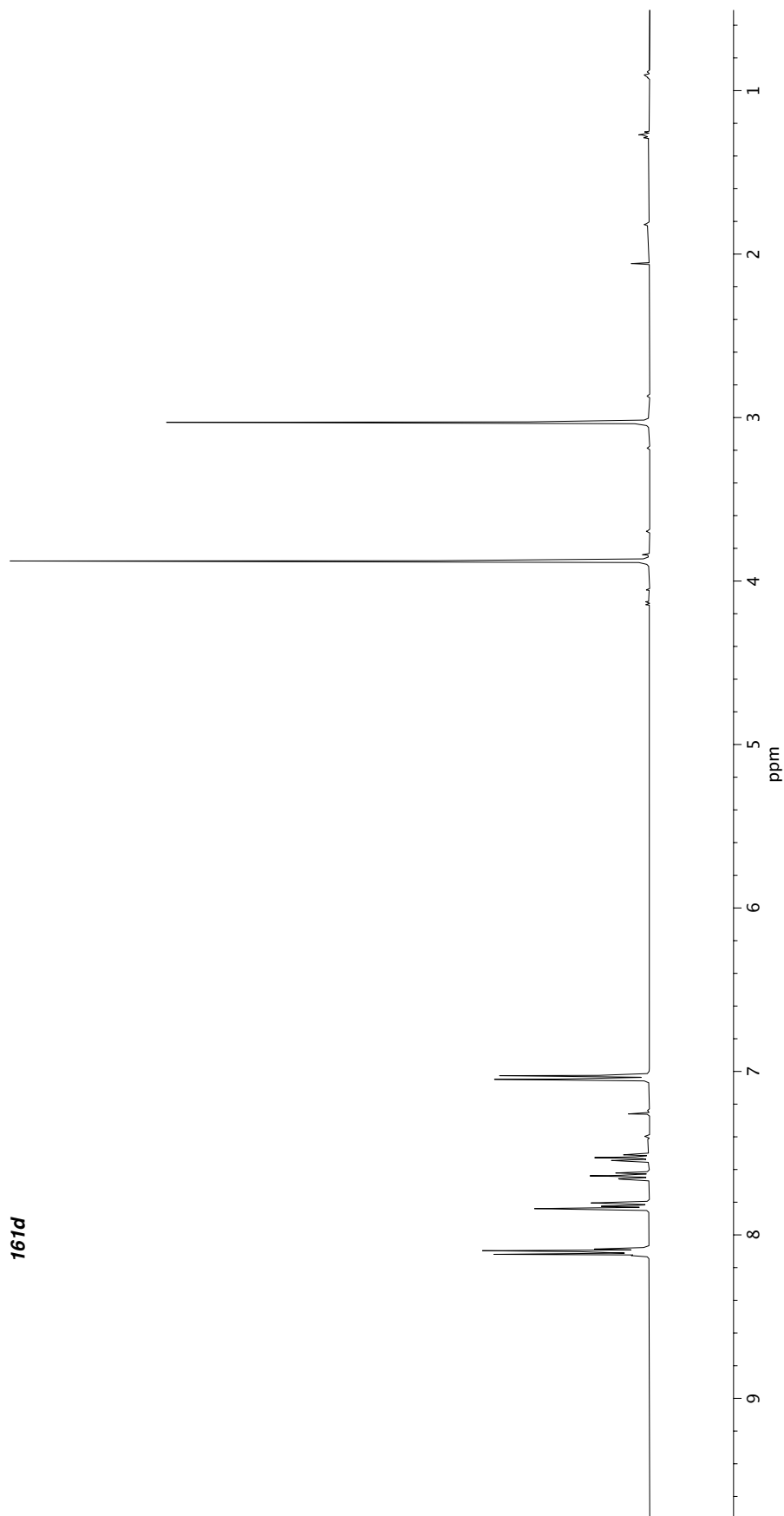
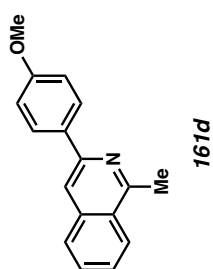




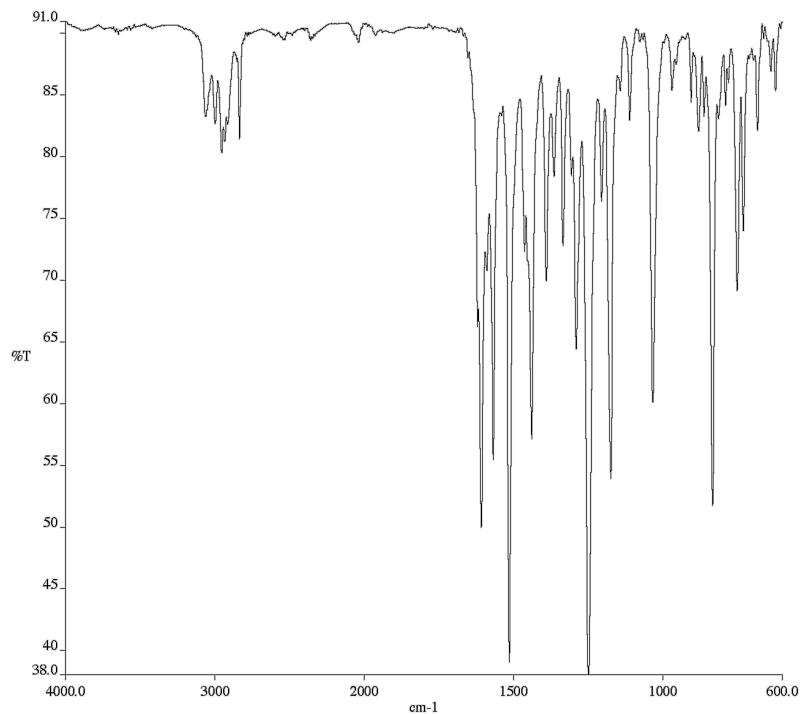
**Figure A1.37** Infrared spectrum (Thin Film, NaCl) of compound **161c**.



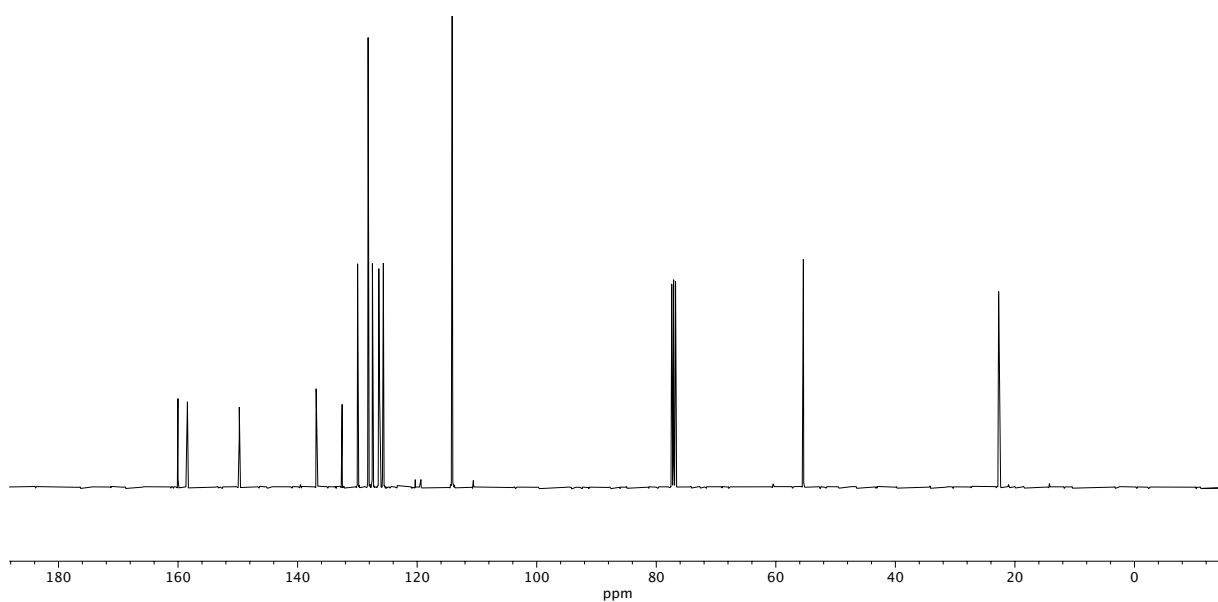
**Figure A1.38** <sup>13</sup>C NMR (100 MHz, CDCl<sub>3</sub>) of compound **161c**.



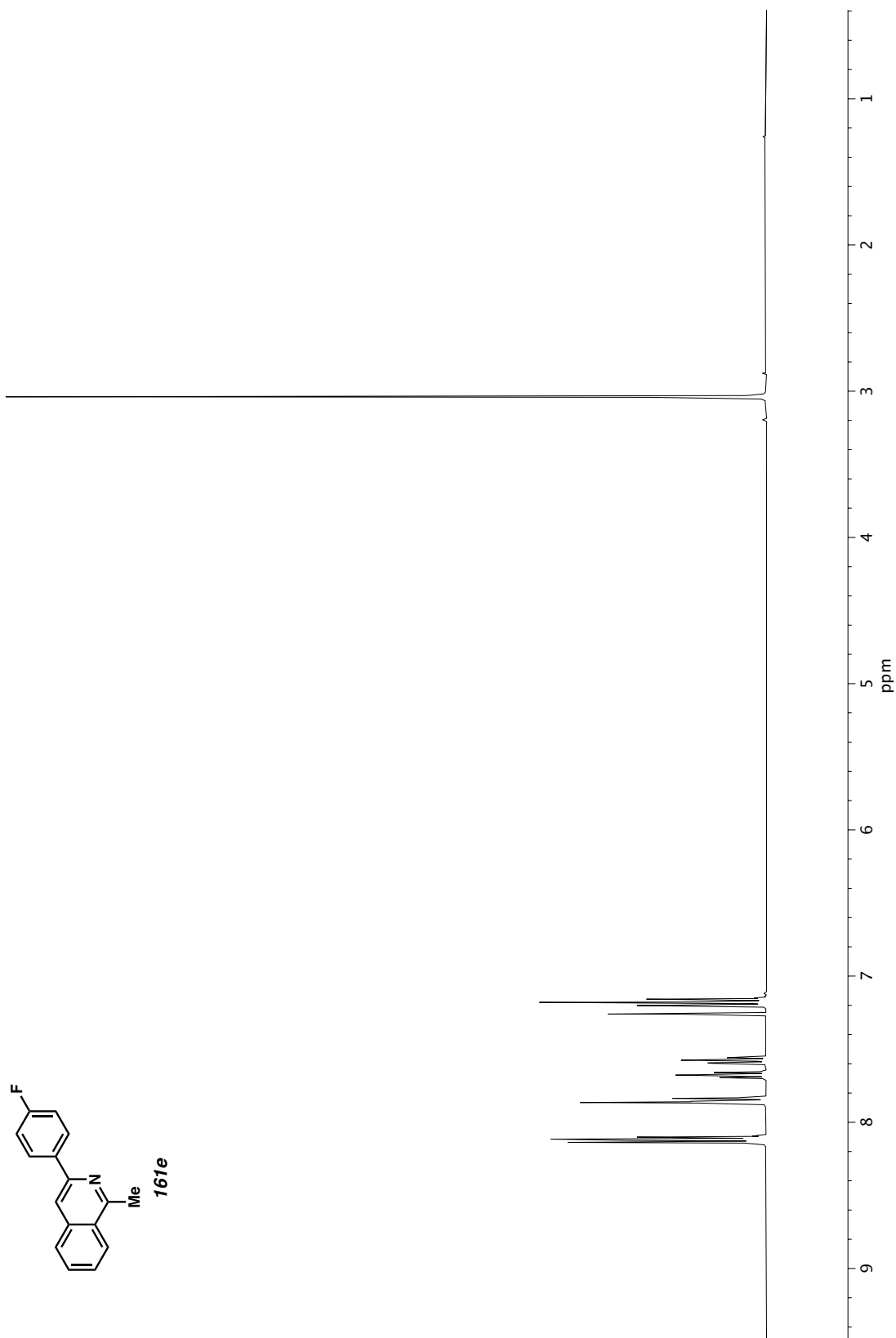
**Figure A1.39** <sup>1</sup>H NMR (400 MHz, CDCl<sub>3</sub>) of compound **161d**.



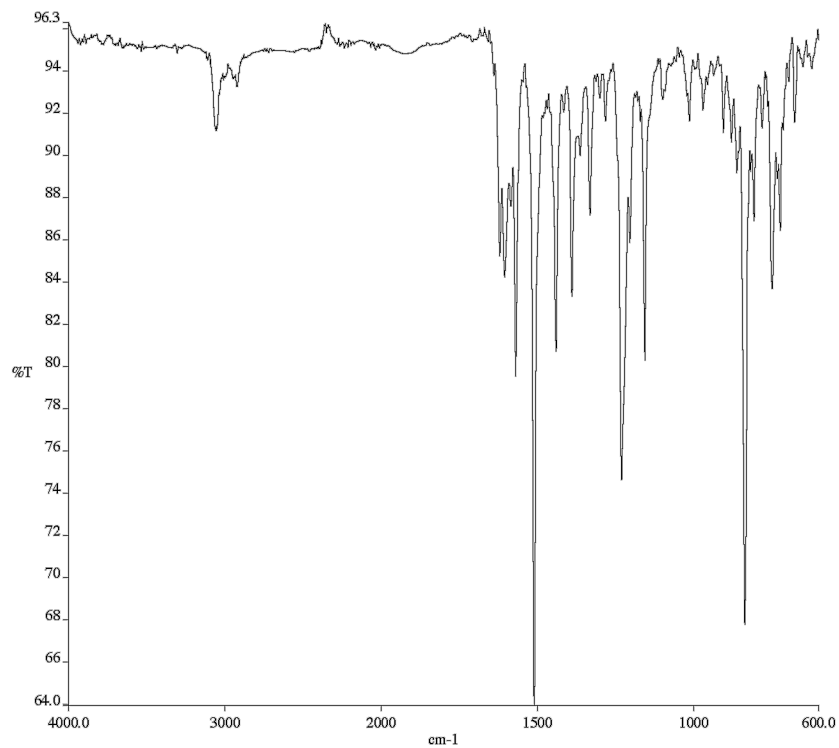
**Figure A1.40** Infrared spectrum (Thin Film, NaCl) of compound **161d**.



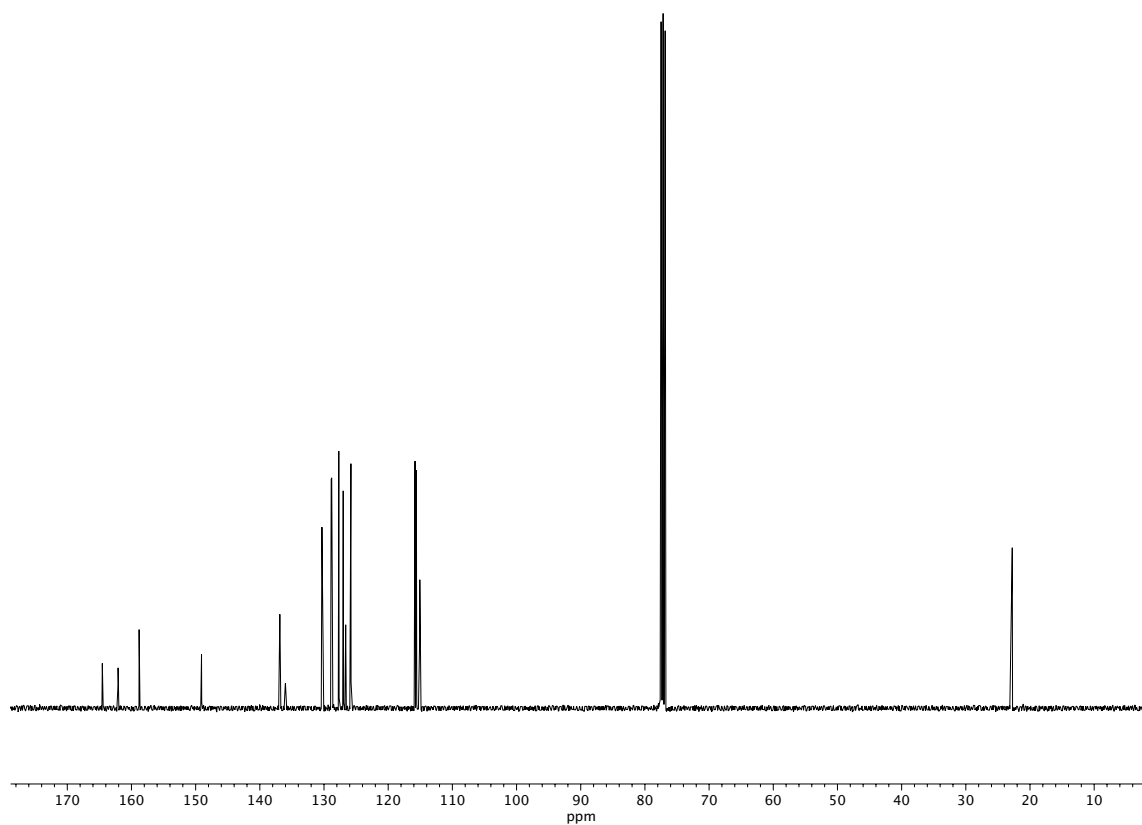
**Figure A1.41** <sup>13</sup>C NMR (100 MHz, CDCl<sub>3</sub>) of compound **161d**.



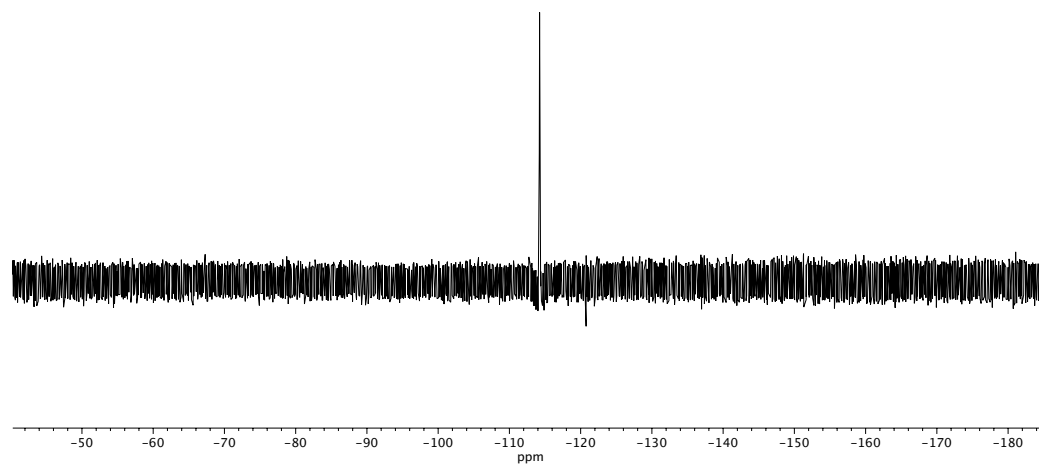
**Figure A1.42**  $^1\text{H}$  NMR (400 MHz,  $\text{CDCl}_3$ ) of compound **161e**.



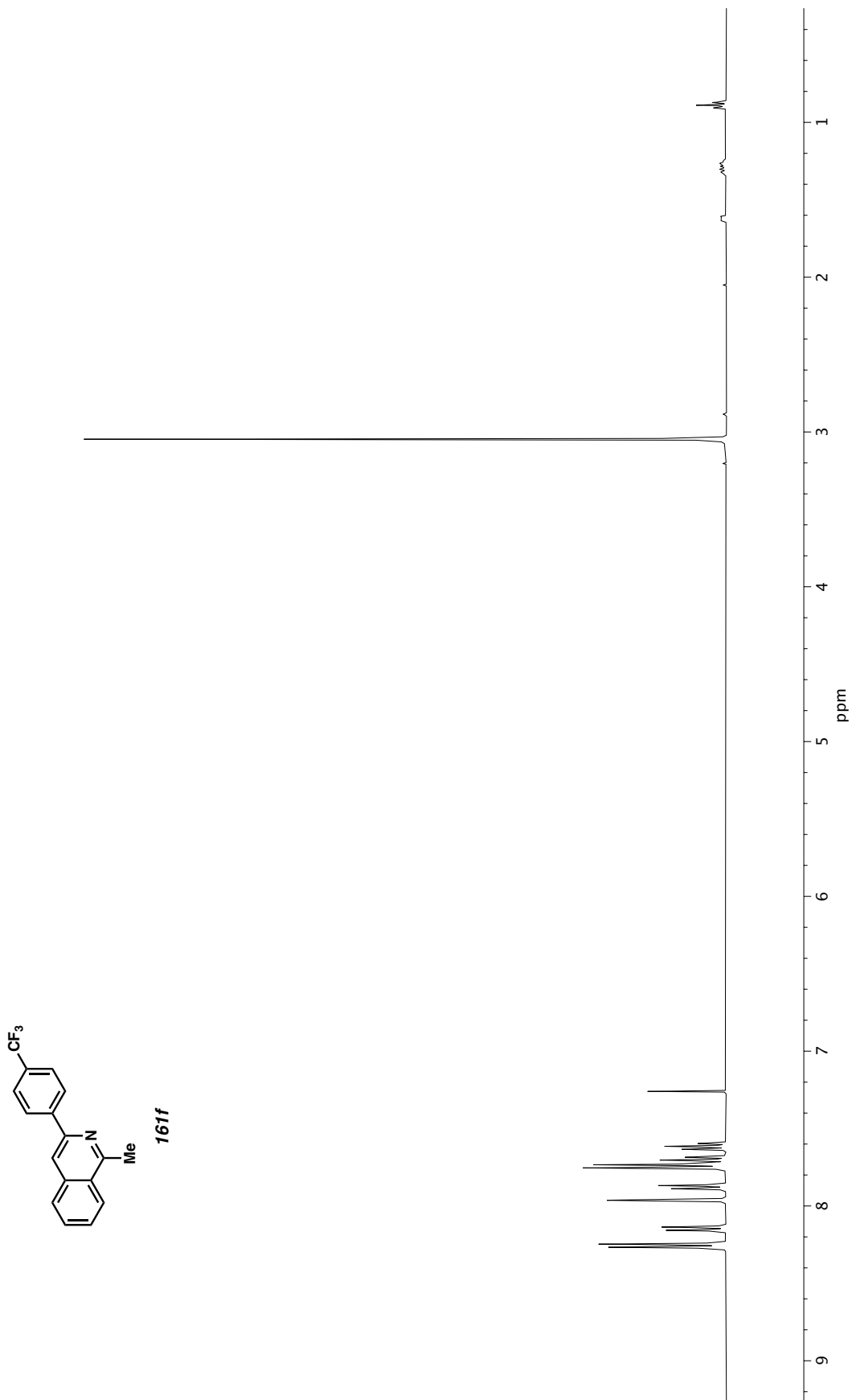
**Figure A1.43** Infrared spectrum (Thin Film, NaCl) of compound **161e**.



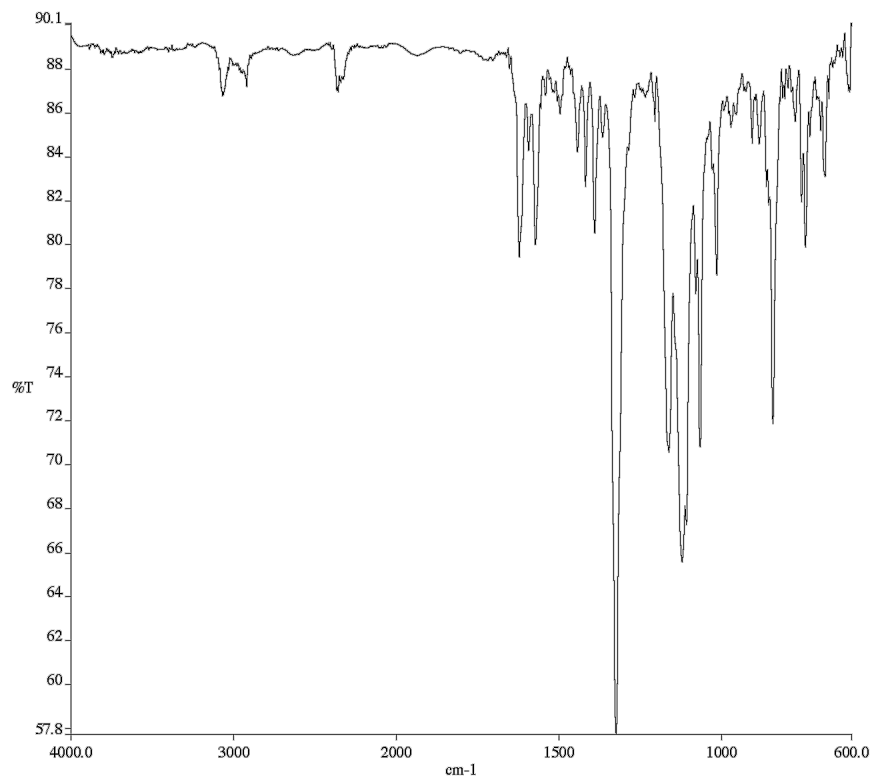
**Figure A1.44** <sup>13</sup>C NMR (100 MHz, CDCl<sub>3</sub>) of compound **161e**.



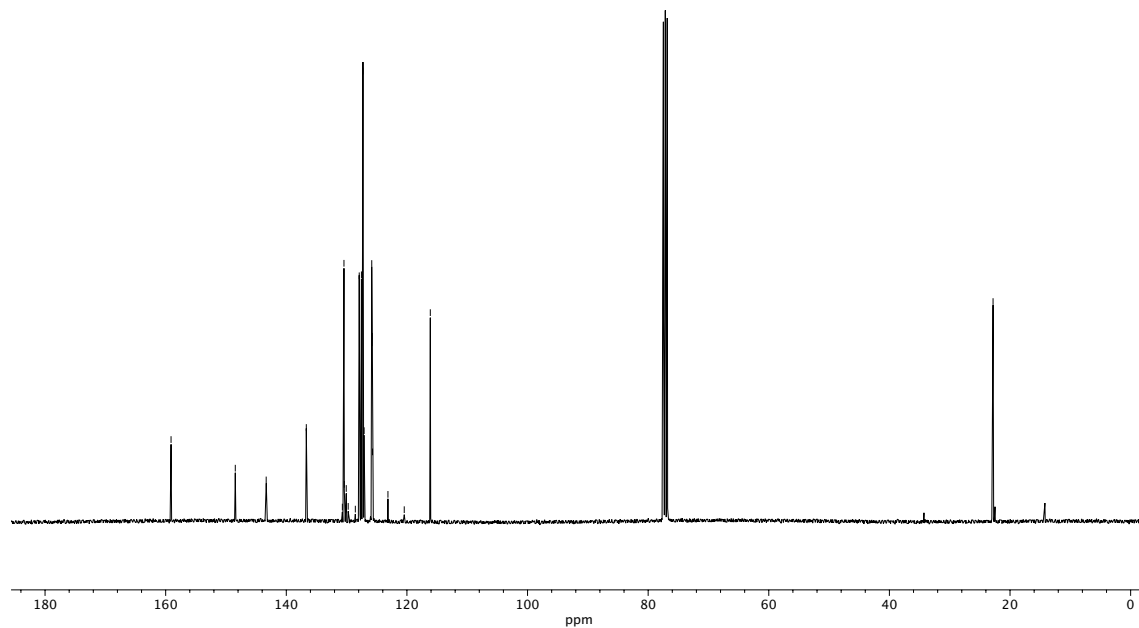
**Figure A1.45**  $^{19}\text{F}$  NMR (282 MHz,  $\text{CDCl}_3$ ) of compound **161e**.



**Figure A1.46**  $^1\text{H}$  NMR (400 MHz,  $\text{CDCl}_3$ ) of compound **161f**.

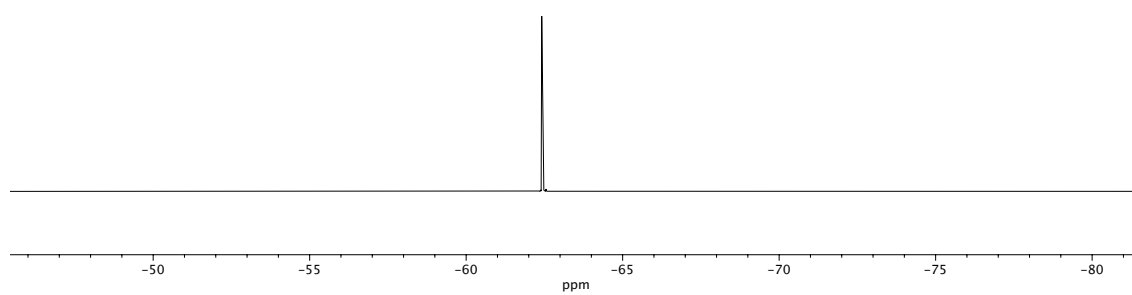


**Figure A1.47** Infrared spectrum (Thin Film, NaCl) of compound **161f**.

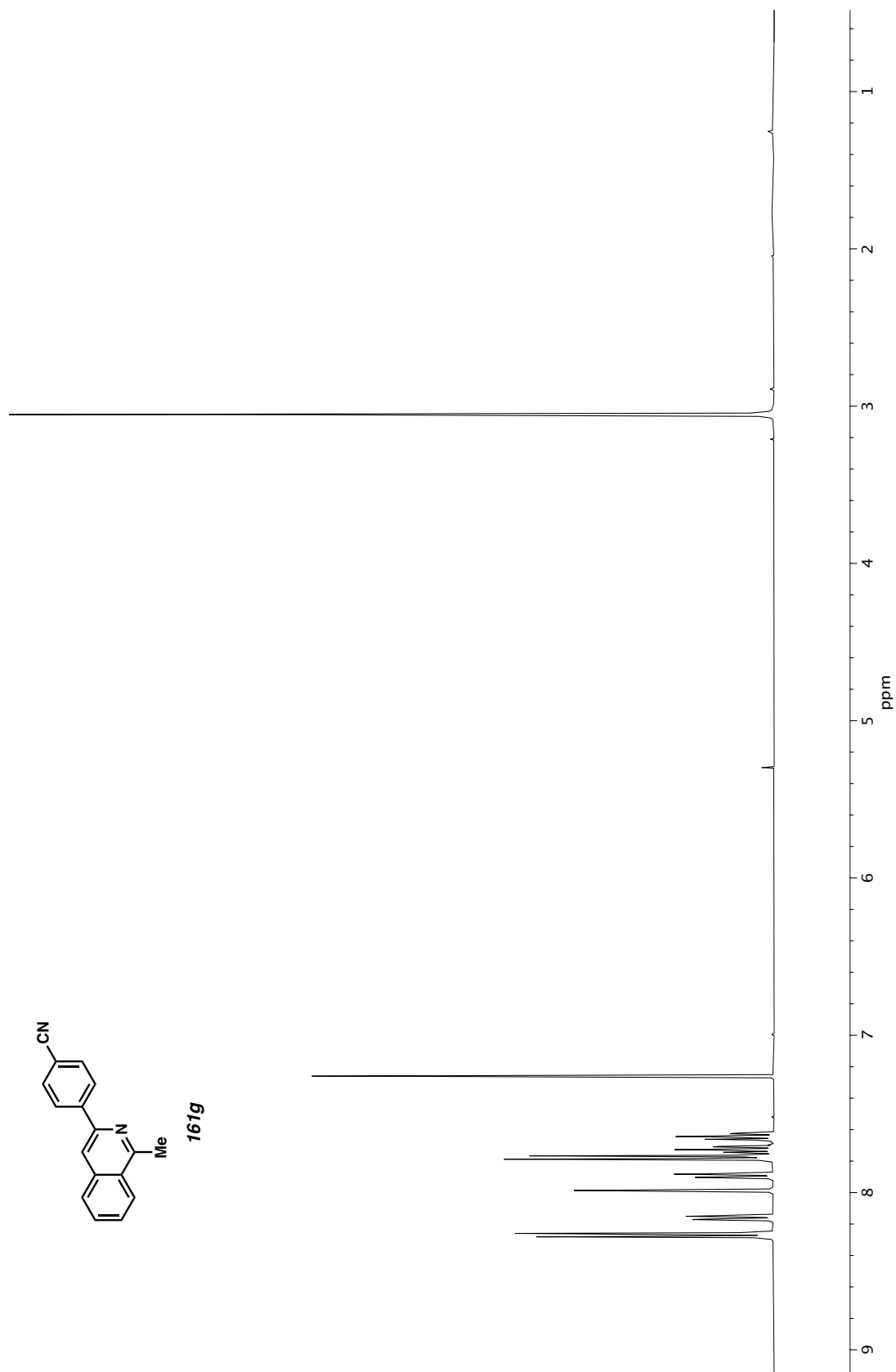


**Figure A1.48** <sup>13</sup>C NMR (100 MHz, CDCl<sub>3</sub>) of compound **161f**.

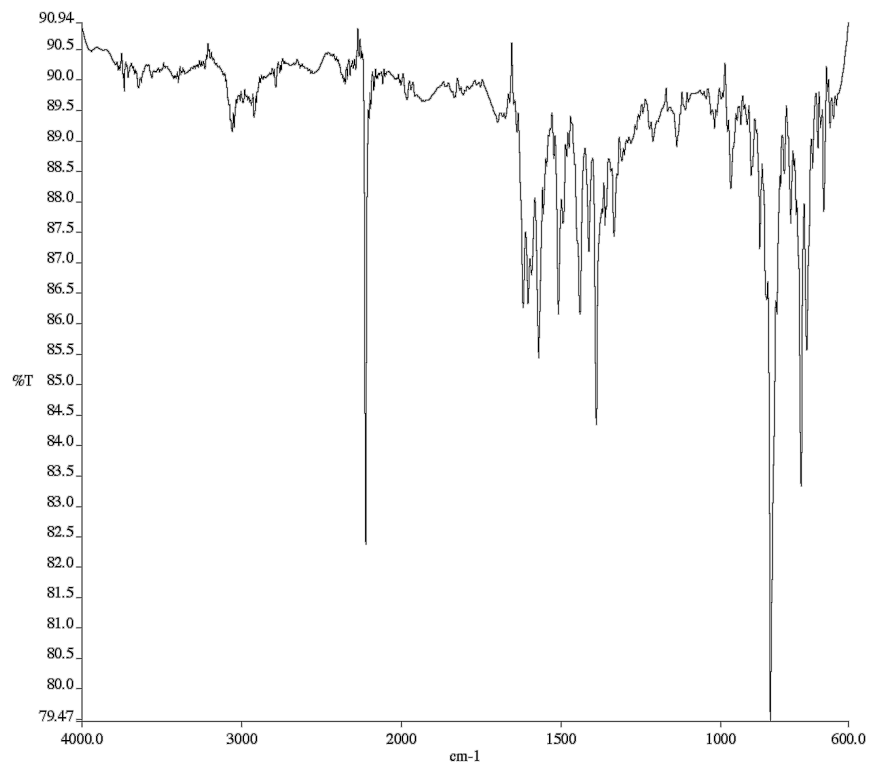




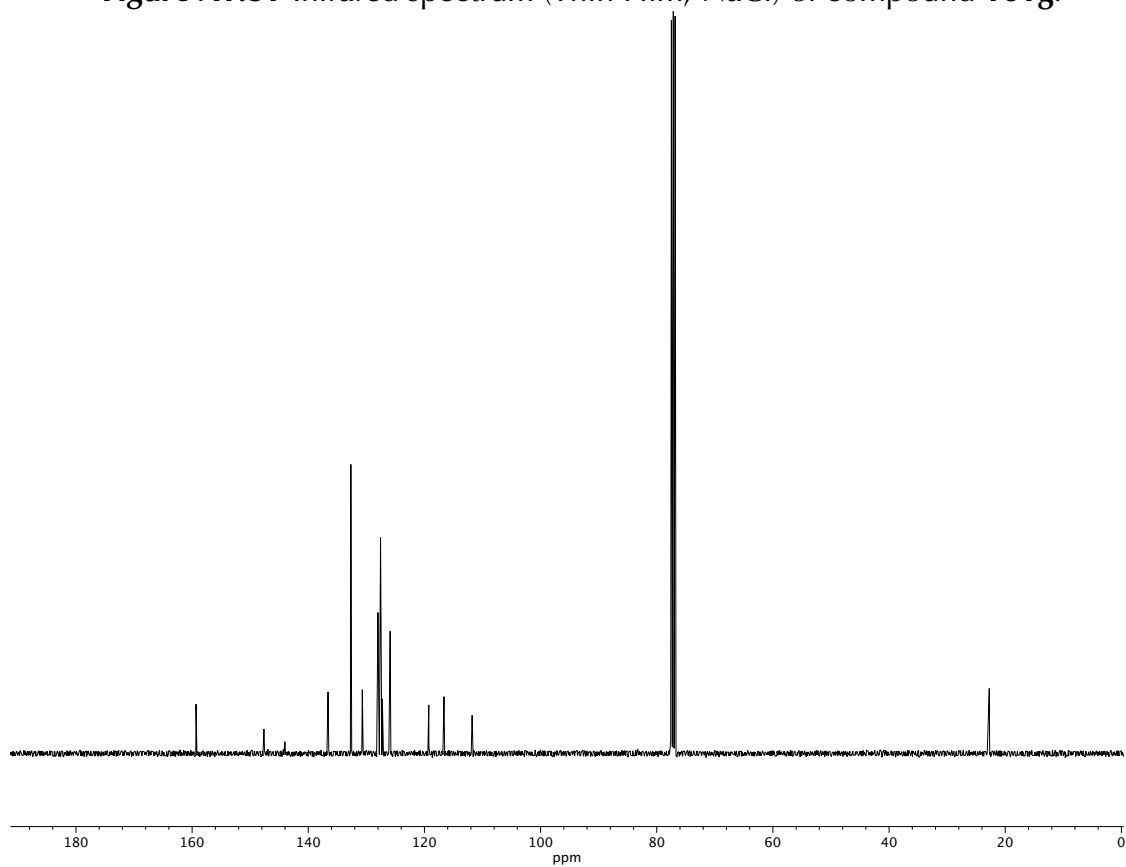
**Figure A1.49**  $^{19}\text{F}$  NMR (282 MHz,  $\text{CDCl}_3$ ) of compound **161f**.



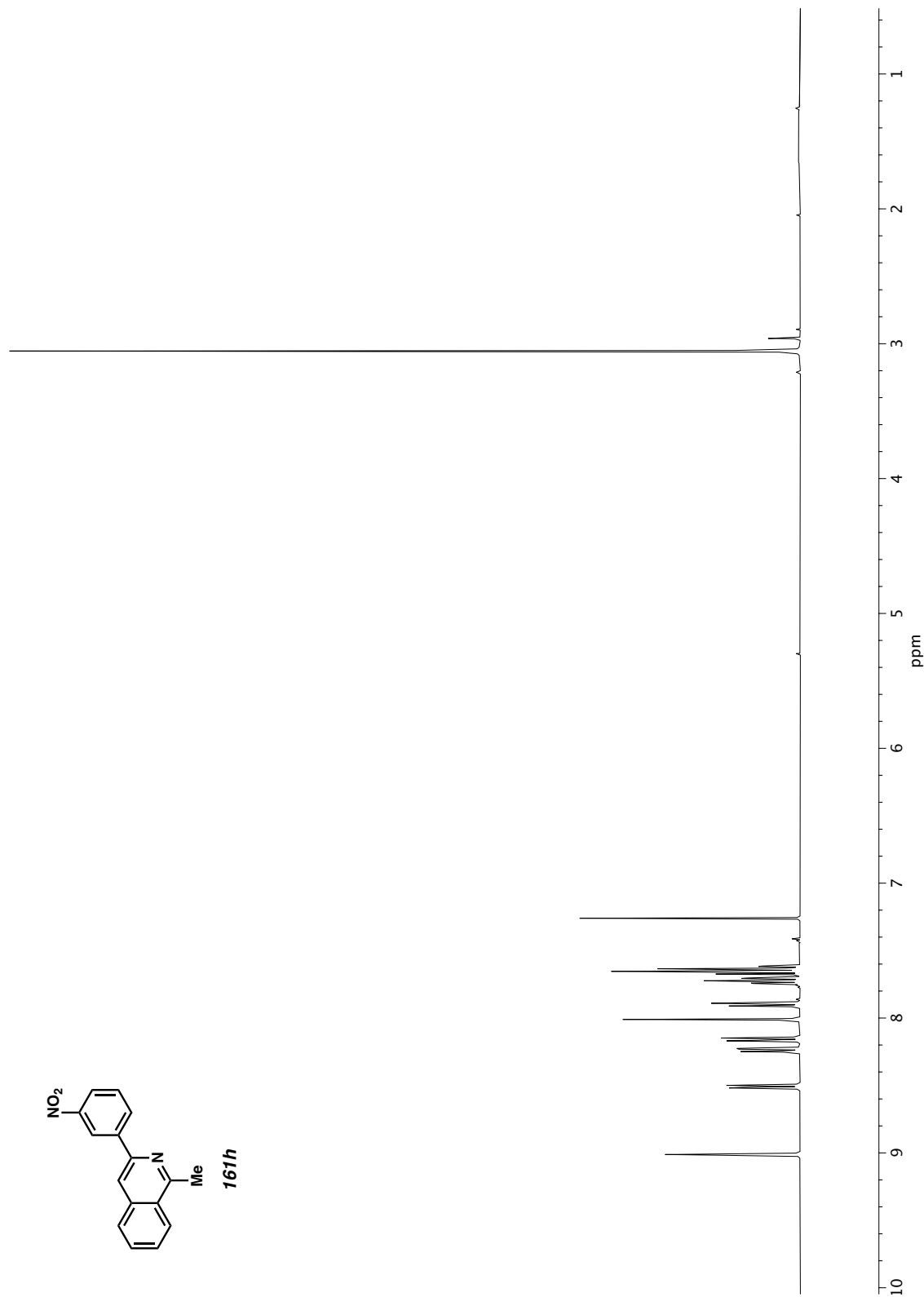
**Figure A1.50**  $^1\text{H}$  NMR (400 MHz,  $\text{CDCl}_3$ ) of compound **161g**.



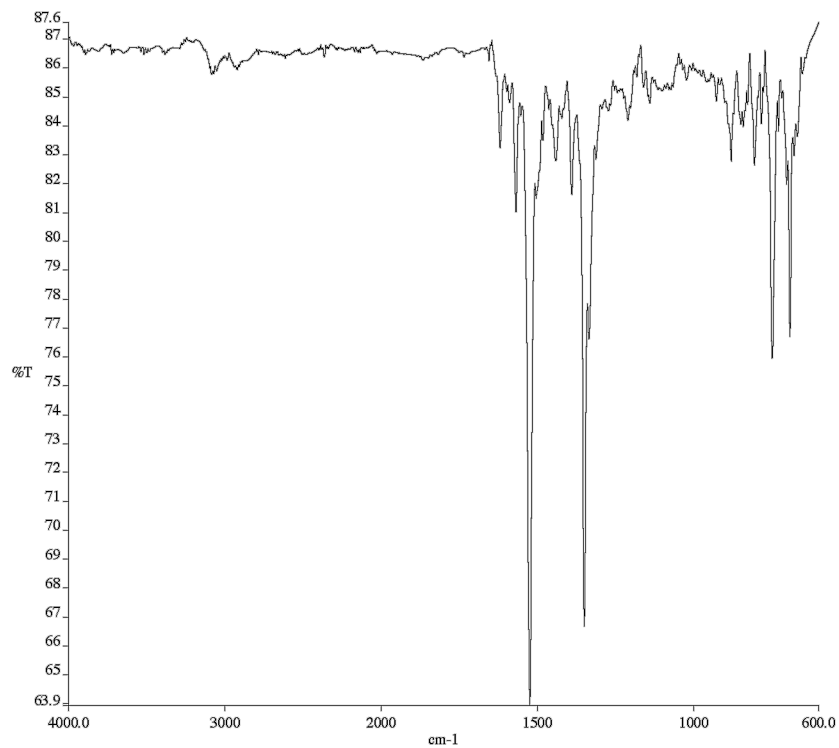
**Figure A1.51** Infrared spectrum (Thin Film, NaCl) of compound **161g**.



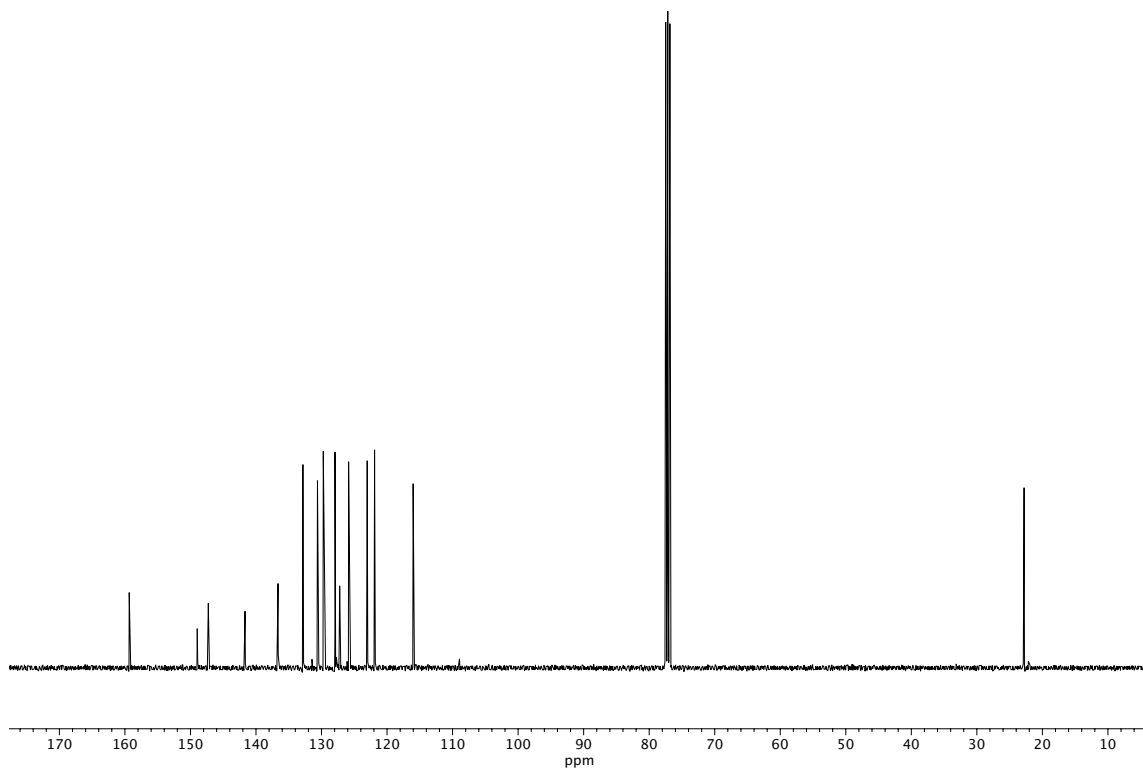
**Figure A1.52** <sup>13</sup>C NMR (100 MHz, CDCl<sub>3</sub>) of compound **161g**.



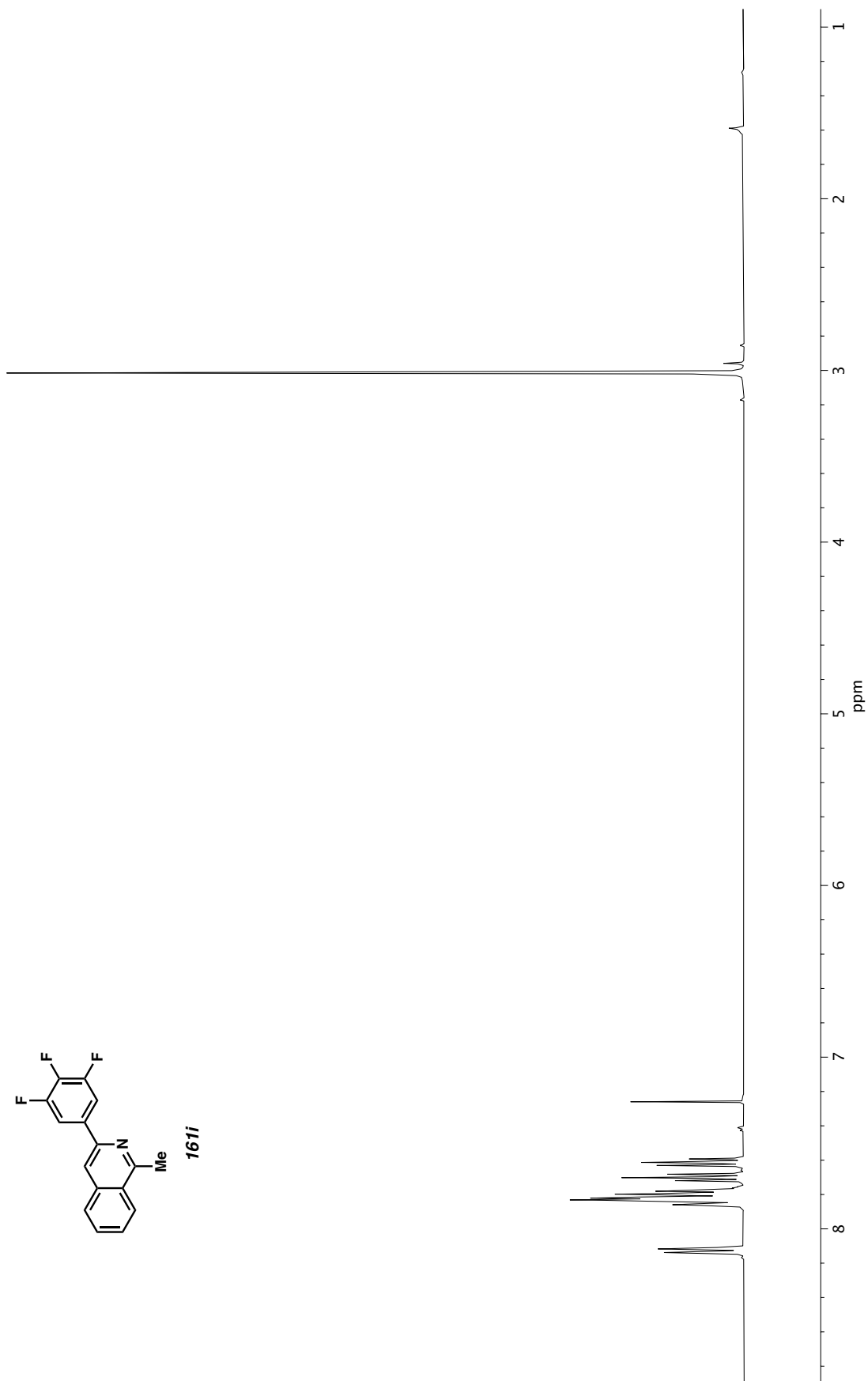
**Figure A1.53** <sup>1</sup>H NMR (400 MHz, CDCl<sub>3</sub>) of compound **161h**.



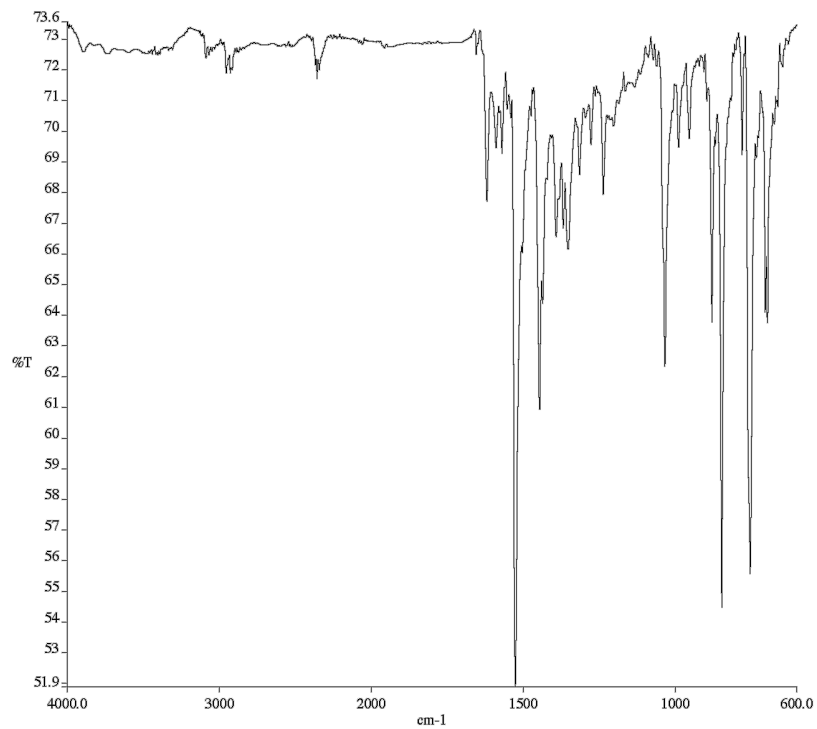
**Figure A1.54** Infrared spectrum (Thin Film, NaCl) of compound **161h**.



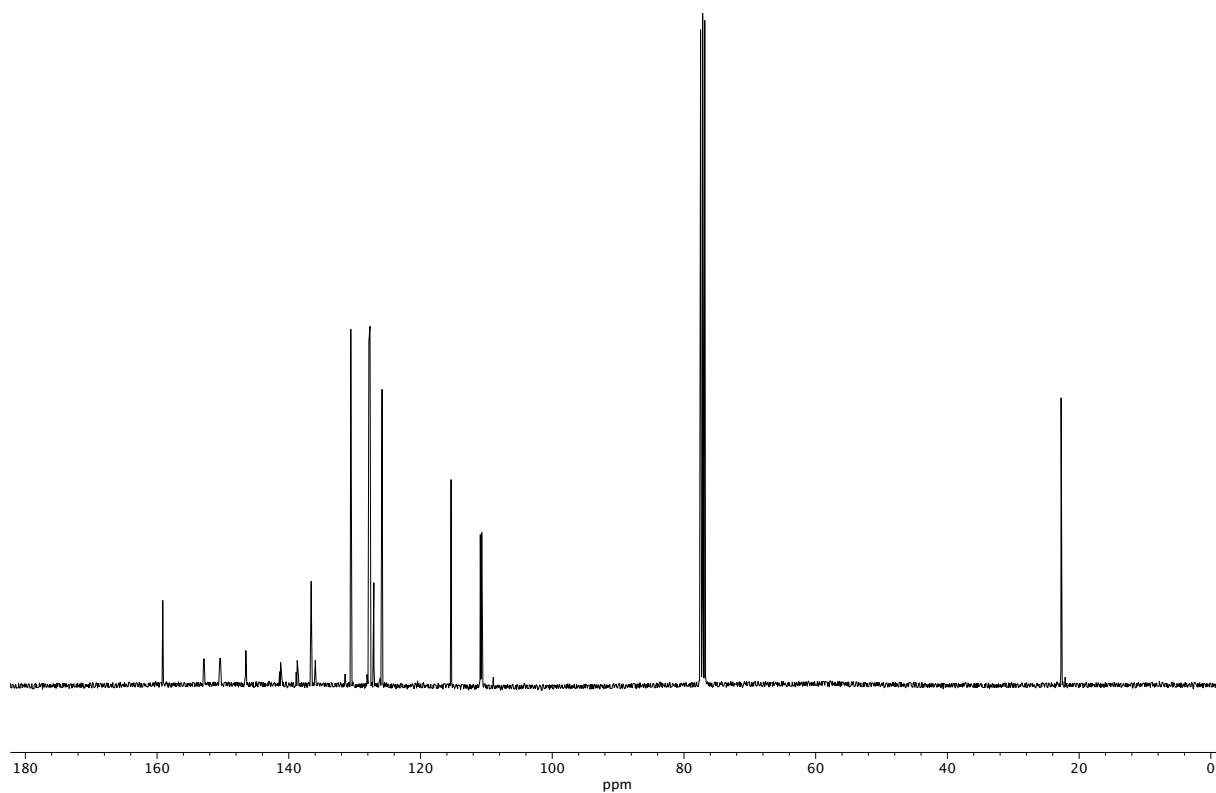
**Figure A1.55** <sup>13</sup>C NMR (100 MHz, CDCl<sub>3</sub>) of compound **161h**.



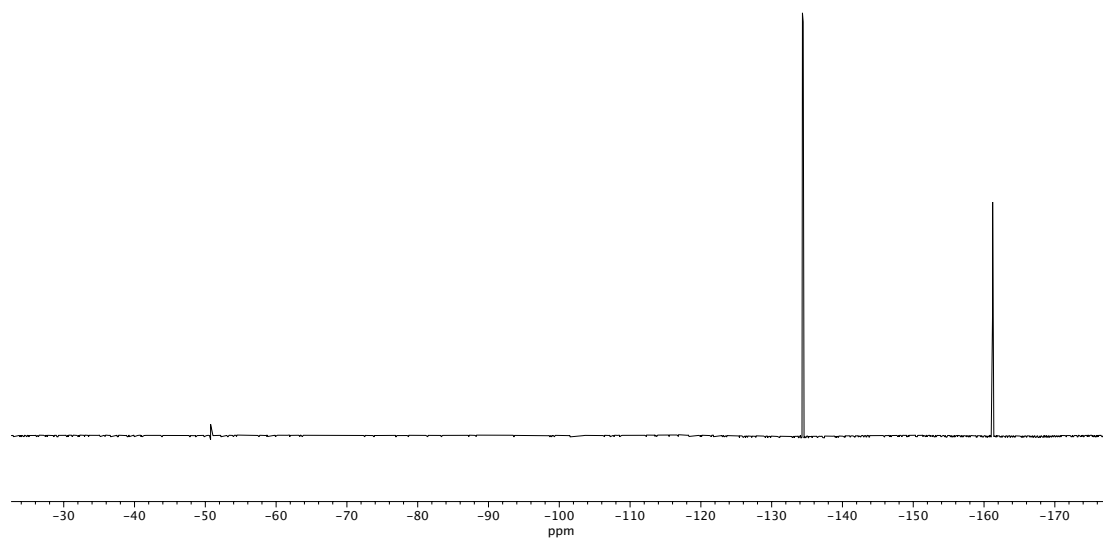
**Figure A1.56** <sup>1</sup>H NMR (400 MHz, CDCl<sub>3</sub>) of compound **161i**.



**Figure A1.57** Infrared spectrum (Thin Film, NaCl) of compound **161i**.

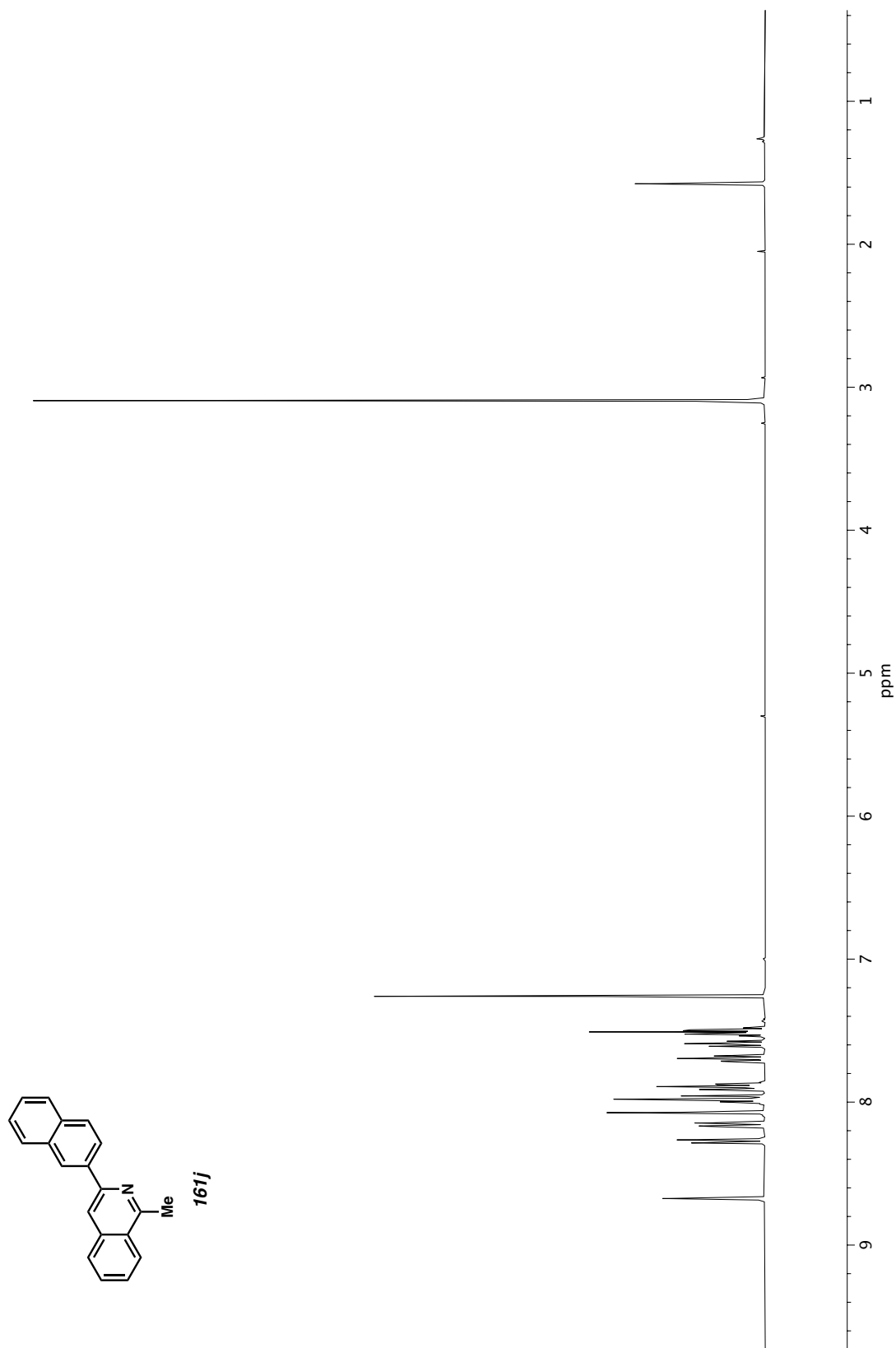


**Figure A1.58** <sup>13</sup>C NMR (100 MHz, CDCl<sub>3</sub>) of compound **161i**.

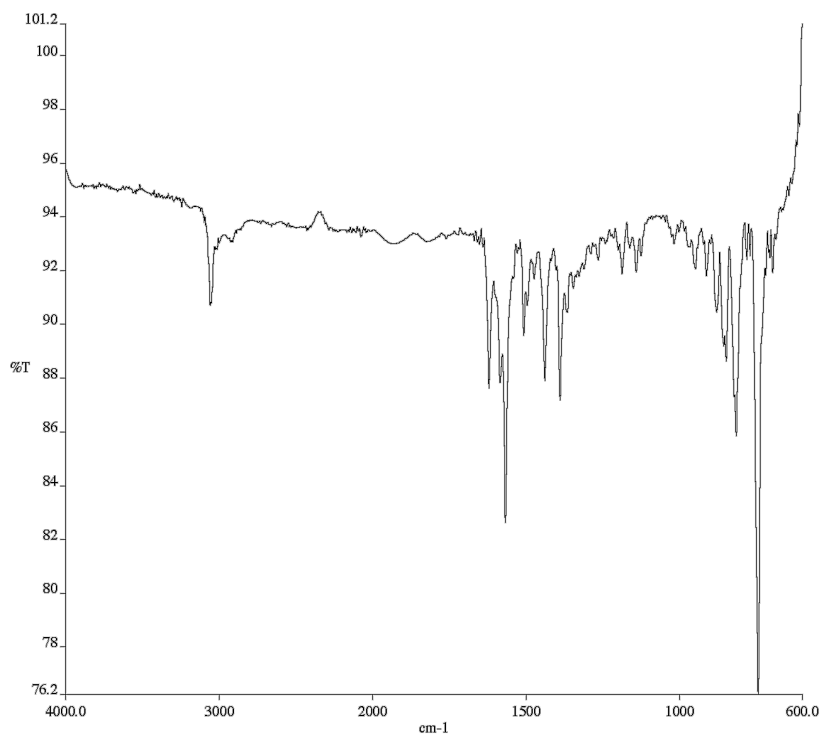


**Figure A1.59**  $^{19}\text{F}$  NMR (282 MHz,  $\text{CDCl}_3$ ) of compound **161i**.

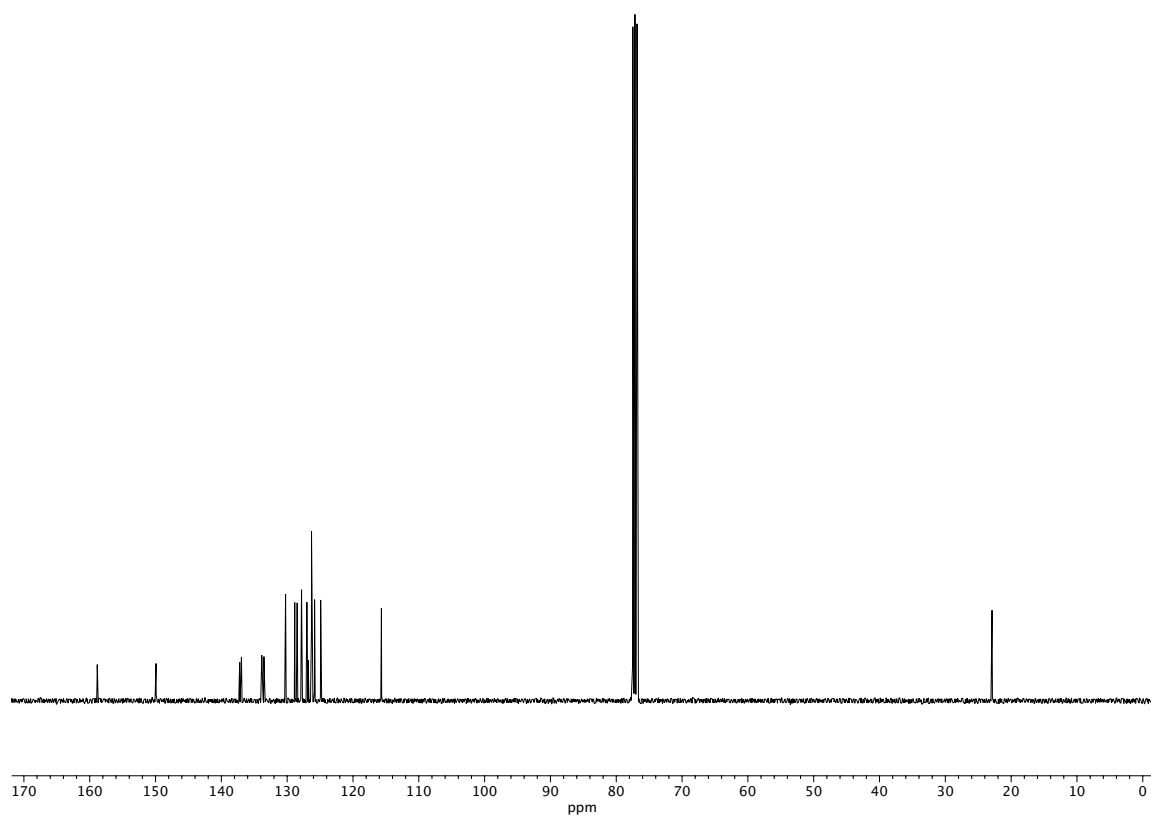




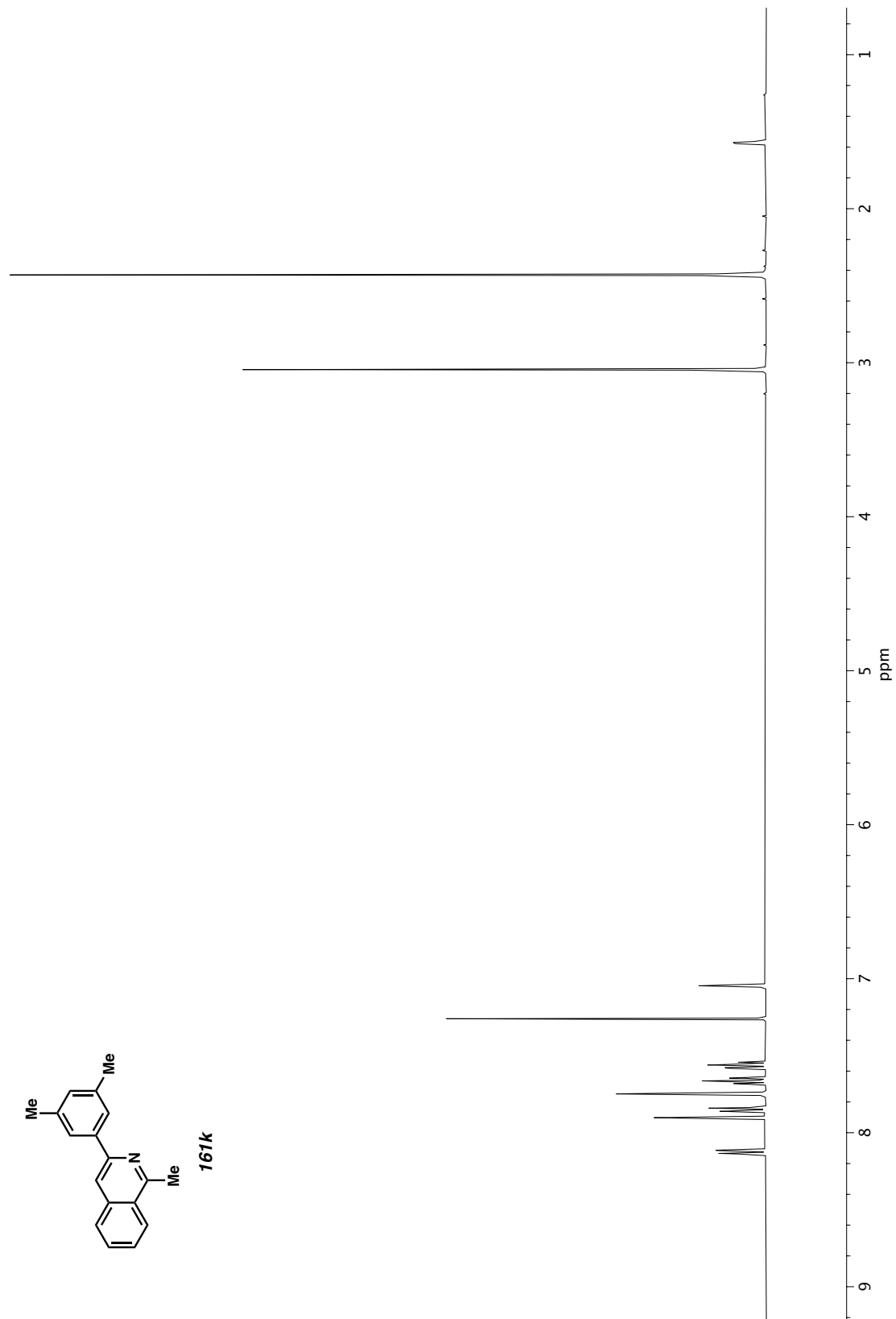
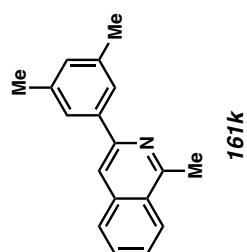
**Figure A1.60** <sup>1</sup>H NMR (400 MHz, CDCl<sub>3</sub>) of compound **161j**.



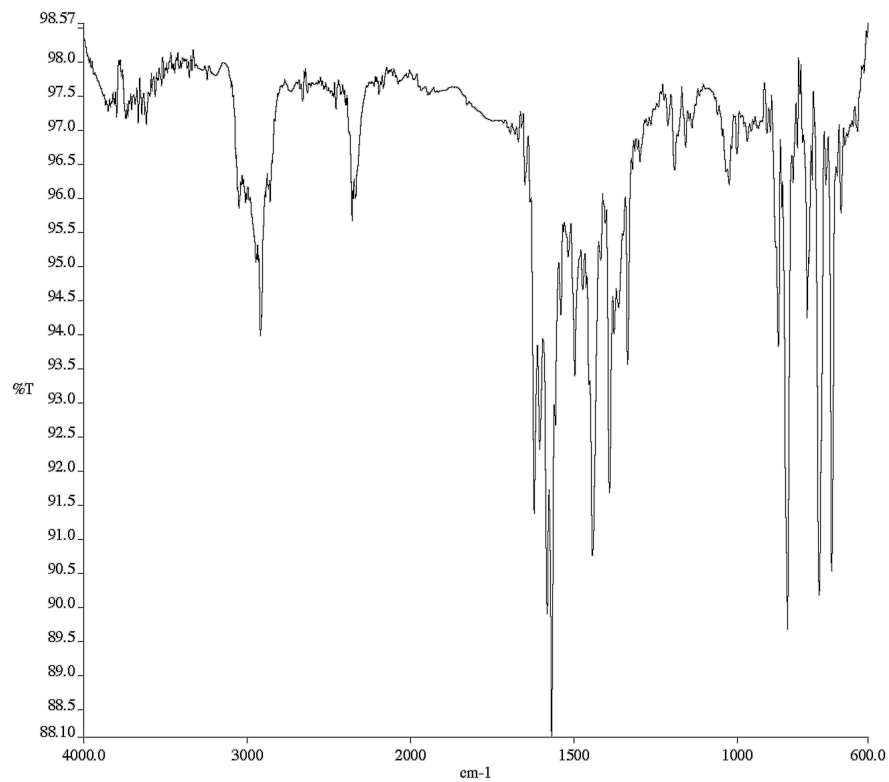
**Figure A1.61** Infrared spectrum (Thin Film, NaCl) of compound **161j**.



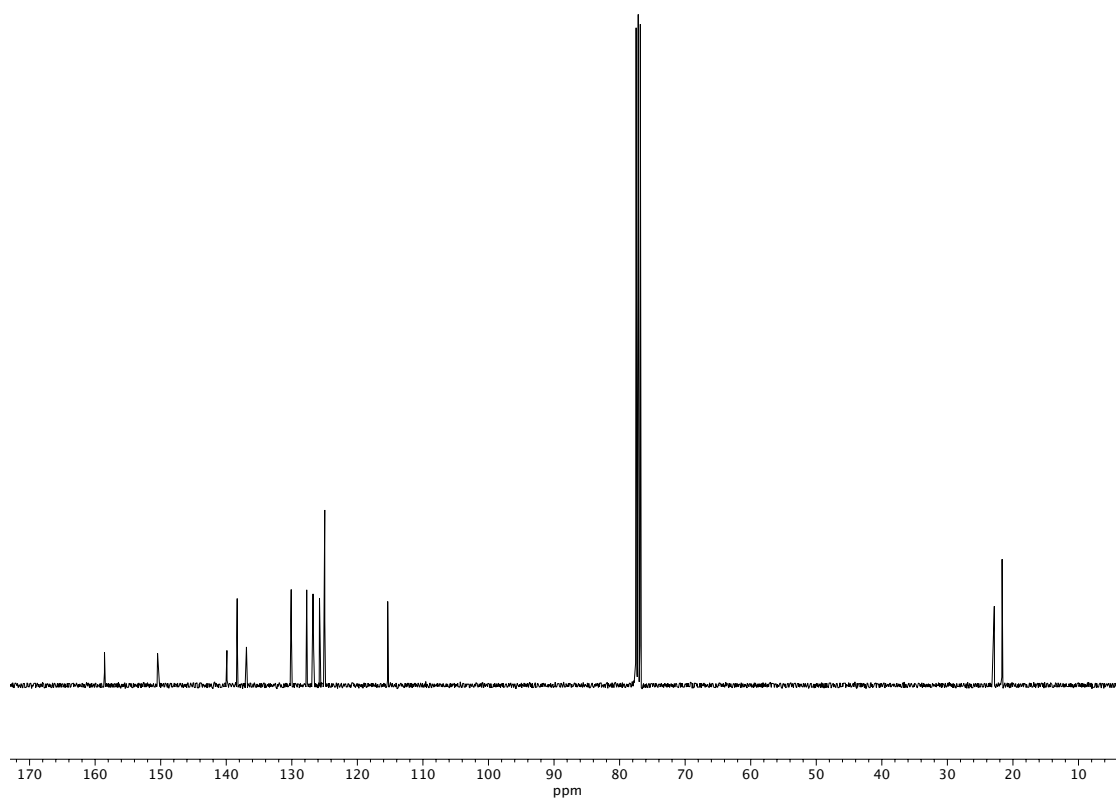
**Figure A1.62** <sup>13</sup>C NMR (100 MHz, CDCl<sub>3</sub>) of compound **161j**.



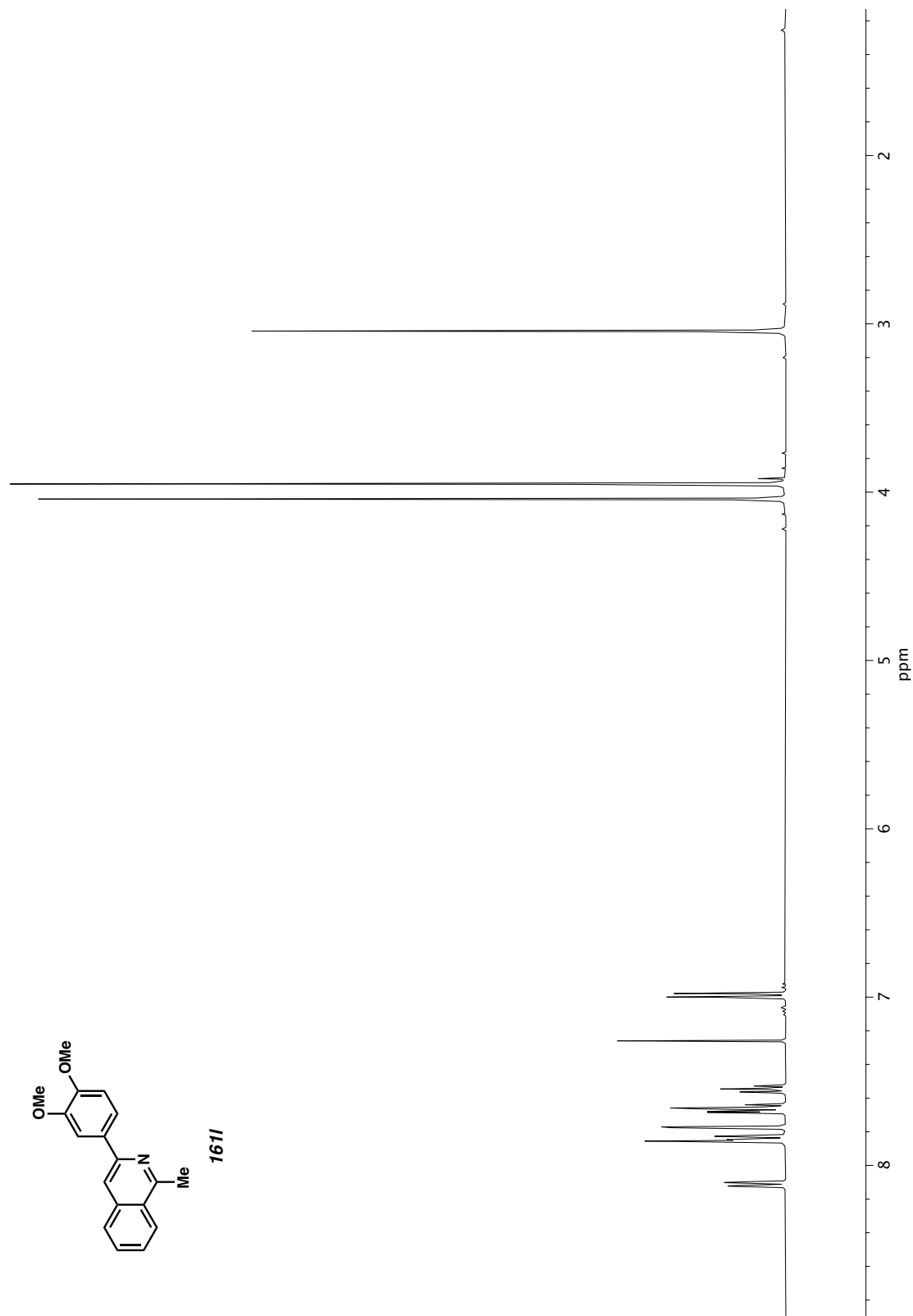
**Figure A1.63**  $^1\text{H}$  NMR (400 MHz,  $\text{CDCl}_3$ ) of compound **161k**.



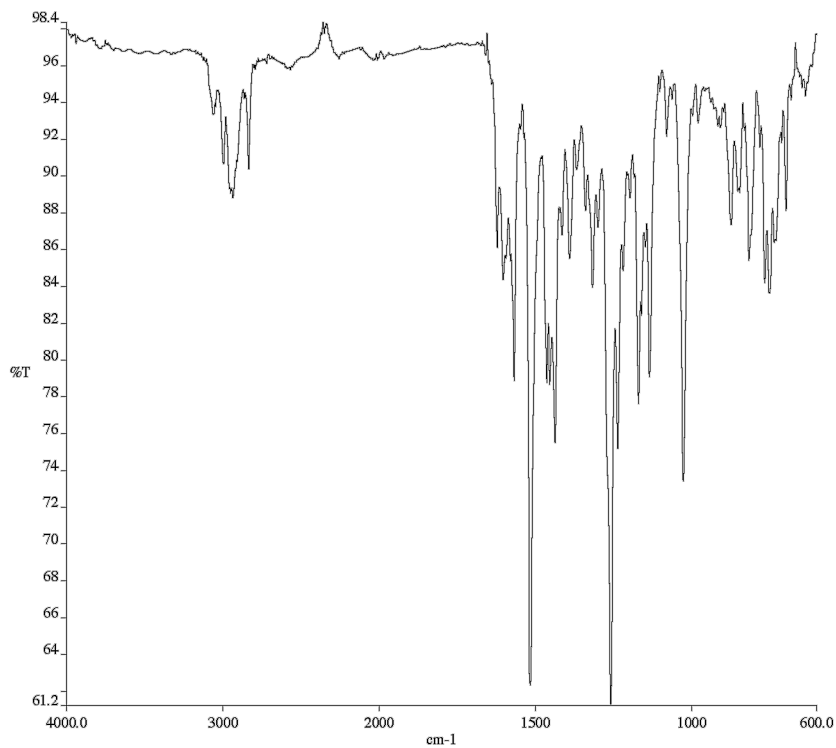
**Figure A1.64** Infrared spectrum (Thin Film, NaCl) of compound **161k**.



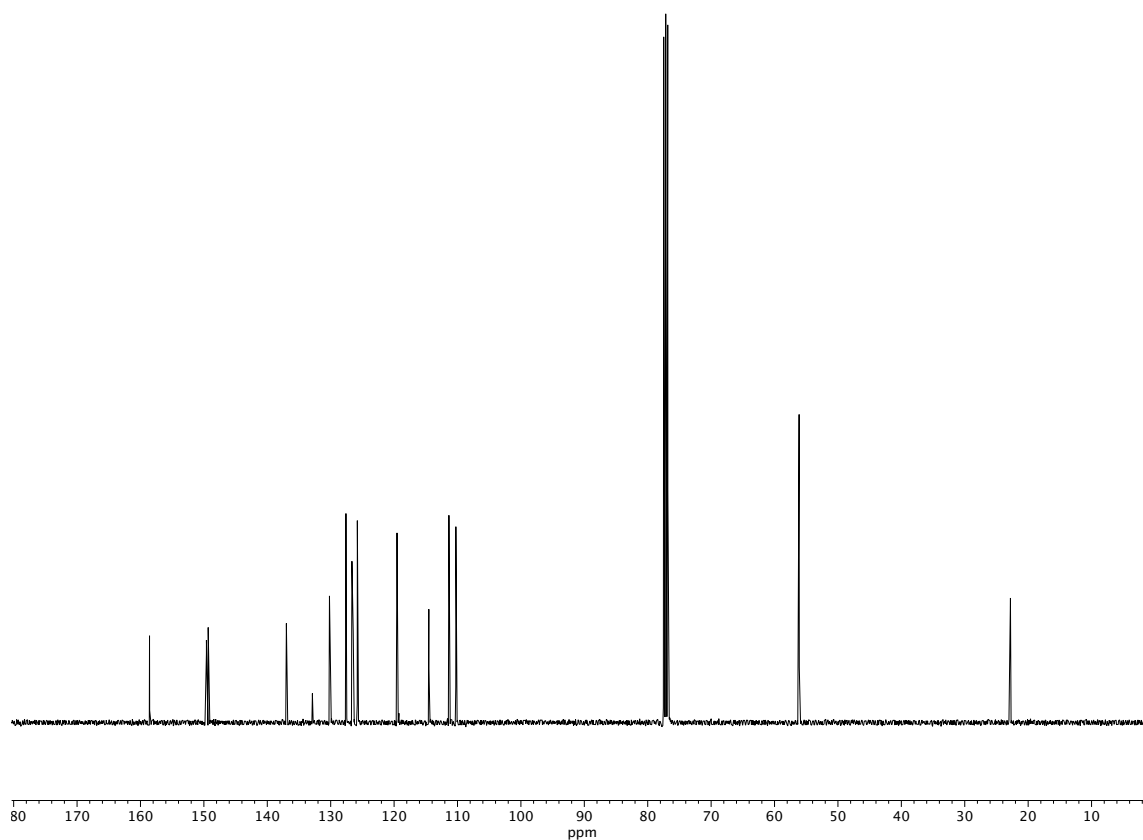
**Figure A1.65** <sup>13</sup>C NMR (100 MHz, CDCl<sub>3</sub>) of compound **161k**.



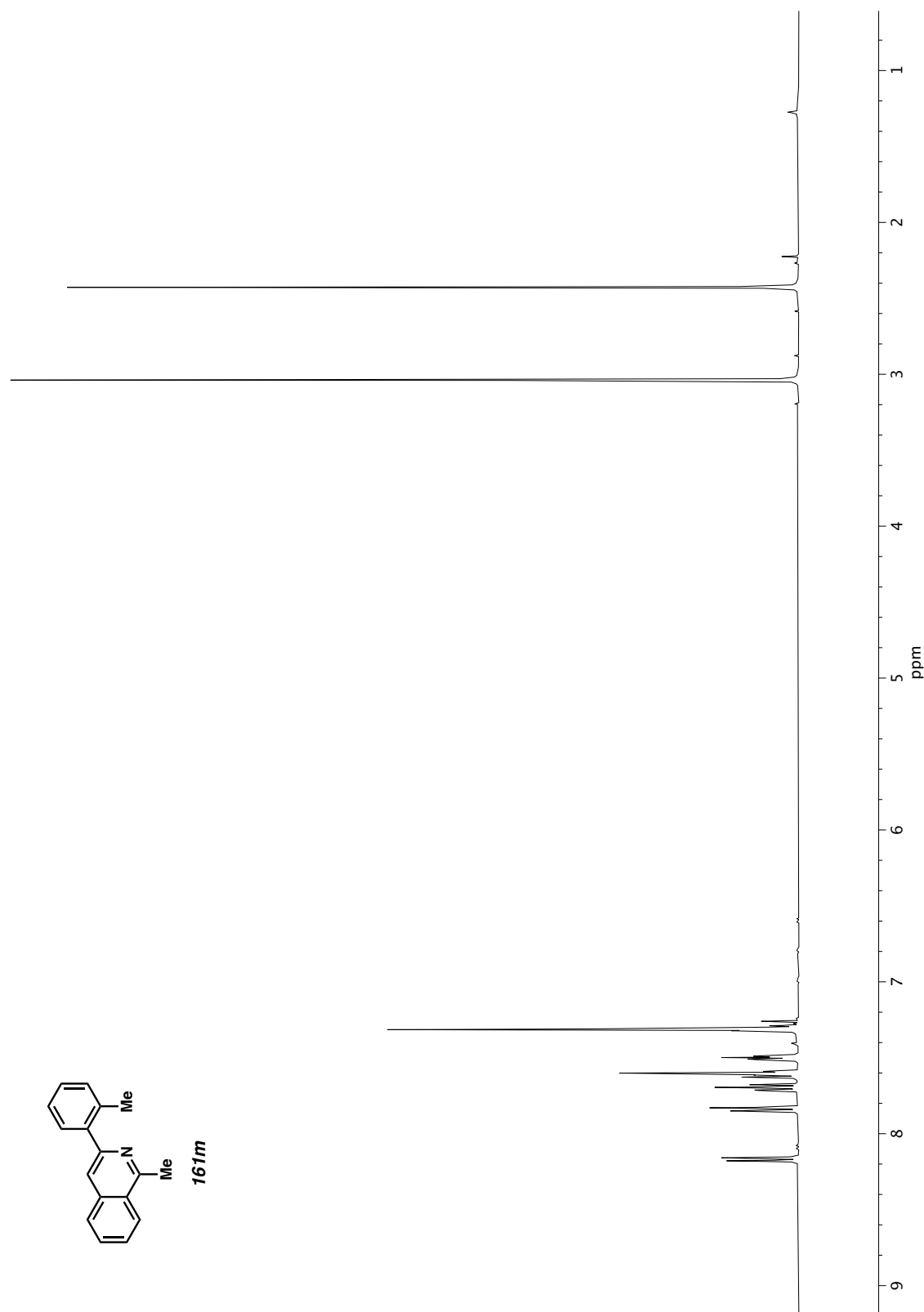
**Figure A1.66**  $^1\text{H}$  NMR (400 MHz,  $\text{CDCl}_3$ ) of compound **161I**.



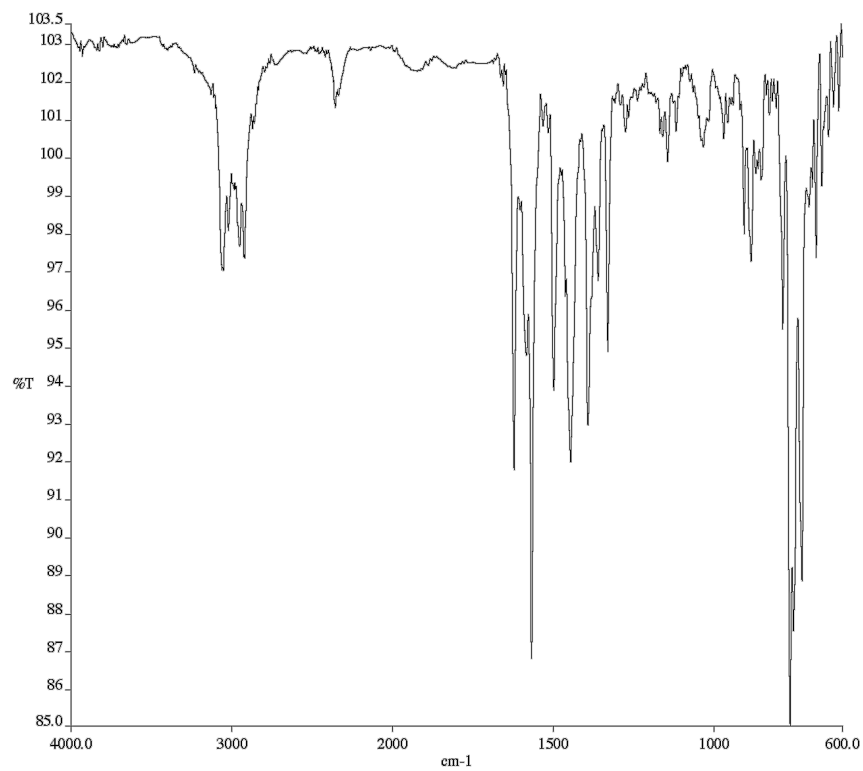
**Figure A1.67** Infrared spectrum (Thin Film, NaCl) of compound **161I**.



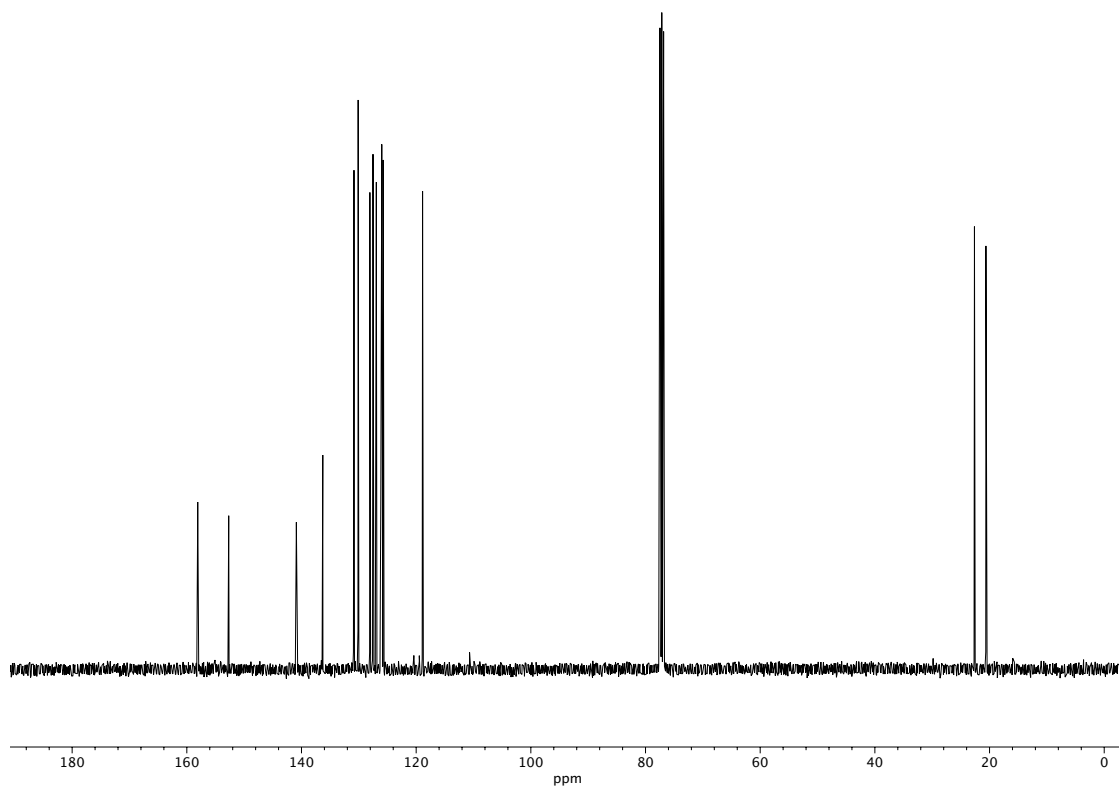
**Figure A1.68** <sup>13</sup>C NMR (100 MHz, CDCl<sub>3</sub>) of compound **161I**.



**Figure A1.69**  $^1\text{H}$  NMR (400 MHz,  $\text{CDCl}_3$ ) of compound **161m**.

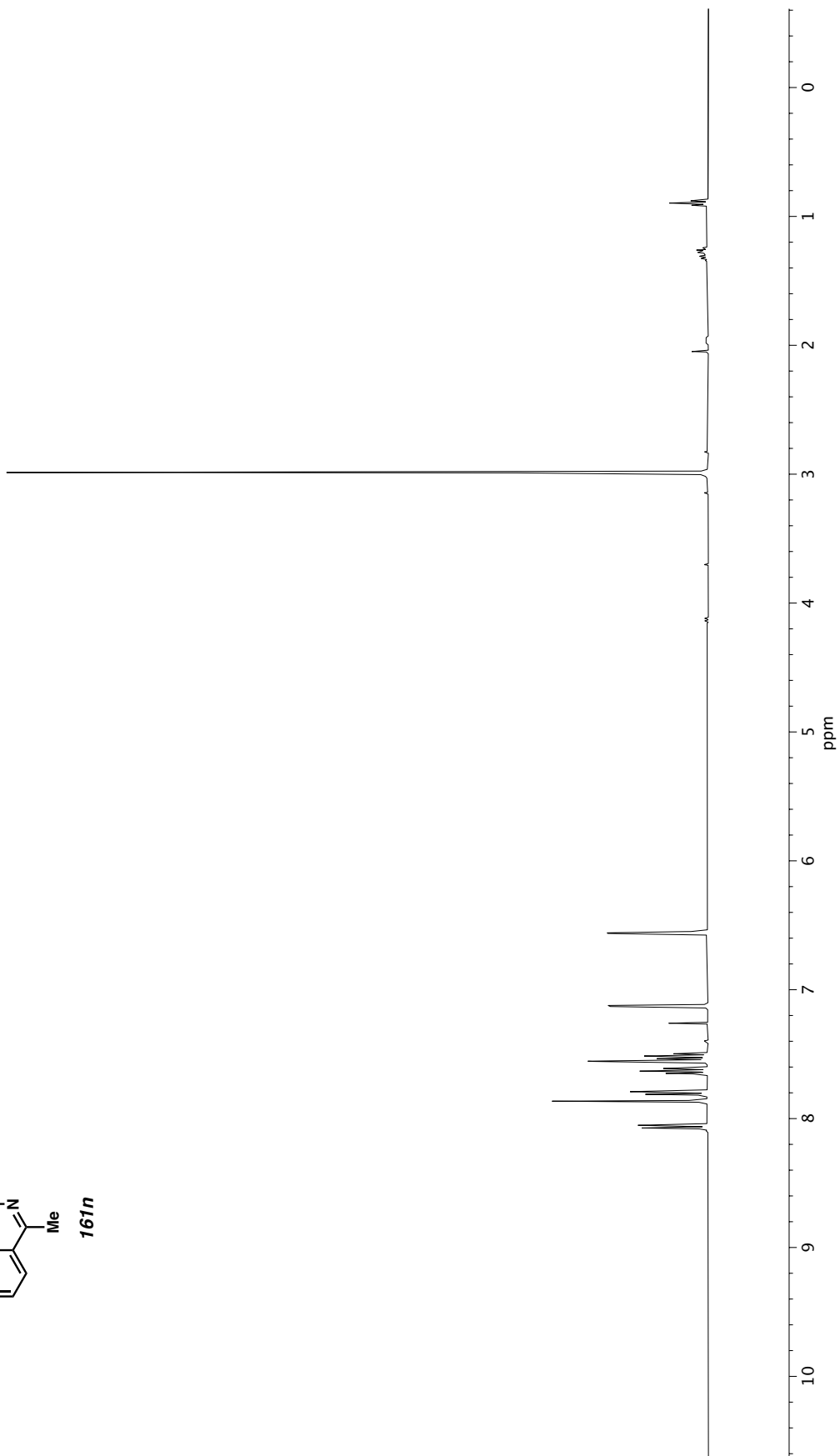
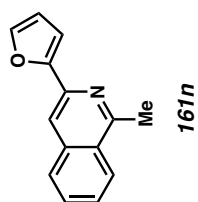


**Figure A1.70** Infrared spectrum (Thin Film, NaCl) of compound **161m**.

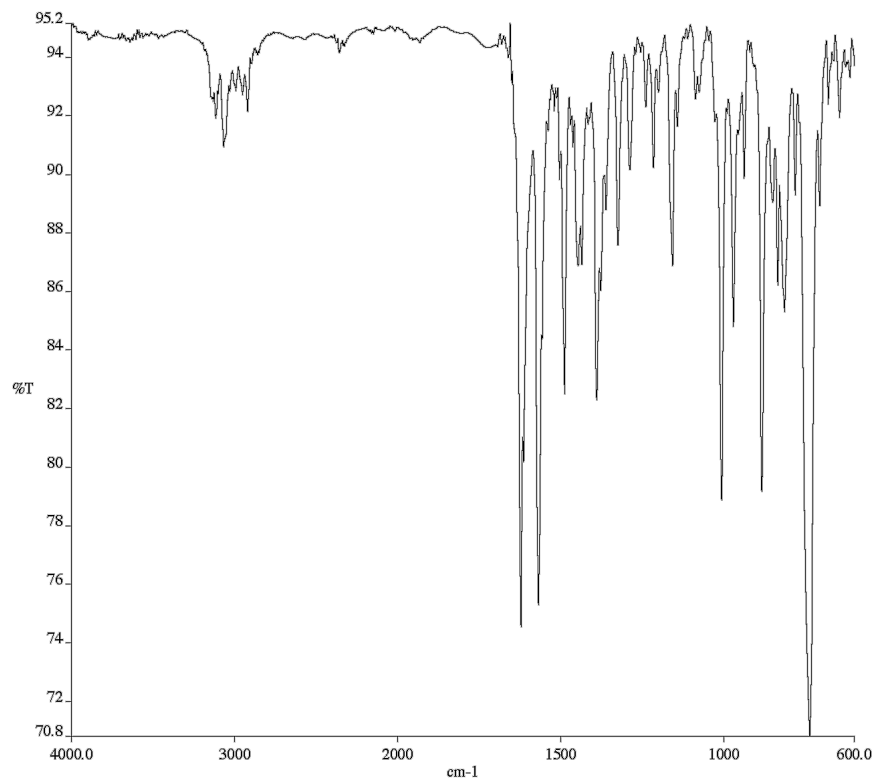


**Figure A1.71** <sup>13</sup>C NMR (100 MHz, CDCl<sub>3</sub>) of compound **161m**.

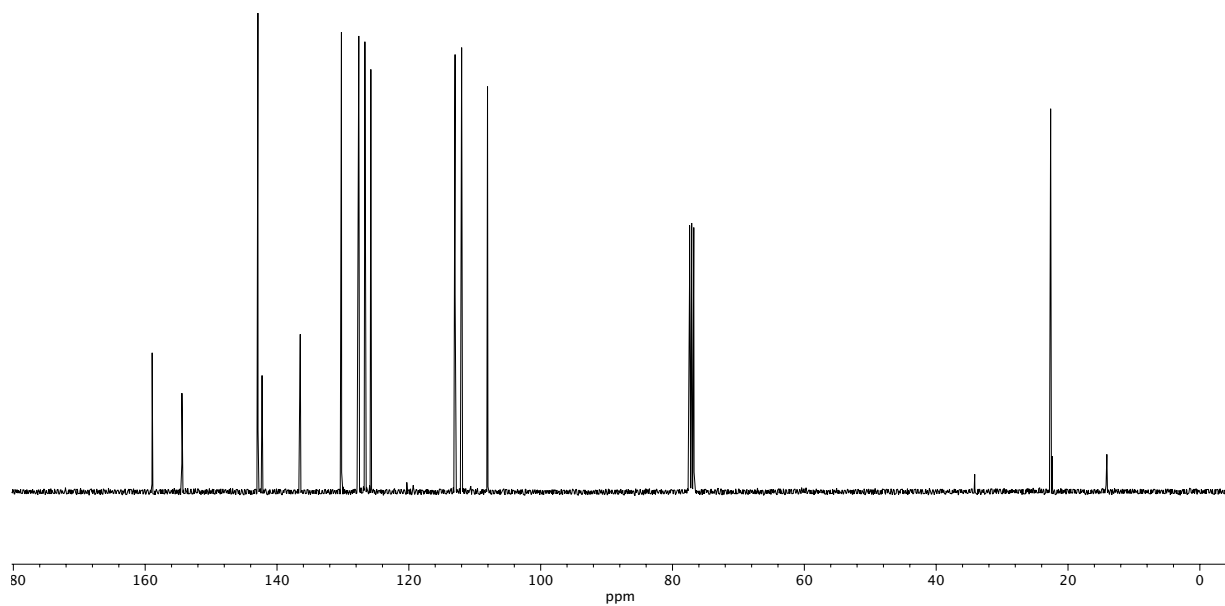




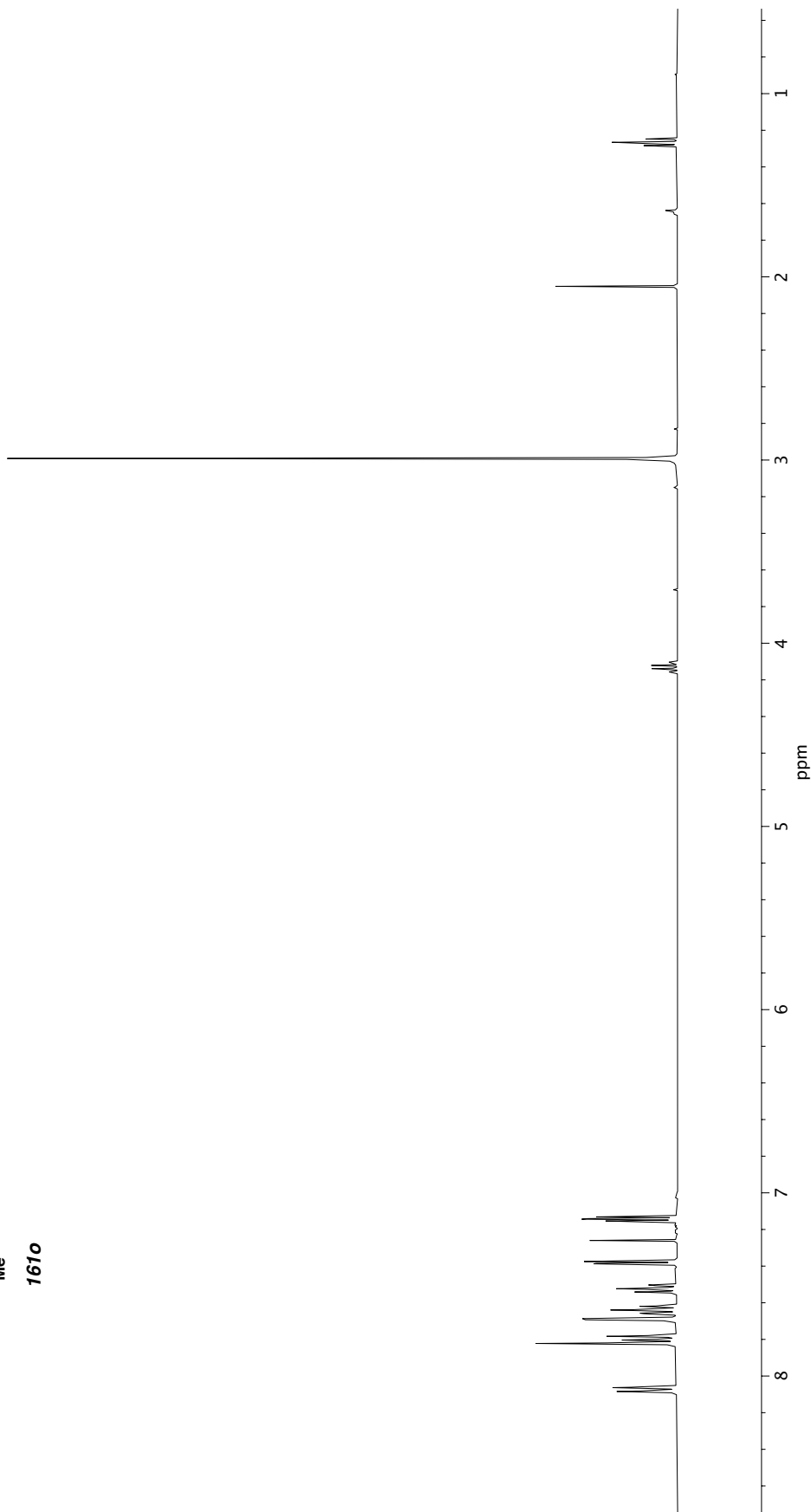
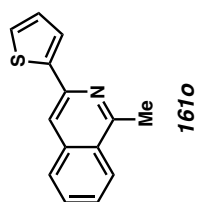
**Figure A1.72** <sup>1</sup>H NMR (400 MHz, CDCl<sub>3</sub>) of compound **161n**.



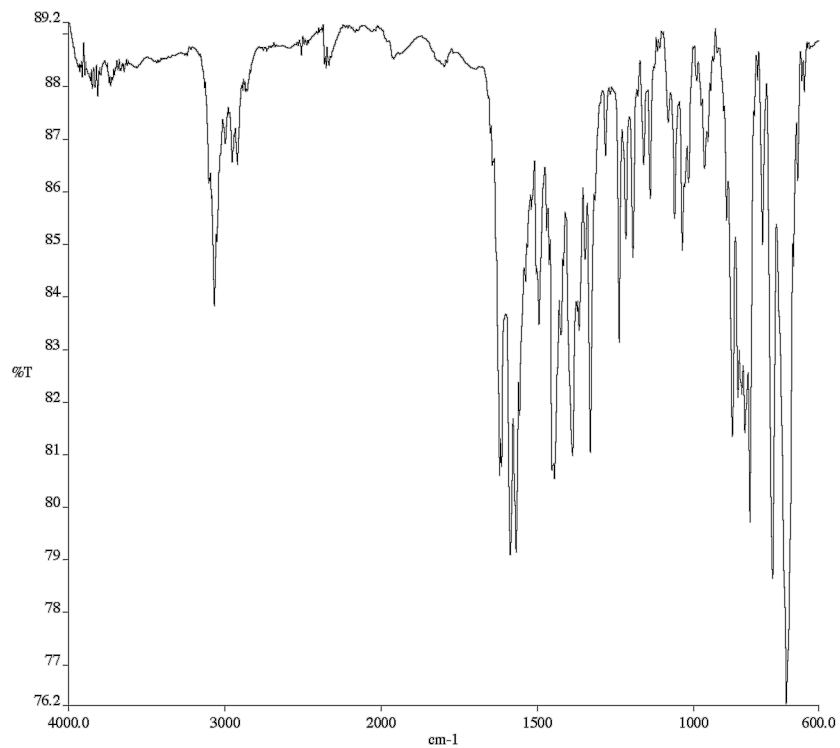
**Figure A1.73** Infrared spectrum (Thin Film, NaCl) of compound **161n**.



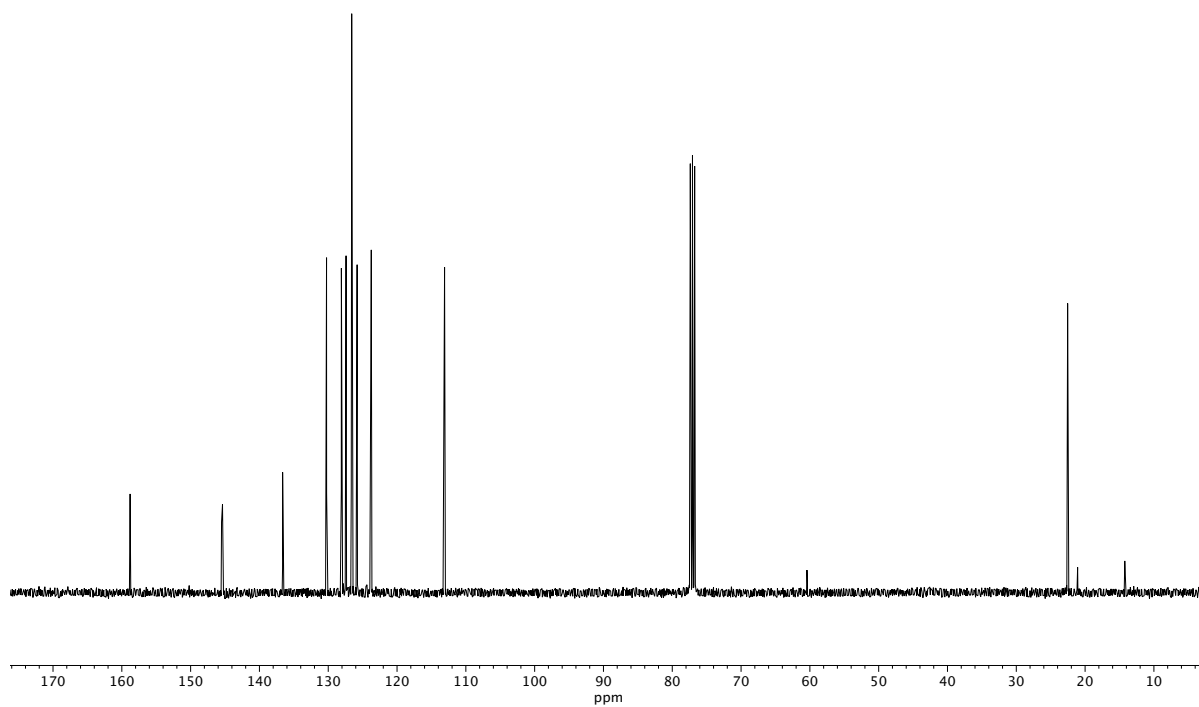
**Figure A1.74** <sup>13</sup>C NMR (100 MHz, CDCl<sub>3</sub>) of compound **161n**.



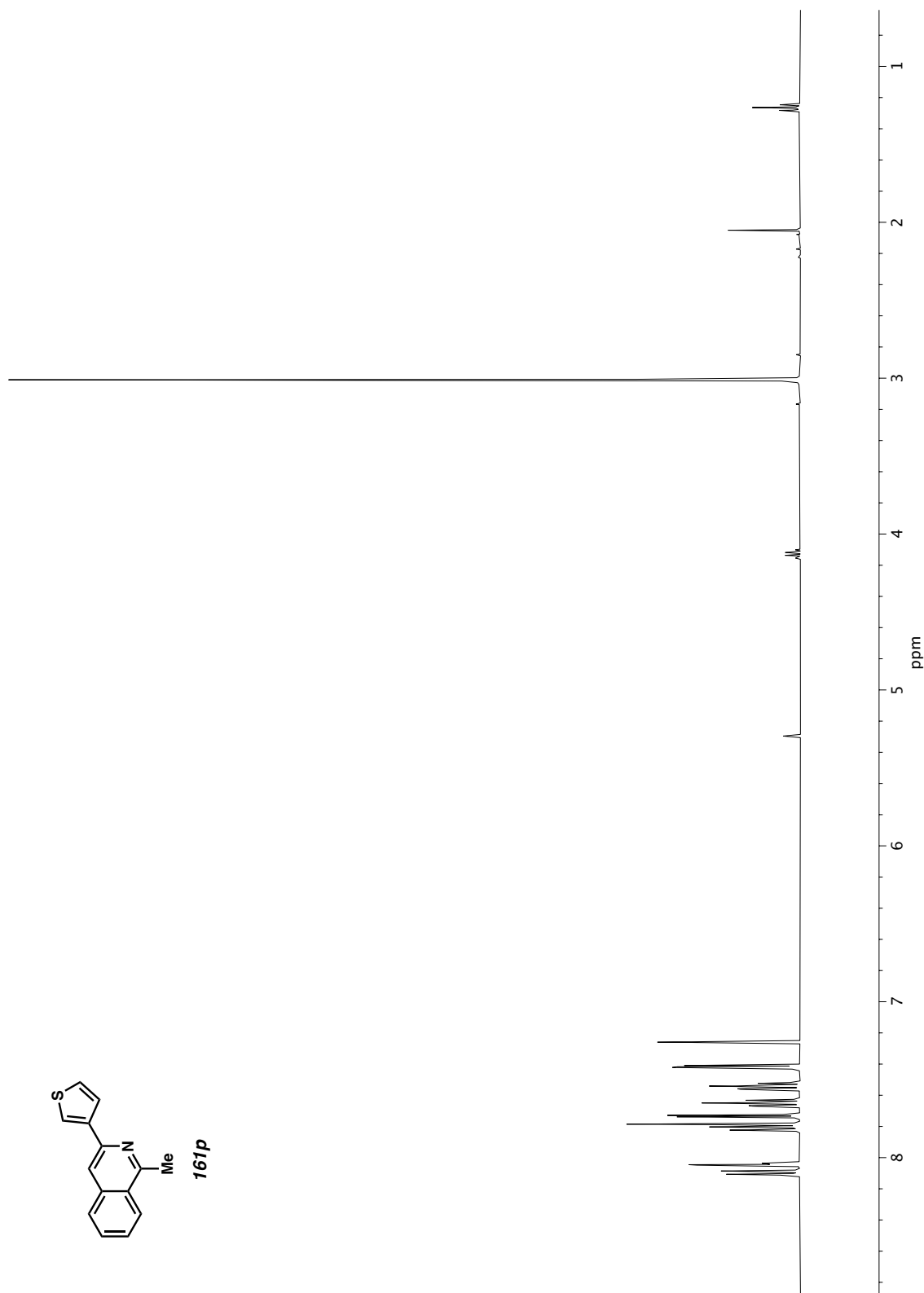
**Figure A1.75**  $^1\text{H}$  NMR (400 MHz,  $\text{CDCl}_3$ ) of compound **1610**.



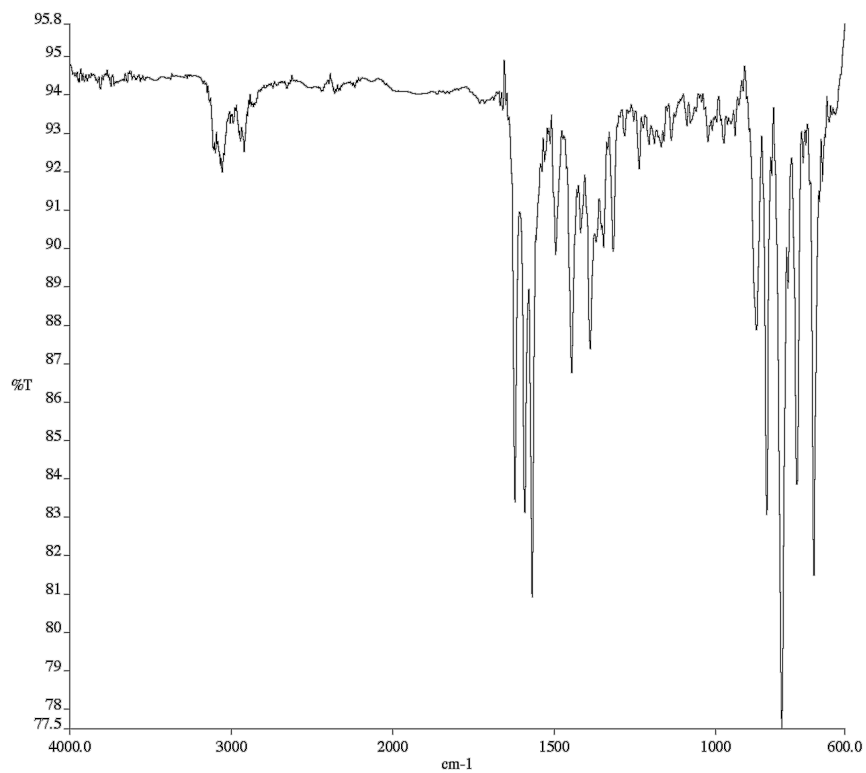
**Figure A1.76** Infrared spectrum (Thin Film, NaCl) of compound **161o**.



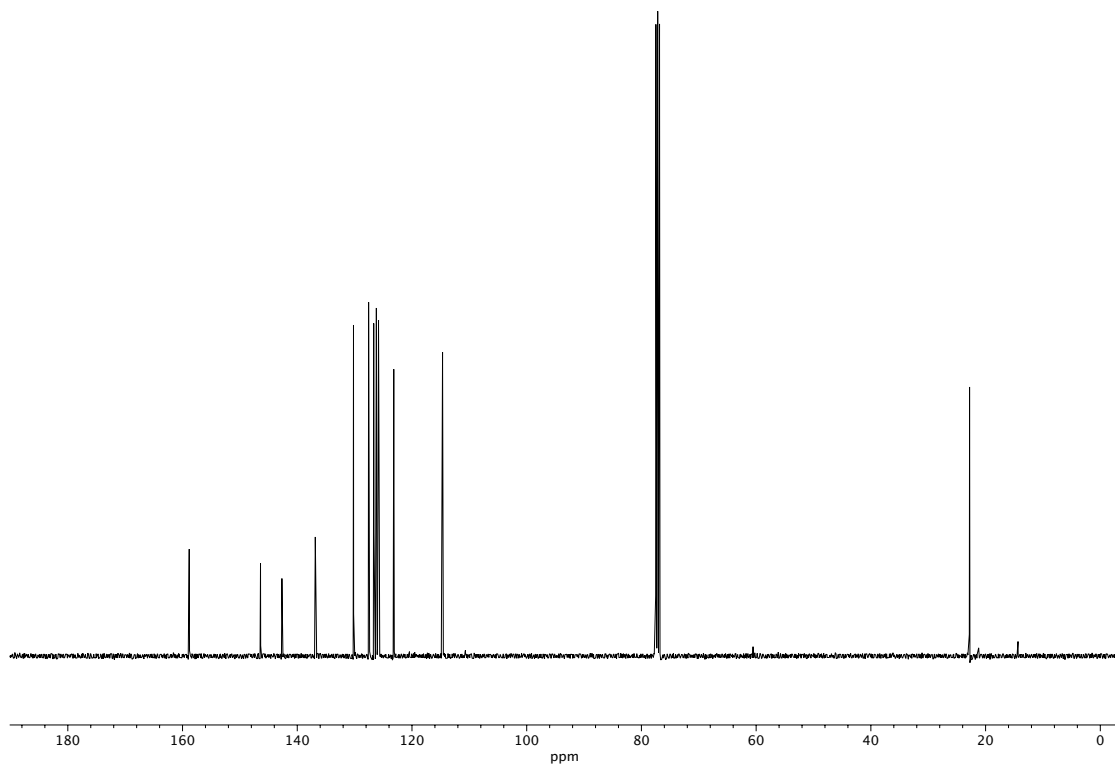
**Figure A1.77** <sup>13</sup>C NMR (100 MHz, CDCl<sub>3</sub>) of compound **161o**.



**Figure A1.78** <sup>1</sup>H NMR (400 MHz, CDCl<sub>3</sub>) of compound **161p**.

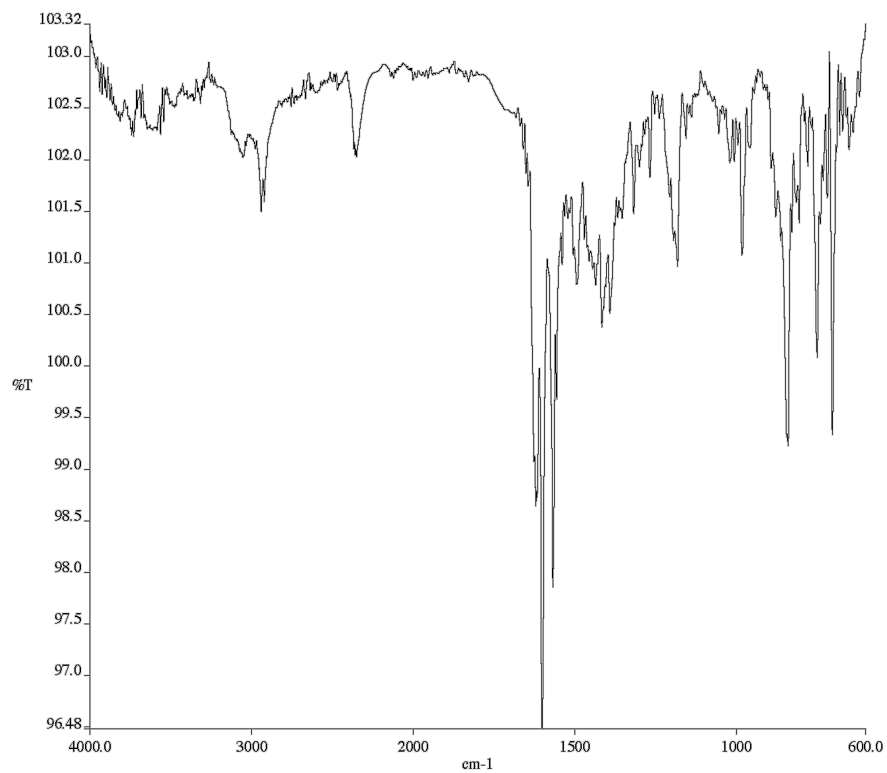


**Figure A1.79** Infrared spectrum (Thin Film, NaCl) of compound **161p**.

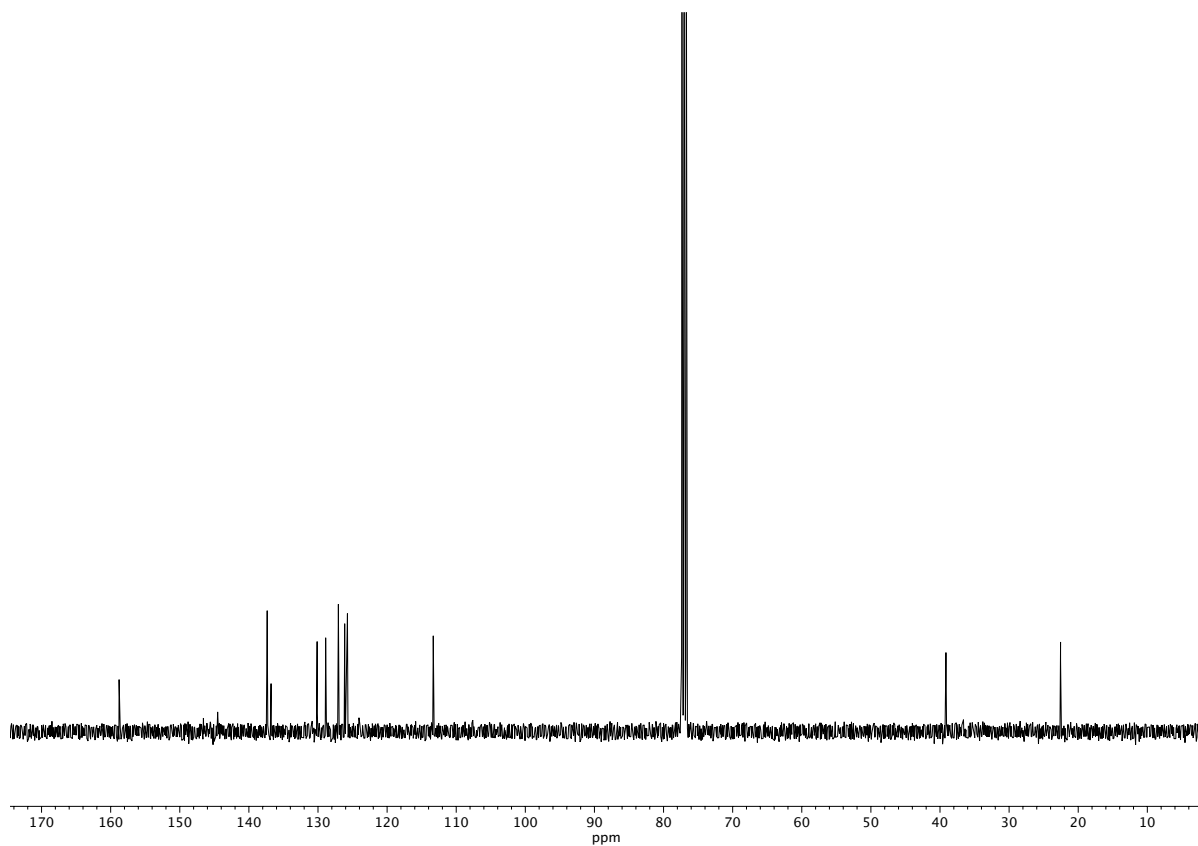


**Figure A1.80** <sup>13</sup>C NMR (100 MHz, CDCl<sub>3</sub>) of compound **161p**.



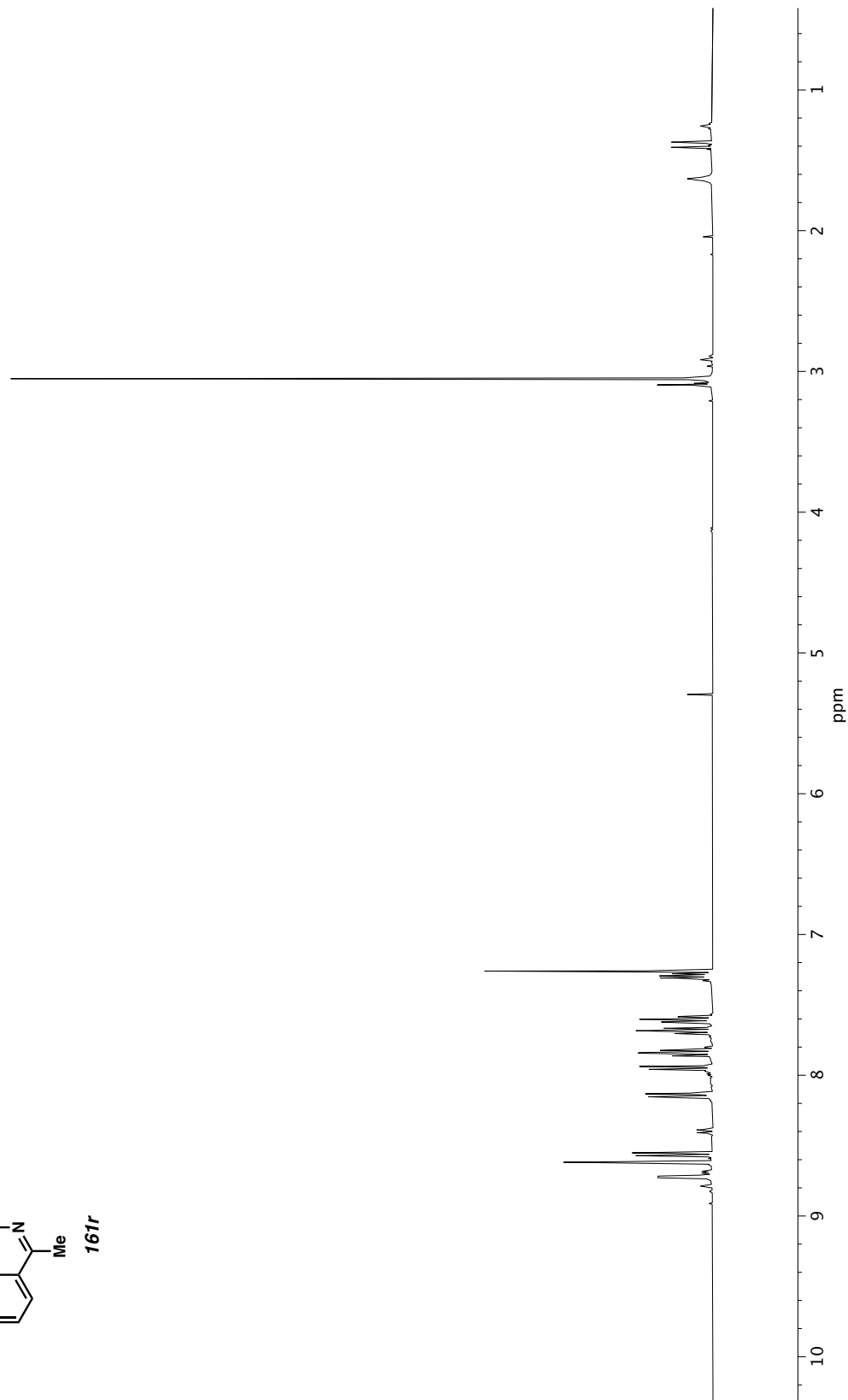
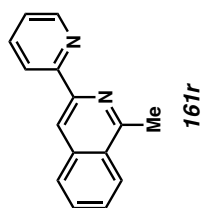


**Figure A1.82** Infrared spectrum (Thin Film, NaCl) of compound **161q**.

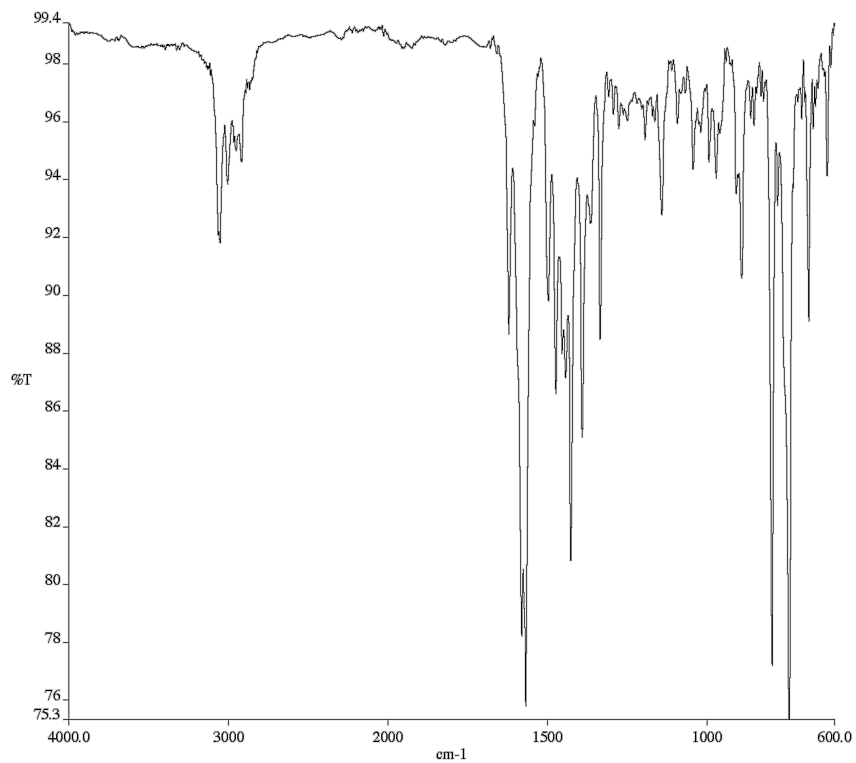


**Figure A1.83** <sup>13</sup>C NMR (100 MHz, CDCl<sub>3</sub>) of compound **161q**.

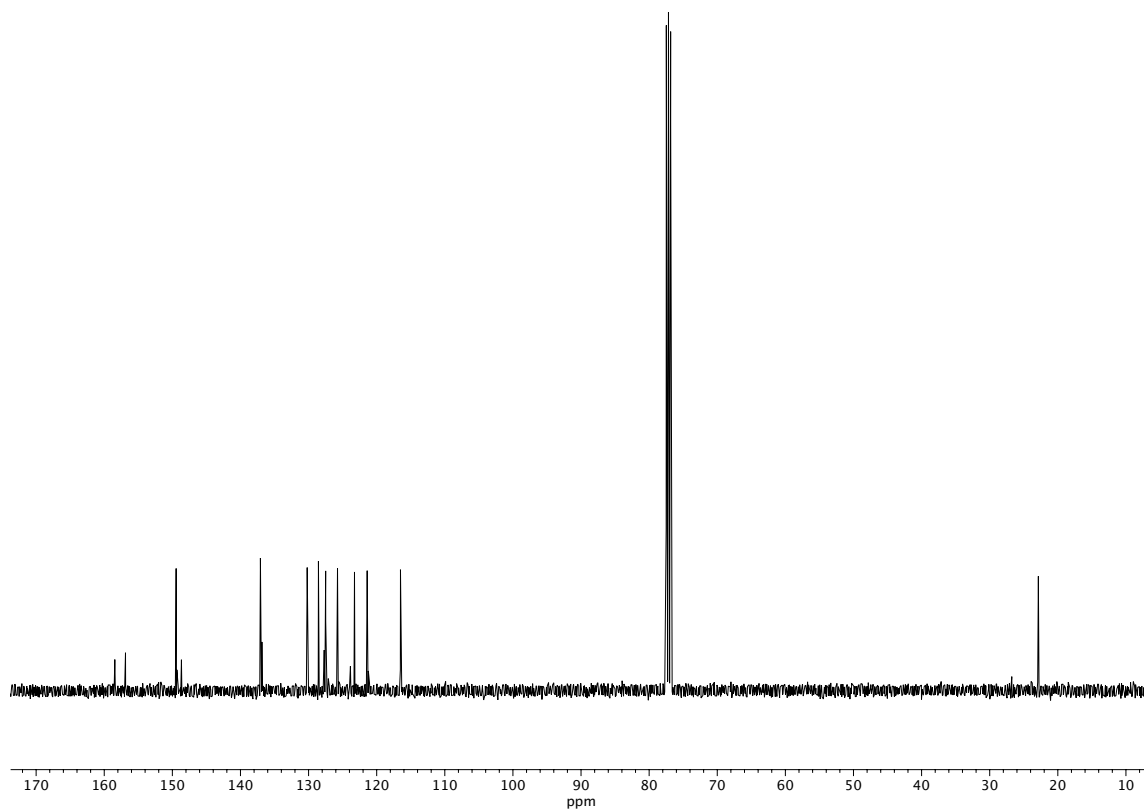




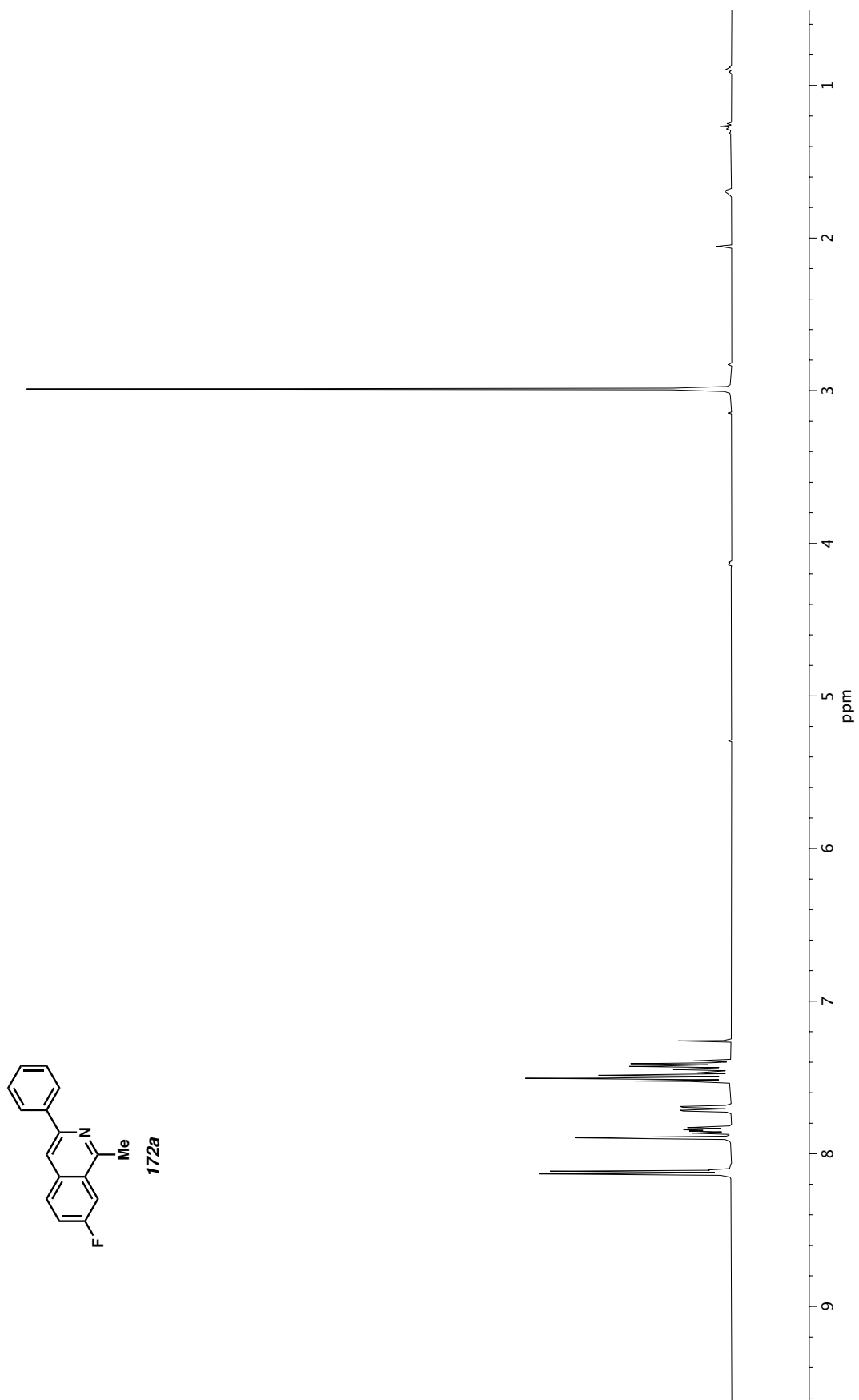
**Figure A1.84**  $^1\text{H}$  NMR (400 MHz,  $\text{CDCl}_3$ ) of compound **161r**.



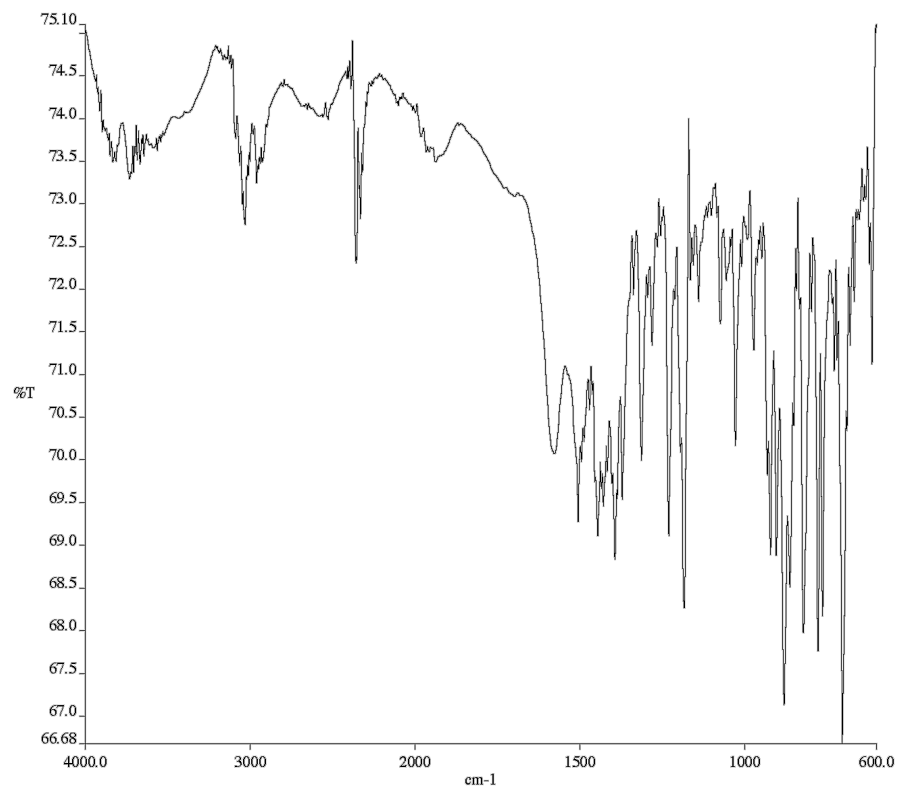
**Figure A1.85** Infrared spectrum (Thin Film, NaCl) of compound **161r**.



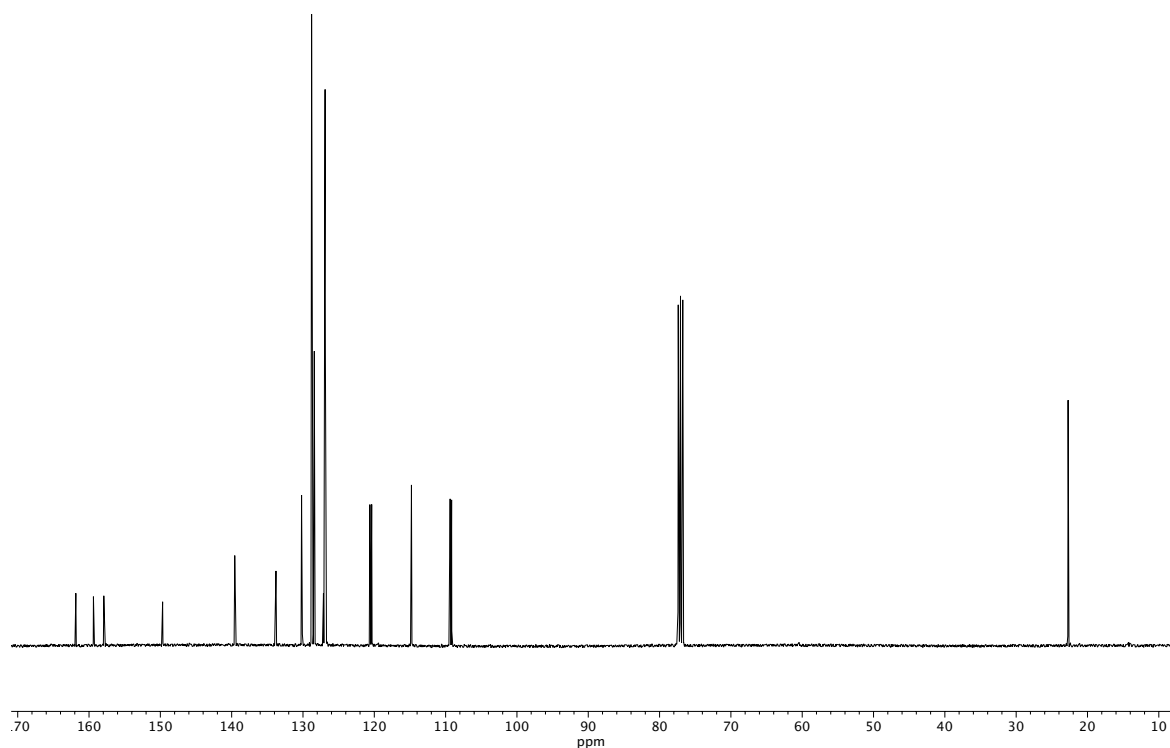
**Figure A1.86** <sup>13</sup>C NMR (100 MHz, CDCl<sub>3</sub>) of compound **161r**.



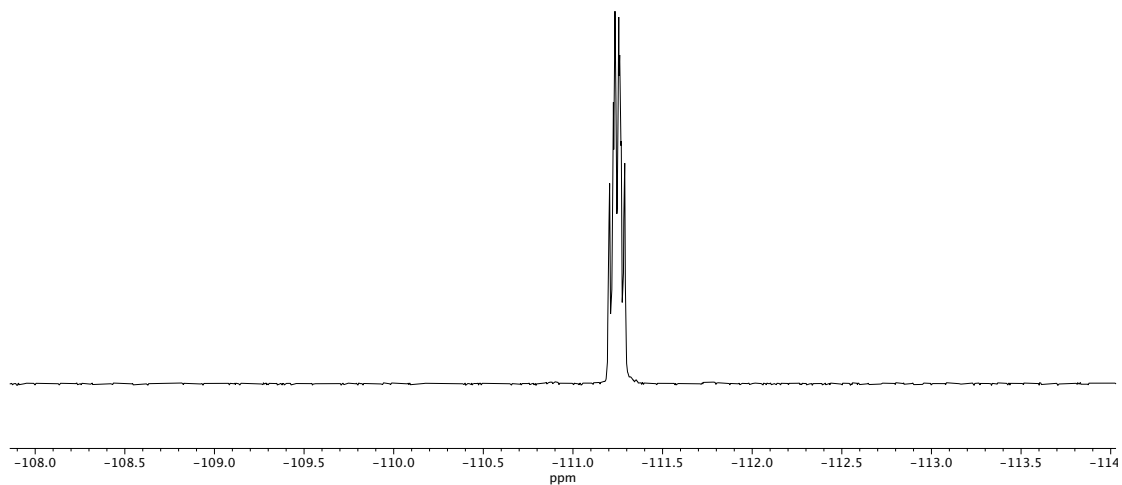
**Figure A1.87**  $^1\text{H}$  NMR (400 MHz,  $\text{CDCl}_3$ ) of compound **172a**.



**Figure A1.88** Infrared spectrum (Thin Film, NaCl) of compound **172a**.

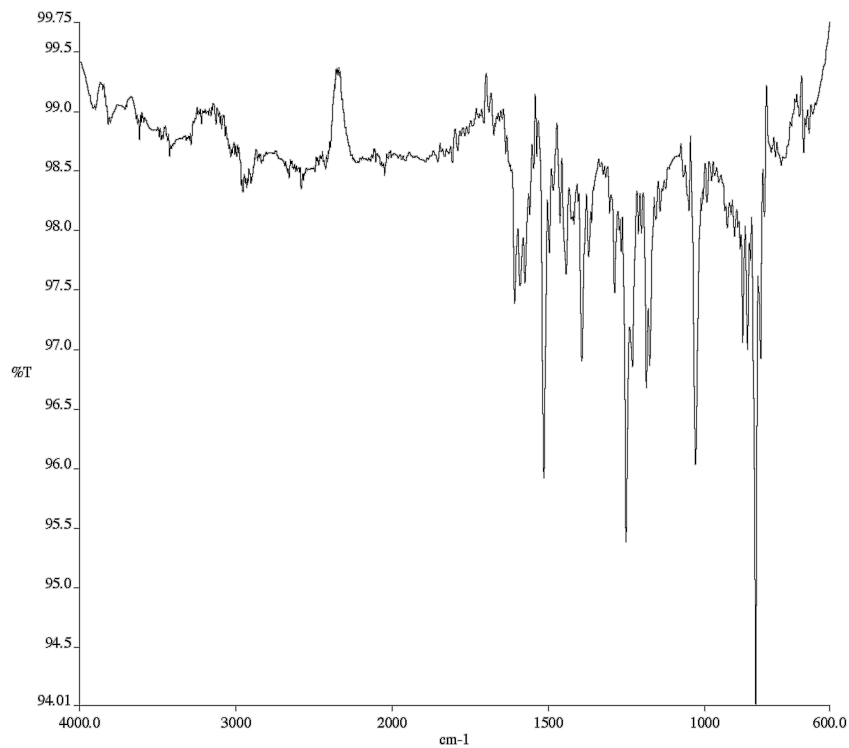


**Figure A1.89** <sup>13</sup>C NMR (100 MHz, CDCl<sub>3</sub>) of compound **172a**.

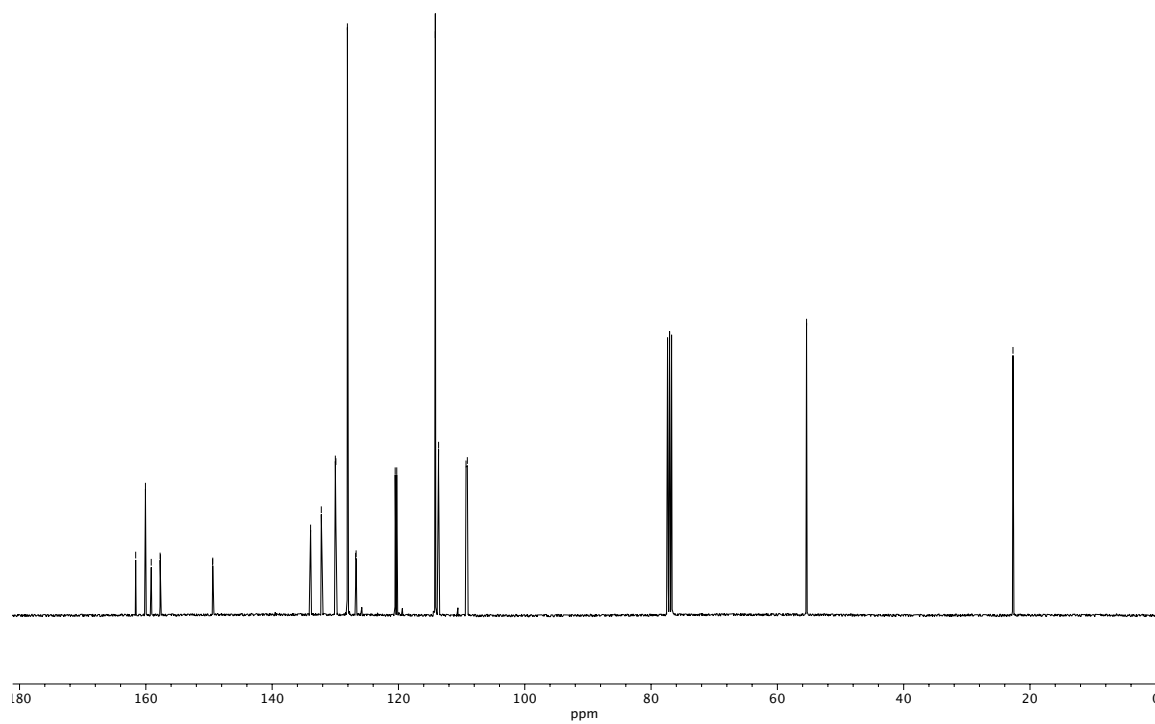


**Figure A1.90**  $^{19}\text{F}$  NMR (282 MHz,  $\text{CDCl}_3$ ) of compound **172a**.

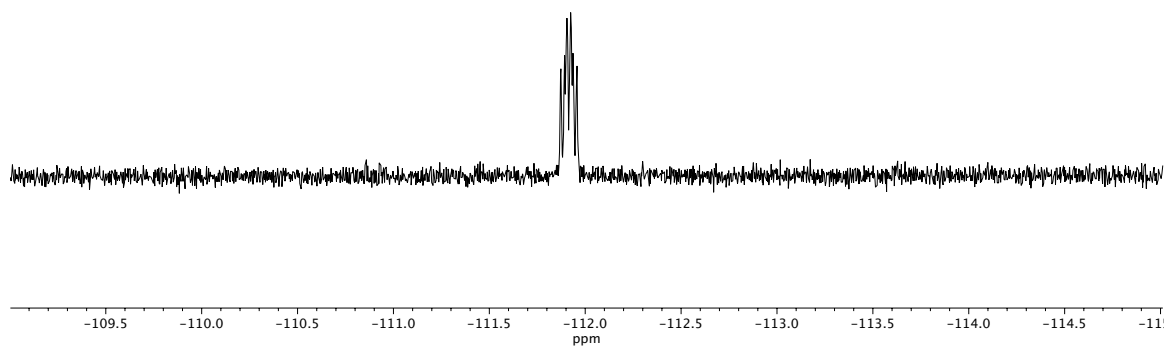




**Figure A1.92** Infrared spectrum (Thin Film, NaCl) of compound **172b**.

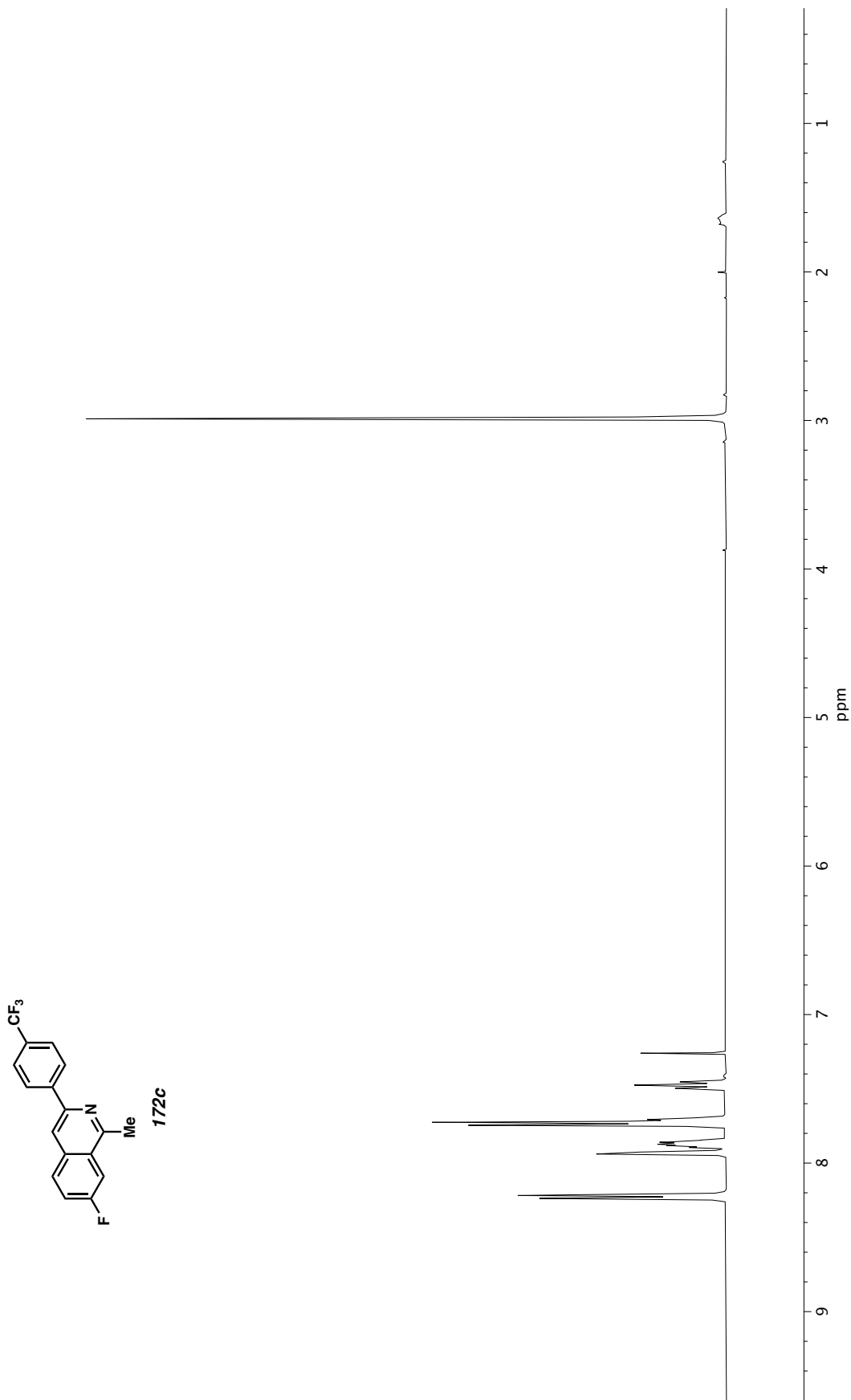


**Figure A1.93** <sup>13</sup>C NMR (100 MHz, CDCl<sub>3</sub>) of compound **172b**.

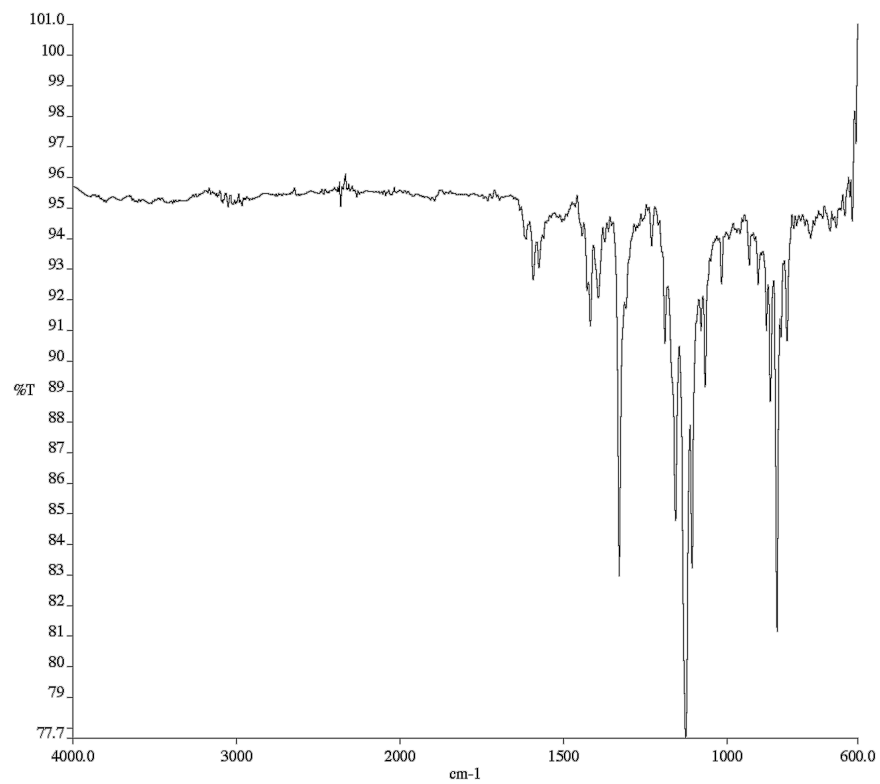


**Figure A1.94**  $^{19}\text{F}$  NMR (282 MHz,  $\text{CDCl}_3$ ) of compound **172b**.

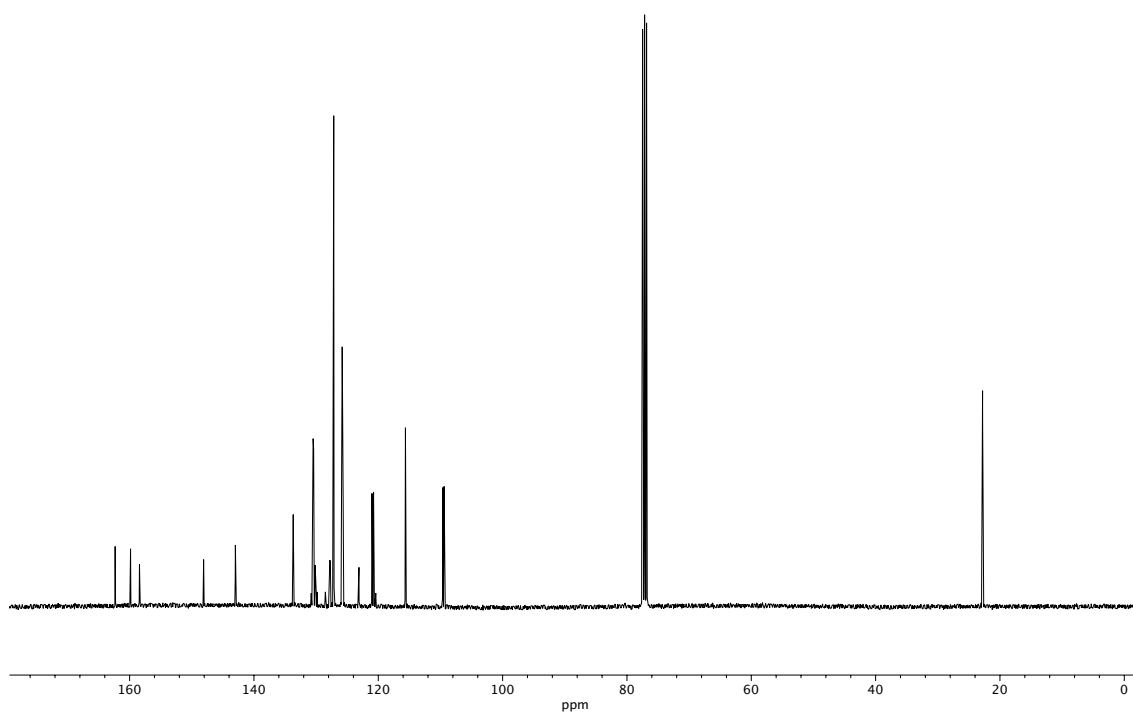




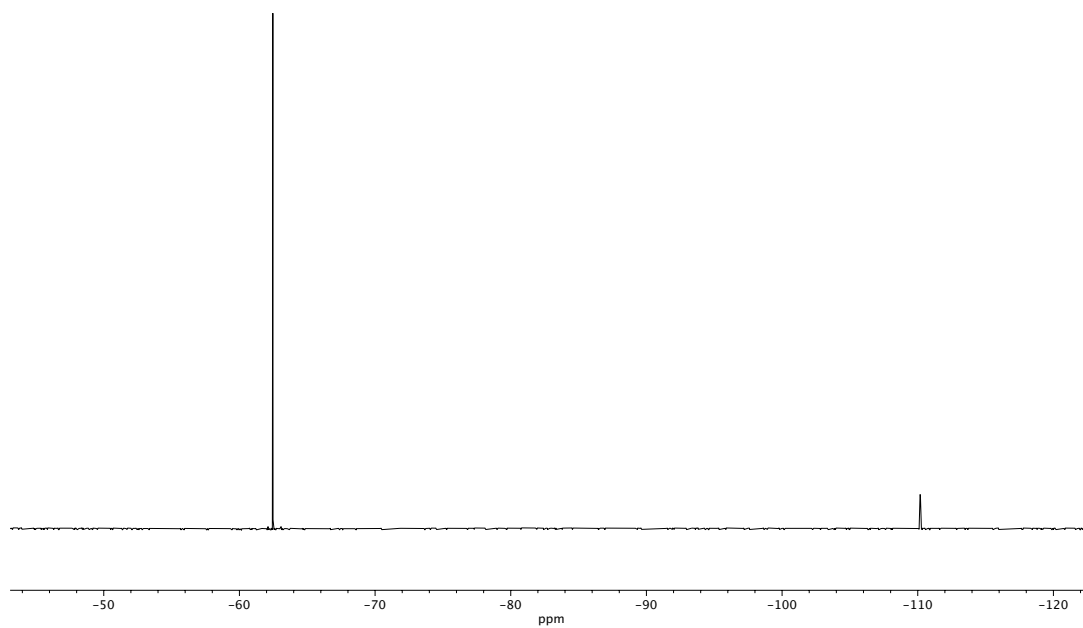
**Figure A1.95**  $^1\text{H NMR}$  (400 MHz,  $\text{CDCl}_3$ ) of compound **172c**.



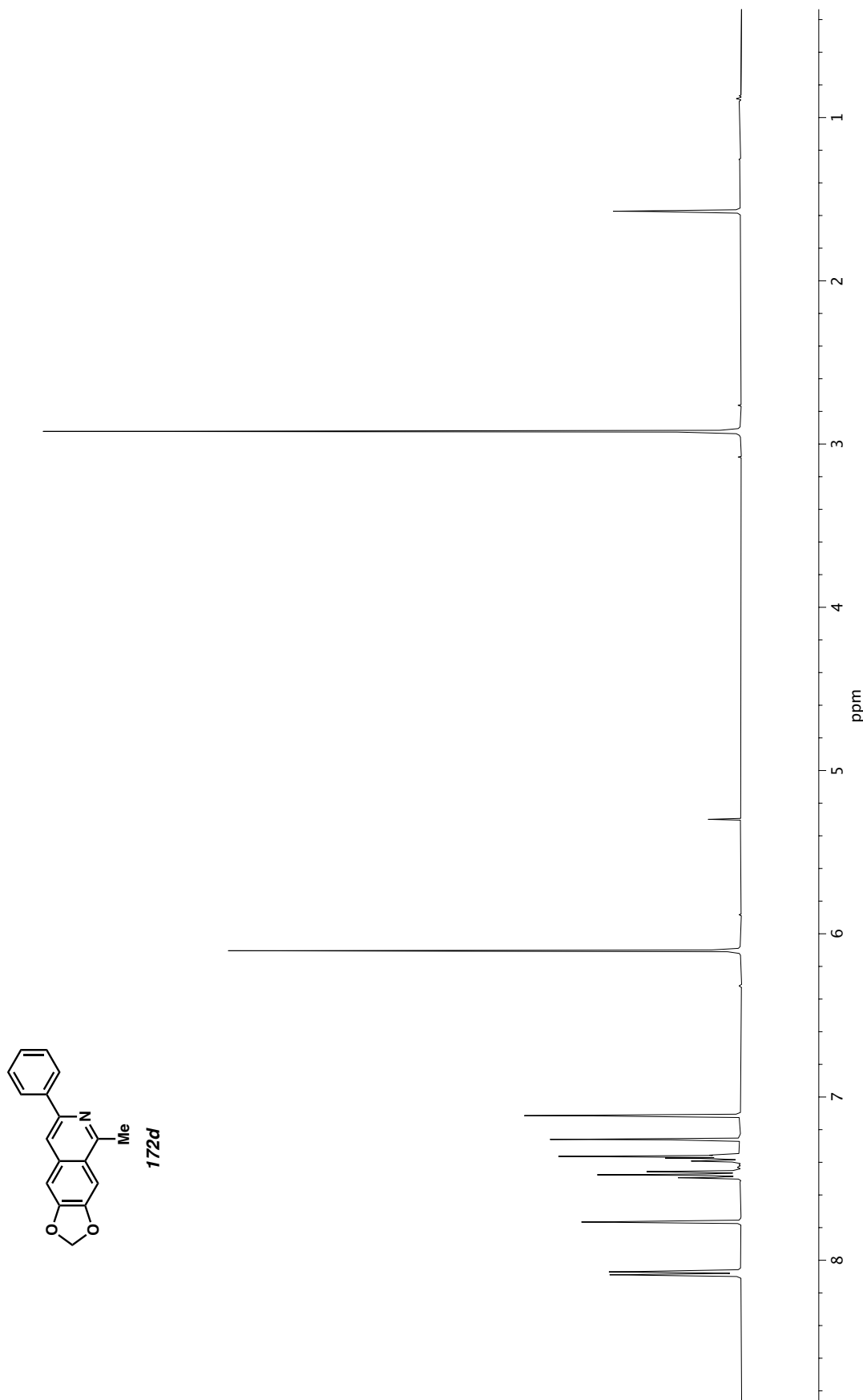
**Figure A1.96** Infrared spectrum (Thin Film, NaCl) of compound **172c**.



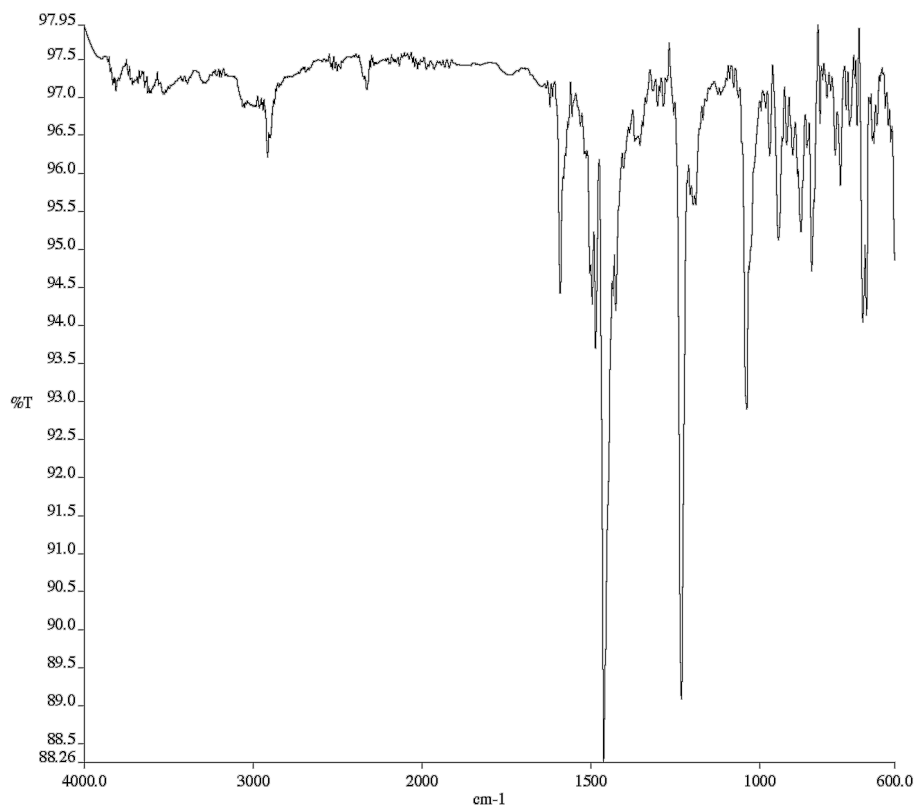
**Figure A1.97** <sup>13</sup>C NMR (100 MHz, CDCl<sub>3</sub>) of compound **172c**.



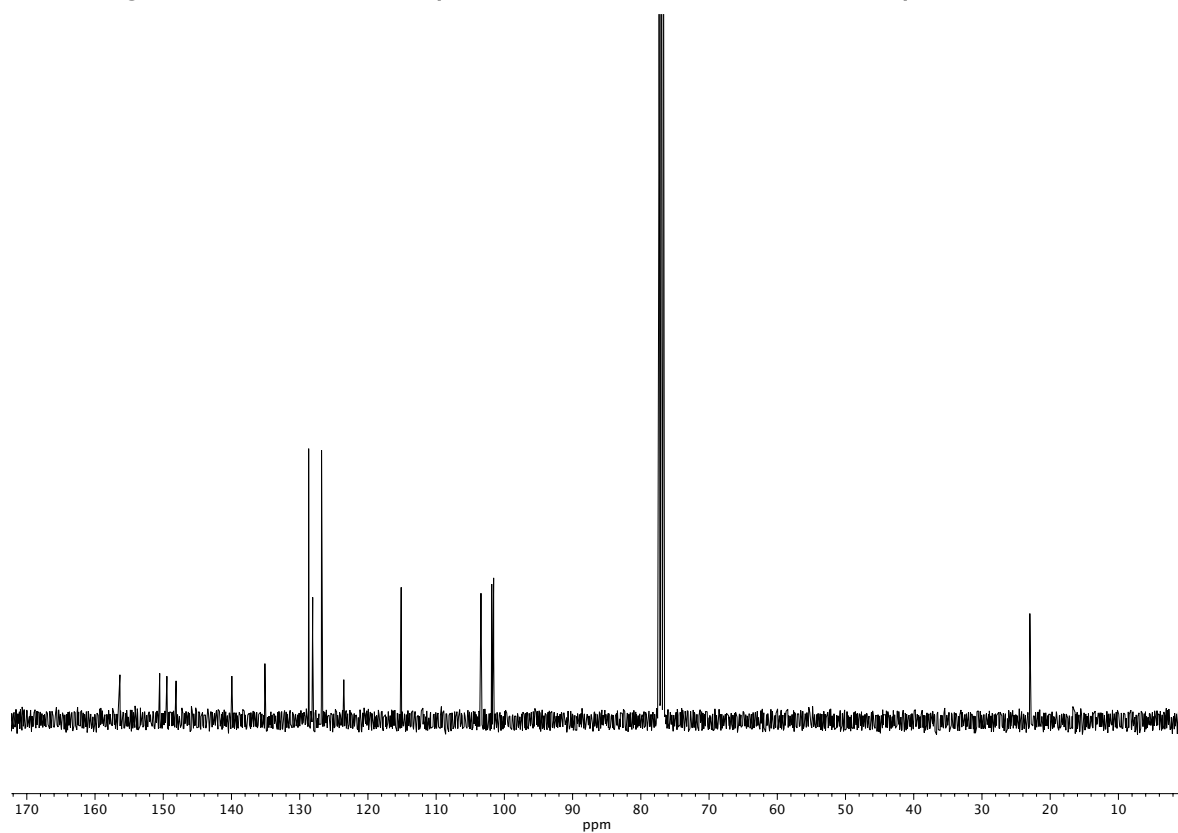
**Figure A1.98**  $^{19}\text{F}$  NMR (282 MHz,  $\text{CDCl}_3$ ) of compound **172c**.



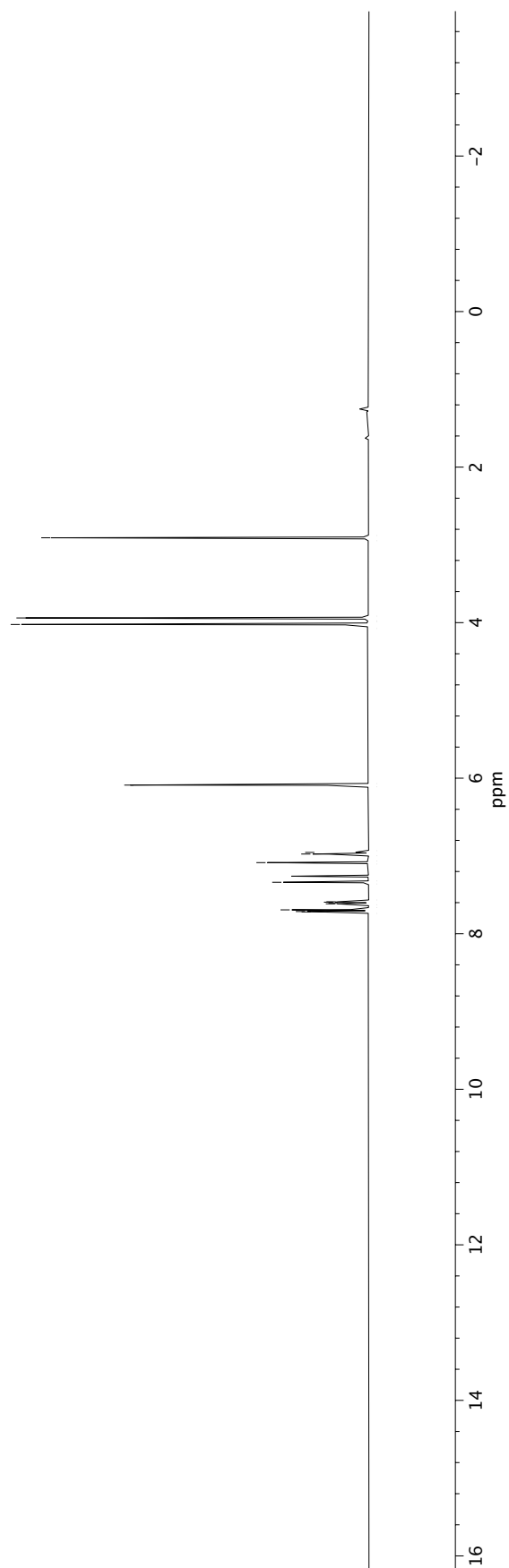
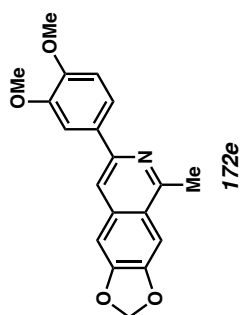
**Figure A1.99**  $^1\text{H}$  NMR (400 MHz,  $\text{CDCl}_3$ ) of compound **172d**.



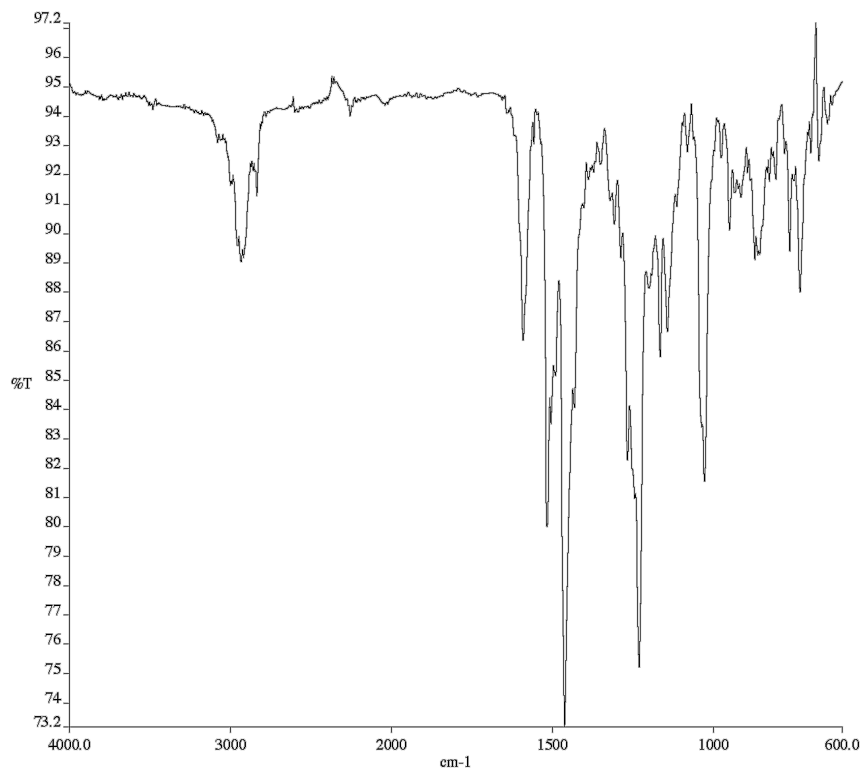
**Figure A1.100** Infrared spectrum (Thin Film, NaCl) of compound **172d**.



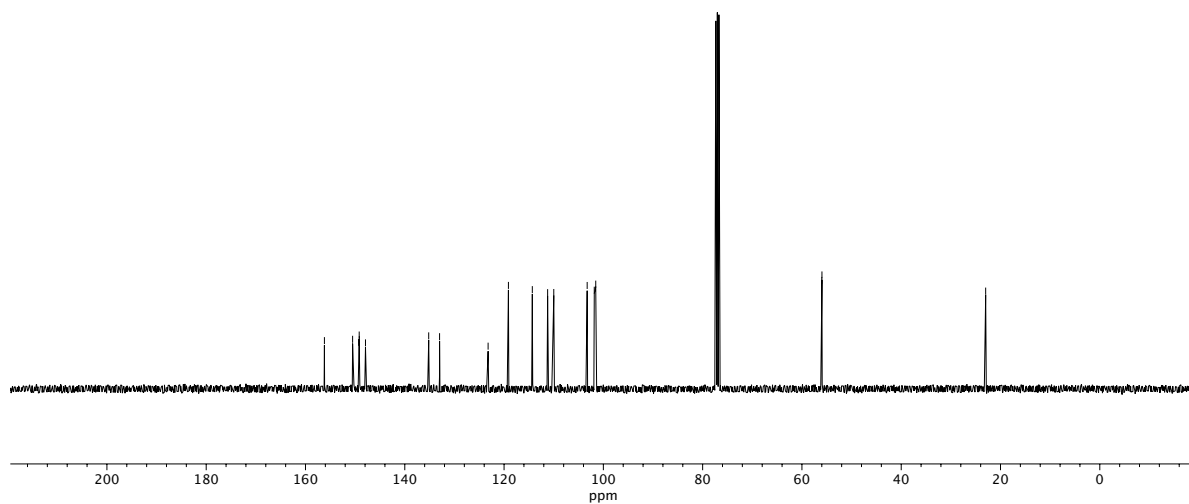
**Figure A1.101** <sup>13</sup>C NMR (100 MHz, CDCl<sub>3</sub>) of compound **172d**.



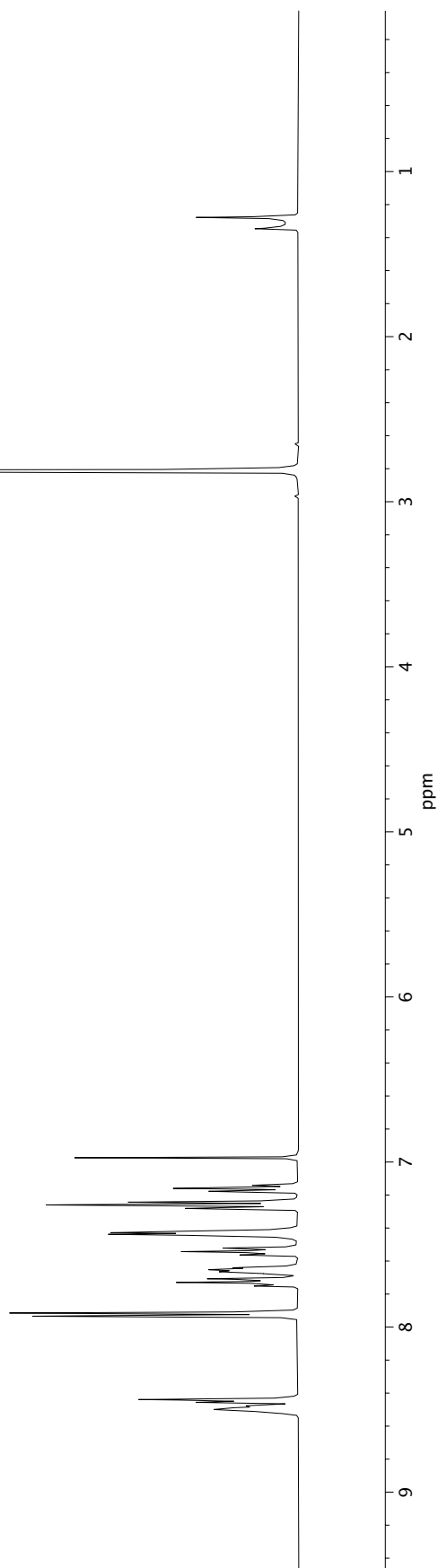
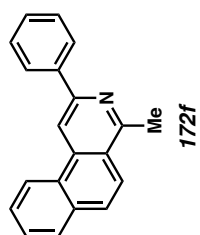
**Figure A1.102** <sup>1</sup>H NMR (400 MHz, CDCl<sub>3</sub>) of compound **172e**.



**Figure A1.103** Infrared spectrum (Thin Film, NaCl) of compound **172e**.

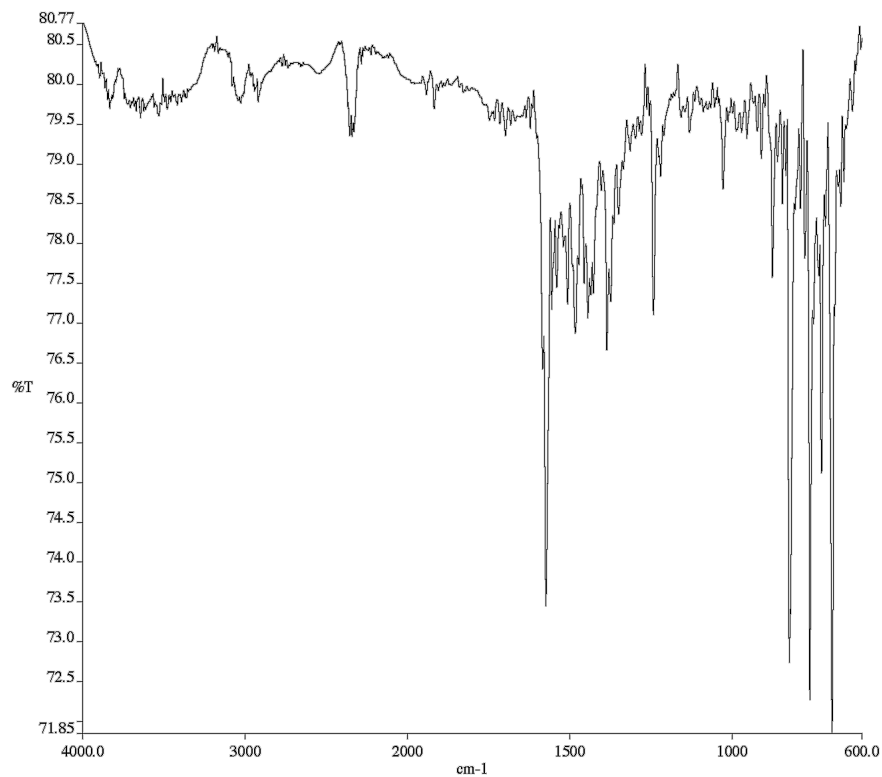


**Figure A1.104** <sup>13</sup>C NMR (100 MHz, CDCl<sub>3</sub>) of compound **172e**.

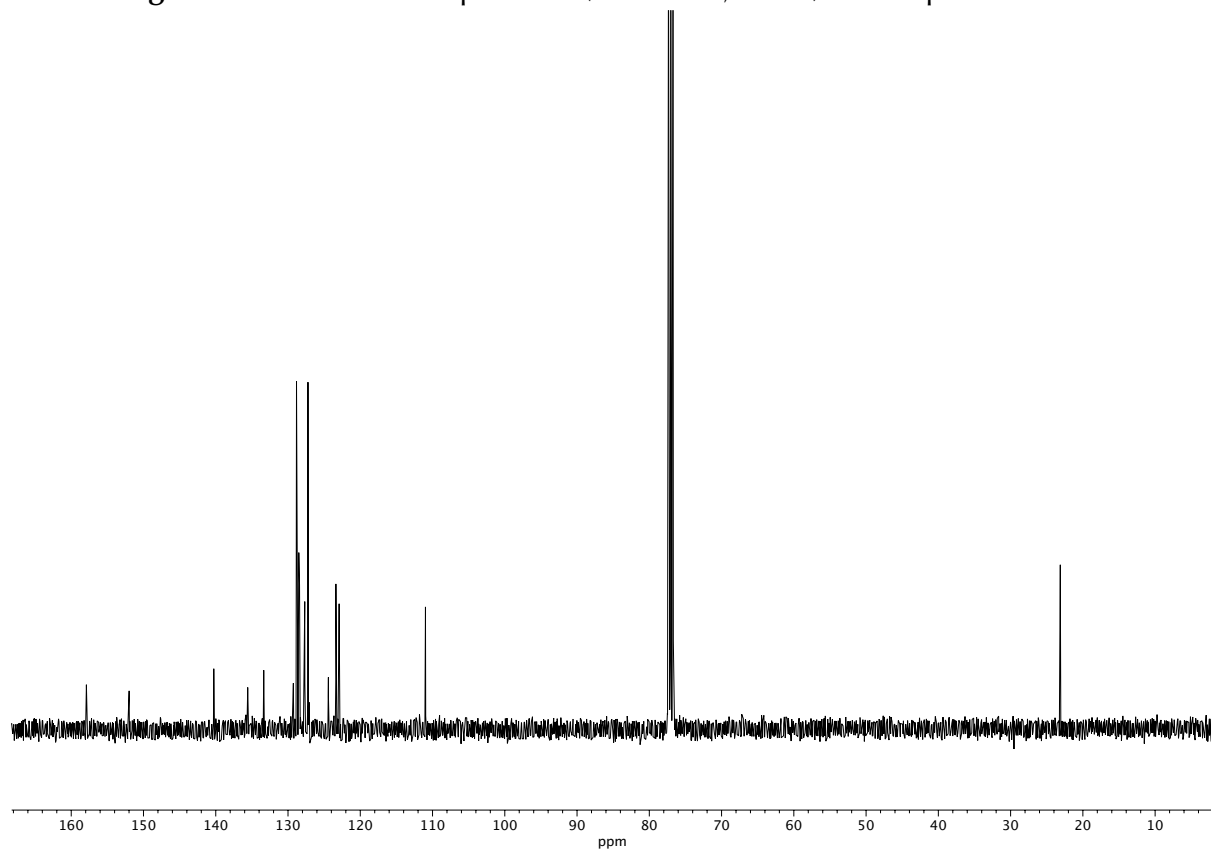


**Figure A1.105** <sup>1</sup>H NMR (400 MHz, CDCl<sub>3</sub>) of compound **172f**.

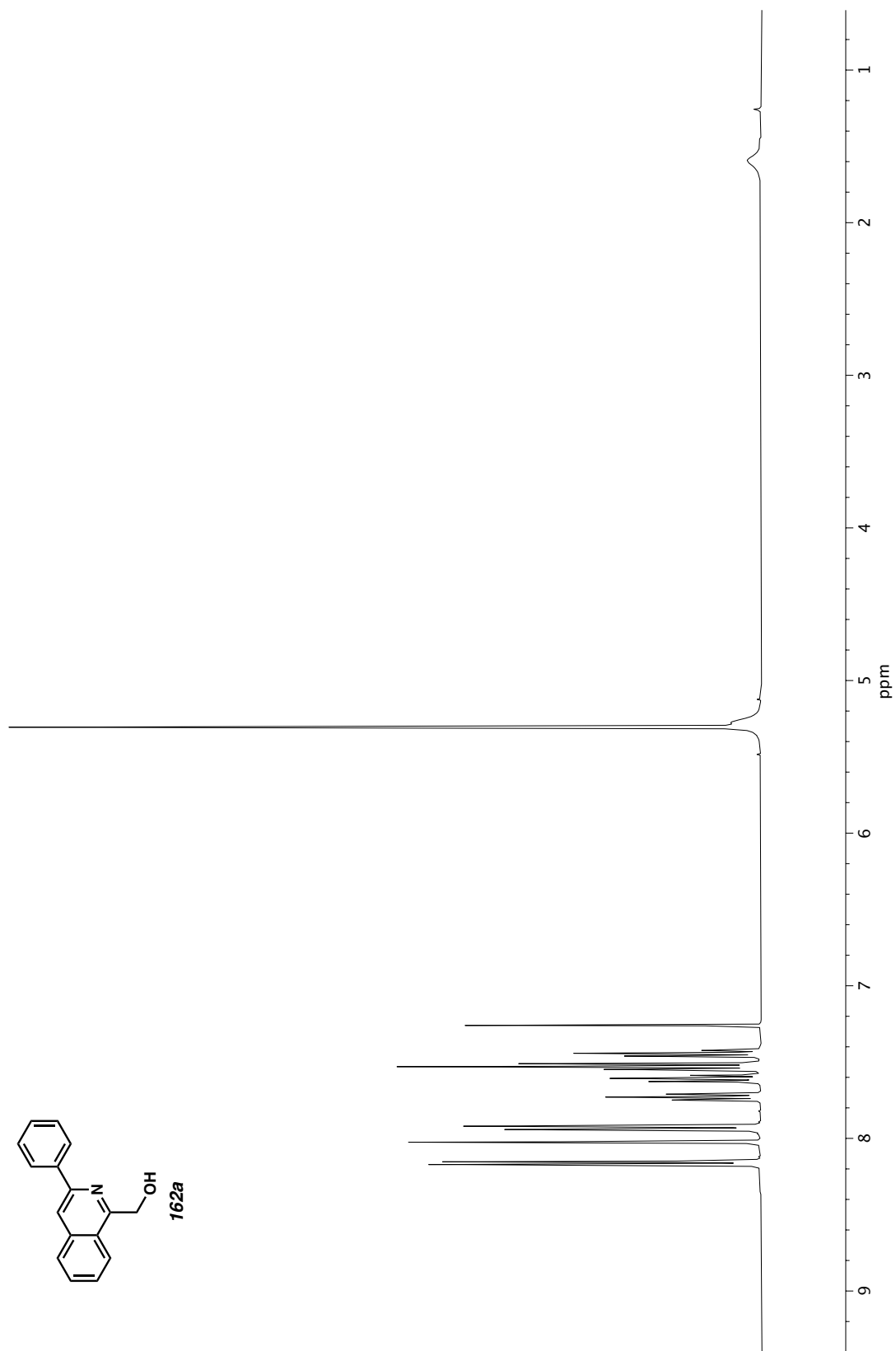




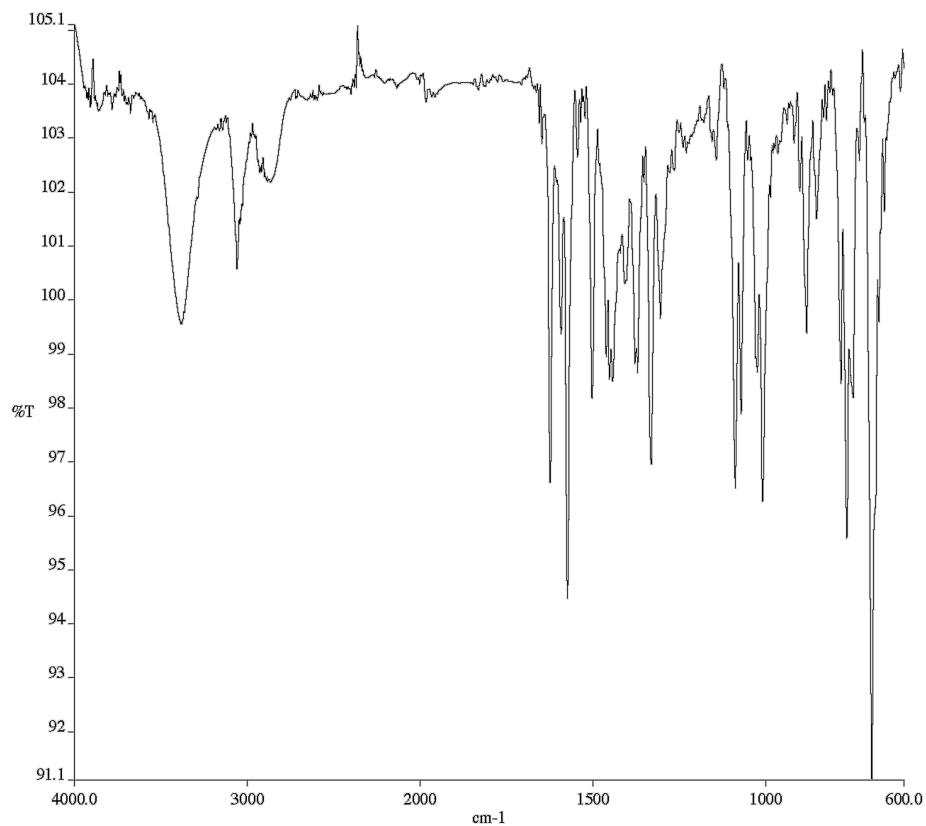
**Figure A1.106** Infrared spectrum (Thin Film, NaCl) of compound **172f**.



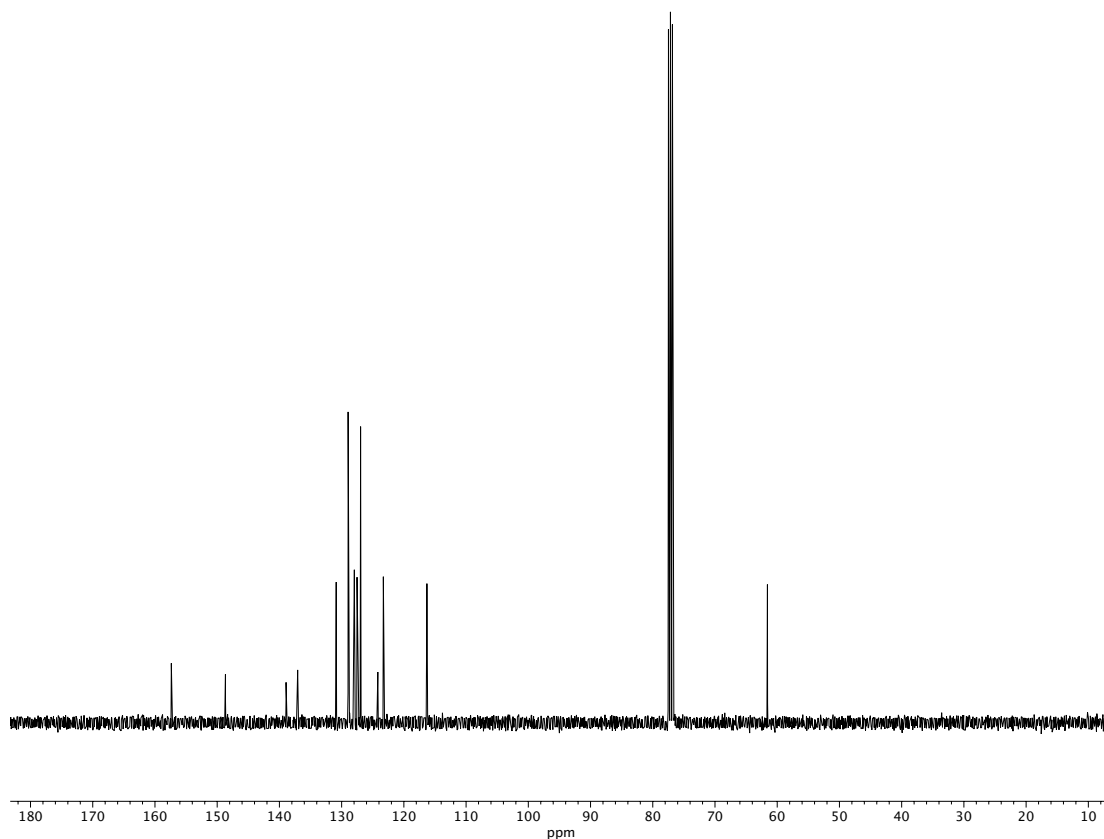
**Figure A1.107**  $^{13}\text{C}$  NMR (100 MHz,  $\text{CDCl}_3$ ) of compound **172f**.



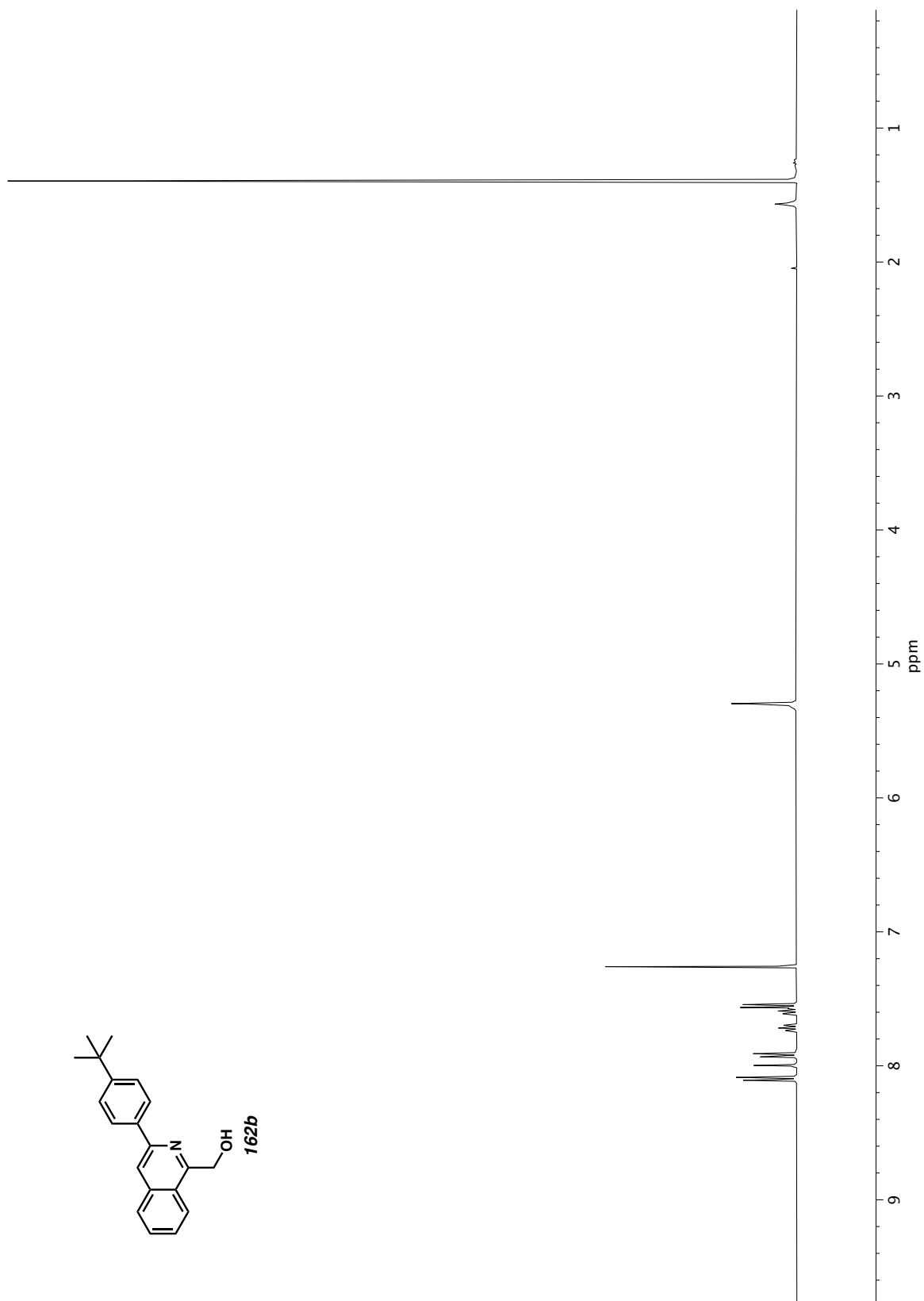
**Figure A1.108** <sup>1</sup>H NMR (400 MHz, CDCl<sub>3</sub>) of compound **162a**.

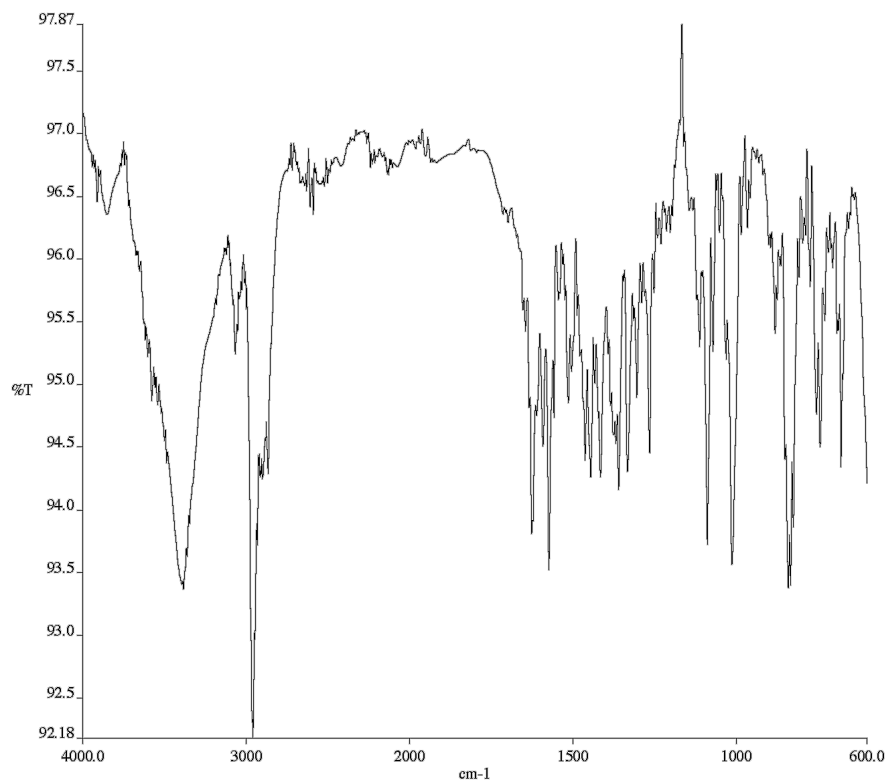


**Figure A1.109** Infrared spectrum (Thin Film, NaCl) of compound **162a**.

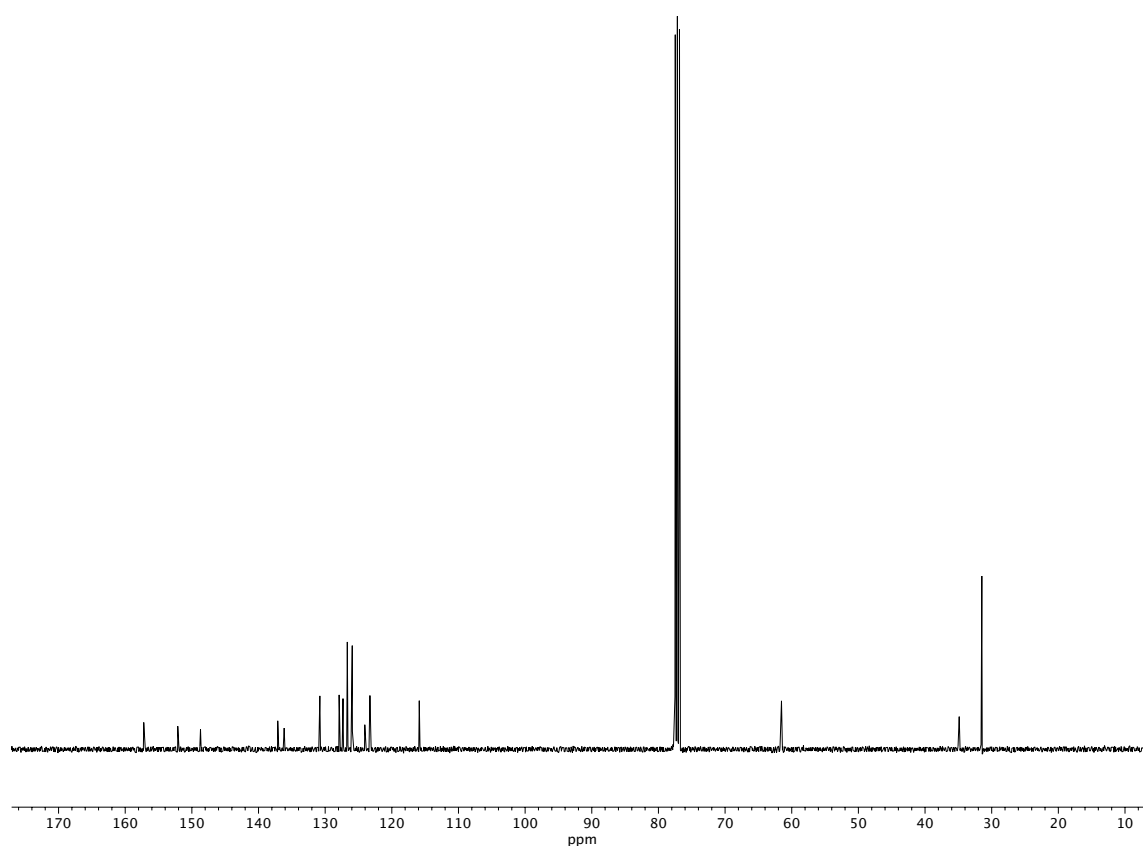


**Figure A1.110** <sup>13</sup>C NMR (100 MHz, CDCl<sub>3</sub>) of compound **162a**.

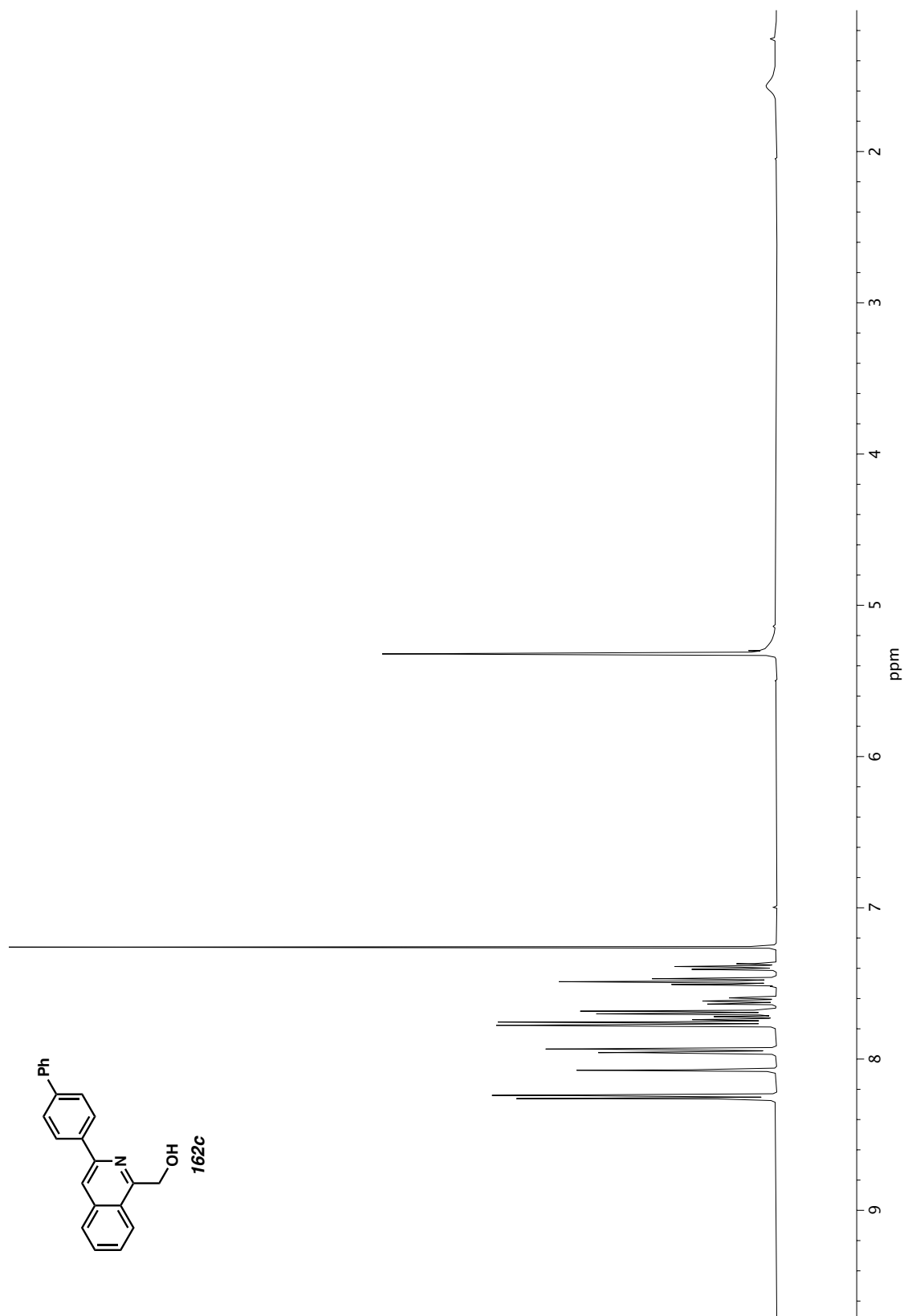


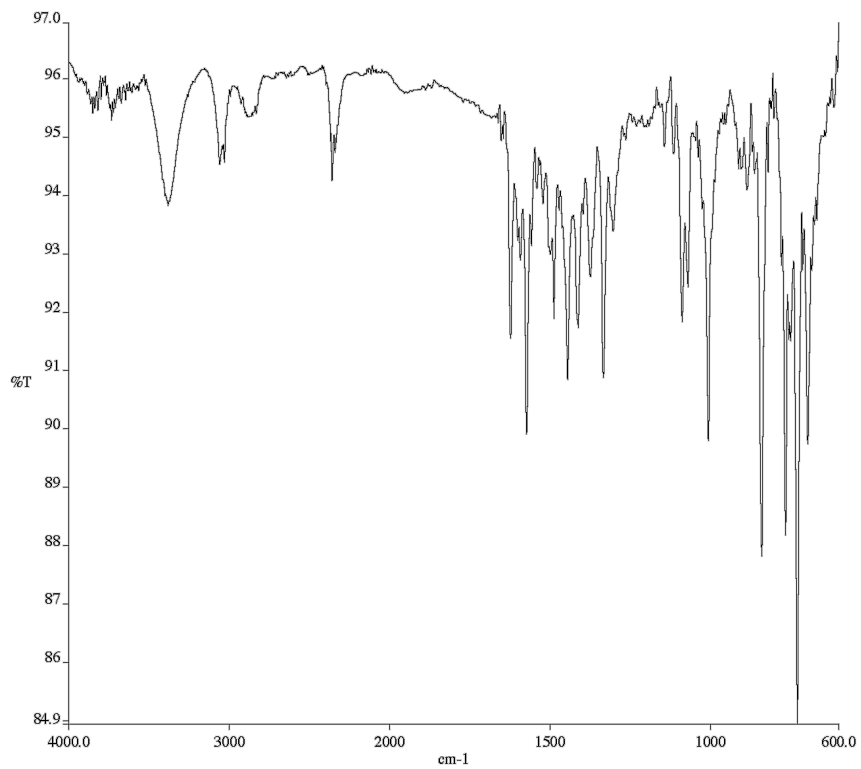


**Figure A1.112** Infrared spectrum (Thin Film, NaCl) of compound **162b**.

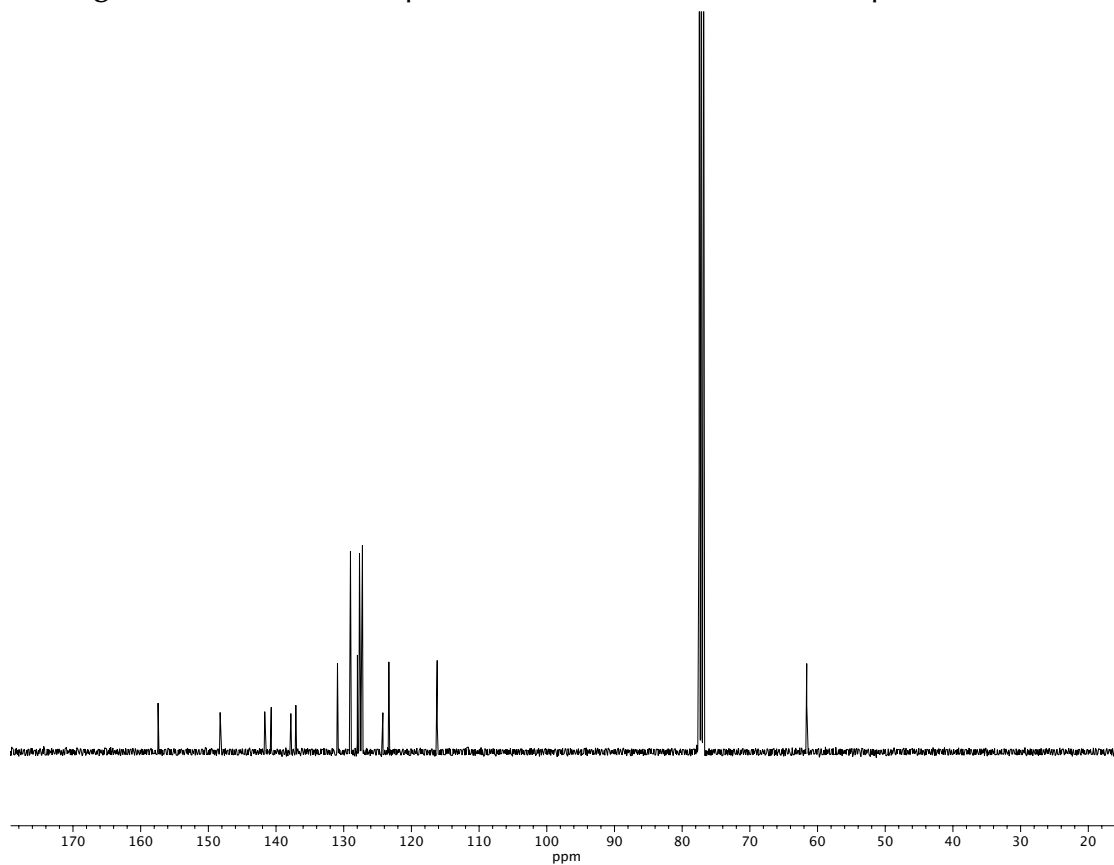


**Figure A1.113** <sup>13</sup>C NMR (100 MHz, CDCl<sub>3</sub>) of compound **162b**.

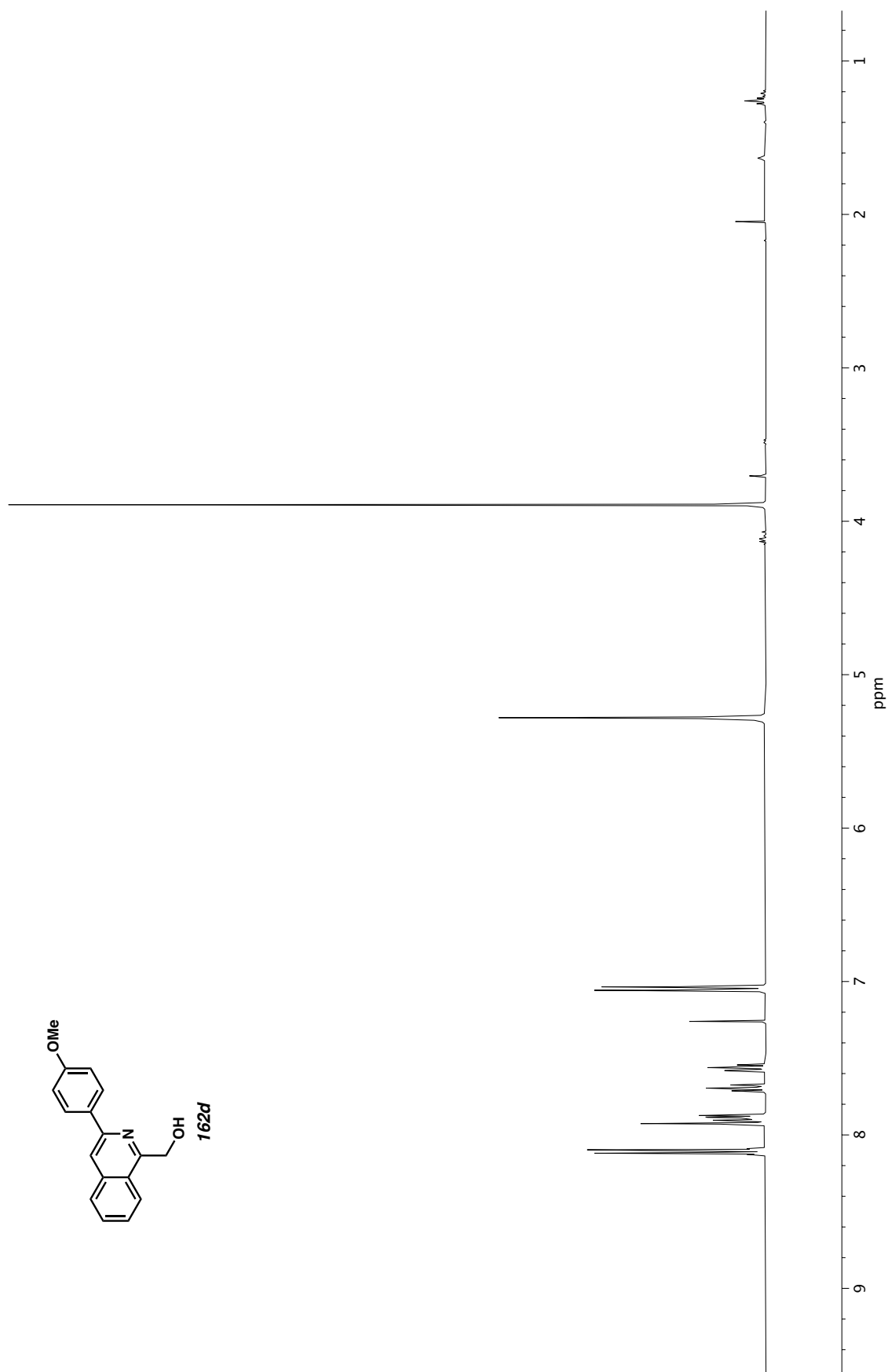




**Figure A1.115** Infrared spectrum (Thin Film, NaCl) of compound **162c**.

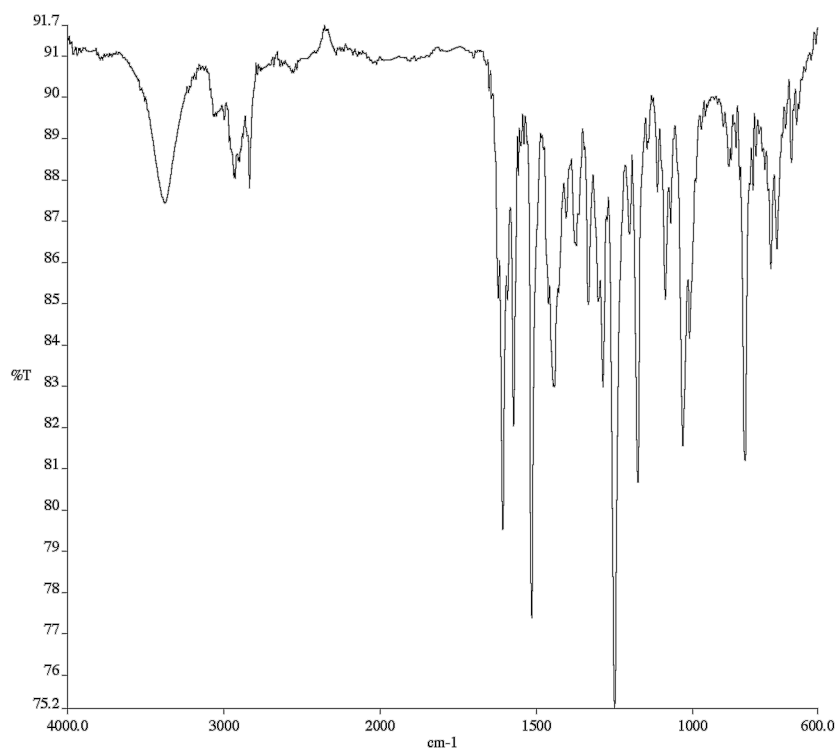


**Figure A1.116** <sup>13</sup>C NMR (100 MHz, CDCl<sub>3</sub>) of compound **162c**.

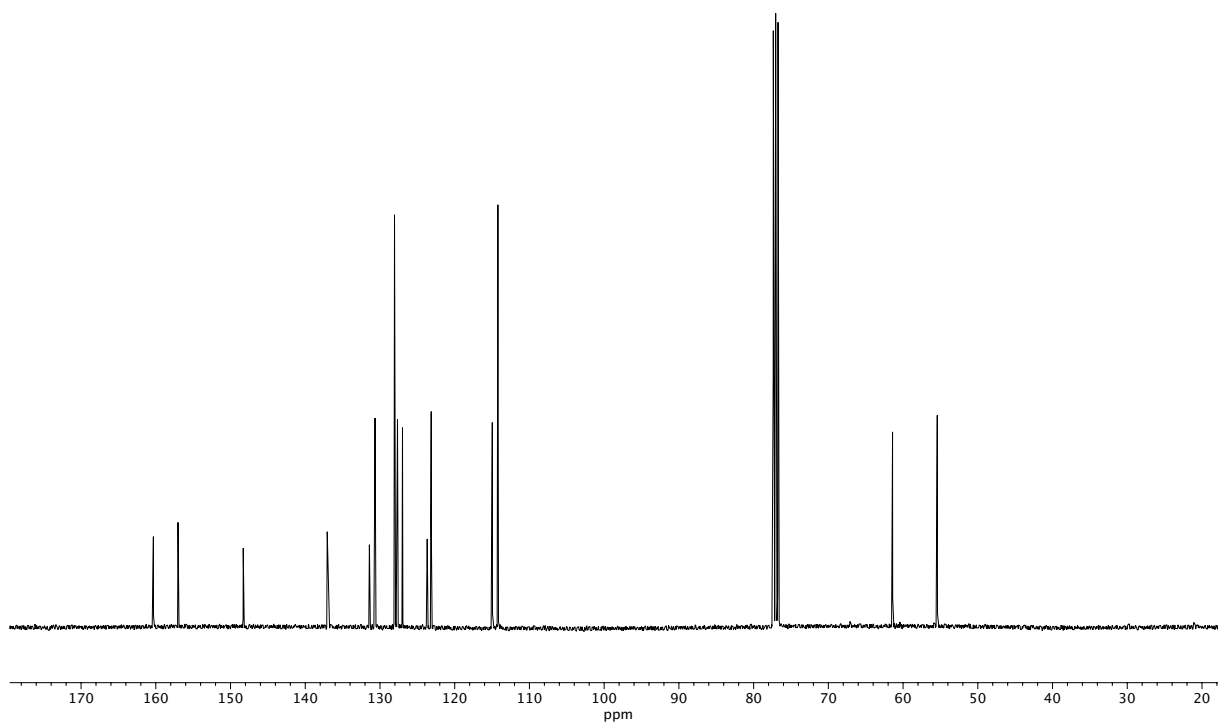


**Figure A1.117** <sup>1</sup>H NMR (400 MHz, CDCl<sub>3</sub>) of compound **162d**.

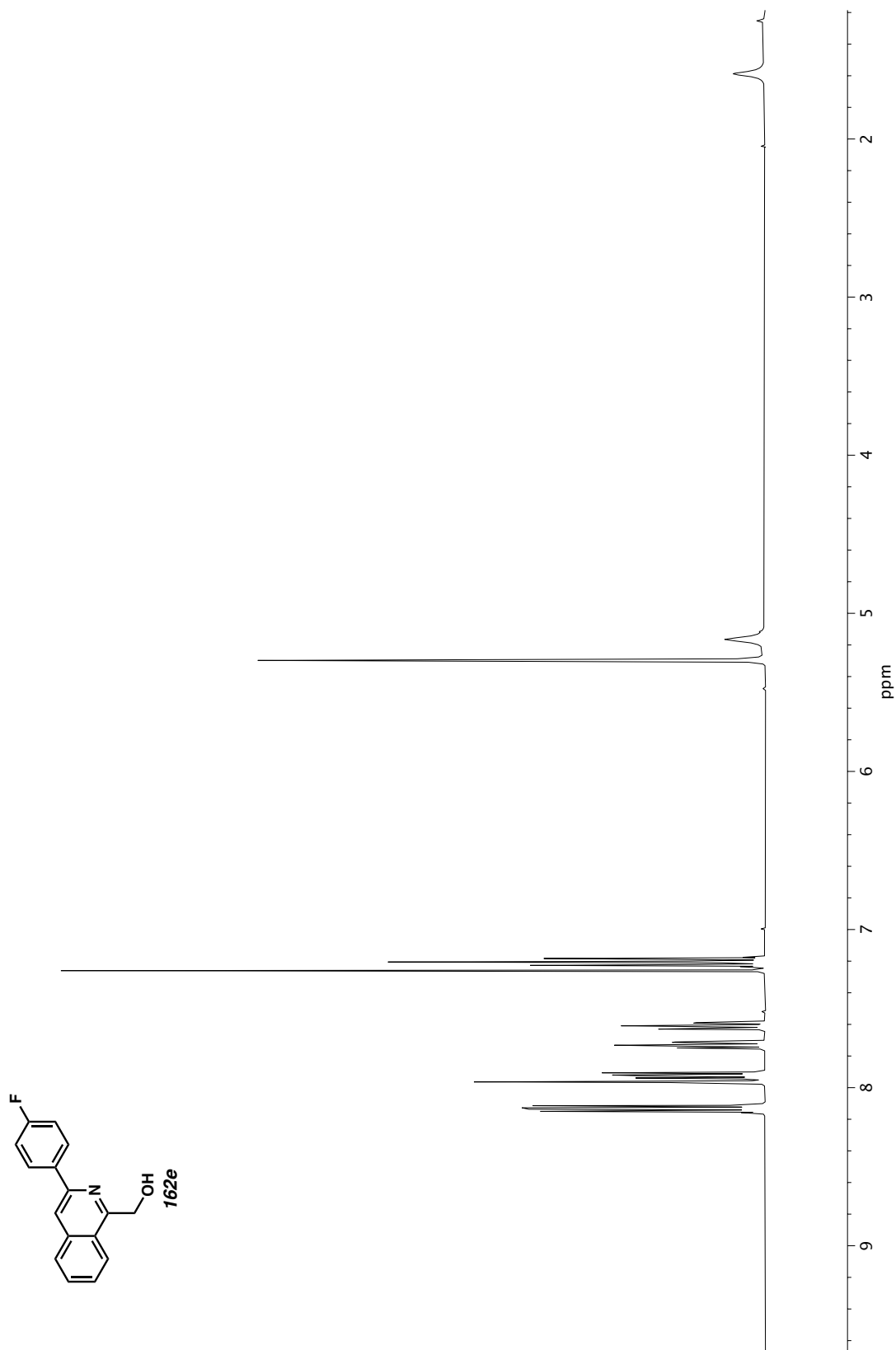




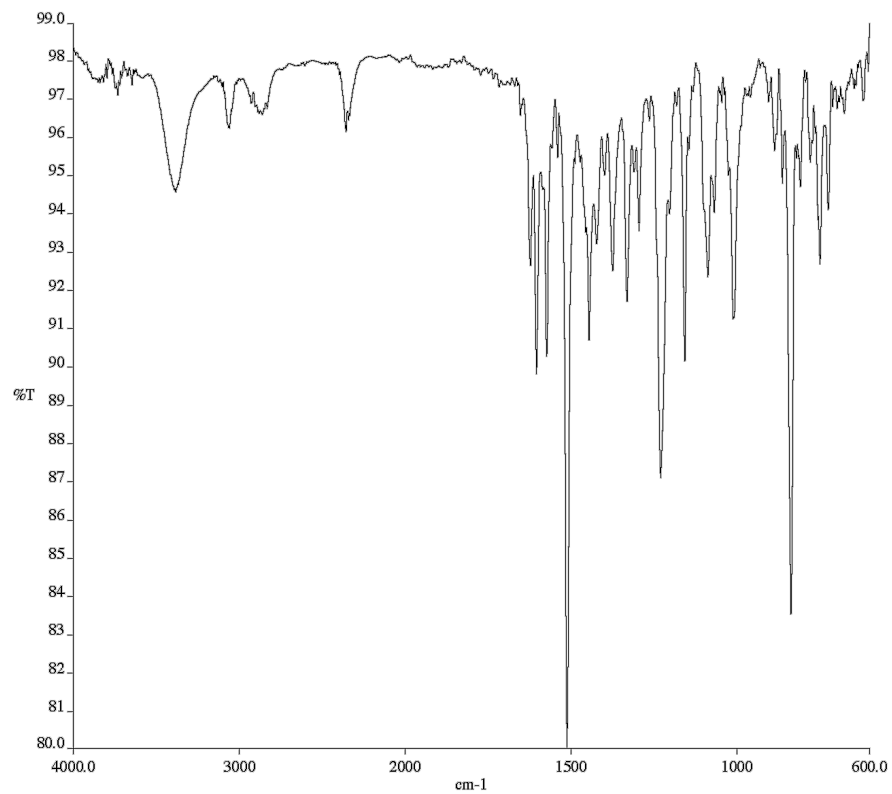
**Figure A1.118** Infrared spectrum (Thin Film, NaCl) of compound **162d**.



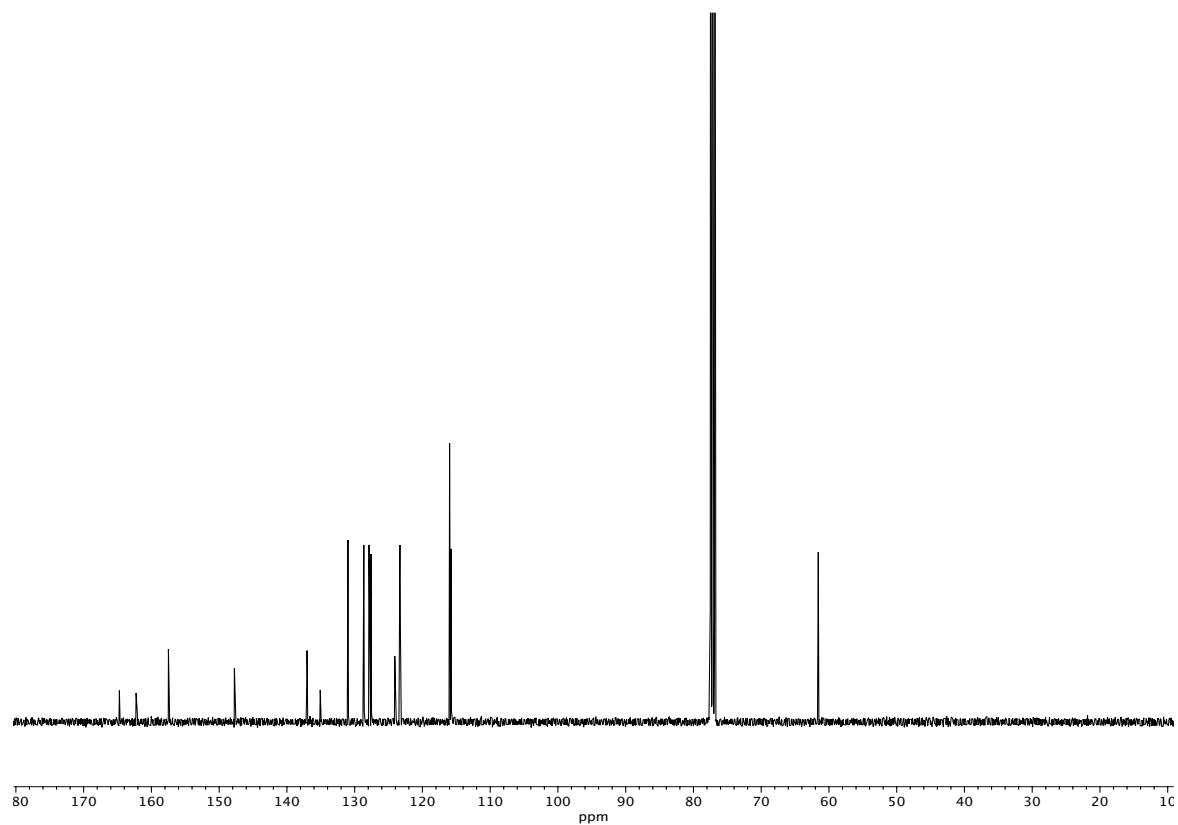
**Figure A1.119** <sup>13</sup>C NMR (100 MHz, CDCl<sub>3</sub>) of compound **162d**.



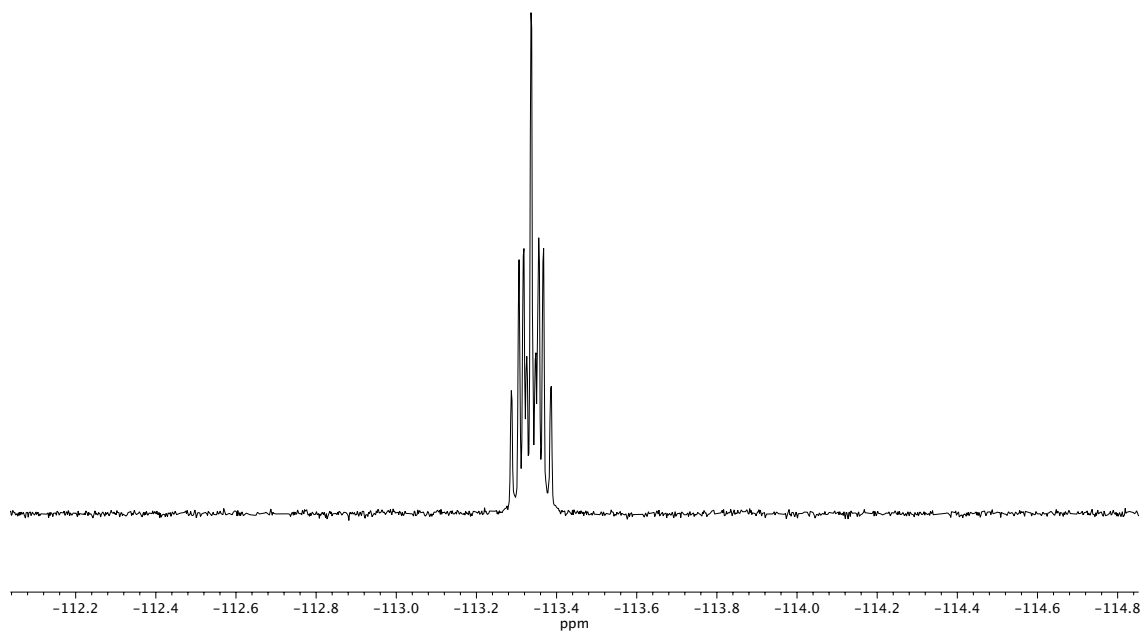
**Figure A1.120**  $^1\text{H}$  NMR (400 MHz,  $\text{CDCl}_3$ ) of compound **162e**.



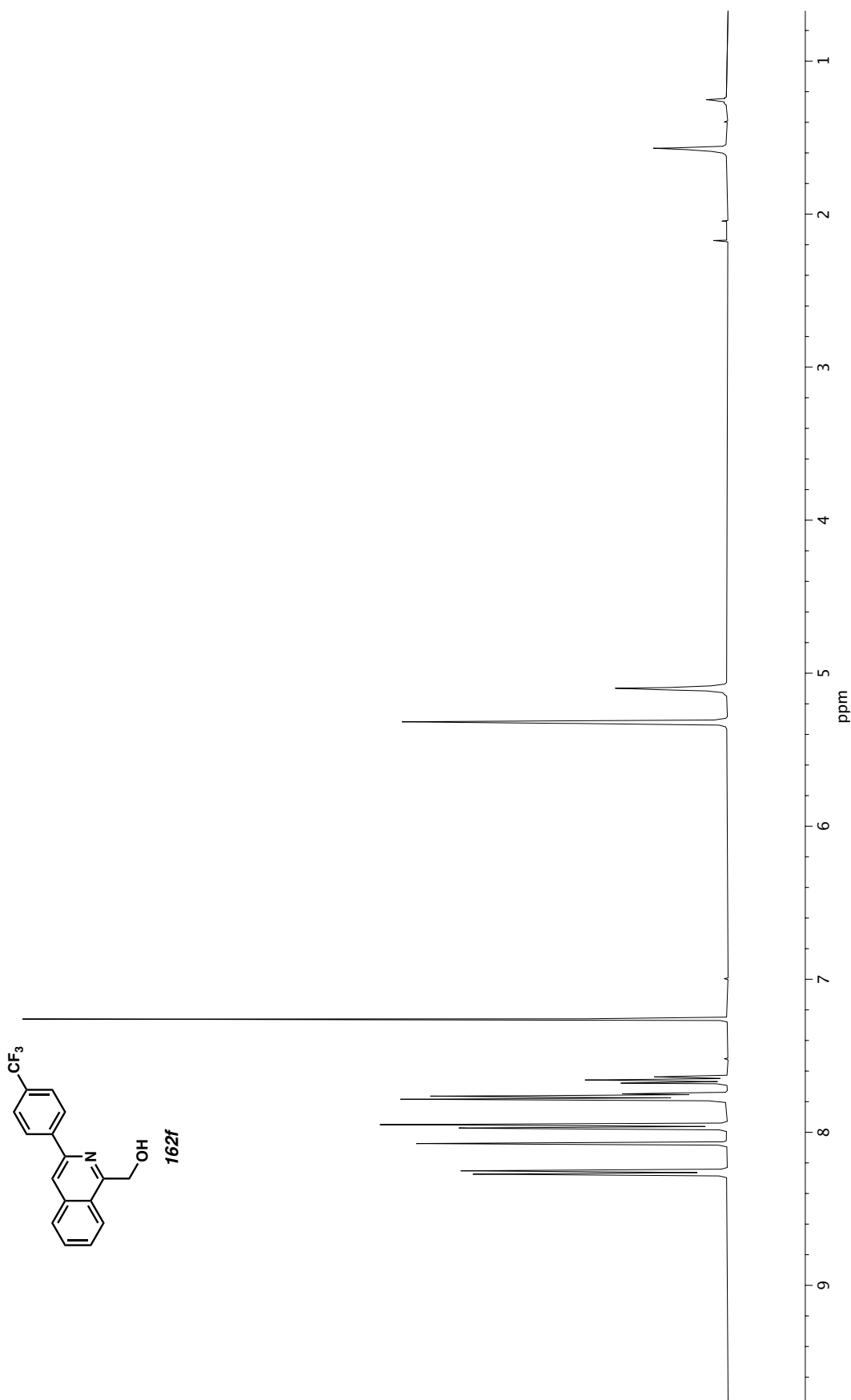
**Figure A1.121** Infrared spectrum (Thin Film, NaCl) of compound **162e**.



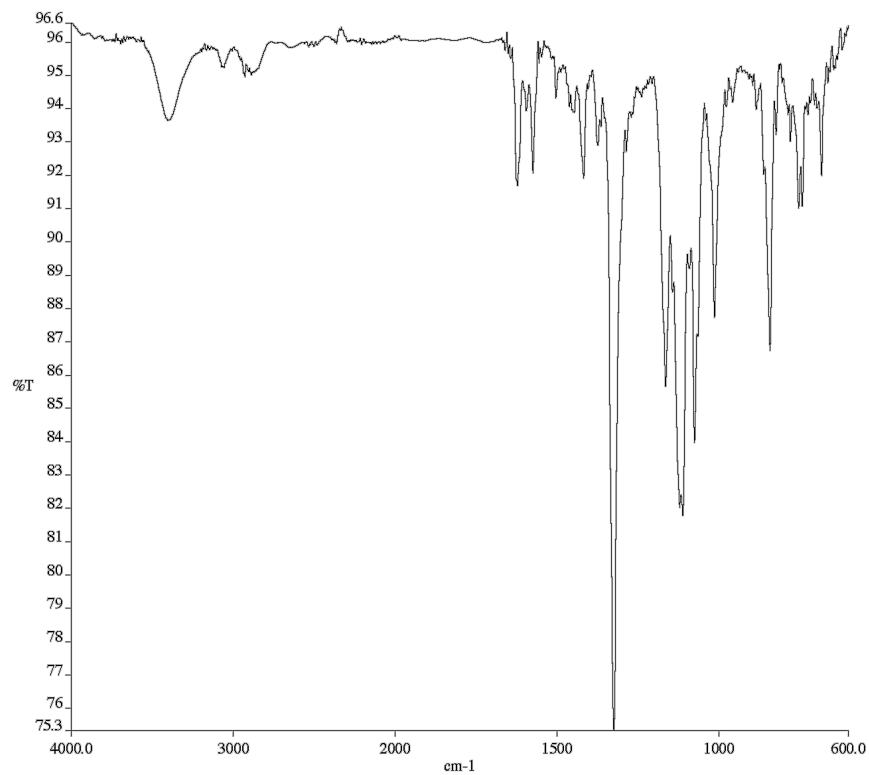
**Figure A1.122** <sup>13</sup>C NMR (100 MHz, CDCl<sub>3</sub>) of compound **162e**.



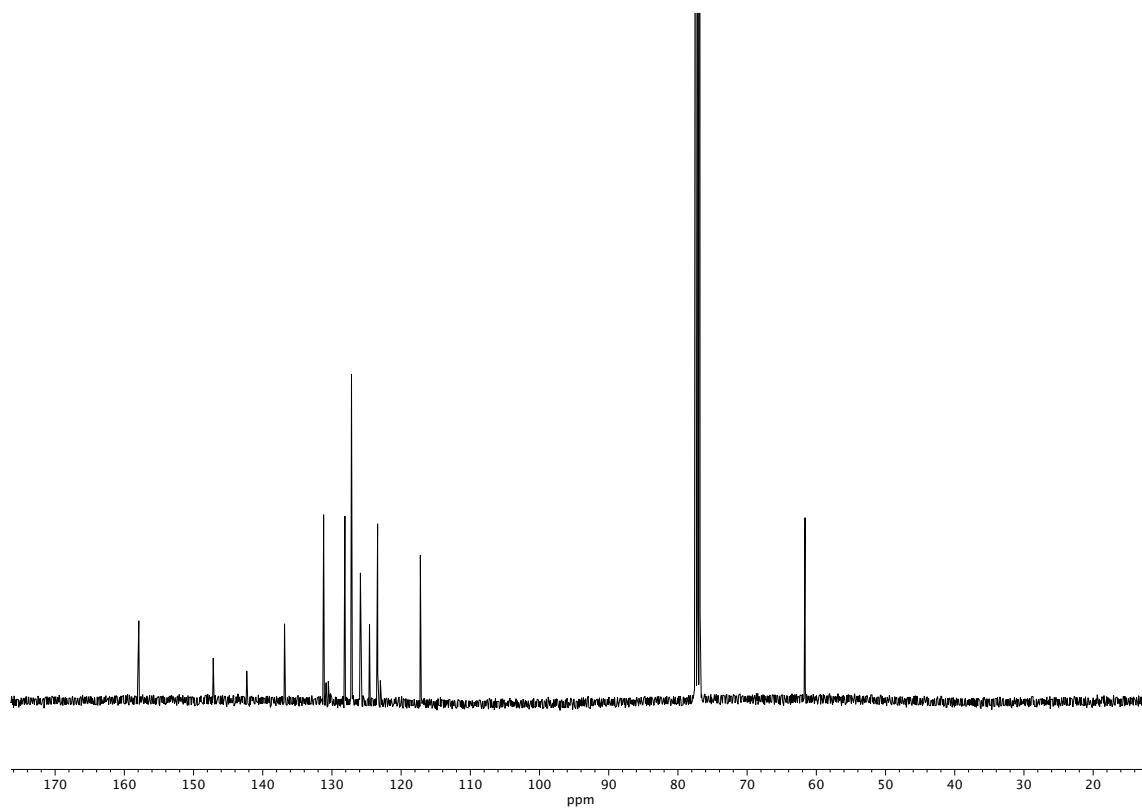
**Figure A1.123**  $^{19}\text{F}$  NMR (282 MHz,  $\text{CDCl}_3$ ) of compound **162e**.



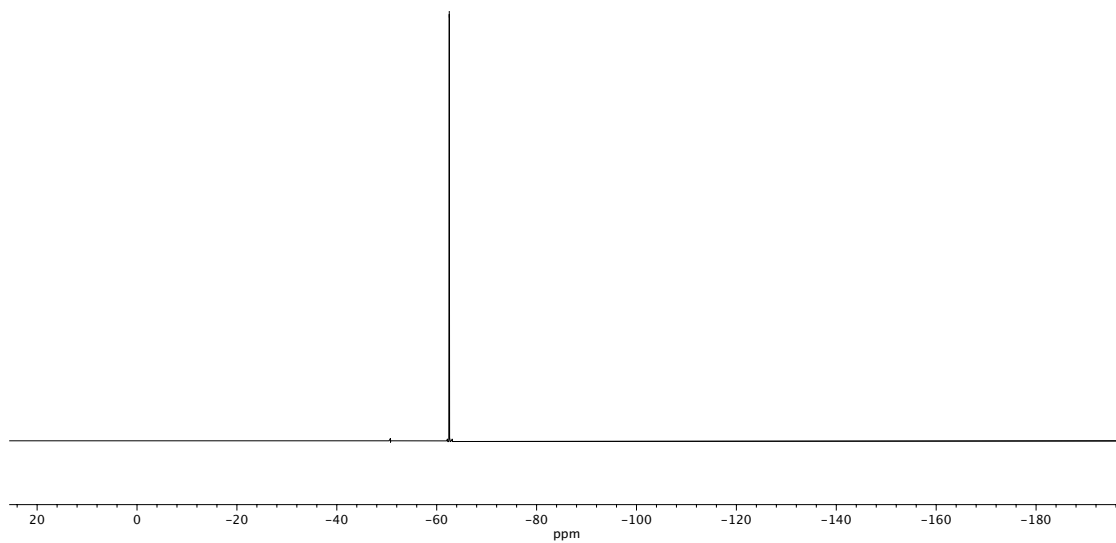
**Figure A1.124**  $^1\text{H}$  NMR (400 MHz,  $\text{CDCl}_3$ ) of compound **162f**.



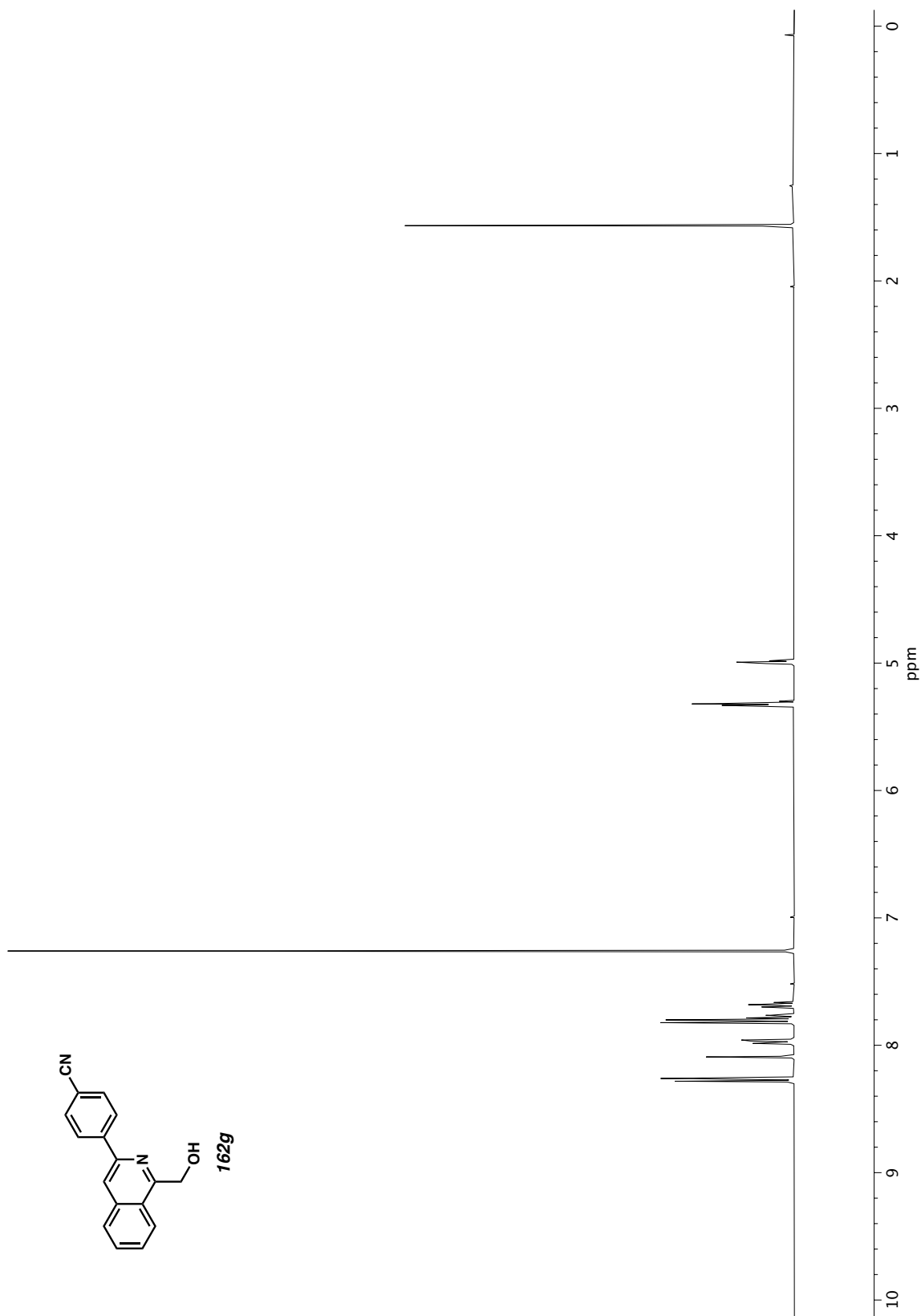
**Figure A1.125** Infrared spectrum (Thin Film, NaCl) of compound **162f**.



**Figure A1.126** <sup>13</sup>C NMR (100 MHz, CDCl<sub>3</sub>) of compound **162f**.

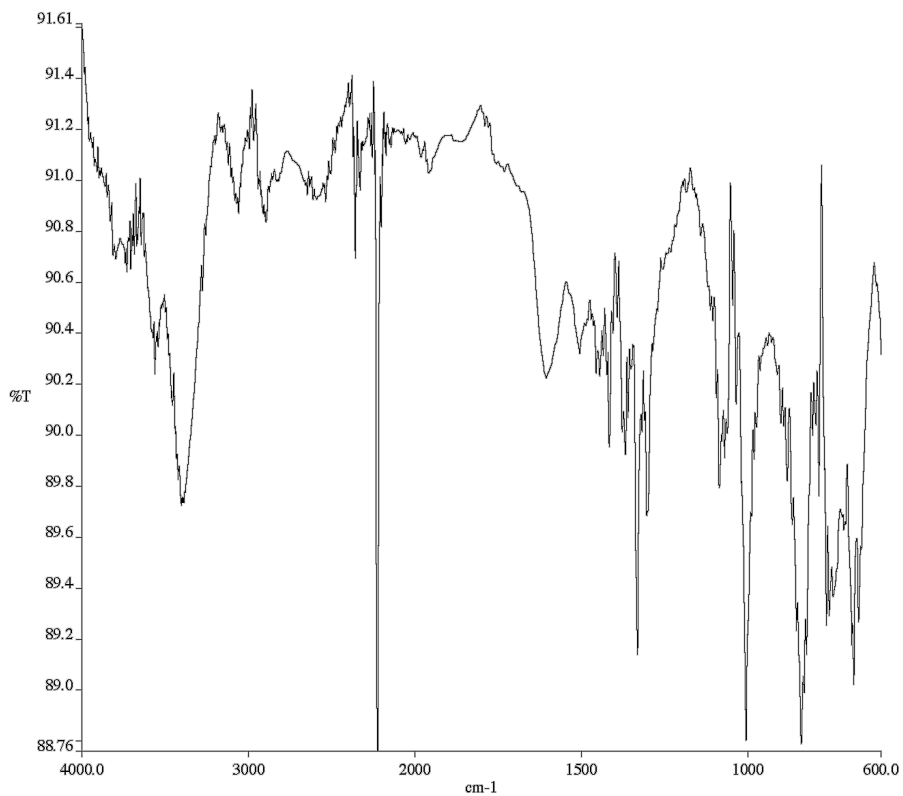


**Figure A1.127**  $^{19}\text{F}$  NMR (282 MHz,  $\text{CDCl}_3$ ) of compound **162f**.

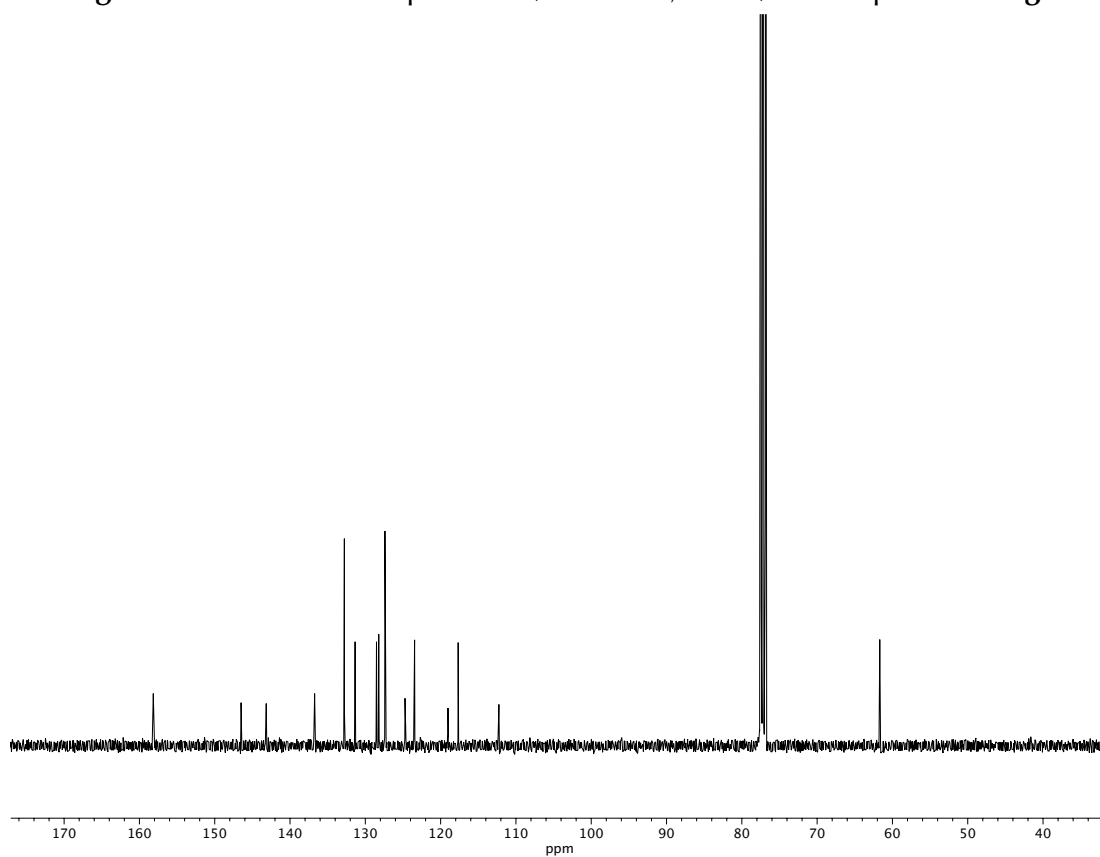


**Figure A1.128** <sup>1</sup>H NMR (400 MHz, CDCl<sub>3</sub>) of compound **162g**.

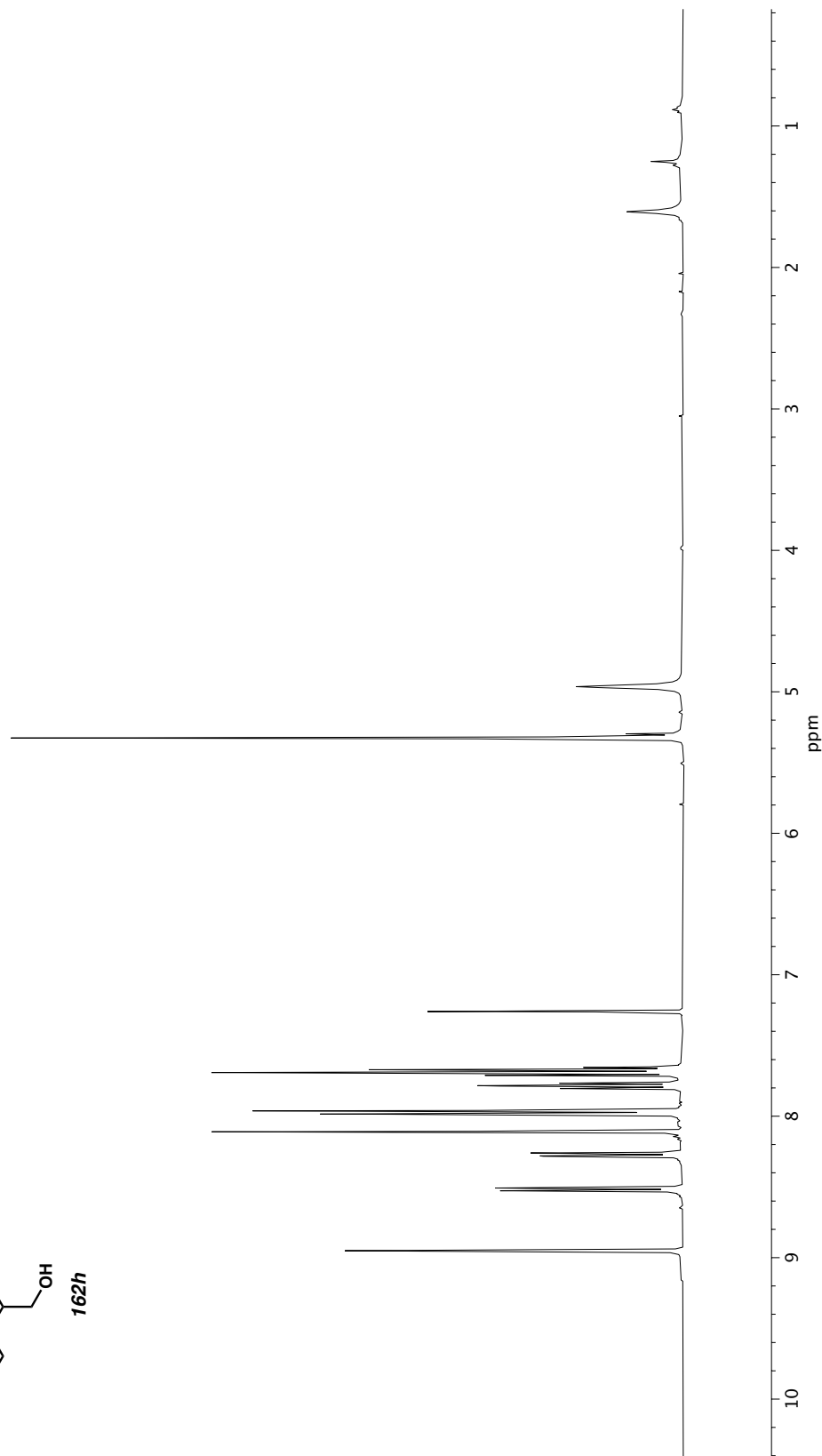
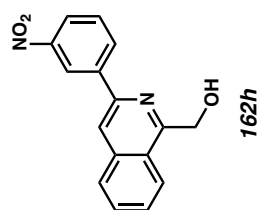




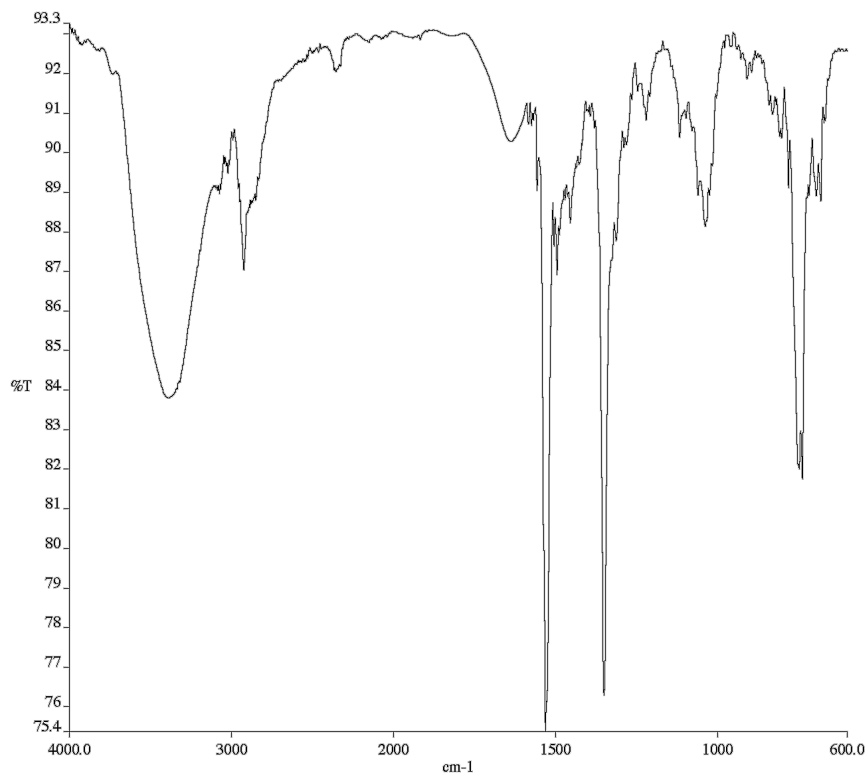
**Figure A1.129** Infrared spectrum (Thin Film, NaCl) of compound **162g**.



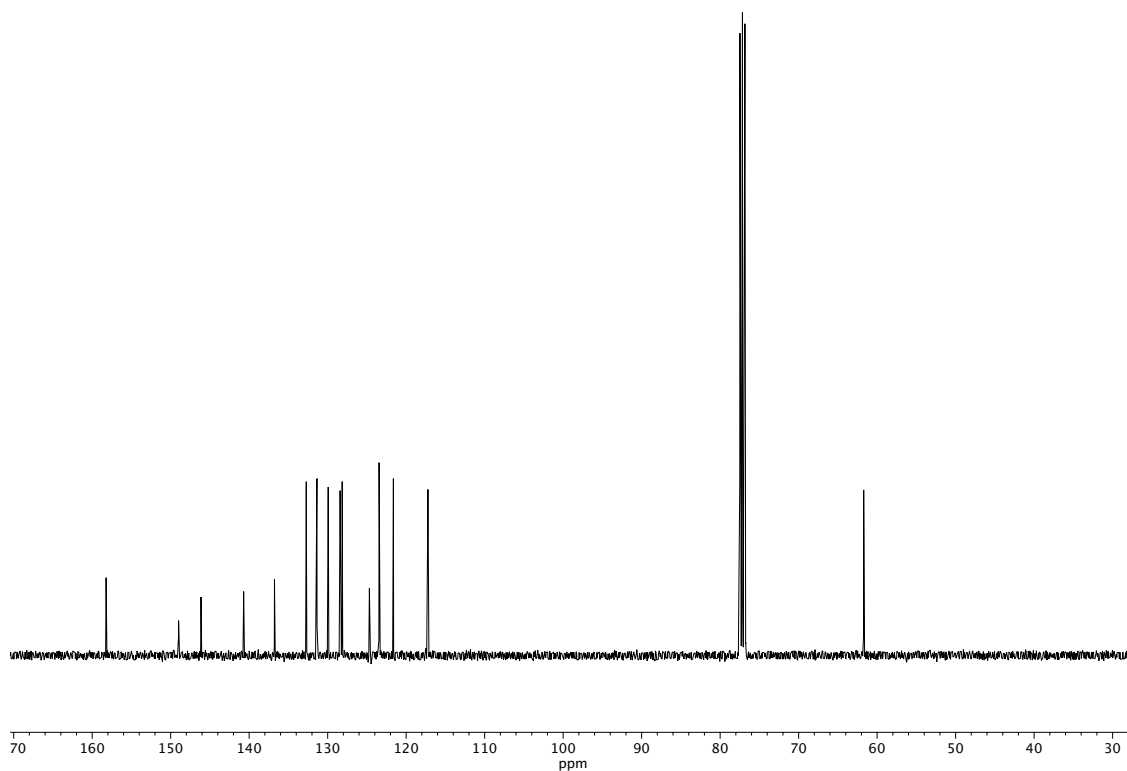
**Figure A1.130** <sup>13</sup>C NMR (100 MHz, CDCl<sub>3</sub>) of compound **162g**.



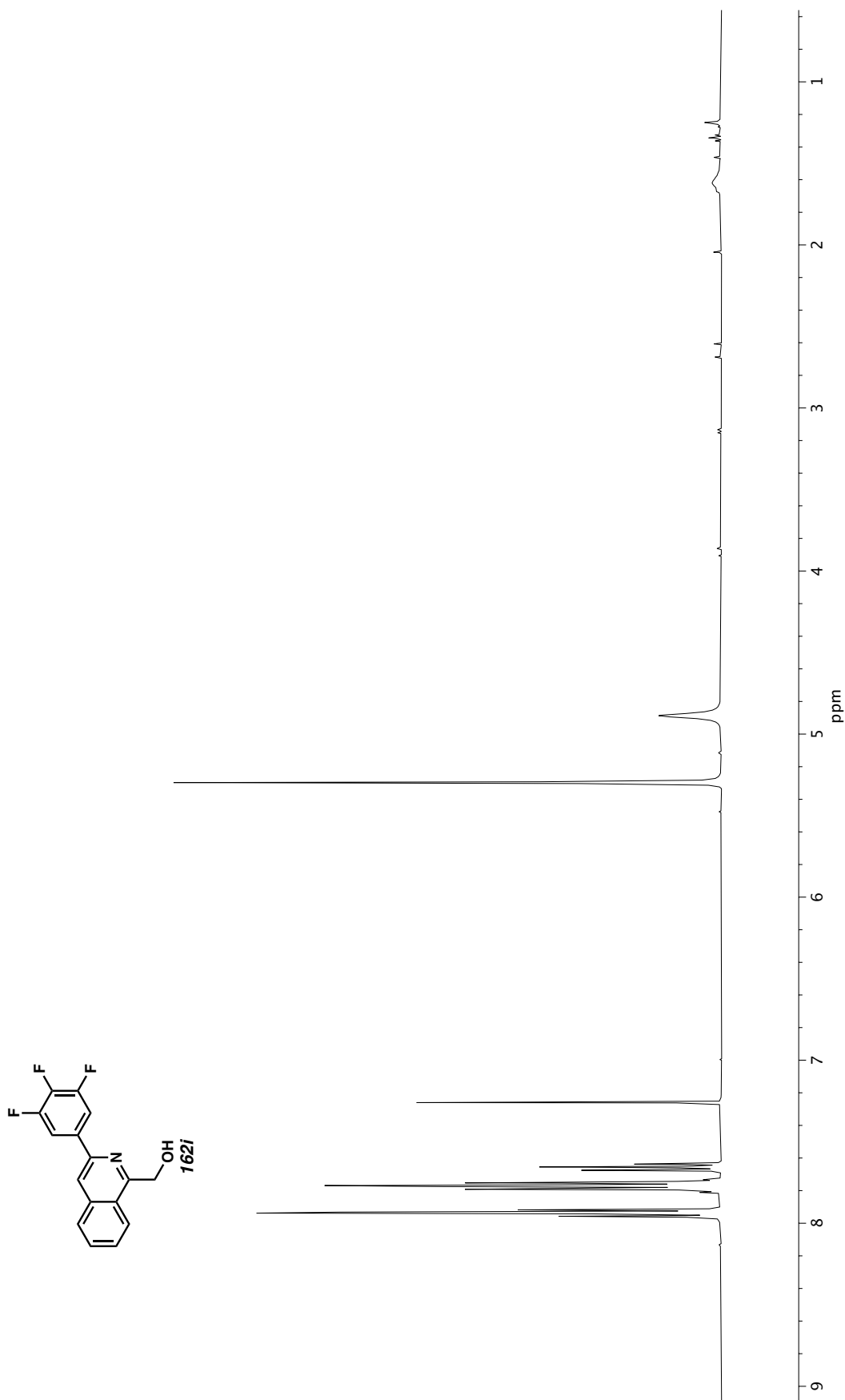
**Figure A1.131** <sup>1</sup>H NMR (400 MHz, CDCl<sub>3</sub>) of compound **162h**.



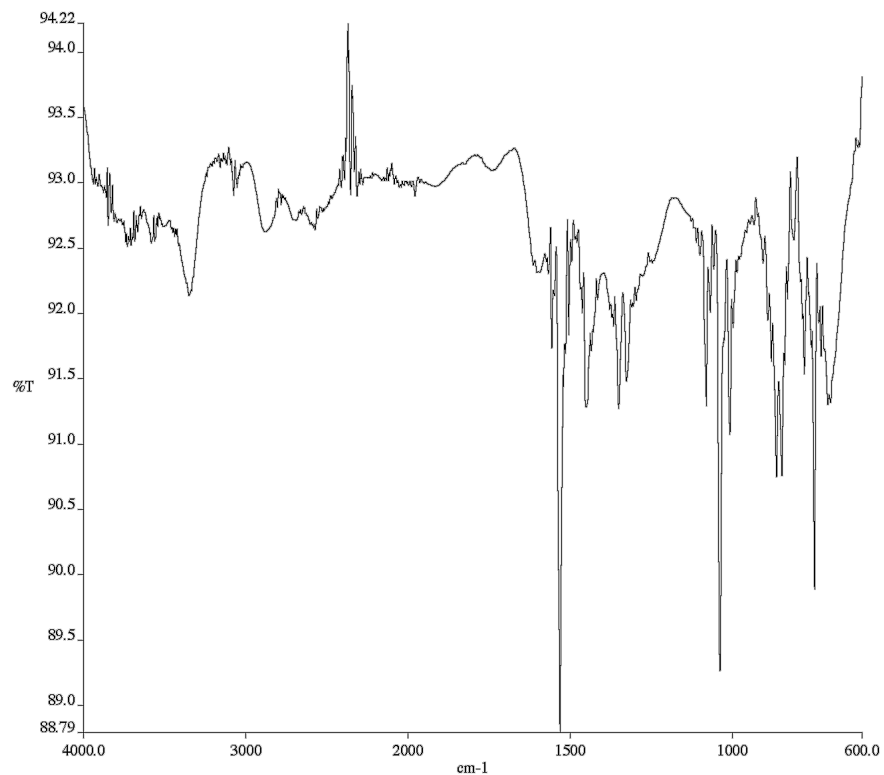
**Figure A1.132** Infrared spectrum (Thin Film, NaCl) of compound **162h**.



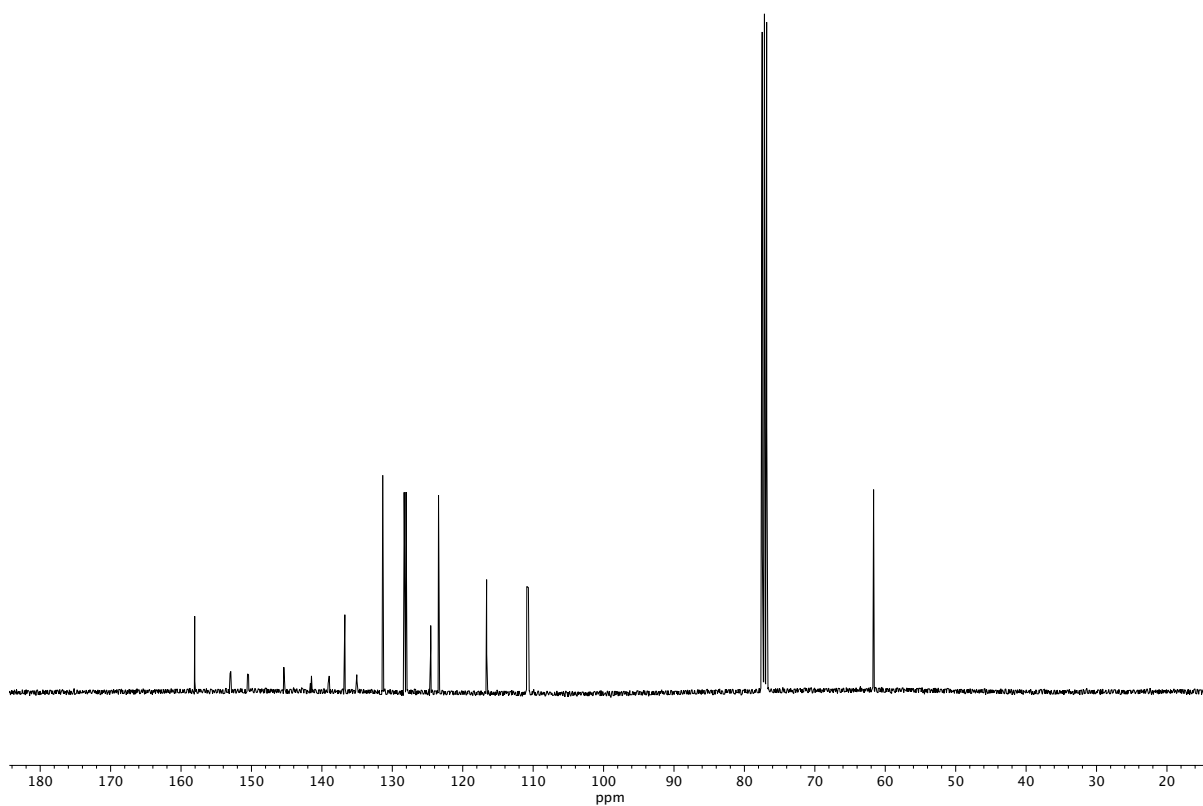
**Figure A1.133** <sup>13</sup>C NMR (100 MHz, CDCl<sub>3</sub>) of compound **162h**.



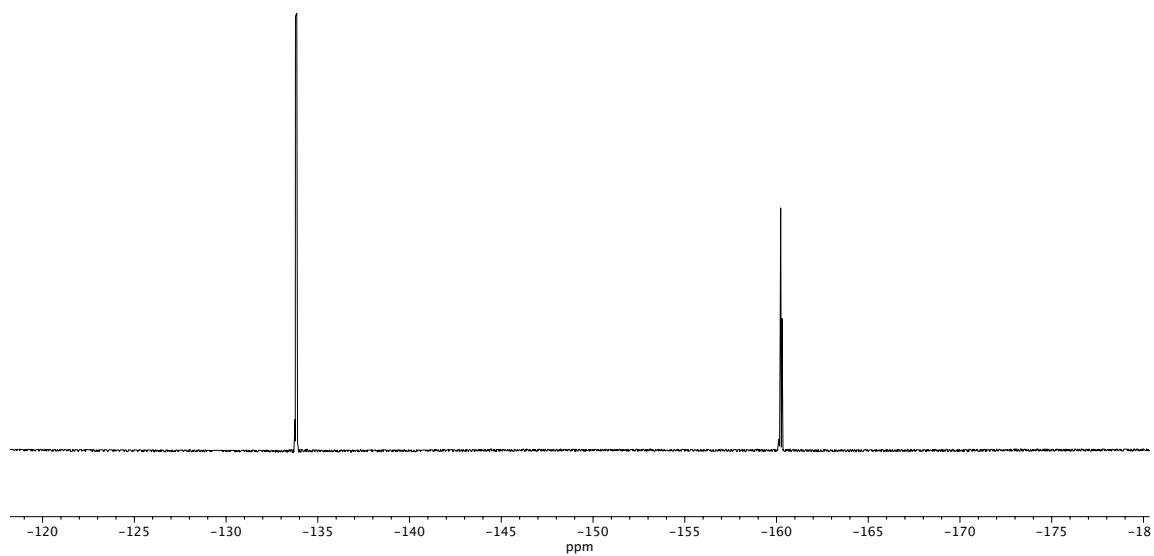
**Figure A1.134** <sup>1</sup>H NMR (400 MHz, CDCl<sub>3</sub>) of compound **162i**.



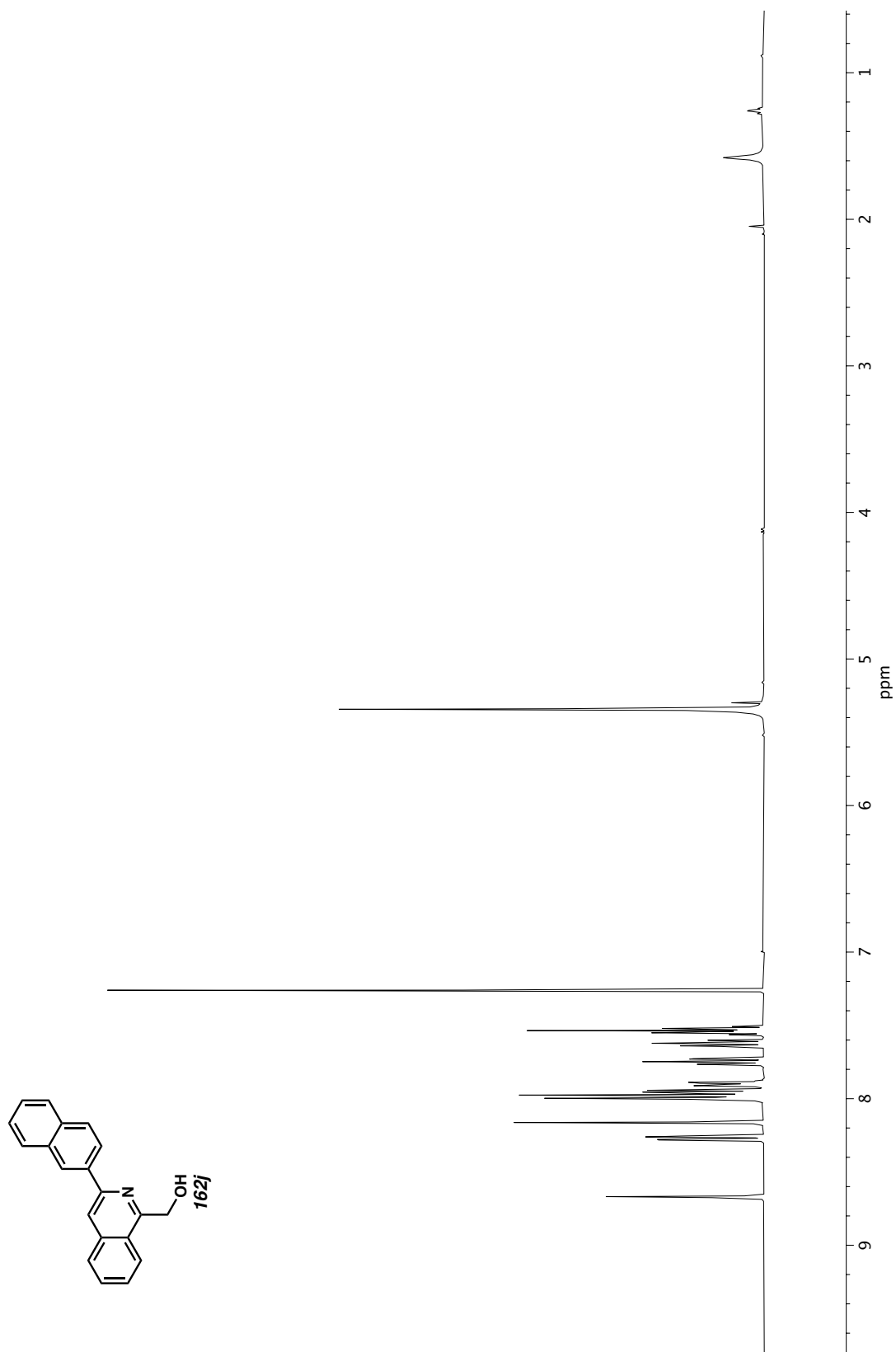
**Figure A1.135** Infrared spectrum (Thin Film, NaCl) of compound **162i**.

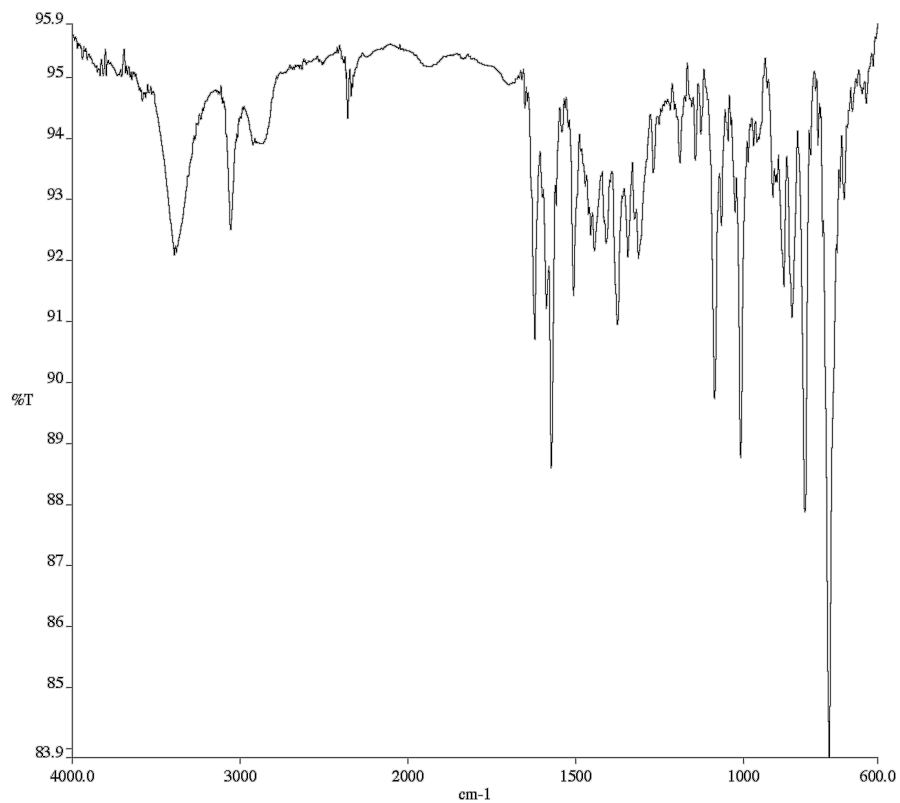


**Figure A1.136** <sup>13</sup>C NMR (100 MHz, CDCl<sub>3</sub>) of compound **162i**.

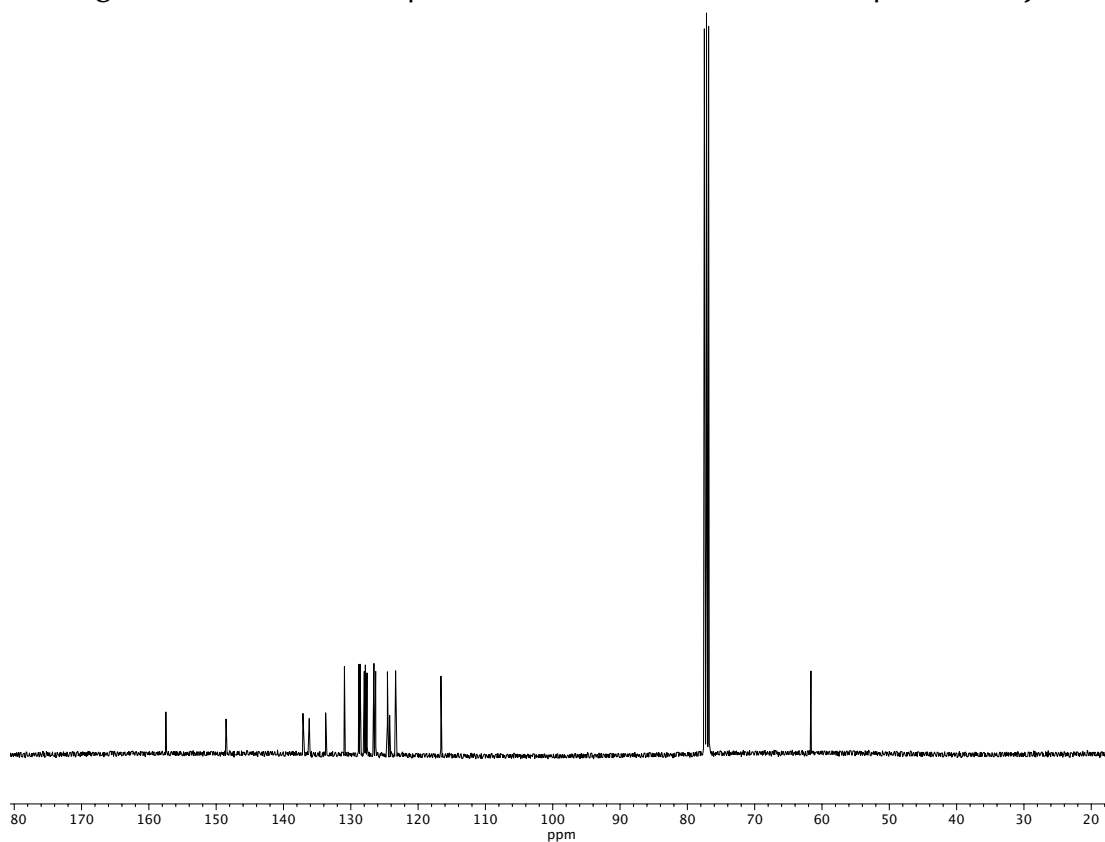


**Figure A1.137**  $^{19}\text{F}$  NMR (282 MHz,  $\text{CDCl}_3$ ) of compound **162i**.



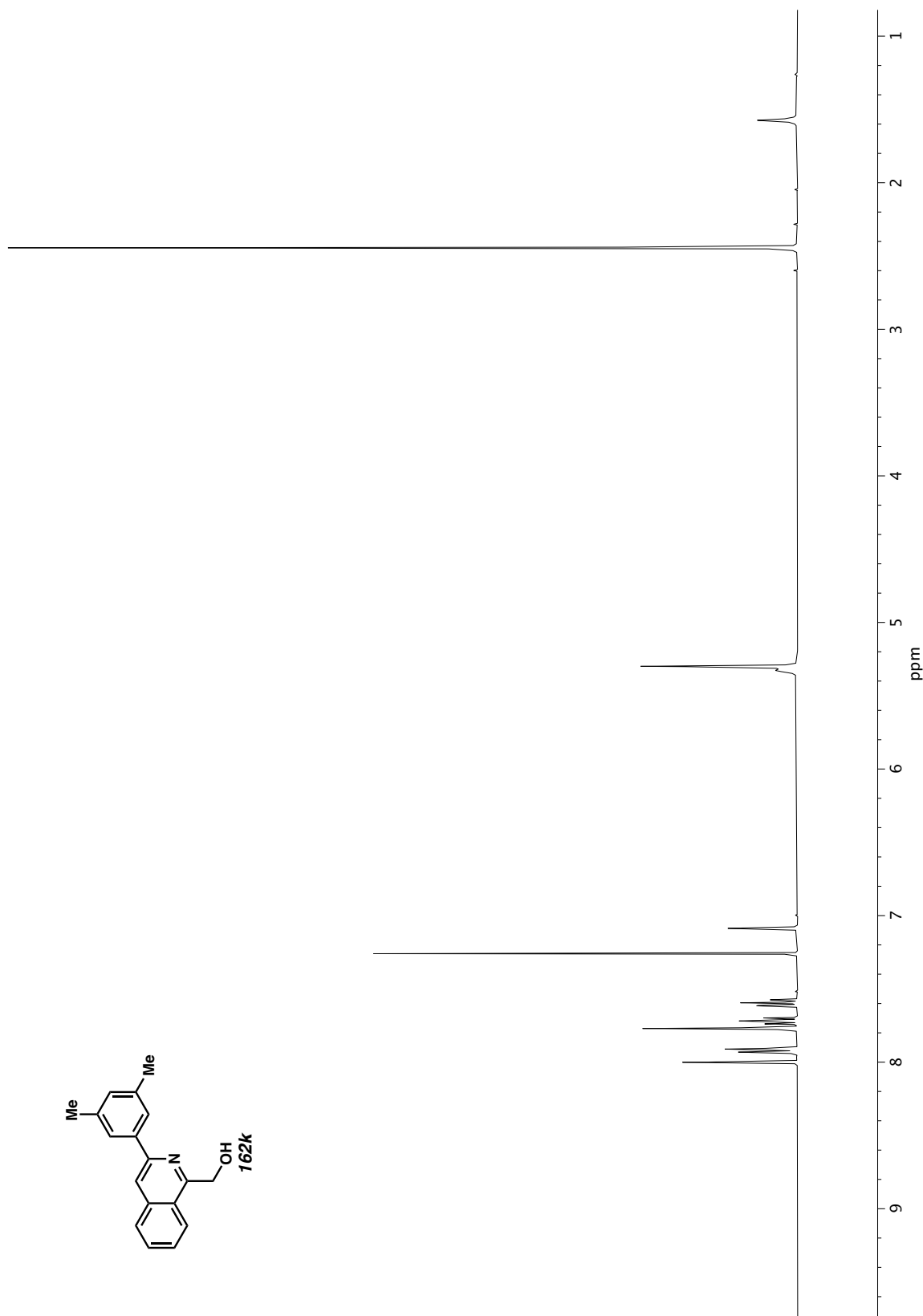


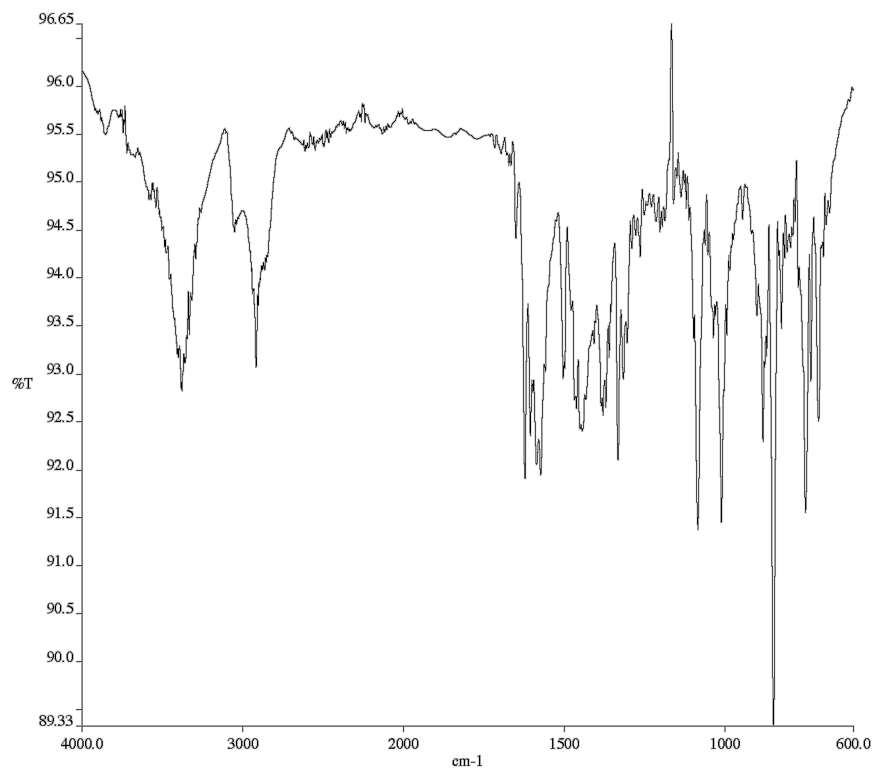
**Figure A1.139** Infrared spectrum (Thin Film, NaCl) of compound **162j**.



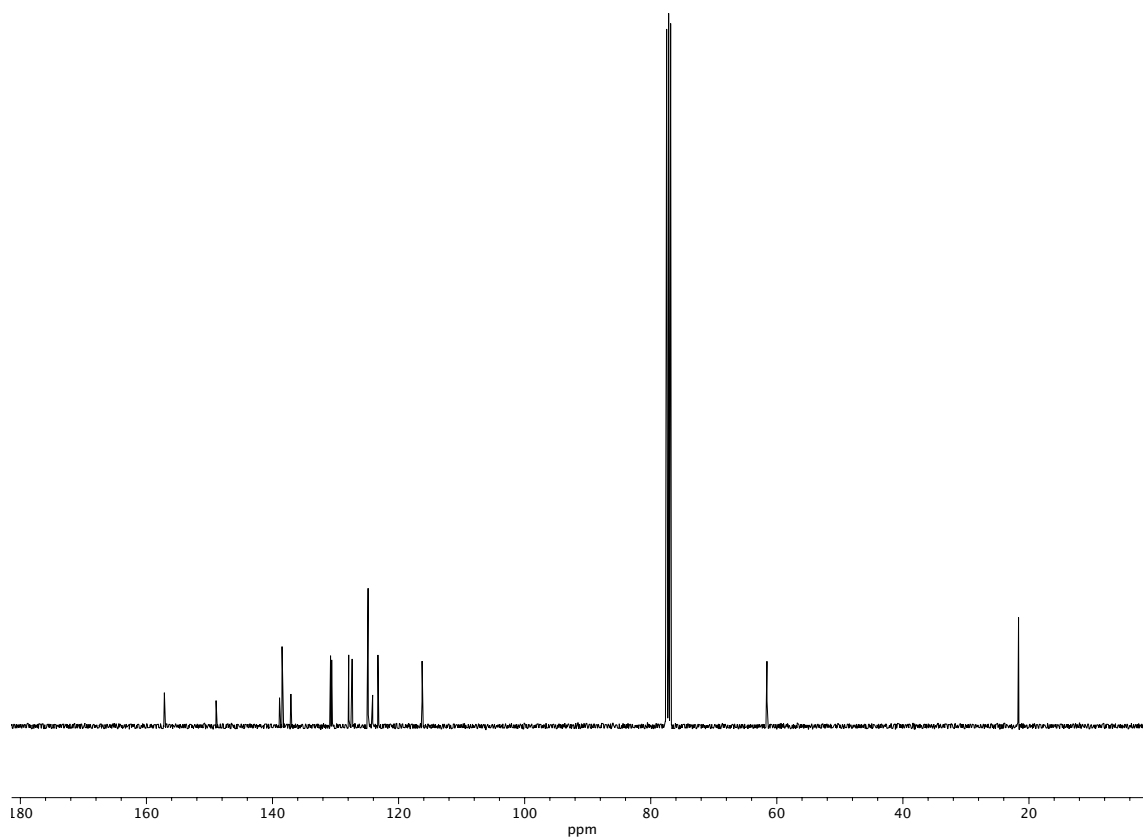
**Figure A1.140** <sup>13</sup>C NMR (100 MHz, CDCl<sub>3</sub>) of compound **162j**.



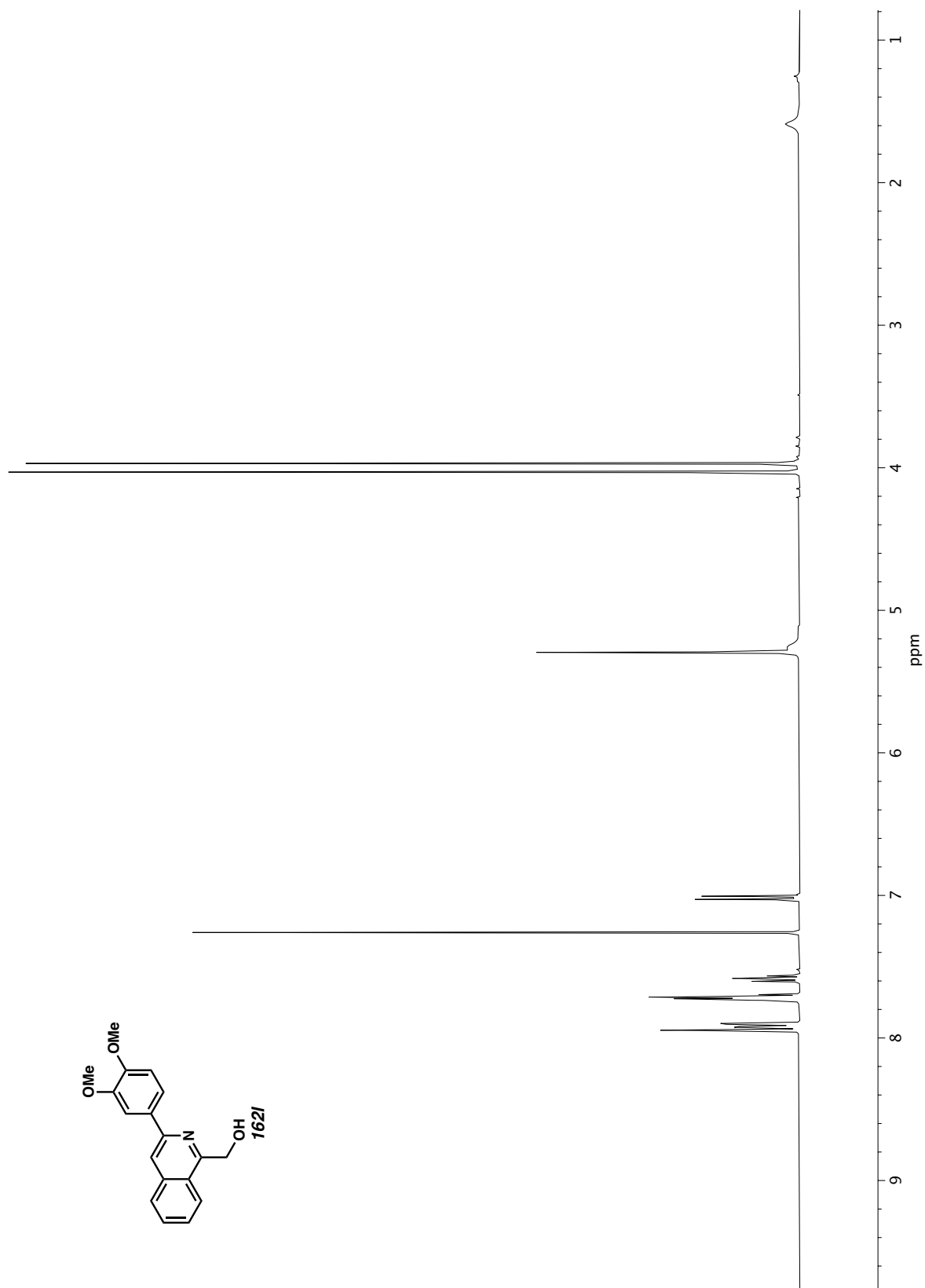


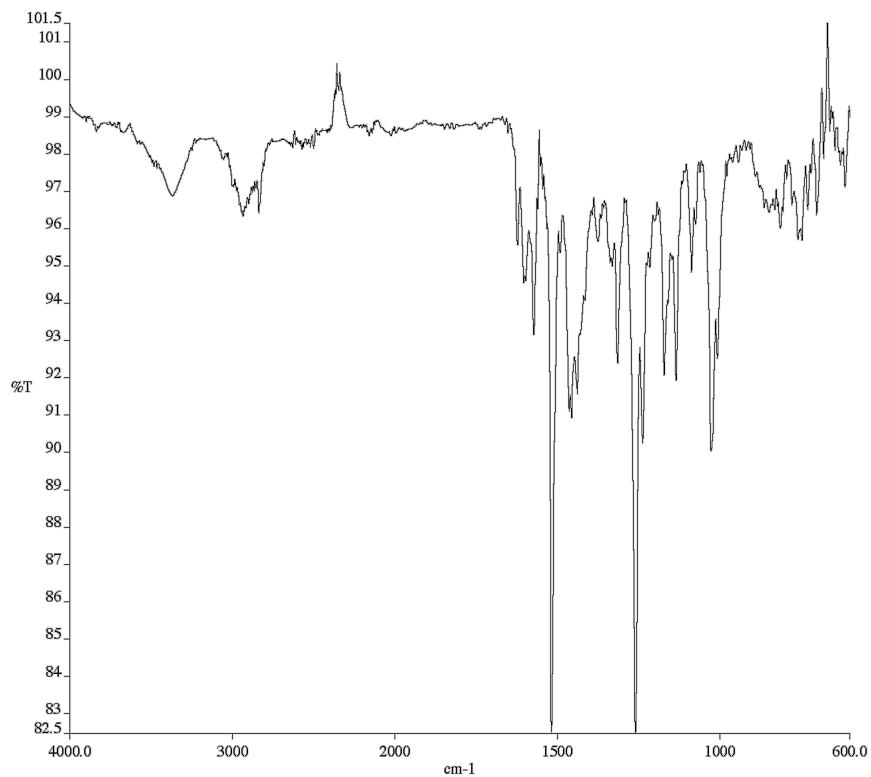


**Figure A1.142** Infrared spectrum (Thin Film, NaCl) of compound **162k**.

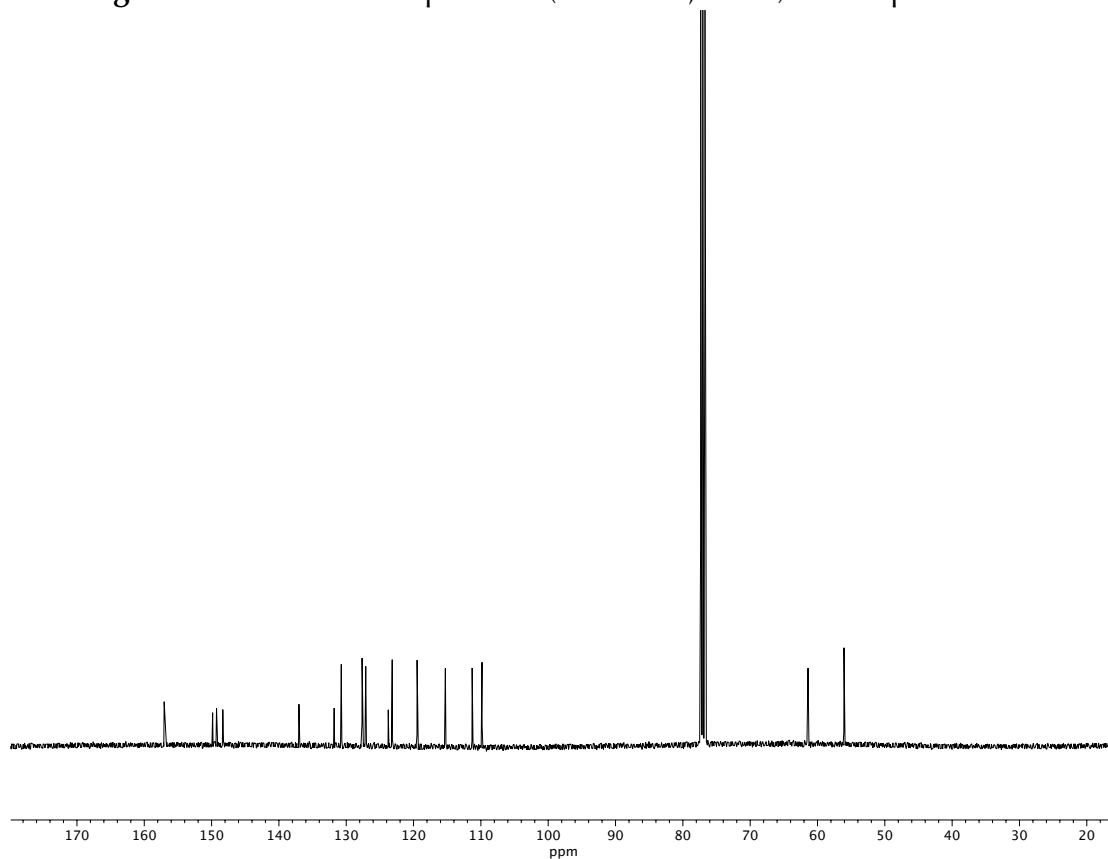


**Figure A1.143** <sup>13</sup>C NMR (100 MHz, CDCl<sub>3</sub>) of compound **162k**.

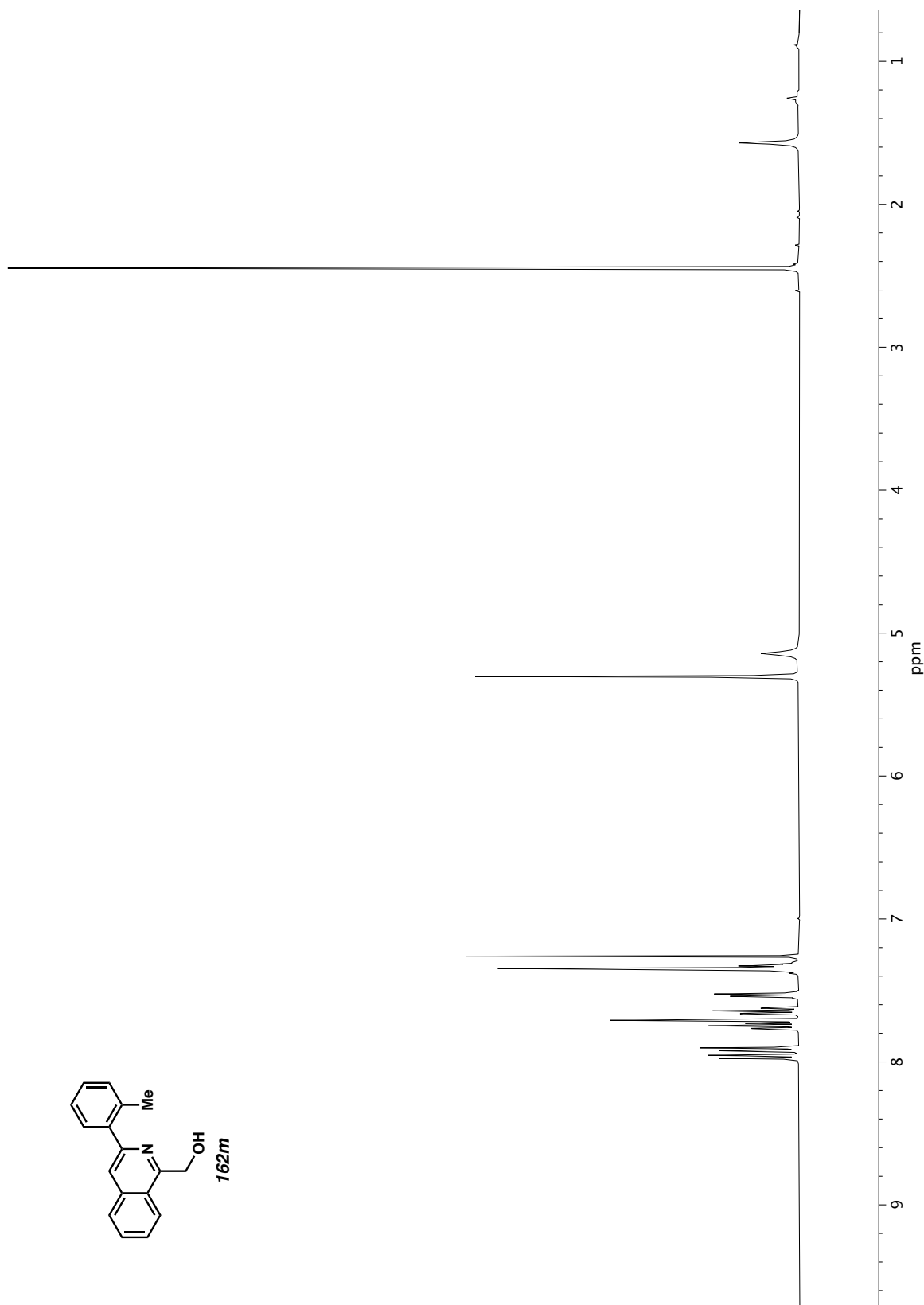


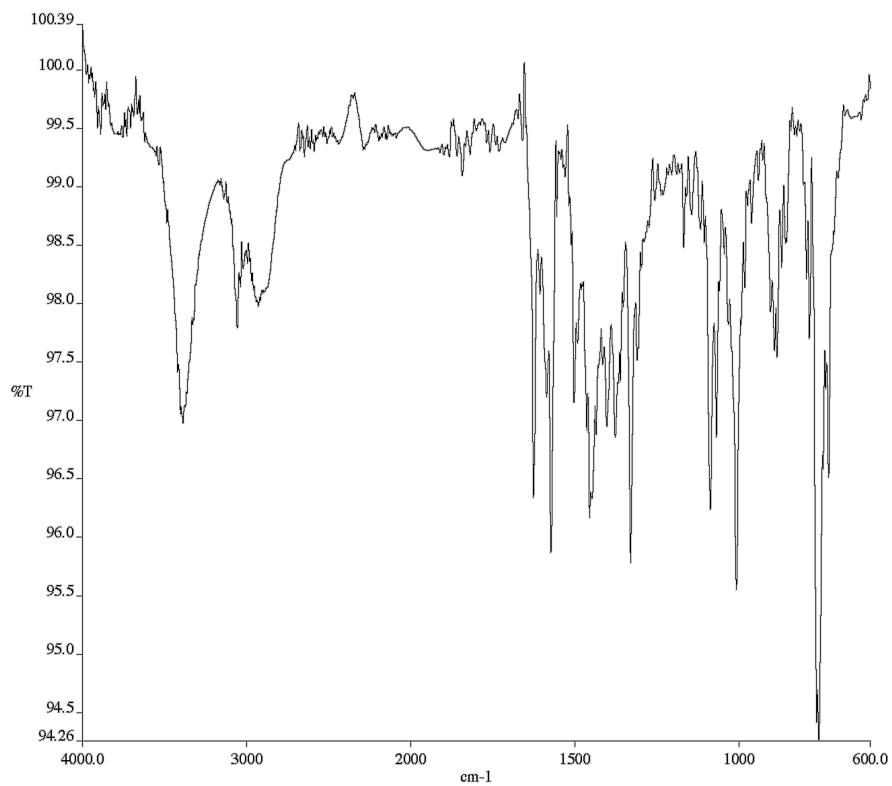


**Figure A1.145** Infrared spectrum (Thin Film, NaCl) of compound **162I**.

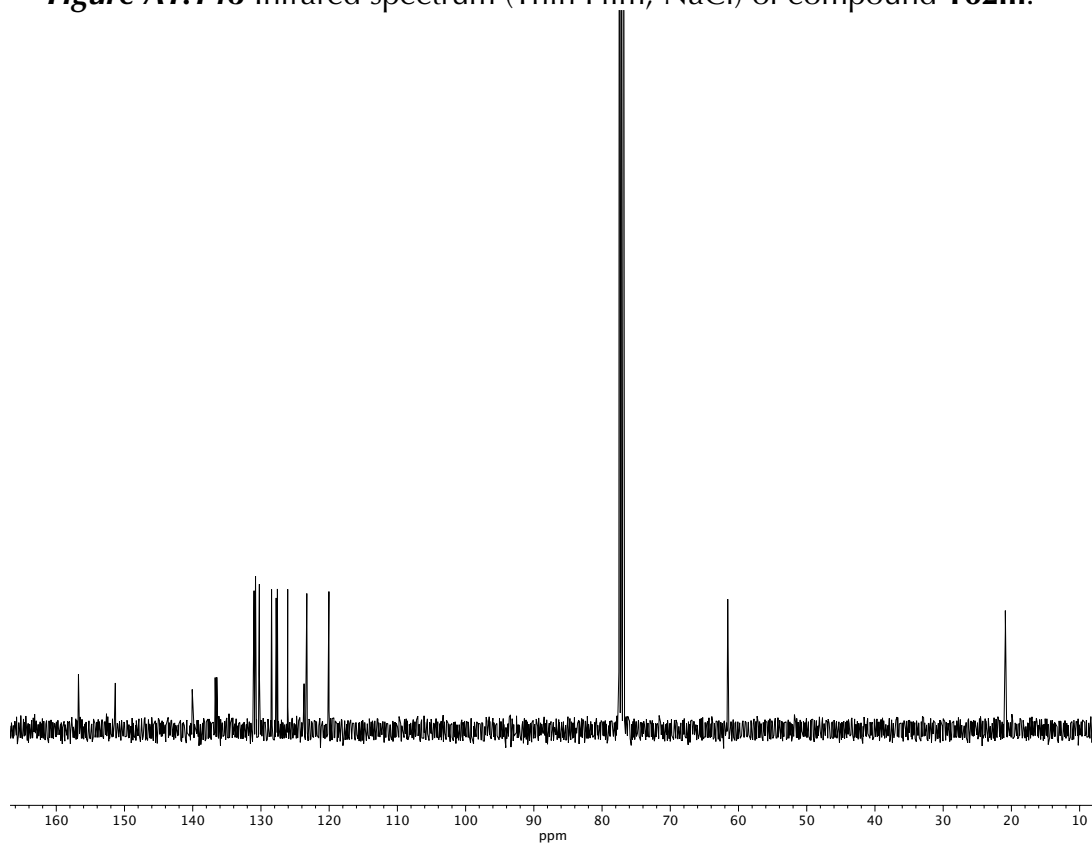


**Figure A1.146** <sup>13</sup>C NMR (100 MHz, CDCl<sub>3</sub>) of compound **162I**.

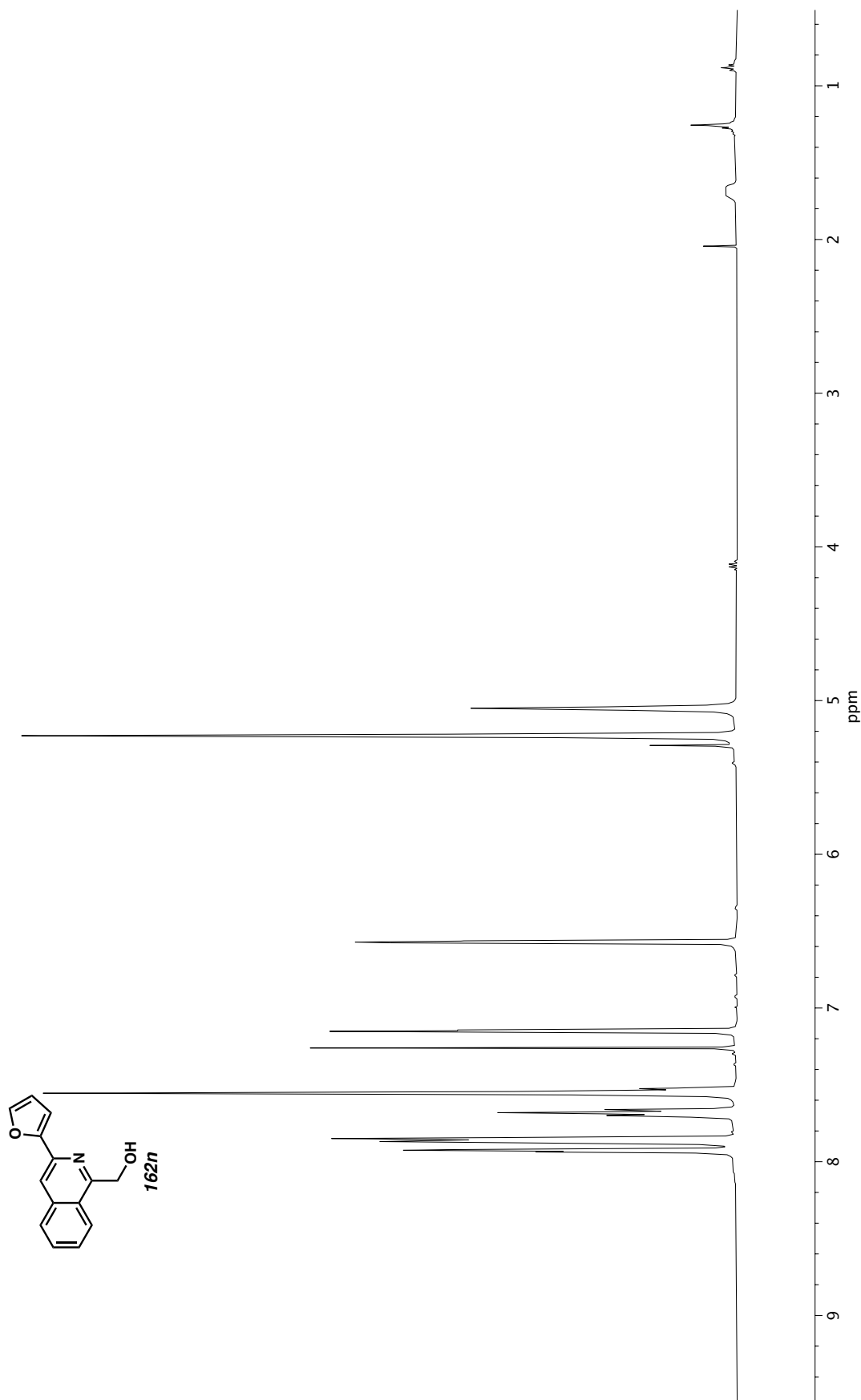




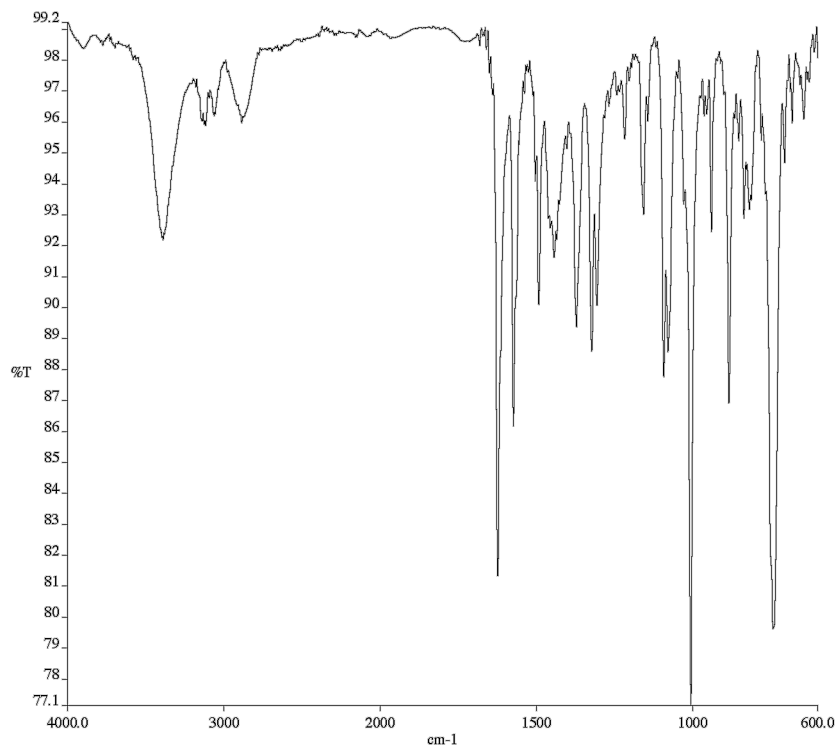
**Figure A1.148** Infrared spectrum (Thin Film, NaCl) of compound **162m**.



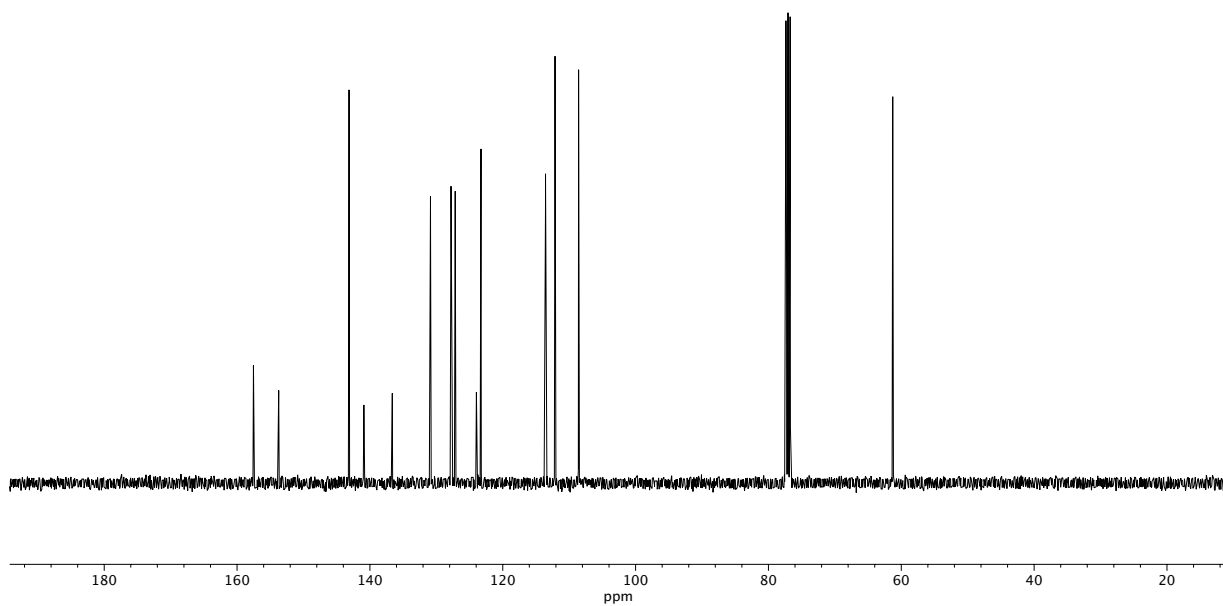
**Figure A1.149** <sup>13</sup>C NMR (100 MHz, CDCl<sub>3</sub>) of compound **162m**.



**Figure A1.150**  $^1\text{H}$  NMR (400 MHz,  $\text{CDCl}_3$ ) of compound **162n**.

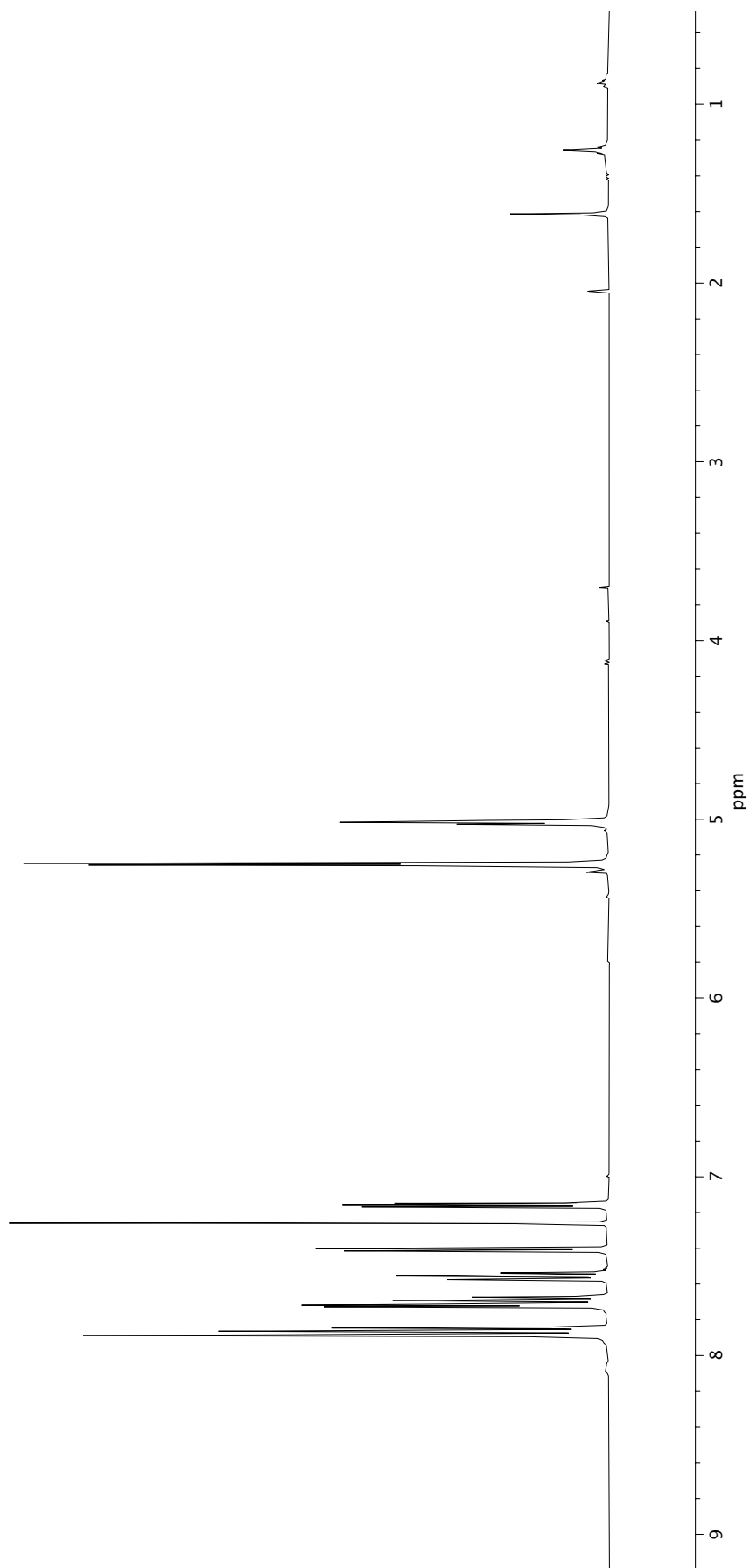
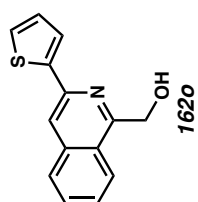


**Figure A1.151** Infrared spectrum (Thin Film, NaCl) of compound **162n**.

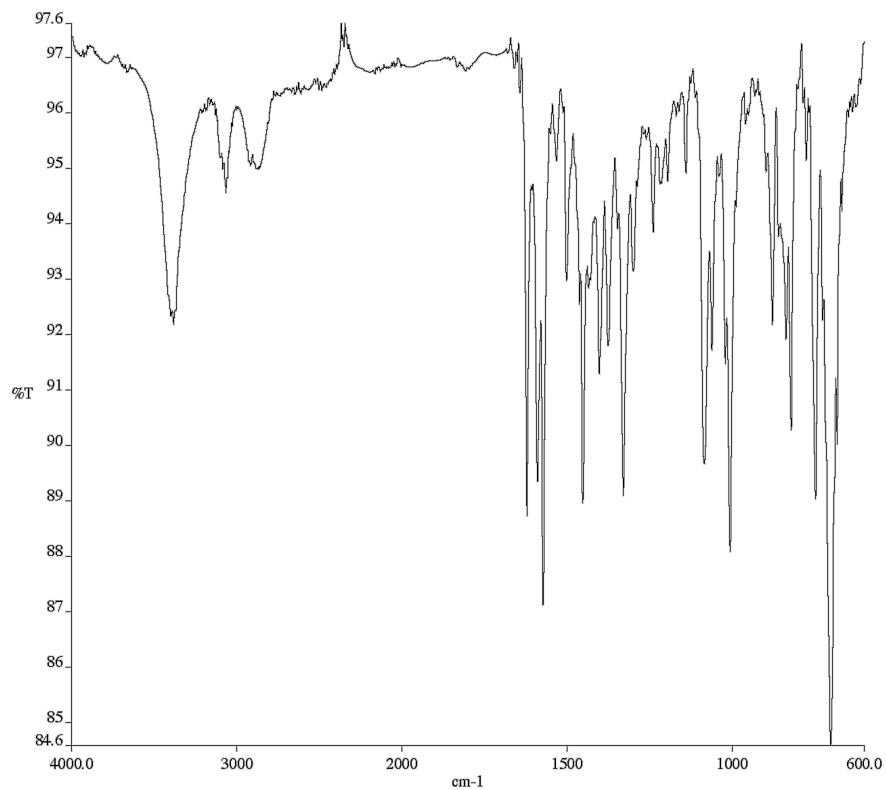


**Figure A1.152** <sup>13</sup>C NMR (100 MHz, CDCl<sub>3</sub>) of compound **162n**.

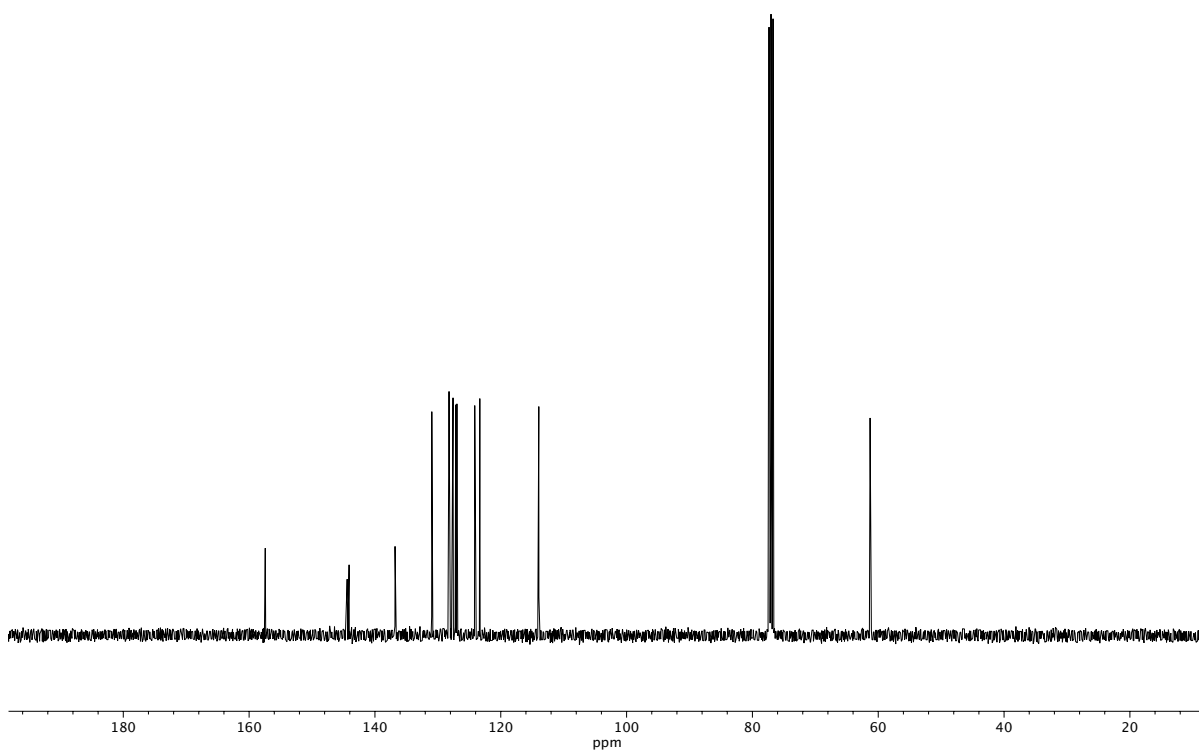




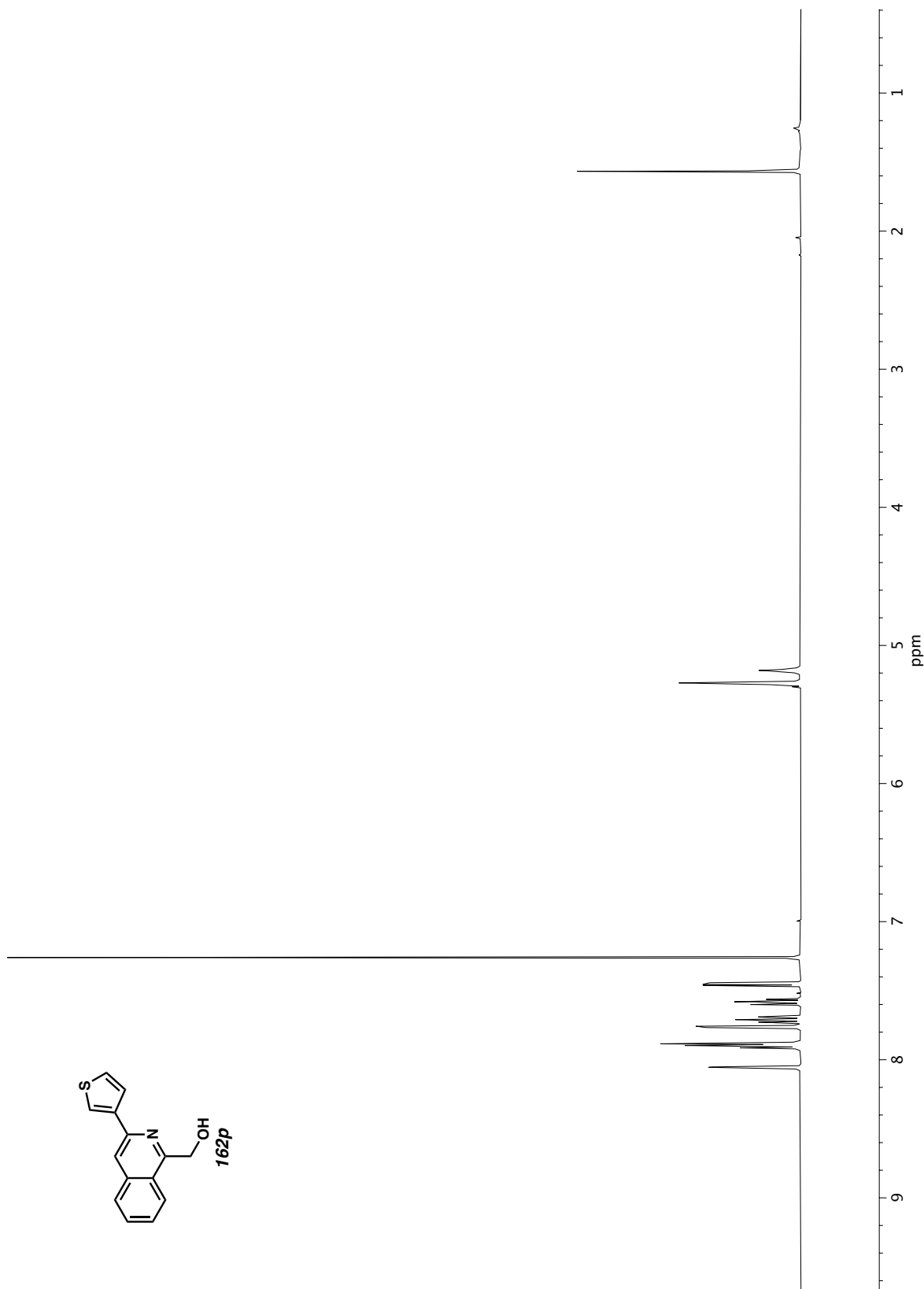
**Figure A1.153** <sup>1</sup>H NMR (400 MHz, CDCl<sub>3</sub>) of compound **1620**.



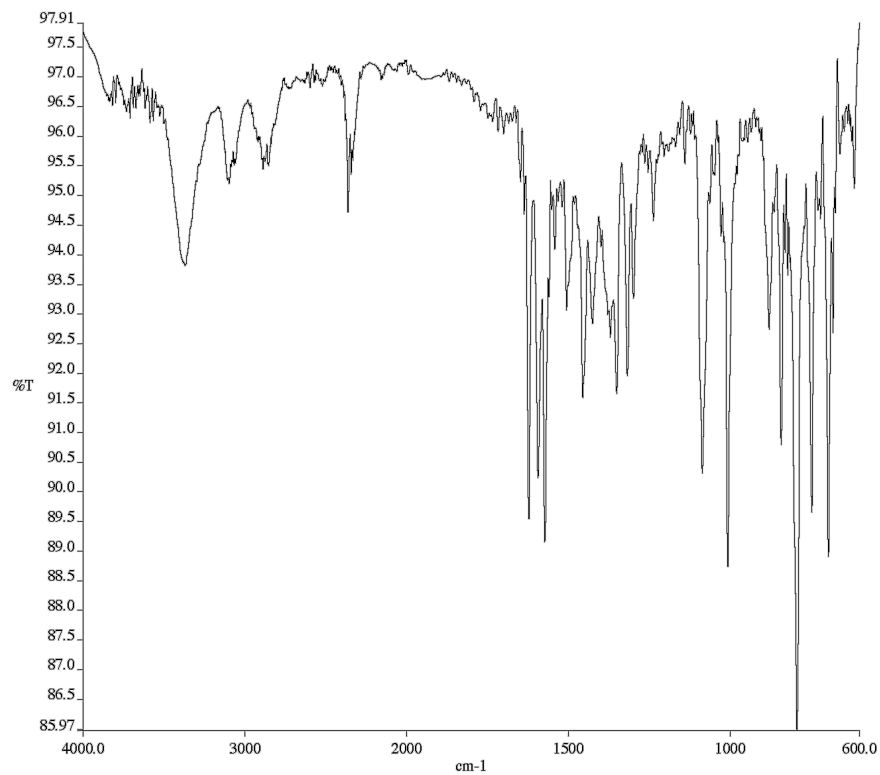
**Figure A1.154** Infrared spectrum (Thin Film, NaCl) of compound **162o**.



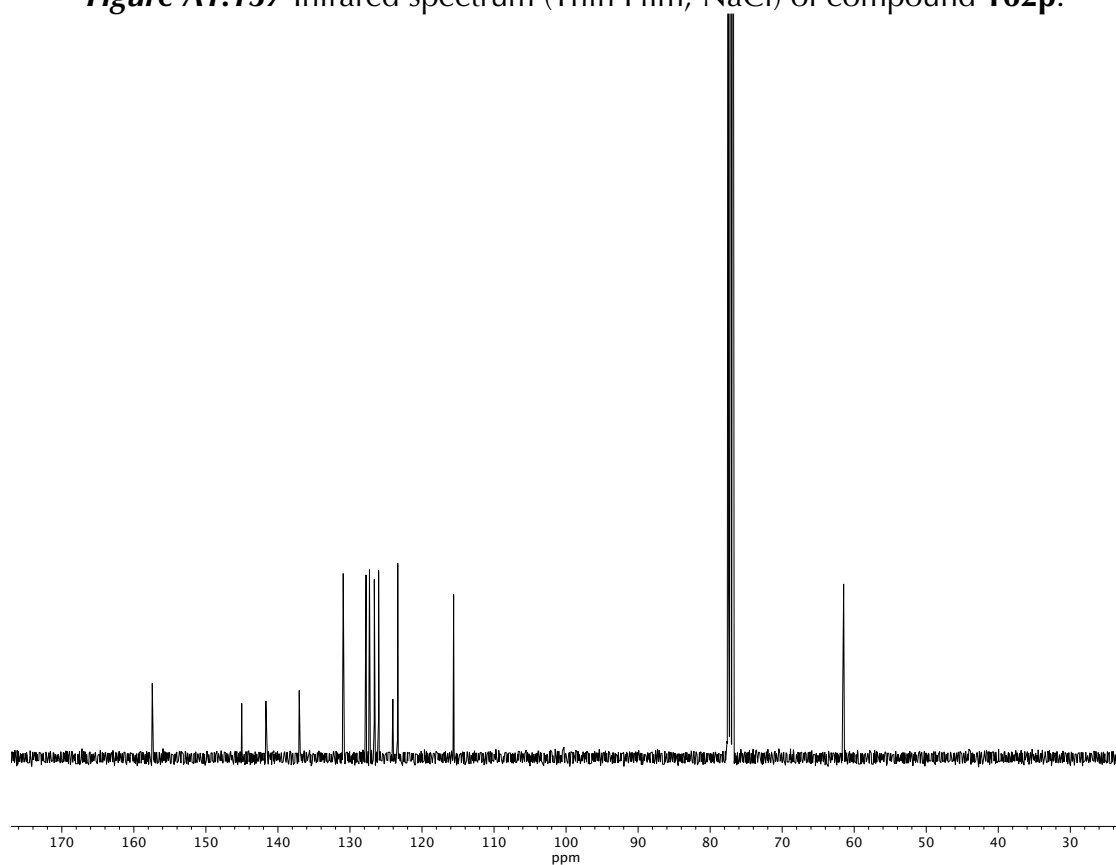
**Figure A1.155** <sup>13</sup>C NMR (100 MHz, CDCl<sub>3</sub>) of compound **162o**.



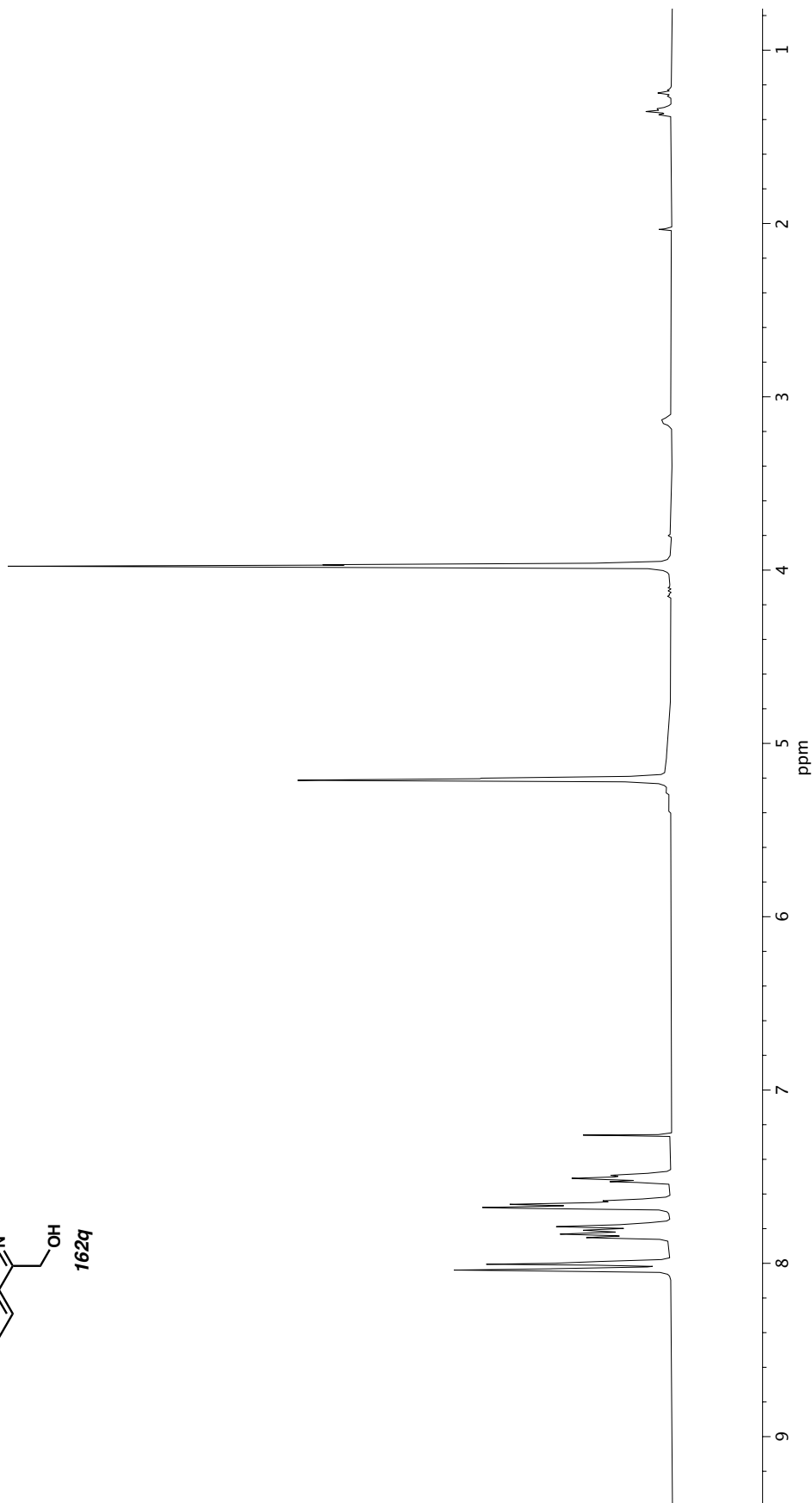
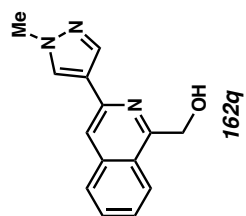
**Figure A1.156** <sup>1</sup>H NMR (400 MHz, CDCl<sub>3</sub>) of compound **162p**.



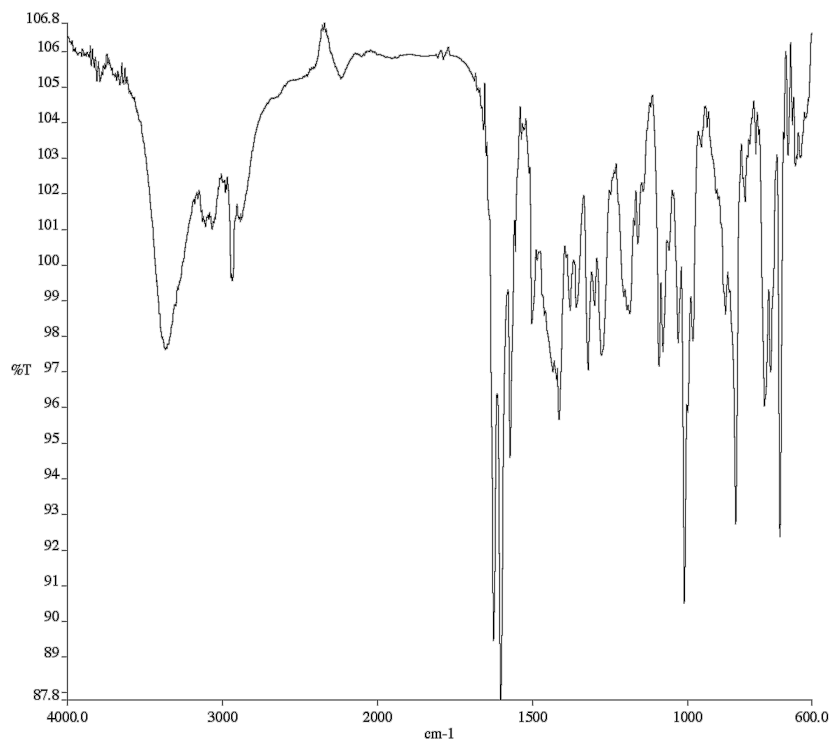
**Figure A1.157** Infrared spectrum (Thin Film, NaCl) of compound **162p**.



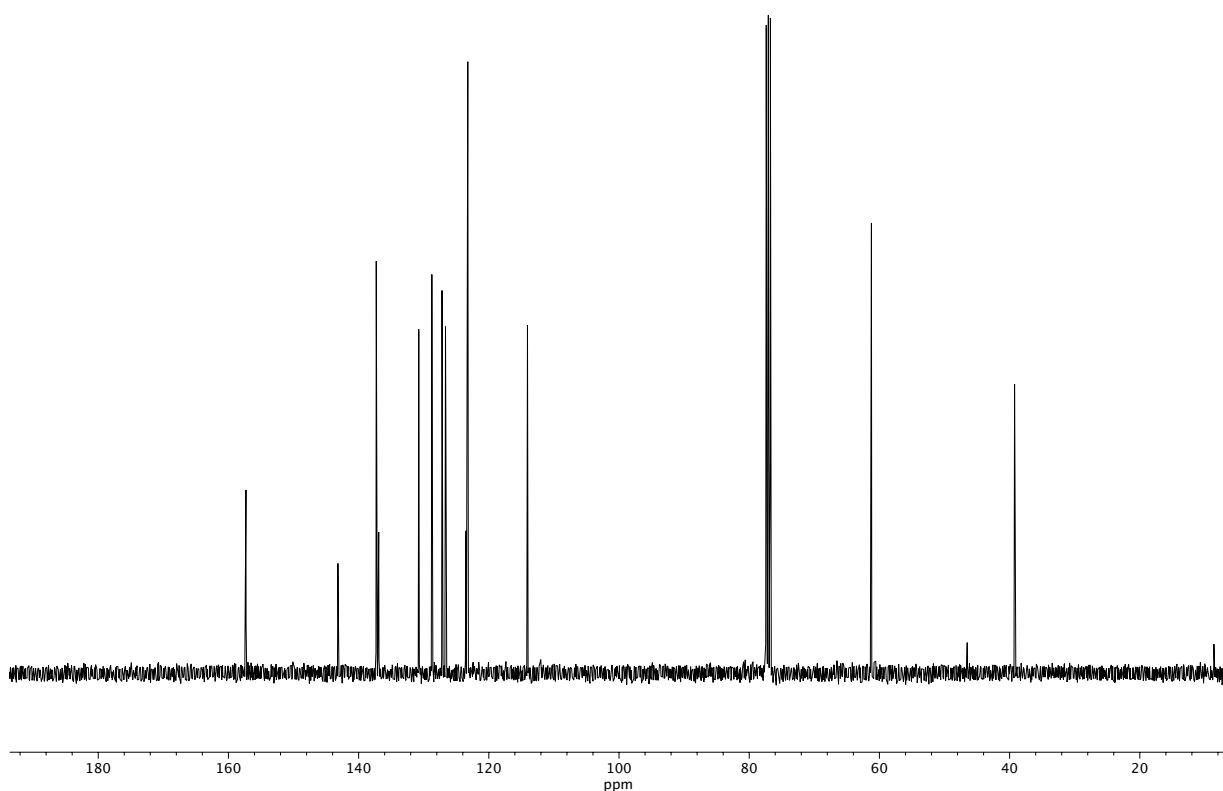
**Figure A1.158** <sup>13</sup>C NMR (100 MHz, CDCl<sub>3</sub>) of compound **162p**.



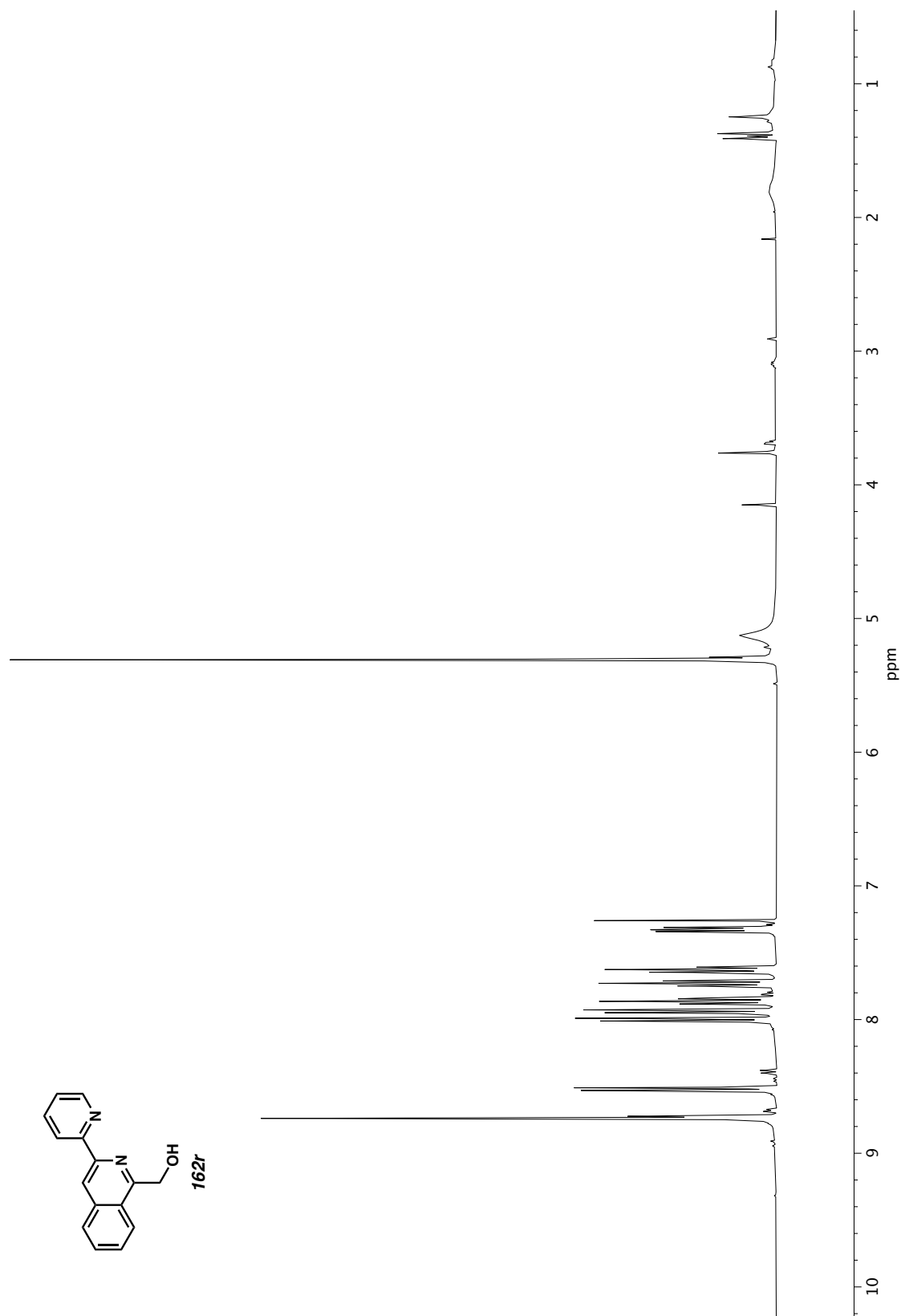
**Figure A1.159** <sup>1</sup>H NMR (400 MHz, CDCl<sub>3</sub>) of compound **162q**.



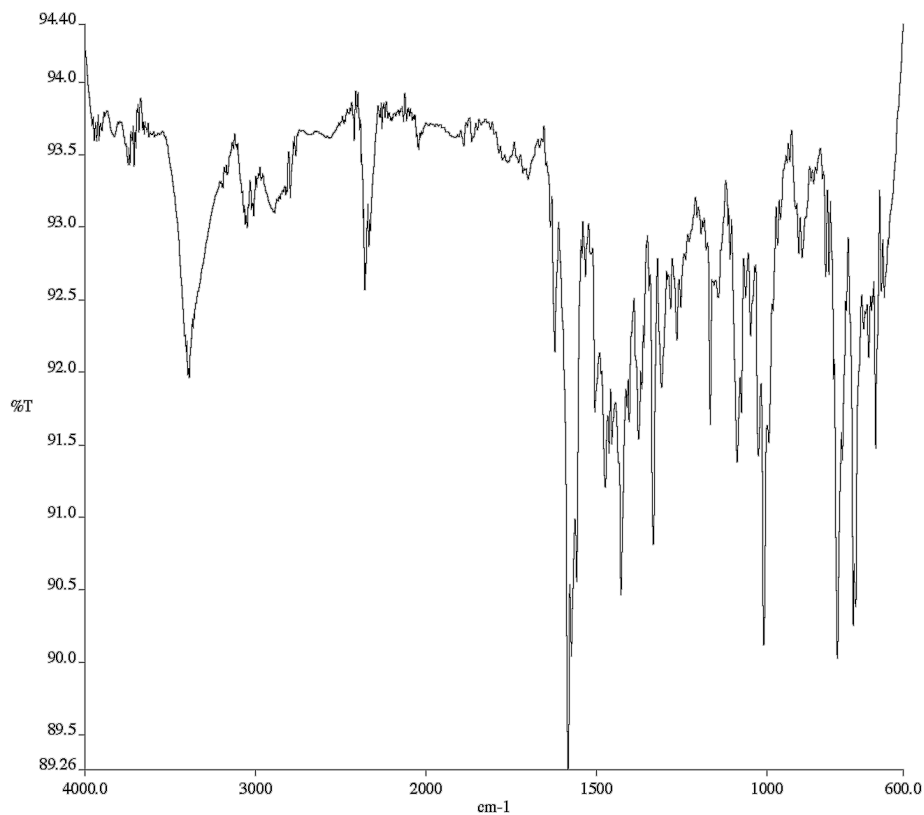
**Figure A1.160** Infrared spectrum (Thin Film, NaCl) of compound **162q**.



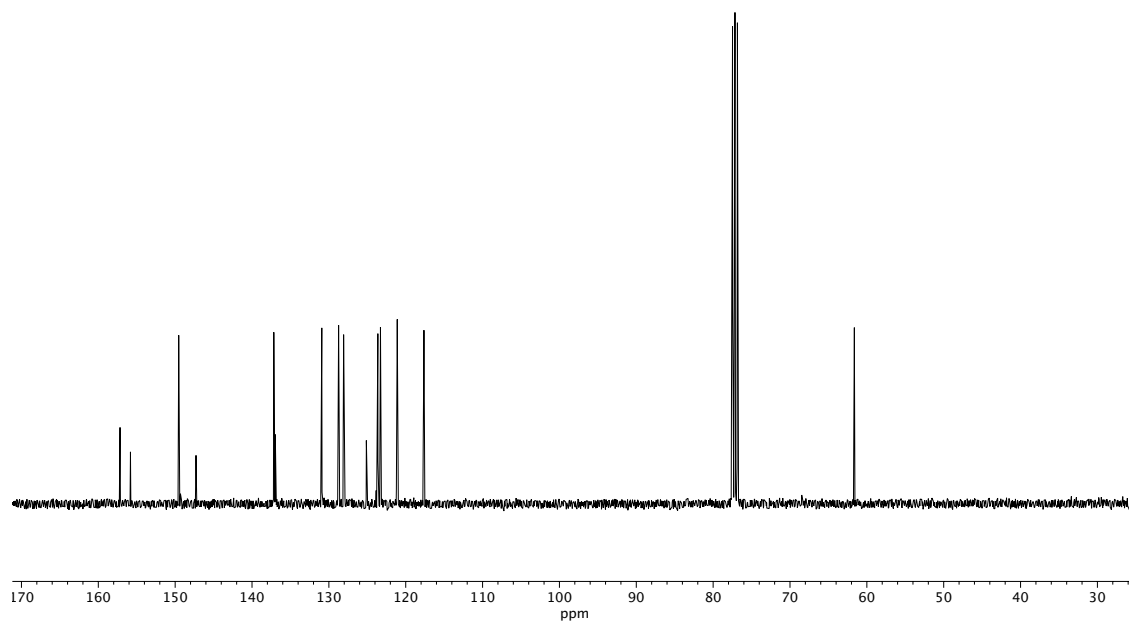
**Figure A1.161** <sup>13</sup>C NMR (100 MHz, CDCl<sub>3</sub>) of compound **162q**.



**Figure A1.162**  $^1\text{H}$  NMR (400 MHz,  $\text{CDCl}_3$ ) of compound **162r**.

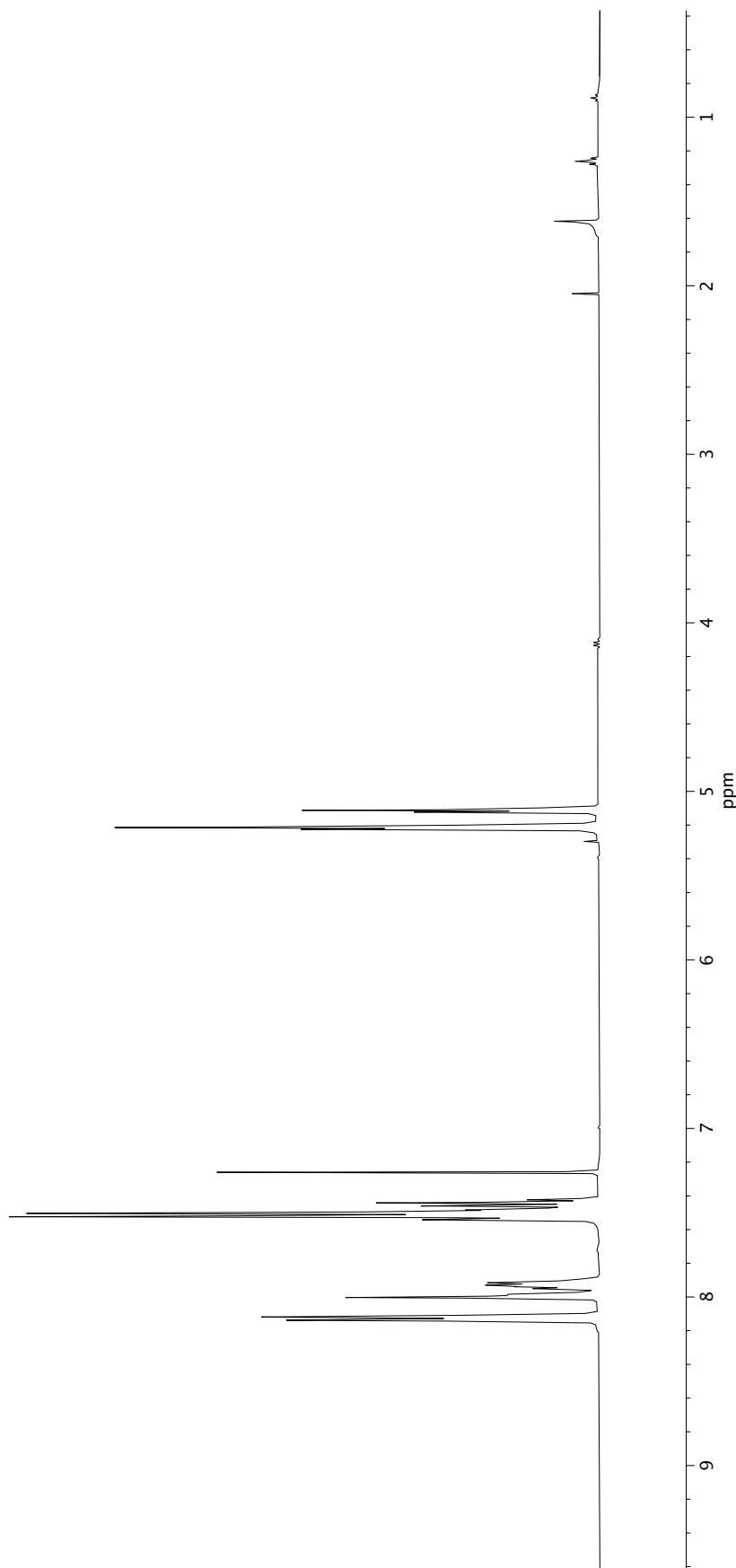
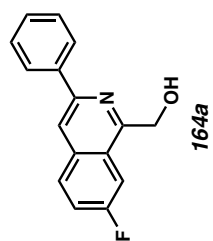


**Figure A1.163** Infrared spectrum (Thin Film, NaCl) of compound **162r**.

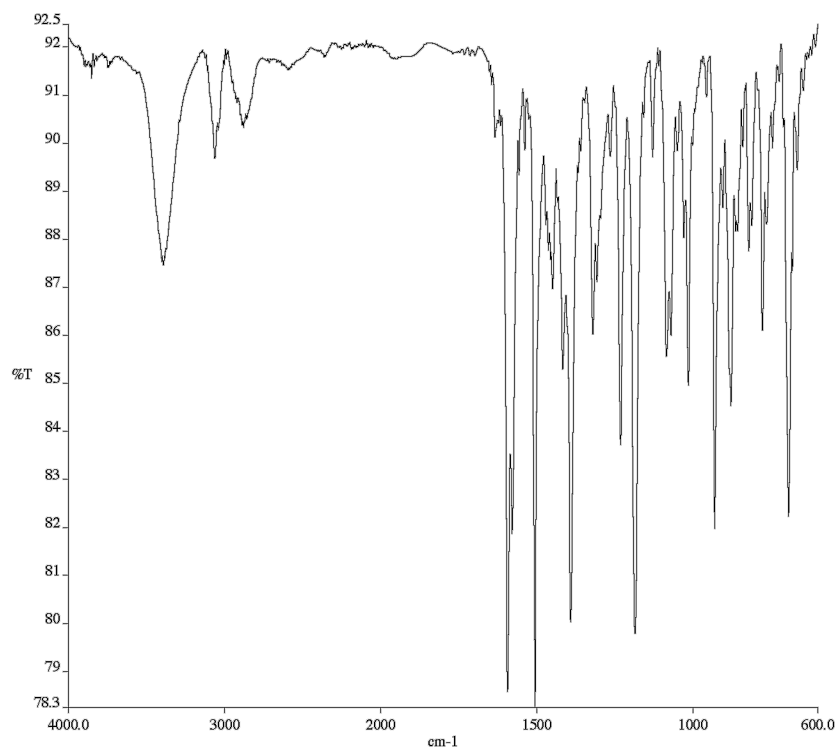


**Figure A1.164** <sup>13</sup>C NMR (100 MHz, CDCl<sub>3</sub>) of compound **162r**.

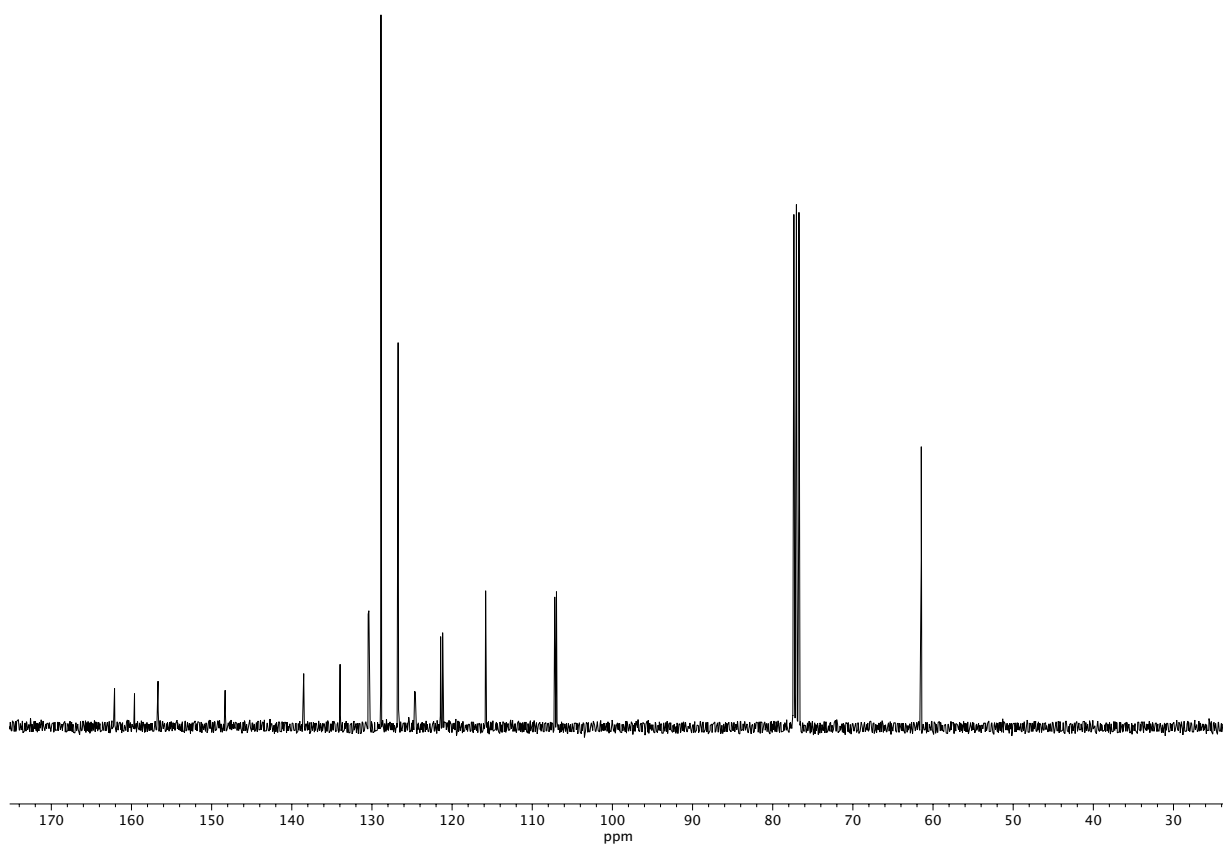




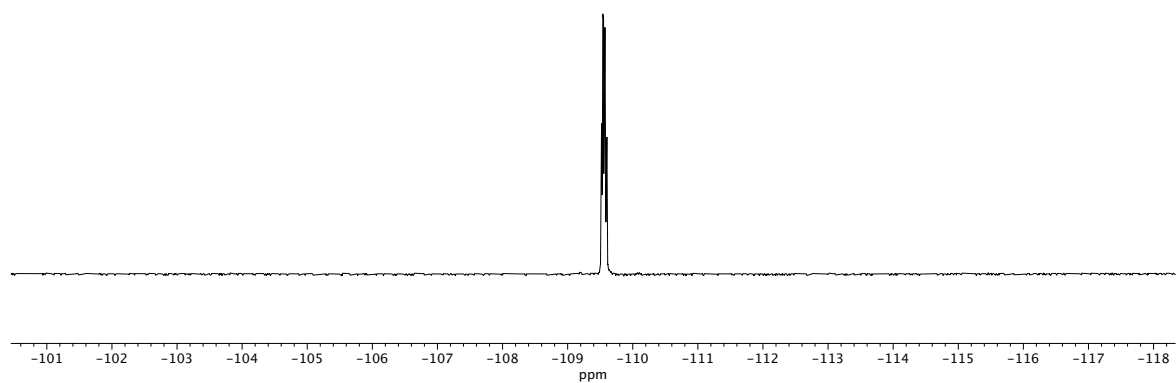
**Figure A1.165** <sup>1</sup>H NMR (400 MHz, CDCl<sub>3</sub>) of compound **164a**.



**Figure A1.166** Infrared spectrum (Thin Film, NaCl) of compound **164a**.

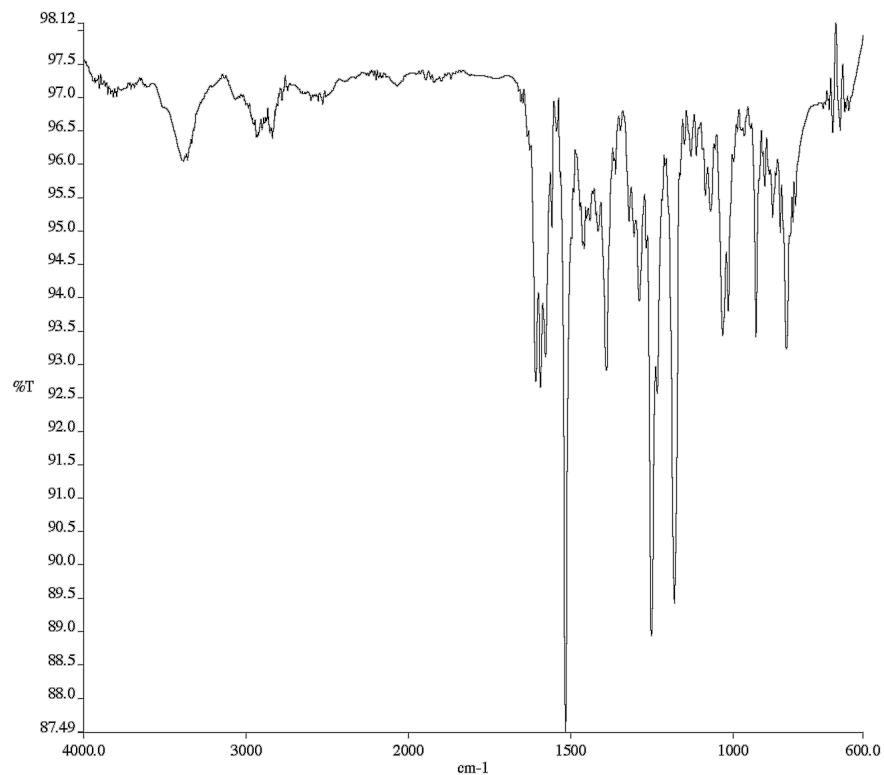


**Figure A1.167** <sup>13</sup>C NMR (100 MHz, CDCl<sub>3</sub>) of compound **164a**.

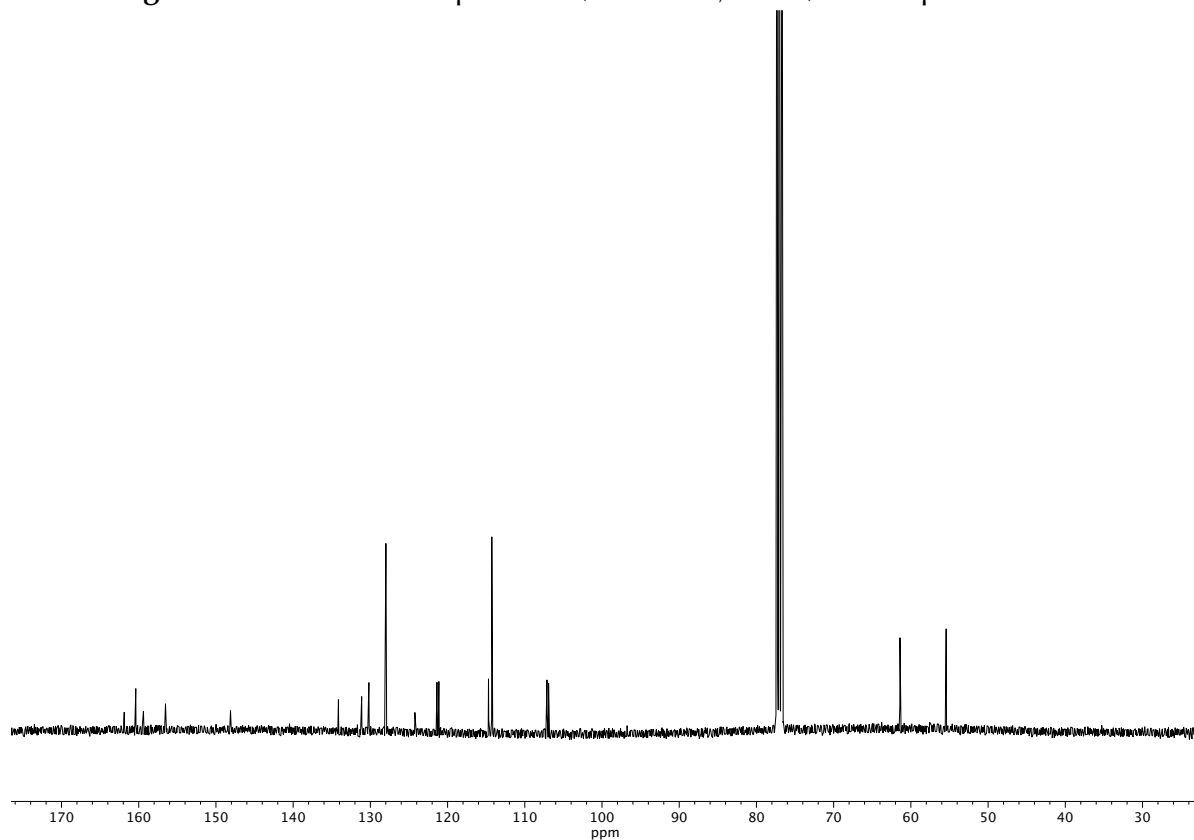


**Figure A1.168**  $^{19}\text{F}$  NMR (282 MHz,  $\text{CDCl}_3$ ) of compound **164a**.

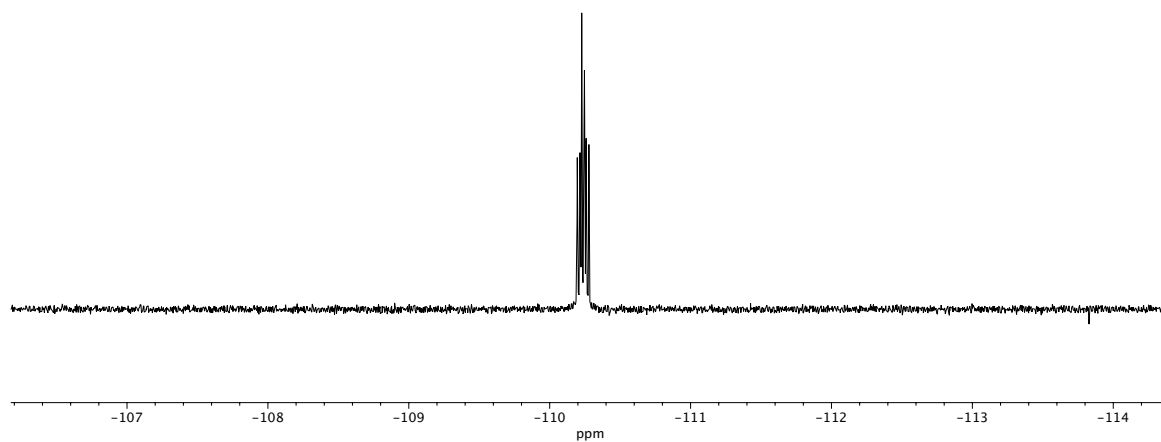




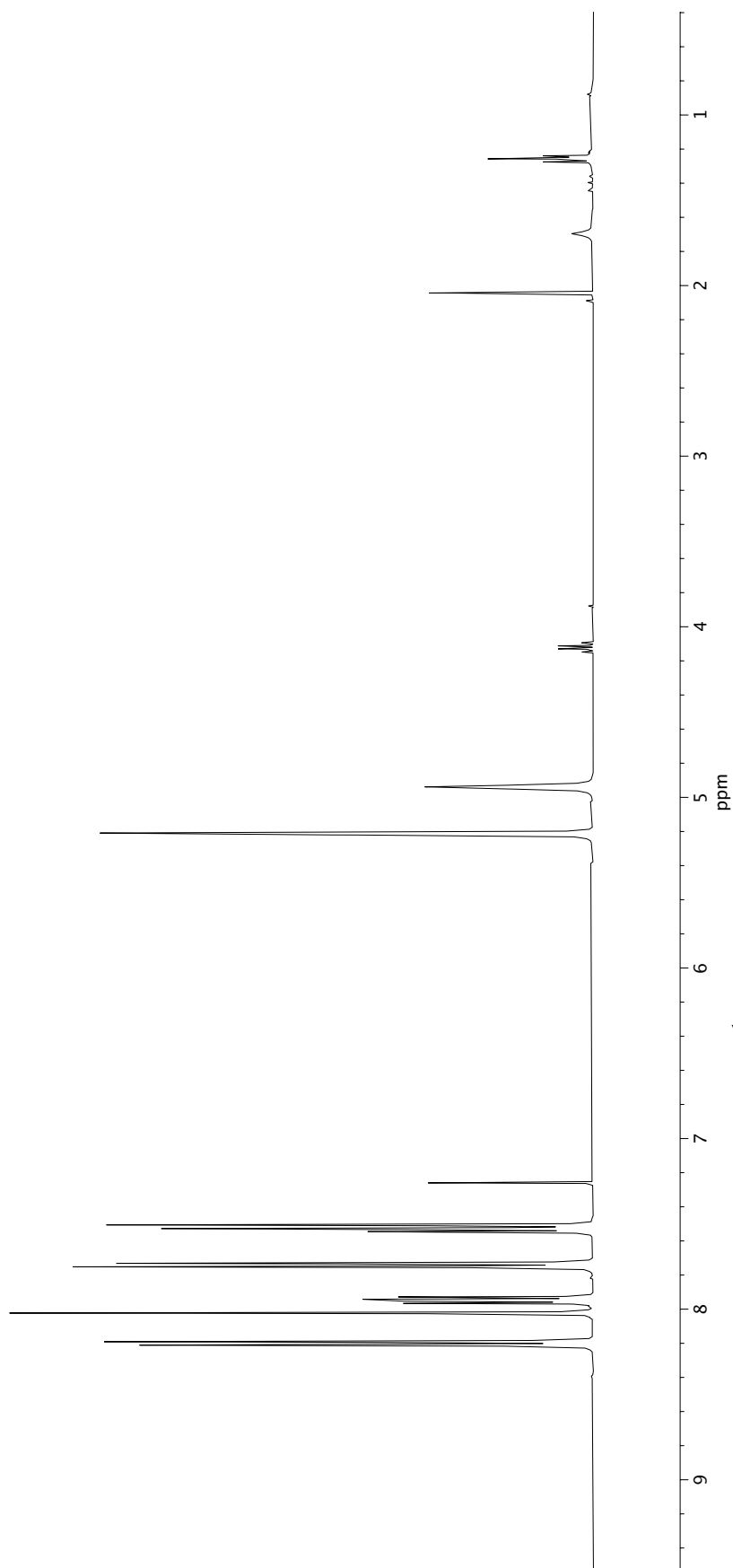
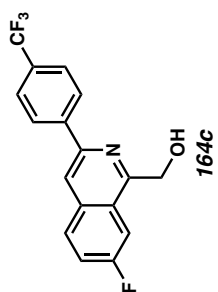
**Figure A1.170** Infrared spectrum (Thin Film, NaCl) of compound **164b**.



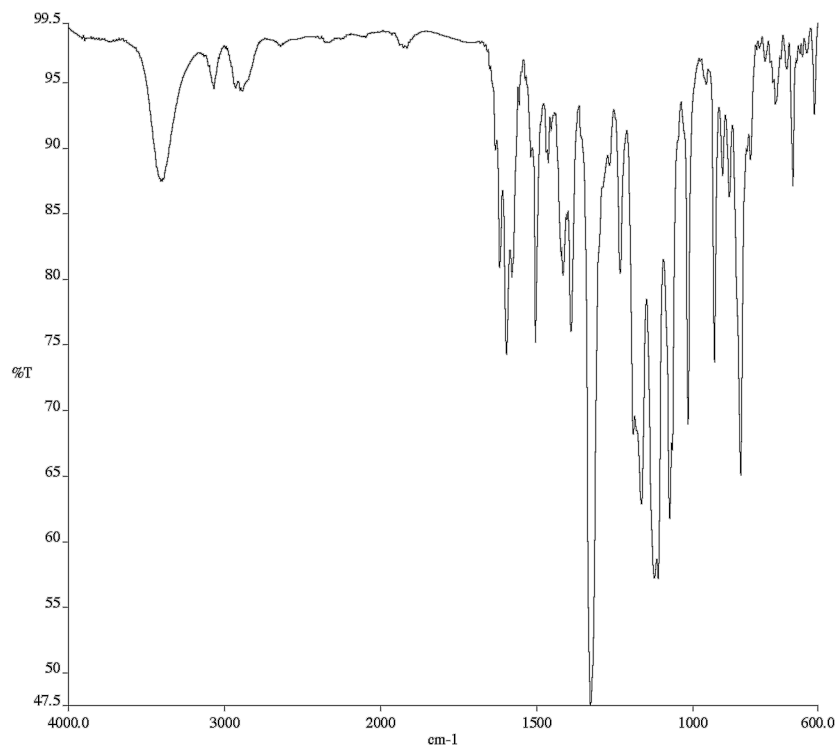
**Figure A1.171** <sup>13</sup>C NMR (100 MHz, CDCl<sub>3</sub>) of compound **164b**.



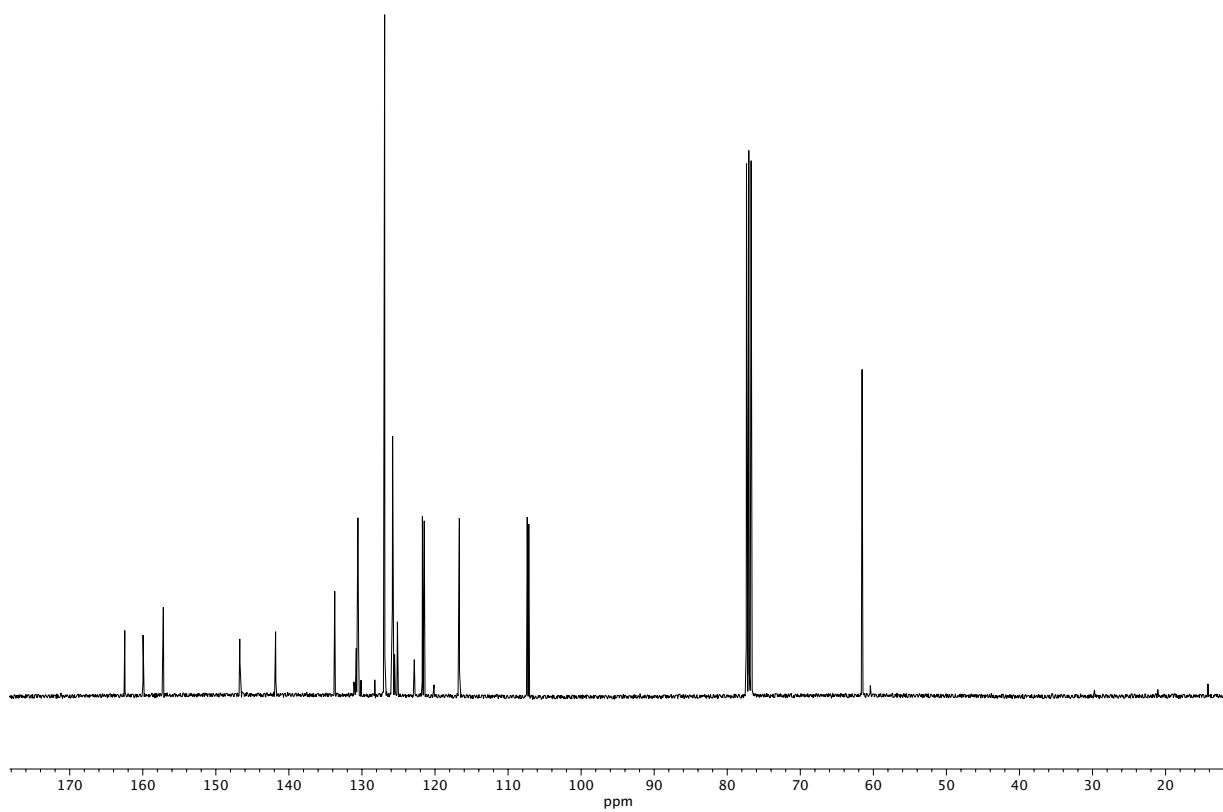
**Figure A1.172**  $^{19}\text{F}$  NMR (282 MHz,  $\text{CDCl}_3$ ) of compound **164b**.



**Figure A1.173** <sup>1</sup>H NMR (400 MHz, CDCl<sub>3</sub>) of compound **164c**.

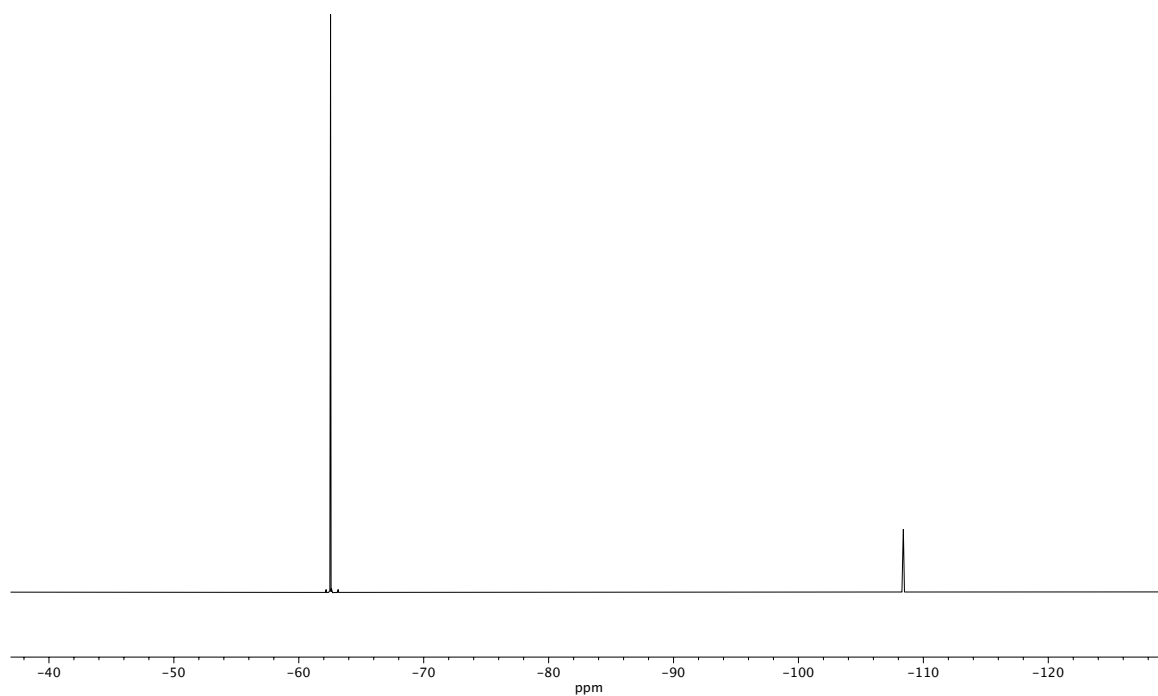


**Figure A1.174** Infrared spectrum (Thin Film, NaCl) of compound **164c**.

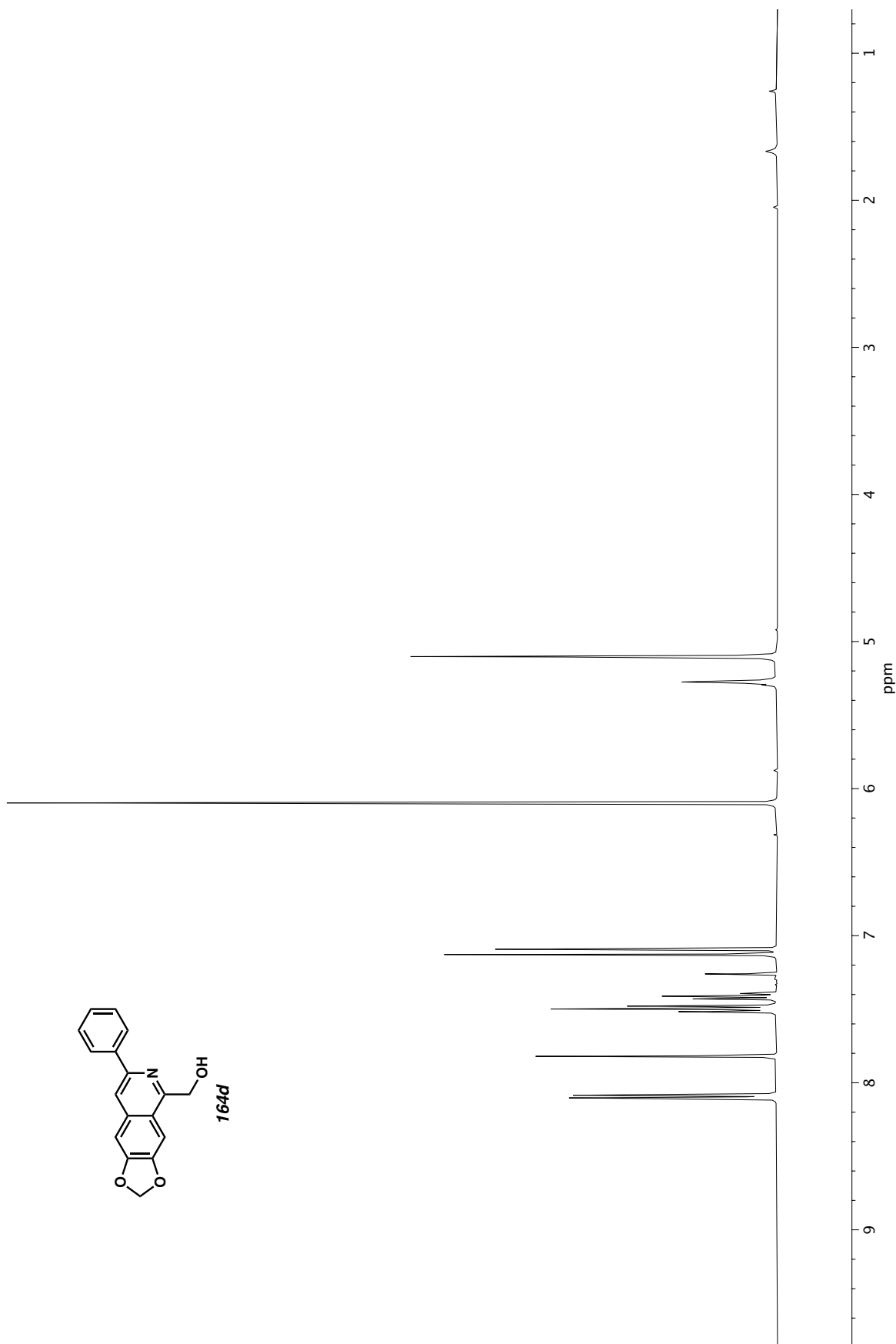


**Figure A1.175** <sup>13</sup>C NMR (100 MHz, CDCl<sub>3</sub>) of compound **164c**.

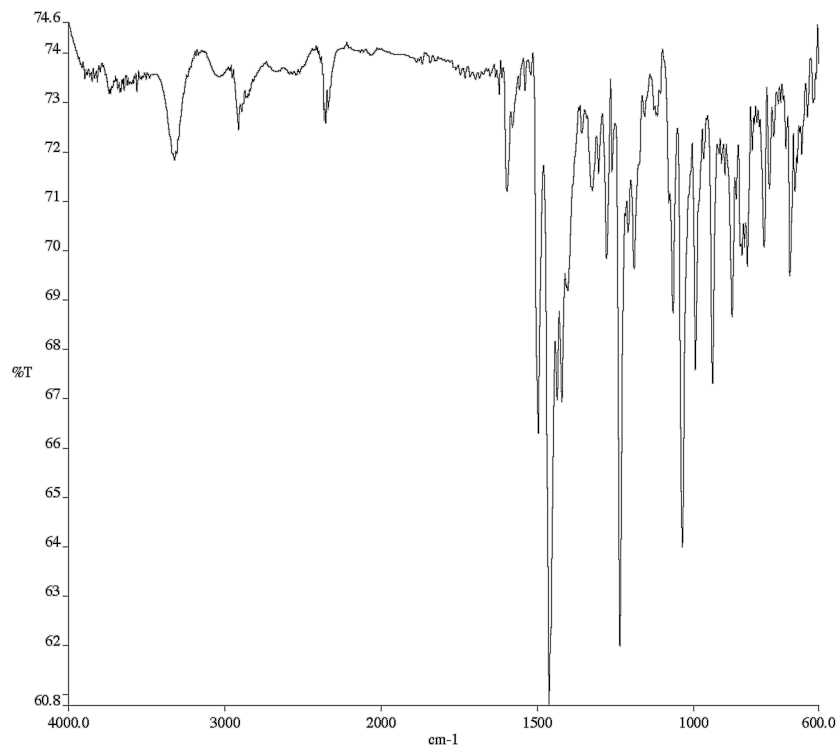




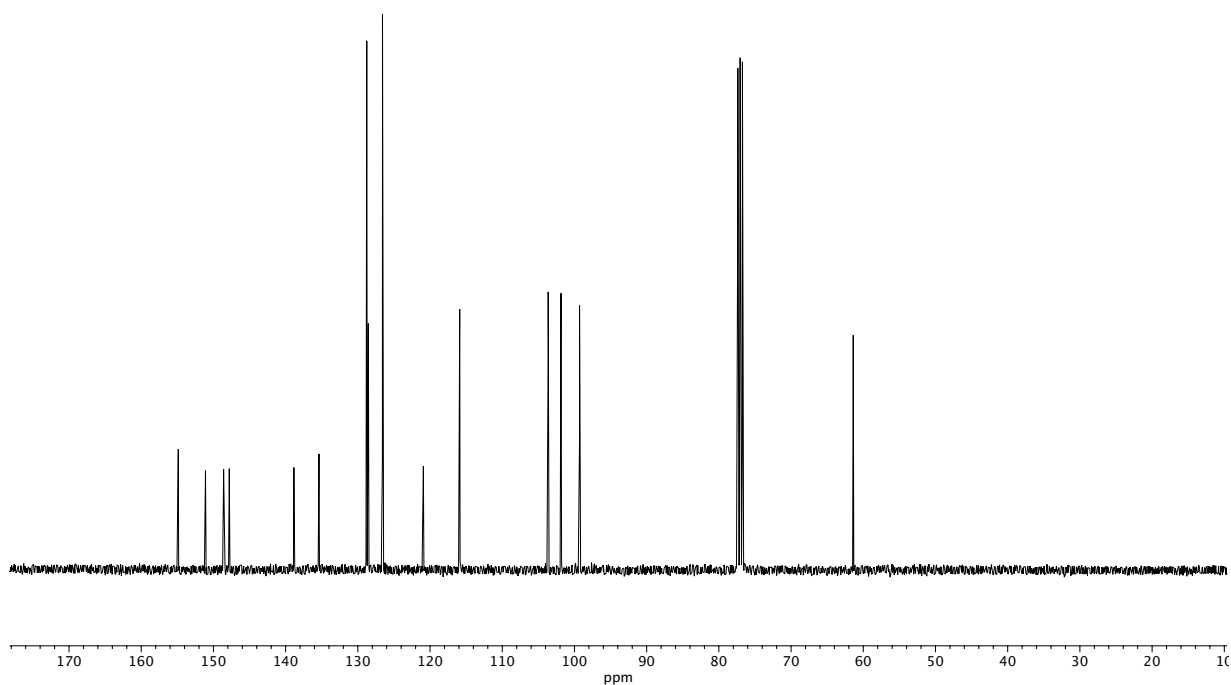
**Figure A1.176**  $^{19}\text{F}$  NMR (282 MHz,  $\text{CDCl}_3$ ) of compound **164c**.



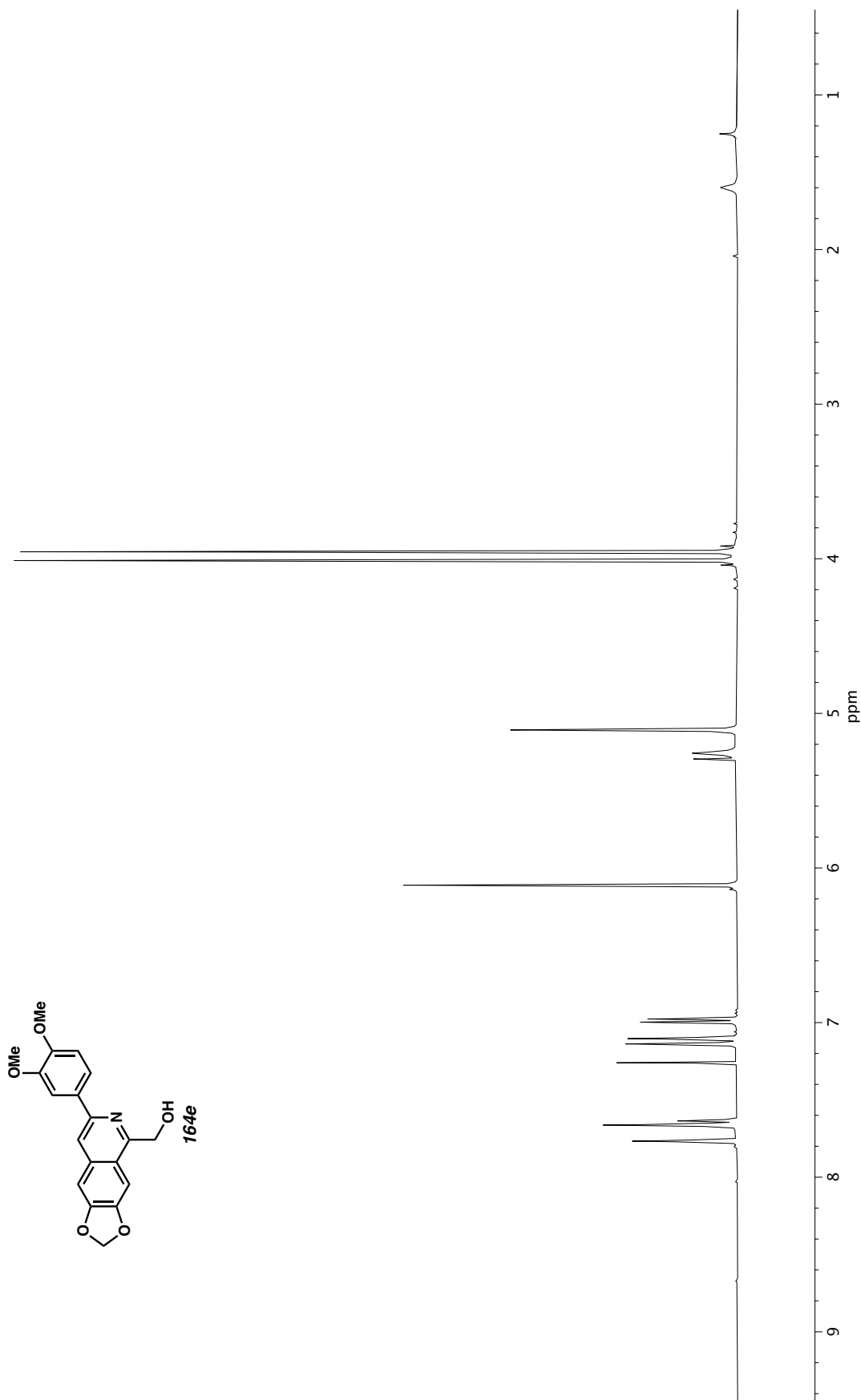
**Figure A1.177**  $^1\text{H}$  NMR (400 MHz,  $\text{CDCl}_3$ ) of compound **164d**.



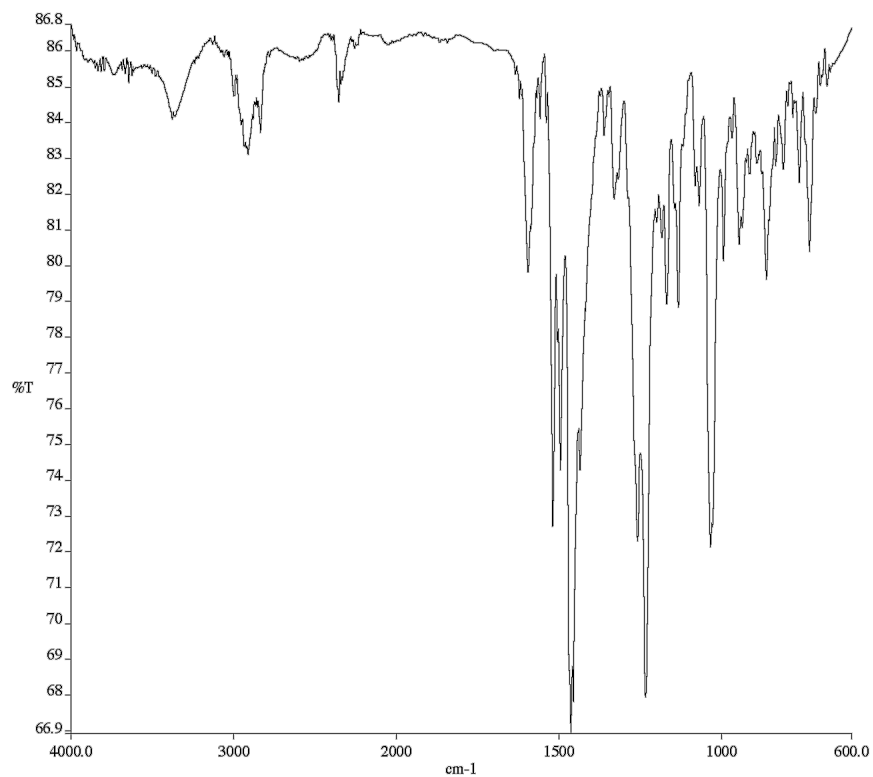
**Figure A1.178** Infrared spectrum (Thin Film, NaCl) of compound **164d**.



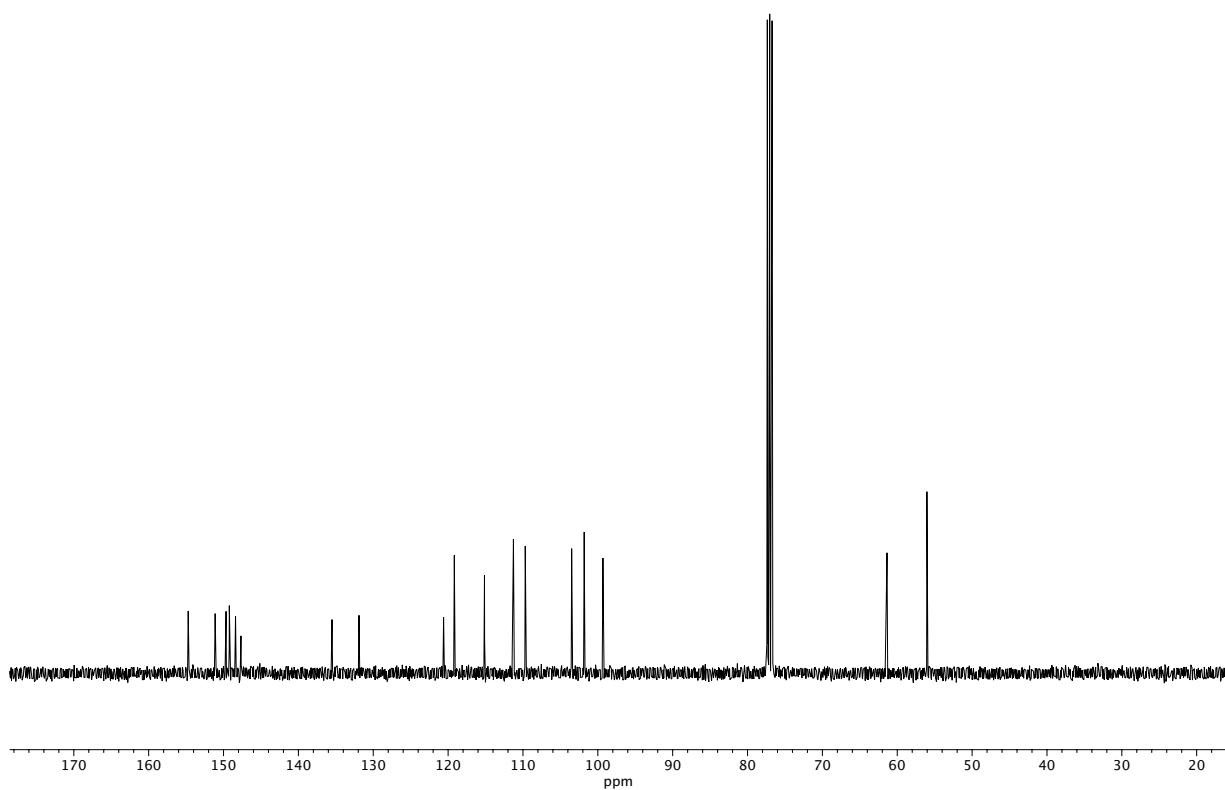
**Figure A1.179** <sup>13</sup>C NMR (100 MHz, CDCl<sub>3</sub>) of compound **164d**.



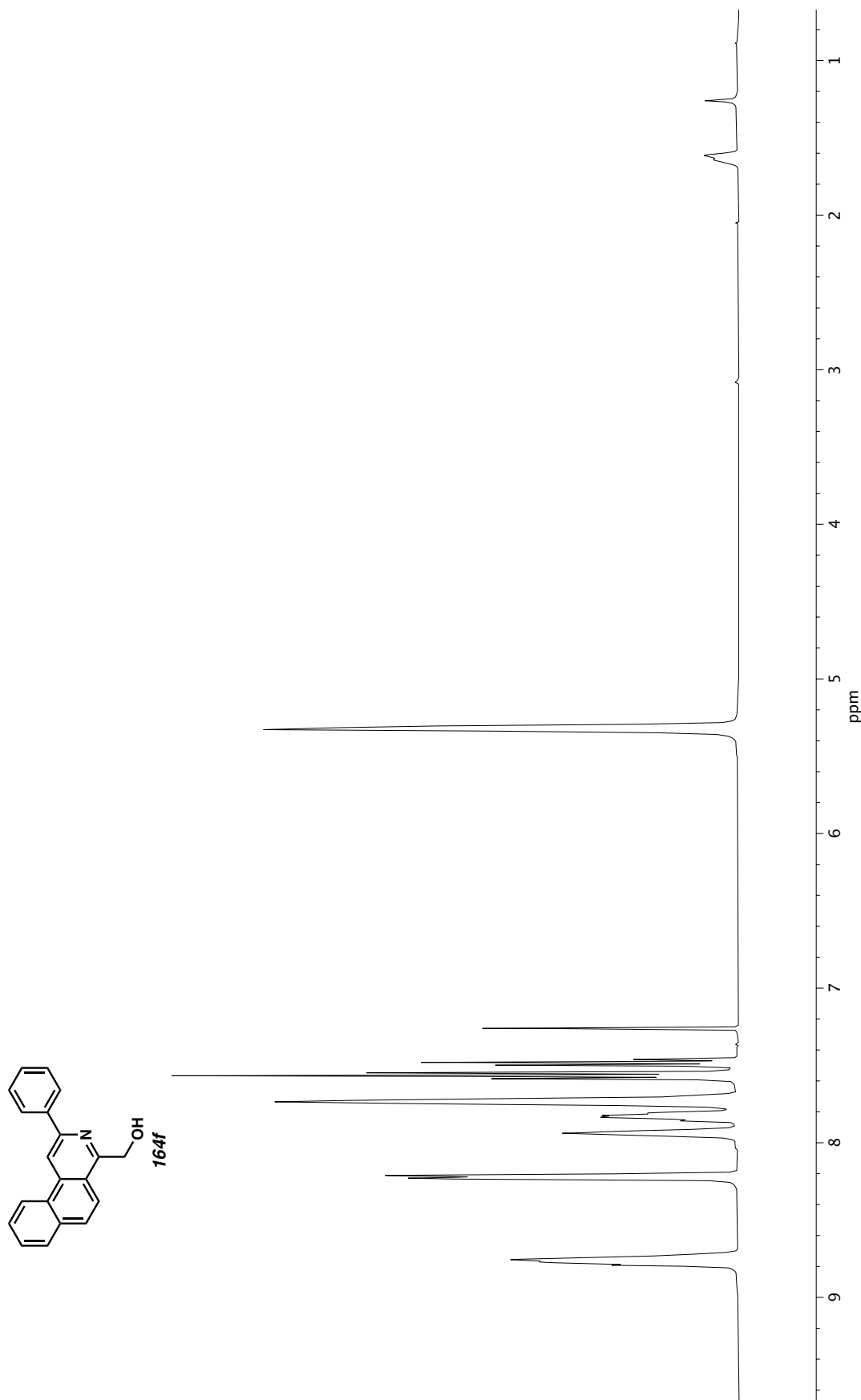
**Figure A1.180**  $^1\text{H}$  NMR (400 MHz,  $\text{CDCl}_3$ ) of compound **164e**.



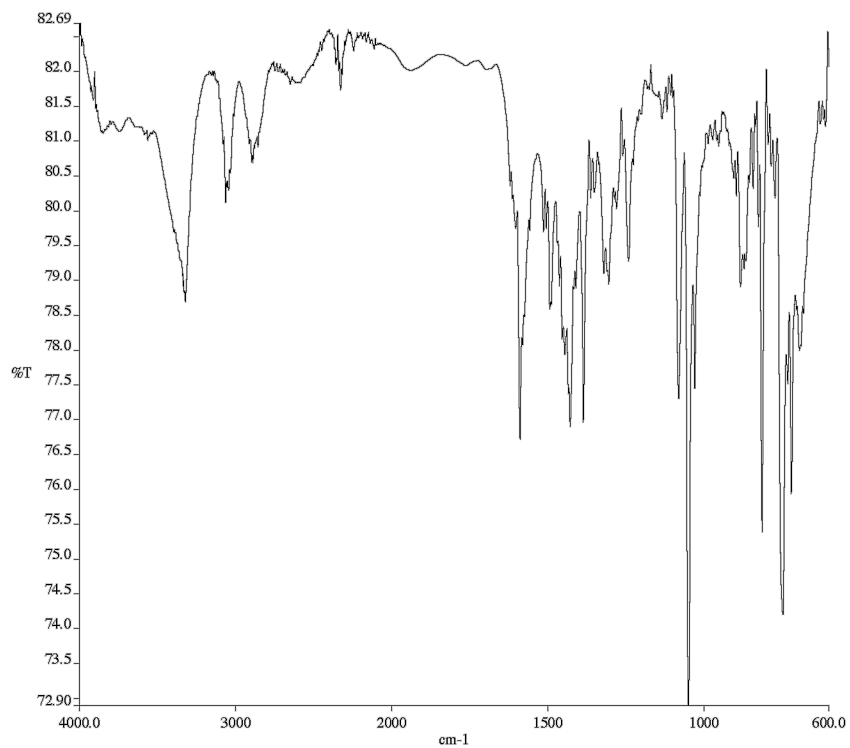
**Figure A1.181** Infrared spectrum (Thin Film, NaCl) of compound **164e**.



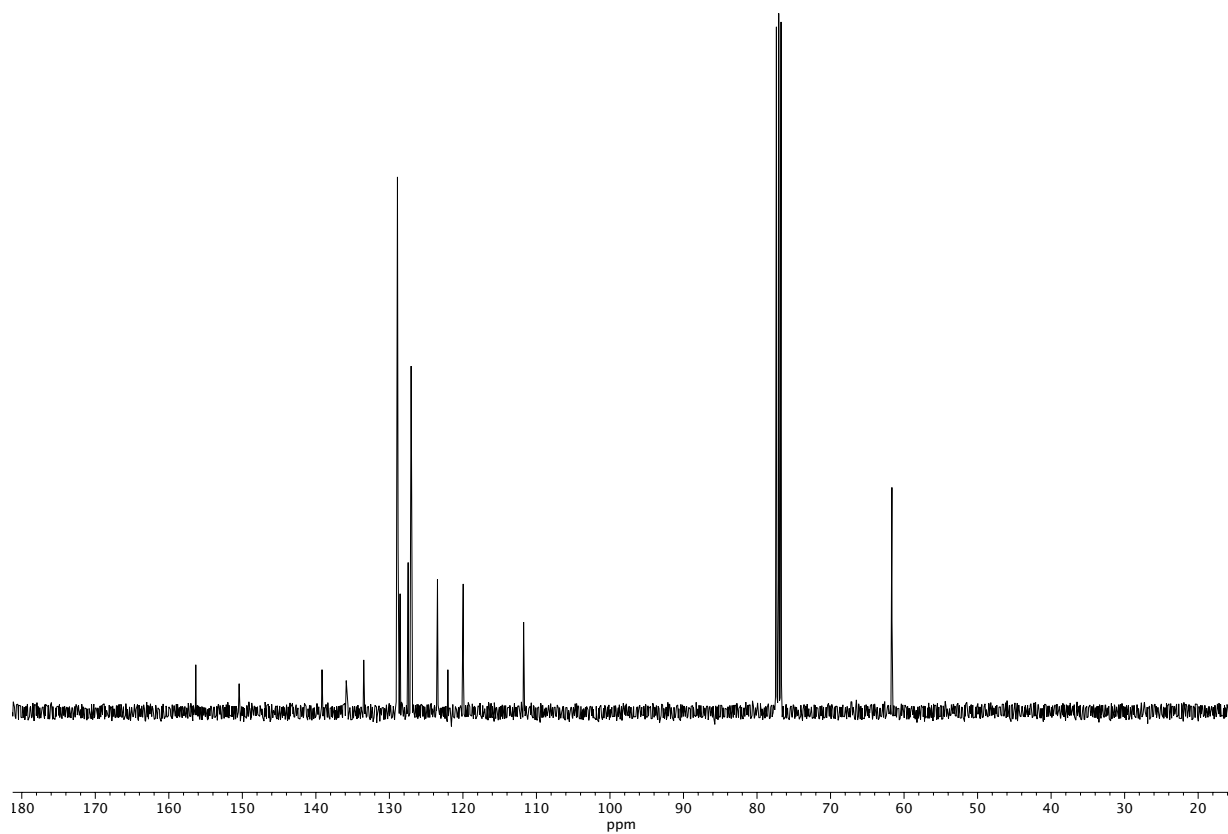
**Figure A1.182** <sup>13</sup>C NMR (100 MHz, CDCl<sub>3</sub>) of compound **164e**.



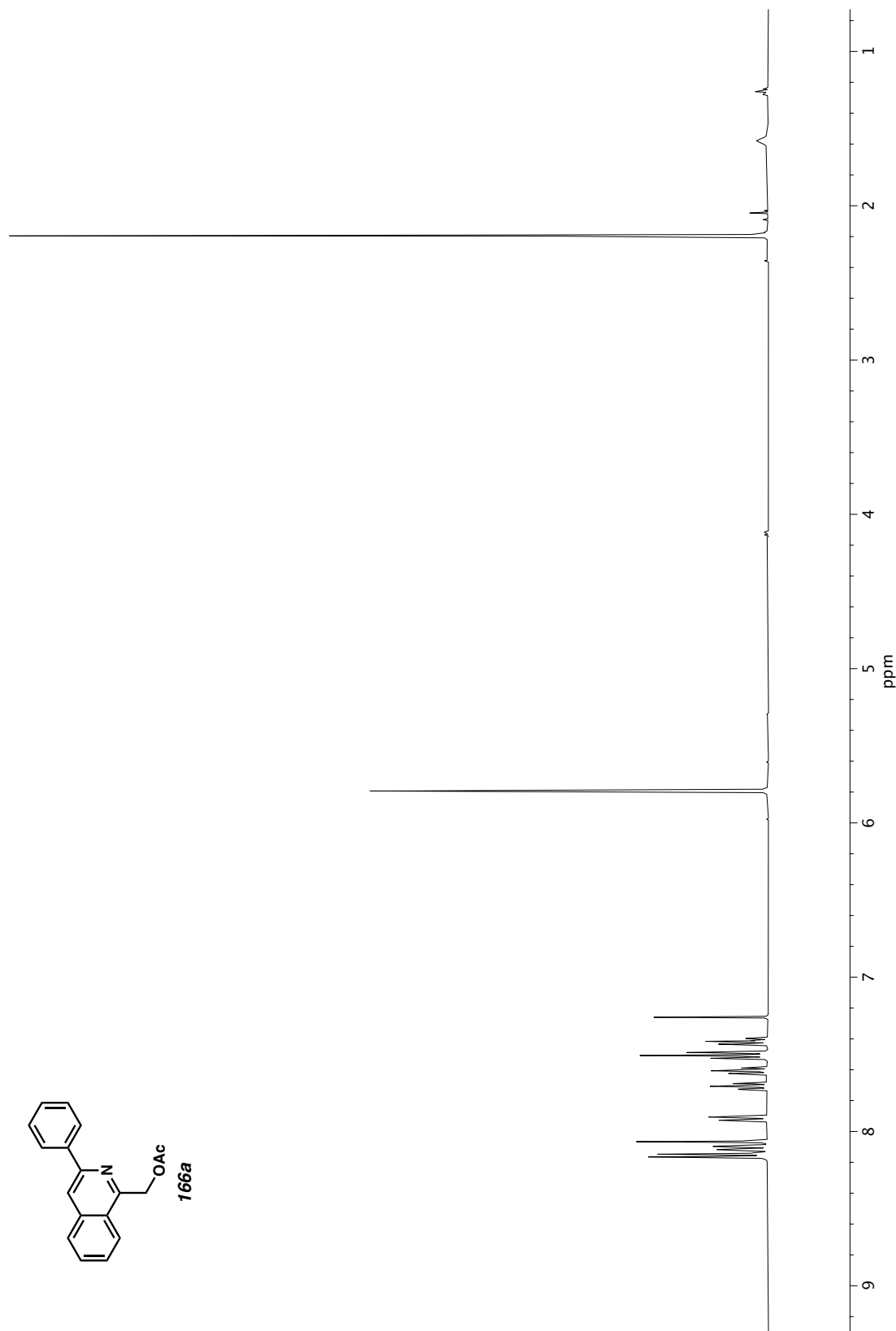
**Figure A1.183**  $^1\text{H}$  NMR (400 MHz,  $\text{CDCl}_3$ ) of compound **164f**.



**Figure A1.184** Infrared spectrum (Thin Film, NaCl) of compound **164f**.

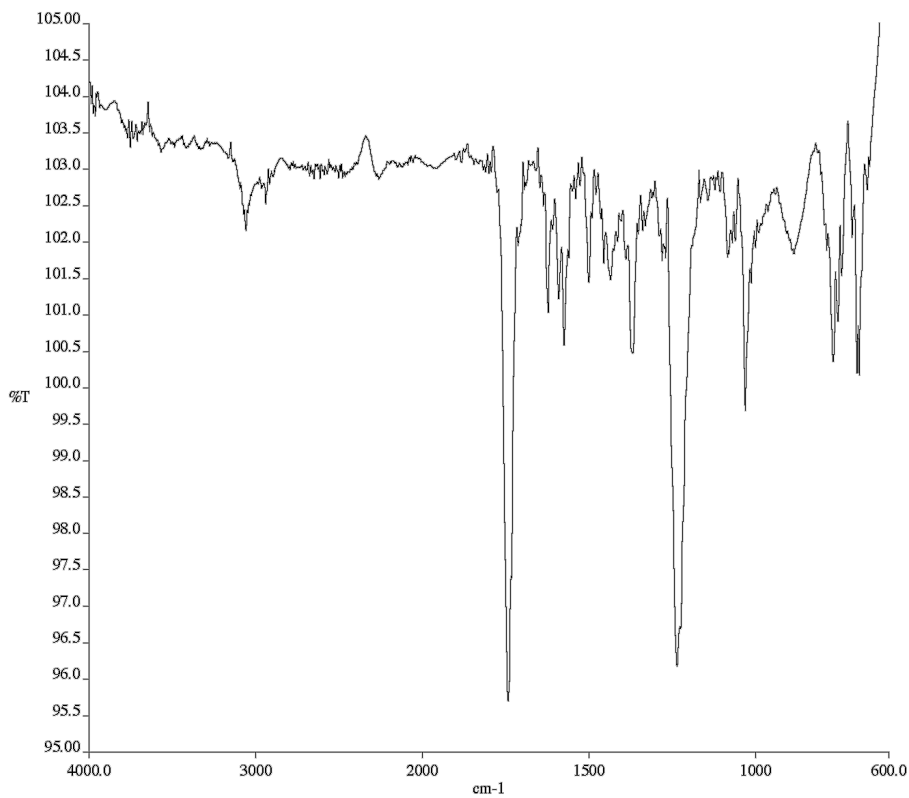


**Figure A1.185** <sup>13</sup>C NMR (100 MHz, CDCl<sub>3</sub>) of compound **164f**.

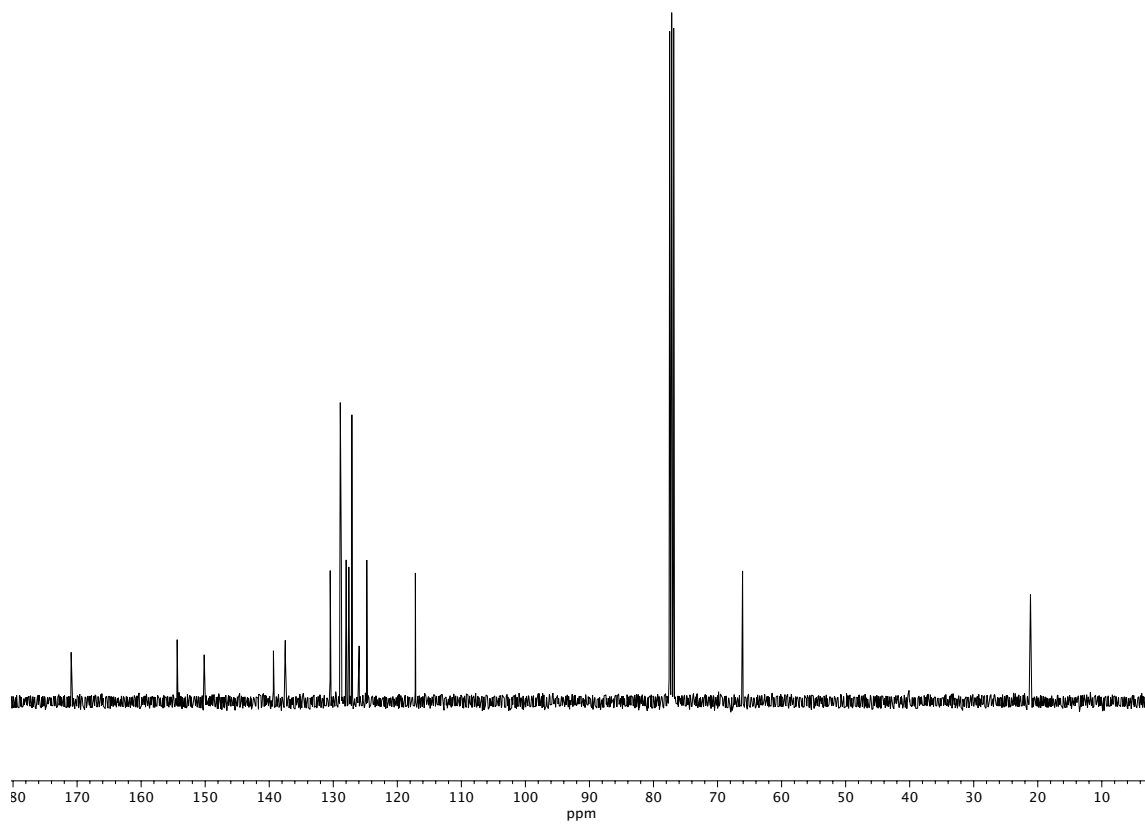


**Figure A1.186** <sup>1</sup>H NMR (400 MHz, CDCl<sub>3</sub>) of compound **166a**.

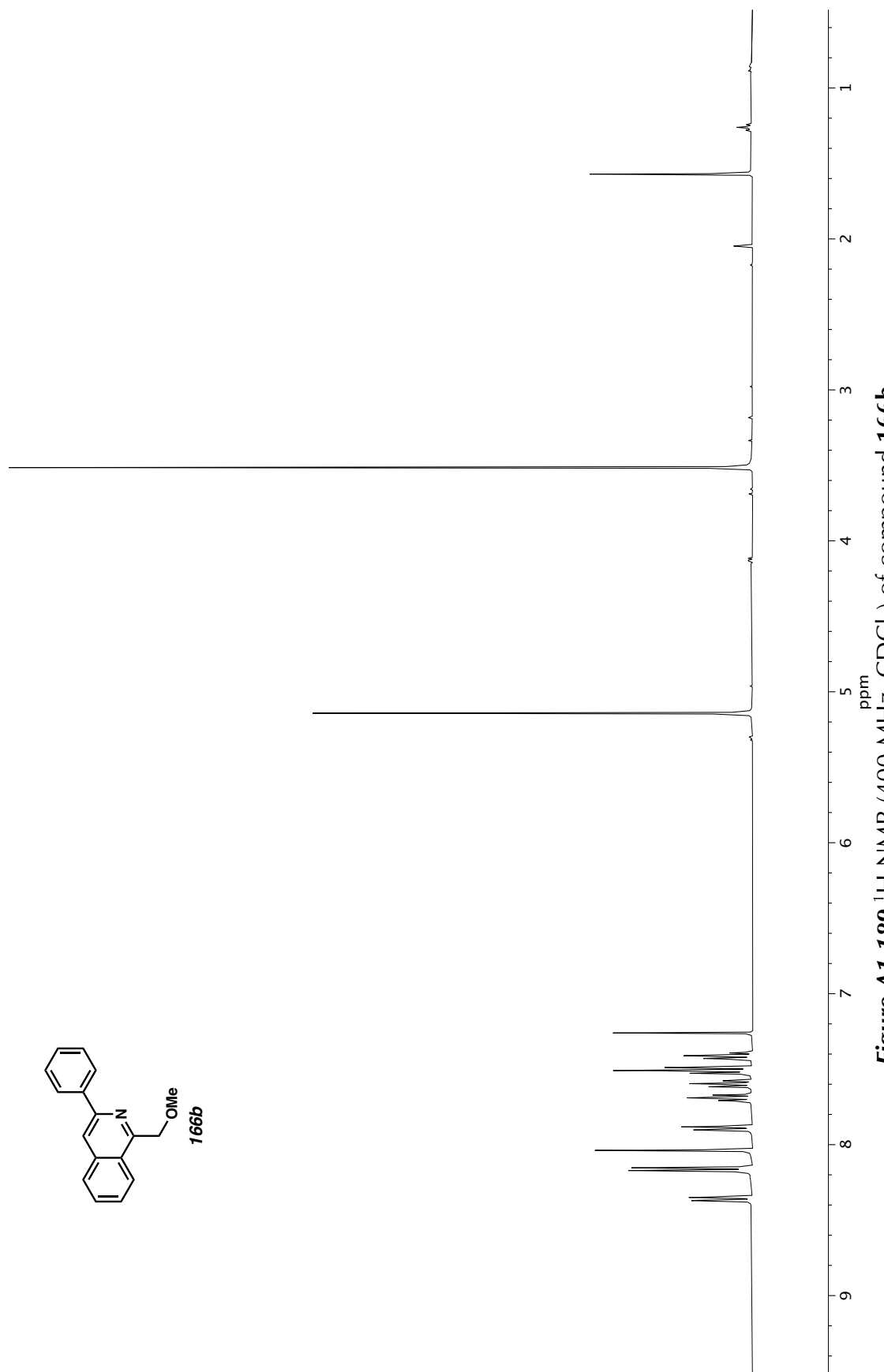


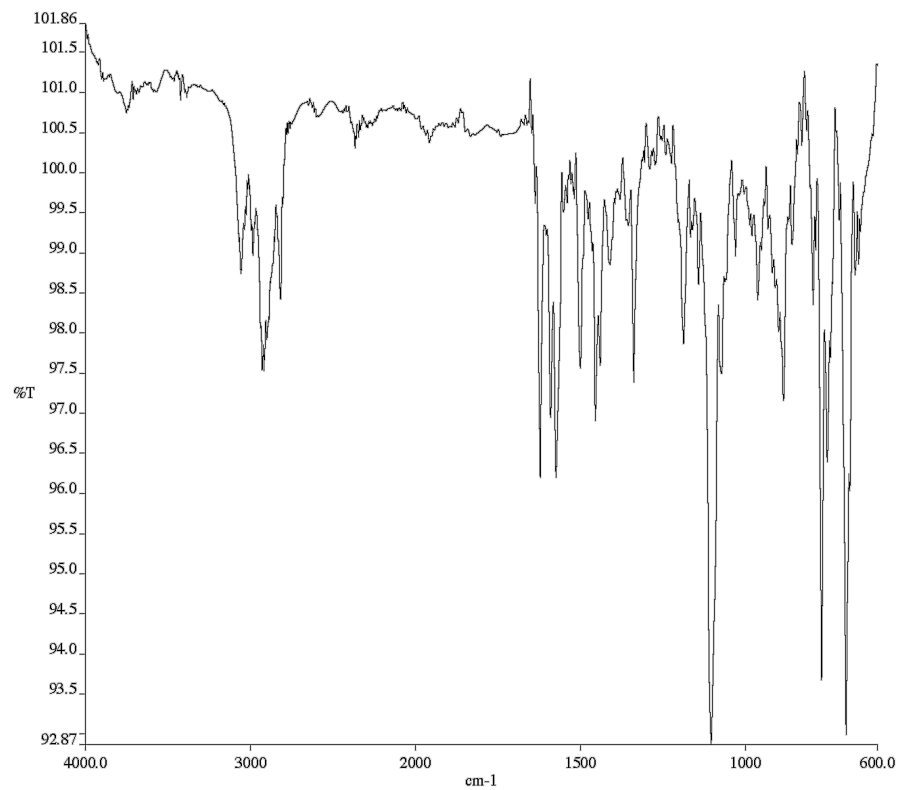


**Figure A1.187** Infrared spectrum (Thin Film, NaCl) of compound **166a**.

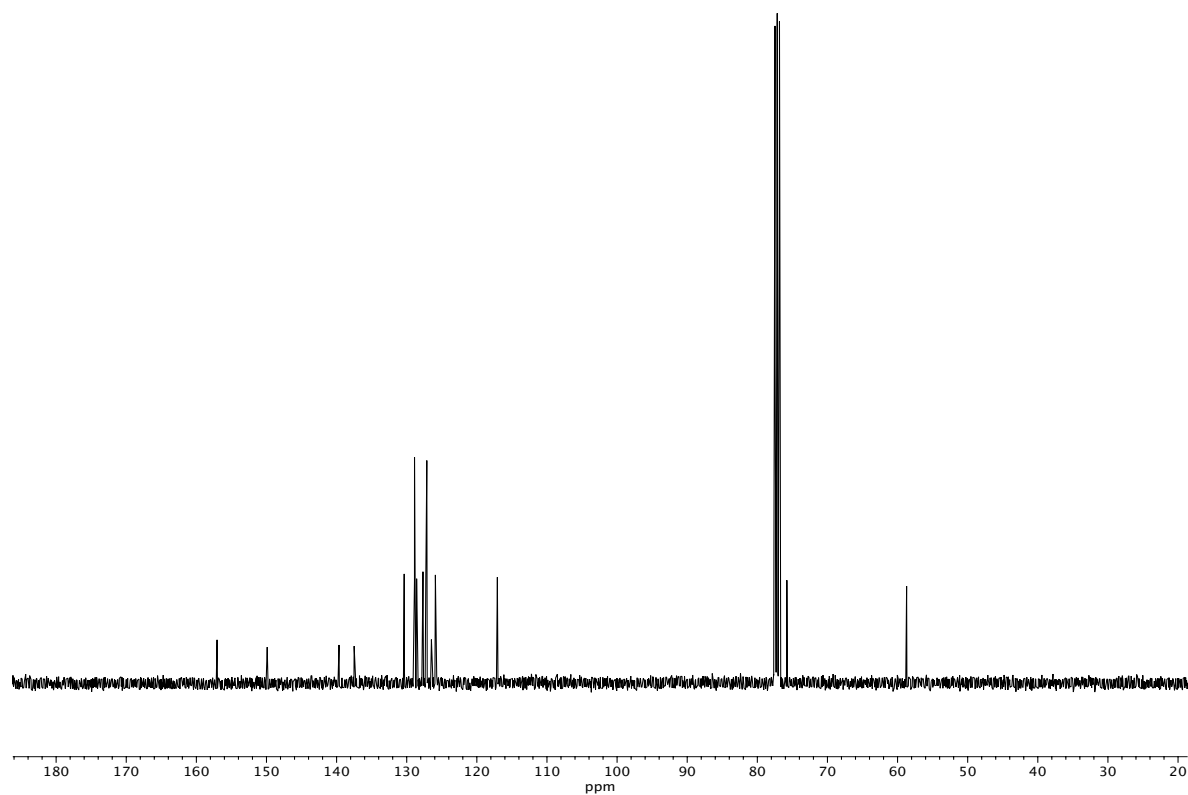


**Figure A1.188** <sup>13</sup>C NMR (100 MHz, CDCl<sub>3</sub>) of compound **166a**.

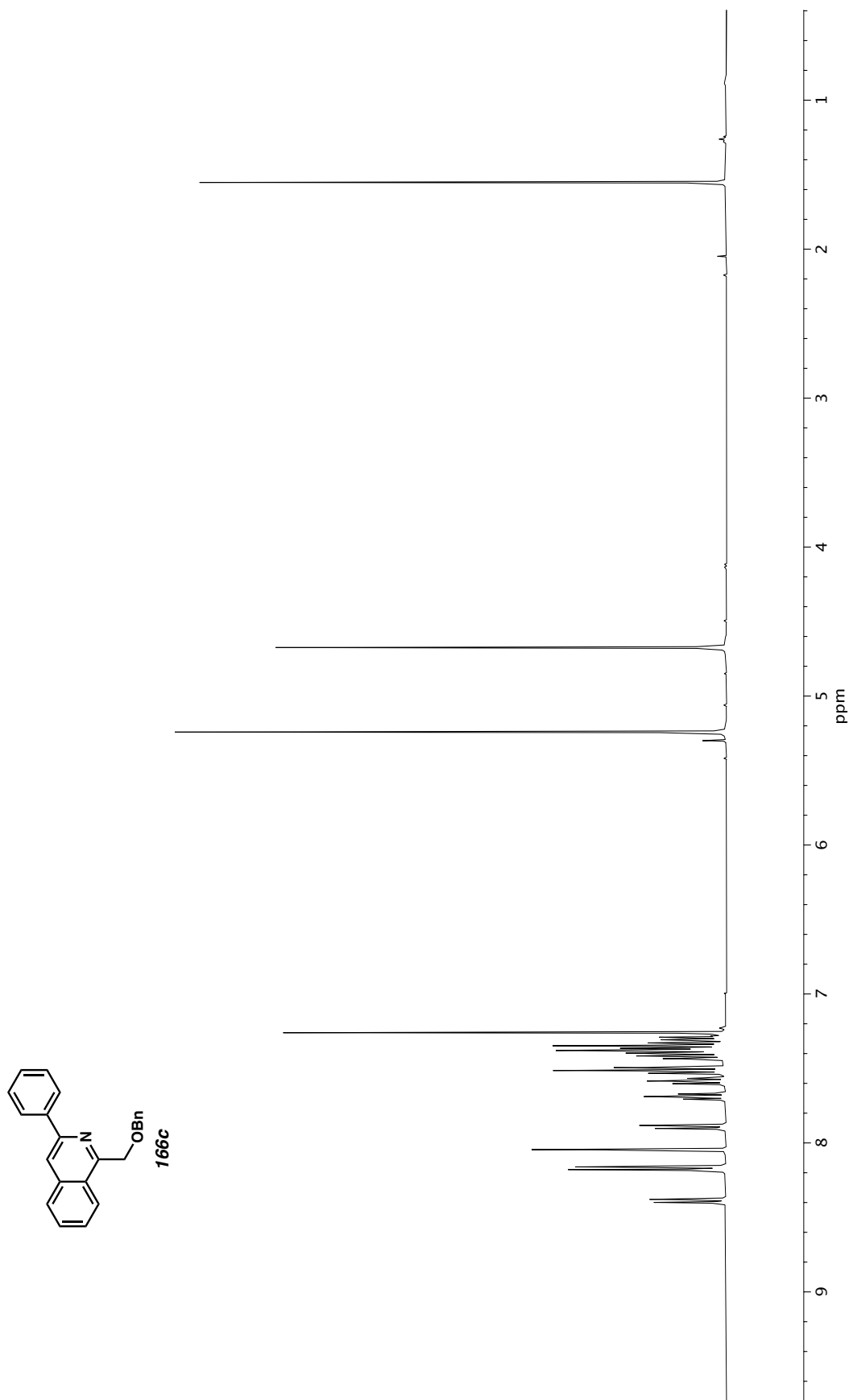


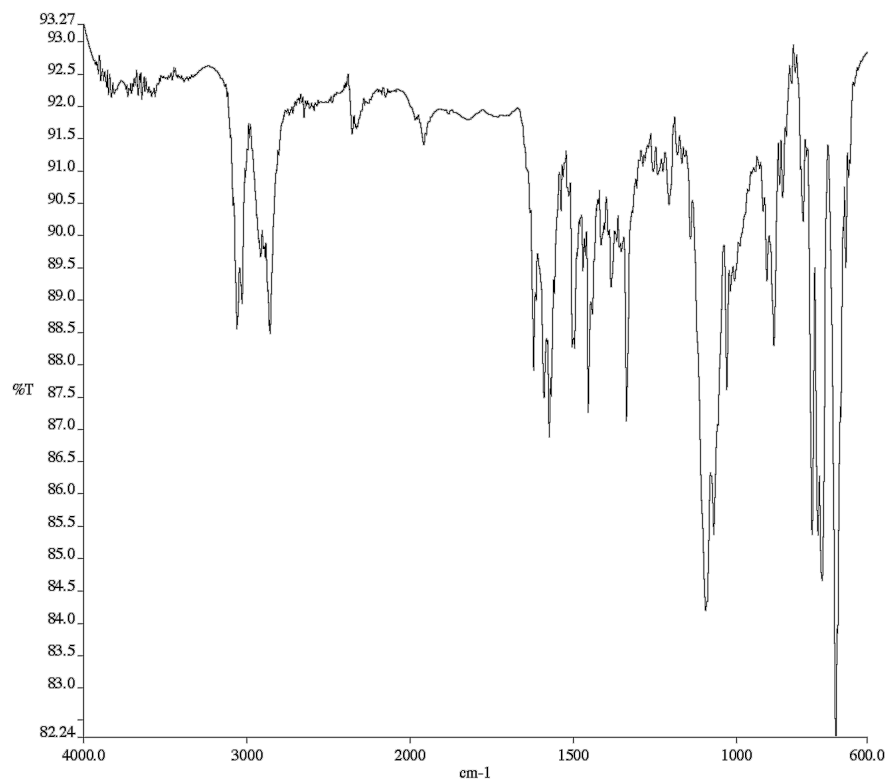


**Figure A1.190** Infrared spectrum (Thin Film, NaCl) of compound **166b**.

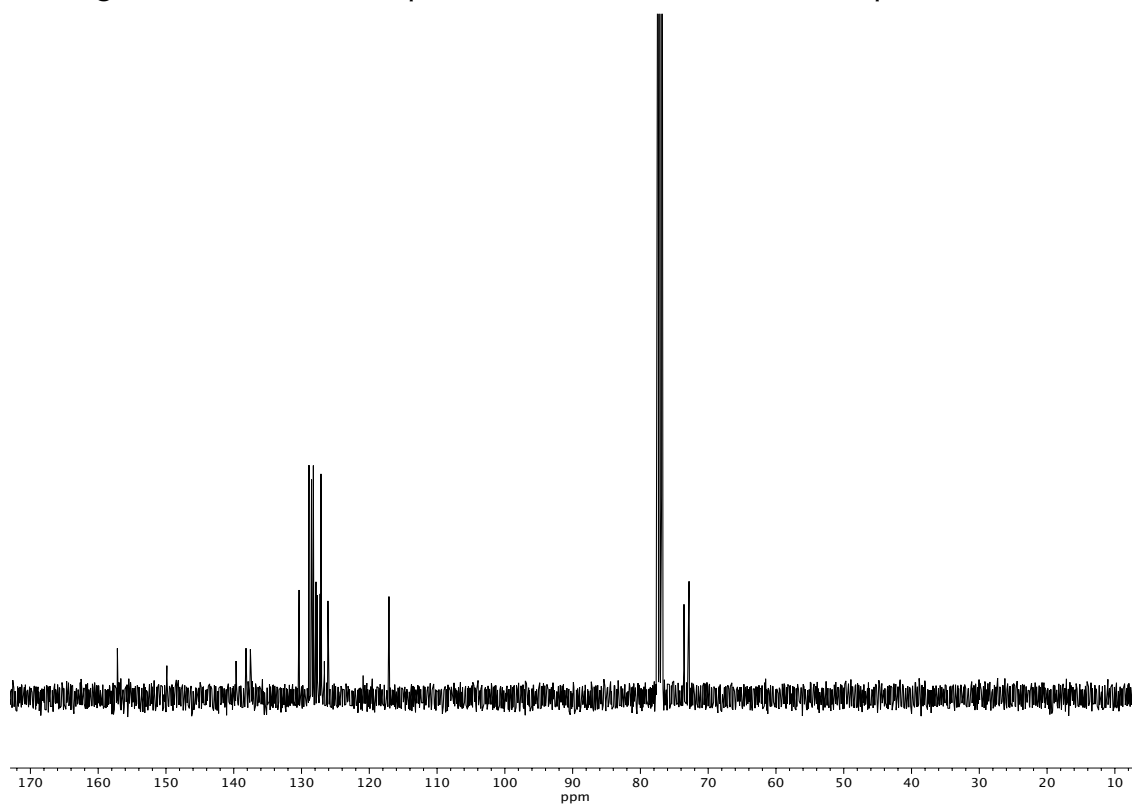


**Figure A1.191** <sup>13</sup>C NMR (100 MHz, CDCl<sub>3</sub>) of compound **166b**.

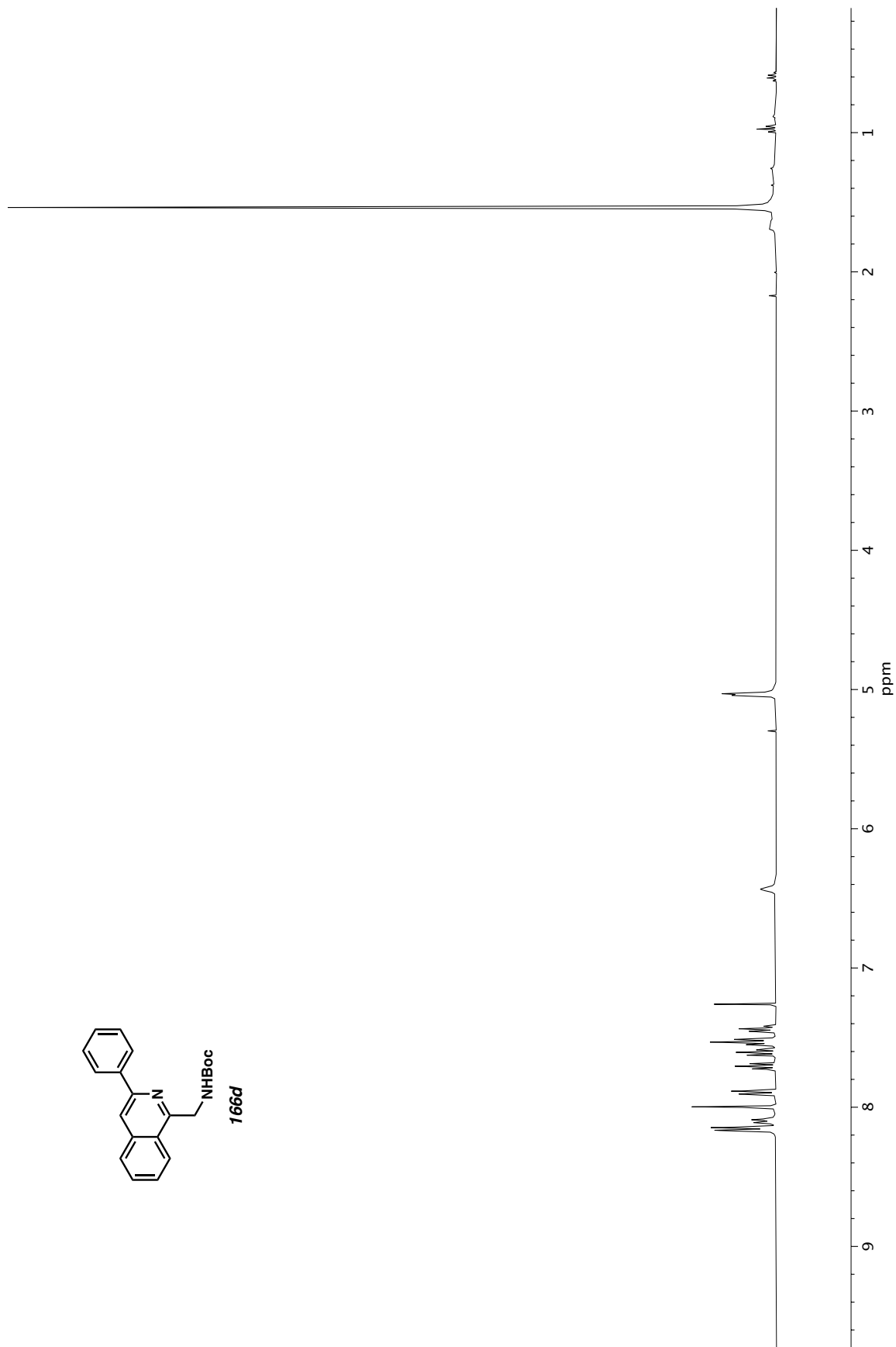




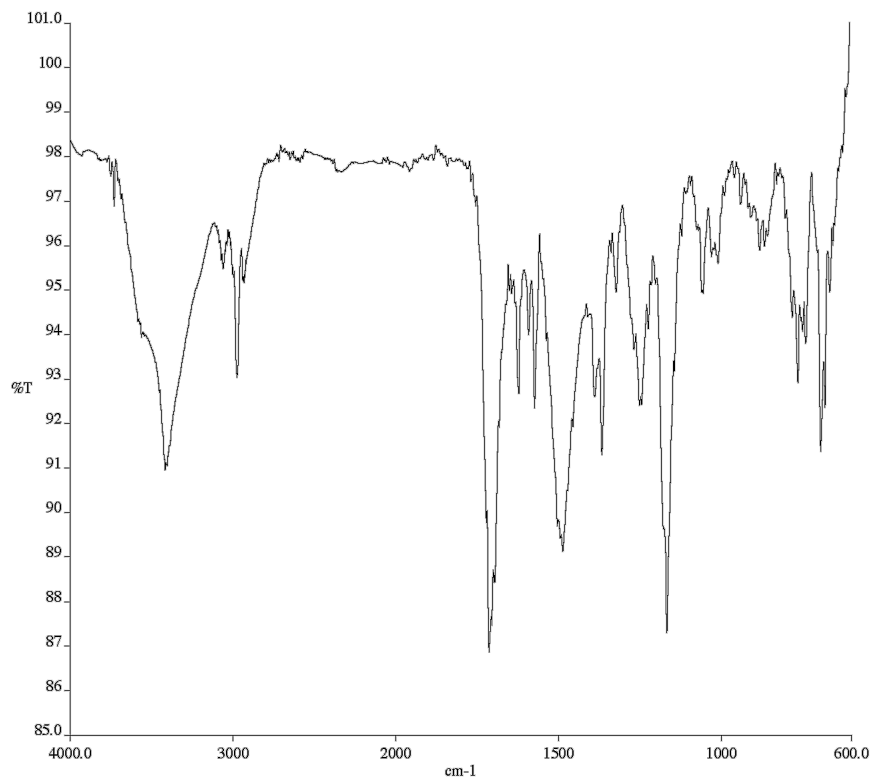
**Figure A1.193** Infrared spectrum (Thin Film, NaCl) of compound **166c**.



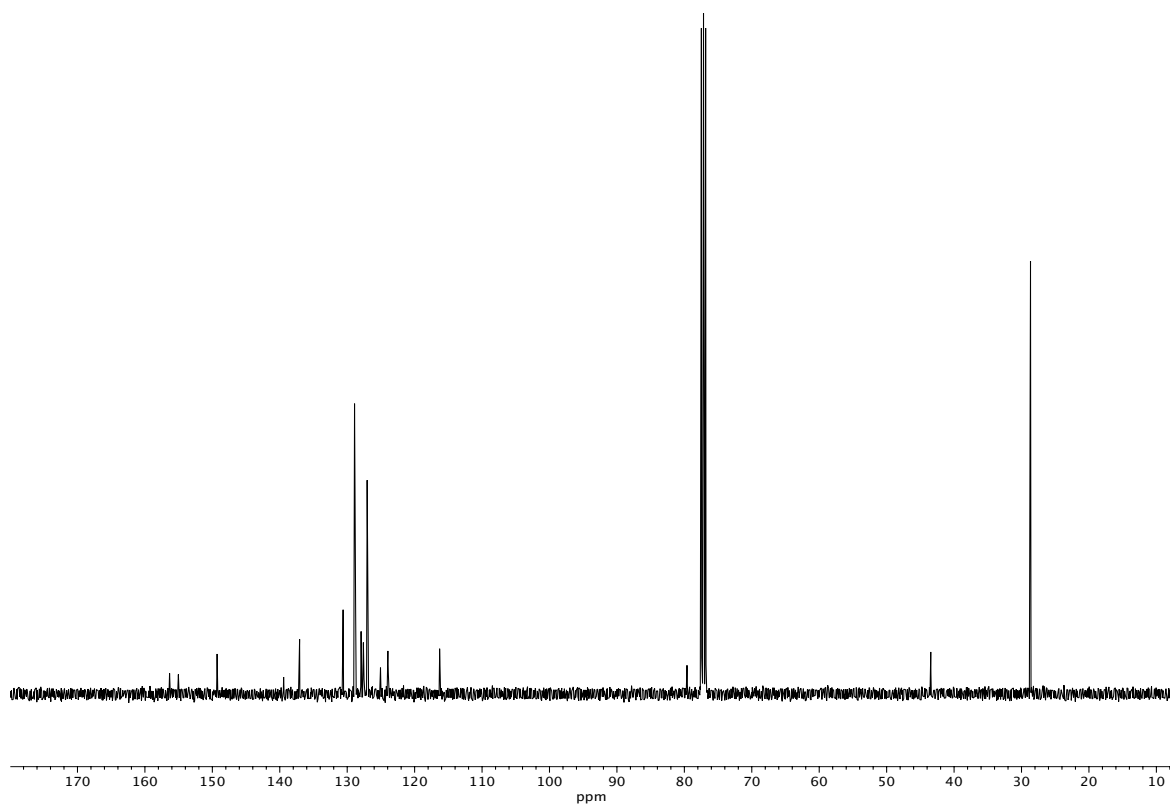
**Figure A1.194** <sup>13</sup>C NMR (100 MHz, CDCl<sub>3</sub>) of compound **166c**.



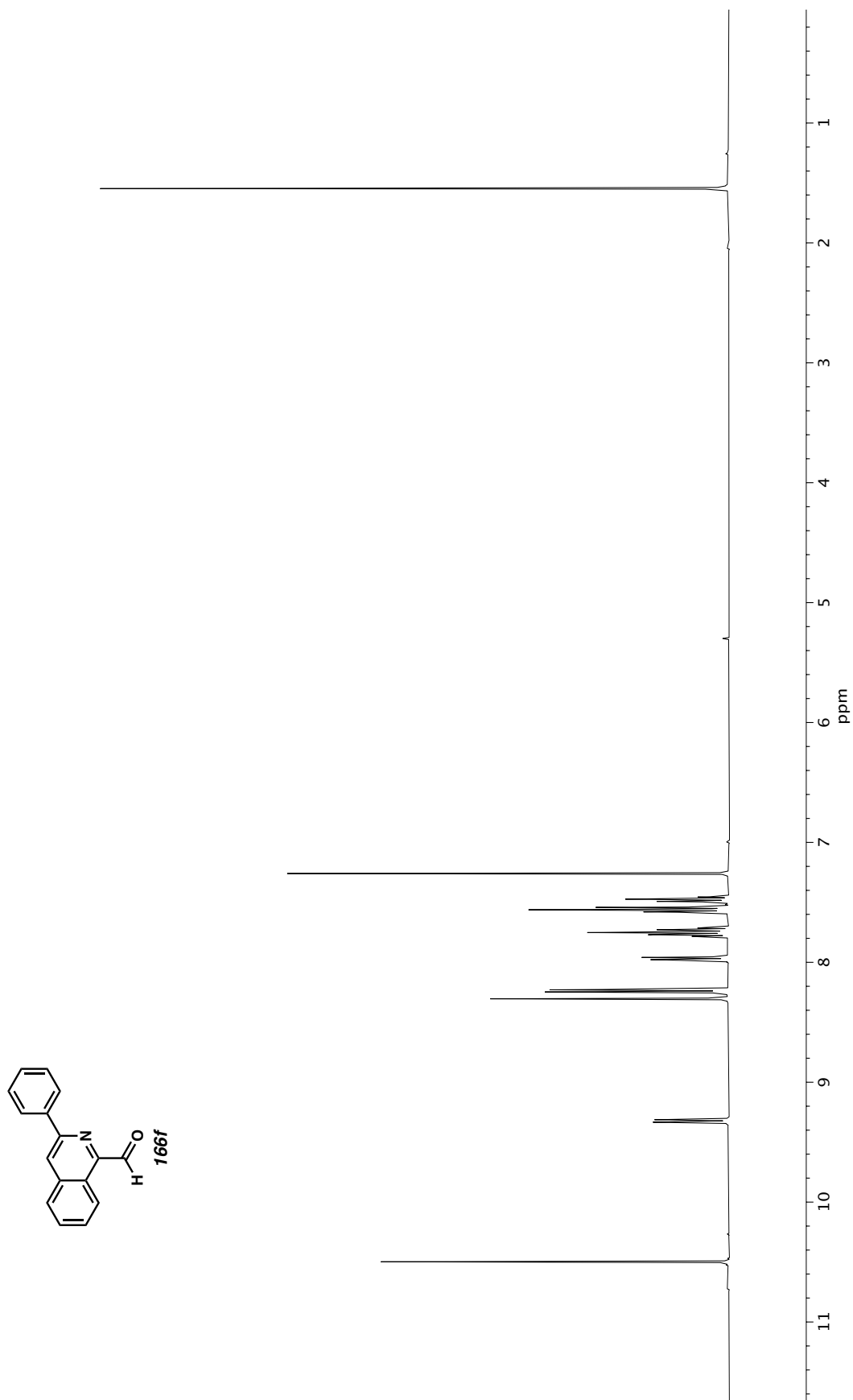
**Figure A1.195**  $^1\text{H}$  NMR (400 MHz,  $\text{CDCl}_3$ ) of compound **166d**.



**Figure A1.196** Infrared spectrum (Thin Film, NaCl) of compound **166d**.

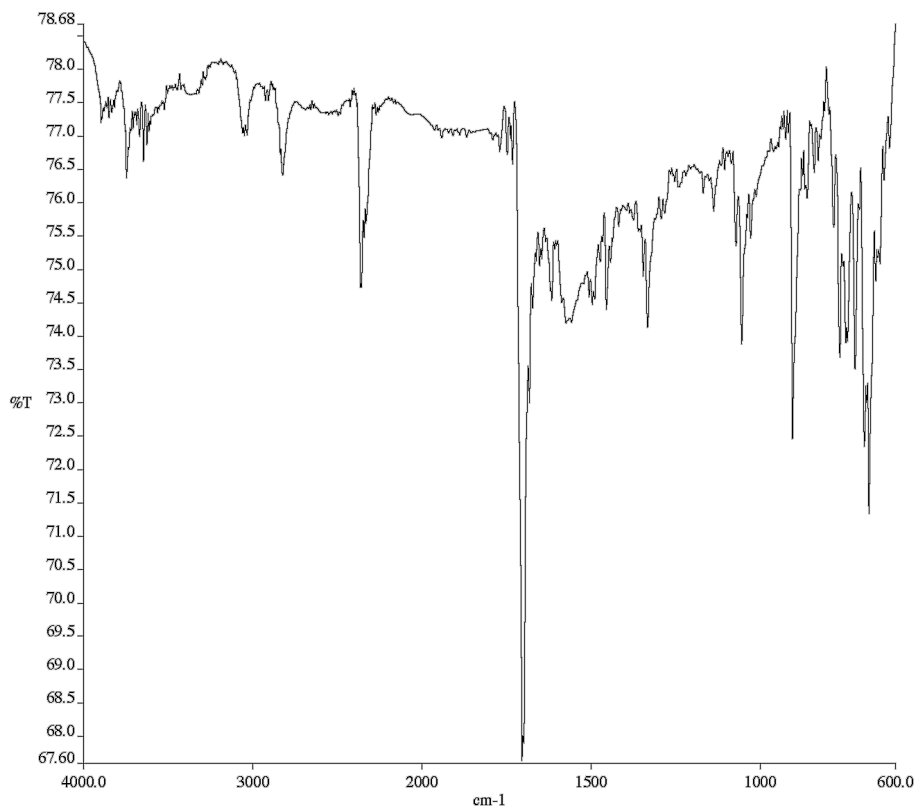


**Figure A1.197** <sup>13</sup>C NMR (100 MHz, CDCl<sub>3</sub>) of compound **166d**.

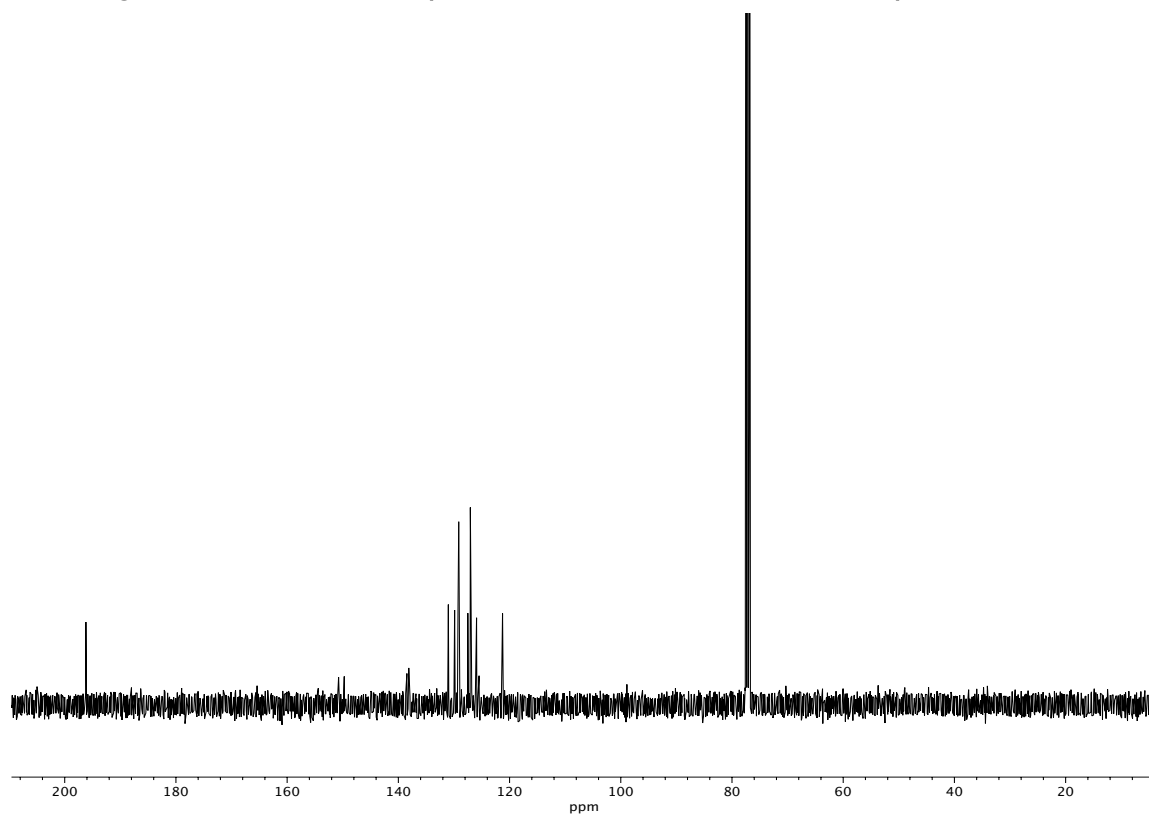


**Figure A1.198**  $^1\text{H}$  NMR (400 MHz,  $\text{CDCl}_3$ ) of compound **166f**.

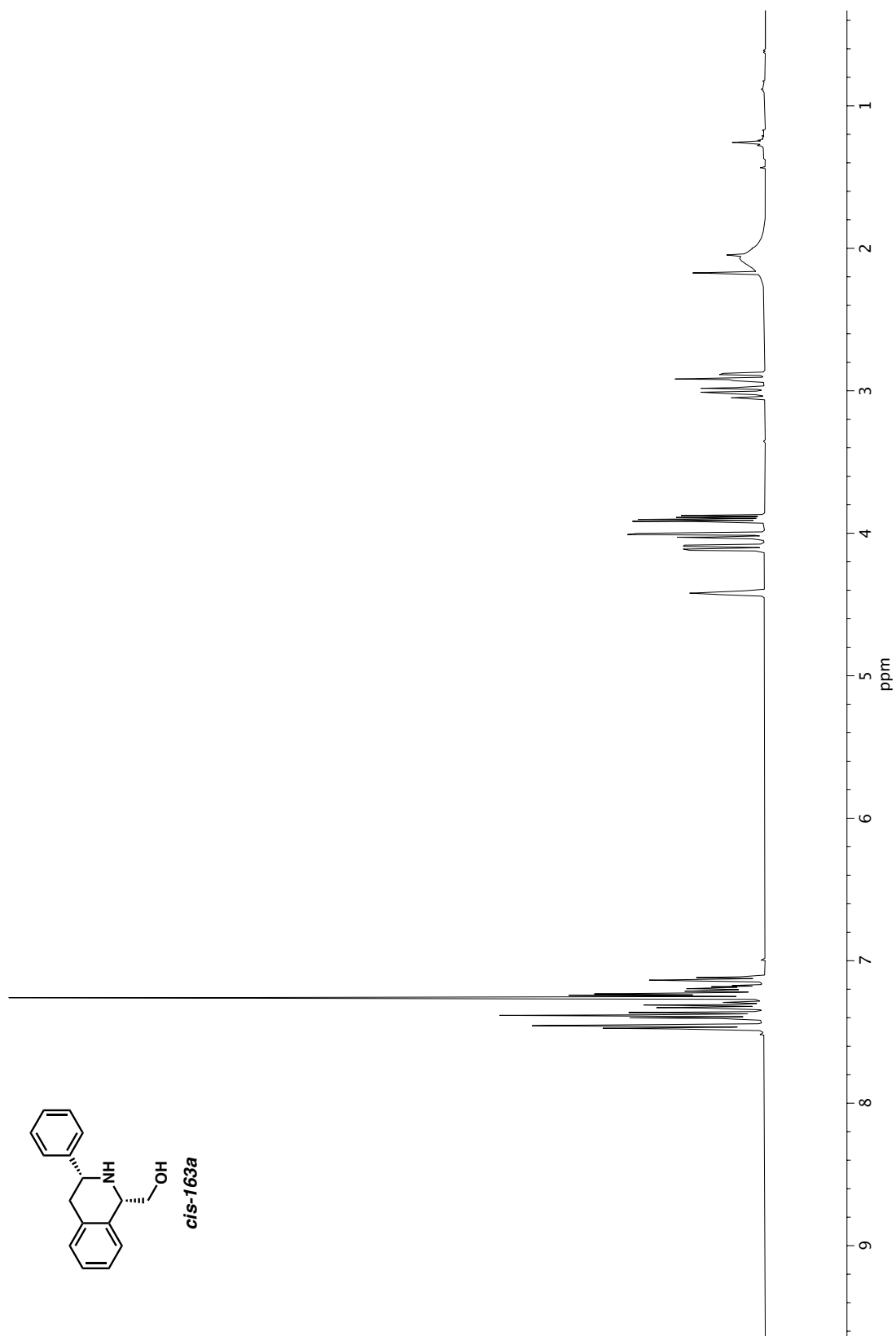




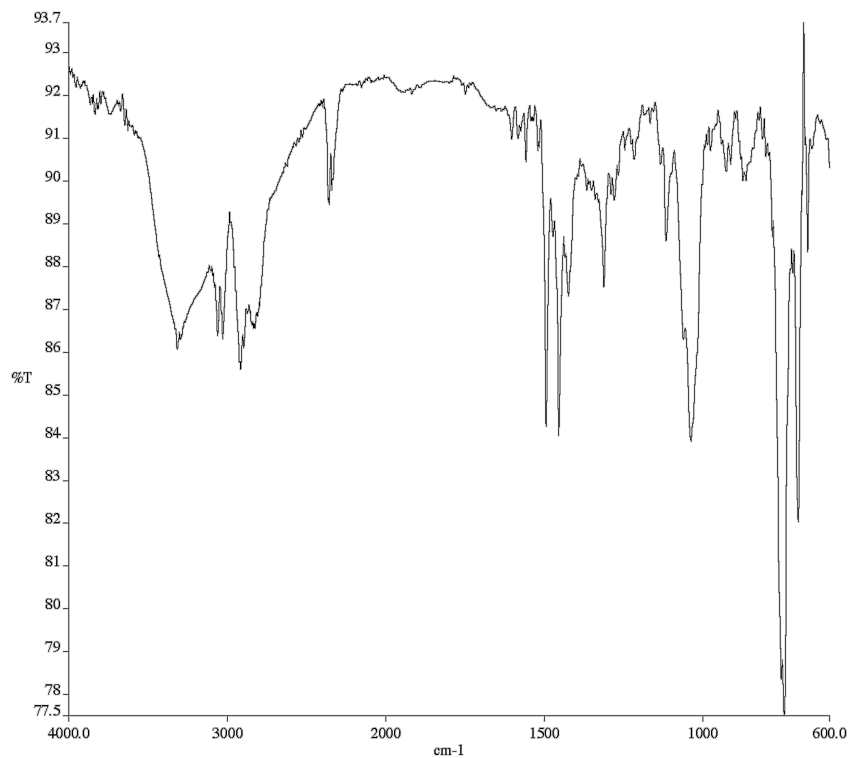
**Figure A1.199** Infrared spectrum (Thin Film, NaCl) of compound **166f**.



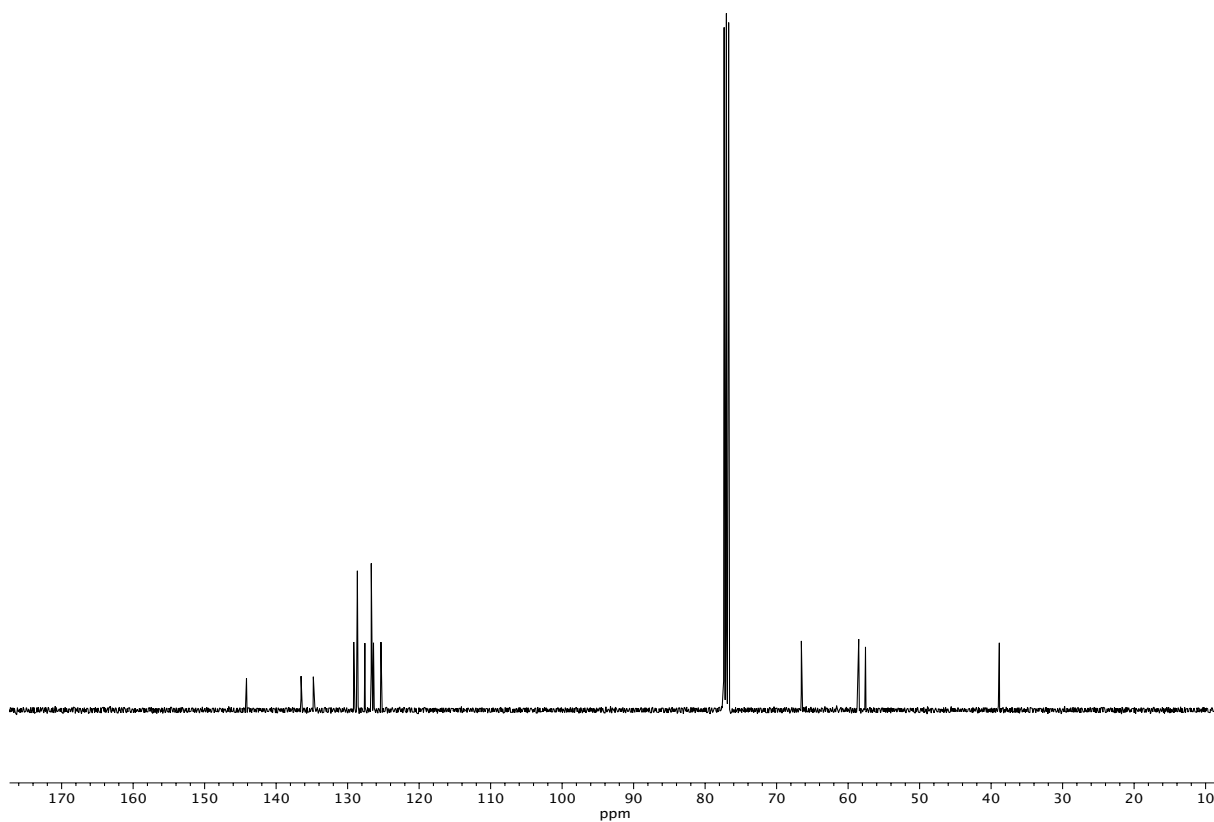
**Figure A1.200** <sup>13</sup>C NMR (100 MHz, CDCl<sub>3</sub>) of compound **166f**.



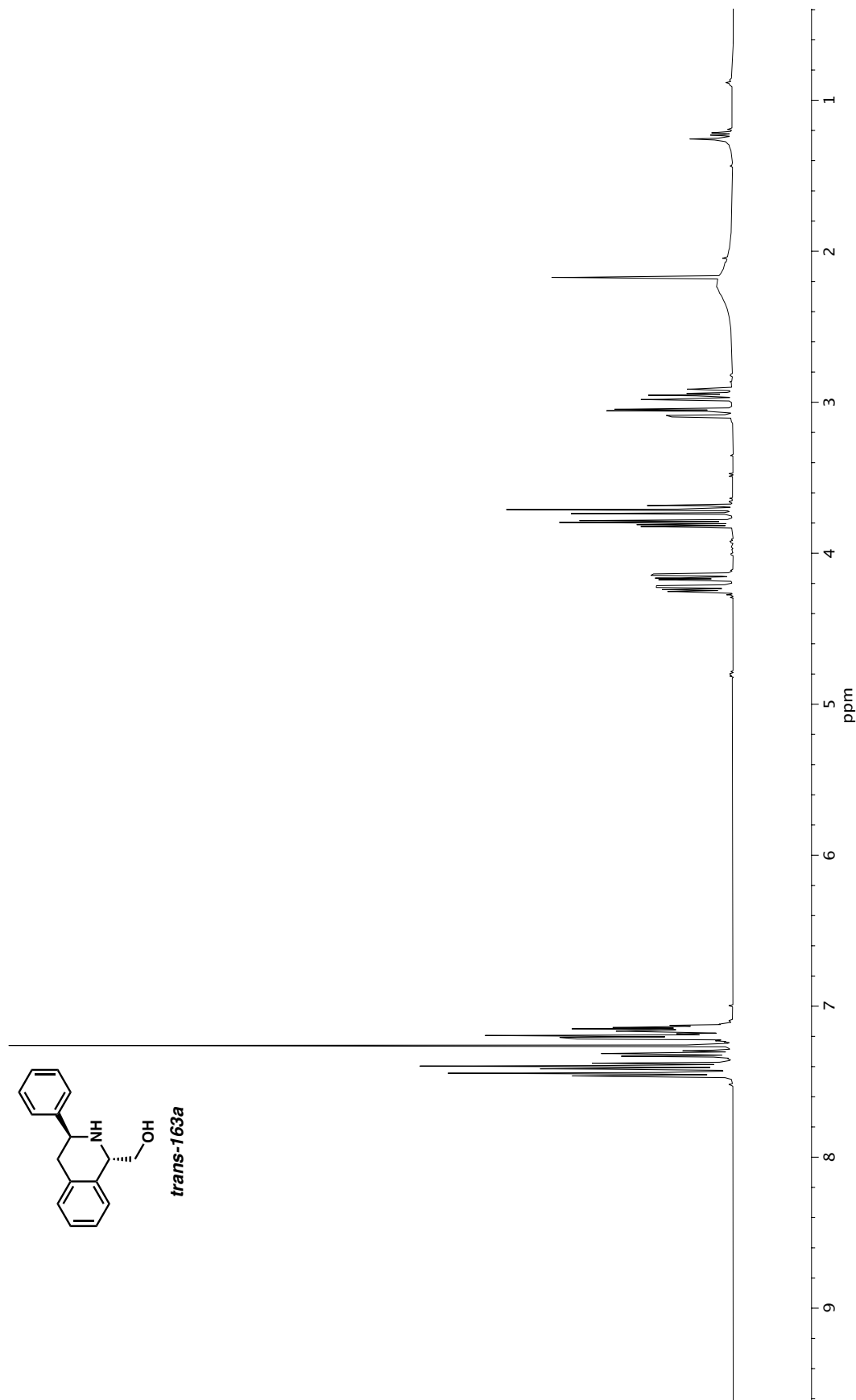
**Figure A1.201** <sup>1</sup>H NMR (400 MHz, CDCl<sub>3</sub>) of compound ***cis*-163a**.



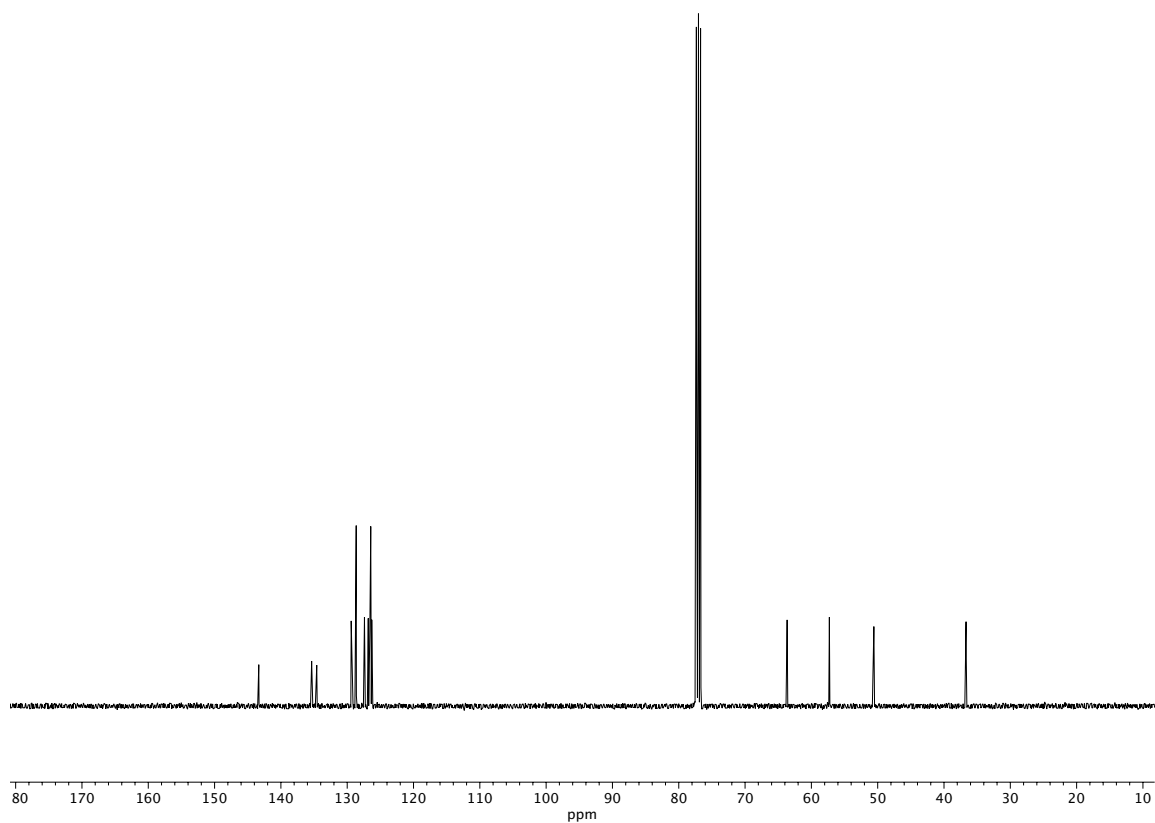
**Figure A1.202** Infrared spectrum (Thin Film, NaCl) of compound **163a**.



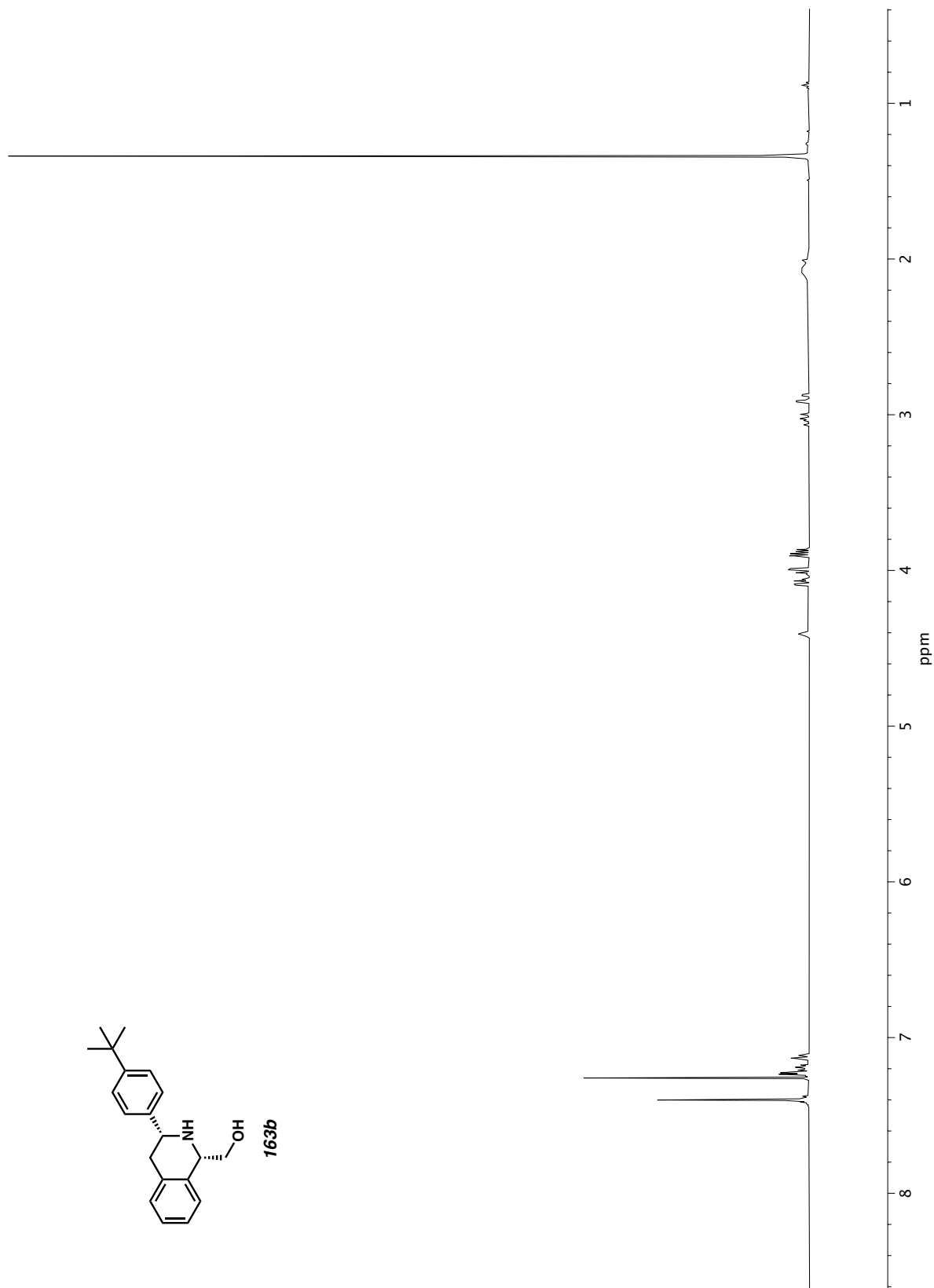
**Figure A1.203** <sup>13</sup>C NMR (100 MHz, CDCl<sub>3</sub>) of compound **163a**.

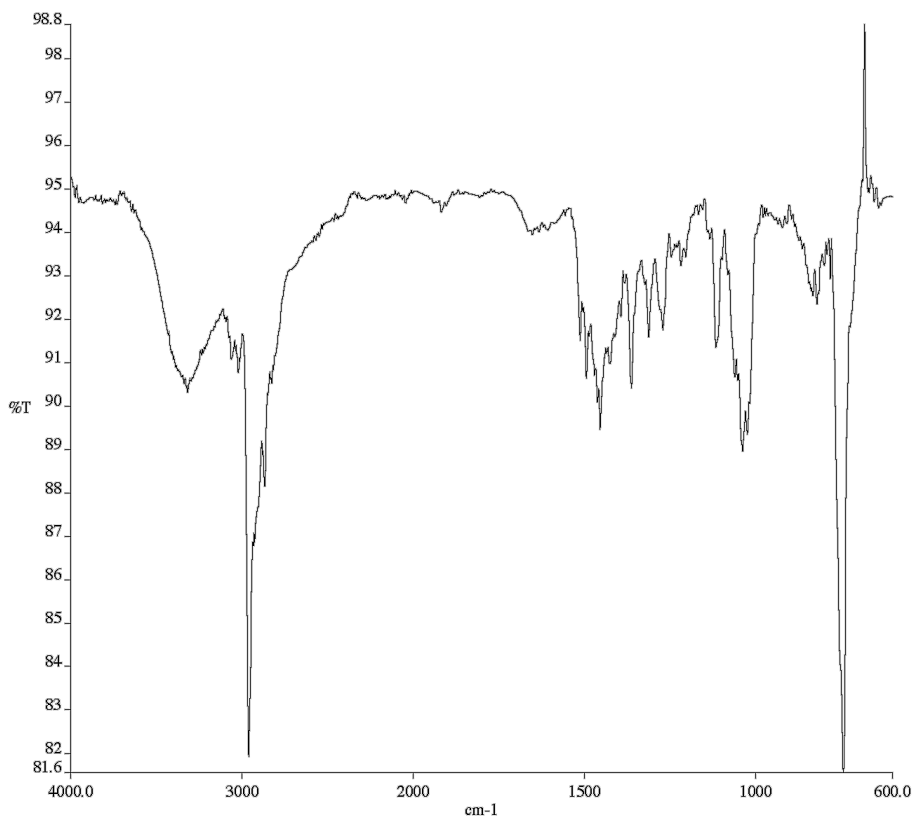


**Figure A1.204** <sup>1</sup>H NMR (400 MHz, CDCl<sub>3</sub>) of compound *trans*-163a.

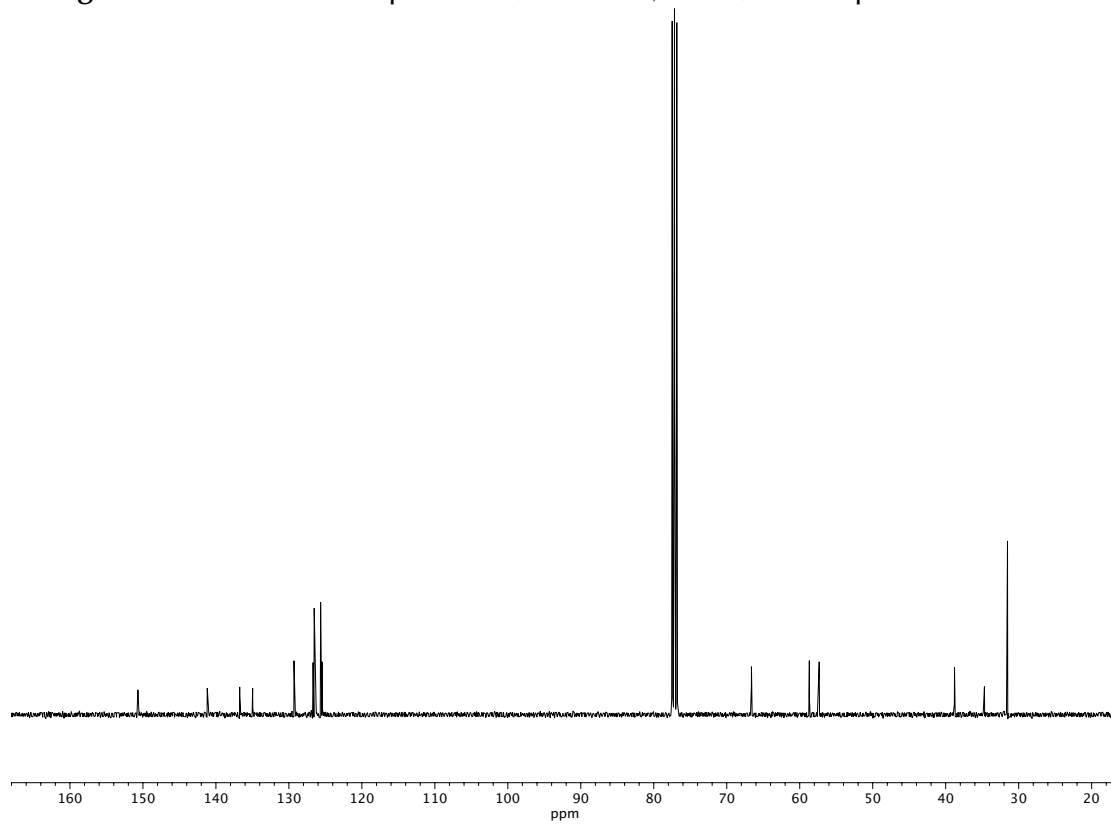


**Figure A1.205**  $^{13}\text{C}$  NMR (100 MHz,  $\text{CDCl}_3$ ) of compound *trans*-163a.

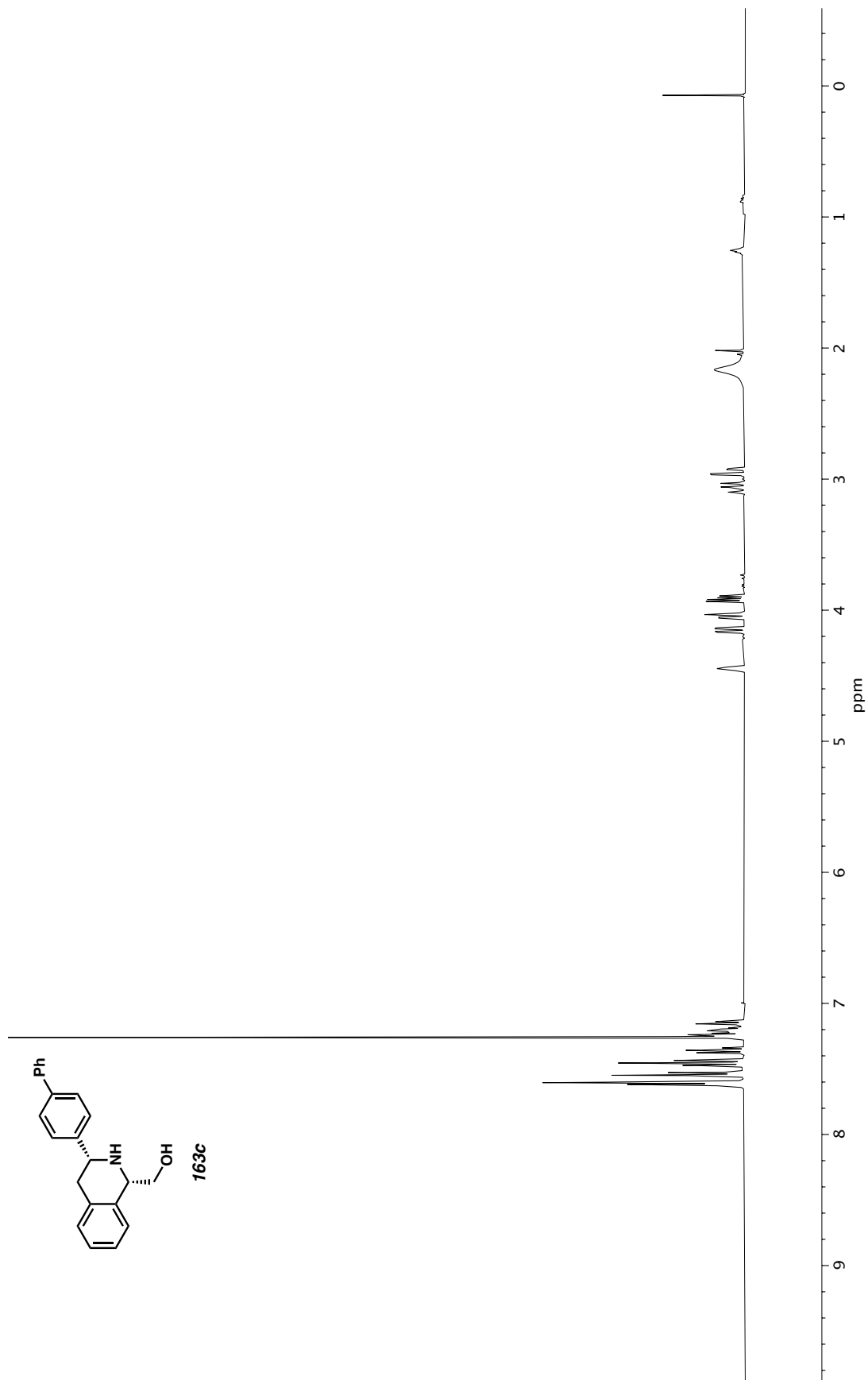




**Figure A1.207** Infrared spectrum (Thin Film, NaCl) of compound **163b**.

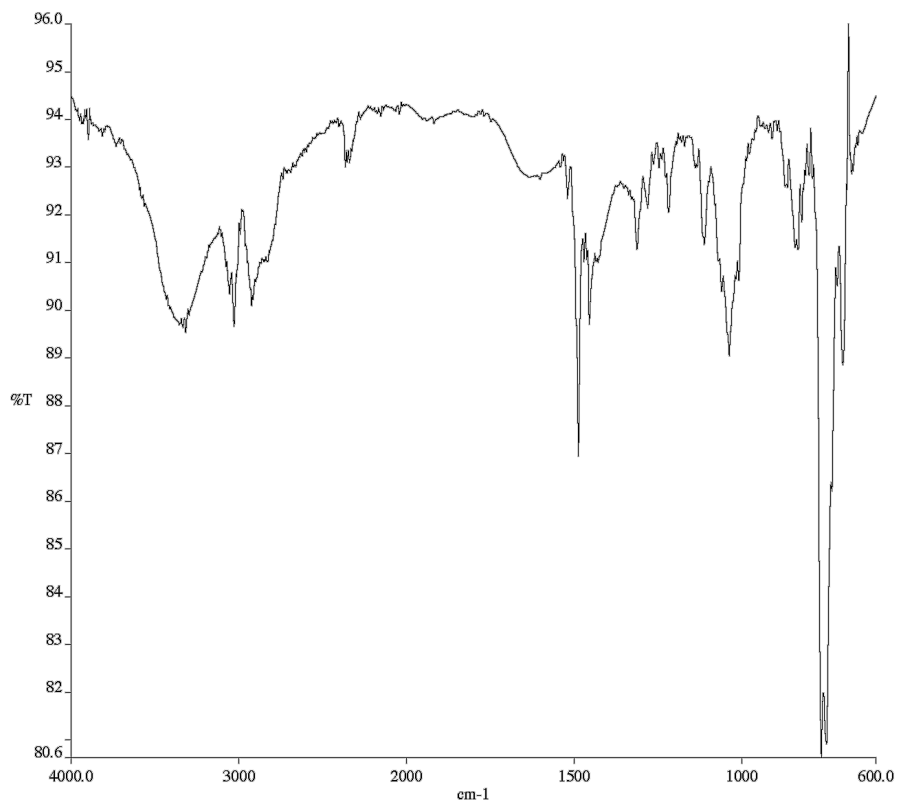


**Figure A1.208** <sup>13</sup>C NMR (100 MHz, CDCl<sub>3</sub>) of compound **163b**.

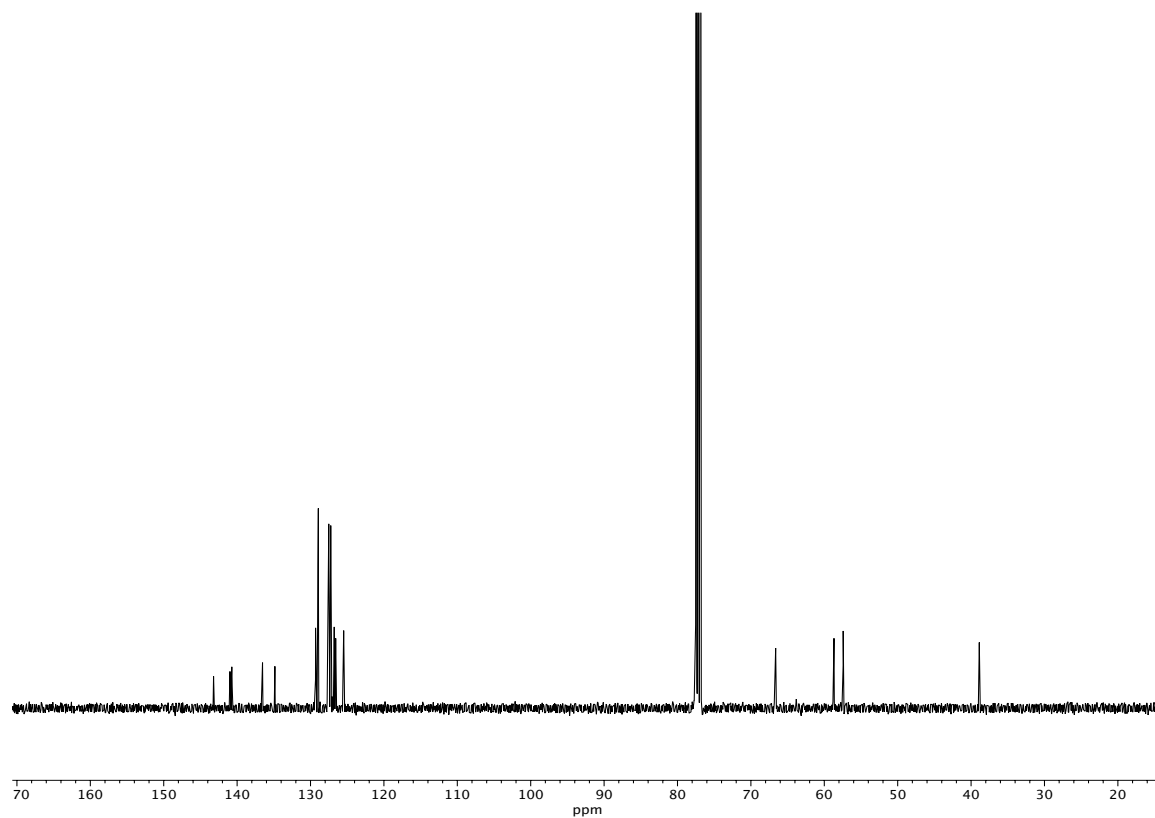


**Figure A1.209**  $^1\text{H}$  NMR (400 MHz,  $\text{CDCl}_3$ ) of compound **163c**.

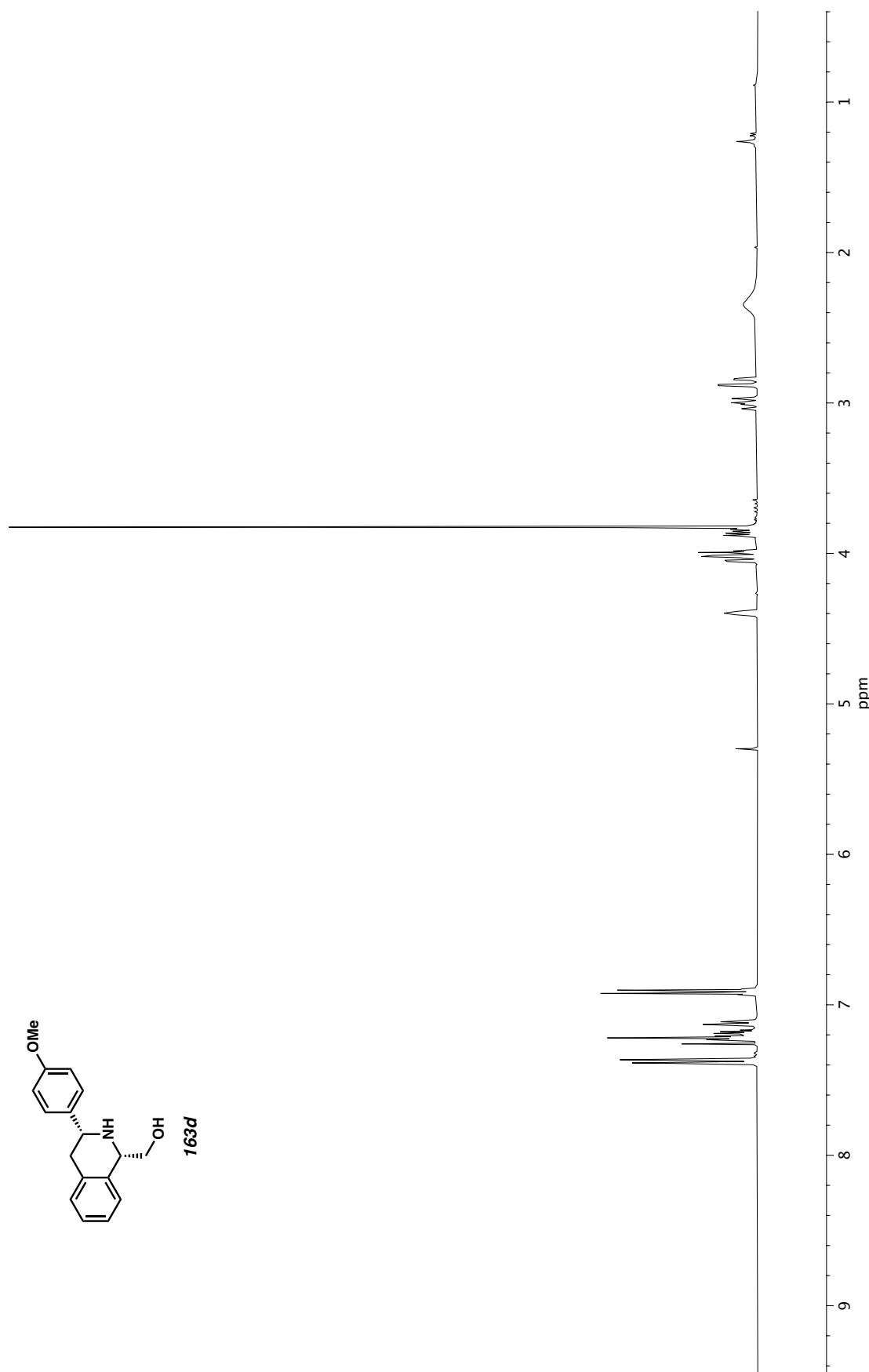


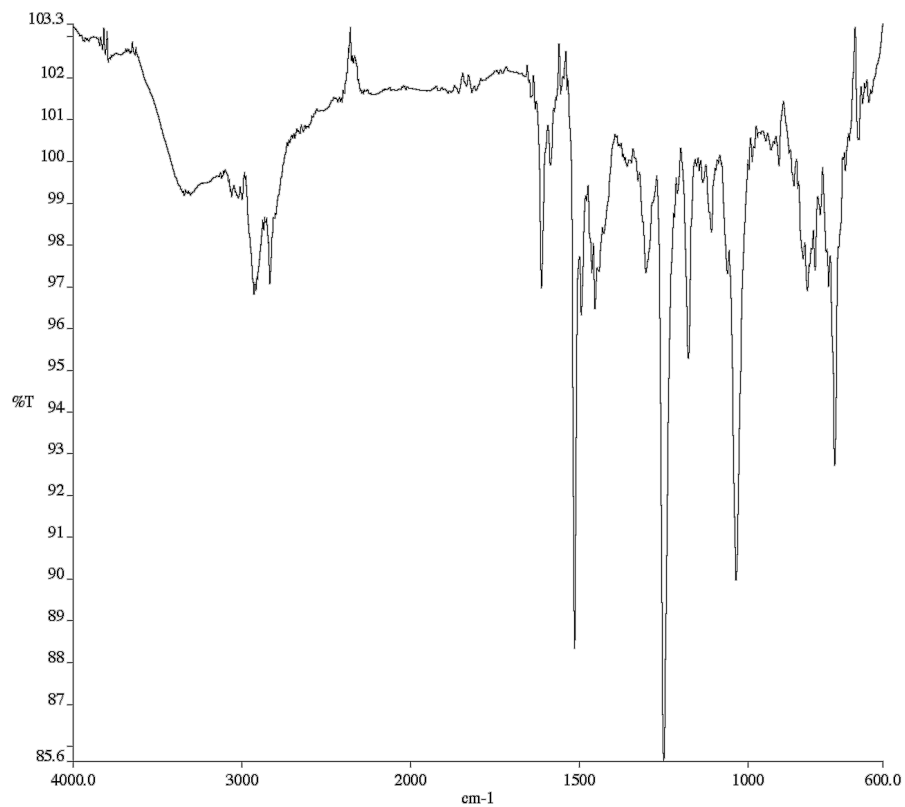


**Figure A1.210** Infrared spectrum (Thin Film, NaCl) of compound **163c**.

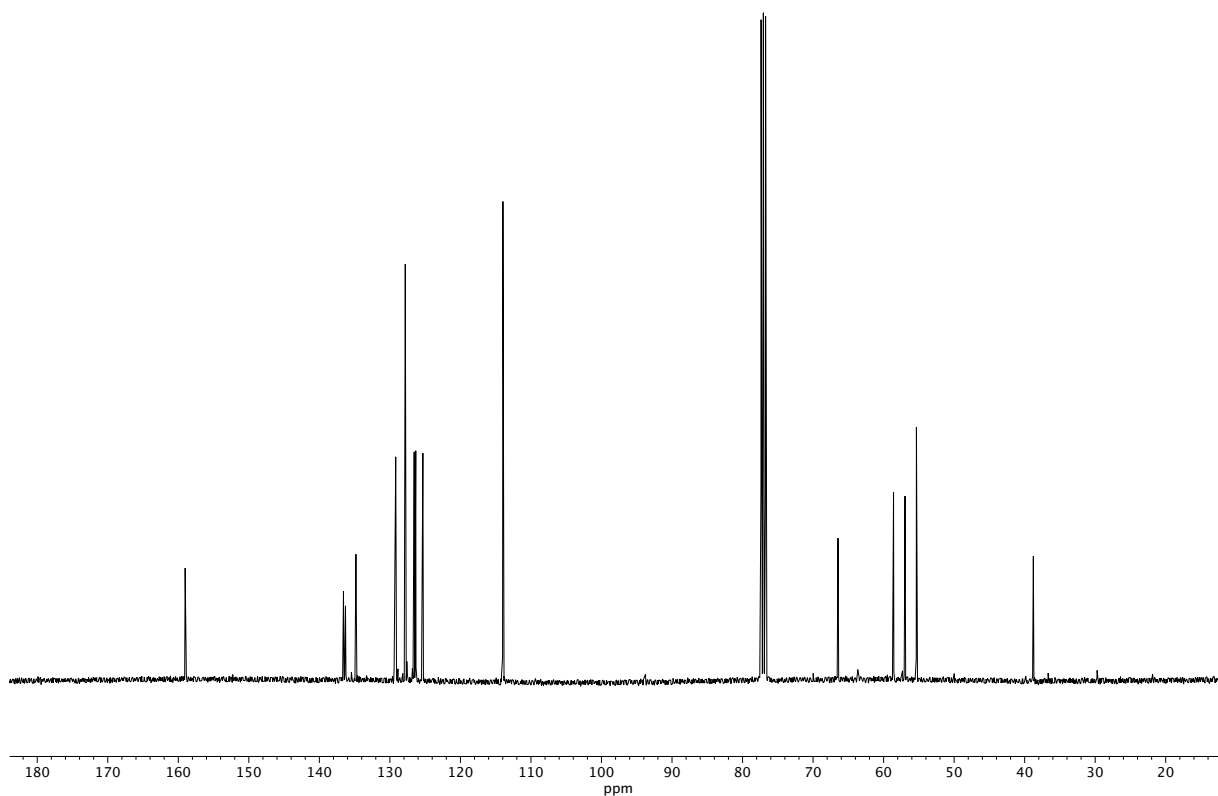


**Figure A1.211** <sup>13</sup>C NMR (100 MHz, CDCl<sub>3</sub>) of compound **163c**.

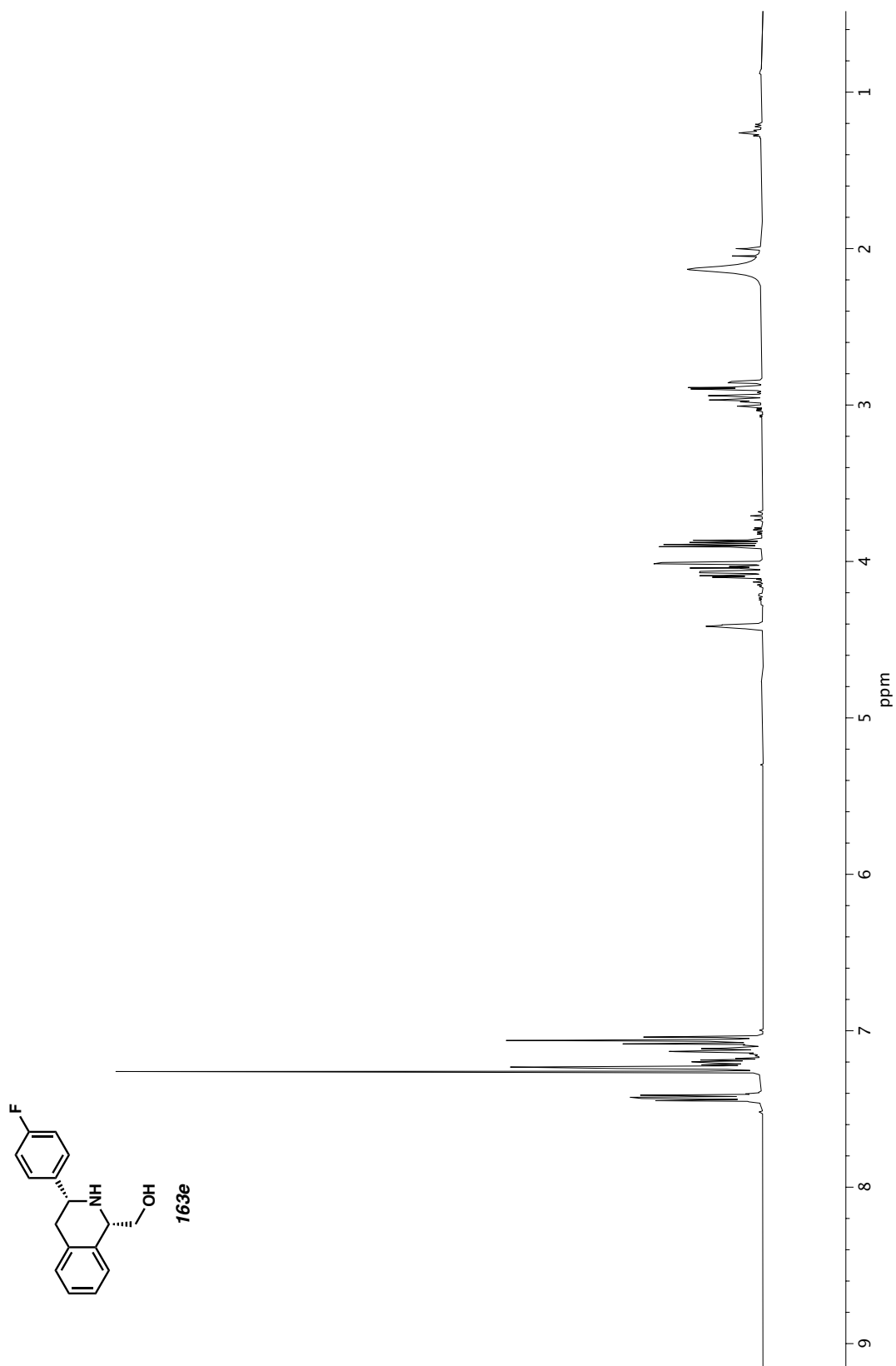




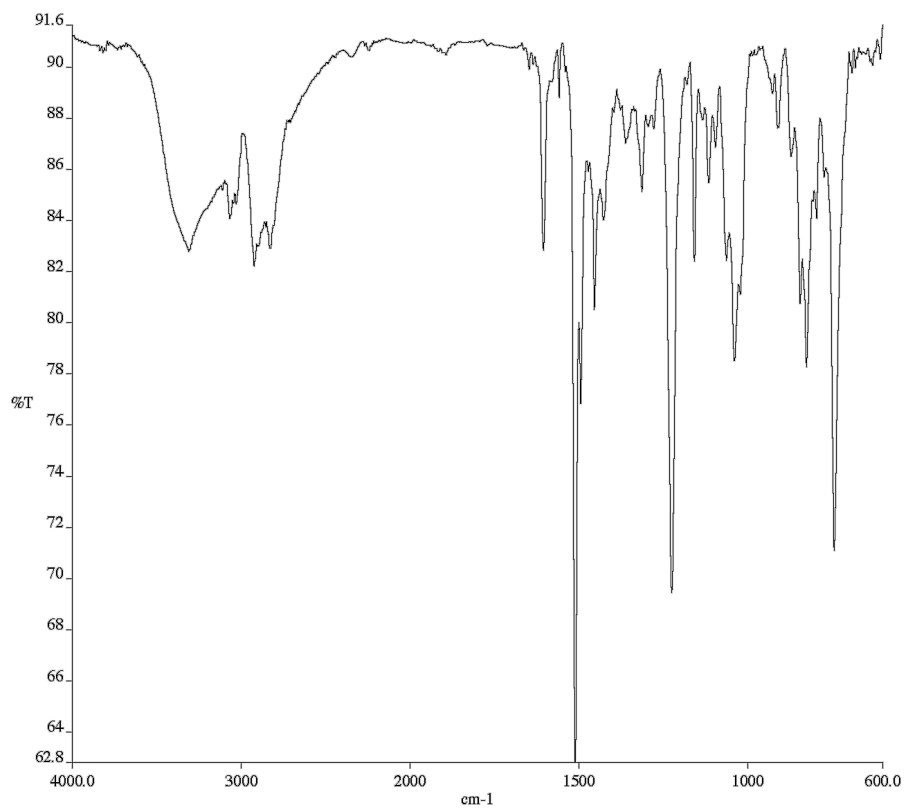
**Figure A1.213** Infrared spectrum (Thin Film, NaCl) of compound **163d**.



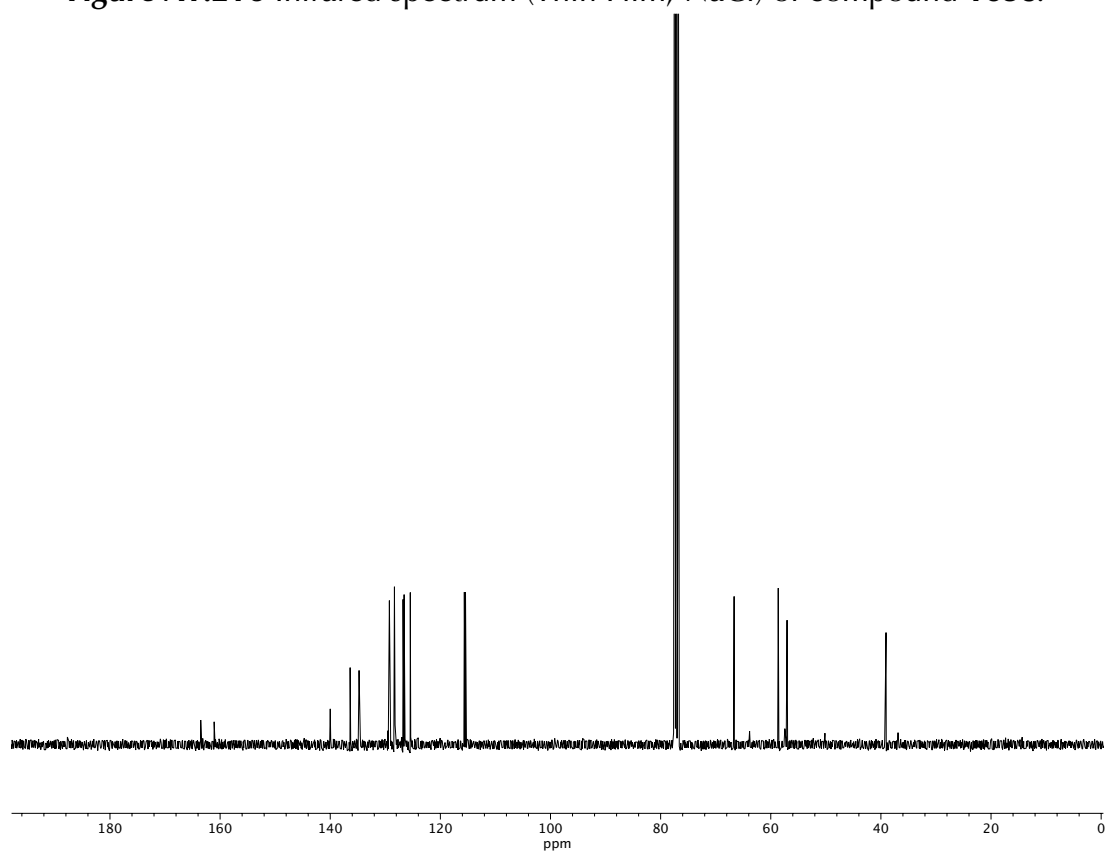
**Figure A1.214** <sup>13</sup>C NMR (100 MHz, CDCl<sub>3</sub>) of compound **163d**.



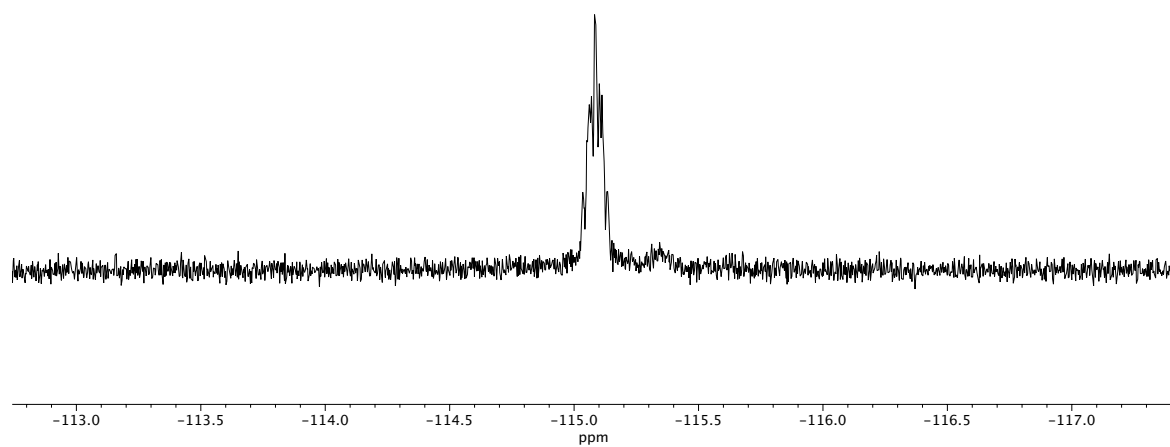
**Figure A1.215**  $^1\text{H}$  NMR (400 MHz,  $\text{CDCl}_3$ ) of compound **163e**.



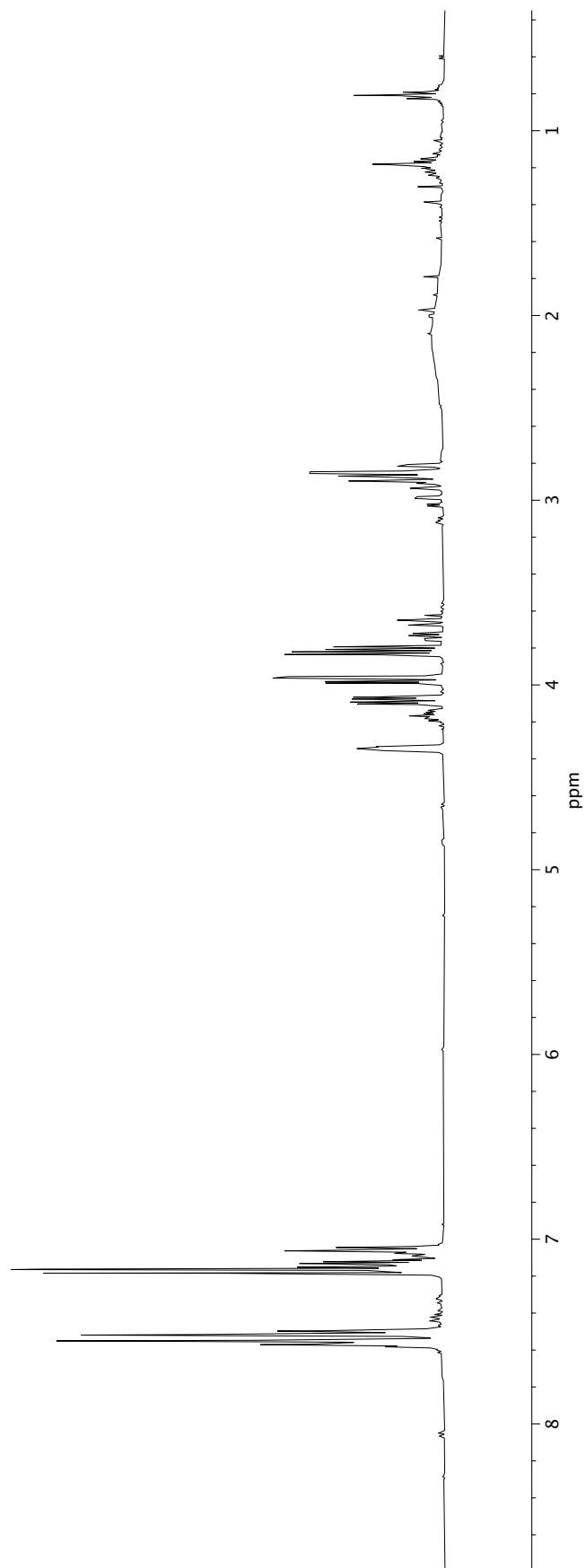
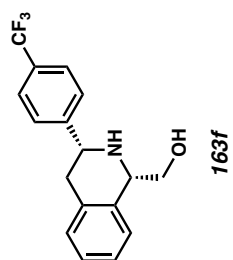
**Figure A1.216** Infrared spectrum (Thin Film, NaCl) of compound **163e**.



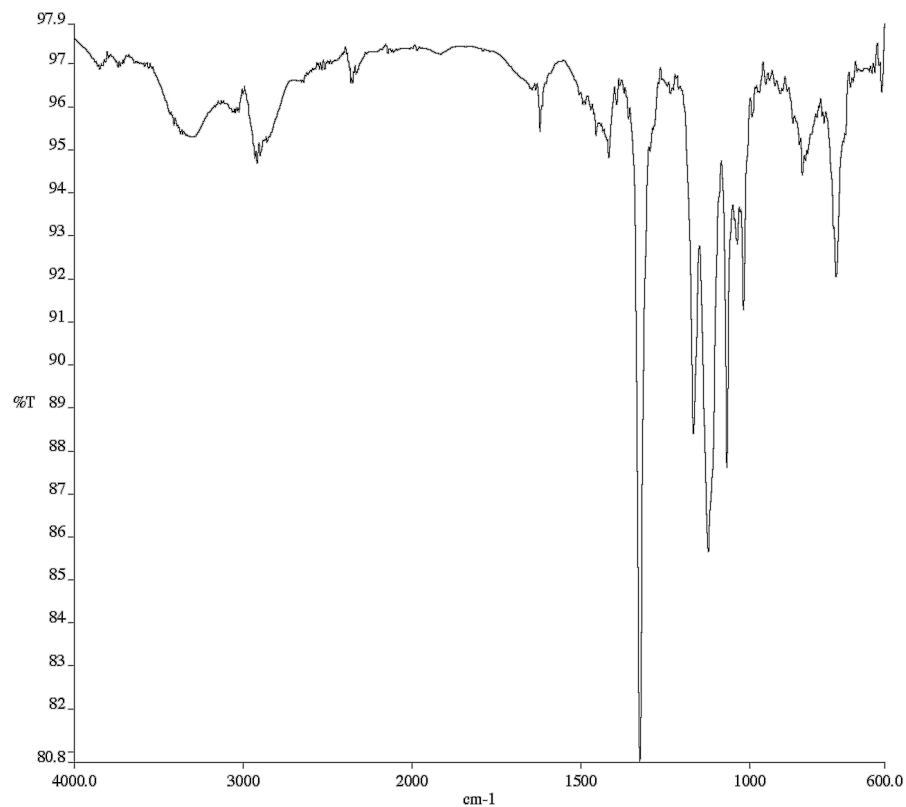
**Figure A1.217** <sup>13</sup>C NMR (100 MHz, CDCl<sub>3</sub>) of compound **163e**.



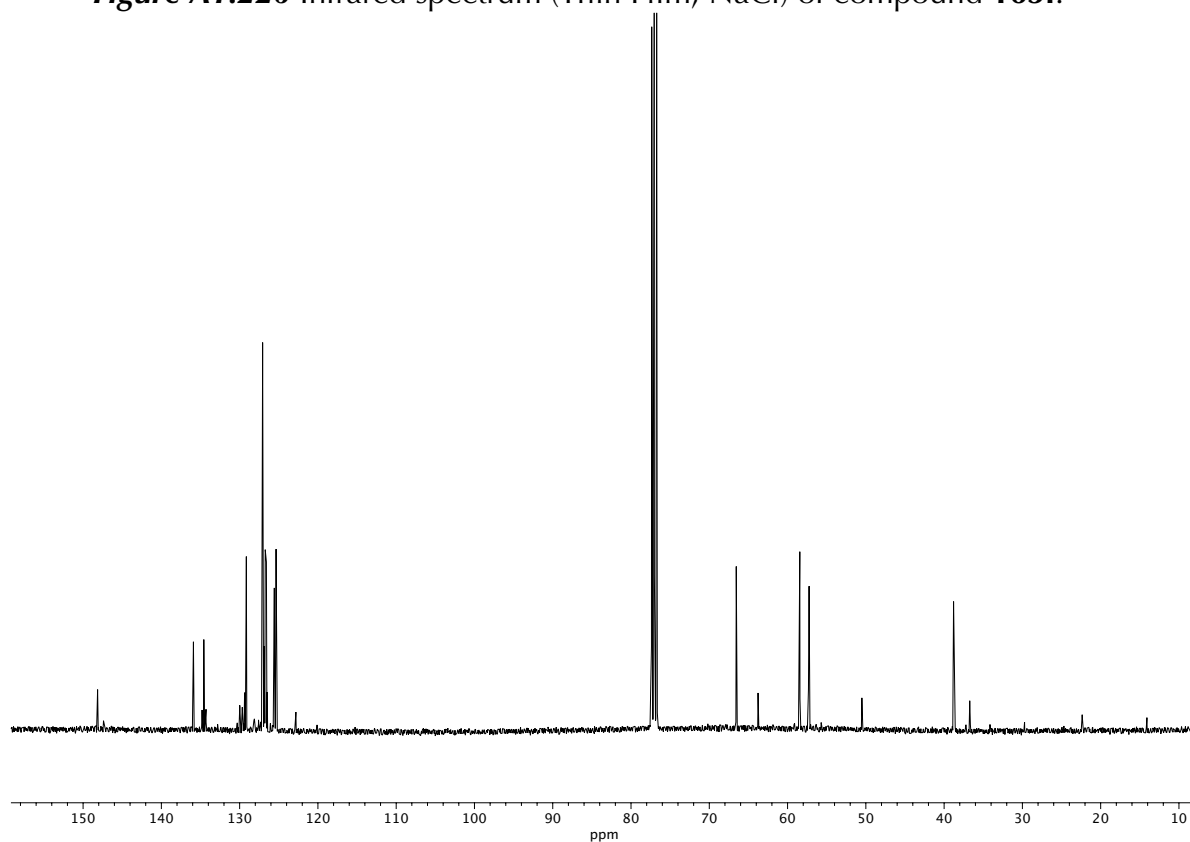
**Figure A1.218**  $^{19}\text{F}$  NMR (282 MHz,  $\text{CDCl}_3$ ) of compound **163e**.



**Figure A1.219** <sup>1</sup>H NMR (400 MHz, CDCl<sub>3</sub>) of compound **163f**.

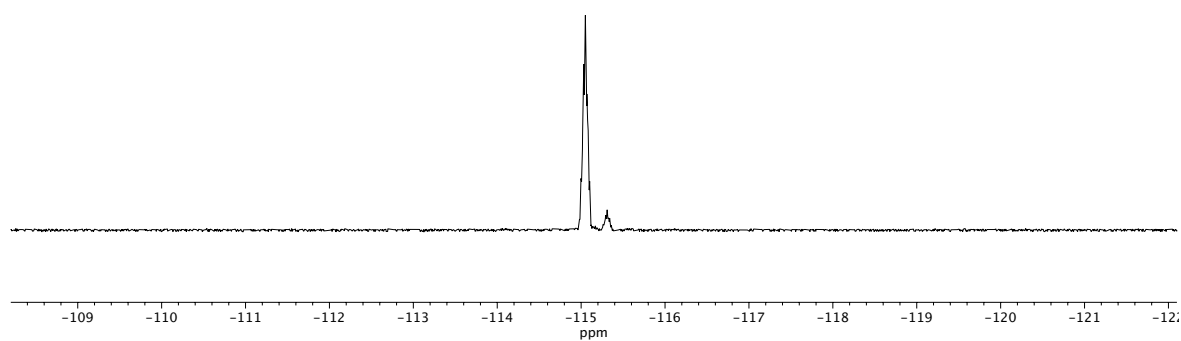


**Figure A1.220** Infrared spectrum (Thin Film, NaCl) of compound **163f**.

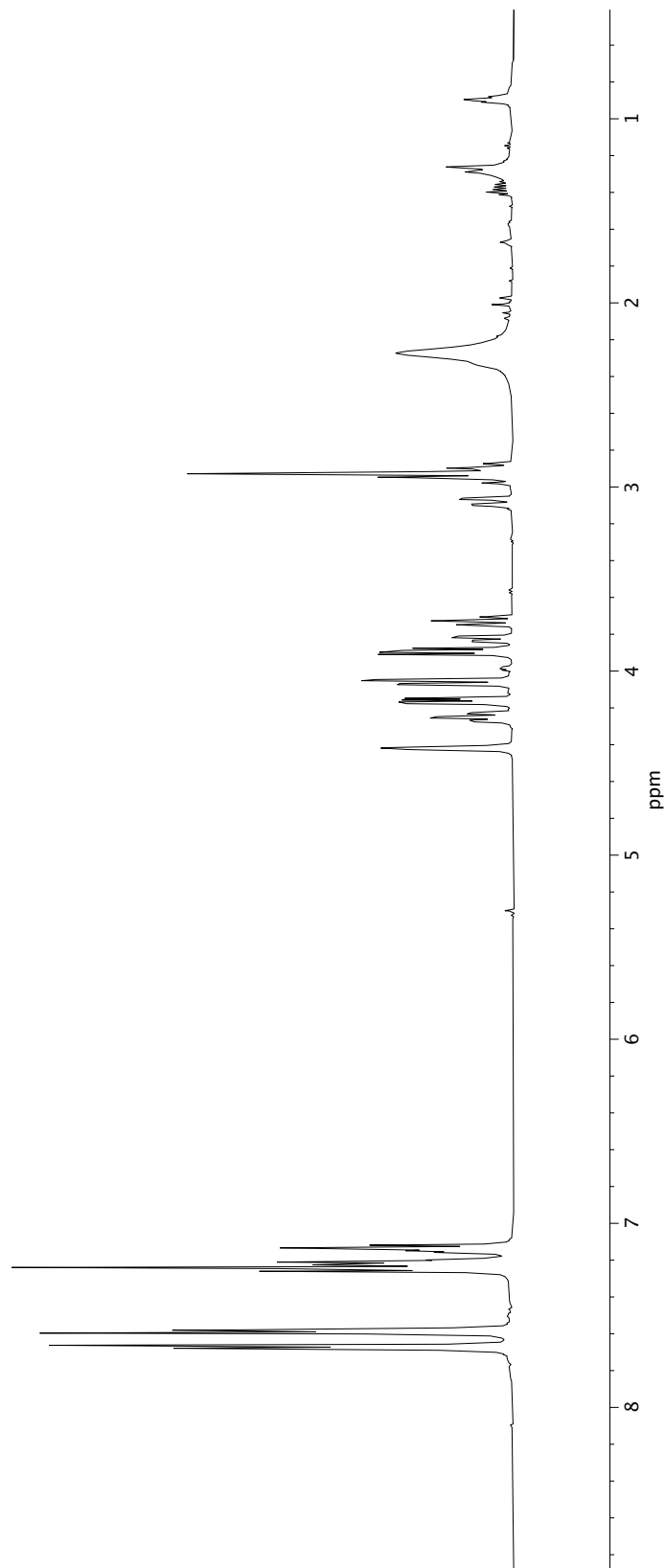
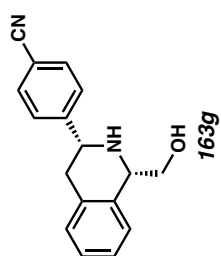


**Figure A1.221** <sup>13</sup>C NMR (100 MHz, CDCl<sub>3</sub>) of compound **163f**.

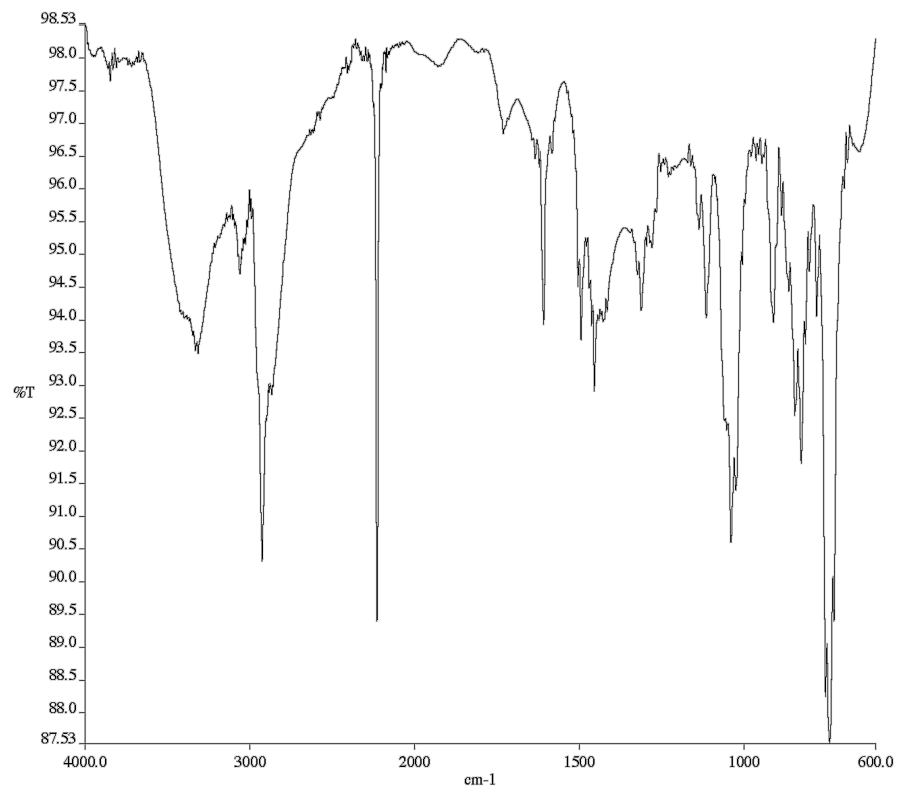




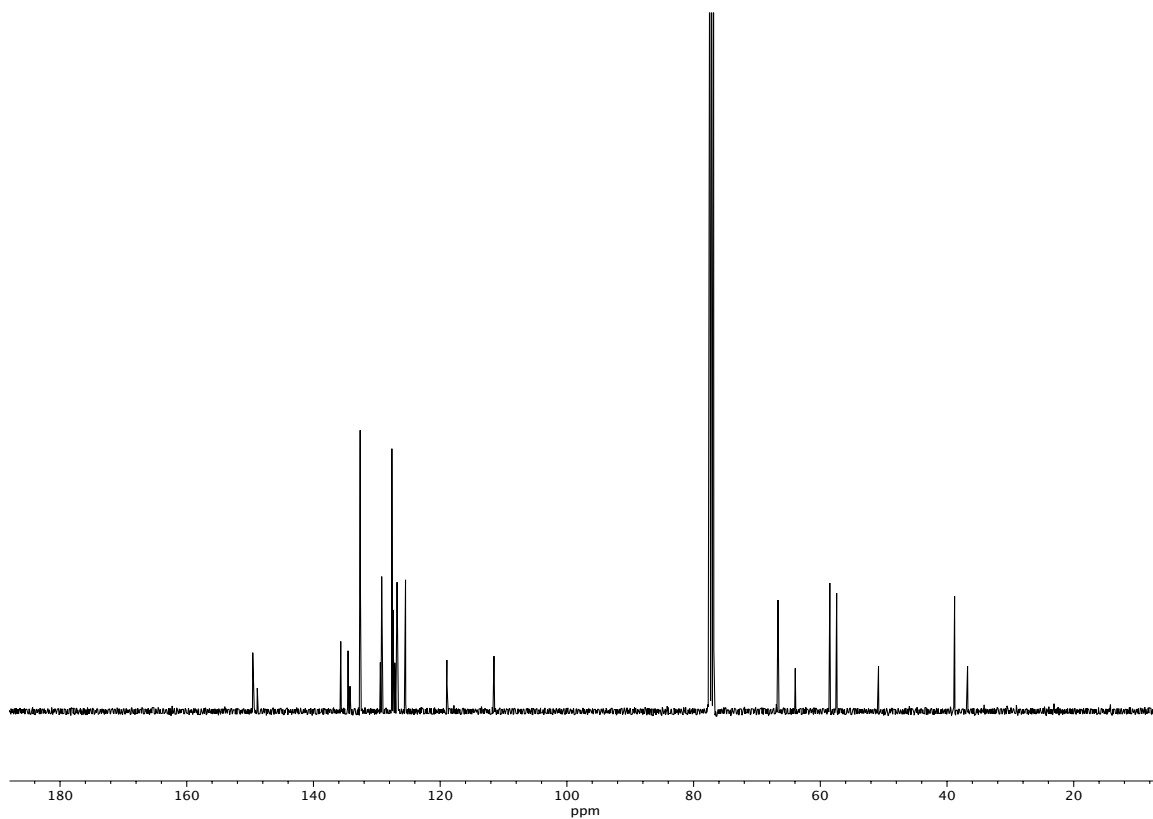
**Figure A1.222**  $^{19}\text{F}$  NMR (282 MHz,  $\text{CDCl}_3$ ) of compound **163f**.



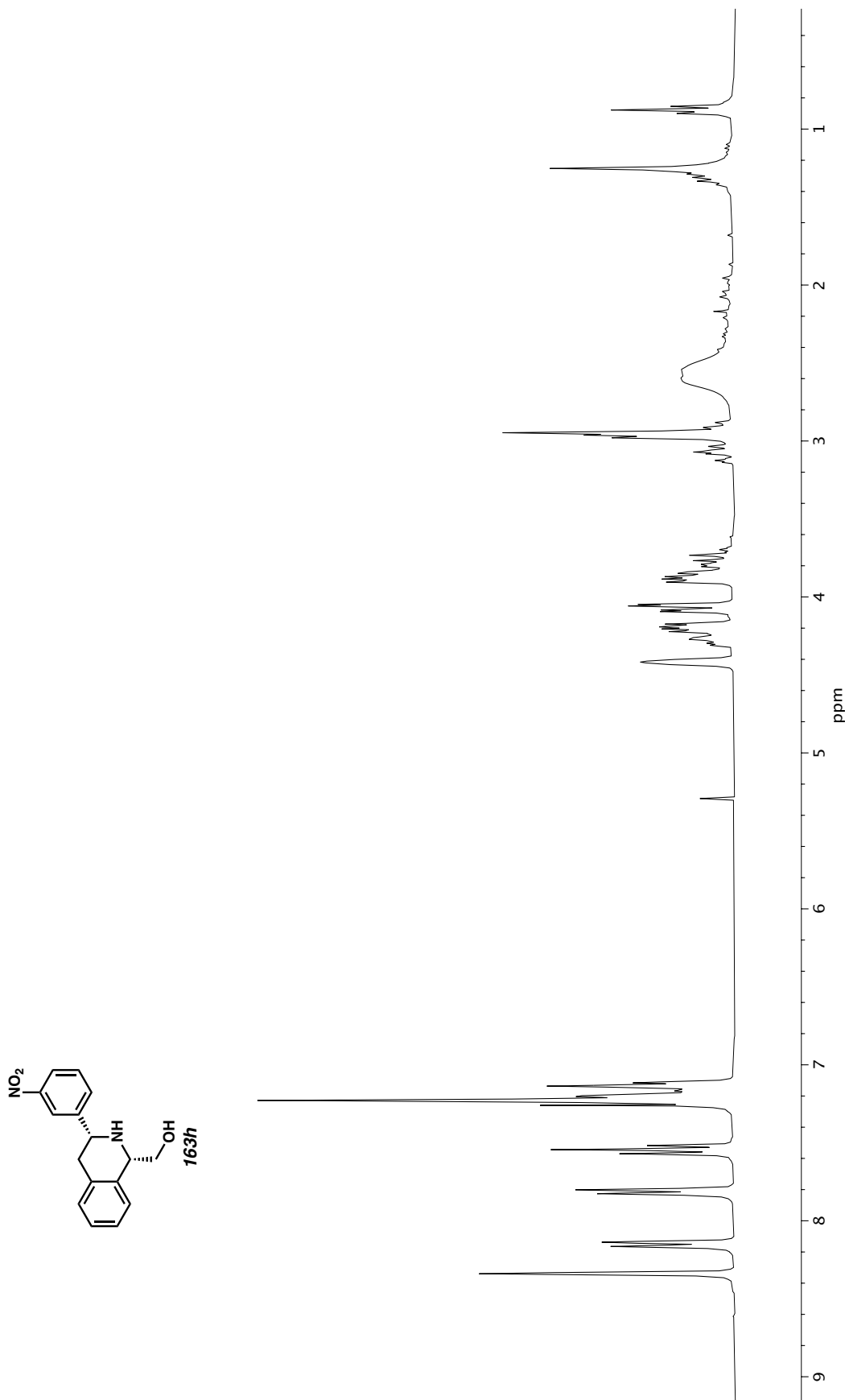
**Figure A1.223** <sup>1</sup>H NMR (400 MHz, CDCl<sub>3</sub>) of compound **163g**.

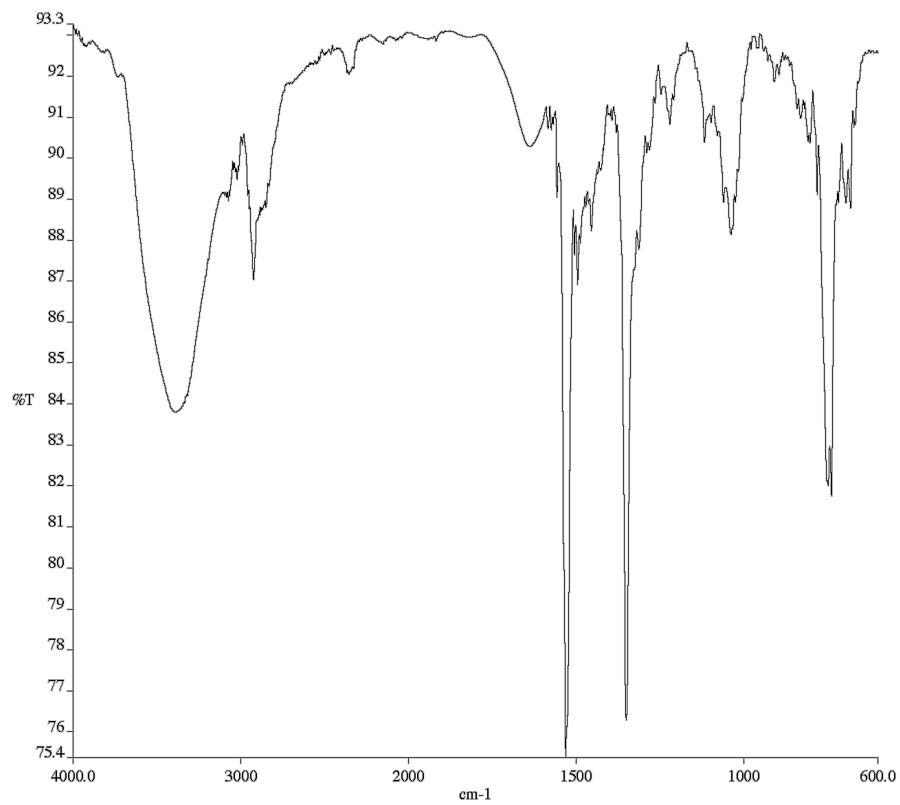


**Figure A1.224** Infrared spectrum (Thin Film, NaCl) of compound **163g**.

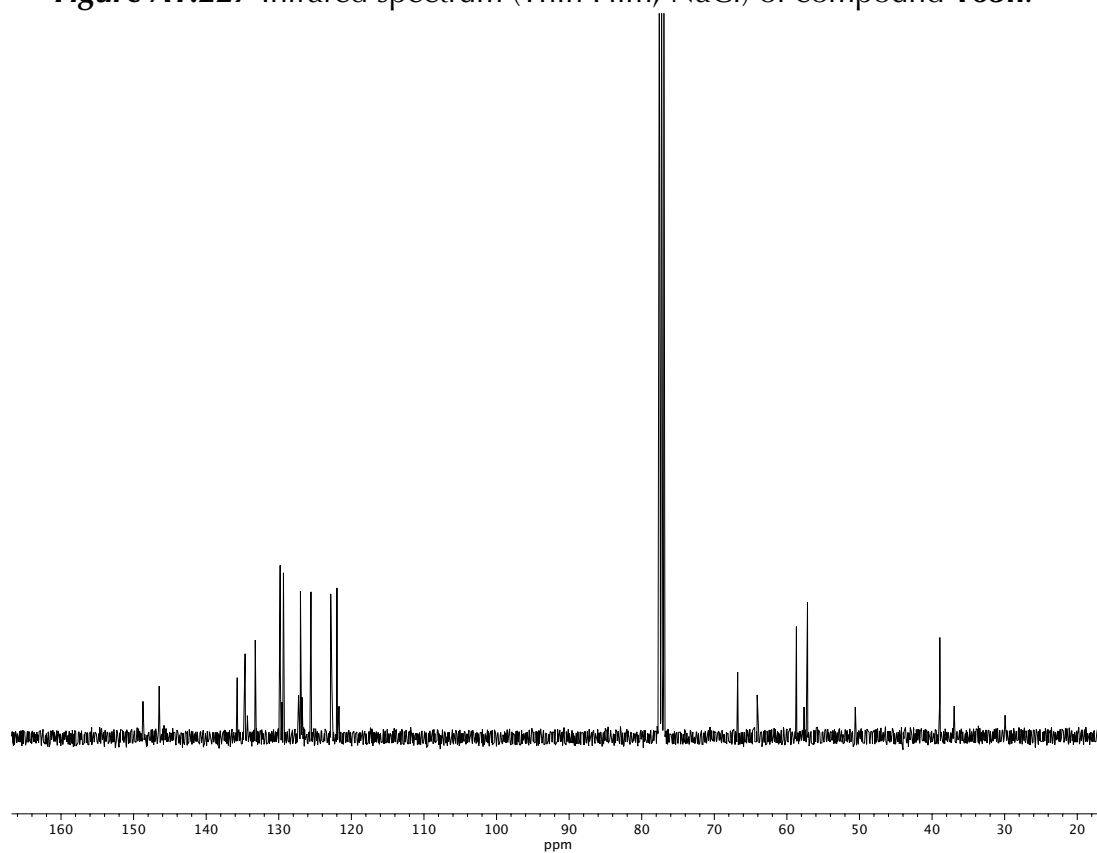


**Figure A1.225** <sup>13</sup>C NMR (100 MHz, CDCl<sub>3</sub>) of compound **163g**.

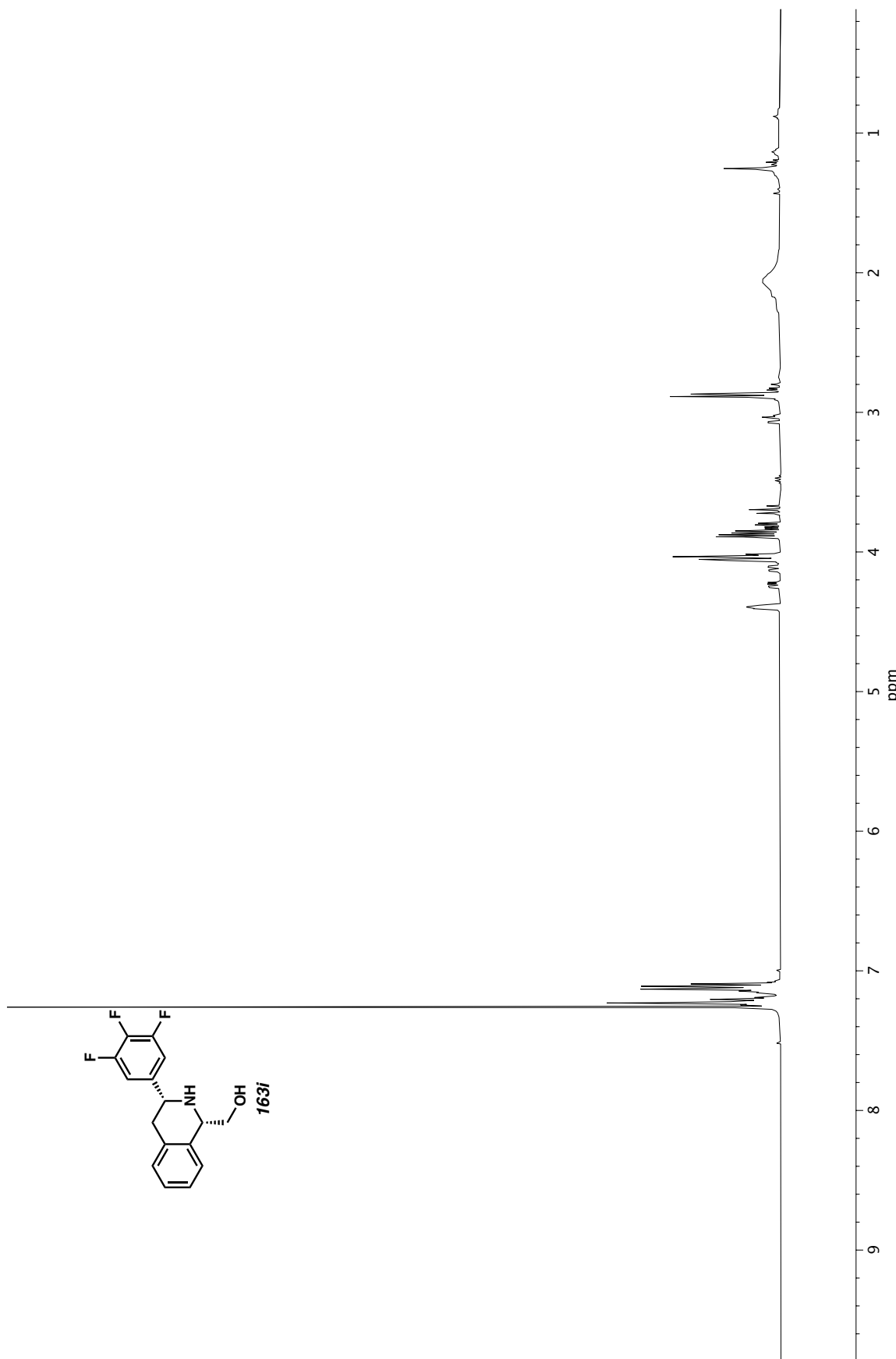


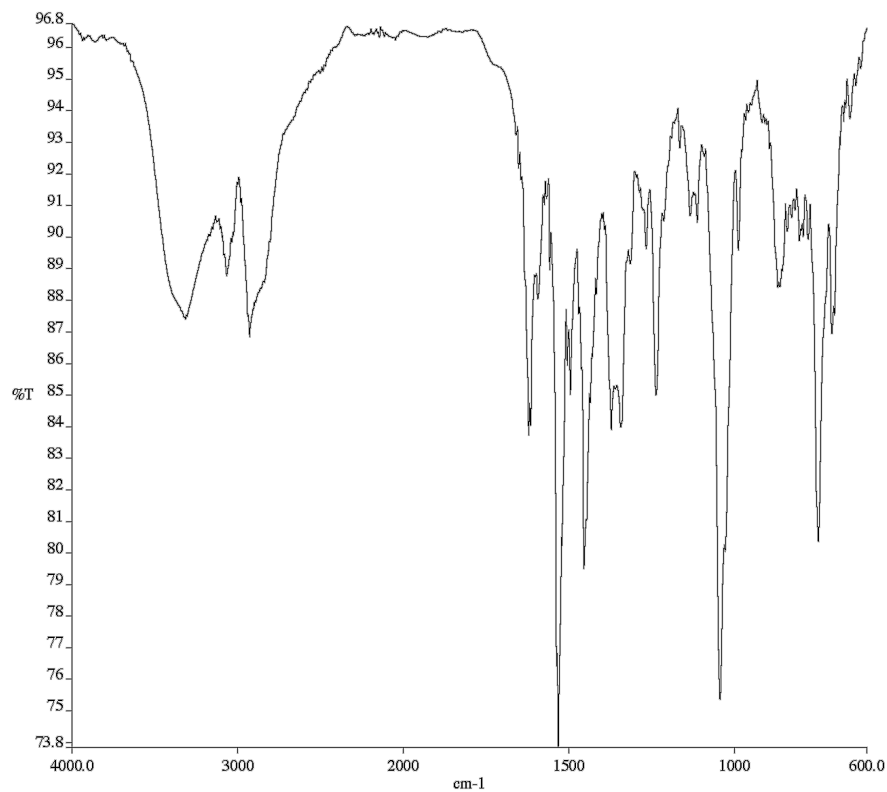


**Figure A1.227** Infrared spectrum (Thin Film, NaCl) of compound **163h**.

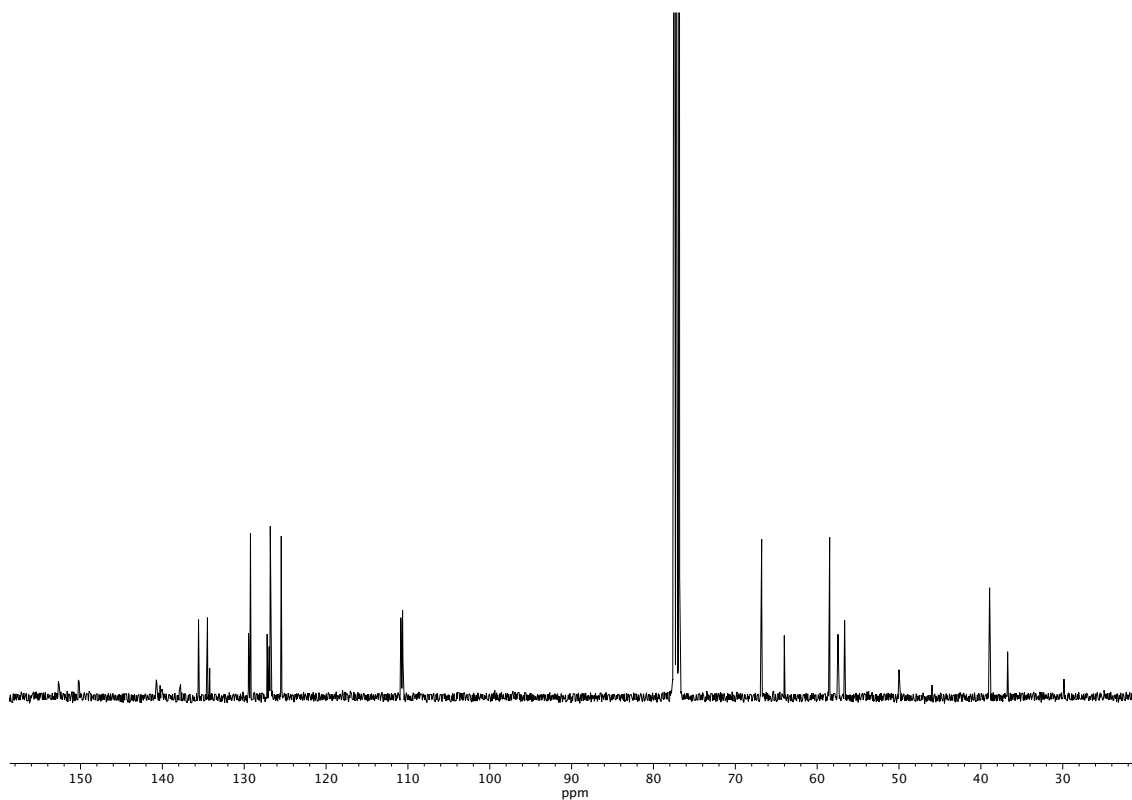


**Figure A1.228** <sup>13</sup>C NMR (100 MHz, CDCl<sub>3</sub>) of compound **163h**.

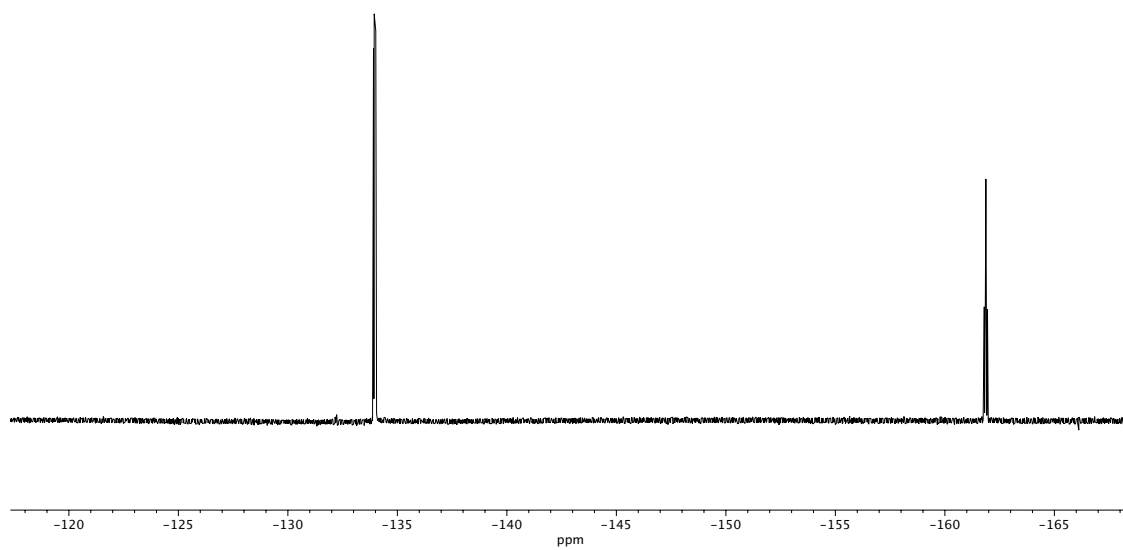




**Figure A1.230** Infrared spectrum (Thin Film, NaCl) of compound **163i**.

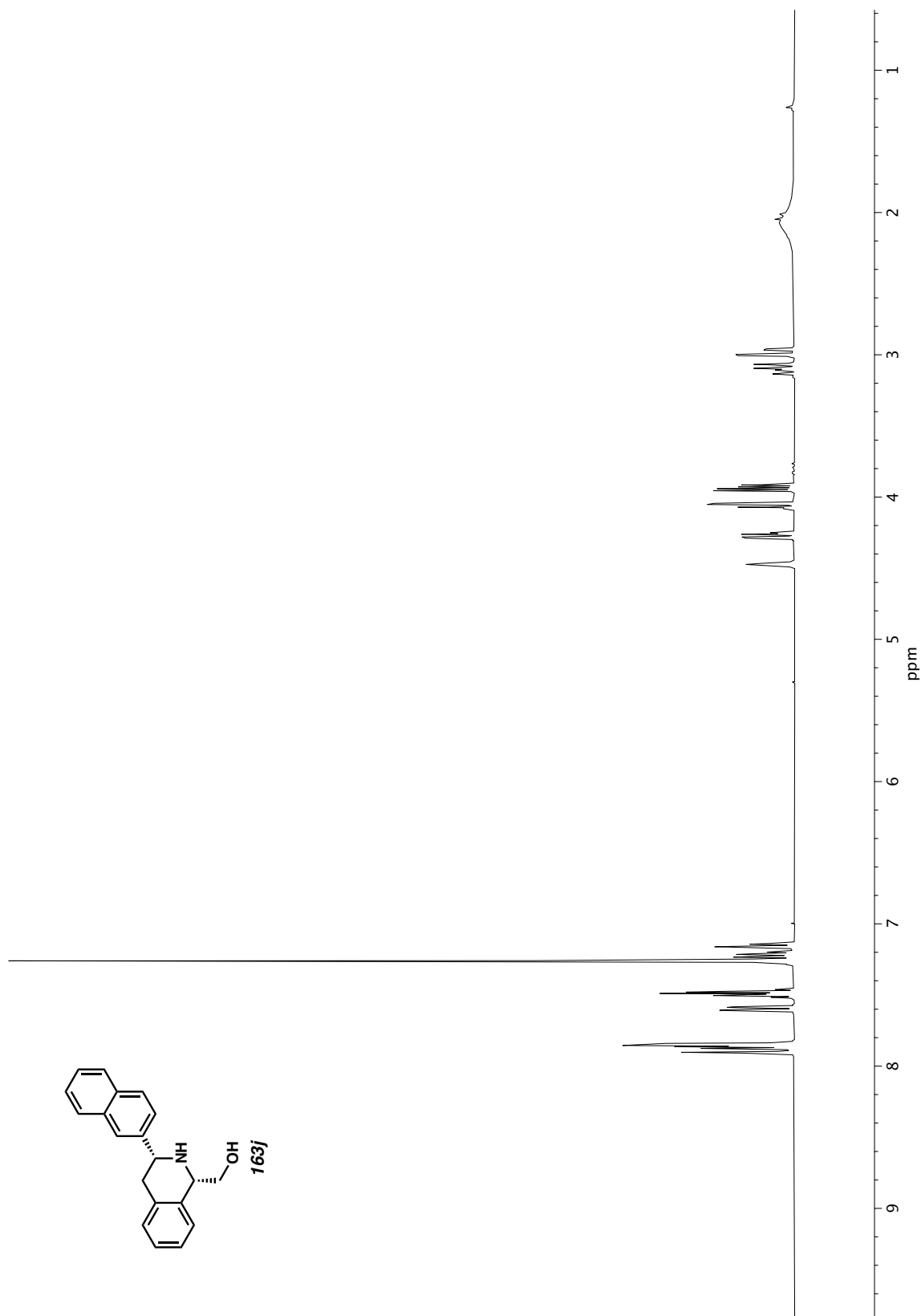


**Figure A1.231** <sup>13</sup>C NMR (100 MHz, CDCl<sub>3</sub>) of compound **163i**.

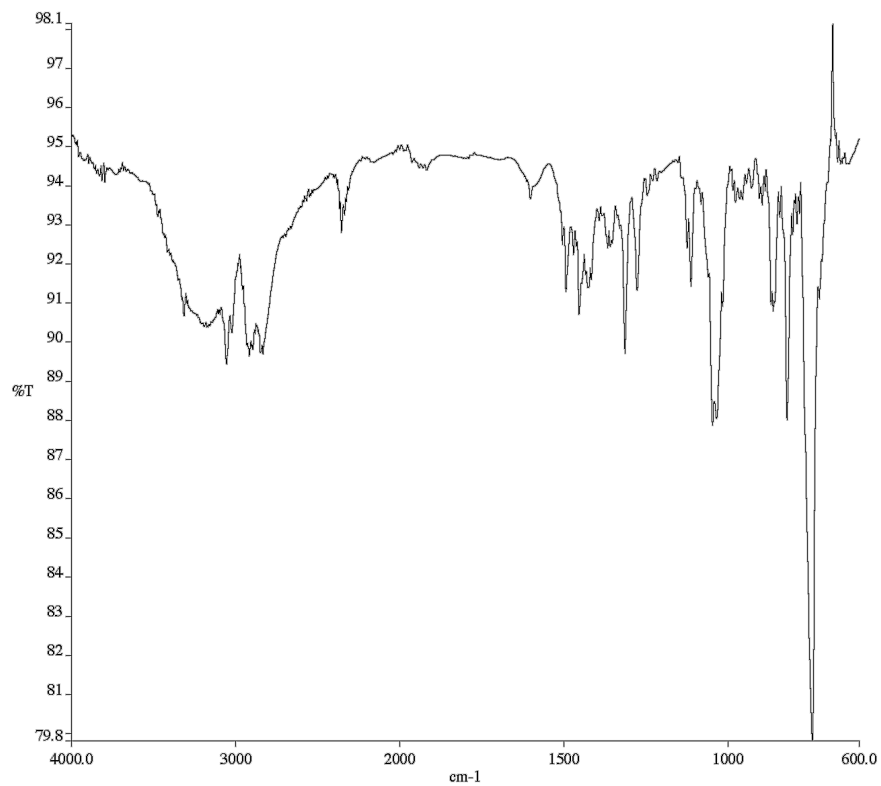


**Figure A1.232**  $^{19}\text{F}$  NMR (282 MHz,  $\text{CDCl}_3$ ) of compound **163i**.

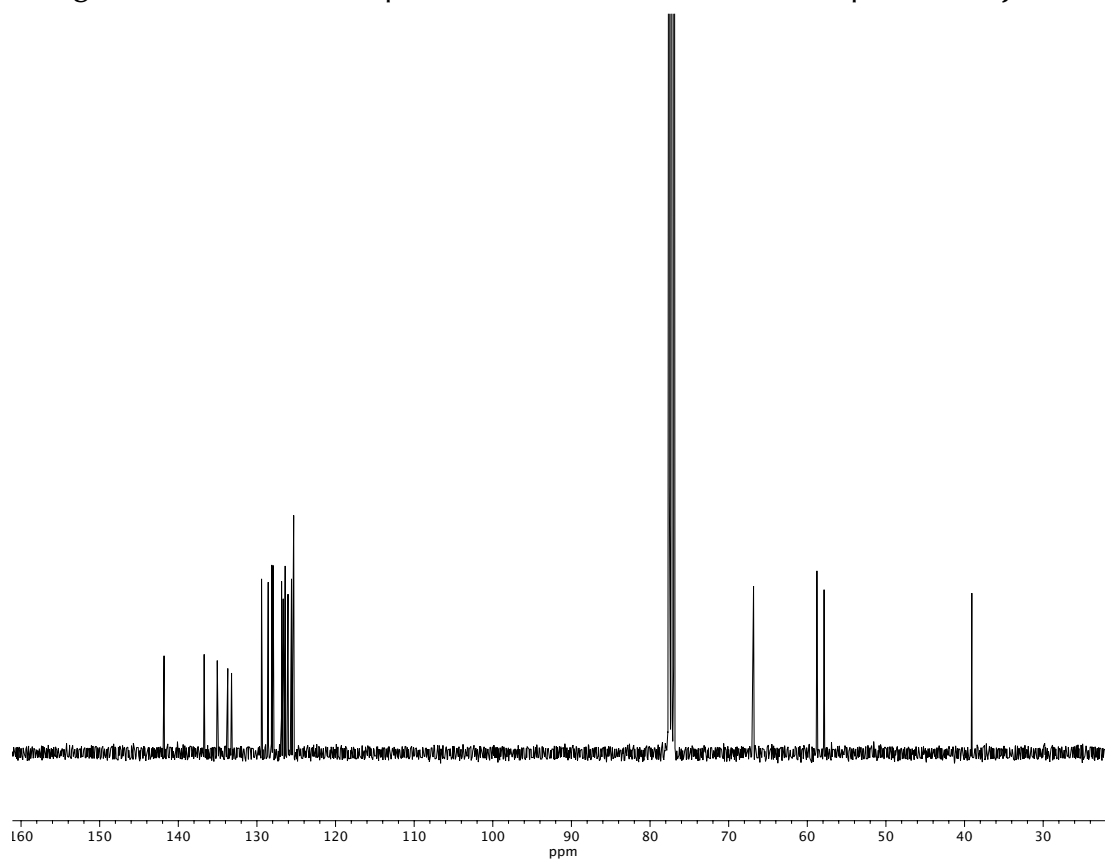




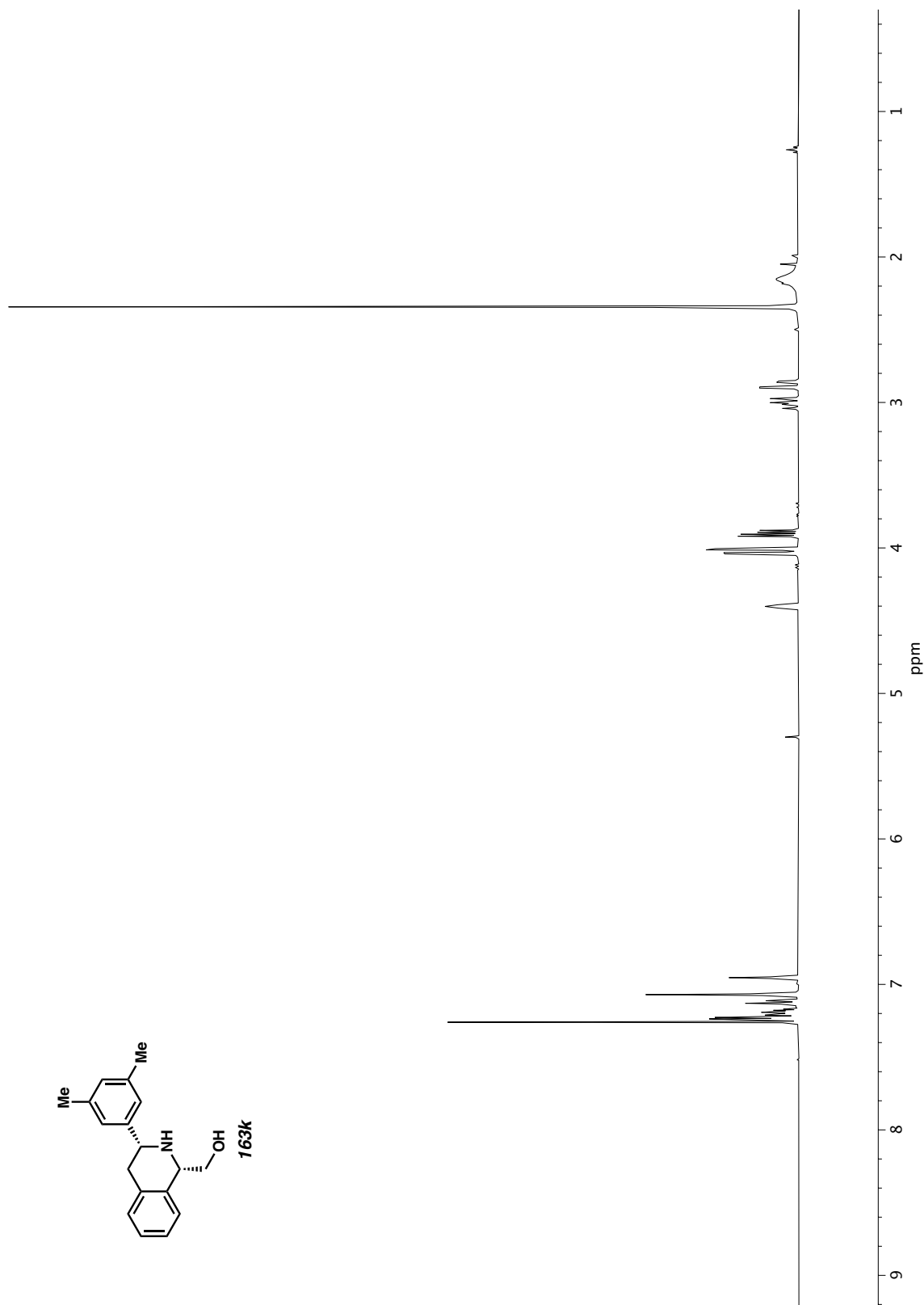
**Figure A1.233** <sup>1</sup>H NMR (400 MHz, CDCl<sub>3</sub>) of compound **163j**.



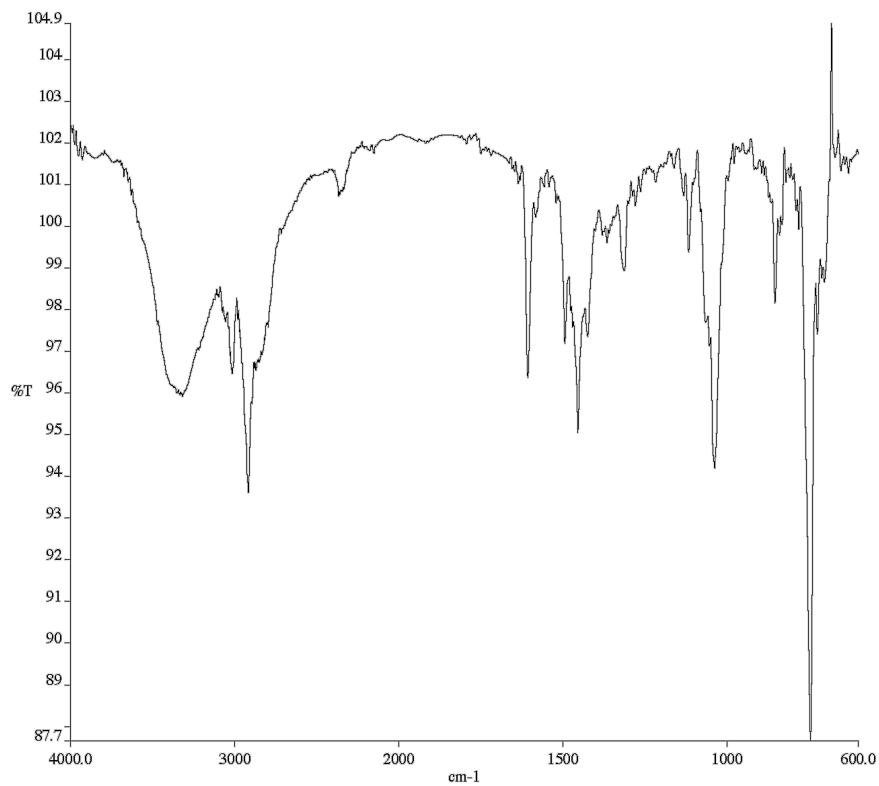
**Figure A1.234** Infrared spectrum (Thin Film, NaCl) of compound **163j**.



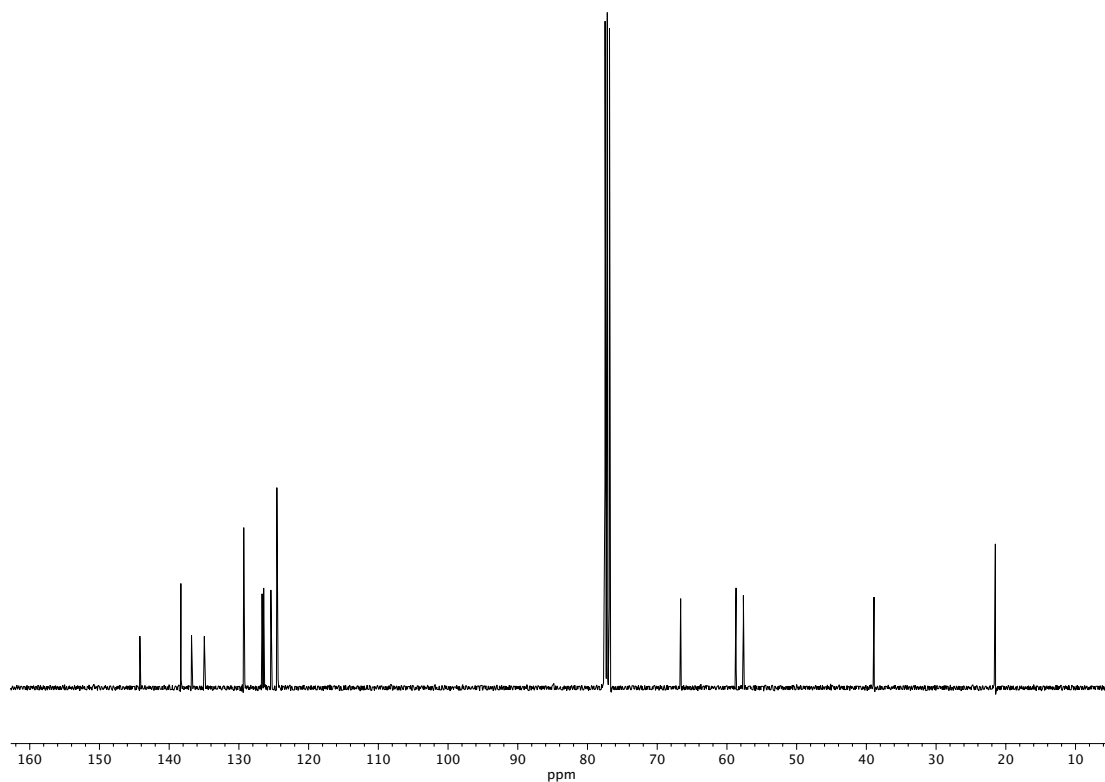
**Figure A1.235** <sup>13</sup>C NMR (100 MHz, CDCl<sub>3</sub>) of compound **163j**.



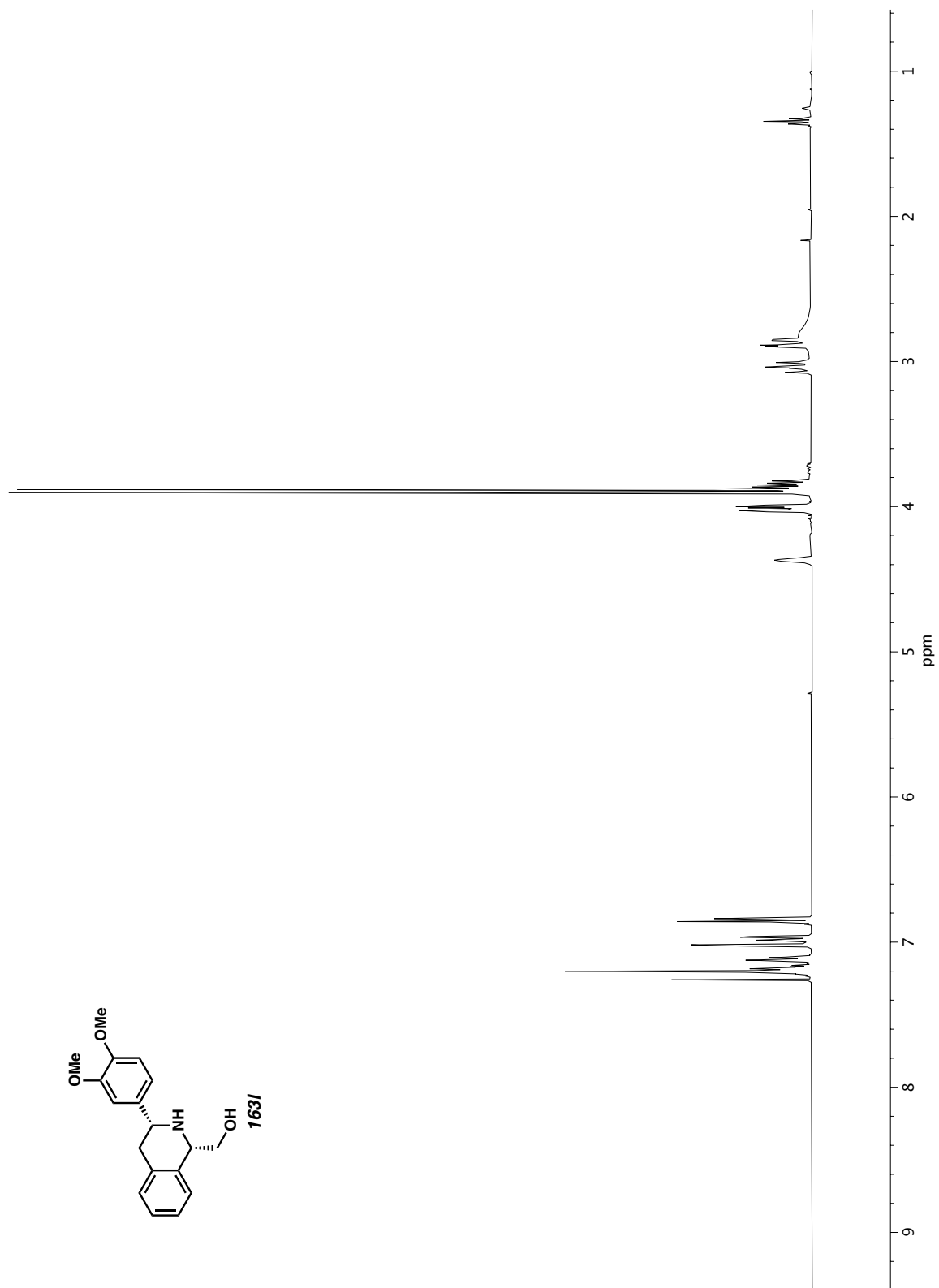
**Figure A1.236**  $^1\text{H}$  NMR (400 MHz,  $\text{CDCl}_3$ ) of compound **163k**.



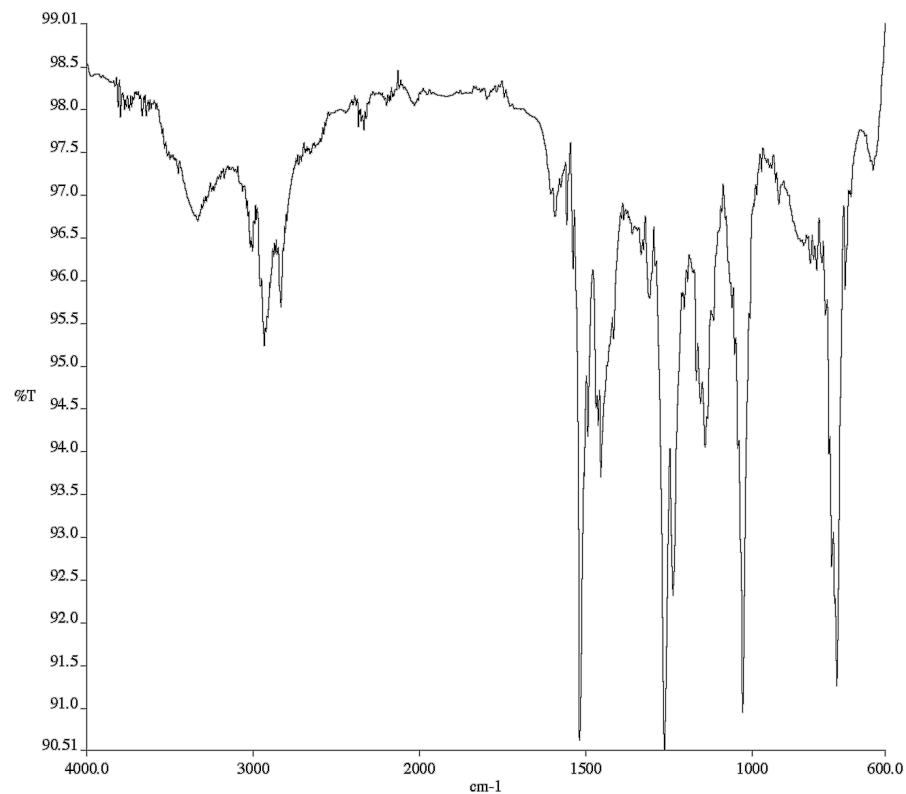
**Figure A1.237** Infrared spectrum (Thin Film, NaCl) of compound **163k**.



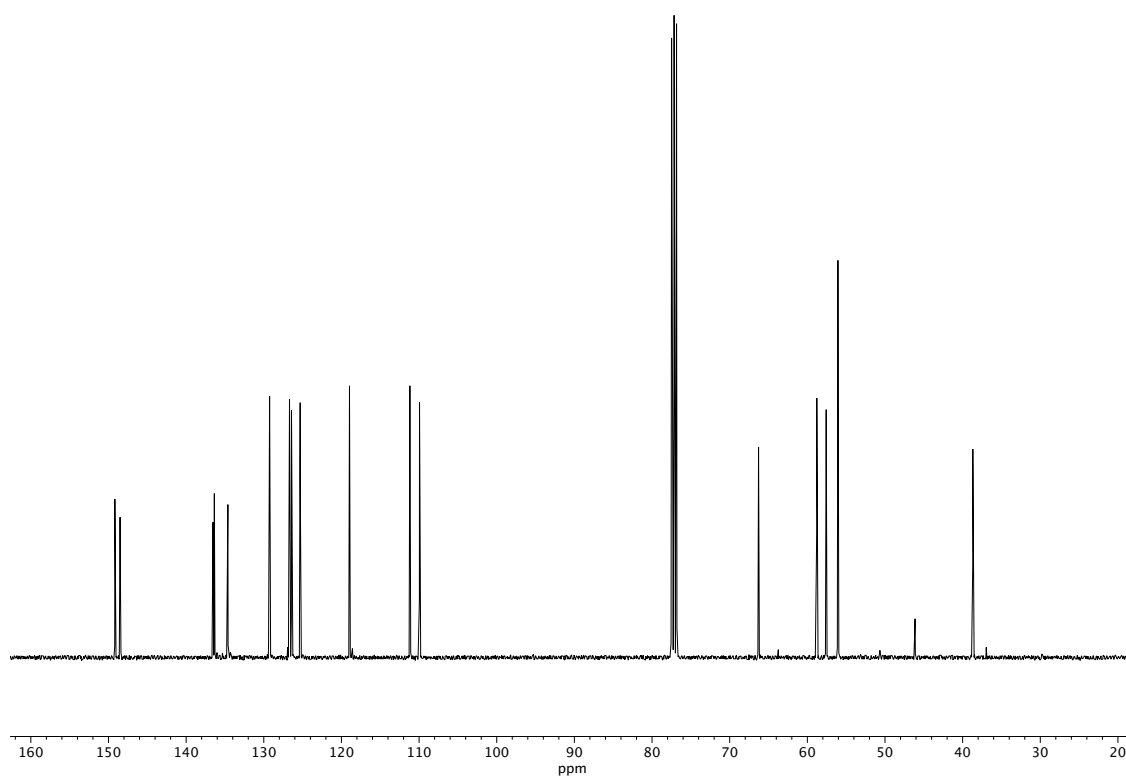
**Figure A1.238** <sup>13</sup>C NMR (100 MHz, CDCl<sub>3</sub>) of compound **163k**.



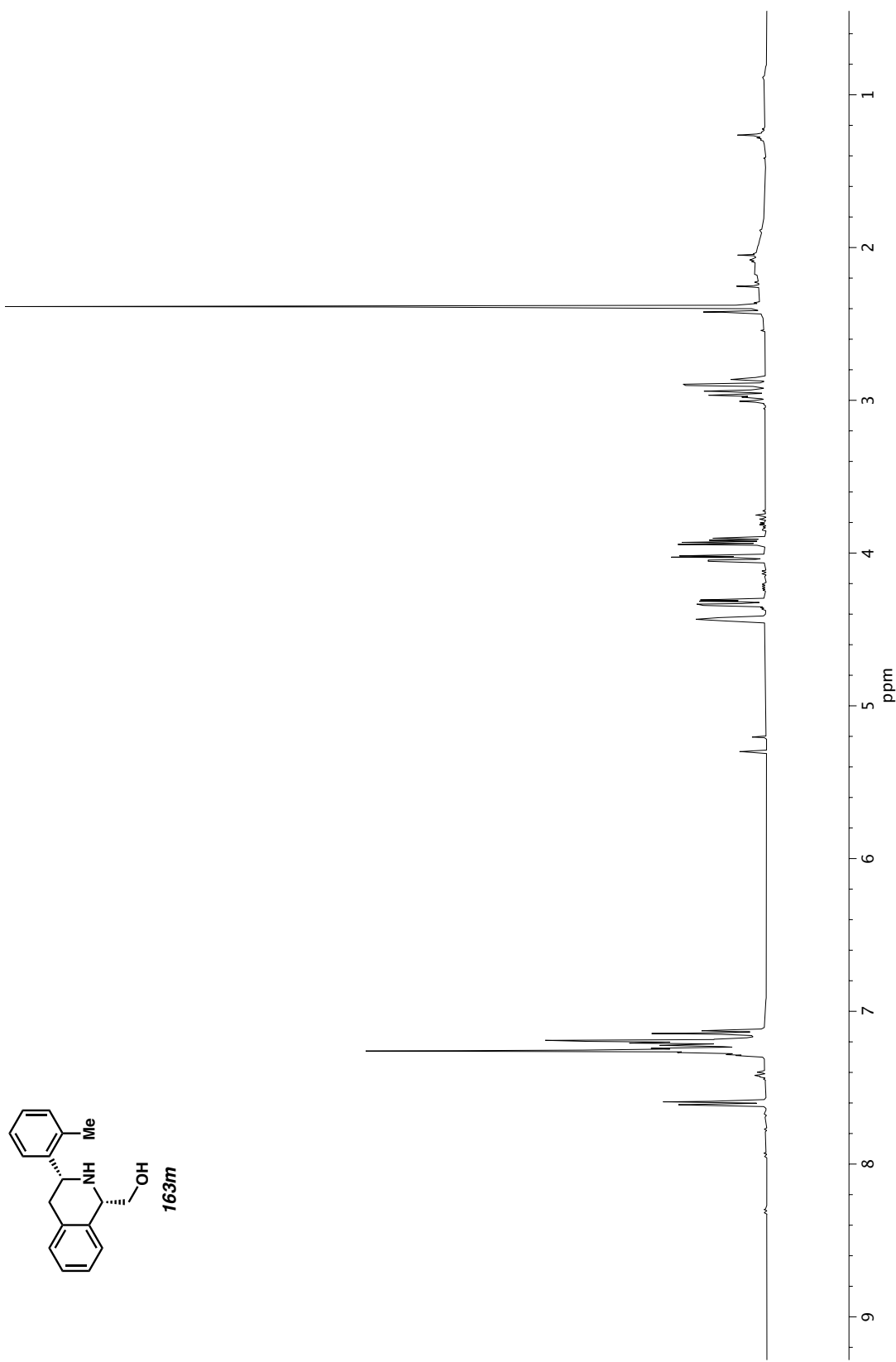
**Figure A1.239**  $^1\text{H}$  NMR (400 MHz,  $\text{CDCl}_3$ ) of compound **163I**.



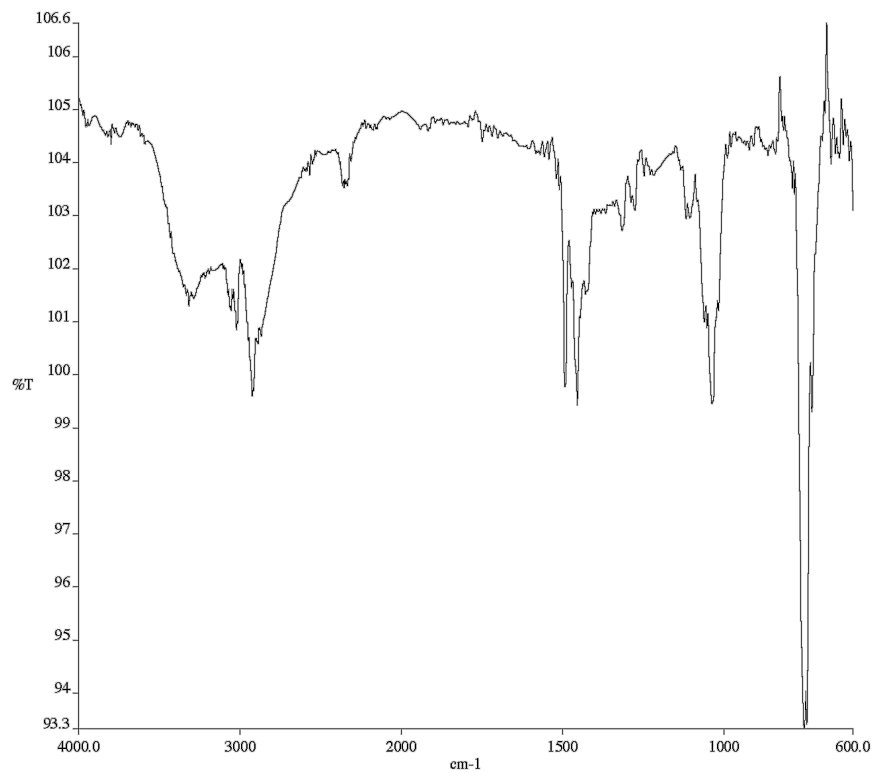
**Figure A1.240** Infrared spectrum (Thin Film, NaCl) of compound **163I**.



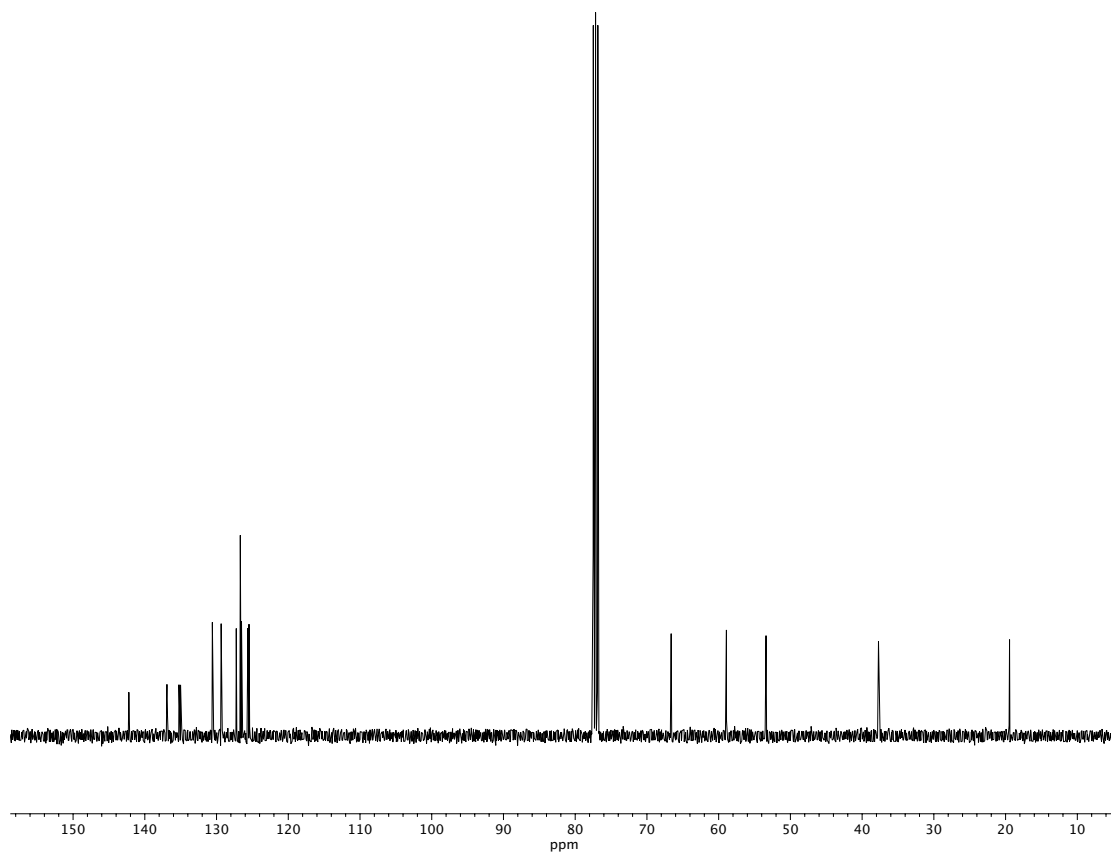
**Figure A1.241** <sup>13</sup>C NMR (100 MHz, CDCl<sub>3</sub>) of compound **163I**.



**Figure A1.242**  $^1\text{H}$  NMR (400 MHz,  $\text{CDCl}_3$ ) of compound **163m**.

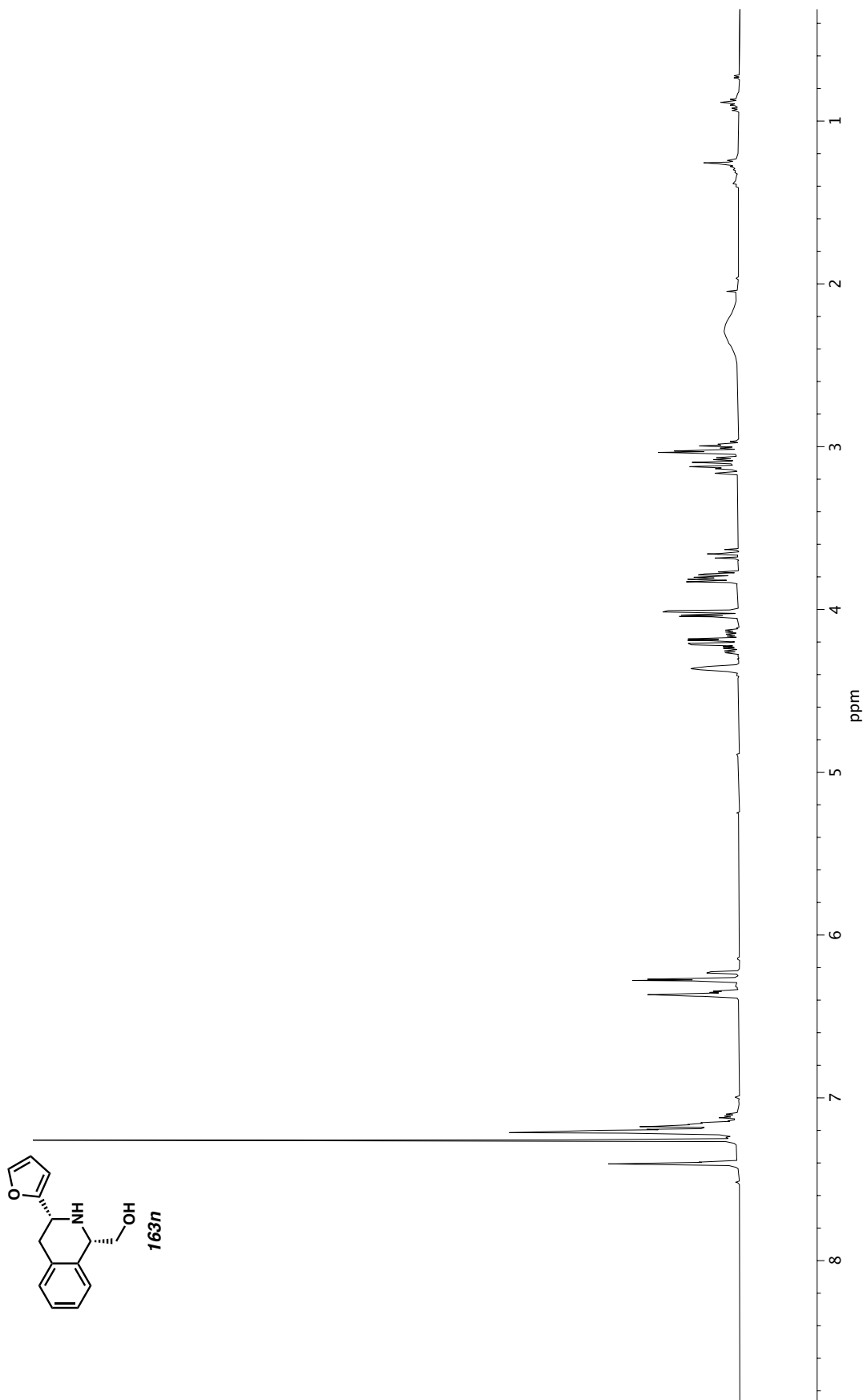


**Figure A1.243** Infrared spectrum (Thin Film, NaCl) of compound **163m**.

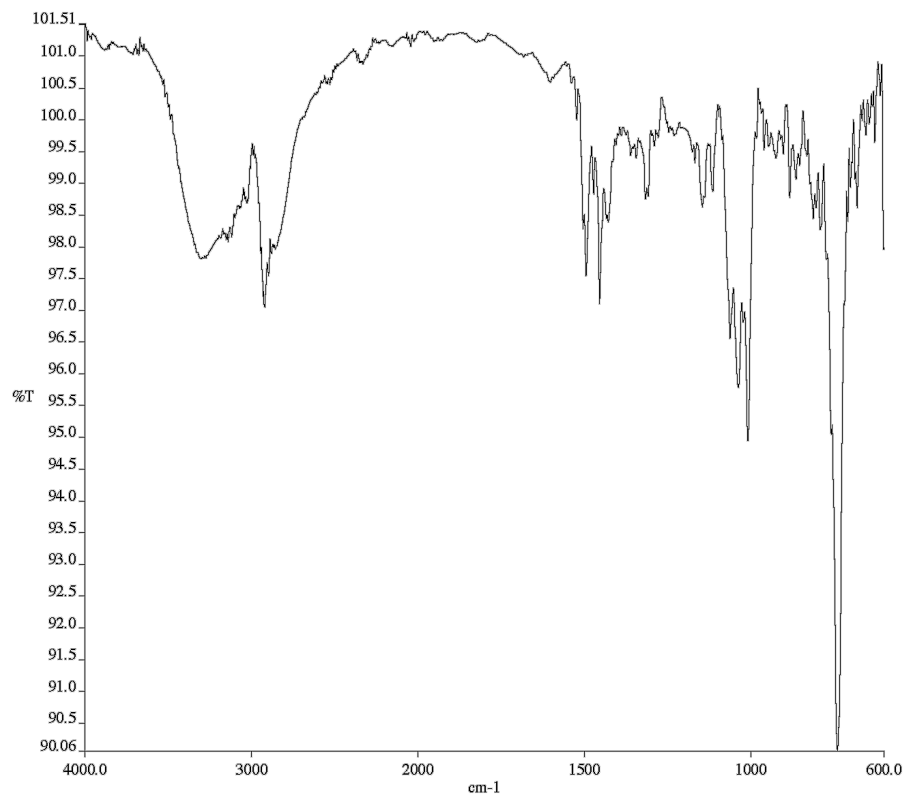


**Figure A1.244** <sup>13</sup>C NMR (100 MHz, CDCl<sub>3</sub>) of compound **163m**.

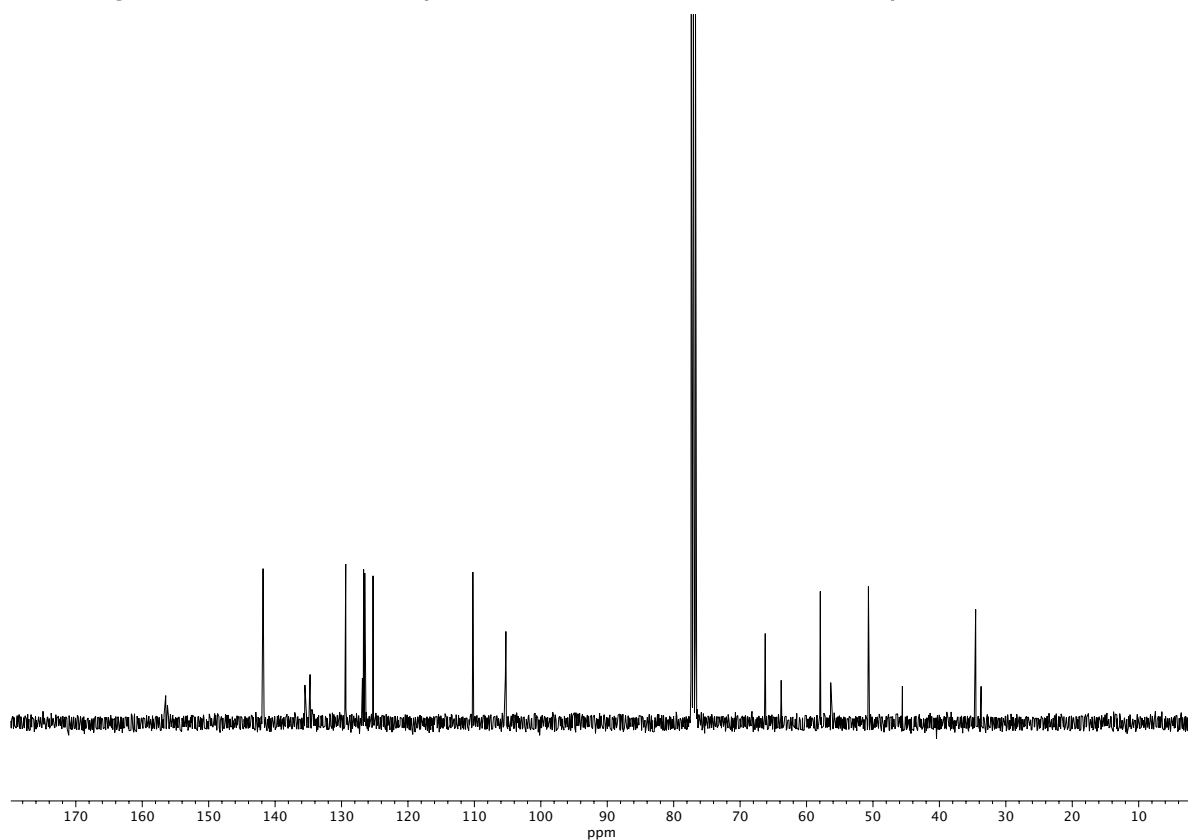




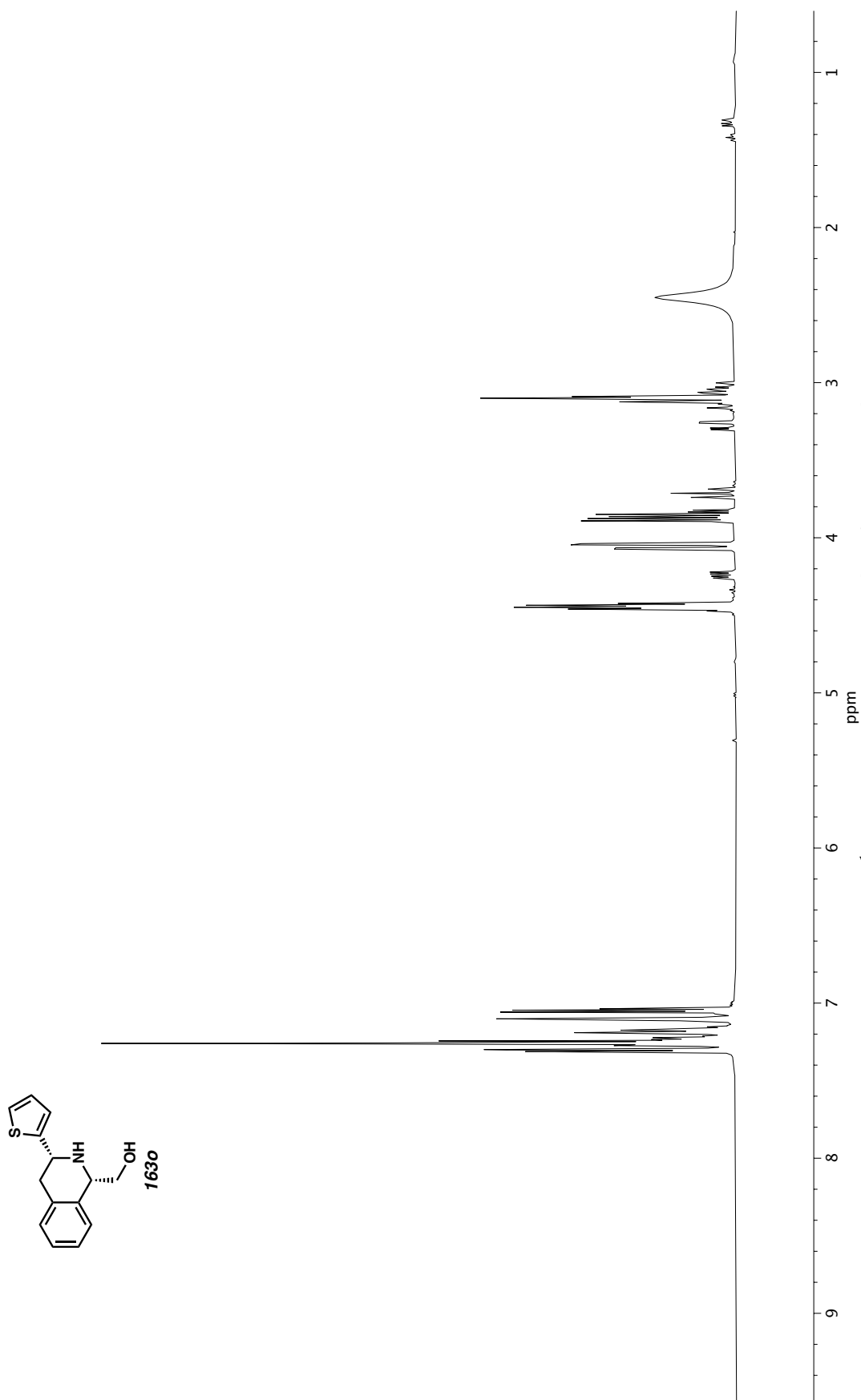
**Figure A1.245** <sup>1</sup>H NMR (400 MHz, CDCl<sub>3</sub>) of compound **163n**.

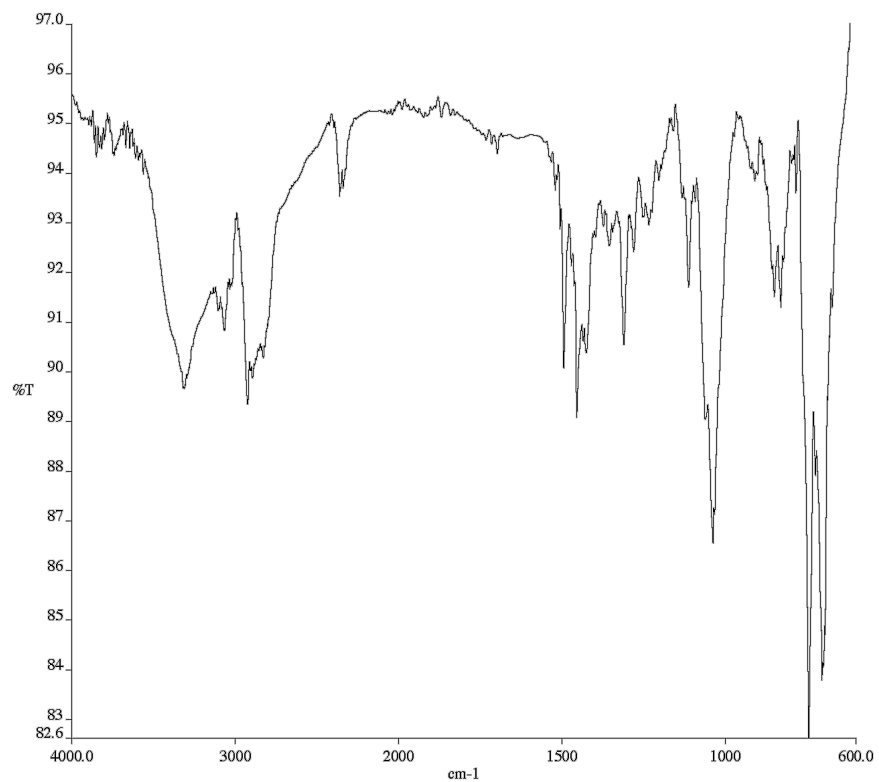


**Figure A1.246** Infrared spectrum (Thin Film, NaCl) of compound **163n**.

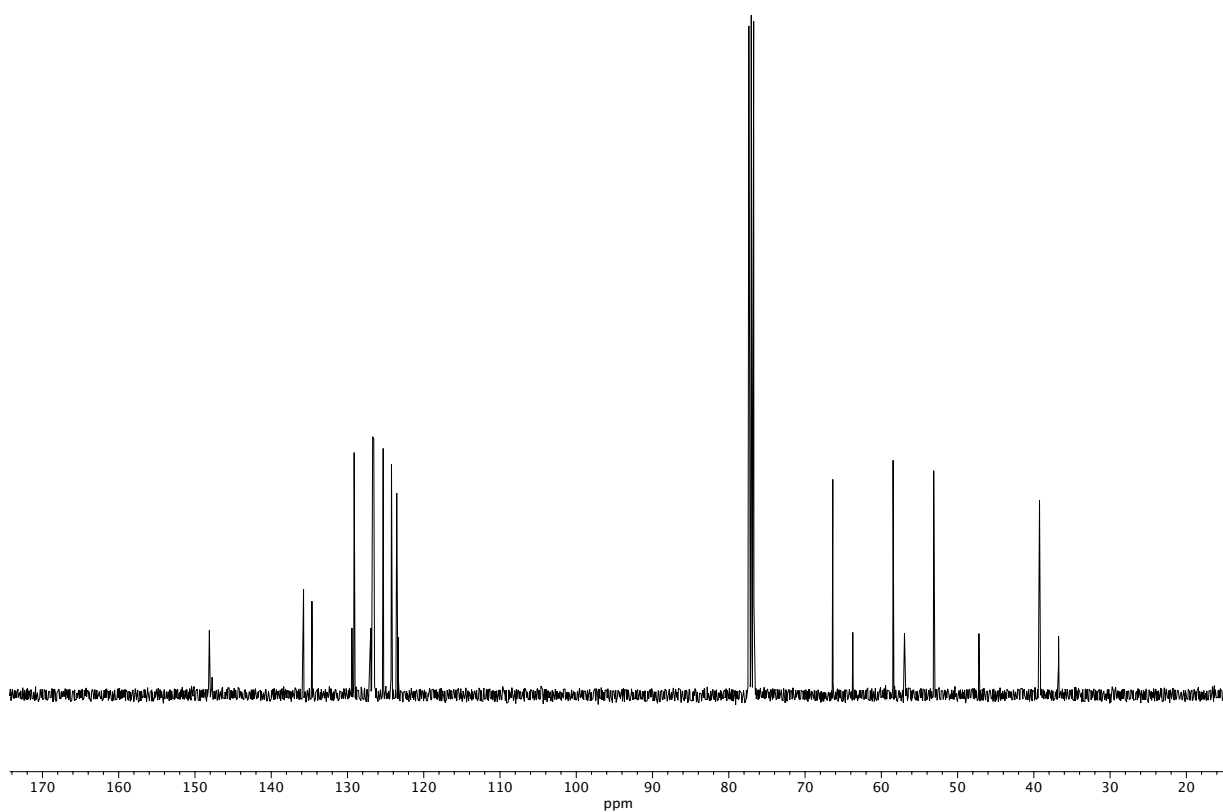


**Figure A1.247** <sup>13</sup>C NMR (100 MHz, CDCl<sub>3</sub>) of compound **163n**.

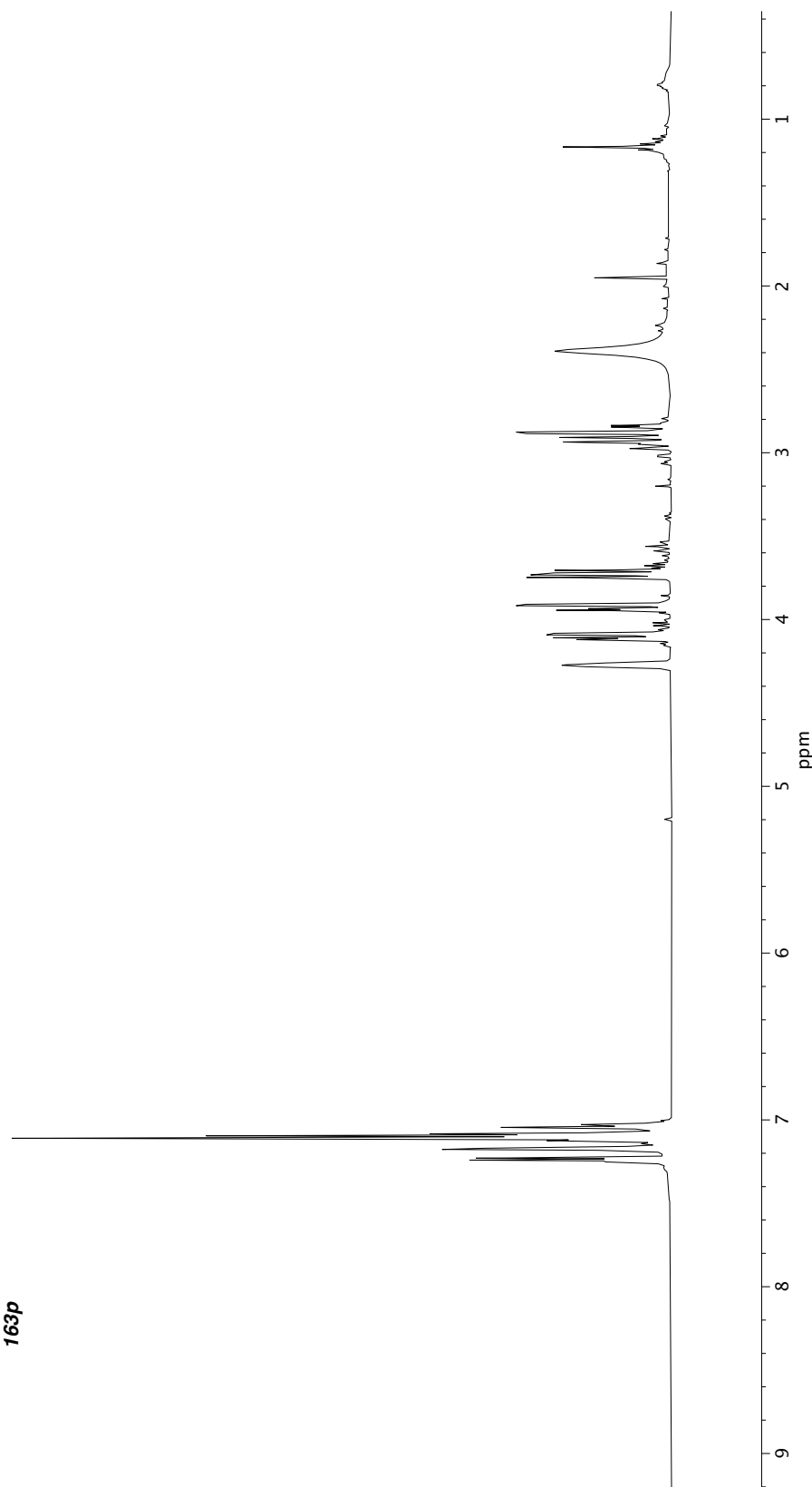
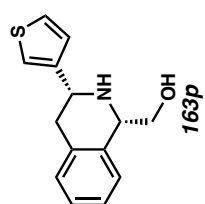




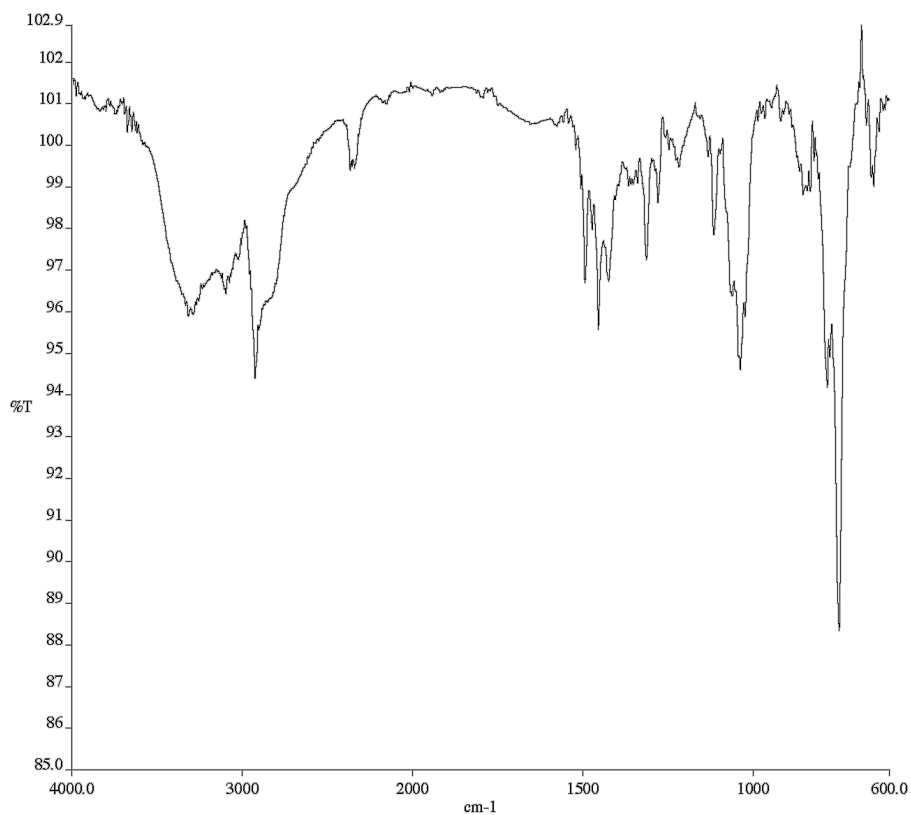
**Figure A1.249** Infrared spectrum (Thin Film, NaCl) of compound **163o**.



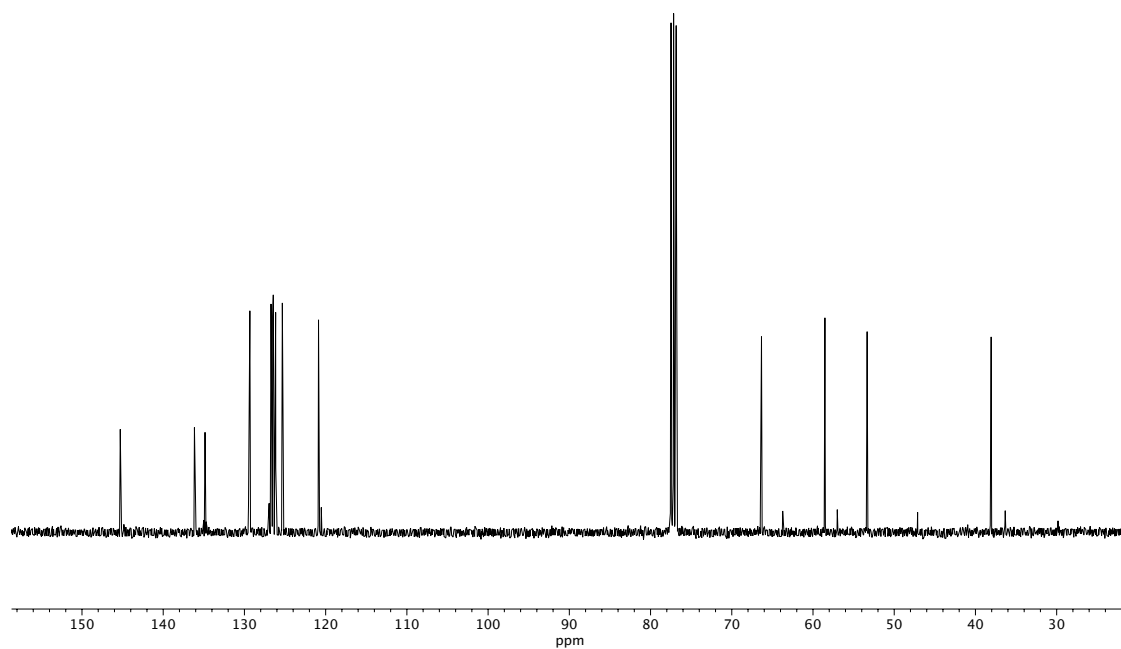
**Figure A1.250** <sup>13</sup>C NMR (100 MHz, CDCl<sub>3</sub>) of compound **163o**.



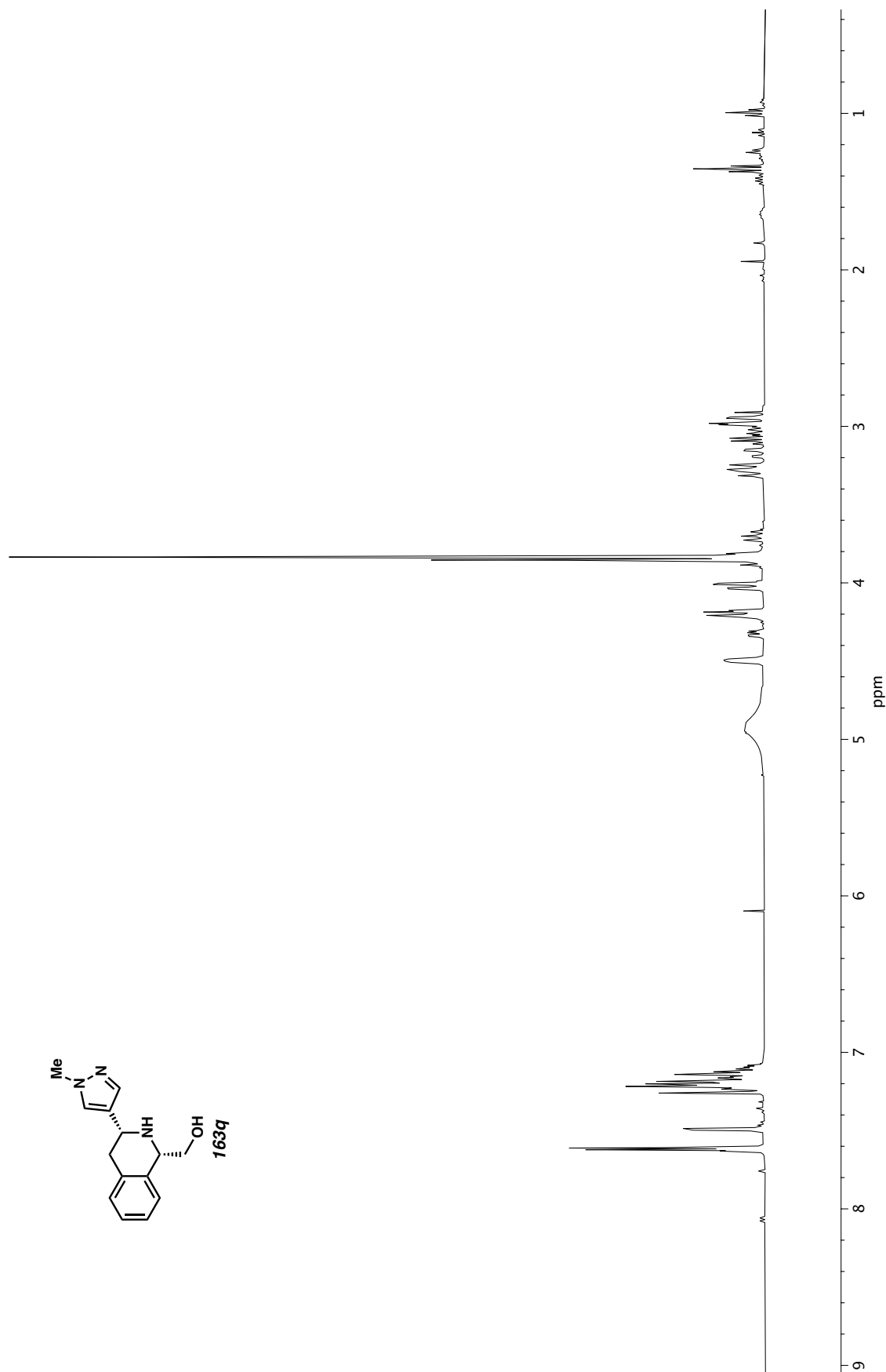
**Figure A1.251**  $^1\text{H}$  NMR (400 MHz,  $\text{CDCl}_3$ ) of compound **163p**.



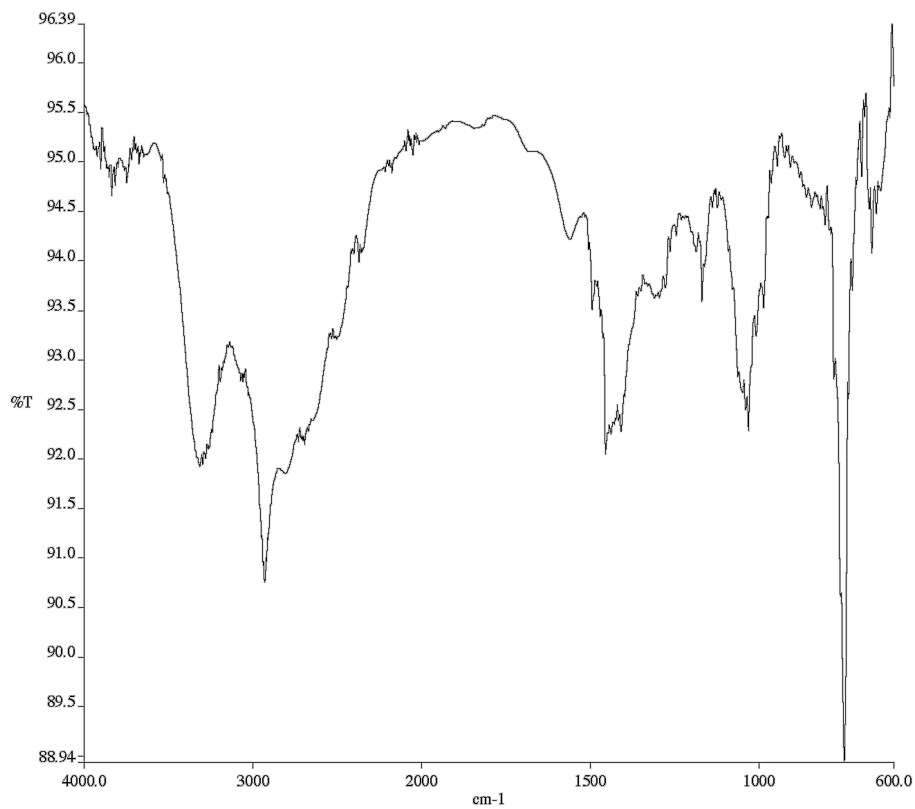
**Figure A1.252** Infrared spectrum (Thin Film, NaCl) of compound **163p**.



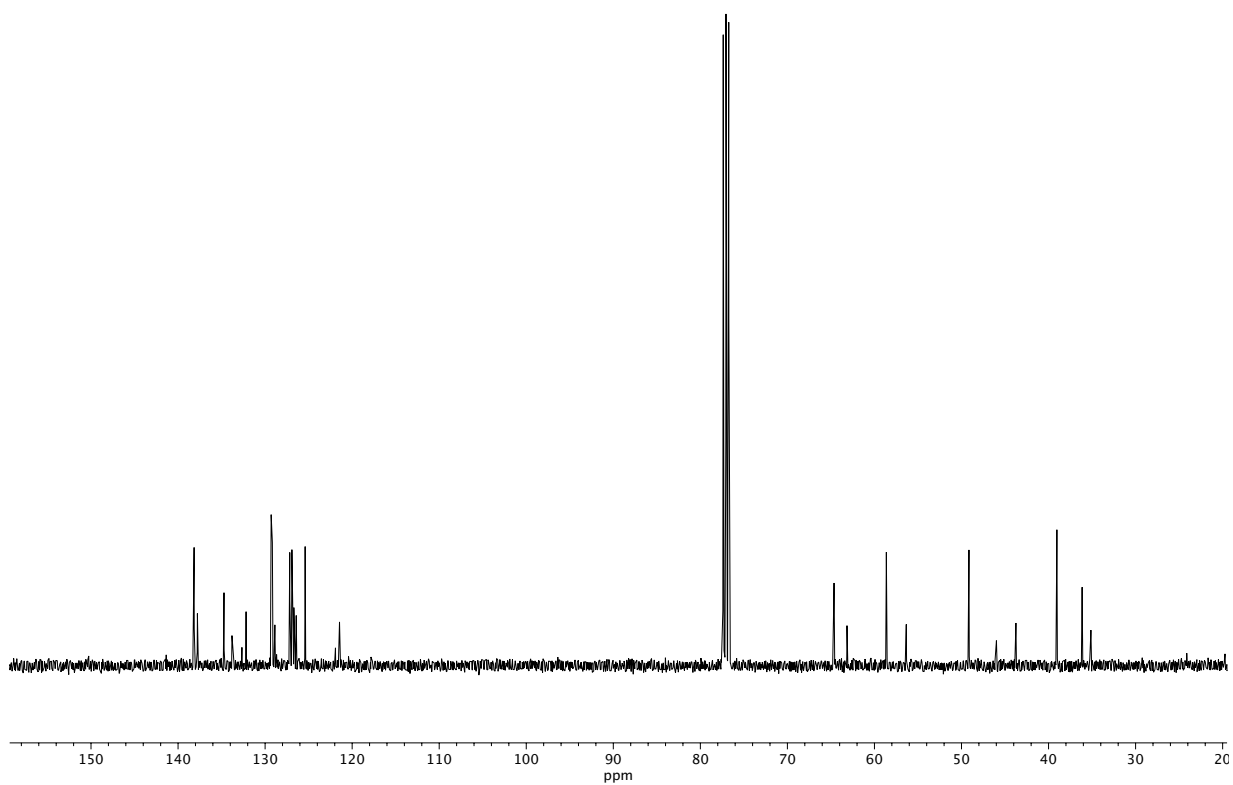
**Figure A1.253**  $^{13}\text{C}$  NMR (100 MHz,  $\text{CDCl}_3$ ) of compound **163p**.



**Figure A1.254** <sup>1</sup>H NMR (400 MHz, CDCl<sub>3</sub>) of compound **163q**.

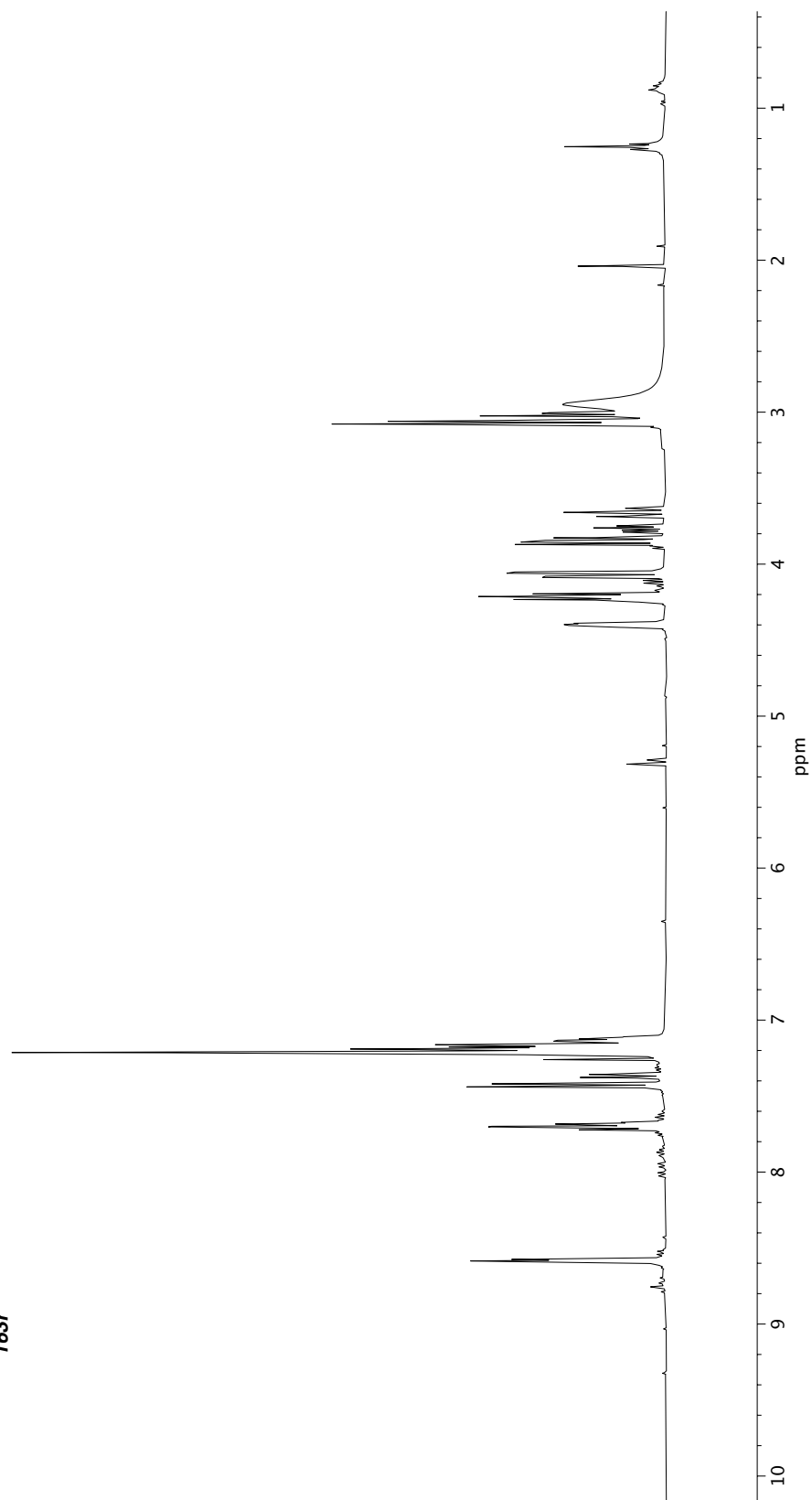
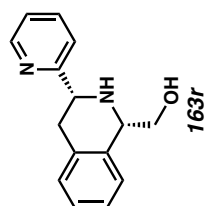


**Figure A1.255** Infrared spectrum (Thin Film, NaCl) of compound **163q**.

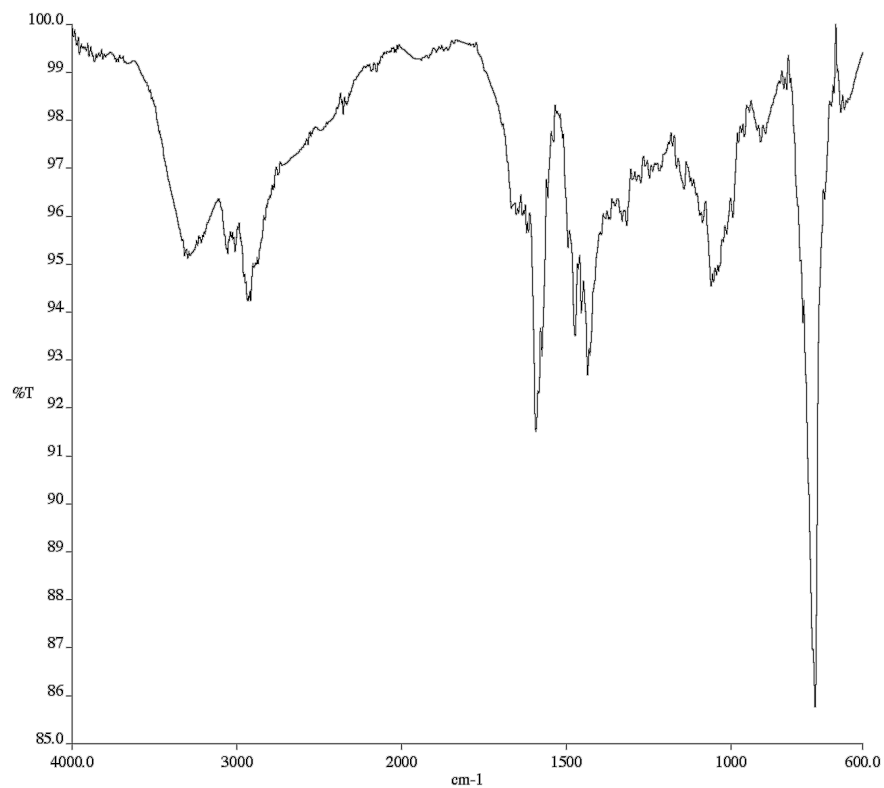


**Figure A1.256** <sup>13</sup>C NMR (100 MHz, CDCl<sub>3</sub>) of compound **163q**.

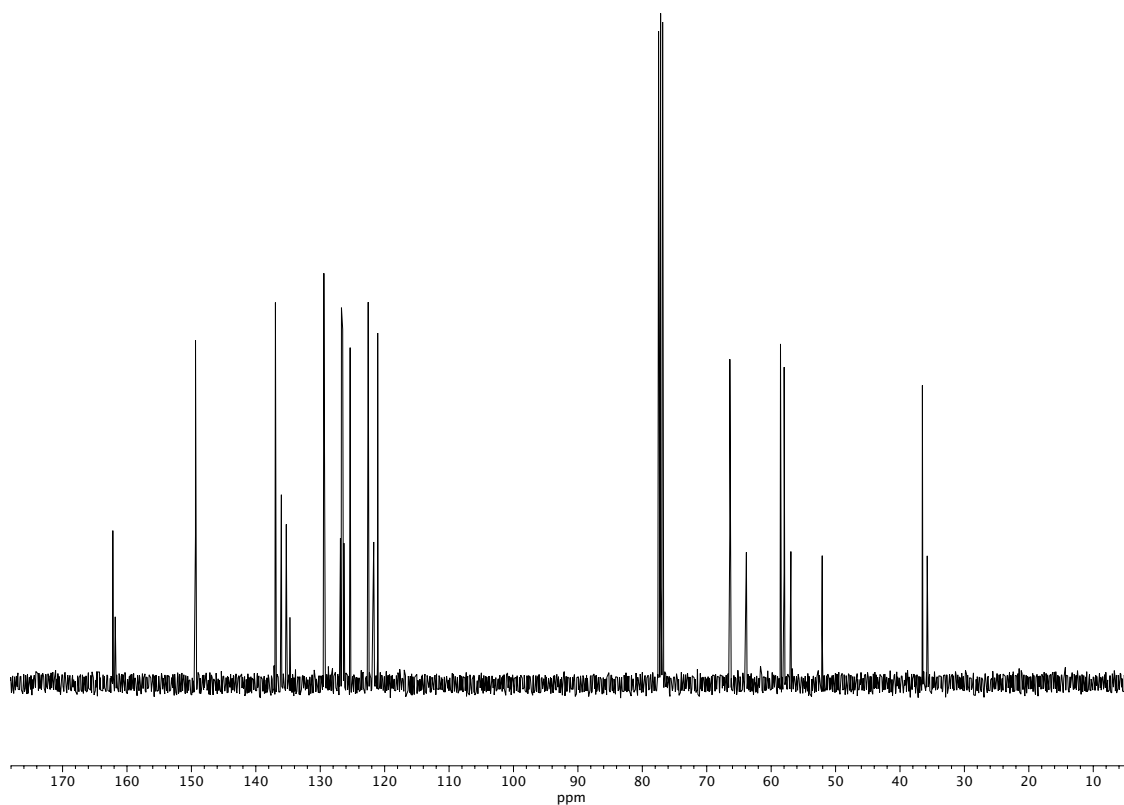




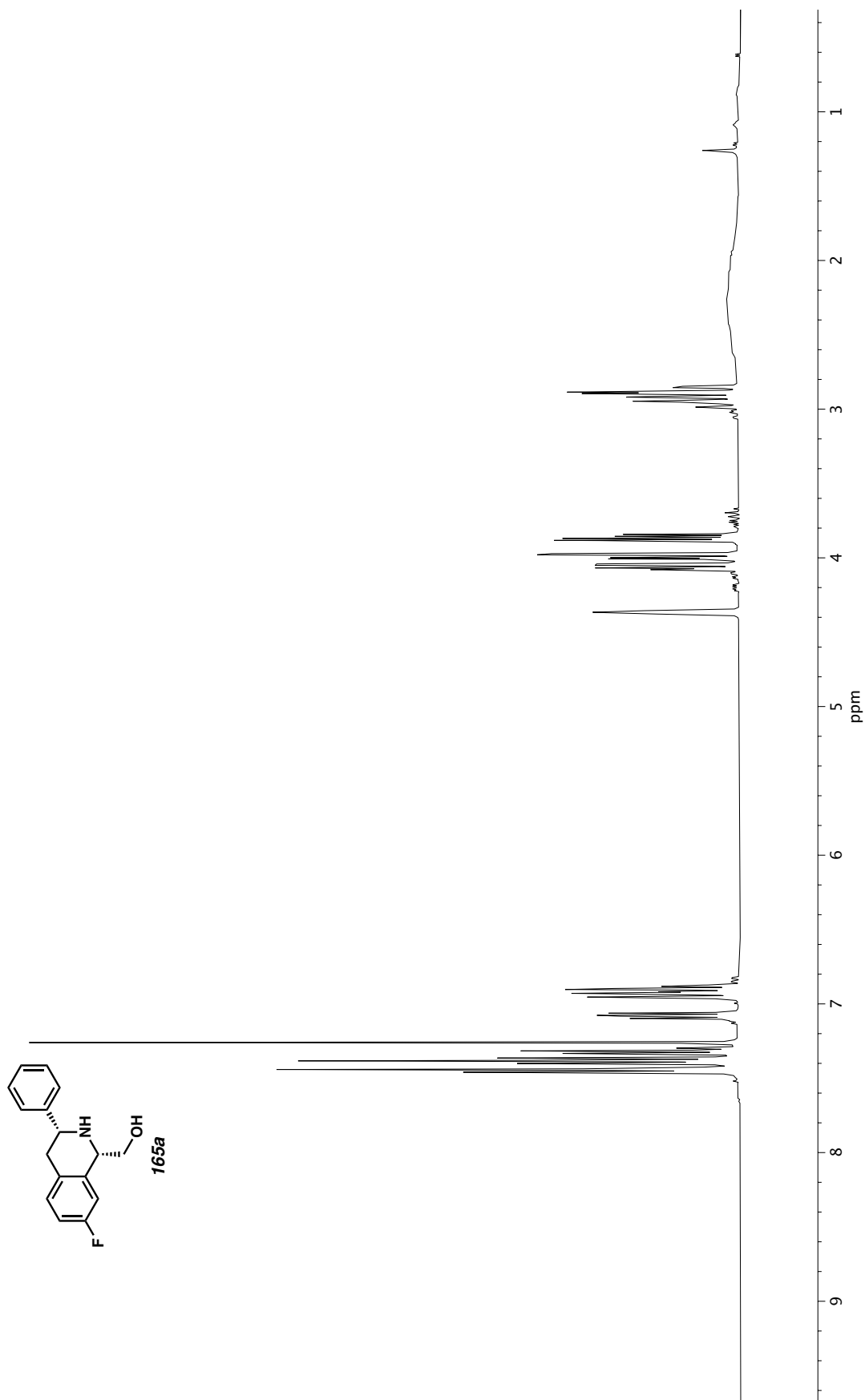
**Figure A1.257** <sup>1</sup>H NMR (400 MHz, CDCl<sub>3</sub>) of compound **163r**.



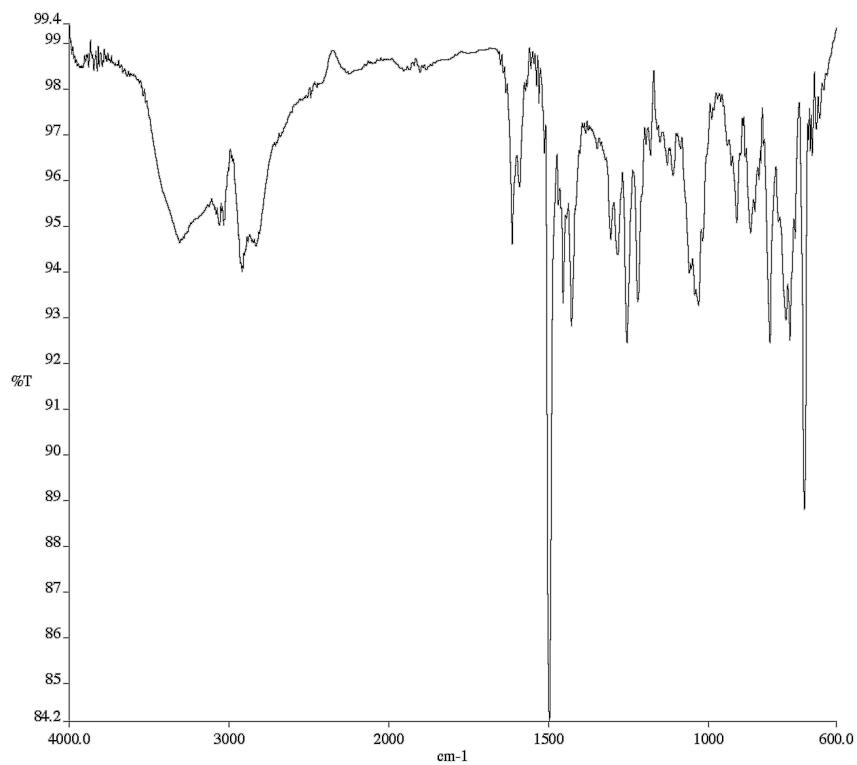
**Figure A1.258** Infrared spectrum (Thin Film, NaCl) of compound **163r**.



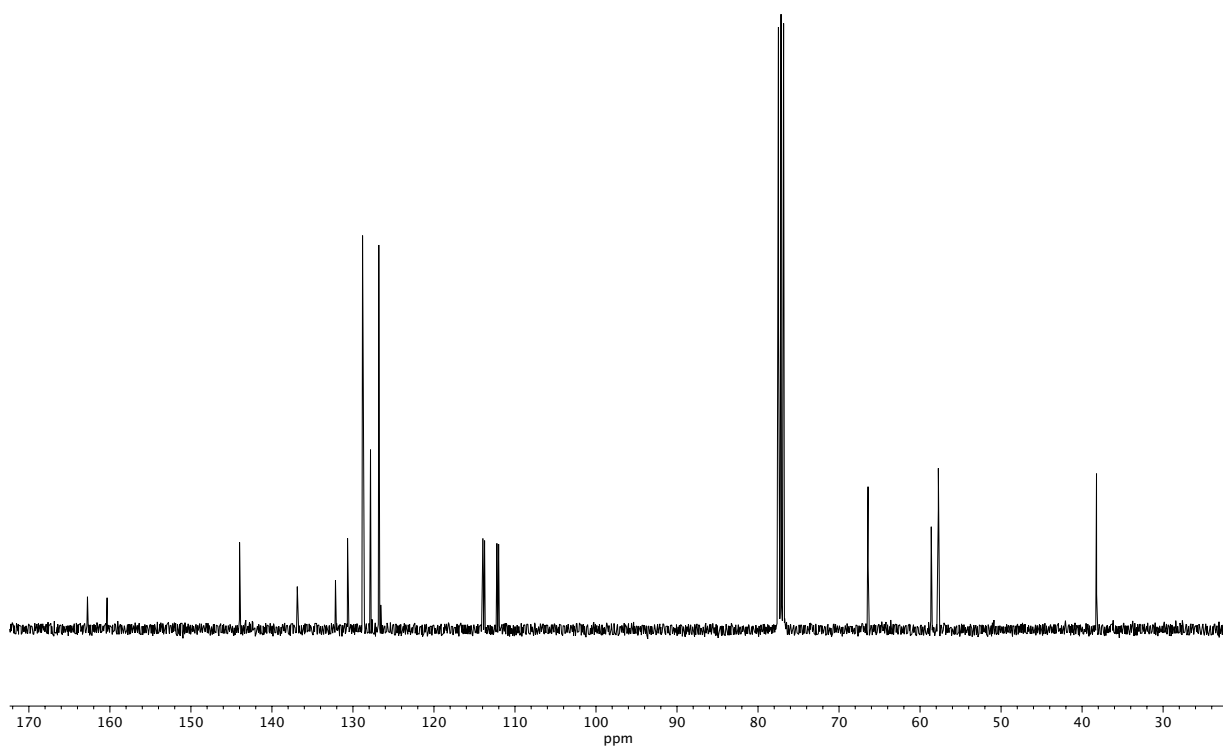
**Figure A1.259** <sup>13</sup>C NMR (100 MHz, CDCl<sub>3</sub>) of compound **163r**.



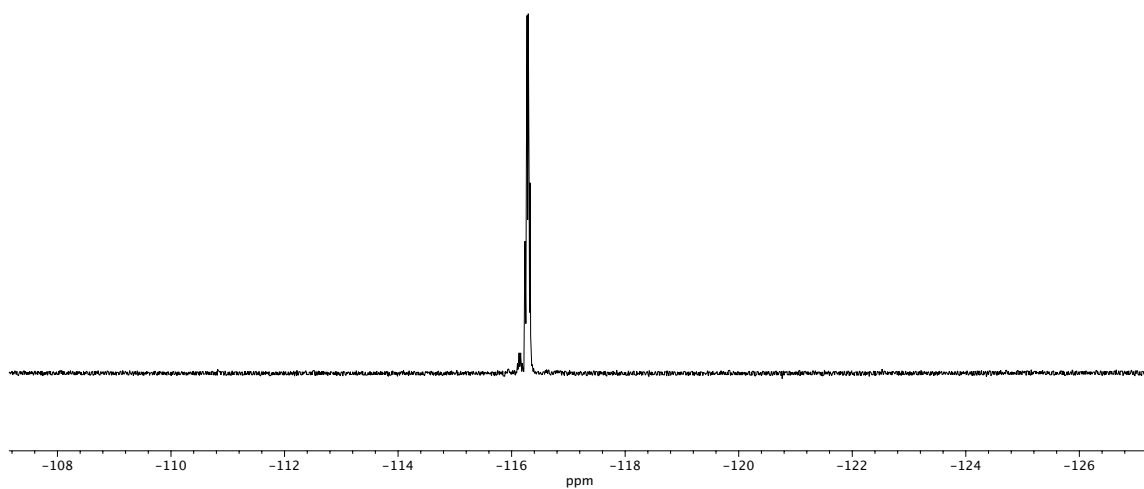
**Figure A1.260**  $^1\text{H}$  NMR (400 MHz,  $\text{CDCl}_3$ ) of compound **165a**.



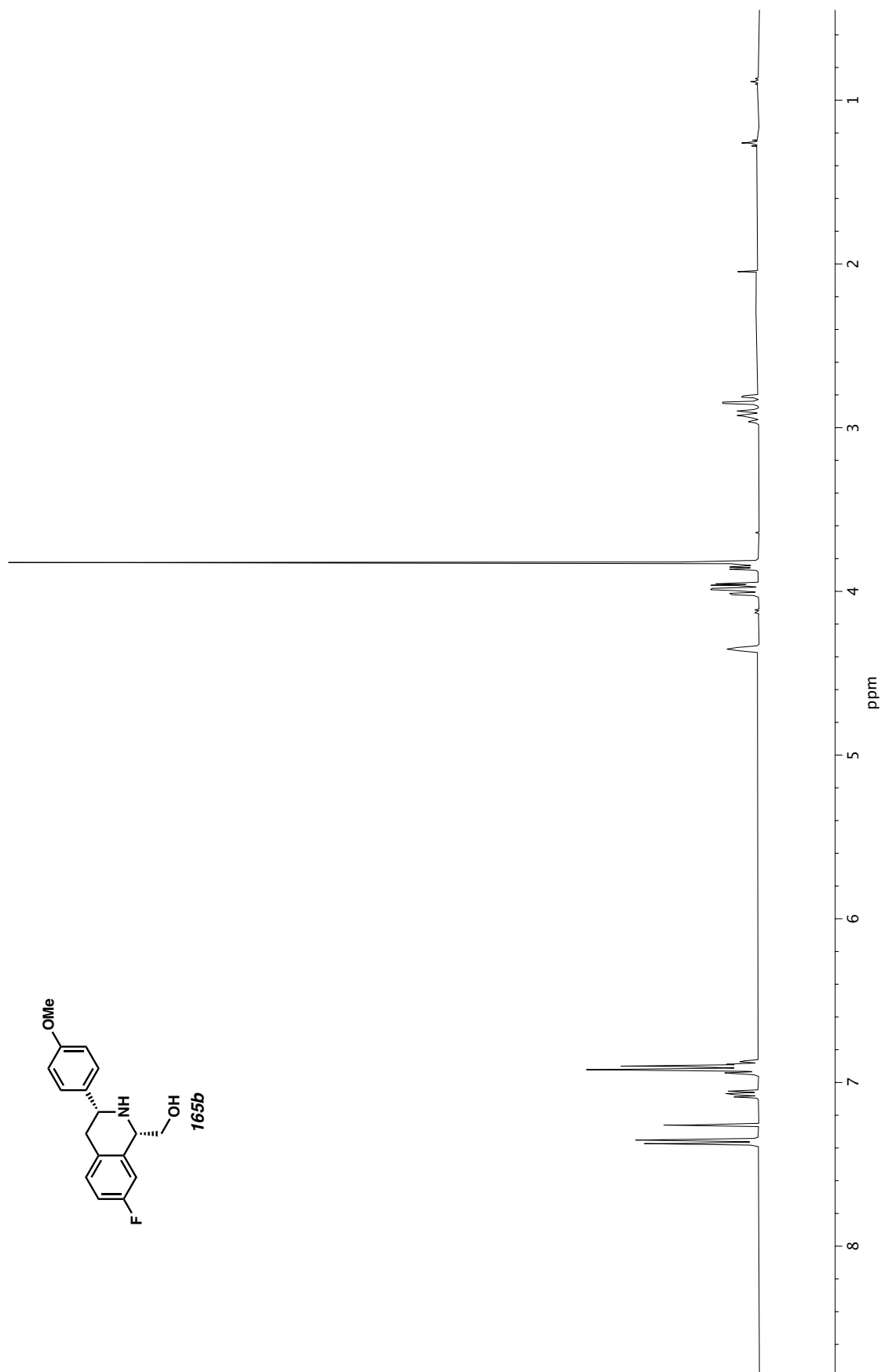
**Figure A1.261** Infrared spectrum (Thin Film, NaCl) of compound **165a**.



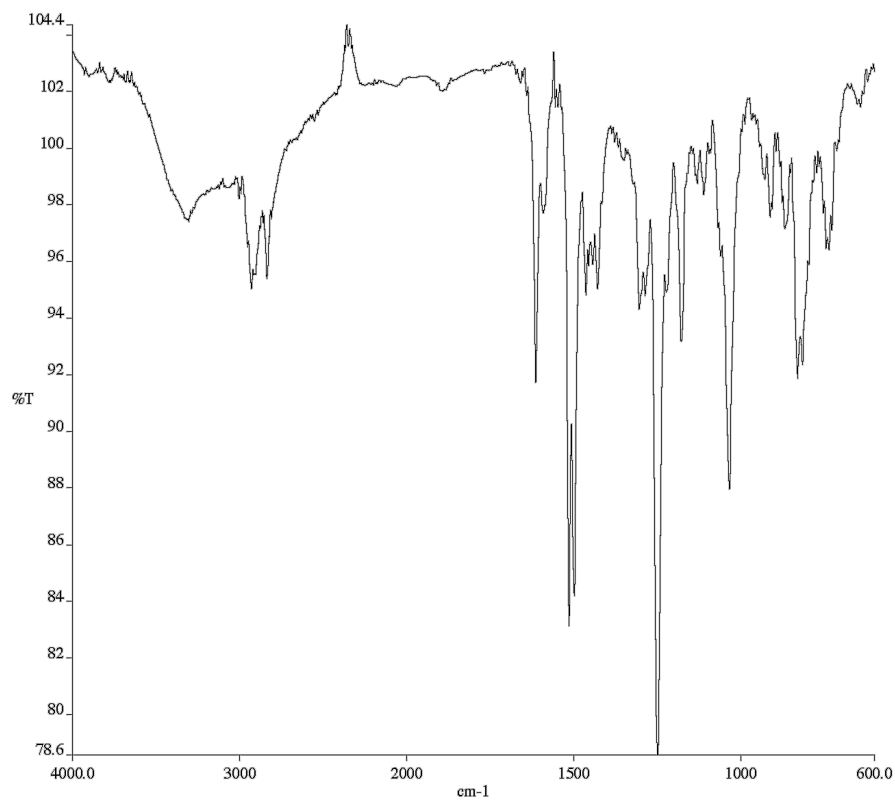
**Figure A1.262** <sup>13</sup>C NMR (100 MHz, CDCl<sub>3</sub>) of compound **165a**.



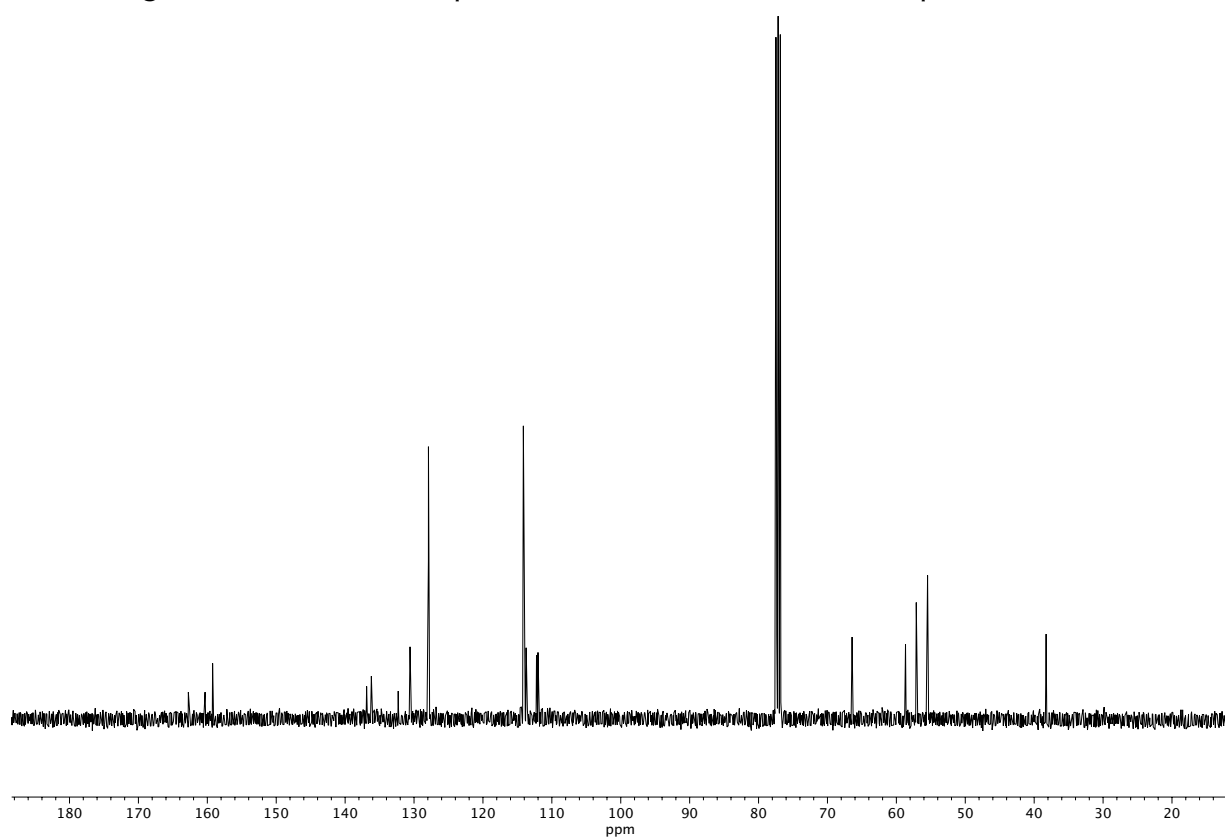
**Figure A1.263**  $^{19}\text{F}$  NMR (282 MHz,  $\text{CDCl}_3$ ) of compound **165a**.



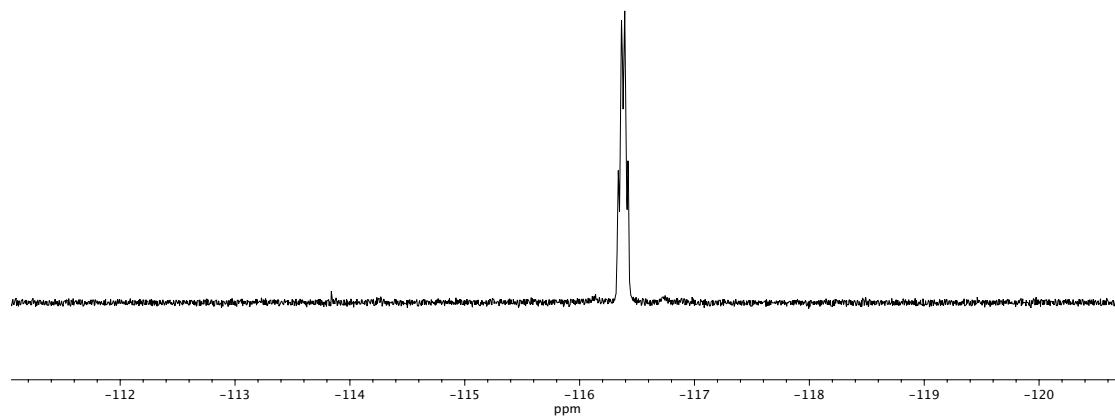
**Figure A1.264**  $^1\text{H}$  NMR (400 MHz,  $\text{CDCl}_3$ ) of compound **165b**.



**Figure A1.265** Infrared spectrum (Thin Film, NaCl) of compound **165b**.

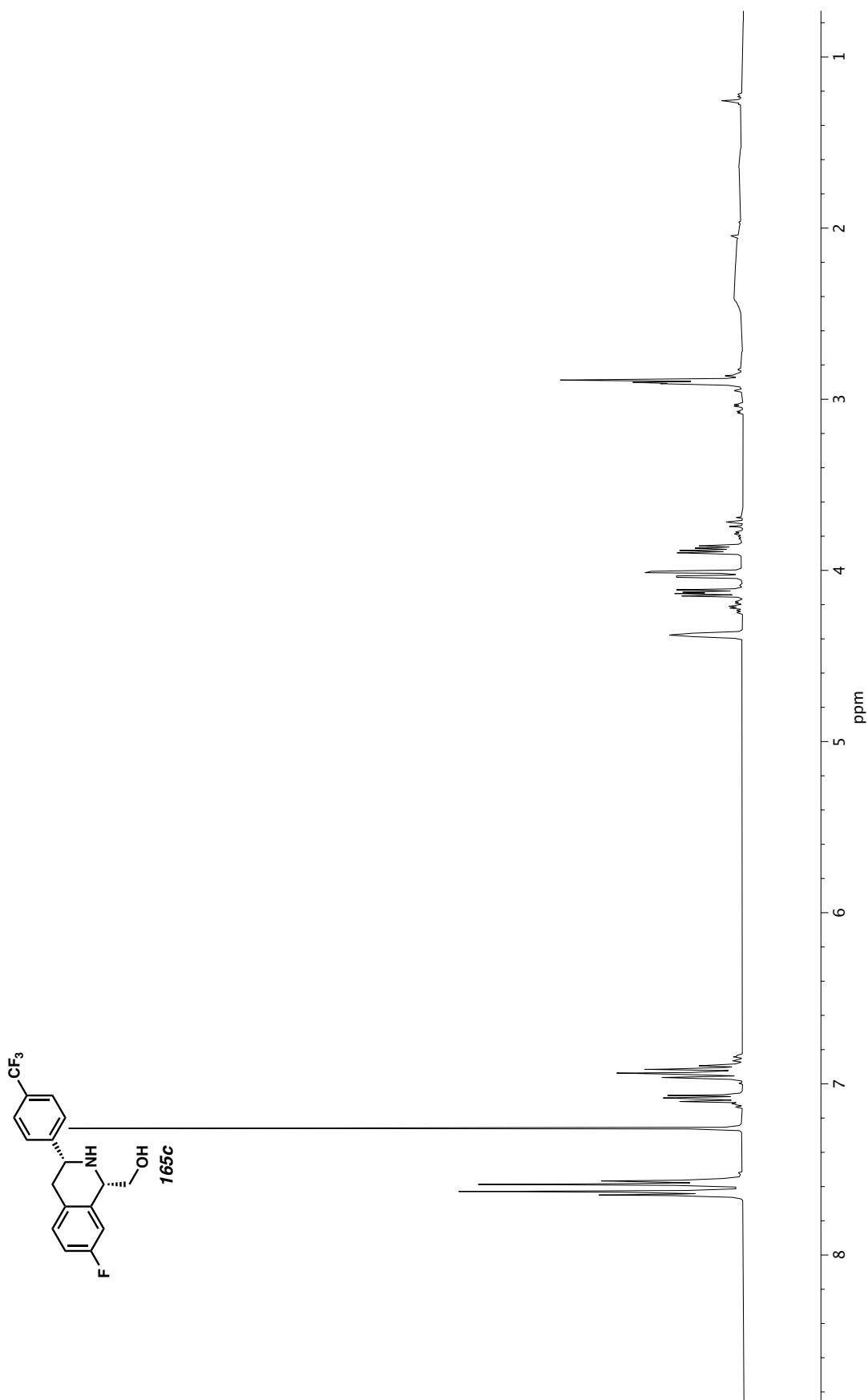


**Figure A1.266** <sup>13</sup>C NMR (100 MHz, CDCl<sub>3</sub>) of compound **165b**.

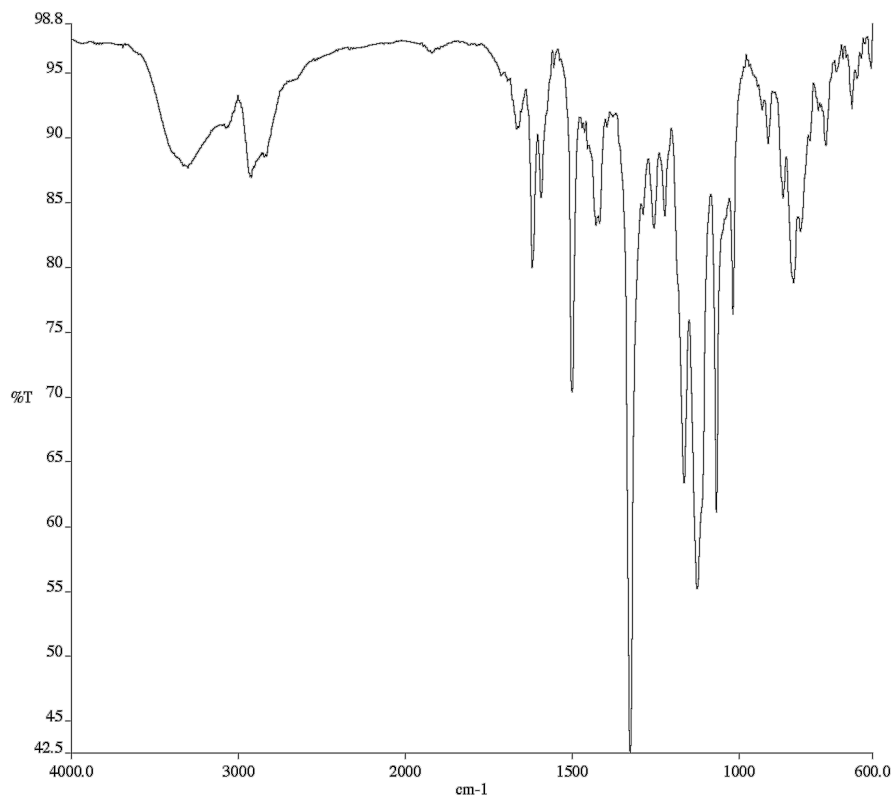


**Figure A1.267**  $^{19}\text{F}$  NMR (282 MHz,  $\text{CDCl}_3$ ) of compound **165b**.

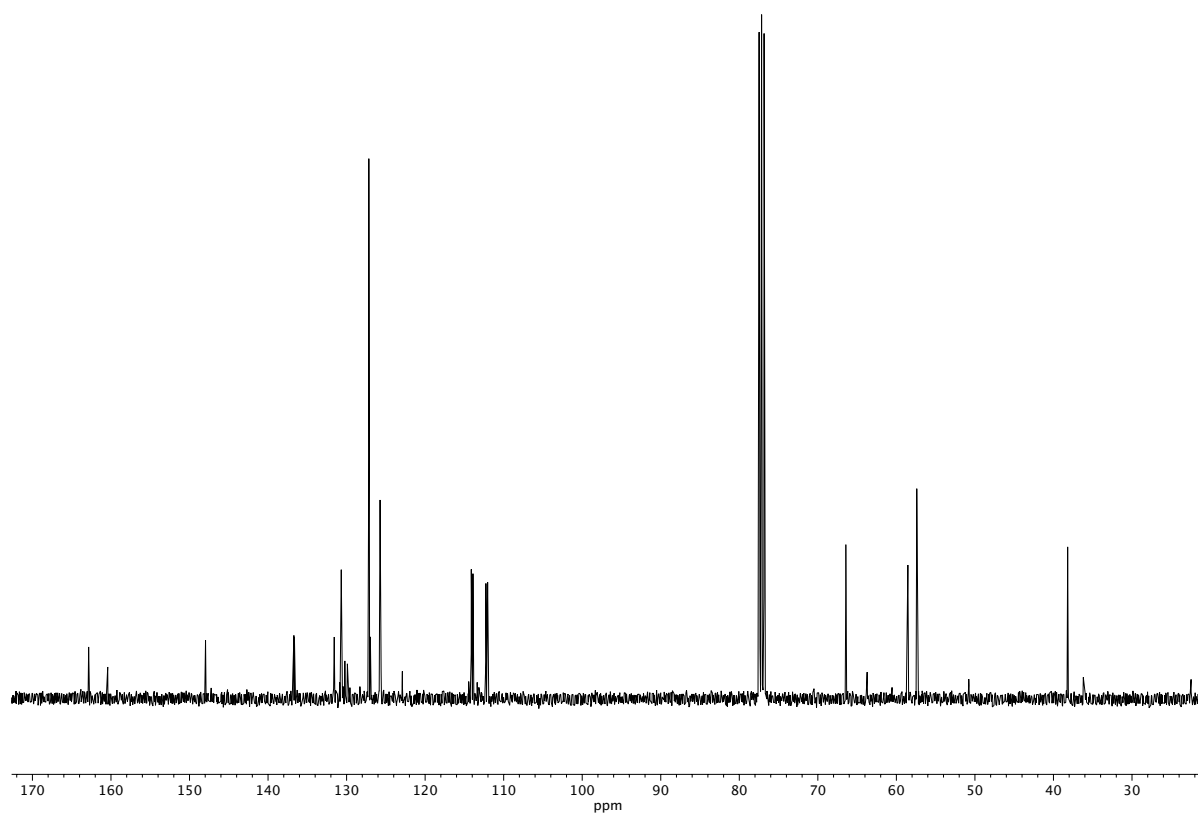




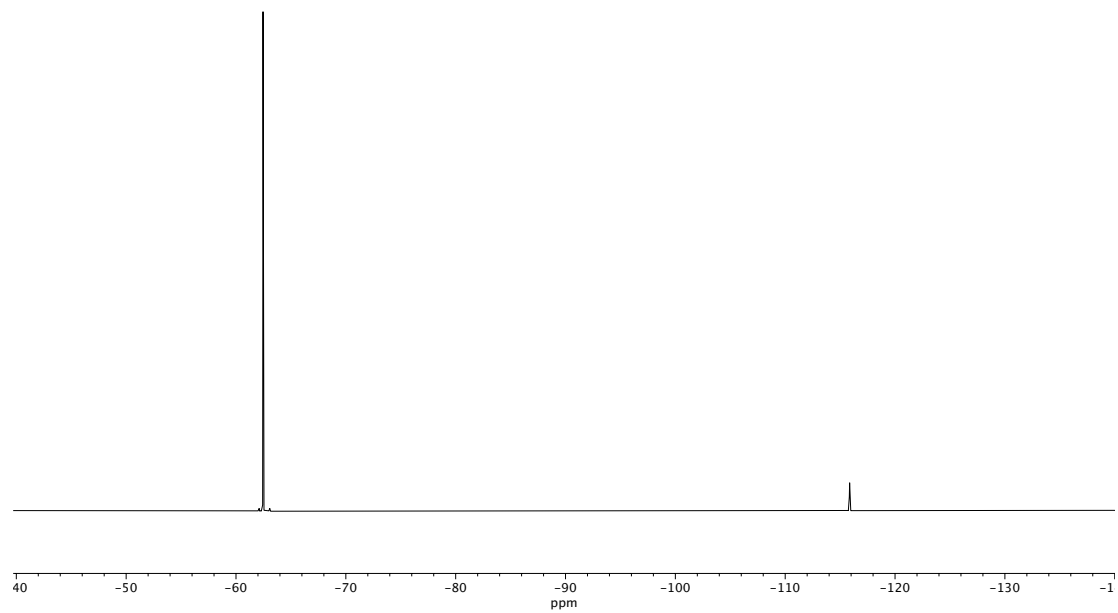
**Figure A1.268** <sup>1</sup>H NMR (400 MHz, CDCl<sub>3</sub>) of compound **165c**.



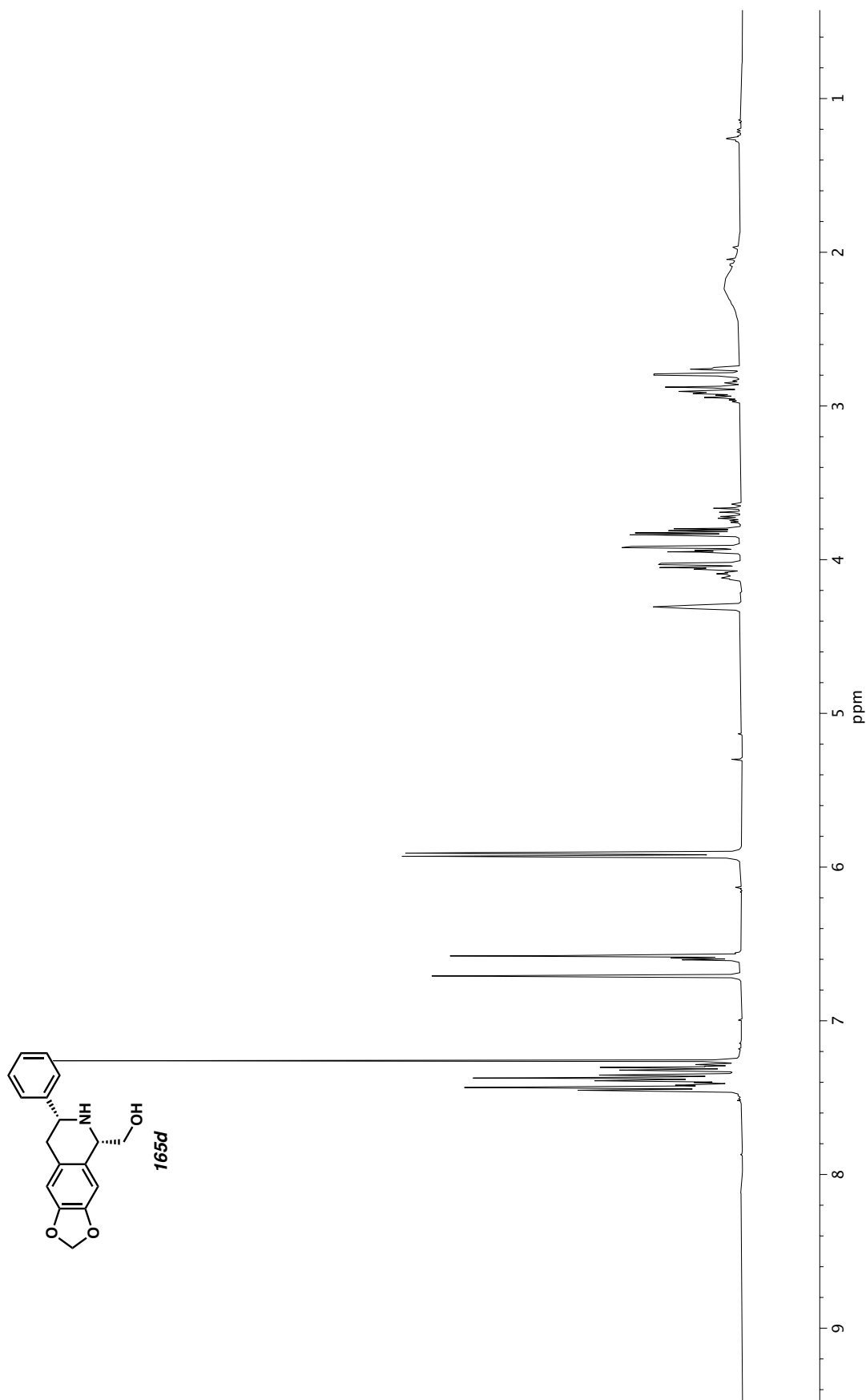
**Figure A1.269** Infrared spectrum (Thin Film, NaCl) of compound **165c**.



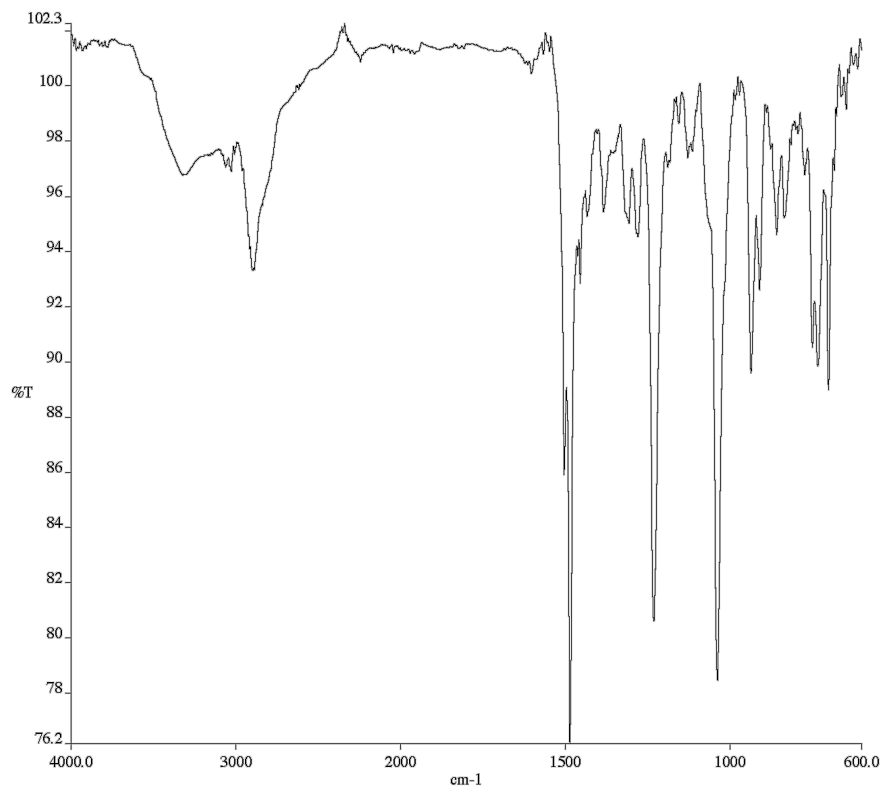
**Figure A1.270** <sup>13</sup>C NMR (100 MHz, CDCl<sub>3</sub>) of compound **165c**.



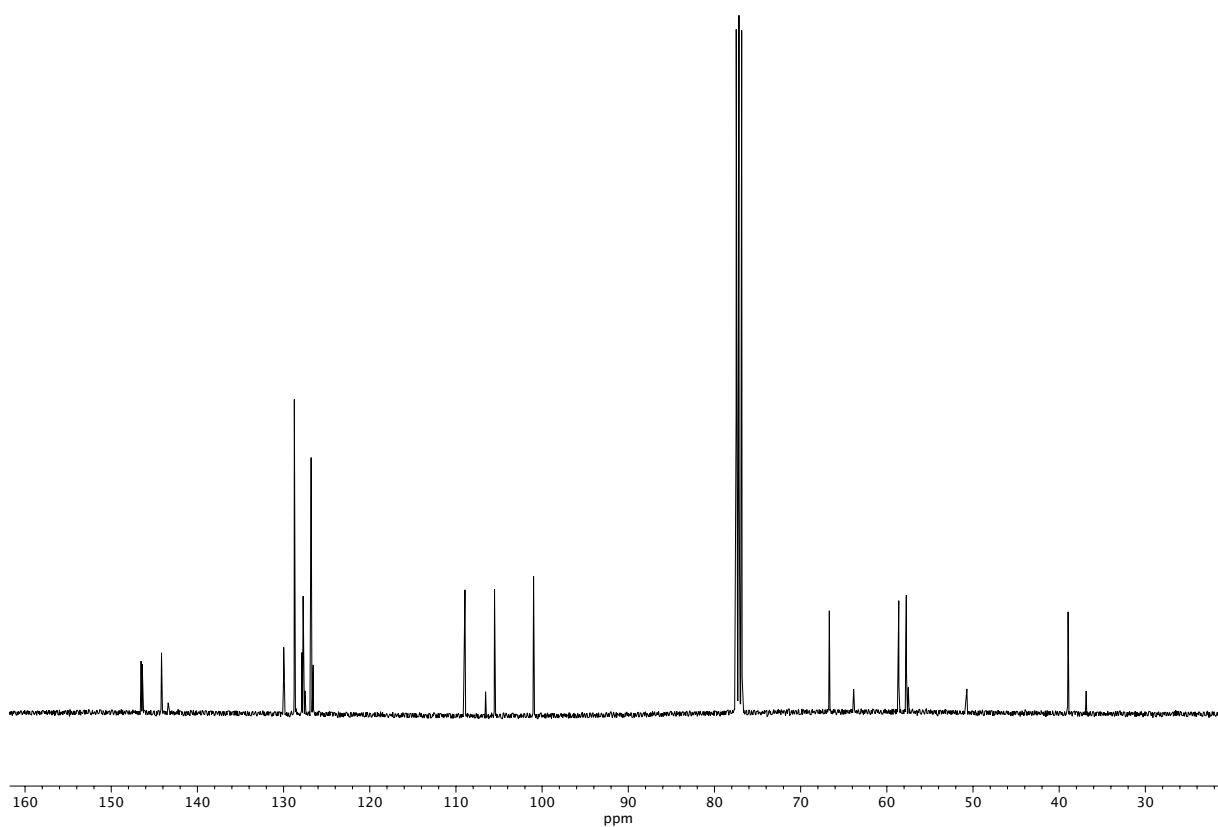
**Figure A1.271**  $^{19}\text{F}$  NMR (282 MHz,  $\text{CDCl}_3$ ) of compound **165c**.



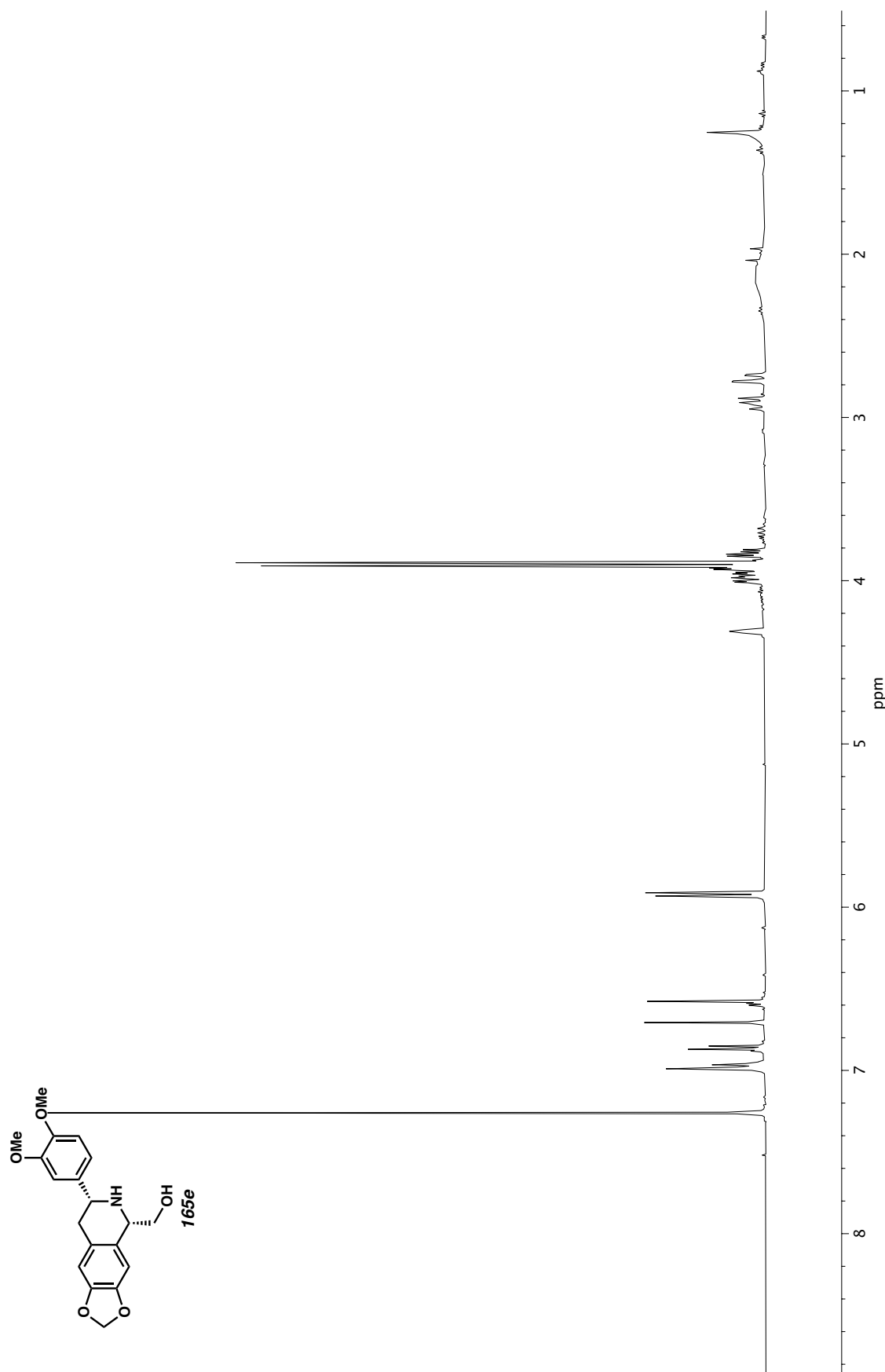
**Figure A1.272**  $^1\text{H}$  NMR (400 MHz,  $\text{CDCl}_3$ ) of compound **165d**.



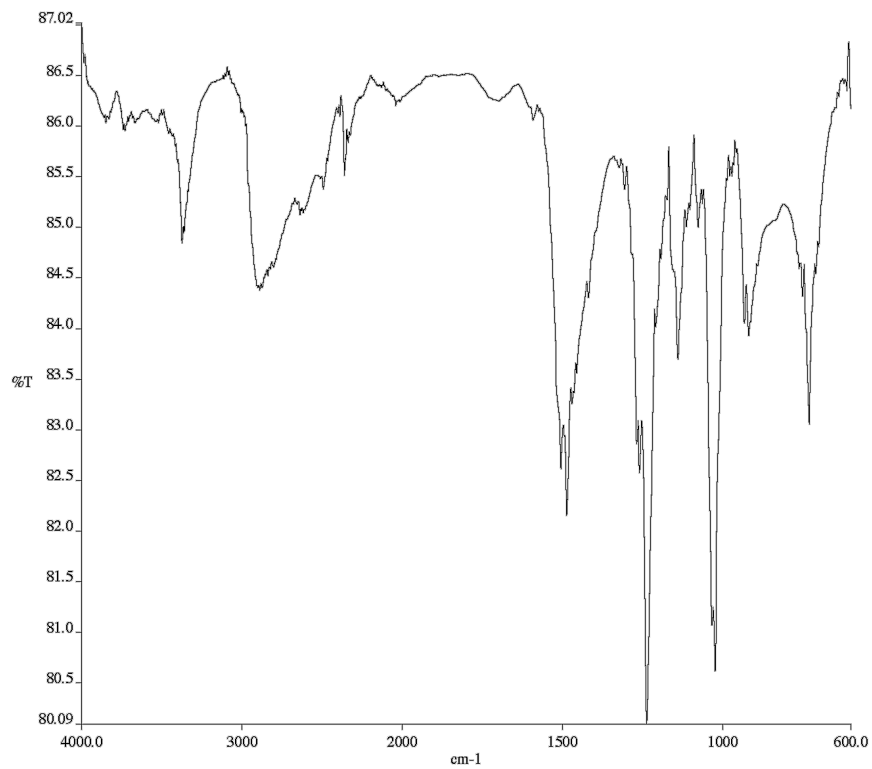
**Figure A1.273** Infrared spectrum (Thin Film, NaCl) of compound **165d**.



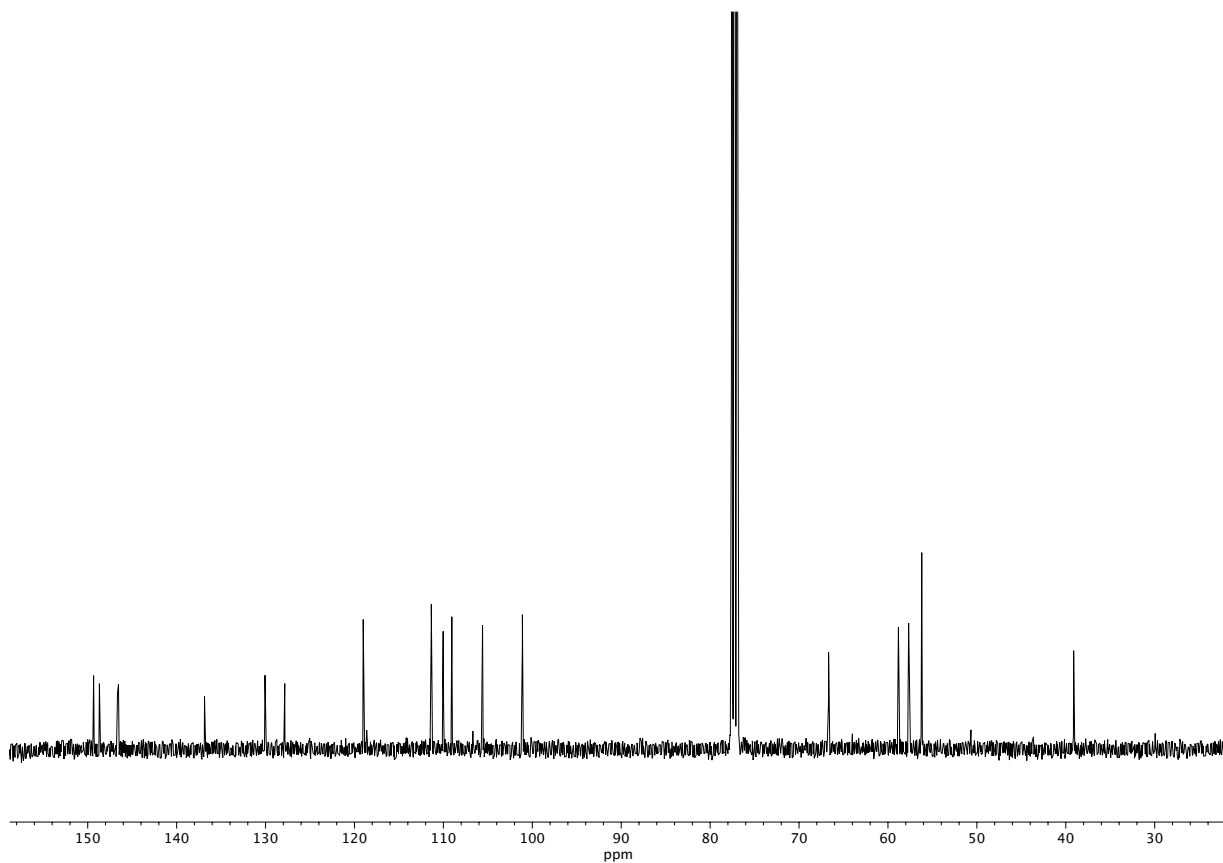
**Figure A1.274** <sup>13</sup>C NMR (100 MHz, CDCl<sub>3</sub>) of compound **165d**.



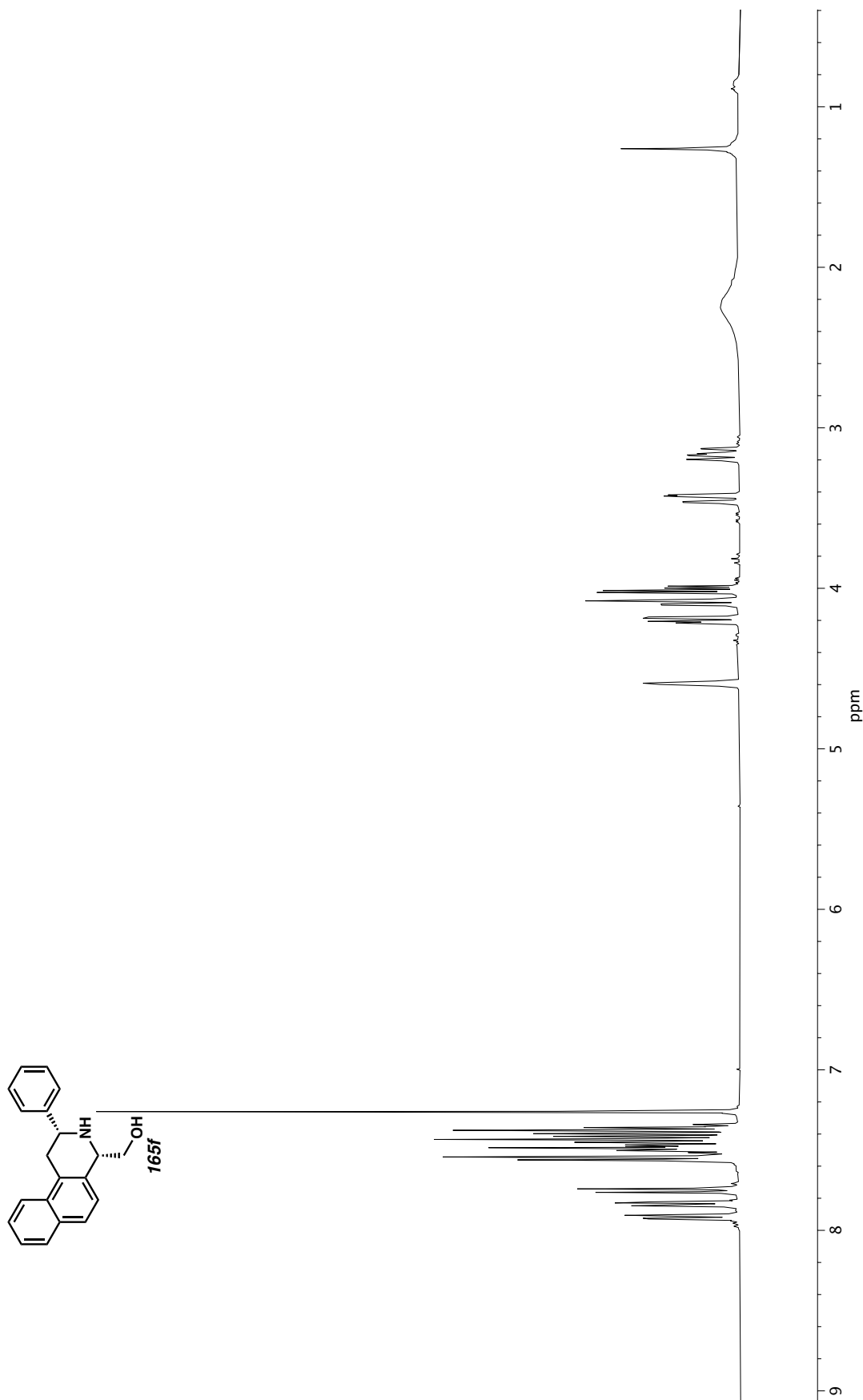
**Figure A1.275**  $^1\text{H}$  NMR (400 MHz,  $\text{CDCl}_3$ ) of compound **165e**.



**Figure A1.276** Infrared spectrum (Thin Film, NaCl) of compound **165e**.

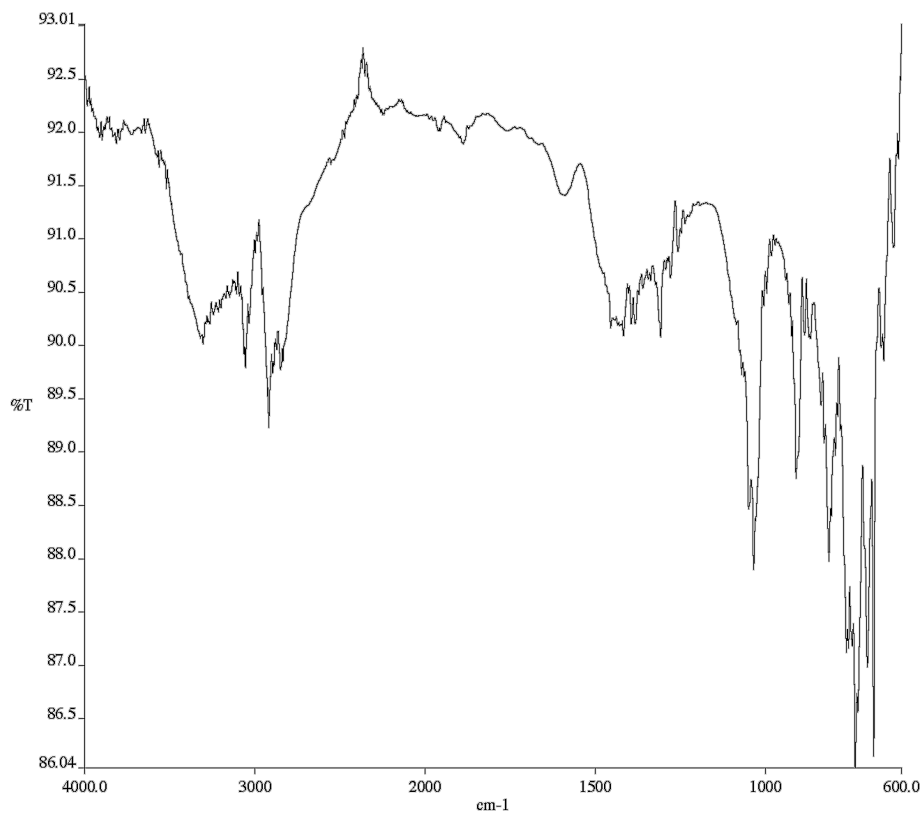


**Figure A1.277** <sup>13</sup>C NMR (100 MHz, CDCl<sub>3</sub>) of compound **165e**.

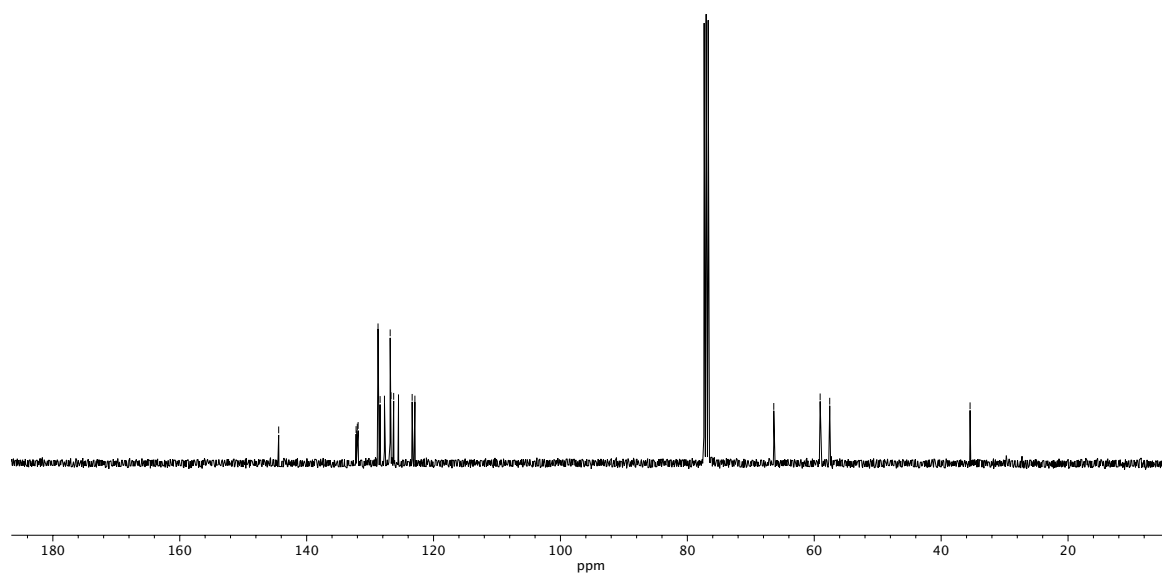


**Figure A1.278**  $^1\text{H}$  NMR (400 MHz,  $\text{CDCl}_3$ ) of compound **165f**.

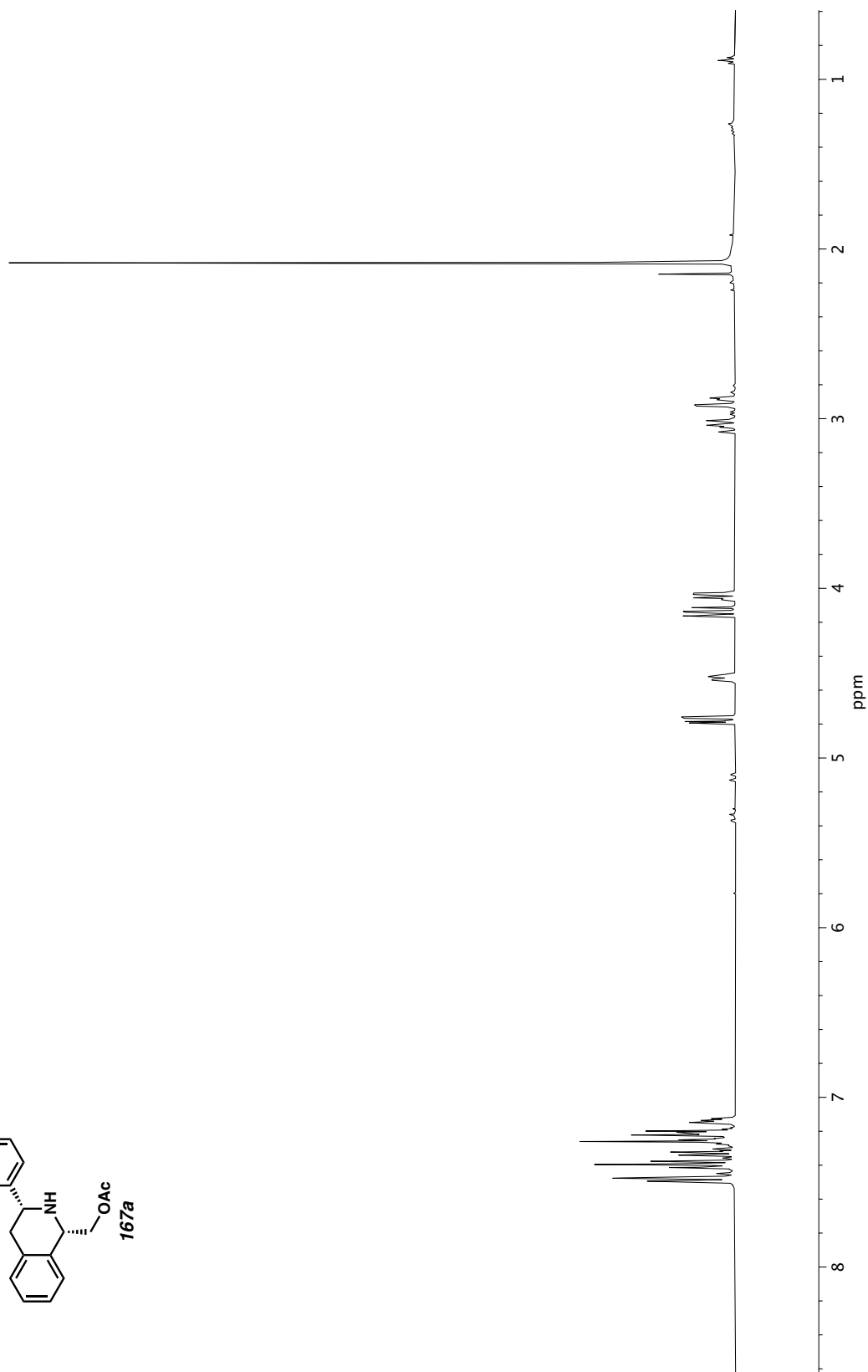
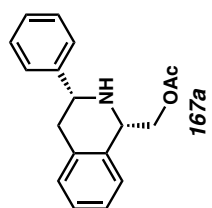




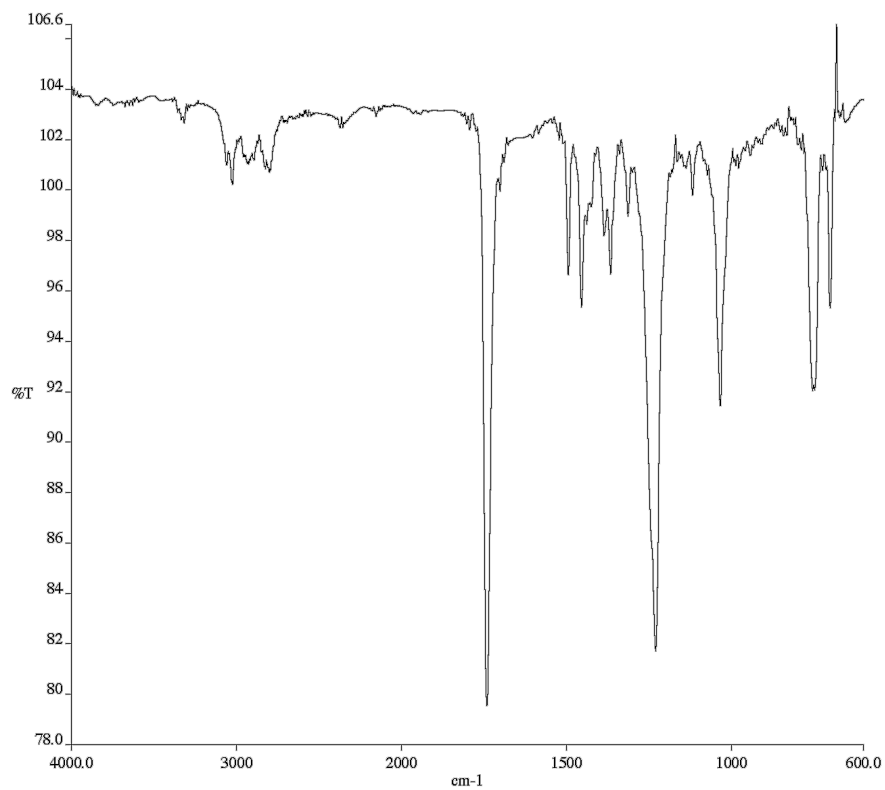
**Figure A1.279** Infrared spectrum (Thin Film, NaCl) of compound **165f**.



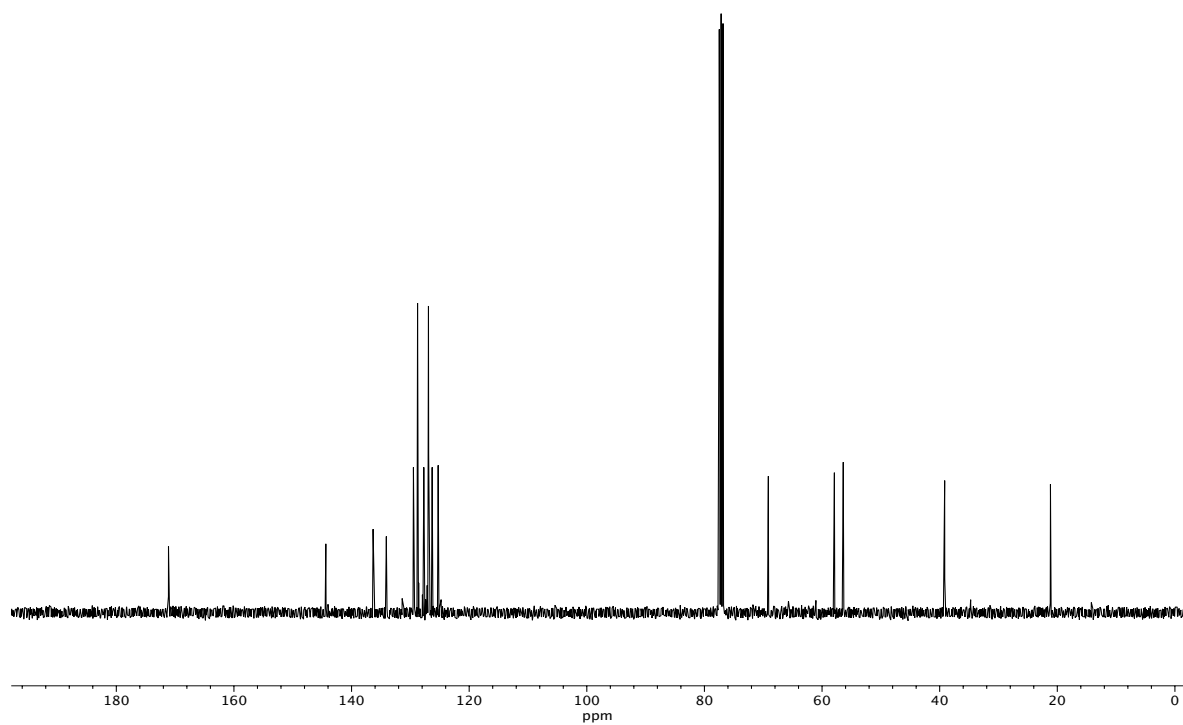
**Figure A1.280** <sup>13</sup>C NMR (100 MHz, CDCl<sub>3</sub>) of compound **165f**.



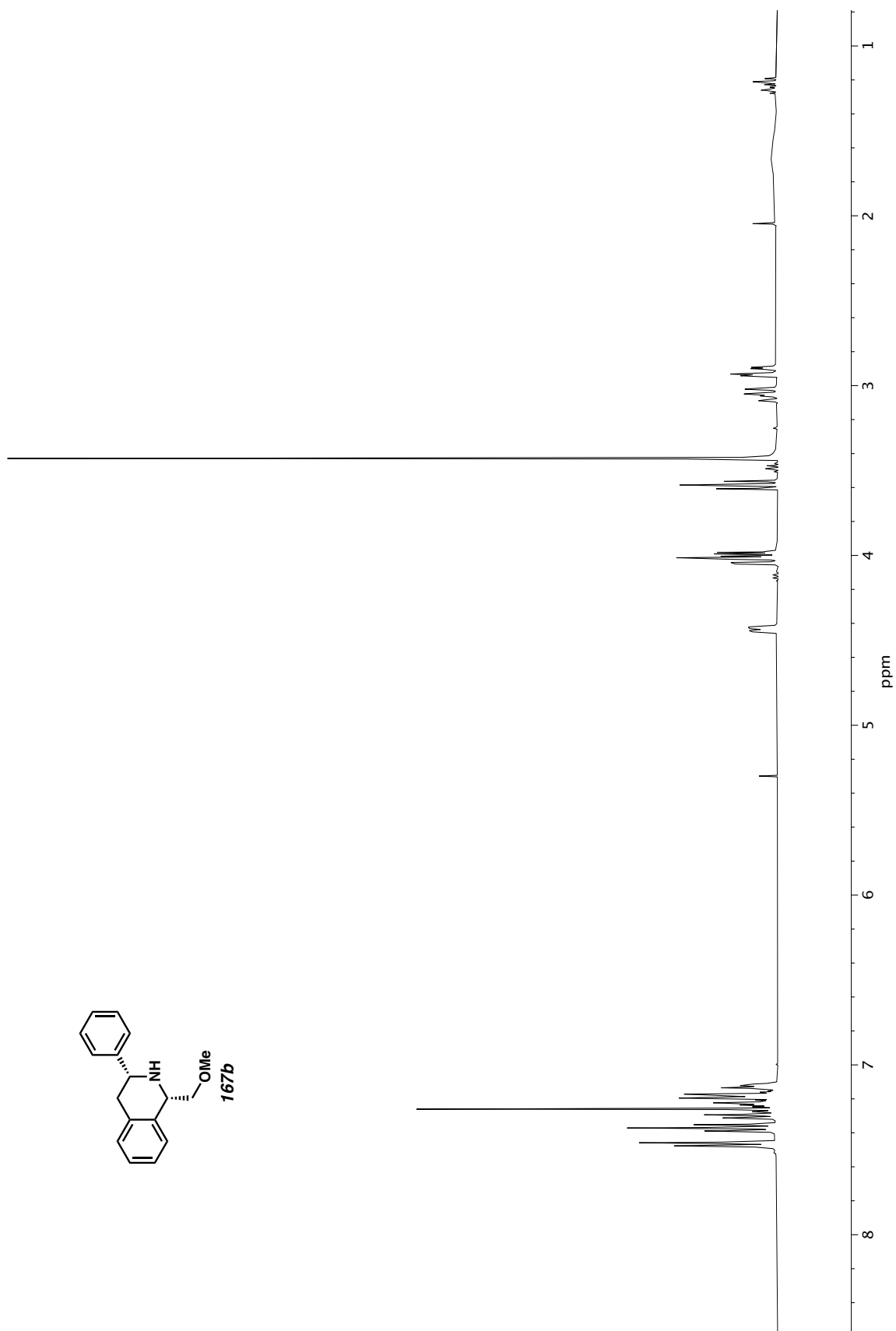
**Figure A1.281** <sup>1</sup>H NMR (400 MHz, CDCl<sub>3</sub>) of compound **167a**.



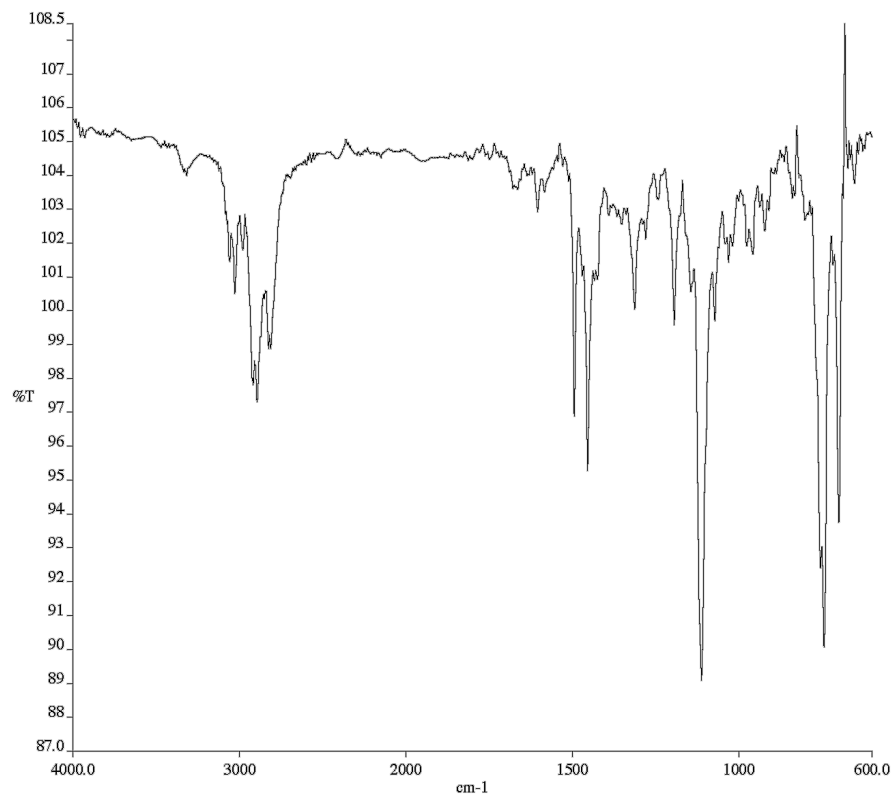
**Figure A1.282** Infrared spectrum (Thin Film, NaCl) of compound **167a**.



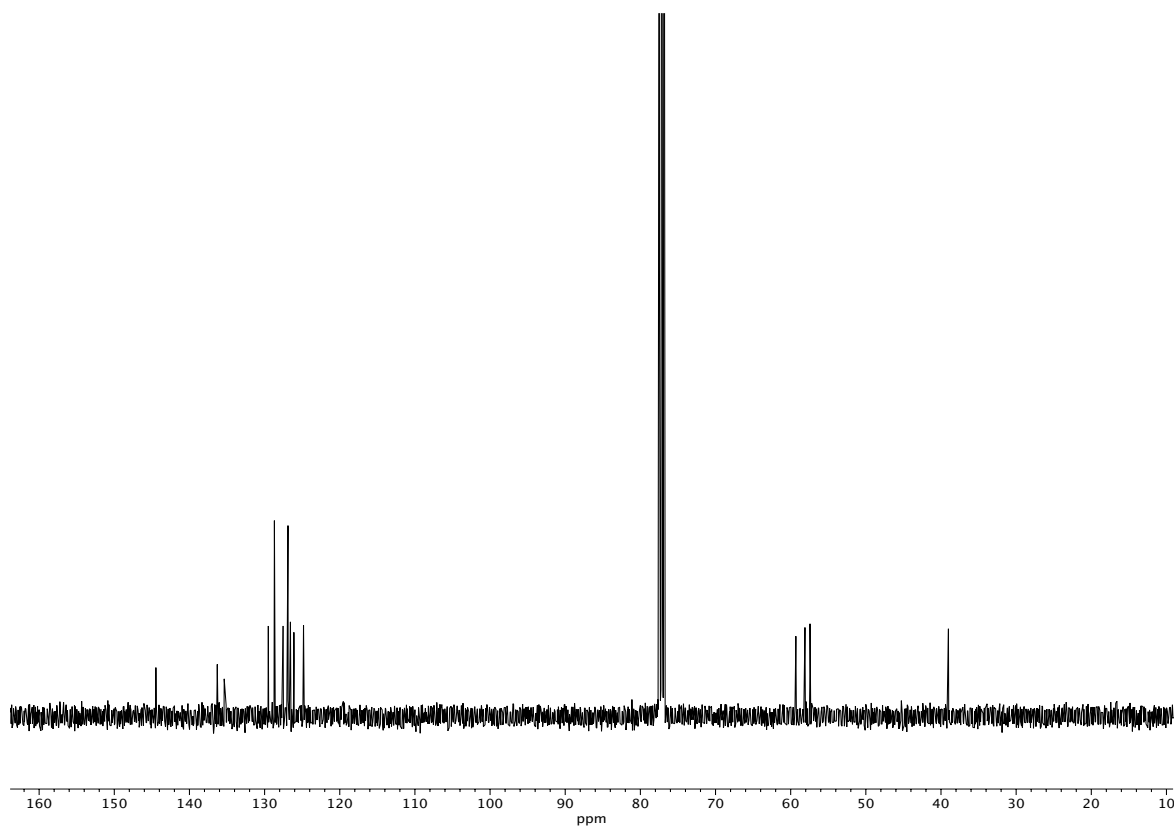
**Figure A1.283** <sup>13</sup>C NMR (100 MHz, CDCl<sub>3</sub>) of compound **167a**.



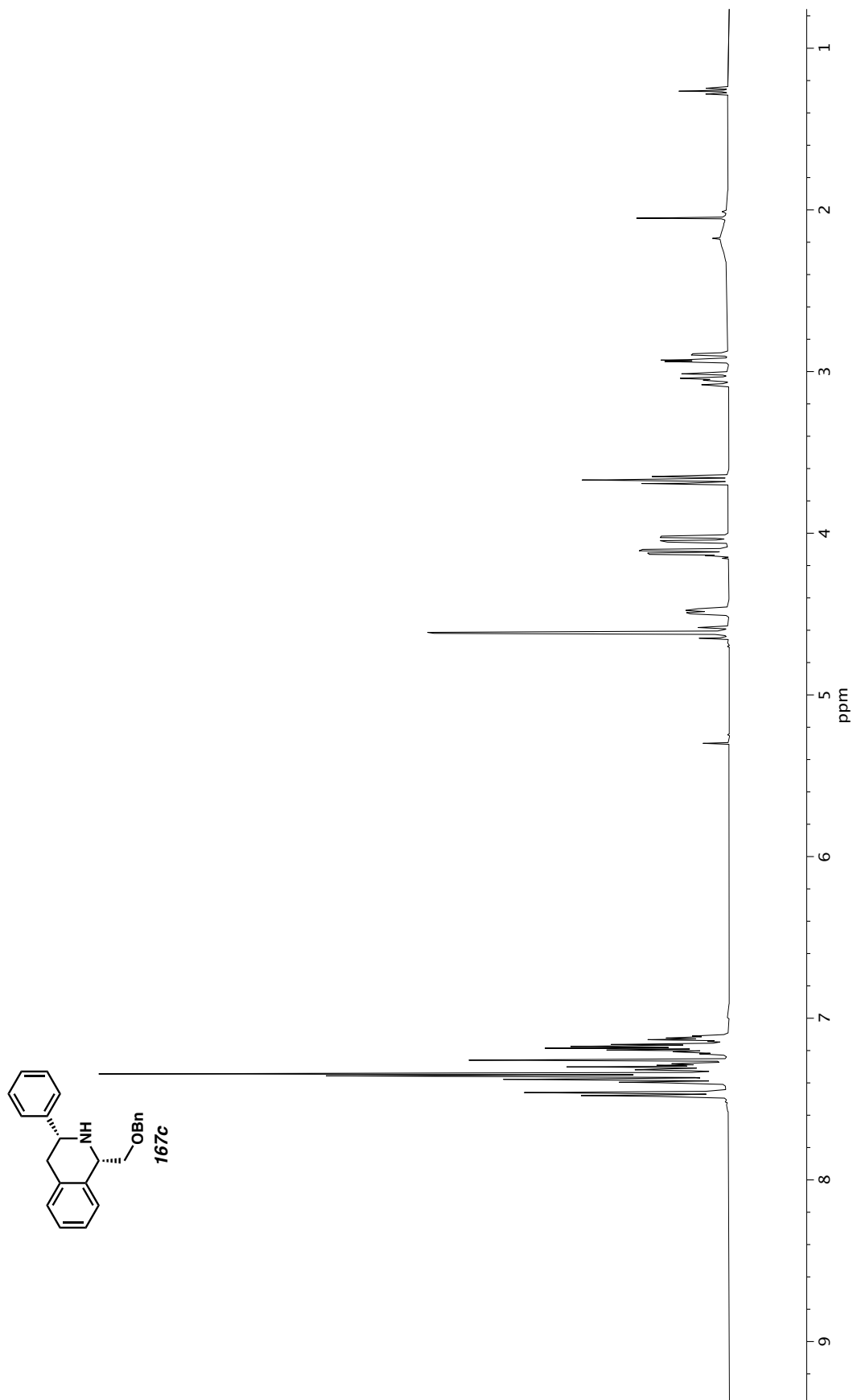
**Figure A1.284**  $^1\text{H}$  NMR (400 MHz,  $\text{CDCl}_3$ ) of compound **167b**.



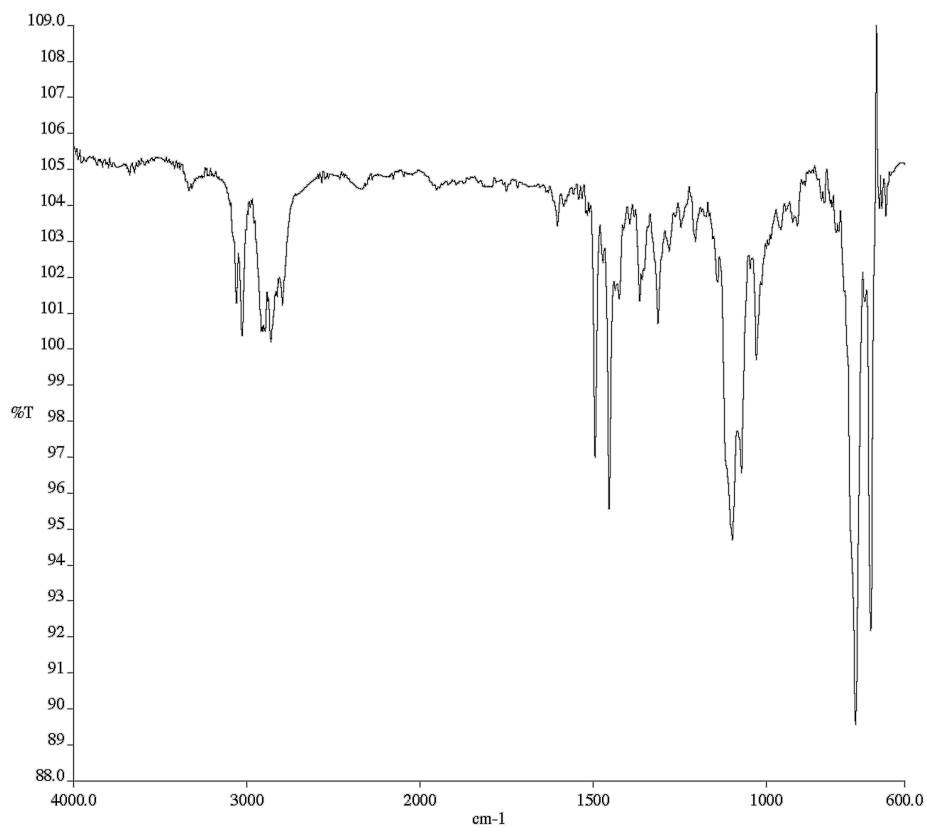
**Figure A1.285** Infrared spectrum (Thin Film, NaCl) of compound **167b**.



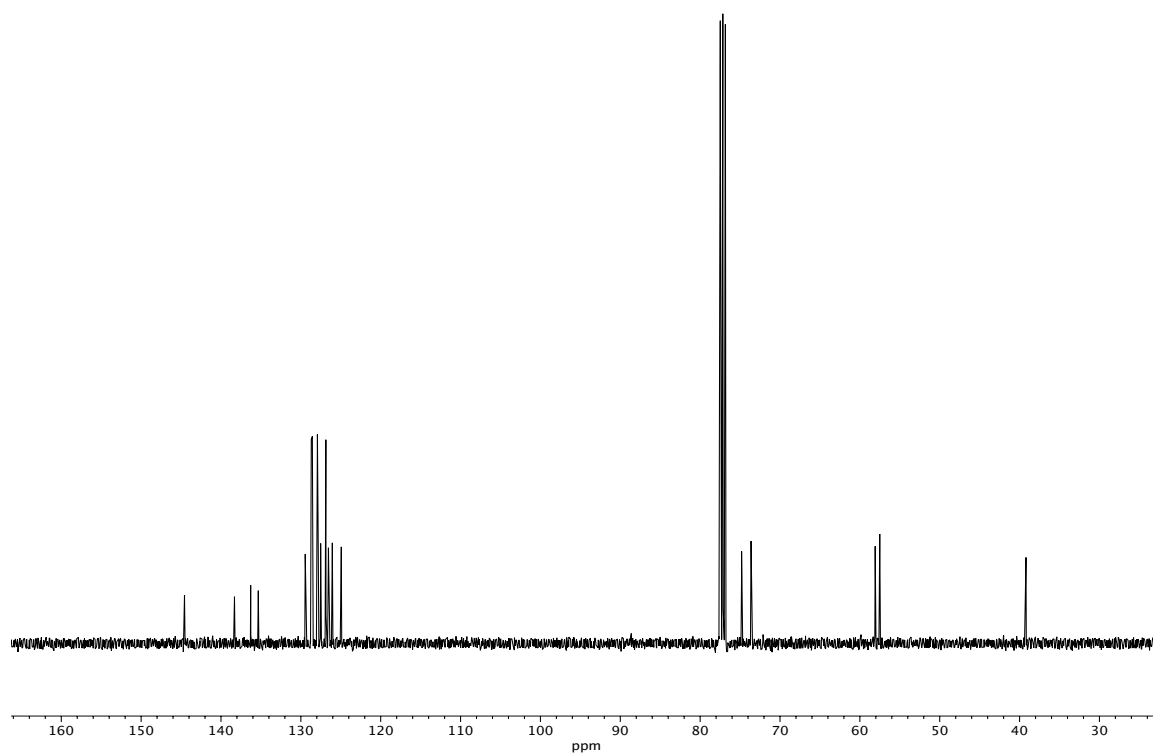
**Figure A1.286** <sup>13</sup>C NMR (100 MHz, CDCl<sub>3</sub>) of compound **167b**.



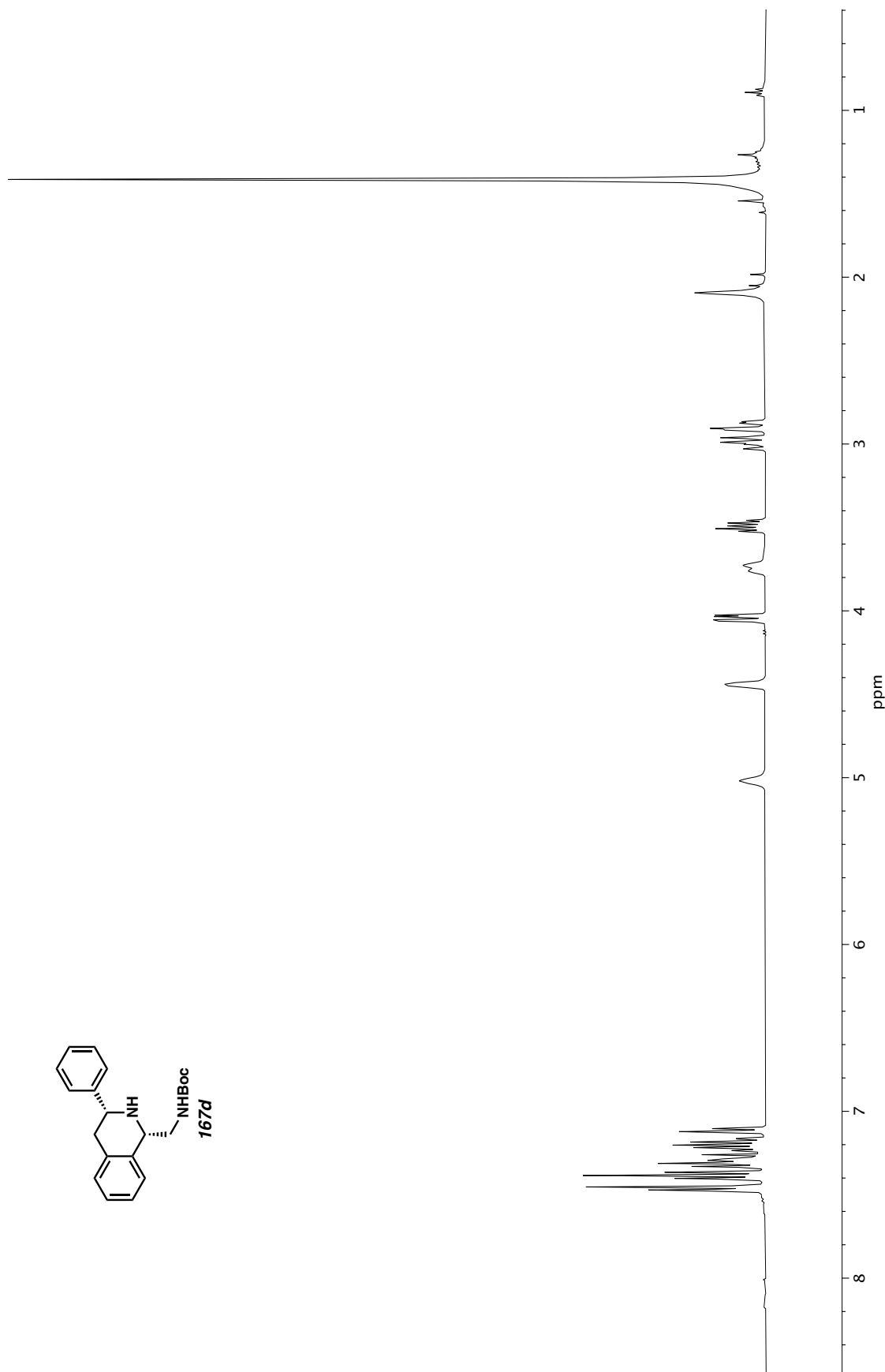
**Figure A1.287**  $^1\text{H}$  NMR (400 MHz,  $\text{CDCl}_3$ ) of compound **167c**.



**Figure A1.288** Infrared spectrum (Thin Film, NaCl) of compound **167c**.

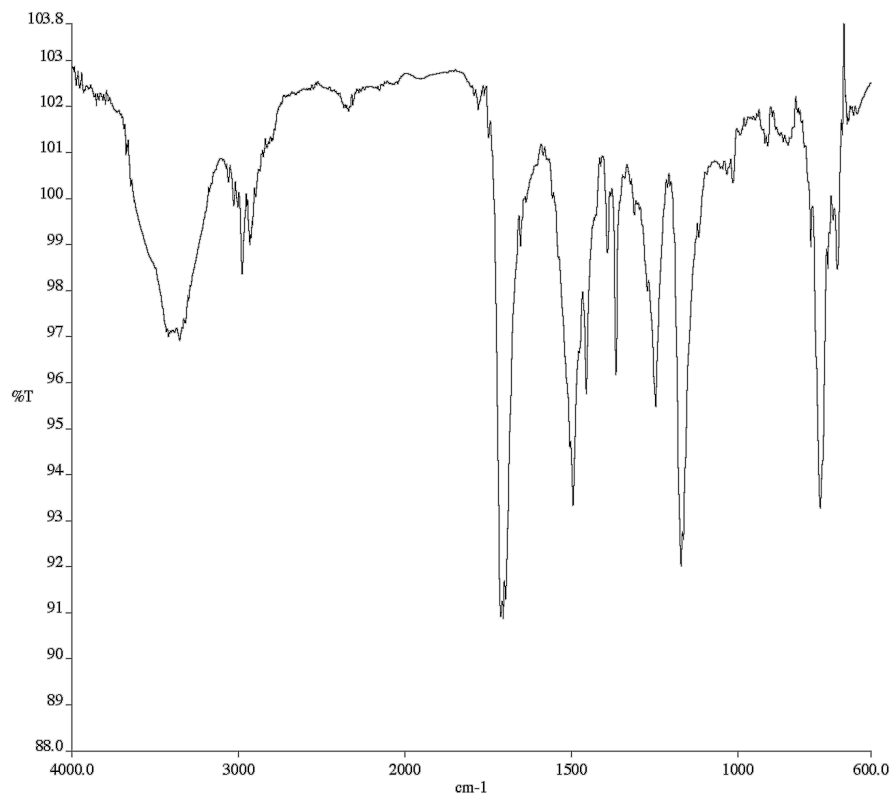


**Figure A1.289** <sup>13</sup>C NMR (100 MHz, CDCl<sub>3</sub>) of compound **167c**.

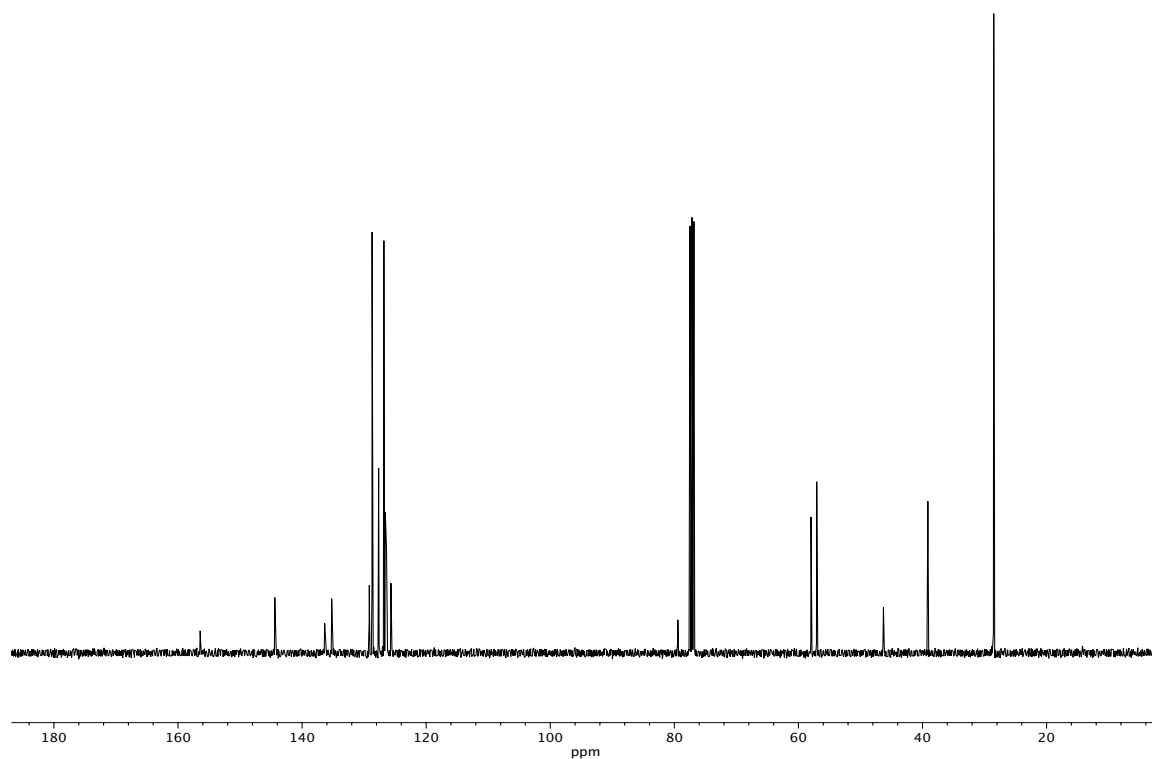


**Figure A1.290**  $^1\text{H}$  NMR (400 MHz,  $\text{CDCl}_3$ ) of compound **167d**.

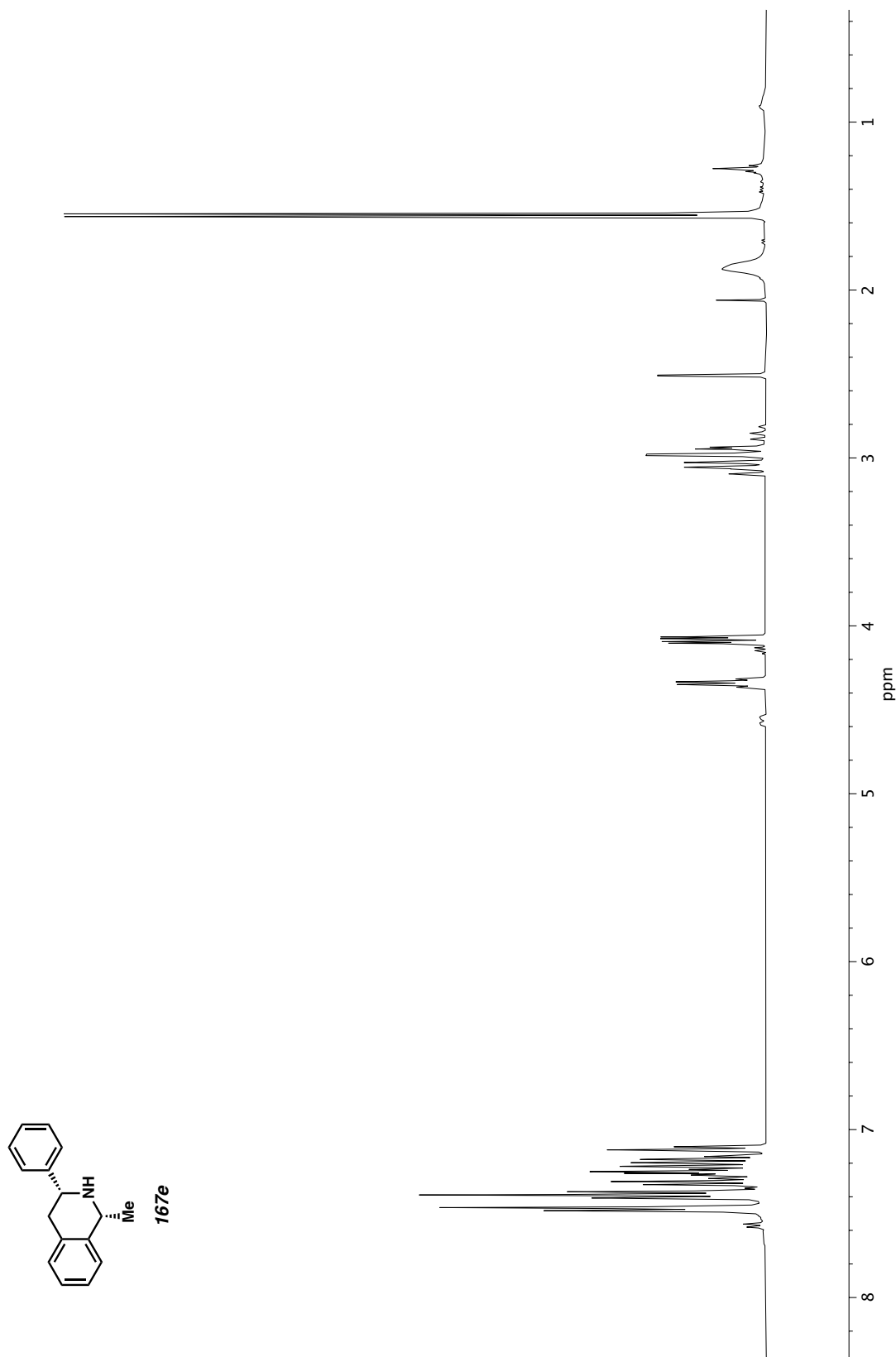




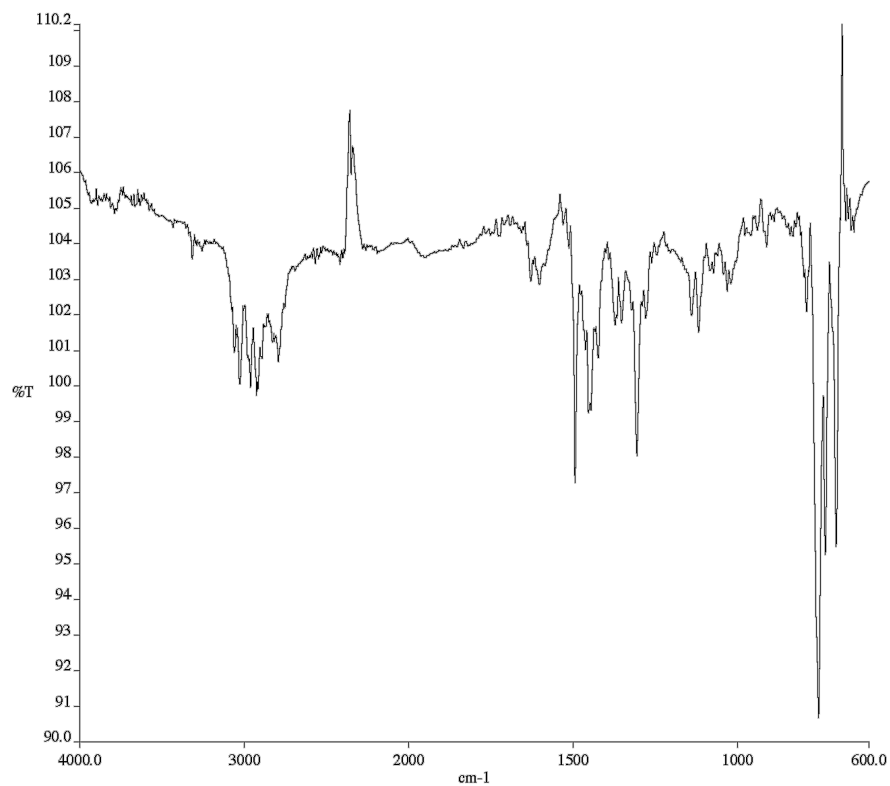
**Figure A1.291** Infrared spectrum (Thin Film, NaCl) of compound **167d**.



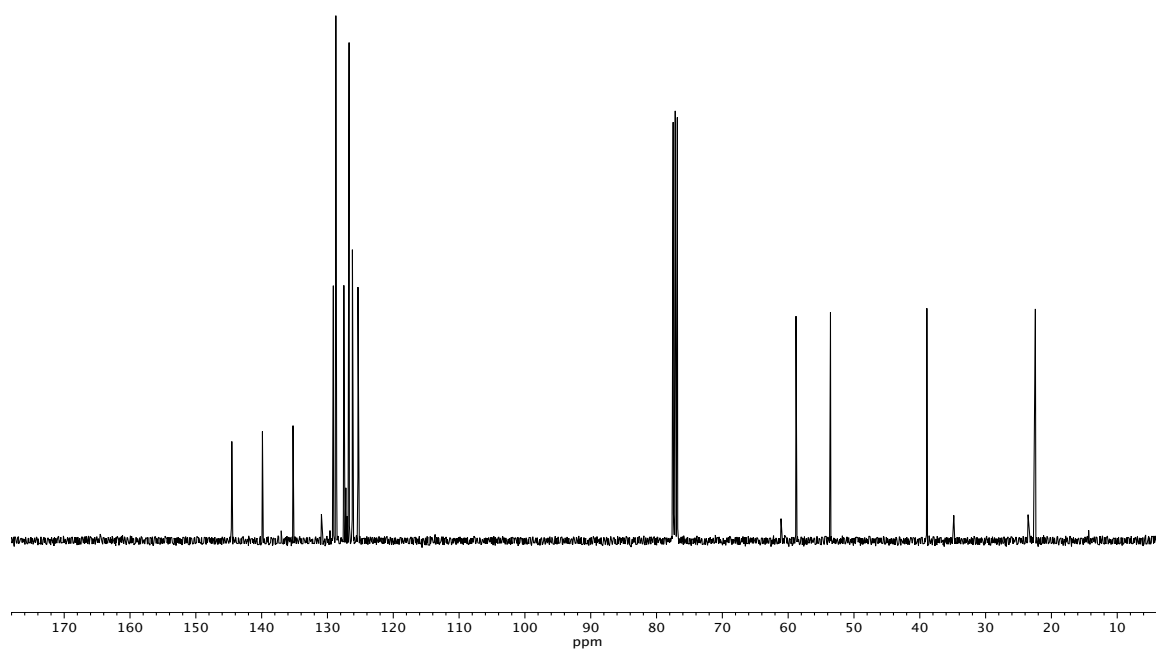
**Figure A1.292** <sup>13</sup>C NMR (100 MHz, CDCl<sub>3</sub>) of compound **167d**.



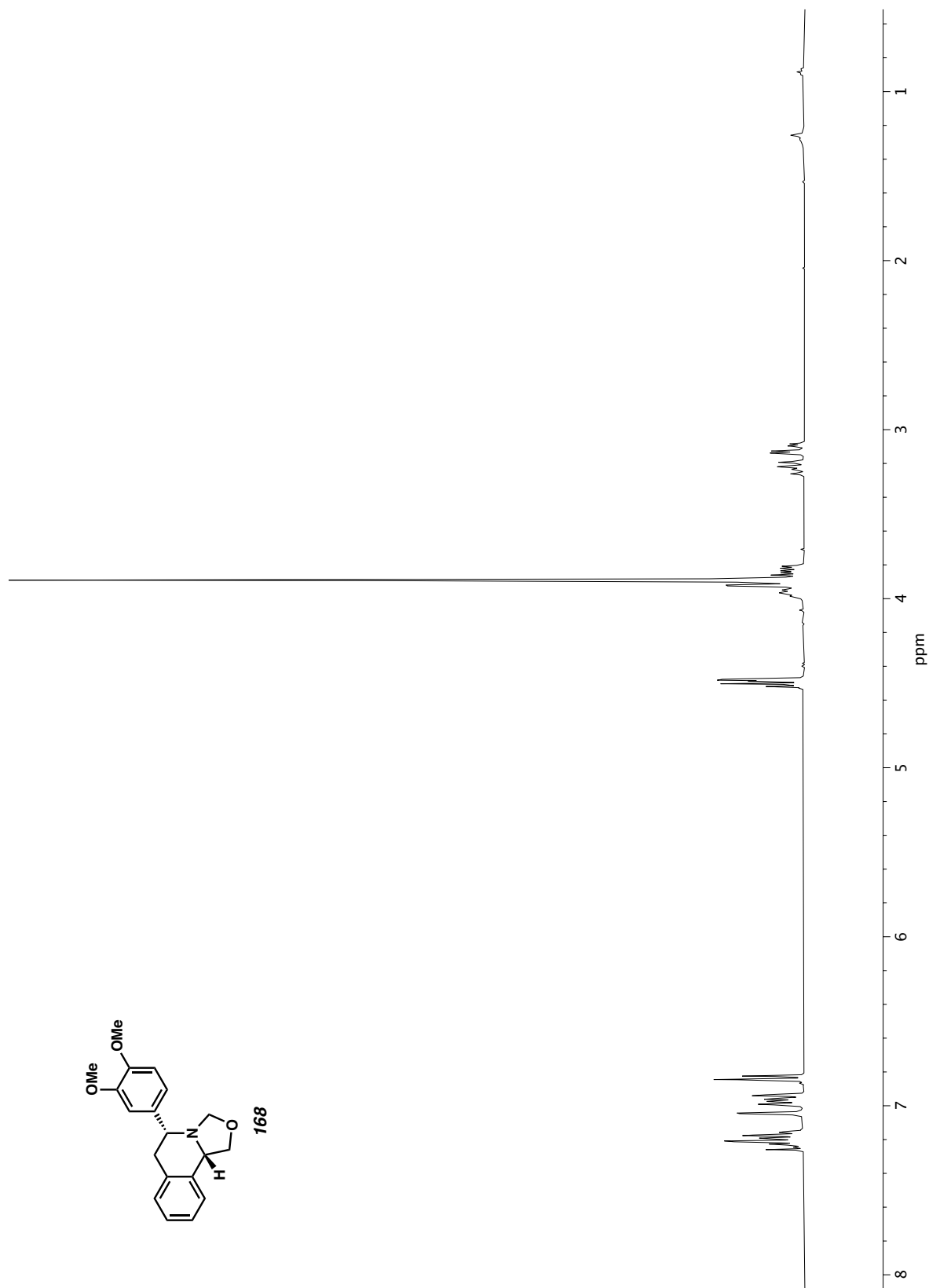
**Figure A1.293** <sup>1</sup>H NMR (400 MHz, CDCl<sub>3</sub>) of compound **167e**.



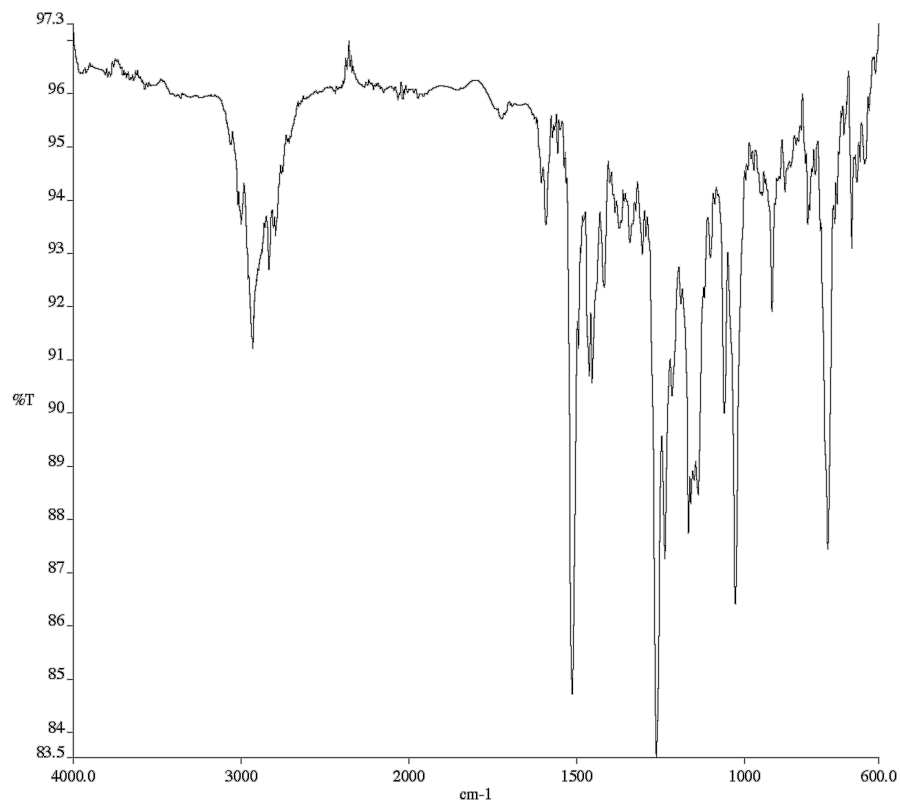
**Figure A1.294** Infrared spectrum (Thin Film, NaCl) of compound **167e**.



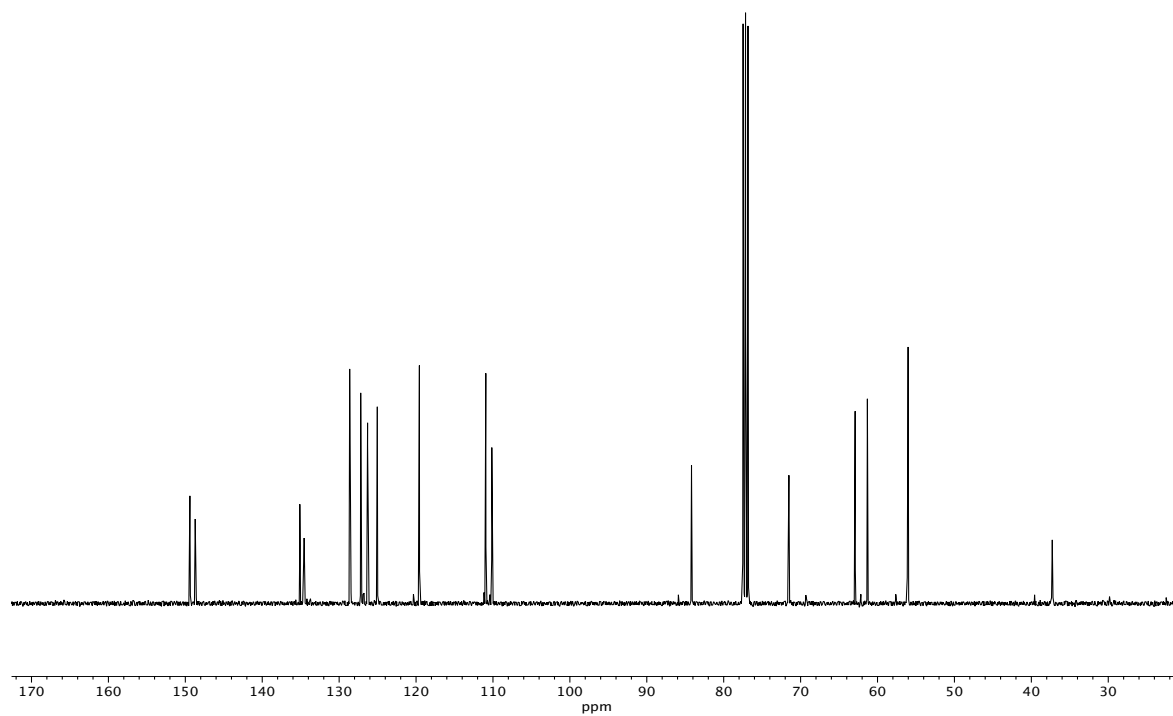
**Figure A1.295** <sup>13</sup>C NMR (100 MHz, CDCl<sub>3</sub>) of compound **167e**.



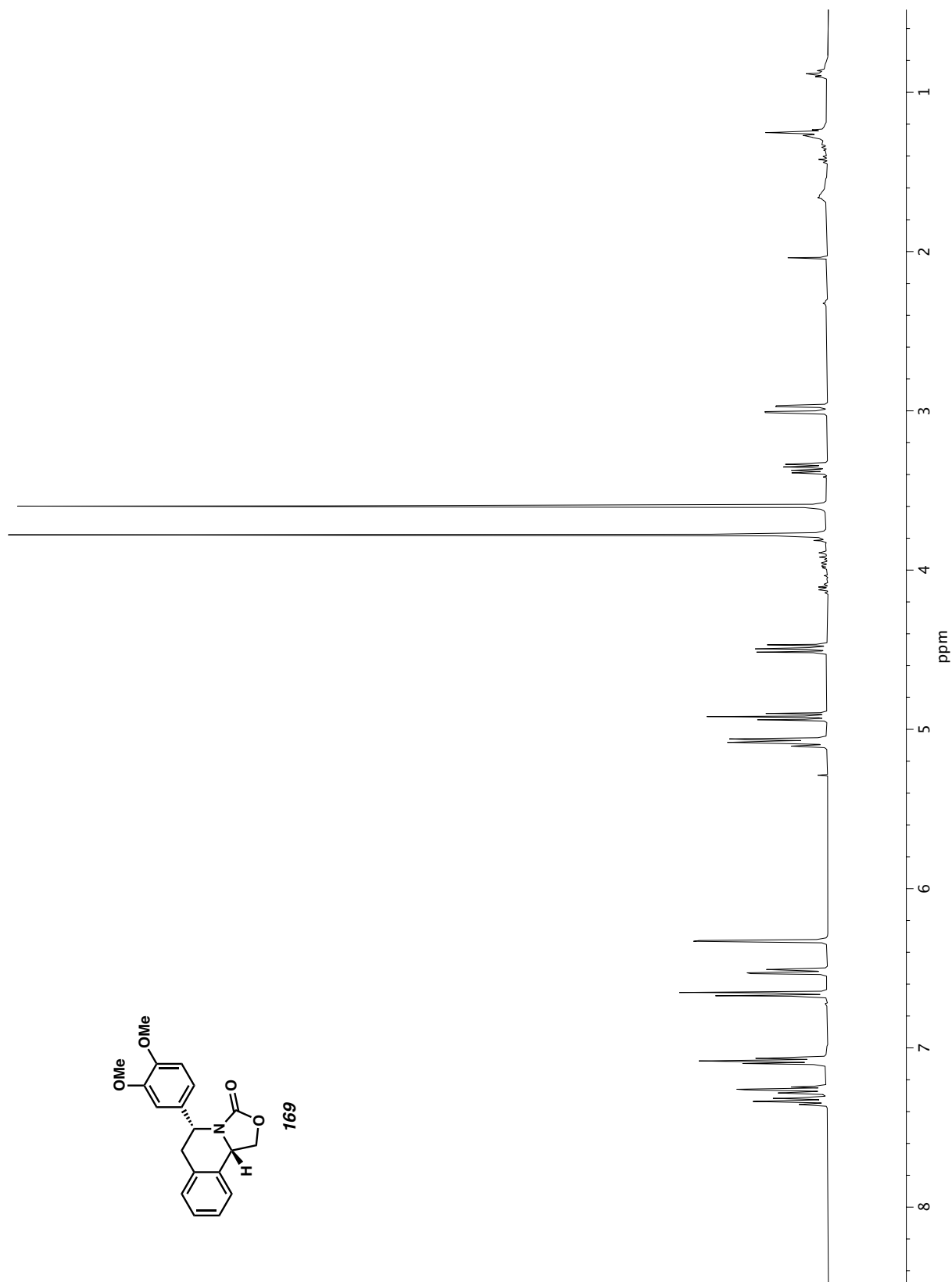
**Figure A1.296**  $^1\text{H}$  NMR (400 MHz,  $\text{CDCl}_3$ ) of compound **168**.



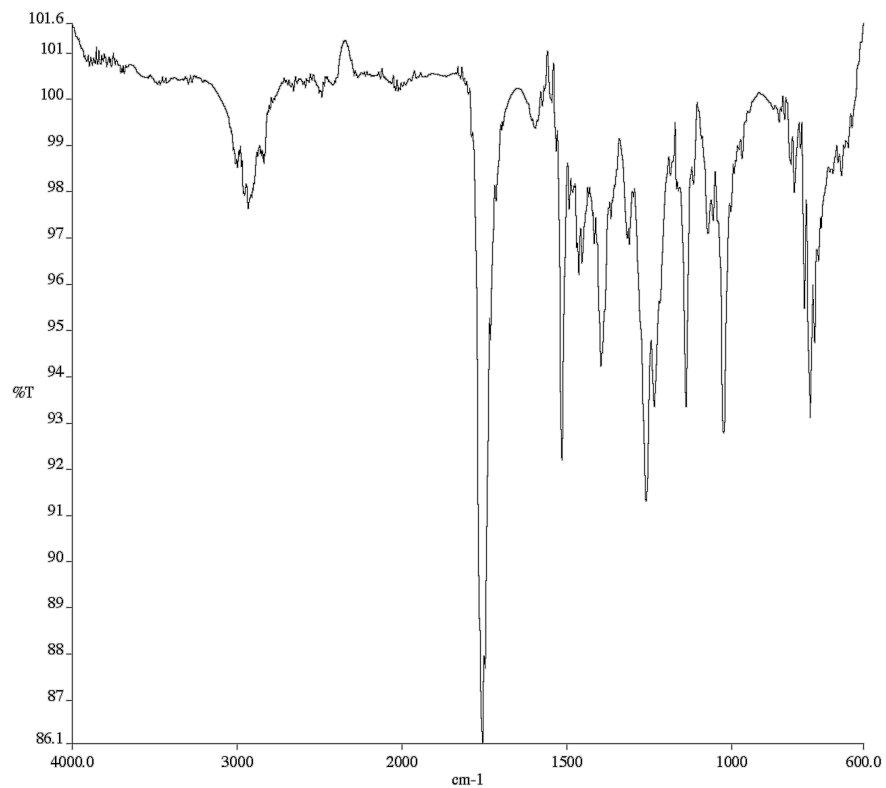
**Figure A1.297** Infrared spectrum (Thin Film, NaCl) of compound **168**.



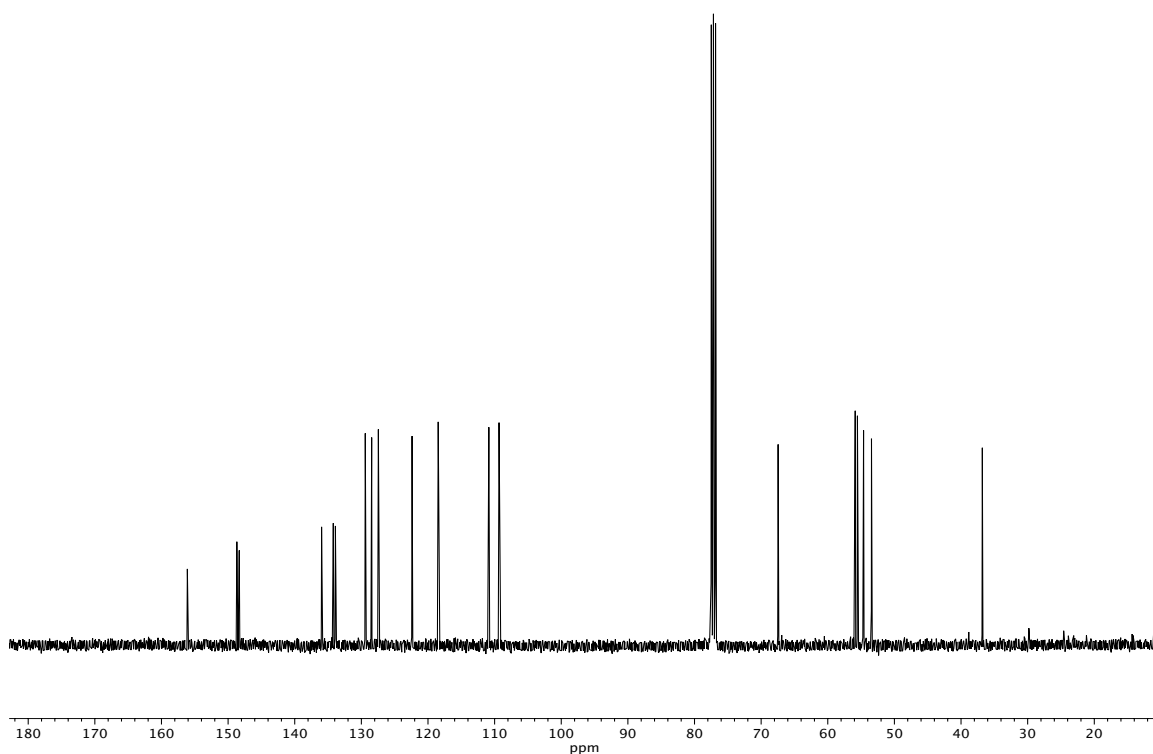
**Figure A1.298** <sup>13</sup>C NMR (100 MHz, CDCl<sub>3</sub>) of compound **168**.



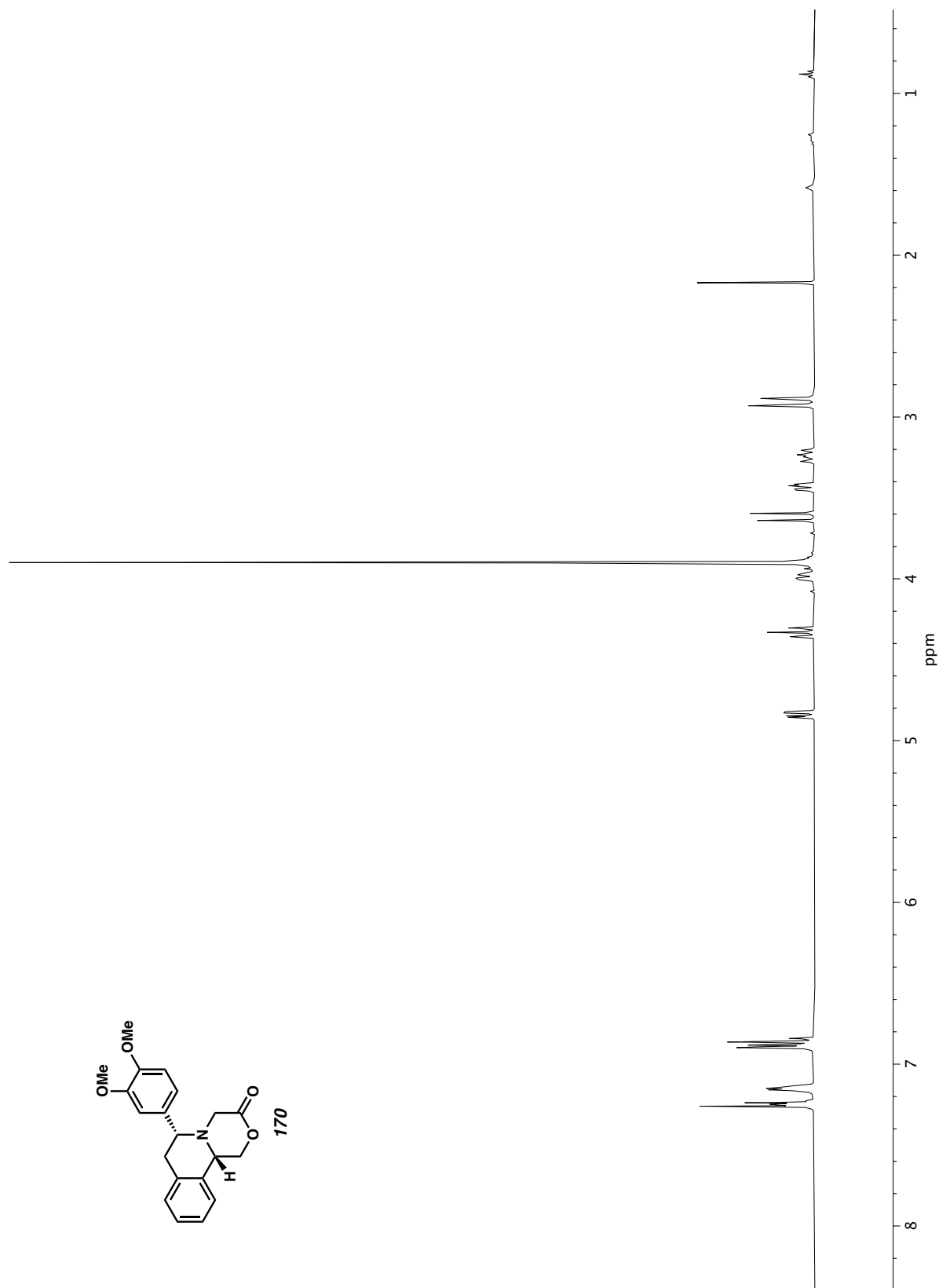
**Figure A1.299**  $^1\text{H NMR}$  (400 MHz,  $\text{CDCl}_3$ ) of compound **169**.



**Figure A1.300** Infrared spectrum (Thin Film, NaCl) of compound **169**.



**Figure A1.301** <sup>13</sup>C NMR (100 MHz, CDCl<sub>3</sub>) of compound **169**.





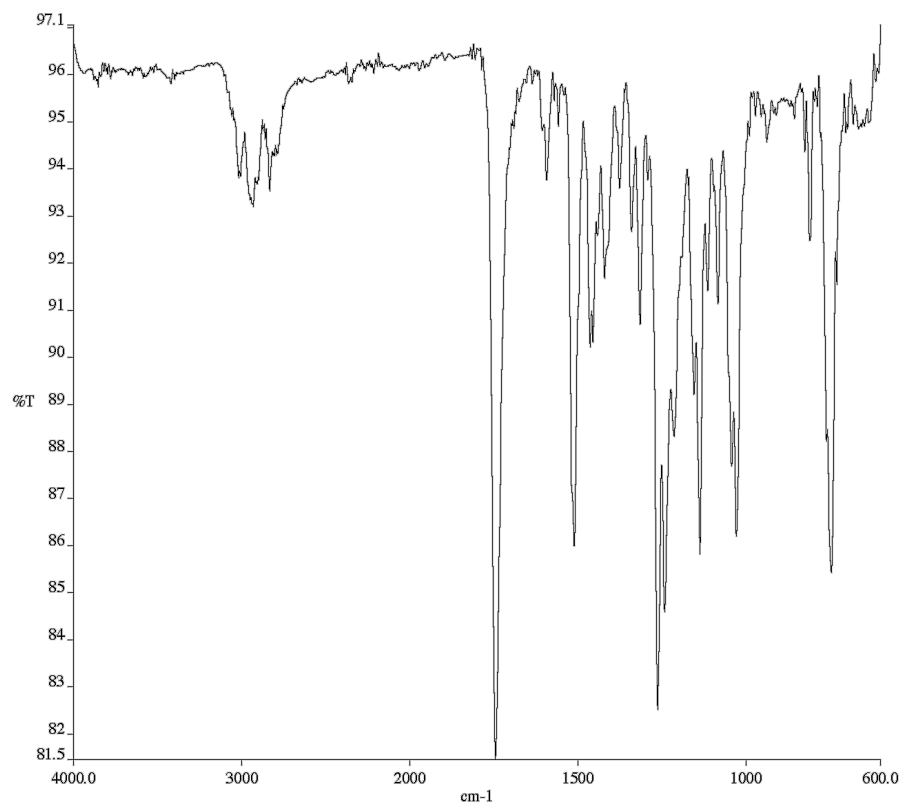


**Figure A1.303** Infrared spectrum (Thin Film, NaCl) of compound **170**.

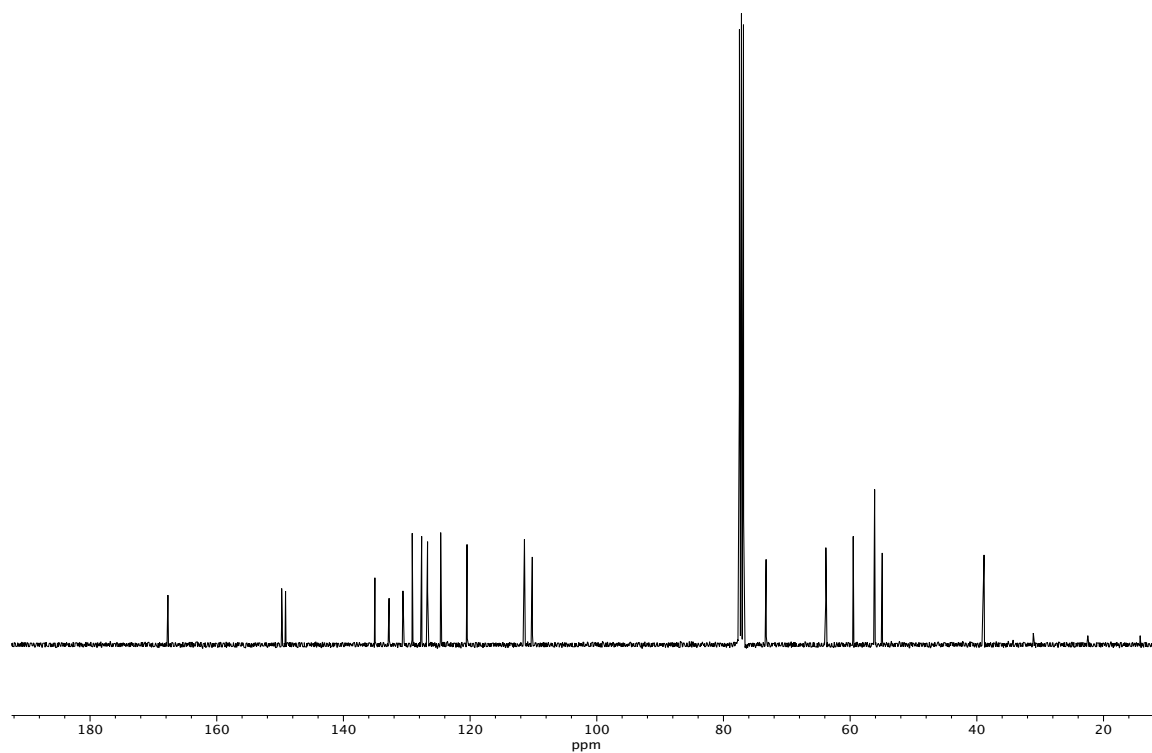


**Figure A1.304** <sup>13</sup>C NMR (100 MHz, CDCl<sub>3</sub>) of compound **170**.

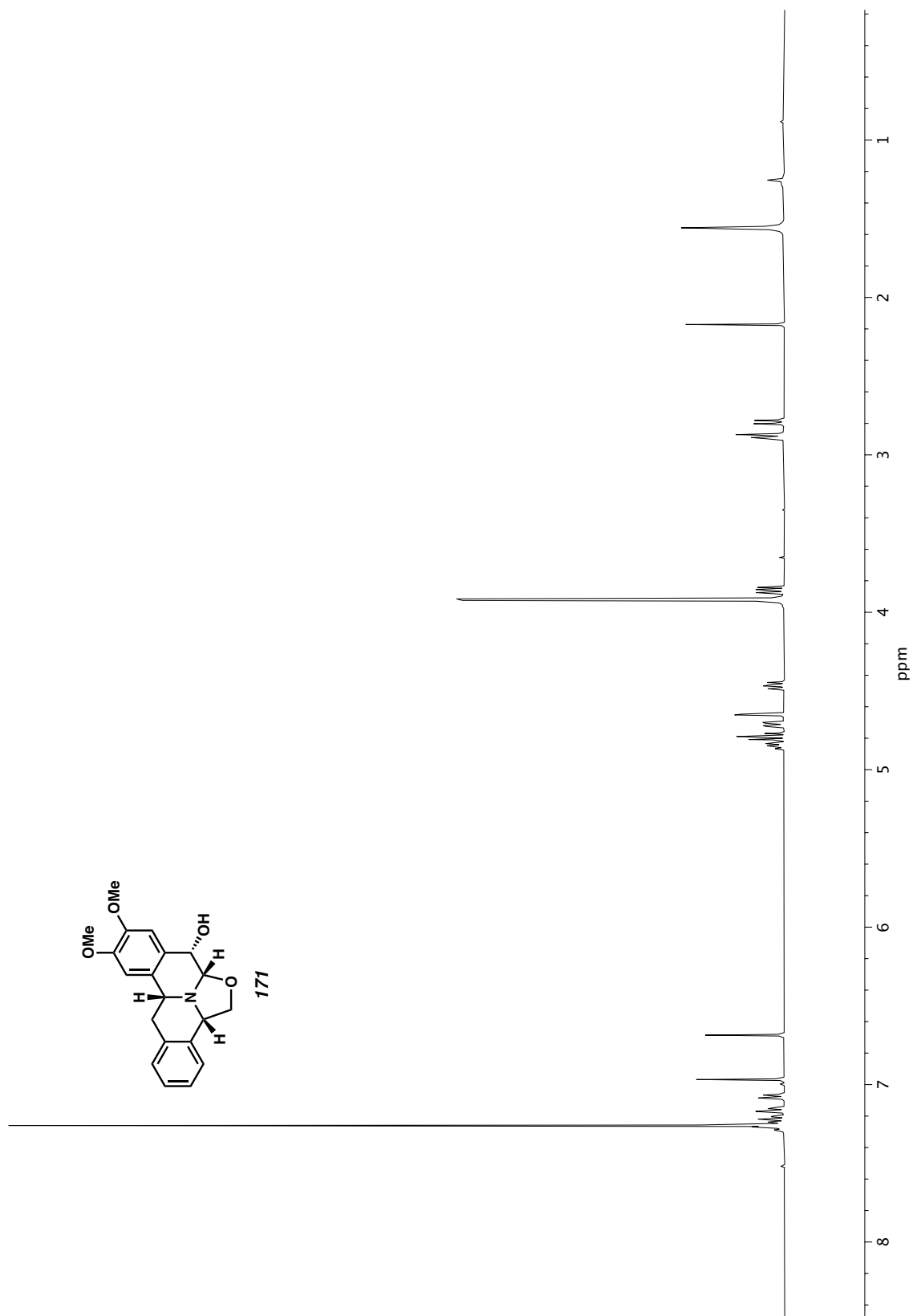


**Figure A1.305** <sup>1</sup>H NMR (400 MHz, CDCl<sub>3</sub>) of compound **171**.

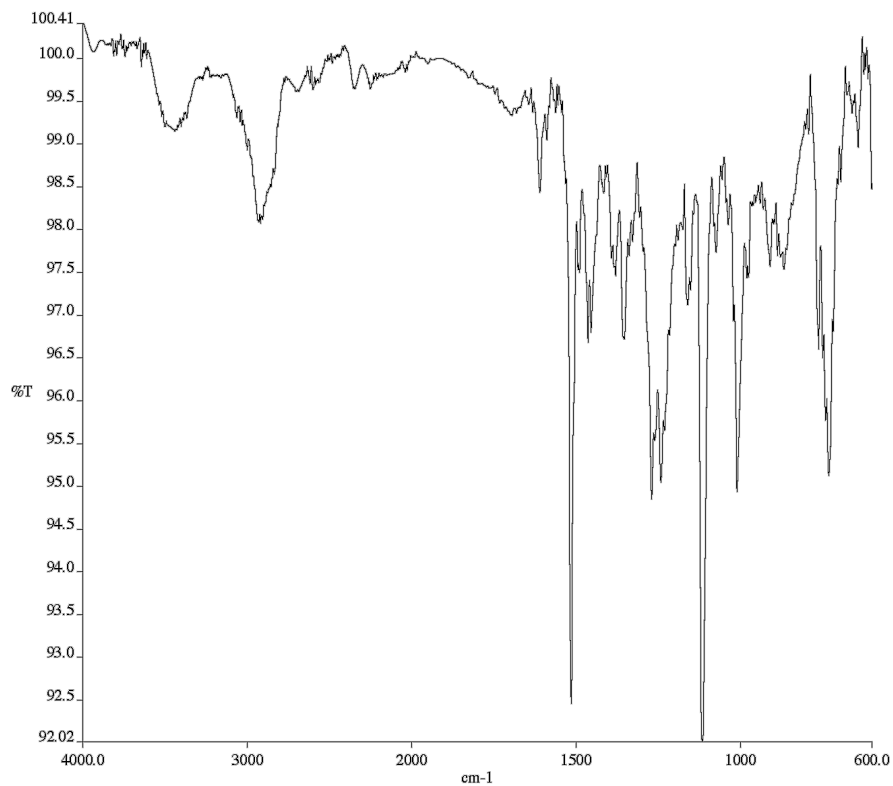


**Figure A1.306** Infrared spectrum (Thin Film, NaCl) of compound **171**.

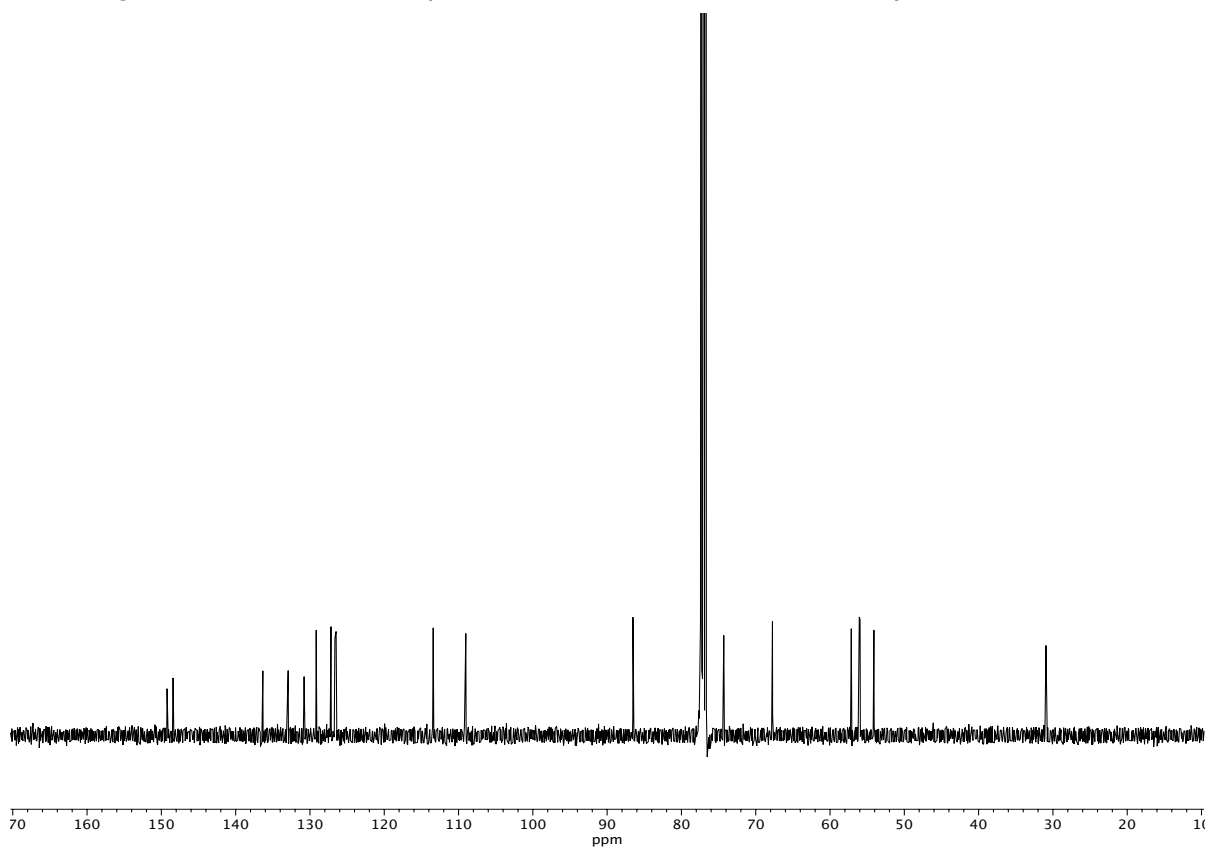


**Figure A1.307** <sup>13</sup>C NMR (100 MHz, CDCl<sub>3</sub>) of compound **171**.

## **APPENDIX 2**

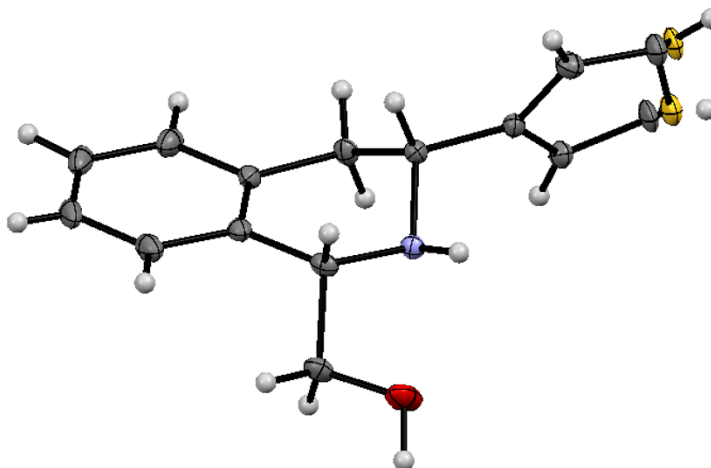
*X-Ray Crystallography Reports Relevant to Chapter 2:  
Iridium-Catalyzed Enantioselective and Diastereoselective  
Hydrogenation of 1,3-Disubstituted Isoquinolines*

## A2.1 GENERAL EXPERIMENTAL

A crystal was mounted on a polyimide MiTeGen loop with STP Oil Treatment and placed under a nitrogen stream. Low temperature (100K) X-ray data were collected with a Bruker AXS KAPPA APEX II diffractometer diffractometer running at 50 kV and 30 mA (Mo  $K_{\alpha}$  = 0.71073 Å; PHOTON 100 CMOS detector with TRIUMPH graphite monochromator). All diffractometer manipulations, including data collection, integration, and scaling were carried out using the Bruker APEX3 software. An absorption correction was applied using SADABS in point group 2. The space group was determined and the structure solved by intrinsic phasing using XT. Refinement was full-matrix least squares on  $F^2$  using XL. All non-hydrogen atoms were refined using anisotropic displacement parameters. Hydrogen atoms were placed in idealized positions and the coordinates refined (each of the two disordered pairs were constrained to the same position). The isotropic displacement parameters of all hydrogen atoms were fixed at 1.2 times (1.5 times for methyl groups and alcohol) the  $U_{eq}$  value of the bonded atom.

## A2.2 X-RAY CRYSTAL STRUCTURE ANALYSIS OF THIQ 163P

The tetrahydroisoquinoline (THIQ) product **163p** (87% ee) was crystallized by slow evaporation from chloroform at 23 °C to provide crystals suitable for X-ray analysis. Compound d19110 (**163p**) crystallizes in the monoclinic space group  $P2_1(\#4)$  with one molecule in the asymmetric unit. The S atom and one C atom were disordered 60:40; the anisotropic displacement parameters of each of the C S bonded pairs were constrained to be the same.

**Figure A2.1** X-ray crystal structure of **THIQ 163p**.**Table A2.1** Crystal data and structure refinement for product **163p**.

Identification code	d19110	
Empirical formula	C <sub>14</sub> H <sub>15</sub> N O S	
Formula weight	245.33	
Temperature	100 K	
Wavelength	0.71073 Å	
Crystal system	Monoclinic	
Space group	P 1 21 1	
Unit cell dimensions	a = 8.3309(19) Å	a = 90°
	b = 6.6556(18) Å	b = 96.337(8)°
	c = 10.916(3) Å	g = 90°
Volume	601.6(3) Å <sup>3</sup>	
Z	2	
Density (calculated)	1.354 g/cm <sup>3</sup>	
Absorption coefficient	0.251 mm <sup>-1</sup>	
F(000)	260	
Crystal size	0.38 x 0.17 x 0.08 mm <sup>3</sup>	
Theta range for data collection	1.877 to 35.613°.	
Index ranges	-13 ≤ h ≤ 13, -10 ≤ k ≤ 10, -17 ≤ l ≤ 17	

Reflections collected	25734
Independent reflections	5228 [R(int) = 0.0337]
Completeness to theta = 25.242°	99.5 %
Absorption correction	Semi-empirical from equivalents
Max. and min. transmission	1.0000 and 0.9299
Refinement method	Full-matrix least-squares on F <sup>2</sup>
Data / restraints / parameters	5228 / 1 / 209
Goodness-of-fit on F <sup>2</sup>	1.058
Final R indices [I>2sigma(I)]	R1 = 0.0383, wR2 = 0.0909
R indices (all data)	R1 = 0.0484, wR2 = 0.0960
Absolute structure parameter [Flack]	0.04(2)
Absolute structure parameter [Hoofit]	0.03(2)
Extinction coefficient	n/a
Largest diff. peak and hole	0.457 and -0.227 e.Å <sup>-3</sup>

**Table A2.2** Atomic coordinates ( $\times 10^5$ ), and equivalent isotropic displacement parameters ( $\text{\AA}^2 \times 10^4$ ), and population for **163p**.  $U(\text{eq})$  is defined as one third of the trace of the orthogonalized  $U_{ij}$  tensor.

	x	y	z	U(eq)	pop
S(1)	-1782(9)	10112(13)	8554(8)	192(2)	0.61(1)
S(1A)	-12835(17)	26880(20)	15351(16)	200(4)	0.40(1)
O(1)	46731(15)	90530(20)	2239(13)	250(3)	1
N(1)	38190(14)	60130(20)	16462(10)	126(2)	1
C(1)	31520(15)	47500(20)	25761(12)	119(2)	1
C(2)	45361(17)	34360(20)	31317(14)	146(2)	1
C(3)	59104(16)	47440(20)	36870(12)	135(2)	1
C(4)	69583(19)	40430(30)	46858(14)	193(3)	1
C(5)	81732(19)	52630(30)	52519(15)	236(3)	1
C(6)	83610(20)	71900(30)	48189(15)	243(4)	1
C(7)	73300(20)	79110(30)	38302(15)	210(3)	1
C(8)	60916(17)	66970(20)	32554(13)	140(2)	1
C(9)	49394(17)	75610(20)	22155(13)	133(2)	1

C(10)	58373(18)	84320(30)	11976(14)	174(3)	1
C(11)	16954(16)	36170(20)	20222(13)	127(2)	1
C(12)	17083(17)	18760(20)	13110(13)	147(2)	1
C(13)	-10370(60)	29940(90)	16190(50)	192(2)	0.61(1)
C(13A)	1840(80)	11730(130)	9760(70)	200(4)	0.40(1)
C(14)	1166(19)	42160(30)	21889(15)	177(3)	1

**Table A2.3** Bond lengths [ $\text{\AA}$ ] and angles [ $^\circ$ ] for **163p**.

S(1)-C(12)	1.6959(16)
S(1)-C(13)	1.755(6)
S(1A)-C(13A)	1.746(9)
S(1A)-C(14)	1.6492(19)
O(1)-H(1)	0.93(3)
O(1)-C(10)	1.419(2)
N(1)-H(1A)	0.90(2)
N(1)-C(1)	1.4732(18)
N(1)-C(9)	1.4799(19)
C(1)-H(1B)	1.03(2)
C(1)-C(2)	1.5193(19)
C(1)-C(11)	1.4985(19)
C(2)-H(2A)	0.98(2)
C(2)-H(2B)	1.00(2)
C(2)-C(3)	1.511(2)
C(3)-C(4)	1.400(2)
C(3)-C(8)	1.396(2)
C(4)-H(4)	0.91(3)
C(4)-C(5)	1.389(2)
C(5)-H(5)	0.93(3)
C(5)-C(6)	1.382(3)
C(6)-H(6)	0.85(3)
C(6)-C(7)	1.388(3)
C(7)-H(7)	0.99(3)
C(7)-C(8)	1.403(2)
C(8)-C(9)	1.517(2)
C(9)-H(9)	0.99(2)
C(9)-C(10)	1.521(2)
C(10)-H(10A)	0.96(3)
C(10)-H(10B)	1.01(3)
C(11)-C(12)	1.395(2)



C(11)-C(14)	1.405(2)
C(12)-C(13A)	1.365(6)
C(12)-H(12)	0.94(2)
C(12)-H(12A)	0.94(2)
C(13)-H(13)	0.91(5)
C(13)-C(14)	1.357(5)
C(13A)-H(13A)	1.04(8)
C(14)-H(14A)	0.90(3)
C(14)-H(14)	0.90(3)
C(12)-S(1)-C(13)	91.08(18)
C(14)-S(1A)-C(13A)	91.0(2)
C(10)-O(1)-H(1)	112.9(17)
C(1)-N(1)-H(1A)	108.6(14)
C(1)-N(1)-C(9)	112.10(10)
C(9)-N(1)-H(1A)	106.4(15)
N(1)-C(1)-H(1B)	110.5(13)
N(1)-C(1)-C(2)	106.04(11)
N(1)-C(1)-C(11)	111.07(11)
C(2)-C(1)-H(1B)	108.3(12)
C(11)-C(1)-H(1B)	106.3(12)
C(11)-C(1)-C(2)	114.61(12)
C(1)-C(2)-H(2A)	112.8(13)
C(1)-C(2)-H(2B)	110.8(13)
H(2A)-C(2)-H(2B)	106(2)
C(3)-C(2)-C(1)	109.66(12)
C(3)-C(2)-H(2A)	108.2(13)
C(3)-C(2)-H(2B)	109.0(13)
C(4)-C(3)-C(2)	120.00(14)
C(8)-C(3)-C(2)	120.42(12)
C(8)-C(3)-C(4)	119.48(14)
C(3)-C(4)-H(4)	117.4(15)
C(5)-C(4)-C(3)	120.85(16)
C(5)-C(4)-H(4)	121.3(15)
C(4)-C(5)-H(5)	120.5(18)
C(6)-C(5)-C(4)	119.70(16)
C(6)-C(5)-H(5)	119.6(18)
C(5)-C(6)-H(6)	122.3(19)
C(5)-C(6)-C(7)	120.17(15)
C(7)-C(6)-H(6)	117.3(19)

C(6)-C(7)-H(7)	122.1(15)
C(6)-C(7)-C(8)	120.68(17)
C(8)-C(7)-H(7)	117.2(15)
C(3)-C(8)-C(7)	119.12(14)
C(3)-C(8)-C(9)	121.50(12)
C(7)-C(8)-C(9)	119.33(14)
N(1)-C(9)-C(8)	111.60(12)
N(1)-C(9)-H(9)	108.5(13)
N(1)-C(9)-C(10)	107.26(12)
C(8)-C(9)-H(9)	111.2(13)
C(8)-C(9)-C(10)	111.69(12)
C(10)-C(9)-H(9)	106.4(14)
O(1)-C(10)-C(9)	107.91(12)
O(1)-C(10)-H(10A)	111.9(15)
O(1)-C(10)-H(10B)	111.6(13)
C(9)-C(10)-H(10A)	109.0(14)
C(9)-C(10)-H(10B)	110.1(14)
H(10A)-C(10)-H(10B)	106(2)
C(12)-C(11)-C(1)	125.94(13)
C(12)-C(11)-C(14)	111.87(13)
C(14)-C(11)-C(1)	122.19(13)
S(1)-C(12)-H(12)	119.9(15)
C(11)-C(12)-S(1)	112.40(11)
C(11)-C(12)-H(12)	127.7(16)
C(11)-C(12)-H(12A)	127.7(16)
C(13A)-C(12)-C(11)	111.7(4)
C(13A)-C(12)-H(12A)	120.6(16)
S(1)-C(13)-H(13)	105(3)
C(14)-C(13)-S(1)	111.3(4)
C(14)-C(13)-H(13)	143(3)
S(1A)-C(13A)-H(13A)	105(3)
C(12)-C(13A)-S(1A)	112.0(5)
C(12)-C(13A)-H(13A)	143(4)
S(1A)-C(14)-H(14A)	120.7(15)
C(11)-C(14)-S(1A)	113.35(14)
C(11)-C(14)-H(14A)	125.9(15)
C(11)-C(14)-H(14)	125.9(15)
C(13)-C(14)-C(11)	113.4(3)
C(13)-C(14)-H(14)	120.7(15)

---

**Table A2.4** Anisotropic displacement parameters ( $\text{\AA}^2 \times 10^4$ ) for **163p**. The anisotropic displacement factor exponent takes the form:  $-2\pi^2 [h^2 a^{*2} U^{11} + \dots + 2 h k a^* b^* U^{12}]$

	U11	U22	U33	U23	U13	U12
S(1)	146(4)	220(4)	204(4)	-44(3)	-7(3)	-76(3)
S(1A)	121(7)	246(7)	223(6)	-49(5)	-15(4)	-92(4)
O(1)	205(6)	302(7)	251(6)	151(5)	60(4)	14(5)
N(1)	133(5)	113(5)	131(5)	14(4)	8(4)	-15(4)
C(1)	109(5)	126(5)	121(5)	0(4)	13(4)	-11(4)
C(2)	129(6)	135(6)	168(6)	39(5)	-7(4)	-20(5)
C(3)	101(5)	182(6)	123(5)	1(5)	14(4)	5(5)
C(4)	157(6)	274(8)	144(6)	12(6)	2(5)	45(5)
C(5)	127(6)	437(10)	143(6)	-57(6)	2(5)	35(6)
C(6)	148(6)	416(11)	167(6)	-123(7)	23(5)	-95(6)
C(7)	191(7)	255(8)	193(6)	-75(6)	54(5)	-94(6)
C(8)	125(5)	173(6)	126(5)	-31(5)	35(4)	-21(5)
C(9)	150(6)	94(5)	161(6)	-5(5)	45(4)	-16(4)
C(10)	171(6)	166(6)	191(6)	30(5)	53(5)	-35(5)
C(11)	124(5)	138(6)	114(5)	5(4)	-2(4)	-20(4)
C(12)	150(6)	141(6)	147(6)	-16(5)	10(4)	-27(5)
C(13)	146(4)	220(4)	204(4)	-44(3)	-7(3)	-76(3)
C(13A)	121(7)	246(7)	223(6)	-49(5)	-15(4)	-92(4)
C(14)	153(6)	197(7)	186(6)	-13(5)	45(5)	-5(5)

**Table A2.5** Hydrogen coordinates ( $\times 10^4$ ) and isotropic displacement parameters ( $\text{\AA}^2 \times 10^3$ ) for **163p**.

	x	y	z	U(eq)
H(1)	5130(30)	9700(50)	-410(30)	38
H(1A)	3010(30)	6680(40)	1220(20)	15
H(1B)	2770(20)	5620(40)	3270(20)	14
H(2A)	4220(30)	2540(40)	3780(20)	18
H(2B)	4930(30)	2550(40)	2490(20)	18
H(4)	6740(30)	2820(40)	5010(20)	23
H(5)	8820(30)	4820(50)	5950(20)	28

H(6)	9050(30)	8010(40)	5180(20)	29
H(7)	7390(30)	9310(40)	3530(20)	25
H(9)	4290(30)	8670(40)	2510(20)	16
H(10A)	6490(30)	9530(40)	1520(20)	21
H(10B)	6600(30)	7400(40)	910(20)	21
H(13)	-2130(60)	2800(70)	1480(40)	23
H(13A)	-450(70)	-40(120)	550(60)	24
H(12)	2610(30)	1210(40)	1060(20)	21
H(12A)	2610(30)	1210(40)	1060(20)	21
H(14A)	-150(30)	5310(40)	2600(20)	21
H(14)	-150(30)	5310(40)	2600(20)	21

**Table A2.6** Torsion angles [°] for **163p**.

S(1)-C(13)-C(14)-C(11)	0.6(4)
N(1)-C(1)-C(2)-C(3)	58.56(14)
N(1)-C(1)-C(11)-C(12)	78.77(18)
N(1)-C(1)-C(11)-C(14)	-102.09(16)
N(1)-C(9)-C(10)-O(1)	52.73(16)
C(1)-N(1)-C(9)-C(8)	44.46(15)
C(1)-N(1)-C(9)-C(10)	167.09(12)
C(1)-C(2)-C(3)-C(4)	151.33(13)
C(1)-C(2)-C(3)-C(8)	-25.09(17)
C(1)-C(11)-C(12)-S(1)	179.50(12)
C(1)-C(11)-C(12)-C(13A)	178.1(4)
C(1)-C(11)-C(14)-S(1A)	-177.87(13)
C(1)-C(11)-C(14)-C(13)	-179.8(3)
C(2)-C(1)-C(11)-C(12)	-41.36(19)
C(2)-C(1)-C(11)-C(14)	137.77(14)
C(2)-C(3)-C(4)-C(5)	-176.42(14)
C(2)-C(3)-C(8)-C(7)	176.81(13)
C(2)-C(3)-C(8)-C(9)	-0.66(19)
C(3)-C(4)-C(5)-C(6)	-0.5(2)
C(3)-C(8)-C(9)-N(1)	-7.99(18)
C(3)-C(8)-C(9)-C(10)	-128.05(14)
C(4)-C(3)-C(8)-C(7)	0.4(2)
C(4)-C(3)-C(8)-C(9)	-177.09(13)
C(4)-C(5)-C(6)-C(7)	0.7(2)
C(5)-C(6)-C(7)-C(8)	-0.3(2)
C(6)-C(7)-C(8)-C(3)	-0.3(2)

C(6)-C(7)-C(8)-C(9)	177.26(14)
C(7)-C(8)-C(9)-N(1)	174.55(12)
C(7)-C(8)-C(9)-C(10)	54.49(17)
C(8)-C(3)-C(4)-C(5)	0.0(2)
C(8)-C(9)-C(10)-O(1)	175.30(13)
C(9)-N(1)-C(1)-C(2)	-71.23(14)
C(9)-N(1)-C(1)-C(11)	163.67(12)
C(11)-C(1)-C(2)-C(3)	-178.55(11)
C(11)-C(12)-C(13A)-S(1A)	0.4(6)
C(12)-S(1)-C(13)-C(14)	-0.3(4)
C(12)-C(11)-C(14)-S(1A)	1.37(18)
C(12)-C(11)-C(14)-C(13)	-0.6(3)
C(13)-S(1)-C(12)-C(11)	0.0(2)
C(13A)-S(1A)-C(14)-C(11)	-0.9(3)
C(14)-S(1A)-C(13A)-C(12)	0.3(5)
C(14)-C(11)-C(12)-S(1)	0.29(16)
C(14)-C(11)-C(12)-C(13A)	-1.1(4)

**Table A2.7** Hydrogen bonds for **163p** [ $\text{\AA}$  and  $^\circ$ ].

D-H...A	d(D-H)	d(H...A)	d(D...A)	$\angle$ (DHA)
O(1)-H(1)...N(1)#1	0.93(3)	1.90(3)	2.8310(18)	177(2)

Symmetry transformations used to generate equivalent atoms: #1 -x+1,y+1/2,-z

## CHAPTER 3

### *Iridium-Catalyzed Asymmetric *Trans*-Selective Hydrogenation of 1,3-Disubstituted Isoquinolines<sup>†</sup>*

#### 3.1 INTRODUCTION

The asymmetric hydrogenation of heteroarenes has recently emerged as a powerful strategy to directly access enantioenriched, saturated heterocycles.<sup>1,2</sup> While significant progress has been made in this field, controlling selectivity in the formation of multiple stereocenters in a single reaction remains challenging. Transition metal-catalyzed hydrogenation of arenes typically proceeds through initial dearomative reduction of the substrate and subsequent rapid hydrogenation, resulting in high *cis*-selectivity of product (Figure 3.1A, path A).<sup>3,4</sup> In contrast, accessing the *trans*-isomer requires a  $\pi$ -facial exchange of the arene to allow hydride delivery from the more sterically hindered face, rendering its synthesis significantly more difficult (Figure 3.1A, path B). While several reports describe the *trans*-selective hydrogenation of arenes, most are limited in scope and not

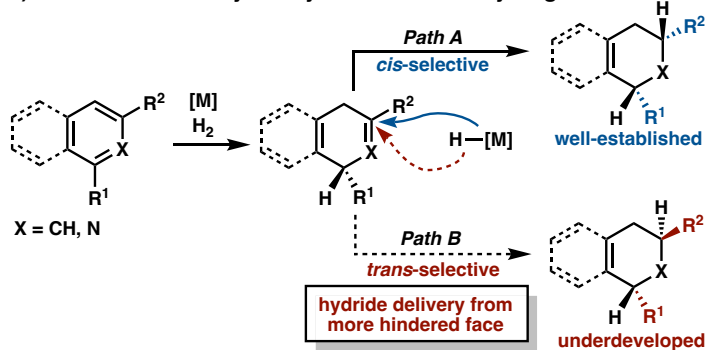
---

<sup>†</sup>This research was performed in collaboration with Dr. Fa Ngamthiporn, and Dr. Michael D. Bartberger. Portions of this chapter have been reproduced with permission from Kim, A. N.; Ngamthiporn, A.; Bartberger, M. D.; Stoltz, B. M. *Chem. Sci.* **2022**, *13*, 3227–3232. © 2022 Royal Society of Chemistry.

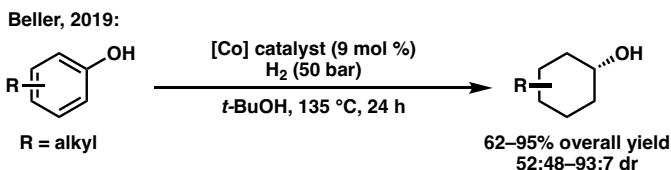
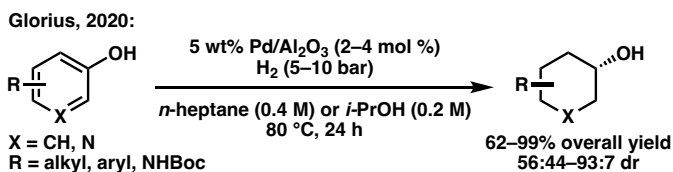
heterocycles, a general method for an asymmetric *trans*-selective hydrogenation of heteroarenes would be a highly desirable and powerful strategy.<sup>7,8</sup>

**Figure 3.1** A) Challenges in diastereoselectivity of *trans*-selective arene hydrogenation. B) Our research on iridium-catalyzed asymmetric hydrogenation of 1,3-disubstituted isoquinolines.

**A. 1) Diastereoselectivity in Asymmetric Arene Hydrogenation**



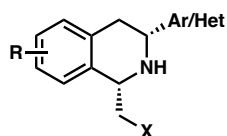
**2) Prior Art in *trans*-selective Hydrogenation**



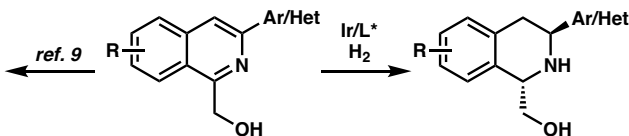
**No general method of a *trans*- and enantioselective hydrogenation of arenes reported**

**B.**

**Previous Research:**



**This Research:**



**trans-selective · enantioselective · mild reaction conditions · broad scope**

Recently, our group has reported the asymmetric hydrogenation of 1,3-disubstituted isoquinolines to access enantioenriched *cis*-1,2,3,4-tetrahydroisoquinolines (THIQs).<sup>9</sup> This

method enables the asymmetric hydrogenation of isoquinolines with Lewis basic functionalities, such as primary alcohols and heteroaryl-substituted isoquinolines, that significantly expanded the scope of the transformation compared to prior reports.<sup>10</sup> During the course of this investigation, we also observed formation of the *trans*-THIQ under certain conditions with excellent enantioselectivity, albeit in small amounts. Herein, we disclose our efforts to develop the first examples of an asymmetric *trans*-selective hydrogenation of 1,3-disubstituted isoquinolines to access enantioenriched *trans*-THIQs (Figure 3.1B).

### 3.2 REACTION OPTIMIZATION

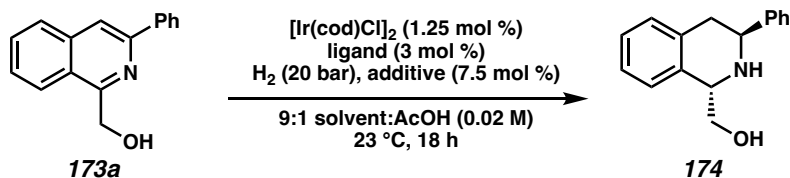
We began our hydrogenation studies with 1-(hydroxymethyl)-3-phenylisoquinoline (**173a**) as our model substrate. An initial experiment employing 1.25 mol % [Ir(cod)Cl]<sub>2</sub>, 3 mol % of chiral Josiphos ligand **L7**, and 7.5 mol % of TBAI in THF delivered the THIQ product with high *cis*-selectivity (Table 3.1, entry 1).<sup>9</sup> We observed that using CH<sub>2</sub>Cl<sub>2</sub> as solvent gave higher levels of diastereoselectivity for *trans*-isomer **174**, with excellent enantioselectivity as well (97% ee, entry 2).<sup>11</sup> Gratified by this result, we explored different additives and observed that smaller halides afforded higher levels of the desired diastereoselectivity, albeit with diminished conversion of **173a**. Overall, TBABr provided the best combination of diastereo- and enantioselectivity (entry 3). Other additives such as TBAPF<sub>6</sub> previously investigated by Pfaltz and coworkers completely shut down the reaction, demonstrating that halide salts were crucial for this transformation (entry 5).<sup>12</sup>

Seeking to improve the diastereoselectivity, we surveyed a variety of chiral ligand scaffolds and found the xylyphos ligand framework to be optimal (Table 3.4). We observed that more electron-rich aryl groups on the chiral ligand provided the *trans*-product with higher selectivity, with the DMM-substituted phosphine **L7** affording the highest

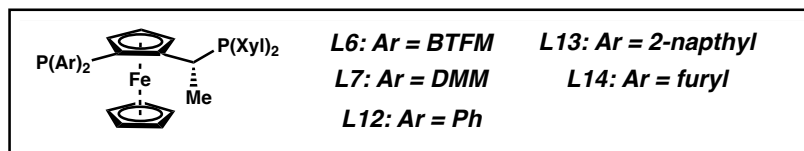


diastereoselectivity of 2:1 *trans*:*cis* (entry 3 vs. entries 6–9). In contrast, more electron-withdrawing aryl groups such as **L6** favored the formation of the *cis*-product (entry 9).

**Table 3.1.** Optimization of the asymmetric *trans*-selective hydrogenation.<sup>a</sup>



entry	ligand	solvent	additive	% conversion <sup>b</sup>	<i>trans</i> : <i>cis</i> <sup>b</sup>	% ee of <i>trans</i> <sup>c</sup>
1	L7	THF	TBAI	>95	1:15.7	–
2	L7	CH <sub>2</sub> Cl <sub>2</sub>	TBAI	>95	1:1.5	97
3	L7	CH <sub>2</sub> Cl <sub>2</sub>	TBABr	>95	2:1	93
4	L7	CH <sub>2</sub> Cl <sub>2</sub>	TBACl	75	2.3:1	80
5	L7	CH <sub>2</sub> Cl <sub>2</sub>	TBAPF <sub>6</sub>	<10	–	–
6	L12	CH <sub>2</sub> Cl <sub>2</sub>	TBABr	>95	1.8:1	94
7	L13	CH <sub>2</sub> Cl <sub>2</sub>	TBABr	95	1.4:1	99
8	L14	CH <sub>2</sub> Cl <sub>2</sub>	TBABr	45	1:2.3	35
9	L6	CH <sub>2</sub> Cl <sub>2</sub>	TBABr	83	1:2.9	81
10	L7	PhMe	TBABr	>95	1.2:1	91
11	L7	EtOAc	TBABr	>95	1:1.1	89
12	L7	CHCl <sub>3</sub>	TBABr	68	2.4:1	93
13	L7	1,2-DCE	TBABr	>95	2.4:1	92

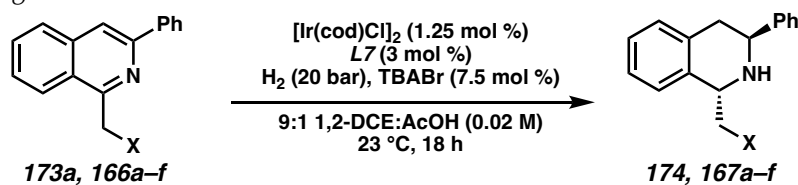


[a] Reaction conditions: 0.04 mmol of **173a**, 1.25 mol % [Ir(cod)Cl]<sub>2</sub>, 3 mol % ligand, 7.5 mol % additive, 20 bar H<sub>2</sub> in 2.0 mL 9:1 solvent:AcOH. [b] Determined from crude <sup>1</sup>H NMR using 1,3,5-trimethoxybenzene as standard. [c] Determined by chiral SFC analysis of Cbz-protected *trans*-product. BTFM = 3,5-bis(trifluoromethyl)phenyl; DMM = 4-methoxy-3,5-dimethylphenyl

Having identified **L7** as the optimal ligand, we briefly investigated different solvents. We observed that non-coordinating chlorinated solvents such as chloroform and 1,2-dichloroethane (1,2-DCE) delivered product **174** with the highest *trans*-selectivity (entries 12–13), while non-chlorinated solvents toluene and ethyl acetate gave nearly a 1:1 diastereomeric ratio (entries 10–11).<sup>13</sup>

We also explored different directing groups at the C1 position to probe their effects on the diastereoselectivity of this reaction. Isoquinolines bearing functionalities such as a methyl ether, benzyl ether, or acetate substituent (**166a–c**) solely provided the *cis*-THIQ, suggesting that they are not functioning as directing groups in the reaction (Table 3.2, entries 1–3). Indeed, the hydrogenation of isoquinoline **166e** that lacks any potential directing group also afforded only the *cis*-diastereomer of product (entry 4).

**Table 3.2.** Investigation of different directing groups to optimize the asymmetric *trans*-selective hydrogenation.



entry	X	% conversion <sup>b</sup>	trans:cis <sup>b</sup>	% ee of trans <sup>c</sup>
1	OAc ( <b>166a</b> )	57	1:>20	–
2	OMe ( <b>166b</b> )	>95	1:17	–
3	OBn ( <b>166c</b> )	>95	1:>20	–
4	H ( <b>166e</b> )	92	1:>20	–
5	NHBoc ( <b>166d</b> )	>95	1.4:1	25
6	NH <sub>2</sub> ( <b>166g</b> )	0	–	–
7	OH ( <b>173a</b> )	>95	2.4:1	92

[a] Reaction conditions: 0.04 mmol of substrate, 1.25 mol % [Ir(cod)Cl]<sub>2</sub>, 3 mol % **L7**, 7.5 mol % TBABr, 20 bar H<sub>2</sub> in 2.0 mL 9:1 1,2-DCE:AcOH. [b] Determined from crude <sup>1</sup>H NMR using 1,3,5-trimethoxybenzene as standard. [c] Determined by chiral SFC analysis of Cbz-protected *trans*-product.

While Boc-protected amine **166d** provided the product in 1.4:1 dr favoring the *trans*-THIQ, basic amine functionalities such as primary amine **166g** gave trace product, potentially due to catalyst deactivation (entries 5–6). Nevertheless, the investigation of different directing groups demonstrates that the hydroxyl functionality serves as the best directing group to selectively access the *trans*-diastereomer by enabling a  $\pi$ -facial exchange

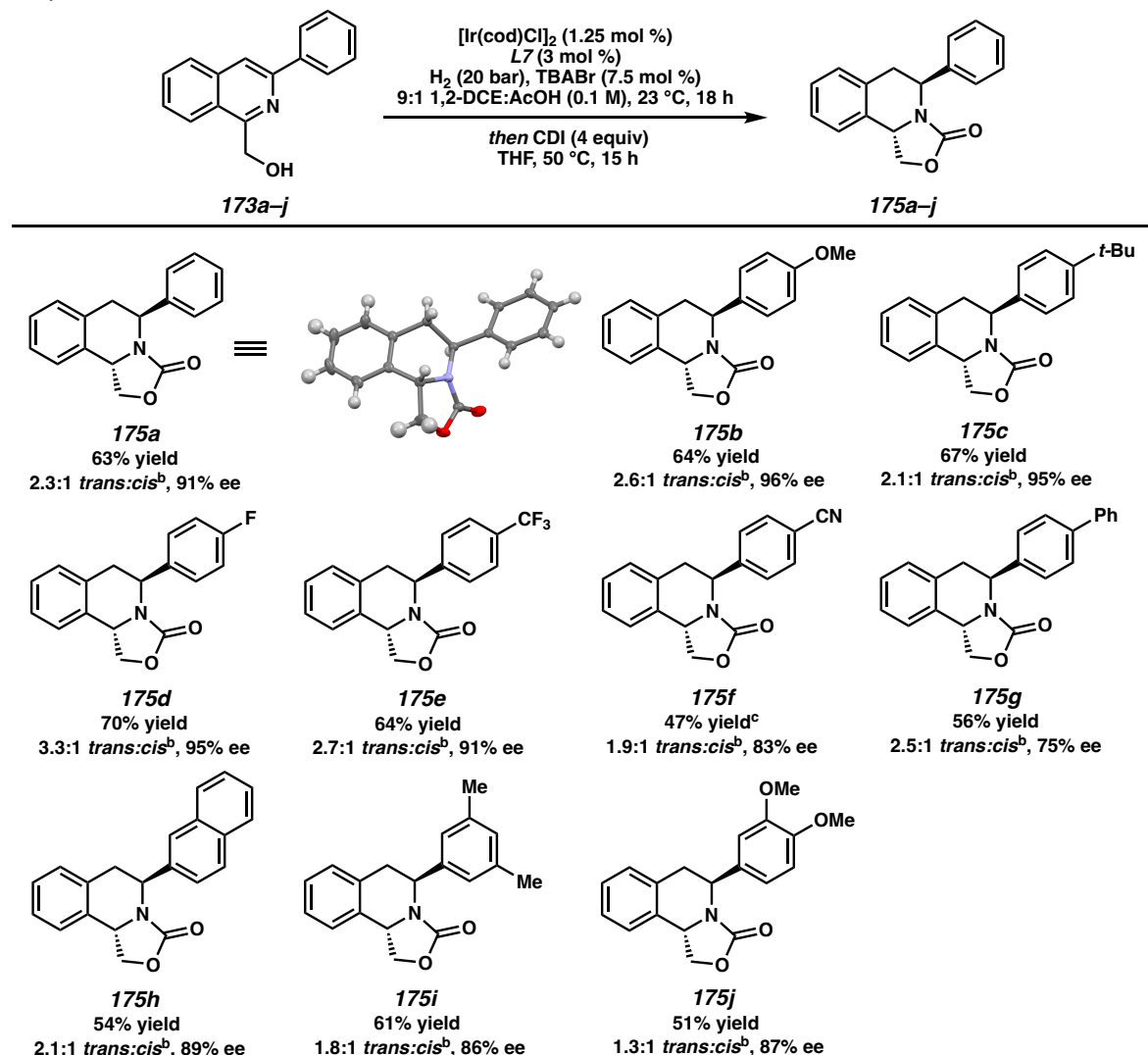
Chapter 3 – Iridium-Catalyzed Asymmetric *Trans*-Selective Hydrogenation of 1,3-Disubstituted Isoquinolines 390  
of the substrate and facilitating hydride delivery from the more sterically hindered face *via* a directed hydrogenation (entry 7).

### 3.3 SUBSTRATE SCOPE

With optimized reaction conditions identified, we explored the substrate scope for this transformation (Scheme 3.1). Due to the inseparable nature of the *cis*- and *trans*-diastereomers of the hydrogenated products, the crude reaction mixture was subsequently treated with 1,1-dicarbonyldiimidazole (CDI) to afford the oxazolidinone-fused THIQs that were then easily separable by column chromatography. From **175a**, the relative and absolute stereochemistry of the *trans*-THIQ product was confirmed by X-ray crystallography.<sup>14</sup>

Gratifyingly, a wide variety of aryl substituents at the 3-position of the isoquinoline were well tolerated, selectively yielding the *trans*-product in moderate to excellent ee.<sup>15</sup> Substitution at the *para*-position of the 3-aryl ring delivered hydrogenated products **175b–175g** in high selectivities, ranging from electron-rich substrates **175b–175c** to more electron-withdrawing substrates **175d–175f**. Sterically encumbered substrates such as 3-naphthyl, 3-xylyl isoquinolines also afforded products **175h–175i** in good isolated yields, with slightly diminished enantioselectivity. Furthermore, the nitrile functional group in **175f** and naphthyl substituent of **175h** were not reduced in this process, highlighting the chemoselectivity of this transformation.

**Scheme 3.1.** Substrate scope of the *trans*-selective hydrogenation of 1,3-disubstituted isoquinolines.<sup>a</sup>

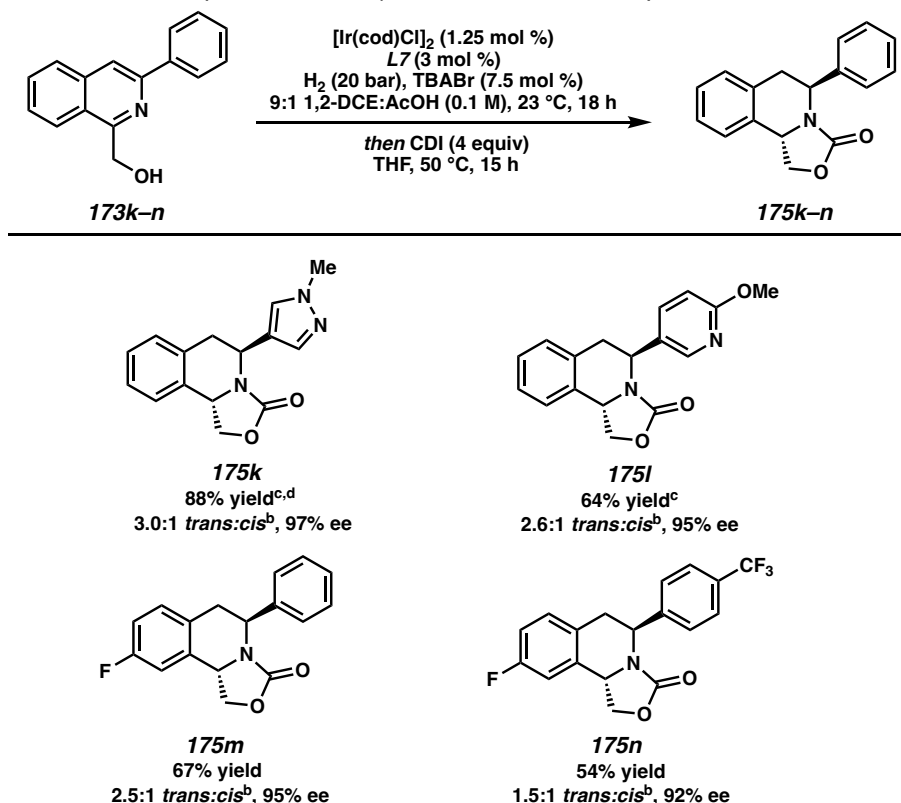


[a] Isolated yields of the *trans*-isomer on a 0.2 mmol scale. SFC analysis was used to determine ee. [b] Determined by <sup>1</sup>H NMR analysis of crude reaction.

Additionally, we were pleased to observe that heteroaryl-substituted isoquinolines were well tolerated at 60 °C and 60 bar H<sub>2</sub> to produce *trans*-THIQs **175k,l** in high enantioselectivities (97% and 94% ee, respectively), and with no erosion of diastereoselectivity (Scheme 3.2). Finally, different electronics of the isoquinoline

carbocycle such as fluorinated isoquinolines (**173m–173n**) were hydrogenated to afford electron-poor THIQs **175m–175n** in high selectivities under our standard conditions.

**Scheme 3.2.** Substrate scope of heteroaryl and fluorinated isoquinolines.<sup>a</sup>



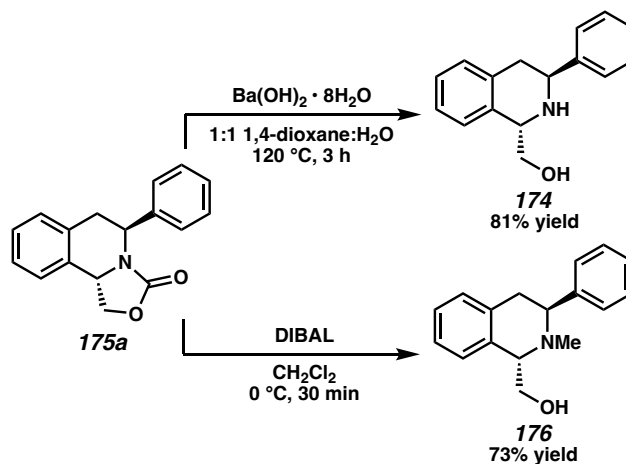
[a] Isolated yields of the *trans*-isomer on a 0.2 mmol scale. SFC analysis was used to determine ee. [b] Determined by <sup>1</sup>H NMR analysis of crude reaction. [c] Performed at 60 bar H<sub>2</sub> and 60 °C. [d] Total isolated yield of inseparable diastereomers.

### 3.4 SYNTHETIC UTILITY

Having demonstrated that this transformation is general for a wide range of 1,3-disubstituted isoquinolines, we sought to derivatize the oxazolidinone-fused THIQs (Scheme 3.3). We were pleased to find that the oxazolidinone functional group could be efficiently removed with Ba(OH)<sub>2</sub> · 8H<sub>2</sub>O to afford THIQ **174** in 81% yield.<sup>16,17</sup> Alternatively, reduction

with DIBAL afforded *N*-methyl THIQ **176** in 73% yield, providing a facile access of our hydrogenated products to *N*-methyl protected THIQs.

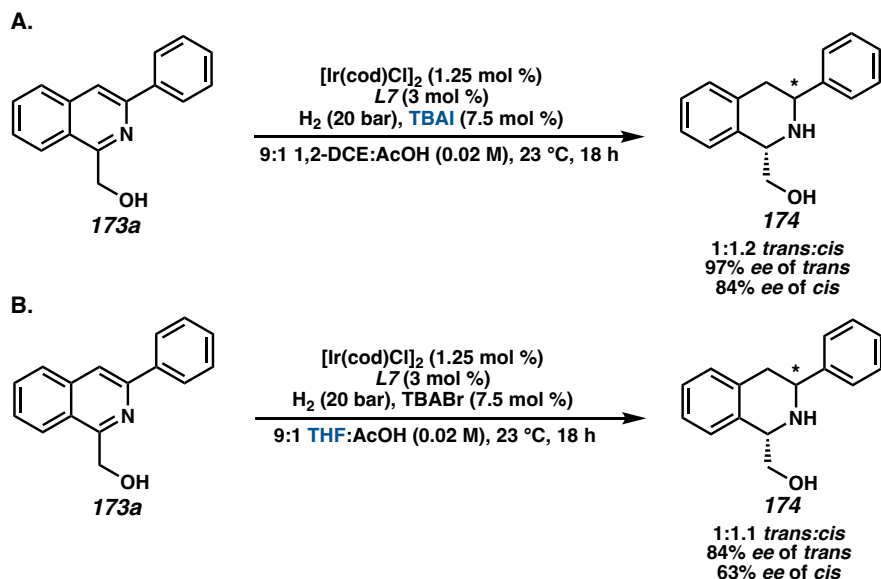
**Scheme 3.3.** Synthetic derivatizations of product **175a**.



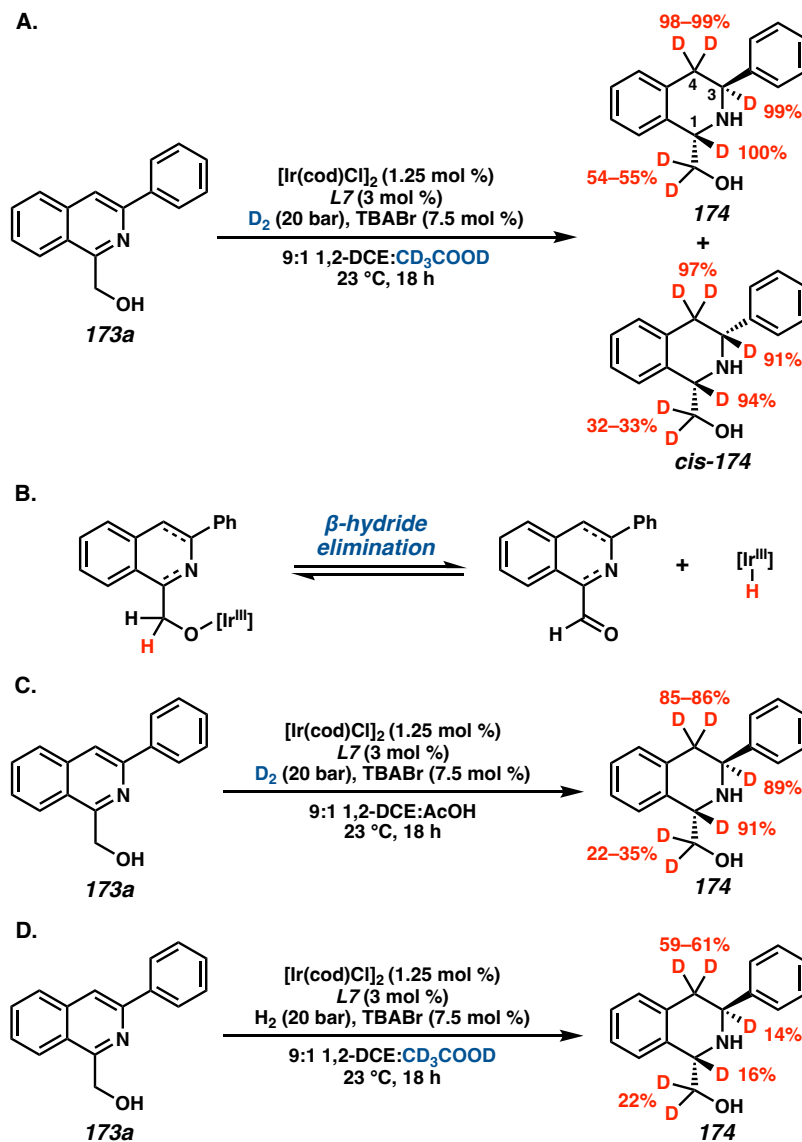
### 3.5 PRELIMINARY MECHANISTIC INSIGHTS

To elucidate the factors controlling the *trans*-selectivity in this transformation, several control experiments were conducted to probe the reaction mechanism (Scheme 3.4). Substituting TBABr for TBAI as the additive gave a 1:1.2 dr favoring the *cis*-product, with high enantioselectivities exhibited for both products. This suggests that the bromide ligand facilitates  $\pi$ -facial exchange of the substrate over iodide to afford higher levels of the *trans*-diastereomer.<sup>18, 19</sup> Replacing 1,2-DCE solvent for THF also delivered similar results, indicating that ethereal solvents inhibit the formation of *trans*-**174** through stronger coordination with iridium (Scheme 3.4B).<sup>20</sup> Overall, the combination of non-coordinating, chlorinated solvents and smaller halides are crucial in governing the observed *trans*-selectivity.

**Scheme 3.4.** Control experiments of the asymmetric *trans*-selective hydrogenation.



Deuterium experiments were also conducted to determine the degree of deuteration of our hydrogenated products (Scheme 3.5). Interestingly, the combination of both  $\text{D}_2$  and  $\text{CD}_3\text{COOD}$  delivered deuterium at the C1-, C3-, and C4-positions of the THIQ, as well as at the methylene carbon of the hydroxymethyl functional group (Scheme 3.5A). We attribute this exocyclic deuteration to a competitive  $\beta$ -hydride elimination pathway that is operative *in situ* under our *trans*-hydrogenation conditions (Scheme 3.5B).<sup>21,22</sup> However, this is likely not a critical pathway toward the *trans*-product, as deuterium incorporation in the corresponding *cis*-isomer (*cis*-174) is also observed. Exchanging either  $\text{D}_2$  or  $\text{CD}_3\text{COOD}$  for their protic counterparts demonstrated deuteride delivery primarily from the gas at the C1- and C3-positions of 174, yet the acid also enables reduction of the isoquinoline ring. This suggests a proton-hydride exchange occurring between the acid and the iridium hydride species for hydrogenation.<sup>19,23</sup> Further investigation of the mechanism and other applications of this technology will be reported in due course.<sup>24</sup>



### 3.6 CONCLUSIONS

In conclusion, we have developed an asymmetric *trans*-selective hydrogenation reaction of 1,3-disubstituted isoquinolines for the syntheses of enantioenriched *trans*-THIQs. Key to this enantio- and diastereoselective reaction is the hydroxymethyl directing group at the C1-position which enables  $\pi$ -facial exchange of the substrate and facilitates hydride



delivery from the sterically more hindered face. This method tolerates a wide range of electronics, Lewis basic functionalities, and substitution at the C1, C3, and C8-positions of the isoquinoline core, representing one of the first examples of an asymmetric hydrogenation technology to selectively access the *trans*-diastereomer of hydrogenated aromatic compounds.

### 3.7 EXPERIMENTAL SECTION

#### 3.7.1 MATERIALS AND METHODS

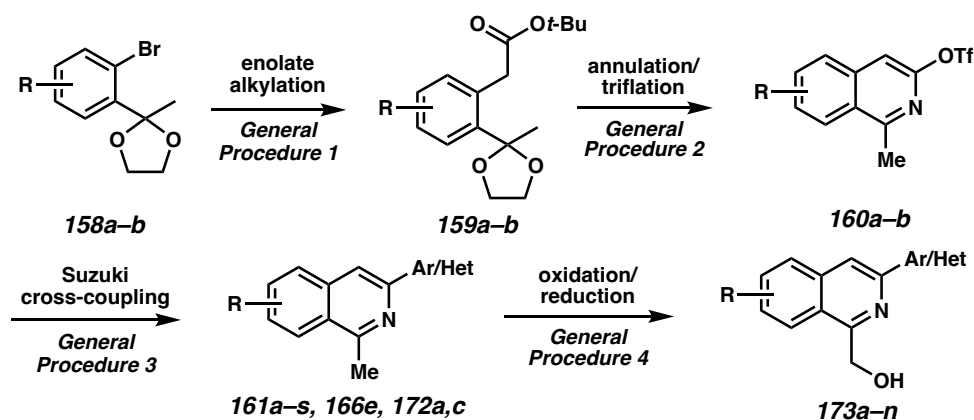
Unless otherwise stated, reactions were performed in flame-dried glassware under an argon or nitrogen atmosphere using dry, deoxygenated solvents. Solvents were dried by passage through an activated alumina column under argon.<sup>25</sup> Reaction progress was monitored by thin-layer chromatography (TLC) or Agilent 1290 UHPLC-MS. TLC was performed using E. Merck silica gel 60 F254 precoated glass plates (0.25 mm) and visualized by UV fluorescence quenching, *p*-anisaldehyde, oxr KMnO<sub>4</sub> staining. Silicycle SiliaFlash® P60 Academic Silica gel (particle size 40–63 μm) was used for flash chromatography. <sup>1</sup>H NMR spectra were recorded on Varian Inova 500 MHz and Oxford 600 MHz spectrometers and are reported relative to residual CHCl<sub>3</sub> (δ = 7.26 ppm) or TMS (δ = 0.00 ppm). <sup>13</sup>C NMR spectra were recorded on a Bruker 400 MHz spectrometer (100 MHz) and are reported relative to CHCl<sub>3</sub> (δ = 77.16 ppm), C<sub>6</sub>D<sub>6</sub> (δ = 128.06 ppm). Data for <sup>1</sup>H NMR are reported as follows: chemical shift (δ ppm) (multiplicity, coupling constant (Hz), integration). Multiplicities are reported as follows: s = singlet, d = doublet, t = triplet, q = quartet, p = pentet, sept = septuplet, m = multiplet, br s = broad singlet, br d = broad doublet. Data for <sup>13</sup>C NMR are reported in terms of chemical shifts (δ ppm). IR spectra were obtained by use

of a Perkin Elmer Spectrum BXII spectrometer or Nicolet 6700 FTIR spectrometer using thin films deposited on NaCl plates and reported in frequency of absorption ( $\text{cm}^{-1}$ ). Optical rotations were measured with a Jasco P-2000 polarimeter operating on the sodium D-line (589 nm), using a 100 mm path-length cell. High resolution mass spectra (HRMS) were obtained from Agilent 6200 Series TOF with an Agilent G1978A Multimode source in electrospray ionization (ESI+), atmospheric pressure chemical ionization (APCI+), or mixed ionization mode (MM: ESI-APCI+). Reagents were purchased from commercial sources and used as received unless otherwise stated.

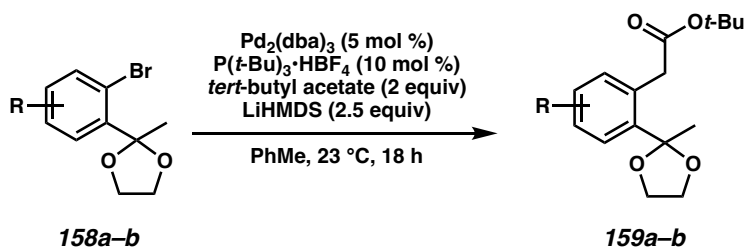
### 3.7.2 EXPERIMENTAL PROCEDURES AND SPECTROSCOPIC DATA

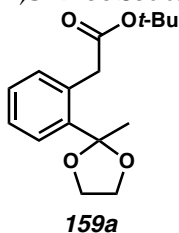
#### 3.7.2.1 Syntheses of hydroxymethyl 1,3-disubstituted isoquinolines

##### General Sequence:

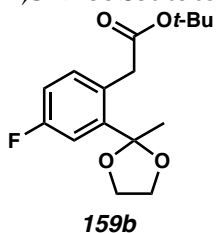


##### General Procedure 1: Enolate Alkylation of Aryl Bromide



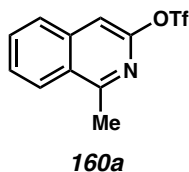
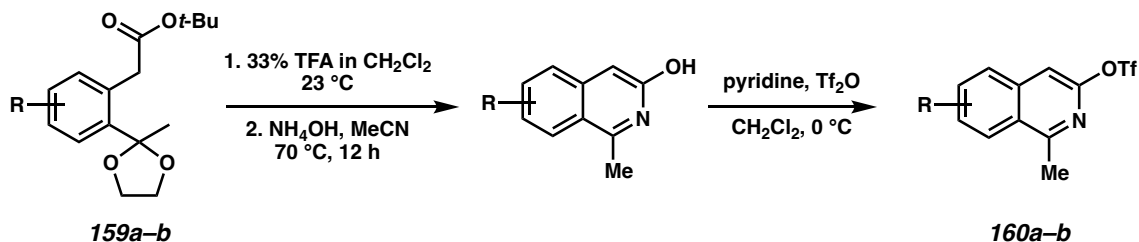


**tert-butyl 2-(2-(2-methyl-1,3-dioxolan-2-yl)phenyl)acetate (159a):** This procedure has been adapted from a previous report.<sup>9</sup> In a Schlenk flask was added  $P(t\text{-Bu})_3 \cdot \text{HBF}_4$  (119 mg, 0.41 mmol),  $\text{Pd}_2(\text{dba})_3$  (188 mg, 0.21 mmol), a solution of 2-(2-bromophenyl)-2-methyl-1,3-dioxolane (**158a**) (1.0 g, 4.1 mmol, 0.42 M), and *tert*-Butyl acetate (0.95 g, 8.2 mmol), respectively. The reaction mixture was cooled to  $-78^\circ\text{C}$  and sparged with nitrogen for 15 minutes. A degassed solution of LiHMDS (1.72 g, 10.25 mmol, 1 M in toluene) was then added via syringe. The reaction mixture was degassed for an additional 15 minutes at  $-78^\circ\text{C}$ , and allowed to slowly warm to room temperature. The reaction was stirred at room temperature for 18 hours, and then quenched with saturated aqueous  $\text{NaHCO}_3$ . The aqueous layer was extracted with  $\text{Et}_2\text{O}$  twice. The combined organic phases were dried over  $\text{MgSO}_4$ , filtered, and the solvent was removed in vacuo. The crude product was purified by silica gel flash chromatography (5% EtOAc in hexanes) to afford **159a** as a yellow oil (1.05 g, 92% yield):  $^1\text{H NMR}$  (400 MHz,  $\text{CDCl}_3$ )  $\delta$  7.53 – 7.45 (m, 1H), 7.20 – 7.06 (m, 3H), 3.96 – 3.83 (m, 2H), 3.71 (s, 2H), 3.68 – 3.55 (m, 2H), 1.60 (s, 3H), 1.39 (s, 9H); All characterization data match those reported.<sup>9</sup>



**tert-butyl 2-(4-fluoro-2-(2-methyl-1,3-dioxolan-2-yl)phenyl)acetate (159b):** Compound **159b** was prepared using general procedure 1 and purified by column chromatography (10% EtOAc in hexanes) to provide a colorless solid (1.9 g, 60% yield);  $^1\text{H}$  NMR (400 MHz,  $\text{CDCl}_3$ )  $\delta$  7.28 (dd,  $J = 10.3, 2.8$  Hz, 1H), 7.15 (dd,  $J = 8.4, 5.7$  Hz, 1H), 6.94 (td,  $J = 8.2, 2.9$  Hz, 1H), 4.06 – 3.90 (m, 2H), 3.74 (s, 2H), 3.72 – 3.69 (m, 2H), 1.65 (s, 3H), 1.45 (s, 9H); All characterization data match those reported.<sup>9</sup>

### General Procedure 2: Isoquinoline Annulation and Triflation

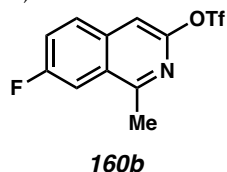


**1-methylisoquinolin-3-yl trifluoromethanesulfonate (160a):** To a RBF was added ester **159a** (2.78 g, 10.0 mmol), anhydrous  $\text{CH}_2\text{Cl}_2$  (75 mL, 0.13 M), and TFA (25 mL, 33% volume of  $\text{CH}_2\text{Cl}_2$ ), respectively. The reaction was stirred at room temperature for 2 hours, and then concentrated in vacuo. The crude was transferred to a Schlenk tube, dissolved in MeCN (10 mL, 1 M), and aqueous  $\text{NH}_4\text{OH}$  (28–30%, 20 mL, 200% volume of MeCN). The

tube was sealed with Kontes valve to prevent loss of gaseous ammonia and stirred at 70 °C.

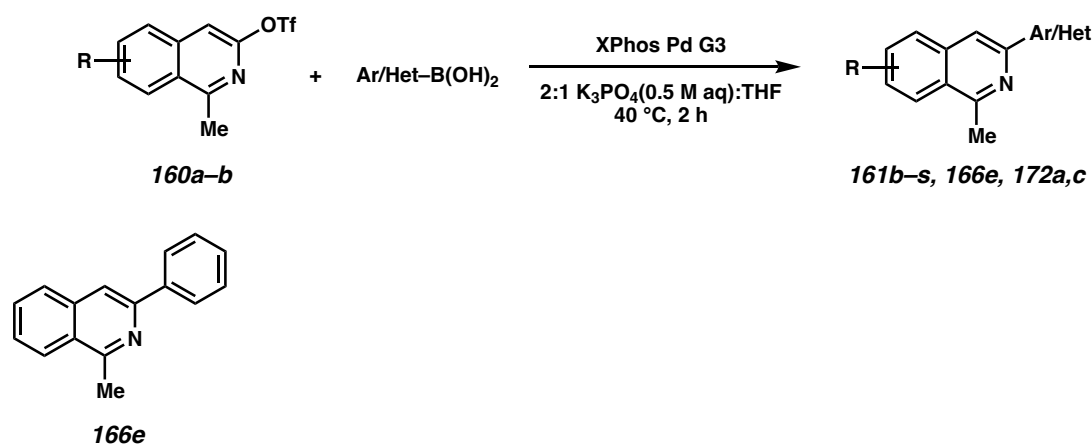
Within 1 hour, the yellow solid of the 3-hydroxyisoquinoline began to precipitate from the reaction solution. After stirring for 18 hours at 70 °C, the reaction was cooled to room temperature, then placed in a -20 °C freezer, and the yellow solid was collected via vacuum filtration. This yellow powder was then washed with cold MeCN and dried at high vacuum to provide 3-hydroxyisoquinoline intermediate (0.70 g, 4.39 mmol). If any starting material remains, the filtrate could be transferred to a flask and concentrated in vacuo to undergo a second condensation reaction.

To a separate flame-dried RBF containing CH<sub>2</sub>Cl<sub>2</sub> (22 mL, 0.2 M) and distilled pyridine (3.6 mL, 44 mmol), the collected yellow powder (0.70 g, 4.39 mmol) was added, and the resulting mixture was cooled to 0 °C. Trifluoromethanesulfonic anhydride (1.5 mL, 8.8 mmol) was then added dropwise at 0 °C, and the reaction was stirred at 0 °C for 1 hour. The reaction was then quenched with saturated aqueous NaHCO<sub>3</sub> at 0 °C, and then slowly warmed to room temperature. The reaction was extracted with CH<sub>2</sub>Cl<sub>2</sub>, dried over Na<sub>2</sub>SO<sub>4</sub>, and concentrated in vacuo. The crude product was purified by column chromatography (10% EtOAc in hexanes) to afford **160a** as a pale yellow oil (1.11 g, 38% yield over 3 steps): <sup>1</sup>H NMR (400 MHz, CDCl<sub>3</sub>) δ 8.17 (dd, *J* = 8.5, 1.0 Hz, 1H), 7.88 (dt, *J* = 8.3, 1.0 Hz, 1H), 7.76 (ddd, *J* = 8.2, 6.9, 1.2 Hz, 1H), 7.67 (ddd, *J* = 8.3, 6.9, 1.3 Hz, 1H), 7.42 (s, 1H), 2.97 (s, 3H); All characterization data match those reported.<sup>9</sup>



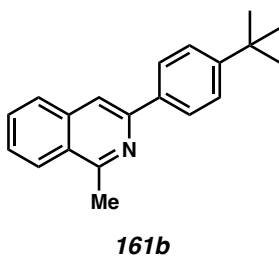
**7-fluoro-1-methylisoquinolin-3-yl trifluoromethanesulfonate (160b):** Compound **160b** was prepared from ester **159b** using general procedure 2 and purified by column chromatography (10% EtOAc in hexanes) to provide a pale brown oil (384 mg, 31% yield over 3 steps):  $^1\text{H NMR}$  (400 MHz,  $\text{CDCl}_3$ )  $\delta$  7.90 (dd,  $J = 9.0, 5.3$  Hz, 1H), 7.76 (dd,  $J = 9.6, 2.5$  Hz, 1H), 7.56 (ddd,  $J = 8.9, 8.0, 2.5$  Hz, 1H), 7.43 (s, 1H), 2.92 (s, 3H); All characterization data match those reported.<sup>9</sup>

### General Procedure 3: Suzuki Cross-Coupling

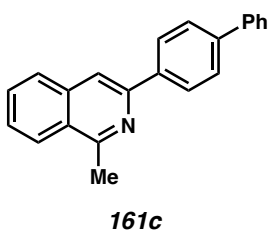


**1-methyl-3-phenylisoquinoline (166e):** To a flame-dried 20-mL scintillation vial capped with a PTFE-lined septum was added XPhos Pd G3 (11.63 mg, 0.014 mmol) and phenyl boronic acid (126 mg, 1.03 mmol). The reaction vial was then evacuated and backfilled with  $\text{N}_2$  three times. The isoquinoline triflate **160a** (200 mg, 0.687 mmol) in degassed THF (2 mL, 0.3 M) was then added to the vial, followed by degassed 0.5 M  $\text{K}_3\text{PO}_4$  solution (4 mL, 0.2 M). The reaction was then stirred at 40 °C for 2 hours. Afterwards, the reaction was diluted with water and the aqueous layer was extracted with  $\text{Et}_2\text{O}$ . The combined organic

phases were dried over Na<sub>2</sub>SO<sub>4</sub>, concentrated in vacuo, and purified by column chromatography (5% EtOAc in hexanes) to afford **166e** as a white solid (138 mg, 92% yield): <sup>1</sup>H NMR (400 MHz, CDCl<sub>3</sub>) δ 8.15 – 8.13 (m, 3H), 7.93 (s, 1H), 7.86 (dt, *J* = 8.3, 1.0 Hz, 1H), 7.67 (ddd, *J* = 8.2, 6.9, 1.2 Hz, 1H), 7.57 (ddd, *J* = 8.2, 6.8, 1.3 Hz, 1H), 7.52 – 7.48 (m, 2H), 7.42 – 7.38 (m, 1H), 3.05 (s, 3H); All characterization data match those reported.<sup>9</sup>

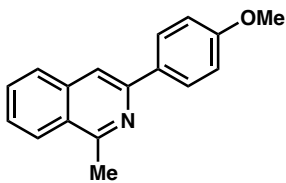


**3-(4-(*tert*-butyl)phenyl)-1-methylisoquinoline (161b):** Compound **161b** was prepared from triflate **160a** using general procedure 3 and purified by column chromatography (5% EtOAc in hexanes) to provide a pale yellow oil (177 mg, 93% yield); <sup>1</sup>H NMR (400 MHz, CDCl<sub>3</sub>) δ 8.12 (d, *J* = 8.4 Hz, 1H) 8.06 (d, *J* = 8.5 Hz, 2H), 7.90 (s, 1H), 7.85 (d, *J* = 8.2 Hz, 1H), 7.66 (ddd, *J* = 8.1, 6.8, 1.2 Hz, 1H), 7.57 – 7.52 (m, 3H), 3.04 (s, 3H), 1.38 (s, 9H); All characterization data match those reported.<sup>9</sup>



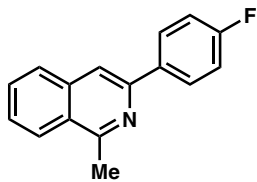
**3-([1,1'-biphenyl]-4-yl)-1-methylisoquinoline (161c):** Compound **161c** was prepared from triflate **160a** using general procedure 3 and purified by column chromatography (5% EtOAc in hexanes) to provide a colorless solid (191 mg, 94% yield); <sup>1</sup>H NMR (400 MHz, CDCl<sub>3</sub>) δ 8.24 – 8.22 (m, 2H), 8.14 (d, *J* = 8.4 Hz, 1H), 7.98 (s, 1H), 7.88 (d, *J* = 8.1 Hz, 1H), 7.75 –

7.73 (m, 2H), 7.70 – 7.67 (m, 3H), 7.58 (ddd,  $J = 8.3, 6.9, 1.3$  Hz, 1H), 7.50 – 7.46 (m, 2H), 7.39 – 7.37 (m, 1H), 3.06 (s, 3H); All characterization data match those reported.<sup>9</sup>



**161d**

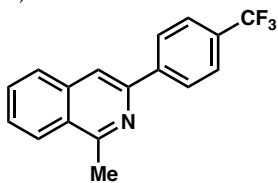
**3-(4-methoxyphenyl)-1-methylisoquinoline (161d):** Compound **161d** was prepared from triflate **160a** using general procedure 3 and purified by column chromatography (5% EtOAc in hexanes) to afford a white solid (79 mg, 93% yield): <sup>1</sup>H NMR (400 MHz, CDCl<sub>3</sub>) <sup>1</sup>H NMR (400 MHz, CDCl<sub>3</sub>)  $\delta$  8.14 – 8.07 (m, 3H), 7.84 (s, 1H), 7.81 (d,  $J = 8.5$ , 1H), 7.64 (ddd,  $J = 8.2, 6.8, 1.2$  Hz, 1H), 7.53 (ddd,  $J = 8.2, 6.8, 1.3$  Hz, 1H), 7.06 – 7.01 (m, 2H), 3.88 (s, 3H), 3.03 (s, 3H); All characterization data match those reported.<sup>9</sup>



**161e**

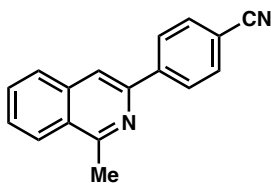
**3-(4-fluorophenyl)-1-methylisoquinoline (161e):** Compound **161e** was prepared from triflate **160a** using general procedure 3 and purified by column chromatography (10% EtOAc in hexanes) to provide a white solid (155 mg, 95% yield); <sup>1</sup>H NMR (400 MHz, CDCl<sub>3</sub>)  $\delta$  8.17 – 8.07 (m, 3H), 7.89 – 7.81 (m, 2H), 7.68 (ddd,  $J = 8.2, 6.9, 1.2$  Hz, 1H), 7.58 (ddd,  $J = 8.2, 6.8, 1.3$  Hz, 1H), 7.20 – 7.16 (m, 2H), 3.04 (s, 3H); All characterization data match those reported.<sup>9</sup>





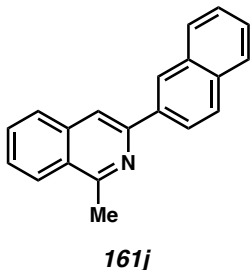
**161f**

**1-methyl-3-(4-(trifluoromethyl)phenyl)isoquinoline (161f):** Compound **161f** was prepared from triflate **160a** using general procedure 3 and purified by column chromatography (2% to 3% EtOAc in hexanes) to afford a white solid (89 mg, 91% yield):  $^1\text{H}$  NMR (400 MHz,  $\text{CDCl}_3$ )  $\delta$  8.26 (d,  $J = 8.1$  Hz, 2H), 8.15 (d,  $J = 8.4$ , 1H), 7.96 (s, 1H), 7.88 (d,  $J = 8.2$  Hz, 1H), 7.78 – 7.73 (m, 2H), 7.73 – 7.67 (m, 1H), 7.63 – 7.59 (m, 1H), 3.05 (s, 3H); All characterization data match those reported.<sup>9</sup>

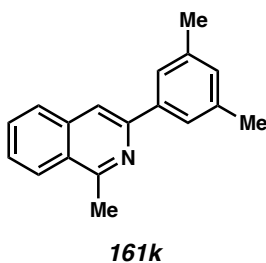


**161g**

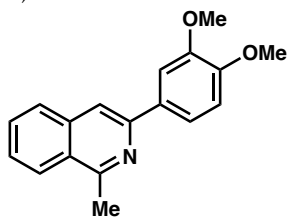
**4-(1-methylisoquinolin-3-yl)benzonitrile (161g):** Compound **161g** was prepared from triflate **160a** using general procedure 3 and purified by column chromatography (10% to 20% EtOAc in hexanes) to provide a white solid (144 mg, 86% yield);  $^1\text{H}$  NMR (400 MHz,  $\text{CDCl}_3$ )  $\delta$  8.38 – 8.22 (m, 2H), 8.16 (d,  $J = 8.3$  Hz, 1H), 7.99 (s, 1H), 7.89 (d,  $J = 8.3$ , 1H), 7.82 – 7.75 (m, 2H), 7.73 (ddd,  $J = 8.1, 6.9, 1.2$  Hz, 1H), 7.64 (ddd,  $J = 8.2, 6.9, 1.3$  Hz, 1H), 3.05 (s, 3H); All characterization data match those reported.<sup>9</sup>



**1-methyl-3-(naphthalen-2-yl)isoquinoline (161j):** Compound **161j** was prepared from triflate **160a** using general procedure 3 and purified by column chromatography (5% EtOAc in hexanes) to provide a white solid (159 mg, 86% yield);  $^1\text{H}$  NMR (400 MHz,  $\text{CDCl}_3$ )  $\delta$  8.68 (s, 1H), 8.27 (dd,  $J = 8.6, 1.8$  Hz, 1H), 8.16 (dq,  $J = 8.3, 1.0$  Hz, 1H), 8.07 (s, 1H), 8.00 – 7.96 (m, 2H), 7.91 – 7.86 (m, 2H), 7.70 (ddd,  $J = 8.2, 6.8, 1.2$  Hz, 1H), 7.59 (ddd,  $J = 8.2, 6.8, 1.3$  Hz, 1H), 7.56 – 7.46 (m, 2H), 3.09 (s, 3H); All characterization data match those reported.<sup>9</sup>

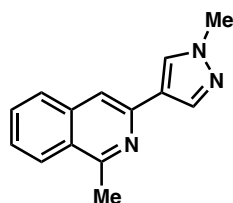


**3-(3,5-dimethylphenyl)-1-methylisoquinoline (161k):** Compound **161k** was prepared from triflate **160a** using general procedure 3 and purified by column chromatography to provide a white solid (156 mg, 92% yield);  $^1\text{H}$  NMR (400 MHz,  $\text{CDCl}_3$ )  $\delta$  8.13 (dd,  $J = 8.4, 1.1$  Hz, 1H), 7.90 (s, 1H), 7.85 (dd,  $J = 8.2, 0.7$  Hz, 1H), 7.75 (s, 2H), 7.66 (ddd,  $J = 8.2, 6.8, 1.2$  Hz, 1H), 7.56 (ddd,  $J = 8.2, 6.9, 1.3$  Hz, 1H), 7.05 (s, 1H), 3.05 (s, 3H), 2.43 (s, 6H); All characterization data match those reported.<sup>9</sup>



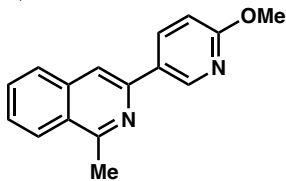
**161l**

**3-(3,4-dimethoxyphenyl)-1-methylisoquinoline (161l):** Compound **161l** was prepared from triflate **160a** using general procedure 3 and purified by column chromatography (20% EtOAc in hexanes) to provide a white solid (195 mg, 99% yield);  $^1\text{H}$  NMR (400 MHz,  $\text{CDCl}_3$ )  $\delta$  8.11 (d,  $J = 8.4$ , 1H), 7.89 – 7.81 (m, 2H), 7.77 (d,  $J = 2.1$  Hz, 1H), 7.71 – 7.61 (m, 2H), 7.55 (ddd,  $J = 8.3$ , 6.9, 1.3 Hz, 1H), 6.99 (d,  $J = 8.4$  Hz, 1H), 4.04 (s, 3H), 3.95 (s, 3H), 3.04 (s, 3H); All characterization data match those reported.<sup>9</sup>



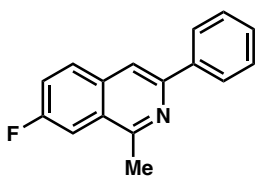
**161q**

**1-methyl-3-(1-methyl-1H-pyrazol-4-yl)isoquinoline (161q):** Compound **161q** was prepared from triflate **160a** using general procedure 3 and purified by column chromatography (50% to 60% EtOAc in hexanes) to provide a white solid (112 mg, 99% yield);  $^1\text{H}$  NMR (400 MHz,  $\text{CDCl}_3$ )  $\delta$  8.07 (d,  $J = 8.4$  Hz, 1H), 8.04 – 8.00 (m, 2H), 7.77 (dd,  $J = 8.2$ , 1.1 Hz, 1H), 7.67 – 7.60 (m, 2H), 7.54 – 7.47 (m, 1H), 3.98 (s, 3H), 2.97 (s, 3H); All characterization data match those reported.<sup>9</sup>



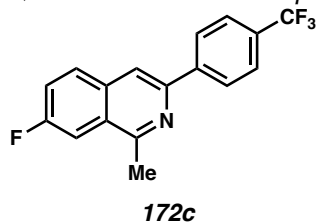
**161s**

**3-(6-methoxypyridin-3-yl)-1-methylisoquinoline (161s):** Compound **161s** was prepared from triflate **160a** using general procedure 3 and purified by column chromatography (15% EtOAc in hexanes) to afford a white solid (232 mg, 90% yield):  $^1\text{H}$  NMR (400 MHz,  $\text{CDCl}_3$ )  $\delta$  8.89 (dd,  $J = 2.5, 0.8$  Hz, 1H), 8.36 (dd,  $J = 8.6, 2.5$  Hz, 1H), 8.11 (dd,  $J = 8.4, 1.0$  Hz, 1H), 7.85 – 7.83 (m, 2H), 7.67 (ddd,  $J = 8.2, 6.9, 1.2$  Hz, 1H), 7.56 (ddd,  $J = 8.1, 6.9, 1.3$  Hz, 1H), 6.87 (dd,  $J = 8.6, 0.8$  Hz, 1H), 4.01 (s, 3H), 3.02 (s, 3H);  $^{13}\text{C}$  NMR (100 MHz,  $\text{CDCl}_3$ )  $\delta$  164.4, 159.0, 147.7, 145.7, 137.6, 136.8, 130.3, 129.2, 127.6, 126.9, 126.6, 125.8, 114.5, 110.8, 53.8, 22.8; IR (Neat Film, NaCl) 2937, 2363, 1604, 1568, 1498, 1443, 1326, 1278, 1254, 1119, 1021, 831, 745; HRMS (MM:ESI-APCI+)  $m/z$  calc'd for  $\text{C}_{16}\text{H}_{15}\text{N}_2\text{O}$   $[\text{M}+\text{H}]^+$ : 251.1184, found 251.1185.



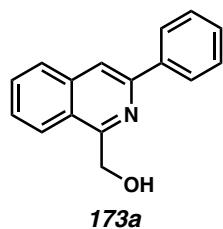
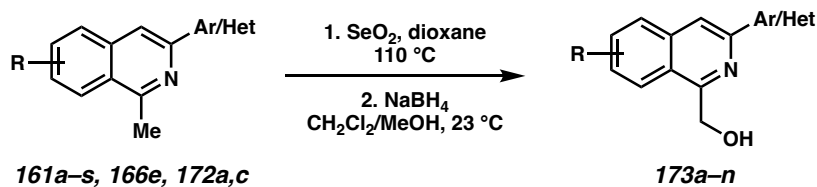
**172a**

**7-fluoro-1-methyl-3-phenylisoquinoline (172a):** Compound **172a** was prepared from triflate **160b** using general procedure 3 and purified by column chromatography (5% EtOAc in hexanes) to provide a white solid (110 mg, 93% yield):  $^1\text{H}$  NMR (400 MHz,  $\text{CDCl}_3$ )  $\delta$  8.14 – 8.11 (m, 2H), 7.90 (s, 1H), 7.85 (dd,  $J = 9.2, 5.7$  Hz, 1H), 7.73 – 7.68 (m, 1H), 7.54 – 7.48 (m, 2H), 7.48 – 7.38 (m, 2H), 2.99 (s, 3H); All characterization data match those reported.<sup>9</sup>



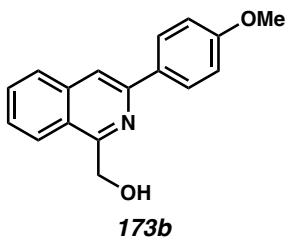
**7-fluoro-1-methyl-3-(4-(trifluoromethyl)phenyl)isoquinoline (172c):** Compound **172c** was prepared from triflate **160b** using general procedure 3 and purified by column chromatography (5% EtOAc in hexanes) to provide a white solid (150 mg, 98% yield):  $^1\text{H}$  NMR (400 MHz,  $\text{CDCl}_3$ )  $\delta$  8.22 (d,  $J = 8.0$  Hz, 2H), 7.94 (s, 1H), 7.90 – 7.85 (m, 1H), 7.74 (d,  $J = 8.0$  Hz, 2H), 7.71 – 7.69 (m, 1H), 7.53 – 7.43 (m, 1H), 2.99 (s, 3H); All characterization data match those reported.<sup>9</sup>

#### General Procedure 4: Oxidation and Reduction to Hydroxymethyl Isoquinoline

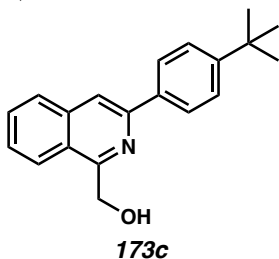


**(3-phenylisoquinolin-1-yl)methanol (173a):** To a 20-mL microwave vial containing a stir bar was added  $\text{SeO}_2$  (140 mg, 1.26 mmol), isoquinoline **166e** (138 mg, 0.63 mmol), and 1,4-dioxane (13 mL, 0.05 M). The reaction vial was then sealed and heated to 110 °C while stirring for 2 hours. The reaction was then cooled to room temperature, filtered through celite, and rinsed with EtOAc. The filtrate was then concentrated in vacuo to afford the aldehyde intermediate, which was used in the next step without further purification.

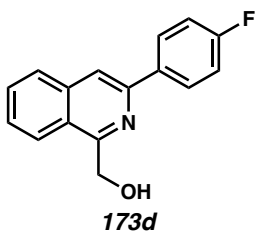
A scintillation vial containing the crude in 4:1 DCM:MeOH (0.1 M) was added sodium borohydride (24 mg, 0.63 mmol) at room temperature. The reaction was stirred until no starting material remained by TLC, and then quenched by the addition of citric acid monohydrate (132 mg, 0.63 mmol). The reaction was stirred for an additional 10 minutes then basified by the addition of saturated aqueous NaHCO<sub>3</sub>. The layers were separated and the aqueous phase was extracted with CH<sub>2</sub>Cl<sub>2</sub>. The combined organic phases were dried over Na<sub>2</sub>SO<sub>4</sub> and concentrated in vacuo. The crude product was purified by column chromatography (20% acetone in hexanes) to afford **173a** as a white solid (100 mg, 68% yield over 2 steps): <sup>1</sup>H NMR (400 MHz, CDCl<sub>3</sub>) δ 8.18 – 8.15 (d, *J* = 7.0 Hz, 2H), 8.03 (s, 1H), 7.94 – 7.92 (m, 2H), 7.73 (ddd, *J* = 8.3, 6.9, 1.1 Hz, 1H), 7.61 (ddd, *J* = 8.1, 6.9, 1.2 Hz, 1H), 7.53 (t, *J* = 7.6 Hz, 2H), 7.46 – 7.42 (m, 1H), 5.31 (s, 2H), 5.26 (br s, 1H, OH); All characterization data match those reported.<sup>9</sup>



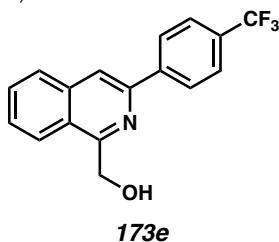
**(3-(4-methoxyphenyl)isoquinolin-1-yl)methanol (173b):** Compound **162d** was prepared using general procedure 4 and purified by column chromatography (20% EtOAc in hexanes) to provide a white solid (48 mg, 73% yield): <sup>1</sup>H NMR (400 MHz, CDCl<sub>3</sub>) δ 8.14 – 8.07 (m, 2H), 7.93 (s, 1H), 7.91 – 7.85 (m, 2H), 7.69 (ddd, *J* = 8.2, 6.9, 1.1 Hz, 1H), 7.56 (ddd, *J* = 8.2, 6.9, 1.2 Hz, 1H), 7.06 – 7.03 (m, 2H), 5.28 (s, 3H), 3.89 (s, 3H); All characterization data match those reported.<sup>9</sup>



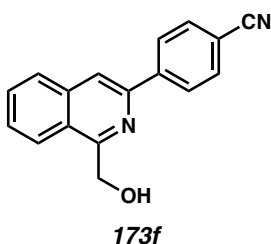
**((3-(4-(*tert*-butyl)phenyl)isoquinolin-1-yl)methanol (173c):** Compound **173c** was prepared using general procedure 4 and purified by column chromatography (20% EtOAc in hexanes) to provide a white solid (162 mg, 95% yield);  $^1\text{H}$  NMR (400 MHz,  $\text{CDCl}_3$ )  $\delta$  8.20 – 8.06 (m, 2H), 8.00 (s, 1H), 7.97 – 7.85 (m, 2H), 7.72 (ddd,  $J = 8.4, 6.9, 1.2$  Hz, 1H), 7.62 – 7.58 (m, 1H), 7.58 – 7.52 (m, 2H), 5.30 (s, 3H), 1.40 (s, 9H); All characterization data match those reported.<sup>9</sup>



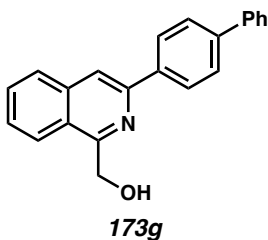
**(3-(4-fluorophenyl)isoquinolin-1-yl)methanol (173d):** Compound **173d** was prepared using general procedure 4 and purified by column chromatography (20% EtOAc in hexanes) to provide a colorless solid (149 mg, 95% yield);  $^1\text{H}$  NMR (400 MHz,  $\text{CDCl}_3$ )  $\delta$  8.13 (dd,  $J = 8.9, 5.4$  Hz, 2H), 7.96 (s, 1H), 7.95 – 7.89 (m, 2H), 7.73 (ddd,  $J = 8.3, 6.9, 1.1$  Hz, 1H), 7.61 (ddd,  $J = 8.1, 6.9, 1.2$  Hz, 1H), 7.21 (dd,  $J = 8.9, 8.5$  Hz, 2H), 5.30 (s, 2H), 5.17 (br s, 1H, OH); All characterization data match those reported.<sup>9</sup>



**(3-(4-(trifluoromethyl)phenyl)isoquinolin-1-yl)methanol (173e):** Compound **173e** was prepared using general procedure 4 and purified by column chromatography (10% to 20% EtOAc in hexanes) to provide a white solid (23 mg, 25% yield);  $^1\text{H}$  NMR (400 MHz,  $\text{CDCl}_3$ )  $\delta$  8.26 (d,  $J = 7.8$  Hz, 2H), 8.07 (s, 1H), 8.00 – 7.92 (m, 2H), 7.82 – 7.73 (m, 3H), 7.70 – 7.61 (m, 1H), 5.32 (s, 2H), 5.10 (br s, 1H, OH); All characterization data match those reported.<sup>9</sup>



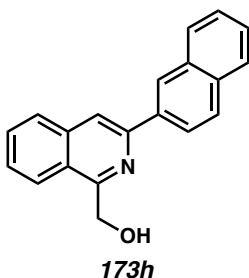
**4-(1-(hydroxymethyl)isoquinolin-3-yl)benzonitrile (173f):** Compound **173f** was prepared using general procedure 4 and purified by column chromatography (30% EtOAc in hexanes) to provide a white solid (138 mg, 92% yield);  $^1\text{H}$  NMR (400 MHz,  $\text{CDCl}_3$ )  $\delta$  8.31 – 8.18 (m, 2H), 8.09 (s, 1H), 7.97 (m, 2H), 7.86 – 7.74 (m, 3H), 7.68 (ddd,  $J = 8.2, 6.9, 1.2$  Hz, 1H), 5.32 (s, 2H), 4.99 (s, 1H); All characterization data match those reported.<sup>9</sup>



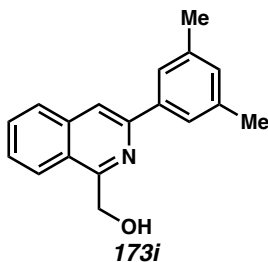
**(3-([1,1'-biphenyl]-4-yl)isoquinolin-1-yl)methanol (173g):** Compound **173g** was prepared using general procedure 4 and purified by column chromatography (20% EtOAc in hexanes)



to provide a colorless solid (181 mg, 92% yield);  $^1\text{H NMR}$  (400 MHz,  $\text{CDCl}_3$ )  $\delta$  8.30 – 8.20 (m, 2H), 8.07 (s, 1H), 7.98 – 7.88 (m, 2H), 7.81 – 7.66 (m, 5H), 7.62 (ddd,  $J = 8.4, 6.9, 1.2$  Hz, 1H), 7.49 (dd,  $J = 8.2, 6.8$  Hz, 2H), 7.43 – 7.34 (m, 1H), 5.32 (s, 3H); All characterization data match those reported.<sup>9</sup>

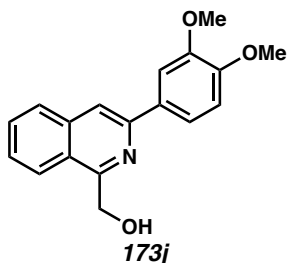


**(3-(naphthalen-2-yl)isoquinolin-1-yl)methanol (173h):** Compound **173h** was prepared using general procedure 4 and purified by column chromatography (20% EtOAc in hexanes) to provide a white solid (158 mg, 97% yield);  $^1\text{H NMR}$  (400 MHz,  $\text{CDCl}_3$ )  $\delta$  8.67 (s, 1H), 8.27 (dd,  $J = 8.6, 1.8$  Hz, 1H), 8.16 (s, 1H), 8.05 – 7.93 (m, 4H), 7.91 – 7.89 (m, 1H), 7.75 (ddd,  $J = 8.2, 6.9, 1.1$  Hz, 1H), 7.62 (ddd,  $J = 8.2, 6.9, 1.2$  Hz, 1H), 7.58 – 7.47 (m, 2H), 5.34 (s, 3H); All characterization data match those reported.<sup>9</sup>

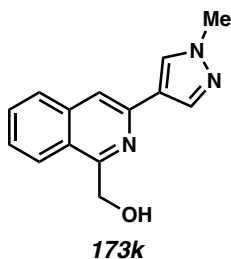


**(3-(3,5-dimethylphenyl)isoquinolin-1-yl)methanol (173i):** Compound **173i** was prepared using general procedure 4 and purified by column chromatography (20% EtOAc in hexanes) to provide a white solid (155 mg, 95% yield);  $^1\text{H NMR}$  (400 MHz,  $\text{CDCl}_3$ )  $\delta$  8.00 (s, 1H), 7.94 – 7.91 (m, 2H), 7.78 – 7.76 (m, 2H), 7.72 (ddd,  $J = 8.3, 6.9, 1.2$  Hz, 1H), 7.60 (ddd,  $J =$

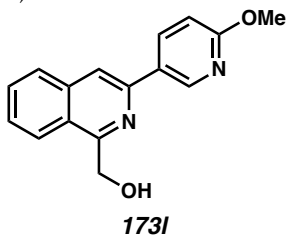
8.2, 6.9, 1.2 Hz, 1H), 7.09 (s, 1H), 5.30 (s, 3H), 2.44 (s, 6H); All characterization data match those reported.<sup>9</sup>



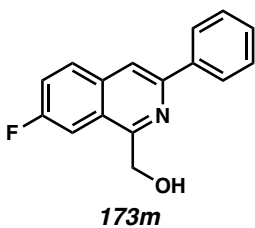
**(3-(3,4-dimethoxyphenyl)isoquinolin-1-yl)methanol (173j):** Compound **173j** was prepared using general procedure 4 and purified by column chromatography (40% EtOAc in hexanes) to provide a white solid (180 mg, 91% yield); <sup>1</sup>H NMR (400 MHz, CDCl<sub>3</sub>) δ 7.95 (s, 1H), 7.93 – 7.90 (m, 2H), 7.77 – 7.67 (m, 3H), 7.58 (ddd, *J* = 8.2, 6.9, 1.2 Hz, 1H), 7.03 – 7.01 (m, 1H), 5.30 (s, 2H), 5.26 (br s, 1H, OH), 4.03 (s, 3H), 3.97 (s, 3H); All characterization data match those reported.<sup>9</sup>



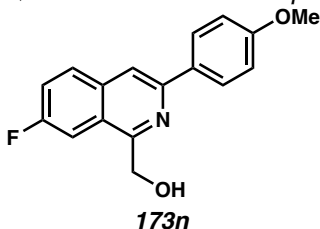
**(3-(1-methyl-1H-pyrazol-4-yl)isoquinolin-1-yl)methanol (173k):** Compound **173k** was prepared using general procedure 4 and purified by column chromatography (70% to 80% EtOAc in hexanes + 1% NEt<sub>3</sub>) to provide a pale beige solid (72 mg, 62% yield); <sup>1</sup>H NMR (400 MHz, CDCl<sub>3</sub>) δ 8.08 – 7.95 (m, 2H), 7.85 – 7.79 (m, 2H), 7.71 – 7.59 (m, 2H), 7.53 – 7.49 (m, 1H), 5.21 (s, 2H), 3.98 (s, 3H); All characterization data match those reported.<sup>9</sup>



**(3-(pyridin-2-yl)isoquinolin-1-yl)methanol (173l):** Compound **173l** was prepared from isoquinoline **161s** using general procedure 4 and purified by column chromatography (20% to 30% EtOAc in hexanes) to provide a white solid (177 mg, 72% yield);  $^1\text{H}$  NMR (400 MHz,  $\text{CDCl}_3$ )  $\delta$  8.94 (dd,  $J = 2.6, 0.7$  Hz, 1H), 8.34 (dd,  $J = 8.7, 2.5$  Hz, 1H), 7.94 – 7.91 (m, 3H), 7.73 (ddd,  $J = 8.2, 6.9, 1.1$  Hz, 1H), 7.61 (ddd,  $J = 8.2, 6.9, 1.2$  Hz, 1H), 6.89 (dd,  $J = 8.7, 0.7$  Hz, 1H), 5.30 (s, 2H), 5.10 (br s, 1H, OH), 4.03 (s, 3H);  $^{13}\text{C}$  NMR (100 MHz,  $\text{CDCl}_3$ )  $\delta$  164.6, 157.7, 146.4, 145.7, 137.2, 137.0, 131.1, 128.2, 127.8, 127.6, 124.1, 123.3, 115.4, 111.1, 61.6, 53.9; IR (Neat Film, NaCl) 3380, 3058, 2948, 2363, 1624, 1606, 1573, 1504, 1447, 1380, 1326, 1286, 1088, 1024, 832, 747  $\text{cm}^{-1}$ ; HRMS (MM:ESI-APCI+)  $m/z$  calc'd for  $\text{C}_{16}\text{H}_{15}\text{N}_2\text{O}_2$   $[\text{M}+\text{H}]^+$ : 267.1128, found 267.1131.

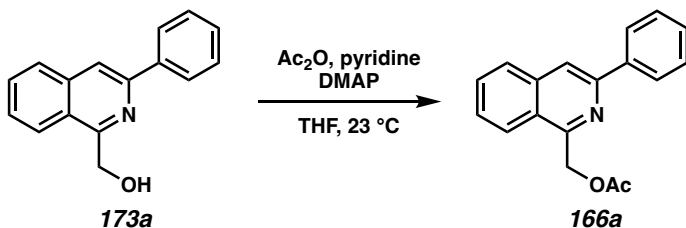


**(7-fluoro-3-phenylisoquinolin-1-yl)methanol (173m):** Compound **173m** was prepared using general procedure 4 and purified by column chromatography (10% EtOAc in hexanes) to provide a white solid (94 mg, 81% yield);  $^1\text{H}$  NMR (400 MHz,  $\text{CDCl}_3$ )  $\delta$  8.13 (d,  $J = 8.0$  Hz, 2H), 8.00 (s, 1H), 7.96 – 7.87 (m, 1H), 7.57 – 7.47 (m, 4H), 7.44 (td,  $J = 6.9, 6.4, 1.4$  Hz, 1H), 5.21 (s, 2H), 5.11 (br s, 1H, OH); All characterization data match those reported.<sup>9</sup>



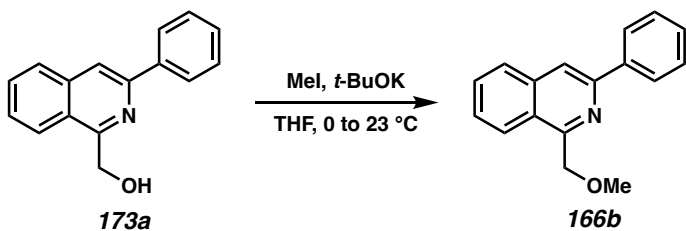
**(7-fluoro-3-(4-(trifluoromethyl)phenyl)isoquinolin-1-yl)methanol (173n):** Compound **173n** was prepared using general procedure 4 and purified by column chromatography (10% EtOAc in hexanes) to provide a white solid (80 mg, 60% yield):  $^1\text{H NMR}$  (400 MHz,  $\text{CDCl}_3$ )  $\delta$  8.20 (d,  $J = 8.1$  Hz, 2H), 8.02 (s, 1H), 7.95 (dd,  $J = 9.8, 5.4$  Hz, 1H), 7.74 (d,  $J = 8.3$  Hz, 2H), 7.58 – 7.47 (m, 2H), 5.21 (s, 2H), 4.94 (br s, 1H, OH); All characterization data match those reported.<sup>9</sup>

### 3.7.2.2 Syntheses of isoquinolines with different directing groups

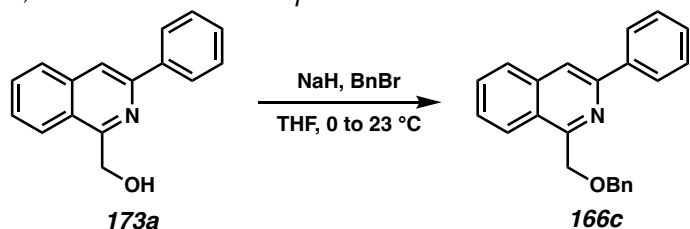


**(3-phenylisoquinolin-1-yl)methyl acetate (166a):** To a scintillation vial containing a stir bar and isoquinoline **173a** (165 mg, 0.70 mmol) in THF (7 mL, 0.1 M) was added DMAP (8.6 mg, 0.07 mmol) and pyridine (0.14 mL, 1.75 mmol). Acetic anhydride (0.1 mL, 1.05 mmol) was then added dropwise. The reaction was stirred overnight at room temperature then diluted with  $\text{Et}_2\text{O}$  and washed with saturated aqueous  $\text{NH}_4\text{Cl}$ . The organic phase was collected, dried over  $\text{Na}_2\text{SO}_4$  and concentrated in vacuo. The crude product was purified by column chromatography (10% EtOAc in hexanes) to afford **166a** as a colorless viscous oil (194 mg, >99% yield):  $^1\text{H NMR}$  (400 MHz,  $\text{CDCl}_3$ )  $\delta$  8.19 – 8.13 (m, 2H), 8.11 (dd,  $J = 8.4, 1.0$  Hz, 1H), 8.07 (s, 1H), 7.92 (dt,  $J = 8.3, 0.9$  Hz, 1H), 7.71 (ddd,  $J = 8.2, 6.8, 1.2$  Hz, 1H),

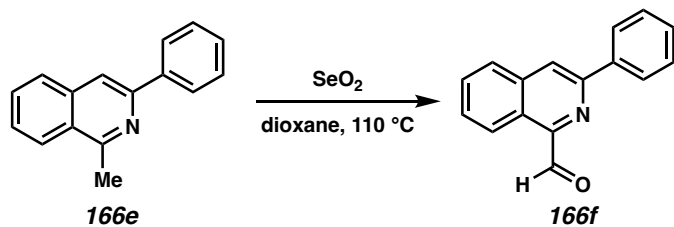
7.61 (ddd,  $J = 8.2, 6.8, 1.3$  Hz, 1H), 7.54 – 7.47 (m, 2H), 7.45 – 7.38 (m, 1H), 5.79 (s, 2H), 2.20 (s, 3H); All characterization data match those reported.<sup>9</sup>



**1-(methoxymethyl)-3-phenylisoquinoline (166b):** To a scintillation vial containing a stir bar and isoquinoline **173a** (165 mg, 0.70 mmol) in THF (7 mL, 0.1 M) was added KO*t*-Bu (86 mg, 0.77 mmol) at room temperature. The resulting mixture was stirred for 5 minutes, then cooled to 0 °C, and MeI (0.05 mL, 0.77 mmol) was added. The reaction was allowed to slowly warm to room temperature overnight and then was quenched with saturated aqueous NH<sub>4</sub>Cl. The organic phase was collected and the aqueous phase was extracted with EtOAc. The organic phases were combined, dried over MgSO<sub>4</sub>, and concentrated in vacuo. The crude product was purified by column chromatography (5% EtOAc in hexanes) to afford **166b** as a white solid (79 mg, 45% yield): <sup>1</sup>H NMR (400 MHz, CDCl<sub>3</sub>) δ 8.36 (dd,  $J = 8.4, 1.1$  Hz, 1H), 8.20 – 8.13 (m, 2H), 8.04 (s, 1H), 7.89 (d,  $J = 8.3$  Hz, 1H), 7.69 (ddd,  $J = 8.2, 6.8, 1.2$  Hz, 1H), 7.60 (ddd,  $J = 8.2, 6.8, 1.3$  Hz, 1H), 7.51 (td,  $J = 7.3, 6.5, 1.2$  Hz, 2H), 7.45 – 7.37 (m, 1H), 5.14 (s, 2H), 3.51 (s, 3H); All characterization data match those reported.<sup>9</sup>

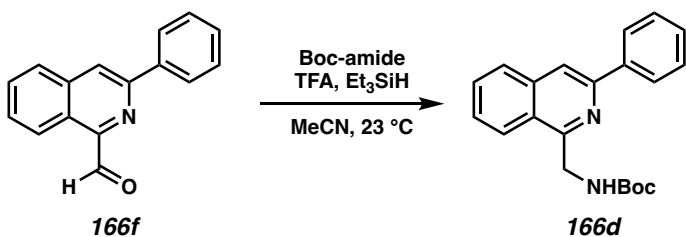


**1-((benzyloxy)methyl)-3-phenylisoquinoline (166c):** This procedure has been adapted from a previous report.<sup>26</sup> To a flame-dried RBF equipped with a stir bar was added NaH (36.4 mg, 60% w/w in oil, 0.91 mmol) and THF (7 mL, 0.1 M). To this suspension, isoquinoline **173a** (165 mg, 0.70 mmol) was added. After 5 minutes of stirring at room temperature, the reaction mixture was cooled to 0 °C and BnBr (0.91 mL, 0.91 mmol) was added. The reaction was allowed to slowly warm to room temperature overnight. Silica (1 g) was then added and the solvent was evaporated under vacuum. The crude product was purified by column chromatography (5% EtOAc in hexanes) to afford **166c** as a colorless viscous oil (153 mg, 67% yield): <sup>1</sup>H NMR (400 MHz, CDCl<sub>3</sub>) δ 8.39 (dd, *J* = 8.4, 1.1 Hz, 1H), 8.21 – 8.14 (m, 2H), 8.04 (s, 1H), 7.89 (d, *J* = 8.3 Hz, 1H), 7.69 (ddd, *J* = 8.2, 6.8, 1.2 Hz, 1H), 7.58 (ddd, *J* = 8.3, 6.8, 1.2 Hz, 1H), 7.51 (dd, *J* = 8.4, 6.9 Hz, 2H), 7.45 – 7.27 (m, 6H), 5.24 (s, 2H), 4.67 (s, 2H); All characterization data match those reported.<sup>9</sup>

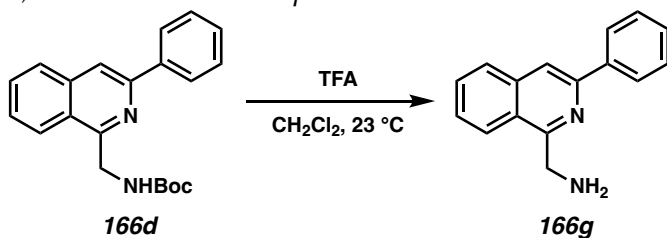


**3-phenylisoquinoline-1-carbaldehyde (166f):** To a Schlenk flask containing a stir bar was added SeO<sub>2</sub> (140 mg, 1.26 mmol) and isoquinoline **166e** (138 mg, 0.63 mmol) in 1,4-dioxane (13 mL, 0.05 M). The reaction vial was then sealed and heated to 110 °C while stirring for 2 hours. The reaction was then cooled to room temperature and filtered through celite rinsing

with EtOAc. The crude product was then purified by column chromatography (5% EtOAc in hexanes) to afford **166f** as a pale yellow solid (1.32 g, 96% yield):  $^1\text{H}$  NMR (400 MHz,  $\text{CDCl}_3$ )  $\delta$  10.50 (s, 1H), 9.32 (d,  $J = 8.2$  Hz, 1H), 8.31 (s, 1H), 8.24 (d,  $J = 8.1$  Hz, 2H), 7.97 (d,  $J = 7.3$  Hz, 1H), 7.84 – 7.67 (m, 2H), 7.56 (t,  $J = 7.5$  Hz, 2H), 7.47 (t,  $J = 7.4$  Hz, 1H); All characterization data match those reported.<sup>9</sup>



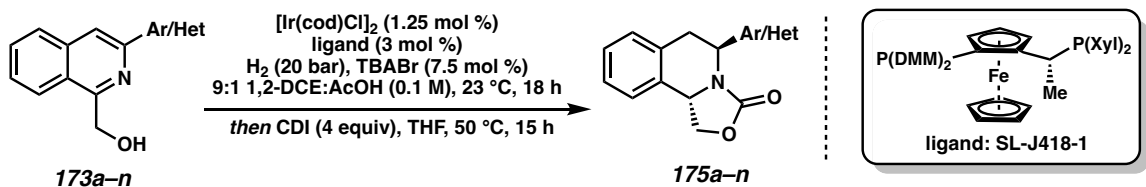
**tert-butyl ((3-phenylisoquinolin-1-yl)methyl)carbamate (166d):** To a solution of aldehyde **166f** (150 mg, 0.64 mmol) and *t*-butyl carbamate (150 mg, 1.28 mmol) in MeCN (6.5 mL, 0.1 M) were added trifluoroacetic acid (0.15 mL, 1.92 mmol) and triethylsilane (1.0 mL, 6.4 mmol). The reaction was stirred at room temperature overnight and then quenched with saturated aqueous  $\text{Na}_2\text{CO}_3$  and extracted with EtOAc. The combined organic phases were washed with brine, dried over  $\text{Na}_2\text{SO}_4$  and concentrated in vacuo. The crude product was purified by column chromatography (15% EtOAc in hexanes) to afford **166d** as a white solid (160 mg, 75% yield):  $^1\text{H}$  NMR (400 MHz,  $\text{CDCl}_3$ )  $\delta$  8.16 (d,  $J = 7.7$  Hz, 2H), 8.10 (d,  $J = 8.4$  Hz, 1H), 8.00 (s, 1H), 7.90 (d,  $J = 8.2$  Hz, 1H), 7.70 (ddd,  $J = 8.1, 6.9, 1.1$  Hz, 1H), 7.61 (ddd,  $J = 8.2, 6.9, 1.2$  Hz, 1H), 7.53 (t,  $J = 7.6$  Hz, 2H), 7.48 – 7.40 (m, 1H), 6.43 (br s, 1H), 5.03 (d,  $J = 4.4$  Hz, 2H), 1.54 (s, 9H); All characterization data match those reported.<sup>9</sup>



**(3-phenylisoquinolin-1-yl)methanamine (166g):** To a solution of carbamate **166d** (225 mg, 0.67 mmol) in  $\text{CH}_2\text{Cl}_2$  (2.2 mL, 0.3 M) was added trifluoroacetic acid (1.03 mL, 13.48 mmol, 20 equiv). The reaction was stirred at 23 °C for 1 hour and then neutralized to neutral pH with 1M NaOH. The organic phase was washed with water and extracted with  $\text{CH}_2\text{Cl}_2$  (2 x 20 mL), then dried over  $\text{Na}_2\text{SO}_4$  and concentrated in vacuo. The crude product was purified by column chromatography (5% MeOH in  $\text{CH}_2\text{Cl}_2$  with 1%  $\text{NEt}_3$ ) to afford **166g** as a yellow solid (113 mg, 72% yield):  $^1\text{H NMR}$  (400 MHz,  $\text{CDCl}_3$ )  $\delta$  8.21 – 8.18 (m, 2H), 8.09 (d,  $J = 8.5$  Hz, 1H), 7.97 (s, 1H), 7.88 (d,  $J = 7.8$  Hz, 1H), 7.68 (ddd,  $J = 8.2, 6.9, 1.2$  Hz, 1H), 7.58 (ddd,  $J = 8.2, 6.9, 1.3$  Hz, 1H), 7.53 – 7.49 (m, 2H), 7.44 – 7.39 (m, 1H), 4.56 (s, 2H), 2.31 (br s, 2H);  $^{13}\text{C NMR}$  (100 MHz,  $\text{CDCl}_3$ )  $\delta$  159.9, 149.5, 139.6, 137.1, 130.3, 128.9, 128.6, 128.0, 127.2, 127.0, 125.2, 124.1, 115.7, 44.6; IR (Neat Film, NaCl) 3276, 3054, 2968, 2924, 1622, 1574, 1501, 1456, 1439, 1365, 1326, 1201, 882, 784, 766, 694  $\text{cm}^{-1}$ ; HRMS (MM:ESI-APCI+)  $m/z$  calc'd for  $\text{C}_{16}\text{H}_{15}\text{N}_2$   $[\text{M}+\text{H}]^+$ : 235.1235, found 235.1231.

### 3.7.2.3 Hydrogenation reactions

#### General Procedure 5: Hydrogenation Reactions

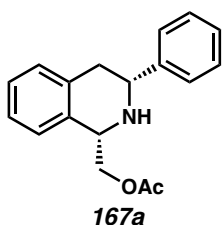




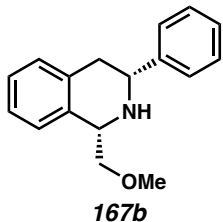
An oven-dried 20-mL scintillation vial containing a magnetic stir bar and an isoquinoline substrate (0.2 mmol) was capped with a PTFE-lined septum and pierced with two 21-gauge needles. The vials were then placed in a Parr bomb and brought into a N<sub>2</sub>-filled glovebox, with the exception of the pressure gauge. In a nitrogen-filled glovebox, a solution of the ligand (SL-J418-1) (4.53 mg, 0.006 mmol per reaction) and [Ir(cod)Cl]<sub>2</sub> (1.68 mg, 0.0025 mmol per reaction) in 1,2-DCE (1.8 mL per reaction) was prepared and allowed to stand for 10 minutes. Meanwhile, a solution of TBABr (4.83 mg, 0.015 mmol per reaction) in AcOH (0.2 mL per reaction) was prepared in a 1-dram vial, and 0.2 mL of the solution was added to each reaction vial by syringe. Afterwards, 1.8 mL of the homogeneous iridium catalyst solution was added to each reaction vial by syringe. After re-capping the vials with caps equipped with needles, the reaction vials were placed in the bomb and the top was covered tightly with plastic wrap secured by a rubber band. The bomb was then removed from the glovebox, and the pressure gauge was quickly screwed in place and tightened. The bomb was charged to 5-10 bar H<sub>2</sub> and slowly released. This process was repeated two more times, before charging the bomb to 20 bar of H<sub>2</sub> (or 60 bar H<sub>2</sub>). The bomb was then left stirring at 200 rpm at 23 °C (or placed in an oil bath and heated to 60 °C) for 18 hours. Then, the bomb was removed from the stir plate and the hydrogen pressure was vented. The reaction vials were removed from the bomb and each solution was basified by the addition of saturated aqueous K<sub>2</sub>CO<sub>3</sub> (2 mL). The layers were separated and the aqueous layer was extracted with EtOAc (3 x 2 mL). The combined organics layers were then dried over Na<sub>2</sub>SO<sub>4</sub> and concentrated in vacuo. The diastereoselectivity of the hydrogenation reaction was determined by crude <sup>1</sup>H NMR analysis.

Then, to a scintillation vial containing the crude reaction mixture in THF (0.05 M) was added 1,1'-carbonyldiimidazole (CDI) (130 mg, 0.8 mmol, 4 equiv) and heated at 50 °C for 15 hours. The reaction mixture was then cooled to 23 °C, concentrated, and purified by column chromatography to separate the diastereomers and isolate the *trans*-product.

Please note that the NMR data listed is for the major diastereomer. The enantiomeric excess was determined by chiral SFC analysis of the *trans*-product (see Table 3.5). The absolute configuration was determined for compound **175a** via X-ray crystallographic analysis, and the absolute configuration for all other products has been inferred by analogy.

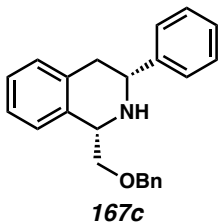


**((1*S*,3*R*)-3-phenyl-1,2,3,4-tetrahydroisoquinolin-1-yl)methyl acetate (**167a**):** Compound **167a** was prepared from isoquinoline **166a** using general procedure 5 and determined by <sup>1</sup>H NMR spectroscopy of the crude reaction mixture to consist of a mixture of diastereomers; (dr = >20:1); <sup>1</sup>H NMR (400 MHz, CDCl<sub>3</sub>) δ 7.51 – 7.45 (m, 2H), 7.41 – 7.37 (m, 2H), 7.34 – 7.30 (m, 1H), 7.27 – 7.24 (m, 1H), 7.23 – 7.18 (m, 2H), 7.16 – 7.10 (m, 1H), 4.78 (dd, *J* = 10.8, 3.5 Hz, 1H), 4.54 – 4.51 (m, 1H), 4.14 (dd, *J* = 10.8, 8.7 Hz, 1H), 4.05 (dd, *J* = 11.1, 3.4 Hz, 1H), 3.08 – 3.01 (m, 1H), 2.90 (dd, *J* = 15.5, 3.6 Hz, 1H), 2.08 (s, 3H); All characterization data match those reported.<sup>9</sup>



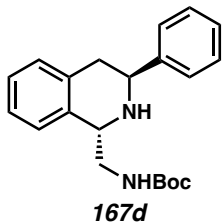
**(1*S*,3*R*)-1-(methoxymethyl)-3-phenyl-1,2,3,4-tetrahydroisoquinoline (167b):**

Compound **167b** was prepared from isoquinoline **166b** using general procedure 5 and determined by <sup>1</sup>H NMR spectroscopy of the crude reaction mixture to consist of a mixture of diastereomers; (dr = 17:1); <sup>1</sup>H NMR (400 MHz, CDCl<sub>3</sub>) δ 7.48 – 7.46 (m, 2H), 7.39 – 7.35 (m, 2H), 7.32 – 7.27 (m, 1H), 7.25 – 7.20 (m, 1H), 7.20 – 7.15 (m, 2H), 7.16 – 7.10 (m, 1H), 4.45 – 4.42 (m, 1H), 4.07 – 3.94 (m, 2H), 3.59 (t, *J* = 8.7 Hz, 1H), 3.43 (s, 3H), 3.06 (dd, *J* = 16.0, 11.1 Hz, 1H), 2.92 (dd, *J* = 16.0, 3.6 Hz, 1H); All characterization data match those reported.<sup>9</sup>



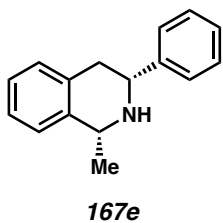
**(1*S*,3*R*)-1-((benzyloxy)methyl)-3-phenyl-1,2,3,4-tetrahydroisoquinoline (167c):**

Compound **167c** was prepared from isoquinoline **166c** using general procedure 5 and determined by <sup>1</sup>H NMR spectroscopy of the crude reaction mixture to consist of a mixture of diastereomers; (dr = >20:1); <sup>1</sup>H NMR (400 MHz, CDCl<sub>3</sub>) δ 7.48 – 7.46 (m, 2H), 7.40 – 7.34 (m, 6H), 7.32 – 7.28 (m, 2H), 7.22 – 7.16 (m, 3H), 7.14 – 7.11 (m, 1H), 4.61 (s, 2H), 4.48 (dd, *J* = 8.7, 3.4 Hz, 1H), 4.12 (dd, *J* = 9.0, 3.6 Hz, 1H), 4.04 (dd, *J* = 11.1, 3.5 Hz, 1H), 3.67 (t, *J* = 8.7 Hz, 1H), 3.05 (dd, *J* = 15.9, 11.1 Hz, 1H), 2.91 (dd, *J* = 15.8, 3.5 Hz, 1H); All characterization data match those reported.<sup>9</sup>



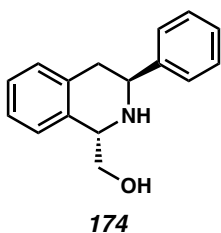
*tert*-butyl (((1*S*,3*R*)-3-phenyl-1,2,3,4-tetrahydroisoquinolin-1-yl)methyl)carbamate

**(167d):** Compound **167d** was prepared from isoquinoline **166d** using general procedure 5 and determined by  $^1\text{H}$  NMR spectroscopy of the crude reaction mixture as a mixture of diastereomers; (dr = 1.4:1); 25% ee for major diastereomer;  $[\alpha]_{\text{D}}^{25} -1.3$  ( $c$  0.53,  $\text{CHCl}_3$ ); Major diastereomer:  $^1\text{H}$  NMR (400 MHz,  $\text{CDCl}_3$ )  $\delta$  7.47 – 7.45 (m, 2H), 7.40 – 7.36 (m, 2H), 7.32 – 7.28 (m, 1H), 7.20 – 7.18 (m, 3H), 7.14 – 7.12 (m, 1H), 5.12 (br s, 1H), 4.18 (dd,  $J = 10.7, 4.0$  Hz, 1H), 3.59 – 3.54 (m, 1H), 3.39 (ddd,  $J = 14.2, 10.7, 4.9$  Hz, 1H), 3.02 (dd,  $J = 16.3, 4.2$  Hz, 1H), 2.94 (dd,  $J = 16.3, 10.8$  Hz, 1H), 1.44 (s, 9H);  $^{13}\text{C}$  NMR (100 MHz,  $\text{CDCl}_3$ )  $\delta$  155.0, 142.8, 134.5, 134.3, 128.2, 127.6, 126.4, 126.0, 125.7, 125.7, 125.1, 55.2, 50.1, 43.6, 36.1, 28.9, 27.4; IR (Neat Film, NaCl) 3733, 3330, 2924, 2368, 2335, 1699, 1492, 1394, 1366, 1268, 1258, 1171, 754  $\text{cm}^{-1}$ ; HRMS (MM:ESI-APCI+)  $m/z$  calc'd for  $\text{C}_{21}\text{H}_{27}\text{N}_2\text{O}_2$   $[\text{M}+\text{H}]^+$ : 339.2073, found 339.2075; SFC Conditions: 30% IPA, 2.5 mL/min, Chiralpak AD-H column,  $\lambda = 210$  nm,  $t_{\text{R}}$  (min): major = 1.95, minor = 4.28.



**(1*R*,3*R*)-1-methyl-3-phenyl-1,2,3,4-tetrahydroisoquinoline (167e):** Compound **167e** was prepared from isoquinoline **166e** using general procedure 5 and determined by  $^1\text{H}$  NMR spectroscopy of the crude reaction mixture to consist of a mixture of diastereomers; (dr =

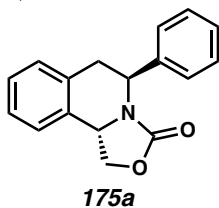
>20:1);  $^1\text{H}$  NMR (400 MHz,  $\text{CDCl}_3$ )  $\delta$  7.49 – 7.46 (m, 2H), 7.41 – 7.37 (m, 2H), 7.33 – 7.29 (m, 1H), 7.28 – 7.23 (m, 1H), 7.23 – 7.14 (m, 2H), 7.11 (d,  $J = 6.9$  Hz, 1H), 4.34 (q,  $J = 6.6$  Hz, 1H), 4.08 (dd,  $J = 11.1, 3.9$  Hz, 1H), 3.12 – 3.01 (m, 1H), 2.96 (dd,  $J = 16.2, 4.1$  Hz, 1H), 1.55 (d,  $J = 6.5$  Hz, 3H); All characterization data match those reported.<sup>9</sup>



**((1*S*,3*R*)-3-phenyl-1,2,3,4-tetrahydroisoquinolin-1-yl)methanol (174):** Compound **174** was prepared from isoquinoline **173a** from general procedure 5 and purified by column chromatography (5% MeOH in  $\text{CH}_2\text{Cl}_2$ ) to provide a tan solid as a mixture of diastereomers (47 mg, 98% yield) (dr = 2.4:1); 92% ee for major diastereomer;  $[\alpha]_{\text{D}}^{25} -8.3$  ( $c$  0.15,  $\text{CHCl}_3$ );

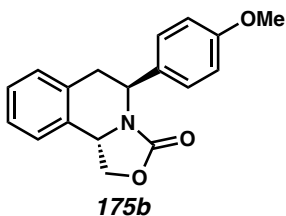
*Trans*-diastereomer:  $^1\text{H}$  NMR (400 MHz,  $\text{CDCl}_3$ )  $\delta$  7.49 – 7.43 (m, 2H), 7.42 – 7.38 (m, 2H), 7.36 – 7.27 (m, 1H), 7.26 – 7.10 (m, 4H), 4.23 (dd,  $J = 10.5, 4.8$  Hz, 1H), 4.16 (dd,  $J = 11.2, 3.9$  Hz, 1H), 3.80 (dd,  $J = 10.8, 4.8$  Hz, 1H), 3.71 (t,  $J = 10.7$  Hz, 1H), 3.07 (dd,  $J = 16.4, 3.9$  Hz, 1H), 2.95 (dd,  $J = 15.9, 11.2$  Hz, 1H);  $^{13}\text{C}$  NMR (100 MHz,  $\text{CDCl}_3$ )  $\delta$  143.5, 135.5, 134.7, 129.5, 128.8, 127.5, 127.0, 126.7, 126.6, 126.4, 63.8, 57.4, 50.7, 36.8.

*Cis*-diastereomer:  $^1\text{H}$  NMR (400 MHz,  $\text{CDCl}_3$ )  $\delta$  7.50 – 7.43 (m, 2H), 7.41 – 7.34 (m, 2H), 7.34 – 7.28 (m, 1H), 7.25 – 7.17 (m, 3H), 7.15 – 7.10 (m, 1H), 4.43 – 4.41 (m, 1H), 4.10 (dd,  $J = 11.1, 3.5$  Hz, 1H), 4.02 (dd,  $J = 10.8, 3.3$  Hz, 1H), 3.90 (dd,  $J = 10.9, 5.4$  Hz, 1H), 3.02 (ddt,  $J = 15.9, 11.1, 1.4$  Hz, 1H), 2.90 (dd,  $J = 15.7, 3.5$  Hz, 1H); All characterization data match those reported.<sup>9</sup>



**(5*S*,10*bS*)-5-phenyl-1,5,6,10*b*-tetrahydro-3*H*-oxazolo[4,3-*a*]isoquinolin-3-one (175a):**

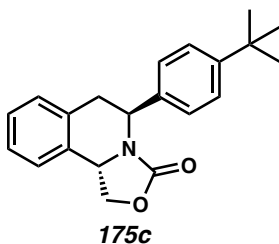
Compound **175a** was prepared from isoquinoline **173a** using general procedure 5 and purified by column chromatography (20% to 40% to 60% EtOAc in hexanes) to provide a clear solid (33 mg, 63% yield); 91% ee;  $[\alpha]_D^{25} +124.3$  (*c* 1.04, CHCl<sub>3</sub>); <sup>1</sup>H NMR (400 MHz, CDCl<sub>3</sub>)  $\delta$  7.28 – 7.19 (m, 8H), 6.91 (d, *J* = 7.3 Hz, 1H), 5.31 (dd, *J* = 6.7, 2.8 Hz, 1H), 4.74 (t, *J* = 8.0 Hz, 1H), 4.69 – 4.66 (m, 1H), 4.29 (dd, *J* = 7.8, 5.9 Hz, 1H), 3.41 (dd, *J* = 16.8, 6.7 Hz, 1H), 3.22 (dd, *J* = 16.7, 2.8 Hz, 1H); <sup>13</sup>C NMR (100 MHz, CDCl<sub>3</sub>)  $\delta$  157.5, 138.8, 134.4, 133.2, 129.4, 128.8, 128.1, 127.9, 127.2, 127.2, 124.4, 68.7, 51.7, 51.5, 31.4; IR (Neat Film, NaCl) 2910, 1751, 1601, 1494, 1452, 1402, 1221, 1114, 1066, 1030, 758, 701 cm<sup>-1</sup>; HRMS (MM:ESI-APCI+) *m/z* calc'd for C<sub>17</sub>H<sub>16</sub>NO<sub>2</sub> [M+H]<sup>+</sup>: 266.1176, found 266.1177; SFC Conditions: 40% MeOH, 3.5 mL/min, Chiralpak IC column,  $\lambda$  = 210 nm, *t<sub>R</sub>* (min): major = 2.61, minor = 2.41.



**(5*S*,10*bS*)-5-(4-methoxyphenyl)-1,5,6,10*b*-tetrahydro-3*H*-oxazolo[4,3-*a*]isoquinolin-3-one (175b):**

Compound **175b** was prepared from isoquinoline **173b** using general procedure 5 and purified by column chromatography (20% to 30% to 40% EtOAc in hexanes) to provide a pale yellow oil (38 mg, 64% yield); 96% ee;  $[\alpha]_D^{25} +150.4$  (*c* 1.01, CHCl<sub>3</sub>); <sup>1</sup>H

NMR (400 MHz, CDCl<sub>3</sub>)  $\delta$  7.29 – 7.24 (m, 3H), 7.22 – 7.20 (m, 2H), 6.94 (d,  $J$  = 8.0 Hz, 1H), 6.82 – 6.78 (m, 2H), 5.32 (dd,  $J$  = 6.7, 2.4 Hz, 1H), 4.77 (t,  $J$  = 8.0 Hz, 1H), 4.71 – 4.67 (m, 1H), 4.30 (dd,  $J$  = 8.0, 6.2 Hz, 1H), 3.75 (s, 3H), 3.44 (dd,  $J$  = 16.6, 6.8 Hz, 1H), 3.23 (dd,  $J$  = 16.7, 2.5 Hz, 1H); <sup>13</sup>C NMR (100 MHz, CDCl<sub>3</sub>)  $\delta$  159.1, 157.4, 134.4, 133.2, 130.7, 129.4, 128.4, 128.1, 127.2, 124.5, 114.1, 68.8, 55.3, 51.6, 50.8, 31.4; IR (Neat Film, NaCl) 2907, 2836, 1750, 1610, 1513, 1402, 1304, 1251, 1178, 1066, 1030, 828, 756 cm<sup>-1</sup>; HRMS (MM:ESI-APCI+)  $m/z$  calc'd for C<sub>18</sub>H<sub>18</sub>NO<sub>3</sub> [M+H]<sup>+</sup>: 296.1281, found 296.1280; SFC Conditions: 10% MeOH, 3.5 mL/min, Chiralcel OJ-H column,  $\lambda$  = 210 nm,  $t_R$  (min): major = 8.66, minor = 7.52.

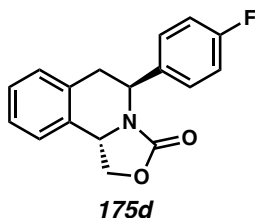


**(5*S*,10*bS*)-5-(4-(*tert*-butyl)phenyl)-1,5,6,10*b*-tetrahydro-3*H*-oxazolo[4,3-*a*]isoquinolin-3-one (175c):** Compound **175c** was prepared from isoquinoline **173c** using general procedure 5 and purified by column chromatography (20% to 30% to 40% EtOAc in hexanes) to provide a clear oil (43 mg, 67% yield); 95% ee;  $[\alpha]_D^{25}$  +115.6 ( $c$  1.01, CHCl<sub>3</sub>); <sup>1</sup>H NMR (400 MHz, CDCl<sub>3</sub>)  $\delta$  7.29 – 7.26 (m, 4H), 7.24 – 7.22 (m, 1H), 7.21 – 7.19 (m, 2H), 6.93 (d,  $J$  = 7.2 Hz, 1H), 5.31 (dd,  $J$  = 6.8, 2.5 Hz, 1H), 4.74 (t,  $J$  = 8.0 Hz, 1H), 4.72 – 4.68 (m, 1H), 4.29 (dd,  $J$  = 7.3, 5.3 Hz, 1H), 3.42 (dd,  $J$  = 16.6, 6.9 Hz, 1H), 3.23 (dd,  $J$  = 16.7, 2.6 Hz, 1H), 1.24 (s, 9H); <sup>13</sup>C NMR (100 MHz, CDCl<sub>3</sub>)  $\delta$  157.5, 150.8, 135.7, 134.5, 133.4, 129.4, 128.1, 127.1, 126.9, 125.7, 124.5, 68.7, 51.6, 51.1, 34.6, 31.4, 31.3; IR (Neat Film, NaCl) 3010, 2962, 1754, 1455, 1401, 1267, 1215, 1115, 1068, 1026, 828, 757 cm<sup>-1</sup>;

HRMS (MM:ESI-APCI+)  $m/z$  calc'd for  $C_{21}H_{24}NO_2$   $[M+H]^+$ : 322.1802, found 322.1801;

SFC Conditions: 20% MeOH, 3.5 mL/min, Chiralpak AD-H column,  $\lambda = 210$  nm,  $t_R$  (min):

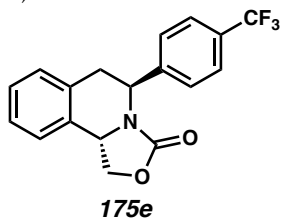
major = 5.04, minor = 5.44.



**(5*S*,10*bS*)-5-(4-fluorophenyl)-1,5,6,10*b*-tetrahydro-3*H*-oxazolo[4,3-*a*]isoquinolin-3-one**

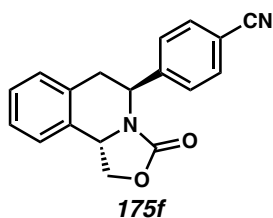
**(175d)**: Compound **175d** was prepared from isoquinoline **173d** using general procedure 5 and purified by column chromatography (20% to 30% to 40% EtOAc in hexanes) to provide a clear oil (40 mg, 70% yield); 95% ee;  $[\alpha]_D^{25} +150.5$  ( $c$  1.01,  $CHCl_3$ );  $^1H$  NMR (400 MHz,  $CDCl_3$ )  $\delta$  7.28 – 7.21 (m, 5H), 6.96 – 6.91 (m, 3H), 5.29 (dd,  $J = 6.8, 2.8$  Hz, 1H), 4.76 (t,  $J = 8$  Hz, 1H), 4.67 (ddd,  $J = 8.7, 6.2, 1.1$  Hz, 1H), 4.30 (dd,  $J = 8.1, 6.2$  Hz, 1H), 3.42 (ddd,  $J = 16.7, 6.6, 1.3$  Hz, 1H), 3.19 (dd,  $J = 16.7, 2.9$  Hz, 1H);  $^{13}C$  NMR (100 MHz,  $CDCl_3$ )  $\delta$  162.3 (d,  $J = 246.8$  Hz), 157.5, 134.6 (d,  $J = 3.3$  Hz), 134.3, 132.9, 129.4, 129.0 (d,  $J = 8.1$  Hz), 128.3, 127.4, 124.5, 115.7 (d,  $J = 21.5$  Hz), 68.7, 51.6, 50.9, 31.6;  $^{19}F$  NMR (282 MHz,  $CDCl_3$ )  $\delta$  –114.4 – –114.5 (m); IR (Neat Film, NaCl) 2910, 1753, 1605, 1510, 1402, 1223, 1161, 1068, 1043, 1029, 885, 828, 758, 745  $cm^{-1}$ ; HRMS (MM:ESI-APCI+)  $m/z$  calc'd for  $C_{17}H_{15}FNO_2$   $[M+H]^+$ : 284.1081, found 284.1078; SFC Conditions: 35% MeOH, 3.5 mL/min, Chiralpak IC column,  $\lambda = 210$  nm,  $t_R$  (min): minor = 2.39, major = 2.58.





**(5*S*,10*bS*)-5-(4-(trifluoromethyl)phenyl)-1,5,6,10*b*-tetrahydro-3*H*-oxazolo[4,3-**

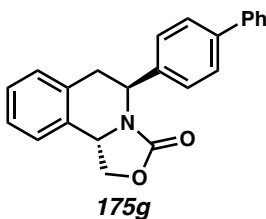
***a*]isoquinolin-3-one (175e):** Compound **175e** was prepared from isoquinoline **173e** using general procedure 5 and purified by column chromatography (20% to 30% to 40% EtOAc in hexanes) to provide a white solid (43 mg, 64% yield); 91% ee;  $[\alpha]_{\text{D}}^{25} +118.2$  ( $c$  1.02,  $\text{CHCl}_3$ );  $^1\text{H}$  NMR (400 MHz,  $\text{CDCl}_3$ )  $\delta$  7.56 (d,  $J = 8.2$  Hz, 2H), 7.45 (d,  $J = 8.0$  Hz, 2H), 7.32 – 7.26 (m, 3H), 7.00 – 6.97 (m, 1H), 5.35 (dd,  $J = 6.7, 3.4$  Hz, 1H), 4.82 (t,  $J = 8.0$  Hz, 1H), 4.76 – 4.72 (m, 1H), 4.38 (dd,  $J = 8.1, 5.9$  Hz, 1H), 3.47 (ddd,  $J = 16.6, 6.6, 1.2$  Hz, 1H), 3.24 (dd,  $J = 16.6, 3.5$  Hz, 1H);  $^{13}\text{C}$  NMR (100 MHz,  $\text{CDCl}_3$ )  $\delta$  157.6, 143.0, 143.0, 134.2, 132.7, 130.2 (q,  $J = 32.6$  Hz), 129.3, 128.4, 127.5, 125.9 (q,  $J = 3.8$  Hz), 124.4, 124.0 (q,  $J = 271.0$  Hz), 68.6, 51.8, 51.5, 31.6;  $^{19}\text{F}$  NMR (282 MHz,  $\text{CDCl}_3$ )  $\delta$  62.7; IR (Neat Film, NaCl) 2916, 1753, 1620, 1402, 1326, 1225, 1162, 1114, 1068, 1017, 889, 829, 757  $\text{cm}^{-1}$ ; HRMS (MM:ESI-APCI+)  $m/z$  calc'd for  $\text{C}_{18}\text{H}_{15}\text{F}_3\text{NO}_2$   $[\text{M}+\text{H}]^+$ : 334.1049, found 334.1048; SFC Conditions: 25% MeOH, 3.5 mL/min, Chiralpak IC column,  $\lambda = 210$  nm,  $t_{\text{R}}$  (min): minor = 2.22, major = 2.37.



**4-((5*S*,10*bS*)-3-oxo-1,5,6,10*b*-tetrahydro-3*H*-oxazolo[4,3-*a*]isoquinolin-5-**

***yl*)benzotrile (175f):** Compound **175f** was prepared from isoquinoline **173f** using general

procedure 5 and purified by column chromatography (25% to 35% to 50% EtOAc in hexanes) to provide a white solid (27 mg, 47% yield); 83% ee;  $[\alpha]_{\text{D}}^{25} +112.3$  ( $c$  1.00,  $\text{CHCl}_3$ );  $^1\text{H}$  NMR (400 MHz,  $\text{CDCl}_3$ )  $\delta$  7.61 – 7.58 (m, 2H), 7.46 – 7.43 (m, 2H), 7.32 – 7.27 (m, 3H), 7.01 – 6.99 (m, 1H), 5.31 (dd,  $J = 6.5, 3.8$  Hz, 1H), 4.83 (t,  $J = 8.4$  Hz, 1H), 4.76 – 4.72 (m, 1H), 4.40 (dd,  $J = 8.3, 5.9$  Hz, 1H), 3.45 (dd,  $J = 16.5, 6.4$  Hz, 1H), 3.20 (dd,  $J = 16.6, 3.9$  Hz, 1H);  $^{13}\text{C}$  NMR (100 MHz,  $\text{CDCl}_3$ )  $\delta$  157.6, 144.5, 134.1, 132.7, 132.5, 129.3, 128.5, 127.9, 127.7, 124.3, 118.6, 111.9, 68.5, 51.9, 51.8, 31.7; IR (Neat Film, NaCl) 2909, 2228, 1747, 1679, 1608, 1402, 1224, 1160, 1114, 1043, 1031, 829, 764, 733  $\text{cm}^{-1}$ ; HRMS (MM:ESI-APCI+)  $m/z$  calc'd for  $\text{C}_{18}\text{H}_{15}\text{N}_2\text{O}_2$   $[\text{M}+\text{H}]^+$ : 291.1134, found 291.1137; SFC Conditions: 40% MeOH, 3.5 mL/min, Chiralpak IC column,  $\lambda = 210$  nm,  $t_{\text{R}}$  (min): minor = 3.97, major = 4.48.

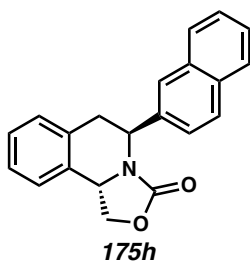


**(5S,10bS)-5-([1,1'-biphenyl]-4-yl)-1,5,6,10b-tetrahydro-3H-oxazolo[4,3-a]isoquinolin-3-one (175g):** Compound **175g** was prepared from isoquinoline **173g** using general procedure 5 and purified by column chromatography (20% to 30% to 40% EtOAc in hexanes) to provide a white solid (38 mg, 56% yield); 75% ee;  $[\alpha]_{\text{D}}^{25} +108.5$  ( $c$  1.01,  $\text{CHCl}_3$ );  $^1\text{H}$  NMR (400 MHz,  $\text{CDCl}_3$ )  $\delta$  7.55 – 7.51 (m, 4H), 7.44 – 7.37 (m, 4H), 7.36 – 7.31 (m, 3H), 7.30 – 7.25 (m, 1H), 6.98 (d,  $J = 7.1$  Hz, 1H), 5.40 (dd,  $J = 6.7, 2.8$  Hz, 1H), 4.83 – 4.76 (m, 2H), 4.39 – 4.32 (m, 1H), 3.49 (dd,  $J = 16.7, 6.7$  Hz, 1H), 3.31 (dd,  $J = 16.7, 2.8$  Hz, 1H);  $^{13}\text{C}$  NMR (100 MHz,  $\text{CDCl}_3$ )  $\delta$  157.5, 140.8, 140.6, 137.8, 134.4, 133.2, 129.4, 128.9, 128.2, 127.6, 127.6, 127.5, 127.3, 127.1, 124.5, 68.7, 51.7, 51.3, 31.5; IR (Neat Film, NaCl) 3028,

2908, 1751, 1487, 1454, 1402, 1220, 1162, 1070, 1042, 886, 830, 760  $\text{cm}^{-1}$ ; HRMS

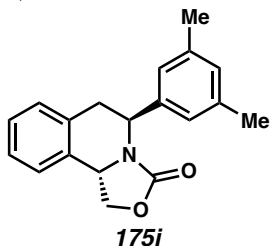
(MM:ESI-APCI+)  $m/z$  calc'd for  $\text{C}_{23}\text{H}_{20}\text{NO}_2$   $[\text{M}+\text{H}]^+$ : 342.1489, found 342.1501; SFC

Conditions: 45% MeOH, 3.5 mL/min, Chiralcel OJ-H column,  $\lambda = 210$  nm,  $t_R$  (min): minor = 5.72, major = 6.80.

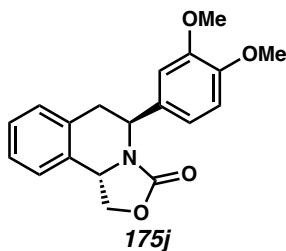


**(5S,10bS)-5-(naphthalen-2-yl)-1,5,6,10b-tetrahydro-3H-oxazolo[4,3-a]isoquinolin-3-**

**one (175h):** Compound **175h** was prepared from isoquinoline **173h** using general procedure 5 and purified by column chromatography (20% to 30% to 40% EtOAc in hexanes) to provide a pale white solid (34 mg, 54% yield); 89% ee;  $[\alpha]_D^{25} +91.3$  ( $c$  1.00,  $\text{CHCl}_3$ );  $^1\text{H}$  NMR (400 MHz,  $\text{CDCl}_3$ )  $\delta$  7.82 – 7.79 (m, 2H), 7.73 – 7.70 (m, 1H), 7.68 (s, 1H), 7.50 (dd,  $J = 8.6, 1.9$  Hz, 1H), 7.47 – 7.42 (m, 2H), 7.38 – 7.30 (m, 2H), 7.27 – 7.23 (m, 1H), 6.93 (d,  $J = 8.0$  Hz, 1H), 5.52 (dd,  $J = 6.5, 3.2$  Hz, 1H), 4.79 (t,  $J = 8.0$  Hz, 1H), 4.74 – 4.70 (m, 1H), 4.35 (dd,  $J = 8.0, 6.0$  Hz, 1H), 3.54 (dd,  $J = 16.7, 6.6$  Hz, 1H), 3.41 (dd,  $J = 16.8, 2.9$  Hz, 1H);  $^{13}\text{C}$  NMR (100 MHz,  $\text{CDCl}_3$ )  $\delta$  157.6, 136.1, 134.4, 133.2, 133.1, 132.9, 129.4, 128.8, 128.2, 128.1, 127.7, 127.2, 126.4, 126.3, 125.9, 125.4, 124.5, 68.8, 51.8, 51.6, 31.3; IR (Neat Film, NaCl) 3017, 1750, 1454, 1401, 1327, 1215, 1070, 1030, 818, 756  $\text{cm}^{-1}$ ; HRMS (MM:ESI-APCI+)  $m/z$  calc'd for  $\text{C}_{21}\text{H}_{18}\text{NO}_2$   $[\text{M}+\text{H}]^+$ : 316.1332, found 316.1332; SFC Conditions: 40% MeOH, 3.5 mL/min, Chiralpak IC column,  $\lambda = 210$  nm,  $t_R$  (min):, minor = 4.21, major = 4.61.

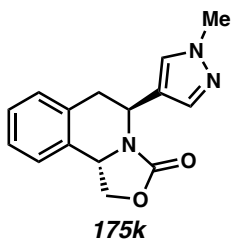


**(5*S*,10*bS*)-5-(3,5-dimethylphenyl)-1,5,6,10*b*-tetrahydro-3*H*-oxazolo[4,3-*a*]isoquinolin-3-one (175*i*):** Compound **175*i*** was prepared from isoquinoline **173*i*** using general procedure 5 and purified by column chromatography (10% to 20% to 30% to 40% EtOAc in hexanes) to provide a pale white solid (36 mg, 61% yield); 86% ee;  $[\alpha]_{\text{D}}^{25} +125.3$  (*c* 1.03, CHCl<sub>3</sub>); <sup>1</sup>H NMR (400 MHz, CDCl<sub>3</sub>) δ 7.30 – 7.23 (m, 3H), 6.97 (d, *J* = 7.1 Hz, 1H), 6.92 (s, 2H), 6.89 (s, 1H), 5.26 (dd, *J* = 6.7, 3.2 Hz, 1H), 4.82 – 4.75 (m, 2H), 4.39 – 4.32 (m, 1H), 3.42 (dd, *J* = 16.6, 6.7 Hz, 1H), 3.24 (dd, *J* = 16.6, 3.2 Hz, 1H), 2.25 (s, 6H); <sup>13</sup>C NMR (100 MHz, CDCl<sub>3</sub>) δ 157.5, 138.9, 138.3, 134.5, 133.4, 129.5, 129.3, 128.1, 127.1, 124.8, 124.3, 68.5, 51.8, 51.5, 31.7, 21.5; IR (Neat Film, NaCl) 3010, 2916, 1752, 1606, 1454, 1402, 1265, 1220, 1070, 1043, 1030, 758, 747 cm<sup>-1</sup>; HRMS (MM:ESI-APCI+) *m/z* calc'd for C<sub>19</sub>H<sub>20</sub>NO<sub>2</sub> [M+H]<sup>+</sup>: 294.1489, found 294.1489; SFC Conditions: 40% MeOH, 3.5 mL/min, Chiralpak IC column, λ = 210 nm, *t<sub>R</sub>* (min): minor = 2.47, major = 2.71.



**(5*S*,10*bS*)-5-(3,4-dimethoxyphenyl)-1,5,6,10*b*-tetrahydro-3*H*-oxazolo[4,3-*a*]isoquinolin-3-one (175*j*):** Compound **175*j*** was prepared from isoquinoline **173*j*** using general procedure 5 and purified by column chromatography (40% to 50% to 75% EtOAc in

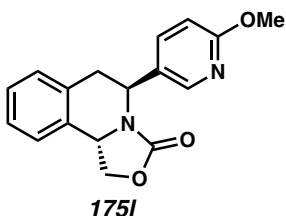
hexanes) to provide a pale yellow oil (33 mg, 51% yield); 87% ee;  $[\alpha]_{\text{D}}^{25} +120.9$  (*c* 1.00, CHCl<sub>3</sub>); <sup>1</sup>H NMR (400 MHz, CDCl<sub>3</sub>) δ 7.30 – 7.28 (m, 2H), 7.27 – 7.23 (m, 1H), 6.95 (d, *J* = 6.8 Hz, 1H), 6.86 (d, *J* = 2.0 Hz, 1H), 6.75 (dd, *J* = 8.3, 2.0 Hz, 1H), 6.71 (d, *J* = 8.3 Hz, 1H), 5.32 (d, *J* = 6.7, 2.3 Hz, 1H), 4.78 (t, *J* = 8.0 Hz, 1H), 4.70 – 4.66 (m, 1H), 4.30 (dd, *J* = 8.1, 6.2 Hz, 1H), 3.81 (s, 3H), 3.79 (s, 3H), 3.45 (dd, *J* = 16.8, 6.5 Hz, 1H), 3.24 (dd, *J* = 16.8, 2.4 Hz, 1H); <sup>13</sup>C NMR (100 MHz, CDCl<sub>3</sub>) δ 157.4, 149.2, 148.7, 134.4, 133.3, 131.1, 129.3, 128.1, 127.2, 124.5, 119.1, 111.0, 110.9, 68.9, 56.0, 56.0, 51.6, 51.1, 31.4; IR (Neat Film, NaCl) 2929, 2836, 1748, 1592, 1516, 1403, 1259, 1237, 1142, 1026, 758, 749 cm<sup>-1</sup>; HRMS (MM:ESI-APCI+) *m/z* calc'd for C<sub>19</sub>H<sub>20</sub>NO<sub>4</sub> [M+H]<sup>+</sup>: 326.1387, found 326.1385; SFC Conditions: 40% MeOH, 3.5 mL/min, Chiralpak AD-H column, λ = 210 nm, *t*<sub>R</sub> (min): major = 2.13, minor = 2.74.



**(5*S*,10*bS*)-5-(1-methyl-1*H*-pyrazol-4-yl)-1,5,6,10*b*-tetrahydro-3*H*-oxazolo[4,3-**

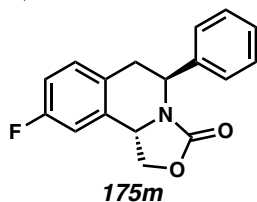
***a*]isoquinolin-3-one (175k):** Compound **175k** was prepared from isoquinoline **173k** using general procedure 5 and purified by column chromatography (80% to 90% to 100% EtOAc in hexanes) to provide a pale yellow oil as a mixture of diastereomers (47 mg, 88% overall yield) (*dr* = 3.0:1); 97% ee for major diastereomer;  $[\alpha]_{\text{D}}^{25} +113.6$  (*c* 1.00, CHCl<sub>3</sub>); Major diastereomer: <sup>1</sup>H NMR (400 MHz, CDCl<sub>3</sub>) δ 7.28 (s, 1H), 7.27 – 7.21 (m, 3H), 7.17 (s, 1H), 6.96 – 6.94 (m, 1H), 5.34 (dd, *J* = 6.6, 2.0 Hz, 1H), 4.77 – 4.74 (m, 2H), 4.29 – 4.23 (m, 1H), 3.78 (s, 3H), 3.42 (dd, *J* = 16.5, 6.7 Hz, 1H), 3.03 (dd, *J* = 16.4, 1.9 Hz, 1H); <sup>13</sup>C NMR (100

MHz, CDCl<sub>3</sub>)  $\delta$  157.1, 138.1, 134.1, 132.8, 129.7, 128.8, 128.0, 127.3, 124.7, 119.7, 69.1, 51.5, 44.2, 39.1, 32.3; IR (Neat Film, NaCl) 2930, 1750, 1444, 1401, 1276, 1216, 1070, 1021, 988, 761, 751 cm<sup>-1</sup>; HRMS (MM:ESI-APCI+)  $m/z$  calc'd for C<sub>15</sub>H<sub>16</sub>N<sub>3</sub>O<sub>2</sub> [M+H]<sup>+</sup>: 270.1237, found 270.1238; SFC Conditions: 40% MeOH, 3.5 mL/min, Chiralpak AD-H column,  $\lambda$  = 210 nm,  $t_R$  (min): minor = 2.24, major = 2.67.

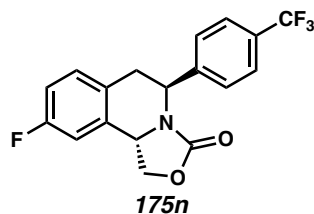


**(5S,10bS)-5-(6-methoxypyridin-3-yl)-1,5,6,10b-tetrahydro-3H-oxazolo[4,3-**

**a]isoquinolin-3-one (175I):** Compound **175I** was prepared from isoquinoline **173I** using general procedure 5 and purified by column chromatography (25% to 35% to 50% EtOAc in hexanes) to provide a pale yellow oil (38 mg, 64% yield); 95% ee;  $[\alpha]_D^{25}$  +124.9 (*c* 1.02, CHCl<sub>3</sub>); <sup>1</sup>H NMR (400 MHz, CDCl<sub>3</sub>)  $\delta$  8.03 (d, *J* = 2.6 Hz, 1H), 7.54 (dd, *J* = 8.7, 2.6 Hz, 1H), 7.29 – 7.27 (m, 2H), 7.25 – 7.23 (m, 1H), 6.95 (dd, *J* = 6.9 Hz, 1H), 6.68 (d, *J* = 8.6 Hz, 1H), 5.31 (dd, *J* = 6.7, 2.5 Hz, 1H), 4.78 (t, *J* = 8.0 Hz, 1H), 4.69 (dd, *J* = 8.8, 6.2 Hz, 1H), 4.31 (dd, *J* = 8.1, 6.0 Hz, 1H), 3.86 (s, 3H), 3.45 (dd, *J* = 16.7, 6.8 Hz, 1H), 3.21 (dd, *J* = 16.8, 2.5 Hz, 1H); <sup>13</sup>C NMR (100 MHz, CDCl<sub>3</sub>)  $\delta$  163.8, 157.4, 145.4, 138.3, 134.1, 132.6, 129.5, 128.3, 127.4, 126.9, 124.6, 111.3, 68.9, 53.5, 51.6, 49.3, 31.1; IR (Neat Film, NaCl) 2945, 1752, 1608, 1494, 1400, 1288, 1262, 1068, 1027, 827, 758, 742 cm<sup>-1</sup>; HRMS (MM:ESI-APCI+)  $m/z$  calc'd for C<sub>17</sub>H<sub>17</sub>N<sub>2</sub>O<sub>3</sub> [M+H]<sup>+</sup>: 297.1234, found 297.1236; SFC Conditions: 40% MeOH, 3.5 mL/min, Chiralpak AD-H column,  $\lambda$  = 210 nm,  $t_R$  (min): minor = 2.80, major = 3.30.



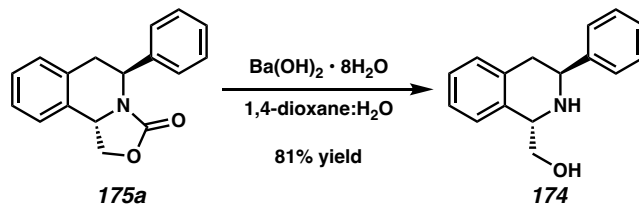
**(5*S*,10*bS*)-9-fluoro-5-phenyl-1,5,6,10*b*-tetrahydro-3*H*-oxazolo[4,3-*a*]isoquinolin-3-one (175m):** Compound **175m** was prepared from isoquinoline **173m** using general procedure 5 and purified by column chromatography (20% to 30% to 40% EtOAc in hexanes) to provide a white solid (38 mg, 67% yield); 95% ee;  $[\alpha]_D^{25} +163.7$  (*c* 1.00, CHCl<sub>3</sub>); <sup>1</sup>H NMR (400 MHz, CDCl<sub>3</sub>)  $\delta$  7.29 – 7.21 (m, 6H), 6.98 (td, *J* = 8.6, 2.5 Hz, 1H), 6.65 (dd, *J* = 8.9, 2.4 Hz, 1H), 5.33 (dd, *J* = 6.6, 2.7 Hz, 1H), 4.74 (t, *J* = 8.5 Hz, 1H), 4.67 – 4.63 (m, 1H), 4.28 (dd, *J* = 8.2, 5.9 Hz, 1H), 3.38 (dd, *J* = 16.6, 6.4 Hz, 1H), 3.22 (dd, *J* = 16.6, 2.8 Hz, 1H); <sup>13</sup>C NMR (100 MHz, CDCl<sub>3</sub>)  $\delta$  161.7 (d, *J* = 246.6 Hz), 157.4, 138.4, 136.1 (d, *J* = 6.6 Hz), 131.0 (d, *J* = 7.8 Hz), 128.9, 128.8 (d, *J* = 3.3 Hz), 128.0, 127.1, 115.4 (d, *J* = 21.3 Hz), 111.4 (d, *J* = 22.1 Hz), 68.4, 51.7 (d, *J* = 2.2 Hz), 51.4, 30.6; <sup>19</sup>F NMR (282 MHz, CDCl<sub>3</sub>)  $\delta$  –114.3 – –114.4 (m); IR (Neat Film, NaCl) 3061, 2914, 1752, 1613, 1593, 1499, 1450, 1430, 1402, 1327, 1241, 1216, 1162, 1069, 1034, 868, 814, 756 cm<sup>-1</sup>; HRMS (MM:ESI-APCI+) *m/z* calc'd for C<sub>17</sub>H<sub>15</sub>FNO<sub>2</sub> [M+H]<sup>+</sup>: 284.1081, found 284.1083; SFC Conditions: 40% MeOH, 3.5 mL/min, Chiralpak IC column,  $\lambda$  = 210 nm, *t<sub>R</sub>* (min): minor = 2.09, major = 2.53.



**(5*S*,10*bS*)-9-fluoro-5-(4-(trifluoromethyl)phenyl)-1,5,6,10*b*-tetrahydro-3*H*-oxazolo[4,3-*a*]isoquinolin-3-one (175n):** Compound **175n** was prepared from isoquinoline **173n** using general procedure 5 and purified by column chromatography (20% to 30% to

40% EtOAc in hexanes) to provide a pale yellow oil (38 mg, 54% yield); 92% ee;  $[\alpha]_D^{25} +115.7$  (*c* 1.02, CHCl<sub>3</sub>); <sup>1</sup>H NMR (400 MHz, CDCl<sub>3</sub>) δ 7.56 (d, *J* = 8.2 Hz, 2H), 7.43 (d, *J* = 8.1 Hz, 2H), 7.29 (dd, *J* = 8.6, 5.4 Hz, 1H), 7.02 (td, *J* = 8.4, 2.5 Hz, 1H), 6.71 (dd, *J* = 8.8, 2.4 Hz, 1H), 5.35 (dd, *J* = 6.6, 3.4 Hz, 1H), 4.80 (t, *J* = 8.5, 1H), 4.69 (dd, *J* = 8.6, 5.9 Hz, 1H), 4.35 (dd, *J* = 8.4, 5.8 Hz, 1H), 3.42 (dd, *J* = 16.6, 6.3 Hz, 1H), 3.22 (dd, *J* = 16.6, 3.4 Hz, 1H); <sup>13</sup>C NMR (100 MHz, CDCl<sub>3</sub>) δ 161.9 (d, *J* = 247.2 Hz), 157.5, 142.7, 136.0 (d, *J* = 6.8 Hz), 131.0 (d, *J* = 7.9 Hz), 130.3 (q, *J* = 32.6 Hz), 128.4 (d, *J* = 3.3 Hz, 1H), 127.5, 125.9 (q, *J* = 3.7 Hz), 124.0 (q, *J* = 271.0 Hz), 115.7 (d, *J* = 21.3 Hz), 111.5 (d, *J* = 22.4 Hz), 68.3, 51.9 (d, *J* = 2.2 Hz), 51.5, 30.8; <sup>19</sup>F NMR (282 MHz, CDCl<sub>3</sub>) δ -62.7, -113.7 – -113.8 (m); IR (Neat Film, NaCl) 2921, 1754, 1620, 1594, 1500, 1402, 1326, 1241, 1162, 1115, 1068, 1018, 839, 759 cm<sup>-1</sup>; HRMS (MM:ESI-APCI+) *m/z* calc'd for C<sub>18</sub>H<sub>14</sub>F<sub>4</sub>NO<sub>2</sub> [M+H]<sup>+</sup>: 352.0955, found 352.0954; SFC Conditions: 40% MeOH, 3.5 mL/min, Chiralpak IC column, λ = 210 nm, *t<sub>r</sub>* (min): minor = 1.43, major = 1.60.

### 3.7.2.4 Product transformations

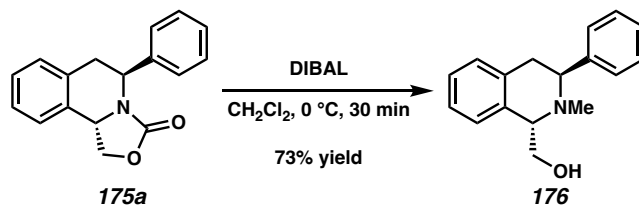


#### ((1*S*,3*S*)-3-phenyl-1,2,3,4-tetrahydroisoquinolin-1-yl)methanol (**174**):

This procedure has been adapted from a previous report.<sup>27</sup> To a 1-dram vial equipped with a stir bar was added a solution of tetrahydroisoquinoline **175a** (4.4 mg, 0.02 mmol) in 1:1 1,4-dioxane:H<sub>2</sub>O (0.4 mL total, 0.05 M). Barium hydroxide octahydrate (24 mg, 4.1 equiv, 0.07 mmol) was then added and the vial was capped with a PTFE-lined septum and sealed with



electrical tape. The reaction mixture was heated to 120 °C and stirred for 3 hours until TLC analysis indicated complete consumption of the starting material. The reaction was then diluted with H<sub>2</sub>O, extracted with EtOAc, and the collected organic layers were dried over Na<sub>2</sub>SO<sub>4</sub> and concentrated under vacuum. The crude product was purified by column chromatography (50% EtOAc in hexanes + 1% NEt<sub>3</sub>) to afford **174** as a white solid (3.2 mg, 81% yield): [ $\alpha$ ]<sub>D</sub><sup>25</sup> –8.3 (*c* 0.15, CHCl<sub>3</sub>); <sup>1</sup>H NMR (400 MHz, CDCl<sub>3</sub>)  $\delta$  7.47 – 7.44 (m, 2H), 7.42 – 7.38 (m, 2H), 7.33 – 7.29 (m, 1H), 7.22 – 7.18 (m, 2H), 7.17 – 7.13 (m, 2H), 4.23 (dd, *J* = 10.6, 4.8 Hz, 1H), 4.15 (dd, *J* = 11.2, 3.9 Hz, 1H), 3.80 (dd, *J* = 10.8, 4.8 Hz, 1H), 3.71 (t, *J* = 10.7 Hz, 1H), 3.07 (dd, *J* = 16.4, 3.9 Hz, 1H), 2.95 (dd, *J* = 16.3, 11.2 Hz, 1H); <sup>13</sup>C NMR (100 MHz, CDCl<sub>3</sub>)  $\delta$  143.5, 135.5, 134.7, 129.5, 128.8, 127.5, 127.0, 126.7, 126.6, 126.4, 63.8, 57.4, 50.7, 36.8; IR (Neat Film, NaCl) 3411, 2357, 2086, 1733, 1716, 1700, 1652, 1558, 1540, 1457, 678 cm<sup>-1</sup>; HRMS (MM:ESI-APCI+) *m/z* calc'd for C<sub>16</sub>H<sub>18</sub>NO [M+H]<sup>+</sup>: 240.1388, found 240.1387.

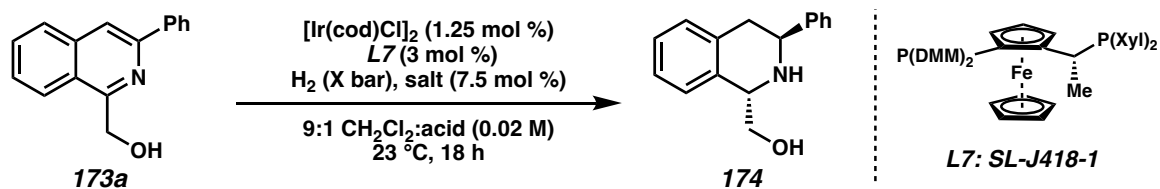


**((1*S*,3*S*)-2-methyl-3-phenyl-1,2,3,4-tetrahydroisoquinolin-1-yl)methanol (**176**):**

This procedure has been adapted from a previous report.<sup>28</sup> To a 1-dram vial equipped with a stir bar was added a solution of tetrahydroisoquinoline **5a** (5.0 mg, 0.02 mmol) in CH<sub>2</sub>Cl<sub>2</sub> (0.4 mL, 0.05 M). The reaction mixture was cooled to 0 °C, and a solution of DIBAL (1.0 M in THF, 0.38 mL, 0.2 mmol) was added dropwise. After stirring for 1 hour, the reaction mixture showed complete consumption of starting material by TLC, and was quenched with MeOH, H<sub>2</sub>O, and saturated aqueous Rochelle's salt and stirred for an additional hour. The

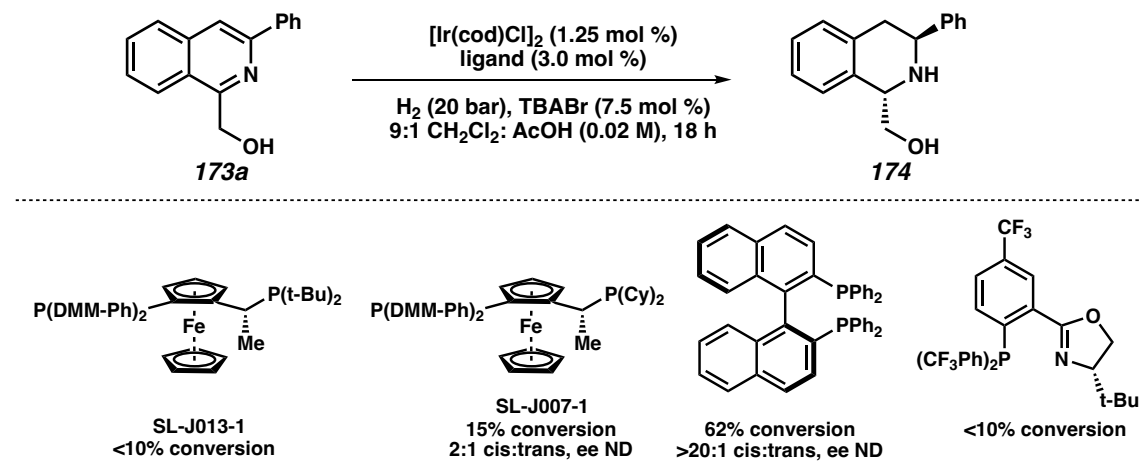
reaction was then diluted with H<sub>2</sub>O, extracted with CH<sub>2</sub>Cl<sub>2</sub> (2 x 5 mL), and the collected organic layers were dried over Na<sub>2</sub>SO<sub>4</sub> and concentrated under vacuum. The crude product was purified by column chromatography (30% EtOAc in hexanes) to afford **6a** as a clear oil (3.5 mg, 73% yield): [ $\alpha$ ]<sub>D</sub><sup>25</sup> +115.8 (*c* 0.50, CHCl<sub>3</sub>); <sup>1</sup>H NMR (400 MHz, CDCl<sub>3</sub>)  $\delta$  7.47 – 7.45 (m, 2H), 7.42 – 7.38 (m, 2H), 7.33 – 7.29 (m, 1H), 7.25 – 7.22 (m, 3H), 7.17 – 7.13 (m, 1H), 4.34 (dd, *J* = 12.2, 4.0 Hz, 1H), 3.93 (dd, *J* = 10.5, 5.3 Hz, 1H), 3.81 (dd, *J* = 10.8, 5.3 Hz, 1H), 3.72 (t, *J* = 10.6 Hz, 1H), 3.37 (dd, *J* = 16.5, 12.2 Hz, 1H), 2.92 (dd, *J* = 16.5, 4.0 Hz, 1H), 2.21 (s, 3H); <sup>13</sup>C NMR (100 MHz, CDCl<sub>3</sub>)  $\delta$  140.9, 134.5, 133.7, 129.5, 128.5, 127.9, 127.8, 127.4, 126.9, 126.7, 65.8, 63.4, 53.2, 35.7, 25.1; IR (Neat Film, NaCl) 3423, 3058, 3024, 2918, 2854, 2366, 1496, 1450, 1406, 1222, 1130, 1044, 774, 752, 699 cm<sup>-1</sup>; HRMS (MM:ESI-APCI+) *m/z* calc'd for C<sub>17</sub>H<sub>20</sub>NO [M+H]<sup>+</sup>: 254.1545, found 254.1543.

### 3.7.3 Additional optimization results

**Table 3.3.** Additional additive, acid, and pressure studies.<sup>a</sup>

entry	salt additive	acid	pressure	% conversion <sup>b</sup>	cis:trans <sup>b</sup>	% ee of trans <sup>c</sup>
1	TBACl	AcOH	20 bar	75	1:2.3	90
2	TBAI	AcOH	20 bar	>95	1.5:1	97
3	TBAPF <sub>6</sub>	AcOH	20 bar	<10	–	–
4	TBABF <sub>4</sub>	AcOH	20 bar	<10	–	–
5	TBABPh <sub>4</sub>	AcOH	20 bar	<10	–	–
6	LiBr	AcOH	20 bar	>95	1:2.3	91
7	NaBr	AcOH	20 bar	90	1:2.3	89
8	KBr	AcOH	20 bar	35	1:2.4	86
9	TBABr	TFA	20 bar	<10	–	–
10	TBABr	MsOH	20 bar	<10	–	–
11	TBABr	AcOH	10 bar	>95	1:2.3	91
12	TBABr	AcOH	60 bar	>95	1:2.6	93

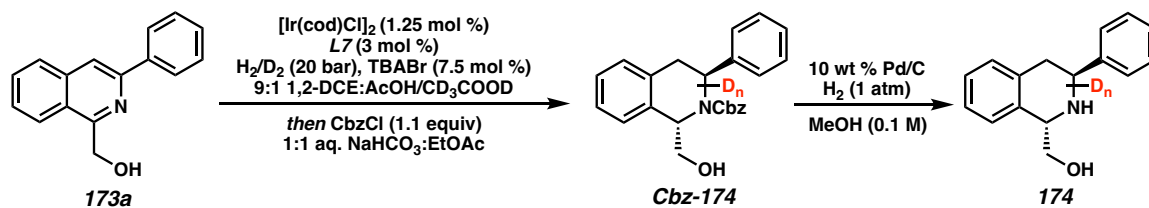
[a] Reaction conditions: 0.04 mmol of **173a**, 1.25 mol %  $[\text{Ir}(\text{cod})\text{Cl}]_2$ , 3 mol % ligand, 7.5 mol % salt additive, 20 bar  $\text{H}_2$  in 0.5 mL 9:1  $\text{CH}_2\text{Cl}_2$ :acid. [b] Determined by crude  $^1\text{H}$  NMR using 1,3,5-trimethoxybenzene as a standard. [c] Determined by chiral SFC analysis of Cbz-protected product.

**Table 3.4.** Additional ligand screen.<sup>a</sup>

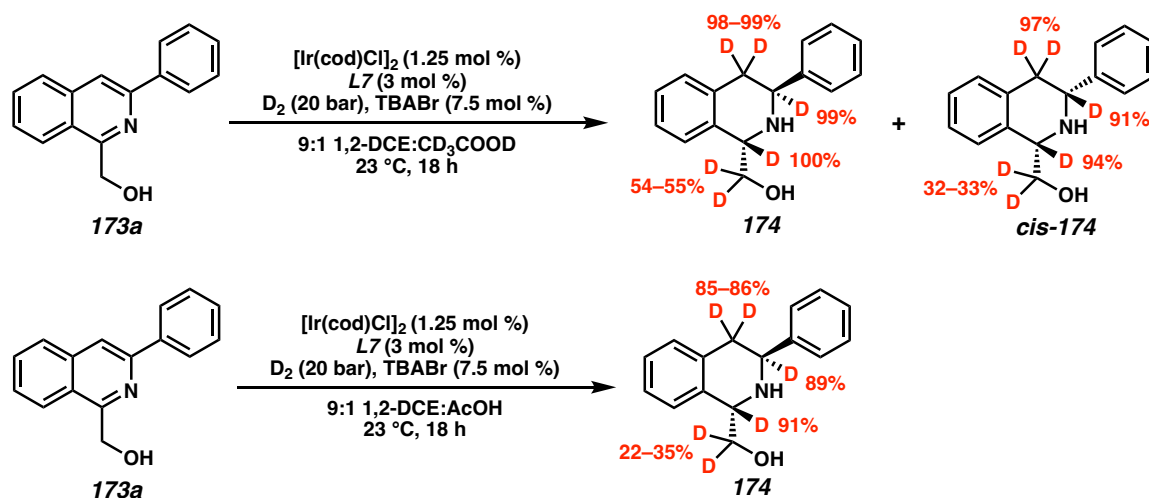
[a] Reaction conditions: 0.04 mmol of **173a**, 1.25 mol %  $[\text{Ir}(\text{cod})\text{Cl}]_2$ , 3 mol % ligand, 7.5 mol % TBABr, 20 bar  $\text{H}_2$  in 0.5 mL 9:1  $\text{CH}_2\text{Cl}_2$ :AcOH. Determined by crude  $^1\text{H}$  NMR using 1,3,5-trimethoxybenzene as a standard.

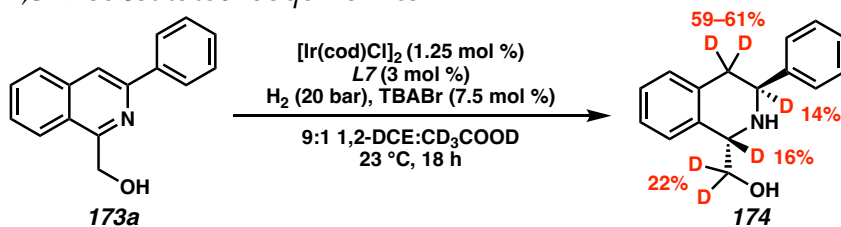
### 3.7.4 Deuterium incorporation experiments

Deuterium experiments were conducted according to general procedure 5 for the hydrogenation of isoquinoline **173a** using deuterium gas instead of hydrogen gas, and/or *d*<sub>4</sub>-AcOH instead of protio acetic acid.



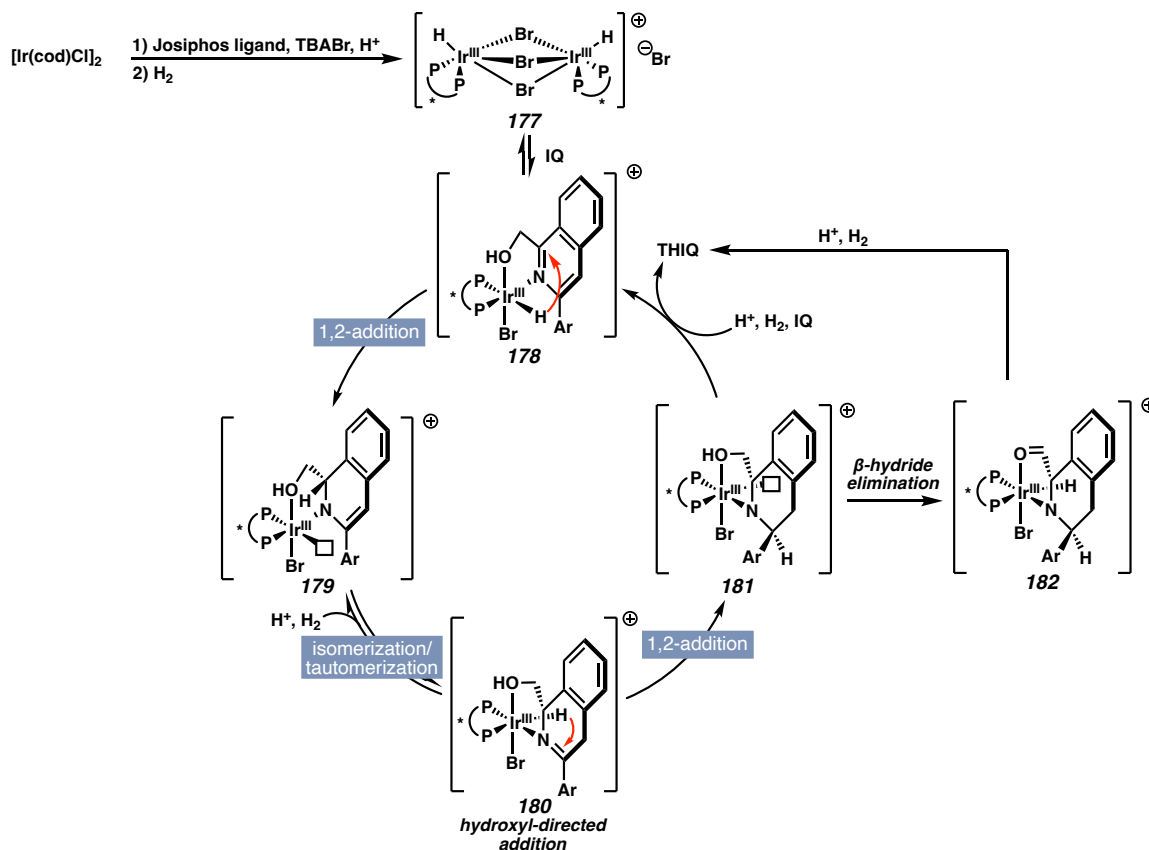
Due to the inseparable nature of the *cis*- and *trans*-diastereomers, the hydrogenated products were subsequently protected with benzyl chloroformate (6.3  $\mu\text{L}$ , 0.044 mmol, 1.1 equiv) in 1:1 saturated aq.  $\text{NaHCO}_3$  and EtOAc (1 mL total). After the reaction showed full conversion of the hydrogenated product, the crude reaction mixture was washed with ethyl acetate and the collected organic layers were dried over  $\text{Na}_2\text{SO}_4$  and concentrated under vacuum. Both the *cis*- and *trans*-isomers were isolated by preparative TLC (40% EtOAc in hexanes) of the Cbz-protected THIQ, then subsequently deprotected using 10 wt% Pd/C catalyst (1 mg) under a  $\text{H}_2$  balloon in MeOH (0.1 M) to afford deuterium-labelled **174**. The major *trans*-isomer was analyzed by  $^1\text{H}$  and  $^2\text{H}$  NMR spectroscopy.





### 3.7.5 Proposed catalytic cycle

Figure 3.2 Proposed catalytic cycle.

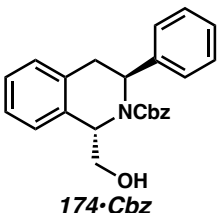
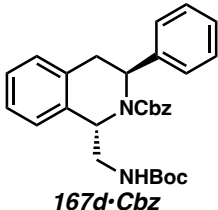


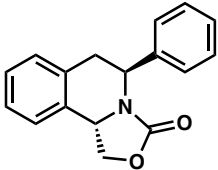
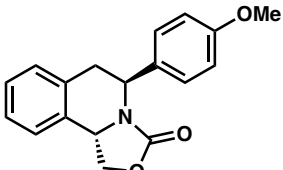
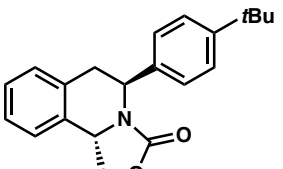
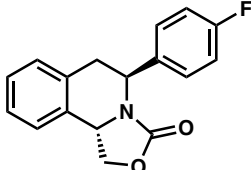
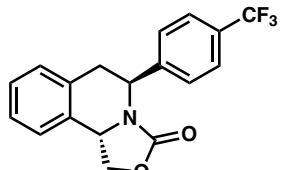
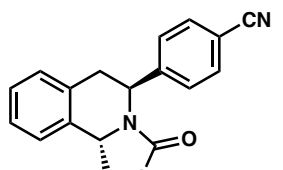
Based on preliminary mechanistic studies and literature precedent, a proposed catalytic cycle for the *trans*-selective asymmetric hydrogenation is described. Pre-formation of the chiral catalyst using  $[\text{Ir}(\text{cod})\text{Cl}]_2$ , chiral ligand, and TBABr, followed by oxidative addition with  $\text{H}_2$  delivers the halogen-bridged dinuclear  $\text{Ir}^{\text{III}}$  catalyst complex **177**. Without the halide, the iridium bisphosphane catalysts tend to irreversibly form dimeric iridium hydride complexes that are catalytically inactive.<sup>10c</sup> Addition of the isoquinoline substrate

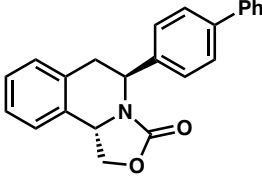
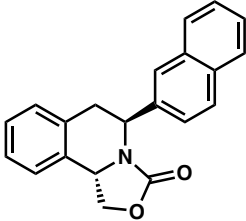
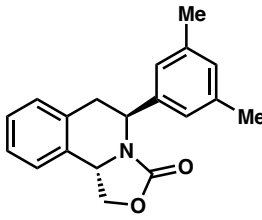
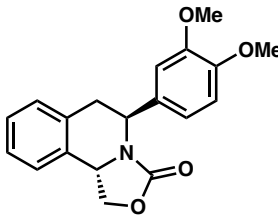
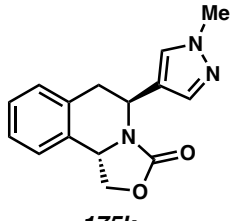
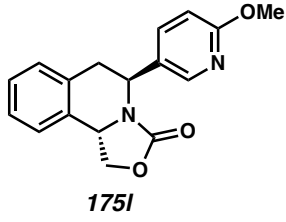
then undergoes bidentate coordination to the metal to generate the corresponding mononuclear Ir<sup>III</sup> complex **178**, followed by a 1,2-hydride addition to establish the C1-stereocenter (**179**).<sup>19</sup> Isomerization and tautomerization of the substrate then enables a directed hydrogenation (**180**) guided by the hydroxymethyl group to deliver the hydride on the opposite face of the molecule. The addition of H<sub>2</sub> in the presence of acid regenerates the catalyst species and liberates the enantioenriched *trans*-THIQ product. Alternatively, based on our deuterium experiments, β-hydride elimination can also proceed from intermediate **181** to generate aldehyde intermediate **182**, which is subsequently reduced to provide the same THIQ product. However, the possibility of β-hydride elimination occurring at other intermediates still cannot be ruled out, and further investigations of the mechanism are currently underway.

### 3.7.6 Determination of enantiomeric excess

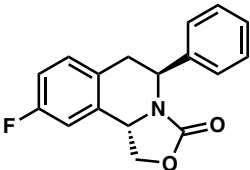
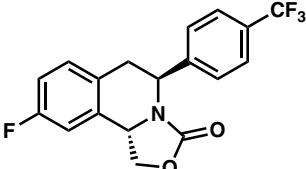
**Table 3.5.** Determination of enantiomeric excess.

entry	compound	SFC analytic conditions	ee (%)
1	 <p><b>174-Cbz</b></p>	Chiralpak AD-H, λ = 210 nm 45% IPA/CO <sub>2</sub> , 3.5 mL/min t <sub>R</sub> (min) major 1.69, minor 2.04	92
2	 <p><b>167d-Cbz</b></p>	Chiralpak AD-H, λ = 210 nm 30% IPA/CO <sub>2</sub> , 2.5 mL/min t <sub>R</sub> (min) major 1.95, minor 4.28	25

entry	compound	SFC analytic conditions	ee (%)
3	 <b>175a</b>	Chiralpak IC, $\lambda = 210$ nm 40% MeOH/CO <sub>2</sub> , 3.5 mL/min $t_R$ (min) minor 2.41, major 2.61	91
4	 <b>175b</b>	Chiralcel OJ-H, $\lambda = 210$ nm 10% MeOH/CO <sub>2</sub> , 3.5 mL/min $t_R$ (min) minor 7.52, major 8.66	96
5	 <b>175c</b>	Chiralpak AD-H, $\lambda = 210$ nm 20% MeOH/CO <sub>2</sub> , 3.5 mL/min $t_R$ (min) major 5.04, minor 5.44	95
6	 <b>175d</b>	Chiralpak IC, $\lambda = 210$ nm 35% MeOH/CO <sub>2</sub> , 3.5 mL/min $t_R$ (min) minor 2.39, major 2.58	95
7	 <b>175e</b>	Chiralpak IC, $\lambda = 210$ nm 25% MeOH/CO <sub>2</sub> , 3.5 mL/min $t_R$ (min) minor 2.22, major 2.37	91
8	 <b>175f</b>	Chiralpak IC, $\lambda = 210$ nm 40% MeOH/CO <sub>2</sub> , 3.5 mL/min $t_R$ (min) minor 3.97, major 4.48	83

entry	compound	SFC analytic conditions	ee (%)
9	 <b>175g</b>	Chiralcel OJ-H, $\lambda = 210$ nm 45% MeOH/CO <sub>2</sub> , 3.5 mL/min $t_R$ (min) minor 5.72, major 6.80	75
10	 <b>175h</b>	Chiralpak IC, $\lambda = 210$ nm 40% MeOH/CO <sub>2</sub> , 3.5 mL/min $t_R$ (min) minor 4.21, major 4.61	89
11	 <b>175i</b>	Chiralpak IC, $\lambda = 210$ nm 40% MeOH/CO <sub>2</sub> , 3.5 mL/min $t_R$ (min) minor 2.47, major 2.71	86
12	 <b>175j</b>	Chiralpak AD-H, $\lambda = 210$ nm 40% MeOH/CO <sub>2</sub> , 3.5 mL/min $t_R$ (min) major 2.13, minor 2.74	87
13	 <b>175k</b>	Chiralpak AD-H, $\lambda = 210$ nm 40% MeOH/CO <sub>2</sub> , 3.5 mL/min $t_R$ (min) minor 2.24, major 2.67	97
14	 <b>175l</b>	Chiralpak AD-H, $\lambda = 210$ nm 40% MeOH/CO <sub>2</sub> , 3.5 mL/min $t_R$ (min) minor 2.80, minor 3.30	95



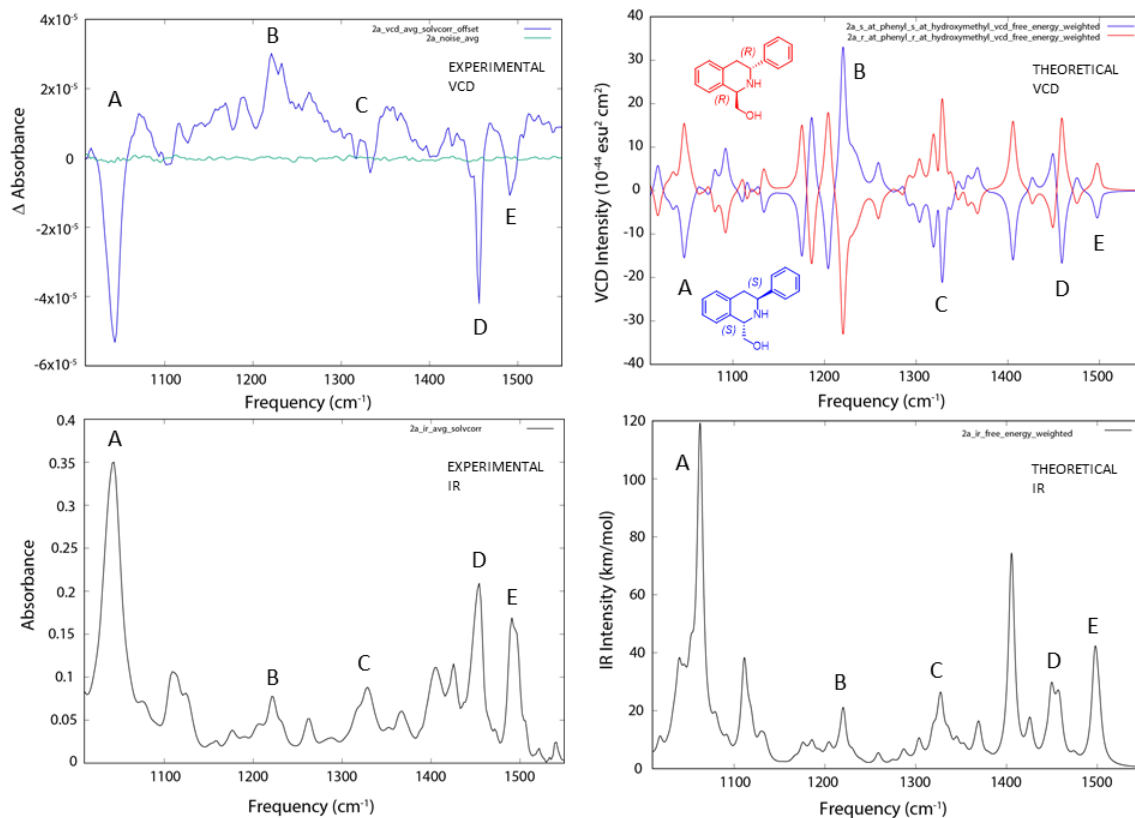
entry	compound	SFC analytic conditions	ee (%)
15	 <b>175m</b>	Chiralpak IC, $\lambda = 210$ nm 40% MeOH/CO <sub>2</sub> , 3.5 mL/min t <sub>R</sub> (min) minor 2.09, major 2.53	95
16	 <b>175n</b>	Chiralpak IC, $\lambda = 210$ nm 40% MeOH/CO <sub>2</sub> , 3.5 mL/min t <sub>R</sub> (min) minor 1.43, major 1.60	92

### 3.7.7 Determination of relative and absolute stereochemistry

**Experimental Protocol.** A solution of the isolated *trans* isomer of **174** (11 mg) was prepared in CDCl<sub>3</sub> (225  $\mu$ L; 49 mg/mL) and loaded into a front-loading SL-4 cell (International Crystal Laboratories) possessing BaF<sub>2</sub> windows and 100  $\mu$ m path length. Infrared (IR) and VCD spectra were acquired on a BioTools ChiralIR-2X VCD spectrometer as a set of 30 one-hour blocks (30 blocks, 3120 scans per block) at 4 cm<sup>-1</sup> resolution in dual PEM mode. A 15-minute acquisition of neat (-)- $\alpha$ -pinene control (separate 75  $\mu$ m BaF<sub>2</sub> cell) yielded a VCD spectrum in agreement with literature spectra and identical to those previously acquired on the same instrument. IR and VCD spectra were background corrected using a 30-minute block IR acquisition of the empty instrument chamber under gentle N<sub>2</sub> purge, and were solvent corrected using a 6-hour (6 blocks, 3120 scans per block) IR/VCD acquisition of CDCl<sub>3</sub> in the same 100  $\mu$ m BaF<sub>2</sub> cell as used for **174**. The reported spectra represent the result of block averaging. The baseline of the resultant VCD spectrum (top left panel below) was vertically offset by a constant such that the y-value was zero at a frequency of 1000 cm<sup>-1</sup> for ease of viewing and assignment.

**Computational Protocol.** The arbitrarily chosen (*R,R*) enantiomer of **174** (ultimately corresponding to *ent*-**174**) was subjected to an initial exhaustive stochastic molecular mechanics-based conformational search (MMFF94 force field, 0.06 Å geometric RMSD cutoff, and 30 kcal/mol energy window) as implemented in MOE 2019.0102 (Chemical Computing Group, Montreal, CA). All conformers retained the (*R,R*) configuration and were subjected to geometry optimization, harmonic frequency calculation, and VCD rotational strength evaluation using density functional theory utilizing the B3PW91 functional, cc-pVTZ basis, and implicit IEFPCM chloroform solvation model. All calculations were performed with the *Gaussian 16* program system (Rev. C.01; Frisch *et al.*, Gaussian, Inc., Wallingford, CT). Resultant IEFPCM-B3PW91/cc-pVTZ harmonic frequencies were scaled by 0.98. All structurally unique conformers possessing all positive Hessian eigenvalues were Boltzmann weighted by relative free energy at 298.15 K. The predicted IR and VCD frequencies and intensities of the retained conformers were convolved using Lorentzian line shapes ( $\gamma = 4 \text{ cm}^{-1}$ ) and summed using the respective Boltzmann weights to yield the final predicted IR and VCD spectra. The predicted VCD spectrum of the (*S,S*) enantiomer (ultimately agreeing with the experimentally measured spectrum of isolated **174**) was generated by inversion of sign. From alignment of the experimentally measured and theoretical IR spectra, in particular regions **A-E** corresponding to unambiguous regions of the experimental VCD spectrum (see below) the absolute configuration of the isolated and measured **174** could be confidently assigned as (*S,S*).

**Figure 3.3** Experimental (left) and theoretical (right) IR and VCD spectra of **174**.



### 3.8 REFERENCES AND NOTES

- (1) For recent reviews of asymmetric hydrogenation of heteroarenes, see: a) Wang, D.-S.; Chen, Q.-A.; Lu, S.-M.; Zhou, Y.-G. *Chem. Rev.* **2012**, *112*, 2557–2590; b) Zhou, Y.-G. *Acc. Chem. Res.* **2007**, *40*, 1357–1366; c) Zhao, D.; Glorius, F. *Angew. Chem. Int. Ed.* **2013**, *52*, 9616–9618; d) Kim, A. N.; Stoltz, B. M. *ACS Catal.* **2020**, *10*, 13834–13851; e) Luo, Y.-E.; He, Y.-M.; Fan, Q.-H. *Chem. Rec.* **2016**, *16*, 2697–2711; f) Fleury-Brégeot, N.; de la Fuente, V.; Castellón, S.; Claver, C. *ChemCatChem* **2010**, *2*, 1346–1371.

- (2) For recent reviews of asymmetric C=N bond hydrogenation, see: a) Cabré, A.; Verdaguer, X.; Riera, A.; *Chem. Rev.* **2022**, *122*, 269–339; b) Abed Ali Abdine, R.; Hedouin, G.; Colobert, F.; Wencel-Delord, J. *ACS Catal.* **2021**, *11*, 215–247; c) Molina Betancourt, R.; Echeverria, P.-G.; Ayad, T.; Phansavath, P.; Ratovelomanana-Vidal, V. *Synthesis* **2021**, *53*, 30–50; d) Barrios-Rivera, J.; Xu, Y.; Wills, M.; Vyas, V. K. *Org. Chem. Front.* **2020**, *7*, 3312–3342; e) Liu, Y.; Yue, X.; Luo, C.; Zhang, L.; Lei, M. *Energy Environ. Mater.* **2019**, *2*, 292–312.
- (3) Wiesenfeldt, M.P.; Nairoukh, Z.; Dalton, T.; Glorius, F. *Angew. Chem. Int. Ed.* **2019**, *58*, 10460–10476.
- (4) Gelis, C.; Heusler, A.; Nairoukh, Z.; Glorius, F. *Chem. Eur. J.* **2020**, *26*, 14090–14094.
- (5) For examples of *trans*-selective arene hydrogenation, see: a) Wollenburg, M.; Heusler, A.; Bergander, K.; Glorius, F. *ACS Catal.* **2020**, *10*, 11365–11370; b) Murugesan, K.; Senthamarai, T.; Alshammari, A. S.; Altamimi, R. M.; Kreyenschulte, C.; Pohl, M.-M.; Lund, H.; Jagadeesh, R. V.; Beller, M. *ACS Catal.* **2019**, *9*, 8581–8591; c) Li, H.; Wang, Y.; Lai, Z.; Huang, K.-W. *ACS Catal.* **2017**, *7*, 4446–4450; d) Tungler, A.; Szabados, E. *Org. Process. Res. Dev.* **2016**, *20*, 1246–1251; e) Maegawa, T.; Akashi, A.; Yaguchi, K.; Iwasaki, Y.; Shigetsura, M.; Monguchi, Y.; Sajiki, H. *Chem.-Eur. J.* **2009**, *15*, 6953–6963; f) Jansat, S.; Picurelli, D.; Pelzer, K.; Philippot, K.; Gómez, M.; Muller, G.; Lecante, P.; Chaudret, B. *New J. Chem.* **2006**, *30*, 115–122.

- (6) For an example of a sequential enantioselective hydrogenation to access the *trans*-diastereomer of product, see: Wiesenfeldt, M. P.; Moock, D.; Paul, D.; Glorius, F. *Chem. Sci.* **2021**, *12*, 5611–5615.
- (7) a) Matsuda, H.; Ninomiya, K.; Shimoda, H.; Nishida, N.; Yoshikawa, M. *Heterocycles* **2001**, *55*, 2043–2050; b) Rochfort, S. J.; Towerzey, L.; Carroll, A.; King, G.; Michael, A.; Pierens, G.; Rali, T.; Redburn, J.; Whitmore, J.; Quinn, R. J. *J. Nat. Prod.* **2005**, *68*, 1080–1082.
- (8) For recent total syntheses of *trans*-THIQ natural products, see: a) Uenishi, S.; Kakigi, R.; Hideshima, K.; Miyawaki, A.; Matsuoka, J.; Ogata, T.; Tomioka, K.; Yamamoto, Y. *Tetrahedron* **2021**, *90*, 132165–132176; b) J. Kayhan, M. J. Wanner, S. Ingemann, J. H. van Maarseveen and H. Hiemstra, *Eur. J. Org. Chem.* **2016**, 3705–3708.
- (9) a) Kim, A. N.; Ngamnithiporn, A.; Welin, E. R.; Daiger, M. T.; Grünanger, C. U.; Bartberger, M. D.; Virgil, S. C.; Stoltz, B. M. *ACS Catal.* **2020**, *10*, 3241–3248; b) Welin, E. R.; Ngamnithiporn, A.; Klatte, M.; Lapointe, G.; Pototschnig, G. M.; McDermott, M. S. J.; Conklin, D.; Gilmore, C. D.; Tadross, P. M.; Haley, C. K.; Negoro, K.; Glibstrup, E.; Grünanger, C.; Allan, K. M.; Virgil, S. C.; Slamon, D. J. Stoltz, B. M. *Science* **2019**, *363*, 270–275.
- (10) For recent reports of Ir-catalyzed asymmetric hydrogenation of 1,3-disubstituted isoquinolines, see: a) Chen, M.-W.; Ji, Y.; Wang, J.; Chen, Q.-A.; Shi, L.; Zhou, Y.-G. *Org. Lett.* **2017**, *19*, 4988–4991; b) Wen, J.; Tan, R.; Liu, S.; Zhao, Q.; Zhang, X. *Chem. Sci.* **2016**, *7*, 3047–3051; c) Kita, Y.; Yamaji, K.; Higashida, K.; Sathaiah, K.; Iimuro, A.; Mashima, K. *Chem. Eur. J.* **2015**, *21*, 1915–1927.

- (11) The absolute configuration of the *trans*-diastereomer was assigned as (*S,S*) by VCD, see Section 3.7.7.
- (12) Smidt, S. P.; Zimmermann, N.; Studer, M.; Pfaltz, A. *Chem. Eur. J.* **2004**, *10*, 4685–4693.
- (13) Attempts to further improve the diastereoselectivity were unsuccessful, see Tables 3.3–3.4.
- (14) The absolute stereochemistry for all other hydrogenated products were assigned by analogy to **175a**.
- (15) Attempts to prepare 3-alkyl substituted isoquinolines were unsuccessful.
- (16) Liu, C.-Y.; Angamuthu, V.; Chen, W.-C.; Hou, D.-R. *Org. Lett.* **2020**, *22*, 2246–2250.
- (17) Cbz-protected **174** was obtained in 91% ee, ruling out any racemization occurring in the reaction.
- (18) Fagnou, K.; Lautens, M. *Angew. Chem. Int. Ed.* **2002**, *41*, 26–47.
- (19) Dorta, R.; Brogini, D.; Stoop, R.; Rügger, H.; Spindler, F.; Togni, A. *Chem. Eur. J.* **2004**, *10*, 267–278.
- (20) Díaz-Torres, R.; Alvarez, S. *Dalton. Trans.* **2011**, *40*, 10742–10750.
- (21) a) Jiménez, M. V.; Fernández-Tornos, J.; Modrego, F. J.; Pérez-Torrente, J. J.; Oro, L. A. *Chem. Eur. J.* **2015**, *21*, 17877–17889; b) Blum, O.; Milstein, D. *J. Am. Chem. Soc.* **1995**, *117*, 4582–4594.
- (22) The same deuterium experiment under the *cis*-selective hydrogenation conditions demonstrates no deuteration at the methylene carbon of **173a**, ruling out an alternative tautomerization mechanism.

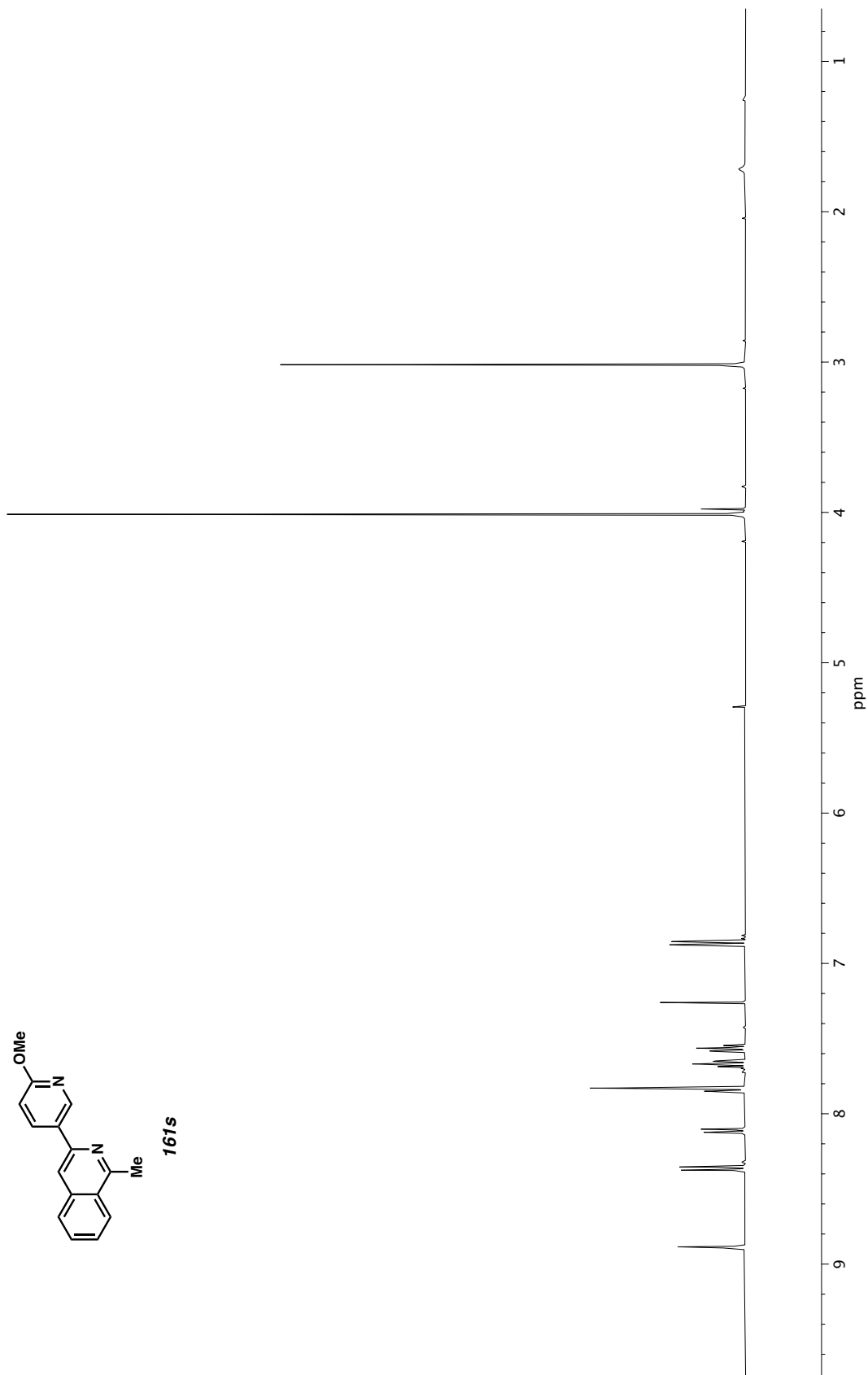
- (23) a) Liu, H.; Wang, W.-H.; Xiong, H.; Nijamudheen, A.; Ertem, M. Z.; Wang, M.; Duan, L. *Inorg. Chem.* **2021**, *60*, 3410–3417; b) Klei, S. R.; Golden, J. T.; Tilley, T. D.; Bergman, R. G. *J. Am. Chem. Soc.* **2002**, *124*, 2092–2093.
- (24) A proposed catalytic cycle is described in the Supporting Information, see Figure 3.1.
- (25) Pangborn, A. M.; Giardello, M. A.; Grubbs, R. H.; Rosen, R. K.; Timmers, F. J. *Organometallics* **1996**, *15*, 1518–1520.
- (26) Legault, C. Y.; Charette, A. B. *J. Am. Chem. Soc.* **2005**, *127*, 8966–8967.
- (27) Liu, C.-Y.; Angamuthu, V.; Chen, W.-C.; Hou, D.-R. *Org. Lett.* **2020**, *22*, 2246–2250.
- (28) Butora, G.; Hudlicky, T.; Fearnley, S. P.; Gum, A. G.; Stabile, M. R.; Abboud, K. *Tetrahedron Lett.* **1996**, *37*, 8155–8158.

## **APPENDIX 3**

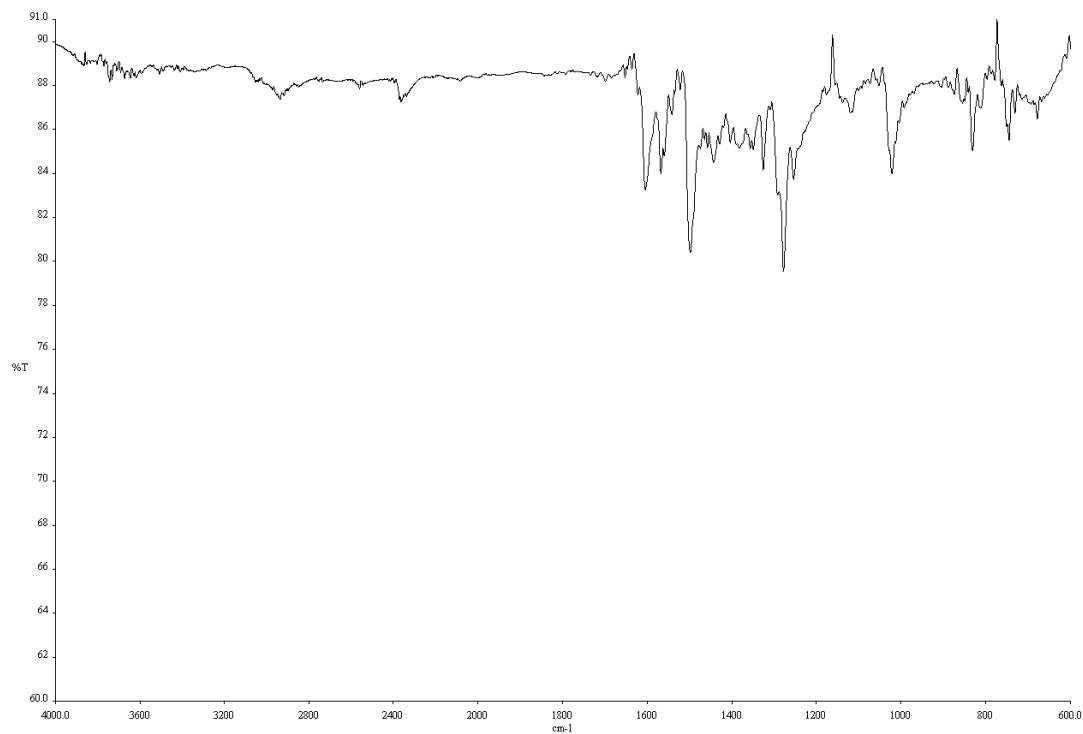
*Spectra Relevant to Chapter 3:*

*Iridium-Catalyzed Asymmetric Trans-Selective  
Hydrogenation of 1,3-Disubstituted Isoquinolines*

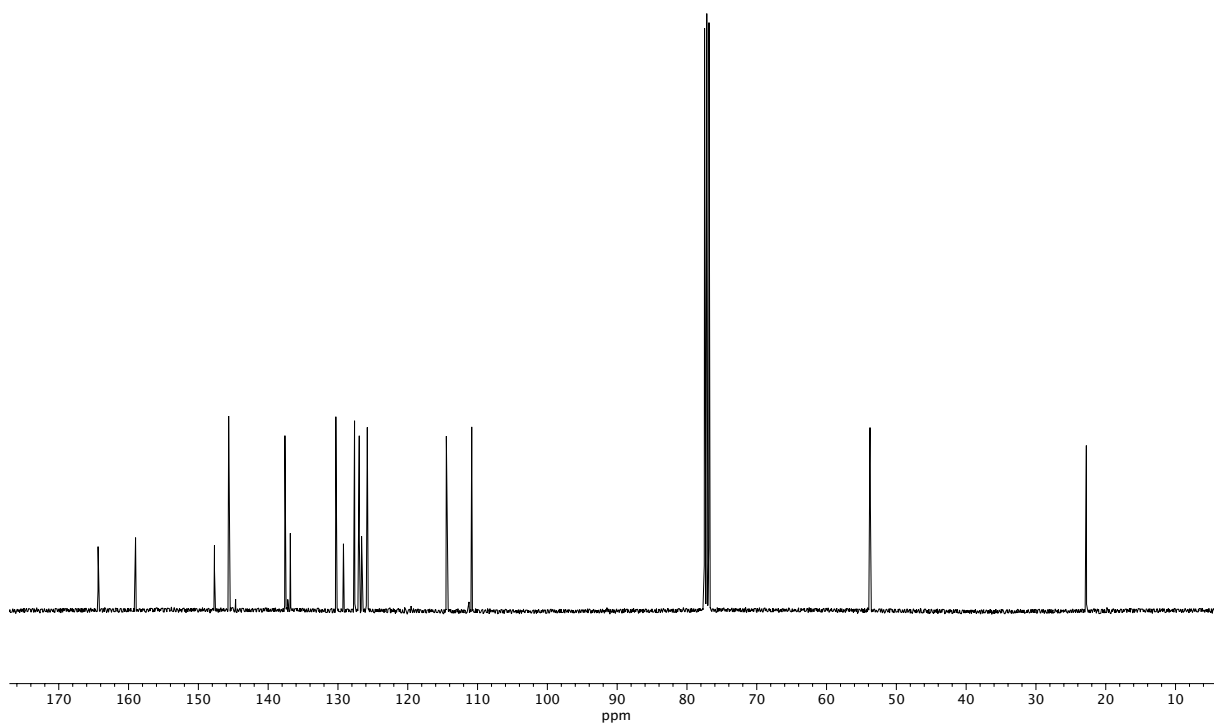




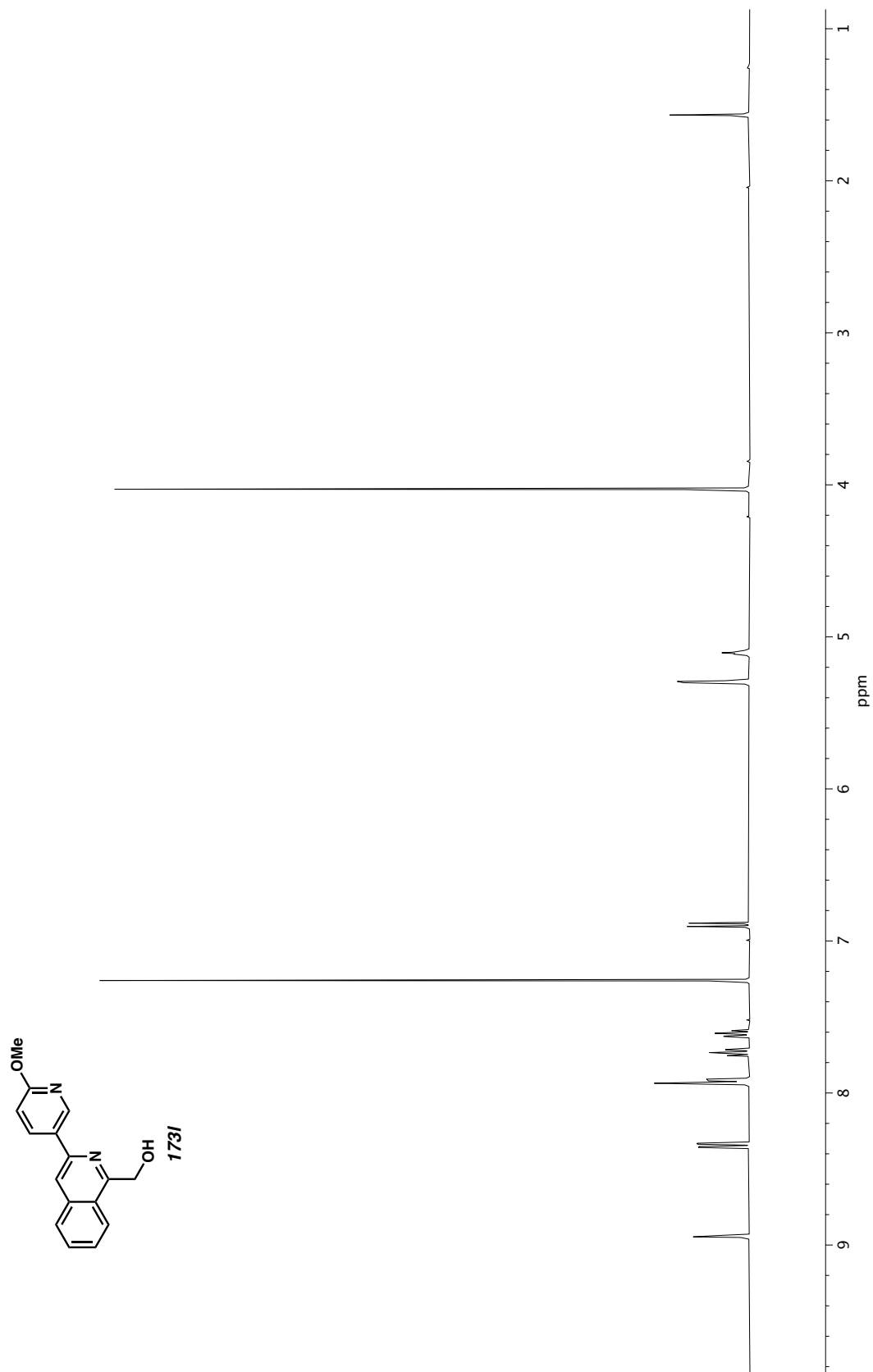
**Figure A3.1** <sup>1</sup>H NMR (400 MHz, CDCl<sub>3</sub>) of compound **161s**.



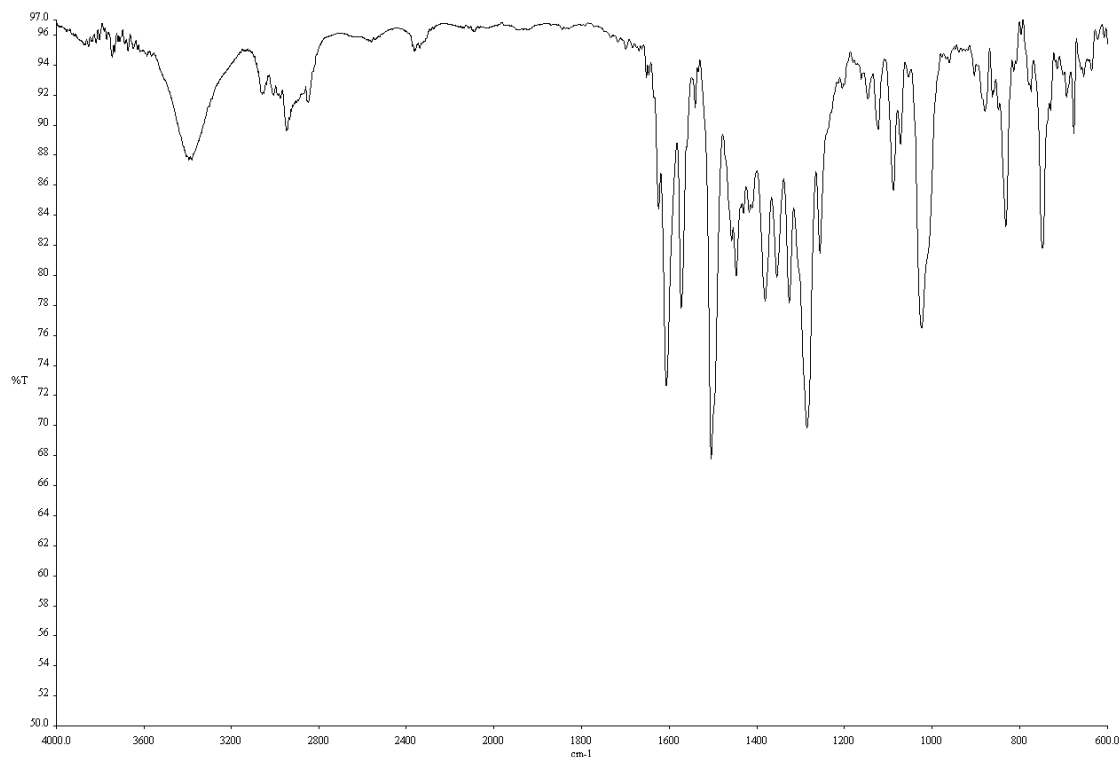
**Figure A3.2** Infrared spectrum (Thin Film, NaCl) of compound **161s**.



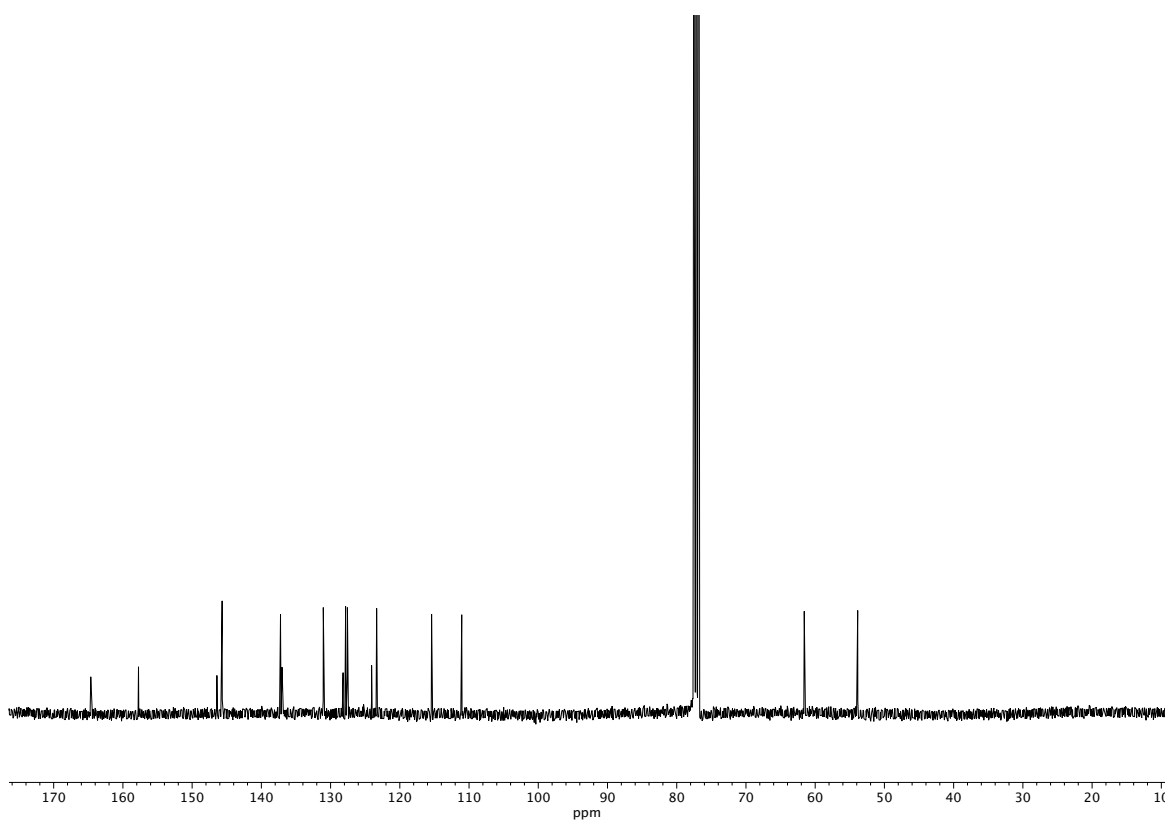
**Figure A3.3** <sup>13</sup>C NMR (100 MHz, CDCl<sub>3</sub>) of compound **161s**.



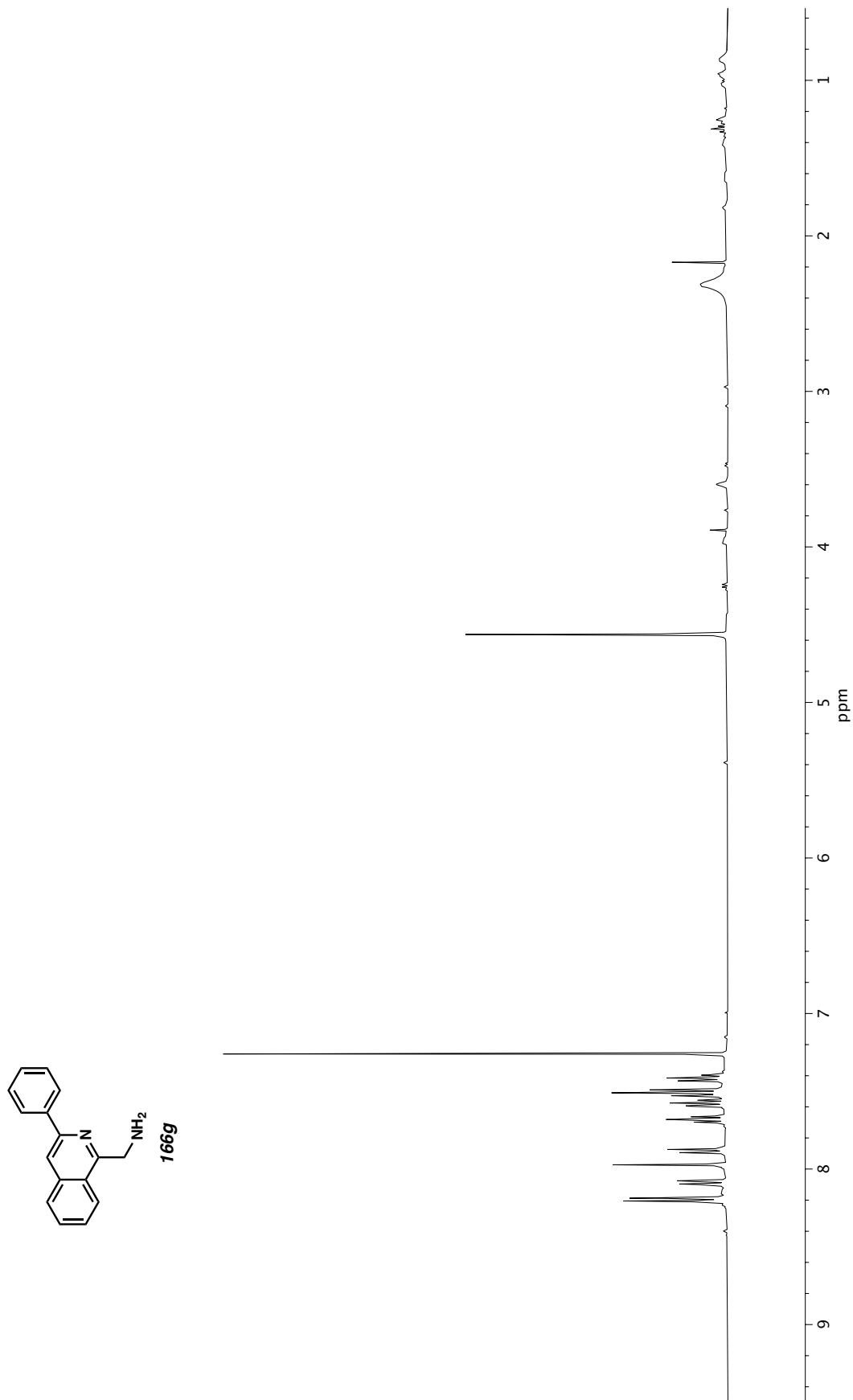
**Figure A3.4** <sup>1</sup>H NMR (400 MHz, CDCl<sub>3</sub>) of compound **173I**.



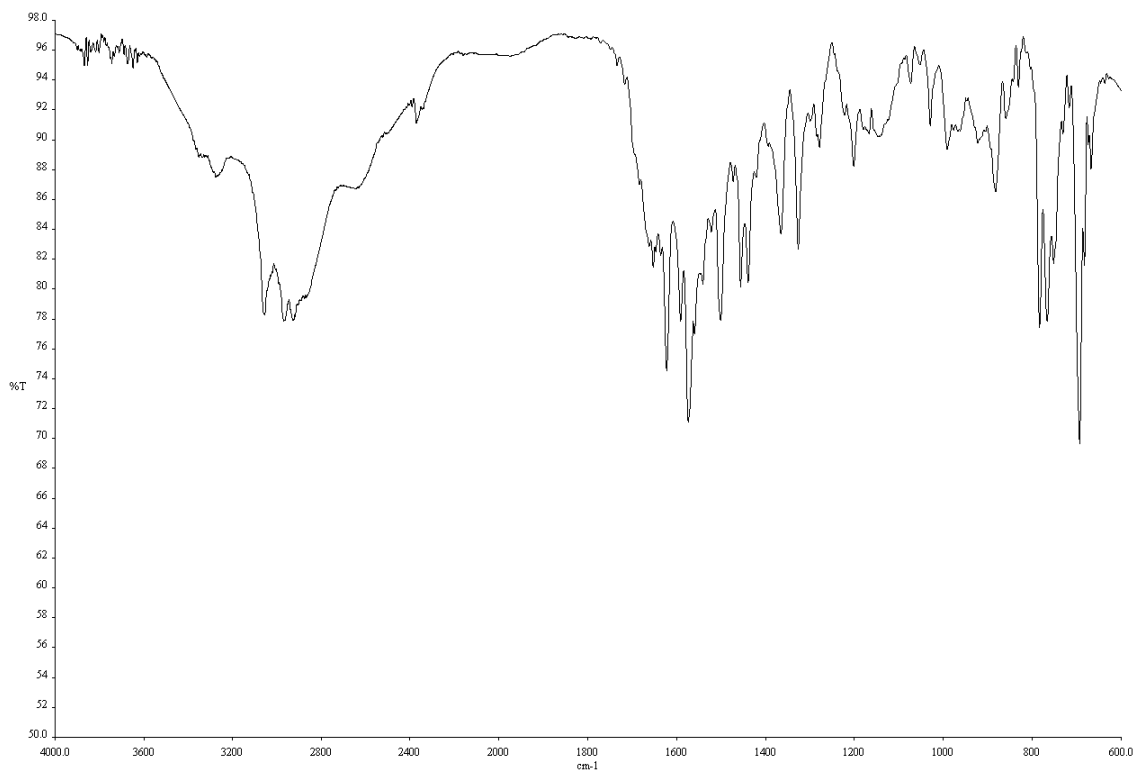
**Figure A3.5** Infrared spectrum (Thin Film, NaCl) of compound **173I**.



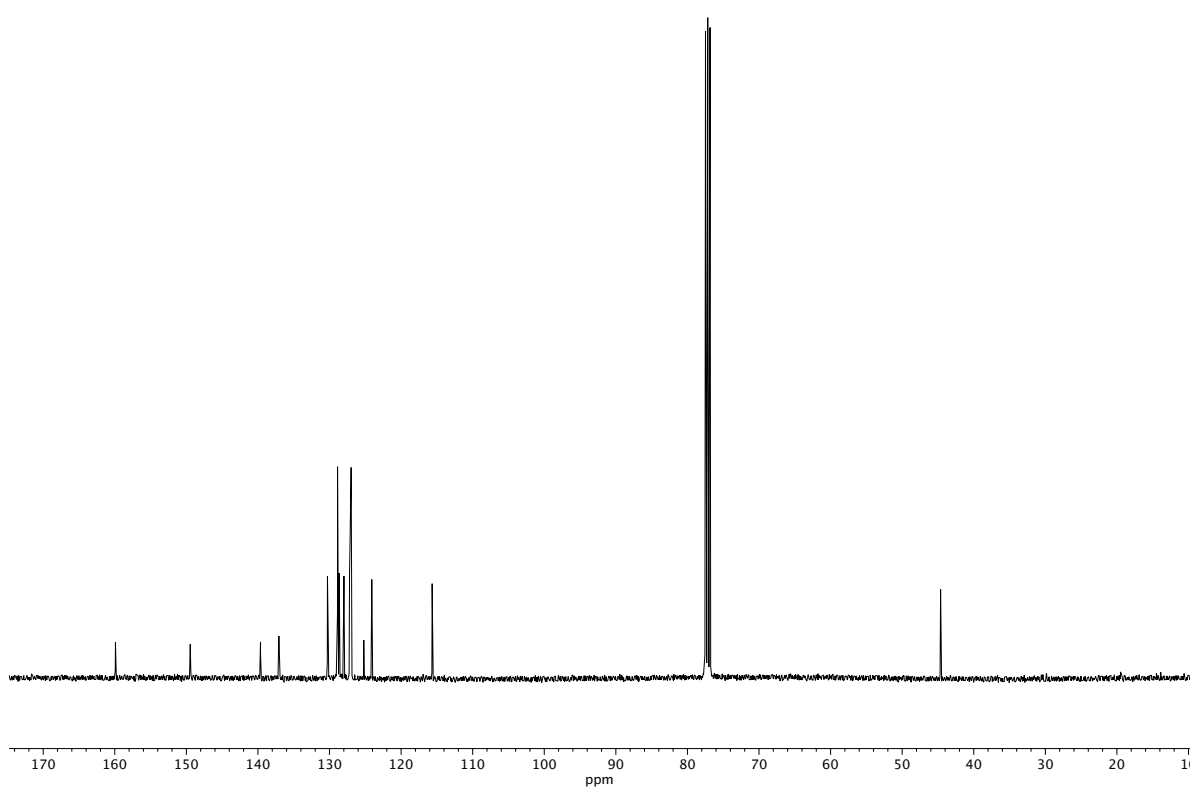
**Figure A3.6** <sup>13</sup>C NMR (100 MHz, CDCl<sub>3</sub>) of compound **173I**.



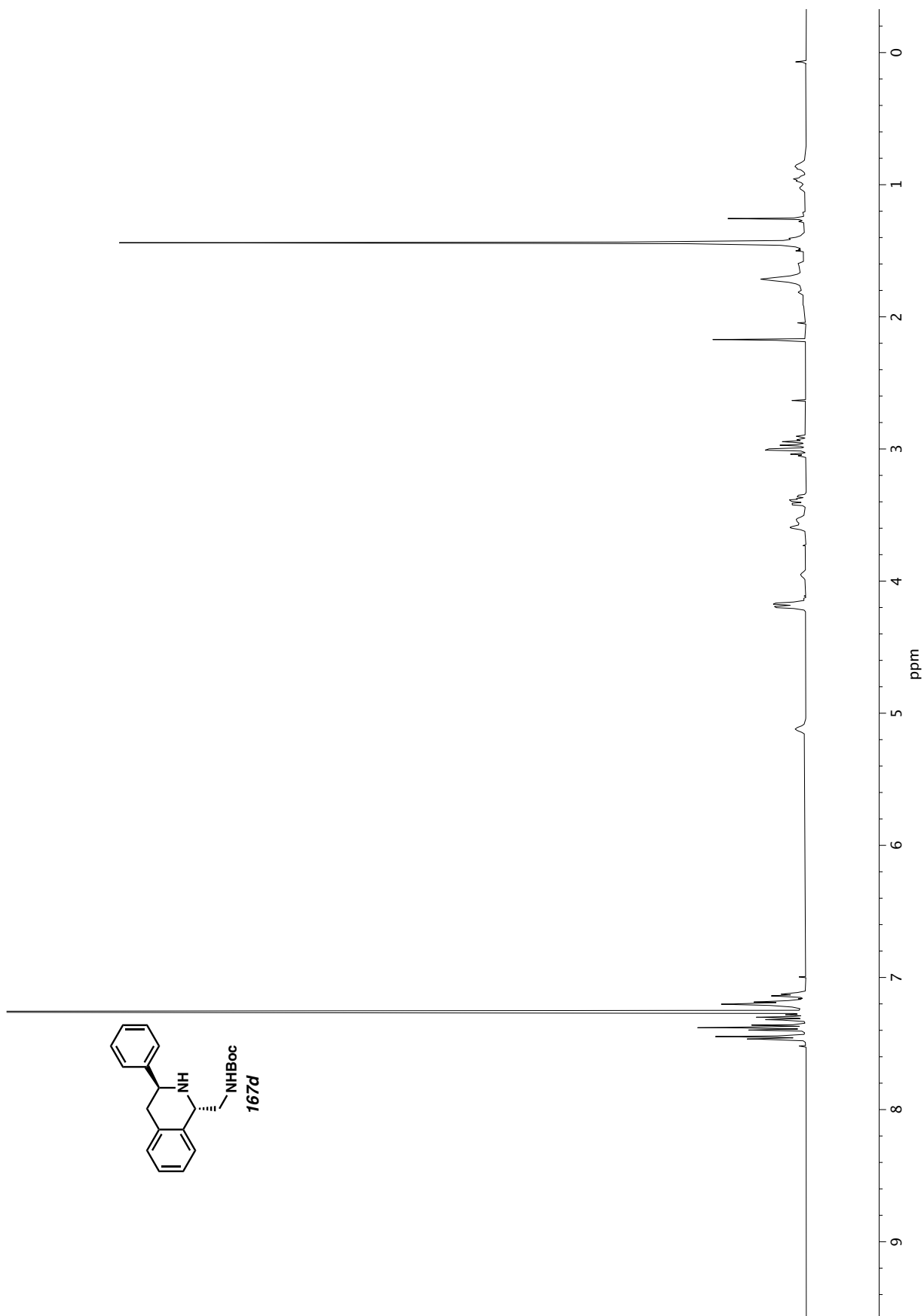
**Figure A3.7** <sup>1</sup>H NMR (400 MHz, CDCl<sub>3</sub>) of compound **166g**.



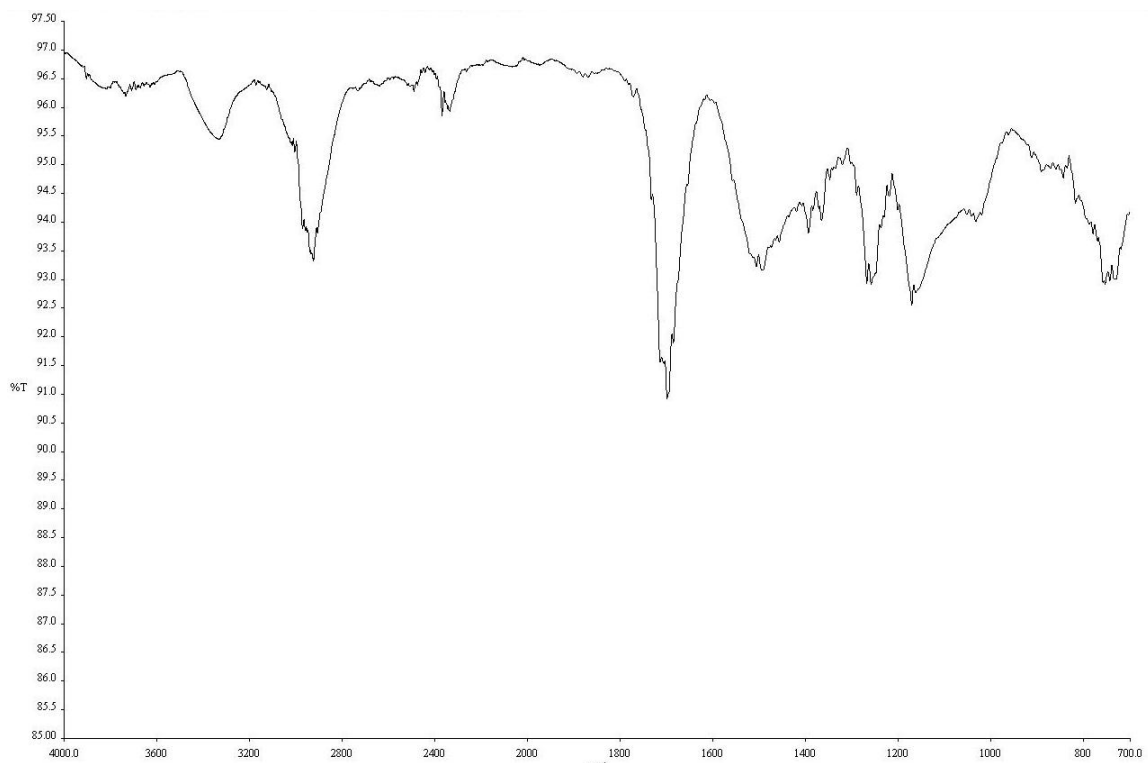
**Figure A3.8** Infrared spectrum (Thin Film, NaCl) of compound **166g**.



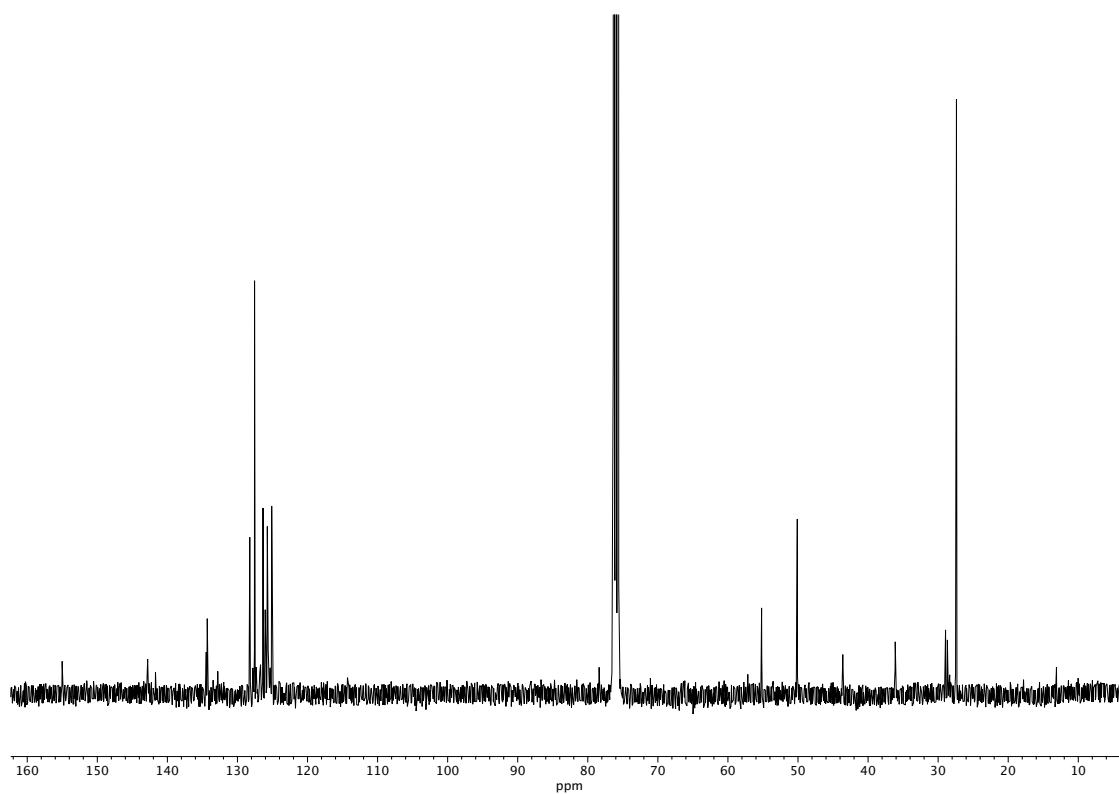
**Figure A3.9**  $^{13}\text{C}$  NMR (100 MHz,  $\text{CDCl}_3$ ) of compound **166g**.



**Figure A3.10**  $^1\text{H}$  NMR (400 MHz,  $\text{CDCl}_3$ ) of compound **167d**.

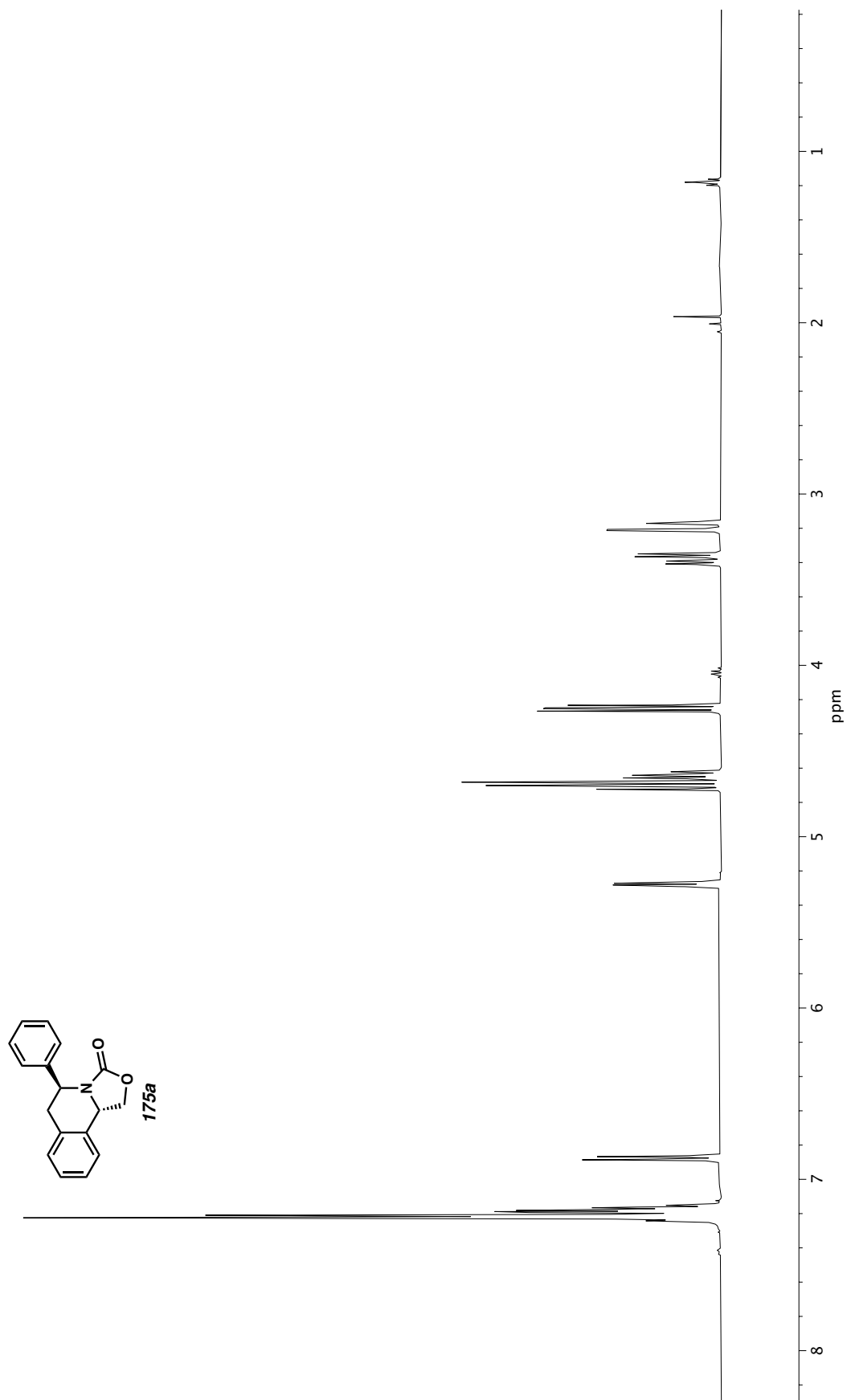


**Figure A3.11** Infrared spectrum (Thin Film, NaCl) of compound **167d**.

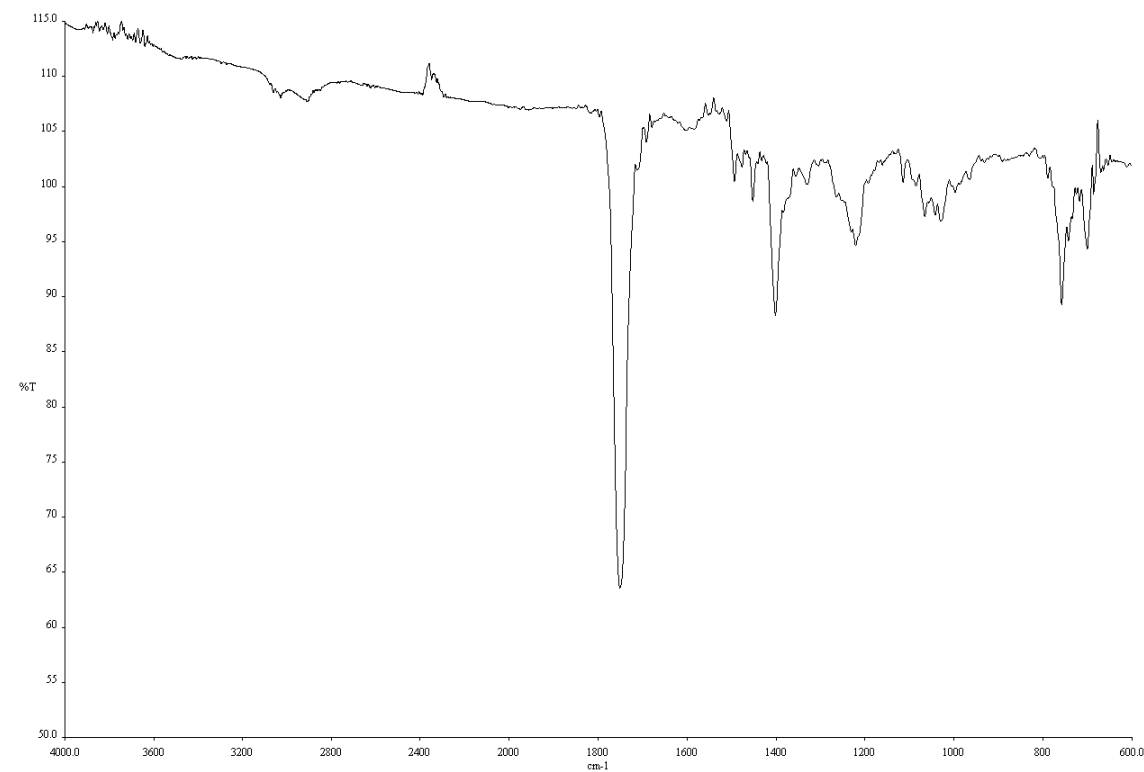


**Figure A3.12**  $^{13}\text{C}$  NMR (100 MHz,  $\text{CDCl}_3$ ) of compound **167d**.

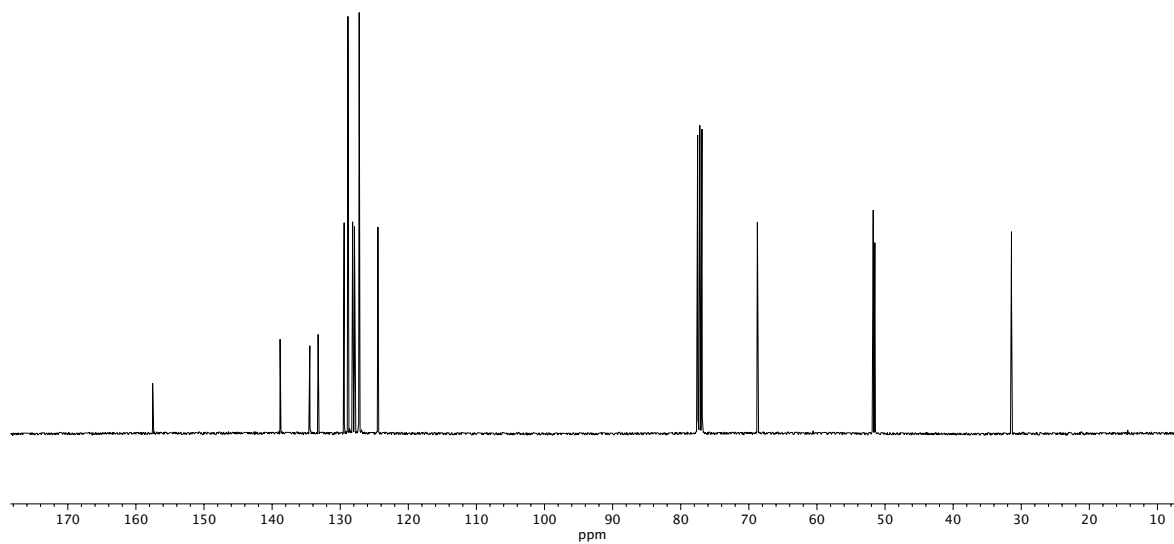




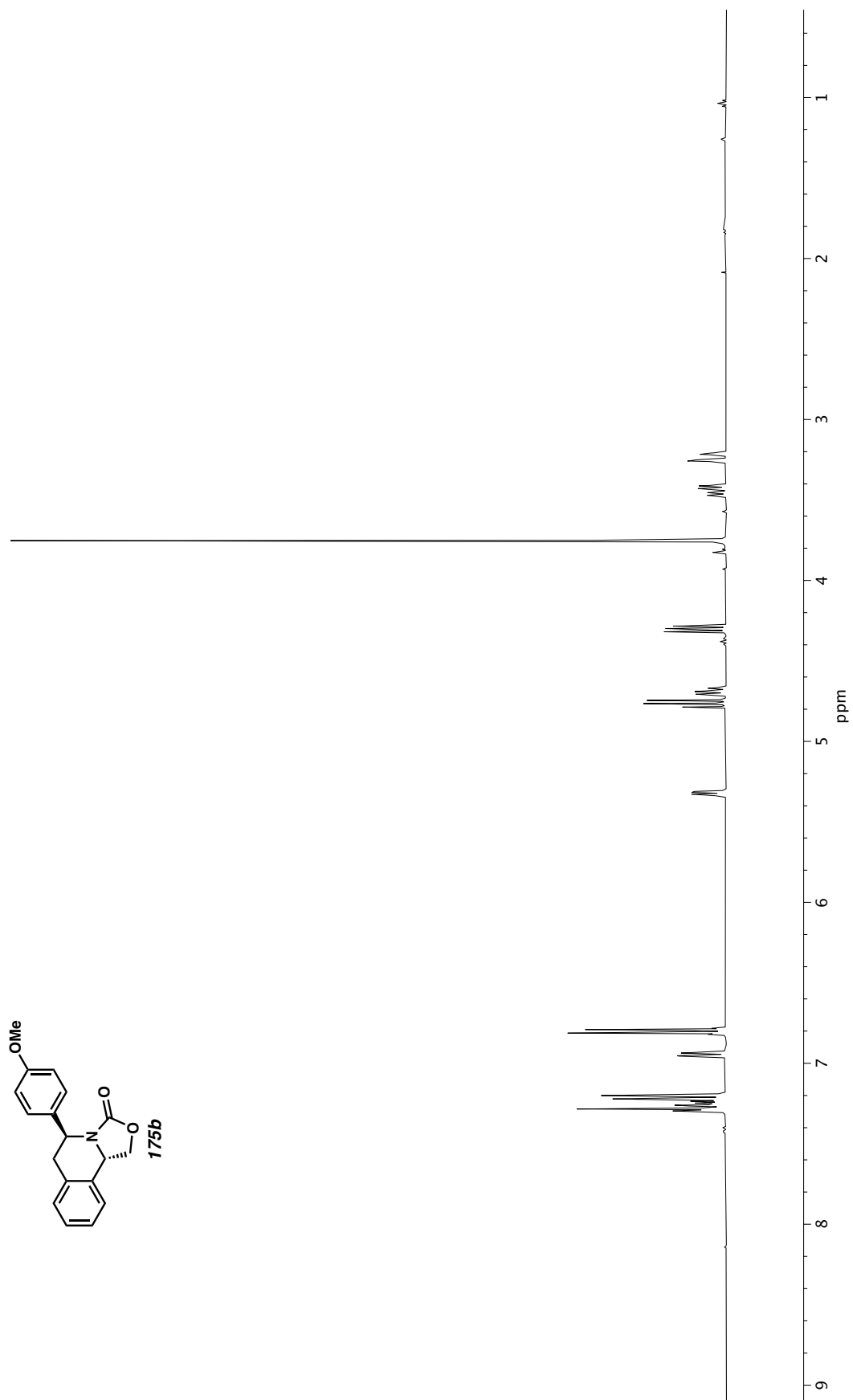
**Figure A3.13**  $^1\text{H}$  NMR (400 MHz,  $\text{CDCl}_3$ ) of compound **175a**.



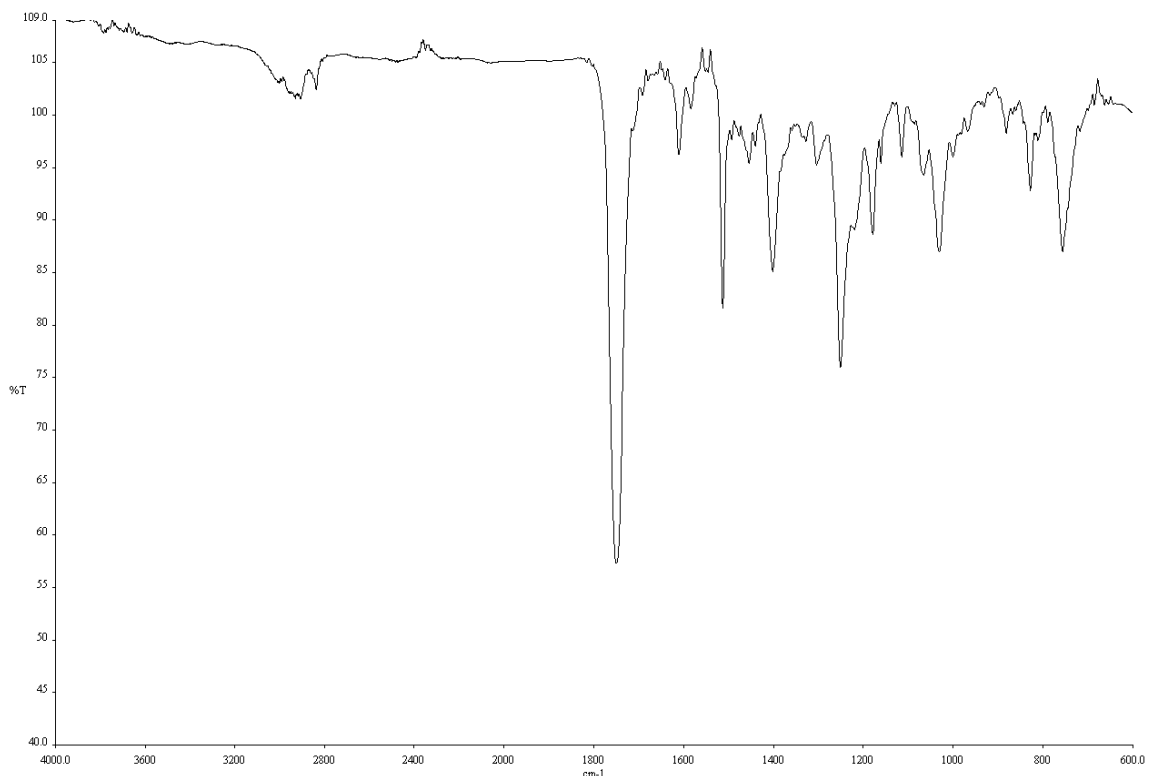
**Figure A3.14** Infrared spectrum (Thin Film, NaCl) of compound **175a**.



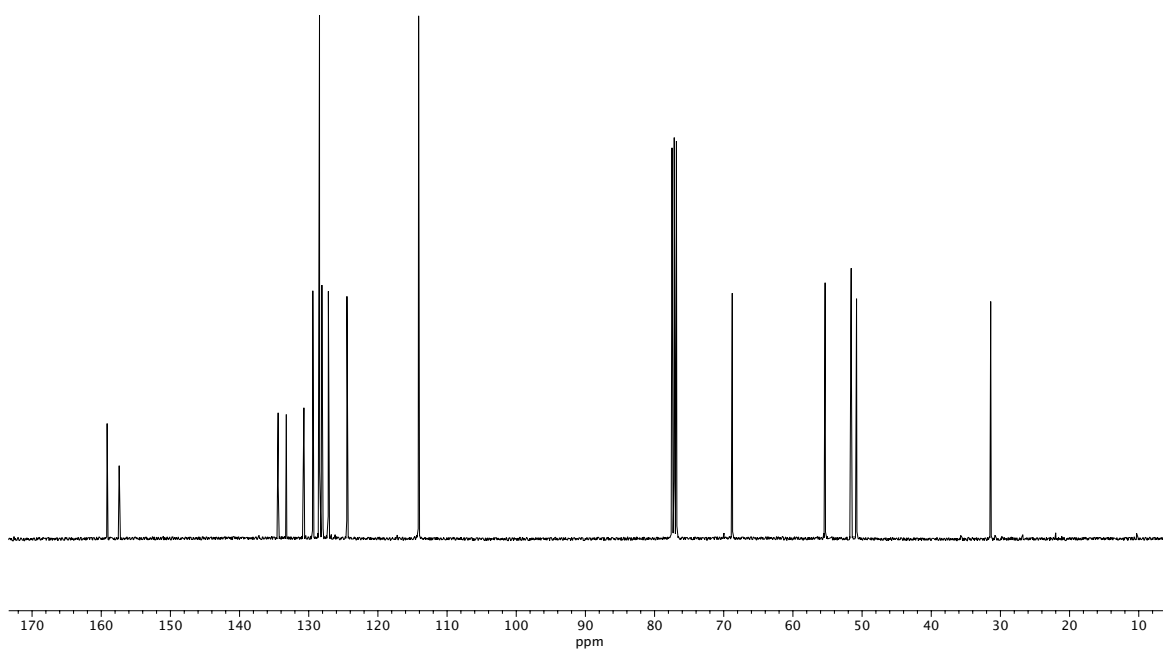
**Figure A3.15** <sup>13</sup>C NMR (100 MHz, CDCl<sub>3</sub>) of compound **175a**.



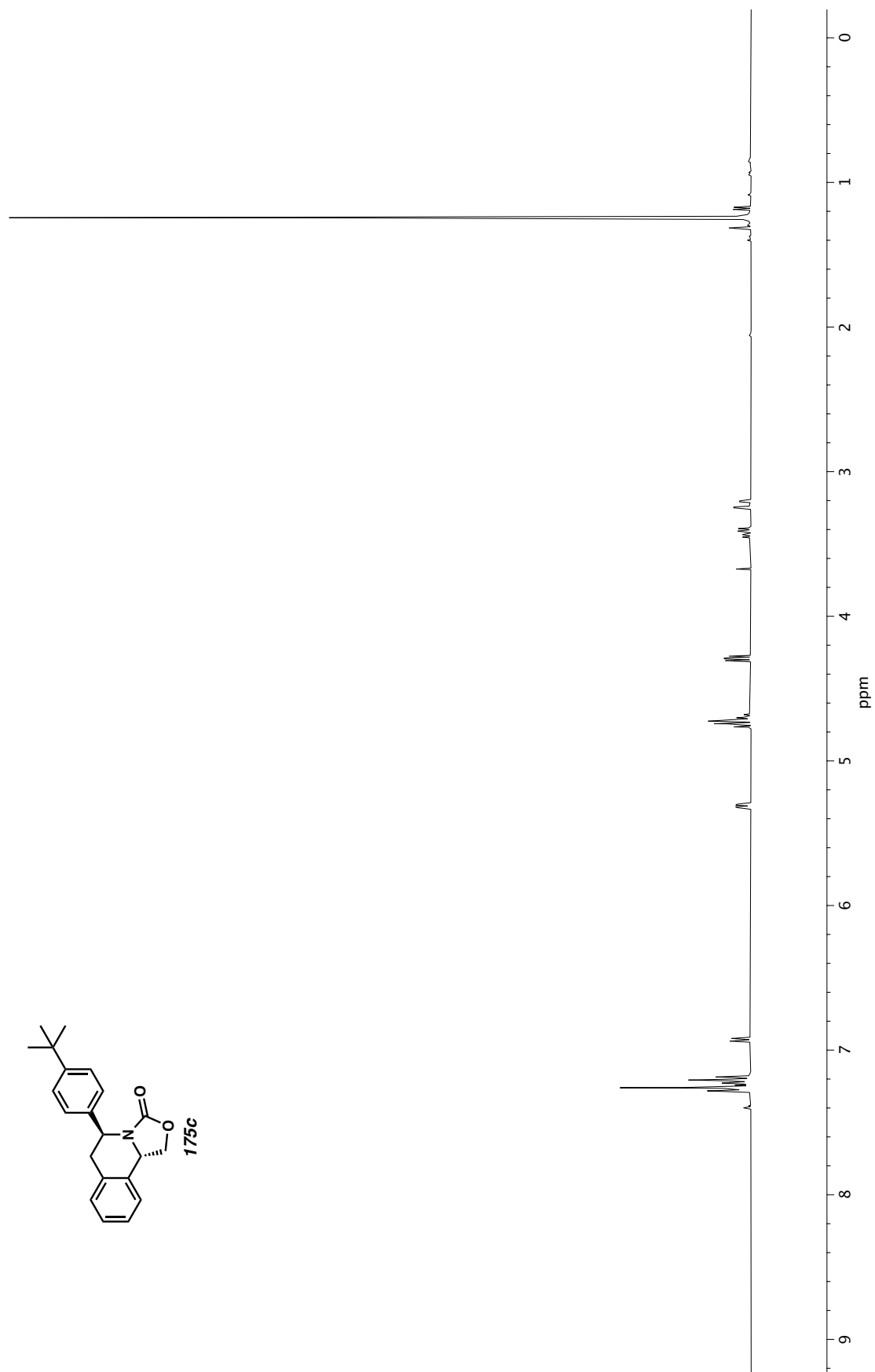
**Figure A3.16** <sup>1</sup>H NMR (400 MHz, CDCl<sub>3</sub>) of compound **175b**.



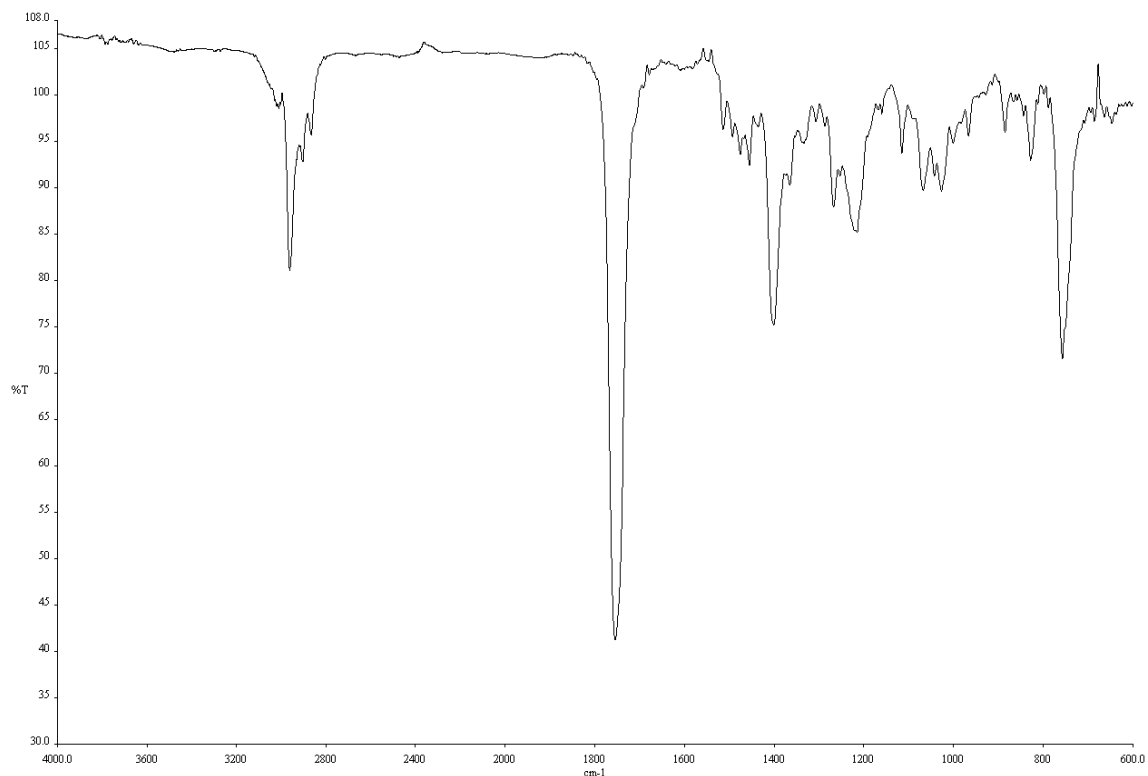
**Figure A3.17** Infrared spectrum (Thin Film, NaCl) of compound **175b**.



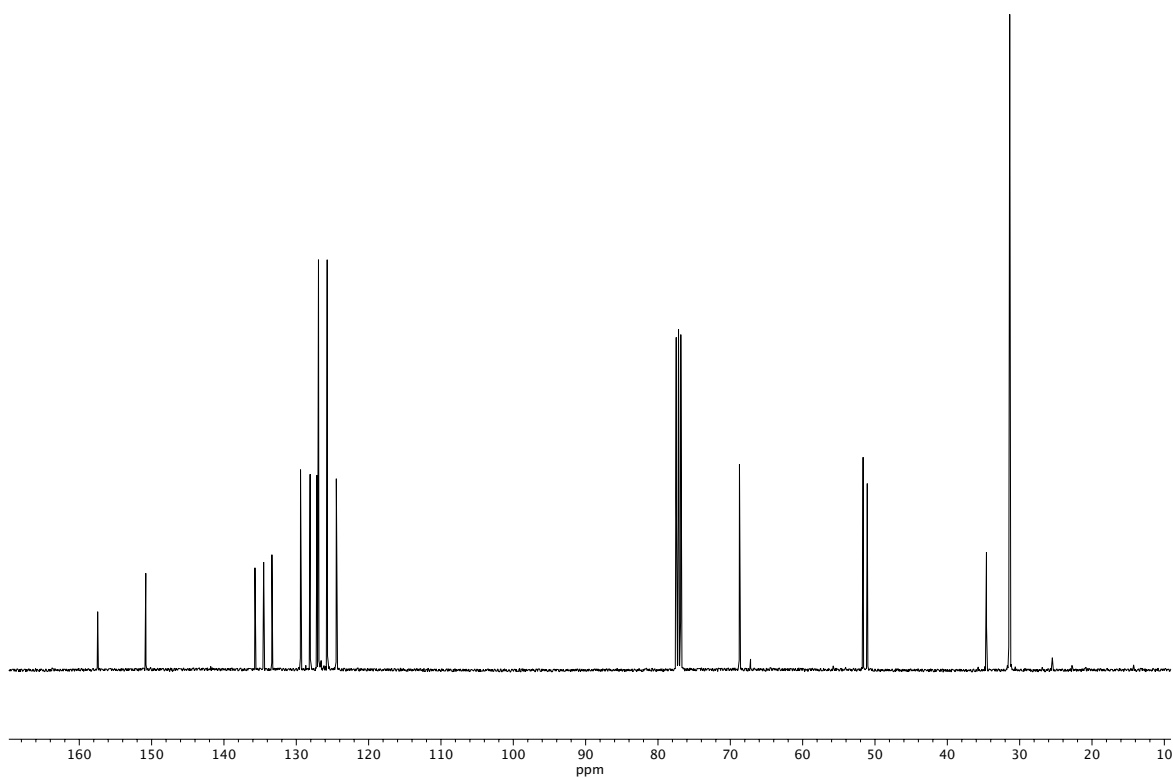
**Figure A3.18**  $^{13}\text{C}$  NMR (100 MHz,  $\text{CDCl}_3$ ) of compound **175b**.



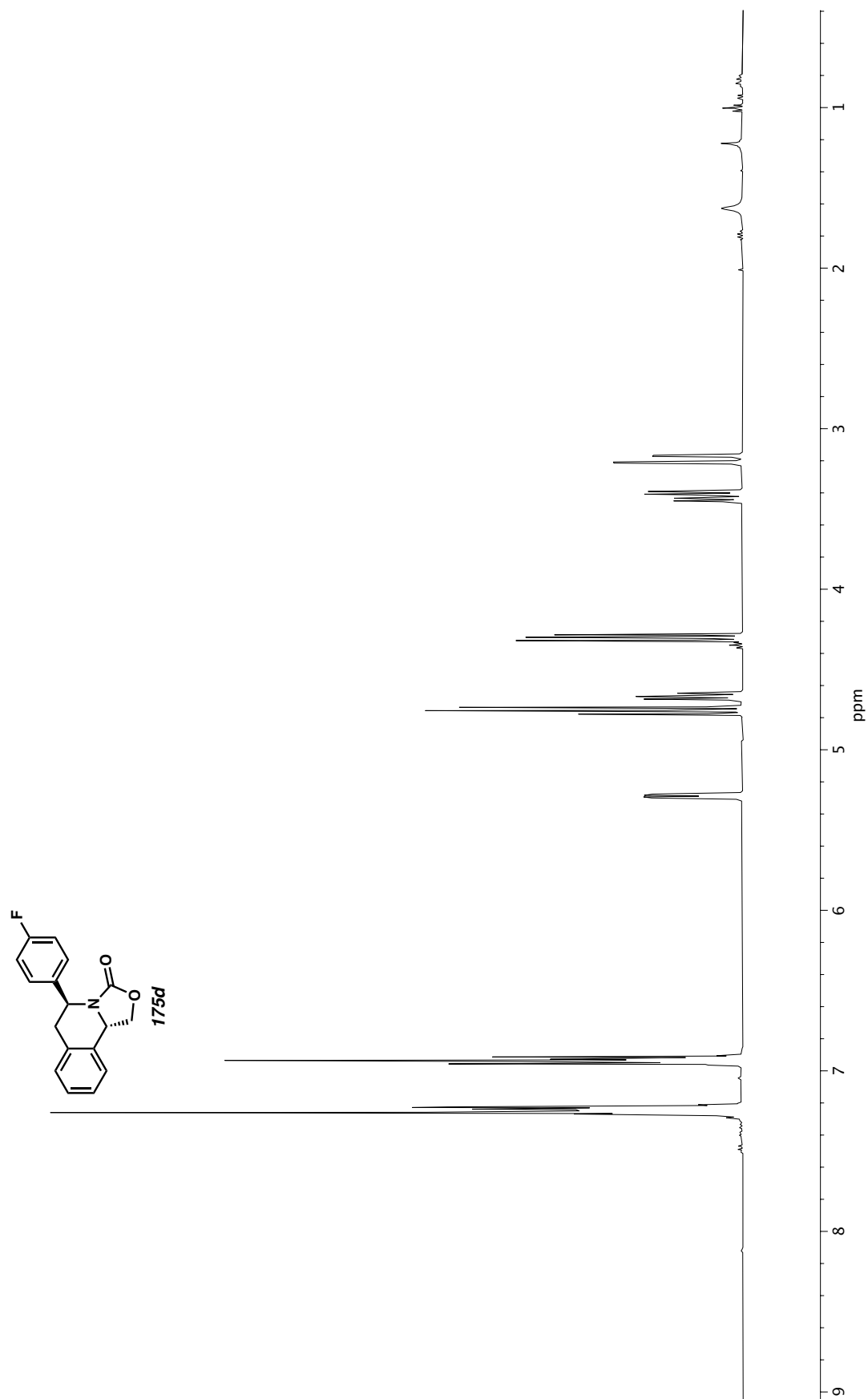
**Figure A3.19**  $^1\text{H}$  NMR (400 MHz,  $\text{CDCl}_3$ ) of compound **175c**.



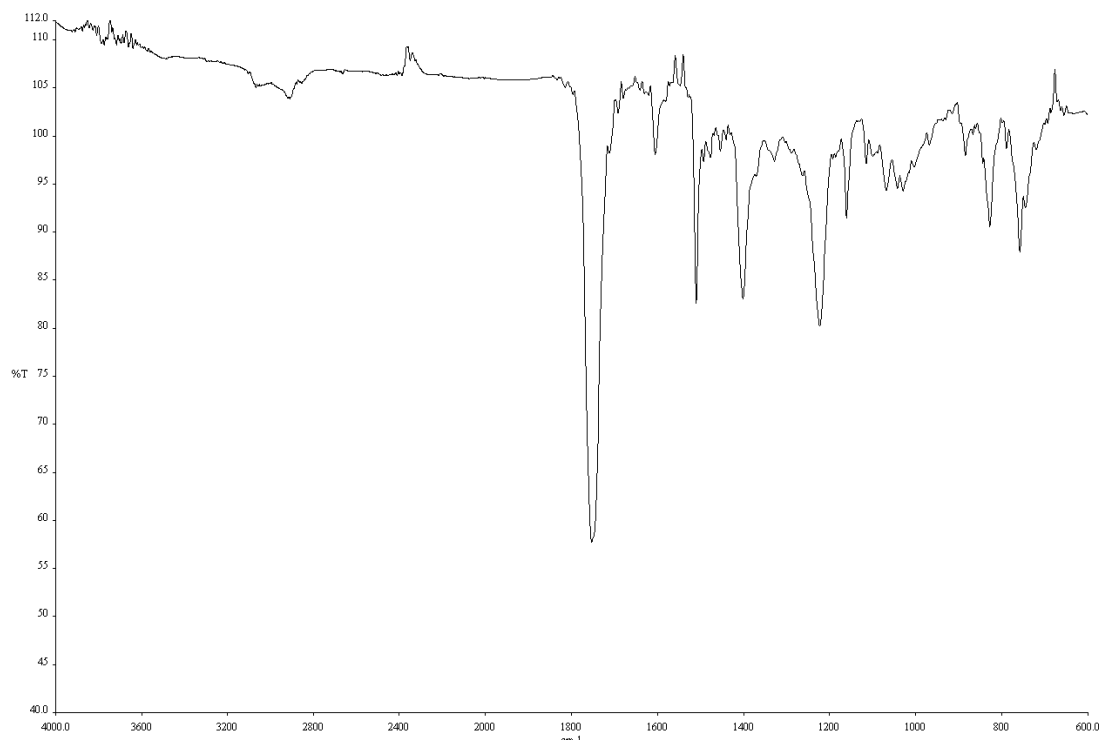
**Figure A3.20** Infrared spectrum (Thin Film, NaCl) of compound **175c**.



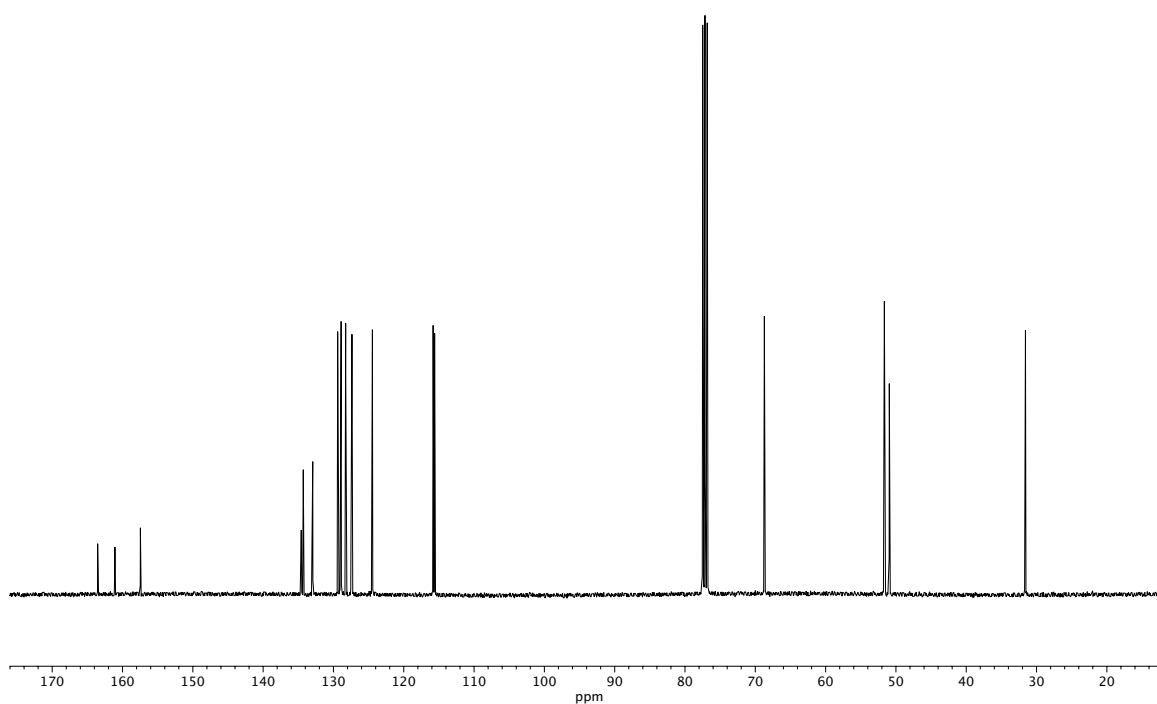
**Figure A3.21**  $^{13}\text{C}$  NMR (100 MHz,  $\text{CDCl}_3$ ) of compound **175c**.



**Figure A3.22**  $^1\text{H}$  NMR (400 MHz,  $\text{CDCl}_3$ ) of compound **175d**.

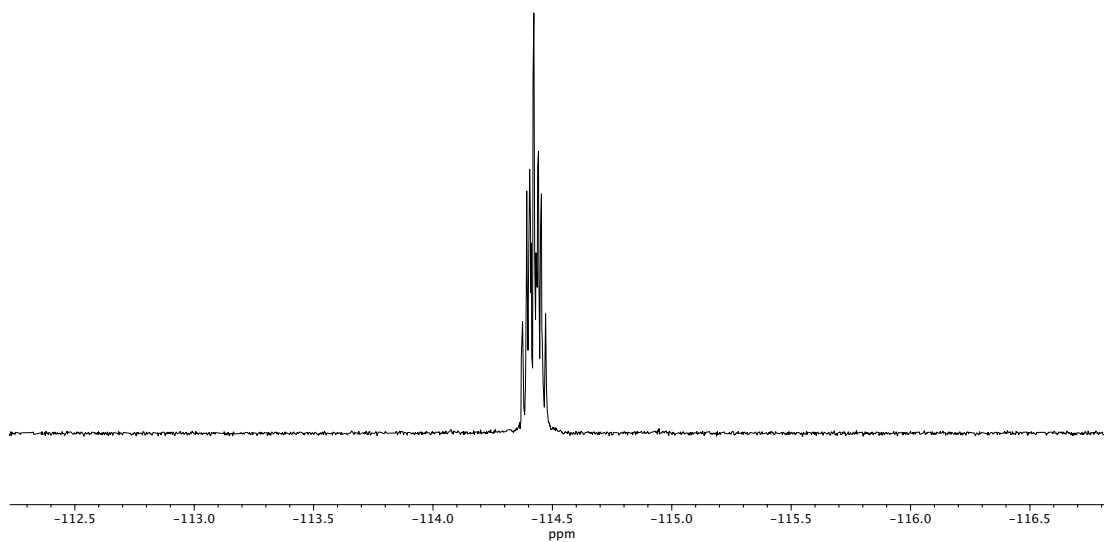


**Figure A3.23** Infrared spectrum (Thin Film, NaCl) of compound **175d**.

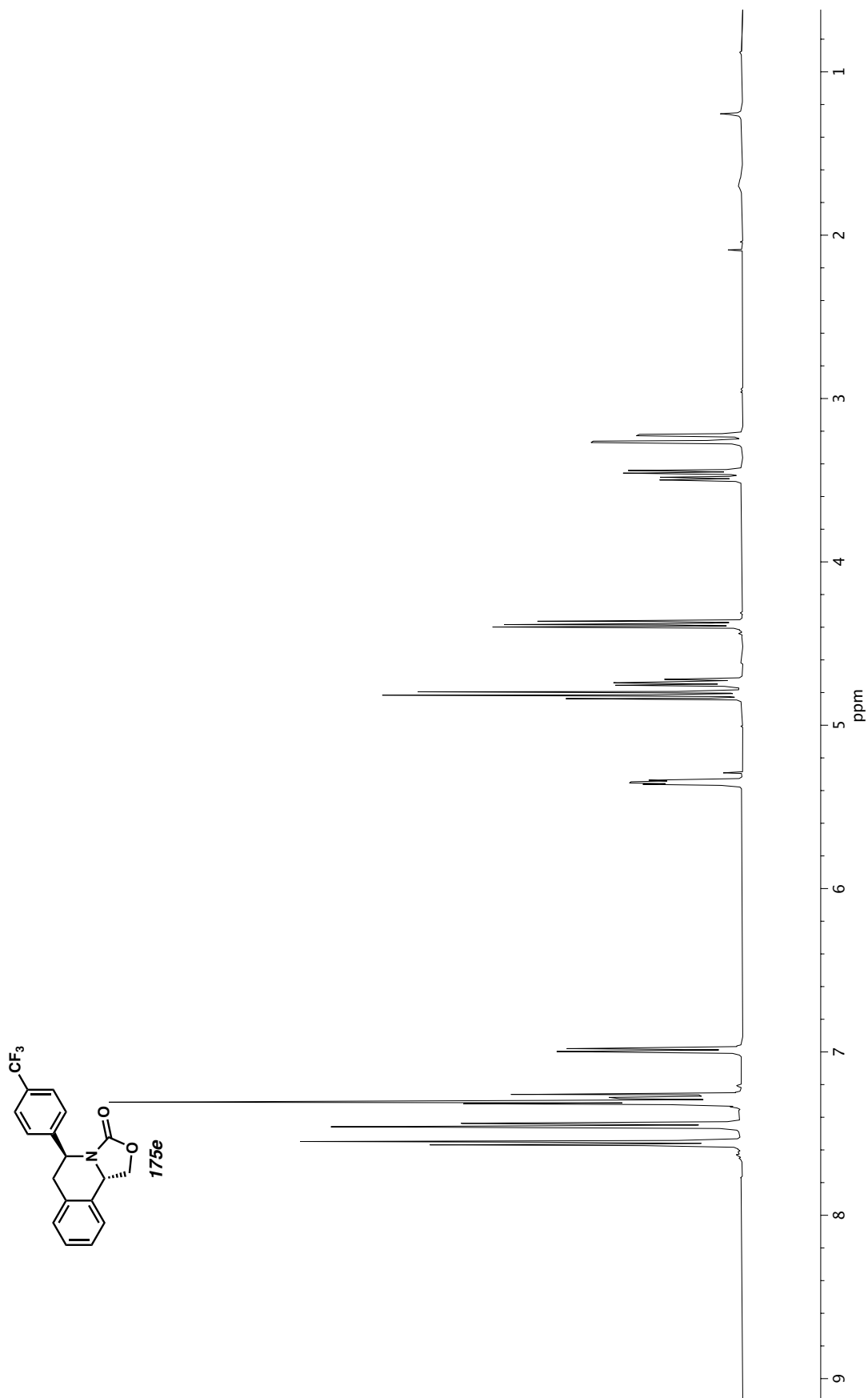


**Figure A3.24** <sup>13</sup>C NMR (100 MHz, CDCl<sub>3</sub>) of compound **175d**.

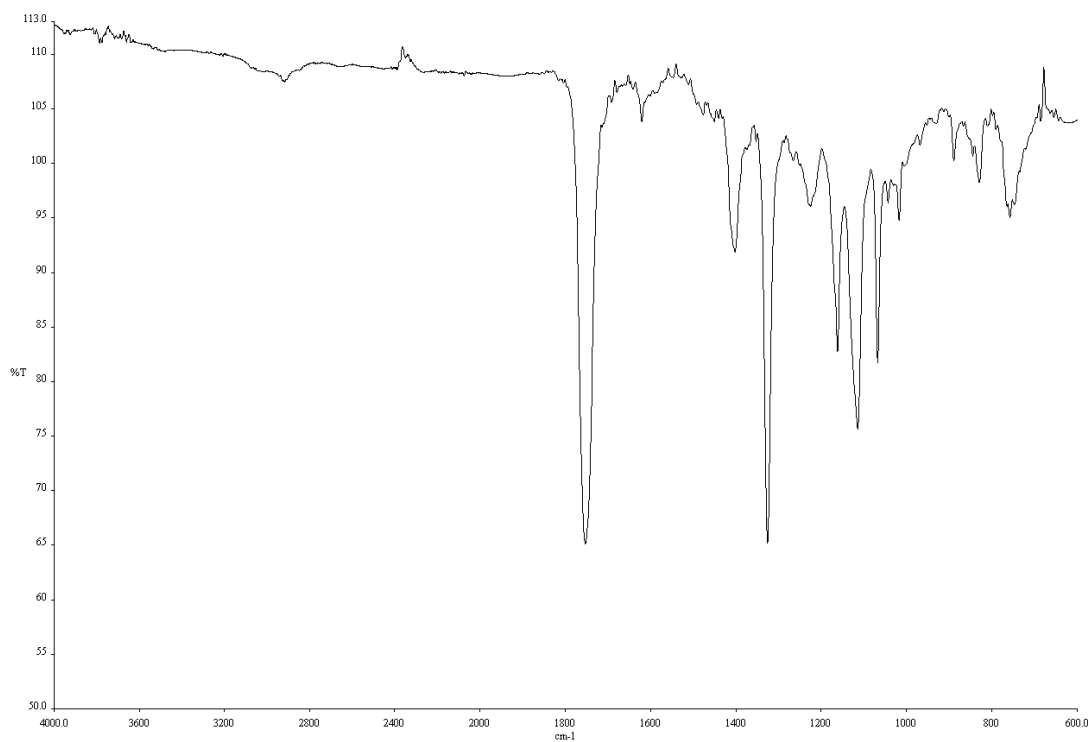




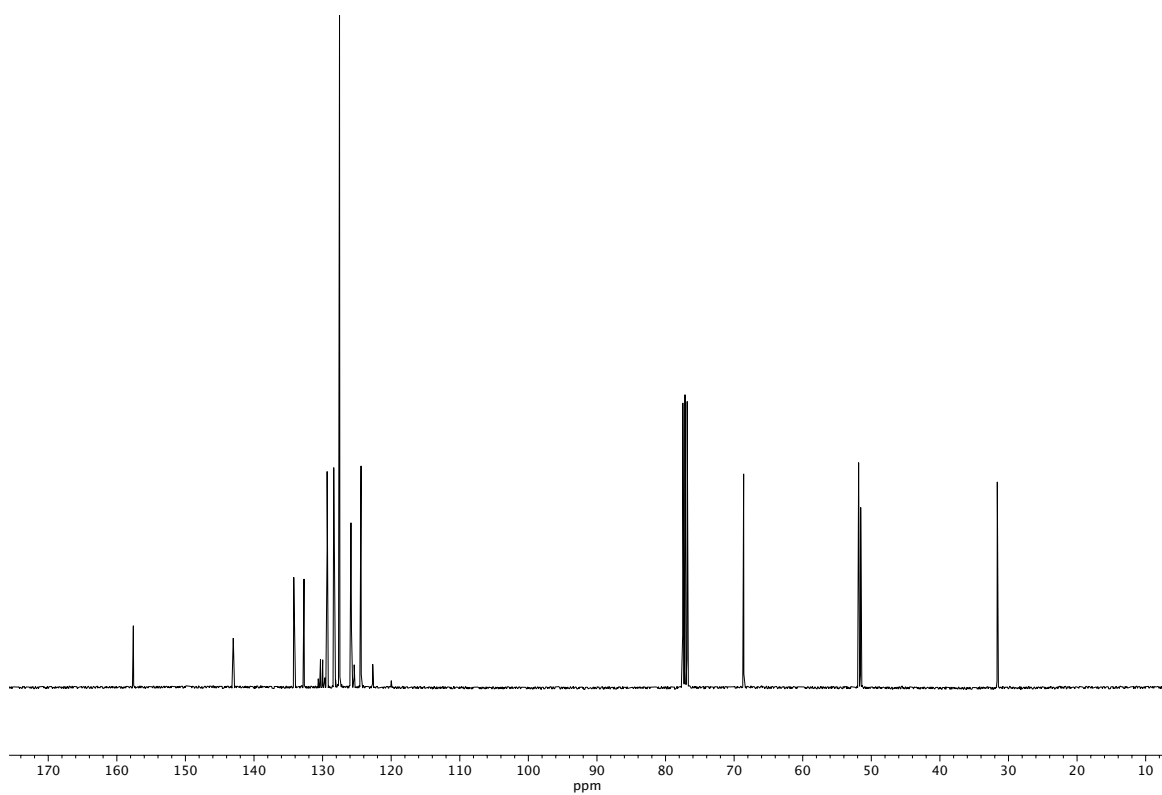
**Figure A3.25**  $^{19}\text{F}$  NMR (282 MHz,  $\text{CDCl}_3$ ) of compound **175d**.



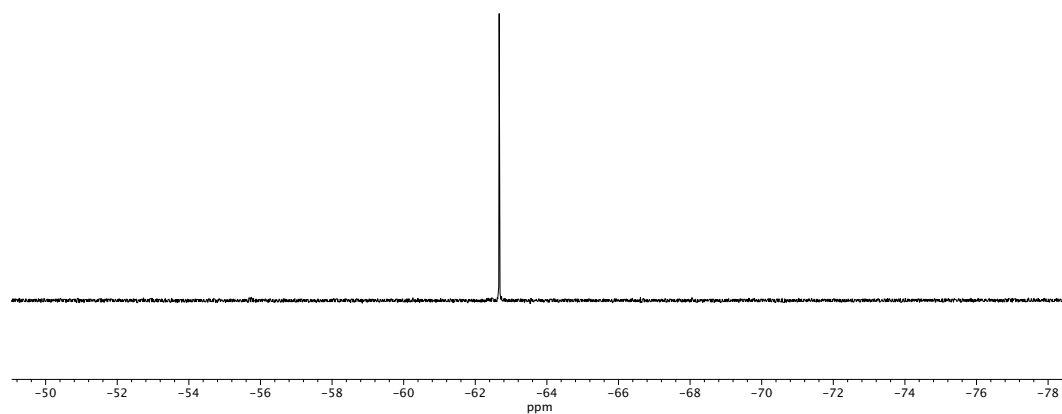
**Figure A3.26**  $^1\text{H}$  NMR (400 MHz,  $\text{CDCl}_3$ ) of compound **175e**.



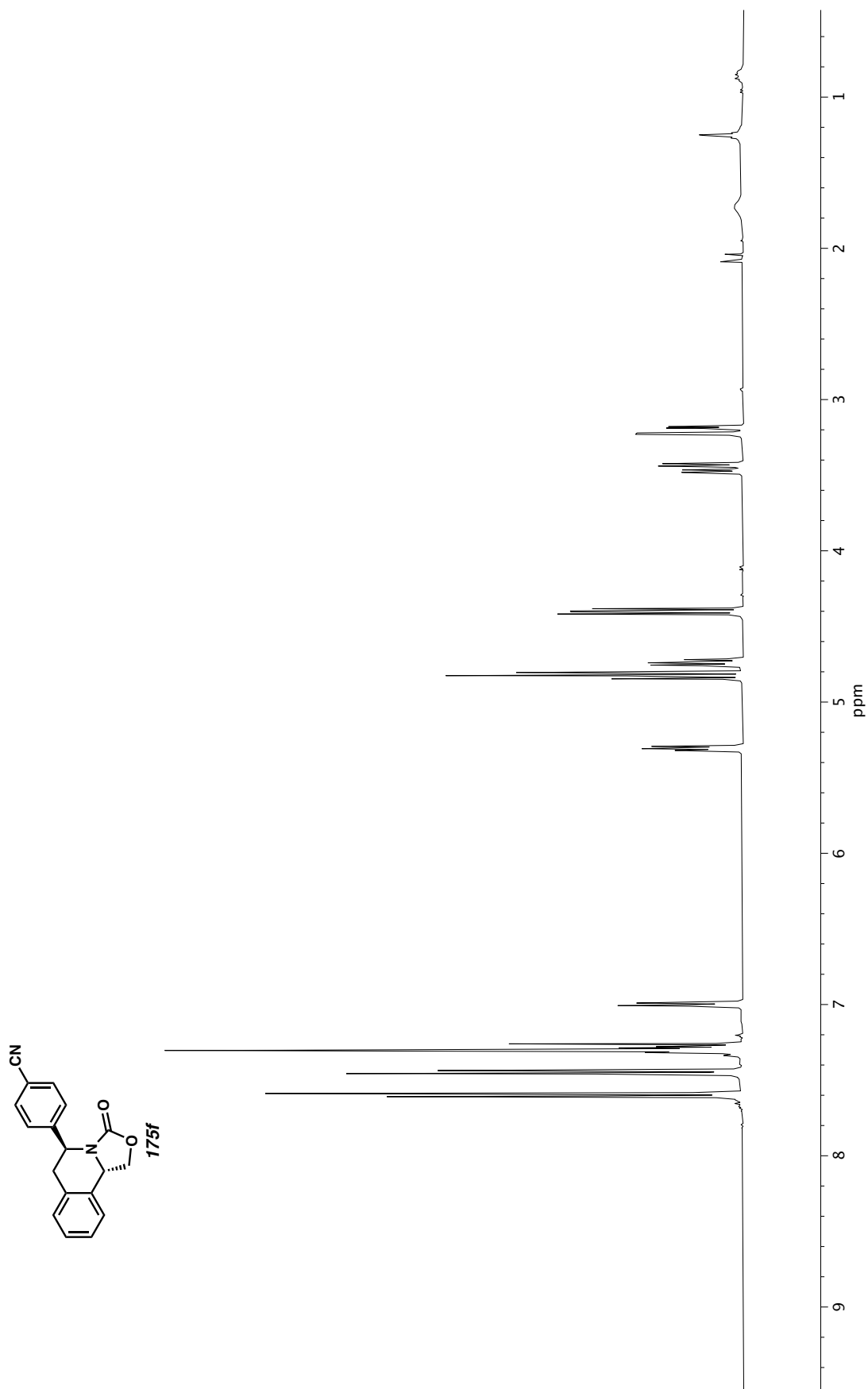
**Figure A3.27** Infrared spectrum (Thin Film, NaCl) of compound **175e**.



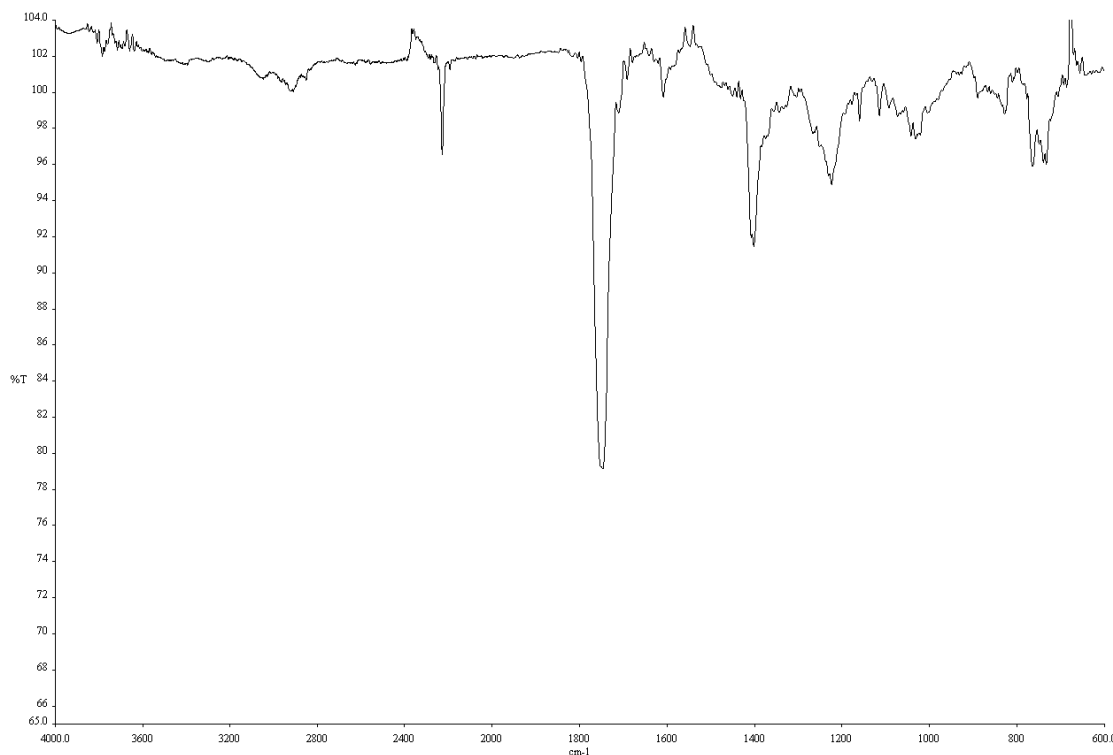
**Figure A3.28**  $^{13}\text{C}$  NMR (100 MHz,  $\text{CDCl}_3$ ) of compound **175e**.



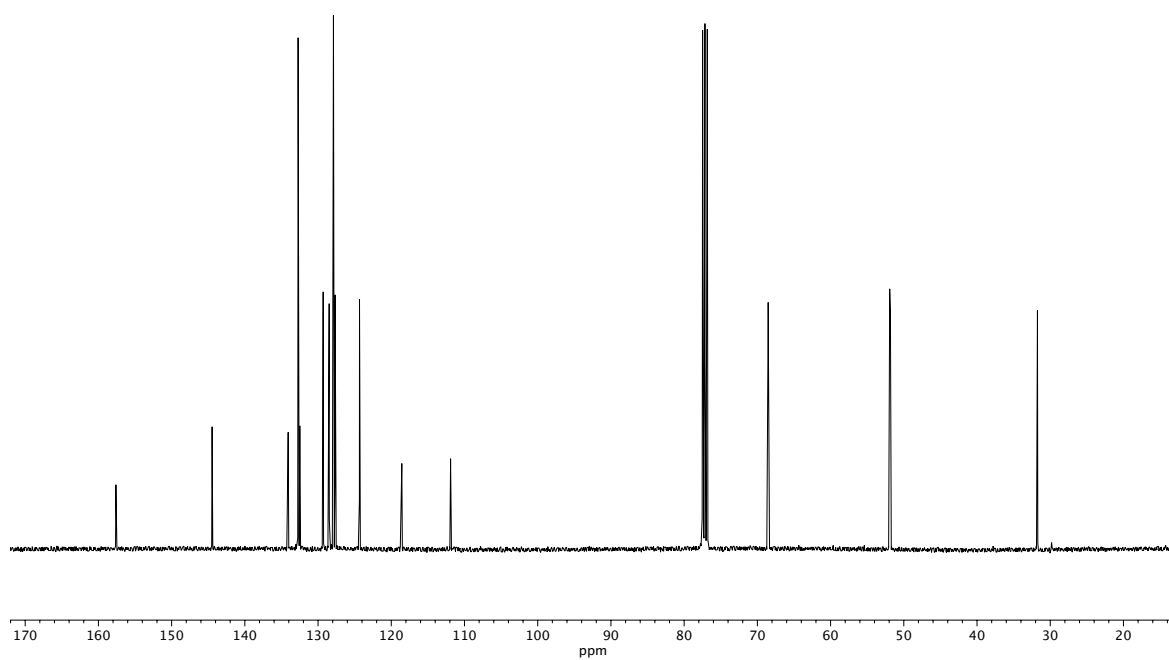
**Figure A3.29**  $^{19}\text{F}$  NMR (282 MHz,  $\text{CDCl}_3$ ) of compound **175e**.



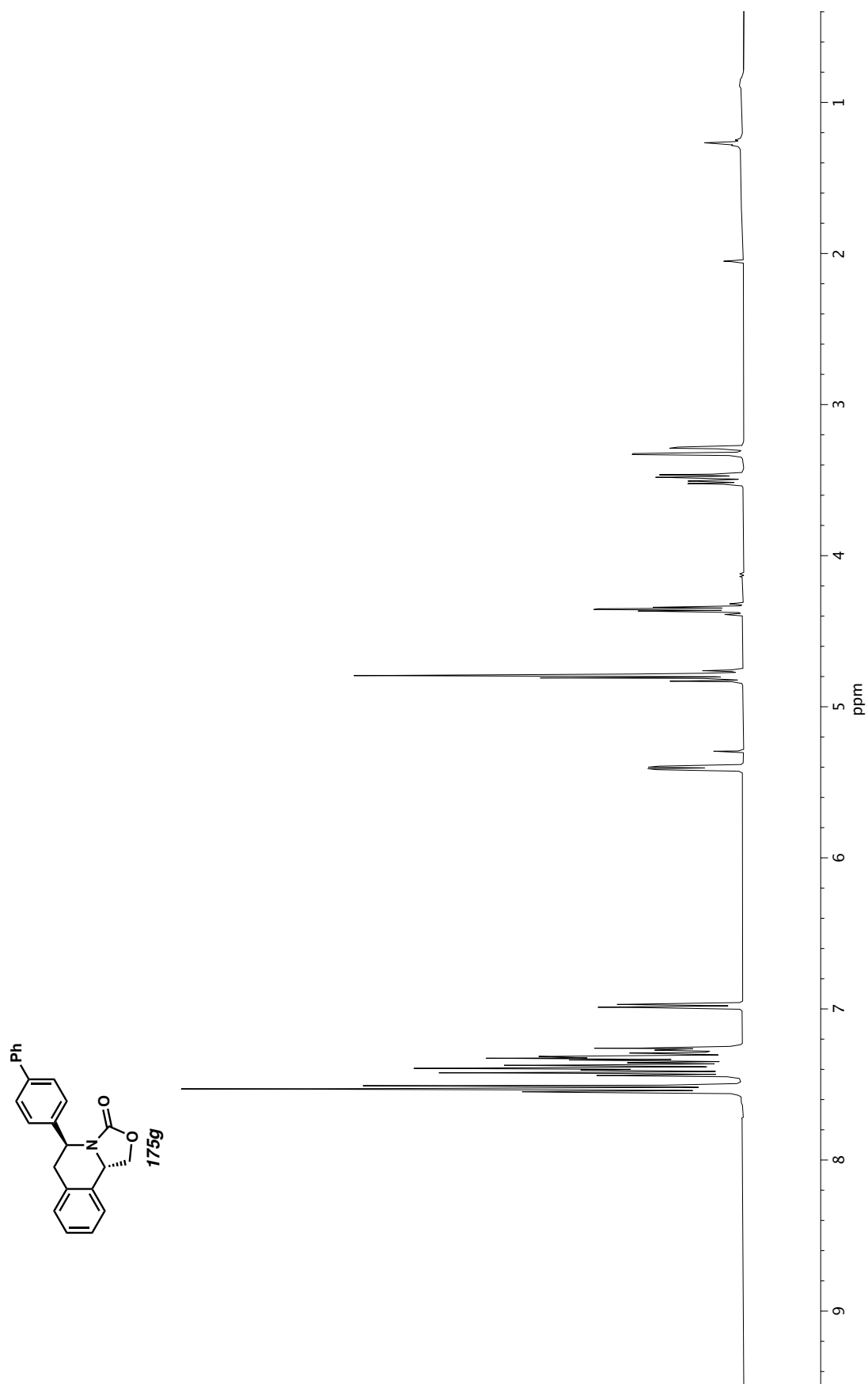
**Figure A3.30**  $^1\text{H}$  NMR (400 MHz,  $\text{CDCl}_3$ ) of compound **175f**.

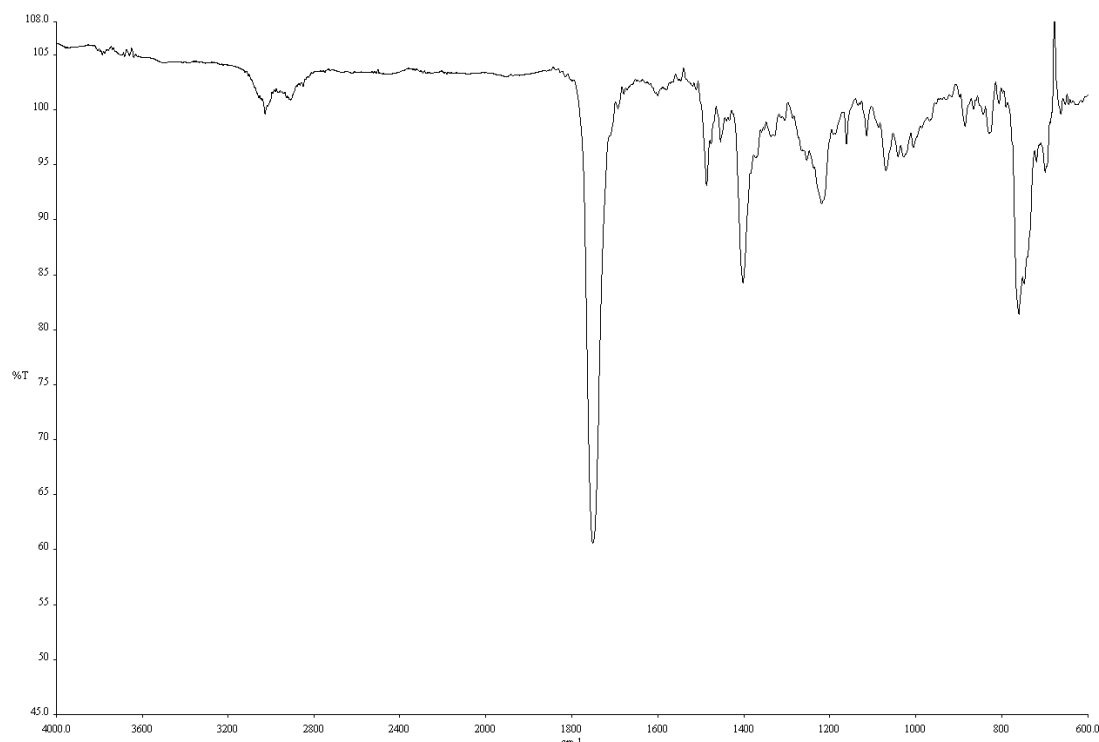


**Figure A3.31** Infrared spectrum (Thin Film, NaCl) of compound **175f**.

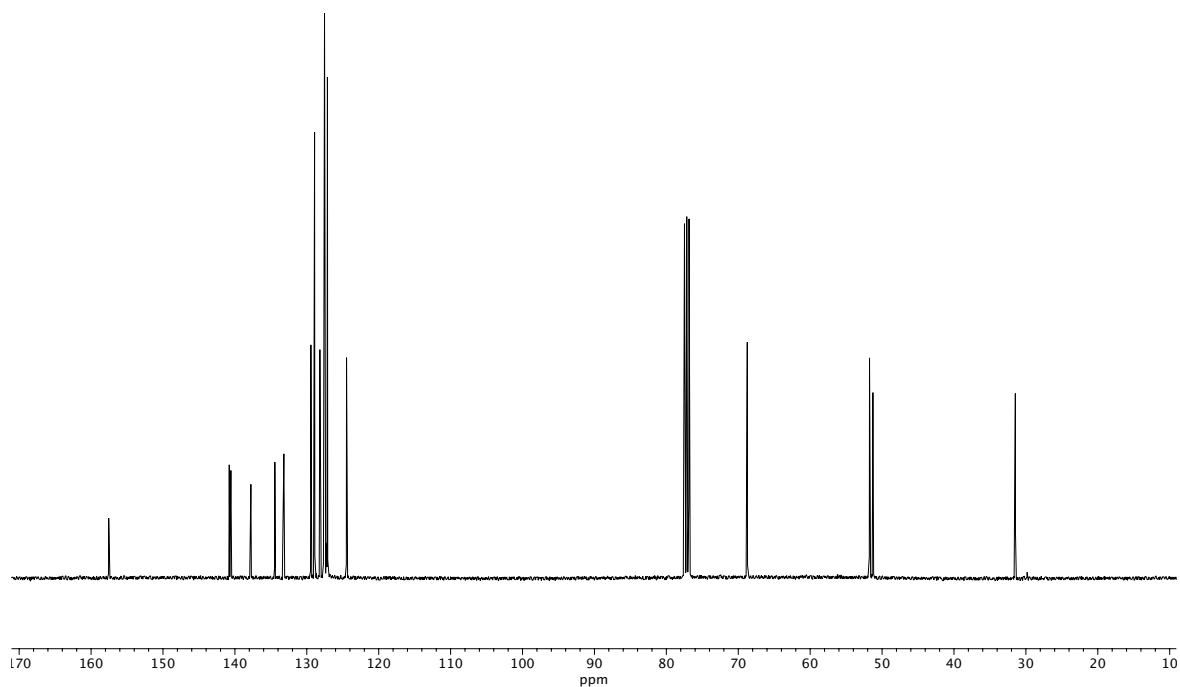


**Figure A3.32** <sup>13</sup>C NMR (100 MHz, CDCl<sub>3</sub>) of compound **175f**.



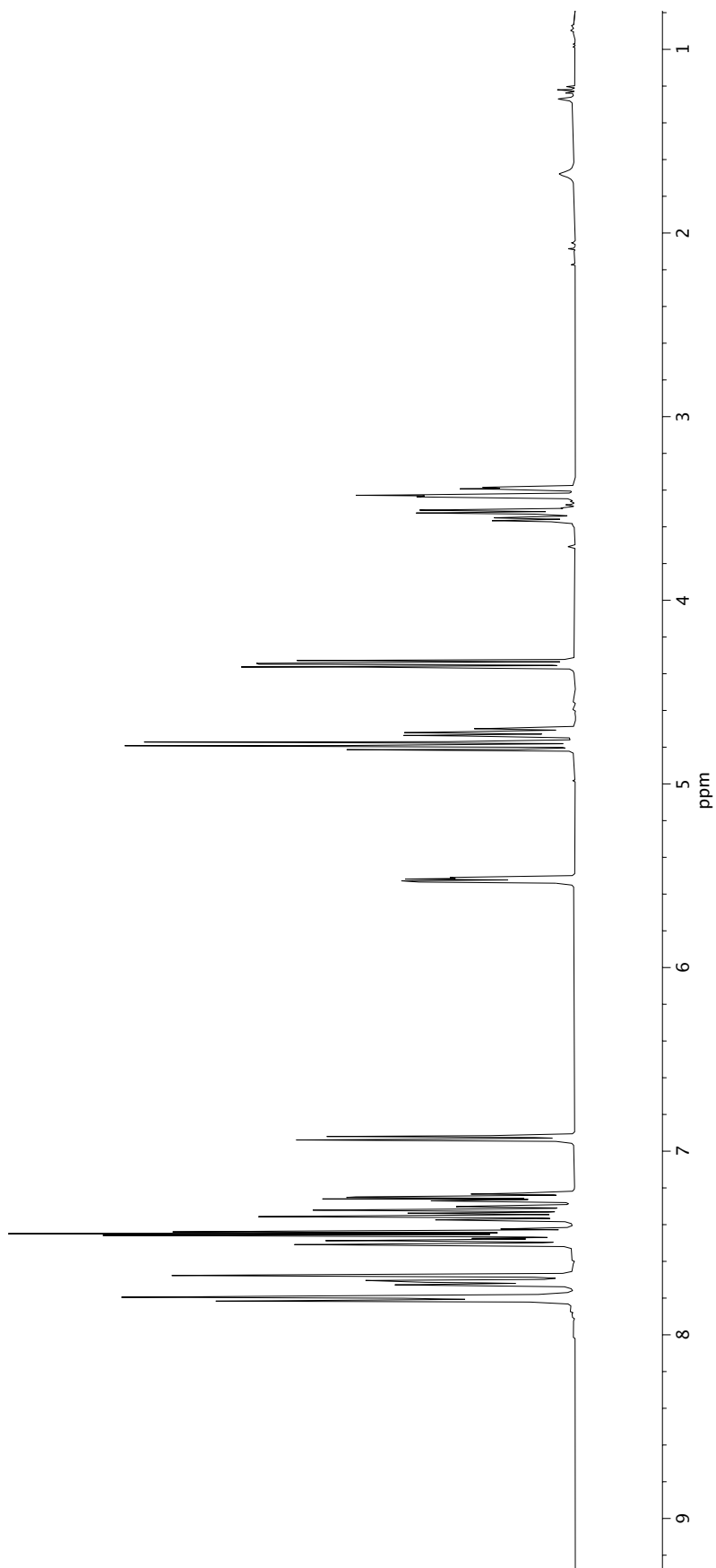
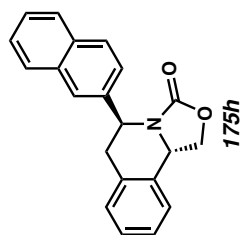


**Figure A3.34** Infrared spectrum (Thin Film, NaCl) of compound **175g**.

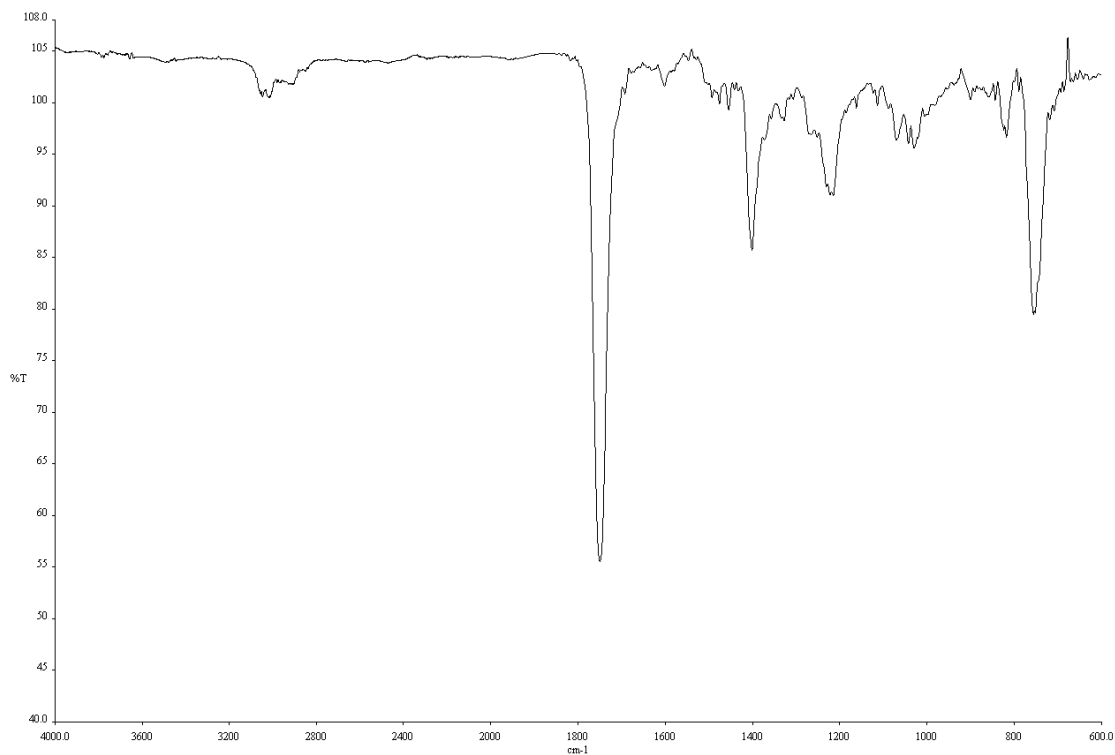


**Figure A3.35** <sup>13</sup>C NMR (100 MHz, CDCl<sub>3</sub>) of compound **175g**.

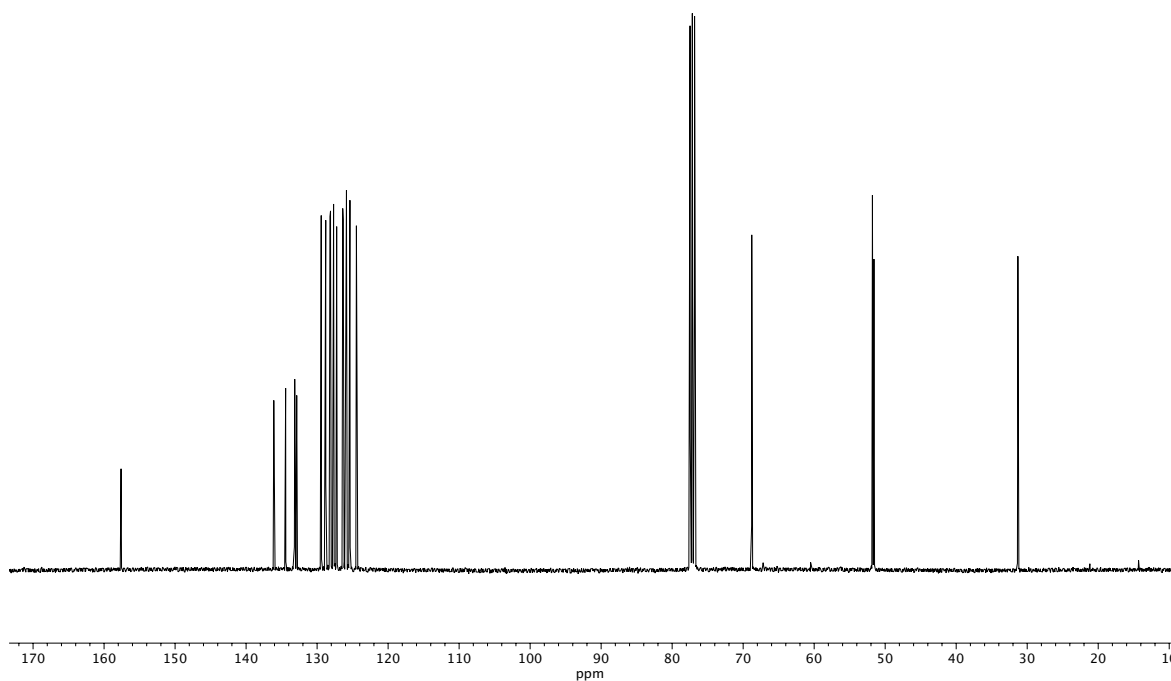




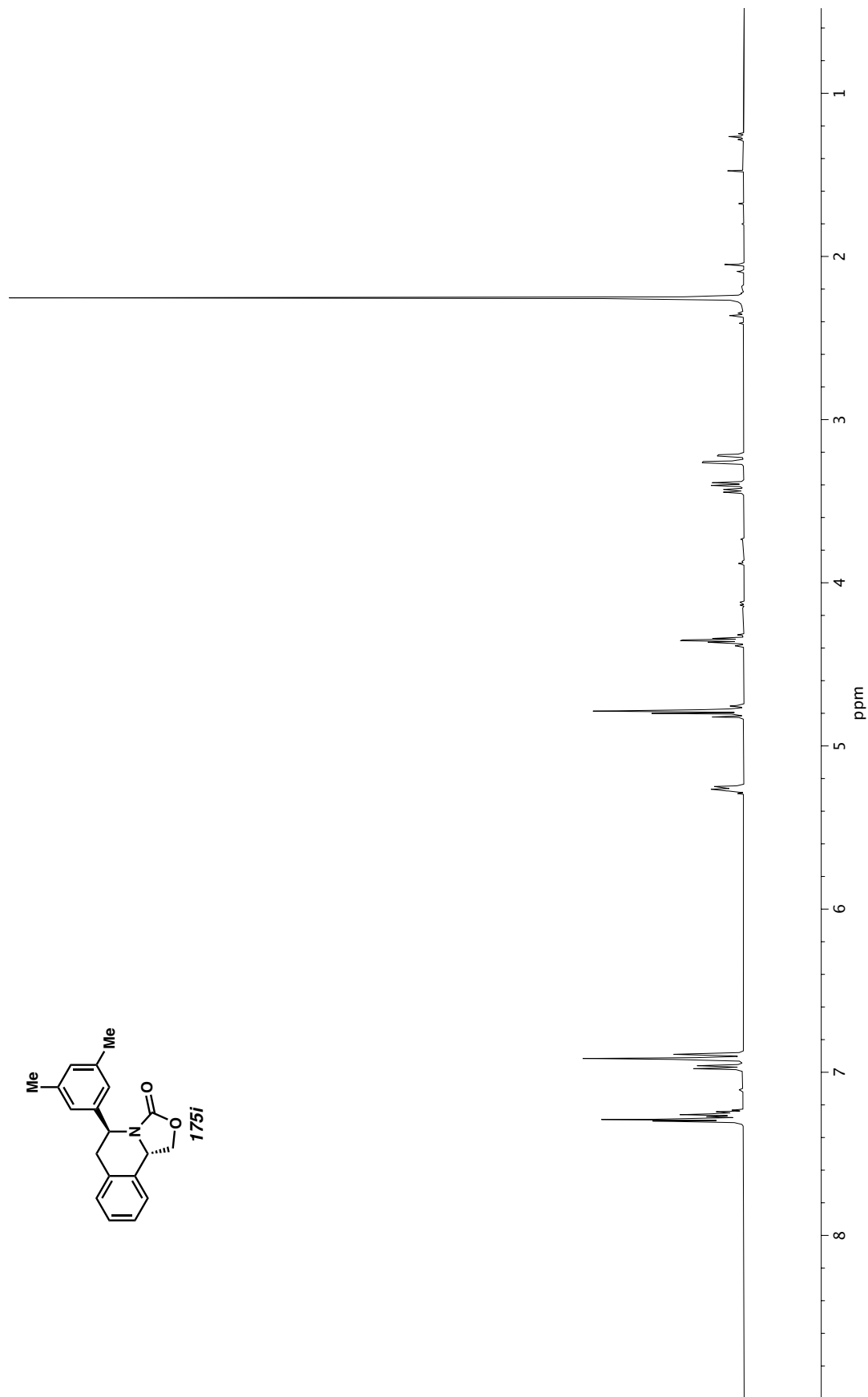
**Figure A3.36**  $^1\text{H}$  NMR (400 MHz,  $\text{CDCl}_3$ ) of compound **175h**.



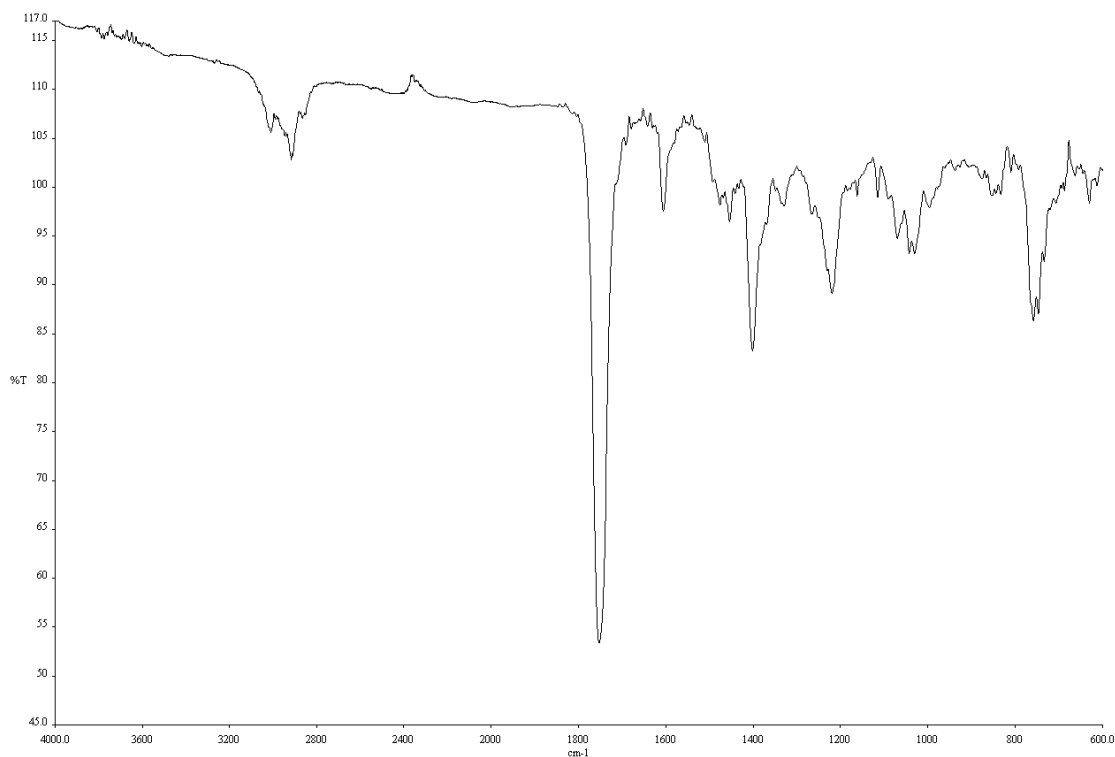
**Figure A3.37** Infrared spectrum (Thin Film, NaCl) of compound **175h**.



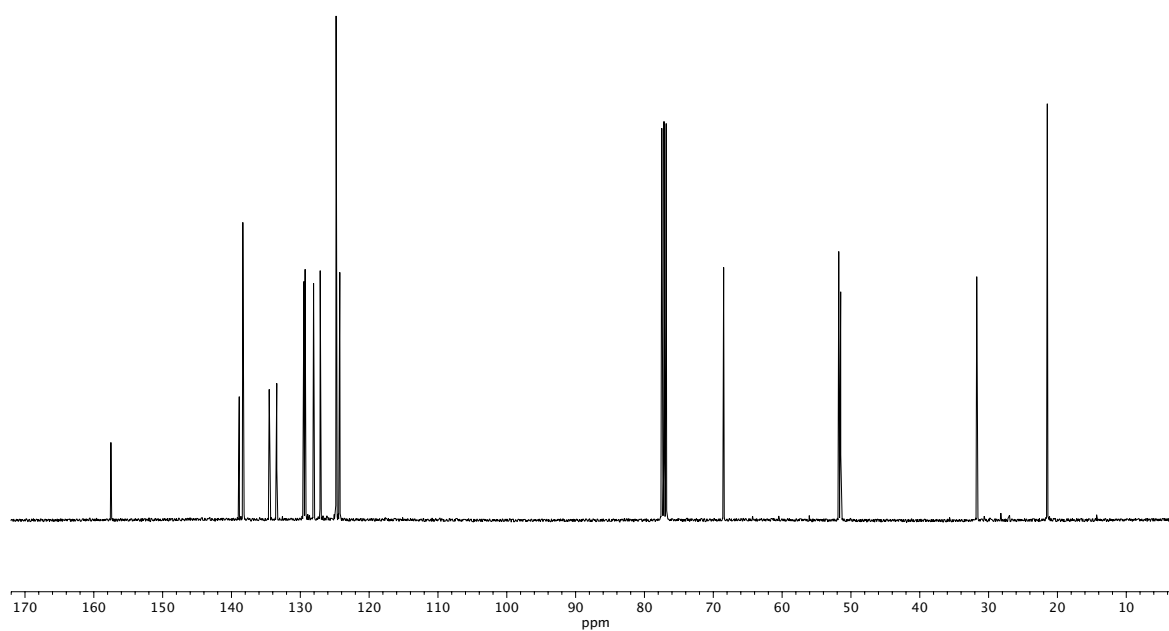
**Figure A3.38** <sup>13</sup>C NMR (100 MHz, CDCl<sub>3</sub>) of compound **175h**.



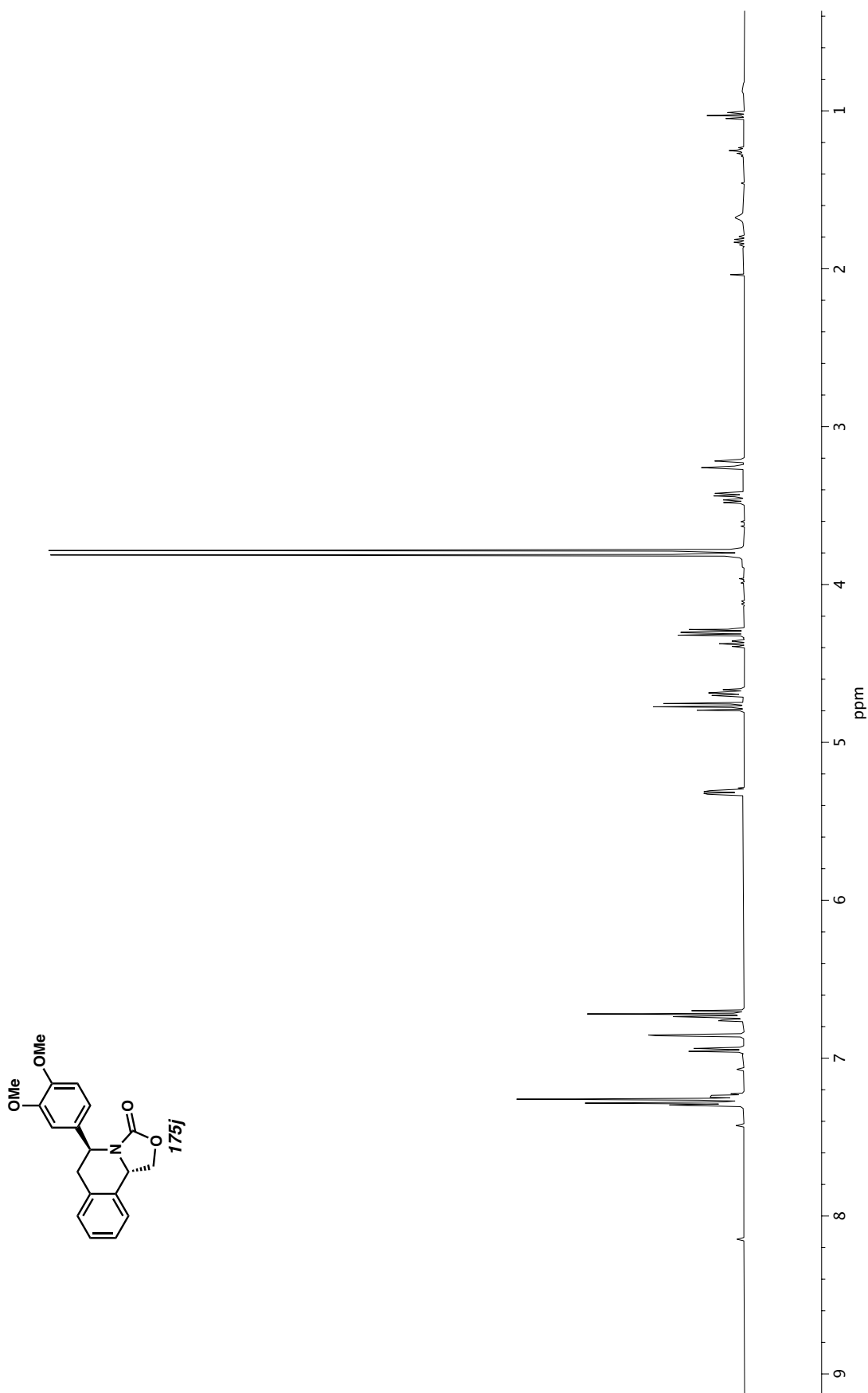
**Figure A3.39**  $^1\text{H}$  NMR (400 MHz,  $\text{CDCl}_3$ ) of compound **175i**.



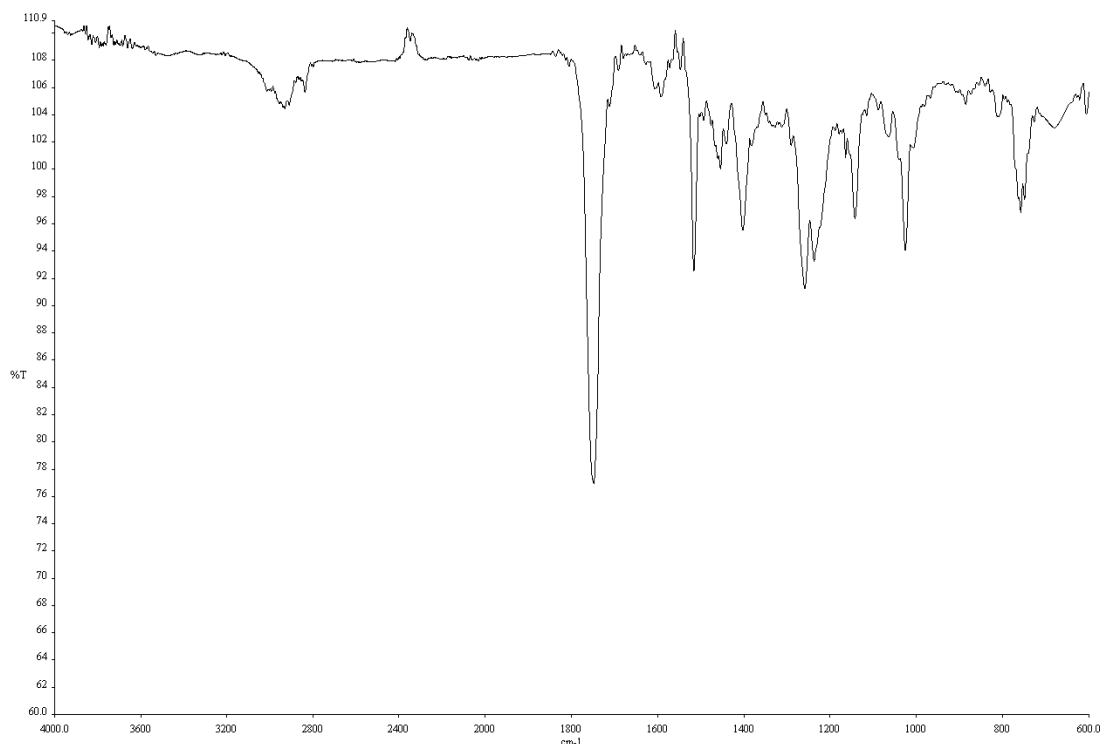
**Figure A3.40** Infrared spectrum (Thin Film, NaCl) of compound **175i**.



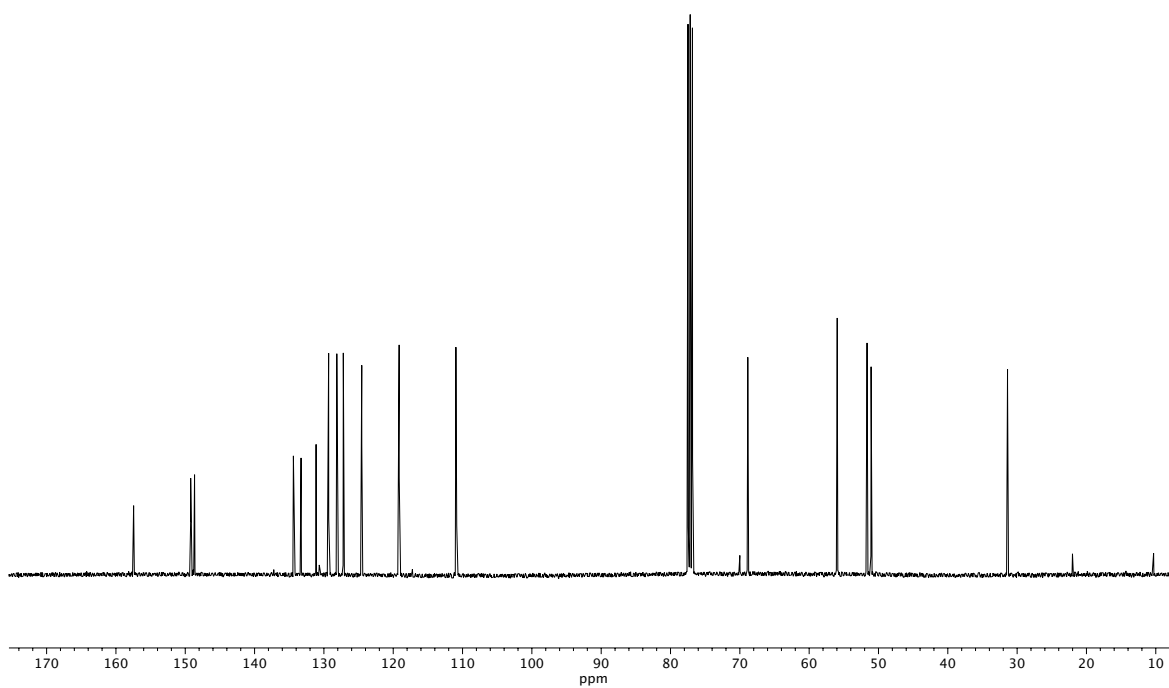
**Figure A3.41**  $^{13}\text{C}$  NMR (100 MHz,  $\text{CDCl}_3$ ) of compound **175i**.



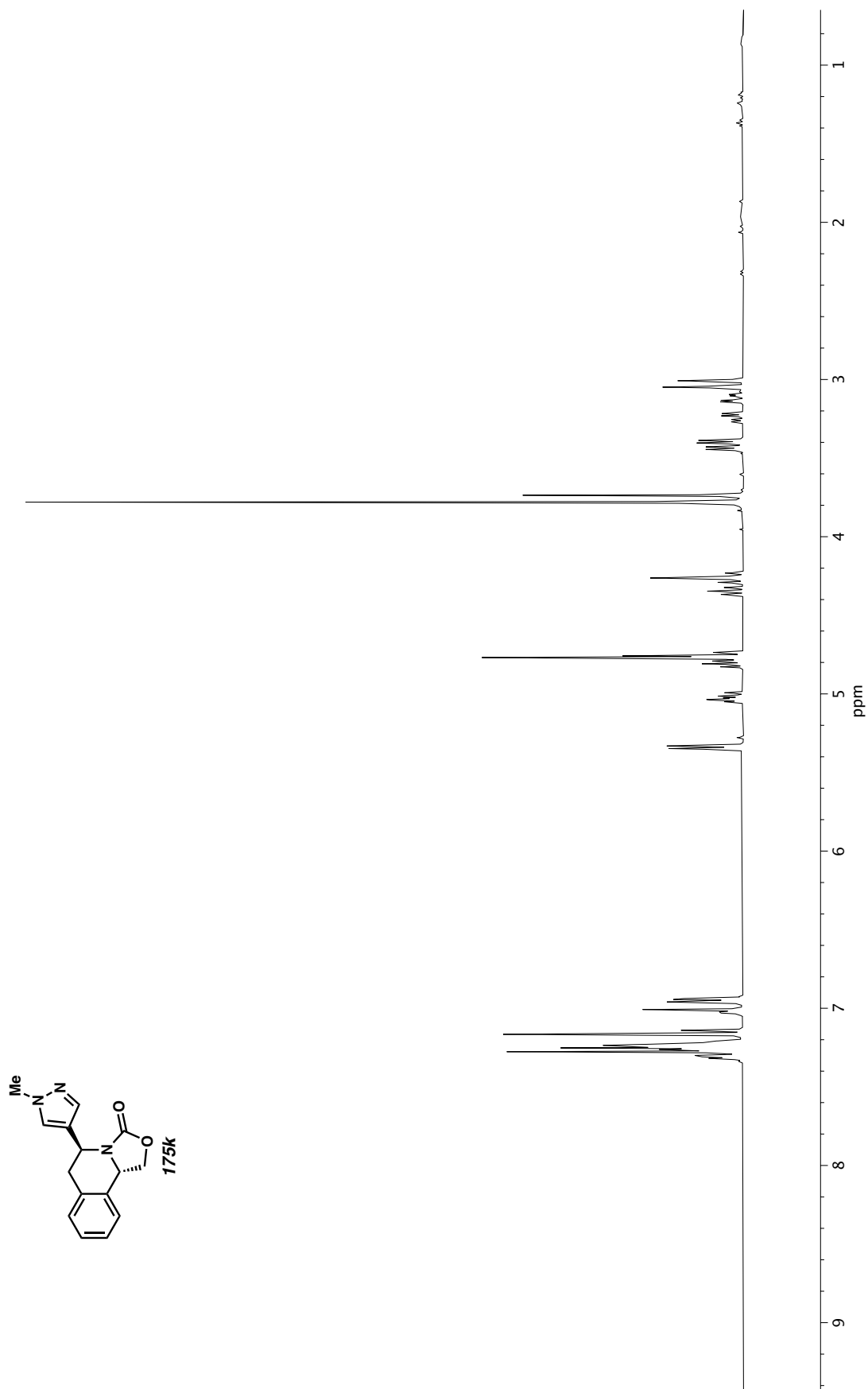
**Figure A3.42**  $^1\text{H}$  NMR (400 MHz,  $\text{CDCl}_3$ ) of compound **175j**.



**Figure A3.43** Infrared spectrum (Thin Film, NaCl) of compound **175j**.



**Figure A3.44** <sup>13</sup>C NMR (100 MHz, CDCl<sub>3</sub>) of compound **175j**.



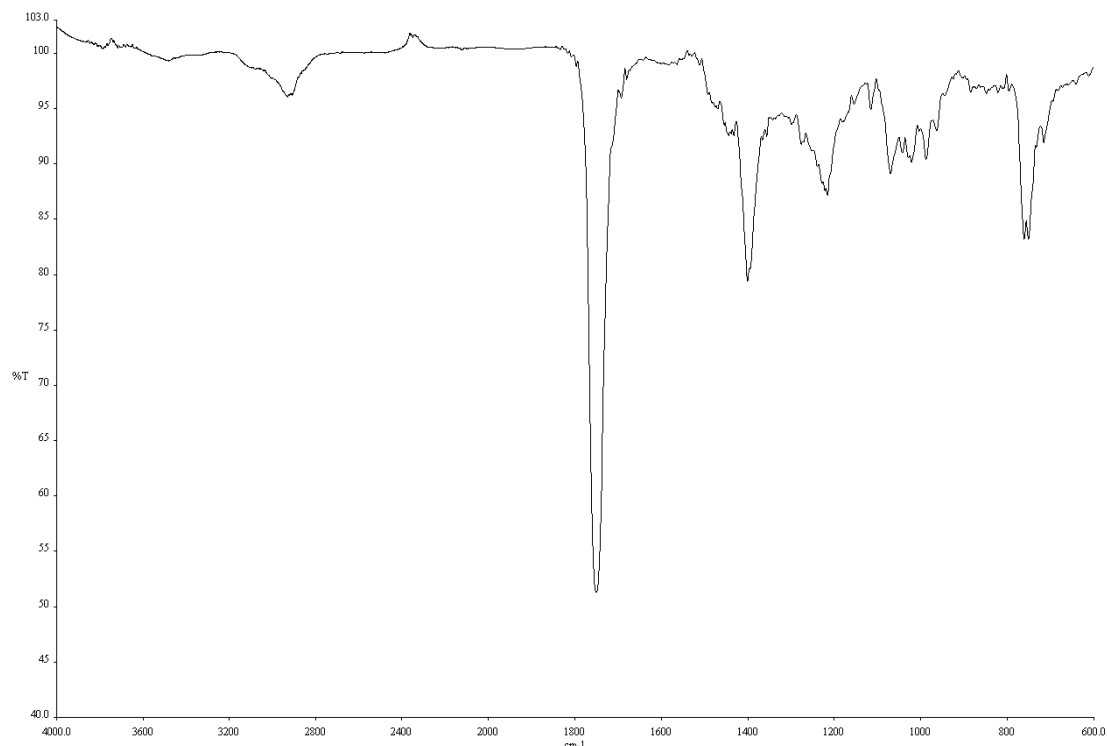


**Figure A3.46** Infrared spectrum (Thin Film, NaCl) of compound **175k**.

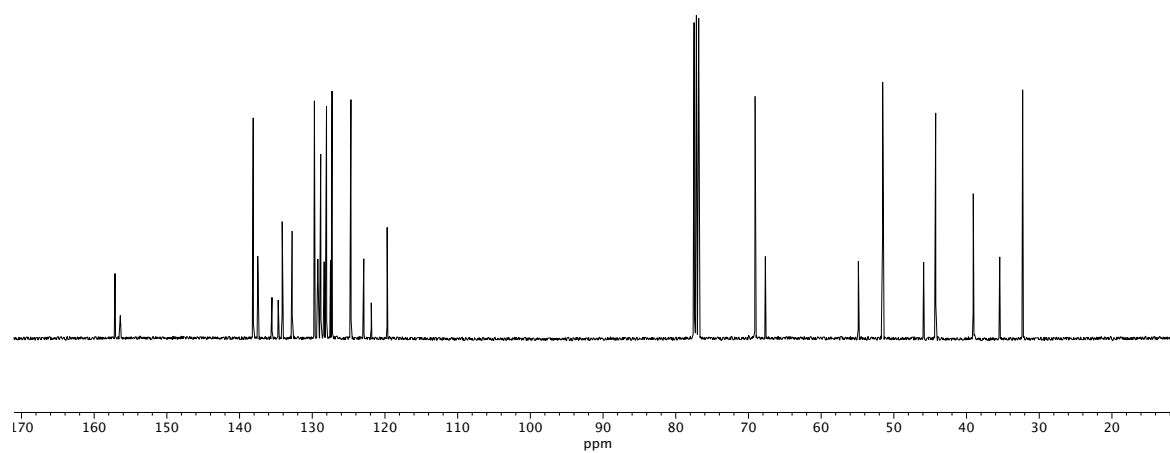


**Figure A3.47** <sup>13</sup>C NMR (100 MHz, CDCl<sub>3</sub>) of compound **175k**.



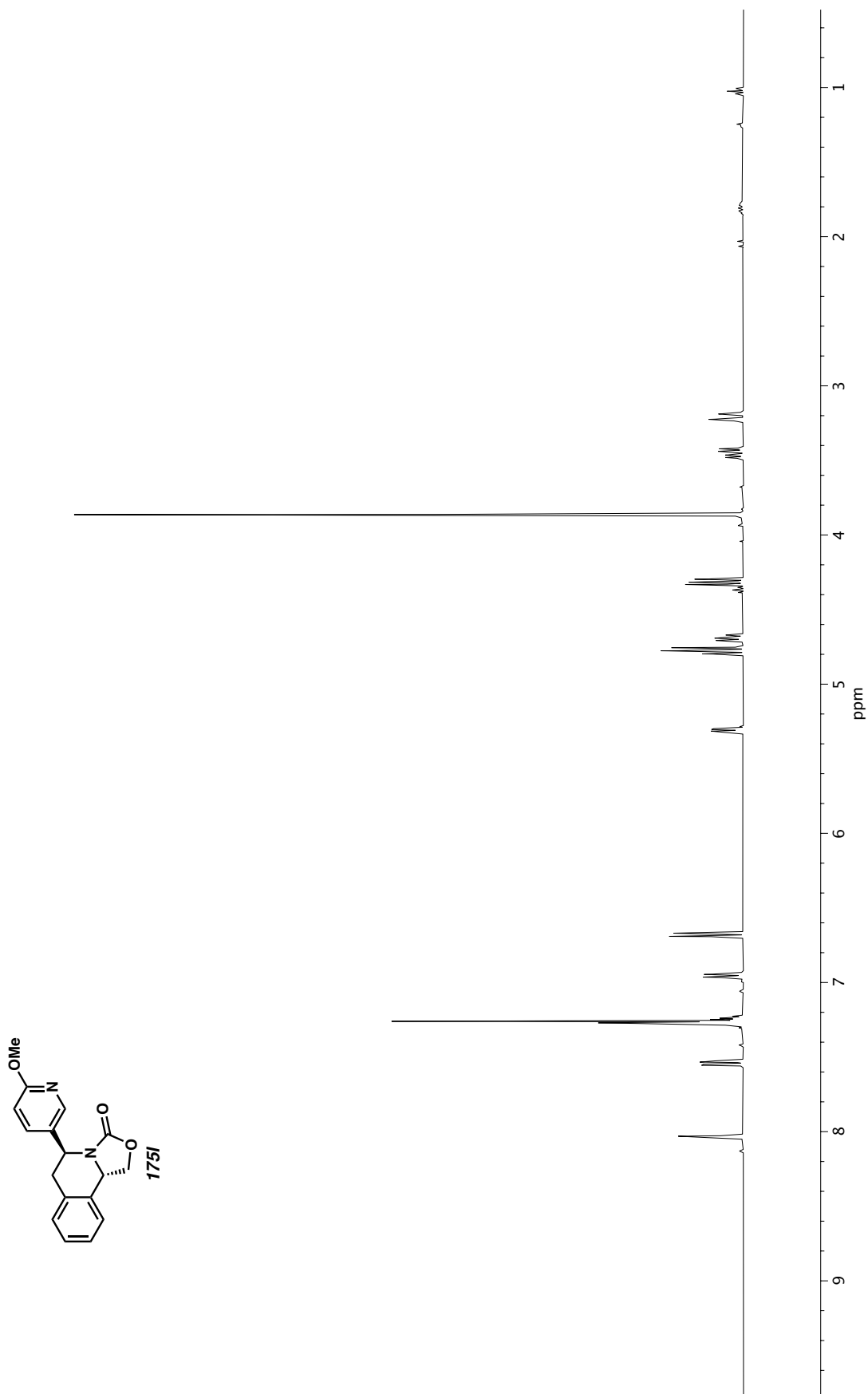


**Figure A3.48**  $^1\text{H}$  NMR (400 MHz,  $\text{CDCl}_3$ ) of compound 175I.

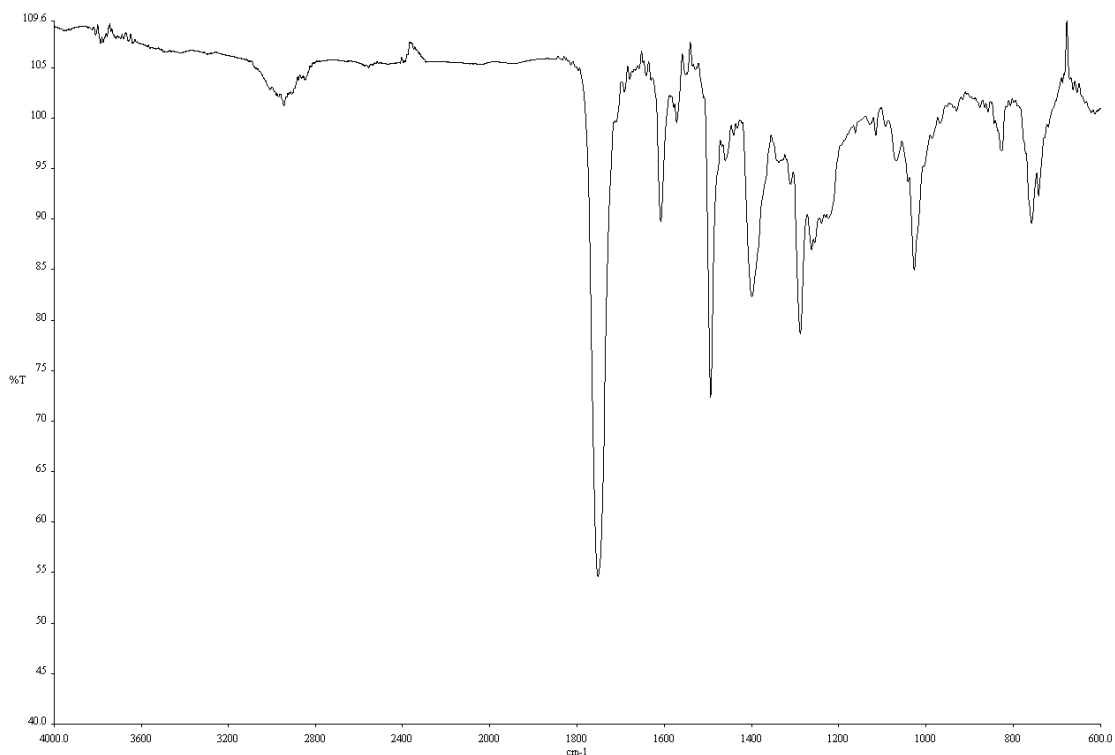


**Figure A3.49** Infrared spectrum (Thin Film, NaCl) of compound **175I**.

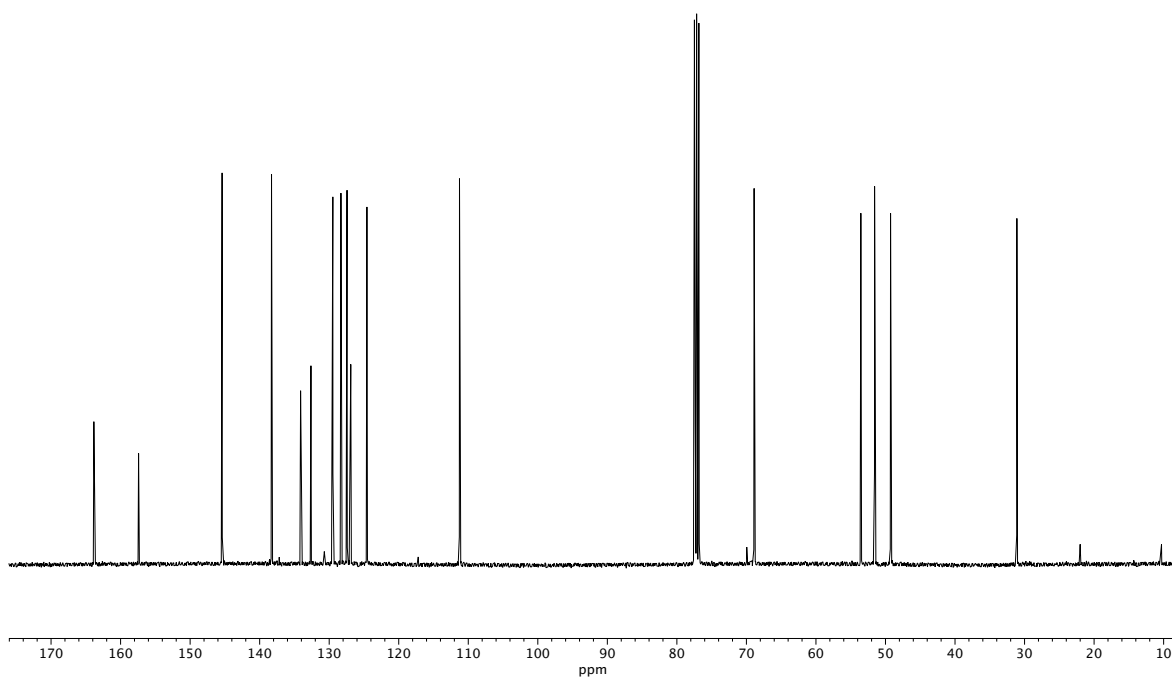


**Figure A3.50** <sup>13</sup>C NMR (100 MHz, CDCl<sub>3</sub>) of compound **175I**.

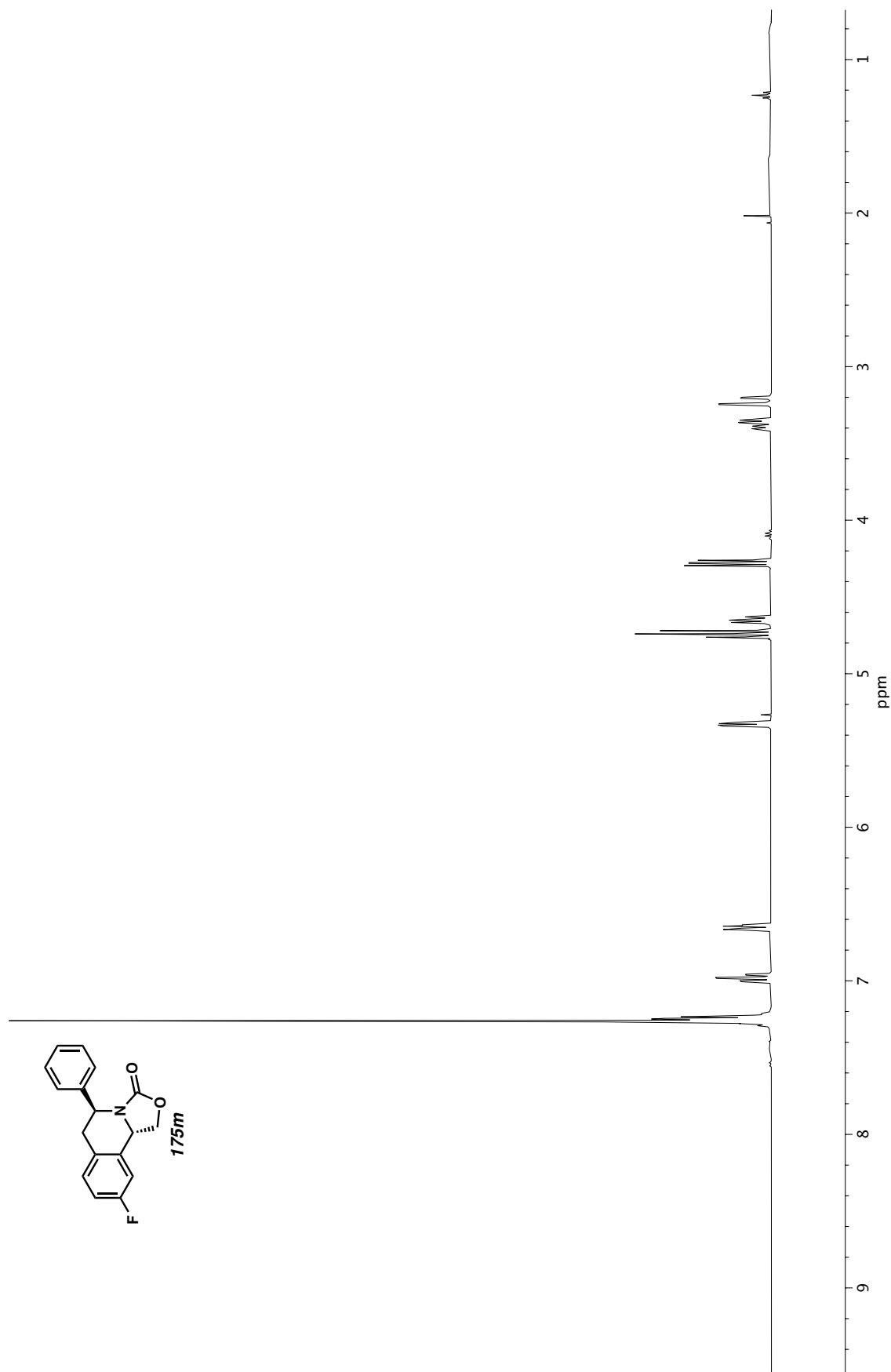


**Figure A3.51** <sup>1</sup>H NMR (400 MHz, CDCl<sub>3</sub>) of compound **175m**.

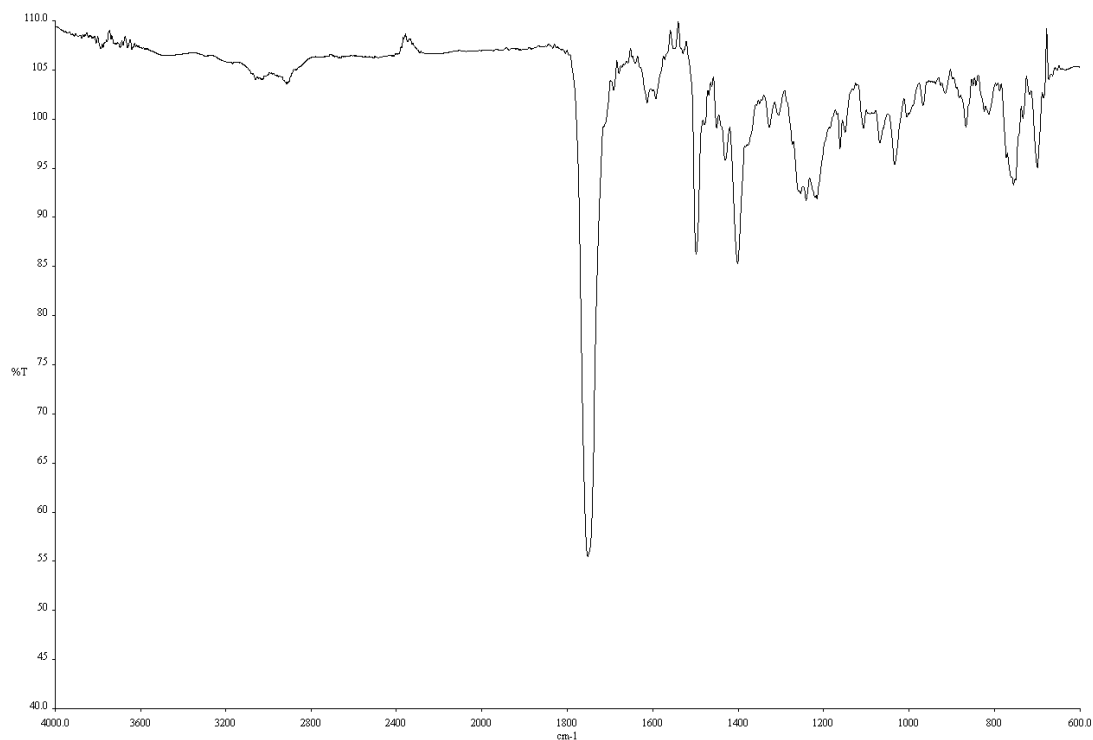


**Figure A3.52** Infrared spectrum (Thin Film, NaCl) of compound **175m**.

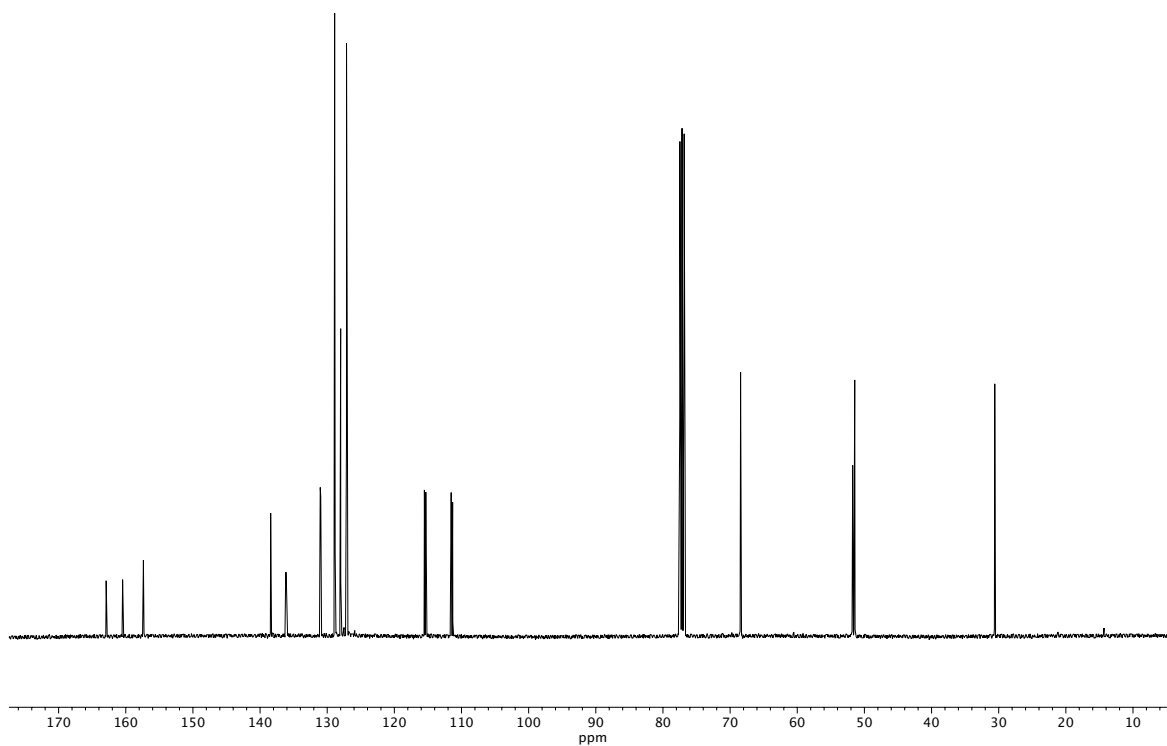


**Figure A3.53** <sup>13</sup>C NMR (100 MHz, CDCl<sub>3</sub>) of compound **175m**.

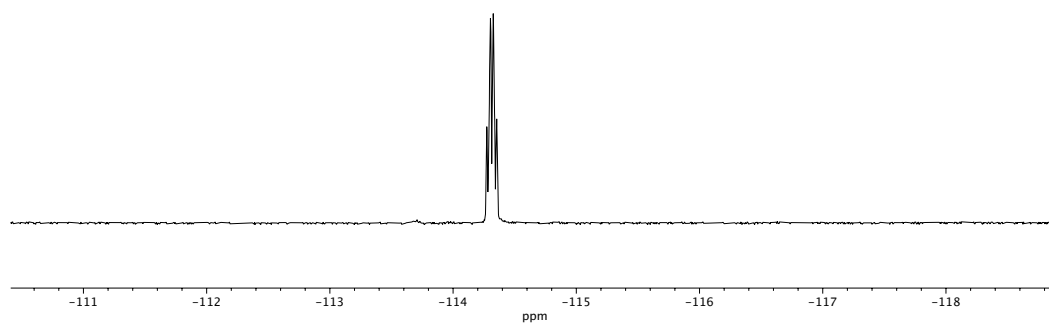


**Figure A3.54**  $^{19}\text{F}$  NMR (282 MHz,  $\text{CDCl}_3$ ) of compound **175m**.

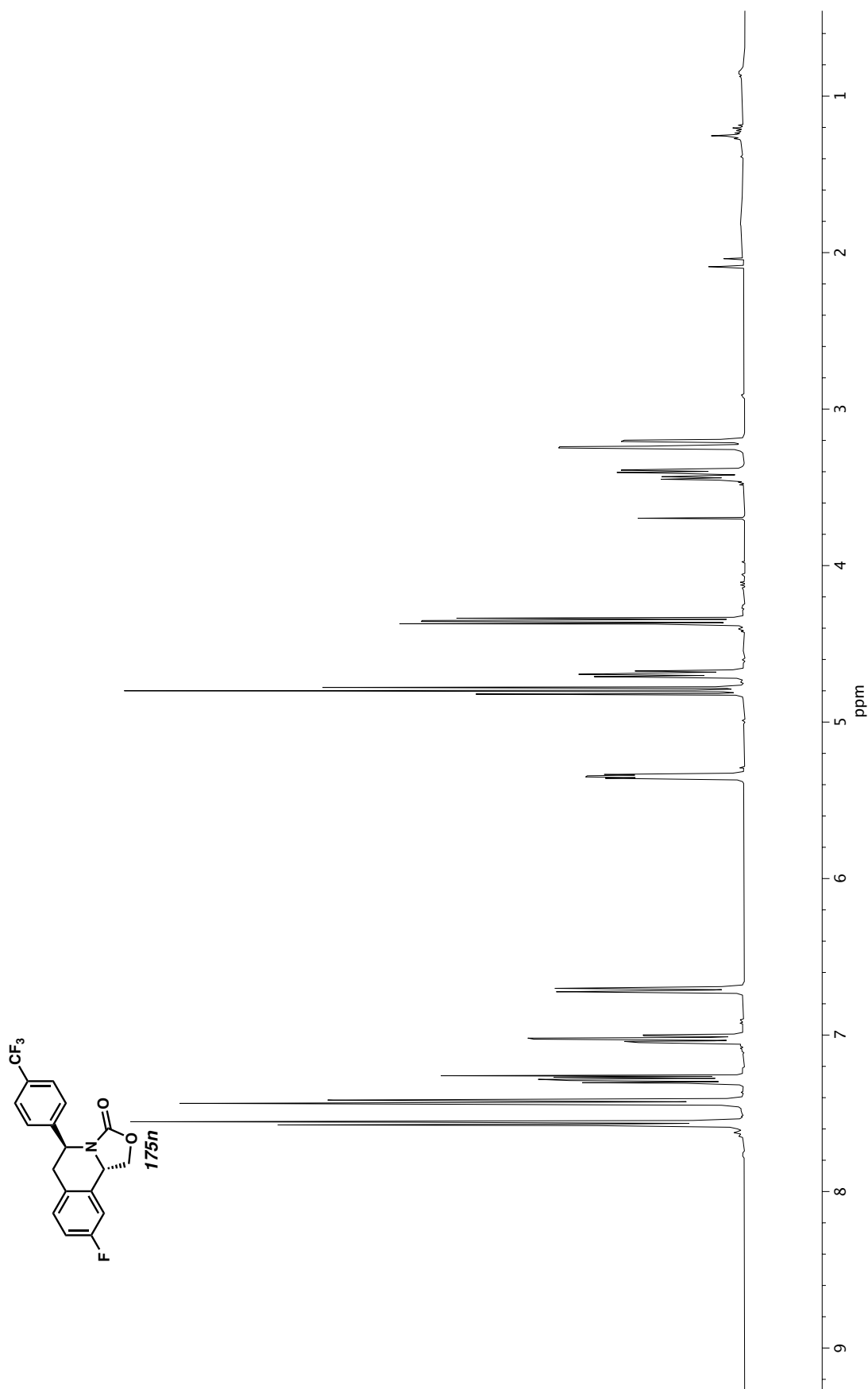


**Figure A3.55**  $^1\text{H}$  NMR (400 MHz,  $\text{CDCl}_3$ ) of compound **175n**.

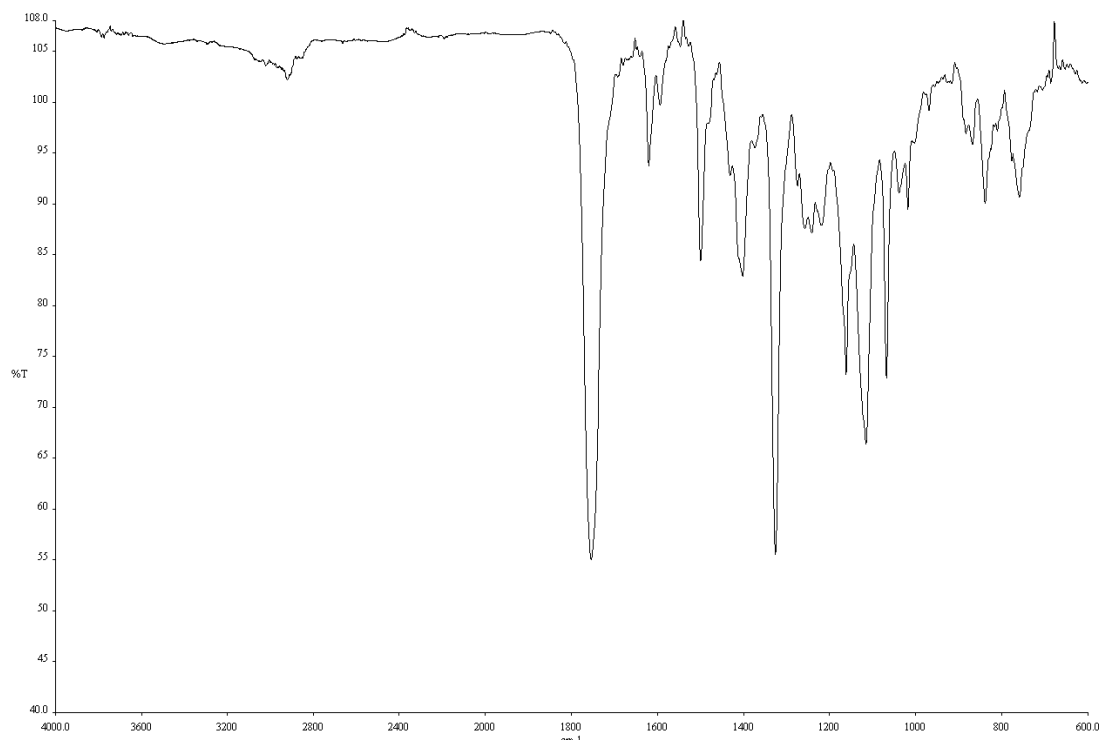


**Figure A3.56** Infrared spectrum (Thin Film, NaCl) of compound **175n**.

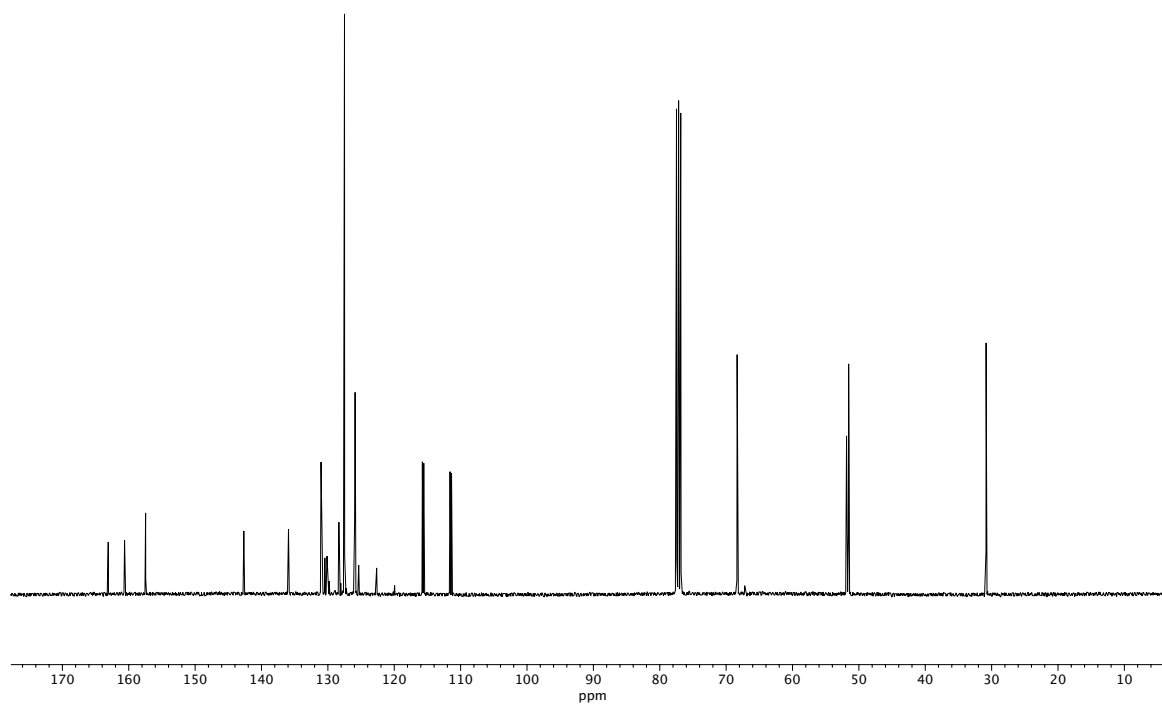


**Figure A3.57**  $^{13}\text{C}$  NMR (100 MHz,  $\text{CDCl}_3$ ) of compound **175n**.

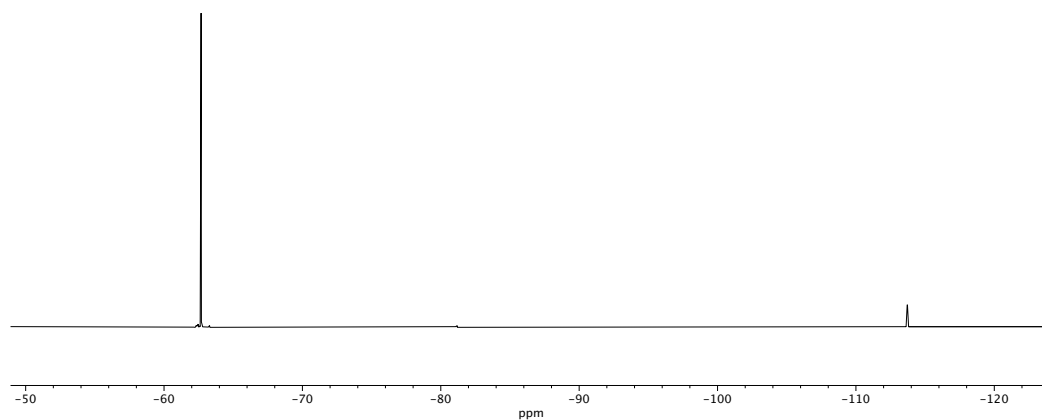


**Figure A3.58**  $^{19}\text{F}$  NMR (282 MHz,  $\text{CDCl}_3$ ) of compound **175n**.



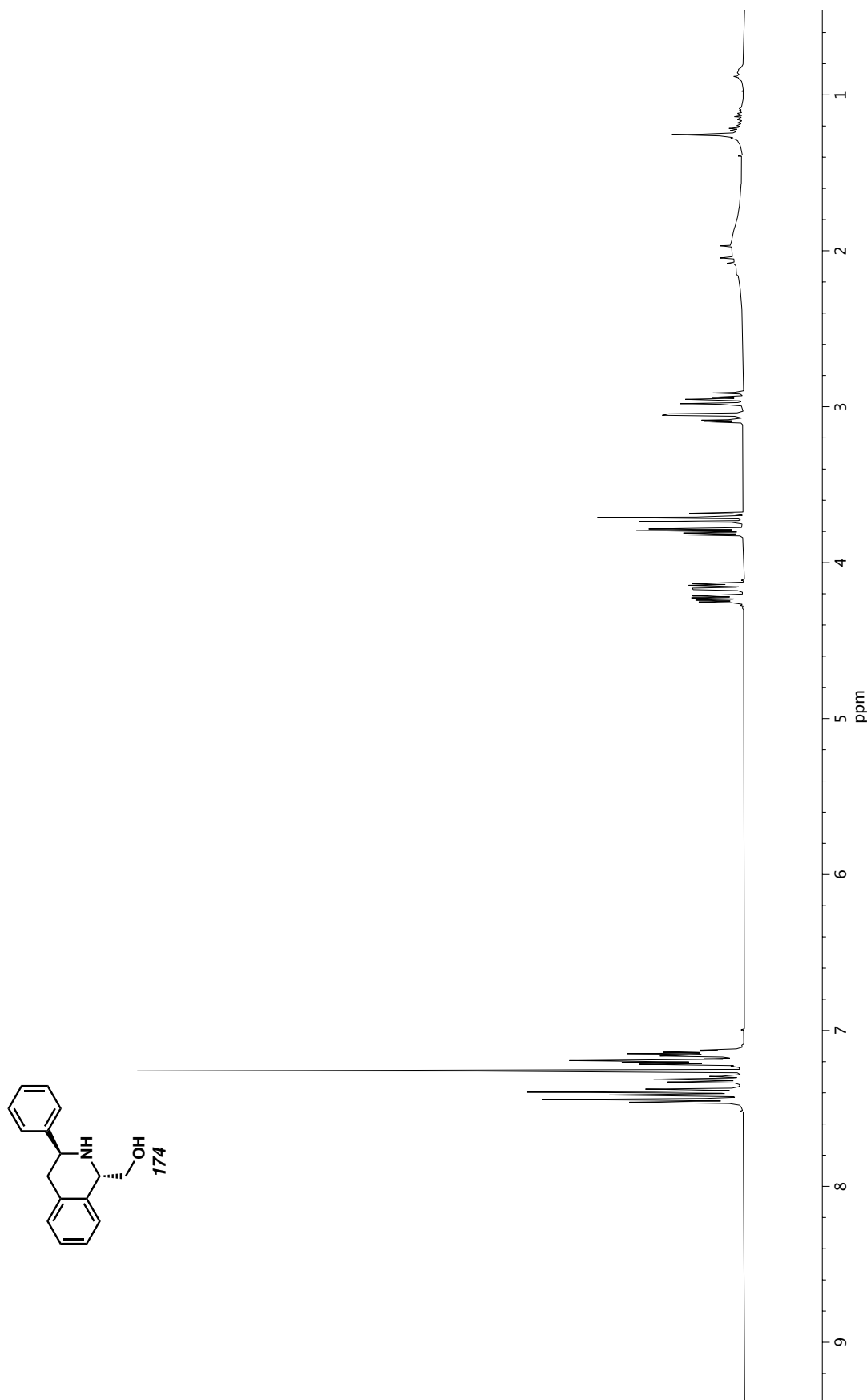


**Figure A3.59**  $^1\text{H}$  NMR (400 MHz,  $\text{CDCl}_3$ ) of compound **174**.

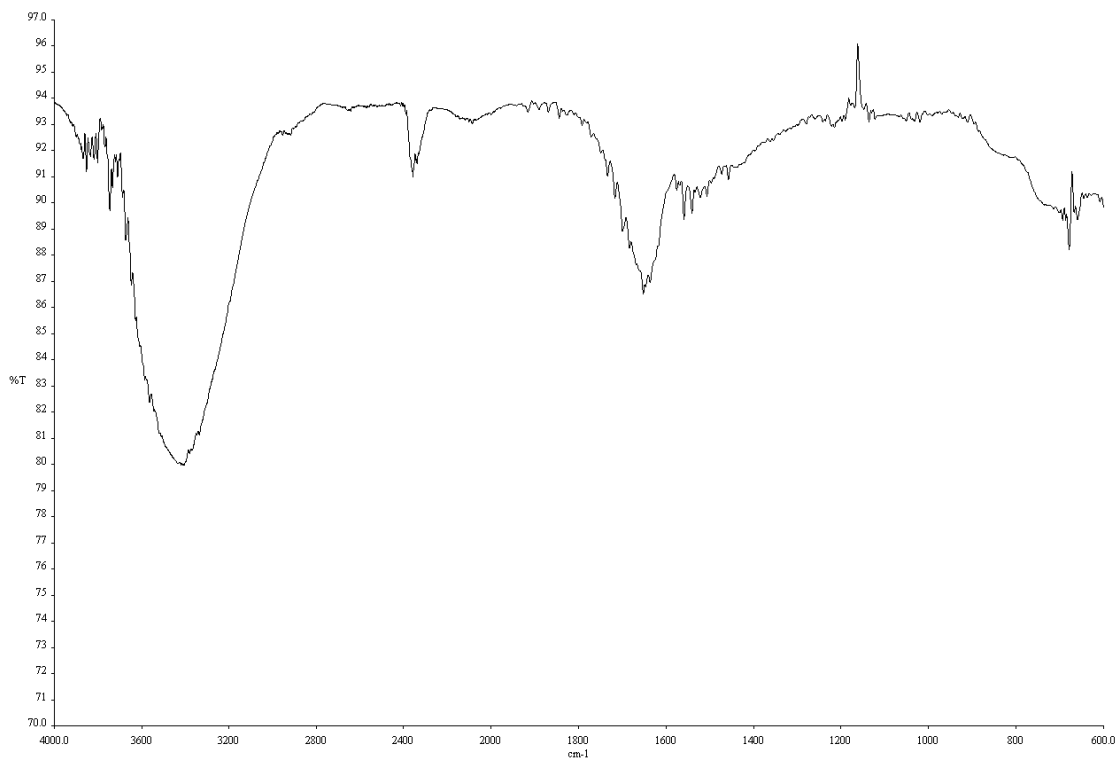


**Figure A3.60** Infrared spectrum (Thin Film, NaCl) of compound **174**.

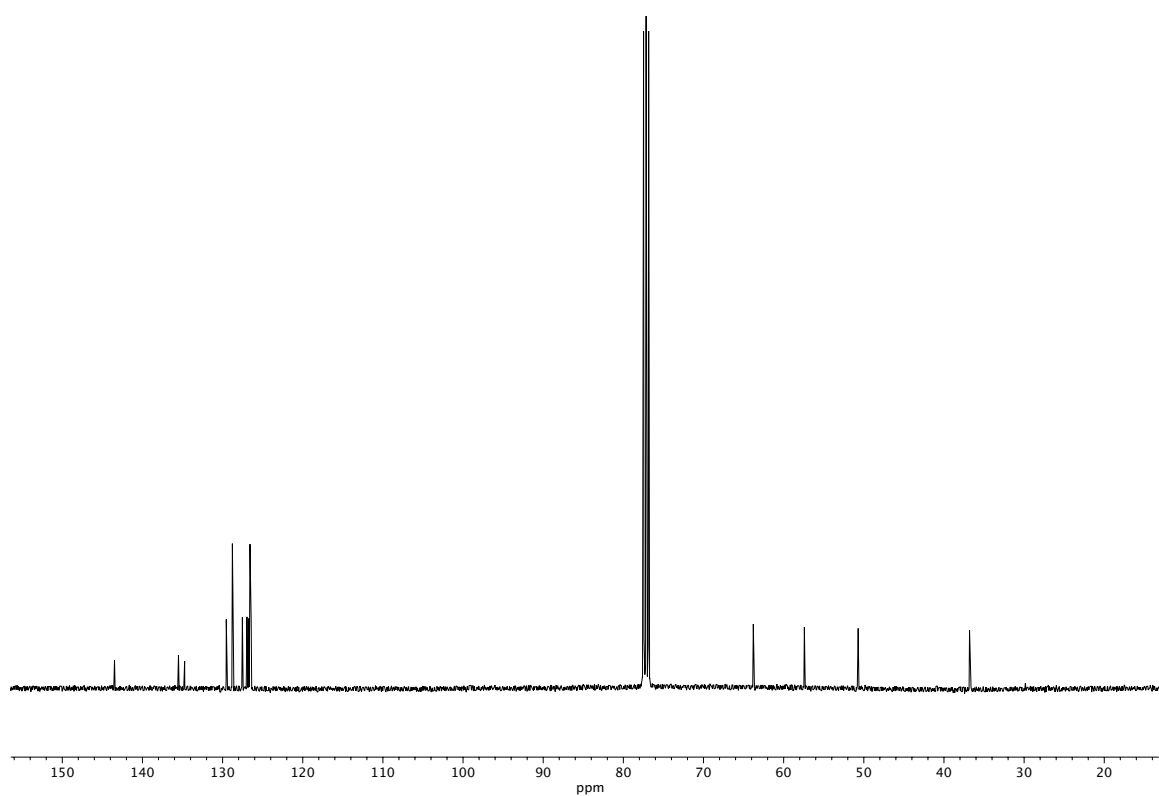


**Figure A3.61** <sup>13</sup>C NMR (100 MHz, CDCl<sub>3</sub>) of compound **174**.

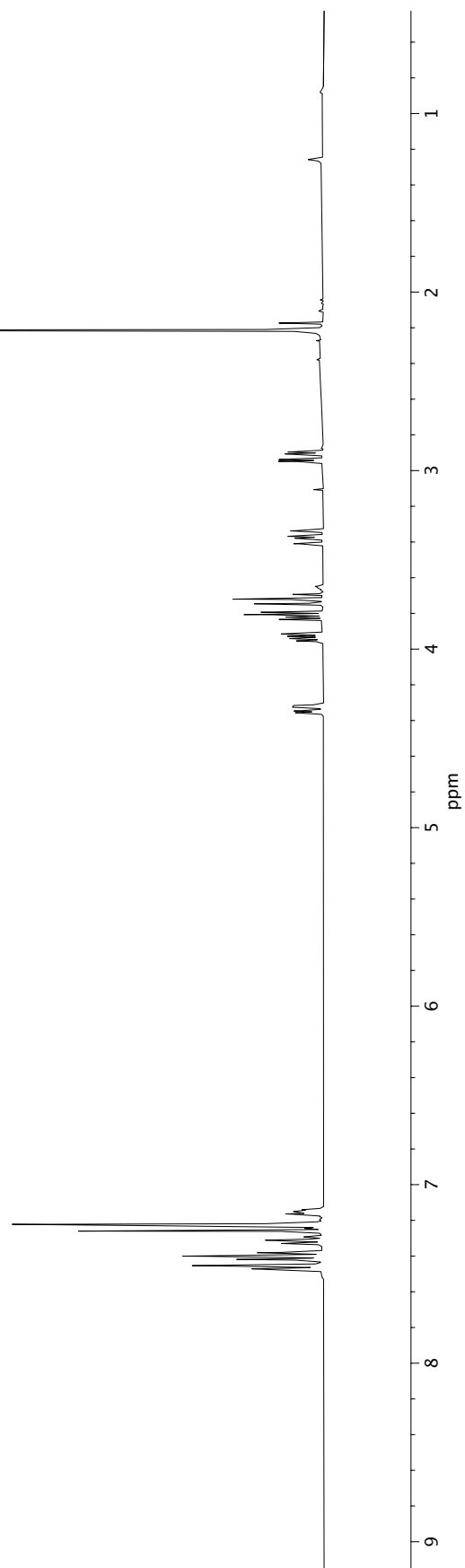
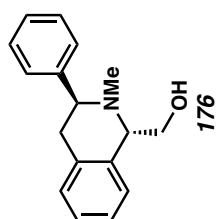
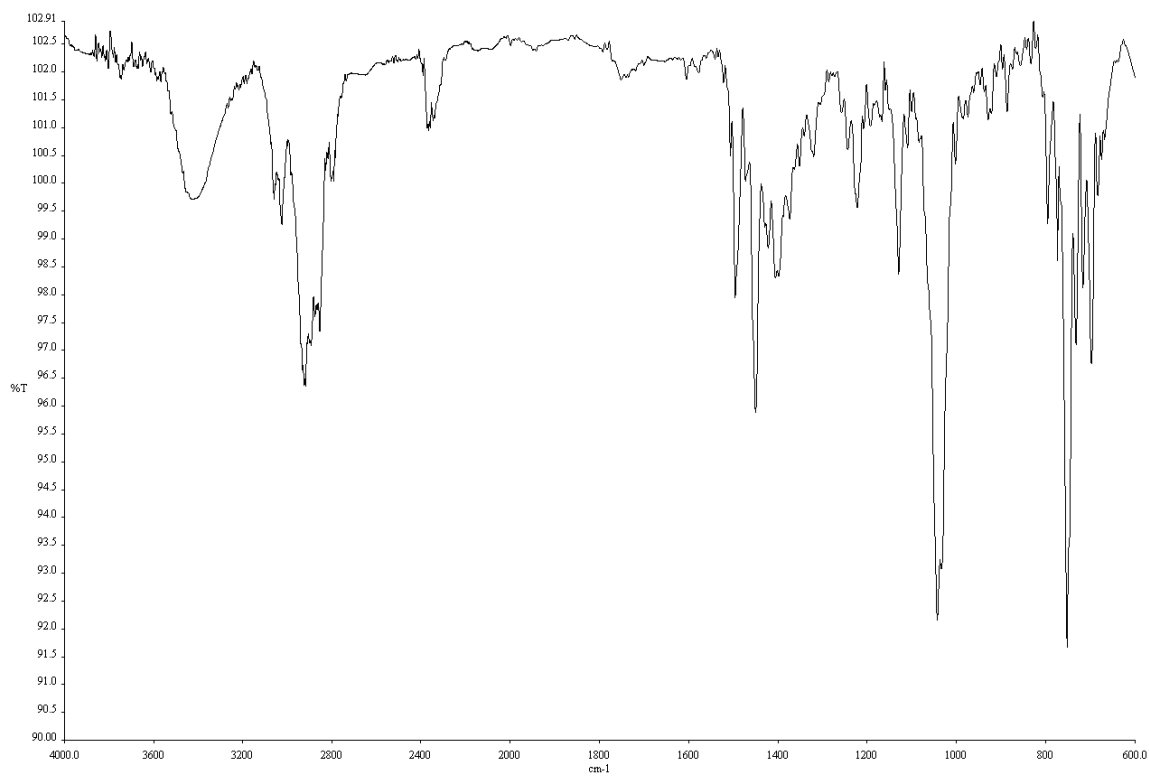
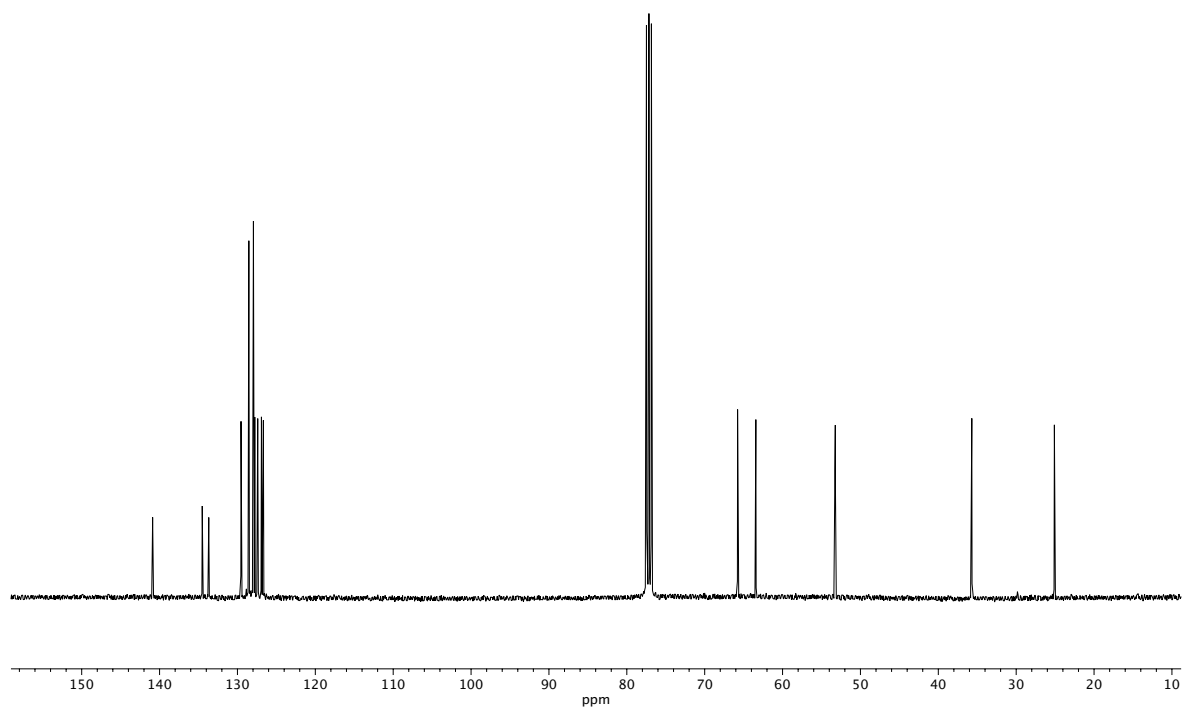


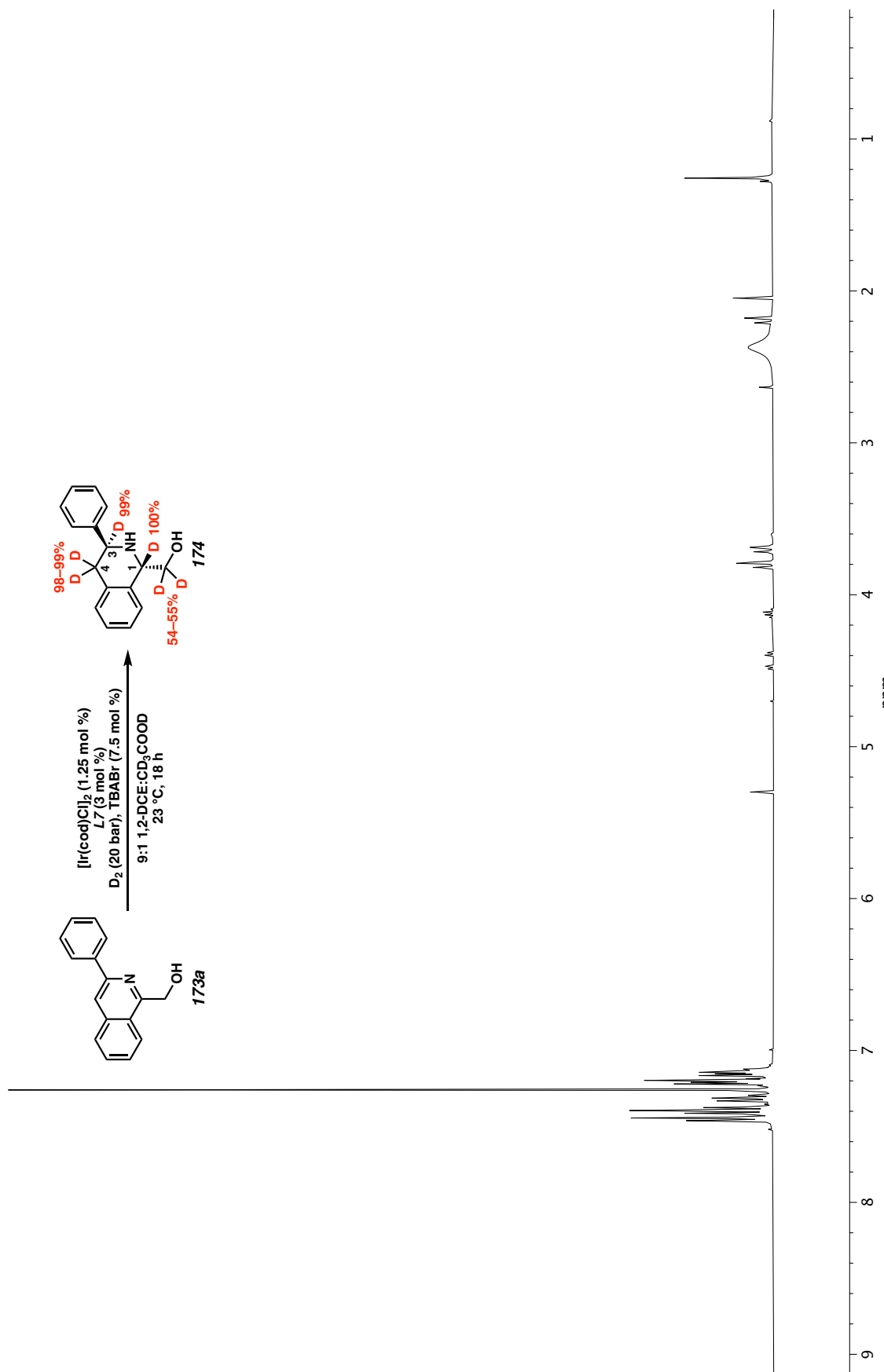
Figure A3.62 <sup>1</sup>H NMR (400 MHz, CDCl<sub>3</sub>) of compound 176.



**Figure A3.63** Infrared spectrum (Thin Film, NaCl) of compound **176**.



**Figure A3.64**  $^{13}\text{C}$  NMR (100 MHz,  $\text{CDCl}_3$ ) of compound **176**.

Figure A3.65  $^1\text{H}$  NMR (400 MHz,  $\text{CDCl}_3$ ) of compound **174**.

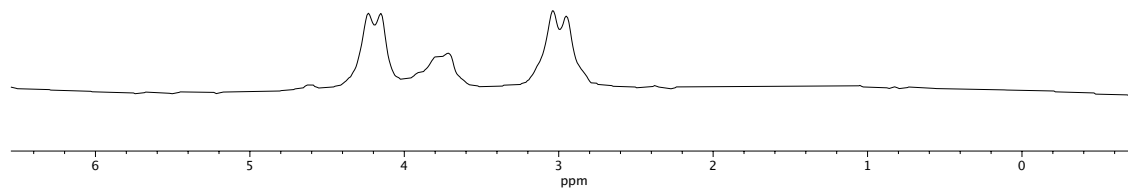


**Figure A3.66**  $^2\text{H}$  NMR (61 MHz,  $\text{CDCl}_3$ ) of compound  $d_5$ -174.

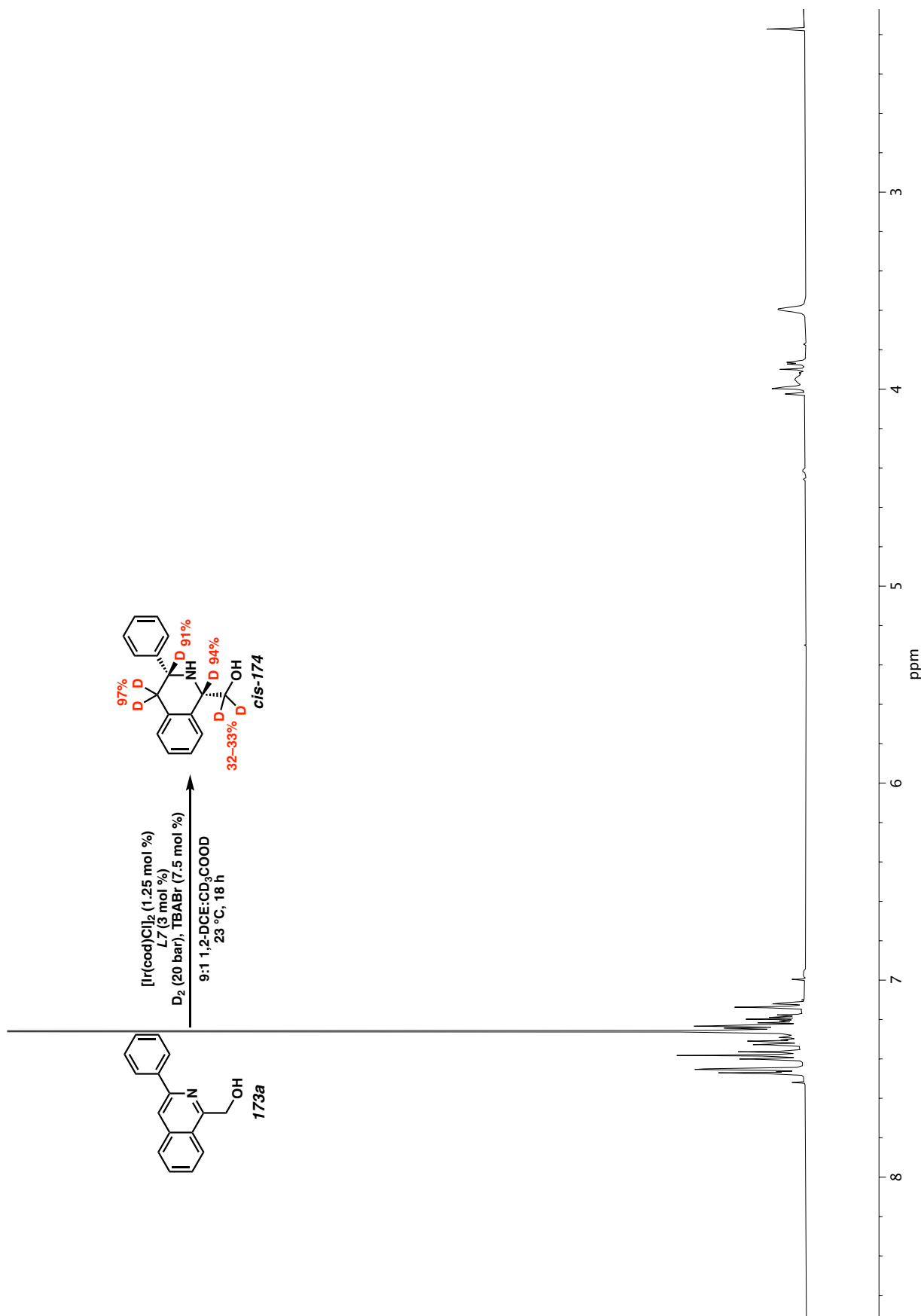


Figure A3.67  $^1\text{H}$  NMR (400 MHz,  $\text{CDCl}_3$ ) of compound **d<sub>n</sub>-cis-174**.

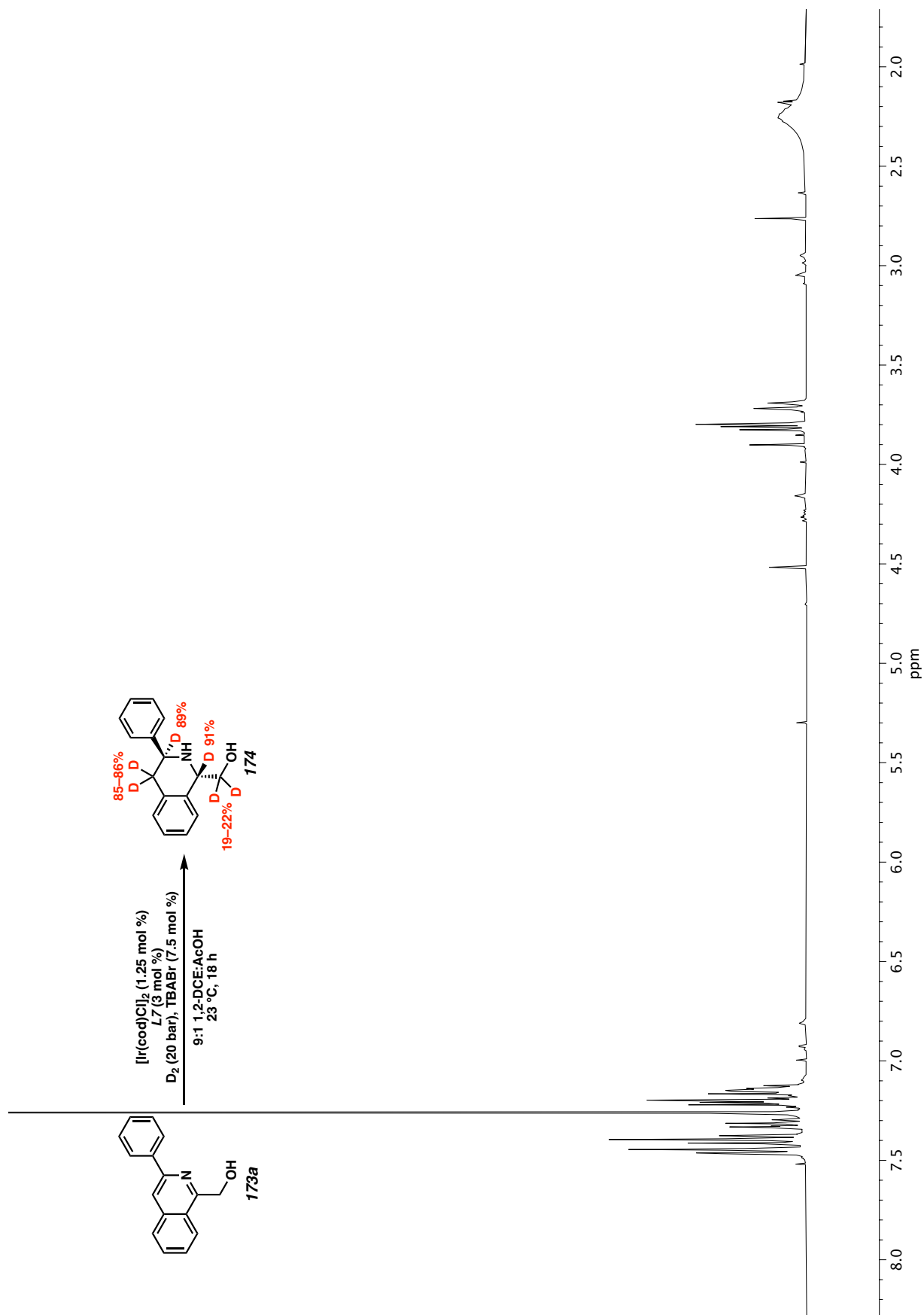
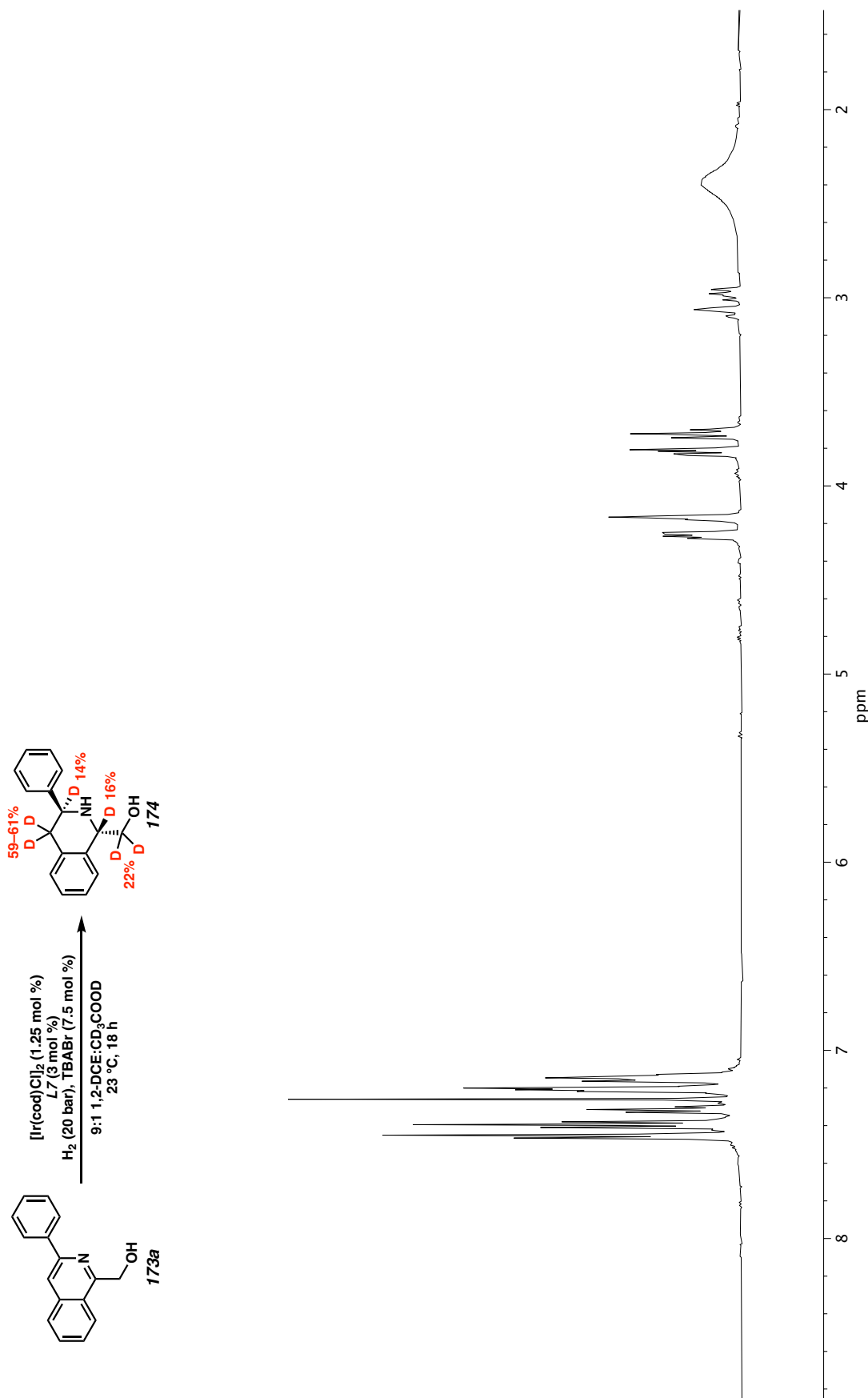


Figure A3.68  $^1\text{H}$  NMR (400 MHz,  $\text{CDCl}_3$ ) of compound **174**.





**Figure A3.69** <sup>1</sup>H NMR (400 MHz, CDCl<sub>3</sub>) of compound **d<sub>r</sub>-174**.

## **APPENDIX 4**

*X-Ray Crystallography Reports Relevant to Chapter 3:*

*Iridium-Catalyzed Asymmetric Trans-Selective*

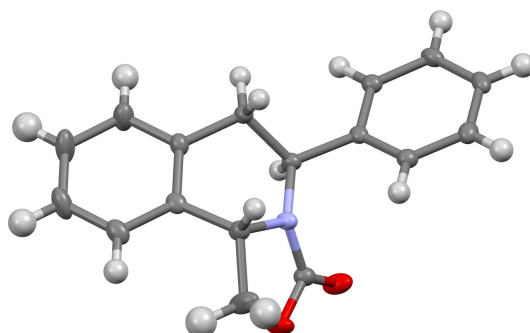
*Hydrogenation of 1,3-Disubstituted Isoquinolines*

#### A4.1 GENERAL EXPERIMENTAL

A crystal was mounted on a polyimide MiTeGen loop with STP Oil Treatment and placed under a nitrogen stream. Low temperature (100K) X-ray data ( $\phi$ - and  $\omega$ -scans) were collected with a Bruker AXS D8 VENTURE KAPPA diffractometer coupled to a PHOTON II CPAD detector with Cu  $K_{\alpha}$  radiation ( $\lambda = 1.54178 \text{ \AA}$ ) from an I $\mu$ S micro-source for the structure of compound V21097. The structure was solved by direct methods using SHELXS and refined against  $F^2$  on all data by full-matrix least squares with SHELXL-2017 using established refinement techniques. All non-hydrogen atoms were refined using anisotropic displacement parameters. Hydrogen atoms were placed in idealized positions and the coordinates refined (each of the two disordered pairs were constrained to the same position). The isotropic displacement parameters of all hydrogen atoms were fixed at 1.2 times (1.5 times for methyl groups and alcohol) the  $U_{eq}$  value of the bonded atom.

#### A4.2 X-RAY CRYSTAL STRUCTURE ANALYSIS OF THIQ 175a

The tetrahydroisoquinoline (THIQ) product **175a** (91% ee) was crystallized by slow evaporation from chloroform at 23 °C to provide crystals suitable for X-ray analysis. Compound V21097 crystallizes in the orthorhombic space group  $P2_12_12_1$  with one molecule in the asymmetric unit.

**Figure A4.1** X-ray crystal structure of **THIQ 175a**.**Table A4.1** Crystal data and structure refinement for product **175a**.

Identification code	V21097	
Empirical formula	C <sub>17</sub> H <sub>15</sub> N O <sub>2</sub>	
Formula weight	265.30	
Temperature	100(2) K	
Wavelength	1.54178 Å	
Crystal system	Orthorhombic	
Space group	P2 <sub>1</sub> 2 <sub>1</sub> 2 <sub>1</sub>	
Unit cell dimensions	a = 6.5620(8) Å	a = 90°.
	b = 14.2320(17) Å	b = 90°.
	c = 14.4563(19) Å	g = 90°.
Volume	1350.1(3) Å <sup>3</sup>	
Z	4	
Density (calculated)	1.305 Mg/m <sup>3</sup>	
Absorption coefficient	0.687 mm <sup>-1</sup>	
F(000)	560	
Crystal size	0.300 x 0.150 x 0.150 mm <sup>3</sup>	
Theta range for data collection	4.359 to 79.624°.	
Index ranges	-8<=h<=8, -17<=k<=18, -18<=l<=18	
Reflections collected	23786	

Independent reflections	2903 [R(int) = 0.0368]
Completeness to theta = 67.679°	100.0 %
Absorption correction	Semi-empirical from equivalents
Max. and min. transmission	0.7543 and 0.6141
Refinement method	Full-matrix least-squares on F <sup>2</sup>
Data / restraints / parameters	2903 / 0 / 181
Goodness-of-fit on F <sup>2</sup>	1.106
Final R indices [I > 2σ(I)]	R1 = 0.0314, wR2 = 0.0806
R indices (all data)	R1 = 0.0317, wR2 = 0.0807
Absolute structure parameter	0.04(5)
Extinction coefficient	n/a
Largest diff. peak and hole	0.157 and -0.228 e.Å <sup>-3</sup>

**Table A4.2** Atomic coordinates ( $\times 10^4$ ), and equivalent isotropic displacement parameters ( $\text{\AA}^2 \times 10^3$ ), and population for **175a**.  $U(\text{eq})$  is defined as one third of the trace of the orthogonalized  $U_{ij}$  tensor.

	x	y	z	U(eq)
C(1)	5632(2)	5374(1)	8245(1)	20(1)
O(1)	7103(2)	4818(1)	8618(1)	26(1)
O(2)	3839(2)	5236(1)	8370(1)	30(1)
C(2)	9070(3)	5142(1)	8341(2)	39(1)
C(3)	8729(2)	6082(1)	7842(1)	20(1)
C(4)	9357(2)	6972(1)	8337(1)	18(1)
C(5)	10846(3)	7016(1)	9020(1)	24(1)
C(6)	11296(3)	7867(2)	9444(1)	32(1)
C(7)	10246(3)	8669(2)	9192(1)	35(1)
C(8)	8766(3)	8632(1)	8500(1)	28(1)
C(9)	8329(2)	7787(1)	8060(1)	19(1)
C(10)	6807(2)	7701(1)	7288(1)	19(1)

C(11)	5305(2)	6893(1)	7469(1)	16(1)
C(12)	3921(2)	6716(1)	6645(1)	16(1)
C(13)	4020(3)	5903(1)	6111(1)	20(1)
C(14)	2681(3)	5771(1)	5375(1)	22(1)
C(15)	1261(3)	6451(1)	5150(1)	23(1)
C(16)	1180(3)	7277(1)	5665(1)	22(1)
C(17)	2487(2)	7401(1)	6413(1)	19(1)
N(1)	6496(2)	6060(1)	7731(1)	19(1)

---

**Table A4.3** Bond lengths [ $\text{\AA}$ ] and angles [ $^\circ$ ] for **175a**.

---

C(1)-O(2)	1.206(2)
C(1)-N(1)	1.352(2)
C(1)-O(1)	1.360(2)
O(1)-C(2)	1.428(2)
C(2)-C(3)	1.536(2)
C(2)-H(2A)	0.9900
C(2)-H(2B)	0.9900
C(3)-N(1)	1.474(2)
C(3)-C(4)	1.512(2)
C(3)-H(3)	1.0000
C(4)-C(5)	1.391(2)
C(4)-C(9)	1.401(2)
C(5)-C(6)	1.389(3)
C(5)-H(5)	0.9500
C(6)-C(7)	1.383(3)
C(6)-H(6)	0.9500
C(7)-C(8)	1.395(3)
C(7)-H(7)	0.9500
C(8)-C(9)	1.390(2)
C(8)-H(8)	0.9500
C(9)-C(10)	1.503(2)
C(10)-C(11)	1.537(2)
C(10)-H(10A)	0.9900

C(10)-H(10B)	0.9900
C(11)-N(1)	1.4693(19)
C(11)-C(12)	1.518(2)
C(11)-H(11)	1.0000
C(12)-C(13)	1.392(2)
C(12)-C(17)	1.395(2)
C(13)-C(14)	1.393(2)
C(13)-H(13)	0.9500
C(14)-C(15)	1.382(3)
C(14)-H(14)	0.9500
C(15)-C(16)	1.391(2)
C(15)-H(15)	0.9500
C(16)-C(17)	1.391(2)
C(16)-H(16)	0.9500
C(17)-H(17)	0.9500
O(2)-C(1)-N(1)	127.52(16)
O(2)-C(1)-O(1)	122.54(15)
N(1)-C(1)-O(1)	109.93(14)
C(1)-O(1)-C(2)	110.03(13)
O(1)-C(2)-C(3)	106.31(14)
O(1)-C(2)-H(2A)	110.5
C(3)-C(2)-H(2A)	110.5
O(1)-C(2)-H(2B)	110.5
C(3)-C(2)-H(2B)	110.5
H(2A)-C(2)-H(2B)	108.7
N(1)-C(3)-C(4)	109.86(13)
N(1)-C(3)-C(2)	100.27(13)
C(4)-C(3)-C(2)	117.83(15)
N(1)-C(3)-H(3)	109.5
C(4)-C(3)-H(3)	109.5
C(2)-C(3)-H(3)	109.5
C(5)-C(4)-C(9)	120.26(15)
C(5)-C(4)-C(3)	124.42(15)
C(9)-C(4)-C(3)	115.32(14)

C(6)-C(5)-C(4)	120.11(17)
C(6)-C(5)-H(5)	119.9
C(4)-C(5)-H(5)	119.9
C(7)-C(6)-C(5)	119.90(17)
C(7)-C(6)-H(6)	120.1
C(5)-C(6)-H(6)	120.1
C(6)-C(7)-C(8)	120.27(17)
C(6)-C(7)-H(7)	119.9
C(8)-C(7)-H(7)	119.9
C(9)-C(8)-C(7)	120.30(17)
C(9)-C(8)-H(8)	119.9
C(7)-C(8)-H(8)	119.9
C(8)-C(9)-C(4)	119.13(15)
C(8)-C(9)-C(10)	123.21(15)
C(4)-C(9)-C(10)	117.66(14)
C(9)-C(10)-C(11)	111.16(13)
C(9)-C(10)-H(10A)	109.4
C(11)-C(10)-H(10A)	109.4
C(9)-C(10)-H(10B)	109.4
C(11)-C(10)-H(10B)	109.4
H(10A)-C(10)-H(10B)	108.0
N(1)-C(11)-C(12)	112.78(13)
N(1)-C(11)-C(10)	107.82(12)
C(12)-C(11)-C(10)	111.92(12)
N(1)-C(11)-H(11)	108.0
C(12)-C(11)-H(11)	108.0
C(10)-C(11)-H(11)	108.0
C(13)-C(12)-C(17)	118.59(15)
C(13)-C(12)-C(11)	122.95(14)
C(17)-C(12)-C(11)	118.46(14)
C(12)-C(13)-C(14)	120.40(15)
C(12)-C(13)-H(13)	119.8
C(14)-C(13)-H(13)	119.8
C(15)-C(14)-C(13)	120.71(15)
C(15)-C(14)-H(14)	119.6



C(13)-C(14)-H(14)	119.6
C(14)-C(15)-C(16)	119.42(15)
C(14)-C(15)-H(15)	120.3
C(16)-C(15)-H(15)	120.3
C(15)-C(16)-C(17)	119.92(15)
C(15)-C(16)-H(16)	120.0
C(17)-C(16)-H(16)	120.0
C(16)-C(17)-C(12)	120.94(15)
C(16)-C(17)-H(17)	119.5
C(12)-C(17)-H(17)	119.5
C(1)-N(1)-C(11)	120.07(13)
C(1)-N(1)-C(3)	111.82(13)
C(11)-N(1)-C(3)	122.70(12)

**Table A4.4** Anisotropic displacement parameters ( $\text{\AA}^2 \times 10^3$ ) for **175a**. The anisotropic displacement factor exponent takes the form:  $-2\pi^2 [h^2 a^{*2} U^{11} + \dots + 2 h k a^* b^* U^{12}]$

	U11	U22	U33	U23	U13	U12
C(1)	20(1)	19(1)	20(1)	2(1)	2(1)	2(1)
O(1)	22(1)	23(1)	34(1)	12(1)	1(1)	5(1)
O(2)	20(1)	26(1)	43(1)	11(1)	7(1)	0(1)
C(2)	20(1)	28(1)	68(1)	18(1)	-9(1)	-2(1)
C(3)	14(1)	21(1)	25(1)	2(1)	1(1)	1(1)
C(4)	14(1)	25(1)	16(1)	1(1)	5(1)	0(1)
C(5)	16(1)	36(1)	20(1)	0(1)	2(1)	4(1)
C(6)	20(1)	49(1)	26(1)	-11(1)	-6(1)	6(1)
C(7)	27(1)	39(1)	39(1)	-21(1)	-7(1)	3(1)
C(8)	23(1)	28(1)	35(1)	-10(1)	-6(1)	4(1)
C(9)	16(1)	24(1)	18(1)	-3(1)	1(1)	0(1)
C(10)	19(1)	17(1)	19(1)	2(1)	-1(1)	-1(1)
C(11)	16(1)	17(1)	16(1)	2(1)	1(1)	1(1)
C(12)	13(1)	19(1)	15(1)	3(1)	2(1)	-2(1)

C(13)	20(1)	20(1)	18(1)	2(1)	2(1)	1(1)
C(14)	25(1)	24(1)	18(1)	0(1)	3(1)	-6(1)
C(15)	21(1)	32(1)	16(1)	5(1)	-2(1)	-8(1)
C(16)	16(1)	27(1)	22(1)	8(1)	0(1)	1(1)
C(17)	17(1)	20(1)	20(1)	2(1)	2(1)	0(1)
N(1)	14(1)	20(1)	22(1)	6(1)	0(1)	0(1)

**Table A4.5** Hydrogen coordinates ( $\times 10^4$ ) and isotropic displacement parameters ( $\text{\AA}^2 \times 10^3$ ) for **175a**.

	x	y	z	U(eq)
H(2A)	9723	4683	7921	47
H(2B)	9959	5231	8888	47
H(3)	9391	6060	7219	24
H(5)	11557	6463	9197	29
H(6)	12322	7897	9906	38
H(7)	10535	9249	9491	42
H(8)	8054	9187	8328	34
H(10A)	7534	7586	6698	22
H(10B)	6043	8297	7227	22
H(11)	4430	7072	8007	20
H(13)	5007	5436	6250	24
H(14)	2744	5208	5024	27
H(15)	348	6356	4649	28
H(16)	234	7755	5505	26
H(17)	2402	7959	6770	22

**Table A4.6** Torsion angles [ $^\circ$ ] for **175a**.

O(2)-C(1)-O(1)-C(2)	179.11(18)
N(1)-C(1)-O(1)-C(2)	-0.1(2)
C(1)-O(1)-C(2)-C(3)	8.0(2)

O(1)-C(2)-C(3)-N(1)	-11.7(2)
O(1)-C(2)-C(3)-C(4)	107.34(18)
N(1)-C(3)-C(4)-C(5)	138.89(15)
C(2)-C(3)-C(4)-C(5)	25.0(2)
N(1)-C(3)-C(4)-C(9)	-41.39(18)
C(2)-C(3)-C(4)-C(9)	-155.28(15)
C(9)-C(4)-C(5)-C(6)	1.2(2)
C(3)-C(4)-C(5)-C(6)	-179.11(16)
C(4)-C(5)-C(6)-C(7)	0.6(3)
C(5)-C(6)-C(7)-C(8)	-1.3(3)
C(6)-C(7)-C(8)-C(9)	0.2(3)
C(7)-C(8)-C(9)-C(4)	1.6(3)
C(7)-C(8)-C(9)-C(10)	-177.85(17)
C(5)-C(4)-C(9)-C(8)	-2.3(2)
C(3)-C(4)-C(9)-C(8)	178.00(15)
C(5)-C(4)-C(9)-C(10)	177.19(14)
C(3)-C(4)-C(9)-C(10)	-2.5(2)
C(8)-C(9)-C(10)-C(11)	-130.25(17)
C(4)-C(9)-C(10)-C(11)	50.33(18)
C(9)-C(10)-C(11)-N(1)	-48.40(16)
C(9)-C(10)-C(11)-C(12)	-172.99(12)
N(1)-C(11)-C(12)-C(13)	-9.5(2)
C(10)-C(11)-C(12)-C(13)	112.26(16)
N(1)-C(11)-C(12)-C(17)	170.44(13)
C(10)-C(11)-C(12)-C(17)	-67.77(18)
C(17)-C(12)-C(13)-C(14)	-1.4(2)
C(11)-C(12)-C(13)-C(14)	178.59(14)
C(12)-C(13)-C(14)-C(15)	1.3(2)
C(13)-C(14)-C(15)-C(16)	0.3(2)
C(14)-C(15)-C(16)-C(17)	-1.7(2)
C(15)-C(16)-C(17)-C(12)	1.5(2)
C(13)-C(12)-C(17)-C(16)	0.0(2)
C(11)-C(12)-C(17)-C(16)	-179.99(14)
O(2)-C(1)-N(1)-C(11)	17.7(3)
O(1)-C(1)-N(1)-C(11)	-163.14(14)

O(2)-C(1)-N(1)-C(3)	172.42(17)
O(1)-C(1)-N(1)-C(3)	-8.43(19)
C(12)-C(11)-N(1)-C(1)	-80.48(17)
C(10)-C(11)-N(1)-C(1)	155.43(14)
C(12)-C(11)-N(1)-C(3)	127.63(15)
C(10)-C(11)-N(1)-C(3)	3.6(2)
C(4)-C(3)-N(1)-C(1)	-112.36(15)
C(2)-C(3)-N(1)-C(1)	12.38(19)
C(4)-C(3)-N(1)-C(11)	41.6(2)
C(2)-C(3)-N(1)-C(11)	166.32(16)

---

## CHAPTER 4

### *Advances in the Total Synthesis of the Tetrahydroisoquinoline Alkaloids (2002 – 2020) †*

#### 4.1 INTRODUCTION

The tetrahydroisoquinoline (THIQ) alkaloids make up one of the largest groups of natural products with a wide range of structural diversity and biological activity.<sup>1</sup> From simple tetrahydroisoquinolines such as salsolidine **183**, to complex tris-tetrahydroisoquinoline systems like Ecteinsacidin 743 **184**, there is a wide variety in structure and activity between the families of isoquinoline alkaloids that possess the 1,2,3,4-tetrahydroisoquinoline ring system (Figure 4.1). Thus, the chemical syntheses of these alkaloids have been extensively investigated toward the development of efficient total syntheses and understanding of their biological activity.<sup>2</sup>

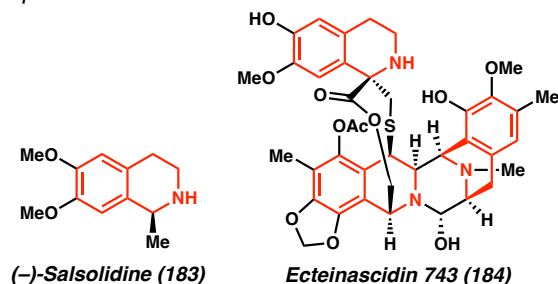
While several review articles on the total synthesis of isoquinoline alkaloids have been published, including Williams' seminal review on the THIQ antitumor antibiotics,<sup>3</sup> there has been no comprehensive review of the chemical syntheses of tetrahydroisoquinoline alkaloids over the past several decades. Moreover, recent total syntheses have emerged

---

<sup>†</sup>This review was conducted in collaboration with Dr. Fa Ngamnithiporn and Emily Du.

harnessing modern chemical methods and novel technology. As these synthetic strategies diverge from biomimetic approaches, they often provide a highly efficient route toward complex THIQ alkaloids compared to previous syntheses. This review will cover literature from 2002 to 2020, highlighting the chemical syntheses of a range of THIQ alkaloids that especially feature creative, novel synthetic approaches (Figure 4.2).

**Figure 4.1** Tetrahydroisoquinoline alkaloids (–)-salsolidine **183** and Ecteinascidin 743 **184**.

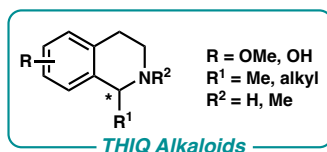


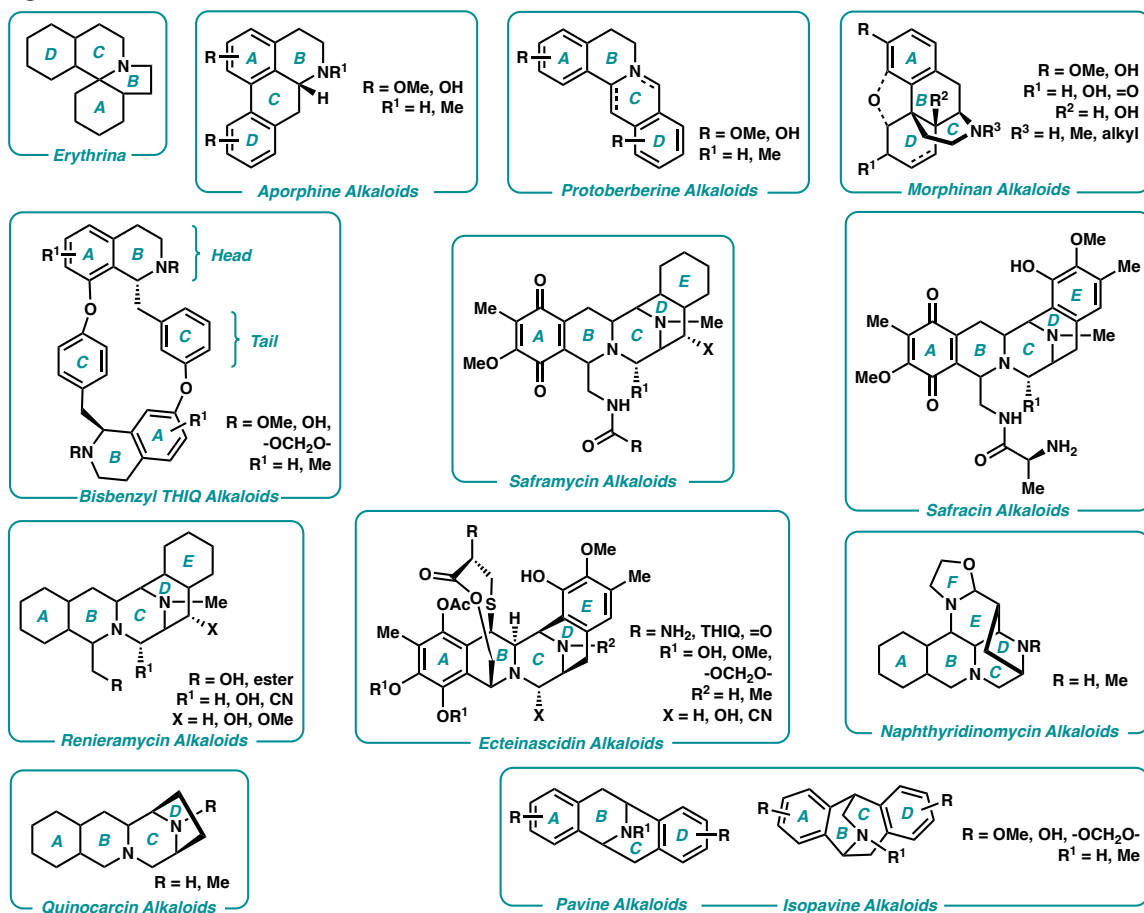
## 4.2 TETRAHYDROISOQUINOLINE ALKALOIDS

### 4.2.1 GENERAL STRUCTURE AND BIOSYNTHESIS

Most simple THIQ alkaloids come from the Cactaceae, Chenopodiaceae, and Fabaceae cacti families.<sup>1</sup> These cactus species contain β-phenylethylamine alkaloids, as well as simple tetrahydroisoquinolines that bear a stereogenic center at the C1 carbon with various oxidation patterns on the arene ring (Figure 4.3).

**Figure 4.3** General structure of simple THIQ alkaloids.



**Figure 4.2** General structures of THIQ alkaloid families.

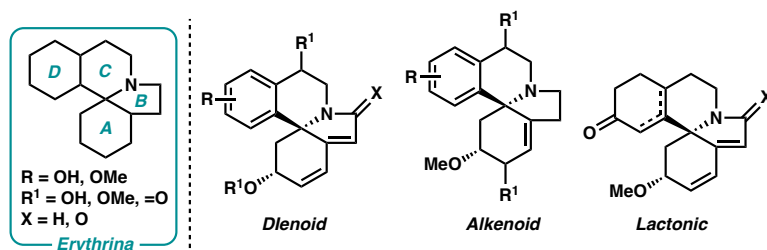
The biosynthesis of these simple THIQs is generally achieved from the condensation of the corresponding  $\beta$ -phenylethylamine with a formaldehyde or acetaldehyde equivalent, accessing the tetrahydroisoquinoline motif as a single enantiomer.<sup>4</sup> These naturally require electron-rich functional groups on the arene ring to undergo electrophilic aromatic substitution chemistry. Throughout this review, this key heterocyclic motif serves as a fundamental scaffold in all THIQ natural products that requires unique and creative synthetic approaches to install.

## 4.3 SPIROCYCLIC TETRAHYDROISOQUINOLINE ALKALOIDS

### 4.3.1. GENERAL STRUCTURE AND BIOSYNTHESIS

From the Fabaceae family, the *Erythrina* genus consists of about 143 alkaloids that are characterized by the spirocyclic motif embedded in the tetracyclic scaffold (Figure 4.4).<sup>1</sup> There are three main classes of *Erythrina* alkaloids referred to as the dienoid, alkenoid, and lactonic alkaloids.<sup>5</sup> The dienoid alkaloids feature a conjugated diene system, whereas the alkenoids have a 1,6-double bond in the A ring, and the lactonic alkaloids possess a lactone ring in ring D. These alkaloids have been discovered to possess an array of biological activity, including antiepileptic, anticonvulsant, and CNS depressing properties.

**Figure 4.4** General structure of the *Erythrina* alkaloids.



The biosynthesis of the *Erythrina* alkaloids is proposed to stem from norreticuline **185** as a key precursor (Figure 4.5).<sup>1,6</sup> Oxidative phenol coupling occurs to generate intermediate **186**, followed by rearrangement and ring opening of the tetrahydroisoquinoline ring to form dibenzazonine **188**. Zenk and coworkers utilizes <sup>13</sup>C-labelling studies to suggest an allylic cation intermediate **189** that undergoes subsequent ring closure to access the natural product skeleton **190**. However, the specific enzymes that catalyze these transformations have not yet been fully elucidated.

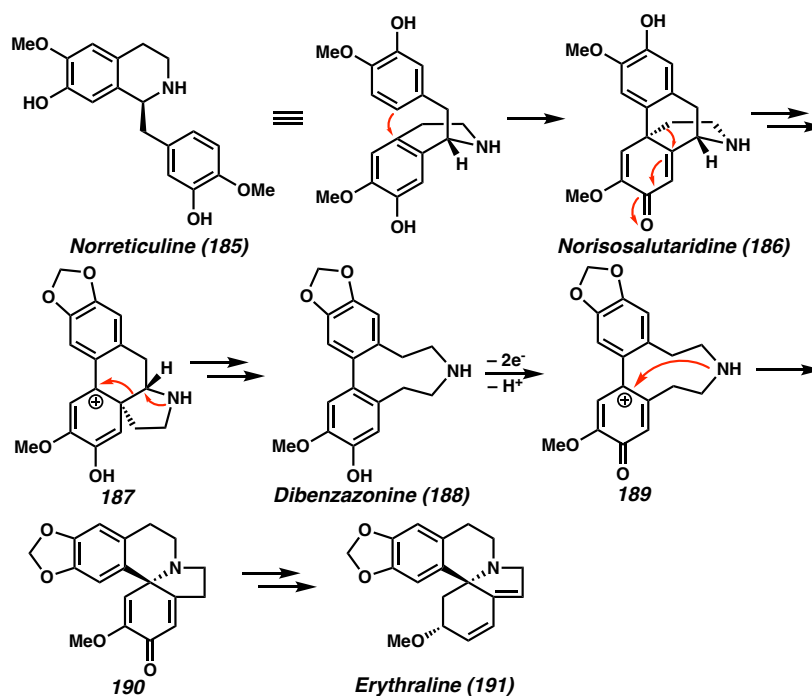
#### 4.3.2. TOTAL SYNTHESIS OF ERYTHRINA ALKALOIDS

Approaches to the synthesis of the core spirocyclic system of the *Erythrina* alkaloids are diverse, accessing several natural product members of this family both in racemic and



enantioselective fashion. Three general strategies toward the construction of the THIQ core have been described, either through the disconnection of the C<sub>1</sub>–C<sub>8a</sub>,<sup>7</sup> C<sub>1</sub>–N,<sup>8</sup> and/or the N–C<sub>3</sub> bond (Figure 4.6). While electrophilic aromatic substitution chemistry through iminium ion cyclization is most common to assemble the scaffold, other novel disconnections have also been explored to build the A, B, and C rings.

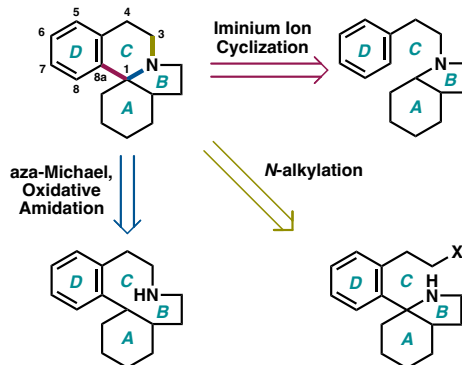
**Figure 4.5** Proposed biosynthesis of the *Erythrina* alkaloids.



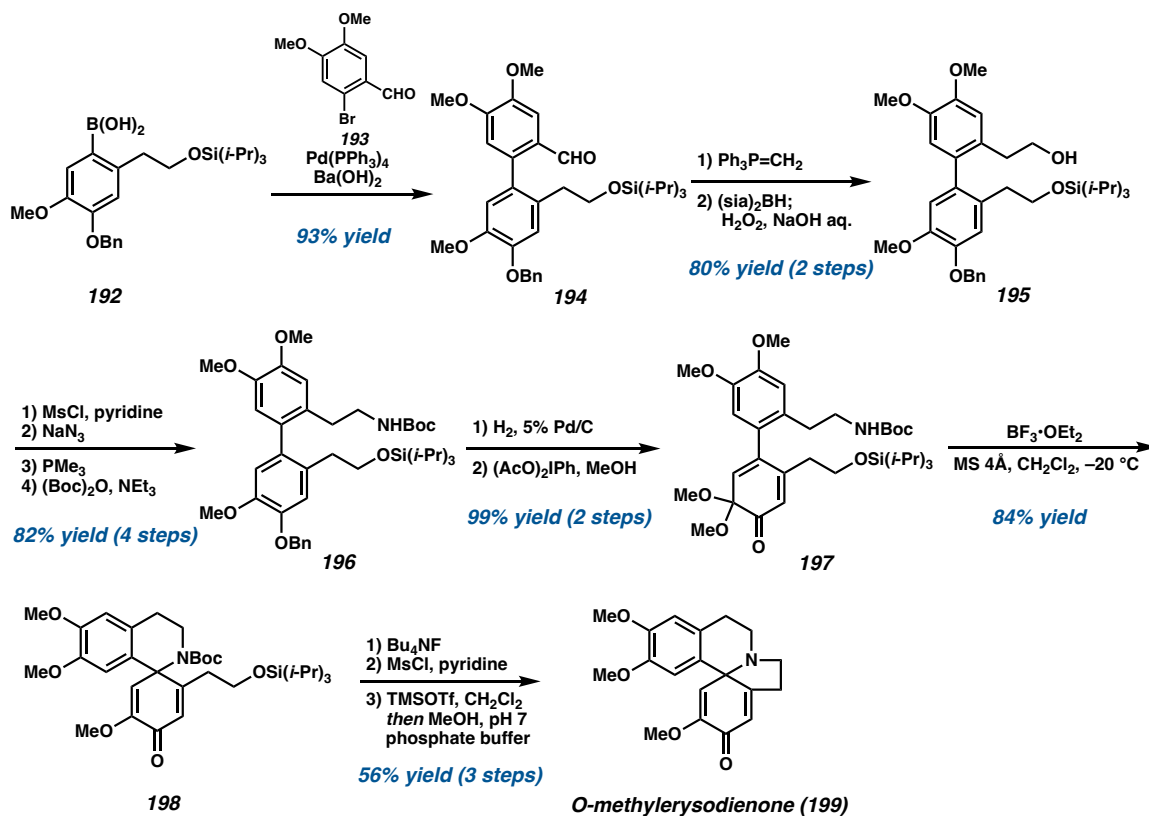
In 2004, Matsumoto sought to construct the *Erythrinan* scaffold utilizing substitution chemistry for the key spirocyclization of *ortho*-quinone monoacetal **197** to establish the C ring.<sup>8a</sup> Toward the synthesis of *O*-methylerysodienone **199**, Matsumoto and coworkers initially access the biphenyl precursor **194** from a Suzuki–Miyaura coupling of arylboronic acid **192** and aryl bromide **193** (Scheme 4.1). Further oxidative manipulations and substitution chemistry results in the installation of the nucleophilic nitrogen functional group in intermediate **196**. The C-ring was then established through the key spirocyclization step

from *ortho*-quinone acetal **197**, using  $\text{BF}_3 \cdot \text{OEt}_2$  as the optimal Lewis acid compared to other metal triflates. Finally, *N*-alkylation to furnish the B-ring occurred smoothly under methanol and phosphate buffer.

**Figure 4.6** Synthetic approaches to *Erythrina* alkaloids.



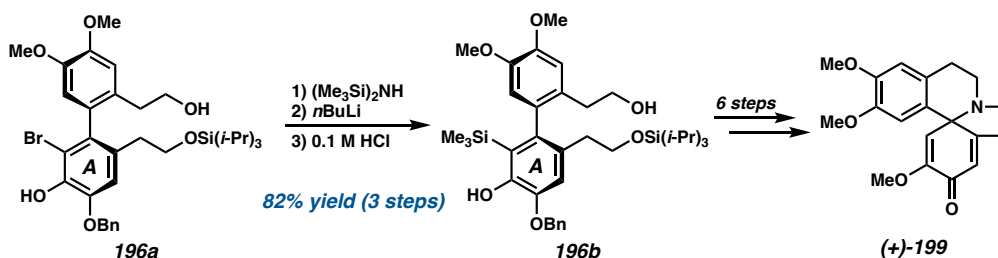
**Scheme 4.1** Matsumoto's total synthesis of *O*-methylerysodienone **199**.



Matsumoto and coworkers also demonstrated the enantioselective synthesis of *O*-methylerysodienone **199** by installing an additional *ortho* substituent on the A-ring,

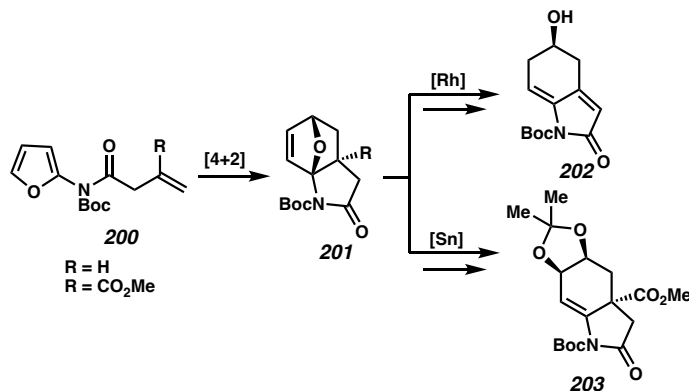
transmitting axial chirality of the biphenyl intermediate from its hindered rotation to the spirocyclic center of the natural product (Scheme 4.1). Adding a trimethylsilyl group *ortho* to the biphenyl bond that was easily cleaved with  $\text{Bu}_4\text{NF}$  allowed separation of both enantiomers and enabled the enantioselective synthesis of (+)-*O*-methylethersodienone.

**Scheme 4.2** Matsumoto's enantioselective synthesis of *O*-methylethersodienone **199**.



Alternatively, Padwa and coworkers sought to construct the A ring of the *Erythrina* alkaloids through an intramolecular Diels–Alder reaction that could yield intermediate **201**. The oxabicyclic adduct could then undergo regioselective ring-opening reactions with rhodium or tin to access building blocks **202** and **203** (Scheme 4.3).<sup>9</sup>

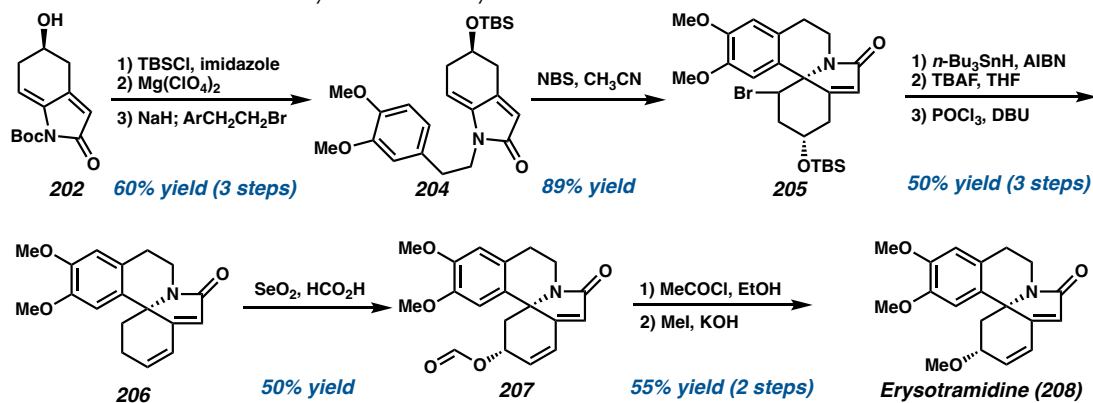
**Scheme 4.3** Padwa's synthetic strategy toward the *Erythrina* alkaloids.



A Rh(I)-catalyzed ring-opening cascade as demonstrated in Pathway A delivers intermediate **202** that undergoes *N*-alkylation with alkyl bromide to yield **204** (Scheme 4.4). The bicyclic lactam then underwent smooth cyclization to generate the spirocyclic

tetrahydroisoquinoline **205** with NBS in CH<sub>3</sub>CN. Reduction of the bromide and elimination of the alcohol then produces **206**, which undergoes stereoselective allylic oxidation, subsequent reduction, and *O*-methylation to synthesize erysotramidine **208**.

**Scheme 4.4** Padwa's total synthesis of erysotramidine **208**.

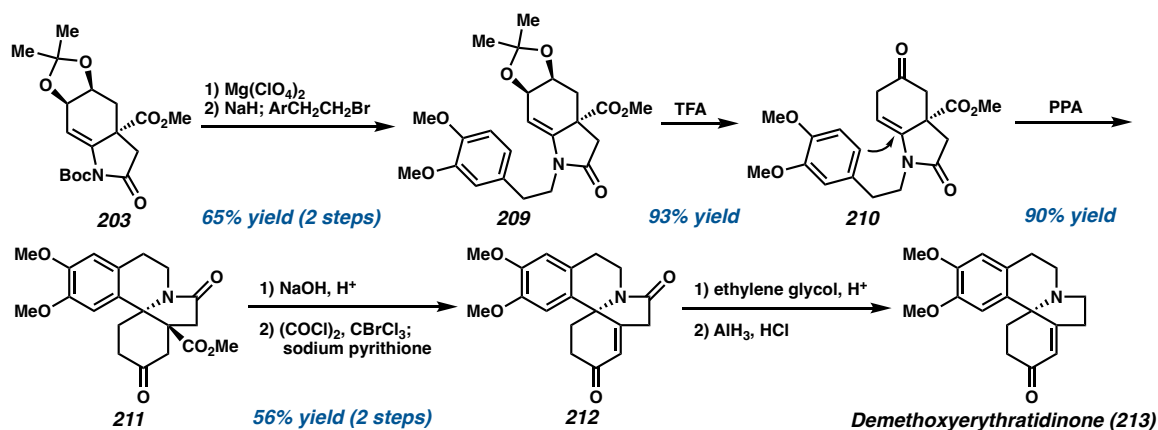


Pathway B commences with ring-opening by SnCl<sub>2</sub> followed by addition of acetone to access acetonide **203** (Scheme 4.5). *N*-alkylation and treatment of acetonide with trifluoroacetic acid led to tetrahydroindolinone **210**. A Pictet–Spengler reaction with PPA then establishes the *Erythrinan* scaffold **211**, which was then subjected to hydrolysis, Barton decarboxylation, and reduction to access demethoxyerythratidinone **213**. This novel strategy toward the tetrahydroindolinone core allows access to several natural products of the *Erythrina* alkaloids, based on an intramolecular Diels–Alder reaction of 2-imido-substituted furans.

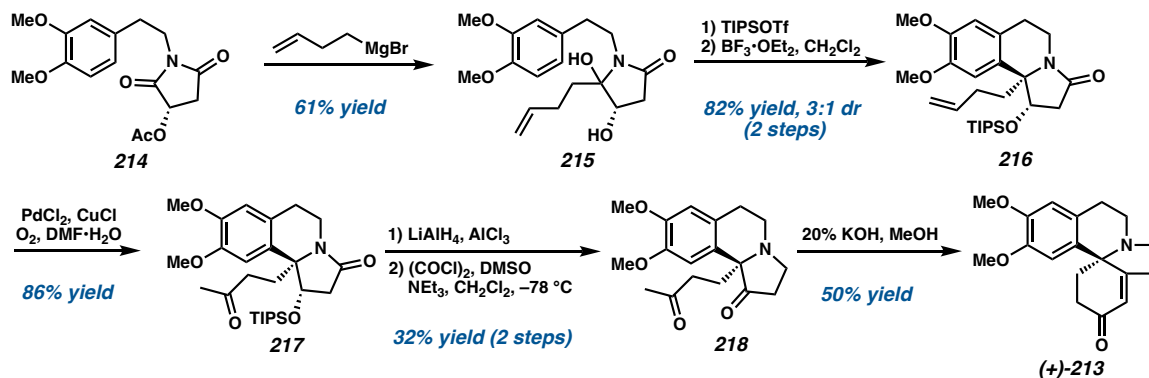
Enantioselective approaches to the synthesis of demethoxyerythratidinone **213** have been explored over the past two decades.<sup>10</sup> Simpkins and coworkers demonstrated an asymmetric total synthesis of **213** through a key *N*-acyliminium ion cyclization using (*S*)-malic acid-derived lactams (Scheme 4.6).<sup>11</sup> Initially, addition of butenyl magnesium bromide to imide **214** resulted in hydroxylactam **215** with excellent regiocontrol. Protection of the

secondary alcohol followed by exposure to  $\text{BF}_3 \cdot \text{OEt}_2$  formed an acyliminium intermediate that allowed cyclization to occur with diastereocontrol. Wacker oxidation of **216** and subsequent reduction removed the amide carbonyl, and aldol cyclization of the two oxidized ketones yielded (+)-demethoxyerythratidinone **213** in 50% yield, allowing access to both enantiomers of the natural product in simply eight steps.

**Scheme 4.5** Padwa's total synthesis of demethoxyerythratidinone **213**.



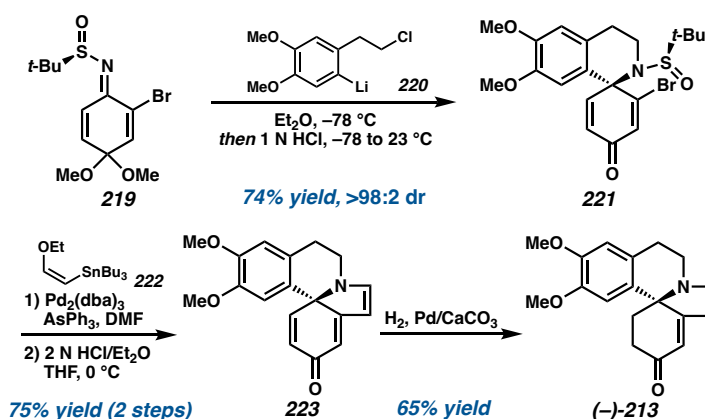
**Scheme 4.6** Simpkin's enantioselective synthesis of (+)-demethoxyerythratidinone **213**.



Distinct from classic electrophilic aromatic substitution strategies to forge the THIQ core, Reisman and coworkers utilized their developed method of installing enantioenriched 4-aminocyclohexadienones to access **213**.<sup>12</sup> Having optimized a method for the

diastereoselective 1,2-addition of organometallic reagents to benzoquinone monoketal-derived sulfinimines, they established spirocyclic THIQ **221** through addition of aryllithium **220** to bromosulfinimine **219** to provide a single diastereomer in 74% yield (Scheme 4.7). Stille coupling then furnished the corresponding enol ether, with sulfinamide deprotection and in situ condensation accessing the natural product scaffold **223**. Selective hydrogenation of triene **223** then completed the elegant and rapid total synthesis of (–)-demethoxyerythratidinone in only six steps and 26% overall yield.

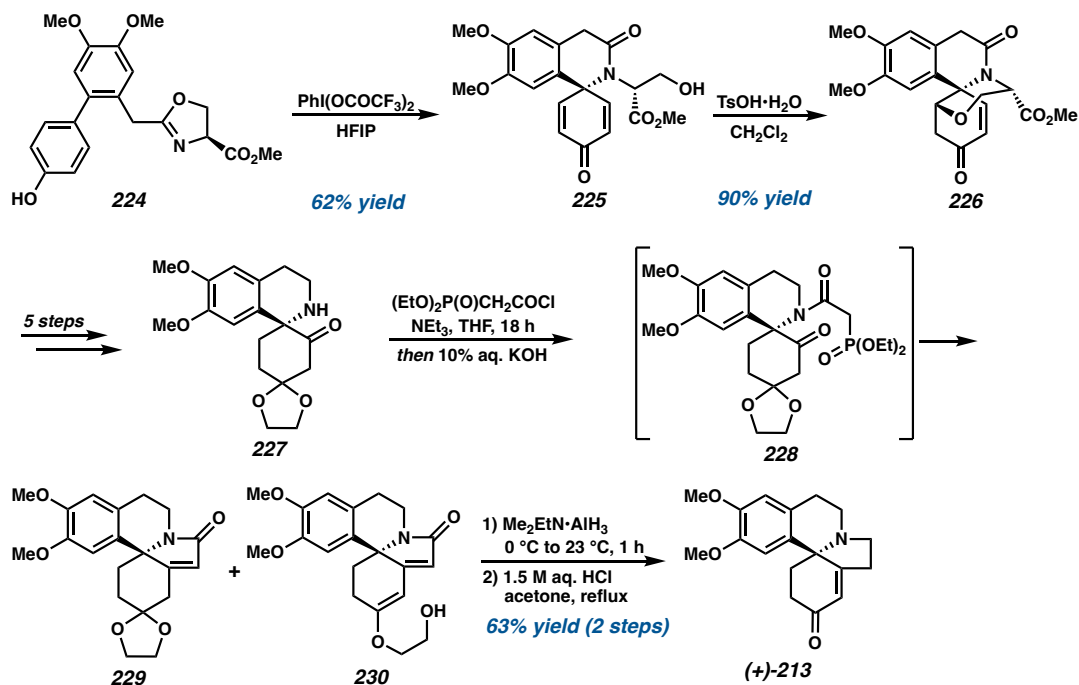
**Scheme 4.7** Reisman's enantioselective synthesis of (–)-demethoxyerythratidinone **213**.



Toward the total syntheses of (+)-demethoxyerythratidinone **213** and (+)-erysotramidine **208**, Ciufolini and coworkers employed an oxidative cyclization of a phenolic oxazoline, establishing the stereogenic center of the spirocycle.<sup>13</sup> Starting from oxazoline **224** prepared in five steps, oxidative amidation occurred smoothly to access **225** in 62% yield (Scheme 4.8). Upon treatment with TsOH, oxa-Michael addition then proceeds to furnish enone **226** as a single diastereomer. After several steps to remove the bridging serine moiety and further oxidative manipulations, late-stage intermediate **227** served as a universal precursor to access both natural products. First, *N*-acylation of **227** with  $(\text{EtO})_2\text{P}(\text{O})\text{CH}_2\text{COCl}$  and subsequent treatment with aq. KOH established a mixture of

lactams **229** and **230**. Reduction of the mixture of products and acidic hydrolysis then resulted in the total synthesis of (+)-**213**.

**Scheme 4.8** Ciufolini's enantioselective synthesis of (+)-demethoxyerythratidinone **213**.

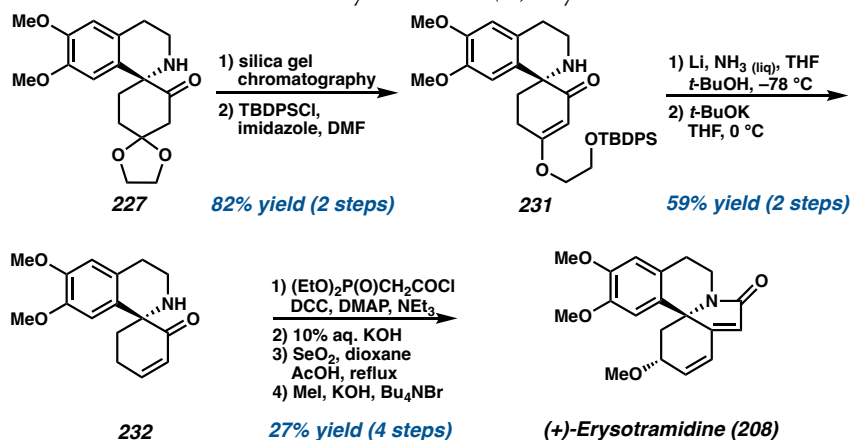


Alternatively, silica gel chromatography of **227** and subsequent protection provided quantitative conversion to **231**, which underwent conjugate reduction with  $\text{Li}/\text{NH}_3$  and elimination with *t*-BuOK to deliver **232** in 64% overall yield (Scheme 4.9). *N*-acylation and cyclization then established the natural product scaffold, which was advanced to (+)-erysotramidine **208** in two subsequent steps. Overall, a unified approach to the *Erythrina* alkaloids was demonstrated through a key oxidative amidation and cyclization strategy.

Kaluza's synthetic strategy toward the asymmetric synthesis of (–)-erysotramidine **208** utilized a late-stage Heck cyclization to assemble the A ring of the natural product scaffold.<sup>14</sup> Starting from imide **233** prepared in two steps from L-tartaric acid, addition of Grignard reagent **234**, and Lewis-acid mediated cyclization provided an epimeric mixture of

diacetate **235** (Scheme 4.10). Silver-catalyzed cyclization then furnished dihydrofuranyl derivative **236**, with further reduction accessing key intermediate **237**. Preparation of the (*Z*)-vinyl iodide for the late-stage Heck cyclization was achieved through Swern oxidation, then Wittig olefination of the crude aldehyde and protection of the hydroxyl group to provide **239**. A Heck cyclization then established the A ring of the natural product scaffold, providing **240** in 62% yield as the sole product. A final methylation step of the alcohol furnished the unnatural enantiomer (–)-erysotramidine **208** in good yield.

**Scheme 4.9** Ciufolini's enantioselective synthesis of (+)-erysotramidine **208**.



#### 4.4 BENZYL TETRAHYDROISOQUINOLINE ALKALOIDS

Benzyltetrahydroisoquinoline alkaloids specifically feature a benzyl group at the C1 position of the isoquinoline ring and comprise one of the largest and most diverse groups of alkaloids. Despite the considerable variation in structure of benzyl THIQ alkaloids, the biosynthesis of these natural products is proposed to share early biosynthetic precursors.<sup>1</sup>

Isoquinoline biosynthesis stems from dopamine **241** and *p*-hydroxyphenylacetaldehyde **242** to yield the central biosynthetic intermediate (*S*)-reticuline **247** (Figure 4.7).<sup>15</sup> Condensation of **241** and **242** is catalyzed by the enzyme norcoclaurine synthase (NCS) to form (*S*)-norcoclaurine **243**. Methylation then occurs by a *S*-adenosyl



methionine-(SAM)-dependent *O*-methyl transferase to access (*S*)-coclaurine **244**. After *N*-methylation to yield intermediate **245**, hydroxylation by *N*-methylcoclaurine 3'-hydroxylase (NMTC) followed by *O*-methylation produces the key precursor (*S*)-reticuline **247**. From this key intermediate, the biosynthetic pathways branch to form a variety of different structural classes of THIQ alkaloids (Figure 4.8).

**Scheme 4.10** Kaluza's enantioselective synthesis of (–)-erysotramidine **208**.

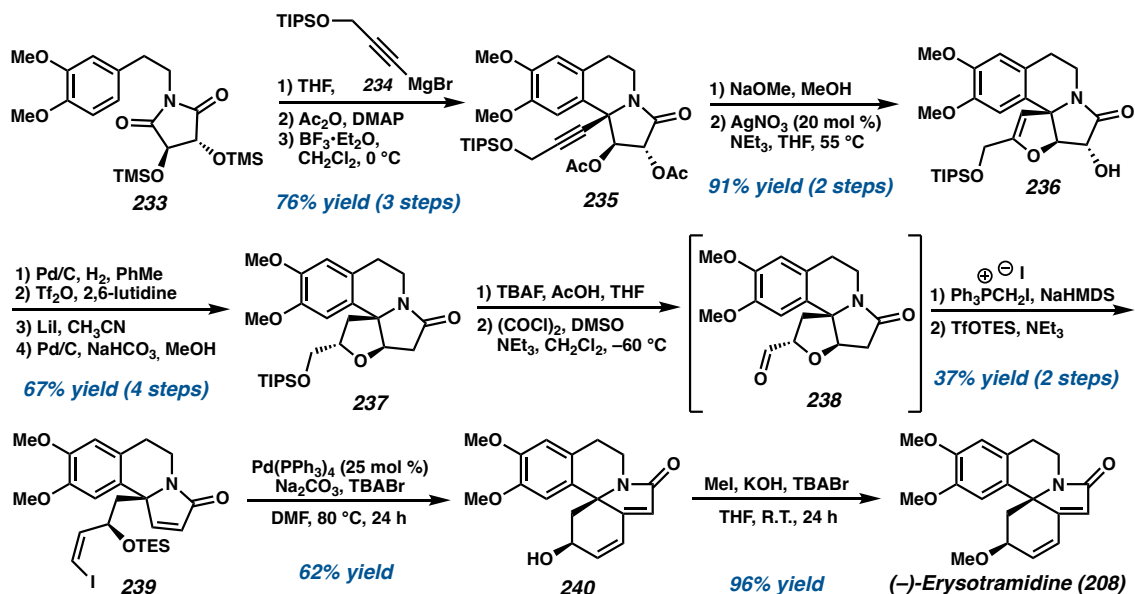
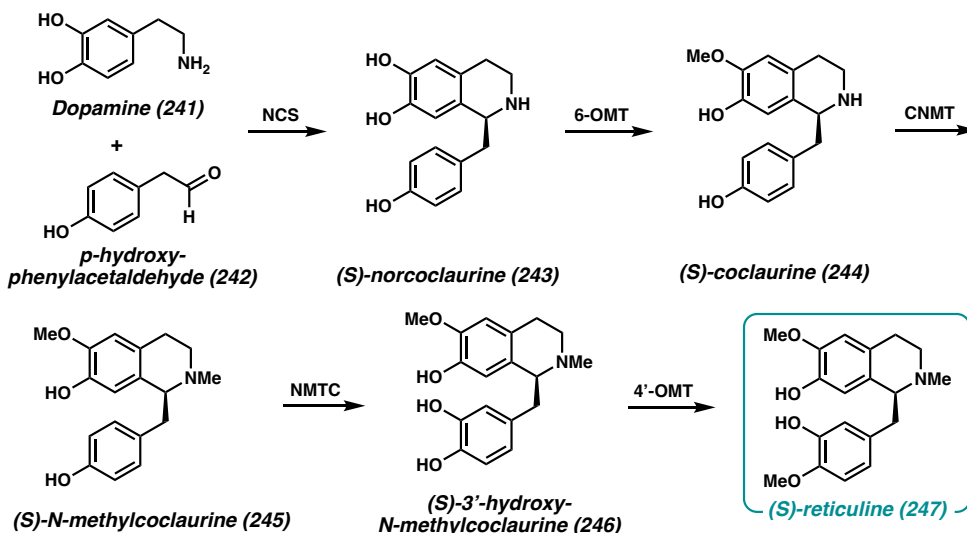


**Figure 4.7** Early biosynthetic pathways to yield (*S*)-reticuline **247**.

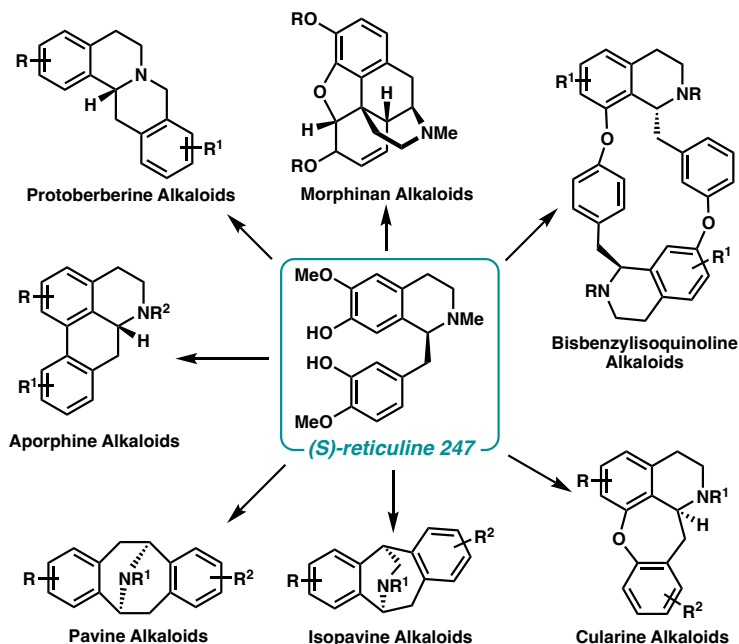


#### 4.4.1 APORPHINE ALKALOIDS

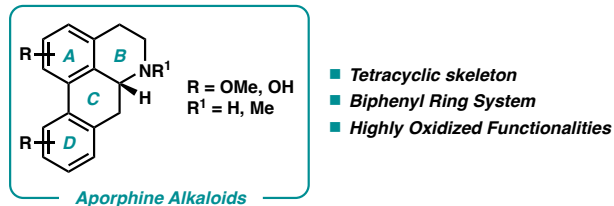
##### 4.4.1.1. GENERAL STRUCTURE AND BIOSYNTHESIS

The aporphine alkaloids are based on the 4H-dibenzo[*de,g*]quinoline structure or its *N*-methyl derivative, with a tetracyclic core as distinguished in Figure 4.9.<sup>16</sup> They contain a biphenyl ring system and highly oxidized substitution patterns, with hydroxyl, methoxy, and methylenedioxy moieties situated over all four rings.

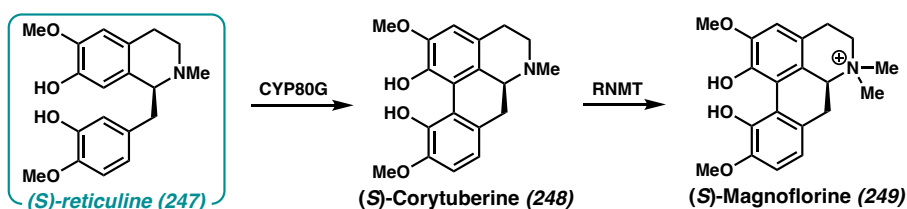
**Figure 4.8** Diverging biosynthetic pathways from (*S*)-reticuline **247** that access a wide variety of structural classes of THIQ alkaloids.



The aporphine alkaloids have been isolated from a variety of plants, including the genera *Glaucium flavum*, *Beilschmiedia elliptica*, and *Nandina domestica*. They are known to be promising agents in the prevention and treatment of metabolic syndrome due to their broad biological activity, including anti-hypertension, anti-diabetes, anti-obesity, anti-oxidation, and anti-inflammation.<sup>17</sup> In particular, many of the aporphines show various levels of preventing insulin resistance and regulating glucose homeostasis. The methoxy and hydroxyl substituents may be important for these biological activities.<sup>17</sup>

**Figure 4.9** General structure of the aporphine alkaloids.

The aporphine alkaloids are presumably derived from reticuline **247**, which undergoes an intramolecular bis-phenol coupling to construct the core.<sup>18</sup> The CYP80G subfamily of cytochrome P450 monooxygenases has been correlated with aporphine biosynthesis, in which CYP80G2 (corytuberine synthase) catalyzes conversion of (*S*)-reticuline **247** to (*S*)-corytuberine **248** via intramolecular C–C coupling (Figure 4.10). *N*-methylation of corytuberine **248** by reticuline *N*-methyl transferase (RNMT) enzyme then delivers one of the aporphine natural products magnoflorine **249**. Other related aporphine members of the family are proposed to arise from a similar route, either delivering the *N*-H, *N*-methyl aporphine or the quaternary aporphine salt.

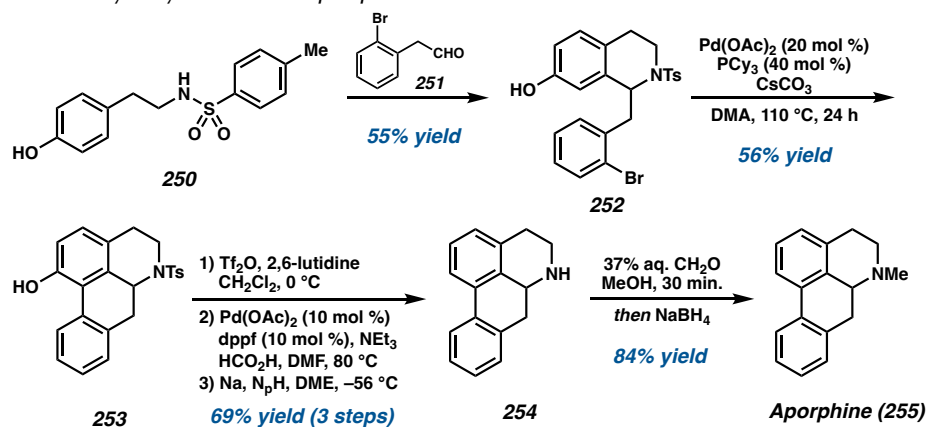
**Figure 4.10** Proposed biosynthesis of aporphine alkaloid (*S*)-magnoflorine **249**.

#### 4.4.1.2. TOTAL SYNTHESIS OF APORPHINE ALKALOIDS

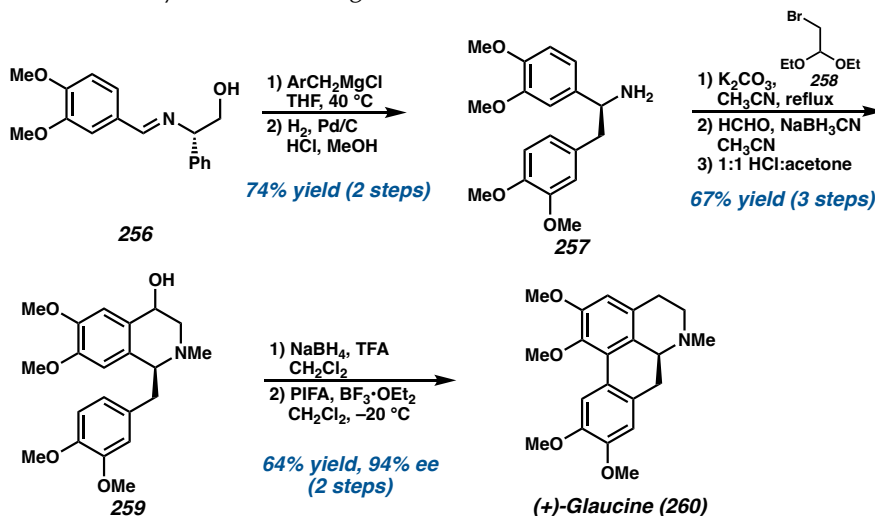
Approaches toward the syntheses of the aporphine alkaloids commonly feature EAS chemistry to establish the THIQ core, followed by an intramolecular phenol arylation to achieve the natural product scaffold. In 2004, Cuny described the synthesis of aporphine **255** utilizing this synthetic strategy starting from *N*-tosyl tyramine **250** (Scheme 4.11).<sup>19</sup> A Pictet–Spengler cyclization with 2-bromophenylacetaldehyde **251** was affected to afford

THIQ **252** in 55% yield. A Pd-catalyzed intramolecular phenol *ortho*-arylation then delivered the key aporphine scaffold **253** in moderate yield. Finally, removal of the hydroxyl group and the sulfonamide followed by reductive amination with 37% aqueous formaldehyde in the presence of NaBH<sub>4</sub> afforded aporphine **255**. Similar synthetic strategies have also been utilized in subsequent reports to access different aporphine natural products.<sup>20</sup>

**Scheme 4.11** Cuny's synthesis of aporphine **255**.



Circumventing the need for prefunctionalization of the arene before direct arylation, Vicario and coworkers reported the total synthesis of (+)-glaucine using an oxidative biaryl coupling to establish the aporphine scaffold (Scheme 4.12).<sup>21</sup> From imine **256**, addition of Grignard benzylic reagents followed by hydrogenation to remove the chiral appendage delivered amine **257**. *N*-alkylation with bromoacetaldehyde diethylacetal (BADA) allowed a Pomeranz–Fritsch cyclization to construct THIQ **259**. After reduction of the hydroxyl group, the final C–C biaryl oxidative coupling was accomplished using hypervalent iodine(III) reagent (bis(trifluoroacetoxy)iodo)benzene (PIFA) that allowed the synthesis of (+)-glaucine **260** cleanly with no racemization observed.

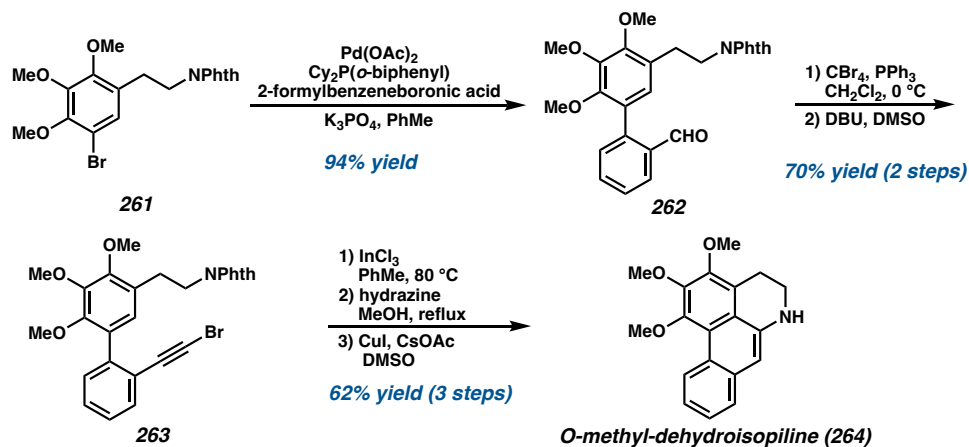
**Scheme 4.12** Vicario's synthesis of (+)-glaucine **260**.

Alternatively, Fürstner and co-workers constructed the aporphine scaffold through a key In-mediated cycloisomerization reaction from biphenyl derivatives.<sup>22</sup> From enamide **261**, a Suzuki coupling with 2-formylbenzeneboronic acid yielded functionalized biphenyl derivative **262**, constructing the C–C biphenyl bond early in the synthesis (Scheme 4.13). Conversion of the aldehyde to alkyne **263** then sets the stage for the key carbocyclization, which was effected using  $\text{InCl}_3$  in toluene. After removal of the phthalimide protecting group, intramolecular amination forged the THIQ ring and completed the total synthesis of *O*-methyl-dehydroisopiline **264**.

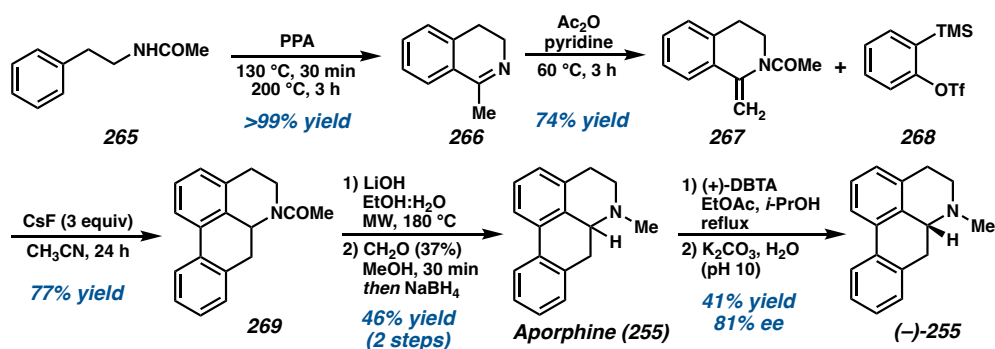
An unusual approach toward the synthesis of the aporphine scaffold employs benzyne chemistry to construct two of the four rings in a single transformation. Raminelli and coworkers described the synthesis of aporphine **255** from amide **265**, which was converted to isoquinoline **266** through a Bischler–Napieralski reaction (Scheme 4.14).<sup>23</sup> Treatment with acetic anhydride then yielded isoquinoline **267**, which served as the nonpolar diene for the [4+2] annulation. Thus, adding **267** and benzyne precursor **268** in the presence of  $\text{CsF}$  delivered aporphine core **269** from a [4+2] reaction followed by hydrogen migration.

Hydrolysis of **269** followed by reductive amination delivered aporphine **255**, which was then subjected to chiral resolution using (+)-DBTA to provide the enantiomer of the aporphine alkaloid. Raminelli and coworkers were further able to demonstrate the syntheses of different aporphine alkaloids using benzyne chemistry to couple isoquinoline derivatives and various silylaryl triflates, allowing rapid access to functionalized aporphine scaffolds.<sup>24</sup>

**Scheme 4.13** Fürstner's synthesis of *O*-methyl-dehydroisopiline **264**.



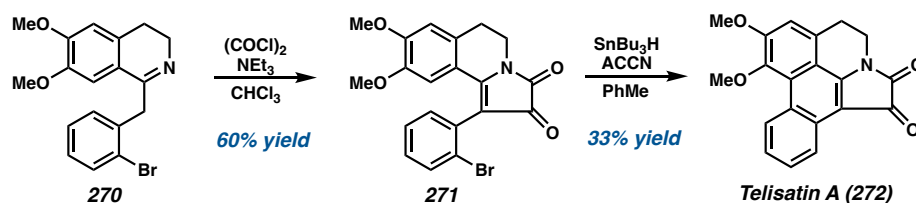
**Scheme 4.14** Raminelli's synthesis of (–)-aporphine **255**.



Beyond the syntheses of the classic aporphine natural product scaffold, others have targeted unique members of the aporphine alkaloids which share the characteristic tetracyclic nucleus but with varying oxygenation patterns and bond connectivity. For instance, Nimgirawath and coworkers completed the total synthesis of telisatin A **272** and other members of the telisatin-type alkaloids that are distinguished by an oxalyl moiety fused to

the THIQ core (Scheme 4.15).<sup>25</sup> From dihydroisoquinoline **270** that was established from a Bischler–Napieralski reaction, treatment with oxalyl chloride and NEt<sub>3</sub> afforded dione **271**. A radical cyclization using SnBu<sub>3</sub>H in the presence of 1,1'-azobis(cyclohexanecarbonitrile) (ACCN) then delivered telisatin A **272** and other telisatin alkaloids in 30–34% yields.

**Scheme 4.15** Nimgirawath's synthesis of telisatin A **272**.



Cuny and coworkers described the syntheses of C7-oxygenated aporphine alkaloids through a diastereoselective reductive cyclization followed by a Pd-catalyzed *ortho*-arylation to form the biaryl C–C bond (Scheme 4.16).<sup>26</sup> From carbamate **273**, selective reduction of the methyl ester using DIBAL, followed by an acid-mediated cyclization with BF<sub>3</sub>•OEt<sub>2</sub> delivered oxazolidinone **274** of both anti- and syn-diastereomers. Demethylation and formation of the dioxolane moiety with CH<sub>2</sub>Br<sub>2</sub> provided **275**, which underwent an *ortho*-phenyl arylation with an XPhos precatalyst to afford (–)-artabonatine A **276**. This natural product has been revised after observing that the specific rotation and <sup>1</sup>H and <sup>13</sup>C NMR spectral data for the natural product possessed the *syn*-configuration rather than its reported structure of the *trans*-diastereomer.

Lastly, the proaporphine alkaloids are recognized as biosynthetic precursors of aporphine alkaloids that are distinguished by the spiro-cyclohexadienone ring system. Toward the construction of this unique spirocycle, Honda and coworkers first reported the total synthesis of stepharine **280** and pronuciferine **281** utilizing an intramolecular aromatic oxidation of a common phenol intermediate (Scheme 4.17A).<sup>27</sup> From aldehyde **277**,

condensation with nitromethane followed by reduction and acetylation delivered amide **278**.

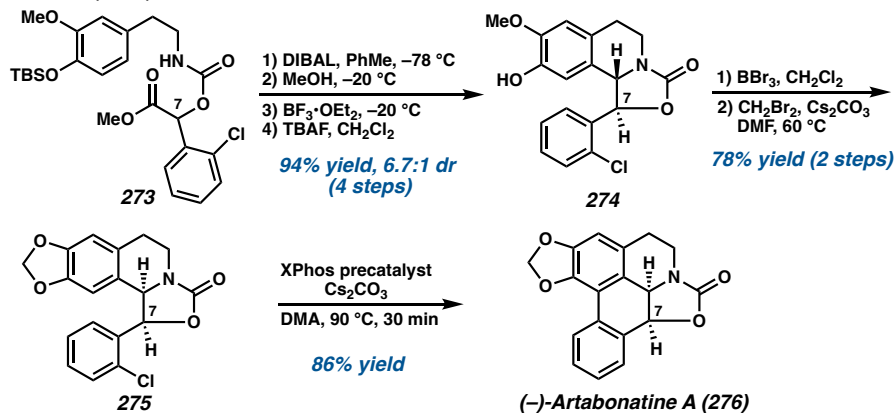
After removal of the benzyl group, a Bischler–Napieralski reaction with POCl<sub>3</sub> then acylation with trifluoroacetic anhydride yielded enamide **279** for the key aromatic oxidation.

Ultimately, the oxidation of **279** with iodobenzene diacetate (PIDA) was successful in allowing cyclization to stepharine **280** in 90% yield. *N*-methylation of **280** further delivered pronuciferine **281**.

Alternatively, Magnus and coworkers demonstrated that the spirocyclization could be achieved through an intramolecular displacement of a mesylate derivative **282** using CsF in NMP at 150 °C to deliver stepharine **280** as well (Scheme 4.17B).<sup>28</sup>

4.17B).<sup>28</sup>

**Scheme 4.16** Cuny's synthesis of (–)-artabonatine A **276**.

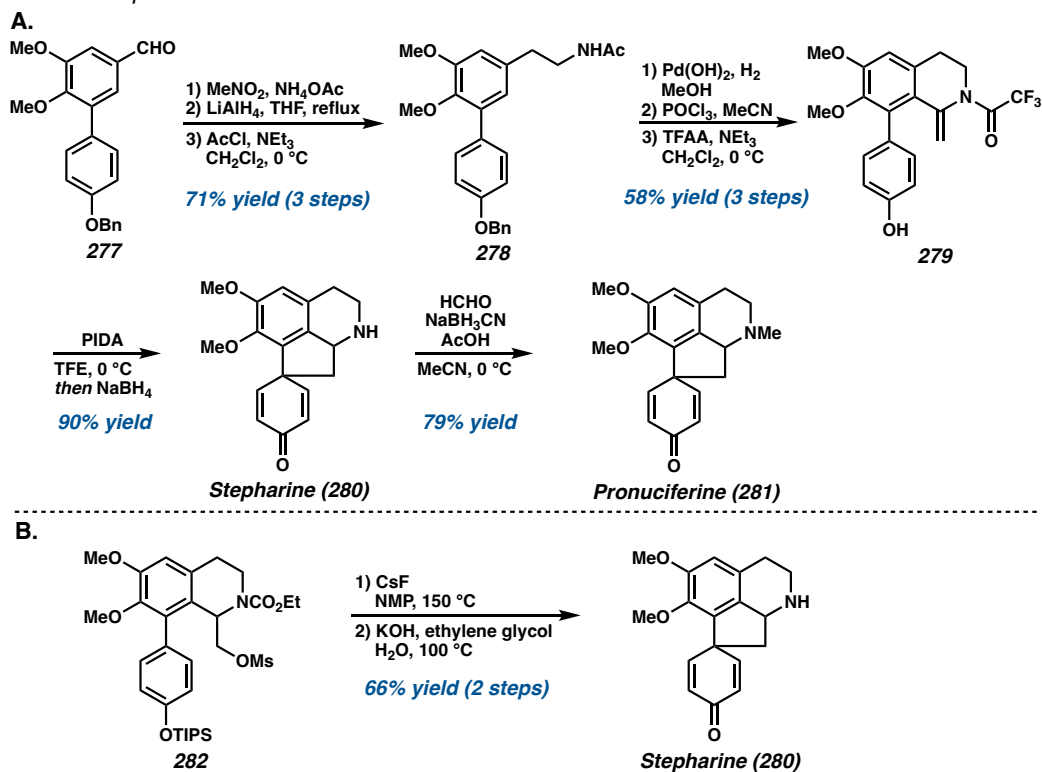


Takao and coworkers reported the enantioselective synthesis of a distinct proaporphine alkaloid (–)-misramine **290** utilizing their previously developed enantioselective Friedel–Crafts 1,4-addition of enones.<sup>29</sup> From phenethyl enone **283**, their key enantioselective intramolecular 1,4-addition was accomplished using *epi*-cinchonine amine **C1** as a catalyst (Scheme 4.18). With enantioenriched spiroindane **284**, a Rubottom oxidation followed by treatment with camphorsulfonic acid (CSA) and trimethyl orthoformate induced an intramolecular hemiacetalization of the phenol and carbonyl to



deliver tetracycle **285**. After several protecting group manipulations, a benzylic oxidation with  $\text{CrO}_3$  furnished ketone **286**. Next, to establish the THIQ core, the 2-oxoethyl group was incorporated into the benzene ring via a Claisen rearrangement to afford the C-allylated product **287**, then ozonolysis followed by deoxygenation to produce aldehyde **289**. Finally, reductive amination and removal of the TBS group afforded (–)-misramine **290** as a single diastereomer.

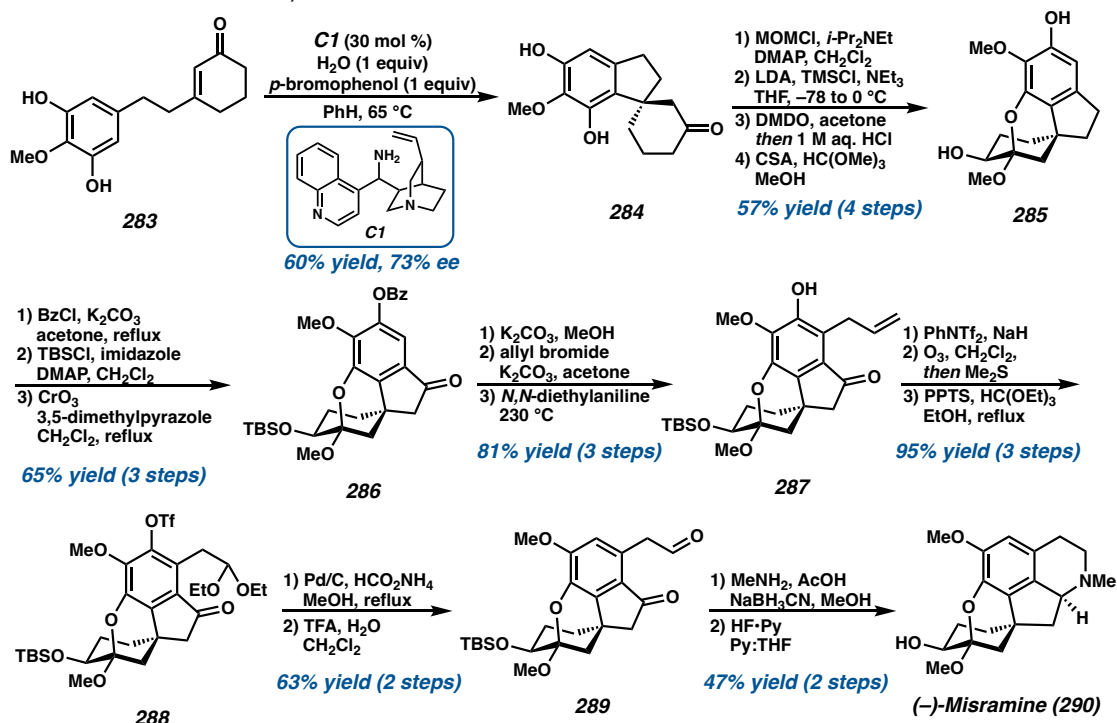
**Scheme 4.17** A. Honda's synthesis of stepharine **280** and pronuciferine **281**. B. Magnus' synthesis of stepharine **280**.



Fagnou and coworkers further utilized the Pd-catalyzed direct arylation of aryl halides for the preparation of aporphine analogues, including C2-substituted aporphines and the syntheses of (*R*)-nornuciferine **302** and (*R*)-nuciferine **301** (Scheme 4.19).<sup>30</sup> First, a Bischler–Napieralski cyclization of differentially substituted amides under either  $\text{POCl}_3$  or polyphosphoric acid yielded the dihydroisoquinoline intermediate which was immediately

reduced to THIQ **292** using NaBH<sub>4</sub> in MeOH. After protection of the secondary amine, the key direct arylation step was explored for each substrate, enabling the direct coupling of aryl bromides, chlorides, and iodides, as well as different *N*-protecting groups (Scheme 4.19A).

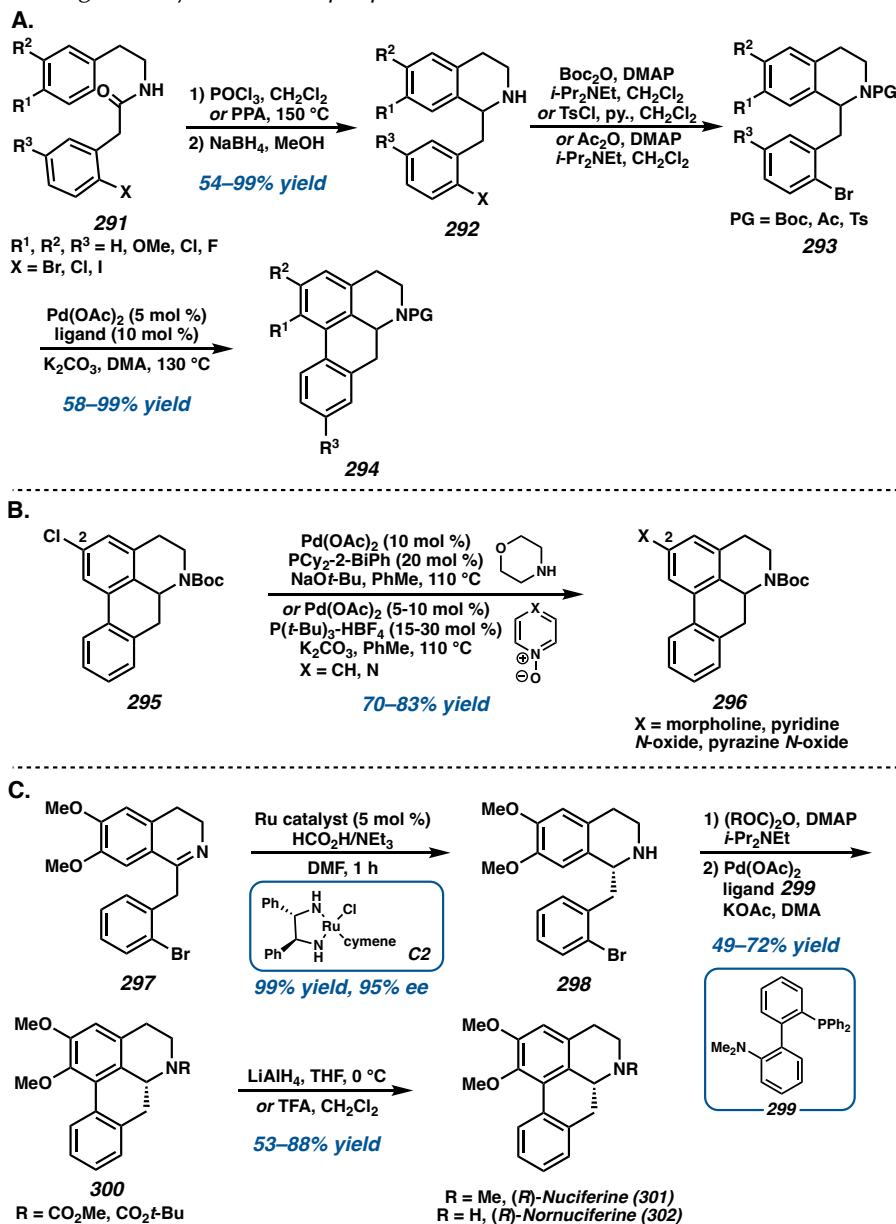
**Scheme 4.18** Takao's synthesis of (–)-misramine **290**.



Fagnou also performed SAR studies to probe the effects of C2-substituents on their biological activity. In this experiment, aporphine derivative **295** was coupled with different nucleophilic coupling partners, installing a range of functionalities such as a morpholine, pyridine, and pyrazine *N*-oxides (Scheme 4.19B). This strategy was also employed for the synthesis of (*R*)-normuciferine **302** and (*R*)-muciferine **301** by utilizing a Ru-catalyzed asymmetric transfer hydrogenation after Bischler–Napieralski cyclization to provide THIQ **298** in 99% yield and with 95% *ee* (Scheme 4.19C) Then, Pd-catalyzed arylation followed by reduction or deprotection of the Boc group delivered both natural products. Overall, these

syntheses highlight the utility of direct arylation methodology for both target-oriented and diversity-oriented synthesis.

**Scheme 4.19** Fagnou's synthesis of aporphine alkaloids.

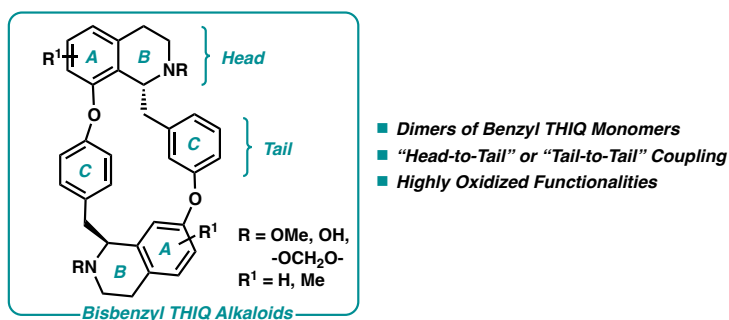


#### 4.4.2. BISBENZYL TETRAHYDROISOQUINOLINE ALKALOIDS

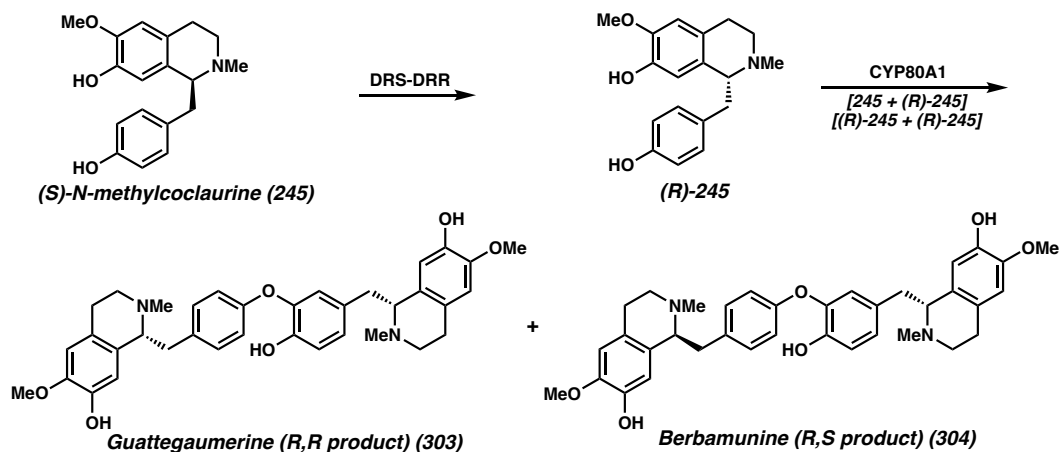
##### 4.4.2.1. GENERAL STRUCTURE AND BIOSYNTHESIS

The bisbenzyltetrahydroisoquinoline alkaloids consist of two monomeric benzyl THIQ fragments linked through diphenyl ether or biphenyl bonds (Figure 4.11). The substitution on the arene mainly consist of hydroxyl, methoxy, or methylenedioxy groups. Over hundreds of bisbenzyl THIQ alkaloids have been isolated and characterized, with the diaryl ether linkage either involved in “tail-to-tail” coupling of the benzyl unit, or “head-to-tail” coupling of the THIQ linked to the benzyl C ring.

**Figure 4.11** General structure of bisbenzyl THIQ alkaloids.



The bisbenzyl THIQ alkaloids have been isolated from an array of plant species, including *Chondrodendron tomentosum*, and opium poppy *Papaver somniferum*.<sup>31</sup> They are widely known for their dopaminergic, antitumor, and neuroprotectant properties. This class of alkaloids is proposed to be formed from the coupling of two monomer units derived from *N*-methylcoclaurine (NMC) **245** in either the (*R*) or (*S*)-configuration, catalyzed by enzyme CYP80A1 (Figure 4.12). First, epimerization of **245** is performed by dehydroreticuline synthase-dehydroreticuline reductase (DRS-DRR) to yield (*R*)-**245**, then either (*R*)+(*R*) coupling or (*R*)+(*S*) coupling delivers guattegaumerine **303** or berbamunine **304**, respectively. However, dimerization of benzyl THIQs can occur either between both benzyl units or between the THIQ moiety to a benzyl unit, and thus the structural diversity of these alkaloids is extensive.<sup>31</sup>

**Figure 4.12** Proposed biosynthesis of bisbenzyl THIQ alkaloids **303** and **304**.

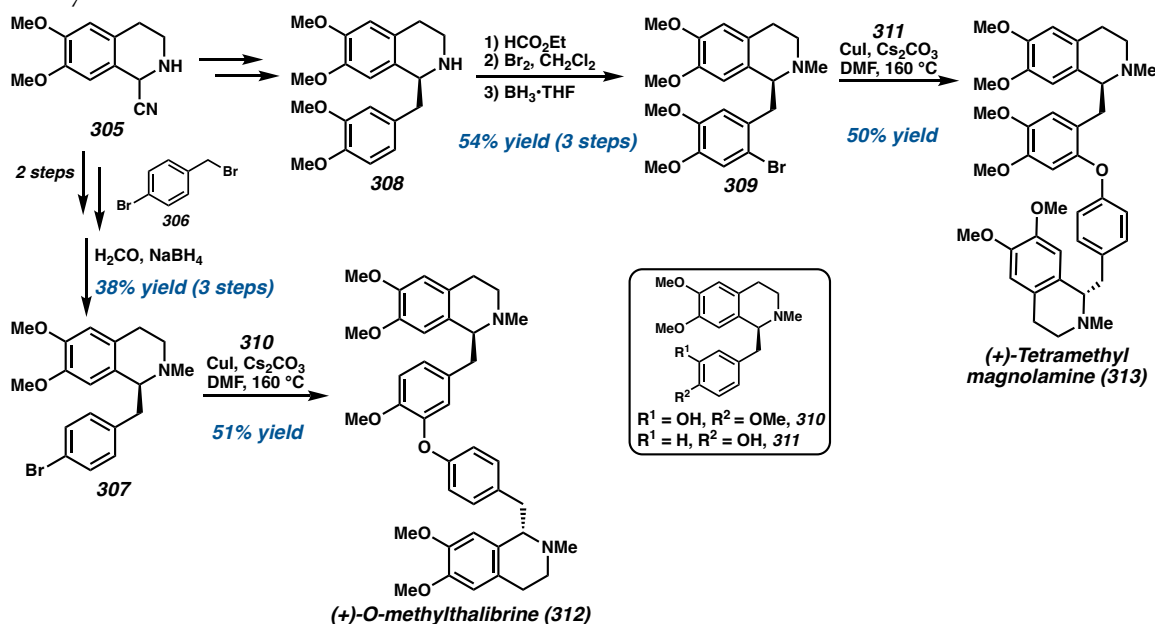
#### 4.4.2.2. TOTAL SYNTHESIS OF BISBENZYL THIQ ALKALOIDS

In 2011, Opatz and coworkers described the modular syntheses of (+)-tetramethylmagnolamine **313** and (+)-*O*-methylthalibrine **312** from a common intermediate THIQ **305** (Scheme 4.20).<sup>32</sup> Alkylation of deprotonated aminonitrile **305** with benzyl bromide **306** and subsequent reductive methylation gives THIQ monomer **307**, while bromination of **308** followed by formamide reduction yielded the other THIQ monomer **309**. Finally, an Ullman coupling of **307** forged the biaryl ether linkage with THIQ **310** to afford (+)-*O*-methylthalibrine dimer **312**, or alternatively with THIQ **309** and **311** to synthesize (+)-tetramethylmagnolamine **313**. Opatz and coworkers utilized a similar synthetic strategy for the C–O coupling of two benzyl THIQ monomers to access the macrocyclic skeleton of the curare alkaloids as well.<sup>32b</sup>

A similar synthetic approach was described by Bracher and coworkers for the total synthesis of tetrandine **321** and isotetrandine **322**, featuring a Pictet–Spengler condensation to construct the THIQ moieties followed by an Ullmann coupling for biaryl ether formation (Scheme 4.21).<sup>33</sup> First, benzyl-THIQ **316** was constructed from a Pictet–Spengler cyclization of carbamate **314** with enol ether **315**, which further underwent a C–O coupling using a

copper(I) bromide-dimethylsulfide complex with Cs<sub>2</sub>CO<sub>3</sub> in pyridine to yield **318**. After deprotection, a second Pictet–Spengler reaction with enol ether **319** delivered *seco*-bisbenzylisoquinoline **320** in 42–46% overall yield. A second Ullmann coupling using the same optimized conditions then afforded the macrocycle and accessed both natural products tetrandine **321** and isotetrandine **322** after reduction with LiAlH<sub>4</sub>.

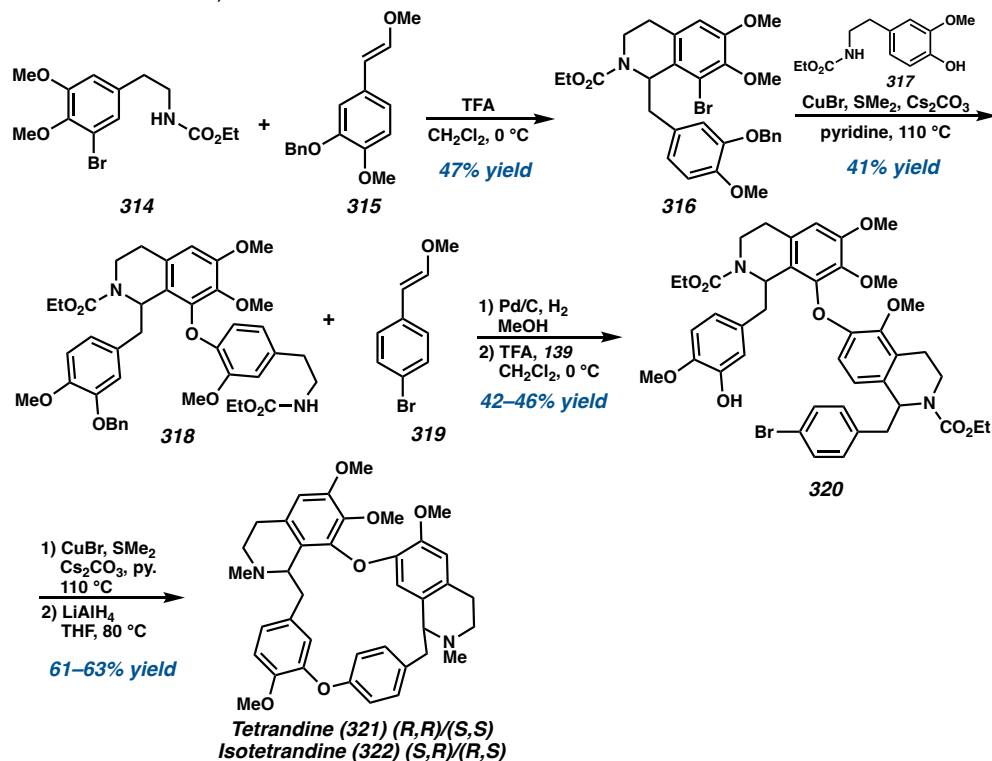
**Scheme 4.20** Opatz's synthesis of (+)-tetramethylmagnolamine **313** and (+)-*O*-methylthalibrine **312**.



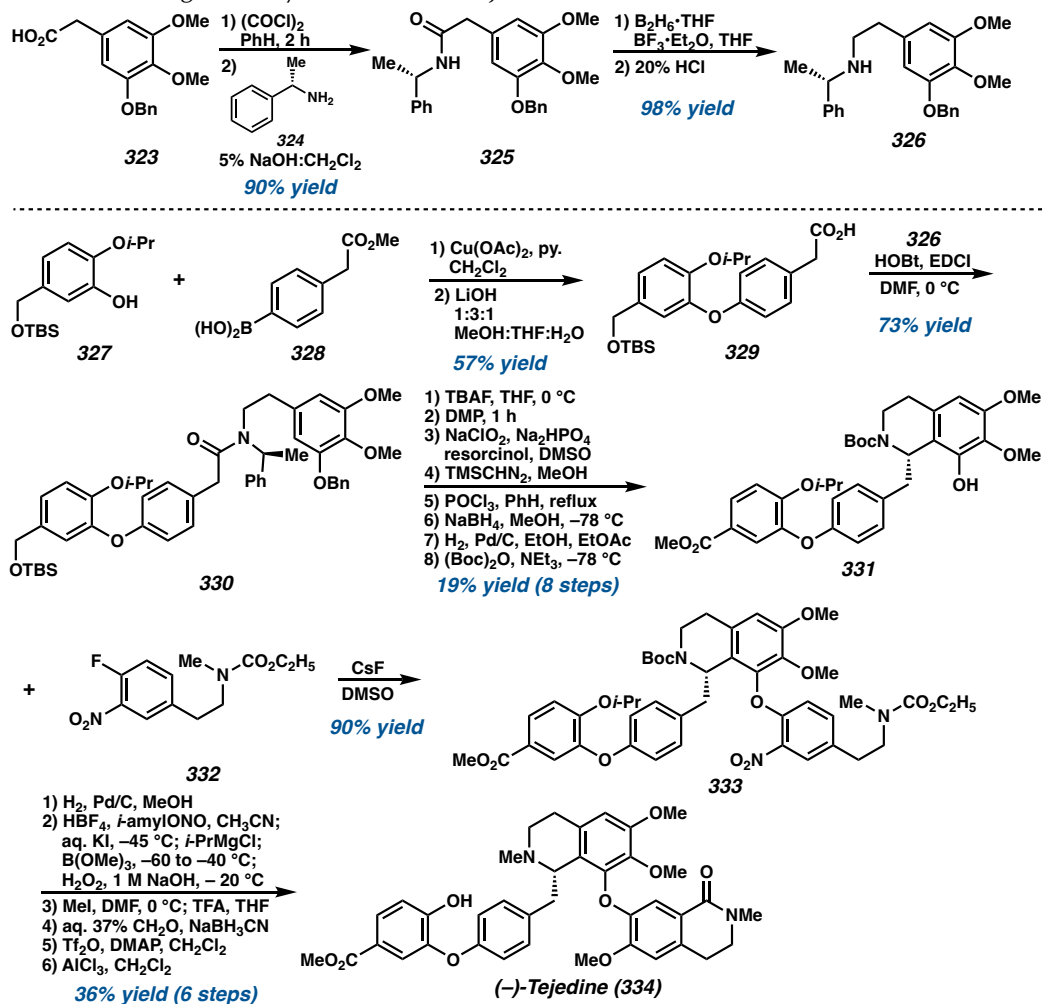
Apart from macrocyclic bisbenzyltetrahydroisoquinoline alkaloids, several novel strategies to access *seco*-bisbenzyltetrahydroisoquinolines have been explored. In 2002, Georghiou and coworkers described the total synthesis of (–)-tejedine **334** from a key Bischler–Napieralski cyclization and diaryl ether coupling (Scheme 4.22).<sup>34</sup> One of the synthons for the key cyclization was synthesized from phenyl acetic acid **323**, which upon reaction with (*S*)-methylbenzylamine **324** delivered amide **325**, and further reduction afforded synthon **326**. The diaryl ether coupling partner was then achieved from a Cu(OAc)<sub>2</sub>-

catalyzed C–O coupling of phenol **327** with phenyl boronic acid **328**, which was then hydrolyzed to carboxylic acid **329**.

**Scheme 4.21** Bracher's synthesis of tetrandine **321** and isotetrandine **322**.



With the two partners in hand, a diastereoselective Bischler–Napieralski reaction was performed using the chiral auxiliary-bearing synthon **326** condensed with **329** to deliver amide **330**, followed by cyclization using  $\text{POCl}_3$  and reduction to deliver THIQ **331** as a single diastereomer. Finally, the dihydroisoquinolone unit was installed from phenylethylamine **332** which underwent a base-mediated  $\text{S}_{\text{N}}\text{Ar}$  coupling with **331** to deliver **333**. After converting the nitro group to a methoxy substituent, *N*-methylation and cyclization afforded (–)-tejedine **334**.

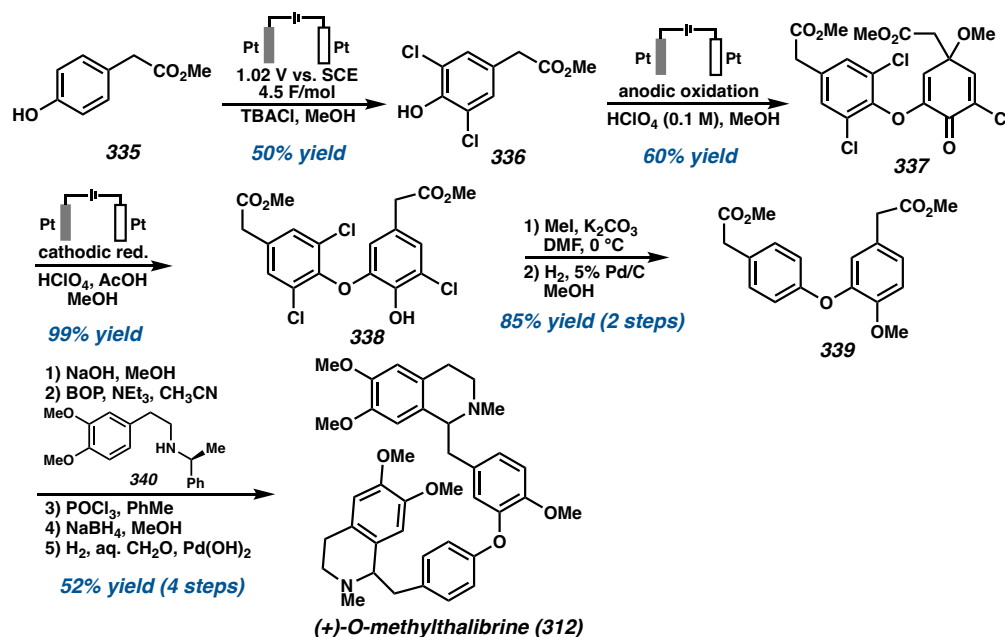
**Scheme 4.22** Georghiou's synthesis of (–)-tejedine **334**.

Toward the synthesis of (+)-*O*-methylthalibrine **312**, Nishiyama and coworkers employed an electrochemical method to construct the diaryl ether core along with a stereoselective Bischler–Napieralski reaction to establish the THIQ moieties.<sup>35</sup> First, the electrochemical halogenation of phenol **335** was optimized to deliver dichlorinated phenol **336** using TBACl as the halogen source (Scheme 4.23). Then, oxidative dimerization of **336** was performed to deliver **337** in 60% yield, followed by cathodic reduction to afford the desired diaryl ether product **338**. After methylation of the phenol, catalytic hydrogenolysis delivered **339** in 85% overall yield. Alternatively, an electrochemical reductive



dechlorination reaction was also developed by passing a methanol solution of **338** through a Pd tube (cathode) and a Pt wire (anode) in aqueous H<sub>2</sub>SO<sub>4</sub> solution outside the flow cell. Hydrogen, which was generated by electrolysis, was absorbed into the Pd tube and thus the successive reduction was conducted to give **339** in 76% yield.<sup>35a</sup> After hydrolysis, the reaction of the resulting diacid with phenylethylamine **340** provided the corresponding bis-amide which underwent a Bischler–Napieralski cyclization followed by reduction to deliver bis-THIQ in 75% overall yield. Finally, a one-pot conversion of removing the chiral auxiliaries and *N*-methylation afforded the natural product **312**.

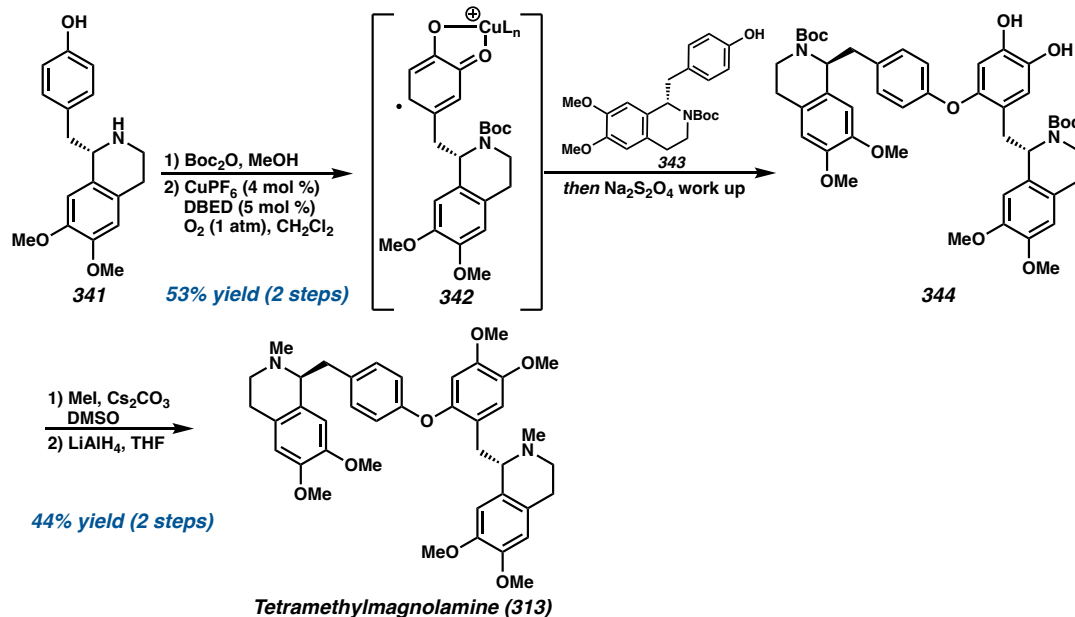
**Scheme 4.23** Nishiyama's electrochemical synthesis of (+)-*O*-methylthalibrine **312**.



Alternatively, Lumb and coworkers adopted a bioinspired strategy for the synthesis of (*S,S*)-tetramethylmagnolamine **313** utilizing a catalytic aerobic desymmetrization of phenols.<sup>36</sup> From THIQ **341**, which was established from a Bischler–Napieralski cyclization followed by asymmetric reduction, a Boc protection and subsequent aerobic oxidative coupling using CuPF<sub>6</sub> and *N,N'*-di-*tert*-butylethylenediamine (DBED) under 1 atm of O<sub>2</sub>

formed oxygenated radical intermediate **342** (Scheme 4.24). Upon treatment of another THIQ molecule **343**, a radical C–O coupling afforded the desymmetrized bis-THIQ dimer **344** after reductive workup. Subsequent methylation and reduction of the Boc groups furnished tetramethylmagnolamine **313** in 7 steps with 21% overall yield. By taking advantage of the natural product’s pseudosymmetry and biosynthesis, this synthetic approach concisely assembles the target by only preparing a single coupling partner.

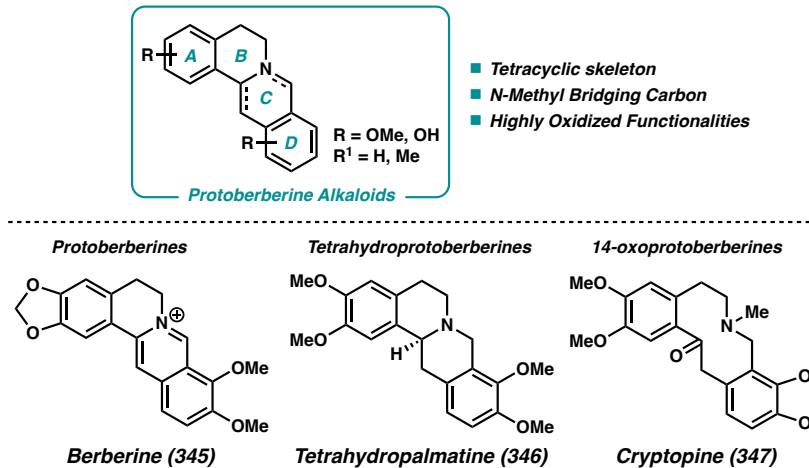
**Scheme 4.24** Lumb’s synthesis of tetramethylmagnolamine **313**.



#### 4.4.3. PROTOBERBERINE ALKALOIDS

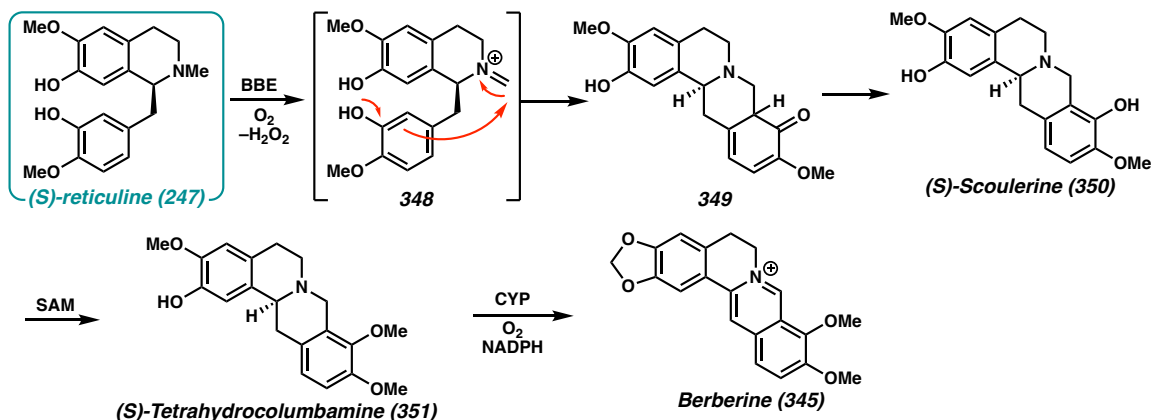
##### 4.4.3.1. GENERAL STRUCTURE AND BIOSYNTHESIS

The protoberberine alkaloids constitute a tetracyclic ring system with varied functionalities on the arene ring. These alkaloids are derived from benzyl THIQs through phenolic oxidation and coupling with the *N*-methyl group, which serves as the “berberine bridge” carbon (Figure 4.13).<sup>37</sup>

**Figure 4.13** General structure of the protoberberine THIQ alkaloids.

Primarily isolated from the Papaveraceae (e.g., *Corydalis*, *Papaver*), Berberidaceae (e.g., *Berberis*, *Mahonia*), and Menispermaceae family, the protoberberine alkaloids consist of several variations of the tetracyclic ring system: the protoberberines such as berberine **345**, the tetrahydroprotoberberines like tetrahydropalmatine **346**, and C14-oxo derivatives, such as cryptopine **347**. These three distinct scaffolds are only several of the myriad number of skeleton types identified.

Plants that contain the protoberberine alkaloids are known to be used as analgesics, sedatives, and antiseptics in traditional medicine. Both the quaternary alkaloid salts and their tetrahydroderivatives have important biological and therapeutic activity, and thus their chemical syntheses have been extensively explored. Their biosynthesis stems from oxidation of reticuline **247** catalyzed by a berberine bridge enzyme (BBE) to generate iminium **348**, with release of H<sub>2</sub>O<sub>2</sub> as by-product (Figure 4.14).<sup>38</sup> Electrophilic aromatic substitution then delivers the protoberberine scaffold (*S*)-scoulerine **350**, which upon methylation by (*S*)-adenosyl methionine (SAM) forms tetrahydroprotoberberine **351**. Further oxidation of the amine by a cytochrome P450-dependent enzyme and formation of the dioxolane ring gives berberine **345**.<sup>39</sup>

**Figure 4.14** Proposed biosynthesis of protoberberine alkaloids **345** and **351**.

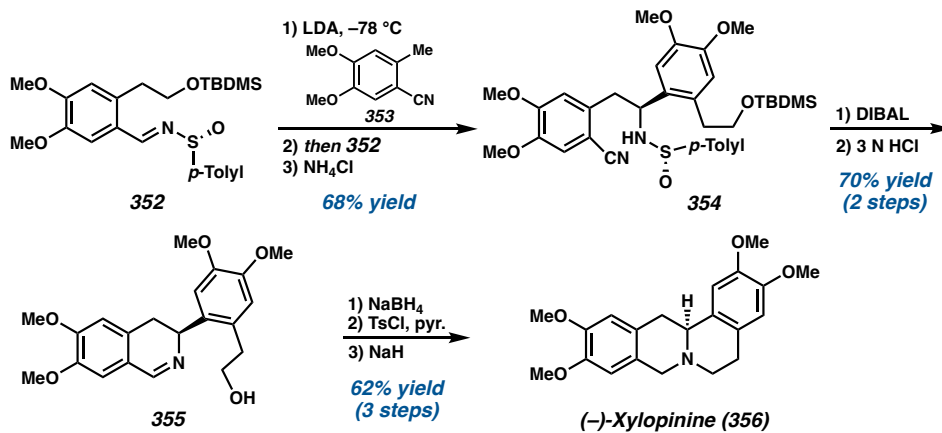
#### 4.4.3.2. TOTAL SYNTHESIS OF PROTOBERBERINE ALKALOIDS

While there have been vast reports on the syntheses of the protoberberine alkaloids, some feature distinct synthetic strategies to access the natural product. In 2002, Davis and coworkers reported the synthesis of protoberberine alkaloid (–)-xylopinine **356** involving the addition of a lithiated *ortho*-tolyl nitrile into an enantiopure sulfinimine.<sup>40</sup> Using enantiopure sulfinimine **352**, which was prepared from condensation of the aldehyde with enantiopure sulfonamide, reaction with lithiated *ortho*-tolyl nitrile **353** delivered sulfonamide **354** as a mixture of diastereomers (Scheme 4.25). Treatment with DIBAL followed by hydrolysis reduced the nitrile and removed the sulfinyl group to allow cyclization to afford dihydroisoquinoline **355**. Reduction of the imine, tosylation, and cyclization of the amine using NaH gave (–)-xylopinine **356** in 73% yield.

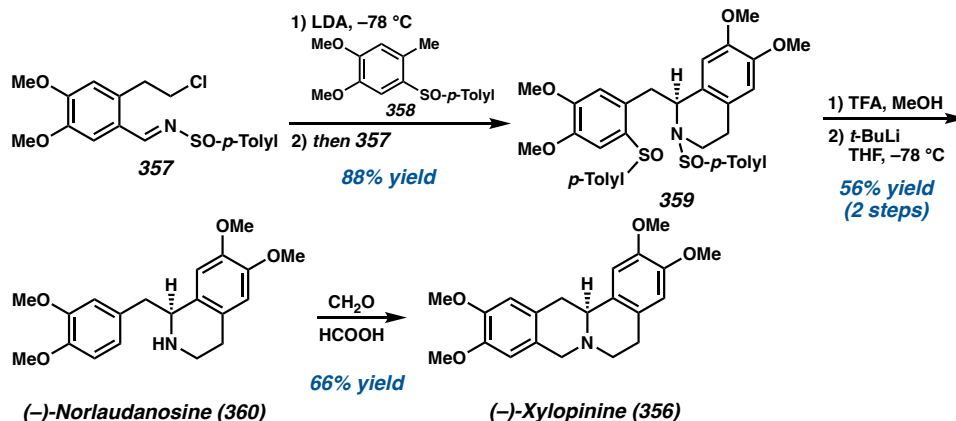
Similarly, Ruano and coworkers harnessed a similar strategy toward the synthesis of (–)-xylopinine **356**, instead using toluenesulfonamide **358** to add into *N*-sulfinylimine **357** that produced benzyl THIQ **359** in 58% yield (Scheme 4.26).<sup>41</sup> Treatment with TFA and *t*-BuLi removed both sulfinyl groups to access (–)-norlaudanosine **360**, and a Pictet–Spengler cyclization with formaldehyde ultimately delivered (–)-xylopinine **356**. Both Yang,<sup>42</sup> and

Rozwadowska<sup>43</sup> have also harnessed this synthetic approach of the addition of nucleophiles to enantiopure sulfinimines to synthesize other members of the protoberberine alkaloid family.

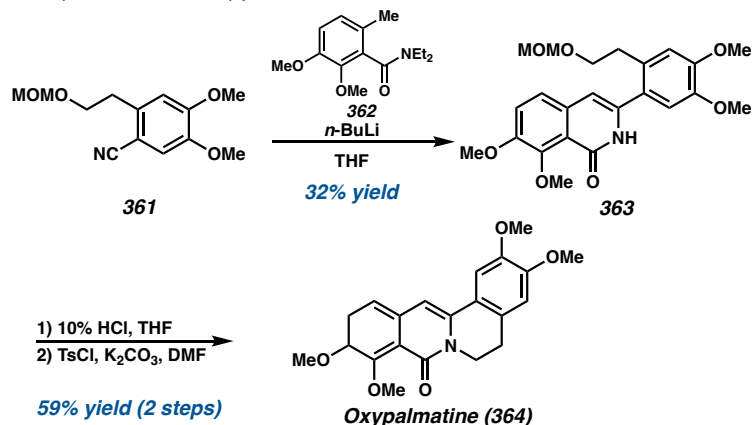
**Scheme 4.25** Davis' synthesis of (-)-xylopinine **356**.



**Scheme 4.26** Ruano's synthesis of (-)-xylopinine **356**.



The convergent synthetic approach of the addition of lithiated nucleophiles to dihydroisoquinolines or benzonitriles have been well explored to quickly build the protoberberine scaffold. Cho and coworkers demonstrated the convergent coupling of benzonitrile **361** and lithiated *ortho*-toluamide **362** to access isoquinolone **363** in 32% yield (Scheme 4.27).<sup>44</sup> Then, removal of protecting groups and reaction with *p*-TsCl in the presence of  $K_2CO_3$  delivered oxypalmatine **364**.

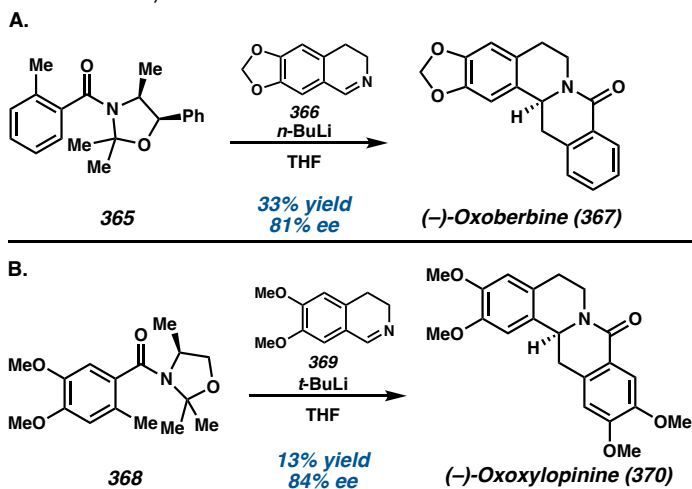
**Scheme 4.27** Cho's synthesis of oxypalmatine **364**.

Utilizing lithiated oxazoline or oxazolidine chiral auxiliaries to add into dihydroisoquinolines, Iwao<sup>45</sup> and Chrzanowska<sup>46</sup> were able to synthesize both enantiomers of the protoberberine alkaloids. From enantioenriched oxazolidine **365**, treatment with *n*-BuLi generated the carbanion followed by addition to dihydroisoquinoline **366** directly afforded oxoberbine **367** in 33% yield with 81% *ee* (Scheme 4.28A). More recently, Chrzanowska and coworkers also applied the same strategy toward the synthesis of (–)-oxylopinine **370** from the addition of lithiated oxazolidine **368** to dihydroisoquinoline **369** (Scheme 4.28B).

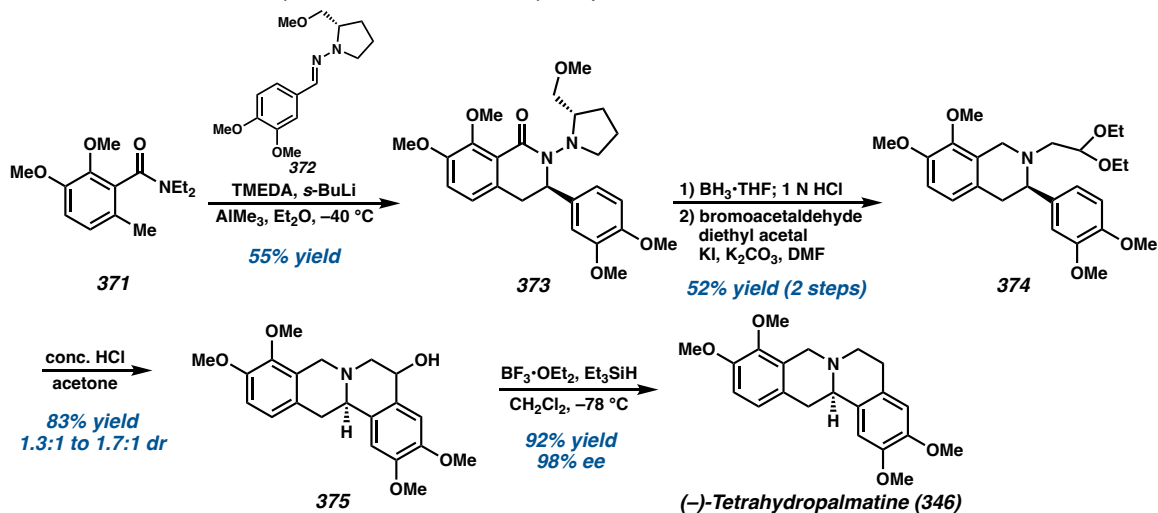
Finally, Enders and coworkers demonstrated the addition of lithiated benzamides to enantioenriched hydrazones to assemble dihydroisoquinolones toward the synthesis of tetrahydropalmatine **346**.<sup>47</sup> Lithiated benzamide **371** was reacted with hydrazone **372**, which was prepared from condensation of enantiopure “SAMP” hydrazines with 3,4-dimethoxybenzaldehyde, to deliver isoquinolone **373** as a single diastereomer (Scheme 4.29). Then, treatment of **373** with BH<sub>3</sub>•THF cleaved the N–N bond of the chiral auxiliary, followed by installation of the diethyl acetal moiety to afford **374**. A Pomeranz–Fritsch cyclization was then induced using concentrated HCl to obtain protoberberine scaffold **375**

as a mixture of diastereomers. Removing the hydroxyl group was achieved using  $\text{BF}_3 \cdot \text{OEt}_2$  and  $\text{Et}_3\text{SiH}$  to ultimately synthesize (–)-tetrahydropalmatine **346** in 92% yield with 98% ee.

**Scheme 4.28** Chrzanowska's synthesis of A. Oxoberberine **367** and B. (–)-oxoxylopinine **370**.



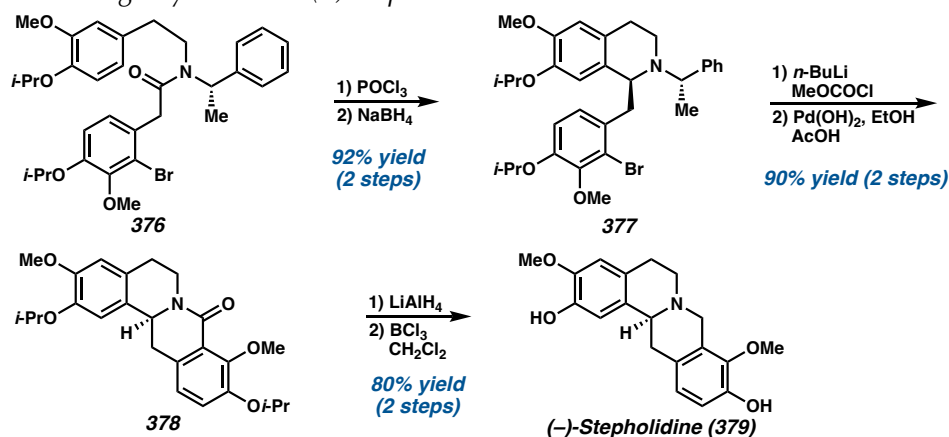
**Scheme 4.29** Ender's synthesis of (–)-tetrahydropalmatine **346**.



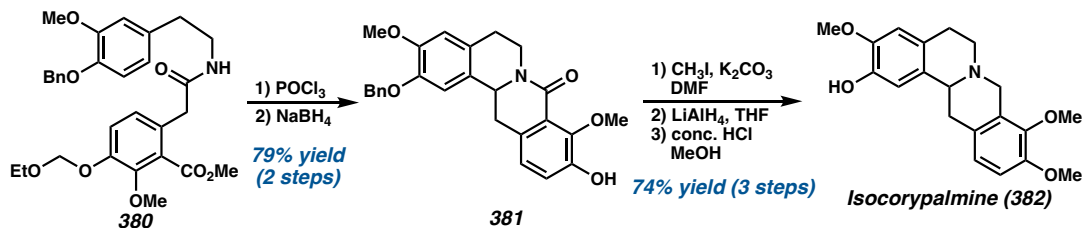
More classic approaches to the protoberberine alkaloids involve electrophilic aromatic substitution chemistry to assemble the THIQ core. Both the Yang<sup>48</sup> and Harding<sup>49</sup> groups demonstrated a Bischler–Napieralski strategy toward building the THIQ core, with a tethered methyl ester allowing cyclization to the protoberberine scaffold. From amide **376**, treatment with  $\text{POCl}_3$  followed by  $\text{NaBH}_4$  reduction established enantioenriched THIQ **377**

induced from the chiral auxiliary (Scheme 4.30). Then, introduction of the methyl ester through a lithium halogen exchange and quenching with methyl chloroformate, and intramolecular cyclization of the amine delivered protoberberine scaffold **378**. Yang was then able to achieve the synthesis of (–)-stepholidine **379** after carbonyl reduction and protecting group removal. Similarly, Harding utilized amide **380** with a pendent methyl ester to undergo Bischler–Napieralski cyclization and reduction to access the protoberberine scaffold **381** directly (Scheme 4.31). Methylation and reduction of the carbonyl then delivered isocorypalmine **382**.

**Scheme 4.30** Yang's synthesis of (–)-stepholidine **379**.



**Scheme 4.31** Harding's synthesis of isocorypalmine **382**.

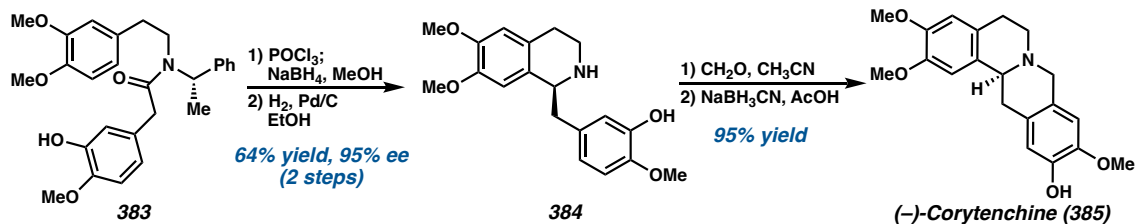


Other electrophilic aromatic substitution strategies utilize formaldehyde or aldehyde equivalents to close the C-ring and access the natural product scaffold. In 2010, Georghiou and coworkers harnessed a chiral auxiliary-assisted Bischler–Napieralski cyclization and

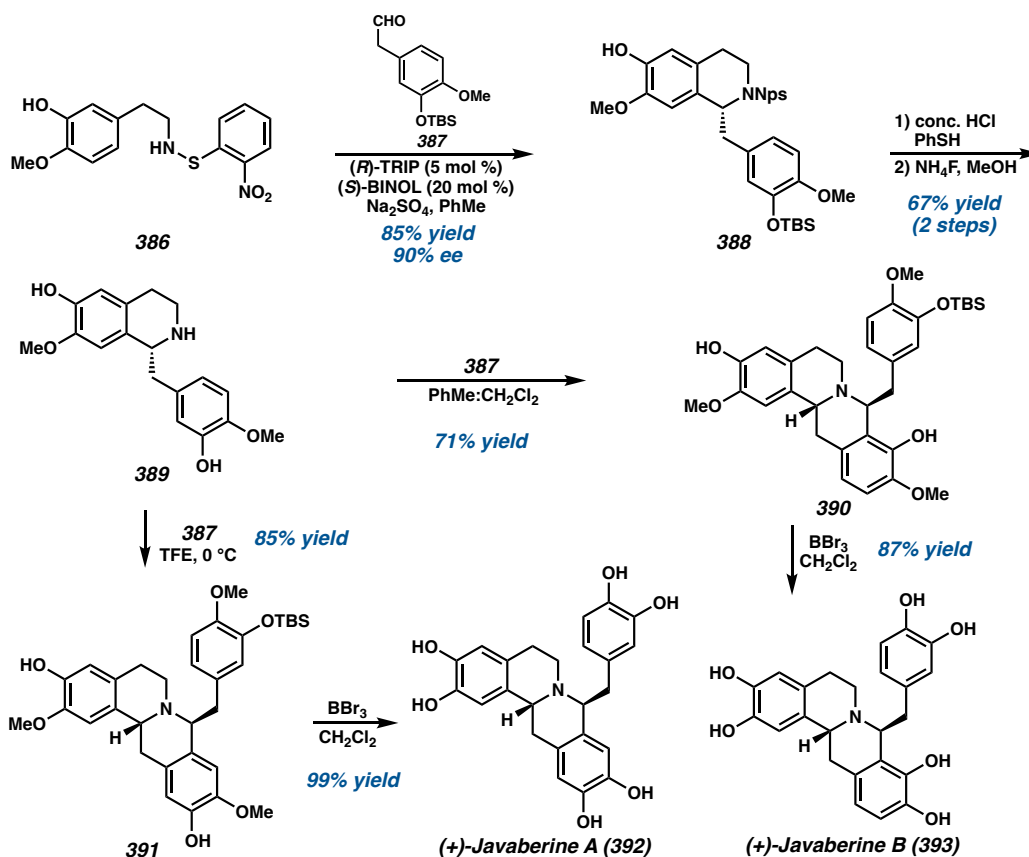
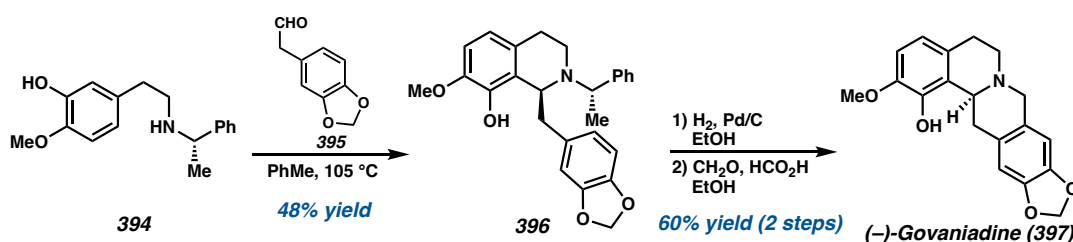


reduction of amide **383** to achieve THIQ **384**, upon which addition of formaldehyde followed by  $\text{NaBH}_3\text{CN}$  reduction delivered (–)-corytenchine **385** (Scheme 4.32).<sup>50</sup>

**Scheme 4.32** Georghiou's synthesis of (–)-corytenchine **385**.



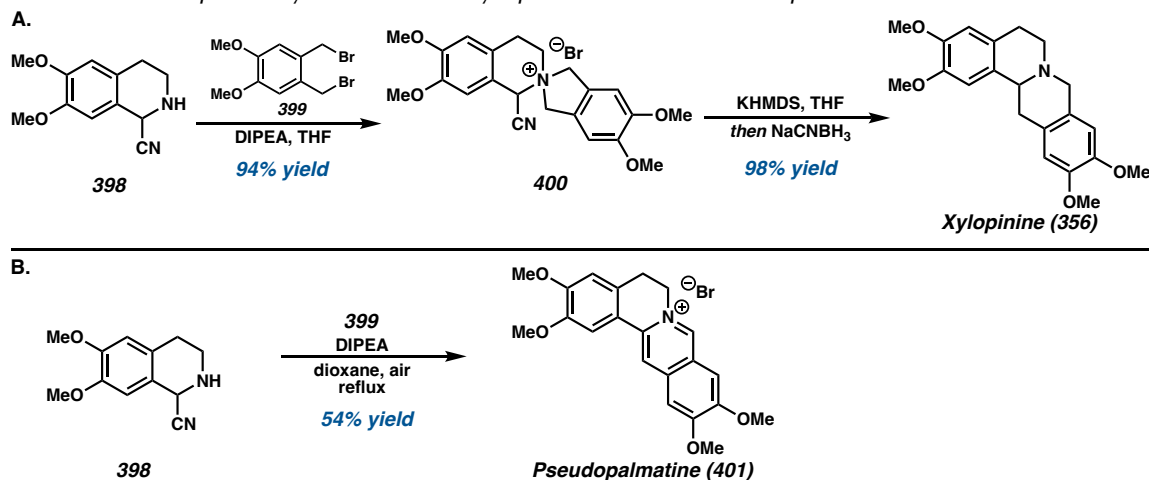
Alternatively, Hiemstra<sup>51</sup> and van Maarseveen<sup>52</sup> and coworkers demonstrated a regioselective *ortho*- or *para*-directed Pictet–Spengler reaction to construct the THIQ core. First, a Pictet–Spengler condensation of protected amine **386** with aldehyde **387** afforded THIQ **388** in 85% yield with 90% ee (Scheme 4.33). Then, a second Pictet–Spengler reaction was effected with another equivalent of aldehyde **387** to deliver either the *para*- or *ortho*-isomer depending on the solvent. Increasing H-bonding character of the solvent such as HFIP and trifluoroethanol increased the amount of *para*-substituted product **391**, while aprotic, apolar solvents such as toluene gave the highest selectivity of *ortho*-isomer **390**. Treatment with  $\text{BBr}_3$  led to the formation of (+)-javaberine A **392** and (+)-javaberine B **393**. Van Maarseveen and coworkers demonstrated an *ortho*-selective Pictet–Spengler reaction using aldehyde **395** with equimolar amounts of **394** in toluene as solvent to achieve the *ortho*-isomer **396** in good selectivity (Scheme 4.34). Debenzylation and cyclization of the C-ring using formaldehyde under acidic conditions produced (–)-govaniadine **397** in 61% yield, allowing access to several other *ortho*-oxygenated alkaloids as well.

**Scheme 4.33** Hiemstra's synthesis of (+)-javaberine A **392** and (+)-javaberine B **393**.**Scheme 4.34** van Maarseveen's synthesis of (–)-govaniadine **397**.

Apart from the classical synthetic approaches to the protoberberine alkaloids, Opatz and coworkers utilize a Stevens rearrangement of ammonium ylides to synthesize the protoberberine alkaloids.<sup>53</sup> From common synthetic intermediate THIQ **398**,<sup>54</sup> reaction with dibromide **399** delivered spirocyclic ammonium salt **400**, which upon deprotonation induced a Stevens rearrangement followed by reduction with  $\text{NaCNBH}_3$  to obtain xylopinine **356** (Scheme 4.35A). This was further optimized to a one-pot cascade synthesis of

pseudopalmatine **401** from **398** and **399** using DIPEA as base, and aromatization under air to protoberberine alkaloid **401** (Scheme 4.35B).<sup>55</sup>

**Scheme 4.35** Opatz's synthesis of A. Xylopinine **356**. B. Pseudopalmatine **401**.

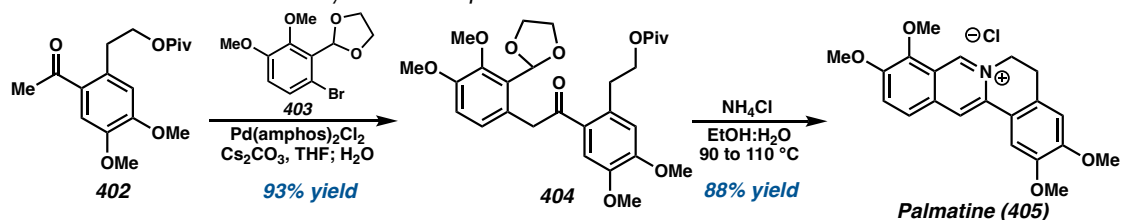


Several transition metal-catalyzed annulations have been developed to apply toward the synthesis of the protoberberine alkaloids. In 2014, Donohoe and coworkers described a Pd-catalyzed enolate arylation of aryl bromides and ketones to generate masked 1,5-dicarbonyl intermediates that could readily cyclize with a source of  $\text{NH}_3$  to an array of isoquinolines.<sup>56</sup> The coupling of ketone **402** and aryl bromide **403** was effected using  $\text{Pd}(\text{amphos})_2\text{Cl}_2$  and  $\text{Cs}_2\text{CO}_3$  to access ketone **404** in 93% yield (Scheme 4.36). Then, a one-pot aromatization and cyclization using  $\text{NH}_4\text{Cl}$  in ethanol and water delivered palmatine **405**. This protocol was successfully utilized for a variety of substituted aryl bromides and ketones for the rapid synthesis of the protoberberine alkaloids.

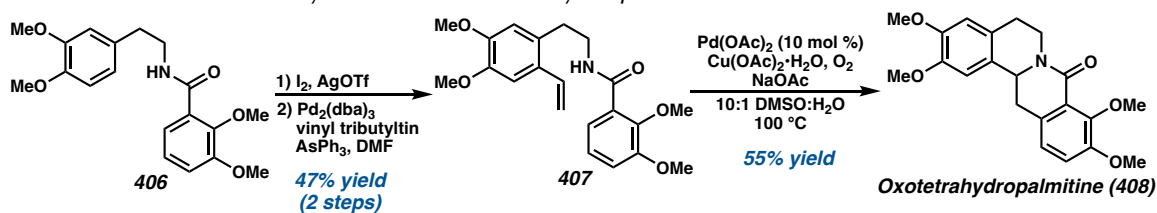
Alternatively, Mhaske and coworkers employed a Pd-catalyzed intramolecular tandem olefin amidation and C–H activation method for the synthesis of the protoberberine core.<sup>57</sup> From amide **406**, iodination and Stille coupling with vinyl tributyltin afforded key precursor **407** (Scheme 4.37). Using  $\text{Pd}(\text{OAc})_2$  as catalyst and  $\text{Cu}(\text{OAc})_2 \cdot \text{H}_2\text{O}$  and  $\text{O}_2$  as

oxidant, **407** first underwent amidation to assemble the THIQ, followed by C–H activation of the arene to allow cyclization to oxotetrahydropalmitine **408** in 55% yield.

**Scheme 4.36** Donohoe's synthesis of palmatine **405**.

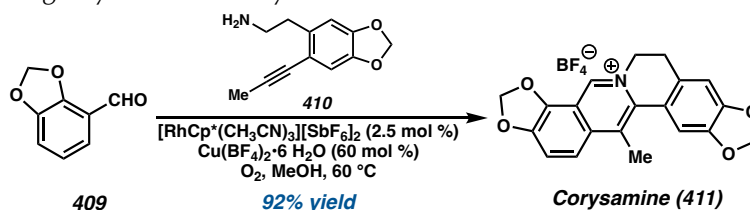


**Scheme 4.37** Mhaske's synthesis of oxotetrahydropalmitine **408**.



In 2016, Cheng and coworkers developed a general Rh-catalyzed C–H activation and annulation method to afford various natural and unnatural protoberberine alkaloids.<sup>58</sup> An array of substituted benzaldehydes, such as **409**, were coupled with alkyne **410** using  $[\text{RhCp}^*(\text{CH}_3\text{CN})_3][\text{SbF}_6]_2$  as catalyst with  $\text{Cu}(\text{BF}_4)_2 \cdot 6 \text{H}_2\text{O}$  and  $\text{O}_2$  as oxidant to deliver protoberberine alkaloid corysamine **411** in 92% yield (Scheme 4.38). This one-pot transformation was successfully employed for a variety of benzaldehydes and alkyne amines to provide a library of protoberberine salts in good yield and selectivity.

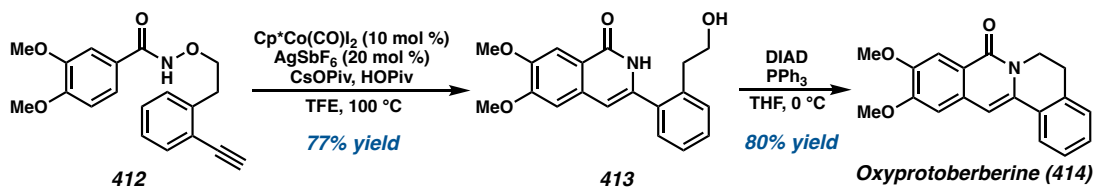
**Scheme 4.38** Cheng's synthesis of corysamine **411**.



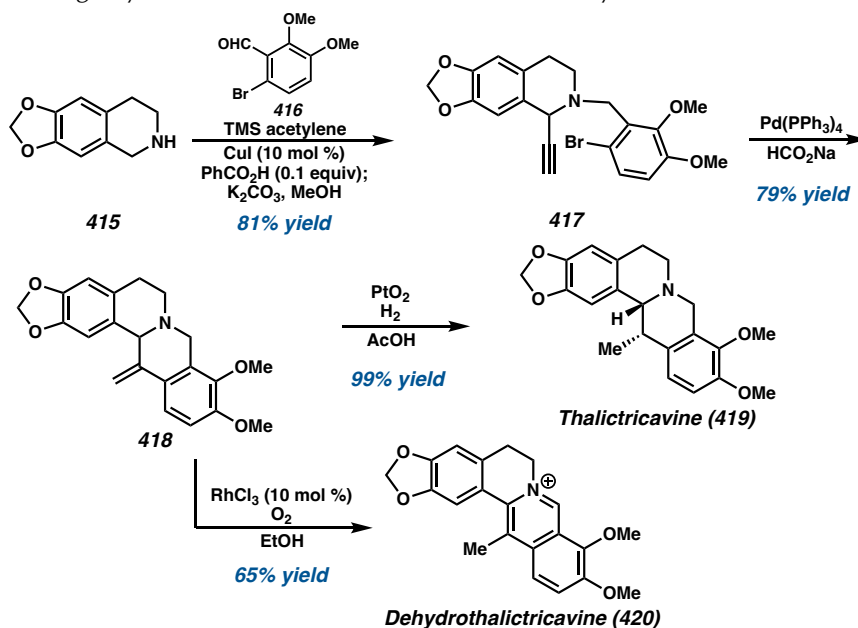
Glorius and coworkers also reported a C–H activation annulation approach of substituted benzamides to install the oxyprotoberberine core.<sup>59</sup> Using  $\text{Cp}^*\text{Co}(\text{CO})\text{I}_2$  as

catalyst, benzamide **412** underwent alkyne insertion, reductive C–N bond formation and N–O bond cleavage to achieve isoquinolone **413** in a single transformation (Scheme 4.39). A Mitsunobu reaction then constructed the oxyprotoberberine scaffold **414** in 80% yield, which could be further elaborated into the protoberberine or tetrahydroprotoberberine alkaloids.

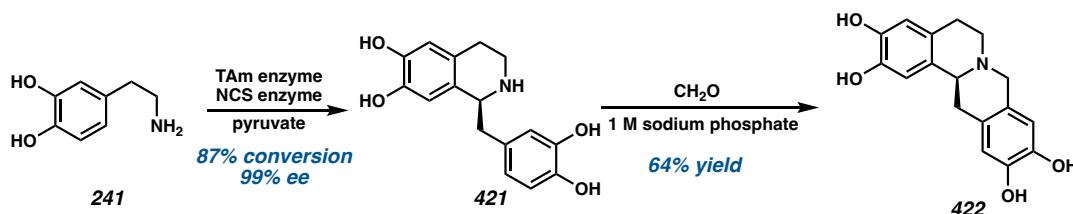
**Scheme 4.39** Glorius' general synthesis of protoberberine alkaloids.



Harnessing a Cu-catalyzed three component coupling reaction of an amine, aldehyde, and alkyne, Tong and coworkers optimized a general annulation strategy that enabled the syntheses of over 30 natural protoberberine alkaloids.<sup>60</sup> To this end, THIQ **415**, benzaldehyde **416**, and trimethylsilylacetylene were employed in a three component condensation reaction to afford THIQ **417** in 81% yield (Scheme 4.40). Then, a Pd-catalyzed reductive carbocyclization reaction successfully provided the desired tetracycle **418** of the protoberberine core. Hydrogenation of the *exo*-olefin delivered the natural product thalictricavine **419** as a single diastereomer. A Rh-catalyzed isomerization of **418** with concomitant oxidation under air also provided the protoberberine salt dehydrothalictricavine **420** in 65% yield. With this highly efficient synthetic route, a variety of 13-methyl-protoberberine alkaloids were synthesized for the first time, including their analogues in excellent overall yields.

**Scheme 4.40** Tong's synthesis of thalictricavine **419** and dehydrothalictricavine **420**.

Finally, Ward and coworkers employed a novel chemoenzymatic cascade toward the synthesis of the tetrahydroprotoberberine alkaloids.<sup>61</sup> From dopamine **241**, first a Pictet–Spengler condensation using a transaminase enzyme (TAm) from CV2025 *Chromobacterium violaceum* and a norcoclaurine synthase enzyme (NCS) delivered THIQ **421** in 87% yield with 99% ee (Scheme 4.41). Then, the addition of formaldehyde induced a second Pictet–Spengler reaction to deliver tetrahydroprotoberberine alkaloid **422** in 64% yield.

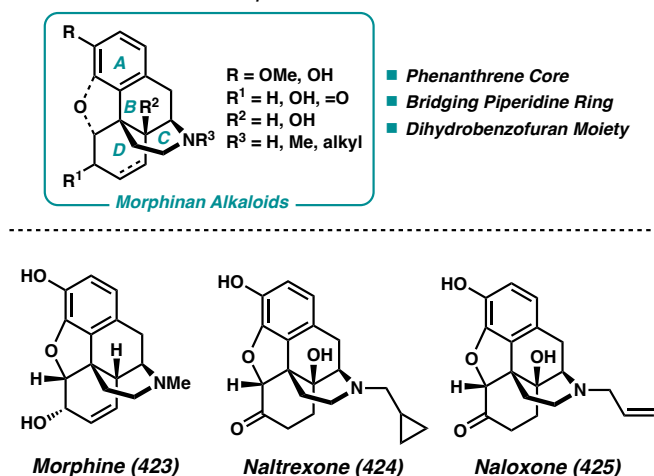
**Scheme 4.41** Ward's chemoenzymatic synthesis of tetrahydroprotoberberine alkaloid **422**.

#### 4.4.4. MORPHINAN ALKALOIDS

##### 4.4.4.1. GENERAL STRUCTURE AND BIOSYNTHESIS

The morphinan alkaloids are distinguished by their phenanthrene core with a bridging piperidine ring and a fused benzodihydrofuran moiety. They are famous THIQ-derived natural products well-known for their analgesic and anesthetic bioactivity. Morphine **423** is commonly used to treat severe pain, while other members such as naltrexone **424** and naloxone **425** are commercially produced for treatment of opiate overdoses and alcohol addiction (Figure 4.15).<sup>62</sup> Isolated primarily from opium poppy *Papaver somniferum*, the global production of opium poppy concentrate is estimated to be around 8700 tons per year, of which morphine and codeine are the principal ingredients.<sup>63</sup>

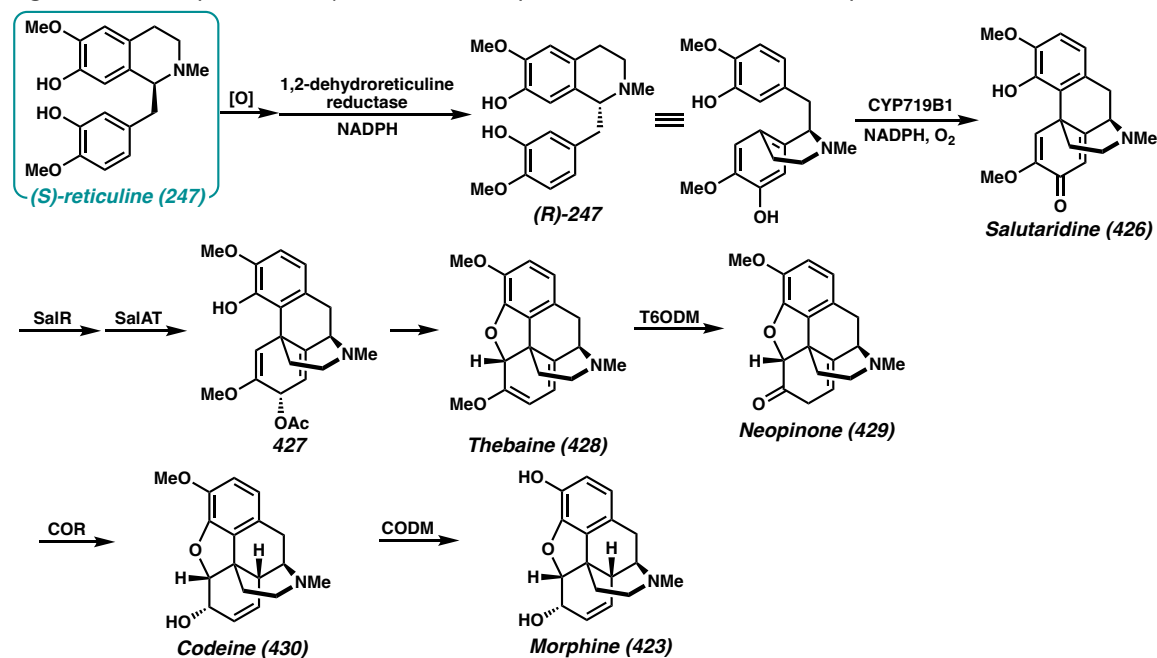
**Figure 4.15** General structure of the morphinan THIQ alkaloids.



The biosynthesis of morphine and its related congeners stems from key intermediate reticuline **247**, which is converted to the (*R*)-enantiomer by 1,2-dehydroreticuline reductase (Figure 4.16).<sup>62</sup> Then, an oxidative phenol coupling catalyzed by salutaridine synthase (CYP719B1) establishes the morphinan skeleton in salutaridine **426**. Tetracycle **426** is then reduced by salutaridine reductase and acetylated by salutaridinol acetyltransferase to deliver salutaridinol-7-*O*-acetate **427**. An S<sub>N</sub>2'-type cyclization then occurs to establish the dihydrobenzofuran moiety in thebaine **428**. Thebaine-6-*O*-demethylase (T6ODM) cleaves

off the methyl group to give neopinone **429**, which can undergo isomerization and reduction of the carbonyl by codeinone reductase (COR) to yield codeine **430**.<sup>64</sup> Finally, demethylation catalyzed by codeine *O*-demethylase (CODM) produces morphine **423**.

**Figure 4.16** Proposed biosynthesis of morphine **423** and related morphinan alkaloids.



#### 4.4.4.2. TOTAL SYNTHESIS OF MORPHINAN ALKALOIDS

Since Gates' first synthesis of morphine in 1952, many others have pursued the synthesis of this alkaloid and other related natural products from this family.<sup>65</sup> The continuing interest in the morphinan alkaloids as synthetic targets have resulted in numerous reviews in the total synthesis of these alkaloids, and thus this section will only cover the most recent syntheses from the past decade.<sup>66</sup>

A myriad number of strategies for the synthesis of morphine have been well explored in the past several decades. In particular, Fukuyama and coworkers have disclosed several syntheses of morphine featuring an intramolecular Mannich cyclization to construct the THIQ core.<sup>67</sup> However, their most recent synthesis of (–)-morphine utilizes chiral substrate

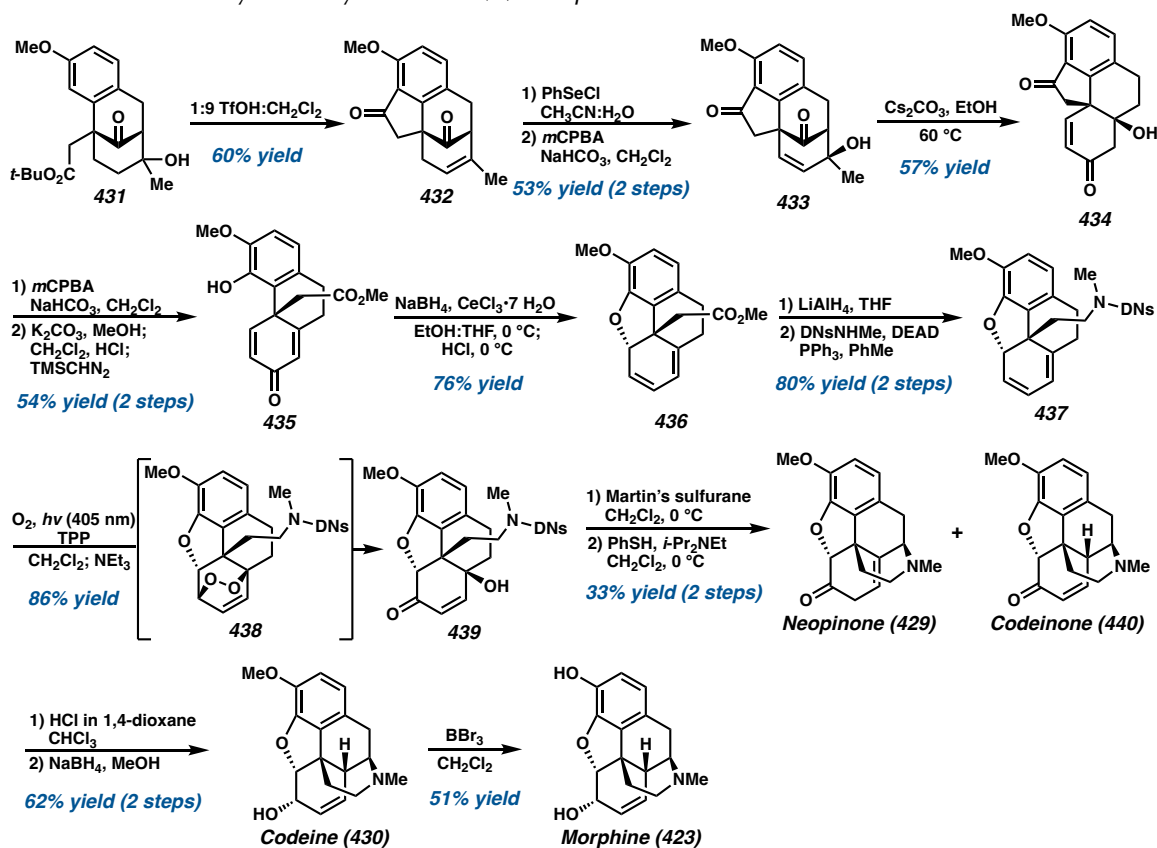


**431** to construct the morphine skeleton via a Friedel–Crafts cyclization and dehydration to deliver **432** (Scheme 36).<sup>68</sup> Hydroxyselenenylation of the resulting olefin followed by oxidation and elimination generates allylic alcohol **433** which undergoes a retro-aldol/aldol sequence to furnish enone **434**. Construction of the dihydrofuran ring commenced with Baeyer–Villiger oxidation and methanolysis of the lactone to afford dienone **435**. Luche reduction of the enone followed by treatment with HCl then caused formation of a dienyl cation and interception with the phenol to furnish the dihydrofuran ring **436**. With the tetracyclic scaffold in place, functional manipulations with the pendent methyl ester moiety to the protected tertiary amine **437** set up for oxidation with singlet oxygen to give endoperoxide **438**. Treatment with triethylamine induced cleavage of the O–O bond to afford hydroxyenone **439**, with dehydration of the alcohol and removal of the DN<sub>s</sub> group facilitating 1,6-addition to access natural products neopinone **429** and codeinone **440**, with further reduction to deliver codeine **430** and morphine **423**.

In an alternative fashion, Chida and coworkers sought to access (–)-morphine **423** through an elegant sequential Claisen rearrangement of an allylic vicinal diol, resulting in the stereoselective formation of two C–C bonds and two contiguous stereocenters in a single operation (Scheme 4.43).<sup>69</sup> Starting from allylic vicinal diol **441**, a Johnson-type Claisen rearrangement with MeC(OEt)<sub>3</sub> in the presence of 2-nitrophenol initiated the sequential Claisen/Claisen rearrangement to provide **442**. In this transformation, both vicinal quaternary and tertiary stereocenters were installed in a single transformation. Construction of the benzofuran moiety then was accomplished by treatment of **442** with *m*CPBA, inducing demethylative etherification of the epoxide to deliver **443**. Further oxidative manipulations afforded enone **444**, and following reduction, protection of the resulting alcohol, global

reduction, and Swern oxidation, dialdehyde **445** was accessed to construct the tetracyclic scaffold. A Friedel–Crafts cyclization using *p*-TsOH•H<sub>2</sub>O allowed the installation of the tetracycle **446** with concomitant removal of the TBS group. Finally, reductive amination and protection of the secondary amine generated late-stage intermediate **447**, which was only two steps away from the natural product synthesis.<sup>65,70</sup>

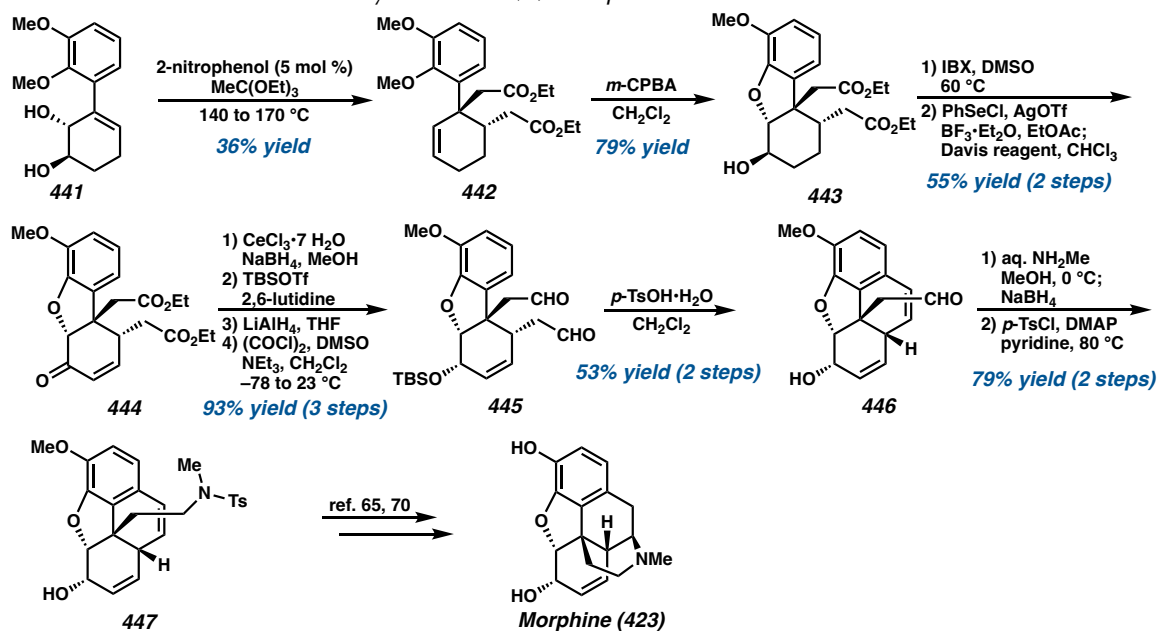
**Scheme 4.42** Fukuyama's synthesis of (–)-morphine **423**.



Toward the synthesis of (±)-morphine, Smith and coworkers utilized a diastereoselective light-mediated cyclization to establish the benzofuran moiety, and a cascade ene-yne-ene ring closing metathesis to forge the tetracyclic scaffold (Scheme 4.44).<sup>71</sup> First, a challenging sp<sup>3</sup>-sp<sup>2</sup> Suzuki–Miyaura cross-coupling of vinyl bromide **448** with β-amino borane derivative **449** was accomplished using Pd(dppf)Cl<sub>2</sub>•CH<sub>2</sub>Cl<sub>2</sub> as

catalyst. Photocyclization of **450** then proceeded smoothly to deliver *cis*-fused **451** as the sole product. After subsequent functional group manipulations to install the terminal alkyne and vinyl ketone in **452**, the cascade ene-yne-ene metathesis was accomplished using Hoveyda–Grubbs II catalyst (**C3**). It is proposed that the transformation proceeds via reaction of the ruthenium catalyst with the allyl component of **452** first, followed by an intramolecular reaction with the alkyne to generate alkylidene intermediate **453**. Ring closing metathesis with the vinyl ketone then afforded tetracycle **454** which was subjected further to deprotection of the amine and 1,6-addition to afford the morphine scaffold **455**. Diastereoselective reduction of the ketone delivered codeine **430** as a single diastereomer, as well as morphine **423** after demethylation.

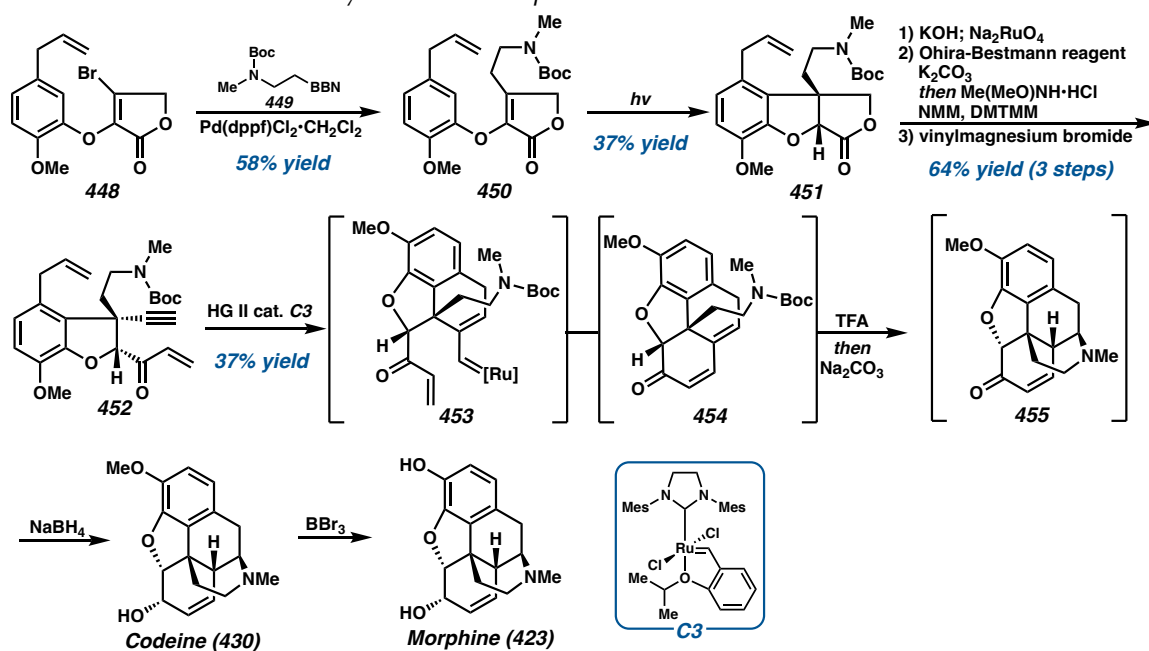
**Scheme 4.43** Chida's formal synthesis of (–)-morphine **423**.



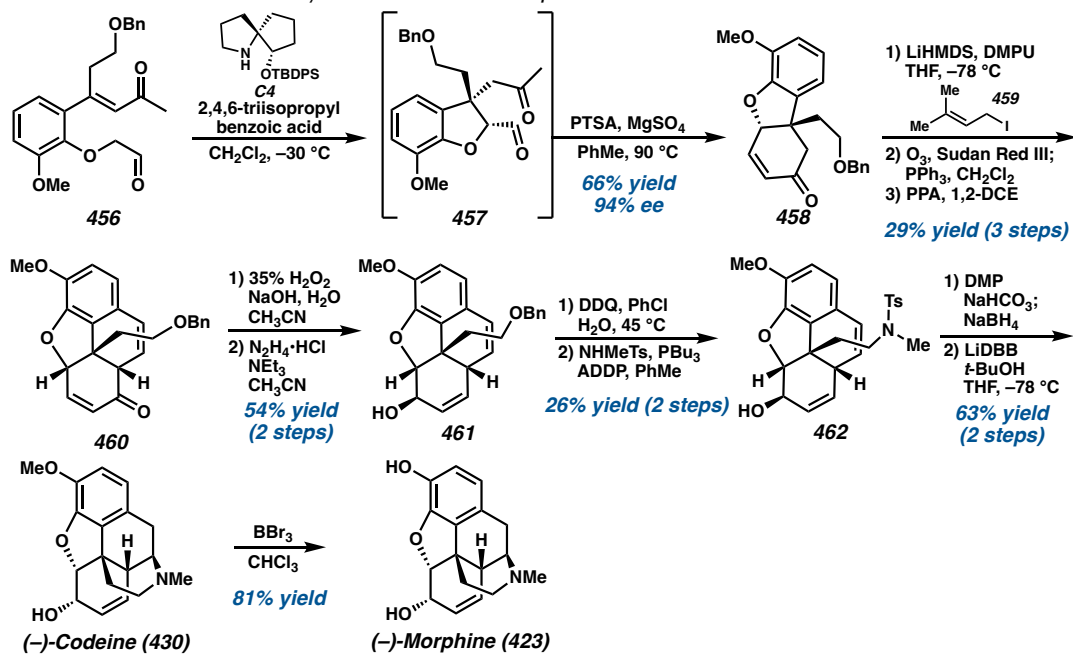
Most recently, Tu and coworkers disclosed an enantioselective synthesis of (–)-morphine harnessing a catalytic enantioselective Robinson annulation to rapidly construct the benzofuran moiety of the natural product.<sup>72</sup> From enone **456**, which was prepared in four

steps from commercially available materials, an intramolecular Michael addition followed by Robinson annulation was thoroughly investigated and optimized. Ultimately, spiropyrrolidine catalyst **C4** with triisopropylbenzoic acid as an additive proved to be most effective in delivering tricycle **458** in 66% yield with 94% ee (Scheme 4.45). This key transformation performed well on up to a 5-gram scale to rapidly build stereochemical complexity toward the morphine scaffold.

**Scheme 4.44** Smith's total synthesis of morphine **423**.



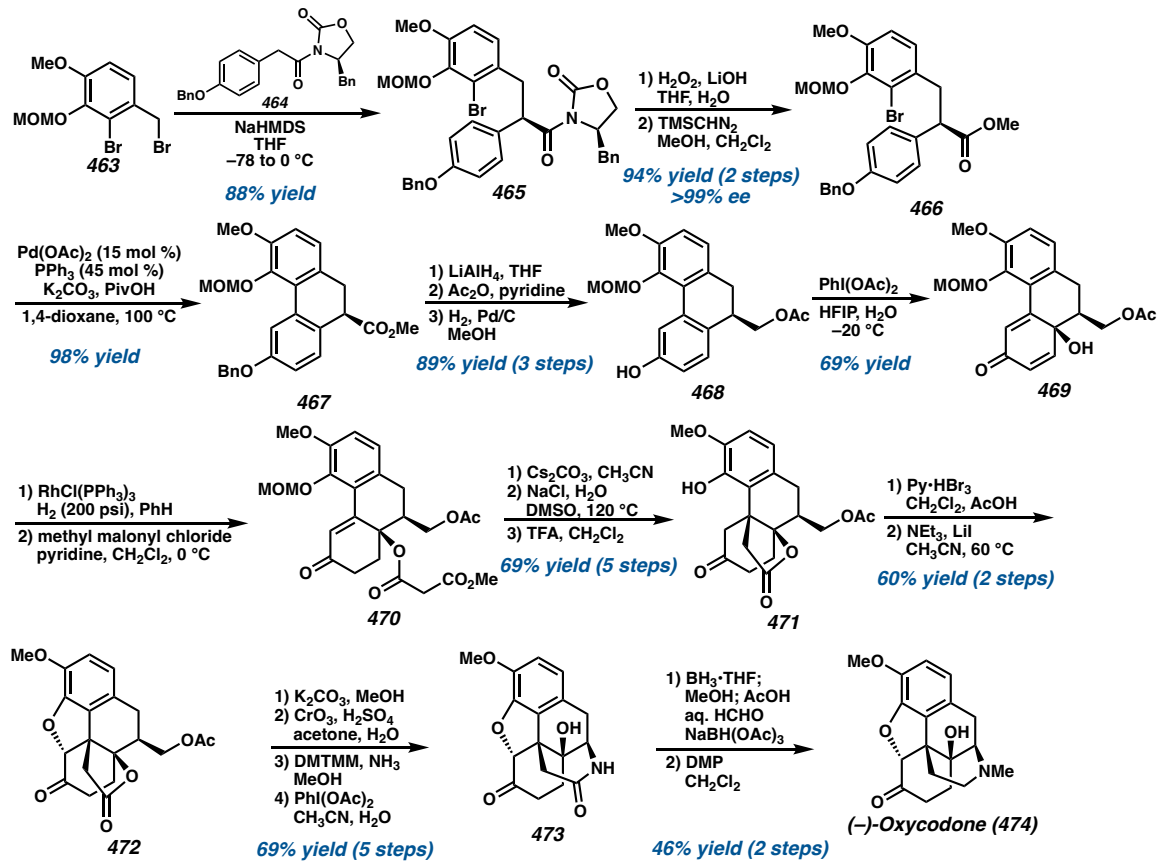
With large amounts of **458** in hand, prenylation followed by ozonolysis and treatment with a catalytic amount of polyphosphoric acid induced a Friedel–Crafts cyclization to afford tetracycle **460**. After selective epoxidation and Wharton reaction to achieve allylic alcohol **461**, cleavage of the benzyl group and an intermolecular Mitsunobu reaction delivers amine **462**. Inversion of the allylic alcohol stereocenter and deprotection of the tosyl group promoted the hydroamination reaction to access (–)-codeine **430**, and subsequent demethylation to synthesize (–)-morphine **423**.

**Scheme 4.45** Tu's total synthesis of (-)-morphine **423**.

Toward the synthesis of other related morphine alkaloids, Fukuyama and coworkers disclosed the synthesis of oxycodone **474**, which is distinguished from morphine by the ketone and additional hydroxyl functionality.<sup>73</sup> Their synthetic approach commenced with alkylation of arene **463** with the enolate derived from imide **464** to furnish **465** as a single diastereomer (Scheme 4.46). Removal of the chiral auxiliary and subsequent methylation of the acid delivered **466** to set up for the direct arylation. Thus, treatment of **466** with Pd(OAc)<sub>2</sub> resulted in arylation to establish the tricycle, which upon reduction of the ester, acetylation, and debenzoylation gave phenol **468**. Next, a key oxidative dearomatization was attempted to install the hydroxyl group. Reaction of **468** with PhI(OAc)<sub>2</sub> afforded the desired intermediate **469** in 69% yield, followed by selective hydrogenation and acylation to deliver enone **470**. Upon treatment with Cs<sub>2</sub>CO<sub>3</sub>, an intramolecular Michael addition proceeded to deliver the desired lactone **471** after two additional manipulations. Selective  $\alpha$ -bromination of the ketone allowed the formation of the benzofuran moiety **472** by displacement with the phenol.

Functionalization of the acetate to the amide set up for a Hofmann rearrangement, followed by hydrolysis of the resulting isocyanate to the primary amine, and amidation to form the desired lactam **473**. Finally, reduction of the lactam, *N*-methylation, and oxidation of the secondary alcohol furnished (–)-oxycodone **474**.

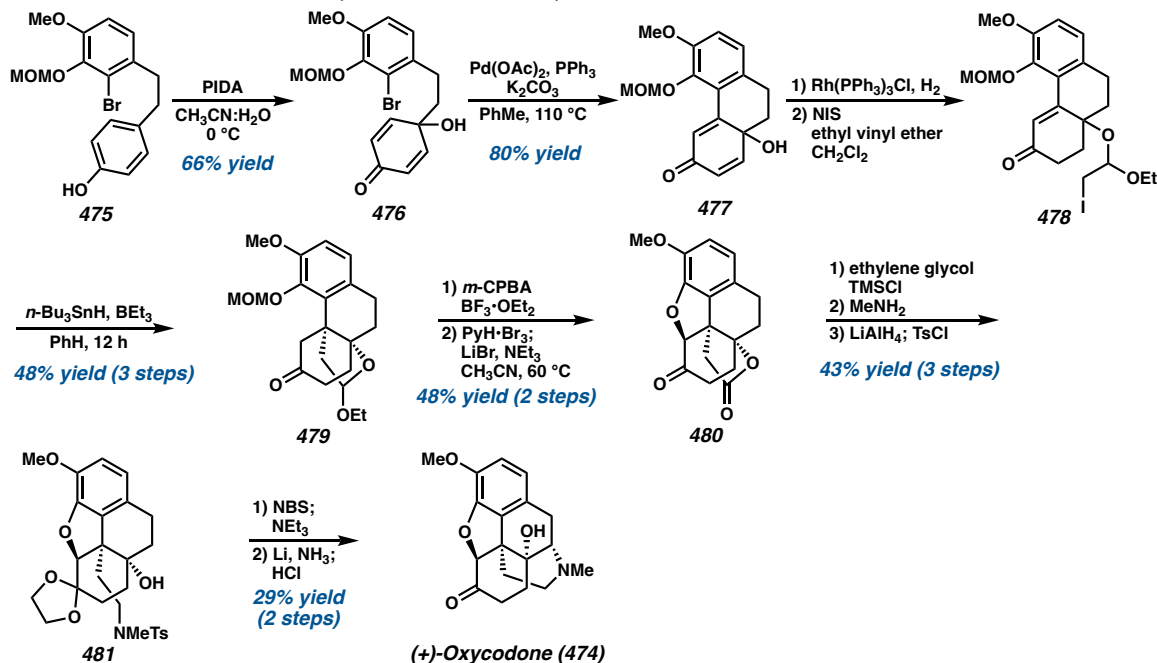
**Scheme 4.46** Fukuyama's total synthesis of (–)-oxycodone **474**.



Other approaches toward the synthesis of oxycodone include a desymmetrization-based strategy reported by Chen and coworkers.<sup>74</sup> To this end, an oxidative dearomatization of phenol **475** under hypervalent iodine conditions afforded hydroxy dienone **476** that could rapidly build tricycle **477** using an intramolecular Heck cyclization (Scheme 4.47). Installation of the all-carbon quaternary stereocenters was accomplished through a radical cyclization of iodoacetal **478** to deliver lactol **479**, which could then be further oxidized to

deliver morphinan scaffold **480**. Protection of the ketone followed by amidation and reduction led to the formation of amine **481**, which furnished oxycodone **474** after desaturation and deprotection steps. This developed sequence demonstrated a shorter step-count in comparison to the original Fukuyama synthesis.

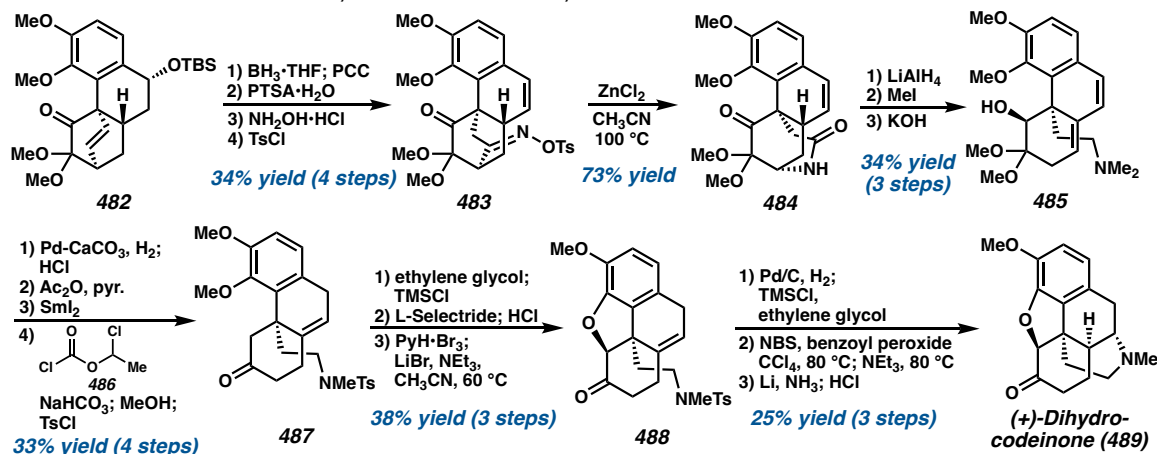
**Scheme 4.47** Chen's total synthesis of (+)-oxycodone **474**.



Chen and coworkers' alternative synthetic approach to the morphinan family of natural products was developed from their method of oxidative dearomatization of atropisomerically pure biaryl phenols to achieve complex intramolecular Diels–Alder products such as **482**.<sup>75</sup> To demonstrate the synthetic utility of these intermediates, **482** was elaborated into lactam **484** via Beckmann rearrangement of oxime **483** (Scheme 4.48). Reduction of the amide followed by Hoffmann elimination induced further cleavage of the bridgehead C–N bond to furnish amine **485**. Selective reduction, deoxygenation, and demethylation were sequentially performed to deliver key intermediate **487**. Then, phenolic demethylation followed by treatment with pyridinium tribromide established the

dihydrobenzofuran ring **488**, with subsequent olefin isomerization and detosylation to synthesize dihydrocodeinone **489**. **489** serves as a valuable intermediate to access a variety of morphinan alkaloids including codeine, morphine, thebaine, and oxycodone.

**Scheme 4.48** Chen's total synthesis of (+)-dihydrocodeinone **489**.

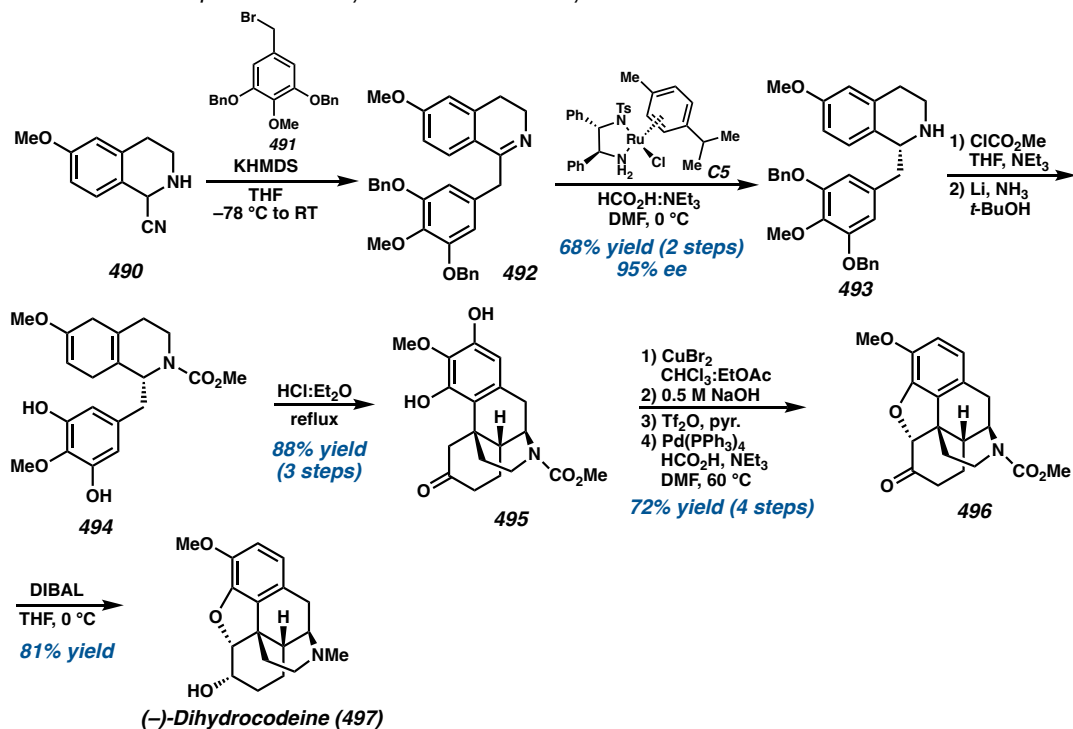


In 2014, Opatz and coworkers have also disclosed a general strategy toward the enantioselective synthesis of (–)-dihydrocodeine **497** and other related morphinan alkaloids (Scheme 4.49).<sup>76</sup> Their key intermediate is prepared from aminonitrile **490**, which upon deprotonation with KHMDS furnished a stabilized  $\alpha$ -aminocarbanion which was alkylated with benzyl bromide **491** to deliver **492** upon spontaneous dehydrocyanation. Enantioselective reduction of **492** using Noyori's asymmetric hydrogenation catalyst **C5** delivered THIQ **493** with 95% ee. With the C1 stereocenter established, the secondary amine was protected, followed by Birch reduction furnishing carbamate **494** which was immediately set up for a Grewe cyclization to establish two new stereogenic centers of the tetracycle **495**.  $\alpha$ -bromination and treatment with NaOH closed the dihydrobenzofuran ring, with subsequent triflation and Pd-catalyzed detriflation furnishing **496** in 80% yield. Treatment with DIBAL ultimately reduced both the ketone and carbamate, accessing



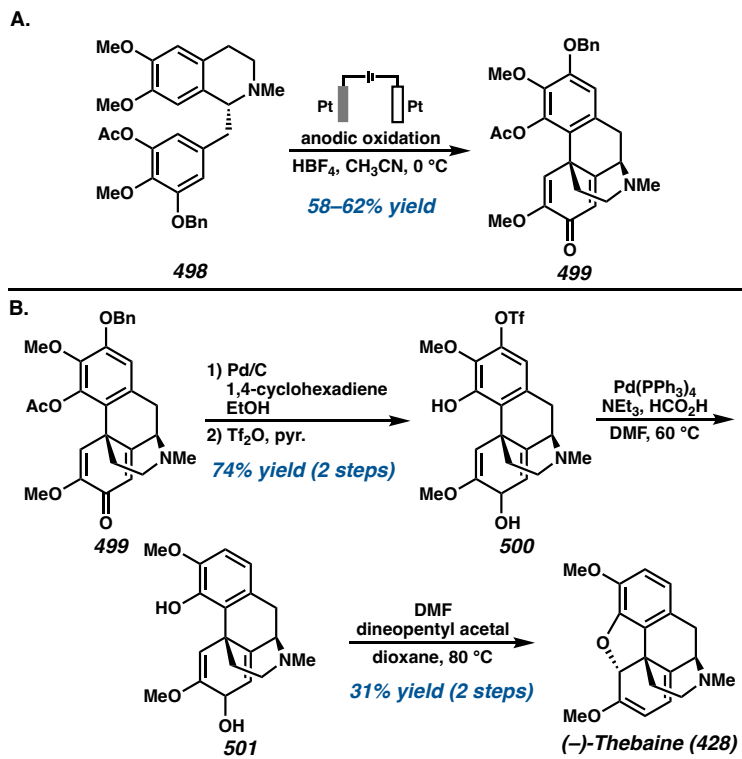
dihydrocodeine **497** in 81% yield. Intermediate **497** also constitutes the formal synthesis of thebaine **428**, while **496** served as a precursor for the synthesis of codeine and morphine.

**Scheme 4.49** Opatz's total synthesis of (–)-dihydrocodeine **497**.



This synthetic strategy toward the morphinan alkaloids as well as their biosynthesis also further inspired the development of an electrochemical oxidative coupling of benzyl THIQs.<sup>77</sup> Toward the synthesis of thebaine **428**, Opatz and coworkers optimized an electrochemical oxidative coupling of THIQ **498** using Pt electrodes in an undivided cell, achieving tetracycle **499** regio- and diastereoselectively (Scheme 4.50A). With this developed methodology, they demonstrated the synthesis of both racemic and (–)-thebaine **428** through several functional group manipulations and a biomimetic  $\text{S}_{\text{N}}2'$ , involving activation of the allylic alcohol **501** with *N,N*-dimethylformamide dineopentyl acetal to close the dihydrobenzofuran ring (Scheme 4.50B). This electrochemical coupling strategy has also been applied toward the total synthesis of (–)-oxycodone **474** from tetracycle **499**.<sup>77b</sup>

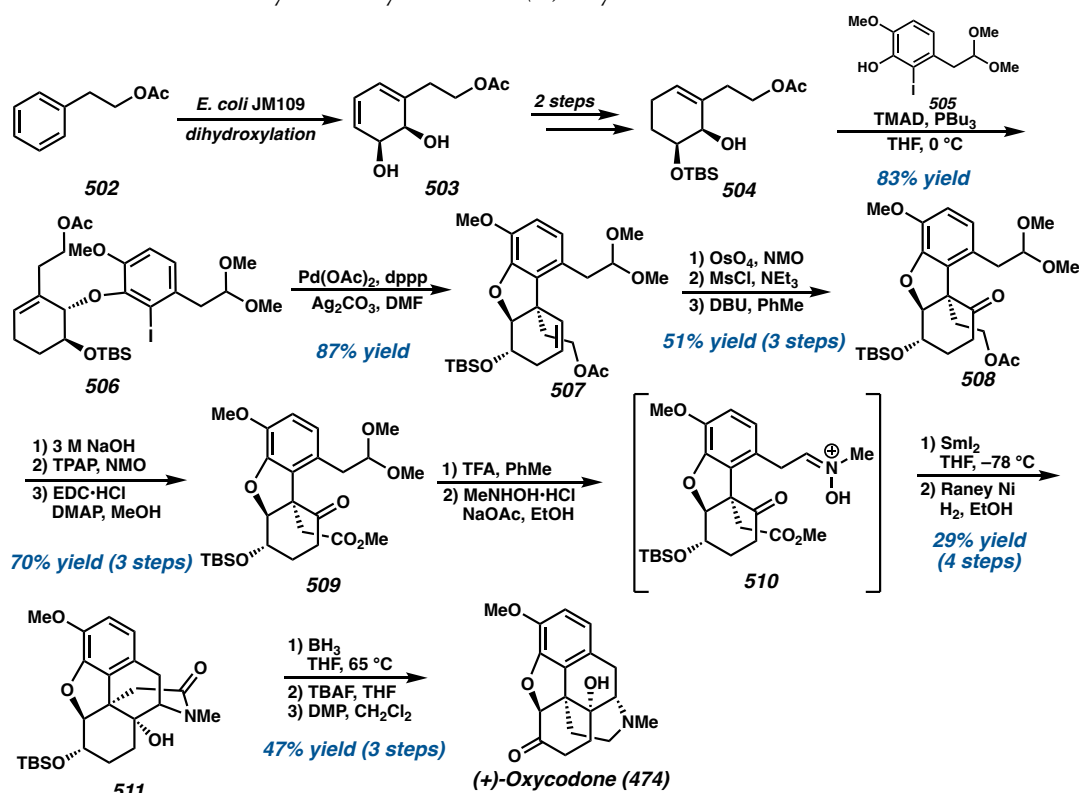
**Scheme 4.50** A. Opatz's electrochemical oxidative coupling. B. Application toward the total synthesis of (–)-thebaine **428**.



The synthesis of the morphinan alkaloids, and in particular oxycodone, has been extensively explored by Hudlicky and coworkers for more than 25 years. Several generations of the chemoenzymatic synthesis of *ent*-oxycodone have been reported, featuring a key Heck cyclization to achieve the dihydrobenzofuran ring and ultimately a keto-nitrone coupling to establish the natural product scaffold.<sup>78</sup> The final synthetic route began with the enzymatic dihydroxylation of phenethyl acetate by whole-cell fermentation with *E. coli* JM109 (pDTG601A) to produce *cis*-diol **503**, which was subsequently reduced and protected as a silyl ether to deliver **504** (Scheme 4.51). A Mitsunobu coupling of the allylic alcohol with phenol **505** then afforded intermediate **506**, which upon an intramolecular Heck reaction constructed the dihydrobenzofuran ring **507**. Dihydroxylation of the olefin followed by DBU-mediated elimination via formation of an intermediate lactol furnished ketone **508** in

63% yield. Oxidative manipulations to transform the acetate to a methyl ester delivered intermediate **509**, then deprotection of the acetal afforded an aldehyde intermediate, which was treated with *N*-methyl hydroxylamine to provide nitrone **510**. Treatment with  $\text{SmI}_2$  then induced cyclization to the lactone with the desired stereochemistry, which upon Raney nickel reduction furnished lactam **511**. Finally, further reduction of the amide carbonyl and oxidation of the alcohol delivered *ent*-oxycodone **474**. Overall, the fourth-generation synthesis of oxycodone was accomplished in 11 steps from phenethyl acetate via a key nitrone intermediate to achieve the correct stereochemistry.

**Scheme 4.51** Hudlicky's total synthesis of (+)-oxycodone **474**.



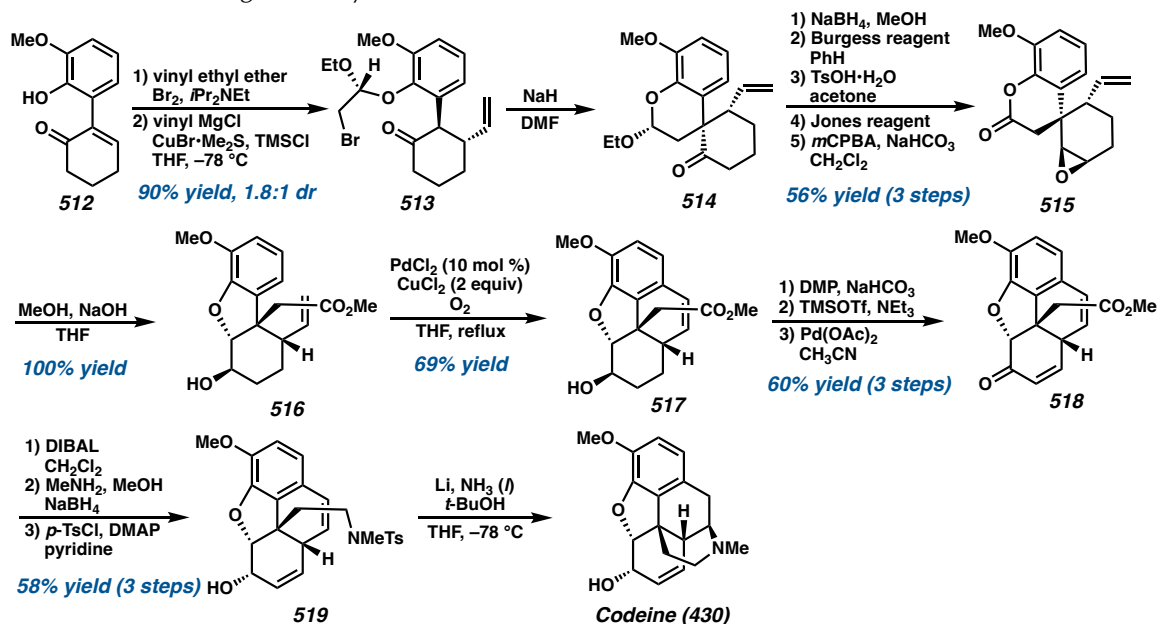
More recent synthetic approaches to the morphinan alkaloids harness C–H activation strategies to efficiently establish the natural product scaffold. For instance, Zhang and coworkers report the total synthesis of codeine and morphine featuring a cascade cyclization

to construct the dihydrofuran ring, and an intramolecular Pd-catalyzed C–H olefination of an unactivated alkene to install the morphinan skeleton (Scheme 4.52).<sup>79</sup> Starting from phenol **512** which was quickly accessed by a Suzuki coupling, treatment with ethyl vinyl ether followed by Michael addition with vinyl magnesium bromide in the presence of copper(I) bromide delivered ketone **513** in 1.8:1 dr relative to the ketal center. The undesired diastereomer could be converted to **513** upon treatment with 2N HCl. Treatment of **513** with NaH afforded spiro-ketone **514** as a single diastereomer, with subsequent manipulations of the ketone to give epoxide **515**. Then, the key cascade cyclization was accomplished using MeOH in the presence of NaOH by opening the lactone ring and attacking the epoxide to deliver **516**. Next, an intramolecular Pd-catalyzed C–H alkenylation was performed to deliver **517** in high regioselectivity. With the tetracycle established, **517** was eventually converted to the natural product using oxidative manipulations to achieve enone **518**, DIBAL reduction and reductive amination to furnish amine **519**, and a radical cyclization to synthesize codeine **430**.

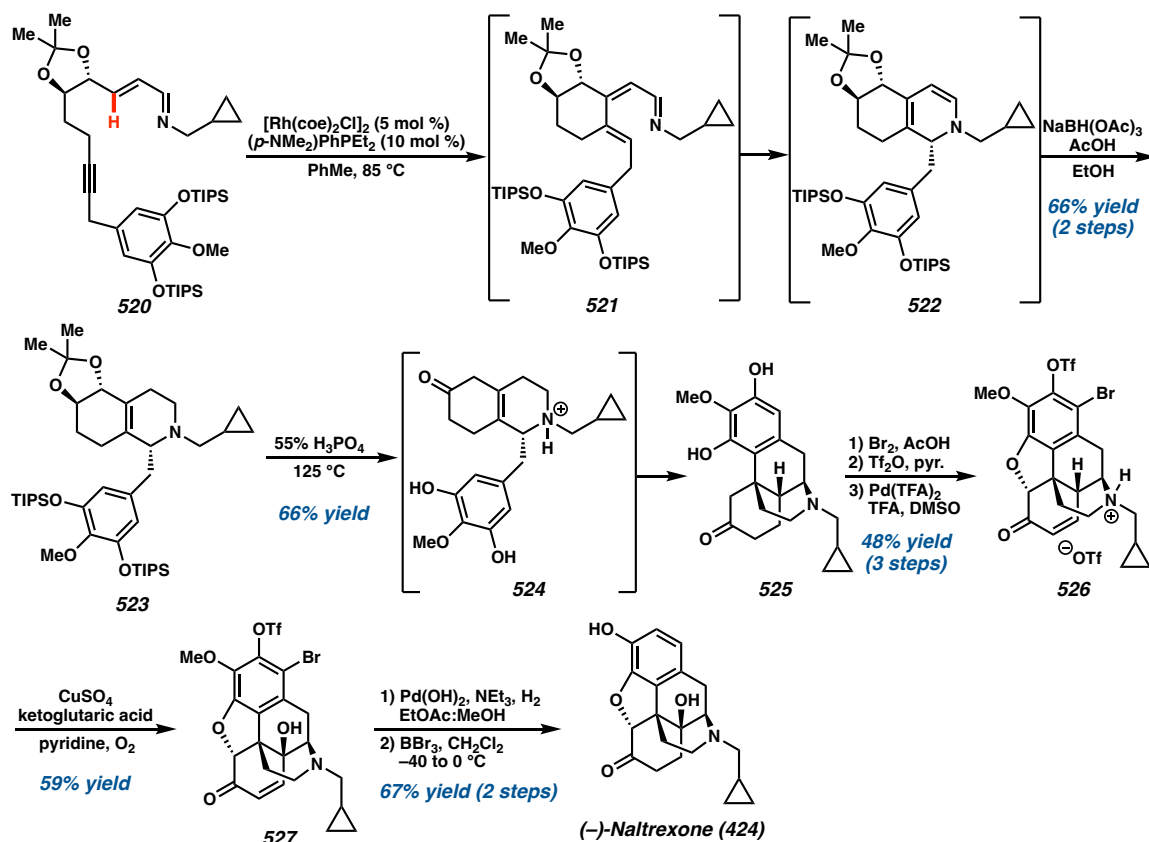
Ellman and coworkers alternatively devised a Rh-catalyzed C–H alkenylation and electrocyclization cascade strategy to synthesize the THIQ framework toward the total synthesis of (–)-naltrexone **424** (Scheme 4.53).<sup>80</sup> From imine **520**, which was prepared in 8 steps from commercial starting materials, a Rh(I)-catalyzed C–H activation of the olefin was initiated, followed by alkyne insertion to deliver an azatriene intermediate **521**. Triene **521** undergoes rapid electrocyclization in situ to access dihydropyridine **522**, which was subsequently reduced to deliver THIQ **523**. Treatment of **523** with dilute H<sub>3</sub>PO<sub>4</sub> then afforded morphinan scaffold **525** in 66% yield. They propose that this transformation likely proceeded through removal of the silyl and acetonide protecting groups, followed by allylic alcohol

ionization and hydride shift to provide ketone **525**. A Grewe cyclization then established the desired morphinan skeleton. Treatment of **525** with Br<sub>2</sub> then afforded a dibrominated intermediate due to facile bromination of the electron-rich aromatic ring, followed by nucleophilic displacement to establish the dihydrofuran ring. Triflation of the phenol followed by dehydrogenation of the ketone using Pd(TFA)<sub>2</sub> installed enone **526**. Finally, a late-stage C–H hydroxylation of enone **526** was explored to access the natural product. Using pyridine as solvent and ketoglutaric acid to reduce the peroxide intermediate, treatment of **526** with CuSO<sub>4</sub> and O<sub>2</sub> successfully installed the hydroxyl group with the correct stereochemistry to yield **527**. Removing the bromide and triflate groups, reduction of the enone, and demethylation with BBr<sub>3</sub> ultimately afforded (–)-naltrexone **424**.

**Scheme 4.52** Zhang's total synthesis of codeine **430**.



In 2020, Metz and coworkers described the total synthesis of thebainone A **536**, harnessing an intramolecular nitron cycloaddition and a Heck cyclization to construct the natural product scaffold (Scheme 4.54).<sup>81</sup>

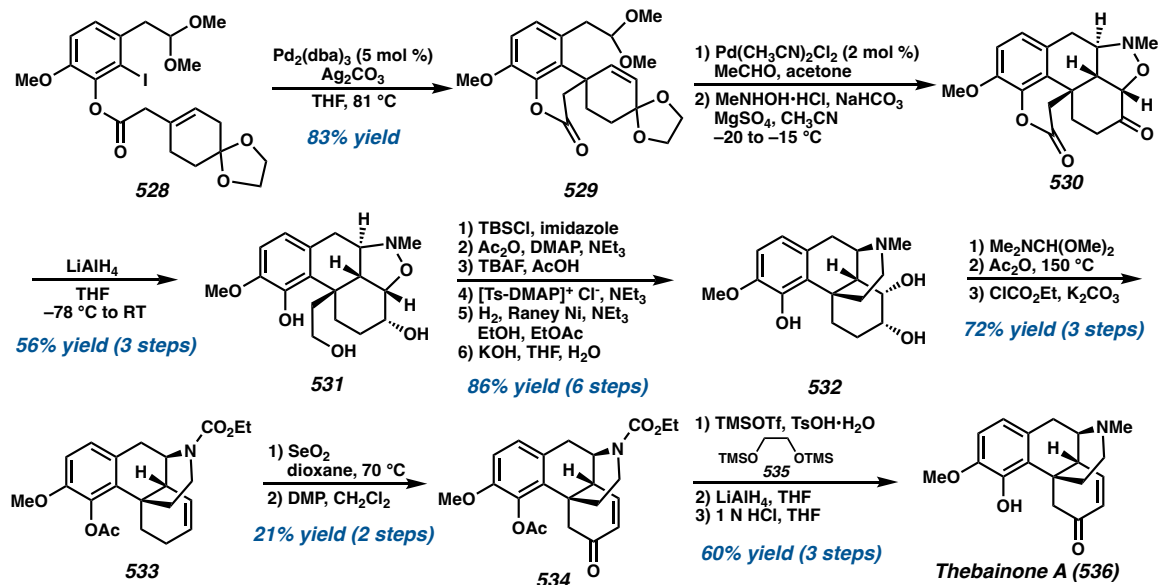
**Scheme 4.53** Ellman's total synthesis of (-)-naltrexone **424**.

From ester **528** which was accessed in 4 steps from isovanillin, a Heck cyclization using  $\text{Pd}_2(\text{dba})_3$  and  $\text{Ag}_2\text{CO}_3$  induced formation of spiro-lactone **529** in 83% yield. Deprotection of the ketone and aldehyde followed by treatment with *N*-methylhydroxylamine induced a diastereoselective nitron cycloaddition to achieve isoxazolidine **530**. Since this ketolactone was rather unstable, subsequent reduction with  $\text{LiAlH}_4$  delivered **531**, and conversion of the primary alcohol to a tosylate was then followed by reductive cleavage of the heterocycle with concomitant nucleophilic substitution to generate **532**. To install the enone moiety, the *cis* diol was reductively eliminated by formamide acetal pyrolysis, with subsequent acetylation and ethyl carbamate formation to give **533**. Allylic oxidation followed by DMP oxidation then successfully installed the enone

**534** in 21% yield over two steps. Finally, protection of the ketone was required to reduce the carbamate and acetate group, and deprotection with 1N HCl ultimately provided thebainone

A **536**.

**Scheme 4.54** Metz's total synthesis of thebainone A **536**.



#### 4.4.5. PAVINE AND ISOPAVINE ALKALOIDS

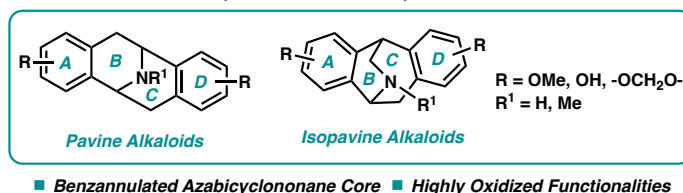
##### 4.4.5.1. GENERAL STRUCTURE AND BIOSYNTHESIS

The pavine and isopavine alkaloids contain a characteristic tetracyclic tetrahydroisoquinoline core structure consisting of a dibenzo-9-azabicyclo[3.3.1]nonane and dibenzo-9-azabicyclo[3.2.2]nonane, respectively (Figure 4.17).<sup>82</sup> They are mainly found in four plant families, the Papaveraceae, Berberidaceae, Lauraceae, and Ranunculaceae families. These alkaloids have been shown to possess interesting bioactivity for the treatment of nerve system disorders such as Alzheimer's, Parkinson's disease, and Huntington's chorea.<sup>83</sup>

Although the complete biosynthesis of the pavine and isopavine alkaloids has not been entirely elucidated, there are some speculations of their biogenetic precursors. It is

likely that they are derived from benzyl THIQ reticuline **247** or a similar analog thereof, which undergoes cyclization at either the C3 or C4 position of the THIQ ring to achieve the pavine or isopavine scaffold, respectively.<sup>84</sup> For the isopavine alkaloids, a 4-hydroxybenzyl THIQ is postulated as a precursor that could undergo dehydration and cyclization to achieve the azabicyclo[3.2.2]nonane core.<sup>85</sup> Alternatively, it has been suggested that pavine alkaloids are derived from a similar intermediate such as 4-hydroxynorlaudanosoline, from which a dehydration reaction and cyclization at the C3 position would yield the pavine skeleton.<sup>84</sup> More recently, Ng and coworkers elucidated the structure of an *N*-methyltransferase enzyme (pavine NMT) that is involved in the *N*-methylation of the pavine alkaloids.<sup>86</sup>

**Figure 4.17** General structure of the pavine and isopavine THIQ alkaloids.



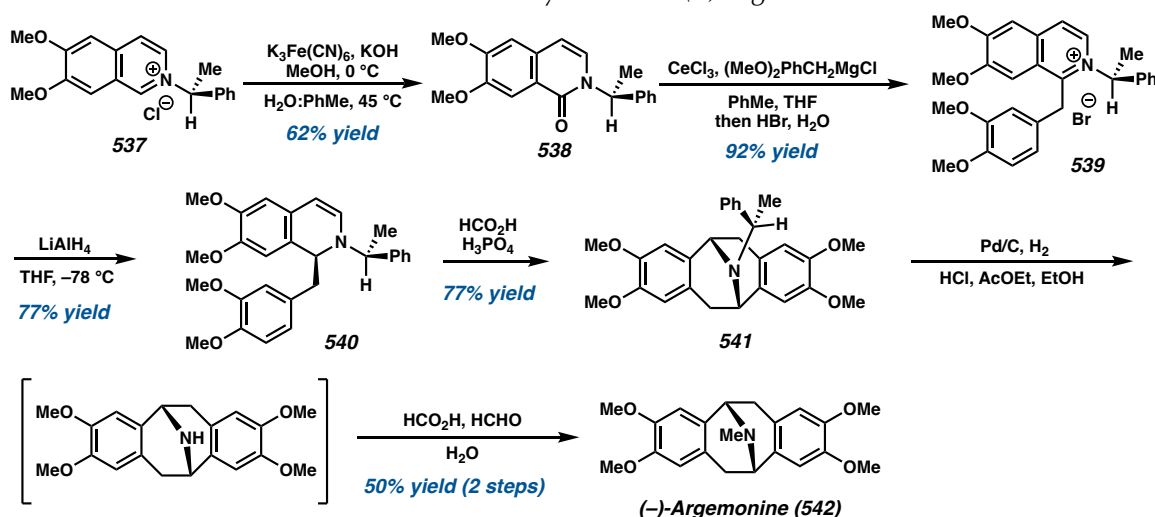
#### 4.4.5.2. TOTAL SYNTHESIS OF PAVINE AND ISOPAVINE ALKALOIDS

In 2004, Marazano reported the synthesis of (–)-argemonine **542**, enabled by a key enantioselective transformation of isoquinolinium salt **537** to 1-benzyl isoquinoline derivative **539** (Scheme 4.55).<sup>87</sup> Isoquinolinium salt **539** was prepared in two steps from salt **537**, and reduction of **539** with LiAlH<sub>4</sub> formed tertiary amine **540**. Cyclization of **540** in the presence of formic acid and H<sub>3</sub>PO<sub>4</sub> supplied benzylamine **541** with 93:7 dr. Hydrogenolysis with Pd/C (10 mol %) and H<sub>2</sub> cleaved the chiral auxiliary, which was dissolved in formic acid and aqueous formaldehyde to furnish the methylated natural product (–)-argemonine **542**.

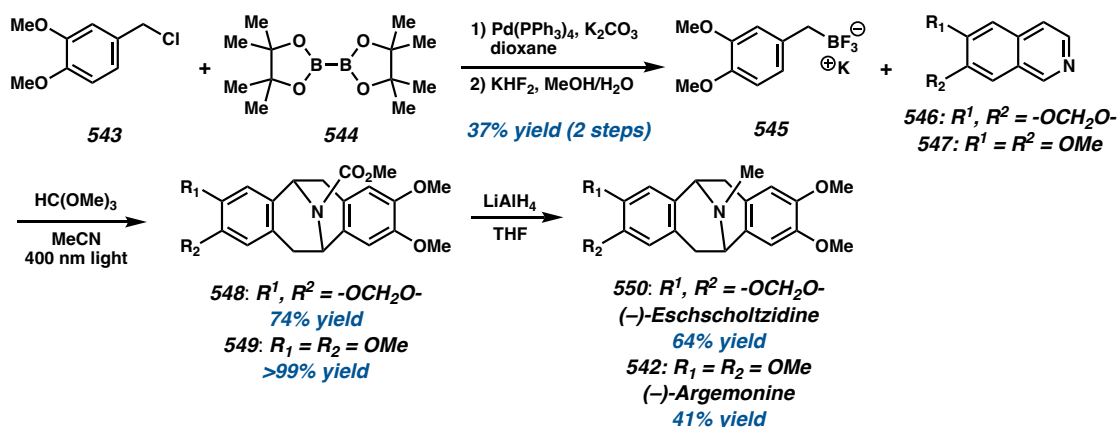


Nishigaichi and coworkers also developed a modular synthesis of argemonine **363** and eschscholtzidine **371** from the coupling of isoquinolines and electron-rich potassium trifluoroborate reagents (Scheme 4.56).<sup>88</sup> After synthesizing potassium trifluoroborate reagent **366** from benzyl chloride **364**, treatment of **366** with isoquinolines **367–368** under thermal or photochemical conditions followed by reduction with LiAlH<sub>4</sub> resulted in the concise syntheses of argemonine **363** and eschscholtzidine **371**.

**Scheme 4.55** Marazano's enantioselective synthesis of (–)-argemonine **542**.



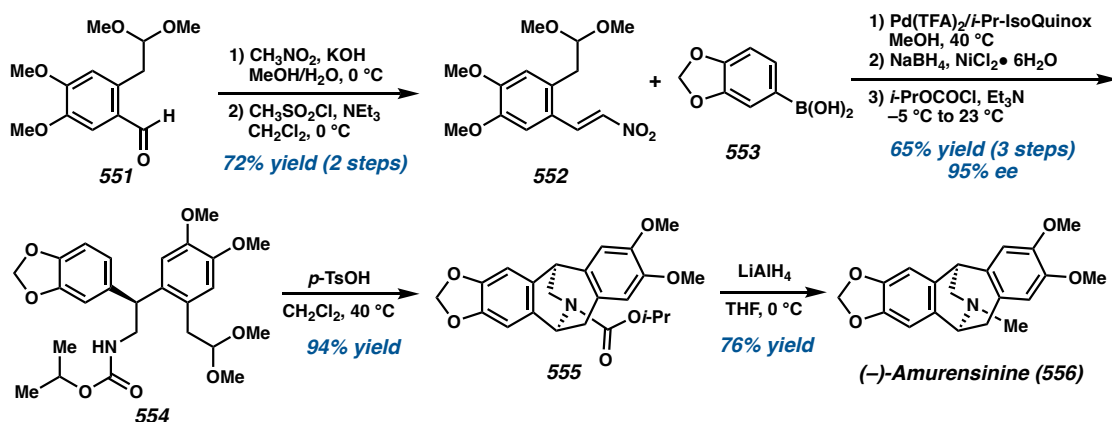
**Scheme 4.56** Nishigaichi's synthesis of argemonine **542** and eschscholtzidine **550**.



Jiang and coworkers reported a general approach to access isopavines, including (–)-amurenisine, (–)-reframidine, (–)-reframine, and other non-natural isopavine

derivatives within five or six steps with >95% ee.<sup>89</sup> Their retrosynthetic strategy began with the formation of bridging C–N and C–C bonds through Pictet–Spengler reaction of an amino dimethyl acetal **554** (Scheme 4.57). From aldehyde **551**, a Henry reaction with nitromethane, followed by dehydration with methanesulfonyl chloride and excess trimethylamine delivered  $\beta$ -nitrostyrene **552**. A Pd-catalyzed asymmetric addition of **552** with aryl boronic acid **553**, followed by reduction and conversion to the carbamate yielded **554**. The Pictet–Spengler reaction of carbamate **554**, followed by reduction of carbamate **555** formed (–)-amurensinine **556**.

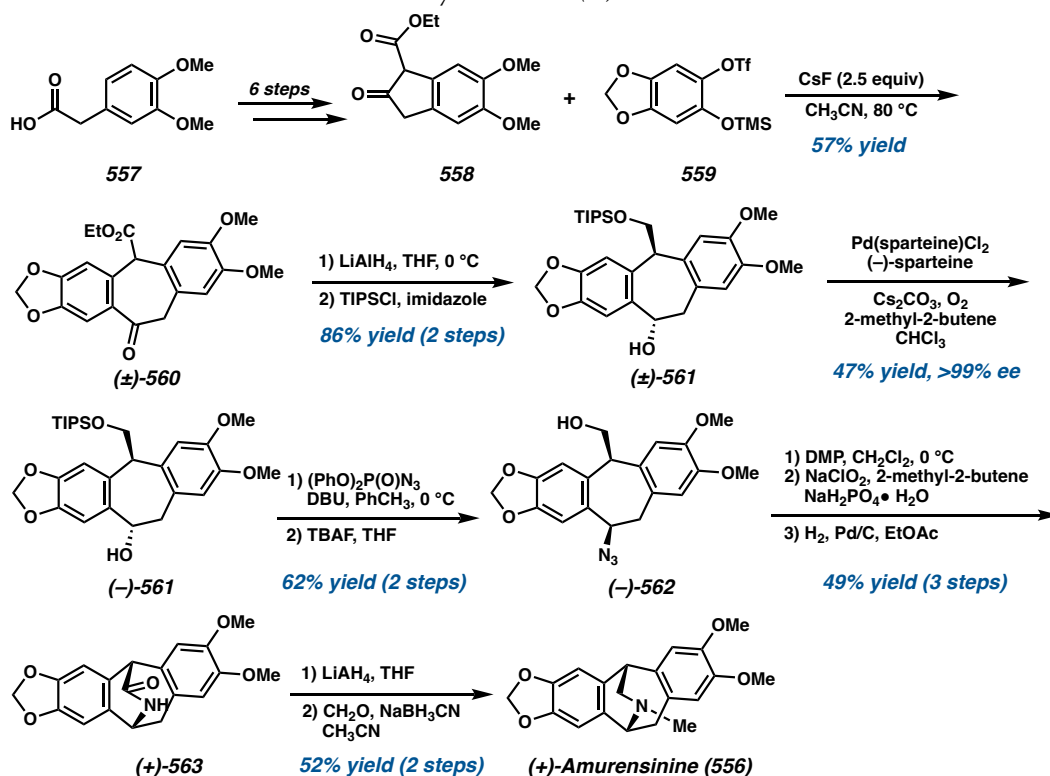
**Scheme 4.57** Jiang's enantioselective synthesis of (–)-amurensinine **556**.



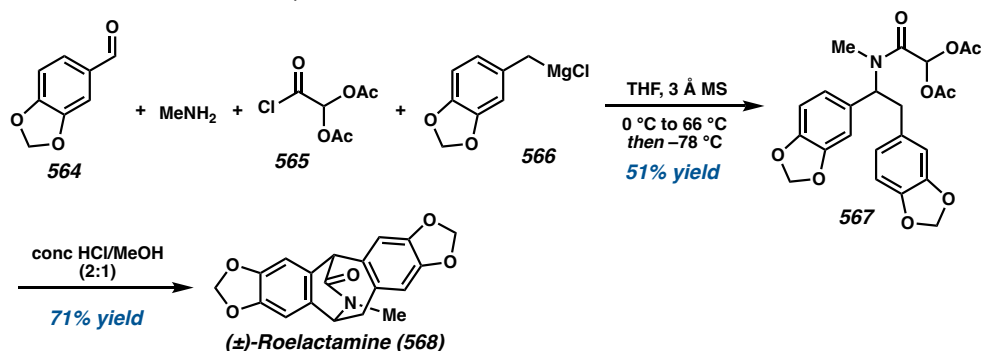
In 2006, Stoltz and coworkers reported the enantioselective total synthesis of amurensinine **556**.<sup>90</sup> They envisioned to apply their developed Pd-catalyzed oxidative kinetic resolution methodology to rapidly access the isopavine core in a modular fashion (Scheme 4.58).<sup>90b</sup> To this end, (3,4-dimethoxyphenyl)acetic acid **557** was treated to form a diazoester compound, then subjected to a  $\text{Rh}_2(\text{OAc})_4$ -catalyzed C–H insertion to produce  $\beta$ -ketoester **558** in 91% yield over 6 steps. Coupling of  $\beta$ -ketoester **558** and aryne precursor **559** in the presence of  $\text{CsF}$  afforded a net C–C insertion to form the central carbocyclic ring of ketoester **560**. Diastereoselective reduction of ketoester **560** and protection of the primary alcohol

provided **561**. Oxidative kinetic resolution using Pd(sparteine)Cl<sub>2</sub> and (–)-sparteine as the chiral ligand provided enantioenriched (–)-**561** with 99% ee. Conversion of the alcohol to the azide with inversion using (PhO)<sub>2</sub>P(O)N<sub>3</sub> (DPPA) produced azido alcohol (–)-**562** with no loss of optical purity. After oxidation of the alcohol, reduction of the azide delivered the desired lactam (+)-**563**. Reductive methylation produced (+)-amurensinine **556** with 99% ee.

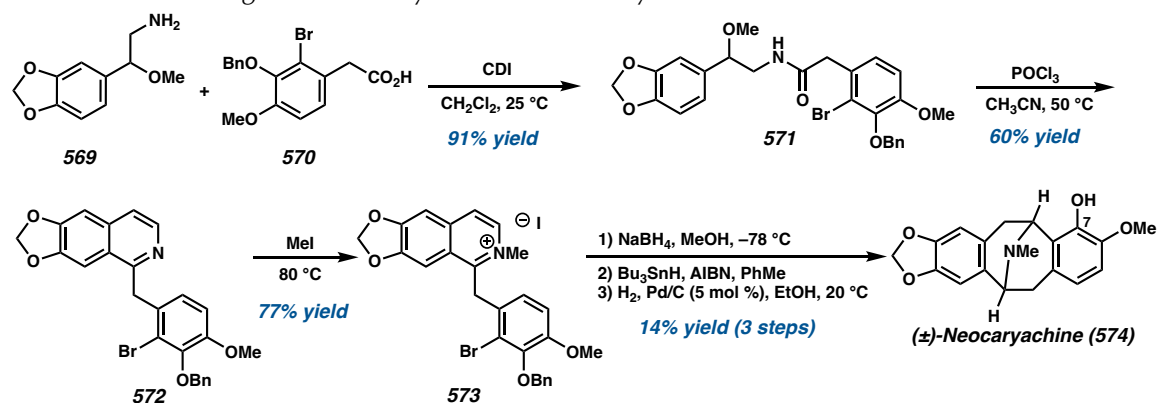
**Scheme 4.58** Stoltz's enantioselective synthesis of (+)-amurensinine **556**.



In 2007, Martin utilized a four-component reaction to rapidly access roelactamine **568** in a racemic fashion from piperonal **564**.<sup>91</sup> The condensation of piperonal with methylamine provided an imine in situ that was then reacted sequentially with benzyl Grignard **566** and acid chloride **565** to furnish amide **567** (Scheme 4.59). Treatment of **567** with a concentrated 2:1 mixture of HCl:MeOH allowed the amide to undergo sequential cyclizations to produce roelactamine **568**.

**Scheme 4.59** Martin's synthesis of roelactamine **568**.

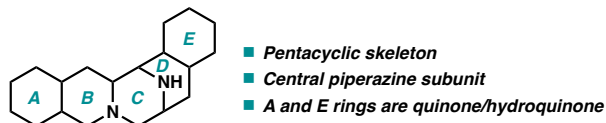
Finally, the first synthesis of a pavine alkaloid with C7 functionalization was reported by Nakagawa-Goto.<sup>92</sup> From amine **569**, which was prepared in three steps, amidation with carboxylic acid **570** using carbonyldiimidazole (CDI) provided amide **571** (Scheme 4.60). A Bischler–Napieralski reaction with  $\text{POCl}_3$  formed benzylisoquinoline **572**. Treatment of **572** with methyl iodide delivered isoquinolinium salt **573**. Subsequent reduction with  $\text{NaBH}_4$  to the enamine, followed by radical cyclization and removal of the benzyl group yielded  $(\pm)$ -neocaryachine **574**.

**Scheme 4.60** Nakagawa-Goto's synthesis of neocaryachine **574**.**4.5. THIQ ALKALOIDS FROM THE SAFRAMYCIN FAMILY**

The saframycin family is the largest subclass of tetrahydroisoquinoline alkaloids, consisting of saframycins, safracins, ranieramycins, and ecteinascidins. The core structure of

natural products in this family features the intricate pentacyclic skeleton, having five six-membered rings condensed into the core scaffold (Figure 4.18). Well known for their potent anticancer/antitumor activities, natural products in this family have been popular targets in numerous synthetic endeavors.

**Figure 4.18** Core skeleton of THIQ alkaloids in the saframycin family.



#### 4.5.1. SAFRAMYCIN ALKALOIDS

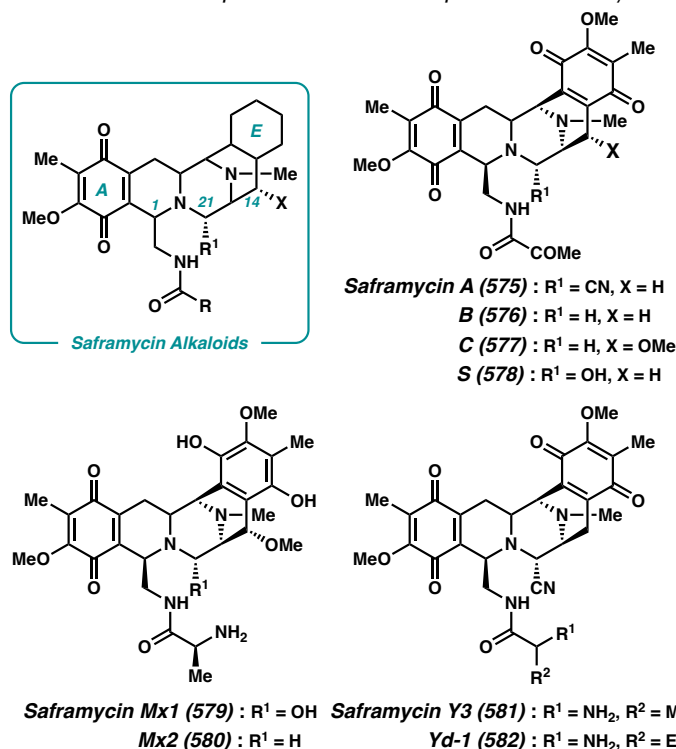
##### 4.5.1.1. GENERAL STRUCTURE AND BIOSYNTHESIS

The very first set of saframycins, namely safrmycins A–E, were isolated in 1977 from bacteria *Streptomyces lavendulae*.<sup>93</sup> In the ensuing studies, four additional saframycins (F, G, H, and R) were isolated from the same species of bacteria,<sup>94</sup> and later in 1988, it was disclosed that myxobacteria *Myxococcus xanthus* strain Mx x48 produced saframycins MX1 and MX2.<sup>95</sup> In addition to the “natural” saframycins, six new saframycins (Y3, Yd-1, Yd-2, Ad-1, Y2b, and Y2b-d) were obtained by a directed biosynthesis through the supplementation of different amino acids.<sup>96</sup>

Among the currently known saframycin alkaloids, the shared structural motif is the amide side chain, which is appended on the B-ring at the C1 position (Figure 4.19). Additionally, the A-ring of all saframycins is in the quinone oxidation state, while the E-ring can be in various oxidation levels, ranging from phenol, hydroquinone, and quinone. The amino nitrile or carbinol amine functionality on the central piperazine subunit functions as a latent electrophilic iminium species, which can alkylate DNA, and is largely responsible for

saframycins' potent antitumor/antimicrobial activity.<sup>97</sup> Saframycins voided of a leaving group at C21 typically exhibit significantly lower biological activities.<sup>93</sup>

**Figure 4.19** General structure and representative examples of saframycin alkaloids.

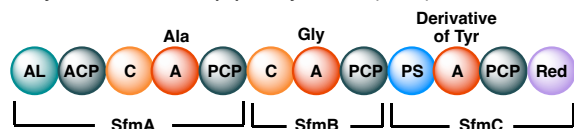


Early biochemical studies of saframycins were conducted via feeding/isotope-labelling experiments, and the results suggest that one alanine, one glycine, and two tyrosine derivatives constitute the backbone of saframycin A.<sup>98</sup> By exploiting the cloned biosynthetic gene cluster and its sequence analysis, it was later proposed that the pentacyclic backbone is assembled by a nonribosomal peptide synthetase (NRPS).<sup>99</sup> Specifically for saframycin A, the NRPS comprises three modules (SfmA, SfmB, and SfmC) in which the first two are responsible for the production of dipeptidyl intermediate **A** from alanine and glycine (Scheme 4.61A). As for the last module, intriguing multi-step transformations catalyzed by SfmC were discovered by Oikawa and coworkers in 2010.<sup>100</sup> The notable domains in this module are a) the Pictet–Spengler reaction domain (PS) which catalyzes two successive

Pictet–Spengler reactions to construct the bis-tetrahydroisoquinoline (bis-THIQ) intermediate, and b) the reduction domain (Red) which reduces the thioester intermediates and releases aldehyde precursors (**B**, **E**, and **F**) for following reactions. Interestingly, they also noted that the relatively less strict substrate specificity of the PS domain might allow for an incorporation of synthetic aldehydes into the core skeleton. Once the pentacycle is constructed, late-stage tailoring modifications, including hydroquinone oxidation, *N*-methylation, and hydrolysis of the fatty acid chain proceed to afford Saframycin A.<sup>101</sup> This thorough understanding of the biosynthetic mechanism serves as a foundation for future developments of a chemoenzymatic total synthesis of saframycin alkaloids and their related analogs (*vide infra*).

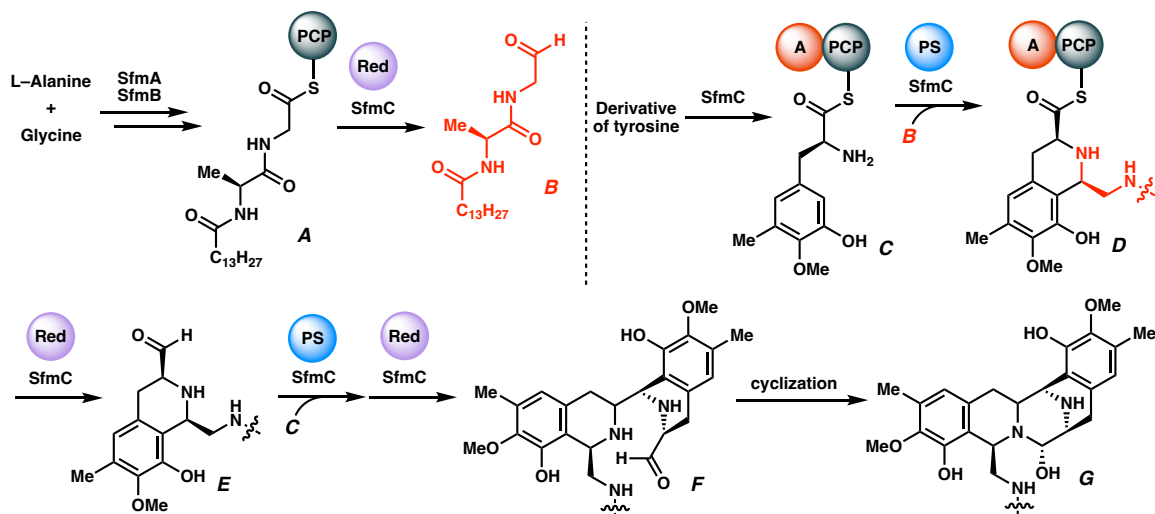
**Scheme 4.61** A. Domain organization of saframycin A NRPS. B. Proposed biosynthetic mechanism for the construction of saframycin A's pentacyclic skeleton.

a) Saframycin A nonribosomal peptide synthetase (NRPS):



AL - acyl-coA ligase, ACP - acyl carrier protein, C - condensation, A - adenylation, PCP - peptidyl carrier protein, PS - Pictet-Spengler, Red - Reduction

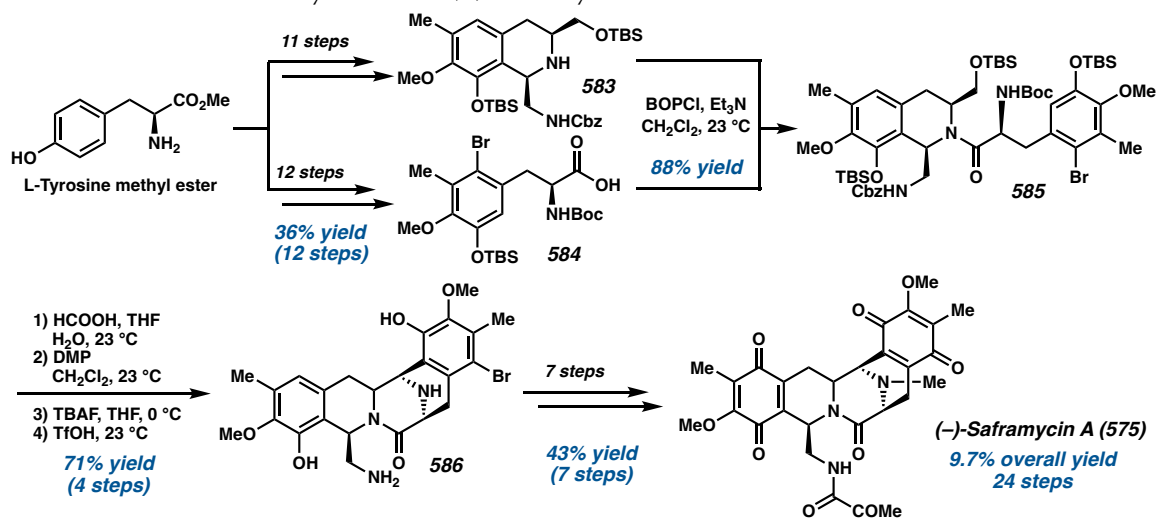
b) Proposed biosynthesis of saframycin A's core



#### 4.5.1.2. TOTAL SYNTHESIS OF SAFRAMYCIN ALKALOIDS

After the publication of a comprehensive review by William in 2002,<sup>3</sup> there have been only three reports detailing the synthesis of saframycin alkaloids, all targeted saframycin A. In 2011, Liu employed L-tyrosine as a chiral building block in the preparation of (–)-saframycin A (Scheme 4.62).<sup>102</sup> They commenced their synthetic studies by converting L-tyrosine methyl ester into the desired amino acid **584** in 12 steps and tetrahydroisoquinoline **583** in 11 steps, which served as the eastern and western portions of the natural product, respectively. Although the regioselectivity issue for mono-hydroxy phenol substrate is a common problem in the Pictet–Spengler cyclization reaction,<sup>103</sup> they noted that the selectivity, in this case, can be controlled by carefully maintaining the reaction temperature at 0 °C with a slow addition of the aldehyde starting material, furnishing THIQ **583** in 86% yield.

**Scheme 4.62** Liu's total synthesis of (–)-saframycin A **575**.



With both halves in hand, they coupled them together to give the amide intermediate **585**. Subsequent functional group manipulations and an intramolecular Pictet–Spengler cyclization with triflic acid (TfOH) afforded pentacycle **586**. It is worth noting here that the

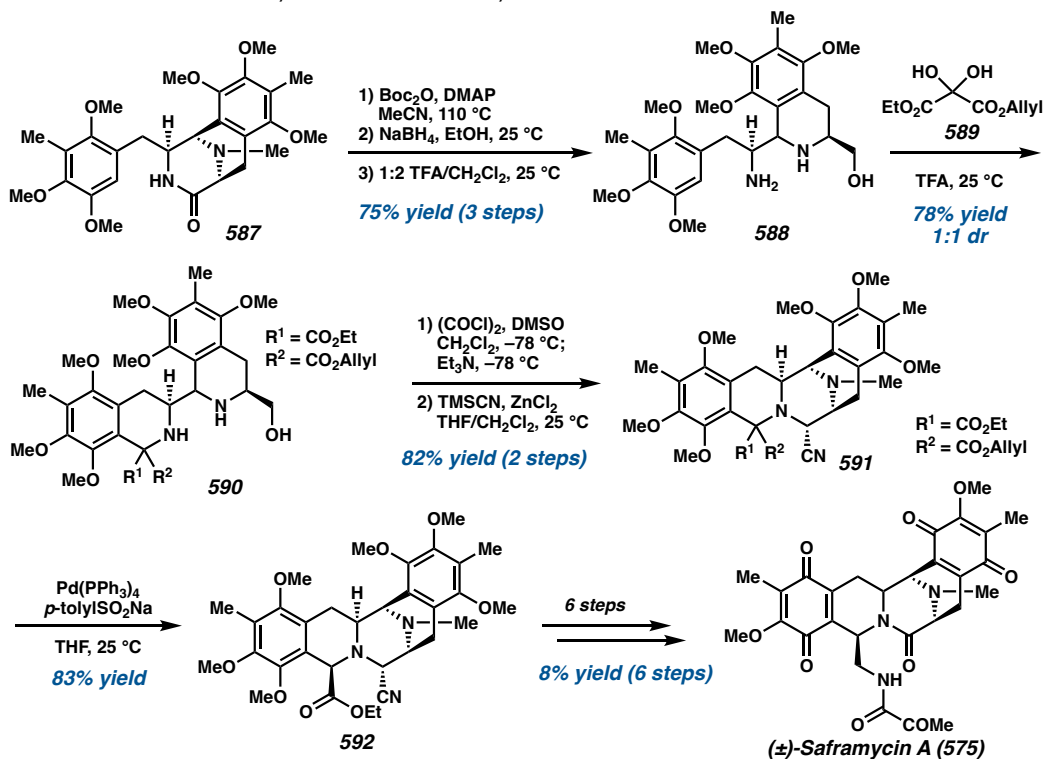


second Pictet–Spengler cyclization requires a bromine atom on the eastern half of the molecule to function as a blocking group and provide the correct regiochemical outcome for the cyclization. They further advanced this intermediate to the targeted natural product via a 7-step peripheral modification, concluding a 24-step total synthesis of (–)-saframycin A **575** in an overall 9.7% yield. Of note, the key synthetic strategy in this report is reminiscent of Corey’s approach to prepare the pentacyclic core of ecteinascidin and phthalascidin where an amide coupling is used to merge the western and eastern halves of the molecule.<sup>104</sup>

In 2018, Saito and coworkers published a racemic synthesis of saframycin A **575** (Scheme 4.63), which is a follow-up study to correct the stereochemistry at the C1 position of the western THIQ.<sup>105</sup> The tricyclic lactam **587**, which was prepared in 14 steps from commercially available material,<sup>106</sup> first underwent reductive cleavage and Boc removal to provide hydroxymethyl isoquinoline **588**. This compound served as a Pictet–Spengler substrate, and cyclization with allyl ethyl oxomalonate ester (**589**) delivered bis-THIQ **590**. From this intermediate, the pentacyclic core **591** was constructed via the Swern oxidation of the primary alcohol to afford the aldehyde, which underwent ring-closure to generate the hemiaminal C-ring. By subjecting TMSCN to the same pot, the amino nitrile formation proceeded to furnish the desired product **591** in 82% yield over 2 steps. They subsequently performed a decarboxylation and stereoselective protonation to correctly install the stereochemistry at the C1 position of the western THIQ (**592**). In the final stage, the ethyl ester in **592** was converted to the pyruvamide through a 4-step sequence, consisting of a)  $\text{LiBH}_4$  reduction, b) Mitsunobu reaction with phthalimide, c) removal of phthalimide to reveal the free amine, and d) acylation of amine with pyruvic acid. Finally, selective

demethylation and ceric ammonium nitrate (CAN) oxidation were performed to deliver (±)-saframycin A **575** in an overall 27 steps for the longest linear sequence.

**Scheme 4.63** Saito's total synthesis of saframycin A **575**.



The most recent total synthesis of saframycin A is a merger of chemical and biosynthesis.<sup>107</sup> Based on the proposed nonribosomal peptide synthetase (NRPS) responsible for the construction of the pentacyclic skeleton (*vide supra*), Oikawa and Oguri specifically designed substrates that successfully participated in the SfmC-catalyzed multistep enzymatic conversion (Scheme 4.61). Once the core skeleton was obtained, they exploited chemical synthesis to further manipulate functional groups, and finally deliver not only saframycin A, but also Jorunnamycin A and N-Fmoc Saframycin Y3. This hybrid strategy is highly efficient and allows for a rapid access to the elaborated pentacyclic scaffolds only in a single day.

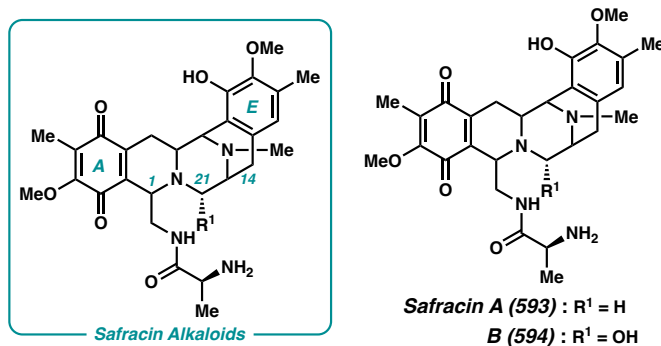
#### 4.5.2. SAFRACIN ALKALOIDS

#### 4.5.2.1. GENERAL STRUCTURE AND BIOSYNTHESIS

Isolated from *Pseudomonas fluorescens*,<sup>108</sup> safracins are structurally similar to the saframycins, except for having a phenol E-ring instead of a quinone/hydroquinone (Figure 4.20). Optimization of the fermentation process of this bacteria resulted in a multikilogram isolation of cyanosafracin B, having a nitrile moiety at the C21 position, which served as an inexpensive precursor to prepare ecteinascidin 743 (Et-743), an anticancer drug.<sup>109</sup>

Biosynthetically, the pentacyclic core of safracins is believed to be assembled from one alanine, one glycine, and two functionalized tyrosine via the nonribosomal peptide synthetase (NRPS), resembling the mechanism reported for the saframycins.<sup>110</sup> In the most recent study, Tang and coworkers essentially established the entire safracin biosynthetic pathway by investigating post-NRPS modifications. These include the A-ring oxidation, *N*-methylation, and removal of the fatty acyl chain.<sup>111</sup>

**Figure 4.20** General structure of safracin alkaloids.



#### 4.5.2.2. TOTAL SYNTHESIS OF SAFRACIN ALKALOIDS

Despite the extensive research in the area of safracin biosyntheses, to the best of our knowledge, there is still no report of a chemical total synthesis of any safracin alkaloid. Since the initial disclosure of efforts toward safracin A by Kubo and coworkers in 1995,<sup>112</sup> not

much progress has been reported. This could perhaps be attributed to the ample quantities of safracins obtained from the isolation process.

### 4.5.3. RENIERAMYCIN ALKALOIDS

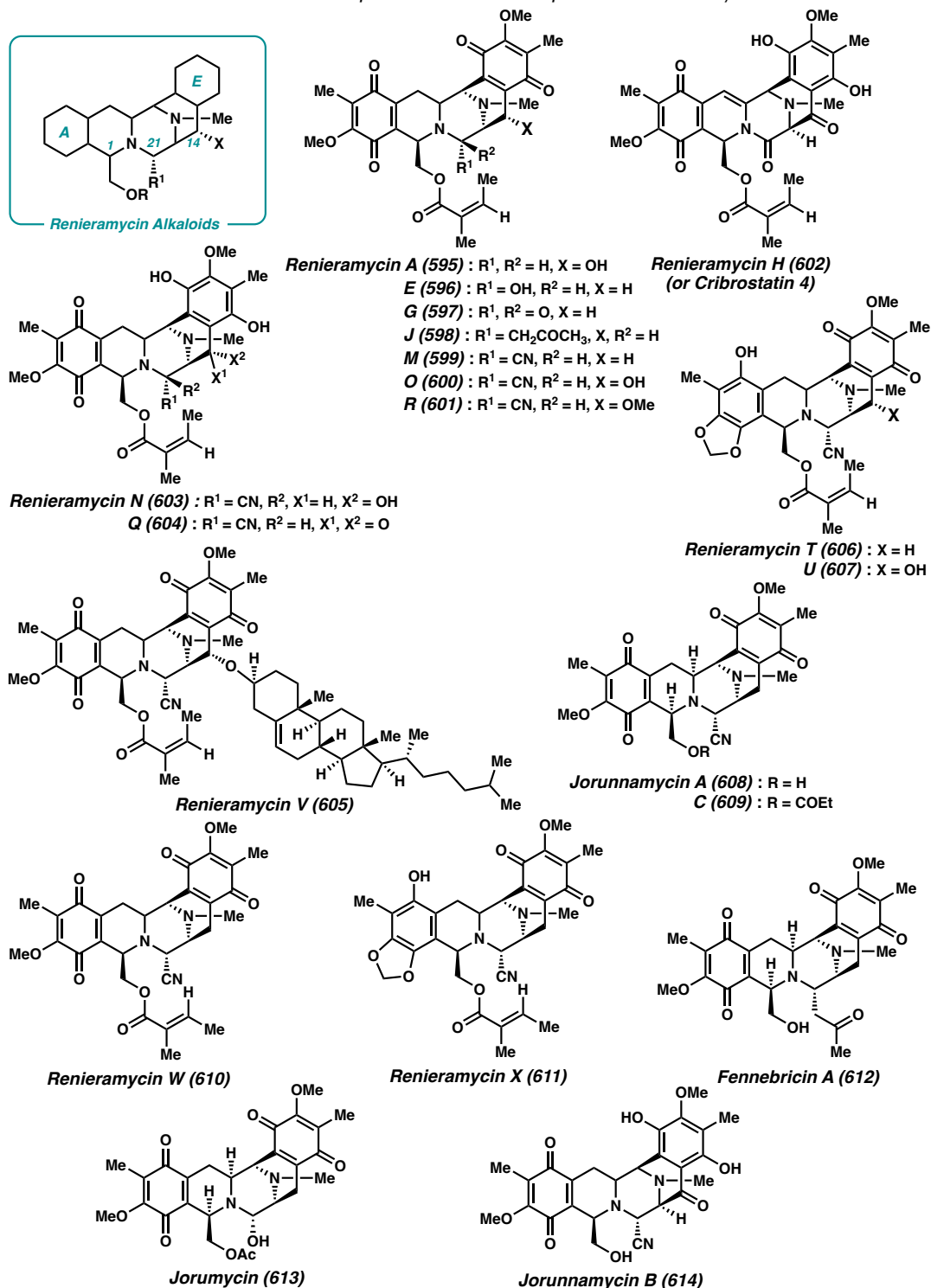
#### 4.5.3.1. GENERAL STRUCTURE AND BIOSYNTHESIS

The general structure of renieramycins is highly similar to that of the saframycin alkaloids. The main difference is at the C1-position, where renieramycins possess an ester or alcohol functionality instead of an amide side chain found in the saframycins (Figure 4.21).

Renieramycin alkaloids are typically isolated from marine organisms, such as different species of blue sponges and nudibranchs, collected in various parts of the world. Before 2002, only the structures of renieramycins A–G, I, cribrostatin 4 (or renieramycin H), and jorumycin were disclosed. However, in the past 20 years, more than 20 new renieramycins were reported.<sup>113</sup> These new compounds are mostly artifacts resulting from the attempts to improve the stability of renieramycin alkaloids.

In 2003–2004, the structures of renieramycins J–O, and Q–S were isolated from the Thai sponge *Xestospongia sp.* pretreated with potassium cyanide (KCN) by Saito, Suwanborirux, and coworkers.<sup>114</sup> They found that the addition of KCN helps stabilizing the labile amino alcohol moiety via the conversion to a more stable amino nitrile and improves the isolated yields of renieramycins by approximately 100-fold. This developed isolation protocol also allowed for the discovery of minor components of renieramycins in *Xestospongia sp.*, including renieramycins T–U which possess an ecteinascidin-renieramycin hybrid structure,<sup>115</sup> as well as renieramycin V which contains a sterol unit appended to the C14-position.<sup>116</sup> Additionally, jorunnamycins A–C were isolated from the aqueous KCN-pretreated *Jorunna funebris* collected in Thailand.<sup>117</sup>

**Figure 4.21** General structure and representative examples of renieramycin alkaloids.



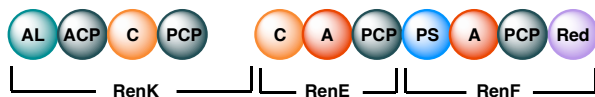
The Saito and Concepcion groups later reported three novel renieramycin-type alkaloids, namely renieramycins W–Y, which were isolated from the KCN-pretreated

*Xestospongia sp.* collected in the Philippines.<sup>118</sup> Structurally, renieramycins W and X are the first to have tiglic acid ester functionality instead of the angelate ester or the alcohol. Most recently, Guo and coworkers successfully isolated and disclosed the structures of fennebricins A–D from the South China Sea nudibranch *J. funebris*.<sup>119</sup>

Biosynthetically, the core pentacyclic skeleton of renieramycins were also reported to be assembled through a non-ribosomal peptide synthetase (NRPS) pathway, similar to the NRPS system of saframycin A.<sup>120</sup> Donia and coworkers recently discovered that there are three NRPS modules, namely, RenE, RenF, and RenK, which are responsible for the production of the renieramycin E core structure (Scheme 4.64A). The first two modules (RenK and RenE) promote the formation of aldehyde building block **615**, while RenF catalyzes multi-step transformations to ultimately deliver pentacycle **617** (Scheme 4.64B). Of note, RenK module is missing an adenylation domain (A) consistent with the fact that renieramycin E is one amino acid shorter than saframycin A.

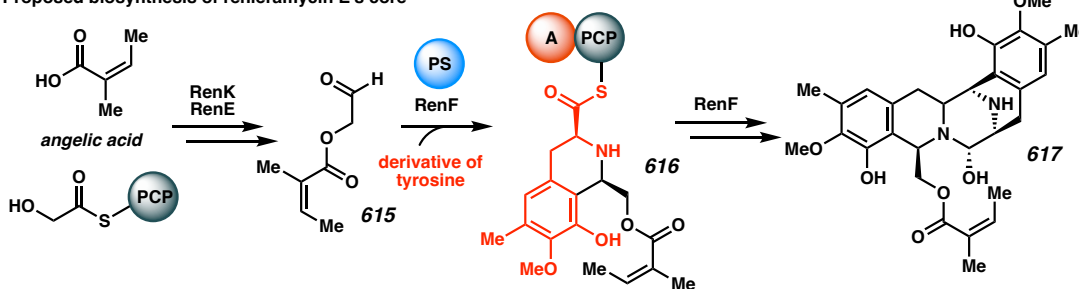
**Scheme 4.64** A. Domain organization of renieramycins NRPS. B. Proposed biosynthetic mechanism for the construction of renieramycin E's pentacyclic skeleton.

a) Renieramycins nonribosomal peptide synthetase (NRPS):



AL - acyl-coA ligase, ACP - acyl carrier protein, C - condensation, A - adenylation, PCP - peptidyl carrier protein, PS - Pictet-Spengler, Red - Reduction

b) Proposed biosynthesis of renieramycin E's core



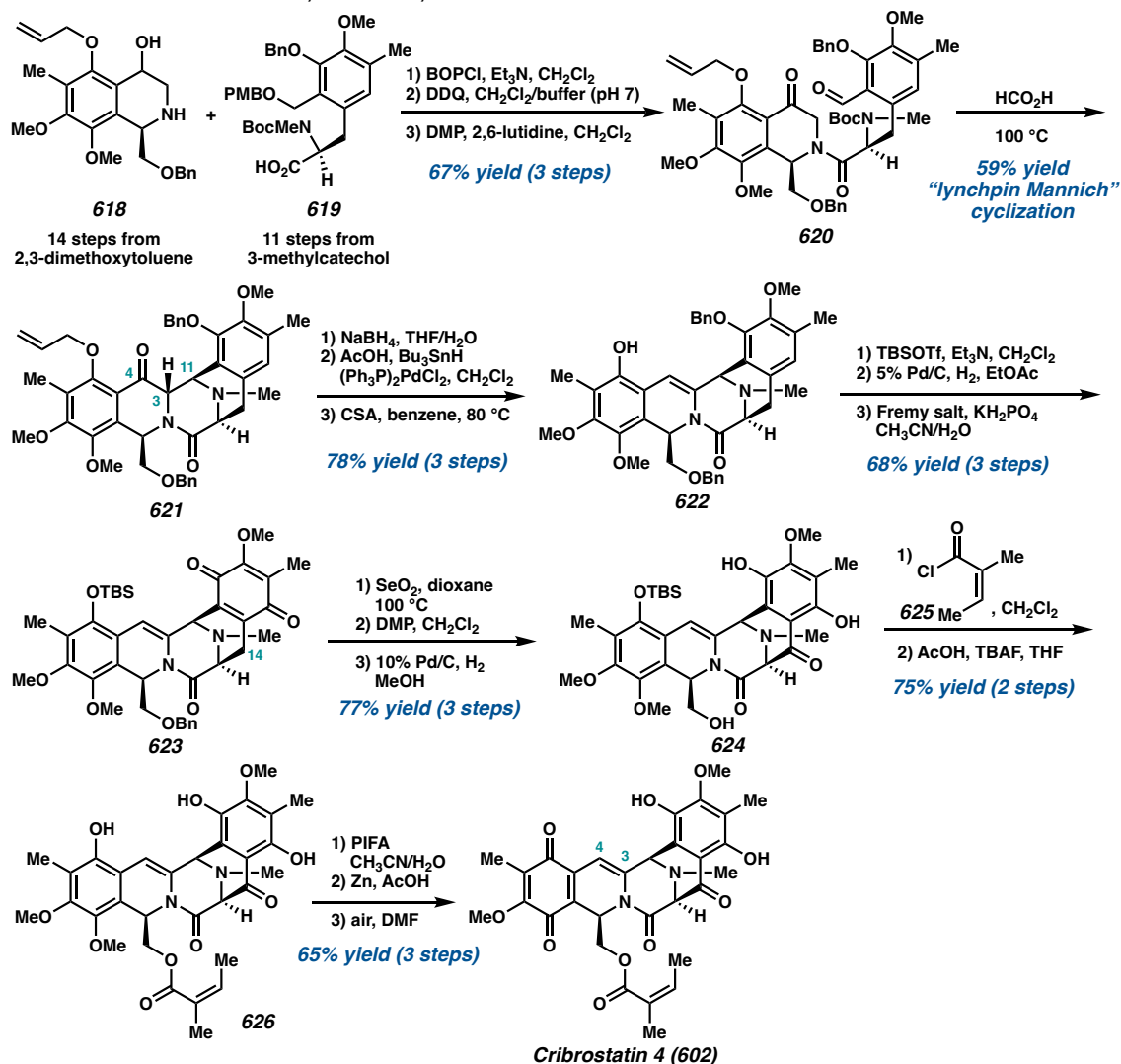
#### 4.5.3.2. TOTAL SYNTHESIS OF RENIERAMYCIN ALKALOIDS

In the past 20 years, chemical syntheses of renieramycins have been an active research area with a number of synthetic studies towards these molecules and >10 reports successfully preparing naturally occurring renieramycin alkaloids. The first total synthesis of (–)-cribrostatin 4 (**602**, aka renieramycin H) was disclosed by Danishefsky and coworkers in 2005 utilizing asymmetric reductions as key transformations to prepare both western and eastern halves of the molecule (Scheme 4.65).<sup>121</sup> With the two enantioenriched fragments in hand, they convergently coupled them together through an amide coupling, followed by a “lynchpin Mannich” cyclization to deliver pentacycle **621**. Of note, the stereochemistry at the C3 position is opposite to that existing in the saframycin-like backbone. Nonetheless, this is inconsequential because the targeted natural product has the C3=C4 benzylic olefin. Accordingly, the ketone functionality at the C4 position was reduced and subsequently eliminated, affording intermediate **622**.

Finally, the last steps of the total synthesis involves the adjustment of oxidation levels of the A- and E- rings, the installation of the ketone at C14, and the introduction of the angeloyl group. By first converting intermediate **622** to monoquinone **623**, regioselective benzylic oxidation with SeO<sub>2</sub> proceeded smoothly, followed by DMP oxidation and quinone reduction to generate bis-hydroquinone **624**. Despite the difficulty met in their initial attempts to perform angelation on a similar substrate, they adjusted the A-ring oxidation state and were able to perform esterification on this specific intermediate using angeloyl chloride **625**, followed by TBS deprotection to prepare **626**. Selective air oxidation of the ring A hydroquinone eventually provided cribrostatin 4 (**602**) in 34 steps for the longest linear sequence from commercially available 2,3-dimethoxytoluene. They additionally noted that

the high stability of the E-ring hydroquinone can be attributed to the presence of the C14 ketone, while the resting state of the A ring is in the quinone oxidation level.

**Scheme 4.65** Danishefsky's total synthesis of (–)-cribrostatin 4 **602**.

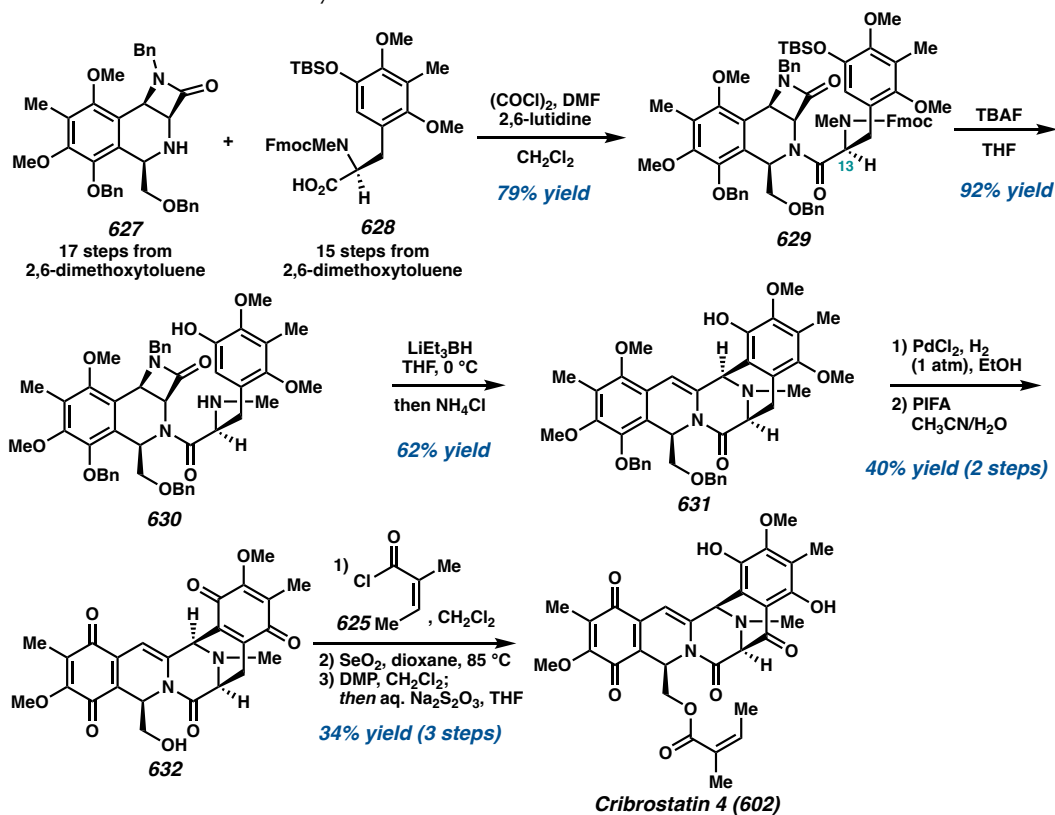


With a longstanding interest in the chemistry and biology of the THIQ antitumor antibiotics, the Williams laboratory also developed an asymmetric total synthesis of (–)-cribrostatin 4 (**602**) (Scheme 4.66).<sup>122</sup> By exploiting a sequential asymmetric Staudinger/Pictet–Spengler cyclization reaction, which was first developed in a separate study,<sup>123</sup> the β-lactam-fused THIQ **627** was prepared to serve as the western portion of the



molecule. On the other hand, the enantioenriched tyrosine derivative **628** was synthesized using chiral glycine template as a chiral auxiliary. The assembly of these two molecules was then performed through an acid chloride intermediate to provide amide **629** without detectable epimerization at the C13 position. Treatment of **629** with TBAF resulted in the removal of both the TBS and Fmoc protecting groups to give **630**.

**Scheme 4.66** William's total synthesis of (-)-cribrostatin 4 **602**.



Following this, the  $\text{LiEt}_3\text{BH}$  reduction of  $\beta$ -lactam **630** initiated the cyclization/elimination cascade, which established the pentacyclic skeleton of cribrostatin 4. Although there are two possible pathways for this transformation, the authors postulated the formation of an *o*-quinone methide intermediate to be operative. Finally, the advancement of pentacycle **631** to cribrostatin 4 consists of a) debenzoylation with  $\text{PdCl}_2$ , b) oxidation of both phenols to bisquinone **632** with PIFA, c) esterification to generate the angelated intermediate,

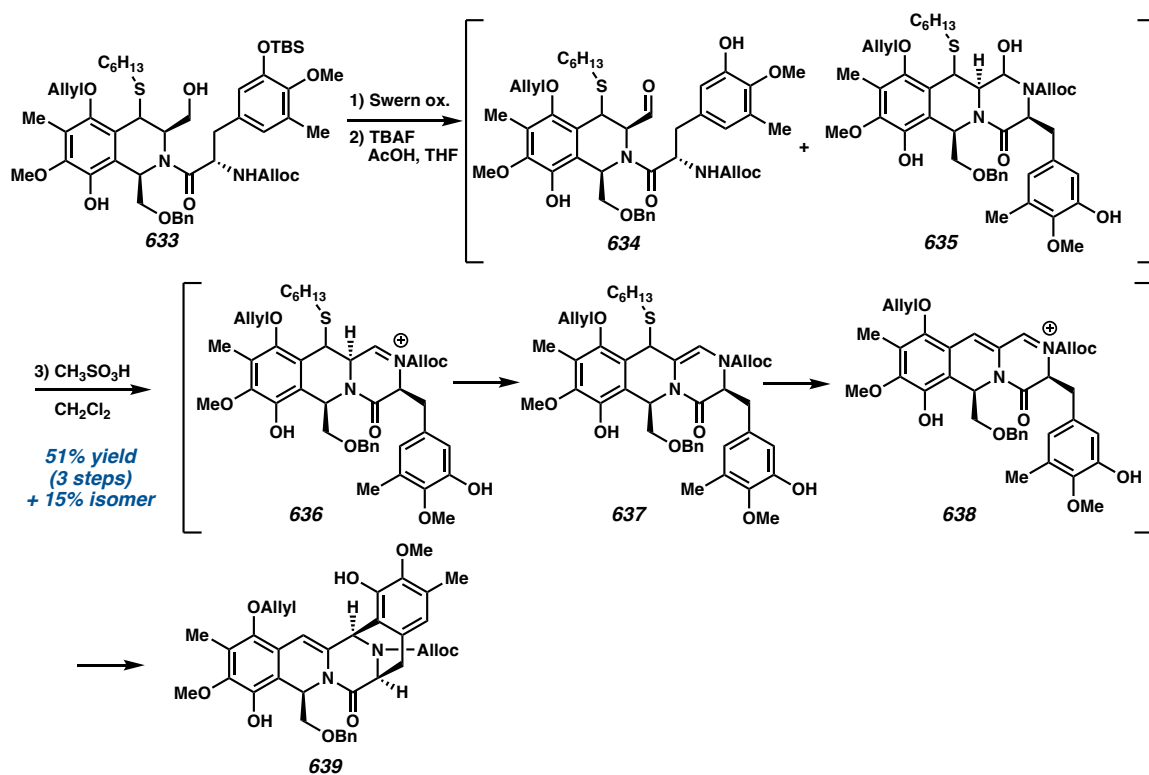
and d) double oxidation to install a ketone functionality at the C14 position. It is worth noting here that the order of this sequence proves critical to the success of this synthesis, as Danishefsky previously found that the pentacyclic alcohol (deangelated cribrostatin 4) was highly unstable, and attempts to perform esterification on this particular intermediate all led to decomposition of the starting material.<sup>121</sup> Overall, Williams and coworkers completed a 25-step (longest linear sequence) asymmetric total synthesis of (–)-cribrostatin 4 (**602**), starting from commercially available 2,6-dimethoxytoluene.

Within the same year, Zhu and coworkers described the third asymmetric total synthesis of (–)-cribrostatin 4 (**602**).<sup>124</sup> The key synthetic strategy to access the pentacyclic skeleton (**639**) features a domino sequence, involving the formation of iminium ion **636**, followed by  $\beta$ -elimination and Pictet–Spengler cyclization, which greatly resembles Williams' strategy (Scheme 4.67). In Zhu's case, the thiol group at the C4 position acts as a leaving group to unveil  $\alpha,\beta$ -unsaturated iminium ion **638**. This intermediate then underwent cyclization to form pentacycle **639** and its constitutional isomer, arising from the undesired regioselectivity, in 51% yield and 15% yield, respectively. The desired isomer (**639**) was transformed into cribrostatin 4 (**602**) following a similar strategy to previous syntheses, providing the natural product in the longest linear sequence of 26 steps from commercially available starting material.

More recently, Saito reported a racemic total synthesis of cribrostatin 4 from commercial material.<sup>125</sup> Instead of building the pentacyclic core from an amide coupling to join the two halves of the molecule, they completed the synthesis by employing diketopiperazine as a central building block and consequently constructing the B- and D-rings to generate the pentacyclic framework. The endgame of this synthesis follows the

sequence reported by Williams.<sup>122</sup> The Saito group also realized an alternative synthetic plan to cribrostatin 4 in 2015,<sup>126</sup> where they slightly modified the order of transformations in the early stage to prepare the pentacyclic skeleton. With this improved strategy, they were able to perform reactions on larger scale and prepared 81 mg of cribrostatin 4 with 8.3% overall yield in addition to renieramycin I, which contains a methoxy substituent at the C14 position.

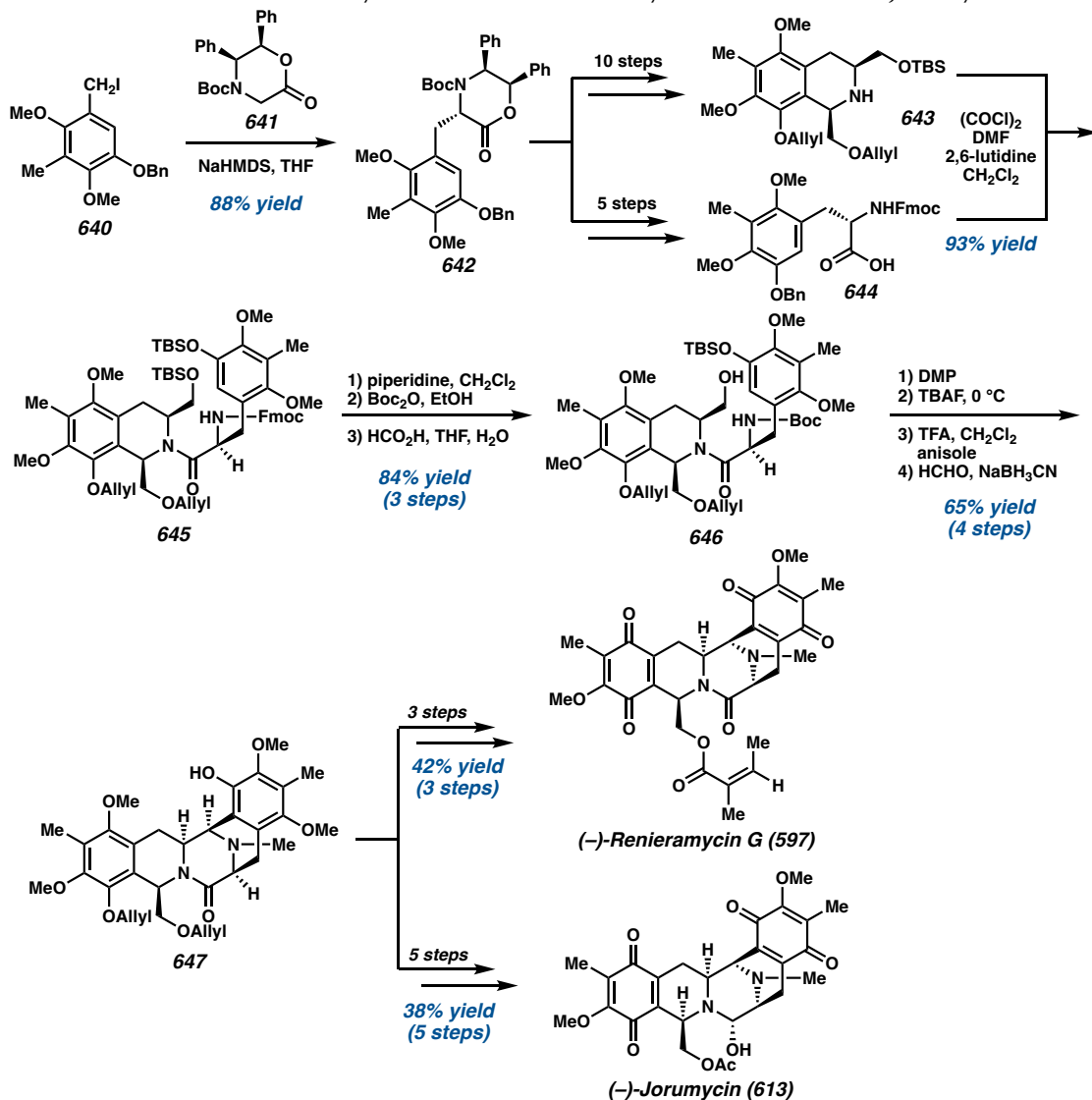
**Scheme 4.67** Zhu's strategy to prepare the pentacyclic skeleton of (-)-cribrostatin 4 **602**.



Apart from cribrostatin 4 (or renieramycin H), renieramycin G (**597**) has also been a popular target, attracting interest from the group of Williams, Magnus, Zhu, Saito, Liu, and Yang to complete its total synthesis. In 2005, Williams and coworkers disclosed the first asymmetric total synthesis of renieramycin G along with another structurally similar natural product, jorumycin (**613**) (Scheme 4.68).<sup>127</sup> They elegantly took advantage of the intrinsic symmetry of the molecule to prepare only one building block (**640**) that can be employed as

both the western and eastern fragments. The use of chiral glycine template **641** as a chiral auxiliary allows for the preparation of benzylated oxazinone **642** which can be further transformed into enantioenriched 1,3-*cis*-THIQ **643** over 10 steps and tyrosine derivative **644** over 5 steps.

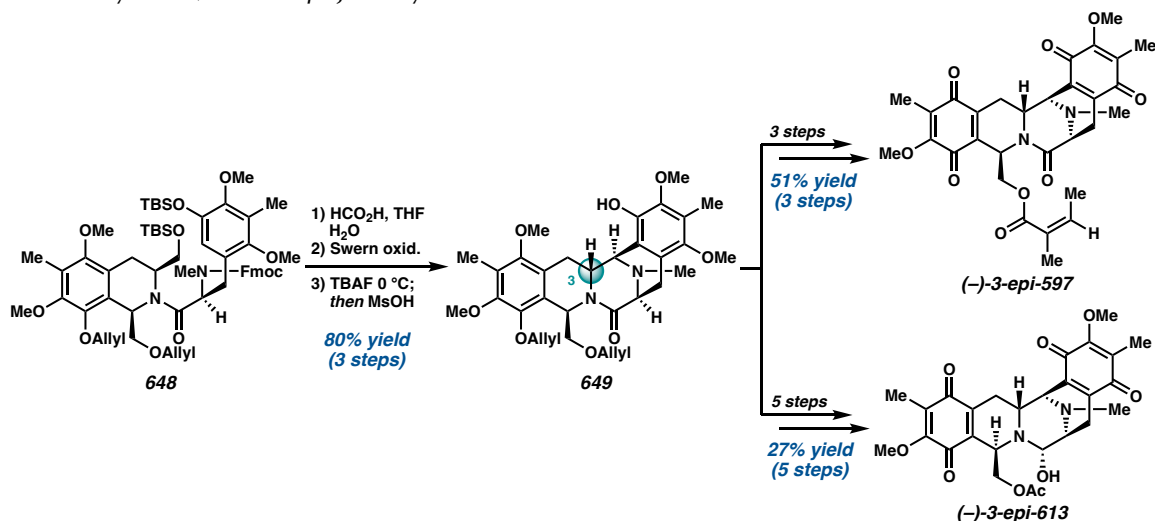
**Scheme 4.68** William's total synthesis of (–)-renieramycin G **597** and (–)-jorumycin **613**.



The coupling of these two molecules via an acid chloride intermediate proceeded smoothly to deliver amide **645** in 93% yield. Fmoc removal with piperidine, reprotection of the free amine with a Boc protecting group, and selective removal of the TBS group were

followed to provide alcohol **646**. The pentacycle was then obtained after oxidation of the primary alcohol, formation of the carbinol amine, and Pictet–Spengler cyclization to construct the D-ring. Reductive amination afforded intermediate **647** that is a precursor to both (–)-renieramycin G (**597**) and (–)-jorumycin (**613**). Interestingly, the use of different protecting groups on the eastern nitrogen atom, which requires basic conditions for deprotection, resulted in the generation of the C3-*epi* variant (**649**) through epimerization (Scheme 4.69). They, nonetheless, successfully advanced this unexpected epimer to 3-*epi*-renieramycin G and 3-*epi*-jorumycin for further biological evaluation studies.

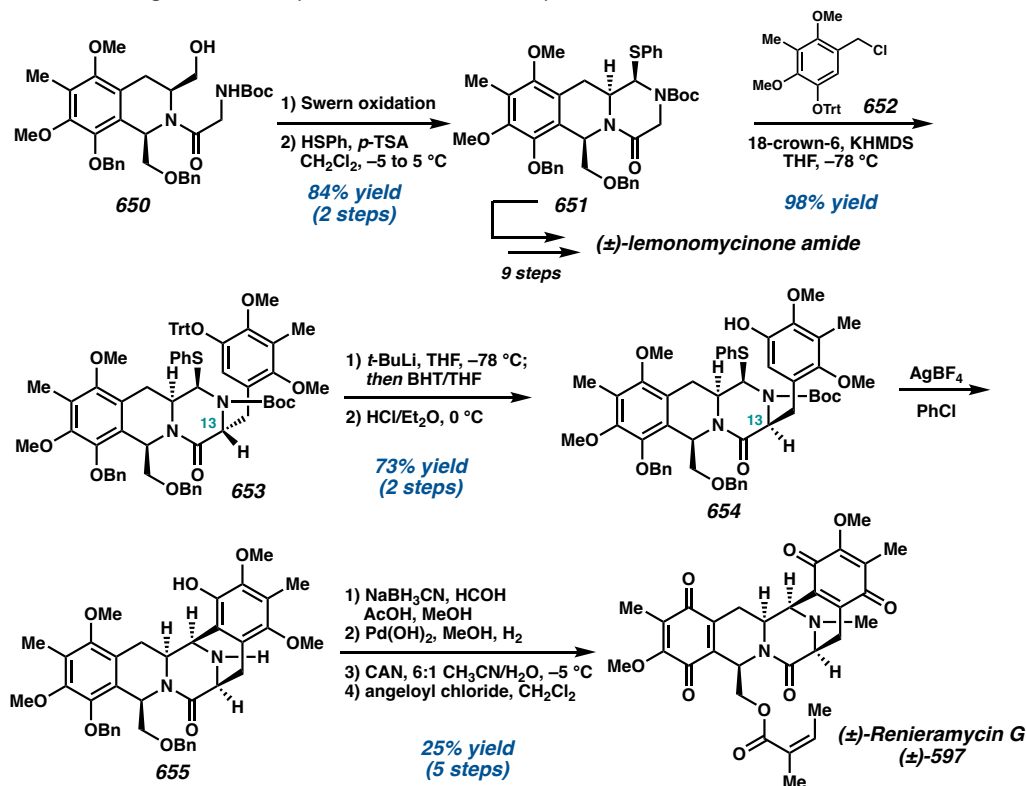
**Scheme 4.69** William’s unexpected C3-epimerization toward the synthesis of 3-*epi*-renieramycin G, and 3-*epi*-jorumycin.



At the same time, Magnus independently developed racemic total syntheses of renieramycin G (**597**) and a lemonomycinone analog (Scheme 4.70).<sup>128</sup> The A–B rings of both molecules were initially prepared through a modified Larock isoquinoline synthesis, followed by an addition at the C1 position, a reduction of the C3=C4 olefin, and a silyl-activated amide coupling to deliver 1,3-*cis*-THIQ **650**. This THIQ intermediate (**650**) then underwent cyclization, and functional group interconversion to thioaminal **651**. At this stage,

thioaminal **651** serves as a diverging point to access renieramycin G or lemonomycinone amide, where a lactam enolate alkylation with benzyl chloride **652** was performed for the synthesis of renieramycin G. This provided the undesired epimer of tetracycle **653** at the C13 position as a single diastereomer, which they were able to correct via a diastereoselective reprotonation with in situ trityl removal to deliver **654**. Treatment of this intermediate (**654**) with  $\text{AgBF}_4$  then triggered cyclization to generate the D-ring in pentacycle **655**. Finally, reductive amination, hydrogenolysis, ceric ammonium nitrate (CAN) oxidation, and esterification afforded racemic renieramycin G (**597**). In this same report, a lemomycinone amide was also prepared by adapting this developed synthetic strategy.

**Scheme 4.70** Magnus' total synthesis of renieramycin G **597**.



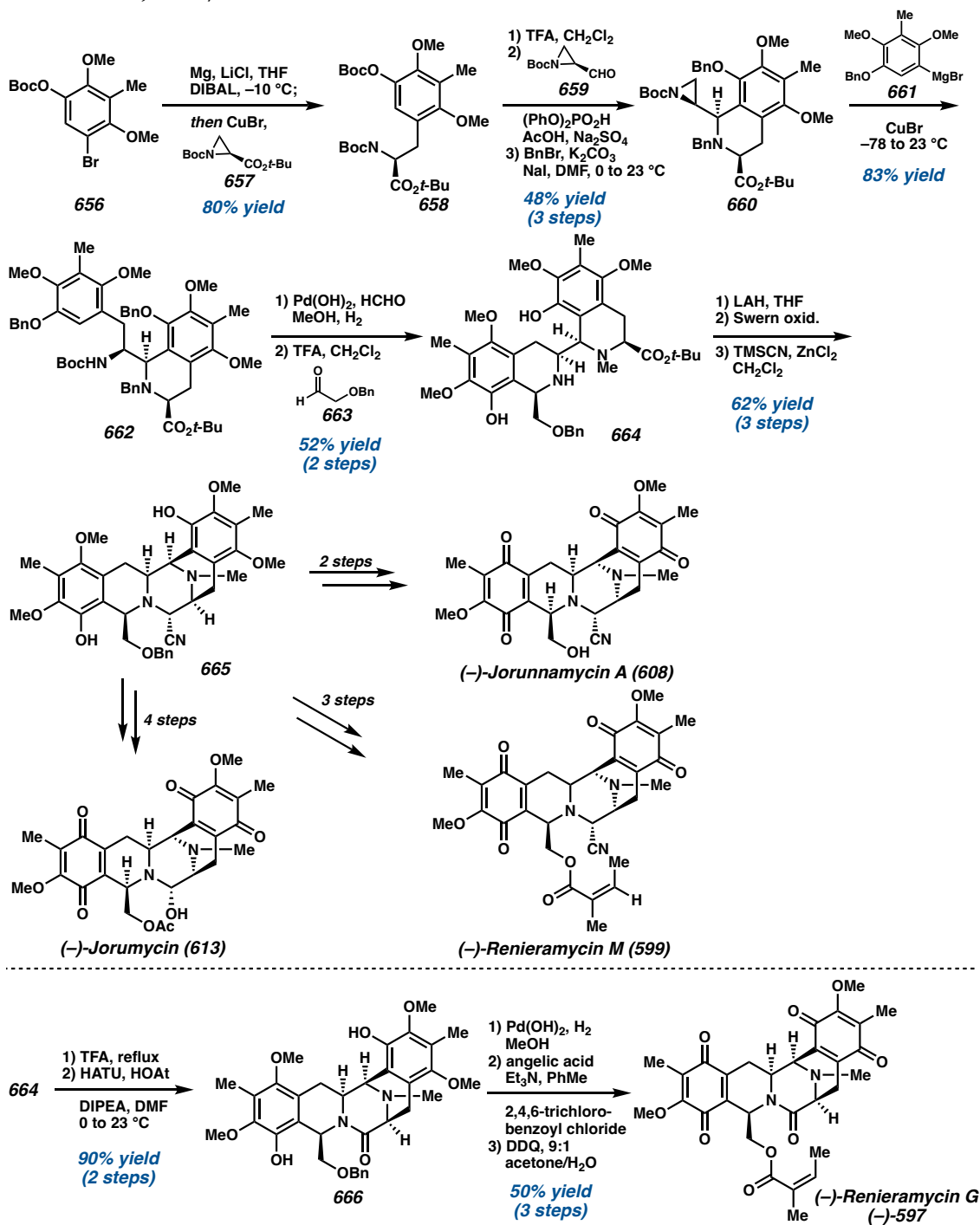
Zhu and coworkers disclosed the asymmetric total syntheses of (–)-renieramycins G, M, (–)-jorunnamycin A, and (–)-jorumycin in 2009 (Scheme 4.71).<sup>129</sup> By employing

aziridine as a lynchpin, they took a different approach to construct the pentacyclic skeleton. Instead of relying on the amide coupling to merge the western and eastern parts of the molecule, they exploited aziridine ring-opening to forge the desired pentacycle. Starting with a CuBr-mediated ring-opening of enantioenriched aziridine **657**, which was prepared from a chiral pool starting material (*N*-trityl-L-serine methyl ester), the Boc-protected amino ester **658** was formed in 80% yield. Following Boc removal, the Pictet–Spengler cyclization of the free amine with formyl aziridine **659** and global benzylation were performed to afford the eastern THIQ building block (**660**). From here, another CuBr-promoted aziridine ring-opening was utilized, and a sequence consisting of a debenylation with in situ methylation and tandem Boc removal/Pictet–Spengler reaction delivered the key bis-THIQ (**664**). This intermediate was then subjected to two different synthetic sequences to prepare a variety of renieramycin alkaloids. First, conversion of the ester to the aldehyde and a Strecker reaction provided pentacycle **665**. This intermediate can be further advanced to jorunnamycin A (**608**), renieramycin M (**599**), and jorumycin (**613**) over 2, 3, and 4 steps, respectively. On the other hand, renieramycin G (**597**) was obtained via a) an amide coupling to form pentacycle **666**, b) hydrogenolysis with Pearlman’s catalyst, c) angelation of the primary alcohol, and c) DDQ oxidation of the bis-phenols.

By exploiting the common strategy in the construction of the bis-THIQ pentacyclic scaffold, i.e., the amide coupling with subsequent elaboration of the C–E rings through Pictet–Spengler cyclization, the Liu group reported an asymmetric total synthesis of (–)-renieramycin G (**597**).<sup>130</sup> The use of L-tyrosine methyl ester as a chiral pool starting material, similar to their total synthesis of saframycin A (*vide supra*), allows for diastereocontrol in

ensuing transformations which ultimately resulted in the successful preparation of enantiopure (–)-renieramycin G in 21 steps for the longest linear sequence.

**Scheme 4.71** Zhu's total synthesis of (–)-renieramycins G **597**, M **599**, (–)-jorunnamycin A **608**, and (–)-jorumycin **613**.

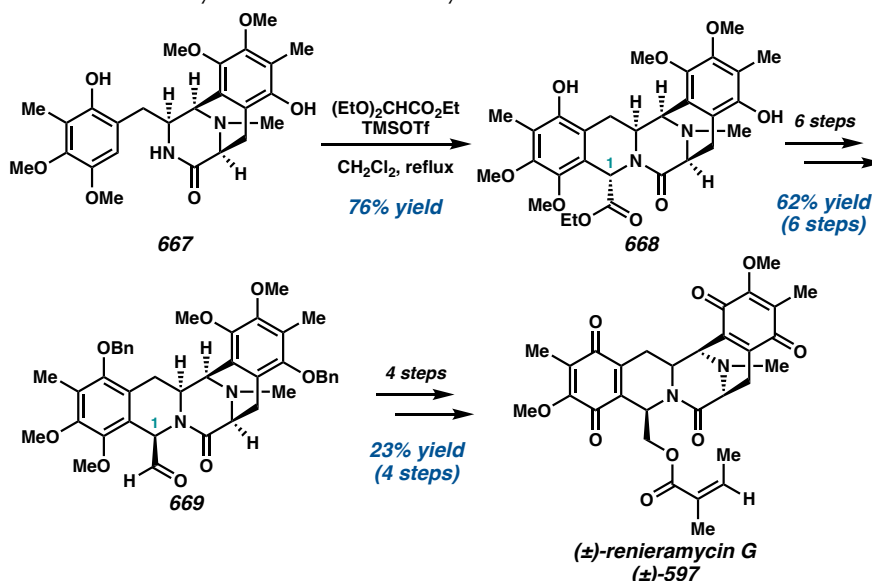




After the disclosure of this report, the group extended this synthetic strategy to prepare 15 analogs of renieramycin G with varying groups at the angelate ester,<sup>131</sup> 15 analogs of jorumycin with varying groups at the primary alcohol,<sup>132</sup> as well as 3 additional stereoisomers of renieramycin G.<sup>133</sup> These analogs were biologically evaluated for their cytotoxic activities against multiple cancer cell lines.

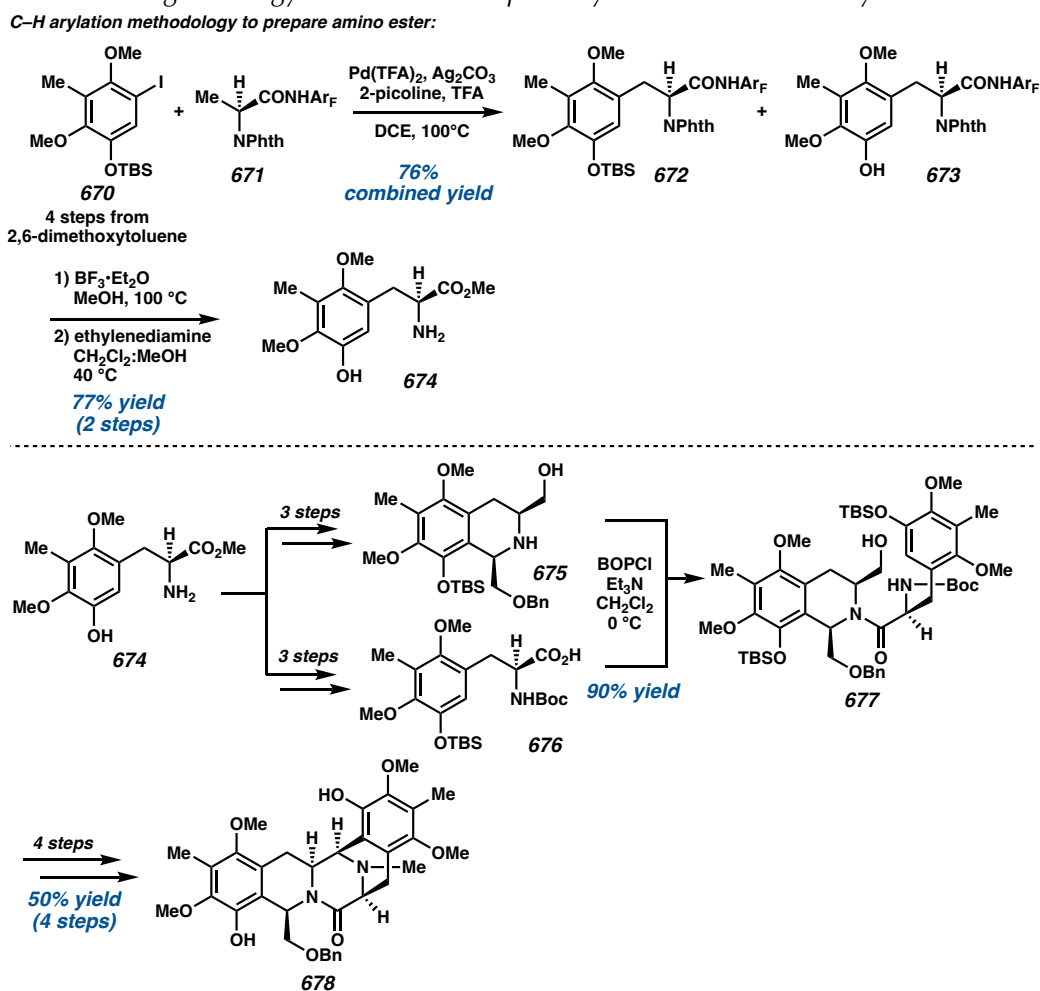
In 2011, Saito and coworkers reported the total synthesis of (±)-renieramycin G (Scheme 4.72),<sup>134</sup> in which the synthetic strategy closely followed their previously reported pathway for the synthesis of saframycin B.<sup>135</sup> From tricyclic lactam **667**, they performed a Pictet–Spengler cyclization with diethoxyacetate, delivering pentacycle **668** in 76% yield, albeit with the opposite stereochemistry at the C1 position. By converting the pendent ester to the aldehyde **669**, they were able to correct this stereochemical problem via a base-mediated epimerization over a total of 6 steps. Finally, the racemic renieramycin G (**597**) was obtained by performing a reduction of the aldehyde to the alcohol, followed by debenzylation, CAN oxidation, and angelation.

**Scheme 4.72** Saito's total synthesis of renieramycin G **597**.



Most recently, Yang and coworkers accomplished the total syntheses of the renieramycin alkaloids by a unified strategy (Scheme 4.73).<sup>136</sup> The key transformations to construct the pentacycle are not significantly different from previous reports (i.e., the amide coupling with subsequent formation of the C,D-rings) however, they were able to expediently prepare tyrosine derivatives **672** and **673** through the utilization of C–H functionalization methodology.

**Scheme 4.73** Yang's strategy to assemble the pentacyclic core of renieramycin alkaloids.



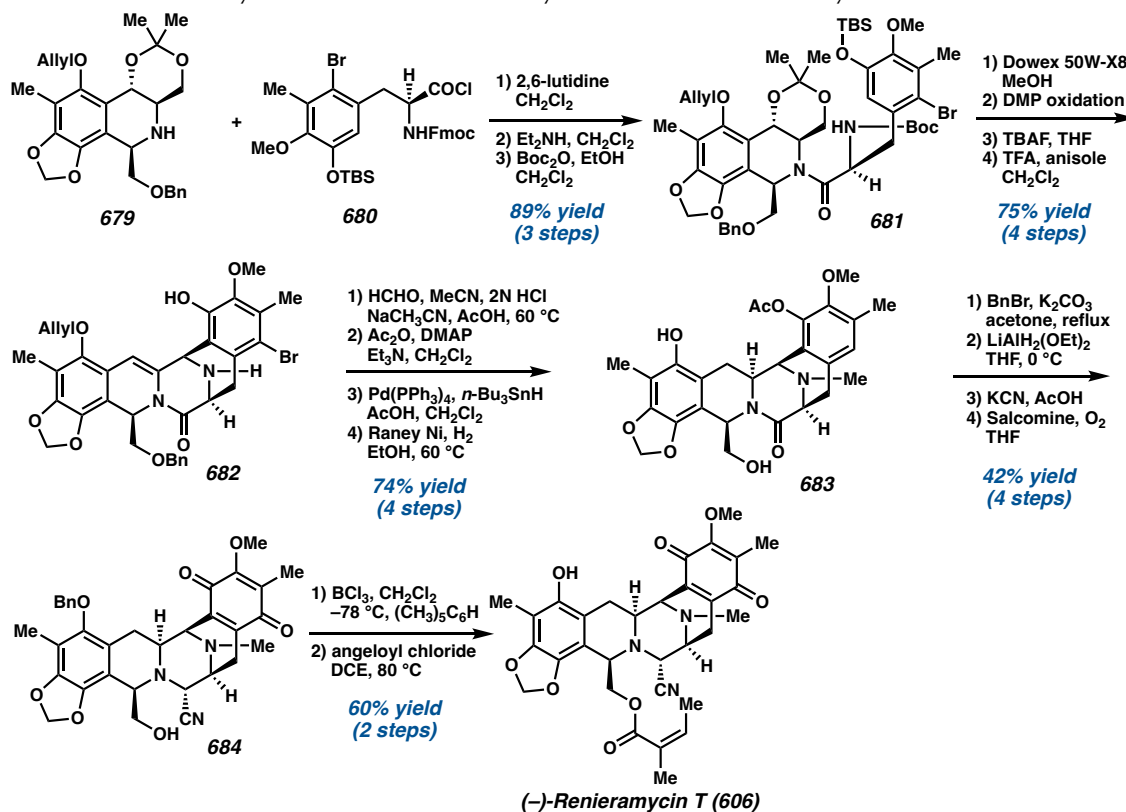
Inspired by Yu's C–H arylation, they performed the coupling of alanine derivative **671** with aryl iodide **670**.<sup>137</sup> This reaction proceeded smoothly to provide a 76% combined

yield of arylated products **672** and **673**, which were transformed into the same amino ester **674** via the removal of the CONHAr<sub>F</sub> directing group and phthalimide protecting group, respectively. Amino ester **674** was used to prepare both the western (**675**) and eastern (**676**) fragments of the renieramycin alkaloids. Treatment of 1,3-cis-THIQ **675** and Boc-protected amino acid **676** with BOPCl and Et<sub>3</sub>N provided amide product **677** in 90% yield. With **677** in hand, pentacycle **678** was obtained from DMP oxidation, removal of the phenolic TBS protecting groups, acid-promoted intramolecular Pictet–Spengler cyclization, and reductive amination. Subsequently, enantioenriched (–)-renieramycins, G, M, J, (–)-jorunnamycin A, and (–)-fennebricin A were prepared from this same pentacycle **678**. Of note, this research represents the first asymmetric total syntheses of renieramycin J and fennebricin A.

The recently isolated renieramycin T (**606**), which features a hybrid structure of ecteinascidin–renieramycin, was also a target for a total synthetic endeavor by Yokoya and Williams.<sup>138</sup> By adapting the strategy used in their total synthetic studies of Et-743,<sup>139</sup> they completed the synthesis of (–)-renieramycin T through the use of L-tyrosine as a chiral pool starting material (Scheme 4.74). Amide coupling of highly decorated THIQ **679** and Fmoc-protected amino acid chloride **680**, followed by swapping of amine protecting groups provided amide **681** in 89% overall yield. Removal of the acetonide, then Dess-Martin oxidation, and intramolecular Pictet–Spengler cyclization delivered pentacycle **682** in 75% yield over 4 steps. From this key intermediate, they performed several functional group manipulations to obtain phenol **683**. This phenolic hydroxyl group was benzyl protected prior to the partial reduction of the central amide, cyanation of the in-situ generated iminium ion, and oxidation of the eastern phenol to afford mono-quinone **684**. Finally, debenylation with BCl<sub>3</sub> and subsequent esterification with angeloyl chloride completed the total synthesis of

renieramycin T (**606**). This natural product along with other compounds in this synthetic sequence were evaluated for their cytotoxicities and revealed to exhibit moderate activities against human cancer cell lines.

**Scheme 4.74** Yokoya's and Williams' total synthesis of (–)-renieramycin T **606**.

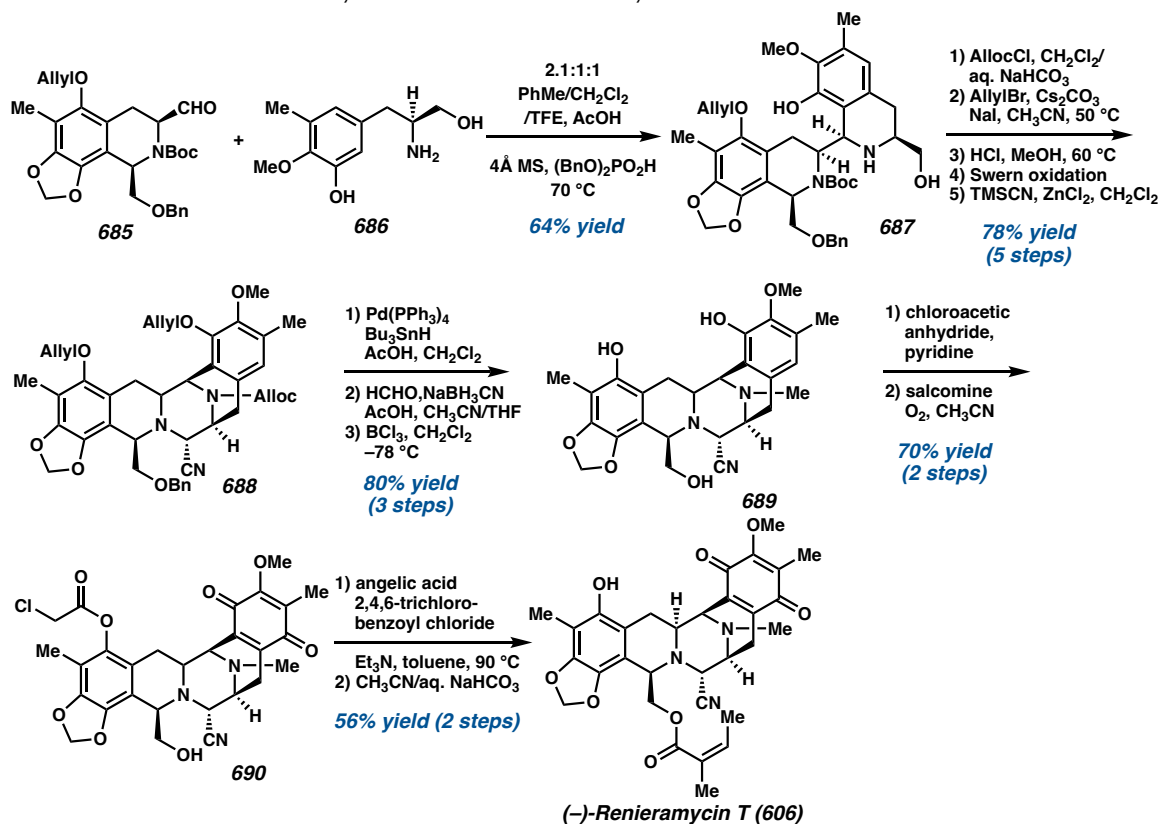


Seeking to develop an alternative strategy for the production of renieramycin T, Saito and coworkers applied the stereoselective decarboxylative reprotonation strategy previously discovered in the synthesis of saframycin A (Scheme 4.63, *vide supra*) in the context of this natural product.<sup>140</sup> To this end, the group completed a formal synthesis of renieramycin T by concluding at intermediate **684** reported by Yokoya and Williams.

The Chen group also achieved a total synthesis of (–)-renieramycin T in 2016.<sup>141</sup> By mimicking the reported biosynthesis of Et-743,<sup>142</sup> they performed a Pictet–Spengler cyclization under a unique ternary solvent system (PhMe, CH<sub>2</sub>Cl<sub>2</sub>, and 2,2,2-trifluoroethanol)

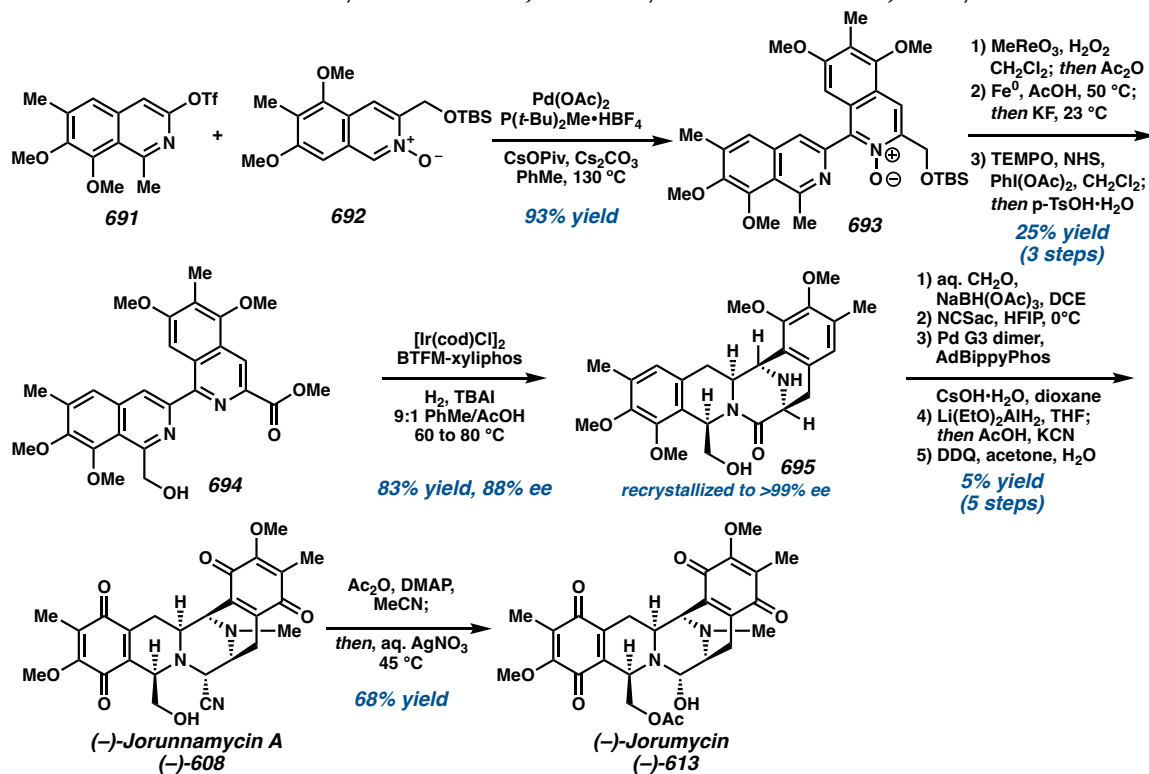
to construct the D-ring of bis-THIQ intermediate **687** (Scheme 4.75). Protection/deprotection chemistry was followed, then a Swern oxidation with a subsequent ZnCl<sub>2</sub>-promoted Strecker reaction eventually closed the C-ring, forming pentacycle **688** in 78% yield over 5 steps. With this intermediate in hand, they discovered that the chloroacetyl protecting group needed to be chemo- and regioselectively installed on the A-ring phenol (**690**) prior to oxidation and installation of the angeloyl group. Accordingly, they successfully prepared (–)-renieramycin T (**606**) in an additional 4 steps with 39% yield. Overall, this asymmetric total synthesis consists of 22 steps for the longest linear sequence, with a 6.2% overall yield from known starting materials. Apart from (–)-renieramycin T, the Chen group successfully prepared three other renieramycin-type alkaloids: (–)-jorunnamycin A, (–)-jorunnamycin C, and (–)-jorumycin through this similar synthetic strategy.<sup>143</sup>

**Scheme 4.75** Chen's total synthesis of (–)-renieramycin T **606**.



Aiming to devise a complementary synthetic route to prepare bis-THIQ alkaloids that specifically avoids the Pictet–Spengler reaction, the Stoltz group completed a synthetic study toward jorumycin (**613**) via a two-part strategy, consisting of a cross-coupling reaction for the convergent construction of the requisite carbon-based skeleton and an enantioselective hydrogenation to install all of the key stereochemistry (Scheme 4.76).<sup>144</sup> Specifically, we successfully exploited the *N*-oxide C–H functionalization developed by Fagnou and coworkers in the coupling of the eastern (**692**) and western (**691**) isoquinoline fragments. With the coupled product **693** in hand, the advancement of this intermediate to the bis-isoquinoline hydrogenation precursor (**694**) was performed through isoquinoline oxidation/mono-*N*-oxide rearrangement, followed by the N–O bond cleavage and oxyl-mediated oxidation.

**Scheme 4.76** Stoltz's total synthesis of (–)-jorunnamycin A **608** and (–)-jorumycin **613**.



Another key transformation in this synthetic strategy is the sequential stereoselective hydrogenation to construct the pentacyclic scaffold of bis-THIQ molecules. The use of  $[\text{Ir}(\text{cod})\text{Cl}]_2$  in conjunction with electron-poor Josiphos BTFM-xylyphos ligand was found to promote the desired hydrogenation-lactamization cascade, providing the pentacycle (**695**) as a single diastereomer in 83% yield, and with 88% ee. Furthermore, this intermediate was recrystallized from a slowly evaporating acetonitrile solution to enantiopurity. The relative and absolute stereochemistry of the product was confirmed via X-ray crystallographic analysis.

The final stage of the synthesis consists of a 5-step sequence. First, reductive amination was employed to methylate the piperazinone N–H. Bis-chlorination of the A- and E-rings with *N*-chlorosaccharin (NCS) was then followed, and the subsequent C–O bond coupling provided a dihydroxylated compound. Lastly, partial reduction of the central lactam with cyanide trapping and DDQ oxidation delivered jorunnamycin A (**608**). Conversion of jorunnamycin A (**608**) into jorumycin (**613**) was achieved in one additional step, concluding the 16-step total synthesis. As a result of his unique approach, access to electronically modulated aromatic substitution patterns are readily attainable.

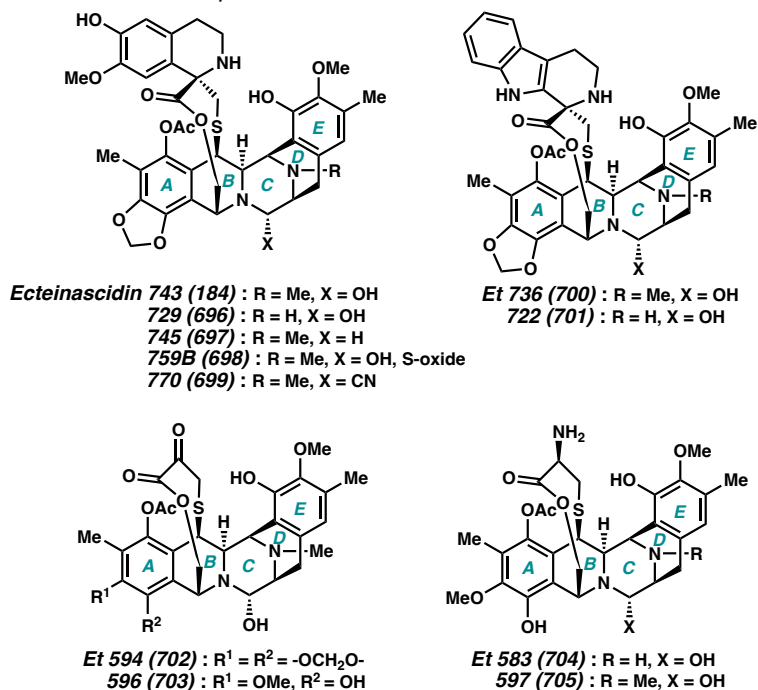
#### 4.5.4. ECTEINASCIDIN ALKALOIDS

##### 4.5.4.1. GENERAL STRUCTURE AND BIOSYNTHESIS

The ecteinascidin alkaloids are known to be extremely potent antitumor agents, with Et-743 **2** (Yondelis<sup>®</sup>) approved for clinical use for the treatment of advanced soft tissue sarcoma.<sup>145</sup> Apart from other THIQ alkaloids, these agents are unique in their structure with the pentacyclic skeleton linked to a 10-membered lactone bridge through a benzylic sulfide linkage (Figure 4.22). Most ecteinascidin alkaloids contain an additional THIQ ring attached

to the lactone bridge as a spirocycle, which is a key distinguishing feature from other THIQ natural product families.

**Figure 4.22** Ecteinascidin natural products.



Early biosynthetic studies of the ecteinascidins revealed that tyrosine and cysteine are the two amino acid building blocks specifically for the synthesis of Et-743.<sup>146</sup> More recently, with the advancement of next-generation sequencing technology, Sherman and coworkers exploited a meta-omic approach to identify the biosynthetic gene cluster responsible for the production of Et-743.<sup>147</sup> In this study, three putative modules of non-ribosomal peptide synthetase (NRPS) is reported to promote transformations for the construction of the pentacyclic core (Scheme 4.77). Similar to the NRPS system of saframycin A (*vide supra*), EtuA2 is a homologue of SfmC which iteratively incorporates two molecules of tyrosine derivatives into the core structure. After the reductive release, also through the EtuA2 module, the aldehyde intermediate undergoes cyclization to generate the



C ring. Hydrolysis of the pendent *N*-acyl moiety subsequently proceeds, and the 10-membered lactone bridge is proposed to be assembled via the tailoring *EtuO* module. This produces *Et*-583 (**704**) as a late-stage intermediate, leading to other isolable ecteinascidins (*Et*-597, *Et*-596, and *Et*-594) and finally *Et*-743.

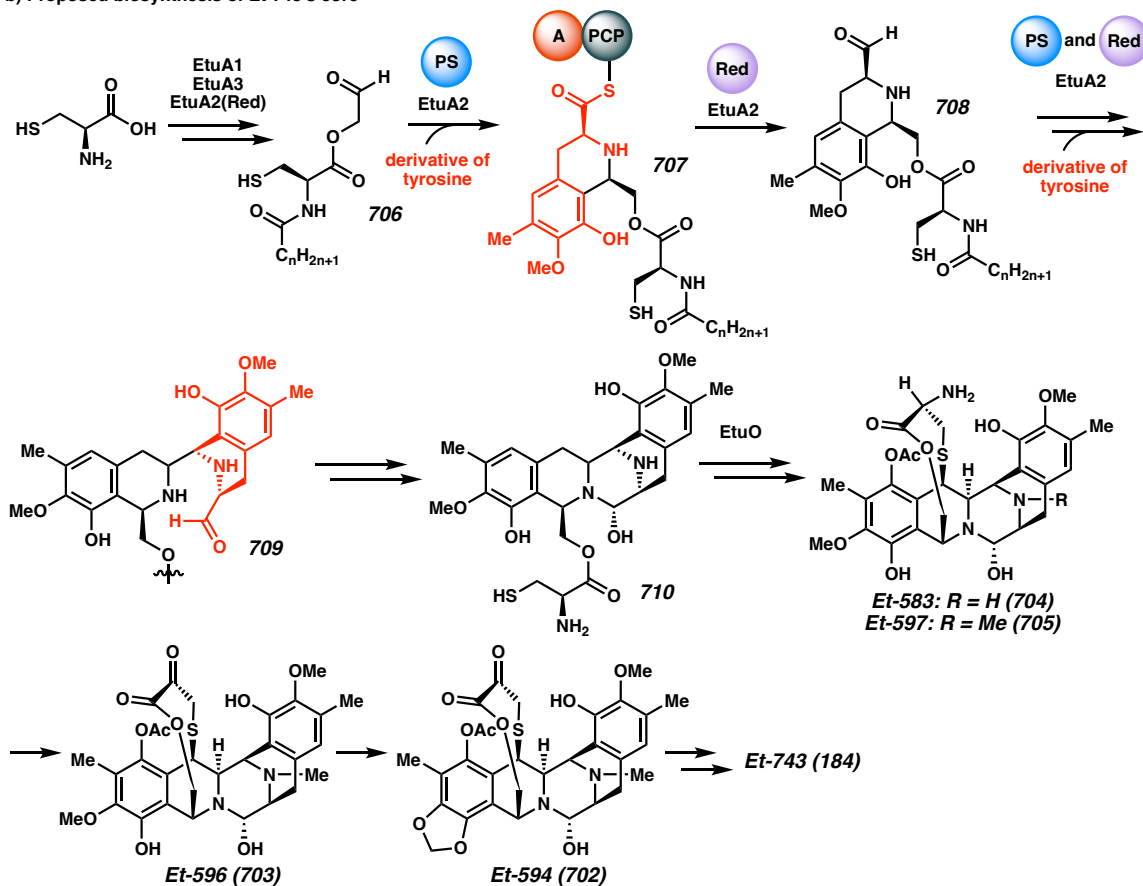
**Scheme 4.77** A. Domain organization of *Et*-743 NRPS. B. Proposed biosynthetic mechanism for the construction of *Et*-743's pentacyclic skeleton.

a) *E*7-743 nonribosomal peptide synthetase (NRPS):



AL - acyl-coa ligase, ACP - acyl carrier protein, C - condensation, A - adenylation, PCP - peptidyl carrier protein, PS - Pictet-Spengler, Red - Reduction

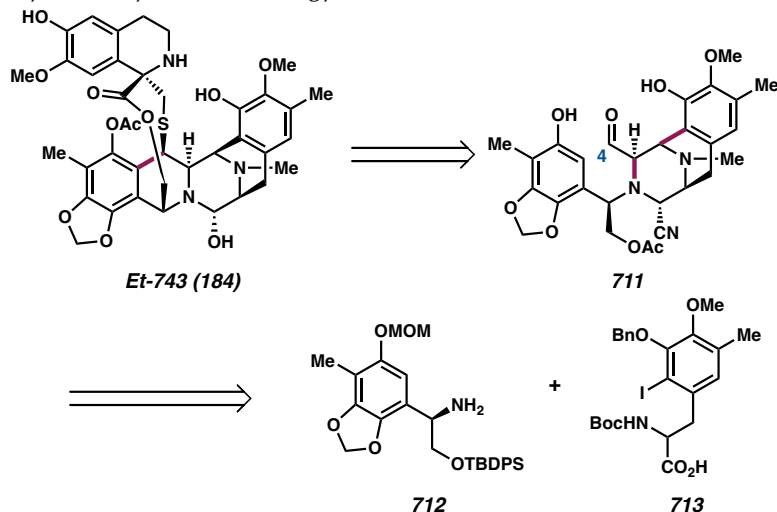
b) Proposed biosynthesis of *Et*-743's core



#### 4.5.4.2. TOTAL SYNTHESIS OF ECTEINASCIDIN ALKALOIDS

Approaches to the chemical syntheses of these natural products generally utilize electrophilic aromatic substitution strategies for construction of the THIQ motifs. After Corey's seminal total synthesis of Et-743 **184** in 1996, other groups have attempted to target this molecule and its congeners with distinct disconnections.<sup>148</sup> In 2002, Fukuyama and coworkers reported the second total synthesis of **184**, envisioning key intermediate **711** to assemble the natural product scaffold through electrophilic aromatic substitution with the requisite oxidation state at the C4 position (Figure 4.23).<sup>149</sup>

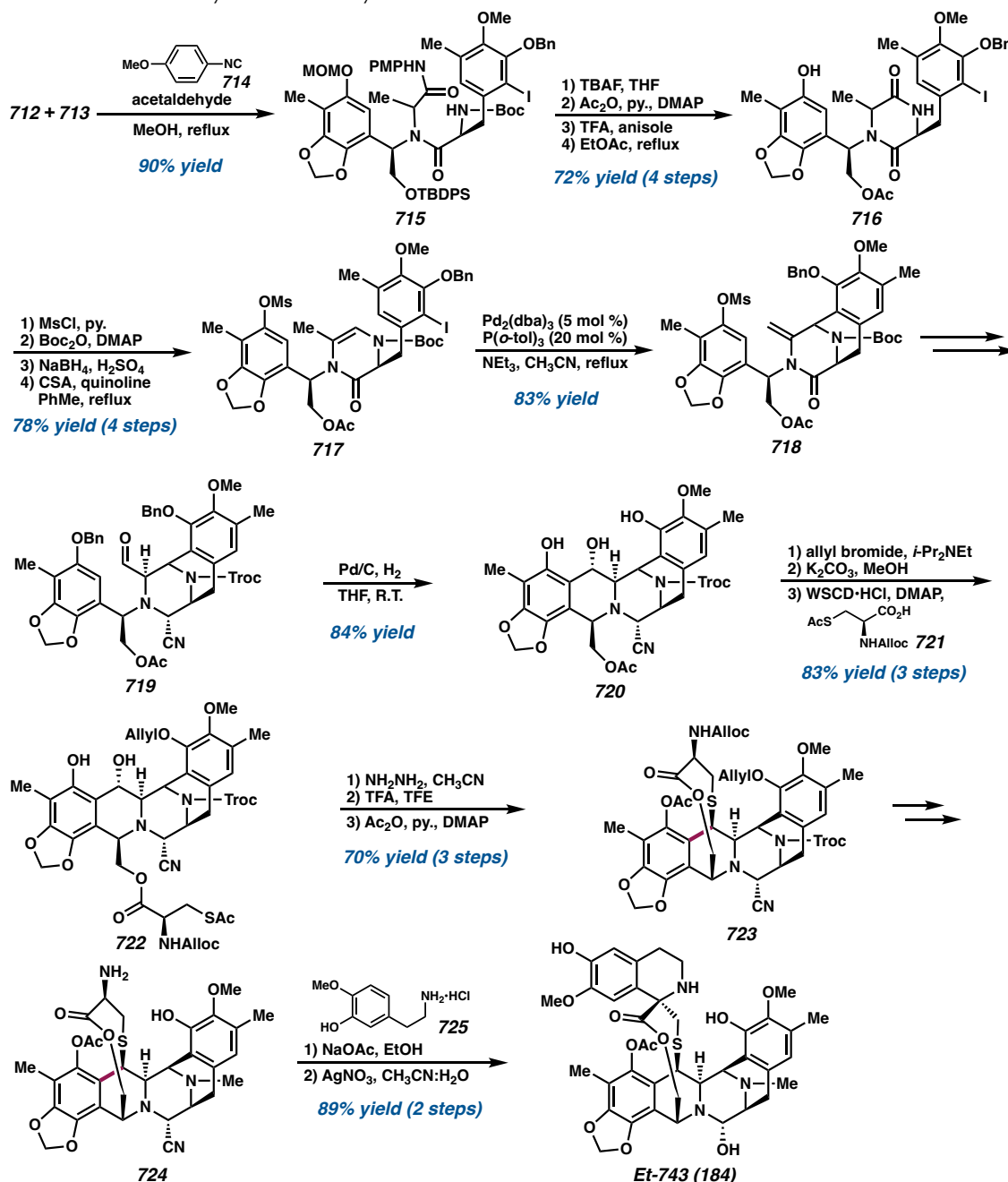
**Figure 4.23** Fukuyama's synthetic strategy toward Et-743 **184**.



With two functionalized fragments **712** and **713**, an Ugi four-component condensation reaction assembled intermediate **715** in high yield, which formed the diketopiperazine C-ring of the core in four subsequent steps (Scheme 4.78). After protection of the phenol and lactam nitrogen of **716**, partial reduction of the carbonyl with NaBH<sub>4</sub>, and dehydration of the hemiaminal intermediate afforded the desired intermediate **717** for the Heck cyclization. Using 5 mol % of Pd<sub>2</sub>(dba)<sub>3</sub> and 20 mol % of P(*o*-tol)<sub>3</sub> ligand, an intramolecular Heck reaction proceeded smoothly to install the D-ring of the natural product scaffold **718** in 83% yield. After several functional group manipulations, the key aldehyde

intermediate **719** then underwent hydrogenolysis of the benzyl ether to induce spontaneous cyclization and deliver the desired pentacycle **720**.

**Scheme 4.78** Fukuyama's total synthesis of Et-743 **184**.



With the desired oxidation already in place at the C4 position, condensation of the alcohol with L-cysteine derivative **721** furnished ester **722**, which smoothly formed the

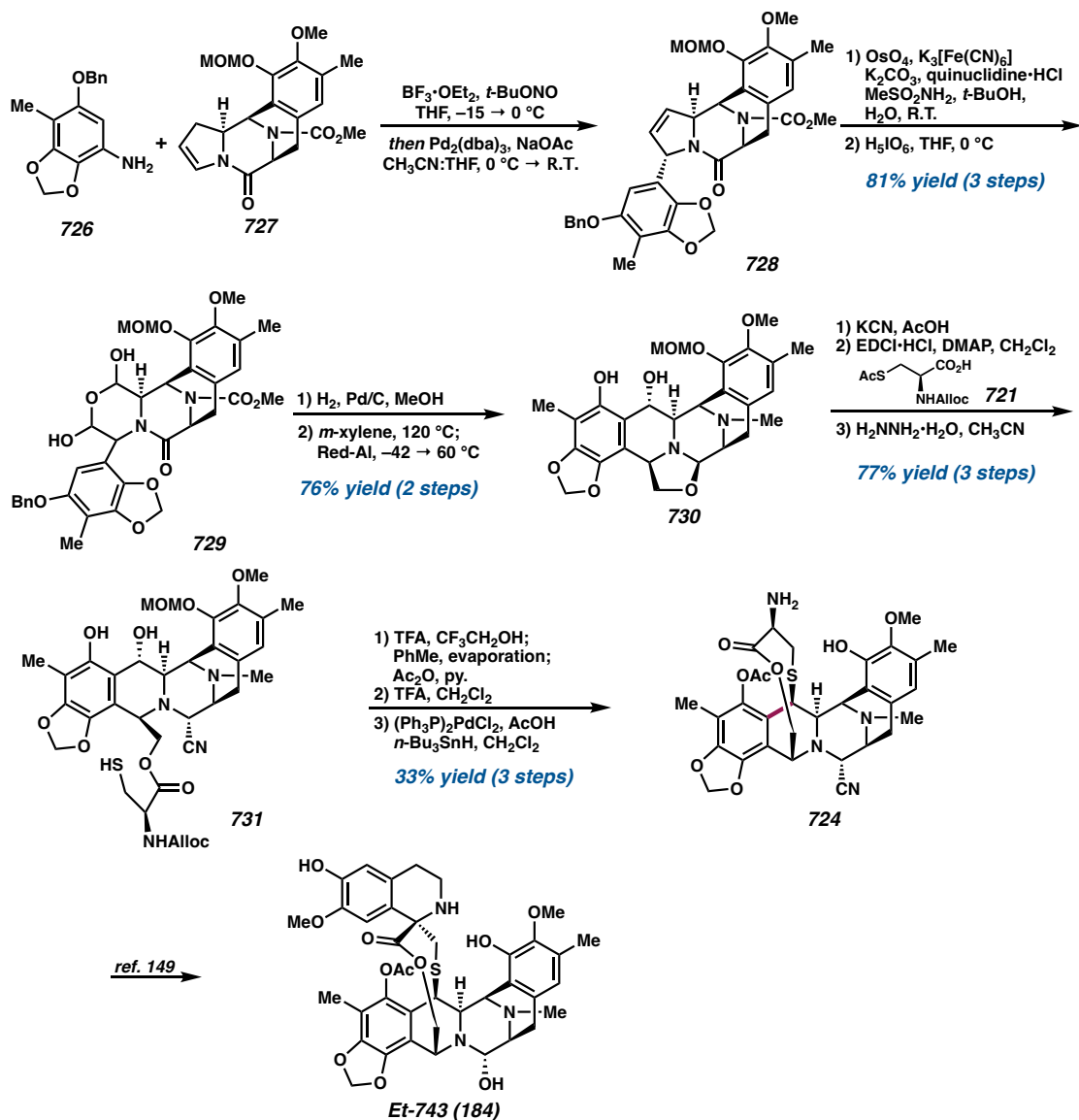
lactone bridge **723** under acidic conditions. A biomimetic transamination reaction afforded the  $\alpha$ -ketolactone **724** to undergo a subsequent Pictet–Spengler reaction with **725** to install the third THIQ moiety. Generating the labile hemiaminal last with AgNO<sub>3</sub> in CH<sub>3</sub>CN and H<sub>2</sub>O completed the natural product **184** in 93% yield.

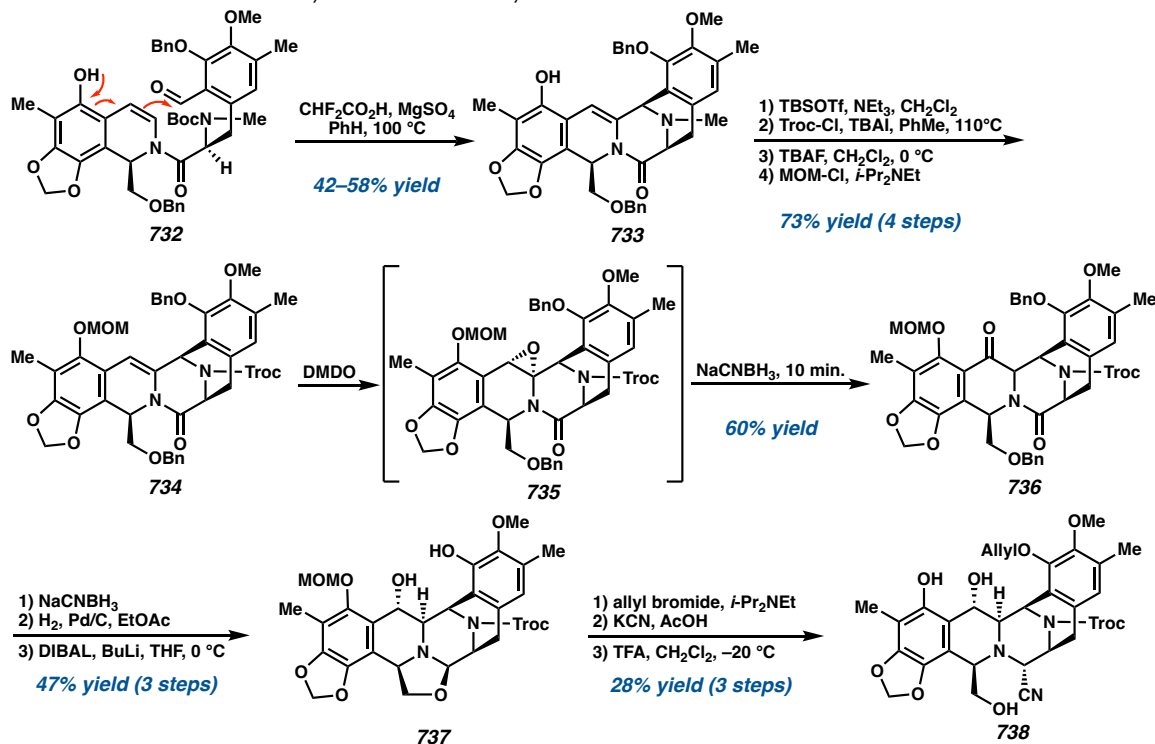
Since their completed total synthesis of **184** in 2002, Fukuyama and coworkers have revised their strategy to render its synthesis more efficient and practical.<sup>150</sup> They instead envisioned accessing intermediate **728** from dihydropyrrole **727**, assembled via a Heck reaction between amine **726** and enamide **727** (Scheme 4.79). Construction of the B-ring and the 10-membered lactone bridge would then proceed according to their initial synthetic strategy. With the functionalized fragments in hand, treatment of **726** with *tert*-butyl nitrite and BF<sub>3</sub>•OEt<sub>2</sub> generated the diazonium salt in situ to undergo the key intermolecular Heck reaction with **727** in the presence of a palladium catalyst. Dihydroxylation of **728** and oxidative cleavage of the resulting 1,2-diol with H<sub>5</sub>IO<sub>6</sub> formed dialdehyde intermediate **729**, which could then be liberated by heating in *m*-xylene and trapped intramolecularly by the electron-rich arene to establish the THIQ B-ring and deliver **730**. Substitution at the C1-position of **731** was then elaborated to construct the 10-membered cyclic sulfide and access the natural product based on their previous synthetic strategy. Overall, the synthetic route to **184** was successfully shortened to 28 steps (as compared to 45 steps in their previous study) and 1.1% overall yield by efficiently constructing the B-ring.

Other synthetic strategies to construct the THIQ B-ring of Et-743 (**184**) were reported in 2006, wherein Danishefsky and coworkers demonstrated a novel vinylogous Pictet–Spengler cyclization from an *ortho*-hydroxystyrene intermediate **732** (Scheme 4.80).<sup>151</sup> Treatment of **734** with DMDO then oxidized the C4 position, which produced ketone **736** as

the major product through either a concerted rearrangement or a 1,2-hydride migration from epoxide **735**. After installation of the nitrile functionality, the MOM group was cleaved to reveal their final intermediate **738**, which constituted a formal total synthesis of Et-743 (**184**).

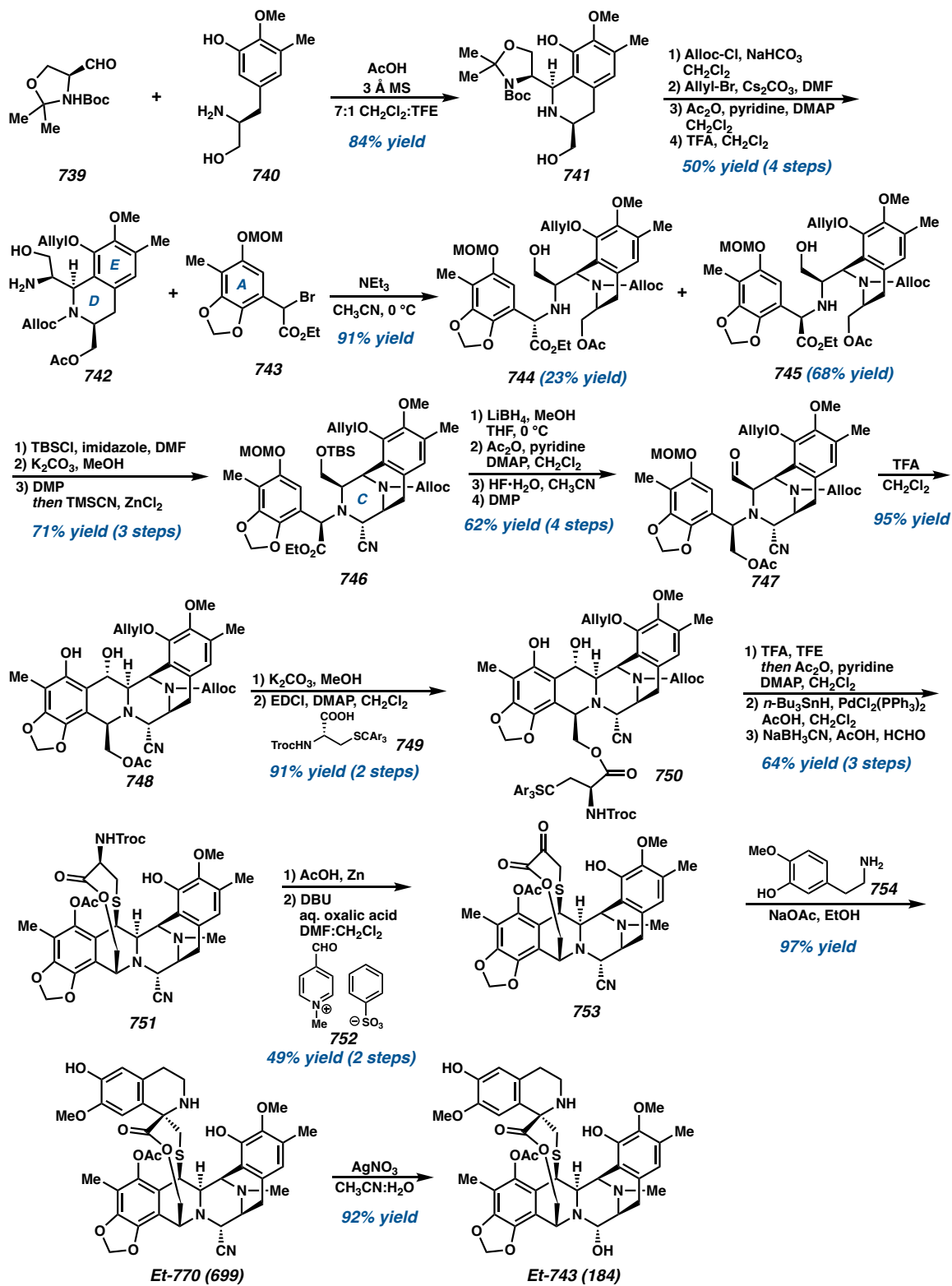
**Scheme 4.79** Fukuyama's revised total synthesis of Et-743 **184**.



**Scheme 4.80** Danishefsky's formal total synthesis of Et-743 **184**.

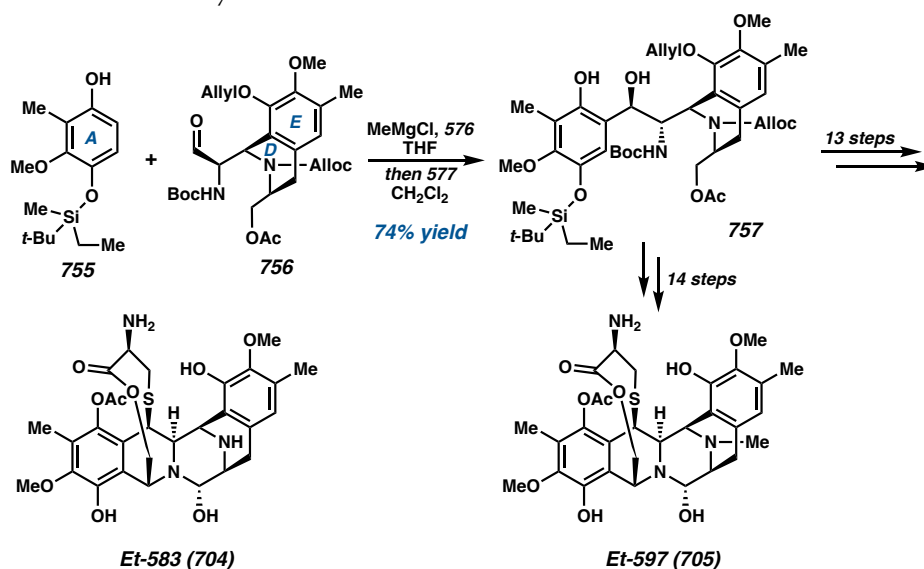
On the other hand, Zhu and coworkers reported the total synthesis of Et-743 (**184**) by retrosynthetically disconnecting the molecule into four building blocks of similar size (Scheme 4.81).<sup>152</sup> Synthesis of the D- and E-ring of **2** commenced with condensation of aldehyde **739** with phenylalaninol **740**, providing access to THIQ **741** in 84% yield as a single diastereomer. Masking the secondary amine as the *N*-allyloxycarbamate, followed by chemoselective protection of the alcohol and removal of the masked amino alcohol delivered **742**. Assembly of this key intermediate with benzyl bromide **743** under  $\text{CH}_3\text{CN}$  in the presence of triethylamine delivered two coupled products **744** and **745** that were isolated in 23% and 68% yield, respectively. The desired diastereomer **745** was carried forward to access the C-ring through a zinc chloride-catalyzed Strecker reaction that provided amino nitrile **746** as a single diastereomer.

**Scheme 4.81** Zhu's total synthesis of ecteinascidin 770 **699** and ecteinascidin 743 **184**.



After several oxidative manipulations to deliver aldehyde **747**, cyclization under acidic conditions afforded **748** with concomitant removal of the MOM-protecting group. After installing the side chain at the C1 position to deliver **750**, the 10-membered lactone bridge was installed from dissolving **750** in TFE containing 1% of TFA through in situ generation of an *ortho*-quinone methide followed by an intramolecular Michael addition to access the key C–S bond in **751**. Following Corey’s protocol, installation of the final THIQ was accomplished via oxidation to the ketoester **753** and Pictet–Spengler cyclization with **754** to provide Et-770 (**699**) in 97% yield.<sup>148a</sup> Treatment of Et-770 with AgNO<sub>3</sub> in a mixture of CH<sub>3</sub>CN and H<sub>2</sub>O provided Et-743 (**184**) in 92% yield. Within the same year, Zhu and coworkers reported a similar synthetic strategy for the total syntheses of Et-597 (**705**) and Et-583 (**704**), instead using phenol **755** to build the natural product scaffold through a sequence of aldol condensations followed by a Pictet–Spengler reaction (Scheme 4.82).<sup>153</sup>

**Scheme 4.82** Zhu’s total synthesis of ecteinascidin 597 **705** and ecteinascidin 583 **704**.



Recently, Ma and coworkers described the total synthesis of Et-743 and lurbinctedin through a convergent Pictet–Spengler coupling event of an elaborated tetrahydroisoquinoline



and tyrosine derivative **758** (Scheme 4.83).<sup>154</sup> Using the same intermediate **758** to construct both the western and eastern fragments of Et-743, a Pictet–Spengler reaction with benzyloxyacetaldehyde **759** and subsequent Boc-protection provided the western THIQ **760** in 83% overall yield. After oxidation of phenol **760** to quinone **761**, a light-mediated C–H bond functionalization using blue LED light in THF allowed cyclization to deliver benzo[1,3]dioxole **762** in 83% yield. The formation of **762** could be scaled up to a multi-decagram scale without compromising the yield.

After protection of the phenol and oxidation of **762** to the aldehyde **763**, an intermolecular Pictet–Spengler reaction with amino alcohol **758** provided cyclization product **764** as the major isomer in 67% yield. This key coupling event allowed efficient construction of the natural product scaffold to install four of the six rings in a single step. Oxidation of the hydroxymethyl group then prepared for a subsequent Strecker reaction to construct the amino nitrile **765**. With decagram quantities of the hexacyclic intermediate **765**, oxidation of the phenol with benzeneseleninic anhydride provided dihydroxy dienone **766**, which underwent elimination and macrocyclization according to Corey’s one-pot procedure to obtain lactone **767**.<sup>148a</sup> Finally, oxidation to the keto ester **753** and Pictet–Spengler reaction with phenethylamine **725** or tryptamine **768** followed by hydrolysis delivered either Et-743 (**184**) or lurbinectedin (**769**), respectively.

#### **4.6. THIQ ALKALOIDS FROM THE NAPHTHYRIDINOMYCIN FAMILY**

##### **4.6.1. GENERAL STRUCTURE AND BIOSYNTHESIS**

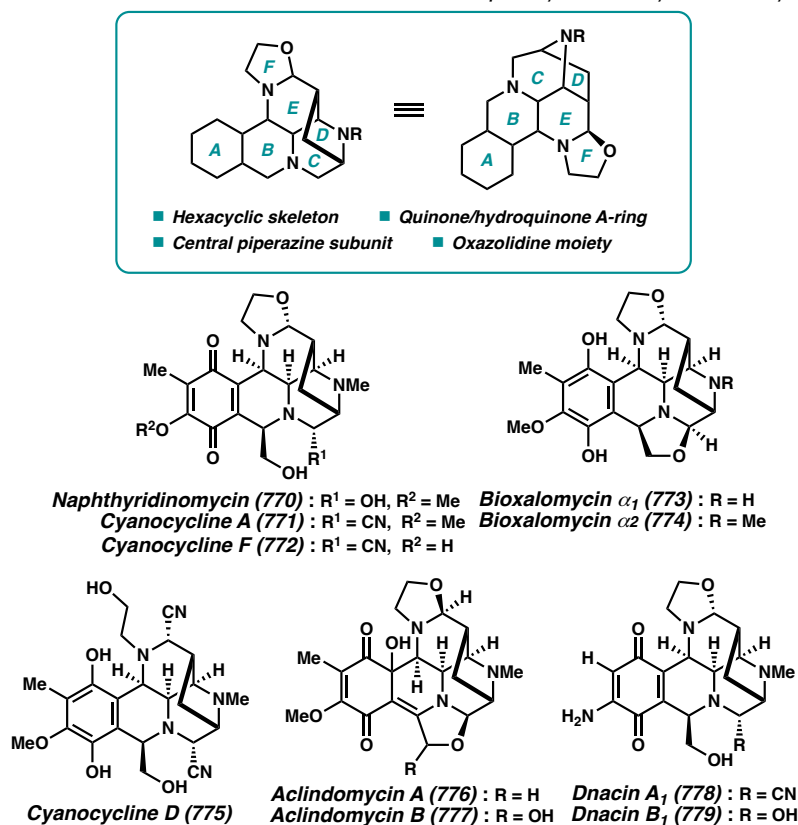
Most alkaloids from the naphthyridinomycin family possess a hexacyclic skeleton, including four six-membered rings, a five-membered bridged ring, and an oxazolidine fragment (Figure 4.24).



The A-ring can either be in the quinone or hydroquinone oxidation state. Members of this family are the naphthyridinomycin (**591**), cyanocyclines (**592–593**, **596**), bioxalomycins (**594–595**), acclidinomycins (**597–598**), and dnacins (**599–600**).

The biosynthesis of cyanocycline A was studied by Zmijewski and coworkers, where they discovered through feeding experiments that the core structure was assembled from tyrosine, methionine, glycine or serine, and ornithine.<sup>155</sup> Later in 2013, the Tang group analyzed the naphthyridinomycin gene cluster and proposed a pathway for the core formation via nonribosomal peptide synthetase (NRPS) NapL and NapJ modules.<sup>156</sup> The completed biosynthetic pathway, especially how the five-membered bridged ring is formed in the core structure, however, still have not been fully elucidated in this study.

**Figure 4.24** Core skeleton of THIQ alkaloids in the naphthyridinomycin family and examples.



#### 4.6.2. TOTAL SYNTHESIS OF NAPHTHYRIDINOMYCIN ALKALOIDS

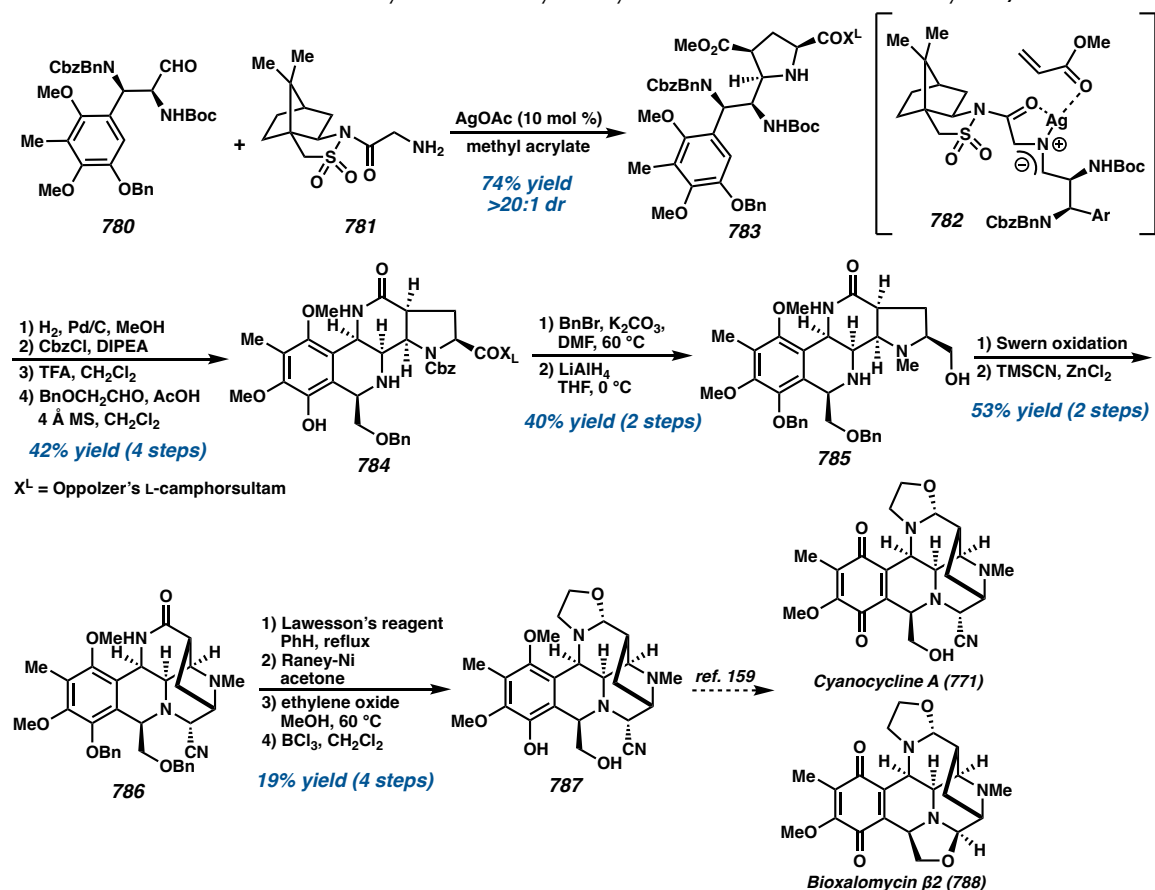
Although no recent total synthesis of the naphthyridinomycin alkaloids have been reported, several approaches for the formal synthesis of these natural products have been explored.<sup>157</sup> In 2007, Garner and coworkers disclosed an efficient synthetic approach toward the cyanocycline and bioxalomycin alkaloids harnessing their developed silver-catalyzed coupling reaction.<sup>158</sup> This key [C+NC+CC] coupling reaction provided rapid access to highly functionalized pyrrolidines which could be converted to the target in one-third of the total number of steps than previously reported total syntheses.

The key coupling reaction was effected by combining aldehyde **780** and Oppolzer's camphorsultam **781** in methyl acrylate solvent with 10 mol% AgOAc (Scheme 4.84). The [3+2] cycloaddition was proposed to proceed through a pre-TS model such as **782**, in which the acrylate dipolarophile approaches the ylide from the least hindered *endo-si* face approach. The *endo*-selective asymmetric coupling allowed the construction of pyrrolidine **783** as a single diastereomer.

To construct the rest of the natural product scaffold, **783** was subjected to hydrogenolysis to construct the lactam, and removal of the Boc group followed by a Pictet–Spengler reaction with benzyloxyacetaldehyde produced THIQ **784**. After protection of the phenol, reduction with LiAlH<sub>4</sub> released the chiral auxiliary and converted the carbamate to the required *N*-methyl group. Oxidation of the primary alcohol **785** allowed construction of the diazobicyclo[3.2.1]octane core followed by cyanide addition to deliver **786**. Finally, the oxazolidine ring was constructed from reduction of **786** to the imine that was reacted with hot ethylene oxide in MeOH to afford the late-stage intermediate **787**, a late-stage Fukuyama intermediate that was two steps away from the synthesis of cyanocycline A **771**.<sup>159</sup>

Bioxalomycin  $\beta$ 2 was known to be convertible from **771**, demonstrating a formal synthesis of this natural product as well. Overall, the successful application of the asymmetric Ag-catalyzed coupling reaction to install functionalized pyrrolidines allowed a rapid approach to this family of natural products.

**Scheme 4.84** Garner's formal synthesis of cyanocycline A **771** and bioxalomycin  $\beta$ 2 **788**.



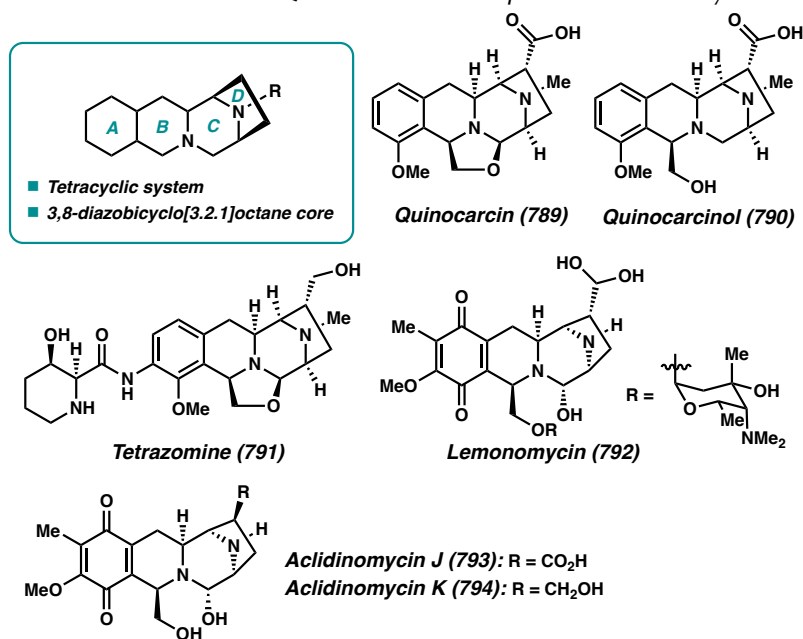
## 4.7. THIQ ALKALOIDS FROM THE QUINOCARCIN FAMILY

### 4.7.1. GENERAL STRUCTURE AND BIOSYNTHESIS

The quinocarcin family of THIQ alkaloids comprise quinocarcin **789**, quinocarcinol **790**, tetrazomine **791**, lemomycin **792**, and acclidinomyins J–K (**793–794**).<sup>160</sup> These compounds are structurally similar, sharing a piperizinohydroisoquinoline motif, as well as

a 3,8-diazobicyclo[3.2.1]octane core (Figure 4.25). Quinocarcin and tetrazomine possess an additional oxazolidine ring, while lemomycin contains a 2,6-dideoxy-4-amino sugar (lemonose) that is rarely found in nature. Compounds within the quinocarcin family display varying levels of antitumor and antibiotic properties. In particular, quinocarcin has exhibited potent antitumor activity against a variety of tumor cell lines and its citrate salt (KW2152) had been in clinical trials in Japan.<sup>161</sup>

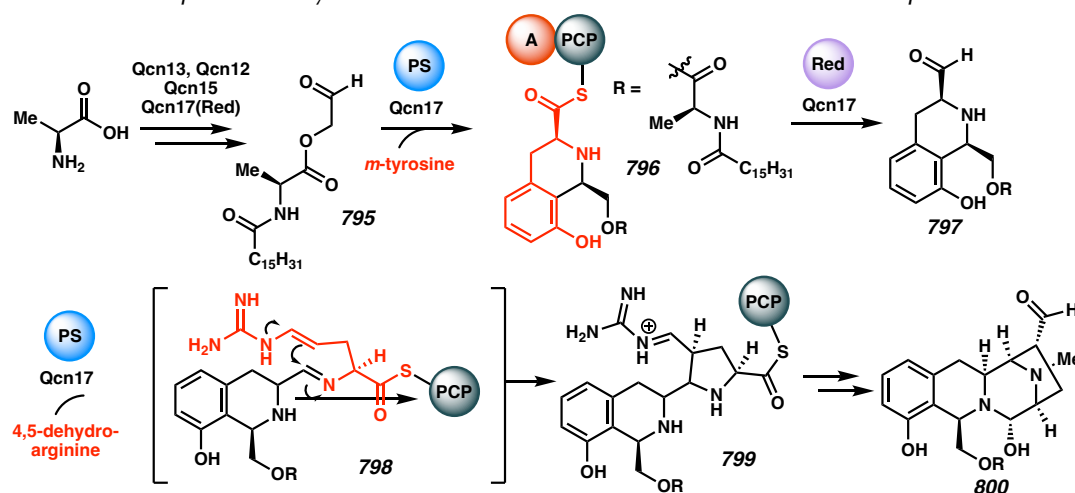
**Figure 4.25** General skeleton of THIQ alkaloids in the quinocarcin family.



In 2013, Oikawa and coworkers identified and analyzed the biosynthetic gene cluster (BGC) of quinocarcin and proposed its core assembly mechanism.<sup>162</sup> There are five modules (Qcn12, 13, 15, 17, and 19) for quinocarcin non-ribosomal peptide synthetase (NRPS). Of these five modules, Qcn 17 and Qcn 19 are the two responsible for key C–C bond formations. Particularly for Qcn17 which contains Pictet–Spengler (PS) and reduction (RE) domains, this module is SfmC-like and promotes successive Pictet–Spengler/Mannich cyclizations to generate pyrrolidine-substituted tetra-hydroisoquinoline intermediate **799** (Scheme 4.85).

The reductive release of this species affords an aldehyde, which spontaneously undergoes an intramolecular cyclization to furnish the C-ring of the quinocarcin scaffold (**800**). In addition to the quinocarcin biosynthetic core assembly mechanism, this study also investigated the biosynthetic pathway for SF-1739, which is a member of the naphthyridinomycin family of THIQ alkaloids. The authors concluded that the mechanisms for the core assembly of these THIQ-pyrrolidine alkaloids are essentially the same but start from amino acids with different substitution patterns on the aromatic portion.

**Scheme 4.85** Proposed biosynthetic mechanism for the construction of the quinocarcin core.



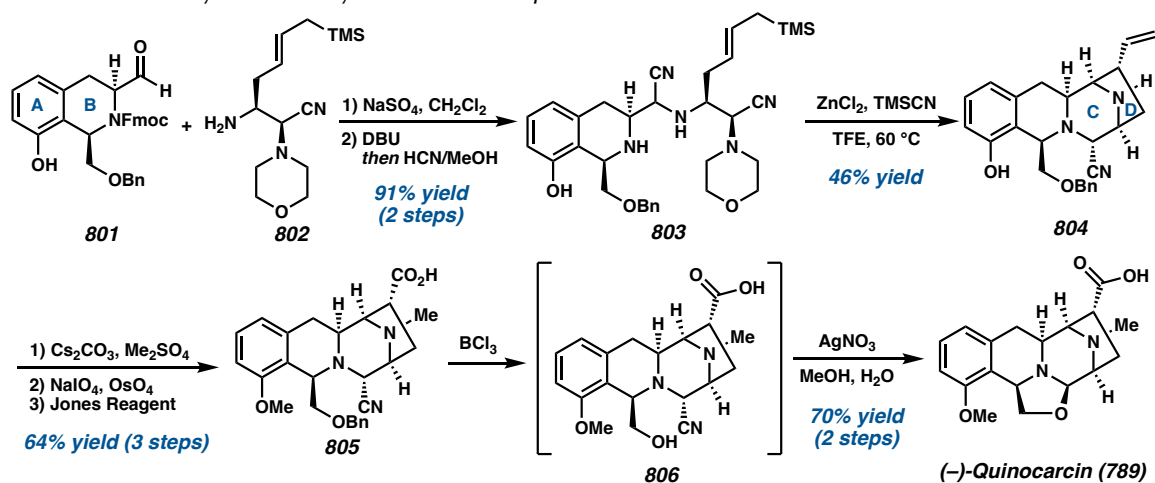
#### 4.7.2. TOTAL SYNTHESIS OF QUINOCARCIN ALKALOIDS

Toward the synthesis of (–)-quinocarcin (**789**), Myers and coworkers designed an extended approach of a previous strategy used by their lab to prepare (–)-saframycin A, involving a directed condensation of *C*- and *N*-protected  $\alpha$ -amino aldehydes.<sup>163</sup> *N*-protected  $\alpha$ -amino aldehyde **801**, comprising the A- and B-rings of the target, and *C*-protected  $\alpha$ -amino aldehyde **802** were subjected to condensation (Scheme 4.86). Without isolation, the product was treated with DBU to cleave the Fmoc group, then addition of methanolic HCN provided Strecker addition product **803**. Treatment of **803** with trimethylsilyl cyanide and ZnCl<sub>2</sub> in

TFE resulted in the cyclization of the C- and D-rings, forming the tetracyclic core **804**.

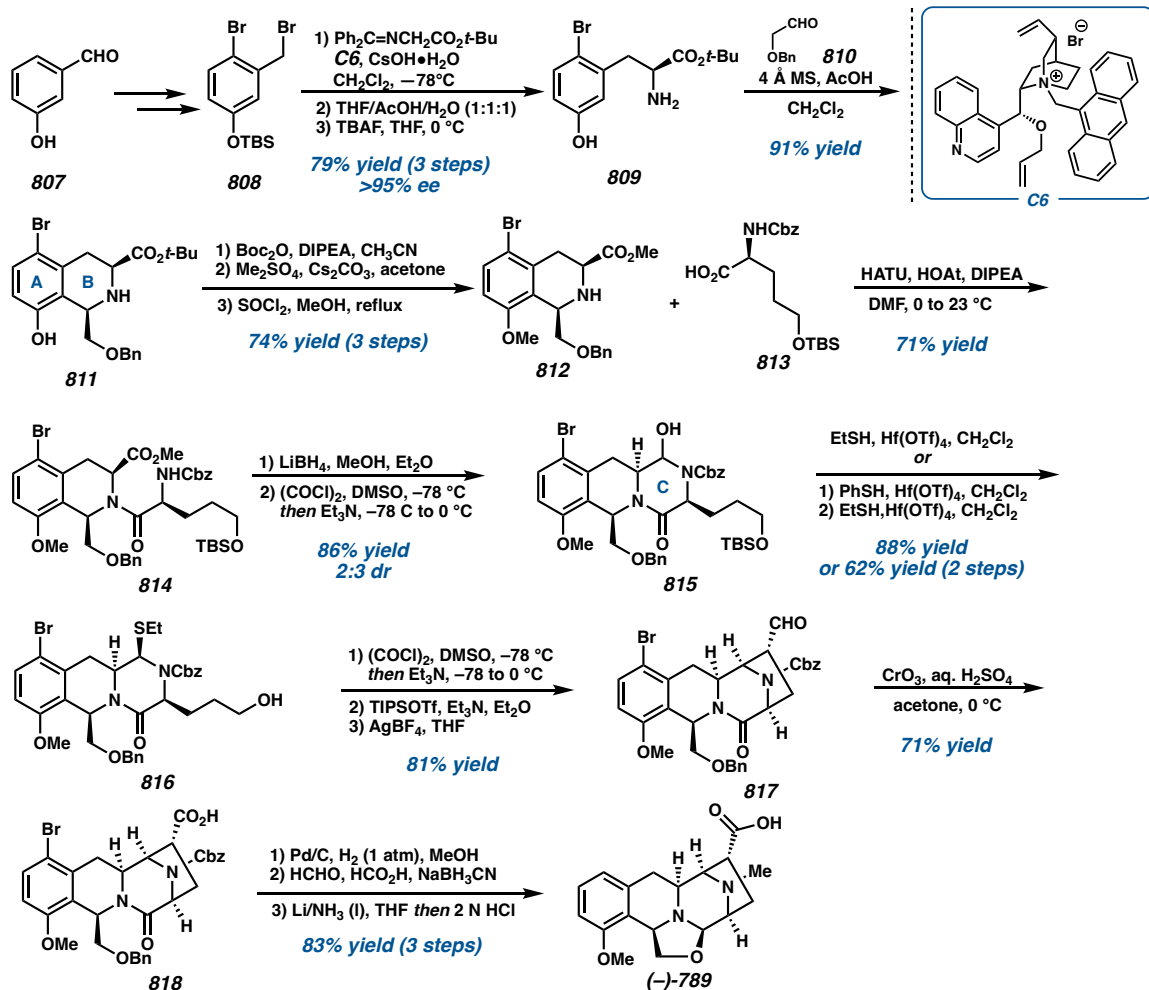
Bismethylation, followed by oxidative cleavage of the olefinic side chain and Jones oxidation furnished acid **805**. Debenzylation in  $\text{BCl}_3$  produced quinocarcin and its uncyclized precursor (DX-52-1) **806**, and treatment with silver nitrate in aqueous methanol converted the mixture entirely to yield (–)-quinocarcin (**789**).

**Scheme 4.86** Myers' total synthesis of (–)-quinocarcin **789**.



In 2008, Zhu and coworkers reported the synthesis of (–)-quinocarcin through sequential ring cyclizations, and construction of the bridged bicycle by an intramolecular Mannich reaction using  $\text{AgBF}_4$ .<sup>164</sup> Selected as the A-ring scaffold, 3-hydroxybenzaldehyde **807** was converted to benzyl bromide **808** (Scheme 4.87). In the presence of Corey–Lygo's phase-transfer catalyst (O-(9)-allyl-N-(9'-anthracenylmethyl) cinchonidium bromide **C6**, **808** was used to alkylate *N*-(diphenylmethylene) glycine *tert*-butyl ester to produce **809** with >95% ee. A Pictet–Spengler reaction of ester **809** with benzoxyacetaldehyde **810** provided tetrahydroisoquinoline **811**, comprising the A- and B-rings. Amine **812** was subsequently acylated with **813** to form THIQ **814**. The ester moiety was selectively reduced before Swern oxidation to afford tricyclic hemiaminal **815** as a mixture of diastereomers.



**Scheme 4.87** Zhu's total synthesis of (-)-quinocarcin **789**.

**815** was then converted to amino thioether **816** in the presence of EtSH and Hf(OTf)<sub>4</sub>.

The undesired diastereomer was recycled in the presence of PhSH and Hf(OTf)<sub>4</sub>, before subjecting the resulting compound to the previous thioether forming conditions again. A chemoselective Swern oxidation, silyl enol ether formation, and intramolecular Mannich reaction in the presence of silver tetrafluoroborate, an activator of the electrophile and nucleophile, led to a 5-*endo*-trig cyclization to furnish tetracyclic compound **817** with an *exo*-oriented aldehyde moiety. Jones oxidation of **817** followed by global deprotection, *N*-

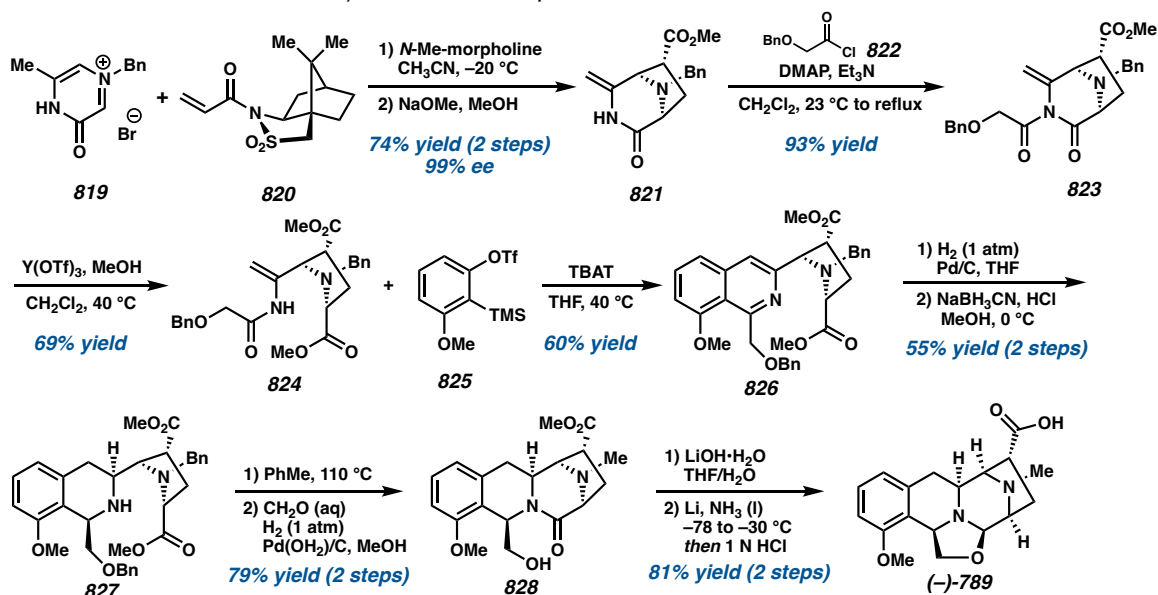
methylation, partial lactam reduction, and ring closure under acidic conditions produced (–)-quinocarcin (**789**).

Harnessing a different approach toward the synthesis of (–)-quinocarcin, Stoltz and coworkers demonstrate the use of an aryne annulation reaction to assemble an isoquinoline precursor toward the THIQ moiety.<sup>165</sup> Drawing from the synthetic strategy used by their group to synthesize (–)-lemonomycin (*vide infra*), Stoltz and coworkers began with the cyclization of a deprotonated oxidopyrazinium bromide **819** with the acrylamide of Oppolzer's sultam **820** to deliver **821** with 99% ee (Scheme 4.88). Basic methanolysis on the desired diastereomeric product, followed by acylation with benzyloxyacetyl chloride **822** produced imide **823**. Regioselective methanolysis at the lactam carbonyl was conducted with yttrium(III) triflate to produce enamine **824**. The enamine and aryne precursor **825** were combined in the presence of tetra-*n*-butylammonium difluorotriphenylsilicate (TBAT) to generate isoquinoline **826**. Two consecutive reductions produced separable THIQs, with desired diastereomer **827** as the major product obtained in 55% yield over two steps. After condensation to form the lactam, Pearlman's catalyst was used to remove the two benzyl groups and methylate the unmasked amine to afford **828**. Saponification of methyl ester **828**, followed by partial reduction of the lactam and treatment of the resulting hemiaminal with a protic source resulted in ring closure to form the oxazolidine ring and afford (–)-quinocarcin (**789**).

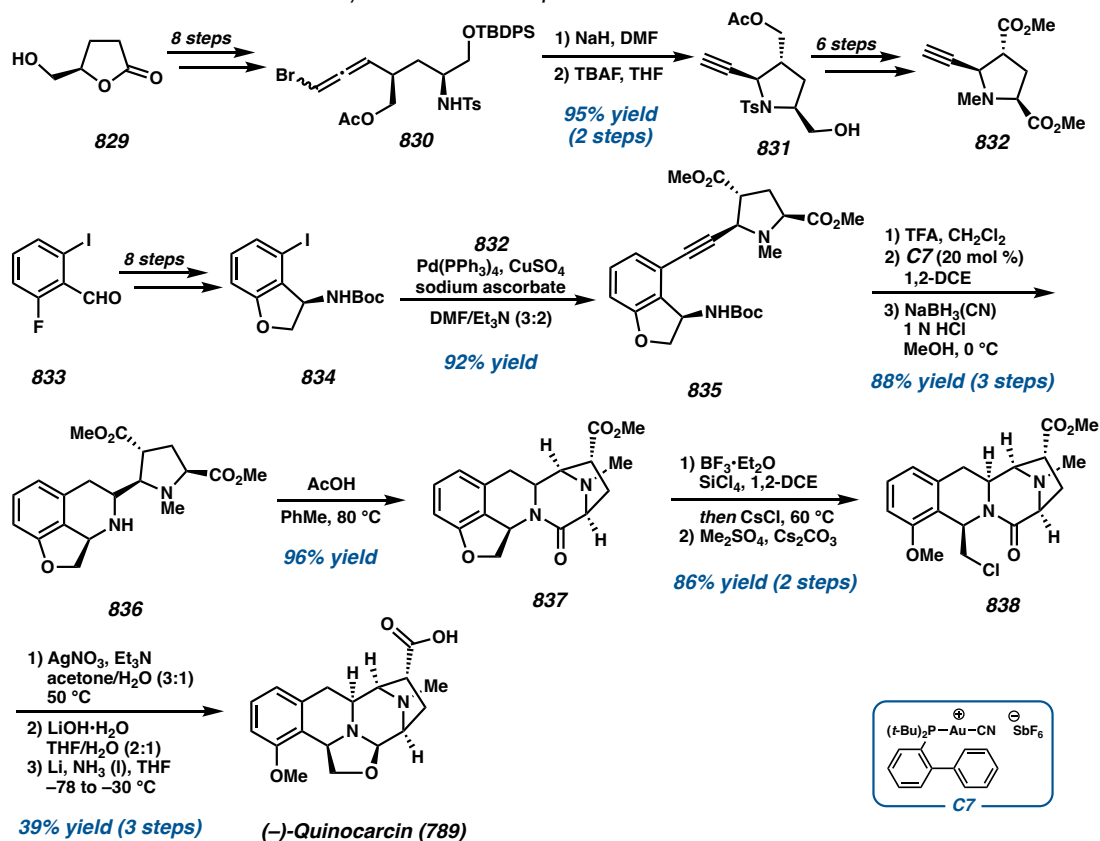
In a convergent approach toward the quinocarcin core, Ohno and coworkers employed a Sonogashira coupling and Au(I)-catalyzed intramolecular alkyne hydroamination to construct the scaffold of the THIQ core.<sup>166</sup> Bromoallene **830** was

constructed from  $\gamma$ -butyrolactone **829** and treated with NaH to provide 2,5-*cis*-pyrrolidine **831** (Scheme 4.89). Further transformation produced pyrrolidine **832**.

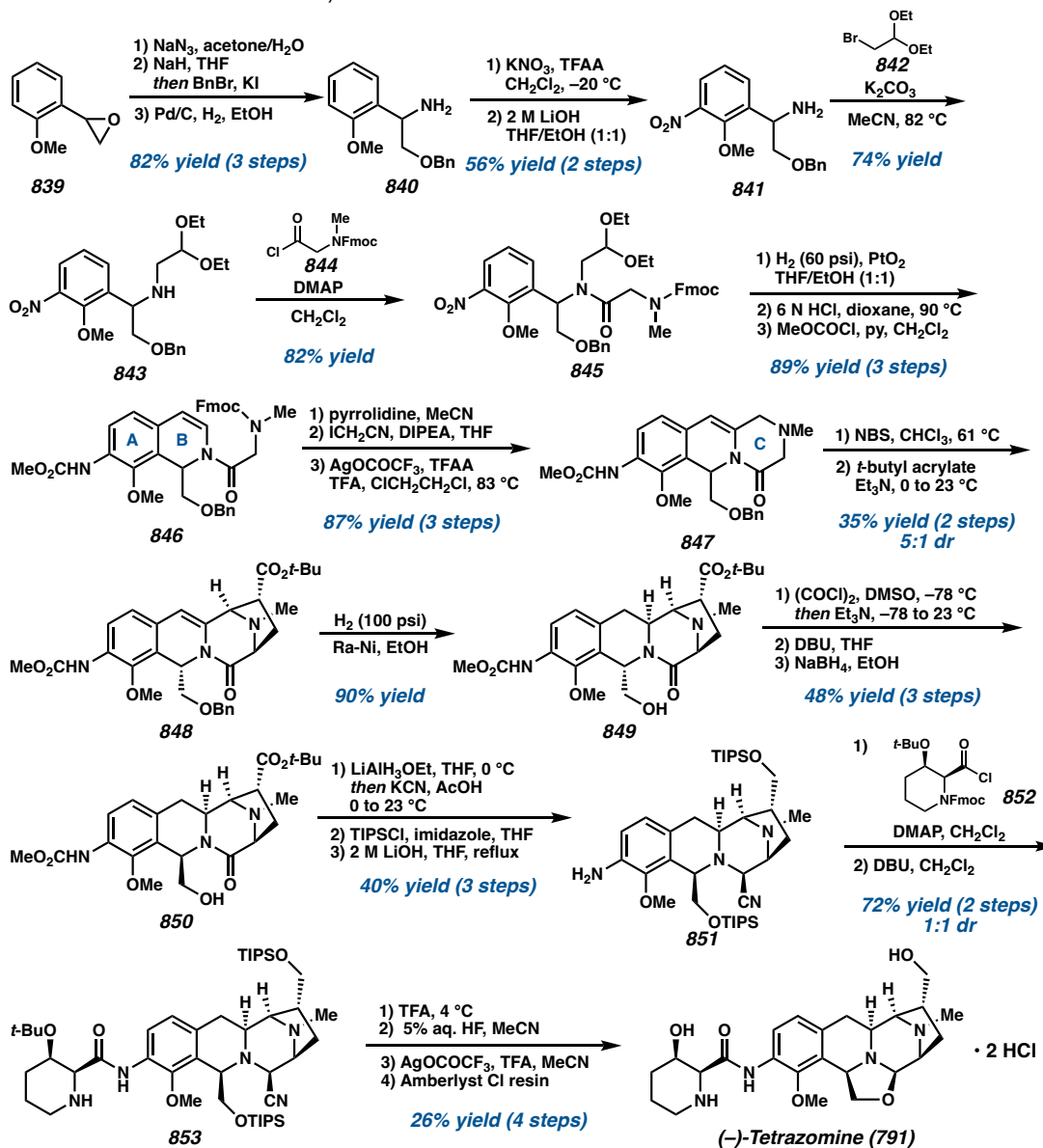
**Scheme 4.88** Stoltz's total synthesis of (–)-quinocarcin **789**.



Enantioenriched dihydrobenzofuran **834** was prepared from aryl iodide **833**. A Sonogashira reaction was then utilized to couple building blocks **832** and **834** to produce coupled product **835**. The Boc group was removed prior to Au(I)-catalyzed 6-*endo*-dig hydroamination using gold catalyst **C7** to form the B-ring of the THIQ. Due to the instability of the enamine generated, the product was directly reduced with NaBH<sub>3</sub>CN without isolation to form secondary amine **836**. Upon heating amine **836** in AcOH, condensation of the amine with one of the esters formed the diazobicyclo[3.2.1]octane core of intermediate **837**. Treatment of **837** with CsCl enabled ring-opening of the dihydrobenzofuran moiety and subsequent methylation of the phenol generated compound **838**. The alkyl halide was finally converted to the alcohol before cyclization to achieve (–)-**789**.

**Scheme 4.89** Ohno's total synthesis of (–)-quinocarcin **789**.**4.7.3. TOTAL SYNTHESIS OF TETRAZOMINE**

In 2002, Williams and coworkers utilized a [1,3]-dipolar cycloaddition in the synthesis of antitumor antibiotic (–)-tetrazomine **791** and its analogues (Scheme 4.90).<sup>167</sup> Starting with the ring-opening of aryl epoxide **839** using sodium azide, the resulting alcohol was protected and the azide was hydrogenated to afford amine **840**. A nitro group was then installed *ortho* to the pre-existing methoxy group and subsequent hydrolysis of the trifluoroacetamide furnished primary amine **841**. Alkylation of the amine with bromoacetaldehyde diethylacetal **842** provided secondary amine **843**, which was acylated with **844** to produce amide **845**. The nitro group was hydrogenated using PtO<sub>2</sub>, and the resulting aniline underwent acid-promoted cyclization to yield dihydroisoquinoline **846**.

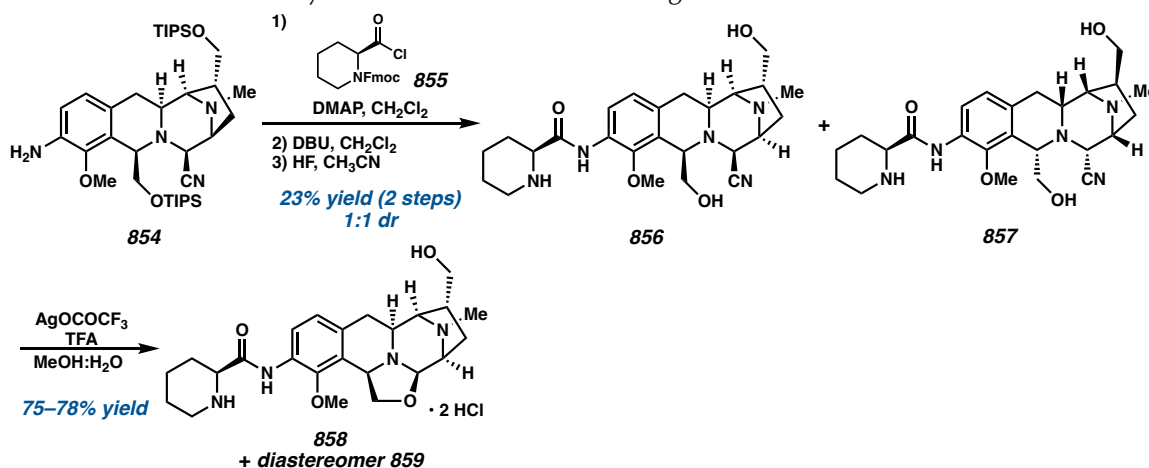
**Scheme 4.90** Williams' total synthesis of (-)-tetrazomine **791**.

Cyclization of amine **846** then proceeded by treatment with  $\text{Ag(I)}$ trifluoroacetate in the presence of TFA and TFAA to deliver allylic amine **847** through a speculated *6-exo-tet* process. The amine **847** was then refluxed in chloroform with NBS to yield an iminium species that was treated with triethylamine and *tert*-butyl acrylate, producing ester **848** with 5:1 dr. Hydrogenation afforded **849**, while the undesired diastereomer was epimerized and hydrogenated to produce the same product. Swern oxidation and treatment with DBU

produced epimerized compound **850**. Subsequent reduction followed by trapping of the resulting carbinolamine afforded the aminonitrile moiety. TIPS protection of the two primary alcohols followed by hydrolysis of the methyl carbamate afforded aniline **851**. Acid chloride **852** was prepared in three steps and coupled with aniline **851** in the presence of DMAP. Subsequent cleavage of the Fmoc group with DBU afforded **853** with 1:1 dr, which were isolable and carried on separately. Treatment of aminonitrile **853** with silver trifluoroacetate induced cyclization to form the oxazolidine ring, and addition of Amberlyst ion-exchange resin (Cl<sup>-</sup> form) followed by filtration and lyophilization afforded tetrazomine **791**. The other diastereomer of **853** was treated to the same steps to afford *ent, epi*-tetrazomine **791**.

In attempts to probe the biological activity of tetrazomine and its analogues, several novel analogues were prepared as shown in Scheme 4.91. Late-stage intermediate **854** was coupled to *N*-Fmoc-L-pipecolic acid chloride **855** followed by cleavage of the Fmoc and TIPS groups to afford both diastereomers **856** and **857** with 1:1 dr. Treatment of both isomers with AgOCOCF<sub>3</sub> and TFA afforded two deoxytetrazomine analogs **858** and **859**.

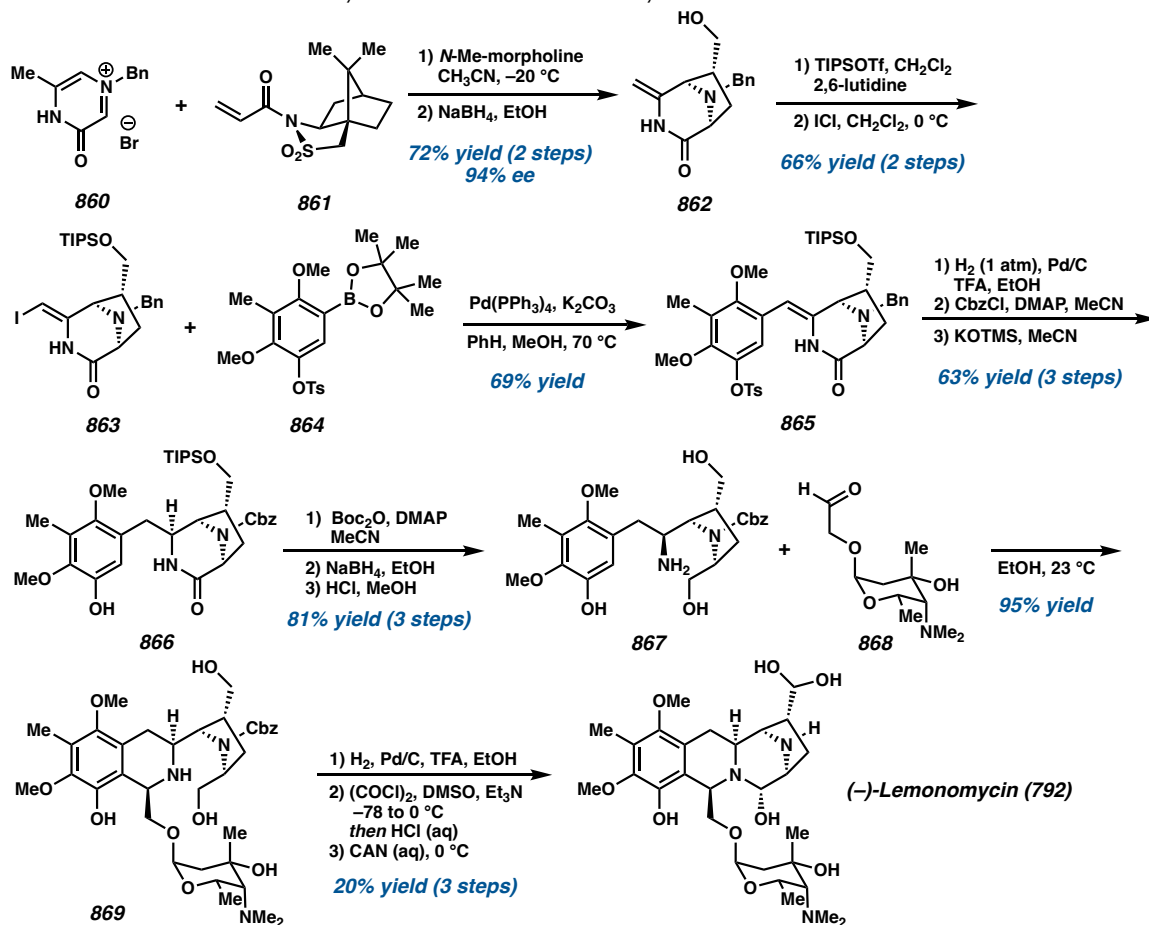
**Scheme 4.91** Williams' synthesis of tetrazomine analogues.



To examine the interaction of tetrazomine **791** and analogues **858–859** with DNA cleavage, these compounds were incubated with a synthetic  $^{32}\text{P}$ -5'-end-labeled 45 bp duplex at pH 7 in phosphate buffer. While some analogues did not exhibit any DNA damage, tetrazomine **791** did display DNA cleavage in a non-sequence-specific manner. Additionally, all four oxazolidine and aminonitrile analogues were assayed against a Gram-(+) bacteria (*Staphylococcus aureus*) and a Gram-(-) bacteria (*Klebsiella pneumoniae*) via the disk diffusion method. Interestingly, deoxy compounds **858** and **859** displayed slightly better activity than either tetrazomine **791** or *ent, epi*-tetrazomine.

#### 4.7.4. TOTAL SYNTHESIS OF LEMONOMYCIN

While there have been reports toward the formal synthesis of lemomycin,<sup>168</sup> Stoltz and coworkers demonstrated a total synthesis of (-)-lemonomycin employing a stereoselective dipolar cycloaddition and diastereoselective Pictet–Spengler cyclization to form the tetracyclic compound.<sup>169</sup> Cyclization of deprotonated bromide salt **860** with Oppolzer's sultam-derived acrylamide **861** provided bicycle **862** with high ee (Scheme 4.92). Enamide **862** was then converted to a silyl ether and treated with ICI to produce *Z*-iodoenamide **863**. Suzuki coupling with aryl boronic ester **864** provided aryl enamide **865** and subsequent hydrogenation and protection of the amine and phenol produced amide **866**. Aminotriol **867** was accessed in three steps with 81% overall yield from simultaneous activation of the amide and protection of the phenol with  $\text{Boc}_2\text{O}$ , reduction with  $\text{NaBH}_4$ , and cleavage of the Boc and TIPS moieties using methanolic HCl. Aldehyde **868** was separately prepared in eight steps (not shown) for Pictet–Spengler reaction with aminotriol **867** to deliver THIQ **869**. Hydrogenolytic cleavage of the Cbz group, Swern oxidation, and treatment with CAN ultimately provided (-)-lemonomycin **792**.

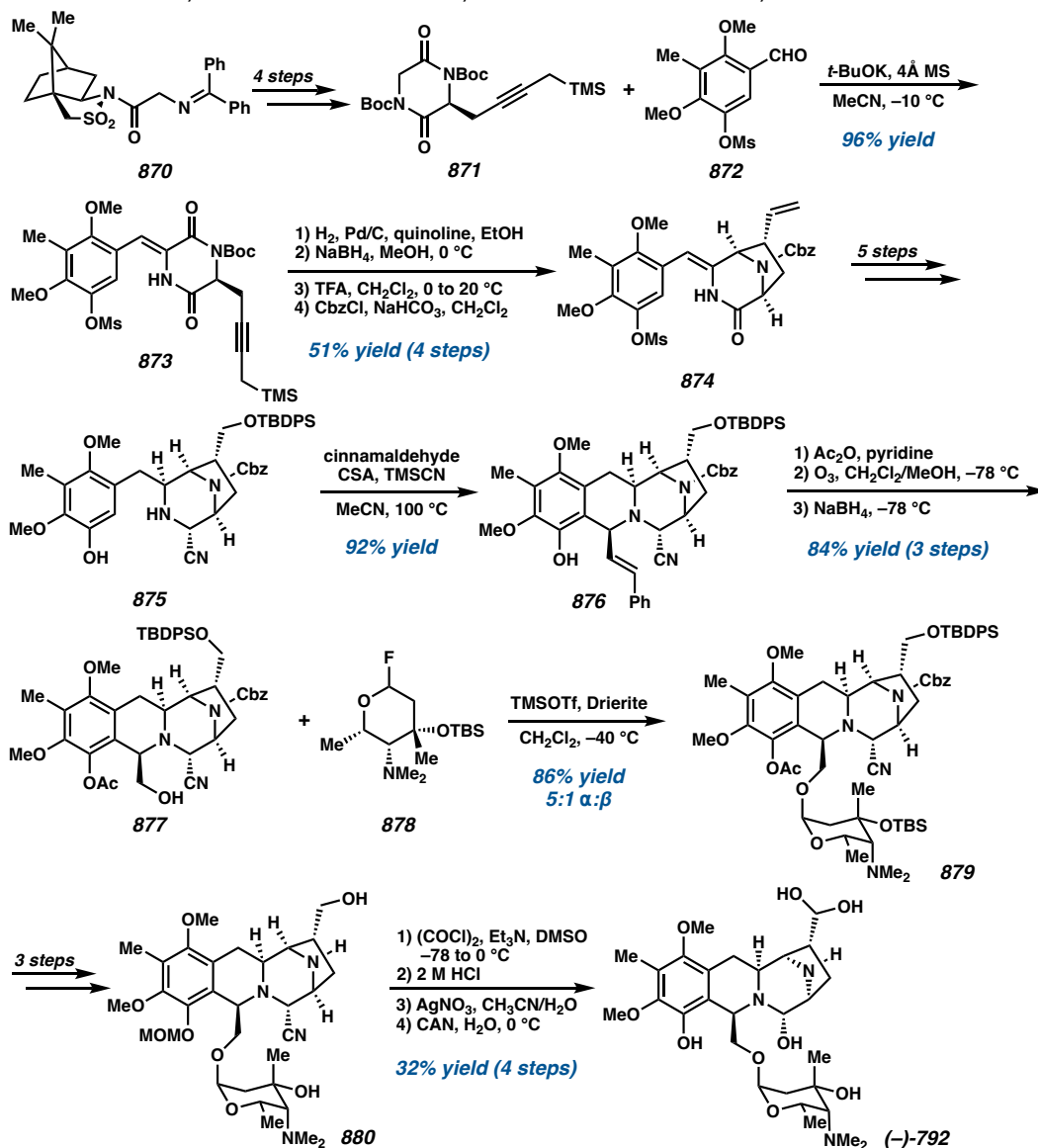
**Scheme 4.92** Stoltz's total synthesis of (–)-lemonomycin **792**.

Toward the synthesis of (–)-lemonomycin, Fukuyama and Kan and coworkers chose to couple the lemonose unit with the tetracyclic aglycon alkaloid subunit through a glycosidation reaction.<sup>170</sup> Oppolzer's chiral auxiliary **870** was transformed to diketopiperazine **871** in four steps (Scheme 4.93). Diketopiperazine **871** was subjected to a Perkin condensation reaction with **872** to give *Z*-enamide **873**, which was reduced and treated with TFA to produce cyclized product **874**. Following several functional group transformations, the B-ring was constructed through a Pictet–Spengler reaction of **875** with cinnamaldehyde in the presence of CSA and TMSCN at 100 °C to deliver THIQ **876**. A one-pot conversion of **876** to aglycon alkaloid **877** was achieved through acetylation of the phenol



group, ozonolysis, and subsequent reduction. Key intermediate **877** was coupled with functionalized lemonose **878** by treatment with TMSOTf and Drierite at  $-40\text{ }^{\circ}\text{C}$  to deliver **879**. After several functional group manipulations, exposure of primary alcohol **880** to Swern oxidation produced the geminal diol, and hemiaminal installation followed by CAN-mediated oxidation of the A-ring produced (–)-lemonomycin **792**.

**Scheme 4.93** Fukuyama and Kan's total synthesis of (–)-lemonomycin **792**.



#### 4.8 CONCLUSIONS

The THIQ natural products are one of the most prominent family of alkaloids that exhibit a diverse range of biological activity as well as structural complexity. It is noteworthy that from simple benzyl THIQ alkaloids to complex ecteinascidin THIQ natural products, all possess interesting biological properties and reactivity that are of great interest to synthetic, biological, and medicinal chemists. From 2002–2020, research in the total synthesis of THIQ alkaloids has advanced greatly, especially in the development of novel methodologies that enable creative synthetic approaches to these molecules. Not only do these modern chemical methods allow efficient chemical syntheses, but they also provide access to a library of natural product analogues to uncover more of their biological activity.

Their challenging molecular architecture along with their important therapeutic effects will surely continue to drive research to develop novel reactions toward their chemical syntheses and uncover new biosynthetic pathways. As of yet, there are still several families of natural products of which their biosynthesis is not fully understood, and the chemical syntheses of some THIQ alkaloids have not yet been explored. Thus, this review hopefully serves as a guide for the recent developments in THIQ alkaloid chemistry, and also addresses some of the remaining challenges in the synthesis of this family of natural products for further medicinal and biological advancement.

#### 4.9 REFERENCES AND NOTES

- (1) Phillipson, J. D.; Roberts, M. F.; Zenk, M. H. *The Chemistry and Biology of Isoquinoline Alkaloids*; Springer, 1985.

- (2) Chrzanowska, M.; Grajewska, A.; Rozwadowska, M. D. *Chem. Rev.* **2016**, *116*, 12369–12465.
- (3) Scott, J. D.; Williams, R. M. *Chem. Rev.* **2002**, *102*, 1669–1730.
- (4) Cassels, B. K. *Nat. Prod. Commun.* **2019**, *14*, 85–90.
- (5) Fahmy, N. M.; Al-Sayed, E.; El-Shazly, M.; Singab, A. N. *Nat. Prod. Res.* **2020**, *34*, 1891–1912.
- (6) a) Barton, D. H. R.; James, R.; Kirby, G. W.; Widdowson, D. A. *Chem. Commun.* **1967**, 266–268; b) Maier, U. H.; Rödl, W.; Deus-Neumann, B.; Zenk, M. H. *Phytochemistry* **1999**, *52*, 373–382.
- (7) a) Zhang, F.; Simpkins, N. S.; Blake, A. J. *Org. Biomol. Chem.* **2009**, *7*, 1963–1979; b) Tietze, L. F.; Tölle, N.; Kratzert, D.; Stalke, D. *Org. Lett.* **2009**, *11*, 5230–5233; c) Mostowicz, D.; Dygas, M.; Kałuża, Z. *J. Org. Chem.* **2015**, *80*, 1957–1963; d) Blackham, E. E.; Booker-Milburn, K. I. *Angew. Chem. Int. Ed.* **2017**, *56*, 6613–6616; e) Luu, H.-T.; Streuff, J. *Eur. J. Org. Chem.* **2019**, 139–149.
- (8) a) Yasui, Y.; Koga, Y.; Suzuki, K.; Matsumoto, T. *Synlett.* **2004**, *4*, 615–618; b) Yasui, Y.; Suzuki, K.; Matsumoto, T. *Synlett.* **2004**, *4*, 619–622; c) Umihara, H.; Yoshino, T.; Shimokawa, J.; Kitamura, M.; Fukuyama, T. *Angew. Chem. Int. Ed.* **2016**, *55*, 6915–6918.
- (9) Padwa, A.; Wang, Q. *J. Org. Chem.* **2006**, *71*, 7391–7402.
- (10) For formal asymmetric syntheses of 3-Demethoxyerythratidinone **208** and **213**, see:  
a) Allin, S. M.; Streetley, G. B.; Slater, M.; James, S. L.; Martin, W. P. *Tetrahedron Lett.* **2004**, *45*, 5493–5496; b) Moon, J. T.; Jung, J. A.; Ha, S. H.; Song, S. H.; Park,

- S. J.; Kim, J.; Choo, D. J.; Lee, Y. S.; Lee, J. Y. *Synth. Commun.* **2011**, *41*, 1282–1292.
- (11) Zhang, F.; Simpkins, N. S.; Wilson, C. *Tetrahedron Lett.* **2007**, *48*, 5942–5947.
- (12) Chuang, K. V.; Navarro, R.; Reisman, S. E. *Chem. Sci.* **2011**, *2*, 1086–1089.
- (13) Paladino, M.; Zaifman, J.; Ciufolini, M. A. *Org. Lett.* **2015**, *17*, 3422–3425.
- (14) Mostowicz, D.; Dygas, M.; Kaluza, Z. *J. Org. Chem.* **2015**, *80*, 1957–1963.
- (15) O'Connor, S. E. Alkaloid Biosynthesis. *Wiley Encycl. Chem. Biol.* **2008**, 1–16.
- (16) Shamma, M.; Slusarchyk, W. A. *Chem. Rev.* **1964**, *64*, 59–79.
- (17) Wang, F.-X.; Zhu, N.; Zhou, F.; Lin, D.-X. *Molecules* **2021**, *26*, 6117–6139.
- (18) Morris, J. S.; Facchini, P. J. *J. Biol. Chem.* **2016**, *291*, 23416–23427.
- (19) Cuny, G. D. *Tetrahedron Lett.* **2004**, *45*, 5167–5170.
- (20) For other syntheses of the aporphine alkaloids, see: a) Lafrance, M.; Blaquièrre, N.; Fagnou, K. *Chem. Commun.* **2004**, 2874–2875; b) Nimgirawath, S.; Udomputtimekakul, P.; Pongphuttichai, S.; Wanbanjob, A.; Taechowisan, T. *Molecules*. **2008**, *13*, 2935–2947; c) Zhong, M.; Jiang, Y.; Chen, Y.; Yan, Q.; Liu, J.; Di, D. *Tetrahedron: Asymmetry*. **2015**, *26*, 1145–1149; d) Pieper, P.; McHugh, E.; Amaral, M.; Tempone, A. G.; Anderson, E. A. *Tetrahedron*. **2020**, *76*, 130814–130821.
- (21) Anakabe, E.; Carrillo, L.; Badía, D.; Vicario, J. L.; Villegas, M. *Synthesis* **2004**, *7*, 1093–1101.
- (22) Fürstner, A.; Mamane, V. *Chem. Commun.* **2003**, 2112–2113.
- (23) Percim, G. P.; Rodrigues, A.; Raminelli, C. A. *Tetrahedron Lett.* **2015**, *56*, 6848–6851.

- (24) a) Rossini, A. F. C.; Muraca, A. C. A.; Casagrande, G. A.; Raminelli, C. *J. Org. Chem.* **2015**, *80*, 10033–10040; b) Perecim, G. P.; Deflon, V. M.; Martins, G. R.; Pinto, L. M. C.; Casagrande, G. A.; Oliveira-Silva, D.; Raminelli, C. *Tetrahedron* **2020**, *76*, 131461–131468.
- (25) Nimgirawath, S.; Udomputtimekakul, P. *Molecules* **2009**, *14*, 917–924.
- (26) a) Ku, A. F.; Cuny, G. D. *Org. Lett.* **2015**, *17*, 1134–1137; b) Ku, A. F.; Cuny, G. D. *J. Org. Chem.* **2016**, *81*, 10062–10070.
- (27) Honda, T.; Shigehisa, H. *Org. Lett.* **2006**, *8*, 657–659.
- (28) Magnus, P.; Marks, K. D.; Meis, A. *Tetrahedron* **2015**, *71*, 3872–3877.
- (29) a) Yoshida, K.; Fujino, Y.; Takamatsu, Y.; Matsui, K.; Ogura, A.; Fukami, Y.; Kitagaki, S.; Takao, K. *Org. Lett.* **2018**, *20*, 5044–5047; b) Yoshida, K.; Itatsu, Y.; Fujino, Y.; Inoue, H.; Takao, K. *Angew. Chem. Int. Ed.* **2016**, *55*, 6734–6738.
- (30) Lafrance, M.; Blaquiere, N.; Fagnou, K. *Eur. J. Org. Chem.* **2017**, 811–825.
- (31) Payne, J. T.; Valentic, T. R.; Smolke, C. D. *Proc. Natl. Acad. Sci. U.S.A.* **2021**, *118*, 1–12.
- (32) a) Blank, N.; Opatz, T. *J. Org. Chem.* **2011**, *76*, 9777–9784; b) Otto, N.; Ferenc, D.; Opatz, T. *J. Org. Chem.* **2017**, *82*, 1205–1217.
- (33) Schütz, R.; Meixner, M.; Antes, I.; Bracher, F. *Org. Biomol. Chem.* **2020**, *18*, 3047–3068.
- (34) Wang, Y.-C.; Georghiou, P. E. *Org. Lett.* **2002**, *4*, 2675–2678.
- (35) a) Kawabata, Y.; Naito, Y.; Saitoh, T.; Kawa, K.; Fuchigami, T.; Nishiyama, S. *Eur. J. Org. Chem.* **2014**, 99–104; b) Naito, Y.; Tanabe, T.; Kawabata, Y.; Ishikawa, Y.; Nishiyama, S. *Tetrahedron Lett.* **2010**, *51*, 4776–4778.

- (36) Huang, Z.; Ji, X.; Lumb, J.-P. *Org. Lett.* **2019**, *21*, 9194–9197.
- (37) Vasconcelos Leitao Da-Cunha, E.; Fecine, I. M.; Guedes, D. N.; Barbosa-Filho, J. M.; Sobral da Silva, M. Protoberberine Alkaloids. In *The Alkaloids: Chemistry and Biology*, Vol. 62; Elsevier Inc., 2005; pp 1–75.
- (38) Kutchan, T. M.; Dittrich, H. *J. Biol. Chem.* **1995**, *270*, 24475–24481.
- (39) Dewick, P. M. *Medicinal Natural Products: A Biosynthetic Approach*, 2<sup>nd</sup> ed.; John Wiley & Sons, 2002.
- (40) a) Davis, F. A.; Mohanty, P. K. *J. Org. Chem.* **2002**, *67*, 1290–1296; b) Davis, F. A.; Melamed, J. Y.; Sharik, S. S. *J. Org. Chem.* **2006**, *71*, 8761–8766.
- (41) Mastranzo, V. M.; Yuste, F.; Ortiz, B.; Sánchez-Obregón, R.; Toscano, R. A.; García Ruano, J. L. *J. Org. Chem.* **2011**, *76*, 5036–5041.
- (42) Cheng, J.; Fu, L.; Ling, C.; Yang, Y. *Heterocycles*. **2010**, *81*, 2581–2592.
- (43) Grajewska, A.; Rozwadowska, M. D. *Tetrahedron: Asymmetry* **2007**, *18*, 2910–2914.
- (44) Nguyen Le, T.; Cho, W.-J. *Bull. Korean Chem. Soc.* **2007**, *28*, 763–766.
- (45) Fukuda, T.; Iwao, M. *Heterocycles* **2007**, *74*, 701–720.
- (46) a) Chrzanowska, M.; Dreas, A.; Rozwadowska, M. D. *Tetrahedron: Asymmetry* **2004**, *15*, 1113–1120; b) Meissner, Z.; Chrzanowska, M. *Tetrahedron: Asymmetry* **2015**, *26*, 225–229.
- (47) Boudou, M.; Enders, D. *J. Org. Chem.* **2005**, *70*, 9486–9494.
- (48) Gao, S.; Cheng, J.-J.; Ling, C.-Y.; Chu, W.-J.; Yang, Y.-S. *Tetrahedron Lett.* **2014**, *55*, 4856–4859.
- (49) Gadhiya, S.; Ponnala, S.; Harding, W. W. *Tetrahedron* **2015**, *71*, 1227–1231.

- (50) Zein, A. L.; Dawe, L. N.; Georghiou, P. E. *J. Nat. Prod.* **2010**, *73*, 1427–1430.
- (51) Kayhan, J.; Wanner, M. J.; Ingemann, S.; van Maarseveen, J. H.; Hiemstra, H. *Eur. J. Org. Chem.* **2016**, 3705–3708.
- (52) Horst, B.; Wanner, M. J.; Jørgensen, S. I.; Hiemstra, H.; van Maarseveen, J. H. *J. Org. Chem.* **2018**, *83*, 15110–15117.
- (53) Pacheco, J. C. O.; Lahm, G.; Opatz, T. *J. Org. Chem.* **2013**, *78*, 4985–4992.
- (54) Stubba, D.; Lahm, G.; Geffe, M.; Runyon, J. W.; Arduengo III, A. J.; Opatz, T. *Angew. Chem. Int. Ed.* **2015**, *54*, 14187–14189.
- (55) Lahm, G.; Deichmann, J.-G.; Rauen, A. L.; Opatz, T. *J. Org. Chem.* **2015**, *80*, 2010–2016.
- (56) Gatland, A. E.; Pilgrim, B. S.; Procopiou, P. A.; Donohoe, T. J. *Angew. Chem. Int. Ed.* **2014**, *53*, 14555–14558.
- (57) Garad, D. N.; Mhaske, S. B. *Org. Lett.* **2016**, *18*, 3862–3865.
- (58) Jayakumar, J.; Cheng, C.-H. *Chem. Eur. J.* **2016**, *22*, 1800–1804.
- (59) Lerchen, A.; Knecht, T.; Koy, M.; Daniliuc, C. G.; Glorius, F. *Chem. Eur. J.* **2017**, *23*, 12149–12152.
- (60) a) Zhou, S.; Tong, R. *Chem. Eur. J.* **2016**, *22*, 7084–7089; b) Yu, J.; Zhang, Z.; Zhou, S.; Zhang, W.; Tong, R. *Org. Chem. Front.* **2018**, *5*, 242–246.
- (61) Lichman, B. R.; Lamming, E. D.; Pesnot, T.; Smith, J. M.; Hailes, H. C.; Ward, J. M. *Green Chem.* **2015**, *17*, 852–855.
- (62) Novak, B. H.; Hudlicky, T.; Reed, J. W.; Mulzer, J.; Trauner, D. *Curr. Org. Chem.* **2000**, *4*, 343–362.
- (63) Blakemore, P. R.; White, J. D. *Chem. Commun.* **2002**, 1159–1168.

- (64) Hagel, J. M.; Facchini, P. J. *Nat. Chem. Biol.* **2010**, *6*, 273–275.
- (65) Gates, M.; Tschudi, G. *J. Am. Chem. Soc.* **1952**, *74*, 1109–1110.
- (66) For recent reviews on the synthesis of morphine, see: a) Rinner, U.; Hudlicky, T. Synthesis of Morphine Alkaloids and Derivatives In *Alkaloid Synthesis. Topics in Current Chemistry*, Vol. 309; Springer, 2011; pp 33–66; b) Zezula, J.; Hudlicky, T. *Synlett* **2005**, 388–405; c) Taber, D. F.; Neubert, T. D.; Schlecht, M. F. in *Strategies and Tactics in Organic Synthesis*; Harnata, M., Ed.; Elsevier: London, 2004, Vol. 5, pp 353–389; d) Novak, B. H.; Hudlicky, T.; Reed, J. W.; Mulzer, J.; Trauner, D. *Curr. Org. Chem.* **2000**, *4*, 343–362.
- (67) a) Uchida, K.; Yokoshima, S.; Kan, T.; Fukuyama, T. *Org. Lett.* **2006**, *8*, 5311–5313; b) Uchida, K.; Yokoshima, S.; Kan, T.; Fukuyama, T. *Heterocycles* **2009**, *77*, 1219–1234; c) Koizumi, H.; Yokoshima, S.; Fukuyama, T. *Chem. Asian. J.* **2010**, *5*, 2192–2198.
- (68) Umihara, H.; Yokoshima, S.; Inoue, M.; Fukuyama, T. *Chem. Eur. J.* **2017**, *23*, 6993–6995.
- (69) Ichiki, M.; Tanimoto, H.; Miwa, S.; Saito, R.; Sato, T.; Chida, N. *Chem. Eur. J.* **2013**, *19*, 264–269.
- (70) Varin, M.; Barré, E.; Iorga, B.; Guillou, C. *Chem. Eur. J.* **2008**, *14*, 6606–6608.
- (71) Chu, S.; Münster, N.; Balan, T.; Smith, M. D. *Angew. Chem. Int. Ed.* **2016**, *55*, 14306–14309.
- (72) Zhang, Q.; Zhang, F.-M.; Zhang, C.-S.; Liu, S.-Z.; Tian, J.-M.; Wang, S.-H.; Zhang, X.-M.; Tu, Y.-Q. *Nat. Commun.* **2019**, *10*, 2507–2513.



- (73) Kimishima, A.; Umihara, H.; Mizoguchi, A.; Yokoshima, S.; Fukuyama, T. *Org. Lett.* **2014**, *16*, 6244–6247.
- (74) Park, K.-H.; Chen, D. Y.-K. *Chem. Commun.* **2018**, *54*, 13018–13021.
- (75) Park, K.-H.; Chen, R.; Chen, D. Y.-K. *Chem. Sci.* **2017**, *8*, 7031–7037.
- (76) Geffe, M.; Opatz, T. *Org. Lett.* **2014**, *16*, 5282–5285.
- (77) a) Lipp, A.; Ferenc, D.; Gütz, C.; Geffe, M.; Vierengel, N.; Schollmeyer, D.; Schäfer, H. J.; Waldvogel, S. R.; Opatz, T. *Angew. Chem. Int. Ed.* **2018**, *57*, 11055–11059; b) Lipp, A.; Selt, M.; Ferenc, D.; Schollmeyer, D.; Waldvogel, S. R.; Opatz, T. *Org. Lett.* **2019**, *21*, 1828–1831.
- (78) Makarova, M.; Endoma-Arias, M. A. A.; Dela Paz, H. E.; Simionescu, R.; Hudlicky, T. *J. Am. Chem. Soc.* **2019**, *141*, 10883–10904.
- (79) Li, Q.; Zhang, H. *Chem. Eur. J.* **2015**, *21*, 16379–16382.
- (80) Dongbang, S.; Pedersen, B.; Ellman, J. A. *Chem. Sci.* **2019**, *10*, 535–541.
- (81) Wang, Y.; Hennig, A.; Küttler, T.; Hahn, C.; Jäger, A.; Metz, P. *Org. Lett.* **2020**, *22*, 3145–3148.
- (82) Gözler, B.; Lantz, M. S.; Shamma, M. *J. Nat. Prod.* **1983**, *46*, 293–309.
- (83) Gee, K. R.; Barnettler, P.; Rhodes, M. R.; McBurney, R. N.; Reddy, N. L.; Hu, L.-Y. R.; Cotter, E.; Hamilton, P. N.; Weber, E.; Keana, J. F. W. *J. Med. Chem.* **1993**, *36*, 1938–1946.
- (84) Brown, D. W.; Dyke, S. F.; Hardy, G.; Sainsbury, M. *Tetrahedron Lett.* **1969**, *19*, 1515–1517.
- (85) Dyke, S. F.; Ellis, A. C. *Tetrahedron* **1971**, *27*, 3803–3809.

- (86) Torres, M. A.; Hoffarth, E.; Eugenio, L.; Savtchouk, J.; Chen, X.; Morris, J. S.; Facchini, P. J.; Ng, K. K.-S. *J. Biol. Chem.* **2016**, *291*, 23403–23415.
- (87) Youte, J.-J.; Barbier, D.; Al-Mourabit, A.; Gnecco, D.; Marazano, C. *J. Org. Chem.* **2004**, *69*, 2737–2740.
- (88) Nishigaichi, Y.; Ohmuro, Y.; Hori, Y.; Ohtani, T. *Chem. Lett.* **2020**, *49*, 118–120.
- (89) Sun, L.; Li, D.; Zhou, X.; Zhang, D.; Wang, J.; He, Z.; Jiang, R.; Chen, W. *J. Org. Chem.* **2017**, *82*, 12899–12907.
- (90) a) Tambar, U. K.; Ebner, D. C.; Stoltz, B. M. *J. Am. Chem. Soc.* **2006**, *128*, 11752–11753; b) Krishnan, S.; Bagdanoff, J. T.; Ebner, D. C.; Ramtohul, Y. K.; Tambar, U. K.; Stoltz, B. M. *J. Am. Chem. Soc.* **2008**, *130*, 13745–13754
- (91) Sunderhaus, J. D.; Dockendorff, C.; Martin, S. F. *Org. Lett.* **2007**, *9*, 4223–4226.
- (92) Miura, Y.; Saito, Y.; Goto, M.; Nakagawa-Goto, K.; *Chem. Pharm. Bull.* **2020**, *68*, 899–902.
- (93) Takahashi, K.; Kubo, A. *J. Antibiot.* **1977**, *30*, 1015–1018.
- (94) a) Mikami, Y.; Takahashi, K.; Yazawa, K.; Hour-Young, C.; Arai, T.; Saito, N.; Kubo, A. *J. Antibiot.* **1988**, *41*, 734–740; b) Lown, J. W.; Hanstock, C. C.; Joshua, A. V.; Arai, T.; Takahashi, K. *J. Antibiot.* **1983**, *36*, 1184–1194.
- (95) Irschik, H.; Trowitzsch-Kienast, W.; Gerth, K.; Hofle, G.; Reichenbach, H. *J. Antibiot.* **1988**, *41*, 993–998.
- (96) Yazawa, K.; Takahashi, K.; Mikami, Y.; Arai, T.; Saito, N.; Kubo, A. *J. Antibiot.* **1986**, *39*, 1639–1650.
- (97) Lown, J. W.; Joshua, A. V.; Lee, J. S. *Biochemistry* **1982**, *21*, 419–428.

- (98) Mikami, Y.; Takahashi, K.; Yazawa, K.; Arai, T.; Namikoshi, M.; Iwasaki, S.; Okuda, S. *J. Biol. Chem.* **1985**, *260*, 344–348.
- (99) Li, L.; Deng, W.; Song, J.; Ding, W.; Zhao, Q.-F; Peng, C.; Song, W.-W; Tang, G.-L; Liu, W. *J. Bacteriol.* **2008**, *190*, 251–263.
- (100) a) Koketsu, K.; Watanabe, K.; Suda, H.; Oguri, H.; Oikawa, H. *Nat. Chem. Biol.* **2010**, *6*, 408–410; b) Koketsu, K.; Minami, A.; Watanabe, K.; Oguri, H.; Oikawa, H. *Curr. Opin. Chem. Biol.* **2012**, *16*, 142–149.
- (101) Song, L.-Q.; Zhang, Y.-Y.; Pu, J.-Y.; Tang, M.-C.; Peng, C.; Tang, G.-L. *Angew. Chem. Int. Ed.* **2017**, *56*, 9116–9120.
- (102) Dong, W.; Liu, W.; Liao, X.; Guan, B.; Chen, S.; Liu, Z. *J. Org. Chem.* **2011**, *76*, 5363–5368.
- (103) Vincent, G.; Lane, J. W.; Williams, R. M. *Tet. Lett.* **2007**, *48*, 3719–3722.
- (104) Martinez, E. J.; Corey, E. J. *Org. Lett.* **2000**, *2*, 993–996.
- (105) Kimura, S.; Saito, N. *Tetrahedron* **2018**, *74*, 4504–4514.
- (106) a) Saito, N.; Kimura, S.; Kawai, S.; Azuma, M.; Koizumi, Y.; Yokoya, M.; Umehara, Y. *Heterocycles* **2015**, *90*, 327–343; b) Matsuo, K.; Okumura, M.; Tanaka, K. *Chem. Pharm. Bull.* **1982**, *30*, 4170–4174.
- (107) Tanifuji, R.; Koketsu, K.; Takakura, M.; Asano, R.; Minami, A.; Oikawa, H.; Oguri, H. *J. Am. Chem. Soc.* **2018**, *140*, 10705–10709.
- (108) Ikeda, Y.; Idemoto, H.; Hirayama, F.; Yamamoto, K.; Iwao, K.; Asao, T.; Munakata, T. *J. Antibiot.* **1983**, *36*, 1279–1283.

- (109) Cuevas, C.; Pérez, M.; Martín, M. J.; Chicharro, J. L.; Fernández-Rivas, C.; Flores, M.; Francesch, A.; Gallego, P.; Zarzuelo, M.; de la Calle, F.; García, J.; Polanco, C.; Rodríguez, I.; Manzanares, I. *Org. Lett.* **2000**, *2*, 2545–2548.
- (110) Velasco, A.; Acebo, P.; Gomez, A.; Schleissner, C.; Rodríguez, P.; Aparicio, T.; Conde, S.; Muñoz, R.; De La Calle, F.; Garcia, J. L.; Sánchez-Puelles, J. M. *Mol. Microbiol.* **2005**, *56*, 144–154.
- (111) Zhang, Y.-Y.; Shao, N.; Wen, W.-H.; Tang, G.-L. *Org. Lett.* **2022**, *24*, 127–131.
- (112) Saito, N.; Harada, S.; Yamashita, M.; Saito, T.; Yamaguchi, K.; Kubo, A. *Tetrahedron* **1995**, *51*, 8213–8230.
- (113) Saito, N. *Chem Pharm. Bull.* **2021**, *69*, 155–177.
- (114) For renieramycins J–O, see a) Suwanborirux, K.; Amnuoyopol, S.; Plubrukarn, A.; Pummangura, S.; Kubo, A.; Tanaka, C.; Saito, N. *J. Nat. Prod.* **2003**, *66*, 1441–1446; For renieramycins Q–S, see b) Amnuoyopol, S.; Suwanborirux, K.; Pummangura, S.; Kubo, A.; Tanaka, C.; Saito, N. *J. Nat. Prod.* **2004**, *67*, 1023–1028; For renieramycin P, see c) Oku, N.; Matsunaga, S.; van Soest, R. W. M.; Fusetani, N. *J. Nat. Prod.* **2003**, *66*, 1136–1139.
- (115) Daikuhara, N.; Tada, Y.; Yamaki, S.; Charupant, K.; Amnuoyopol, S.; Suwanborirux, K.; Saito, N. *Tet. Lett.* **2009**, *50*, 4276–4278.
- (116) Saito, N.; Yoshino, M.; Charupant, K.; Suwanborirux, K. *Heterocycles* **2012**, *84*, 309–314.
- (117) Charupant, K.; Suwanborirux, K.; Amnuoyopol, S.; Saito, E.; Kubo, A.; Saito, N. *Chem. Pharm. Bull.* **2007**, *55*, 81–86.

- (118) Tatsukawa, M.; Punzalan, L. L. C.; Magpantay, H. D. S.; Villaseñor, I. M.; Concepcion, G. P.; Suwanborirux, K.; Yokoya, M.; Saito, N. *Tetrahedron* **2012**, *68*, 7422–7428.
- (119) For fennebricins A–B, see, a) He, W.-F.; Li, Y.; Feng, M.-T.; Gavagnin, M.; Mollo, E.; Mao, S.-C.; Guo, Y.-W. *Fitoterapia* **2014**, *96*, 109–114; for fennebricins C–D, see b) Huang, R.-Y.; Chen, W.-T.; Kurtán, T.; Mándi, A.; Ding, J.; Li, J.; Li, X.-W.; Guo, Y.-W. *Future Med. Chem.* **2016**, *8*, 17–27.
- (120) Tianero, M. D.; Balaich, J. N.; Donia, M. S. *Nat. Microbiol.* **2019**, *4*, 1149–1159.
- (121) Chan, C.; Heid, R.; Zheng, S.; Guo, J.; Zhou, B.; Furuuchi, T.; Danishefsky, S. J. *J. Am. Chem. Soc.* **2005**, *127*, 4596–4598.
- (122) Vincent, G.; Williams, R. M. *Angew. Chem. Int. Ed.* **2007**, *46*, 1517–1520.
- (123) Jin, W.; Metobo, S.; Williams, R. M. *Org. Lett.* **2003**, *5*, 2095–2098.
- (124) Chen, X.; Zhu, J. *Angew. Chem. Int. Ed.* **2007**, *46*, 3962–3965.
- (125) Yokoya, M.; Ito, H.; Saito, N. *Tetrahedron* **2011**, *67*, 9185–9192.
- (126) Yokoya, M.; Kobayashi, K.; Saito, M.; Saito, N. *Marine Drugs* **2015**, *13*, 4915–4933.
- (127) Lane, J. W.; Chen, Y.; Williams, R. M. *J. Am. Chem. Soc.* **2005**, *127*, 12684–12690.
- (128) a) Magnus, P.; Matthews, K. S. *J. Am. Chem. Soc.* **2005**, *127*, 12476–12477; For a full disclosure, see b) Magnus, P.; Matthews, K. S. *Tetrahedron* **2012**, *68*, 6343–6360.
- (129) Wu, Y.-C.; Zhu, J. *Org. Lett.* **2009**, *11*, 5558–5561.
- (130) Liao, X. W.; Liu, W.; Dong, W. F.; Guan, B. H.; Chen, S. Z.; Liu, Z. Z. *Tetrahedron* **2009**, *65*, 5709–5715.

- (131) Liu, W.; Dong, W.; Liao, X.; Yan, Z.; Guan, B.; Wang, N.; Liu, Z. *Bioorg. Med. Chem. Lett.* **2011**, *21*, 1419–1421.
- (132) Liu, W.; Liao, X.; Dong, W.; Yan, Z.; Wang, N.; Liu, Z. *Tetrahedron* **2012**, *68*, 2759–2764.
- (133) Du, E.; Dong, W.; Guan, B.; Pan, X.; Yan, Z.; Li, L.; Wang, N.; Liu, Z. *Tetrahedron* **2015**, *71*, 4296–4303.
- (134) a) Yokoya, M.; Shinada-Fujino, K.; Saito, N. *Tetrahedron Letters* **2011**, *52*, 2446–2449; For a full account with slightly improved synthetic route, see: b) Yokoya, M.; Shinada-Fujino, K.; Yoshida, S.; Mimura, M.; Takada, H.; Saito, N. *Tetrahedron* **2012**, *68*, 4166–4181.
- (135) Kubo, A.; Saito, N.; Yamato, H.; Masubuchi, K.; Nakamura, M. *J. Org. Chem.* **1988**, *53*, 4295–4310.
- (136) Zheng, Y.; Li, X.-D.; Sheng, P.-Z.; Yang, H.-D.; Wei, K.; Yang, Y.-R. *Org. Lett.* **2020**, *22*, 4489–4493.
- (137) Yokoya, M.; Toyoshima, R.; Suzuki, T.; Le, V. H.; Williams, R. M.; Saito, N. *J. Org. Chem.* **2016**, *81*, 4039–4047.
- (138) He, J.; Li, S.; Deng, Y.; Fu, H.; Laforteza, B. N.; Spangler, J. E.; Homs, A.; Yu, J.-Q. *Science* **2014**, *343*, 1216–1220.
- (139) a) Fishlock, D.; Williams, R. M. *Org. Lett.* **2006**, *8*, 3299–3301; b) Fishlock, D.; Williams, R. M. *J. Org. Chem.* **2008**, *73*, 9594–9600.
- (140) Kimura, S.; Saito, N. *ChemistryOpen* **2018**, *7*, 764–771.
- (141) Jia, J.; Chen, R.; Liu, H.; Li, X.; Jia, Y.; Chen, X. *Org. Biomol. Chem.* **2016**, *14*, 7334–7344.

- (142) Rath, C. M.; Janto, B.; Earl, J.; Ahmed, A.; Hu, F. Z.; Hiller, L.; Dahlgren, M.; Kreft, R.; Yu, F.; Wolff, J. J.; Kweon, H. K.; Christiansen, M. A.; Håkansson, K.; Williams, R. M.; Ehrlich, G. D.; Sherman, D. H. *ACS Chem. Biol.* **2011**, *6*, 1244–1256.
- (143) Chen, R.; Liu, H.; Chen, X. *J. Nat. Prod.* **2013**, *76*, 1789–1795.
- (144) Welin, E. R.; Ngamnithiporn, A.; Klatté, M.; Lapointe, G.; Pototschnig, G. M.; McDermott, M. S. J.; Conklin, D.; Gilmore, C. D.; Tadross, P. M.; Haley, C. K.; Negoro, K.; Glibstrup, E.; Grünanger, C. U.; Allan, K. M.; Virgil, S. C.; Slamon, D. J.; Stoltz, B. M. *Science* **2019**, *363*, 270–275.
- (145) Cuevas, C.; Francesch, A. *Nat. Prod. Rep.* **2009**, *26*, 322–337.
- (146) Kerr, R. G.; Miranda, N. F. *J. Nat. Prod.* **1995**, *58*, 1618–1621.
- (147) Rath, C. M.; Janto, B.; Earl, J.; Ahmed, A.; Hu, F. Z.; Hiller, L.; Dahlgren, M.; Kreft, R.; Yu, F.; Wolff, J. J.; Kweon, H. K.; Christiansen, M. A.; Håkansson, K.; Williams, R. M.; Ehrlich, G. D.; Sherman, D. H. *ACS Chem. Biol.* **2011**, *6*, 1244–1256.
- (148) a) Corey, E. J.; Gin, D. Y.; Kania, R. S. *J. Am. Chem. Soc.* **1996**, *118*, 9202–9203; b) Cuevas, C.; Pérez, M.; Martín, M. J.; Chicharro, J. L.; Fernández-Rivas, C.; Flores, M.; Francesch, A.; Gallego, P.; Zarzuelo, M.; de la Calle, F.; García, J.; Polanco, C.; Rodríguez, I.; Manzanares, I. *Org. Lett.* **2000**, *2*, 2545–2548.
- (149) Endo, A.; Yanagisawa, A.; Abe, M.; Tohma, S.; Kan, T.; Fukuyama, T. *J. Am. Chem. Soc.* **2002**, *124*, 6552–6554.
- (150) Kawagishi, F.; Toma, T.; Inui, T.; Yokoshima, S.; Fukuyama, T. *J. Am. Chem. Soc.* **2013**, *135*, 13684–13687.
- (151) Zheng, S.; Chan, C.; Furuuchi, T.; Wright, B. J. D.; Zhou, B.; Guo, J.; Danishefsky, S. J. *Angew. Chem. Int. Ed.* **2006**, *45*, 1754–1759.

- (152) Chen, J.; Chen, X.; Bois-Choussy, M.; Zhu, J. *J. Am. Chem. Soc.* **2006**, *128*, 87–89.
- (153) Chen, J.; Chen, X.; Willot, M.; Zhu, J. *Angew. Chem. Int. Ed.* **2006**, *45*, 8028–8032.
- (154) He, W.; Zhang, Z.; Ma, D. *Angew. Chem. Int. Ed.* **2019**, *58*, 3972–3975.
- (155) a) Zmijewski, M. J. Jr.; Mikolajczak, M.; Viswanatha, V.; Hruby, V. J. *J. Am. Chem. Soc.* **1982**, *104*, 4969–4971; b) Zmijewski, M. J.; Palaniswamy, V. A.; Gould, S. J. *J. Chem. Soc., Chem. Commun.* **1985**, *18*, 1261–1262.
- (156) Pu, J.-Y.; Peng, C.; Tang, M.-C.; Zhang, Y.; Guo, J.-P.; Song, L.-Q.; Hua, Q.; Tang, G.-L. *Org. Lett.* **2013**, *15*, 3674–3677.
- (157) Woo, G. H. C.; Kim, S.-H.; Wipf, P. *Tetrahedron* **2006**, *62*, 10507–10517.
- (158) a) Ümit Kaniskan, H.; Garner, P. *J. Am. Chem. Soc.* **2007**, *129*, 15460–15461; b) Garner, P.; Ümit Kaniskan, H.; Keyari, C. M.; Weerasinghe, L. *J. Org. Chem.* **2011**, *76*, 5283–5294.
- (159) Fukuyama, T.; Li, L.; Laird, A. A.; Keith Frank, R. *J. Am. Chem. Soc.* **1987**, *109*, 1587–1589.
- (160) Aclidinomycins J–K were recently isolated, see: Yang, J.; Song, Y.; Tang, M.-C.; Li, M.; Deng, J.; Wong, N.-K.; Ju, J. *J. Org. Chem.* **2021**, *86*, 11107–11116.
- (161) Kanamaru, R.; Konishi, Y.; Ishioka, C.; Kakuta, H.; Sato, T.; Ishikawa, A.; Asamura, M.; Wakui, A. *Cancer Chemother. Pharmacol.* **1988**, *22*, 197–200.
- (162) Hiratsuka, T.; Koketsu, K.; Minami, A.; Kaneko, S.; Yamazaki, C.; Watanabe, K.; Oguri, H.; Oikawa, H. *Chemistry & Biology* **2013**, *20*, 1523–1535.
- (163) Kwon, S.; Myers, A. G. *J. Am. Chem. Soc.* **2005**, *127*, 16796–16797.
- (164) Wu, Y.-C.; Liron, M.; Zhu, J. *J. Am. Chem. Soc.* **2008**, *130*, 7148–7152.
- (165) Allan, K. M.; Stoltz, B. M. *J. Am. Chem. Soc.* **2008**, *130*, 17270–17271.



- (166) a) Chiba, H.; Oishi, S.; Fujii, N.; Ohno, H. *Angew. Chem. Int. Ed.* **2012**, *51*, 9169–9172; b) Chiba, H.; Sakai, Y.; Ohara, A.; Oishi, S.; Fujii, N.; Ohno, H. *Chem. Eur. J.* **2013**, *19*, 8875–8883.
- (167) Scott, J. D.; Williams, R. M. Total Synthesis of (–)-Tetrazomine. *J. Am. Chem. Soc.* **2002**, *124*, 2951–2956.
- (168) For formal synthesis of (–)-lemonomycin, see: Siengalewicz, P.; Brecker, L.; Mulzer, J. *Synlett.* **2008**, *16*, 2443–2446.
- (169) Ashley, E. R.; Cruz, E. G.; Stoltz, B. M. *J. Am. Chem. Soc.* **2003**, *125*, 15000–15001.
- (170) Yoshida, A.; Akaiwa, M.; Asakawa, T.; Hamashima, Y.; Yokoshima, S.; Fukuyama, T.; Kan, T. *Chem. Eur. J.* **2012**, *18*, 11192–11195.

## CHAPTER 5

### *Progress Toward the Total Synthesis of (+)-Cyanocycline A†*

#### 5.1 INTRODUCTION

The tetrahydroisoquinoline (THIQ) alkaloids make up one of the largest groups of natural products with a wide range of structural diversity and biological activity.<sup>1</sup> In particular, THIQ alkaloids of the naphthyridinomycin family have long served as challenging synthetic targets due to their structural complexity and significant bioactivity as antibiotic and antitumor agents (Figure 5.1).<sup>2</sup> Its congeners possess a hexacyclic carbon framework containing the THIQ core, a pyrrolidine-bridged ring, and a labile oxazolidine moiety as the F-ring. Members of this family include naphthyridinomycin (**770**), cyanocyclines (**771–772**, **775**), bioxalomycins (**773–774**), aclindomycins (**776–777**), and dnacins (**778–779**).

In 1982, cyanocycline A (**771**) was isolated from the fermentation broth of *Streptomyces flavogriseus* No. 49 that displayed significant antibiotic and antitumor activity.<sup>3</sup> Cyanocycline A (**771**) possesses a caged, hexacyclic scaffold that is characterized by the aminonitrile moiety at C(22) in place of a carbinolamine or hydroxyl functionality

---

†This research was performed in collaboration with Camila Suarez and Dr. Veronica Hubble. Early synthetic efforts were conducted by Dr. Eric Welin and Dr. Nick Hafeman.

(Figure 5.2). Cyanocycline A (771) contains eight stereocenters, five of which are contiguous stereocenters centered on the piperidine E-ring. Three basic tertiary amines, a quinone, aminonitrile, and oxazolidine moieties are particularly distinguished functionalities of cyanocycline A that render this natural product a formidable synthetic challenge.

**Figure 5.1** General skeleton of THIQ alkaloids in the naphthyridinomycin family and examples.

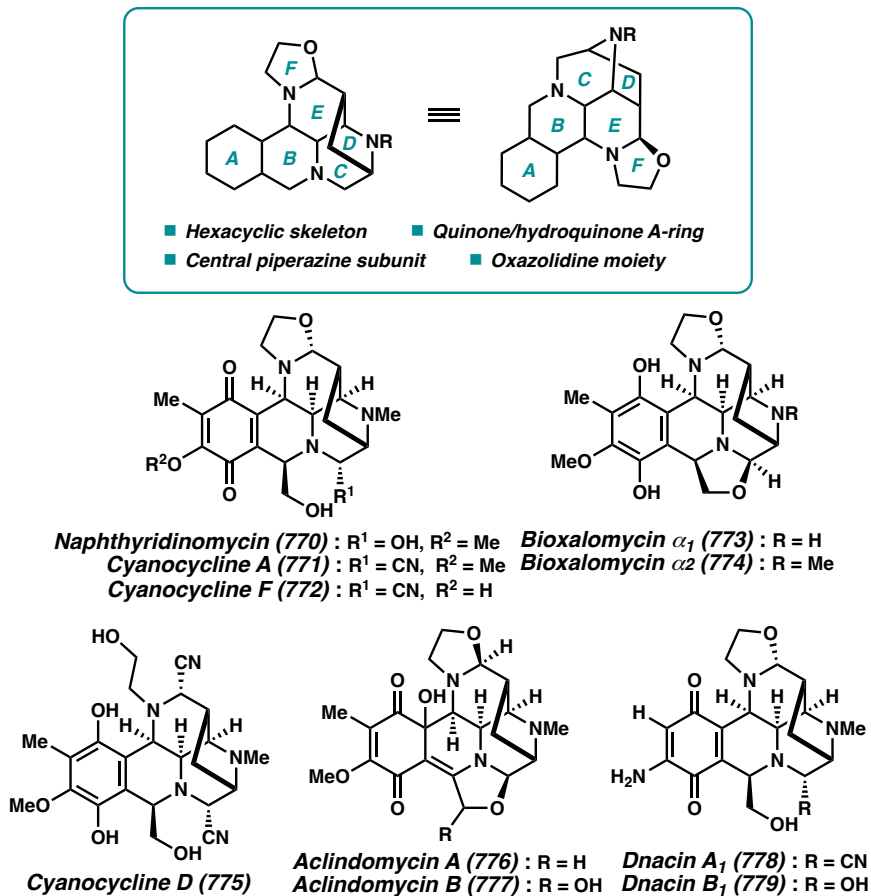
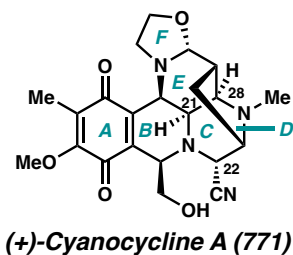


**Figure 5.2.** Structure of Cyanocycline A (771).



The biosynthesis of cyanocycline A and related congeners was studied by Zmijewski and coworkers, where they discovered through feeding experiments that the core structure was assembled from tyrosine, methionine, glycine or serine, and ornithine.<sup>4</sup> Later in 2013, the Tang group analyzed the naphthyridinomycin gene cluster and proposed a pathway for the core formation via nonribosomal peptide synthetase (NRPS) NapL and NapJ modules.<sup>5</sup> The completed biosynthetic pathway, especially how the five-membered bridged ring is formed in the core structure, however, still have not been fully elucidated in this study.

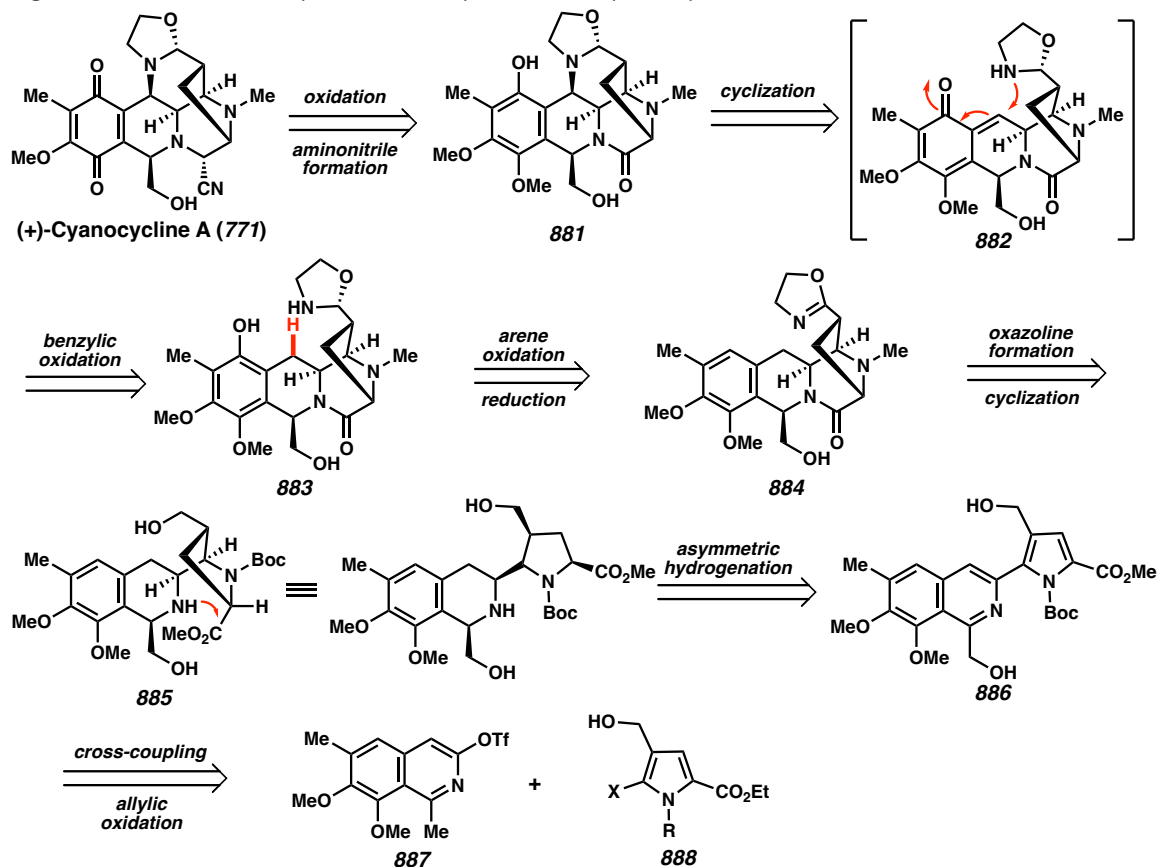
To date, only two completed syntheses of cyanocycline A have been reported by Evans and coworkers in 1986,<sup>6</sup> and Fukuyama and coworkers in 1987.<sup>7</sup> Both groups have later reported an asymmetric synthesis of (+)-cyanocycline A (**771**) utilizing a similar synthetic strategy, accomplishing the synthesis of the natural product in over 30 linear steps.<sup>8,9</sup> More recently, Garner and coworkers disclosed an efficient formal synthesis of cyanocycline A (**771**) and the bioxalomycin alkaloids harnessing their developed silver-catalyzed [C+NC+CC] coupling reaction (Scheme 4.83, *vide supra*).<sup>10</sup> Thus, the natural product scaffold was efficiently synthesized in one-third of the total number of steps than the previously reported total syntheses, constituting a formal synthesis of cyanocycline A (**771**) and bioxalomycin  $\beta$ 2 (**788**).

While these previously reported strategies pioneered the syntheses of the naphthyridinomycin alkaloids, they all feature electrophilic aromatic substitution chemistry for the construction of the THIQ core. Alternatively, we envision a novel, nonbiomimetic route to these alkaloids that could construct the natural product scaffold with high efficiency harnessing modern transition-metal catalysis.

## 5.2 RETROSYNTHETIC ANALYSIS

Inspired by our development of an asymmetric hydrogenation technology to reduce heteroaryl-substituted isoquinolines, we sought to target cyanocycline A (**771**) by a key global hydrogenation event of a pyrrole-substituted isoquinoline intermediate (Chapter 2–3, *vide supra*). To this end, our first retrosynthetic analysis accessed cyanocycline A (**771**) by oxidation of arene **881** to afford the quinone, and aminonitrile formation via partial lactam reduction and cyanide trapping (Figure 5.3). To construct the piperidine E-ring, we envision a late-stage benzylic oxidation event of phenol **883** to generate an *ortho*-quinone methide intermediate **882** in situ, enabling cyclization of the pendent oxazolidine ring to afford the hexacyclic scaffold **881**. Usage of highly reactive *ortho*-quinone methide intermediates for the construction of complex natural products have been precedented, including the total synthesis of a THIQ alkaloid Et-743 (**184**) reported by Corey and coworkers.<sup>11,12</sup>

Phenol **883** will be accessed from arene oxidation of THIQ **884**, with reduction of the oxazoline ring to deliver the oxazolidine, which we anticipate will reduce from the more sterically accessible convex face. Oxazoline formation and cyclization of the secondary amine onto the pendent methyl ester of the pyrrolidine ring in **885** then delivers **884**. THIQ **885** is then forged from a key asymmetric hydrogenation event of isoquinoline **886**, utilizing our developed hydrogenation technology to sequentially reduce both the isoquinoline and pyrrole ring that could potentially enable cyclization to the amide as well.<sup>13</sup> Finally, a cross-coupling event of two heterocyclic fragments **887** and **888** followed by allylic oxidation will afford the key hydrogenation precursor **886**.

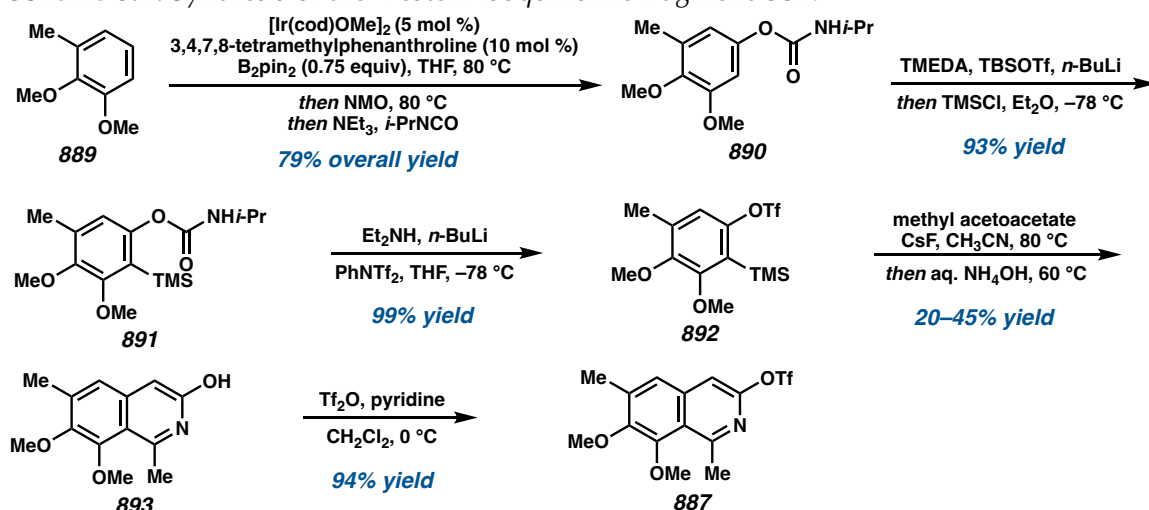
**Figure 5.3.** Initial retrosynthetic analysis of (+)-cyanocycline A (**771**).

### 5.3 FIRST GENERATION APPROACH

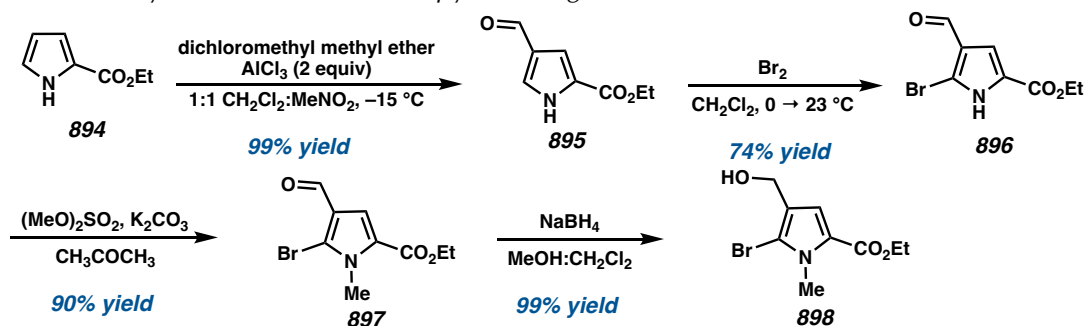
First, we focused on forging the C(21)–C(28) bond of the natural product from two heterocyclic fragments (Figure 5.2). The synthesis of the isoquinoline fragment (**887**) utilizes aryne annulation methodology extensively developed in our lab, with applications in the total synthesis of jorumycin (Scheme 5.1).<sup>14</sup> Our synthesis of isoquinoline triflate **887** began with an iridium-catalyzed borylation of 2,3-dimethoxytoluene **889**, followed by oxidation and carbamate installation to deliver arene **890** in 79% overall yield. Silylation of the arene then proceeded through a carbamoyl-directed *ortho*-metalation event with *n*-BuLi, then trapping with TMSCl to afford arene **891** in 93% yield. Next, the aryne

precursor was accessed from carbamate cleavage and triflation of the intermediary phenol to synthesize the silyl triflate **892** in 99% yield. Silyl aryl triflate **892** was then treated with cesium fluoride to generate the aryne intermediate in situ, which underwent aryne acyl-alkylation with in situ condensation to deliver 3-hydroxy-isoquinoline **893** in a range of 20–45% yield. Finally, triflation of isoquinoline **893** with trifluoromethanesulfonic anhydride provided the electrophilic coupling partner **887** in 94% yield.

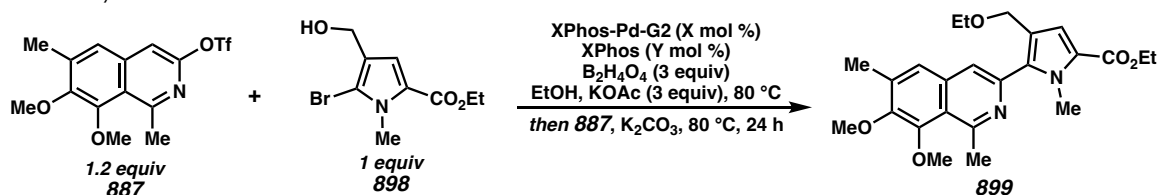
**Scheme 5.1.** Synthesis of the western isoquinoline fragment **887**.



On the other hand, synthesis of the pyrrole fragment commenced from commercially available ethyl 1H-pyrrole-2-carboxylate **894** which underwent Vilsmeier–Haack formylation to deliver C3-substituted aldehyde **895** in 99% yield (Scheme 5.2).<sup>15</sup> Treatment of **895** with  $\text{Br}_2$  installed the bromide **896** at the C2-position to serve as a functional handle for the key cross-coupling event. Then, subsequent *N*-methylation using dimethyl sulfate provided pyrrole **897** in 90% yield, which was then reduced with  $\text{NaBH}_4$  to afford alcohol **898**.<sup>16</sup>

**Scheme 5.2.** Synthesis of the eastern pyrrole fragment **898**.

With the two coupling partners in hand, we then explored the first key cross-coupling event of heterocycles **887** and **898**. We were inspired by Molander and coworkers' report on a one-pot Miyaura borylation and Suzuki cross-coupling method between aryl and heteroaryl halides, which we envisioned could be applicable to our system.<sup>17</sup> Thus, treatment of pyrrole **898** with XPhos Pd G2 catalyst, XPhos ligand, KOAc, and bis-boronic acid underwent Miyaura borylation to generate the boronic acid in situ, followed by addition of isoquinoline triflate **887** to effect a Suzuki cross-coupling event of the two heterocycles (Scheme 5.3).

**Scheme 5.3.** One-pot Pd-catalyzed borylation/Suzuki cross-coupling reaction of heterocycles **887** and **898**.

entry	conditions	results
1	X = 1 mol % Y = 2 mol %	13% yield of <b>899</b> 44% conversion of <b>887</b>
2	X = 5 mol % Y = 10 mol %	19% yield of <b>899</b> 43% protodetriflation of <b>887</b>

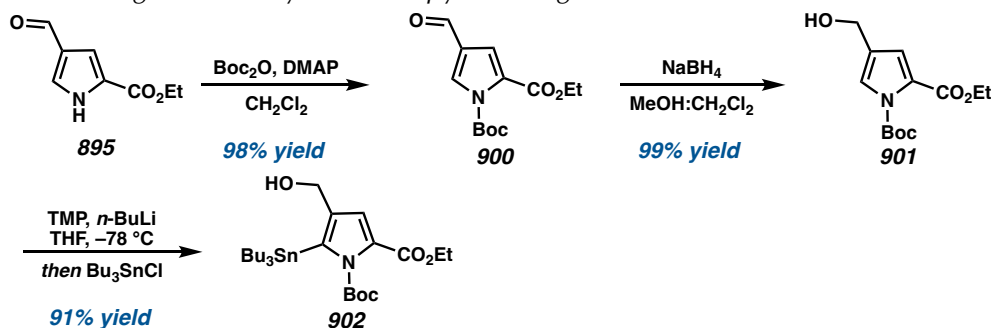
Initially, we observed that employing 1 mol % of the palladium catalyst afforded 13% yield of cross-coupled product **899**, with concomitant expulsion of the hydroxyl group



and ethanol addition to the iminium generated (entry 1). Increasing the catalyst loading to 5 mol % afforded full conversion of isoquinoline triflate **887**, but with only 19% yield of product **899** and 43% yield of protodetriflation observed (entry 2).<sup>18</sup> Thus, we turned to other cross-coupling strategies to improve the convergent coupling of the two heterocyclic fragments.

We next investigated Stille cross-coupling reactions to improve the key cross-coupling event. To this end, pyrrole **895** was protected with a Boc group instead to provide pyrrole **900** in 98% yield, followed by reduction of the aldehyde to deliver alcohol **901** in 99% yield (Scheme 5.4). Next,  $\alpha$ -lithiation of the pyrrole directed by the Boc group was performed using LiTMP, and the generated lithiated species was trapped with  $\text{Bu}_3\text{SnCl}$  to deliver the nucleophilic coupling partner **902** in 91% yield.<sup>19</sup>

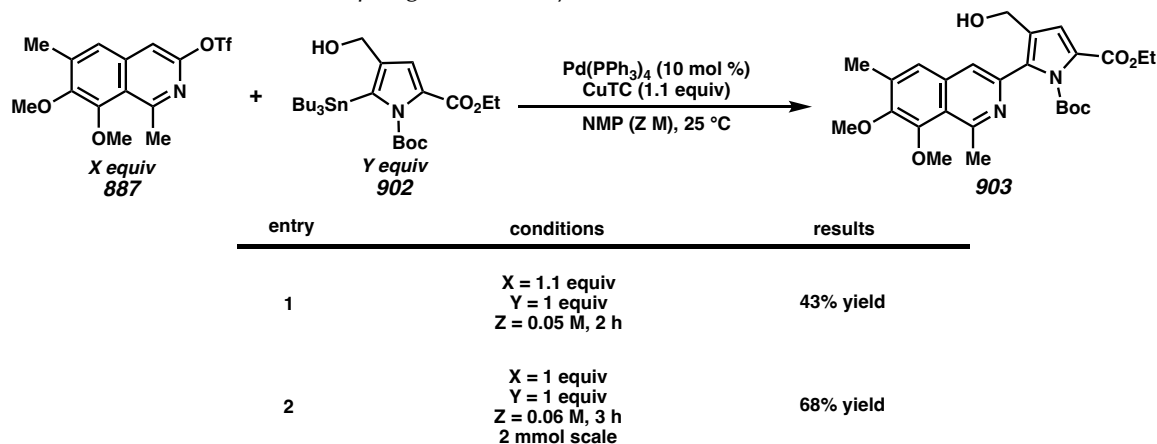
**Scheme 5.4.** 2<sup>nd</sup> generation synthesis of pyrrole fragment **902**.



With the revised pyrrole coupling partner **902**, we then explored Stille cross-coupling conditions. Gratifyingly, employing  $\text{Pd}(\text{PPh}_3)_4$  and CuTC as an additive produced the desired cross-coupled product **903** in 43% yield (Scheme 5.5, entry 1).<sup>20</sup> Further optimization of the reaction conditions using 1:1 equivalents of both partners, increased concentration, and extended reaction time improved the yield to 68% on a 2 mmol scale (entry 2). Having developed a convergent coupling reaction to access a highly

functionalized pyrrole-substituted isoquinoline **903**, we were then poised to explore our key asymmetric hydrogenation step.

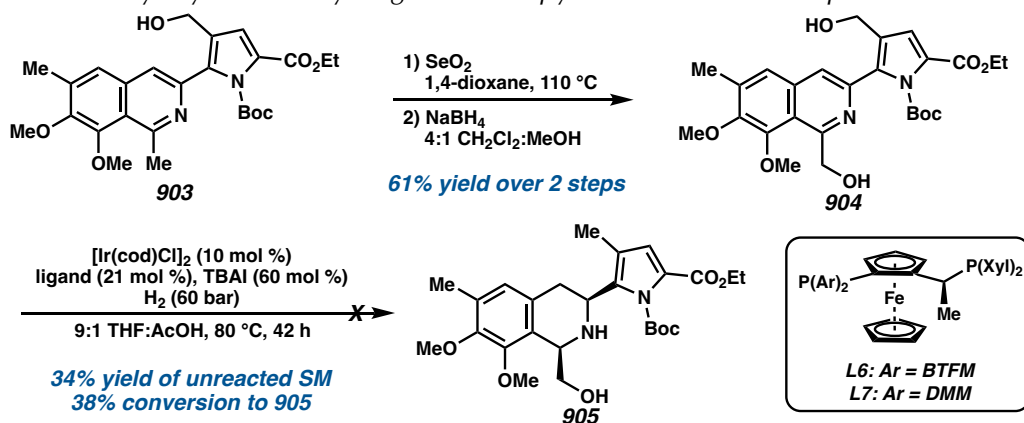
**Scheme 5.5.** Stille cross-coupling of heterocycles **887** and **902**.



We first installed the hydroxymethyl functionality at the C1 position of the isoquinoline to assist directing the asymmetric hydrogenation.<sup>13</sup> Allylic oxidation using  $\text{SeO}_2$  followed by reduction of the aldehyde intermediate with  $\text{NaBH}_4$  delivered isoquinoline **904** in 61% yield over 2 steps (Scheme 5.6). Then, we subjected isoquinoline **904** to our optimized asymmetric hydrogenation conditions using  $[\text{Ir}(\text{cod})\text{Cl}]_2$ , 4-methoxy-3,5-dimethylphenyl-substituted (DMM) Josiphos ligand **L7**, TBAI, and 60 bar of  $\text{H}_2$ . However, even after a reaction time of 42 hours at 80 °C, we mostly observed unreacted starting material, and 38% elimination of the C3-hydroxyl group on the pyrrole ring. Briefly surveying the 3,5-bis(trifluoromethyl)phenyl-substituted (BTFM) phosphine ligand **L6** optimized for the jorumycin synthesis also resulted in poor conversion of isoquinoline **904** and expulsion of the hydroxyl group. Overall, having the alcohol oxidation state at the C3-position of the pyrrole ring proved to be incompatible with our

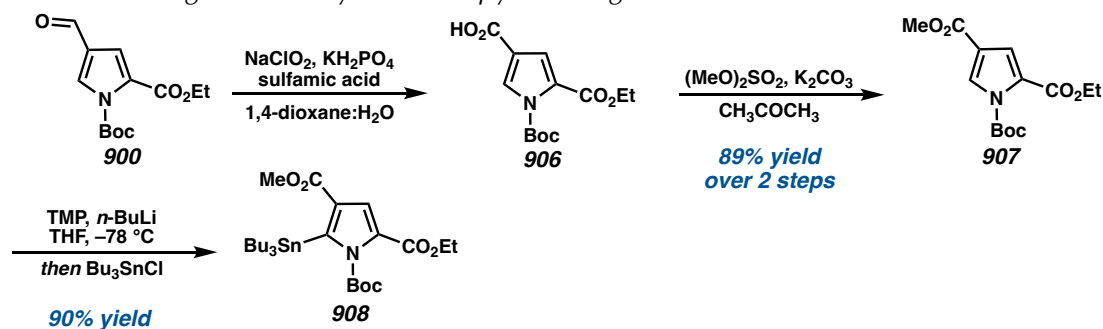
key hydrogenation reaction, prompting us to explore other functionalities that could be later utilized to install the oxazoline ring.

**Scheme 5.6.** Key asymmetric hydrogenation of pyrrole-substituted isoquinoline **903**.



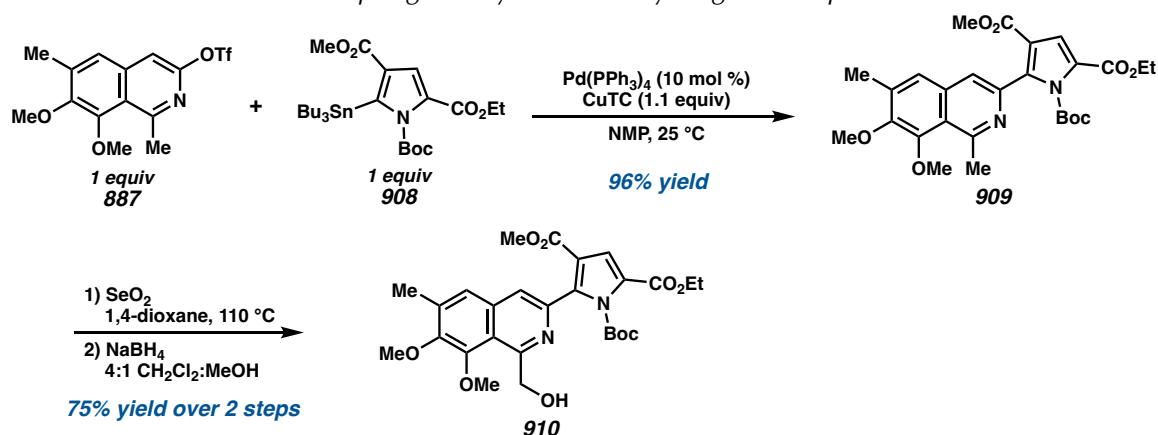
Instead, we envisioned installing a methyl ester at the C3-position of the pyrrole fragment by subjecting pyrrole **900** to a Pinnick oxidation, accessing the carboxylic acid **906** (Scheme 5.7). Then, subsequent methylation of the acid delivered methyl ester **907** in 89% yield over 2 steps. From pyrrole **907**,  $\alpha$ -lithiation and stannylation conditions proceeded efficiently to deliver organostannane **908** in 90% yield. Having the methyl ester functionality at the C3-position serves not only to circumvent hydroxyl elimination pathways, but also to induce a stronger electron-withdrawing effect for pyrrole hydrogenation to be feasible.

**Scheme 5.7.** 3<sup>rd</sup> generation synthesis of pyrrole fragment **908**.



We then revisited the Stille cross-coupling of heterocyclic fragments **887** and **908** to advance to the key hydrogenation precursor (Scheme 5.8). We were pleased to see that we could even further optimize the Stille coupling to obtain a 96% yield of cross-coupled intermediate **909** employing 1:1 equivalents of both coupling partners. Further elaboration of the C1-substituent of the isoquinoline using the same oxidation sequence afforded the hydroxymethyl group **910** in an improved 75% yield over 2 steps. With a more efficient synthetic route to access hydrogenation precursor **910**, we were poised to extensively investigate our key hydrogenation step.

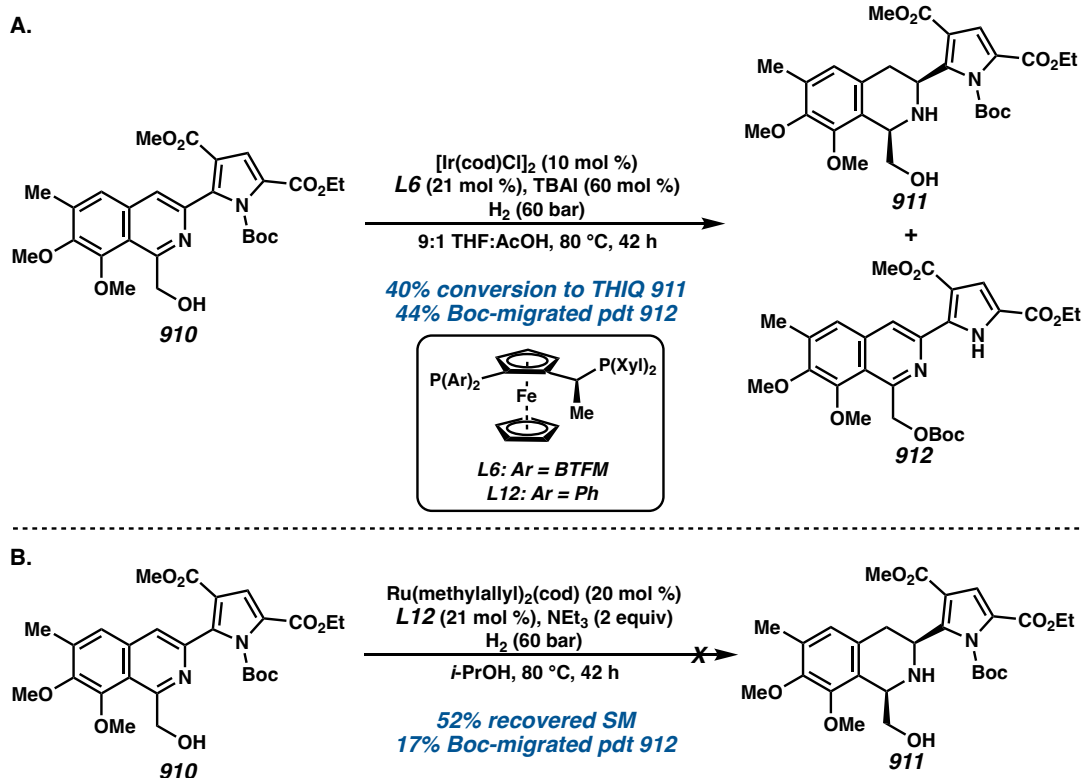
**Scheme 5.8.** Stille cross-coupling and synthesis of hydrogenation precursor **910**.



First, we investigated iridium-catalyzed asymmetric hydrogenation conditions for the reduction of isoquinoline **910**. Using optimized conditions for the jorumycin synthesis, we observed only a 40% yield of the THIQ product **911**, but no trace of pyrrole hydrogenation after 42 hours at 80 °C (Scheme 5.9A).<sup>14</sup> Instead, we observed Boc-migration product **912** from the protected nitrogen atom to the hydroxyl group, likely occurring due to the stronger electron-withdrawing effect of the pyrrole ring that enables

facile abstraction of the Boc group.<sup>21</sup> Revealing the unprotected NH-pyrrole then impedes further hydrogenation presumably due to catalyst deactivation.<sup>22</sup>

**Scheme 5.9.** Key asymmetric hydrogenation attempts of isoquinoline **910**.



We also employed other asymmetric hydrogenation conditions, such as a ruthenium catalyst system developed by Kuwano and coworkers for the asymmetric hydrogenation of 2,3,5-trisubstituted pyrroles (Scheme 5.9B).<sup>23</sup> However, we did not detect any reduction under the optimized Ru-catalyzed conditions, employing Ru(methylallyl)<sub>2</sub>(cod) and Ph-substituted Josiphos ligand **L12**, and instead recovered 52% of starting material and observed 17% yield of the Boc-migrated product **912**.<sup>24</sup> It became clear to us at this stage of the synthesis that the pyrrole ring was difficult to hydrogenate under these asymmetric hydrogenation conditions, and that hydrogenation precursor **910** was generally unreactive to undergo reduction.

To better understand the reactivity of isoquinoline precursor **910** and whether the system can be reduced, we investigated heterogeneous hydrogenation conditions utilizing a variety of metal catalysts. Under 60 bars of H<sub>2</sub> in AcOH, we observed mostly DHIQ intermediate **912** using 1 equivalent of PtO<sub>2</sub>, however we were pleased to see we could access the fully hydrogenated product **915** of both the isoquinoline and pyrrole rings (Scheme 5.10). Using Pd/C as catalyst afforded a range of byproducts, including both the Boc-protected and deprotected THIQ **911** and **913**, respectively (entry 2).

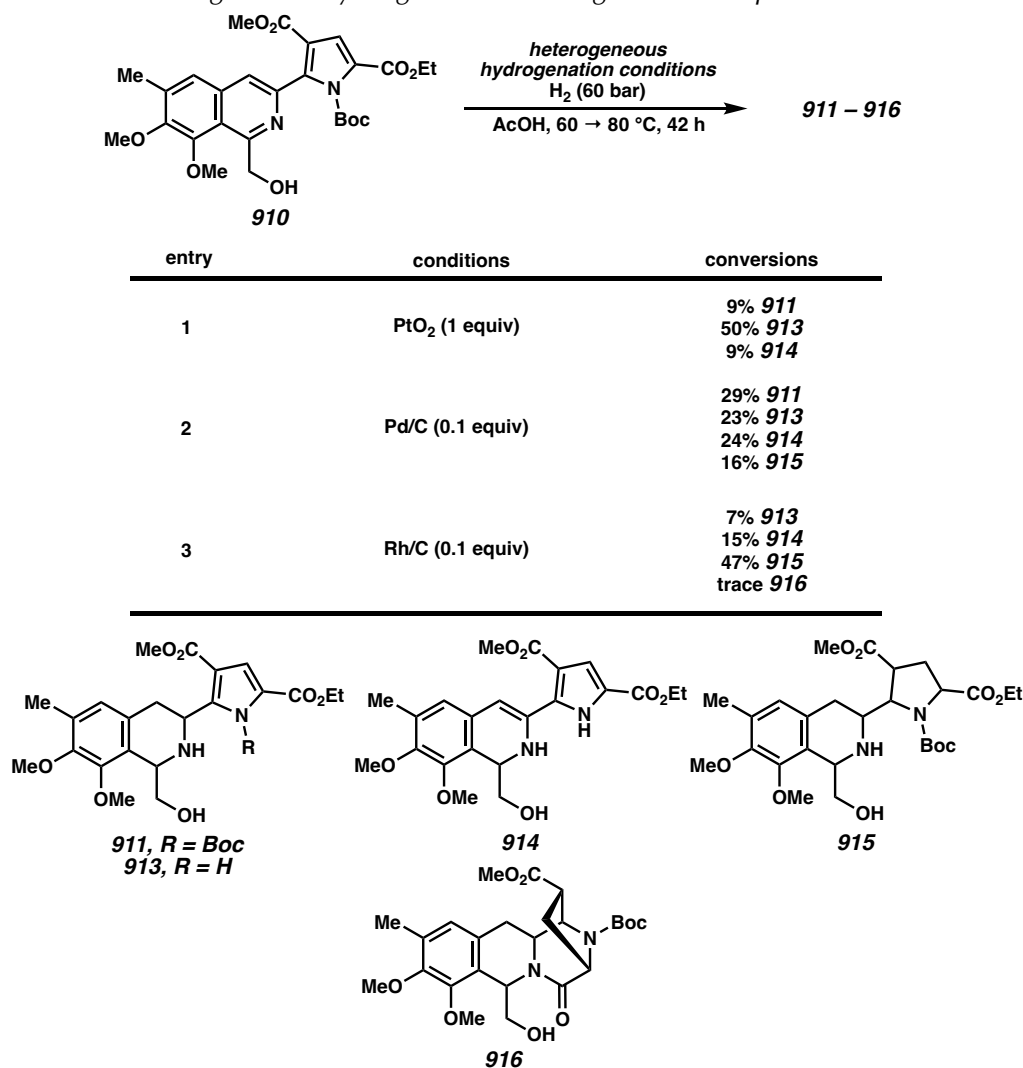
Gratifyingly, when using Rh/C as catalyst, we could now achieve 47% conversion of the fully hydrogenated intermediate **915**, and additionally observe trace amounts of the cyclized product **916** from the secondary amine condensing onto the ethyl ester. Overall, Rh/C and PtO<sub>2</sub> provided cleaner reaction profiles, but provided significant amounts of deprotected byproducts under acetic acid solvent and heat.

We next investigated different solvents of the heterogeneous hydrogenation to suppress any deprotection pathways of the Boc group that impedes further hydrogenation (Scheme 5.11). Using 5% Rh/C and acetic acid as solvent, we observe 27% conversion to the fully hydrogenated intermediate **915** as well as the deprotected THIQ **913** and DHIQ **914** (entry 1).

However, under less acidic solvents such as HFIP and TFE, there was no conversion to pyrrolidine **915**, instead resulting in high levels of deprotected THIQ **913** and DHIQ **914** (entries 2 & 3). On the other hand, little conversion to the deprotected byproducts **913** and **914** was observed using PtO<sub>2</sub> in less acidic solvents. Under TFE

solvent, hydrogenation to the pyrrolidine **915** occurred in 5% conversion, as well as 50% conversion to THIQ intermediate **911** (entry 6).

**Scheme 5.10.** Heterogeneous hydrogenation investigation of isoquinoline **910**.<sup>a</sup>

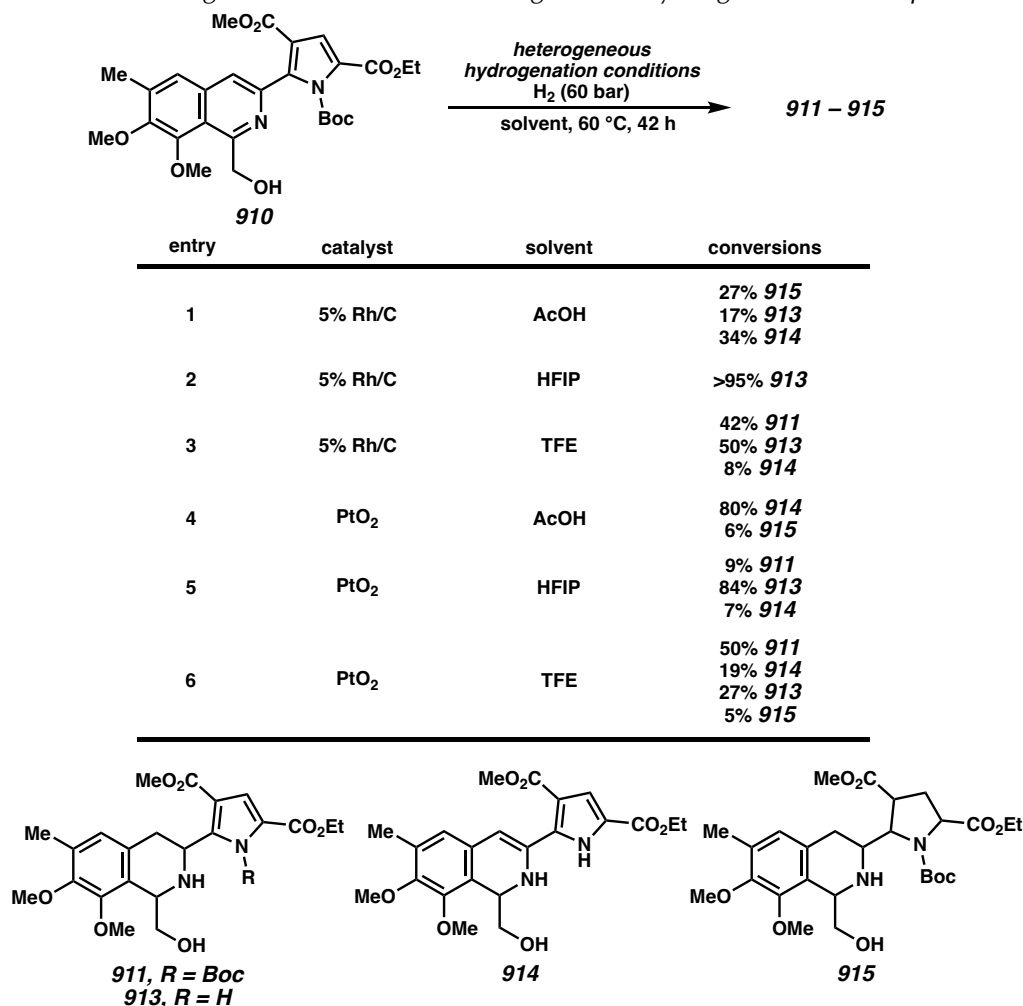


[a] Reaction conditions: 0.01 mmol of **910** in 0.5 mL solvent. Relative levels of conversion determined by LC/MS analysis.

Considering this trend, we further investigated the hydrogenation using PtO<sub>2</sub> at ambient temperature. Under acidic solvents, significant levels of conversion to the deprotected DHIQ intermediate **914** were detected. However, we were pleased to see that

at ambient temperature using  $\text{CHCl}_3$  as solvent, we observed 53% conversion to fully hydrogenated intermediate **915** (Scheme 5.12, entry 4). Overall, key to the hydrogenation of both the isoquinoline and pyrrole ring was the suppression of deprotection pathways that results in byproducts **913** and **914** by using less acidic solvents and ambient temperature.

**Scheme 5.11.** Investigation of solvent in heterogeneous hydrogenation of isoquinoline **910**.



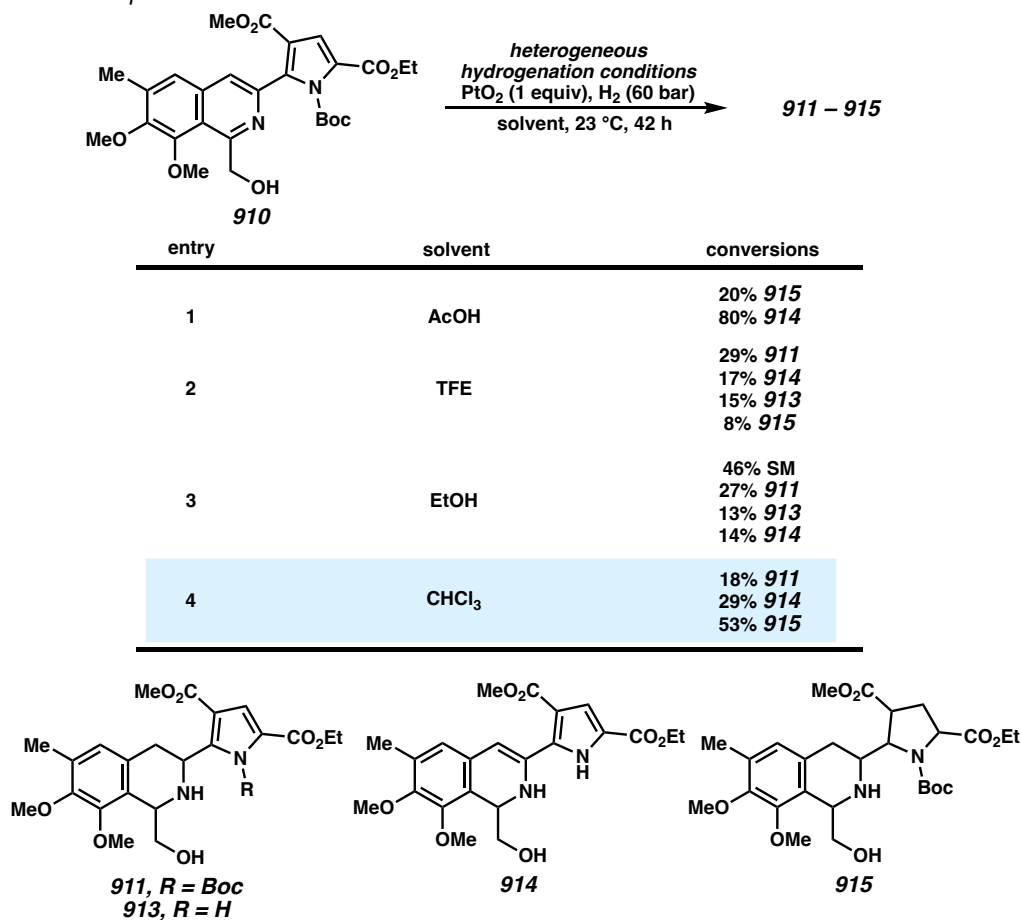
[a] Reaction conditions: 0.01 mmol of **910** in 0.5 mL solvent. Relative levels of conversion determined by LC/MS analysis.

Although we could achieve the fully hydrogenated intermediate **915** in 53% yield, the diastereoselectivity is low and isolated as a mixture of inseparable diastereomers.<sup>25</sup>



Moreover, in attempts to cyclize pyrrolidine **915** to the desired tetracycle **916** by hydrolyzing the ester, we observe competitive cyclization onto the methyl ester moiety at the C3-position of the pyrrolidine as well to deliver **917** (Scheme 5.13).

**Scheme 5.12.** Investigation of solvent in heterogeneous hydrogenation of isoquinoline **910** at ambient temperature.

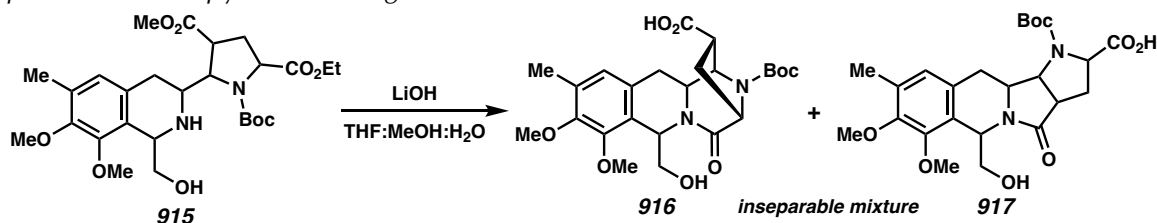


[a] Reaction conditions: 0.01 mmol of **910** in 0.5 mL solvent. Relative levels of conversion determined by LC/MS analysis.

Considering the poor diastereoselectivity of the heterogeneous hydrogenation, competitive cyclization to the less strained tetracycle **917**, and the inability to change the protecting group on the nitrogen atom from the cross-coupled intermediate, we considered

a different approach toward (+)-cyanocycline A (**771**) that would enable faster reduction and higher diastereoselectivity toward tetracycle **916**.

**Scheme 5.13.** Competitive cyclization of secondary amine on to esters at C3- and C5-positions of the pyrrolidine ring.



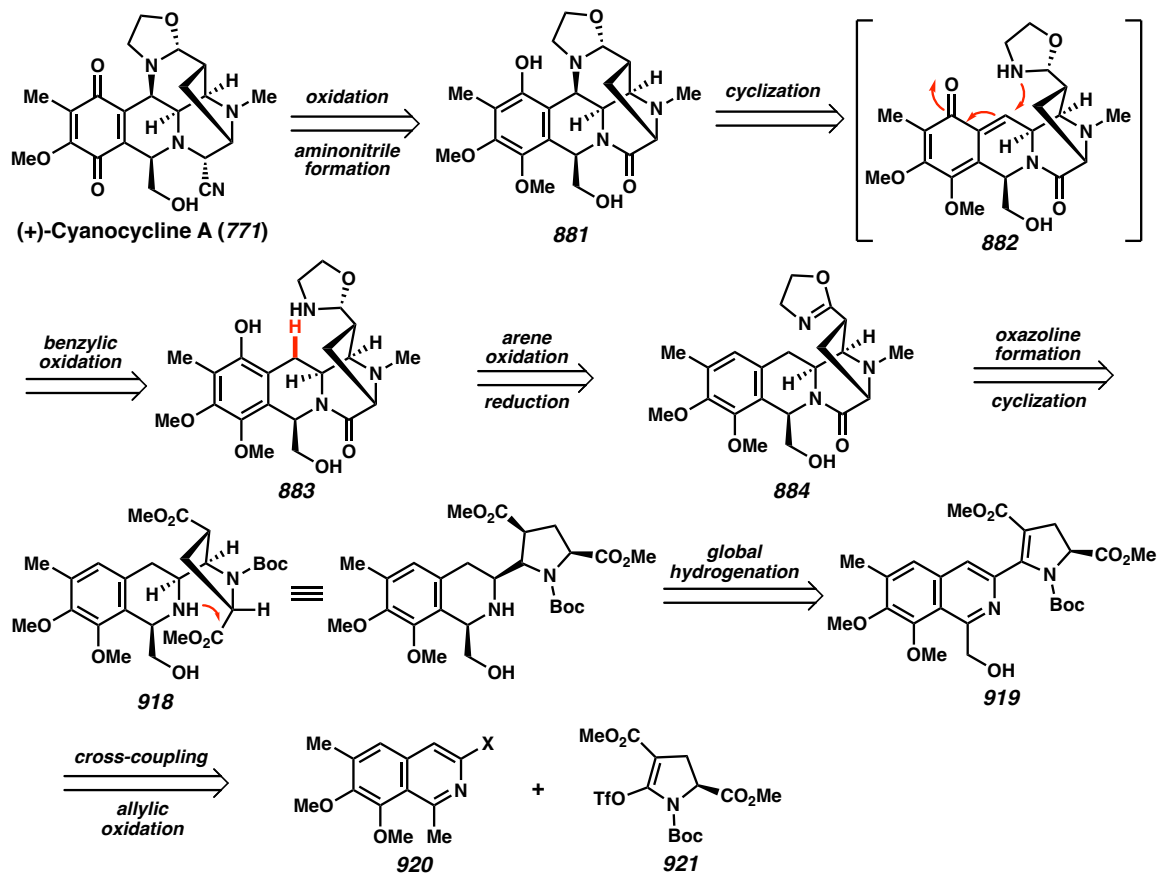
## 5.4 SECOND GENERATION APPROACH

To increase the diastereoselectivity of the global hydrogenation event, we considered installing a dearomatized dihydropyrrole fragment instead to enable facile reduction of the olefin. The ester adjacent to the nitrogen atom of the pyrrolidine ring would be brought in from chiral pool starting materials, which we envisioned would arise from glutamic acid derivatives. Thus, our revised retrosynthetic analysis of (+)-cyanocycline A (**771**) involves a different cross-coupling event of fragments **920** and **921** that switches the previously electrophilic partner of the isoquinoline fragment to a nucleophilic coupling partner (Figure 5.4). After allylic oxidation, global hydrogenation of intermediate **919** should be more efficient, as only the isoquinoline ring and the tetrasubstituted olefin of the dihydropyrrole ring are reduced to afford pyrrolidine **918**.

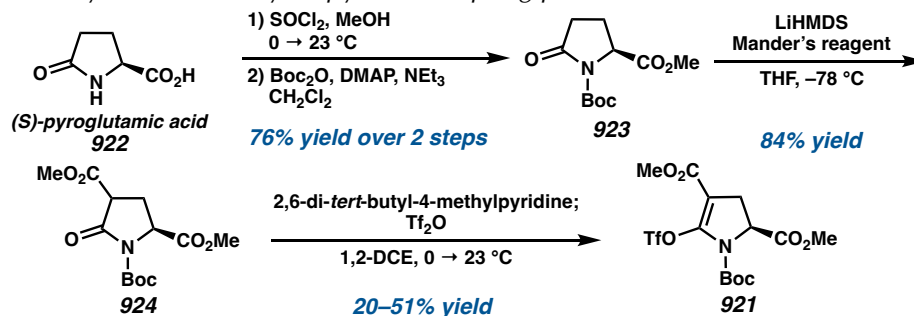
Synthesis of the dihydropyrrole fragment commences with commercially available (*S*)-pyroglutamic acid **922**, which undergoes esterification and Boc-protection to afford lactam **923** (Scheme 5.14). Acylation of lactam **923** is then performed with LiHMDS and Mander's reagent to install the methyl ester moiety at the C3-position to access lactam **924**. Finally, treatment of **924** with 2,6-di-*tert*-butyl-4-methylpyridine and trapping the

generated enolate with  $\text{TiF}_4$  delivers vinyl triflate **921** in 51% yield. However, further attempts to optimize the yield of the triflation were unsuccessful due to the instability of intermediate **921**.

**Figure 5.4.** 2<sup>nd</sup> generation retrosynthetic analysis of (+)-cyanocycline A (**771**).

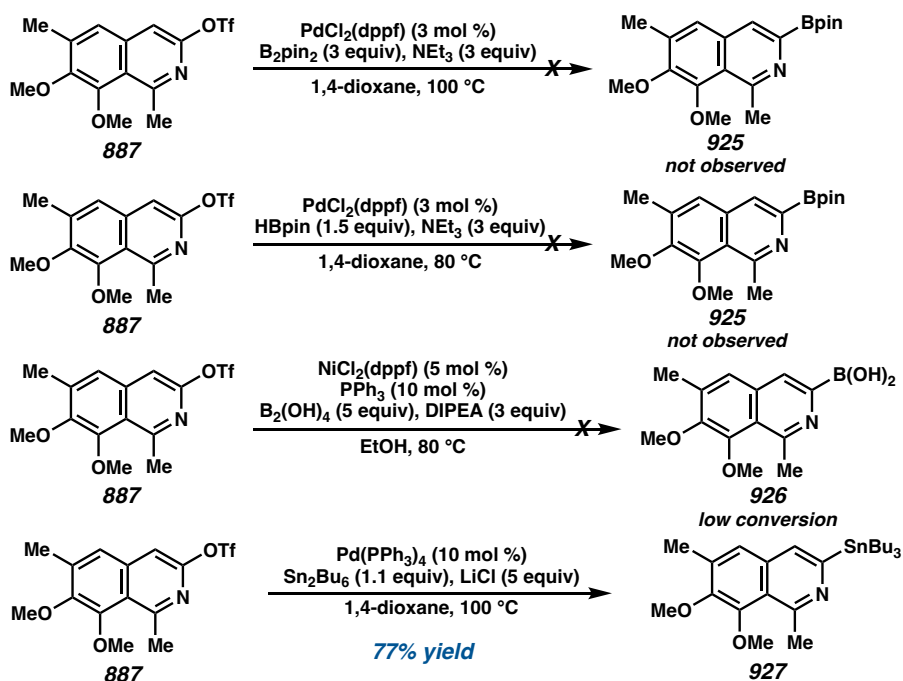


**Scheme 5.14.** Synthesis of dihydropyrrole coupling partner **921**.



Conversion of the isoquinoline triflate **887** to a nucleophilic coupling partner was more challenging than anticipated. We first attempted Pd-catalyzed borylation conditions using B<sub>2</sub>pin<sub>2</sub> and HBpin, but no conversion of starting material was observed (Scheme 5.15).<sup>26</sup> Using nickel-catalyzed borylation conditions developed by Molander and coworkers resulted in little conversion to the boronic acid **926**, but mostly produced leftover starting material and protodetriflation.<sup>27</sup> To our delight, Pd-catalyzed stannylation conditions inspired by Nechaev and coworkers gave smooth conversion of the isoquinoline triflate **887** to organostannane **927** in 77% yield.<sup>28</sup>

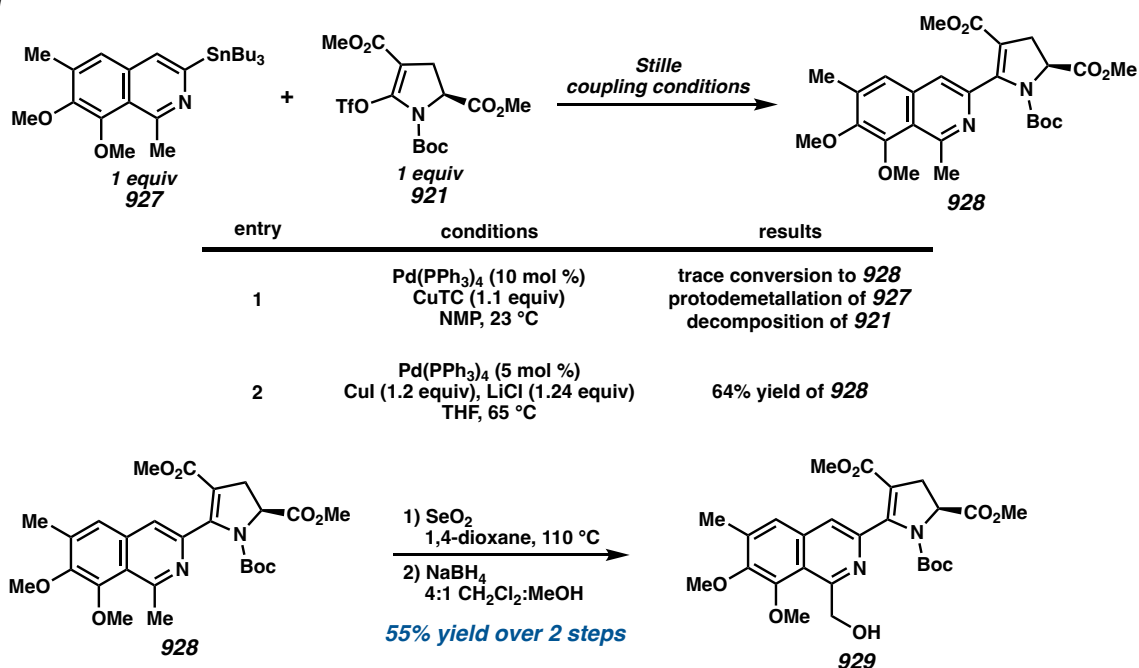
**Scheme 5.15.** Conversion of isoquinoline triflate **887** to a nucleophilic coupling partner.



With both coupling partners in hand, we then explored Stille cross-coupling conditions of isoquinoline stannane **927** and vinyl triflate **921**. Interestingly, using the same optimized conditions for the Stille coupling of isoquinoline triflate **887** and pyrrole stannane **908** resulted in a complex reaction profile of protodemetalation and

decomposition of the vinyl triflate **921** (Scheme 5.16, entry 1). When we explored other additives, we observed that adding LiCl that is known to accelerate the oxidative addition event of the vinyl triflate to palladium improved the yield to 64% (entry 2).<sup>29</sup> Thus, using Pd(PPh<sub>3</sub>)<sub>4</sub>, CuI, LiCl, and 1:1 equivalents of both coupling partners, we could achieve cross-coupled product **928** by reversing the electronics of both fragments.

**Scheme 5.16.** Cross-coupling of heterocycles **921** and **927** and synthesis of hydrogenation precursor.



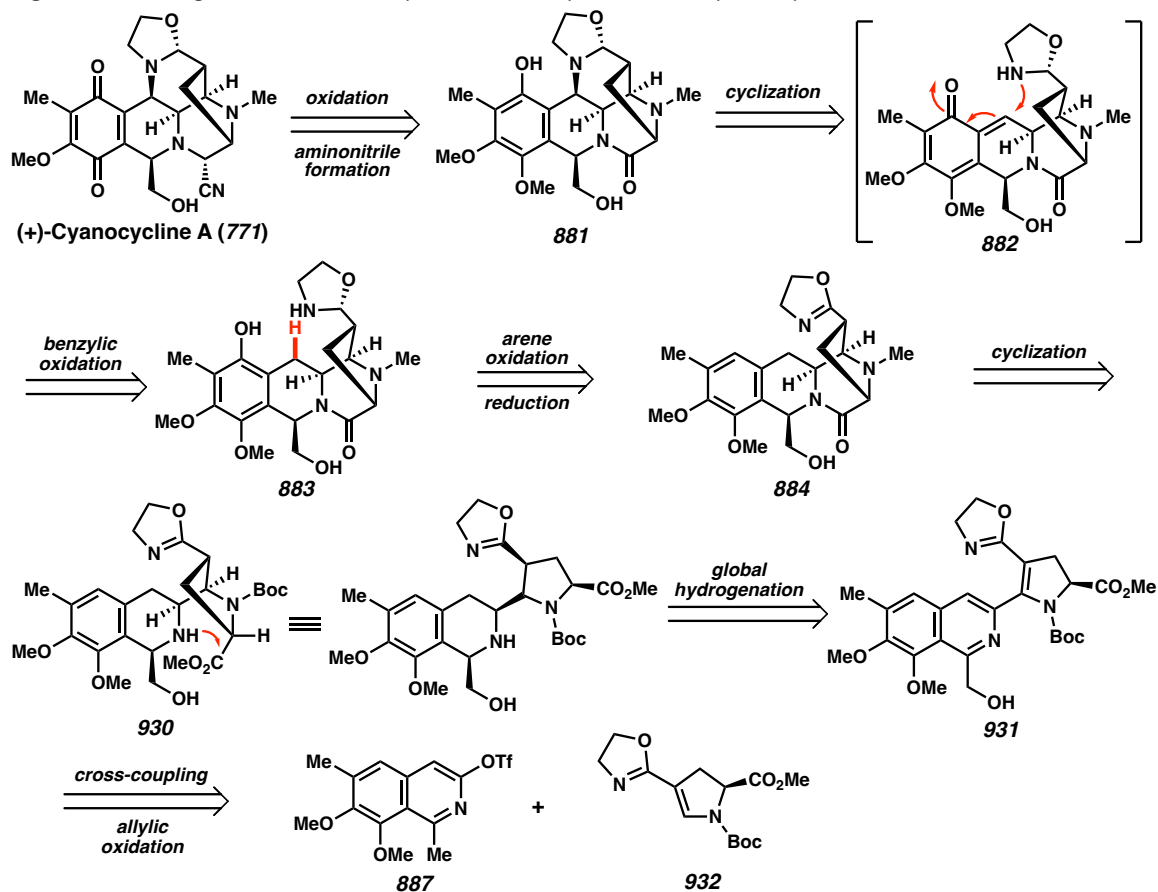
From cross-coupled intermediate **928**, we could access the hydrogenation precursor **929** from allylic oxidation and subsequent reduction of the aldehyde intermediate, observing no deleterious pathways of oxidation of the dihydropyrrole ring and potential aromatization. However, due to the instability of vinyl triflate **921** that resulted in inconsistent yields of 20 to 51%, and to avoid undesired cyclization onto the methyl ester at the C3-position,<sup>30</sup> we envisioned designing an elaborated dihydropyrrole fragment to enable a more convergent strategy for the two heterocycles.

## 5.5 THIRD GENERATION APPROACH

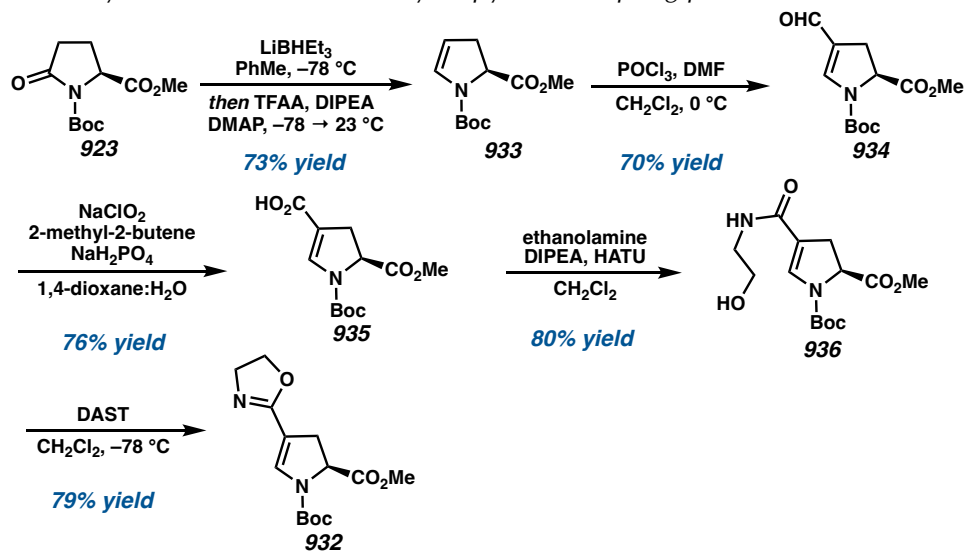
To this end, we considered installing the oxazoline ring onto the dihydropyrrole fragment (**932**) that maps directly onto ring F of the natural product. Not only would this reduce the number of subsequent steps from the global hydrogenation event to install the oxazoline ring, but would also impart a significant electron-withdrawing effect to enable reduction of the tetrasubstituted olefin (Figure 5.5). Moreover, we sought to utilize the oxazoline ring as a potential directing group for the cross-coupling with isoquinoline triflate **887** through either a Heck or a Pd-catalyzed concerted metalation deprotonation (CMD) reaction of the dihydropyrrole olefin.<sup>31</sup> Such transformations using unactivated cyclic enamides are not well precedented, which we envision could be an opportunity for novel reaction development for the coupling of enamides and heteroaryl electrophiles.<sup>32</sup>

Synthesis of the oxazoline-appended dihydropyrrole **932** commences with lactam **923**, which instead undergoes a dehydration event to access dihydropyrrole **933** (Scheme 5.17).<sup>33</sup> Vilsmeier–Haack formylation using POCl<sub>3</sub> in DMF affords aldehyde **934** in 70% yield, which is subjected to Pinnick oxidation to deliver carboxylic acid **935** in 76% yield. Then, amidation of **935** with ethanolamine and HATU reagent gives amide **936** in 80% yield that can be treated with DAST reagent at –78 °C to cleanly afford the oxazoline coupling partner **932** in 79% yield.

With efficient access to dihydropyrrole fragment **932**, we were then poised to explore the key cross-coupling event of isoquinoline triflate **887** and dihydropyrrole **932** without prefunctionalization of the olefin. First, a variety of Pd-catalyzed conditions were investigated based on precedent of direct C–H arylation reactions (Scheme 5.18).<sup>34</sup>

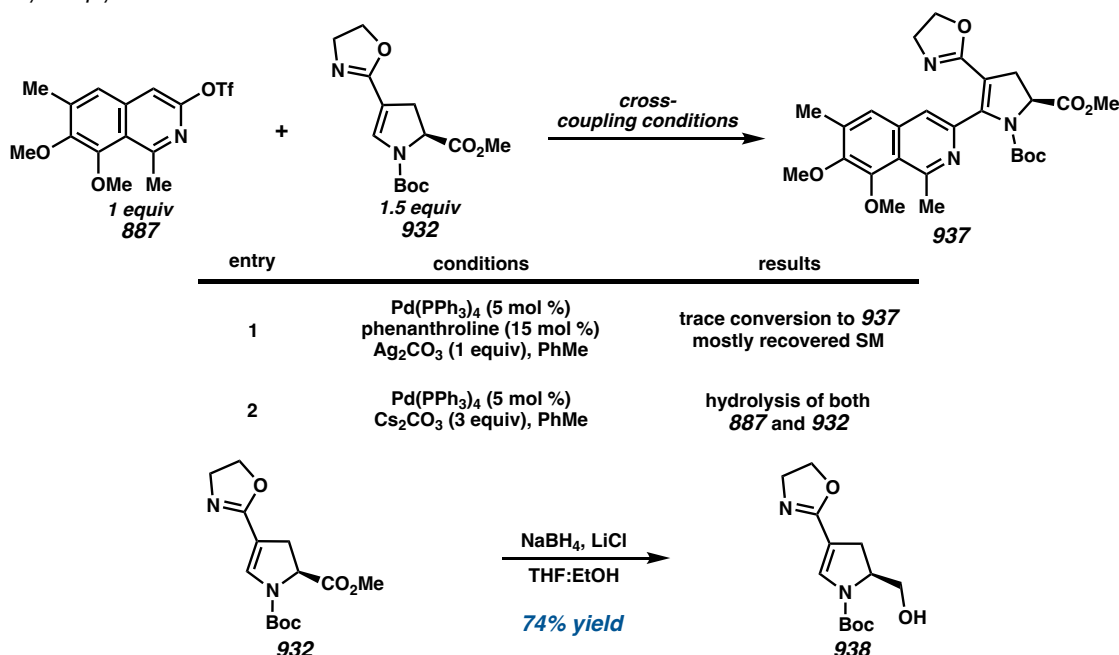
Figure 5.5. 3<sup>rd</sup> generation retrosynthetic analysis of (+)-cyanocycline A (771).

Scheme 5.17. Synthesis of oxazoline dihydropyrrole coupling partner 932.



After surveying a wide range of transition-metal catalysts, we were pleased to see that an initial reaction employing Pd(PPh<sub>3</sub>)<sub>4</sub>, phenanthroline as ligand, and Ag<sub>2</sub>CO<sub>3</sub> as base gave trace conversion to product (entry 1). Surveying a variety of carbonate bases did not improve conversion to product **937**, but Cs<sub>2</sub>CO<sub>3</sub> in particular showed full consumption of starting material **932** to the hydrolyzed carboxylic acid (entry 2). Considering the unique reactivity of Cs<sub>2</sub>CO<sub>3</sub>, we hypothesized whether reducing the ester moiety to the alcohol to avoid hydrolysis of the substrate would activate the substrate toward cross-coupling. Thus, dihydropyrrole **932** was converted to the primary alcohol **938** via LiBH<sub>4</sub> generated in situ.<sup>35</sup>

**Scheme 5.18.** Initial Pd-catalyzed CMD cross-coupling reaction of triflate **887** and dihydropyrrole **932**.

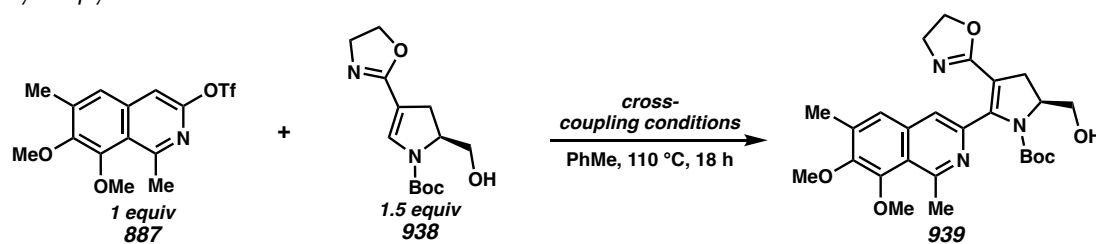


Optimization of the Pd-catalyzed cross-coupling was then explored with triflate **887** and alcohol **938**. To our delight, using P(*t*-Bu)<sub>3</sub> as ligand and 1.0 equivalent of Cs<sub>2</sub>CO<sub>3</sub> afforded a 10% NMR yield of cross-coupled intermediate **939** as a single isomer (Scheme 5.19, entry 1). Increasing the amount of base to 3.5 equivalents and diluting the



concentration to 0.04 M improved the yield to 25%, suggesting that a concerted metalation deprotonation (CMD) reaction pathway may be taking place over a Heck-type mechanism.<sup>36</sup> Yet, the reaction suffers from significant protodetriflation and homocoupling of isoquinoline triflate **887**.

**Scheme 5.19.** Optimization of Pd-catalyzed CMD cross-coupling reaction of triflate **887** and dihydropyrrole **938**.<sup>a</sup>



entry	conditions	results
1	Pd(OAc) <sub>2</sub> (10 mol %), P $\dagger$ -Bu <sub>3</sub> (25 mol %) Cs <sub>2</sub> CO <sub>3</sub> (1 equiv), PhMe (0.07 M)	10% yield 16% homocoupling 45% protodetriflation
2	Pd(OAc) <sub>2</sub> (10 mol %), P $\dagger$ -Bu <sub>3</sub> (25 mol %) Cs <sub>2</sub> CO <sub>3</sub> (3.5 equiv), PhMe (0.04 M)	25% yield 19% homocoupling 41% protodetriflation
3	Pd(OAc) <sub>2</sub> (10 mol %), P $\dagger$ -Bu <sub>3</sub> (20 mol %) Cs <sub>2</sub> CO <sub>3</sub> (3.5 equiv), CsOPiv (50 mol %)	11% yield 14% homocoupling 9% protodetriflation
4	Pd(OAc) <sub>2</sub> (2.5 mol %), P $\dagger$ -Bu <sub>3</sub> (5 mol %) Cs <sub>2</sub> CO <sub>3</sub> (3.5 equiv), CsOPiv (12.5 mol %)	36% yield 8% homocoupling 5% protodetriflation
5	Pd(OAc) <sub>2</sub> (2.5 mol %), PPh <sub>3</sub> (5 mol %) Cs <sub>2</sub> CO <sub>3</sub> (3.5 equiv), CsOPiv (12.5 mol %)	34% yield 3% homocoupling 9% protodetriflation
6	Pd(OAc) <sub>2</sub> (2.5 mol %), PCy <sub>3</sub> (5 mol %) Cs <sub>2</sub> CO <sub>3</sub> (3.5 equiv), CsOPiv (12.5 mol %)	47% yield 8% homocoupling 10% protodetriflation

[a] Reaction conditions: 0.014 mmol of **887** in 0.34 mL solvent. Yields determined from crude <sup>1</sup>H NMR using 1,3,5-trimethoxybenzene as standard.

Employing CsOPiv as an additive that is known to be directly involved in the rate-determining C–H bond cleavage/palladation event decreased the amount of protodetriflation and homocoupling byproducts, affording **939** in 11% yield.<sup>37</sup> Lowering the catalyst loading to 2.5 mol % of palladium and 5 mol % of phosphine ligand also

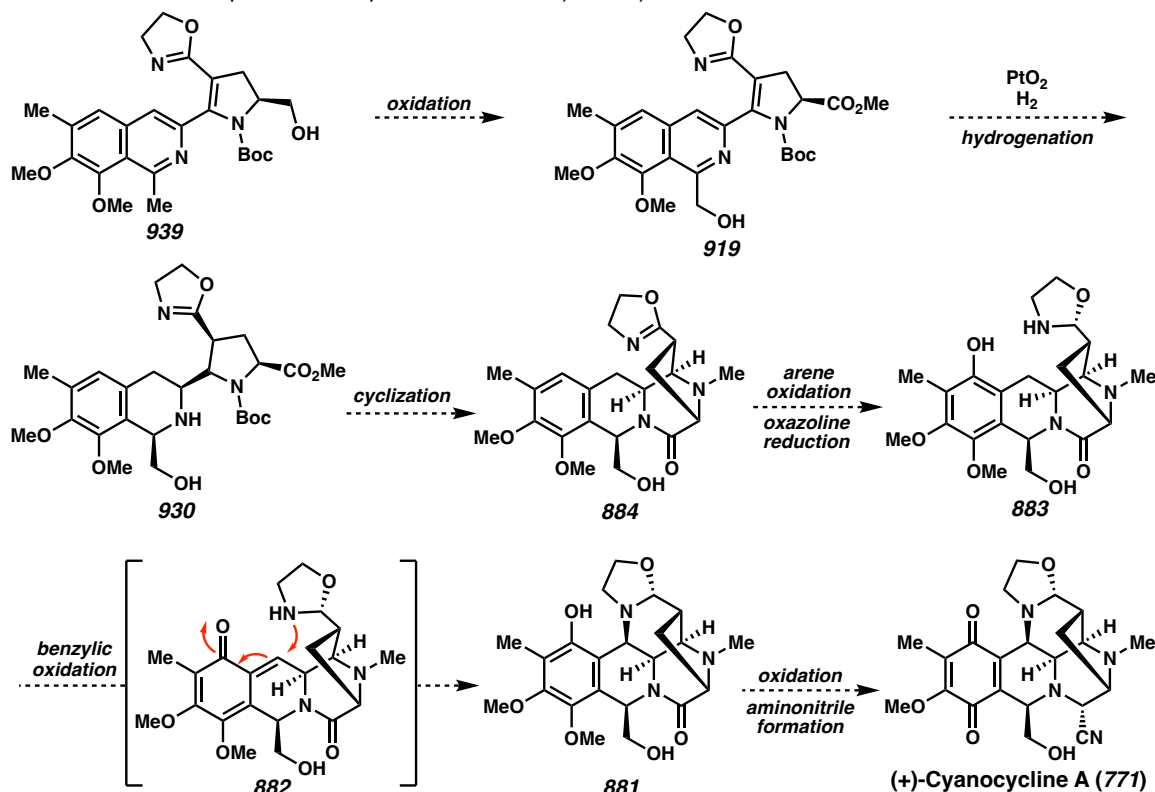
significantly reduced the levels of homocoupling and protodetriflation while increasing the yield of **939** to 36% (entry 4). Finally, exploring more electron-deficient phosphine ligands such as PPh<sub>3</sub> and PCy<sub>3</sub> ultimately improved the yield of the cross-coupling to 47% while suppressing other undesired reaction pathways (entries 5 & 6). Efforts to continue improving the yield of this key cross-coupling reaction and access the hydrogenation precursor are currently ongoing.

## 5.6 CONCLUSION AND FUTURE DIRECTIONS

Toward the total synthesis of (+)-cyanocycline A (**771**), we have developed a highly convergent strategy to cross-couple isoquinoline triflate **887** and dihydropyrrole **938** that installs four out of six rings of the natural product in a single transformation. With intermediate **939** in hand, we anticipate that oxidation of **939** will be relatively facile using previously employed oxidation conditions that installs the hydroxymethyl group at the C1-position of the isoquinoline (Scheme 5.20). With hydrogenation precursor **931**, a global hydrogenation event using PtO<sub>2</sub> will be explored to access **930**, which has already been demonstrated to reduce both the isoquinoline and pyrrole ring (e.g., **915**). Due to the presence of one methyl ester substituent, cyclization of the secondary amine onto the ester should be selective to yield bicycle **884** with the oxazoline ring already in place. After arene oxidation to deliver phenol **883** which has been performed on a similar substrate in the jorumycin synthesis,<sup>14</sup> benzylic oxidation of either oxazolidine **883** or the oxazoline will be extensively explored to generate an *ortho*-quinone methide intermediate **882** that enables cyclization of the pendent heterocycle to access the natural product scaffold **881**.

Finally, oxidation of the arene to the quinone and aminonitrile formation are both well precedented in previous syntheses of THIQ alkaloids to deliver (+)-cyanocycline A (**771**).<sup>2</sup>

**Scheme 5.20.** Proposed completion of (+)-cyanocycline A (**771**).



In conclusion, we have developed a novel cross-coupling strategy of two heterocyclic fragments that installs all of the requisite carbon and nitrogen atoms of (+)-cyanocycline A (**771**). Key to this reaction is an appended oxazoline ring on the dihydropyrrole fragment that enables deprotonation of the  $\text{C}(\text{sp}^2)\text{-H}$  bond and palladation to couple with a functionalized isoquinoline triflate. Furthermore, extensive investigation into both the asymmetric hydrogenation and heterogeneous hydrogenation of a pyrrole-substituted isoquinoline were explored to probe its reactivity and stereoselectivity. Although a variety of asymmetric hydrogenation conditions were not successful in reducing the pyrrole-substituted isoquinoline efficiently, we have developed a

hydrogenation method using PtO<sub>2</sub> and 60 bar H<sub>2</sub> at ambient temperature that enables the reduction of both the isoquinoline and pyrrole ring. We anticipate application of this technology to our most advanced intermediate to reduce a dearomatized dihydropyrrole-substituted isoquinoline effectively. Efforts are currently underway to access this hydrogenation precursor toward the total synthesis of (+)-cyanocycline A (**771**).

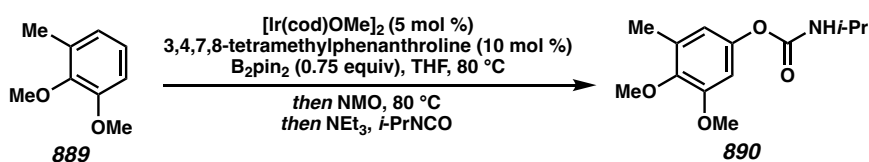
## 5.7 EXPERIMENTAL SECTION

### 5.7.1 MATERIALS AND METHODS

Unless otherwise stated, reactions were performed in flame-dried glassware under an argon or nitrogen atmosphere using dry, deoxygenated solvents. Solvents were dried by passage through an activated alumina column under argon.<sup>38</sup> Reaction progress was monitored by thin-layer chromatography (TLC) or Agilent 1290 UHPLC-MS. TLC was performed using E. Merck silica gel 60 F254 precoated glass plates (0.25 mm) and visualized by UV fluorescence quenching, *p*-anisaldehyde, or KMnO<sub>4</sub> staining. Silicycle SiliaFlash® P60 Academic Silica gel (particle size 40–63 μm) was used for flash chromatography. <sup>1</sup>H NMR spectra were recorded on Varian Inova 500 MHz and Oxford 600 MHz spectrometers and are reported relative to residual CHCl<sub>3</sub> (δ = 7.26 ppm) or TMS (δ = 0.00 ppm). <sup>13</sup>C NMR spectra were recorded on a Bruker 400 MHz spectrometer (100 MHz) and are reported relative to CHCl<sub>3</sub> (δ = 77.16 ppm), C<sub>6</sub>D<sub>6</sub> (δ = 128.06 ppm). Data for <sup>1</sup>H NMR are reported as follows: chemical shift (δ ppm) (multiplicity, coupling constant (Hz), integration). Multiplicities are reported as follows: s = singlet, d = doublet, t = triplet, q = quartet, p = pentet, sept = septuplet, m = multiplet, br s = broad singlet, br d = broad

doublet. Data for  $^{13}\text{C}$  NMR are reported in terms of chemical shifts ( $\delta$  ppm). IR spectra were obtained by use of a Perkin Elmer Spectrum BXII spectrometer or Nicolet 6700 FTIR spectrometer using thin films deposited on NaCl plates and reported in frequency of absorption ( $\text{cm}^{-1}$ ). Optical rotations were measured with a Jasco P-2000 polarimeter operating on the sodium D-line (589 nm), using a 100 mm path-length cell. High resolution mass spectra (HRMS) were obtained from Agilent 6200 Series TOF with an Agilent G1978A Multimode source in electrospray ionization (ESI+), or mixed ionization mode (MM: ESI-APCI+). Reagents were purchased from commercial sources and used as received unless otherwise stated.

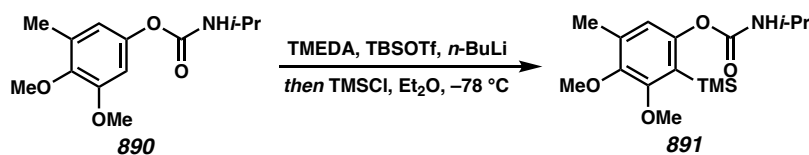
### 5.7.2 EXPERIMENTAL PROCEDURES AND SPECTROSCOPIC DATA



#### 3,4-dimethoxy-5-methylphenyl isopropylcarbamate (**890**)

Compound **890** was prepared according to literature procedure.<sup>14a</sup> In a nitrogen-filled glovebox,  $[\text{Ir}(\text{cod})\text{OMe}]_2$  (22.3 mg, 0.034 mmol, 0.005 equiv) and 3,4,7,8-tetramethyl-1,10-phenanthroline (15.9 mg, 0.067 mmol, 0.01 equiv) were dissolved in 5 mL THF and stirred for 30 min. Then, 2,3-dimethoxytoluene (1.00 mL, 6.73 mmol, 1 equiv) and  $\text{B}_2\text{Pin}_2$  (1.28 g, 5.05 mmol, 0.75 equiv) were weighed into a 20 mL sealable microwave vial in the glovebox with a teflon-coated stir bar and 5 mL THF was added. Upon complete dissolution, the catalyst solution was transferred to the microwave vial, which was sealed prior to removing from the glovebox. The vial was then placed in a preheated 80 °C oil bath and stirred 48 h, at which time TLC (20% EtOAc in hexanes) revealed complete

conversion to a single borylated product. The vial was cooled to room temperature and the cap was removed. *N*-methylnmorpholine-*N*-oxide (2.37 g, 20.2 mmol, 3 equiv) was added in a few small portions and the vial was resealed and returned to the 80 °C oil bath for 3 h, at which time TLC (20% EtOAc in hexanes) indicated complete oxidation to the intermediate phenol. NEt<sub>3</sub> (4.7 mL, 33.7 mmol, 5 equiv) and isopropyl isocyanate (2.6 mL, 26.9 mmol, 4 equiv) were added at room temperature and the solution was stirred 16 h, at which time TLC (50% EtOAc/hex) indicated complete conversion to carbamate **890**. 10% aq. Na<sub>2</sub>S<sub>2</sub>O<sub>3</sub> was added to quench the remaining oxidant and citric acid hydrate (4.5 g, >3 equiv) was added to chelate the boron. This solution was stirred 1 h, and concentrated HCl was added 1 mL at a time until an acidic pH was achieved. The layers were separated and the aqueous phase was extracted with EtOAc. The combined organic phases were then washed with aqueous K<sub>2</sub>CO<sub>3</sub>, dried over MgSO<sub>4</sub> and concentrated. The product was purified by silica column chromatography (25% EtOAc in hexanes) to afford a colorless solid (1.35 g, 4.6 mmol, 79% yield); <sup>1</sup>H NMR (400 MHz, CDCl<sub>3</sub>) δ 6.55 (d, *J* = 2.6, 1H), 6.52 (d, *J* = 2.8, 1H), 4.84 (d, *J* = 7.8 Hz, 1H), 3.88 (ddd, *J* = 16.1, 13.9, 7.6 Hz, 1H), 3.82 (s, 3H), 3.76 (s, 3H), 2.24 (s, 3H), 1.23 (s, 3H), 1.21 (s, 3H); All characterization data match those reported.

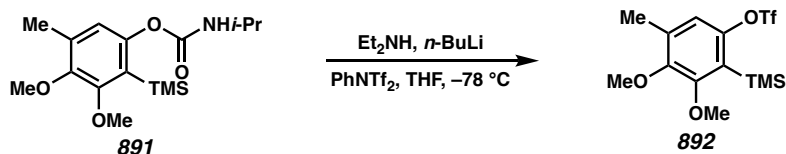


### 3,4-dimethoxy-5-methyl-2-(trimethylsilyl)phenyl isopropylcarbamate (**891**)

Compound **891** was prepared according to literature procedure.<sup>14a</sup> Carbamate **890** (17.30 g, 68.2 mmol, 1 equiv) was dissolved in Et<sub>2</sub>O (340 mL, 0.2 M) *N,N,N',N'*-

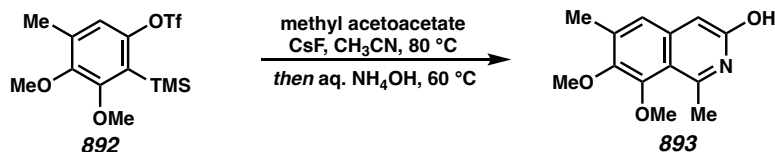
tetramethylethylenediamine (TMEDA, 11.3 mL, 75.1 mmol, 1.1 equiv) was added and the solution was cooled to 0 °C before *tert*-butyldimethylsilyl triflate (TBSOTf, 17.25 mL, 75.1 mmol, 1.1 equiv) was added in a slow stream. The solution was stirred 10 min at 0 °C, removed from the ice bath and stirred at room temperature for 30 min. A second portion of TMEDA (41 mL, 273 mmol, 4 equiv) was added and the solution was cooled to –78 °C. *n*-Butyllithium (2.4 M, 114 mL, 274 mmol, 4 equiv) was added in a dropwise fashion through a flame-dried addition funnel over the course of 1 h, being sure to not let the temperature rise significantly. The resulting yellow suspension was stirred vigorously for 4 h at –78 °C, taking care not to let the temperature rise during the course of the reaction. Trimethylsilyl chloride (61 mL, 478 mmol, 7 equiv) was then added dropwise via addition funnel over the course of 30 min and the suspension was stirred at –78 °C for 30 min, then was removed from the dry ice bath and stirred at room temperature for 16 h. The reaction was quenched by the addition of 300 mL aqueous NH<sub>4</sub>Cl (30 mL saturated solution diluted to 300 mL) through an addition funnel, the first 50 mL of which were added dropwise, followed by the addition of the remainder in a slow stream. The aqueous phase was then further acidified by the addition of small portions of concentrated HCl until an acidic pH was achieved (~30 mL required). The layers were separated and the aqueous phase was extracted twice with Et<sub>2</sub>O. The combined organic phases were washed with saturated aqueous NH<sub>4</sub>Cl, dried over MgSO<sub>4</sub> and concentrated. The product was purified by silica column chromatography (20 → 30% Et<sub>2</sub>O in hexanes) to afford a colorless solid (20.61 g, 63.3 mmol, 93% yield); <sup>1</sup>H NMR (400 MHz, CDCl<sub>3</sub>) δ 6.63 (s, 1H), 4.69 (d, *J* = 8.1 Hz,

1H), 3.96–3.85 (m, 1H), 3.83 (s, 3H), 3.76 (s, 3H), 2.23 (s, 3H), 1.24 (s, 3H), 1.22 (s, 3H), 0.30 (s, 9H); All characterization data match those reported.



### 3,4-dimethoxy-5-methyl-2-(trimethylsilyl)phenyl trifluoromethanesulfonate (892)

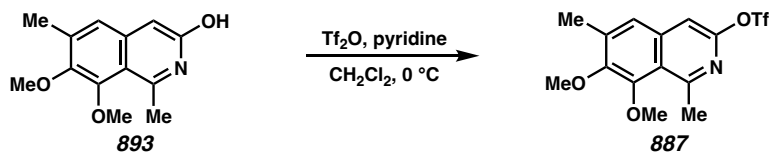
Compound **892** was prepared according to literature procedure.<sup>14a</sup> Carbamate **891** (8.08 g, 24.8 mmol, 1 equiv) was dissolved in THF (100 mL, 0.25 M) and diethylamine (3.85 mL, 37.2 mmol, 1.5 equiv) was added and the solution was cooled to  $-78$  oC. *n*-Butyllithium (2.5 M, 15 mL, 37.5 mmol, 1.5 equiv) was added slowly over the course of 15 min. The solution was stirred at that temperature for 30 min, then removed from its bath and stirred at 23 oC for 30 min. *N*-Phenyl triflimide (10.6 g, 29.8 mmol, 1.2 equiv) was added in one portion and the solution was stirred 30 min. A second portion of diethylamine (4.6 mL, 44.7 mmol, 1.8 equiv) was added and the solution was stirred 2 h. The solution was filtered through a 1 inch pad of silica gel with 50% Et<sub>2</sub>O in hexanes and concentrated. The product was purified by silica column chromatography (10% Et<sub>2</sub>O in hexanes) to afford a colorless oil (9.15 g, 24.6 mmol, 99% yield); <sup>1</sup>H NMR (400 MHz, CDCl<sub>3</sub>)  $\delta$  6.87 (s, 1H), 3.87 (s, 3H), 3.78 (s, 3H), 2.28 (d,  $J = 0.7$  Hz, 3H), 0.38 (s, 9H); All characterization data match those reported.



### 7,8-dimethoxy-1,6-dimethylisoquinolin-3-ol (893)

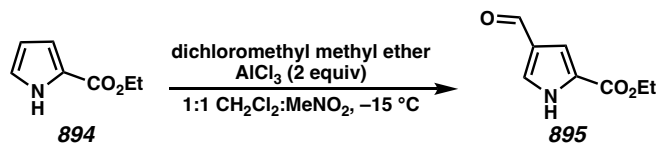


Compound **893** was prepared according to literature procedure.<sup>14a</sup> Cesium fluoride (204 mg, 1.34 mmol, 2.5 equiv) was dissolved in acetonitrile (5.4 mL, 0.1 M) in a 20 mL microwave vial and water (9.7  $\mu$ L, 0.537 mmol, 1.0 equiv) and methyl acetoacetate (58  $\mu$ L, 0.537 mmol, 1.0 equiv) were added. Aryne precursor **892** (250 mg, 0.671 mmol, 1.25 equiv) was added neat via syringe, and the vial was placed in a preheated 80 °C oil bath. After 2 h, TLC revealed complete consumption of **892**, so NH<sub>4</sub>OH (28–30%, 5.4 mL) was added in one portion. The vial was moved to a preheated 60 °C oil bath and stirred for 8 h. The solution was poured into brine inside a separatory funnel and the solution was extracted with EtOAc (2x 30 mL). The aqueous phase was brought to pH 7 by the addition of concentrated HCl and was extracted with EtOAc (2x 30 mL). The aqueous phase was discarded. The organic phase was then extracted with 2M HCl (5x 20 mL). The organic phase was checked by LCMS to confirm that all of product **893** had transferred to the aqueous phase and was subsequently discarded. The aqueous phase was then brought back to pH 7 by the addition of 100 mL 2M NaOH and was extracted with EtOAc (5x 20 mL). The combined organic phases were washed with brine, dried over Na<sub>2</sub>SO<sub>4</sub> and concentrated, providing product **893** as a yellow solid (56.9 mg, 0.243 mmol, 45% yield); <sup>1</sup>H NMR (400 MHz, CDCl<sub>3</sub>)  $\delta$  6.92 (d,  $J$  = 0.7 Hz, 1H), 6.51 (s, 1H), 3.90 (s, 3H), 3.81 (s, 3H), 3.03 (d,  $J$  = 0.7 Hz, 3H), 2.28 (d,  $J$  = 1.0 Hz, 3H); All characterization data match those reported.



### 7,8-dimethoxy-1,6-dimethylisoquinolin-3-yl trifluoromethanesulfonate (**887**)

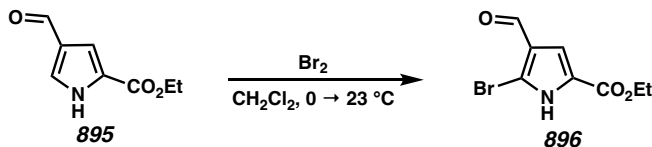
Compound **887** was prepared according to literature procedure.<sup>14a</sup> Isoquinoline **893** (2.60 g, 11.1 mmol, 1 equiv) was dissolved in CH<sub>2</sub>Cl<sub>2</sub> (70 mL, 0.16 M) and pyridine (11.4 mL, 140.6 mmol, 12.7 equiv) was added and the solution was cooled to 0 °C. Trifluoromethanesulfonic anhydride (Tf<sub>2</sub>O, 3.00 mL, 17.8 mmol, 1.6 equiv) was added dropwise, causing the yellow solution to turn dark red. After 30 min TLC (10% EtOAc/hex) revealed complete conversion, so the reaction was quenched by the addition of saturated aqueous NaHCO<sub>3</sub> (70 mL). The solution was stirred vigorously until bubbling ceased, at which time the layers were separated. The organic phase was extracted with CH<sub>2</sub>Cl<sub>2</sub> and the combined organic phases were dried over Na<sub>2</sub>SO<sub>4</sub> and concentrated. The product was purified by silica column chromatography (10% Et<sub>2</sub>O in hexanes) to afford a yellow oil (3.82 g, 10.5 mmol, 94% yield); <sup>1</sup>H NMR (400 MHz, CDCl<sub>3</sub>) δ 7.39 (d, *J* = 1.0 Hz, 1H), 7.21 (s, 1H), 3.98 (s, 3H), 3.93 (s, 3H), 3.07 (d, *J* = 0.7 Hz, 3H), 2.44 (d, *J* = 1.0 Hz, 3H); All characterization data match those reported.



#### Ethyl 4-formyl-1H-pyrrole-2-carboxylate (**895**)

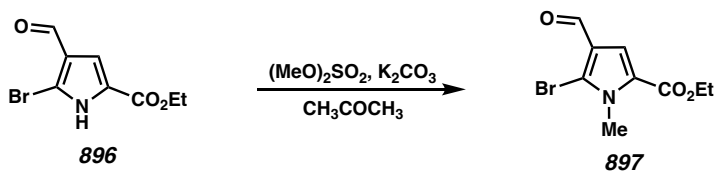
Compound **895** was prepared according to literature procedure.<sup>15</sup> To a stirred solution of pyrrole **894** (20.0 g, 100 mmol, 1.0 equiv) in dry CH<sub>2</sub>Cl<sub>2</sub> and MeNO<sub>2</sub> (600 mL, 1:1) was added powdered AlCl<sub>3</sub> (39.2 g, 144.4 mmol, 2 equiv) in portions. After stirring for 5 min, dichloromethyl methyl ether (98.0 g, 300 mmol, 1.2 equiv) was added dropwise at -15 °C over 10 minutes. The resulting mixture was stirred for 2 hours at -15 °C. Upon full consumption of starting material determined by LCMS analysis, the mixture was quenched

with H<sub>2</sub>O (30 mL) and extracted with EtOAc (2 x 30 mL). The organic layer was washed with saturated aq. NaHCO<sub>3</sub> (30 mL), brine (30 mL), dried over Na<sub>2</sub>SO<sub>4</sub>, and concentrated in vacuo. The residue was crystallized using 10% EtOAc in hexanes to afford pyrrole **895** as a green solid (35.61 g, 114.36 mmol, 99% yield); <sup>1</sup>H NMR (400 MHz, CDCl<sub>3</sub>) δ 9.86 (s, 1H), 9.74 (br s, 1H), 7.57 (dd, *J* = 3.3, 1.5 Hz, 1H), 7.33–7.32 (m, 1H), 4.37 (q, *J* = 7.2 Hz, 2H), 1.38 (t, *J* = 7.2 Hz, 3H); All characterization data match those reported.



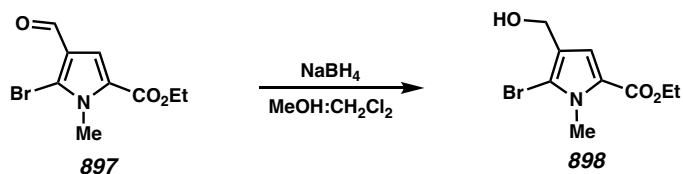
#### Ethyl 5-bromo-4-formyl-1*H*-pyrrole-2-carboxylate (**896**)

A flame-dried round bottom flask was charged with pyrrole **895** (1.34 g, 8 mmol, 1.0 equiv) in DCM (70 mL) and cooled to 0 °C. A solution of Br<sub>2</sub> (0.45 mL, 8.8 mmol, 1.1 equiv) in 10 mL DCM was then added dropwise, and the solution was stirred overnight at room temperature. After 18 hours, the reaction was quenched with saturated aqueous Na<sub>2</sub>S<sub>2</sub>O<sub>3</sub> (35 mL) and extracted with DCM (3 x 30 mL). The combined organic layers were dried over Na<sub>2</sub>SO<sub>4</sub>, filtered, and concentrated. The crude reaction mixture was then purified by silica column chromatography (20 → 30% EtOAc in hexanes) to afford pyrrole **896** as a yellow solid (1.96 g, 5.9 mmol, 74% yield); <sup>1</sup>H NMR (400 MHz, CDCl<sub>3</sub>) δ 9.80 (s, 1H), 7.28 (d, *J* = 2.7 Hz, 1H), 4.37 (q, *J* = 7.1 Hz, 2H), 1.38 (t, *J* = 7.1 Hz, 3H); <sup>13</sup>C NMR (100 MHz, CDCl<sub>3</sub>) δ 184.8, 160.2, 125.8, 124.6, 114.9, 112.9, 61.7, 14.4; IR (Neat Film, NaCl) 3210, 2987, 1698, 1674, 1653, 1554, 1462, 1446, 1377, 1250, 1208, 1012, 847, 821, 773 cm<sup>-1</sup>; HRMS (ESI+) *m/z* calc'd for C<sub>8</sub>H<sub>9</sub>BrNO<sub>3</sub> [M+H]<sup>+</sup>: 245.9760, found 245.9759.



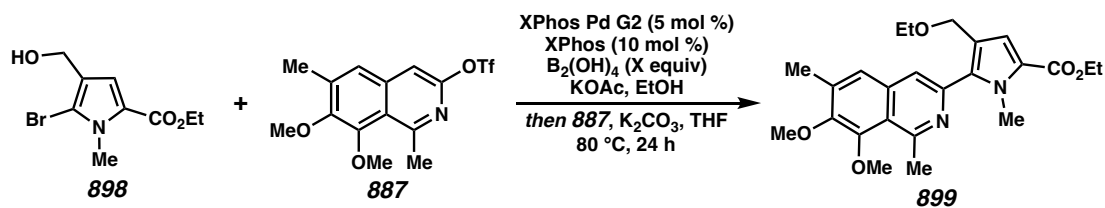
### Ethyl 5-bromo-4-formyl-1-methyl-1H-pyrrole-2-carboxylate (897)

A flame-dried round bottom flask was charged with pyrrole **896** (500 mg, 2 mmol, 1 equiv) and K<sub>2</sub>CO<sub>3</sub> (1.4 g, 10.2 mmol, 5 equiv) in degassed acetone (20 mL, 0.1 M). Dimethyl sulfate (0.25 mL, 2.64 mmol, 1.3 equiv) was then added dropwise, and the reaction was stirred for 1 hour at room temperature. After full consumption of starting material by TLC analysis, the reaction was quenched with saturated aqueous NH<sub>4</sub>Cl (50 mL), and extracted with EtOAc (3 x 20 mL). The combined organic layers were dried over Na<sub>2</sub>SO<sub>4</sub>, filtered, and concentrated. The crude reaction mixture was then purified by silica column chromatography (10 → 20% EtOAc in hexanes) to afford pyrrole **897** as a pink-red solid (468 mg, 1.8 mmol, 90% yield); <sup>1</sup>H NMR (400 MHz, CDCl<sub>3</sub>) δ 9.81 (s, 1H), 7.42 (s, 1H), 4.30 (q, *J* = 7.1 Hz, 2H), 4.00 (s, 3H), 1.35 (t, *J* = 7.1 Hz, 3H); <sup>13</sup>C NMR (100 MHz, CDCl<sub>3</sub>) δ 185.0, 160.4, 126.1, 122.9, 119.4, 117.3, 61.0, 34.9, 14.4; IR (Neat Film, NaCl) 2978, 1713, 1668, 1651, 1469, 1442, 1369, 1352, 1293, 1281, 1242, 1203, 1081, 1036, 764, 739, 667 cm<sup>-1</sup>; HRMS (ESI+) *m/z* calc'd for C<sub>9</sub>H<sub>11</sub>BrNO<sub>3</sub> [M+H]<sup>+</sup>: 259.9917, found 259.9921.



### Ethyl 5-bromo-4-(hydroxymethyl)-1-methyl-1H-pyrrole-2-carboxylate (898)

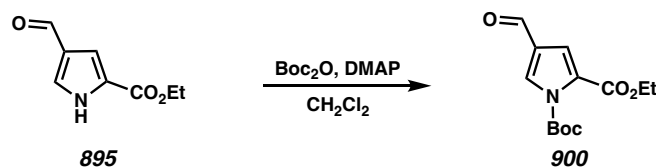
A flame-dried round bottom flask was charged with pyrrole **897** (436 mg, 1.7 mmol, 1 equiv) in 4:1 DCM:MeOH (13.6 mL:3.4 mL, 0.1 M total) and cooled to 0 °C. NaBH<sub>4</sub> (190 mg, 5 mmol, 3 equiv) was then added to the flask, and the reaction was stirred for 30 minutes. After full consumption of starting material by TLC analysis, the reaction was quenched by adding citric acid monohydrate (714 mg, 2 equiv) and stirring rapidly for 10 minutes. The solution was then basified by the slow addition of saturated aqueous NaHCO<sub>3</sub> (20 mL) and extracted with DCM (3 x 20 mL). The combined organic layers were dried over Na<sub>2</sub>SO<sub>4</sub>, filtered, and concentrated. The crude reaction mixture was then purified by silica column chromatography (10 → 20% EtOAc in hexanes) to afford pyrrole **898** as a yellow oil (440 mg, 1.68 mmol, 99% yield); <sup>1</sup>H NMR (400 MHz, CDCl<sub>3</sub>) δ 7.04 (s, 1H), 4.50 (s, 2H), 4.27 (q, *J* = 7.1 Hz, 2H), 3.93 (s, 3H), 1.33 (t, *J* = 7.1 Hz, 3H); <sup>13</sup>C NMR (100 MHz, CDCl<sub>3</sub>) δ 160.6, 123.9, 122.9, 117.5, 112.0, 60.3, 58.1, 34.8, 14.5; IR (Neat Film, NaCl) 3414, 2978, 2945, 2877, 1702, 1553, 1507, 1463, 1437, 1405, 1244, 1156, 1105, 1081, 1057, 999, 833, 759, 667 cm<sup>-1</sup>; HRMS (ESI+) *m/z* calc'd for C<sub>9</sub>H<sub>13</sub>BrNO<sub>3</sub> [M+H]<sup>+</sup>: 262.0073, found 262.0080.



#### Ethyl 5-(7,8-dimethoxy-1,6-dimethylisoquinolin-3-yl)-4-(ethoxymethyl)-1-methyl-1H-pyrrole-2-carboxylate (**899**)

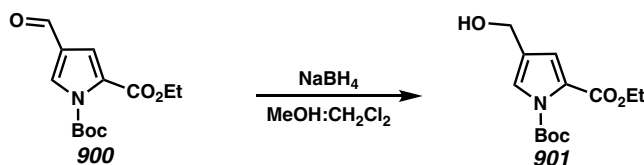
This procedure was adapted from the method of Molander *et al.*<sup>17</sup> In a flame-dried  $\mu$ W vial was charged with XPhos Pd G2 catalyst (9.44 mg, 0.012 mmol, 5 mol %), XPhos ligand (11.4 g, 0.024 mmol, 10 mol %), bis-boronic acid (65 mg, 0.72 mmol, 3

equiv), KOAc (71 mg, 0.72 mmol, 3 equiv), and pyrrole **898** (63 mg, 0.24 mmol, 1 equiv). The vial was then sealed, and vacuum purged/refilled with N<sub>2</sub> four times. Then, 0.14 M degassed EtOH (1.7 mL) was added, and heated to 80 °C for 1 to 2 hours until no starting material was observed. Upon full conversion of starting material, the vial was cooled to room temperature, and 1.8 M of degassed aq. K<sub>2</sub>CO<sub>3</sub> solution (0.4 mL) was added to the vial. After stirring for 5 minutes, triflate **887** (105 mg, 0.29 mmol, 1.2 equiv) in 0.4 mL THF was added to the vial, then heated to 80 °C over 18 hours. The reaction vial was then cooled to room temperature, filtered over celite, and washed with EtOAc (2 x 1 mL). The crude reaction mixture was concentrated and directly purified by silica column chromatography (30% EtOAc in hexanes + 1% NEt<sub>3</sub>) to yield isoquinoline **899** as a brown oil (19 mg, 0.046 mmol, 19% yield); <sup>1</sup>H NMR (400 MHz, CDCl<sub>3</sub>) δ 7.66 (s, 1H), 7.37 (s, 1H), 7.10 (s, 1H), 4.34–4.24 (m, 4H), 4.01 (s, 3H), 4.00 (s, 3H), 3.95 (s, 3H), 3.52 (q, *J* = 7.0 Hz, 2H), 3.13 (s, 3H), 2.46 (s, 3H), 1.36 (t, *J* = 7.1 Hz, 3H); <sup>13</sup>C NMR (100 MHz, CDCl<sub>3</sub>) δ 161.7, 157.0, 151.0, 149.8, 141.5, 138.9, 137.7, 134.8, 124.1, 123.2, 121.6, 120.7, 120.1, 118.8, 65.4, 65.3, 60.9, 60.3, 59.9, 34.7, 27.3, 17.1, 15.5, 14.6; IR (Neat Film, NaCl) 2971, 2930, 2858, 2367, 1701, 1591, 1557, 1492, 1462, 1438, 1390, 1330, 1239, 1207, 1086, 1005, 907, 831, 765 cm<sup>-1</sup>; HRMS (ESI+) *m/z* calc'd for C<sub>24</sub>H<sub>31</sub>N<sub>2</sub>O<sub>5</sub> [M+H]<sup>+</sup>: 427.2227, found 427.2240.



**1-(tert-butyl) 2-ethyl 4-formyl-1H-pyrrole-1,2-dicarboxylate (900)**

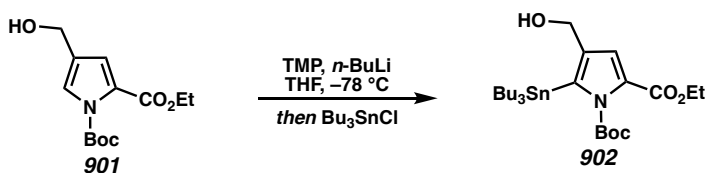
A flame-dried round bottom flask was charged with pyrrole **895** (2 g, 12 mmol, 1 equiv), DMAP (146 mg, 1.2 mmol, 10 mol %), and a magnetic stirring bar in DCM (5 mL, 2.4 M). A solution of Boc<sub>2</sub>O (2.9 g, 13.2 mmol, 1.1 equiv) in DCM (6 mL, 2 M) was then added dropwise, and stirred overnight at room temperature. Upon full consumption of the starting material, the crude reaction was quenched with 1 M HCl (10 mL) and extracted with Et<sub>2</sub>O (3 x 10 mL). The combined organic layers were dried over MgSO<sub>4</sub>, filtered, and concentrated. The crude reaction mixture was then purified by silica column chromatography (10 → 30% EtOAc in hexanes) to yield pyrrole **900** as a clear oil (3.1 g, 11.8 mmol, 98% yield); <sup>1</sup>H NMR (400 MHz, CDCl<sub>3</sub>) δ 9.83 (s, 1H), 7.88 (d, *J* = 1.8 Hz, 1H), 7.18 (d, *J* = 1.8 Hz, 1H), 4.33 (q, *J* = 7.2 Hz, 2H), 1.61 (s, 9H), 1.36 (t, *J* = 7.2 Hz, 3H); <sup>13</sup>C NMR (100 MHz, CDCl<sub>3</sub>) δ 185.1, 160.3, 147.5, 132.3, 127.7, 126.3, 117.0, 86.8, 61.6, 27.7, 14.3; IR (Neat Film, NaCl) 3127, 2981, 2812, 1766, 1731, 1687, 1560, 1417, 1371, 1340, 1281, 1225, 1152, 1112, 1074, 1012, 832, 774, 667 cm<sup>-1</sup>; HRMS (ESI+) *m/z* calc'd for *N*-H **900** C<sub>8</sub>H<sub>9</sub>NO<sub>3</sub> [M+H]<sup>+</sup>: 168.0655, found 168.0656.



#### 1-(*tert*-butyl) 2-ethyl 4-(hydroxymethyl)-1*H*-pyrrole-1,2-dicarboxylate (**901**)

A flame-dried round bottom flask was charged with pyrrole **900** (500 mg, 2 mmol, 1 equiv) in 4:1 DCM:MeOH (19 mL, 0.1 M total) and cooled to 0 °C. NaBH<sub>4</sub> (213 mg, 5.6 mmol, 3 equiv) was then added in portions, and stirred for 30 minutes at room temperature. After full consumption of starting material by TLC analysis, the reaction was quenched by adding citric acid monohydrate (840 mg, 2 equiv) and stirred rapidly for 10 minutes. The

solution was then basified by the slow addition of saturated aqueous NaHCO<sub>3</sub> (20 mL) and extracted with DCM (3 x 20 mL). The combined organic layers were dried over Na<sub>2</sub>SO<sub>4</sub>, filtered, and concentrated. The crude reaction mixture was then purified by silica column chromatography (20 → 30% EtOAc in hexanes) to afford pyrrole **901** as a clear oil (533 mg, 1.98 mmol, 99% yield); <sup>1</sup>H NMR (400 MHz, CDCl<sub>3</sub>) δ 7.29 (d, *J* = 1.8 Hz, 1H), 6.84 (d, *J* = 1.8 Hz, 1H), 4.52 (d, *J* = 5.4 Hz, 2H), 4.30 (q, *J* = 7.1 Hz, 2H), 1.57 (s, 9H), 1.34 (t, *J* = 7.1 Hz, 3H); <sup>13</sup>C NMR (100 MHz, CDCl<sub>3</sub>) δ 160.9, 148.3, 126.3, 124.2, 120.0, 119.9, 85.0, 61.1, 58.1, 27.8, 14.4; IR (Neat Film, NaCl) 3437, 2979, 2938, 2876, 1750, 1720, 1475, 1410, 1370, 1329, 1276, 1232, 1155, 1072, 1019, 980, 848, 831, 775 cm<sup>-1</sup>; HRMS (ESI+) *m/z* calc'd for *N*-H **901** C<sub>8</sub>H<sub>12</sub>NO<sub>3</sub> [M+H]<sup>+</sup>: 170.0812, found 170.0808.

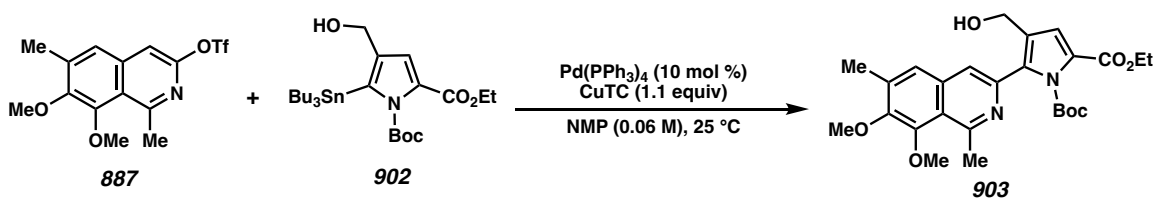


**1-(*tert*-butyl) 2-ethyl 4-(hydroxymethyl)-5-(tributylstannyl)-1*H*-pyrrole-1,2-dicarboxylate (902)**

A flame-dried round bottom flask was charged with 2,2,6,6-tetramethylpiperidine (TMP) (0.5 mL, 2.93 mmol, 2.05 equiv) in THF (5.4 mL, 0.26 M) and cooled to -78 °C. *n*-BuLi (2.5 M in hexanes, 1.2 mL, 2.93 mmol, 2.05 equiv) was then added dropwise, and stirred for 10 minutes at -78 °C, then 30 minutes at 0 °C. The solution was cooled again to -78 °C, and pyrrole **901** (385 mg, 1.43 mmol, 1 equiv) in THF (1.8 mL, 0.79 M) was added dropwise, and stirred for 20 minutes at -78 °C. Then, Bu<sub>3</sub>SnCl (0.78 mL, 2.86 mmol, 2 equiv) was added dropwise, and stirred for 4 hours as the cooling bath slowly warms to room temperature. After full consumption of starting material by TLC analysis, the reaction



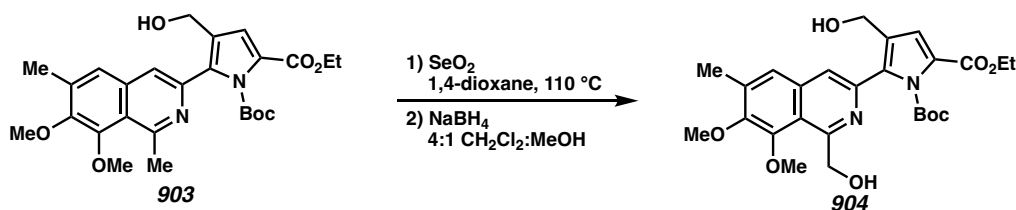
was quenched with H<sub>2</sub>O (10 mL), extracted with Et<sub>2</sub>O (3 x 10 mL). The combined organic phases were dried over Na<sub>2</sub>SO<sub>4</sub>, filtered, and concentrated. The crude reaction mixture was then purified by silica column chromatography (0 → 5% → 10% EtOAc in hexanes) to afford pyrrole **902** as a clear oil (726 mg, 1.3 mmol, 91% yield); <sup>1</sup>H NMR (400 MHz, CDCl<sub>3</sub>) δ 6.92 (s, 1H), 4.46 (d, *J* = 5.6 Hz, 2H), 4.28 (q, *J* = 7.1 Hz, 2H), 1.55 (s, 9H), 1.51–1.42 (m, 6H), 1.37–1.26 (m, 7H), 1.21 (t, *J* = 7.1 Hz, 3H), 1.13–1.05 (m, 5H), 0.88 (t, *J* = 7.3 Hz, 9H); <sup>13</sup>C NMR (100 MHz, CDCl<sub>3</sub>) δ 161.3, 151.1, 141.4, 135.9, 129.2, 121.5, 84.9, 66.0, 60.9, 59.1, 29.3, 27.6, 27.4, 13.8, 12.3; IR (Neat Film, NaCl) 3448, 2955, 2927, 2870, 1727, 1550, 1477, 1463, 1369, 1321, 1236, 1206, 1158, 1073, 1043, 995, 847, 779, 667 cm<sup>-1</sup>; HRMS (ESI +) *m/z* calc'd for C<sub>25</sub>H<sub>46</sub>NO<sub>5</sub>Sn [M+H]<sup>+</sup>: 552.2419, found 552.2412.



**1-(*tert*-butyl) 2-ethyl 5-(7,8-dimethoxy-1,6-dimethylisoquinolin-3-yl)-4-(hydroxymethyl)-1*H*-pyrrole-1,2-dicarboxylate (903)**

A flame-dried round bottom flask was charged with isoquinoline **887** (261 mg, 0.72 mmol, 1 equiv) and a magnetic stirring bar, and brought in a N<sub>2</sub>-filled glovebox. A solution of organostannane **902** (399 mg, 0.72 mmol, 1 equiv) in NMP (11.9 mL, 0.06 M) was then added to the flask, and stirred in the glovebox for 10 minutes at ambient temperature. Then, Pd(PPh<sub>3</sub>)<sub>4</sub> (83 mg, 0.072 mmol, 10 mol %) was added, followed by addition of CuTC (150 mg, 0.79 mmol, 1.1 equiv). The flask was brought out of the glovebox and stirred for 2 hours at room temperature. Upon full consumption of starting material, the reaction was quenched with saturated aq. NaHCO<sub>3</sub> (10 mL) and extracted with EtOAc (3 x 10 mL). The

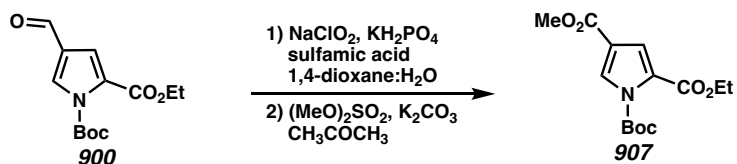
combined organic phases were washed again with 5% aq. LiCl solution (2 x 10 mL), brine (10 mL), and dried over Na<sub>2</sub>SO<sub>4</sub>. The crude reaction mixture was filtered, concentrated, and purified by silica column chromatography (20 → 40% EtOAc in hexanes) to yield isoquinoline **903** as a yellow solid (8.06 g, 30.6 mmol, 94% yield); <sup>1</sup>H NMR (400 MHz, CDCl<sub>3</sub>) δ 7.59 (s, 1H), 7.33 (s, 1H), 6.96 (s, 1H), 4.52 (s, 1H), 4.43 (s, 2H), 4.33 (q, *J* = 7.1 Hz, 2H), 3.99 (s, 3H), 3.94 (s, 3H), 3.11 (s, 3H), 2.44 (s, 3H), 1.49 (s, 9H), 1.36 (t, *J* = 7.1 Hz, 3H); <sup>13</sup>C NMR (100 MHz, CDCl<sub>3</sub>) δ 160.4, 157.2, 151.2, 150.0, 149.9, 140.6, 138.5, 136.1, 134.5, 126.4, 124.2, 123.9, 121.8, 119.9, 118.4, 85.8, 61.1, 60.9, 60.8, 60.3, 57.5, 27.5, 17.1, 14.6; IR (Neat Film, NaCl) 3391, 2978, 2934, 1763, 1717, 1596, 1558, 1492, 1448, 1393, 1370, 1331, 1282, 1220, 1154, 1078, 1005, 914, 845 cm<sup>-1</sup>; HRMS (ESI+) *m/z* calc'd for C<sub>26</sub>H<sub>33</sub>N<sub>2</sub>O<sub>7</sub> [M+H]<sup>+</sup>: 485.2282, found 485.2310.



**1-(*tert*-butyl) 2-ethyl 4-(hydroxymethyl)-5-(1-(hydroxymethyl)-7,8-dimethoxy-6-methylisoquinolin-3-yl)-1*H*-pyrrole-1,2-dicarboxylate (904)**

In a flame-dried μW vial was charged with SeO<sub>2</sub> (105 mg, 0.95 mmol, 2 equiv) and a magnetic stir bar. The vial was vacuum purged/refilled with N<sub>2</sub> three times. A solution of isoquinoline **903** (229 mg, 0.47 mmol, 1 equiv) in 1,4-dioxane (9.5 mL, 0.05 M) was then added to the vial, and heated to reflux for 2 hours. After full consumption of starting material observed by LCMS analysis, the vial was cooled to room temperature and the crude reaction mixture was filtered through celite, rinsing with EtOAc. The crude reaction was concentrated, then dissolved in 4:1 DCM:MeOH (4.7 mL, 0.1 M total).

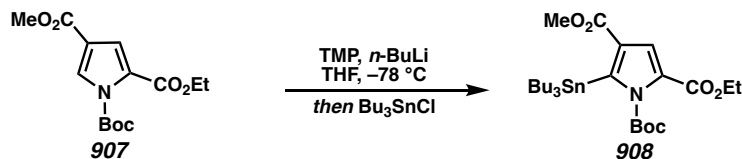
NaBH<sub>4</sub> (18 mg, 0.47 mmol, 1 equiv) was then added, and the reaction was stirred for 30 minutes at room temperature. After full conversion of the aldehyde intermediate observed by LCMS analysis, the reaction was quenched with citric acid monohydrate (199 mg, 0.95 mmol, 2 equiv) and water, and the solution was stirred rapidly for 10 minutes. The solution was then basified by the addition of saturated aq. NaHCO<sub>3</sub> (10 mL), the layers were separated and the aqueous phase was extracted with DCM (3 x 10 mL). The combined organic phases were dried over Na<sub>2</sub>SO<sub>4</sub>, filtered, and concentrated. The crude reaction mixture was purified by silica column chromatography (40 → 50% EtOAc in hexanes) to yield isoquinoline **904** as a white solid (8.06 g, 30.6 mmol, 61% yield); <sup>1</sup>H NMR (400 MHz, CDCl<sub>3</sub>) δ 7.72 (s, 1H), 7.45 (s, 1H), 7.03 (s, 1H), 5.29 (s, 2H), 4.52 (s, 2H), 4.34 (q, *J* = 7.1 Hz, 2H), 4.03 (s, 3H), 3.93 (s, 3H), 2.46 (s, 3H), 1.43 (s, 9H), 1.37 (t, *J* = 7.1 Hz, 3H); <sup>13</sup>C NMR (100 MHz, CDCl<sub>3</sub>) δ 160.3, 157.5, 151.0, 149.5, 149.3, 139.6, 138.8, 135.4, 134.5, 124.5, 124.3, 124.2, 119.8, 119.8, 118.1, 85.8, 64.8, 60.9, 60.9, 60.3, 57.5, 27.4, 17.1, 14.6; IR (Neat Film, NaCl) 3409, 2979, 2937, 2365, 1766, 1713, 1560, 1494, 1447, 1381, 1329, 1217, 1153, 1076, 1006, 911, 833, 734, 668 cm<sup>-1</sup>; HRMS (ESI+) *m/z* calc'd for C<sub>26</sub>H<sub>33</sub>N<sub>2</sub>O<sub>8</sub> [M+H]<sup>+</sup>: 501.2231, found 501.2242.



### 1-(*tert*-butyl) 2-ethyl 4-methyl 1*H*-pyrrole-1,2,4-tricarboxylate (**907**)

A flame-dried round bottom flask was charged with pyrrole **900** (1 g, 3.8 mmol, 1 equiv) in 1:1 1,4-dioxane:H<sub>2</sub>O (100 mL, 0.04 M total). The flask was then cooled to 0 °C, and sulfamic acid (2.18 g, 22 mmol, 6 equiv) was added in portions. A solution of NaClO<sub>2</sub>

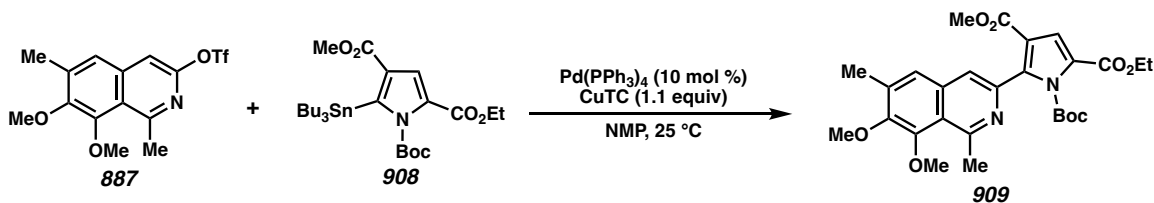
(440 mg, 4.9 mmol, 1.3 equiv) and  $\text{KH}_2\text{PO}_4$  (6.1 g, 44.9 mmol, 12 equiv) in 40 mL of  $\text{H}_2\text{O}$  was then added dropwise via an addition funnel over 30 minutes. The flask was then removed from the ice bath and stirred overnight at room temperature. After full conversion of the starting material was observed, the reaction was extracted with EtOAc (3 x 20 mL). The organic phases were washed with brine (20 mL), dried over  $\text{Na}_2\text{SO}_4$ , filtered, and concentrated. The crude reaction mixture was then dissolved in sparged acetone (38 mL, 0.1 M). Solid  $\text{K}_2\text{CO}_3$  (2.6 g, 18.7 mmol, 5 equiv) was added, then dimethyl sulfate (0.46 mL, 4.9 mmol, 1.3 equiv) was added dropwise. The reaction was stirred at room temperature until full consumption of the starting material was observed. The reaction was then quenched with saturated aq.  $\text{NH}_4\text{Cl}$  (20 mL), extracted with EtOAc (3 x 10 mL), and the combined organic phases were dried over  $\text{Na}_2\text{SO}_4$ . The crude reaction mixture was then filtered, concentrated, and purified by silica column chromatography (5 → 10% EtOAc in hexanes) to yield pyrrole **907** as a clear oil (1.1 g, 3.38 mmol, 89% yield);  $^1\text{H}$  NMR (400 MHz,  $\text{CDCl}_3$ )  $\delta$  7.85 (d,  $J = 1.8$  Hz, 1H), 7.17 (d,  $J = 1.8$  Hz, 1H), 4.31 (q,  $J = 7.1$  Hz, 2H), 3.83 (s, 3H), 1.59 (s, 9H), 1.35 (t,  $J = 7.1$  Hz, 3H);  $^{13}\text{C}$  NMR (100 MHz,  $\text{CDCl}_3$ )  $\delta$  163.8, 160.3, 147.6, 130.3, 126.4, 119.8, 117.4, 86.3, 61.4, 51.8, 27.7, 14.3; IR (Neat Film, NaCl) 3141, 2982, 2902, 2365, 1762, 1724, 1570, 1479, 1396, 1371, 1283, 1237, 1152, 1073, 997, 847, 776, 763, 567  $\text{cm}^{-1}$ ; HRMS (ESI+)  $m/z$  calc'd for  $N\text{-H}$  **907**  $\text{C}_9\text{H}_{12}\text{NO}_4$   $[\text{M}+\text{H}]^+$ : 198.0761, found 198.0754.



**1-(*tert*-butyl) 2-ethyl 4-methyl 5-(tributylstannyl)-1*H*-pyrrole-1,2,4-tricarboxylate (908)**

A flame-dried round bottom flask was charged with 2,2,6,6-tetramethylpiperidine (TMP) (0.19 mL, 1.1 mmol, 1.1 equiv) in THF (2.5 mL, 0.4 M) and cooled to  $-78\text{ }^\circ\text{C}$ . *n*-BuLi (2.5 M in hexanes, 0.48 mL, 1.2 mmol, 1.2 equiv) was then added dropwise, and stirred for 10 minutes at  $-78\text{ }^\circ\text{C}$ , then 30 minutes at  $0\text{ }^\circ\text{C}$ . The solution was cooled again to  $-78\text{ }^\circ\text{C}$ , and pyrrole **907** (297 mg, 1 mmol, 1 equiv) in THF (2.5 mL, 0.4 M) was added dropwise, and stirred for 20 minutes at  $-78\text{ }^\circ\text{C}$ . Then,  $\text{Bu}_3\text{SnCl}$  (0.3 mL, 1.1 mmol, 1.1 equiv) was added dropwise, and stirred for 4 hours as the cooling bath slowly warms to room temperature. After full consumption of starting material by TLC analysis, the reaction was quenched with  $\text{H}_2\text{O}$  (10 mL), extracted with  $\text{Et}_2\text{O}$  (3 x 10 mL). The combined organic phases were dried over  $\text{Na}_2\text{SO}_4$ , filtered, and concentrated. The crude reaction mixture was then purified by silica column chromatography (0  $\rightarrow$  2.5%  $\rightarrow$  5% EtOAc in hexanes) to afford pyrrole **908** as a clear oil (527 mg, 0.9 mmol, 90% yield);  $^1\text{H}$  NMR (400 MHz,  $\text{CDCl}_3$ )  $\delta$  7.22 (s, 1H), 4.29 (q,  $J = 7.1\text{ Hz}$ , 2H), 3.80 (s, 3H), 3.83 (s, 3H), 1.58 (s, 9H), 1.51–1.43 (m, 5H), 1.37–1.27 (m, 11H), 1.12–1.08 (m, 5H), 0.87 (t,  $J = 7.2\text{ Hz}$ , 9H);  $^{13}\text{C}$  NMR (100 MHz,  $\text{CDCl}_3$ )  $\delta$  165.6, 160.6, 150.4, 150.0, 128.8, 126.6, 120.4, 85.9, 61.0, 51.6, 29.1, 27.6, 27.4, 13.9, 12.6; IR (Neat Film, NaCl) 2955, 2924, 2870, 1750, 1719, 1534, 1461, 1424, 1370, 1308, 1253, 1224, 1203, 1156, 1076, 1020, 848, 780, 667  $\text{cm}^{-1}$ ;

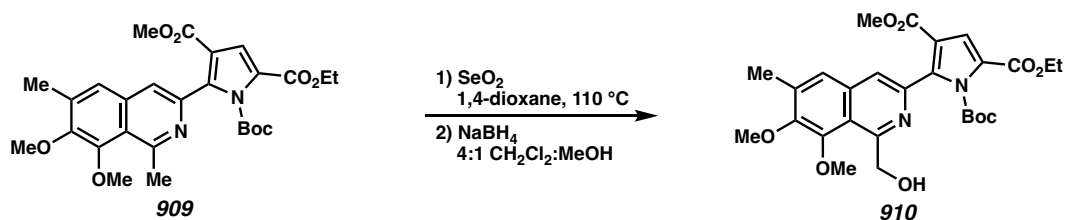
HRMS (MM:ESI-APCI+)  $m/z$  calc'd for  $C_{26}H_{46}NO_6Sn$   $[M+H]^+$ : 580.2368, found 580.2370.



**1-(*tert*-butyl) 2-ethyl 4-methyl 5-(7,8-dimethoxy-1,6-dimethylisoquinolin-3-yl)-1*H*-pyrrole-1,2,4-tricarboxylate (909)**

A flame-dried round bottom flask was charged with isoquinoline **887** (198 mg, 0.54 mmol, 1 equiv) and a magnetic stirring bar, and brought in a N<sub>2</sub>-filled glovebox. A solution of organostannane **908** (319 mg, 0.54 mmol, 1 equiv) in NMP (9.3 mL, 0.06 M) was then added to the flask, and stirred in the glovebox for 10 minutes at ambient temperature. Then, Pd(PPh<sub>3</sub>)<sub>4</sub> (63 mg, 0.054 mmol, 10 mol %) was added, followed by addition of CuTC (114 mg, 0.6 mmol, 1.1 equiv). The flask was brought out of the glovebox and stirred for 2 hours at room temperature. Upon full consumption of starting material, the reaction was quenched with saturated aq. NaHCO<sub>3</sub> (10 mL) and extracted with EtOAc (3 x 10 mL). The combined organic phases were washed again with 5% aq. LiCl solution (2 x 10 mL), brine (10 mL), and dried over Na<sub>2</sub>SO<sub>4</sub>. The crude reaction mixture was filtered, concentrated, and purified by silica column chromatography (10 → 20% EtOAc in hexanes) to yield isoquinoline **909** as a yellow solid (265 mg, 0.52 mmol, 96% yield); <sup>1</sup>H NMR (400 MHz, CDCl<sub>3</sub>) δ 7.80 (s, 1H), 7.43 (s, 1H), 7.33 (s, 1H), 4.34 (q,  $J = 7.1$  Hz, 2H), 3.98 (s, 3H), 3.94 (s, 3H), 3.70 (s, 3H), 3.07 (s, 3H), 2.43 (s, 3H), 1.40 (s, 9H), 1.37 (t,  $J = 7.1$  Hz, 3H); <sup>13</sup>C NMR (100 MHz, CDCl<sub>3</sub>) δ 163.9, 160.0, 156.3, 151.3, 149.7, 147.5, 148.3, 140.0, 137.6, 134.2, 124.4, 124.3, 122.2, 121.7, 118.9, 85.8, 61.1, 60.9, 60.3, 51.5,

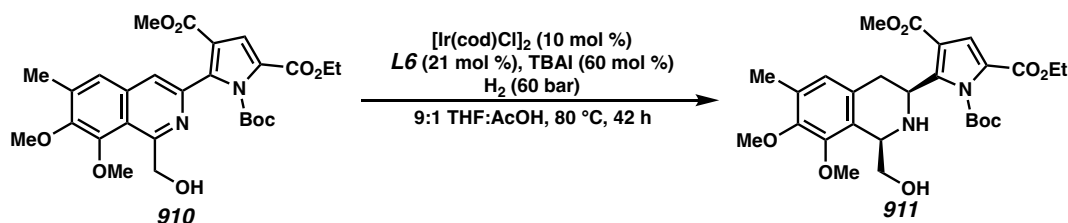
27.4, 17.0, 14.5; IR (Neat Film, NaCl) 2978, 2903, 2365, 1775, 1715, 1555, 1506, 1442, 1394, 1332, 1281, 1237, 1215, 1152, 1080, 1045, 1005, 834, 757  $\text{cm}^{-1}$ ; HRMS (ESI+)  $m/z$  calc'd for  $\text{C}_{27}\text{H}_{33}\text{N}_2\text{O}_8$   $[\text{M}+\text{H}]^+$ : 513.2231, found 513.2246.



**1-(*tert*-butyl) 2-ethyl 4-methyl 5-(1-(hydroxymethyl)-7,8-dimethoxy-6-methylisoquinolin-3-yl)-1*H*-pyrrole-1,2,4-tricarboxylate (910)**

In a flame-dried  $\mu\text{W}$  vial was charged with  $\text{SeO}_2$  (115 mg, 1.03 mmol, 2 equiv) and a magnetic stir bar. The vial was vacuum purged/refilled with  $\text{N}_2$  three times. A solution of isoquinoline **909** (265 mg, 0.52 mmol, 1 equiv) in 1,4-dioxane (10 mL, 0.05 M) was then added to the vial, and heated to reflux for 2 hours. After full consumption of starting material observed by LCMS analysis, the vial was cooled to room temperature and the crude reaction mixture was filtered through celite, rinsing with EtOAc. The crude reaction was concentrated, then dissolved in 4:1 DCM:MeOH (5 mL, 0.1 M total).  $\text{NaBH}_4$  (20 mg, 0.52 mmol, 1 equiv) was then added, and the reaction was stirred for 30 minutes at room temperature. After full conversion of the aldehyde intermediate observed by LCMS analysis, the reaction was quenched with citric acid monohydrate (218 mg, 1.04 mmol, 2 equiv) and water, and the solution was stirred rapidly for 10 minutes. The solution was then basified by the addition of saturated aq.  $\text{NaHCO}_3$  (10 mL), the layers were separated and the aqueous phase was extracted with DCM (3 x 10 mL). The combined organic phases were dried over  $\text{Na}_2\text{SO}_4$ , filtered, and concentrated. The crude reaction mixture was

purified by silica column chromatography (20 → 30% EtOAc in hexanes) to yield isoquinoline **910** as a white solid (207 mg, 0.39 mmol, 75% yield);  $^1\text{H}$  NMR (400 MHz,  $\text{CDCl}_3$ )  $\delta$  7.91 (s, 1H), 7.49 (s, 1H), 7.36 (s, 1H), 5.28 (d,  $J = 4.3$  Hz, 2H), 4.35 (q,  $J = 7.1$  Hz, 2H), 3.93 (s, 3H), 3.72 (s, 3H), 2.45 (s, 3H), 1.38–1.36 (m, 12H);  $^{13}\text{C}$  NMR (100 MHz,  $\text{CDCl}_3$ )  $\delta$  163.9, 160.0, 156.7, 151.2, 149.3, 148.5, 138.6, 138.4, 134.1, 124.5, 124.4, 122.7, 120.2, 118.7, 114.8, 86.6, 64.3, 61.2, 60.9, 51.6, 27.2, 17.0, 14.5; IR (Neat Film, NaCl) 3413, 2980, 2939, 2836, 2365, 1774, 1716, 1558, 1443, 1382, 1330, 1237, 1215, 1152, 1077, 1005, 905, 736, 668  $\text{cm}^{-1}$ ; HRMS (ESI+)  $m/z$  calc'd for  $\text{C}_{27}\text{H}_{33}\text{N}_2\text{O}_9$   $[\text{M}+\text{H}]^+$ : 529.2181, found 529.2199.



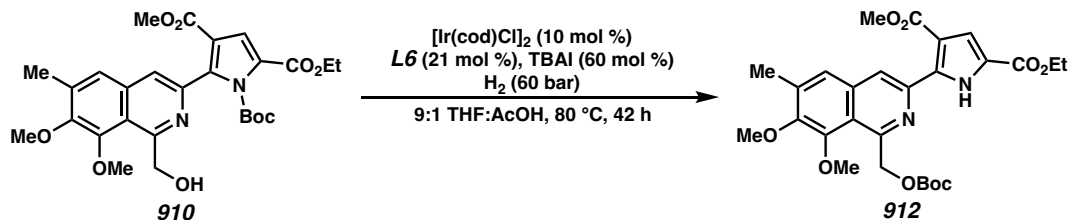
**1-(*tert*-butyl) 2-ethyl 4-methyl 5-(1-(hydroxymethyl)-7,8-dimethoxy-6-methylisoquinolin-3-yl)-1*H*-pyrrole-1,2,4-tricarboxylate (911)**

To an oven-dried 1-dram vial equipped with a stir bar and isoquinoline **910** (5 mg, 0.01 mmol, 1 equiv) was capped with a PTFE-lined septum and pierced with one 21 gauge green needle. The vial was then placed in a Parr bomb and brought into the glovebox, with the exception of the pressure gauge. A layer of plastic wrap and a rubber band were also brought in to seal the top of the bomb. In a nitrogen-filled glovebox, a solution of the BTFM-xylyphos ligand (SL-J008-2) (1.9 mg, 0.0021 mmol, 21 mol %) and  $[\text{Ir}(\text{cod})\text{Cl}]_2$  (0.67 mg, 0.001 mmol, 10 mol %) in THF (0.45 mL per reaction) was prepared and allowed to stand for 10 minutes. Meanwhile, a solution of TBAI (2.2 mg, 0.006 mmol, 0.6 equiv)



in AcOH (0.05 mL per reaction) was prepared in a 1-dram vial, and 0.05 mL of the solution was added to each reaction vial via a syringe. Afterwards, 0.45 mL of the homogeneous iridium catalyst solution was added to each reaction vial via a syringe. After re-capping the vials with caps equipped with needles, the reactions were placed in the bomb and the top was covered tightly with plastic wrap secured by a rubber band. The bomb was then removed from the glovebox, and the pressure gauge was quickly screwed in place and tightened. The bomb was charged to 5-10 bar H<sub>2</sub> and slowly released. This process was repeated two more times, before charging the bomb to 60 bar H<sub>2</sub>. The bomb was then placed in an oil bath and heated to 80 °C for 42 hours. Then, the bomb was removed from the stir plate and the hydrogen pressure was vented. The reaction vials were removed from the bomb and each solution was basified by the addition of saturated aqueous K<sub>2</sub>CO<sub>3</sub> (1 mL). The layers were separated, and the aqueous layer was extracted with EtOAc (3 x 1 mL). The combined organics layers were then dried over Na<sub>2</sub>SO<sub>4</sub>, and concentrated in vacuo. The crude reaction mixture was purified by silica column chromatography (50 → 75% EtOAc in hexanes + 1% NEt<sub>3</sub>) to yield isoquinoline **911** as a white solid (2 mg, 0.004 mmol, 40% yield); <sup>1</sup>H NMR (400 MHz, CDCl<sub>3</sub>) δ 7.26 (s, 1H), 6.48 (s, 1H), 4.83 (dd, *J* = 11.2, 3.6 Hz, 1H), 4.06 (dd, *J* = 11.1, 3.4 Hz, 1H), 3.84–3.82 (m, 2H), 3.81 (s, 3H), 3.79 (s, 3H), 3.65 (s, 3H), 3.24–3.18 (m, 1H), 2.70 (dd, *J* = 15.7, 11.2 Hz, 1H), 2.13 (s, 3H), 1.40 (s, 9H); <sup>13</sup>C NMR (100 MHz, CDCl<sub>3</sub>) δ 163.9, 160.0, 156.7, 151.2, 149.3, 148.5, 138.6, 138.4, 134.1, 124.5, 124.4, 122.7, 120.2, 118.7, 114.8, 86.6, 64.3, 61.2, 60.9, 51.6, 27.2, 17.0, 14.5; IR (Neat Film, NaCl) 2979, 2877, 2835, 2364, 1697, 1682, 1674, 1582,

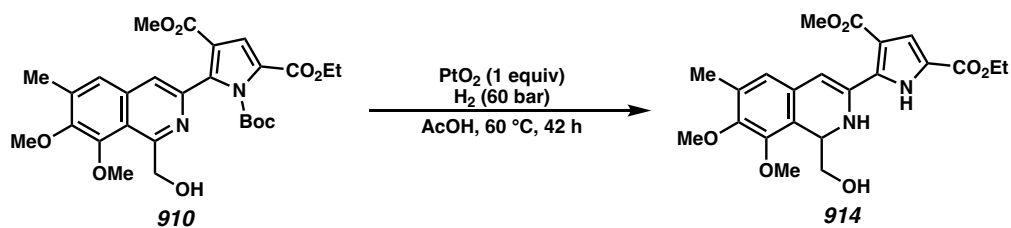
1362, 1293, 1202, 1136, 1084, 1025, 911, 832, 775, 737, 667  $\text{cm}^{-1}$ ; HRMS (ESI+)  $m/z$  calc'd for  $N\text{-H}$  **911**  $\text{C}_{22}\text{H}_{29}\text{N}_2\text{O}_7$   $[\text{M}+\text{H}]^+$ : 433.1969, found 433.1985.



**2-ethyl 4-methyl 5-(1-(((*tert*-butoxycarbonyl)oxy)methyl)-7,8-dimethoxy-6-methylisoquinolin-3-yl)-1*H*-pyrrole-2,4-dicarboxylate (912)**

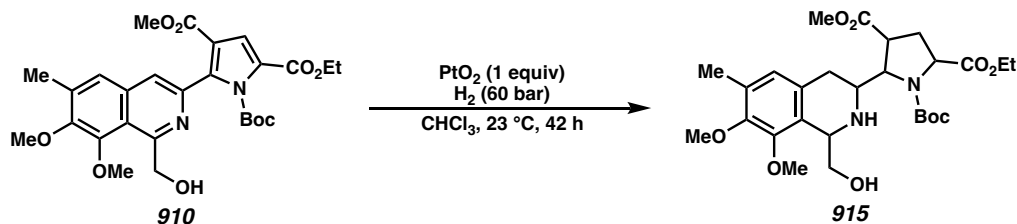
To an oven-dried 1-dram vial equipped with a stir bar and isoquinoline **910** (5 mg, 0.01 mmol, 1 equiv) was capped with a PTFE-lined septum and pierced with one 21 gauge green needle. The vial was then placed in a Parr bomb and brought into the glovebox, with the exception of the pressure gauge. A layer of plastic wrap and a rubber band were also brought in to seal the top of the bomb. In a nitrogen-filled glovebox, a solution of the BTFM-xylyphos ligand (SL-J008-2) (1.9 mg, 0.0021 mmol, 21 mol %) and  $[\text{Ir}(\text{cod})\text{Cl}]_2$  (0.67 mg, 0.001 mmol, 10 mol %) in THF (0.45 mL per reaction) was prepared and allowed to stand for 10 minutes. Meanwhile, a solution of TBAI (2.2 mg, 0.006 mmol, 0.6 equiv) in AcOH (0.05 mL per reaction) was prepared in a 1-dram vial, and 0.05 mL of the solution was added to each reaction vial via a syringe. Afterwards, 0.45 mL of the homogeneous iridium catalyst solution was added to each reaction vial via a syringe. After re-capping the vials with caps equipped with needles, the reactions were placed in the bomb and the top was covered tightly with plastic wrap secured by a rubber band. The bomb was then removed from the glovebox, and the pressure gauge was quickly screwed in place and tightened. The bomb was charged to 5-10 bar  $\text{H}_2$  and slowly released. This process was

repeated two more times, before charging the bomb to 60 bar H<sub>2</sub>. The bomb was then placed in an oil bath and heated to 80 °C for 42 hours. Then, the bomb was removed from the stir plate and the hydrogen pressure was vented. The reaction vials were removed from the bomb and each solution was basified by the addition of saturated aqueous K<sub>2</sub>CO<sub>3</sub> (1 mL). The layers were separated, and the aqueous layer was extracted with EtOAc (3 x 1 mL). The combined organics layers were then dried over Na<sub>2</sub>SO<sub>4</sub>, and concentrated in vacuo. The crude reaction mixture was purified by silica column chromatography (40% EtOAc in hexanes) to yield isoquinoline **912** as a white solid (2.1 mg, 0.004 mmol, 40% yield); (207 mg, 0.39 mmol, 44% yield); <sup>1</sup>H NMR (400 MHz, CDCl<sub>3</sub>) δ 10.69 (br s, 1H), 9.43 (s, 1H), 7.46 (s, 1H), 7.16 (s, 1H), 5.70 (s, 2H), 4.38 (q, *J* = 7.1 Hz, 2H), 4.01 (s, 3H), 3.98 (s, 3H), 3.91 (s, 3H), 2.35 (s, 3H), 1.52 (s, 9H), 1.41 (t, *J* = 7.1 Hz, 3H); <sup>13</sup>C NMR (100 MHz, CDCl<sub>3</sub>) δ 165.0, 160.7, 159.2, 155.3, 153.6, 151.7, 138.4, 128.0, 126.4, 121.8, 120.1, 116.7, 113.6, 108.6, 97.8, 82.9, 68.2, 60.9, 56.0, 51.7, 31.1, 27.9, 14.6, 9.9; IR (Neat Film, NaCl) 2975, 2900, 2364, 1787, 1715, 1555, 1510, 1442, 1394, 1337, 1281, 1240, 1215, 1170, 1080, 1058, 934, 830, 750 cm<sup>-1</sup>; HRMS (ESI+) *m/z* calc'd for C<sub>27</sub>H<sub>33</sub>N<sub>2</sub>O<sub>9</sub> [M+H]<sup>+</sup>: 529.2181, found 529.2199.



**2-ethyl**      **4-methyl**      **5-(1-(hydroxymethyl)-7,8-dimethoxy-6-methyl-1,2-dihydroisoquinolin-3-yl)-1H-pyrrole-2,4-dicarboxylate (914)**

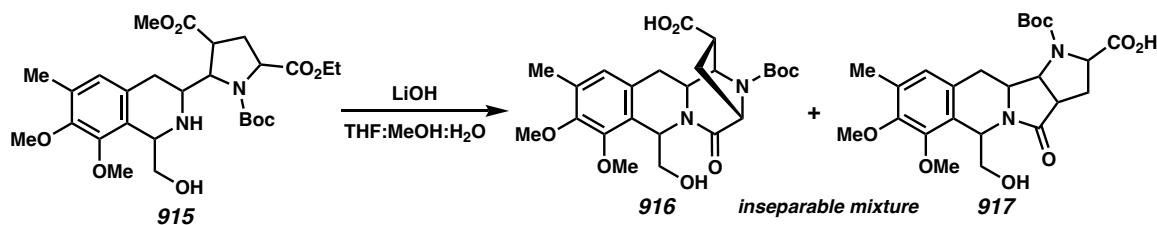
To an oven-dried scintillation vial equipped with a stir bar and isoquinoline **910** (50 mg, 0.1 mmol, 1 equiv) was charged with PtO<sub>2</sub> (21 mg, 0.1 mmol, 1 equiv). The reaction mixture was dissolved in AcOH (0.95 mL, 0.1 M), and was capped with a PTFE-lined septum and pierced with two 21 gauge green needles. The reaction vial was then placed in the bomb reactor, and the pressure gauge was quickly screwed in place and tightened. The bomb was charged to 5-10 bar H<sub>2</sub> and slowly released. This process was repeated two more times, before charging the bomb to 60 bar H<sub>2</sub>. The bomb was then placed in an oil bath and heated to 60 °C for 42 hours. Then, the bomb was removed from the stir plate and the hydrogen pressure was vented. The reaction vials were removed from the bomb and each solution was basified by the addition of saturated aqueous K<sub>2</sub>CO<sub>3</sub> (1 mL). The layers were separated, and the aqueous layer was extracted with EtOAc (3 x 1 mL). The combined organics layers were then dried over Na<sub>2</sub>SO<sub>4</sub>, and concentrated in vacuo. The crude reaction mixture was purified by silica column chromatography (20 → 40% EtOAc in hexanes) to yield isoquinoline **914** as a white solid (34 mg, 0.08 mmol, 80% yield); <sup>1</sup>H NMR (400 MHz, CDCl<sub>3</sub>) δ 9.70 (br s, 1H), 7.32 (s, 1H), 6.79 (s, 1H), 6.42 (s, 1H), 5.96 (dd, *J* = 9.4, 3.8 Hz, 1H), 4.32 (q, *J* = 7.1 Hz, 2H), 3.93 (s, 3H), 3.82 (s, 3H), 3.81 (s, 3H), 3.75–3.69 (m, 1H), 3.63–3.56 (m, 1H), 2.24 (s, 3H), 1.34 (t, *J* = 7.1 Hz, 3H); <sup>13</sup>C NMR (100 MHz, CDCl<sub>3</sub>) δ 164.5, 160.7, 153.1, 151.6, 148.7, 132.1, 127.0, 124.0, 123.2, 121.5, 118.0, 117.6, 113.9, 81.4, 62.1, 61.0, 61.0, 60.2, 51.8, 27.8, 16.0, 14.5; IR (Neat Film, NaCl) 3483, 3264, 2978, 2938, 2251, 1712, 1697, 1572, 1477, 1462, 1369, 1327, 1258, 1200, 1117, 1076, 911, 766, 733 cm<sup>-1</sup>; HRMS (ESI+) *m/z* calc'd for C<sub>22</sub>H<sub>27</sub>N<sub>2</sub>O<sub>7</sub> [M+H]<sup>+</sup>: 431.1813, found 431.1829.



**1-(*tert*-butyl) 2-ethyl 4-methyl 5-(1-(hydroxymethyl)-7,8-dimethoxy-6-methyl-1,2,3,4-tetrahydroisoquinolin-3-yl)pyrrolidine-1,2,4-tricarboxylate (915)**

To an oven-dried scintillation vial equipped with a stir bar and isoquinoline **910** (50 mg, 0.1 mmol, 1 equiv) was charged with PtO<sub>2</sub> (21 mg, 0.1 mmol, 1 equiv). The reaction mixture was dissolved in CHCl<sub>3</sub> (0.95 mL, 0.1 M), and was capped with a PTFE-lined septum and pierced with two 21 gauge green needles. The reaction vial was then placed in the bomb reactor, and the pressure gauge was quickly screwed in place and tightened. The bomb was charged to 5-10 bar H<sub>2</sub> and slowly released. This process was repeated two more times, before charging the bomb to 60 bar H<sub>2</sub>, and stirred at room temperature for 42 hours. Then, the bomb was removed from the stir plate and the hydrogen pressure was vented. The reaction vials were removed from the bomb and each solution was basified by the addition of saturated aqueous K<sub>2</sub>CO<sub>3</sub> (1 mL). The layers were separated, and the aqueous layer was extracted with EtOAc (3 x 1 mL). The combined organics layers were then dried over Na<sub>2</sub>SO<sub>4</sub>, and concentrated in vacuo. The crude reaction mixture was purified by silica column chromatography (1:1 DCM:EtOAc + 1% MeOH + 1% NEt<sub>3</sub>) to yield tetrahydroisoquinoline **915** as a colorless oil (24 mg, 0.04 mmol, 44% yield); *Due to the inseparable nature of diastereomers and the poor diastereoselectivity of this reaction, the dr cannot be determined and only the major diastereomer is reported.* <sup>1</sup>H NMR (400 MHz, CDCl<sub>3</sub>) δ 6.73 (s, 1H), 5.14 (s, 1H), 5.03–5.00 (m, 1H), 4.57–4.52 (m, 1H), 4.34–4.25 (m,

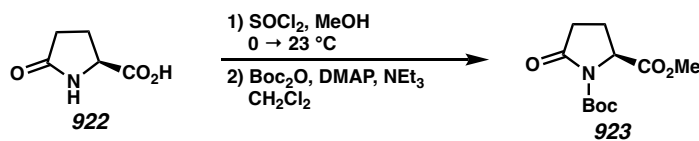
2H), 4.20 (q,  $J = 7.1$  Hz, 2H), 3.89 (s, 3H), 3.78 (s, 3H), 3.77 (s, 3H), 3.55–3.48 (m, 1H), 3.25–3.14 (m, 1H), 3.06–2.99 (m, 1H), 2.68–2.58 (m, 2H), 2.51–2.36 (m, 2H), 2.23 (s, 3H), 1.45 (s, 9H), 1.28 (t,  $J = 7.1$  Hz, 3H);  $^{13}\text{C}$  NMR (100 MHz,  $\text{CDCl}_3$ )  $\delta$  173.3, 150.4, 150.3, 133.4, 131.8, 126.0, 125.7, 83.6, 81.4, 64.3, 62.1, 61.5, 60.4, 60.0, 59.2, 54.9, 53.1, 31.7, 30.9, 28.6, 28.3, 28.1, 15.8, 14.2, 14.0; IR (Neat Film, NaCl) 3388, 2977, 2946, 2890, 2836, 2521, 1783, 1738, 1695, 1461, 1392, 1371, 1198, 1177, 1163, 1082, 910, 821, 736  $\text{cm}^{-1}$ ; HRMS (ESI+)  $m/z$  calc'd for  $\text{C}_{27}\text{H}_{41}\text{N}_2\text{O}_9$   $[\text{M}+\text{H}]^+$ : 537.2807, found 537.2825.



### Tetracycle (**916** + **917**)

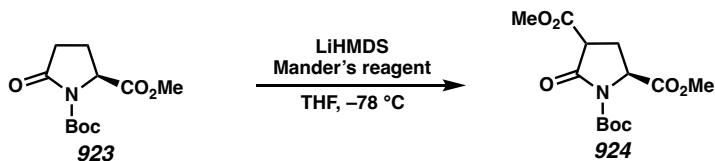
In a flame-dried 1-dram vial was charged with tetrahydroisoquinoline **915** (4.6 mg, 0.009 mmol, 1 equiv) in 2:1 THF:H<sub>2</sub>O (0.3 mL, 0.03 M total). LiOH (1 mg, 0.043 mmol, 5 equiv) was then added to the vial, and heated to 50 °C for 1 hour. After full consumption of starting material observed by LC-MS analysis, the crude reaction mixture was directly purified using reverse-phase ( $\text{C}_{18}$ ) preparative HPLC (MeCN/0.1% TFA in water, 5.0 mL/min, monitor wavelength = 230 nm, 20–75% MeCN over 8 minutes, hold at 80% for 2 minutes. Product **916** and **917** has  $t_{\text{R}} = 4.2$  minutes). Yellow film, (1 mg, 0.002 mmol, 23% yield); *Due to the inseparable nature of both cyclized products **916** and **917**, we are unable to assign each structure, respectively, by  $^1\text{H}$  NMR (see Figure A6.51). However, we are confident that the two isomers are indeed two different cyclized products, as we observe*

trace formations of both cyclized products with either the appended methyl (i.e., **916**) or ethyl ester (i.e., **917**) during this reaction by LC-MS analysis.



### 1-(*tert*-butyl) 2-methyl (*S*)-5-oxopyrrolidine-1,2-dicarboxylate (**921**)

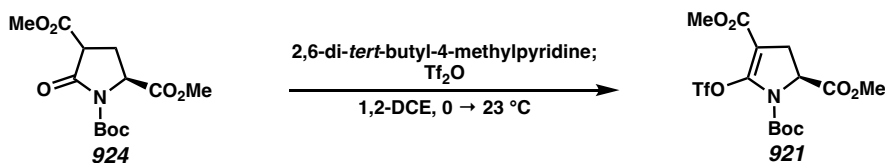
A flame-dried round bottom flask was charged with (*S*)-pyroglutamic acid **922** (1 g, 7.7 mmol, 1 equiv) in MeOH (30 mL, 0.26 M) and cooled to 0 °C. Thionyl chloride (0.06 mL, 0.8 mmol, 0.1 equiv) was then added dropwise, and the mixture was allowed to warm up to room temperature and stirred for 24 hours. Upon full consumption of starting material, solid K<sub>2</sub>CO<sub>3</sub> (790 mg, 9.2 mmol, 1.2 equiv) was added to the reaction mixture, and the resulting solution was filtered over celite. The crude reaction was then concentrated and carried forward to the next step. The crude reaction mixture was dissolved in DCM (7.7 mL, 1 M), and charged with DMAP (94 mg, 0.77 mmol, 0.1 equiv) and NEt<sub>3</sub> (1 mL, 7.7 mmol, 1 equiv). Then, a solution of Boc<sub>2</sub>O (3.4 g, 15.4 mmol, 2 equiv) in DCM (2.7 mL, 2.9 M) was added dropwise, and the resulting reaction mixture was stirred for 18 hours at room temperature. Upon full consumption of starting material, the reaction was quenched with 1 N HCl (10 mL) and extracted with DCM (3 x 10 mL). The combined organic phases were washed with brine (10 mL), dried over Na<sub>2</sub>SO<sub>4</sub>, and concentrated. The crude reaction mixture was purified by silica column chromatography (40 → 50% EtOAc in hexanes) to yield lactam **923** as a clear oil (1.4 g, 5.9 mmol, 76% yield); <sup>1</sup>H NMR (400 MHz, CDCl<sub>3</sub>) δ 4.20 (dd, *J* = 8.2, 4.3 Hz, 1H), 3.70 (s, 3H), 3.60–3.30 (m, 2H), 2.30–1.75 (m, 2H), 1.40 (s, 9H); All characterization data match those reported.<sup>33</sup>



### 1-(*tert*-butyl) 2,4-dimethyl (2*S*)-5-oxopyrrolidine-1,2,4-tricarboxylate (**921**)

A flame-dried round bottom flask was charged with lactam **923** (535 mg, 2.2 mmol, 1 equiv) in THF (13 mL, 0.17 M) and cooled to  $-78\text{ }^\circ\text{C}$ . A solution of LiHMDS (1 M in THF, 4.4 mL, 4.4 mmol, 2 equiv) was then added dropwise, and the mixture was stirred for 30 minutes at  $-78\text{ }^\circ\text{C}$ . Mander's reagent (0.21 mL, 2.64 mmol, 1.2 equiv) was then added dropwise, and the resulting solution was stirred for 1 hour. Upon full consumption of starting material, the reaction was quenched with saturated aq.  $\text{NH}_4\text{Cl}$  (10 mL) at  $-78\text{ }^\circ\text{C}$ , and the resulting solution was warmed to room temperature. The reaction mixture was extracted with EtOAc (3 x 10 mL), dried over  $\text{Na}_2\text{SO}_4$ , and concentrated. The crude reaction mixture was purified by silica column chromatography (20  $\rightarrow$  50% EtOAc in hexanes) to yield lactam **924** as a clear oil (556 mg, 1.85 mmol, 84% yield) (dr = 1.5:1);  $[\alpha]_{\text{D}}^{25} -12.6$  (*c* 0.99,  $\text{CHCl}_3$ );  $^1\text{H NMR}$  (400 MHz,  $\text{CDCl}_3$ )  $\delta$  4.67 (dd,  $J = 9.5, 2.6$  Hz, 1H), 3.78 (s, 3H), 3.77 (s, 3H), 3.67 (dd,  $J = 10.2, 9.0$  Hz, 1H), 2.72 (ddd,  $J = 13.5, 10.2, 9.5$  Hz, 1H), 2.57–2.51 (m, 1H), 1.48 (s, 9H);  $^{13}\text{C NMR}$  (100 MHz,  $\text{CDCl}_3$ )  $\delta$  171.5, 168.6, 167.9, 149.1, 84.4, 57.2, 53.2, 52.9, 48.5, 27.9, 25.4; IR (Neat Film, NaCl) 3470, 2978, 2955, 2345, 1795, 1741, 1652, 1458, 1437, 1394, 1370, 1312, 1293, 1265, 1253, 1024, 903, 771, 736  $\text{cm}^{-1}$ ; HRMS (MM:ESI+)  $m/z$  calc'd for *N*-H-**924**  $\text{C}_8\text{H}_{11}\text{NO}_5$   $[\text{M}+\text{H}]^+$ : 202.0710, found 202.0716.

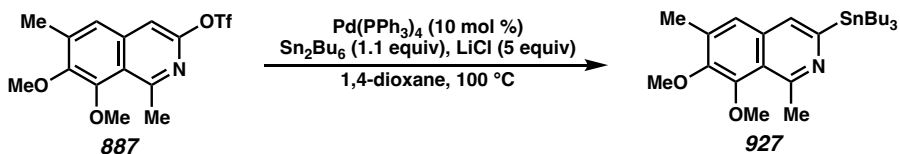




**1-(*tert*-butyl) 2,4-dimethyl (*S*)-5-(((trifluoromethyl)sulfonyl)oxy)-2,3-dihydro-1*H*-pyrrole-1,2,4-tricarboxylate (**921**)**

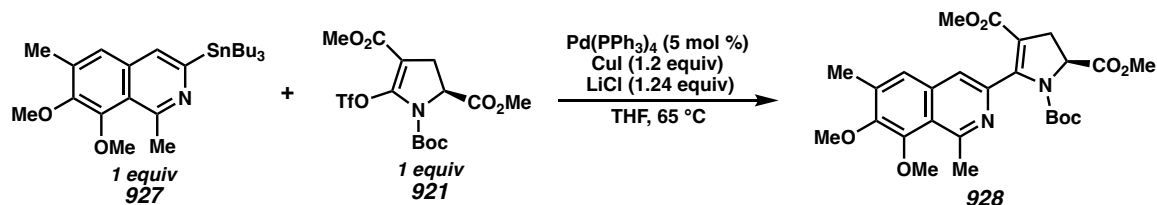
A flame-dried round bottom flask was charged with 2,6-di-*tert*-butyl-4-methylpyridine (43 mg, 0.21 mmol, 2.1 equiv), and the flask was vacuum purged/refilled with  $\text{N}_2$  three times. A solution of lactam **924** (30 mg, 0.1 mmol, 1 equiv) in 1,2-DCE (0.5 mL, 0.2 M) was then added to the reaction mixture, stirred for 10 minutes, and cooled to 0  $^\circ\text{C}$ . Freshly distilled  $\text{Tf}_2\text{O}$  (0.02 mL, 0.12 mmol, 1.2 equiv) was added dropwise at 0  $^\circ\text{C}$ , then the ice bath was removed and allowed to warm to room temperature over 3 hours. Upon full consumption of starting material, the reaction flask was cooled to 0  $^\circ\text{C}$ , and quenched with saturated aq.  $\text{NaHCO}_3$  (2 mL), and the resulting solution was warmed to room temperature. The reaction mixture was extracted with DCM (3 x 1 mL), dried over  $\text{Na}_2\text{SO}_4$ , and concentrated. The crude reaction mixture was purified by silica column chromatography (15  $\rightarrow$  35% EtOAc in hexanes) to yield dihydropyrrole **921** as a colorless oil (22 mg, 0.05 mmol, 51% yield);  $[\alpha]_{\text{D}}^{25}$   $-58.3$  ( $c$  1.07,  $\text{CHCl}_3$ );  $^1\text{H}$  NMR (400 MHz,  $\text{CDCl}_3$ )  $\delta$  4.73 (dd,  $J = 12.1, 4.1$  Hz, 1H), 3.78 (s, 3H), 3.75 (s, 3H), 3.19 (dd,  $J = 16.4, 12.1$  Hz, 1H), 2.84 (dd,  $J = 16.4, 4.0$  Hz, 1H), 1.47 (s, 9H);  $^{13}\text{C}$  NMR (100 MHz,  $\text{CDCl}_3$ )  $\delta$  170.5, 162.8, 149.3, 145.5, 118.5 (q,  $J = 321.1$  Hz), 99.6, 84.6, 57.8, 52.9, 51.9, 29.1, 28.0;  $^{19}\text{F}$  NMR (282 MHz,  $\text{CDCl}_3$ )  $\delta$   $-73.4$ ; IR (Neat Film, NaCl) 2981, 2957, 2356, 2341, 1747, 1714, 1658, 1651, 1439, 1395, 1372, 1269, 1251, 1228, 1177, 1134, 907, 828, 767  $\text{cm}^{-1}$ ;

HRMS (MM:ESI+)  $m/z$  calc'd for *N*-H-**921** C<sub>9</sub>H<sub>10</sub>F<sub>3</sub>NO<sub>7</sub>S [M+H]<sup>+</sup>: 334.0203, found 334.0197.



### 7,8-dimethoxy-1,6-dimethyl-3-(tributylstannyl)isoquinoline (**927**)

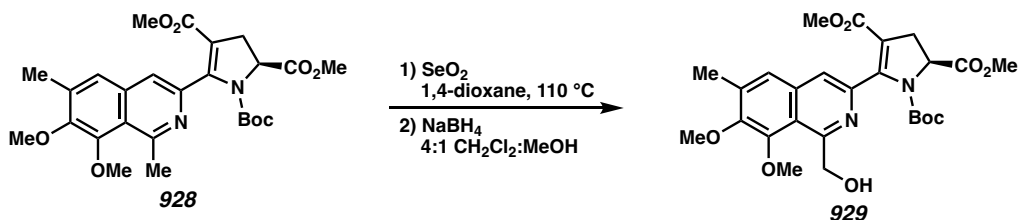
In a flame-dried  $\mu$ W vial was charged with isoquinoline **887** (40 mg, 0.11 mmol, 1 equiv) and a magnetic stirring bar, and brought in a N<sub>2</sub>-filled glovebox. To the reaction vial was added LiCl (23 mg, 0.55 mmol, 5 equiv), Pd(PPh<sub>3</sub>)<sub>4</sub> (13 mg, 0.01 mmol, 0.1 equiv), and then Sn<sub>2</sub>Bu<sub>6</sub> (0.06 mL, 0.12 mmol, 1.1 equiv) dissolved in 1,4-dioxane (3.7 mL, 0.03 M). The reaction vial was then sealed and taken out of the glovebox and heated to 100 °C over 18 hours. Upon full consumption of starting material, the reaction flask was cooled to room temperature, and filtered over celite rinsing with EtOAc. The crude reaction mixture was directly purified by silica column chromatography (0 → 5% → 10% EtOAc in hexanes + 1% NEt<sub>3</sub>) to yield isoquinoline **927** as a clear oil (43 mg, 0.08 mmol, 77% yield); <sup>1</sup>H NMR (400 MHz, CDCl<sub>3</sub>)  $\delta$  8.57 (s, 1H), 7.52 (s, 1H), 4.00 (s, 3H), 3.96 (s, 3H), 3.21 (s, 3H), 2.45 (s, 3H), 1.68–1.54 (m, 7H), 1.36 (h,  $J = 7.1$  Hz, 6H), 1.16–1.09 (m, 5H), 0.89 (t,  $J = 7.2$  Hz, 9H); <sup>13</sup>C NMR (100 MHz, CDCl<sub>3</sub>)  $\delta$  156.7, 150.6, 148.1, 137.0, 134.0, 128.9, 128.7, 124.8, 115.1, 60.9, 60.3, 29.3, 27.7, 27.5, 17.1, 13.9, 10.0; IR (Neat Film, NaCl) 3052, 2952, 2923, 2843, 1616, 1572, 1555, 1474, 1433, 1394, 1368, 1326, 1241, 1144, 1117, 1080, 1002, 889, 683 cm<sup>-1</sup>; HRMS (ESI+)  $m/z$  calc'd for C<sub>25</sub>H<sub>42</sub>NO<sub>2</sub>Sn [M+H]<sup>+</sup>: 500.2258, found 500.2262.



**1-(*tert*-butyl) 2,4-dimethyl (*S*)-5-(7,8-dimethoxy-1,6-dimethylisoquinolin-3-yl)-2,3-dihydro-1*H*-pyrrole-1,2,4-tricarboxylate (928)**

In a flame-dried  $\mu$ W vial was charged with triflate **921** (18.7 mg, 0.045 mmol, 1 equiv) and a magnetic stirring bar, and brought in a  $N_2$ -filled glovebox. To the reaction vial was added CuI (10 mg, 0.052 mmol, 1.2 equiv), LiCl (2.3 mg, 0.054 mmol, 1.24 equiv), and Pd(PPh<sub>3</sub>)<sub>4</sub> (2.5 mg, 0.002 mmol, 0.05 equiv). Then, a solution of isoquinoline **927** (22 mg, 0.045 mmol, 1 equiv) in THF (0.5 mL, 0.1 M) was added to the reaction vial and sealed. The reaction vial was taken out of the glovebox and heated to 65 °C over 18 hours. Upon full consumption of starting material, the reaction was quenched with saturated aq. NaHCO<sub>3</sub> (1 mL) and extracted with EtOAc (3 x 1 mL). The combined organic phases were dried over Na<sub>2</sub>SO<sub>4</sub>, filtered, and concentrated. The crude reaction mixture was purified by silica column chromatography (40% EtOAc in hexanes + 1% NEt<sub>3</sub>) to yield isoquinoline **928** as a white solid (14 mg, 0.03 mmol, 64% yield);  $[\alpha]_D^{25} -99.5$  (*c* 0.70, CHCl<sub>3</sub>); <sup>1</sup>H NMR (400 MHz, CDCl<sub>3</sub>)  $\delta$  7.44 (s, 1H), 7.36 (s, 1H), 4.91 (dd, *J* = 12.3, 5.0 Hz, 1H), 3.96 (s, 3H), 3.92 (s, 3H), 3.83 (s, 3H), 3.47 (s, 3H), 3.33 (dd, *J* = 16.5, 12.3 Hz, 1H), 3.10 (s, 3H), 2.94 (dd, *J* = 16.5, 5.0 Hz, 1H), 2.42 (s, 3H), 1.02 (s, 9H); <sup>13</sup>C NMR (100 MHz, CDCl<sub>3</sub>)  $\delta$  172.1, 171.3, 164.8, 156.2, 150.9, 149.7, 142.5, 137.3, 134.4, 124.1, 122.2, 118.7, 110.2, 81.9, 60.8, 60.5, 60.3, 60.2, 52.7, 51.3, 32.7, 27.7, 27.1, 17.0; IR (Neat Film, NaCl) 2950, 2597, 1744, 1703, 1641, 1591, 1556, 1483, 1442, 1394, 1330, 1236, 1176,

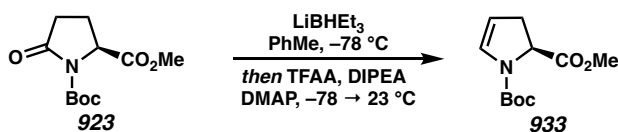
1147, 1118, 1006, 892, 768, 733  $\text{cm}^{-1}$ ; HRMS (ESI+)  $m/z$  calc'd for  $\text{C}_{26}\text{H}_{33}\text{N}_2\text{O}_8$   $[\text{M}+\text{H}]^+$ : 501.2231, found 501.2210.



**1-(*tert*-butyl) 2,4-dimethyl (*S*)-5-(1-(hydroxymethyl)-7,8-dimethoxy-6-methylisoquinolin-3-yl)-2,3-dihydro-1*H*-pyrrole-1,2,4-tricarboxylate (929)**

In a flame-dried  $\mu\text{W}$  vial was charged with  $\text{SeO}_2$  (2.8 mg, 0.03 mmol, 1.5 equiv) and a magnetic stir bar. The vial was vacuum purged/refilled with  $\text{N}_2$  three times. A solution of isoquinoline **928** (8.4 mg, 0.02 mmol, 1 equiv) in 1,4-dioxane (0.5 mL, 0.04 M) was then added to the vial, and heated to reflux for 2 hours. After full consumption of starting material observed by LCMS analysis, the vial was cooled to room temperature and the crude reaction mixture was filtered through celite, rinsing with EtOAc. The crude reaction was concentrated, then dissolved in 4:1 DCM:MeOH (0.2 mL, 0.1 M total).  $\text{NaBH}_4$  (0.6 mg, 0.02 mmol, 1 equiv) was then added, and the reaction was stirred for 30 minutes at room temperature. After full conversion of the aldehyde intermediate observed by LCMS analysis, the reaction was quenched with citric acid monohydrate (8.4 mg, 0.04 mmol, 2 equiv) and water, and the solution was stirred rapidly for 10 minutes. The solution was then basified by the addition of saturated aq.  $\text{NaHCO}_3$  (1 mL), the layers were separated and the aqueous phase was extracted with DCM (3 x 1 mL). The combined organic phases were dried over  $\text{Na}_2\text{SO}_4$ , filtered, and concentrated. The crude reaction mixture was purified by silica column chromatography (40% EtOAc in hexanes) to yield

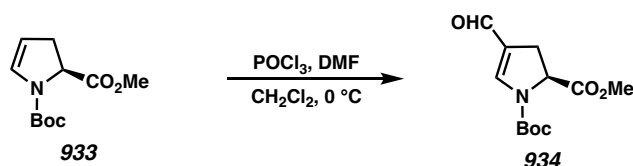
isoquinoline **929** as a white solid (4.8 mg, 0.01 mmol, 55% yield);  $[\alpha]_{\text{D}}^{25} -35.9$  ( $c$  0.75,  $\text{CHCl}_3$ );  $^1\text{H NMR}$  (400 MHz,  $\text{CDCl}_3$ )  $\delta$  7.59 (s, 1H), 7.43 (s, 1H), 5.53 (br s, 1H), 5.28 (s, 2H), 4.93 (dd,  $J = 12.0, 4.5$  Hz, 1H), 4.00 (s, 3H), 3.91 (s, 3H), 3.85 (s, 3H), 3.51 (s, 3H), 3.37 (dd,  $J = 16.6, 12.1$  Hz, 1H), 2.99 (dd,  $J = 16.6, 4.5$  Hz, 1H), 2.43 (s, 3H), 1.06 (s, 9H);  $^{13}\text{C NMR}$  (100 MHz,  $\text{CDCl}_3$ )  $\delta$  172.0, 164.7, 156.1, 150.9, 150.8, 149.3, 138.2, 134.1, 124.2, 120.4, 120.2, 110.5, 82.1, 64.2, 60.8, 60.6, 60.3, 60.2, 52.8, 51.4, 33.0, 27.7, 27.1, 17.0; IR (Neat Film, NaCl) 3362, 2946, 2928, 2903, 1751, 1736, 1700, 1637, 1560, 1466, 1436, 1387, 1328, 1236, 1175, 1154, 1013, 892, 763  $\text{cm}^{-1}$ ; HRMS (ESI+)  $m/z$  calc'd for  $\text{C}_{26}\text{H}_{33}\text{N}_2\text{O}_9$   $[\text{M}+\text{H}]^+$ : 517.2181, found 517.2195.



### 1-(*tert*-butyl) 2-methyl (*S*)-2,3-dihydro-1*H*-pyrrole-1,2-dicarboxylate (**933**)

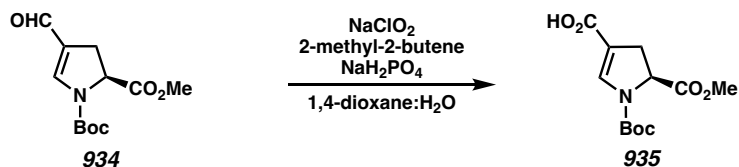
In a flame-dried round bottom flask was charged with lactam **923** (1 g, 4.1 mmol, 1 equiv) in PhMe (5.6 mL, 0.7 M) and cooled to  $-78$  °C. A solution of  $\text{LiBHET}_3$  (1M in PhMe, 4.5 mL, 4.5 mmol, 1.1 equiv) was then added dropwise to the reaction flask at  $-78$  °C, and stirred for 1 hour. Upon full consumption of starting material by TLC analysis, DMAP (5 mg, 0.04 mmol, 0.01 equiv) and DIPEA (4 mL, 23 mmol, 5.7 equiv) was then added to the reaction mixture at  $-78$  °C, followed by TFAA (0.7 mL, 4.9 mmol, 1.2 equiv) dropwise. The dry ice bath was then removed and allowed to warm to room temperature over 6 hours. Upon full consumption of the lactol, the reaction was quenched with  $\text{H}_2\text{O}$  (10 mL), extracted with  $\text{Et}_2\text{O}$  (3 x 10 mL), dried over  $\text{Na}_2\text{SO}_4$ , and concentrated. The crude reaction mixture was purified by silica column chromatography (5  $\rightarrow$  10% EtOAc in

hexanes) to yield dihydropyrrole **933** as a clear oil (679 mg, 3 mmol, 73% yield) (rr = 1.1:1);  $^1\text{H NMR}$  (400 MHz,  $\text{CDCl}_3$ )  $\delta$  6.65 (s, 1H), 4.96 (s, 1H), 4.59 (dd,  $J = 11.9, 5.4$  Hz, 1H), 3.76 (s, 3H), 3.12–3.01 (m, 1H), 2.72–2.62 (m, 1H), 1.44 (s, 9H); All characterization data match those reported.<sup>33</sup>



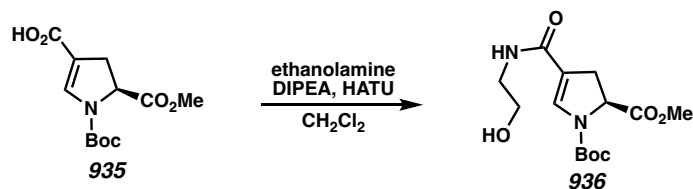
**1-(tert-butyl) 2-methyl (S)-4-formyl-2,3-dihydro-1H-pyrrole-1,2-dicarboxylate (934)**

In a flame-dried round bottom flask was charged with DMF (0.62 mL, 8 mmol, 4 equiv) and cooled to 0 °C.  $\text{POCl}_3$  (0.38 mL, 4 mmol, 2 equiv) was then added dropwise to the reaction flask, and stirred rapidly at 0 °C for 30 minutes. The reaction was diluted with DCM (11 mL, 0.18 M), and a solution of dihydropyrrole **933** (457 mg, 2 mmol, 1 equiv) in DCM (4.5 mL, 0.44 M) was added dropwise at 0 °C and stirred for 1 hour. Upon full consumption of starting material, the reaction flask was poured into a separatory funnel with ice-cold 2M NaOH (10 mL), extracted with DCM (3 x 10 mL), dried over  $\text{Na}_2\text{SO}_4$ , and concentrated. The crude reaction mixture was purified by silica column chromatography (20  $\rightarrow$  30% EtOAc in hexanes) to yield dihydropyrrole **934** as a clear oil (357 mg, 1.4 mmol, 70% yield) (rr = 1.3:1);  $^1\text{H NMR}$  (400 MHz,  $\text{CDCl}_3$ )  $\delta$  9.57 (s, 1H), 7.54 (s, 1H), 4.80 (dd,  $J = 12.4, 5.1$  Hz, 1H), 3.78 (s, 3H), 3.28–3.18 (m, 1H), 2.94–2.80 (m, 1H), 2.11 (s, 9H); All characterization data match those reported.<sup>35</sup>



**(S)-1-(tert-butoxycarbonyl)-5-(methoxycarbonyl)-4,5-dihydro-1H-pyrrole-3-carboxylic acid (935)**

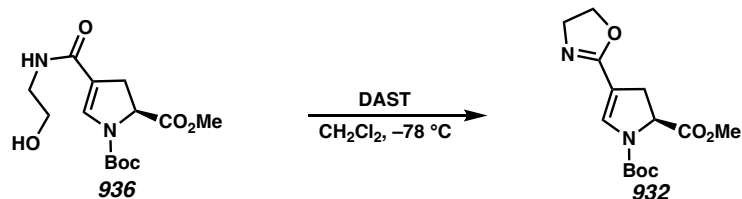
In a flame-dried round bottom flask was charged with aldehyde **934** (1.7 g, 6.5 mmol, 1 equiv) in 3:1 1,4-dioxane:H<sub>2</sub>O (40 mL, 0.16 M total). To this solution was added NaH<sub>2</sub>PO<sub>4</sub> (3.92 g, 32.7 mmol, 5 equiv) and 2-methyl-2-butene (2.8 mL, 26.2 mmol, 4 equiv), then NaClO<sub>2</sub> (416 mg, 4.6 mmol, 0.7 equiv) was added in one portion and stirred for 18 hours at room temperature. Upon full consumption of starting material, the reaction was quenched with saturated aq. NaHCO<sub>3</sub> (20 mL) and stirred for 30 minutes. The reaction mixture was washed with 1 M HCl (20 mL), extracted with EtOAc (3 x 10 mL), dried over Na<sub>2</sub>SO<sub>4</sub>, and concentrated. The crude reaction mixture was purified by silica column chromatography (20 → 70% EtOAc in hexanes + 1% AcOH) to yield dihydropyrrole **935** as a white solid (1.3 g, 4.94 mmol, 76% yield) (rr = 1.3:1); [α]<sub>D</sub><sup>25</sup> -41.7 (*c* 0.99, CHCl<sub>3</sub>); <sup>1</sup>H NMR (400 MHz, CDCl<sub>3</sub>) δ 7.53 (s, 1H), 4.80 (dd, *J* = 12.2, 5.0 Hz, 1H), 3.78 (s, 3H), 3.29–3.17 (m, 1H), 2.91–2.83 (m, 1H), 1.51 (s, 9H); <sup>13</sup>C NMR (100 MHz, CDCl<sub>3</sub>) δ 171.0, 170.3, 150.5, 142.5, 109.6, 83.3, 59.5, 52.8, 32.3, 28.2; IR (Neat Film, NaCl) 2978, 2362, 1754, 1727, 1673, 1620, 1434, 1371, 1268, 1240, 1214, 1166, 1150, 1023, 921, 890, 836, 766, 753 cm<sup>-1</sup>; HRMS (ESI+) *m/z* calc'd for *N*-H-**935** C<sub>7</sub>H<sub>9</sub>NO<sub>4</sub> [M+H]<sup>+</sup>: 172.0604, found 172.0598.



**1-(*tert*-butyl) 2-methyl (*S*)-4-((2-hydroxyethyl)carbamoyl)-2,3-dihydro-1*H*-pyrrole-1,2-dicarboxylate (936)**

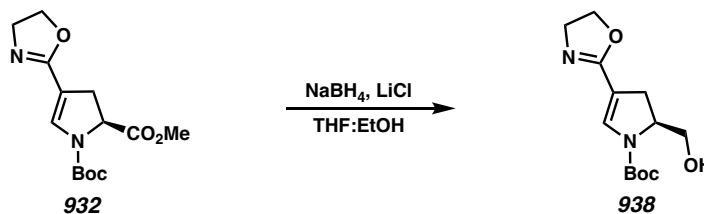
In a flame-dried round bottom flask was charged with carboxylic acid **935** (469 mg, 1.73 mmol, 1 equiv) in DCM (35 mL, 0.05 M) and sparged with N<sub>2</sub> for 10 minutes. To the resulting mixture was added DIPEA (0.45 mL, 2.6 mmol, 1.5 equiv) and ethanolamine (0.13 mL, 2.1 mmol, 1.2 equiv), and the reaction mixture was stirred for 15 minutes. HATU (798 mg, 2.1 mmol, 1.2 equiv) was then added in one portion, and stirred for 18 hours at room temperature. Upon full consumption of starting material, the reaction was filtered, concentrated, and directly purified by silica column chromatography (2 → 10% MeOH in DCM) to yield amide **936** as a white amorphous solid (435 mg, 1.4 mmol, 80% yield) (rr = 1.1:1);  $[\alpha]_D^{25} -51.4$  (*c* 1.04, CHCl<sub>3</sub>); <sup>1</sup>H NMR (400 MHz, CDCl<sub>3</sub>) δ 7.32 (s, 1H), 6.65 (br s, 1H), 4.67 (dd, *J* = 12.2, 5.1 Hz, 1H), 3.74 (s, 3H), 3.69–3.67 (m, 2H), 3.43–3.41 (m, 2H), 3.29–3.11 (m, 1H), 2.89–2.77 (m, 1H), 1.40 (s, 9H); <sup>13</sup>C NMR (100 MHz, CDCl<sub>3</sub>) δ 171.6, 165.4, 151.0, 135.5, 113.8, 82.5, 62.1, 59.5, 52.6, 42.5, 34.2, 28.1; IR (Neat Film, NaCl) 3333, 3108, 2978, 2359, 1748, 1715, 1643, 1540, 1455, 1368, 1285, 1256, 1155, 1062, 975, 918, 848, 763, 679 cm<sup>-1</sup>; HRMS (ESI+) *m/z* calc'd for C<sub>14</sub>H<sub>23</sub>N<sub>2</sub>O<sub>6</sub> [M+H]<sup>+</sup>: 315.1551, found 315.1560.





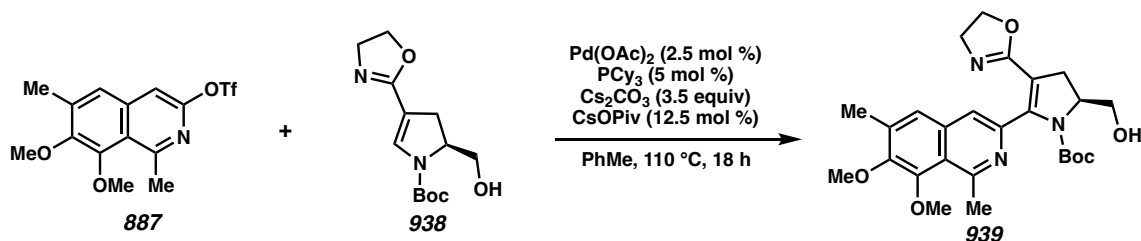
**1-(tert-butyl) 2-methyl (S)-4-(4,5-dihydrooxazol-2-yl)-2,3-dihydro-1H-pyrrole-1,2-dicarboxylate (932)**

In a flame-dried round bottom flask was charged with amide **936** (389 mg, 1.24 mmol, 1 equiv) in DCM (11.3 mL, 0.11 M) and cooled to  $-78$  °C. To this solution was added DAST (0.18 mL, 1.37 mmol, 1.1 equiv) dropwise at  $-78$  °C, and stirred for 1 hour. Upon full consumption of starting material, the reaction was quenched with saturated aq. NaHCO<sub>3</sub> (10 mL), extracted with DCM (3 x 5 mL), dried over Na<sub>2</sub>SO<sub>4</sub>, and concentrated. The crude reaction mixture was purified by silica column chromatography (100% EtOAc) to yield dihydropyrrole **932** as a colorless amorphous solid (290 mg, 0.98 mmol, 79% yield) (rr = 1.3:1);  $[\alpha]_{\text{D}}^{25}$   $-38.4$  (*c* 1.09, CHCl<sub>3</sub>); <sup>1</sup>H NMR (400 MHz, CDCl<sub>3</sub>)  $\delta$  7.13 (s, 1H), 4.75 (dd, *J* = 12.1, 4.9 Hz, 1H), 4.26 (t, *J* = 9.2 Hz, 2H), 3.88 (t, *J* = 9.3 Hz, 2H), 3.75 (s, 3H), 3.35–3.22 (m, 1H), 2.96–2.86 (m, 1H), 1.48 (s, 9H); <sup>13</sup>C NMR (100 MHz, CDCl<sub>3</sub>)  $\delta$  171.3, 161.6, 150.9, 135.4, 107.5, 82.5, 67.4, 58.8, 54.9, 52.7, 33.5, 28.3; IR (Neat Film, NaCl) 3127, 2976, 2877, 2364, 1754, 1715, 1660, 1610, 1478, 1370, 1328, 1263, 1163, 1046, 970, 905, 830, 762, 690 cm<sup>-1</sup>; HRMS (ESI+) *m/z* calc'd for C<sub>14</sub>H<sub>21</sub>N<sub>2</sub>O<sub>5</sub> [M+H]<sup>+</sup>: 297.1445, found 297.1449.



***tert*-butyl (*S*)-4-(4,5-dihydrooxazol-2-yl)-2-(hydroxymethyl)-2,3-dihydro-1*H*-pyrrole-1-carboxylate (**938**)**

In a flame-dried round bottom flask was charged with NaBH<sub>4</sub> (102 mg, 2.69 mmol, 3 equiv), LiCl (114 mg, 2.69 mmol, 3 equiv) in EtOH (3.7 mL, 0.24 M). The reaction flask was cooled to 0 °C, and stirred for 10 minutes. To the resulting mixture was added a solution of dihydropyrrole **932** (263 mg, 0.89 mmol, 1 equiv) in THF (3.7 mL, 0.24 M) dropwise at 0 °C. The ice bath was then removed and allowed to warm to room temperature over 18 hours. Upon full consumption of starting material, the reaction was quenched with H<sub>2</sub>O (5 mL), extracted with Et<sub>2</sub>O (3 x 5 mL), dried over Na<sub>2</sub>SO<sub>4</sub>, and concentrated. The crude reaction mixture was purified by silica column chromatography (10% MeOH in EtOAc) to yield dihydropyrrole **938** as a white solid (177 mg, 0.66 mmol, 74% yield);  $[\alpha]_{\text{D}}^{25} -118.9$  (*c* 1.07, CHCl<sub>3</sub>); <sup>1</sup>H NMR (400 MHz, CD<sub>3</sub>OD)  $\delta$  7.15 (s, 1H), 4.87 (s, 2H), 4.35–4.30 (m, 2H), 3.90–3.85 (m, 2H), 3.64–3.61 (m, 1H), 3.06–3.00 (m, 1H), 2.88–2.77 (m, 1H), 1.51 (s, 9H); <sup>13</sup>C NMR (100 MHz, CD<sub>3</sub>OD)  $\delta$  164.6, 137.6, 109.3, 83.0, 68.6, 63.2, 61.2, 54.8, 33.4, 32.3, 28.5; IR (Neat Film, NaCl) 3258, 2976, 2933, 2878, 2357, 2330, 1708, 1653, 1476, 1455, 1430, 1369, 1307, 1240, 1164, 1048, 997, 825, 761 cm<sup>-1</sup>; HRMS (ESI+) *m/z* calc'd for C<sub>13</sub>H<sub>21</sub>N<sub>2</sub>O<sub>4</sub> [M+H]<sup>+</sup>: 269.1496, found 269.1510.



***tert*-butyl (*S*)-4-(4,5-dihydrooxazol-2-yl)-5-(7,8-dimethoxy-1,6-dimethylisoquinolin-3-yl)-2-(hydroxymethyl)-2,3-dihydro-1*H*-pyrrole-1-carboxylate (**939**)**

In a flame-dried  $\mu$ W vial was charged with isoquinoline **887** (5 mg, 0.014 mmol, 1 equiv), dihydropyrrole **938** (5.5 mg, 0.02 mmol, 1.5 equiv) and a magnetic stirring bar, and brought in a N<sub>2</sub>-filled glovebox. In the glovebox, Cs<sub>2</sub>CO<sub>3</sub> (15.6 mg, 0.05 mmol, 3.5 equiv) and CsOPiv (0.4 mg, 0.0017 mmol, 0.125 equiv) were weighed out and added to the reaction vial. A stock solution of the catalyst was prepared by adding Pd(OAc)<sub>2</sub> (0.08 mg, 0.0003 mmol for each reaction vial, 2.5 mol %) and PCy<sub>3</sub> (0.2 mg, 0.0007 mmol for each reaction vial, 5 mol %) dissolved in PhMe (0.34 mL for each reaction vial, 0.04 M) in a separate 1-dram vial. Upon complete dissolution of the catalyst, 0.34 mL of the solution was transferred to the reaction vial. The vial was then removed from the glovebox, and placed in an oil bath to stir for 18 hours at 110 °C. Upon full consumption of starting material, the reaction vial was cooled to room temperature, and filtered over celite. The crude reaction mixture was directly purified by silica column chromatography (1:1 DCM:EtOAc + 1% MeOH + 1% NEt<sub>3</sub>) to yield isoquinoline **939** as a yellow oil (3.1 mg, 0.006 mmol, 47% yield);  $[\alpha]_{\text{D}}^{25} -99.5$  (*c* 0.70, CHCl<sub>3</sub>); <sup>1</sup>H NMR (400 MHz, CDCl<sub>3</sub>)  $\delta$  7.18 (s, 1H), 6.67 (s, 1H), 4.74–4.63 (m, 1H), 4.50 (dd, *J* = 9.8, 3.7 Hz, 1H), 4.42–4.36 (m, 1H), 4.27 (t, *J* = 9.3 Hz, 2H), 3.94 (s, 3H), 3.91 (t, *J* = 9.3 Hz, 2H), 3.89 (s, 3H), 3.17–3.12 (m, 1H), 3.03 (dd, *J* = 4.1, 1.5 Hz, 1H), 3.01 (s, 3H), 2.38 (s, 3H), 1.49 (s, 9H); <sup>13</sup>C NMR (100

MHz, CDCl<sub>3</sub>) δ 164.7, 158.9, 156.4, 149.8, 148.2, 138.4, 137.4, 135.5, 122.4, 119.3, 108.7, 98.4, 81.8, 67.3, 66.1, 60.8, 60.3, 57.6, 54.9, 53.6, 28.4, 27.3, 26.8, 17.1; IR (Neat Film, NaCl) 3332, 2927, 1994, 1797, 1711, 1652, 1508, 1440, 1360, 1326, 1269, 1236, 1123, 1036, 1008, 902, 828, 749, 680 cm<sup>-1</sup>; HRMS (ESI+) *m/z* calc'd for C<sub>26</sub>H<sub>34</sub>N<sub>3</sub>O<sub>6</sub> [M+H]<sup>+</sup>: 484.2442, found 484.2446.

## 5.8 REFERENCES AND NOTES

- (1) Phillipson, J. D.; Roberts, M. F.; Zenk, M. H. *The Chemistry and Biology of Isoquinoline Alkaloids*; Springer, 1985.
- (2) Siengalewicz, P.; Rinner, U.; Mulzer, J. *Chem. Soc. Rev.* **2008**, *37*, 2676–2690.
- (3) Hayashi, T.; Noto, T.; Nawata, Y.; Okazaki, H.; Sawada, M.; Ando, K. *J. Antibiot.* **1982**, *35*, 771–777.
- (4) a) Zmijewski, M. J. Jr.; Mikolajczak, M.; Viswanatha, V.; Hruby, V. J. *J. Am. Chem. Soc.* **1982**, *104*, 4969–4971; b) Zmijewski, M. J.; Palaniswamy, V. A.; Gould, S. J. *J. Chem. Soc., Chem. Commun.* **1985**, *18*, 1261–1262.
- (5) Pu, J.-Y.; Peng, C.; Tang, M.-C.; Zhang, Y.; Guo, J.-P.; Song, L.-Q.; Hua, Q.; Tang, G.-L. *Org. Lett.* **2013**, *15*, 3674–3677.
- (6) Evans, D. A.; Illig, C. R.; Saddler, J. C. *J. Am. Chem. Soc.* **1986**, *108*, 2478–2479.
- (7) Fukuyama, T.; Li, L.; Laird, A. A.; Frank, R. K. *J. Am. Chem. Soc.* **1987**, *109*, 1587–1589.
- (8) Illig, C. R. Ph.D. Dissertation, Harvard University, Cambridge, MA, 1987.
- (9) Fukuyama, T. *Adv. Heterocycl. Nat. Prod. Synth.* **1992**, *2*, 189–249.

- (10) a) Ümit Kaniskan, H.; Garner, P. *J. Am. Chem. Soc.* **2007**, *129*, 15460–15461; b) Garner, P.; Ümit Kaniskan, H.; Keyari, C. M.; Weerasinghe, L. *J. Org. Chem.* **2011**, *76*, 5283–5294.
- (11) Willis, N. J.; Bray, C. D. *Chem. Eur. J.* **2012**, *18*, 9160–9173.
- (12) Corey, E. J.; Gin, D. Y.; Kania, R. S. *J. Am. Chem. Soc.* **1996**, *118*, 9202–9203.
- (13) a) Kim, A. N.; Ngamnithiporn, A.; Welin, E. R.; Daiger, M. T.; Grünanger, C. U.; Bartberger, M. D.; Virgil, S. C.; Stoltz, B. M. *ACS Catal.* **2020**, *10*, 3241–3248; b) Kim, A. N.; Ngamnithiporn, A.; Bartberger, M. D.; Stoltz, B. M. *Chem. Sci.* **2022**, *13*, 3227–3232.
- (14) a) Welin, E. R.; Ngamnithiporn, A.; Klatte, M.; Lapointe, G.; Pototschnig, G. M.; McDermott, M. S. J.; Conklin, D.; Gilmore, C. D.; Tadross, P. M.; Haley, C. K.; Negoro, K.; Glibstrup, E.; Grünanger, C. U.; Allan, K. M.; Virgil, S. C.; Slamon, D. J.; Stoltz, B. M. *Science*. **2019**, *363*, 270–275; b) Allan, K. M.; Hong, B. D.; Stoltz, B. M. *Org. Biomol. Chem.* **2009**, *7*, 4960–4964.
- (15) Warashina, T.; Matsuura, D.; Sengoku, T.; Takahashi, M.; Yoda, H.; Kimura, Y. *Org. Process Res. Dev.* **2019**, *23*, 614–618.
- (16) Protection of the aldehyde as the acetal resulted in low conversions, so we elected to reduce the aldehyde to the alcohol oxidation state.
- (17) Molander, G. A.; Trice, S. L.; Kennedy, S. M. *J. Org. Chem.* **2012**, *77*, 8678–8688.
- (18) Protection of the alcohol to circumvent expulsion of the hydroxyl group resulted in trace conversion of the pyrrole.

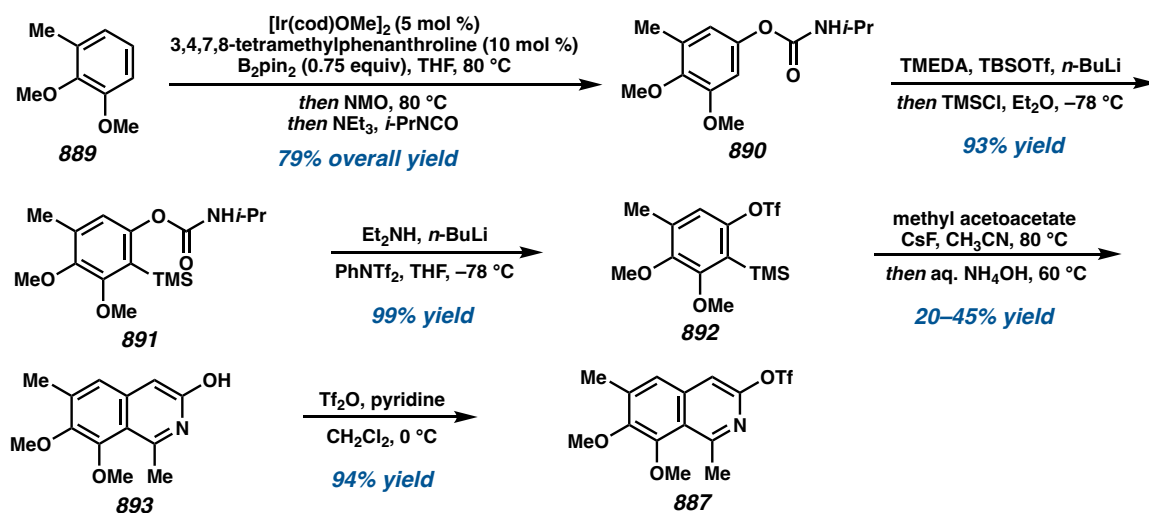
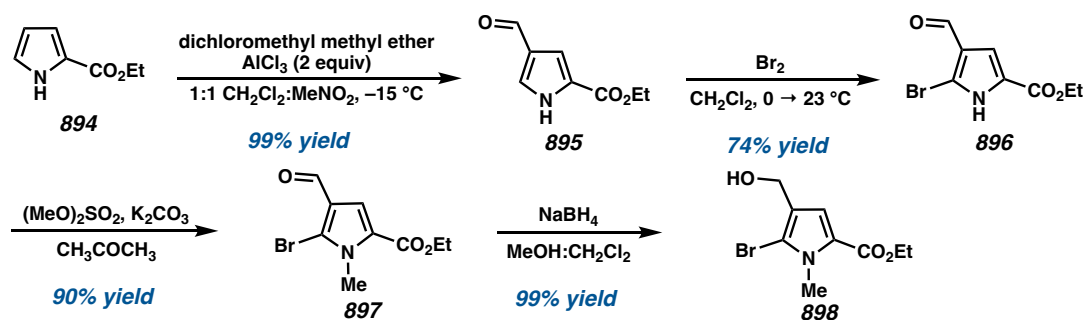
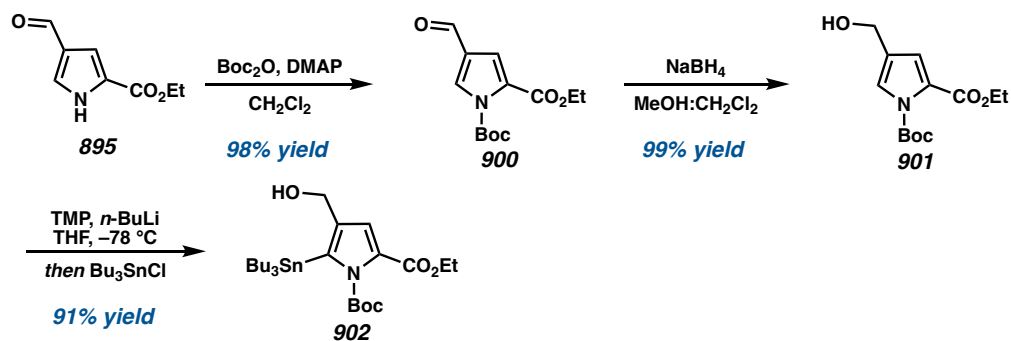
- (19) Hasan, I.; Marinelli, E. R.; Lin, L.-C. C.; Fowler, F. W.; Levy, A. B. *J. Org. Chem.* **1981**, *46*, 157–164.
- (20) a) Reimann, C. E.; Ngamnithiporn, A.; Hayashida, K.; Saito, D.; Korch, K. M.; Stoltz, B. M. *Angew. Chem. Int. Ed.* **2021**, *60*, 17957–17962; b) Fürstner, A.; Funel, J.-A.; Tremblay, M.; Bouchez, L. C.; Nevado, C.; Waser, M.; Ackerstaff, J.; Stimson, C. C. *Chem. Commun.* **2008**, 2783–2875.
- (21) Xue, F.; Silverman, R. B. *Tetrahedron Lett.* **2010**, *51*, 2536–2538.
- (22) Hegedús, L.; Máthé, T. *Appl. Catal., A* **2002**, *226*, 319–322.
- (23) Kuwano, R.; Kashiwabara, M.; Ohsumi, M.; Kusano, H. *J. Am. Chem. Soc.* **2008**, *130*, 808–809.
- (24) Protection of the hydroxymethyl group to prevent the Boc-migration pathway resulted in no conversion of starting material.
- (25) Due to the low diastereoselectivity and inseparable nature of the diastereomers, the dr cannot be determined, however, we observe at least 4 diastereomers after isolation.
- (26) a) Thompson, A. L. S.; Kabalka, G. W.; Akula, M. R.; Huffman, J. W. *Synthesis* **2005**, *4*, 547–550; b) Murata, M.; Oyama, T.; Watanabe, S.; Masuda, Y. *J. Org. Chem.* **2000**, *65*, 164–168.
- (27) Molander, G. A.; Cavalcanti, L. N.; García-García, C. *J. Org. Chem.* **2013**, *78*, 6427–6439.
- (28) Griбанov, P. S.; Golenko, Y. D.; Topchiy, M. A.; Minaeva, L. I.; Asachenko, A. F.; Nechaev, M. S. *Eur. J. Org. Chem.* **2018**, *2018*, 120–125.

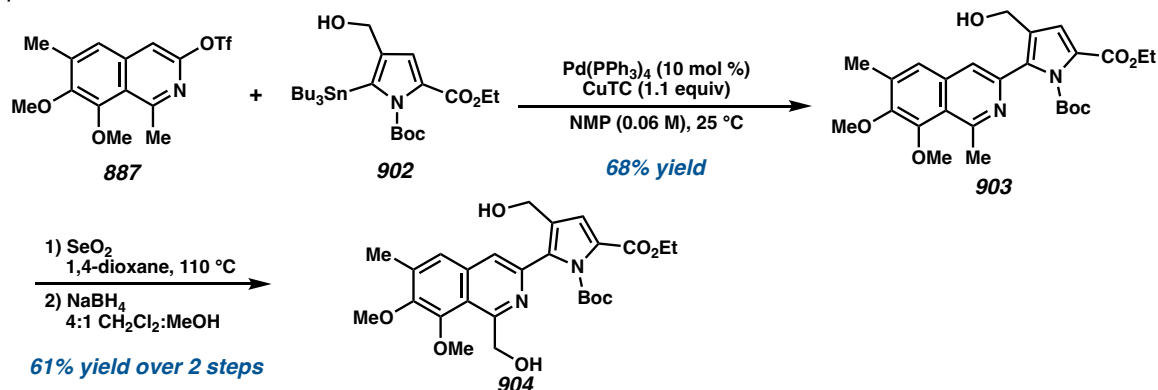
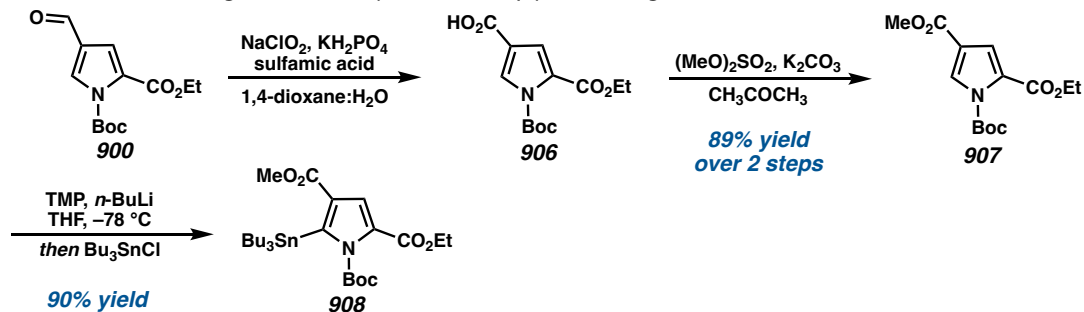
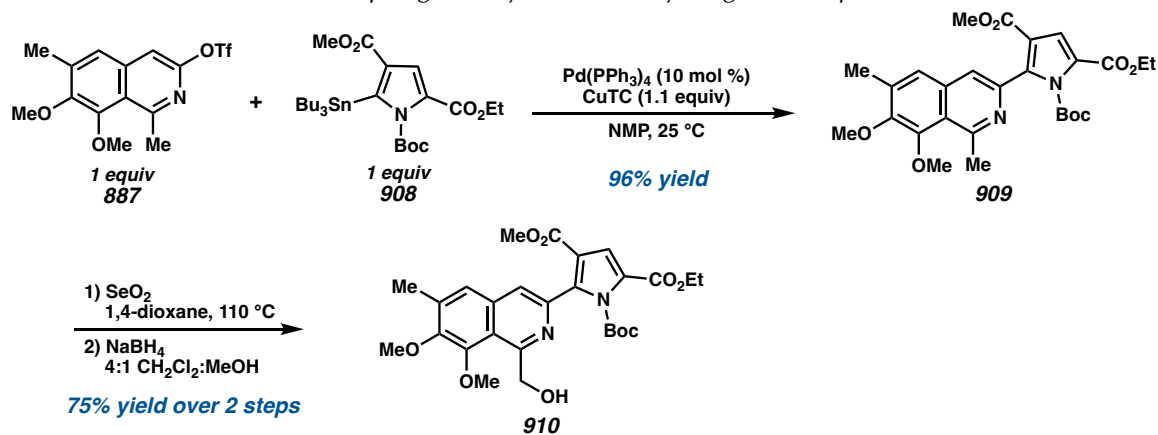
- (29) Casado, A. L.; Espinet, P.; Gallego, A. M. *J. Am. Chem. Soc.* **2000**, *122*, 11771–11782.
- (30) Variation of the substituent at the C3-position of the dihydropyrrole was attempted to differentiate between the two ester functionalities but were unsuccessful, providing much lower yields of the triflation and Stille cross-coupling.
- (31) Gorelsky, S. I.; Lapointe, D.; Fagnou, K. *J. Am. Chem. Soc.* **2008**, *130*, 10848–10849.
- (32) For examples of cyclic enamide cross-couplings, see: a) Evans, P.; McCabe, T.; Morgan, B. S.; Reau, S. *Org. Lett.* **2005**, *7*, 43–46; b) Beng, T. K.; Langevin, S.; Braunstein, H.; Khim, M. *Org. Biomol. Chem.* **2016**, *14*, 830–834.
- (33) Oliveira, D. F.; Miranda, P. C. M. L.; Correia, C. R. D. *J. Org. Chem.* **1999**, *64*, 6646–6652.
- (34) For examples of Pd-catalyzed C–H direct arylation reactions, see: a) Verrier, C.; Lassalas, P.; Théveau, L.; Quéguiner, G.; Trécourt, F.; Marsais, F.; Hoarau, C. *Beilstein J. Org. Chem.* **2011**, *7*, 1584–1601; b) Joucla, L.; Djakovitch, L. *Adv. Synth. Catal.* **2009**, *351*, 673–714; c) Ackermann, L.; Vicente, R.; Kapdi, A. R. *Angew. Chem. Int. Ed.* **2009**, *48*, 9792–9826; d) Phipps, R. J.; Grimster, N. P.; Gaunt, M. J. *J. Am. Chem. Soc.* **2008**, *130*, 8172–8174; e) Wang, L.; Carrow, B. P. *ACS Catal.* **2019**, *9*, 6821–6836.
- (35) Woo, G. H. C.; Kim, S.-H.; Wipf, P. *Tetrahedron* **2006**, *62*, 10507–10517.
- (36) Lapointe, D.; Fagnou, K. *Chem. Lett.* **2010**, *39*, 1118–1126.
- (37) Lafrance, M.; Fagnou, K. *J. Am. Chem. Soc.* **2006**, *128*, 16496–16497.

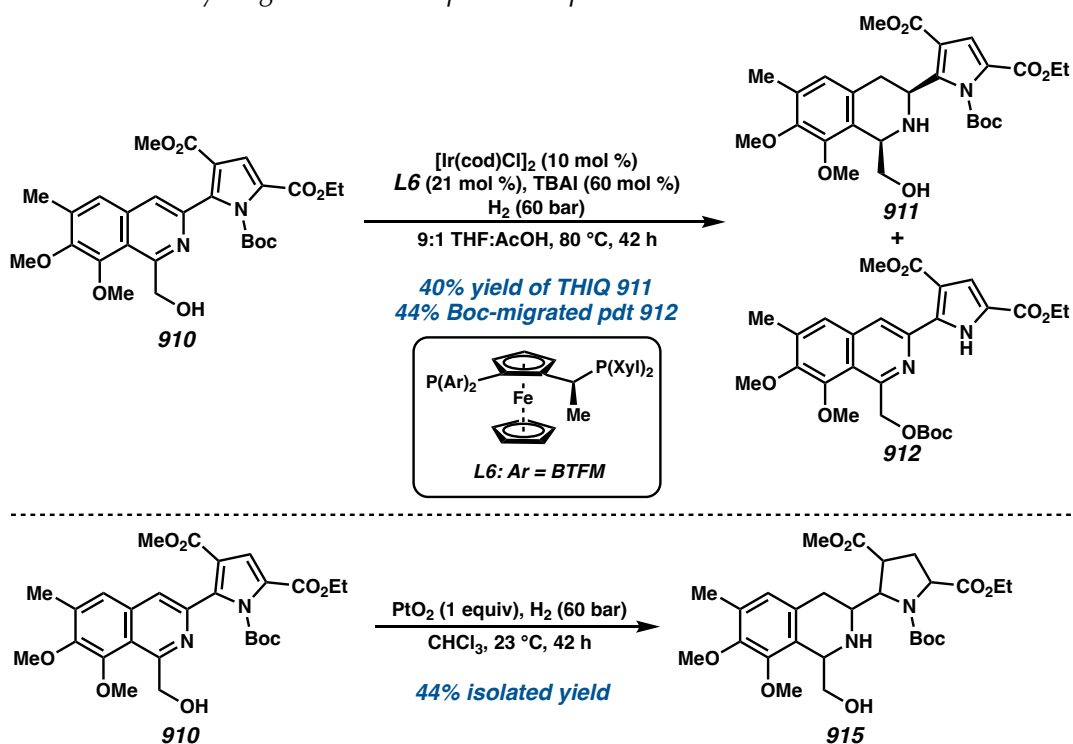
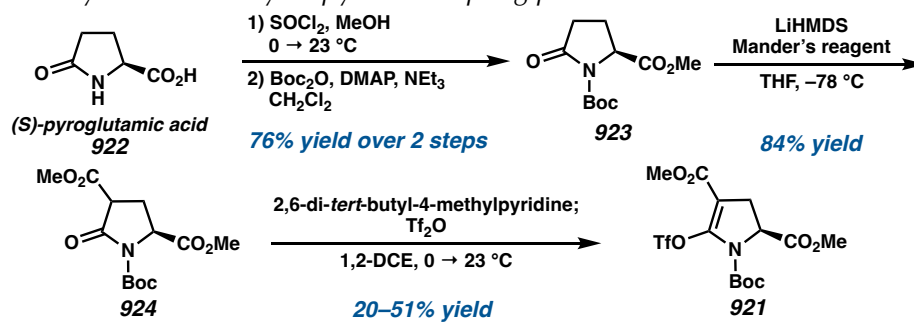
## **APPENDIX 5**

*Synthetic Summary for Chapter 5:  
Progress Toward the Total Synthesis  
of (+)-Cyanocycline A*

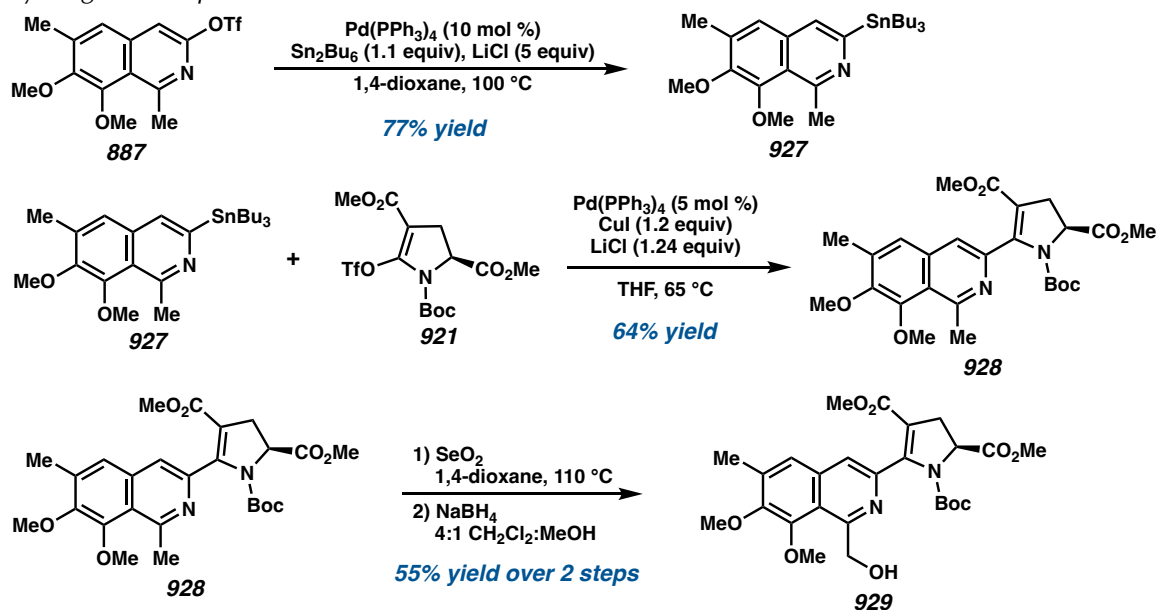


**Scheme A5.1** Synthesis of the western isoquinoline fragment **887**.**Scheme A5.2** Synthesis of the eastern pyrrole fragment **898**.**Scheme A5.3** 2<sup>nd</sup> generation synthesis of pyrrole fragment **902**.

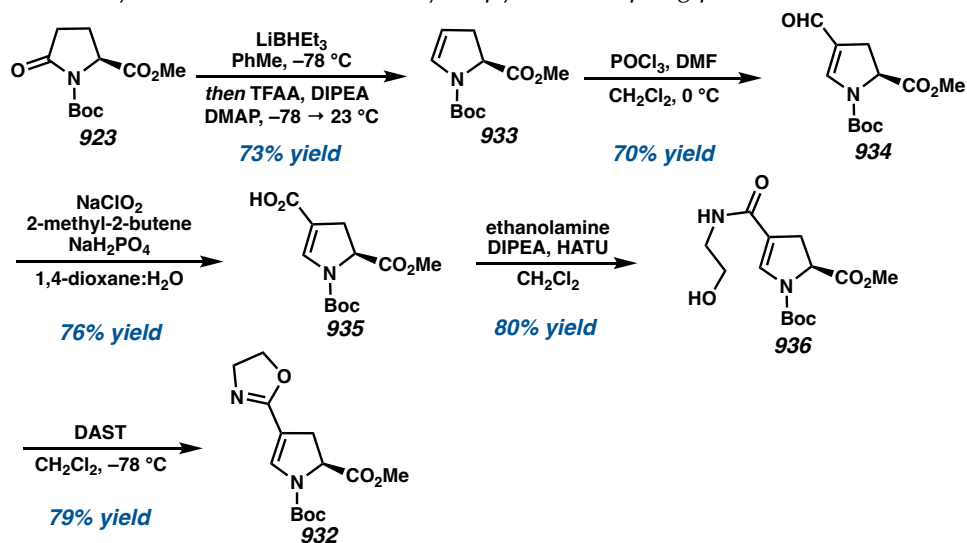
**Scheme A5.4** Cross-coupling of heterocycles **887** and **902**, and synthesis of hydrogenation precursor **904**.**Scheme A5.5** 3<sup>rd</sup> generation synthesis of pyrrole fragment **908**.**Scheme A5.6** Stille cross-coupling and synthesis of hydrogenation precursor **910**.

**Scheme A5.7** Hydrogenation attempts of isoquinoline **910**.**Scheme A5.8** Synthesis of dihydropyrrole coupling partner **921**.

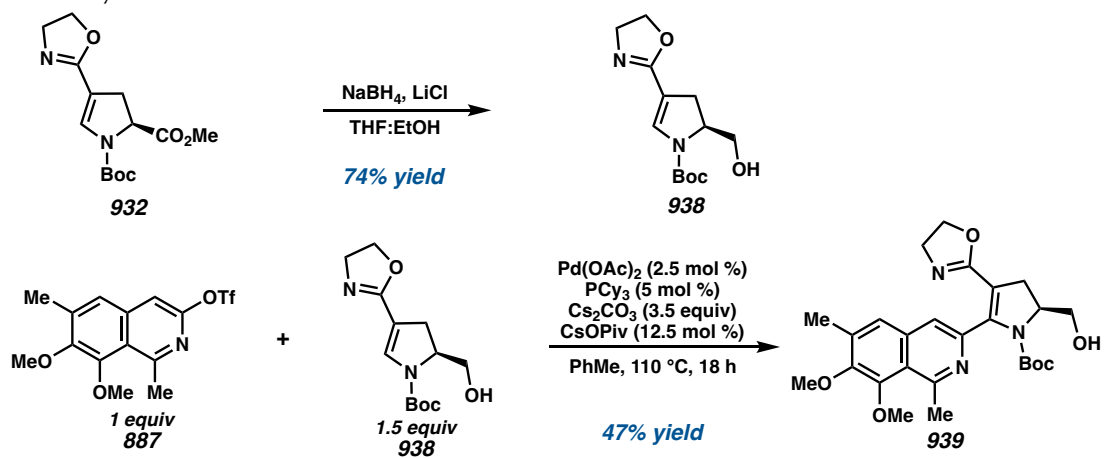
**Scheme A5.9** Stannylation of isoquinoline triflate **887** and synthesis of dihydropyrrole hydrogenation precursor **929**.



**Scheme A5.10** Synthesis of oxazoline dihydropyrrole coupling partner **932**.

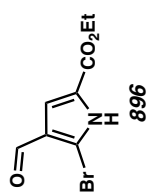


**Scheme A5.11** Reduction of oxazoline **932** and Pd-catalyzed CMD cross-coupling of heterocycles **887** and **938**.



## ***APPENDIX 6***

*Spectra Relevant to Chapter 5:  
Progress Toward the Total Synthesis  
of (+)-Cyanocycline A*



896

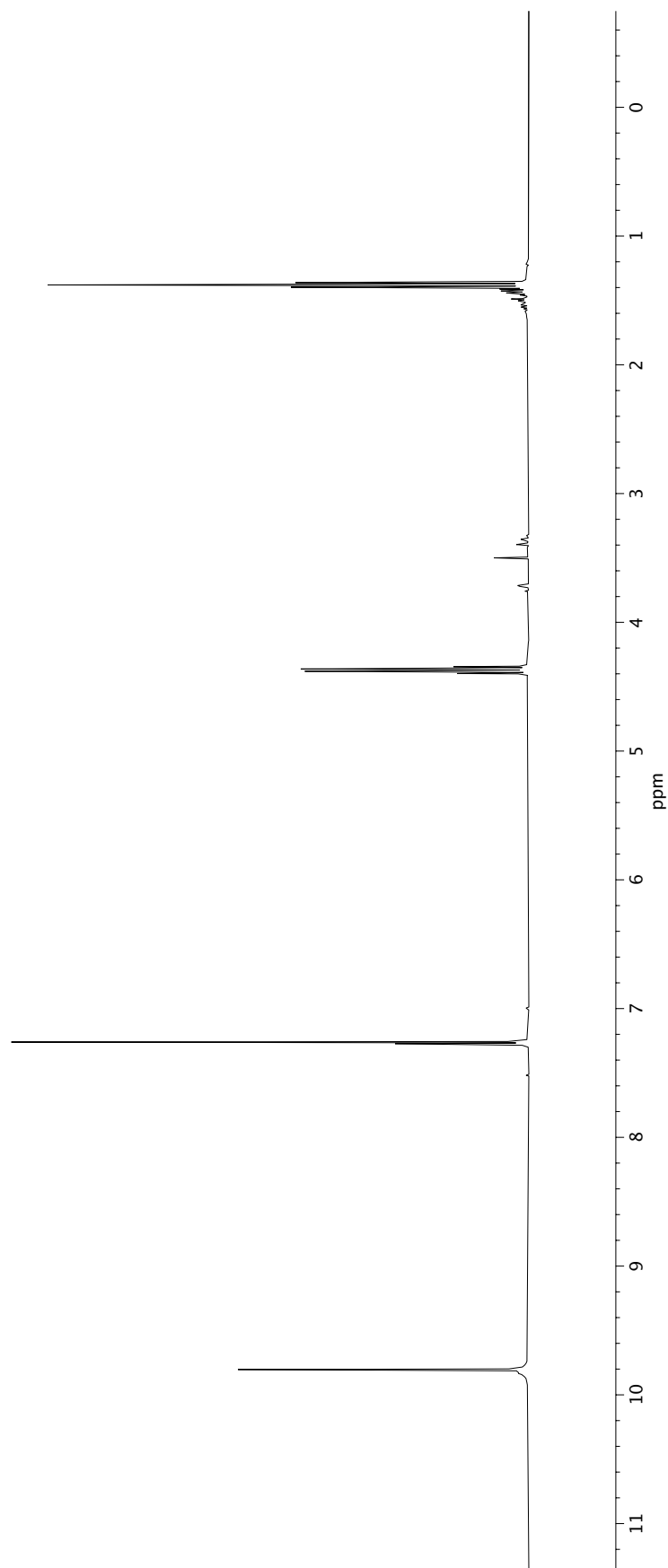


**Figure A6.1**  $^1\text{H}$  NMR (400 MHz,  $\text{CDCl}_3$ ) of compound **896**.

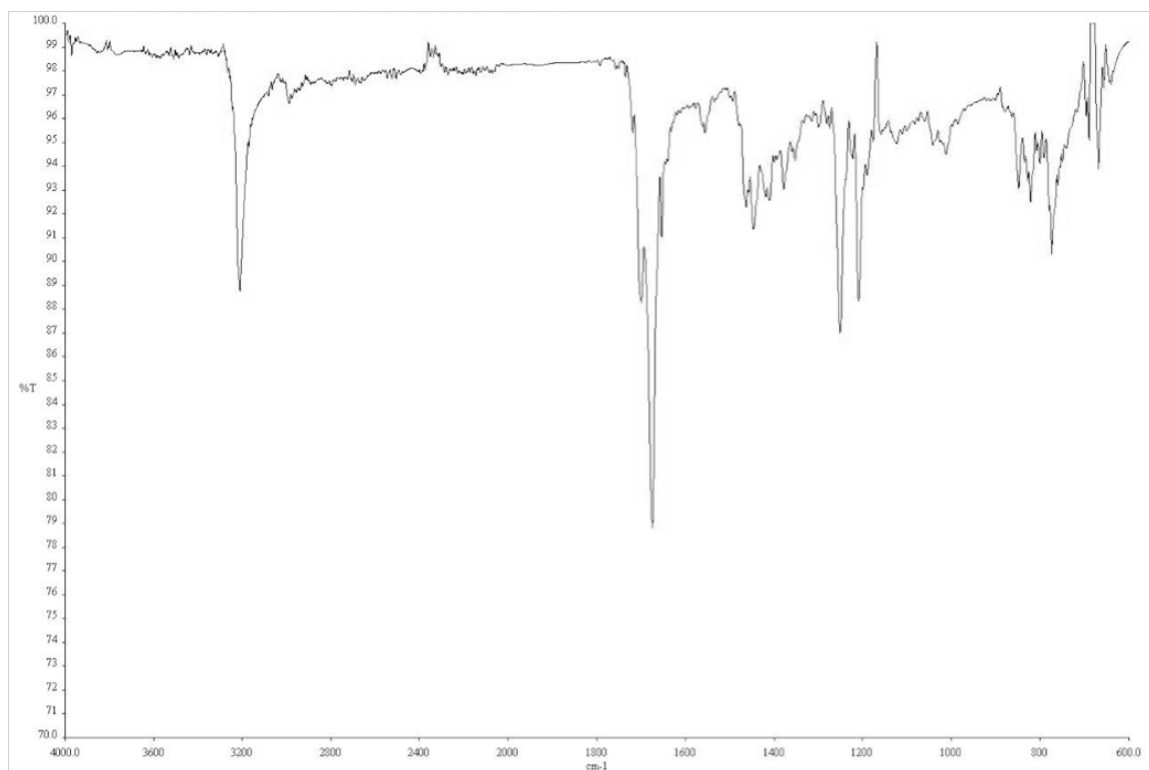


**Figure A6.2** Infrared spectrum (Thin Film, NaCl) of compound **896**.

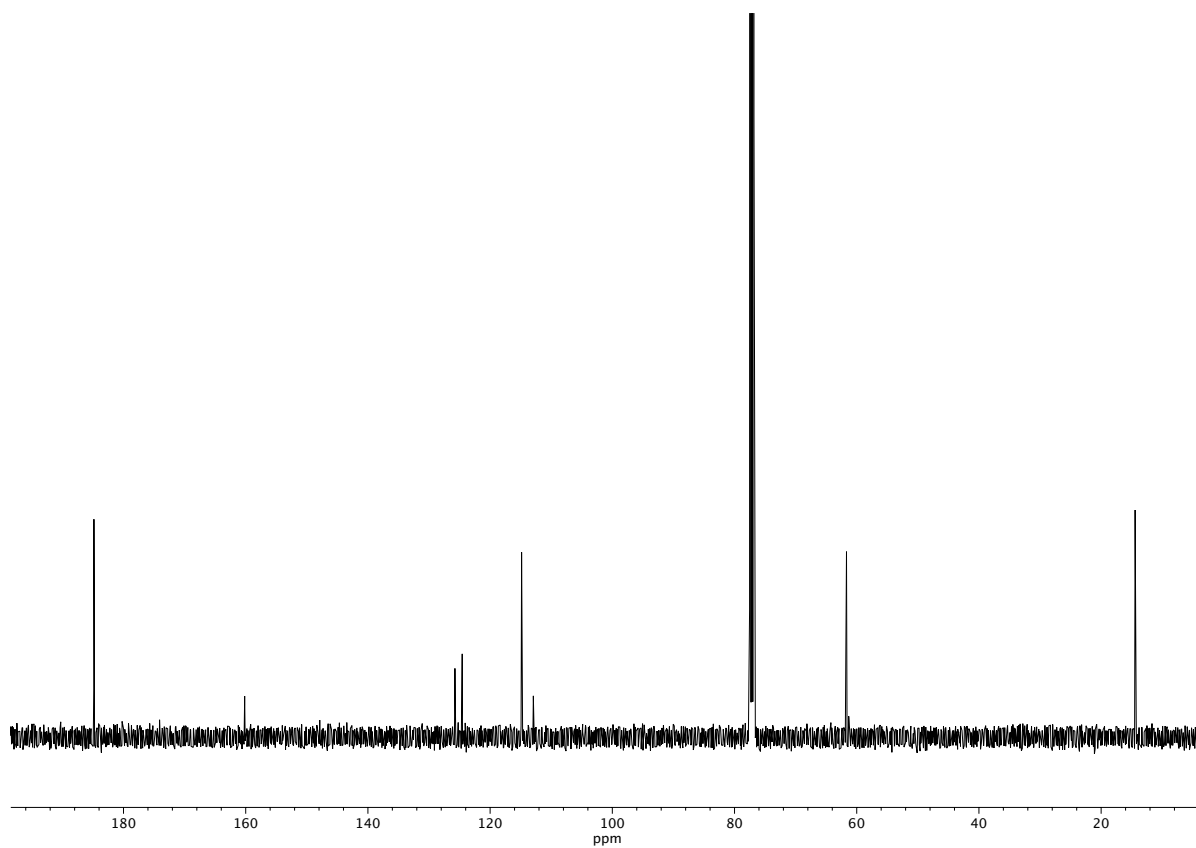


**Figure A6.3** <sup>13</sup>C NMR (100 MHz, CDCl<sub>3</sub>) of compound **896**.



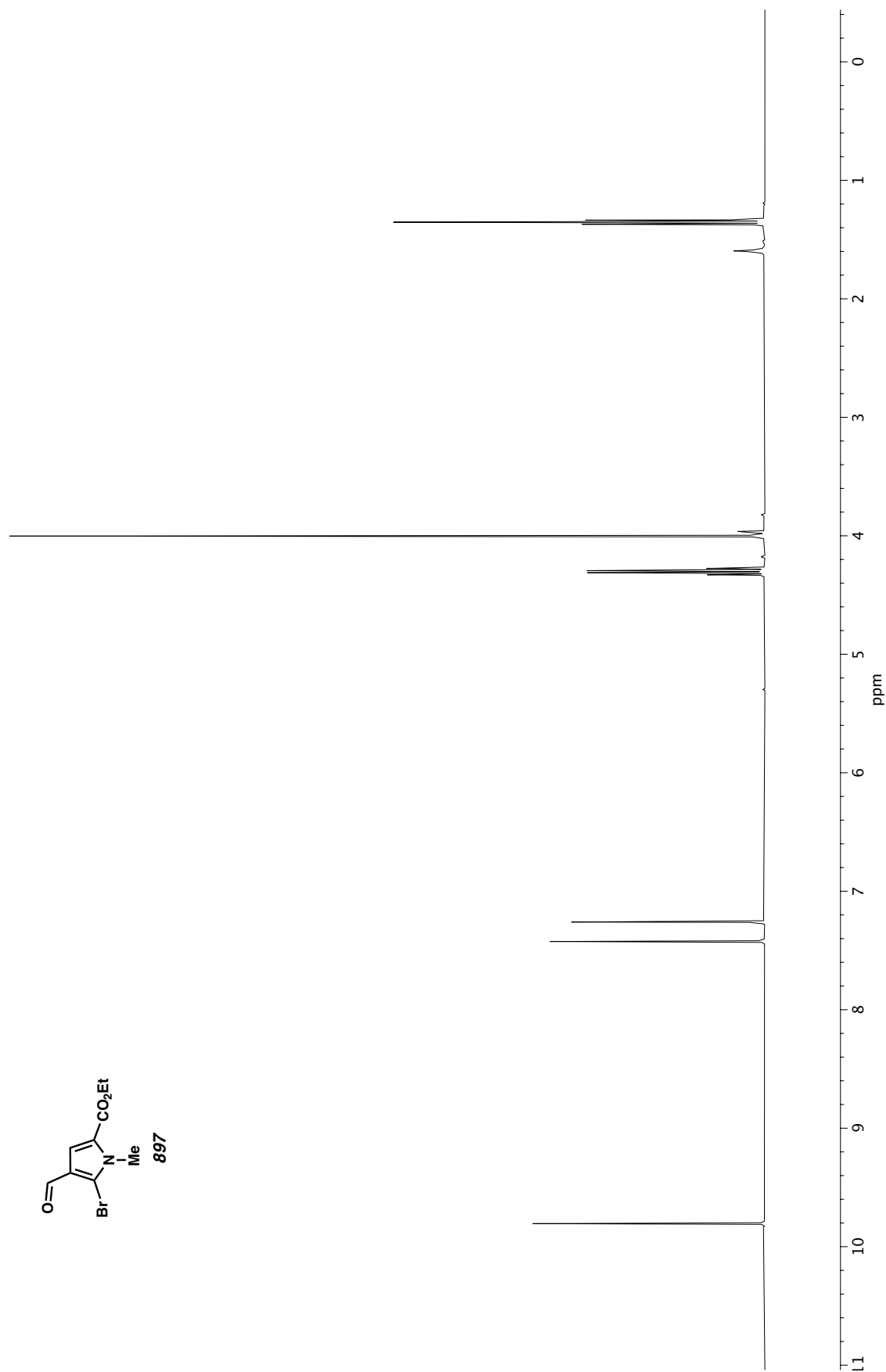


**Figure A6.4**  $^1\text{H}$  NMR (400 MHz, CDCl<sub>3</sub>) of compound **897**.

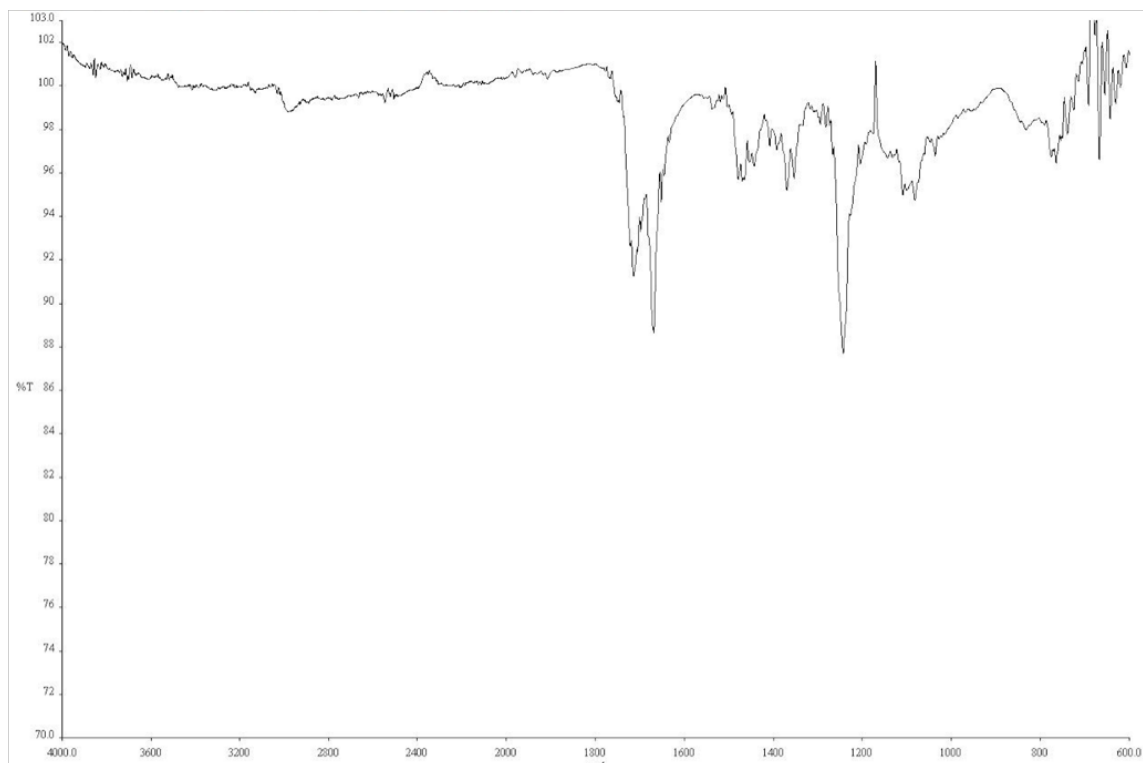


**Figure A6.5** Infrared spectrum (Thin Film, NaCl) of compound **897**.

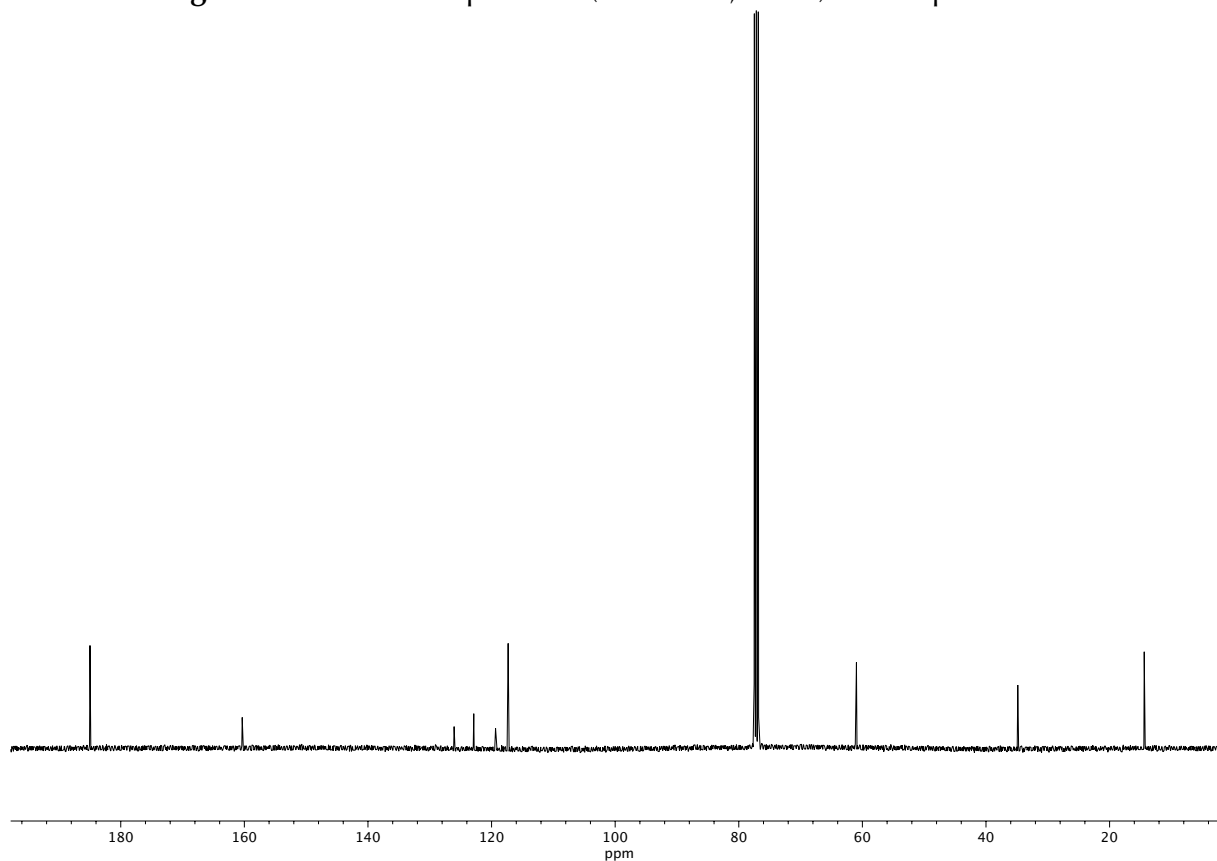


**Figure A6.6** <sup>13</sup>C NMR (100 MHz, CDCl<sub>3</sub>) of compound **897**.

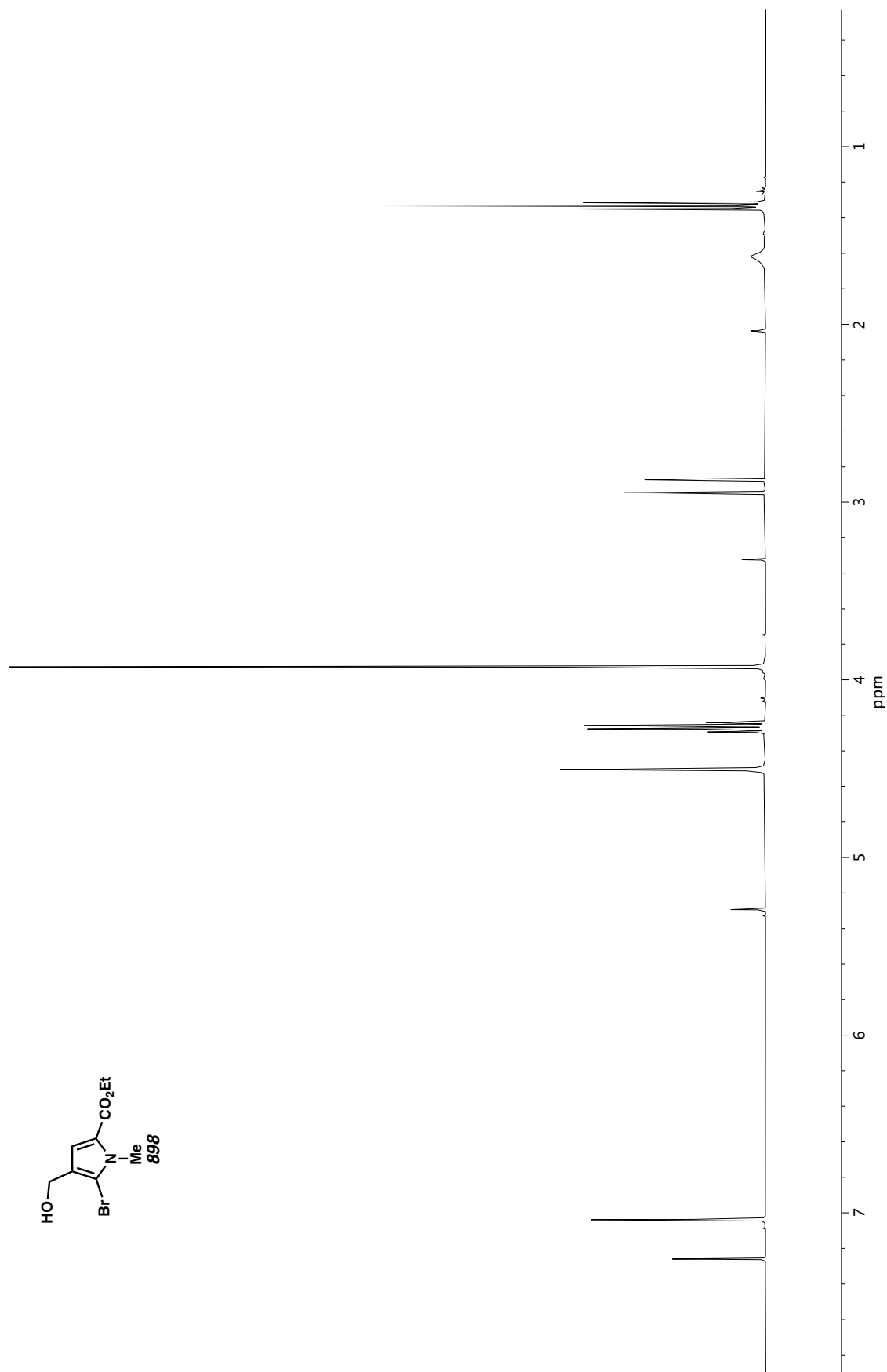


**Figure A6.7**  $^1\text{H}$  NMR (400 MHz, CDCl<sub>3</sub>) of compound **898**.

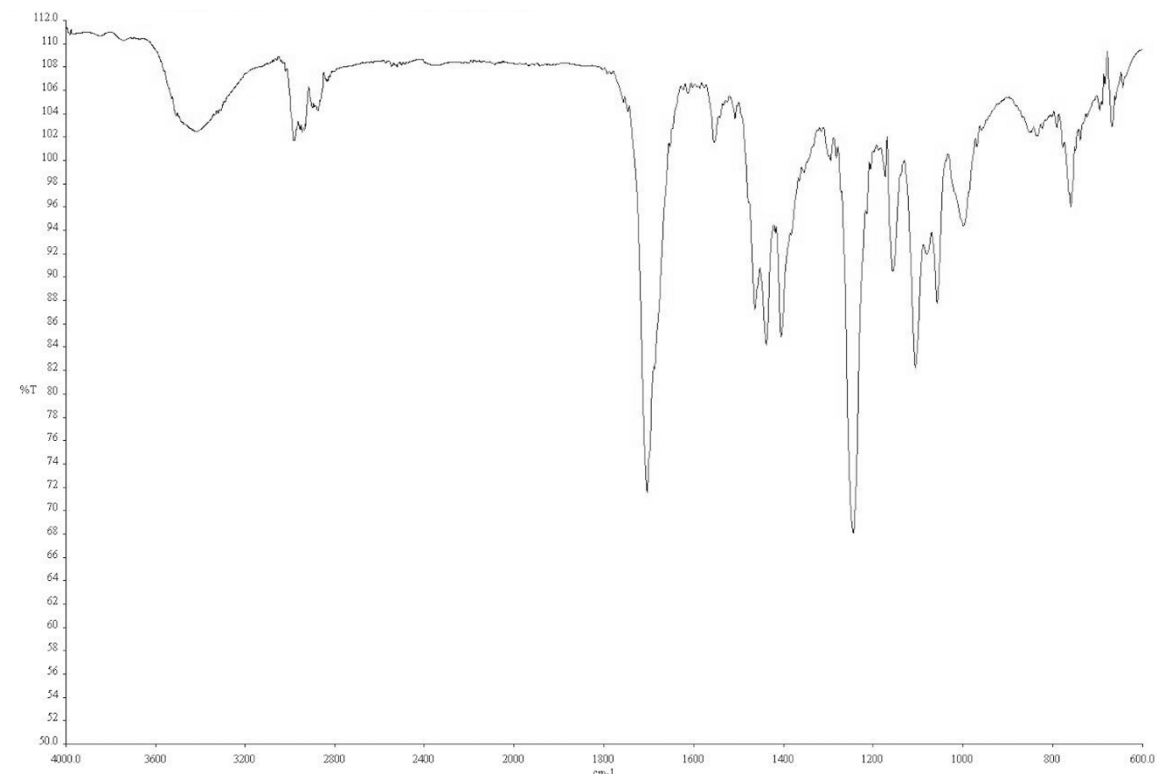


**Figure A6.8** Infrared spectrum (Thin Film, NaCl) of compound **898**.

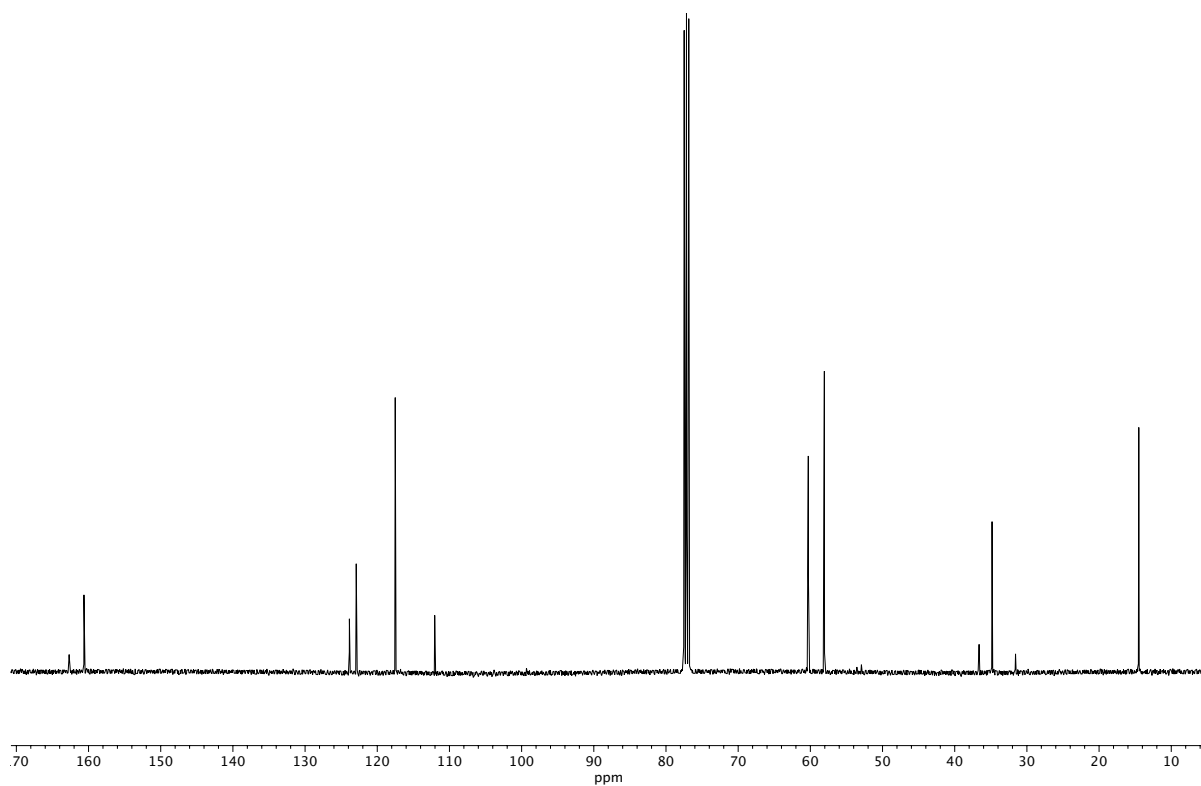


**Figure A6.9**  $^{13}\text{C}$  NMR (100 MHz,  $\text{CDCl}_3$ ) of compound **898**.

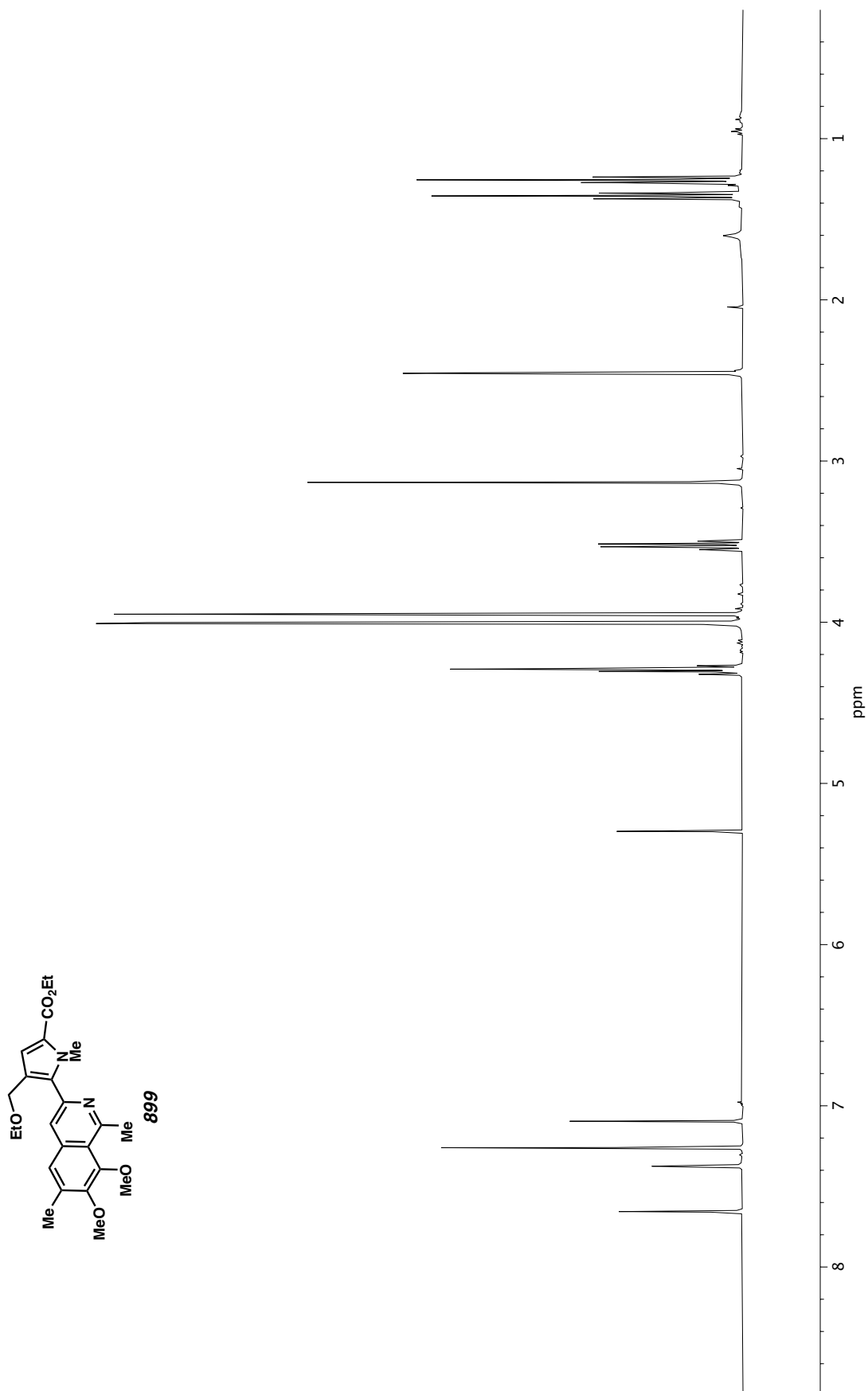


**Figure A6.10**  $^1\text{H}$  NMR (400 MHz,  $\text{CDCl}_3$ ) of compound **899**.

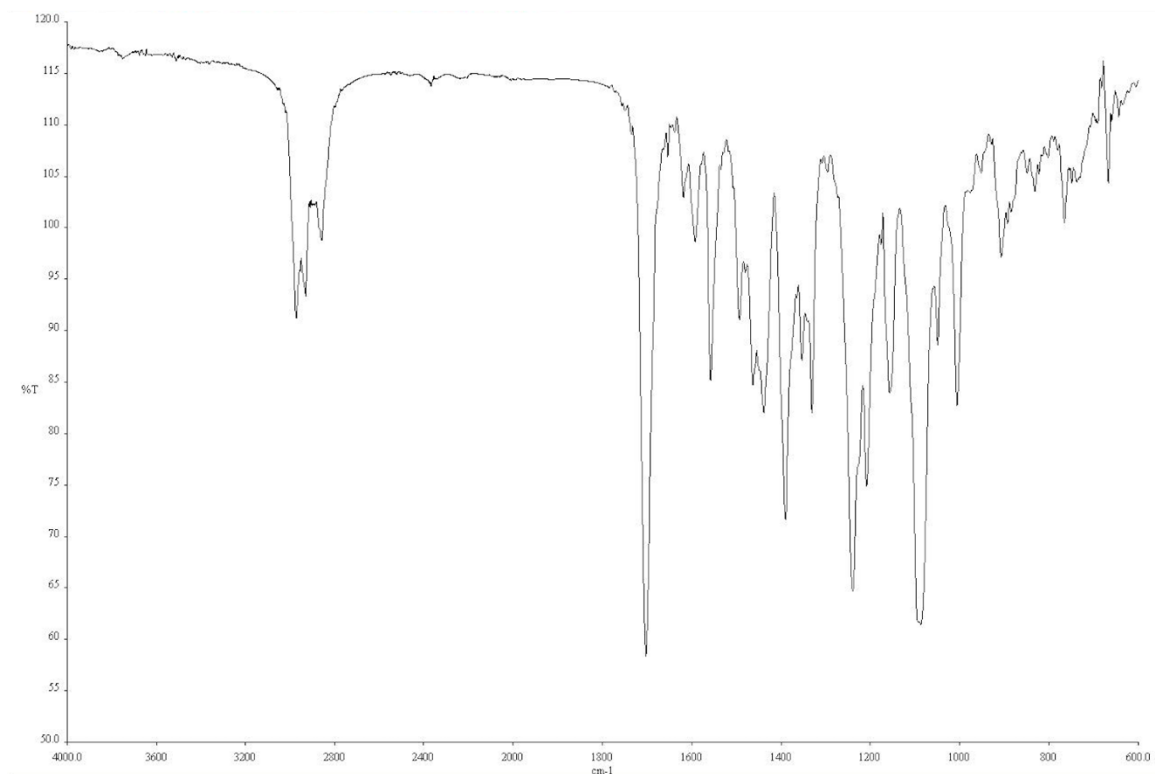


**Figure A6.11** Infrared spectrum (Thin Film, NaCl) of compound **899**.

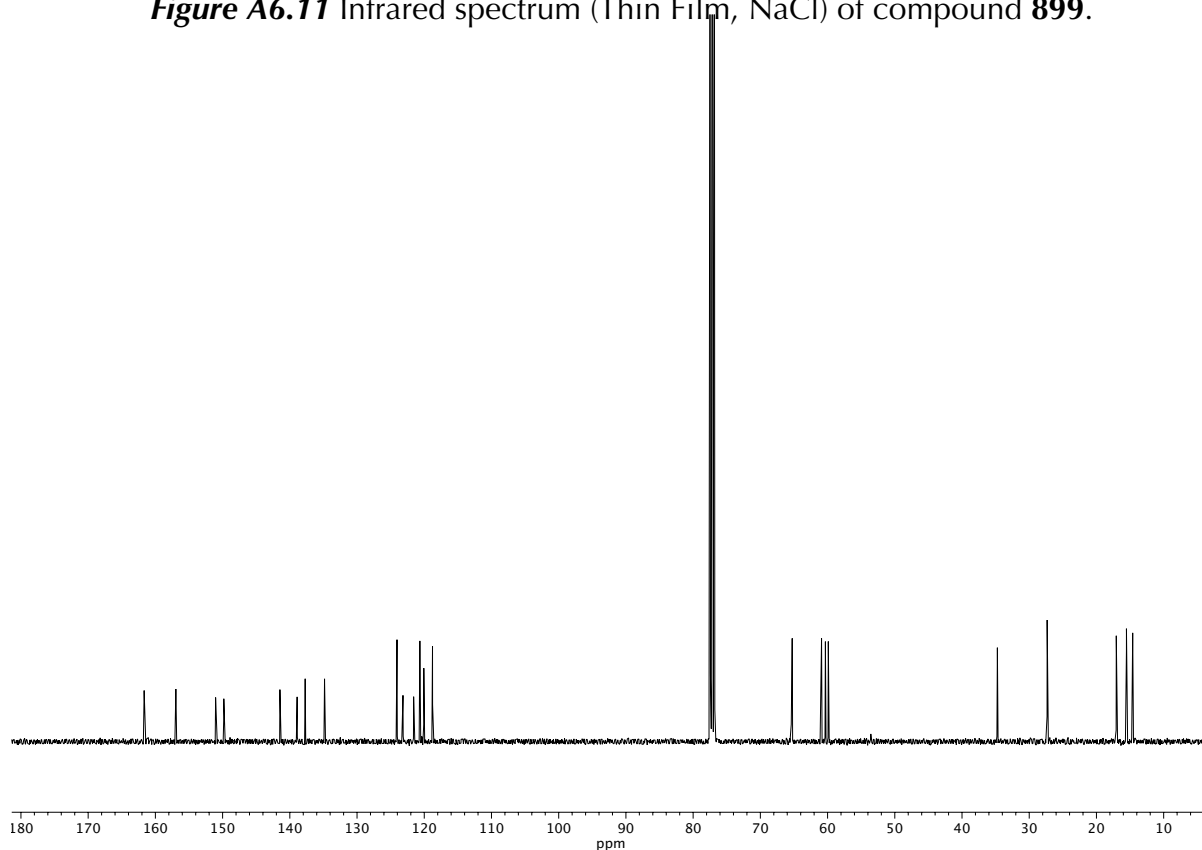


**Figure A6.12**  $^{13}\text{C}$  NMR (100 MHz,  $\text{CDCl}_3$ ) of compound **899**.

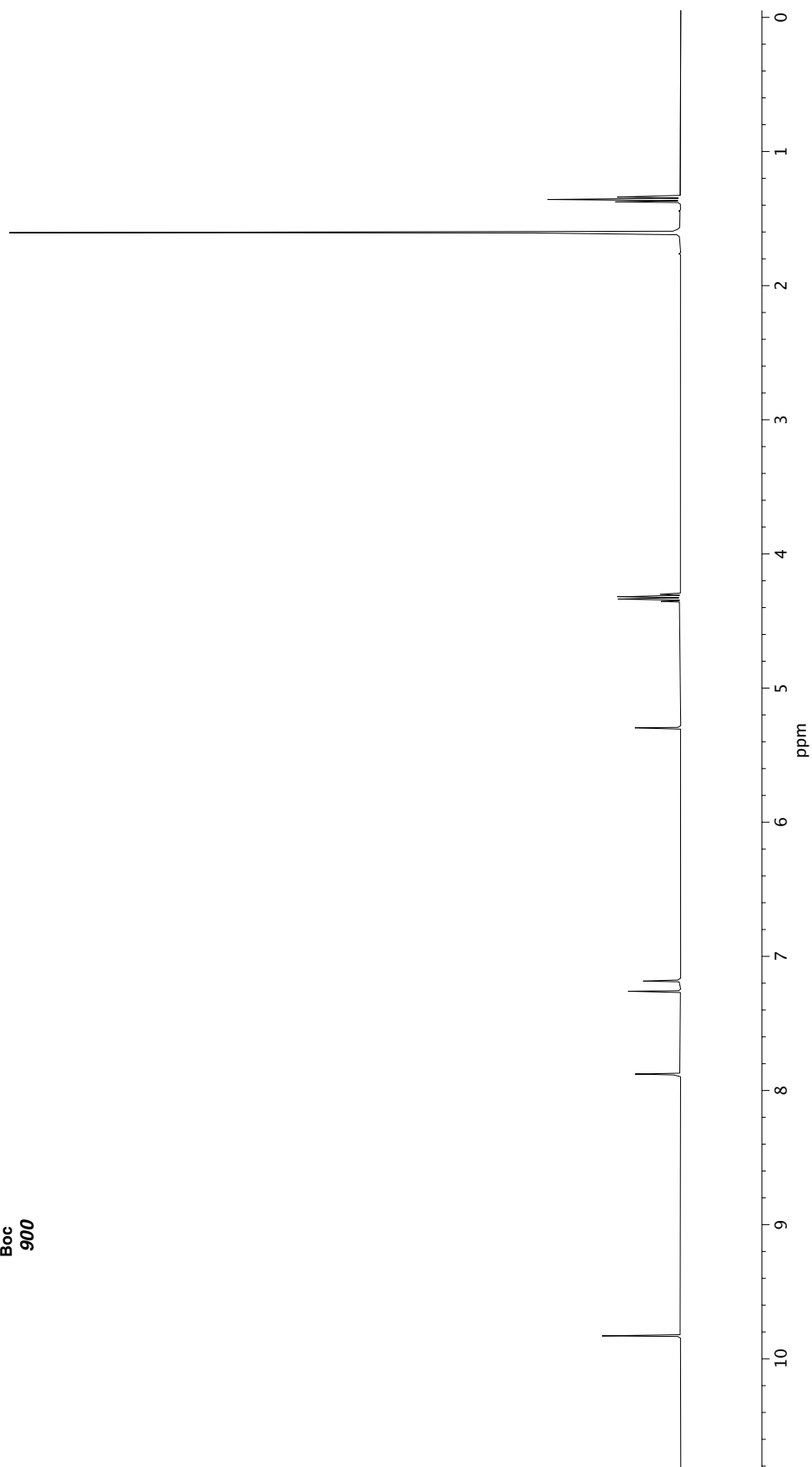
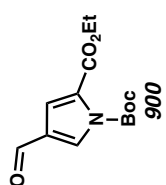


**Figure A6.13** <sup>1</sup>H NMR (400 MHz, CDCl<sub>3</sub>) of compound **900**.

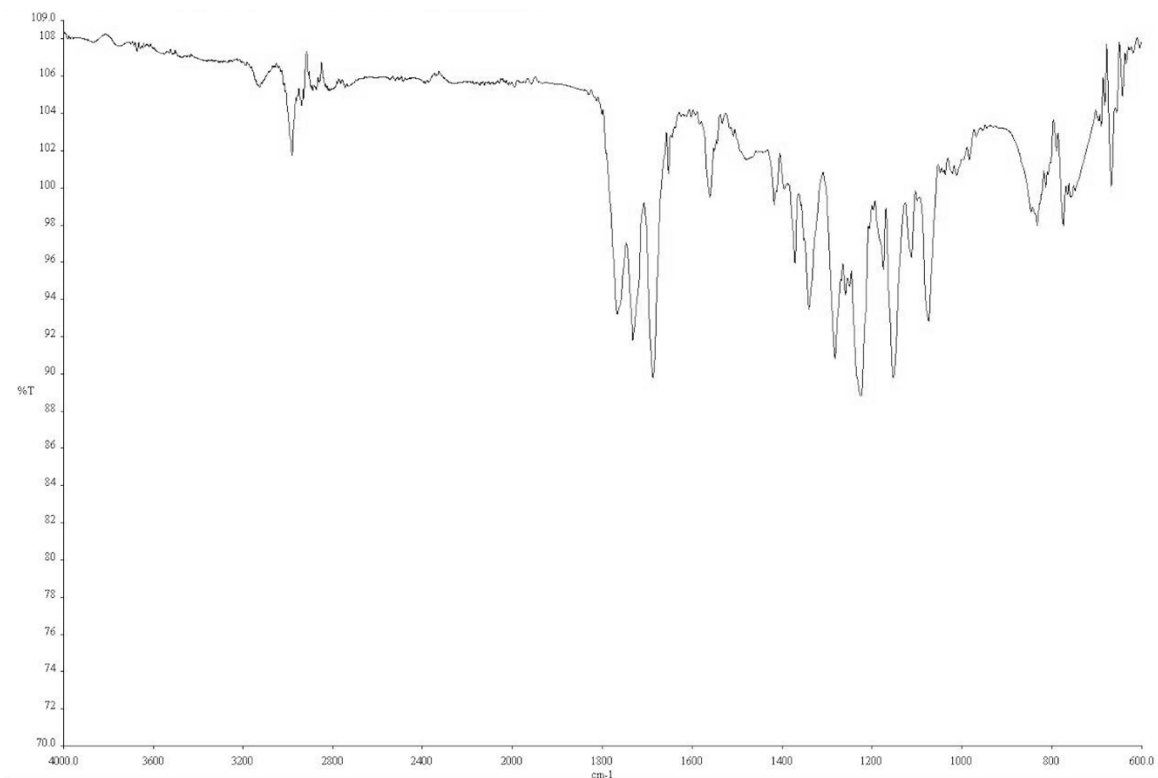


**Figure A6.14** Infrared spectrum (Thin Film, NaCl) of compound **900**.

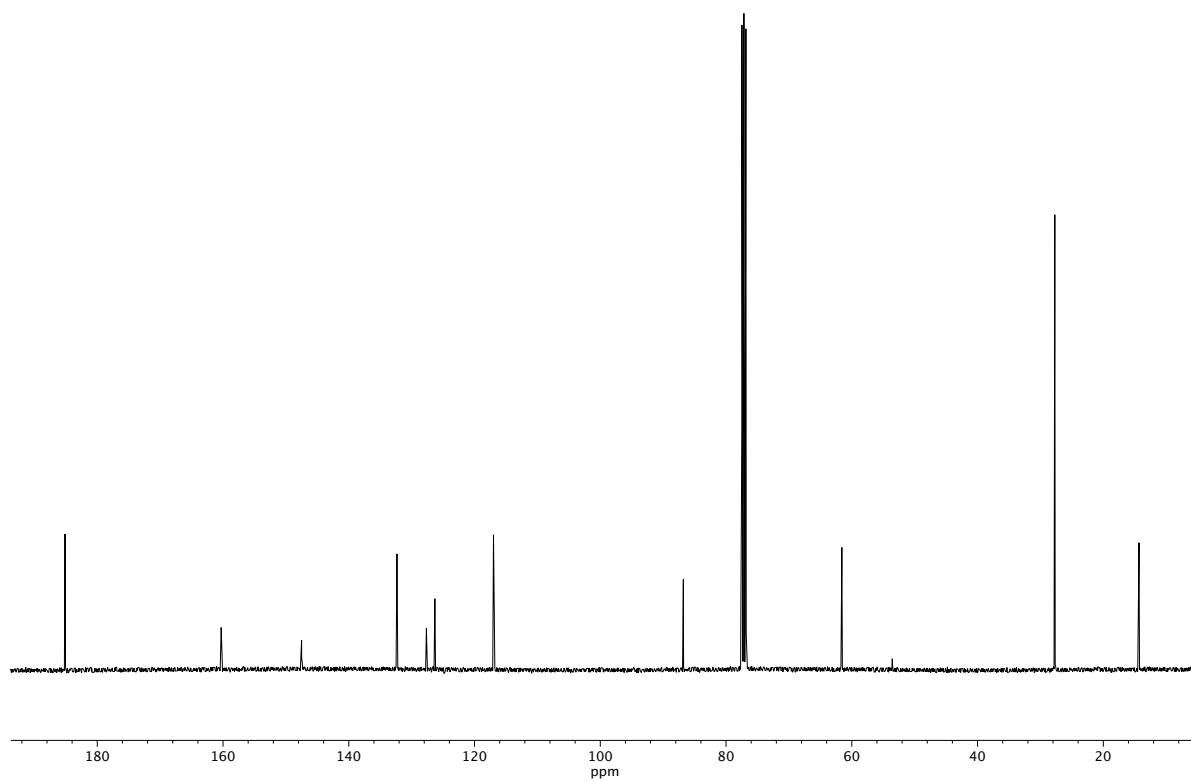


**Figure A6.15** <sup>13</sup>C NMR (100 MHz, CDCl<sub>3</sub>) of compound **900**.



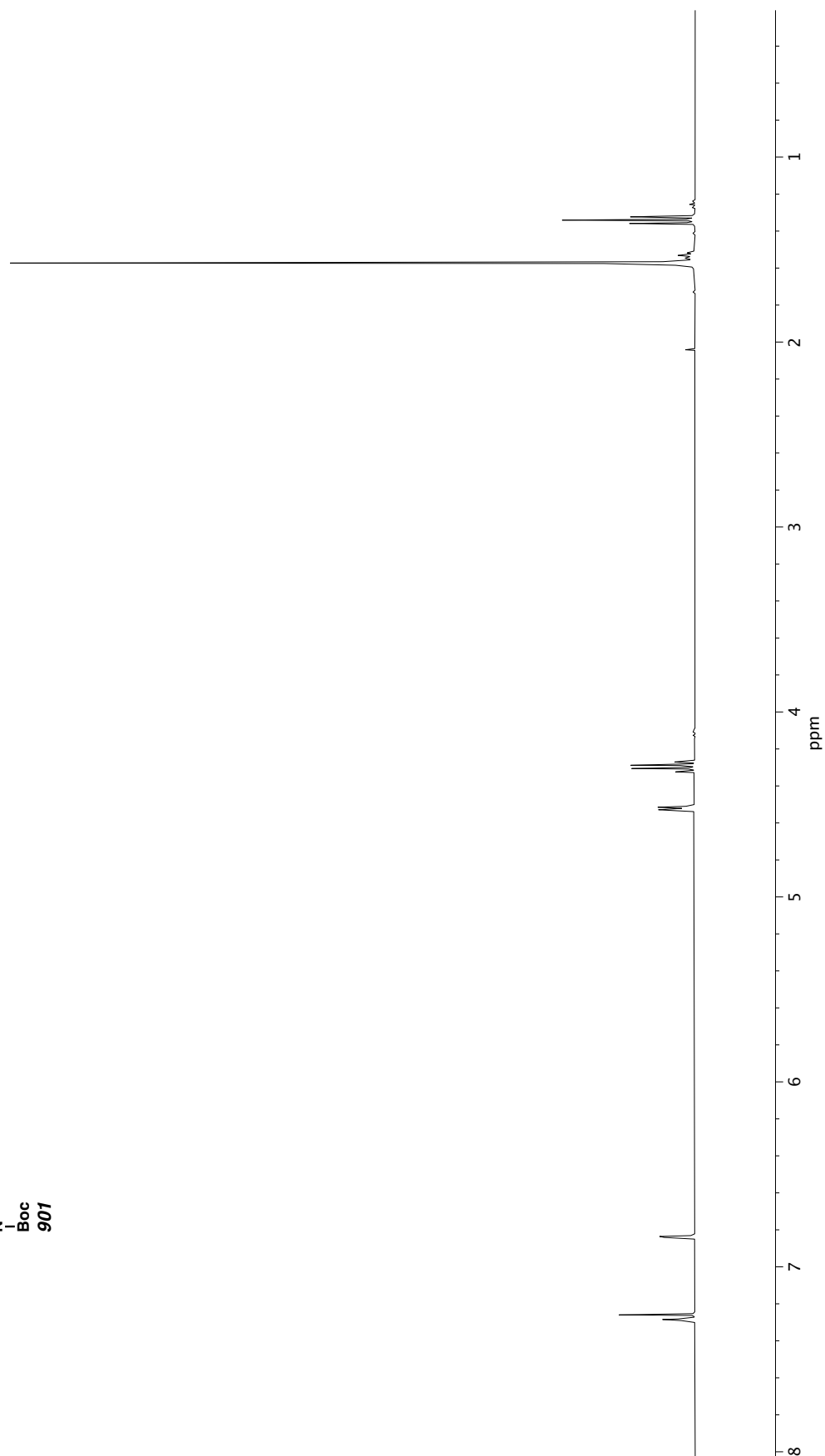
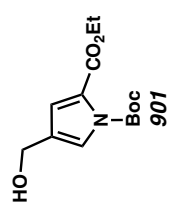


**Figure A6.16** <sup>1</sup>H NMR (400 MHz, CDCl<sub>3</sub>) of compound **901**.

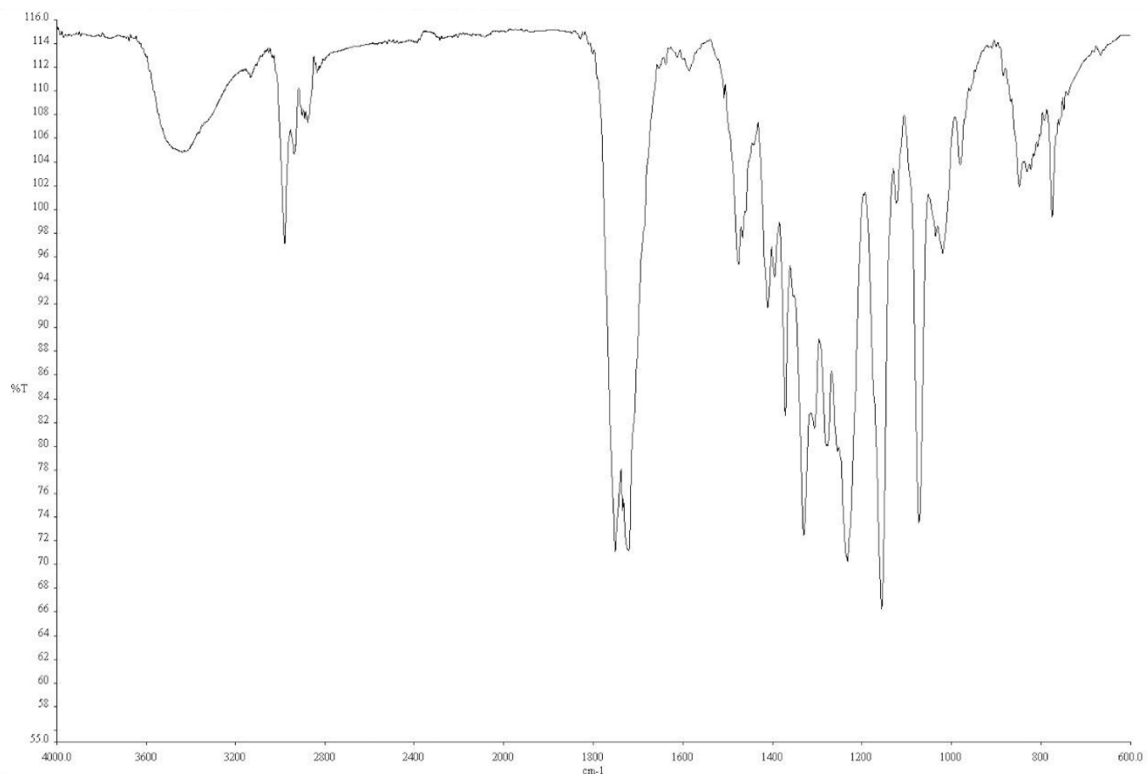


**Figure A6.17** Infrared spectrum (Thin Film, NaCl) of compound **901**.

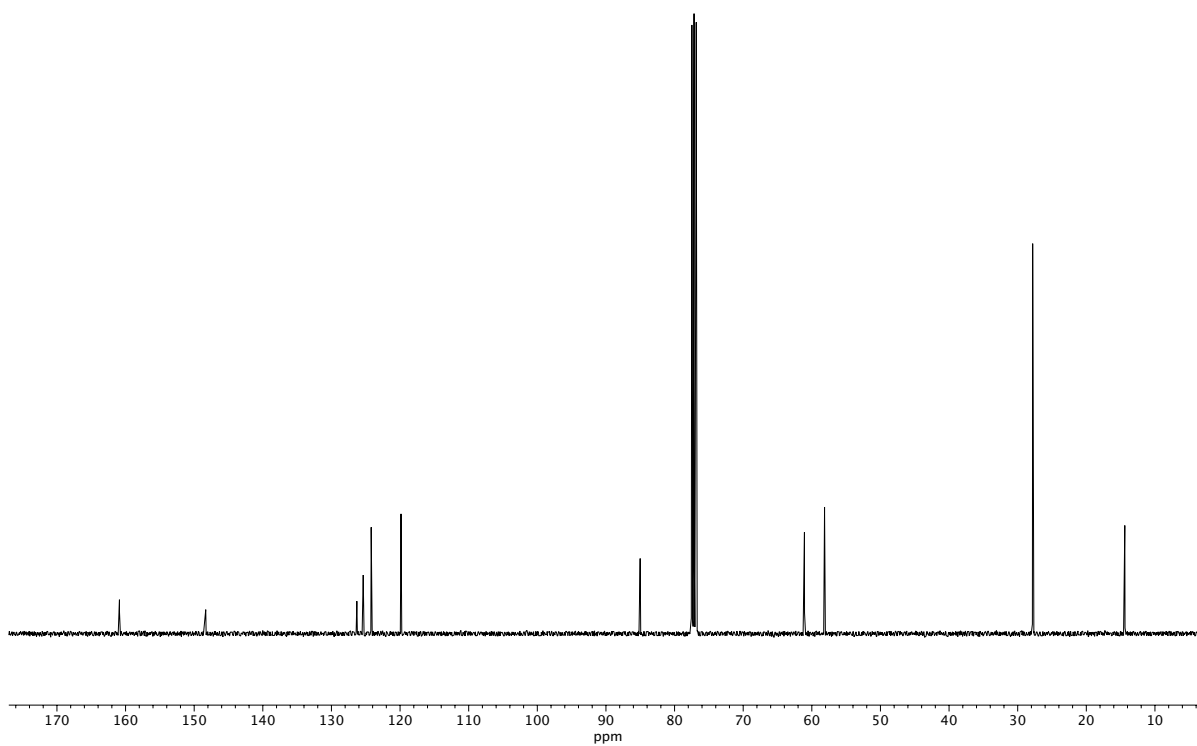


**Figure A6.18**  $^{13}\text{C}$  NMR (100 MHz,  $\text{CDCl}_3$ ) of compound **901**.

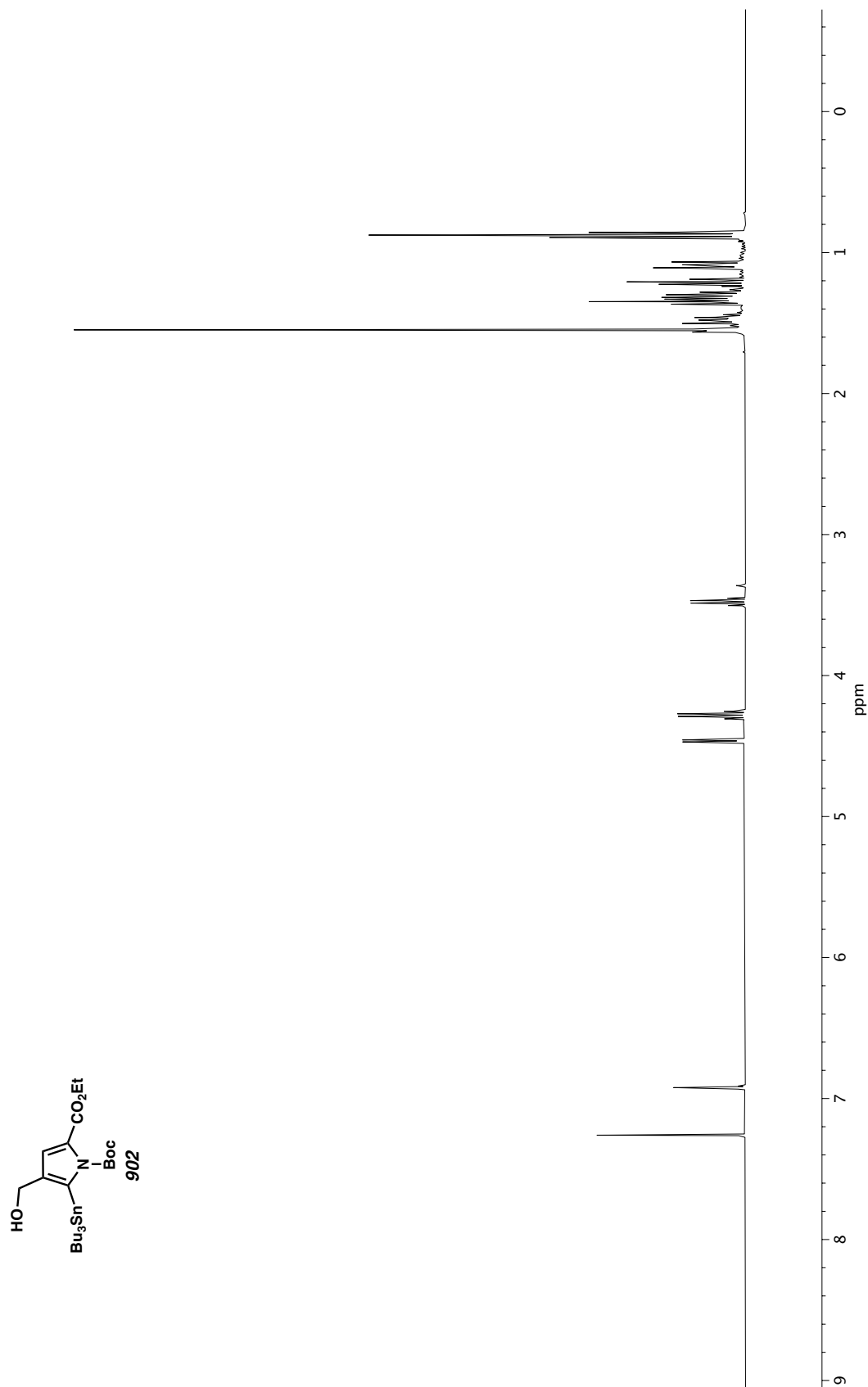


**Figure A6.19**  $^1\text{H}$  NMR (400 MHz,  $\text{CDCl}_3$ ) of compound **902**.

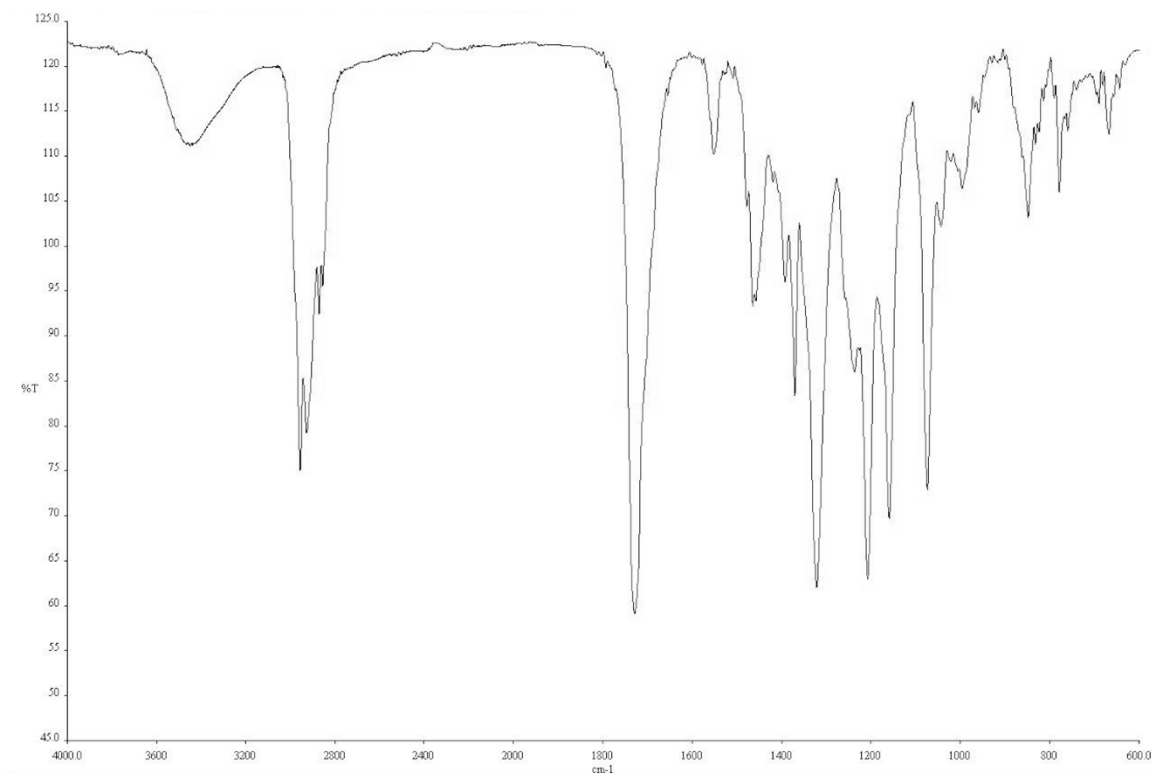


**Figure A6.20** Infrared spectrum (Thin Film, NaCl) of compound **902**.

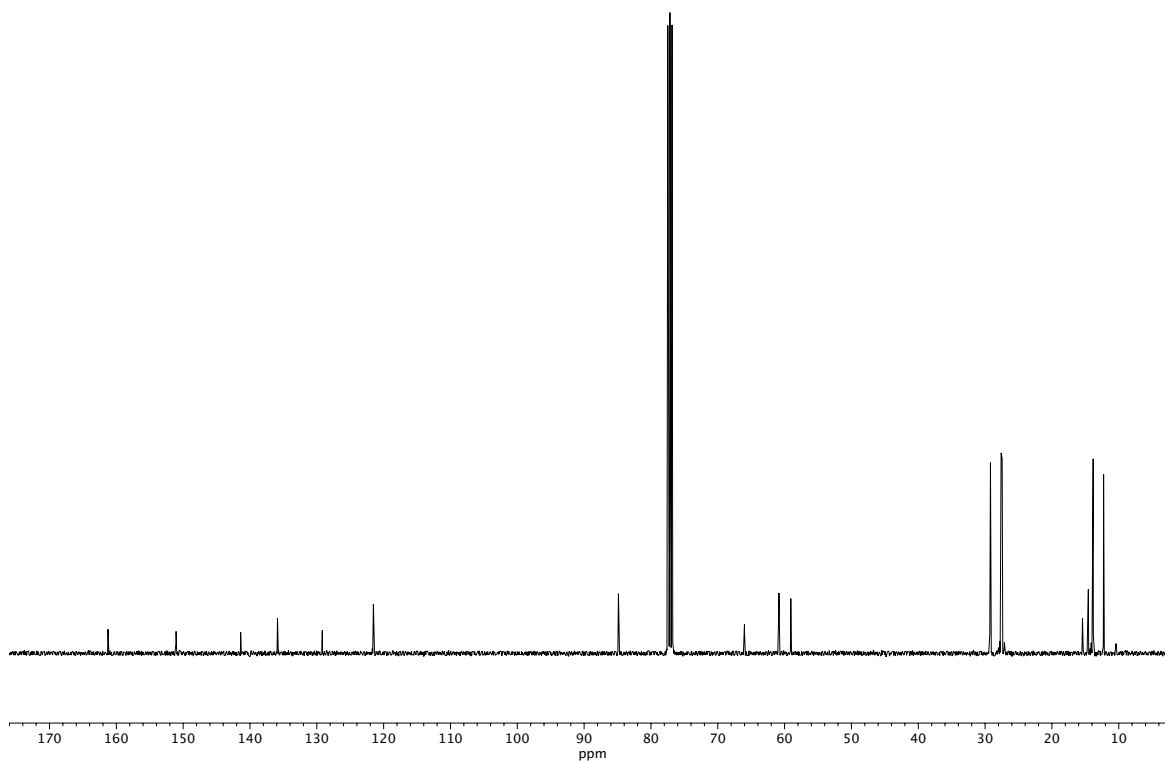


**Figure A6.21**  $^{13}\text{C}$  NMR (100 MHz,  $\text{CDCl}_3$ ) of compound **902**.

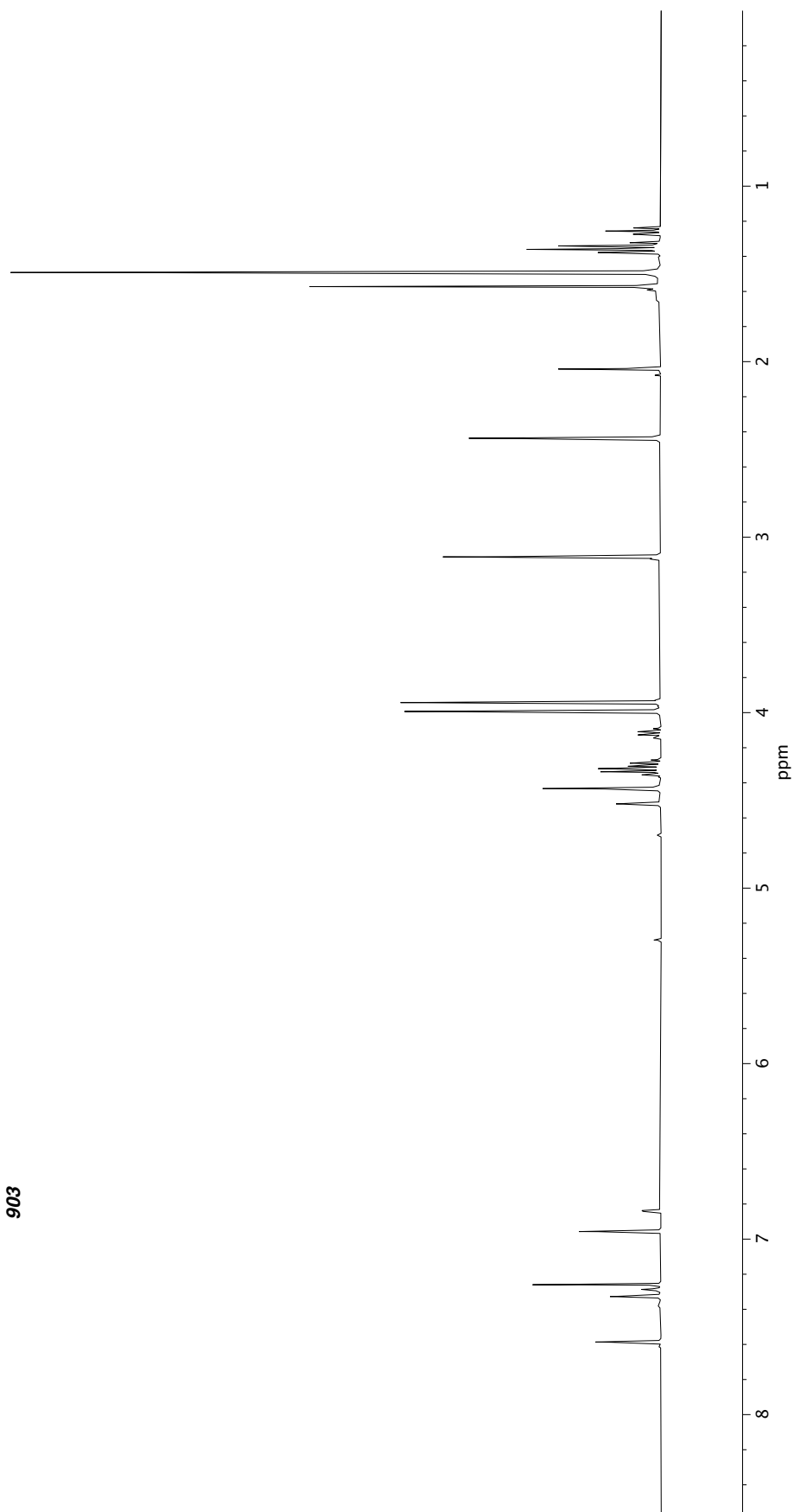
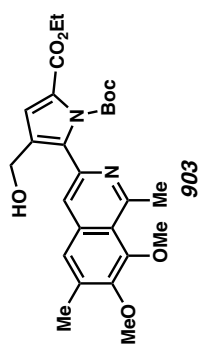
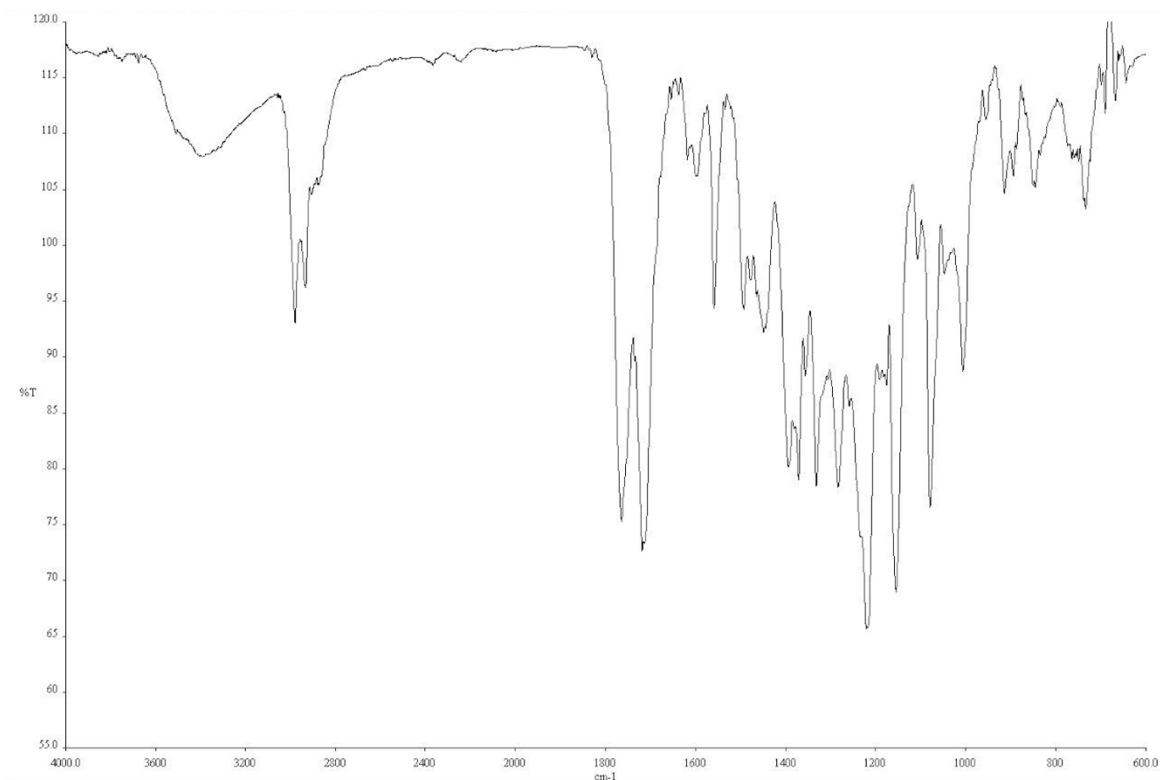
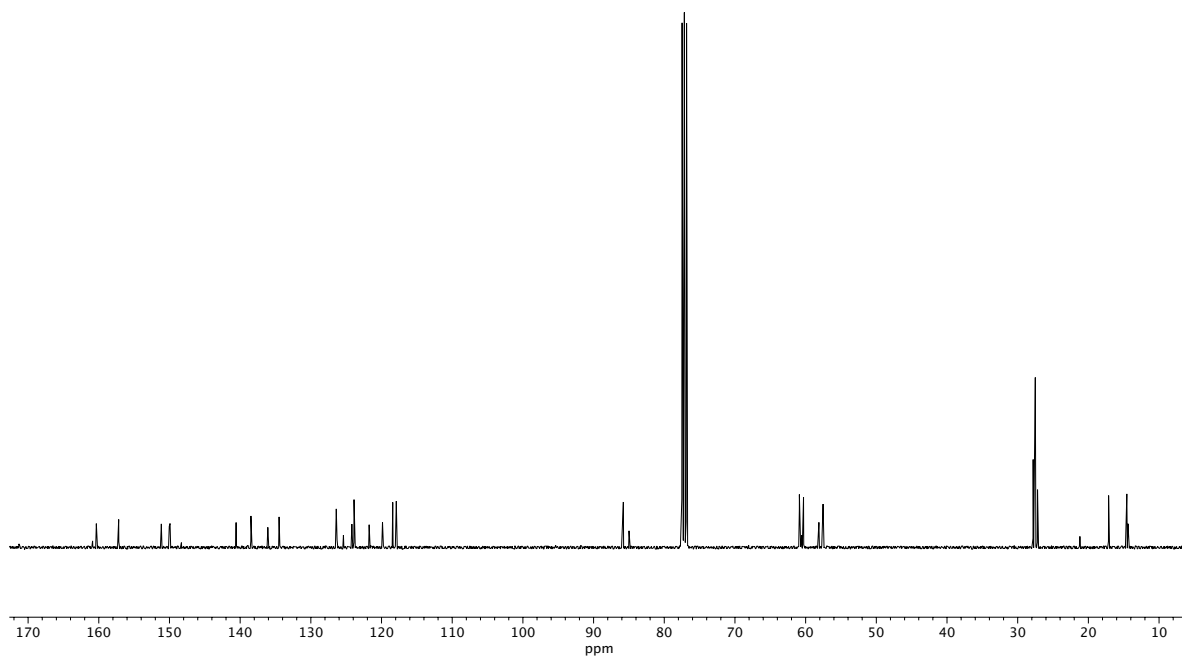


Figure A6.22 <sup>1</sup>H NMR (400 MHz, CDCl<sub>3</sub>) of compound 903.



**Figure A6.23** Infrared spectrum (Thin Film, NaCl) of compound **903**.



**Figure A6.24** <sup>13</sup>C NMR (100 MHz, CDCl<sub>3</sub>) of compound **903**.

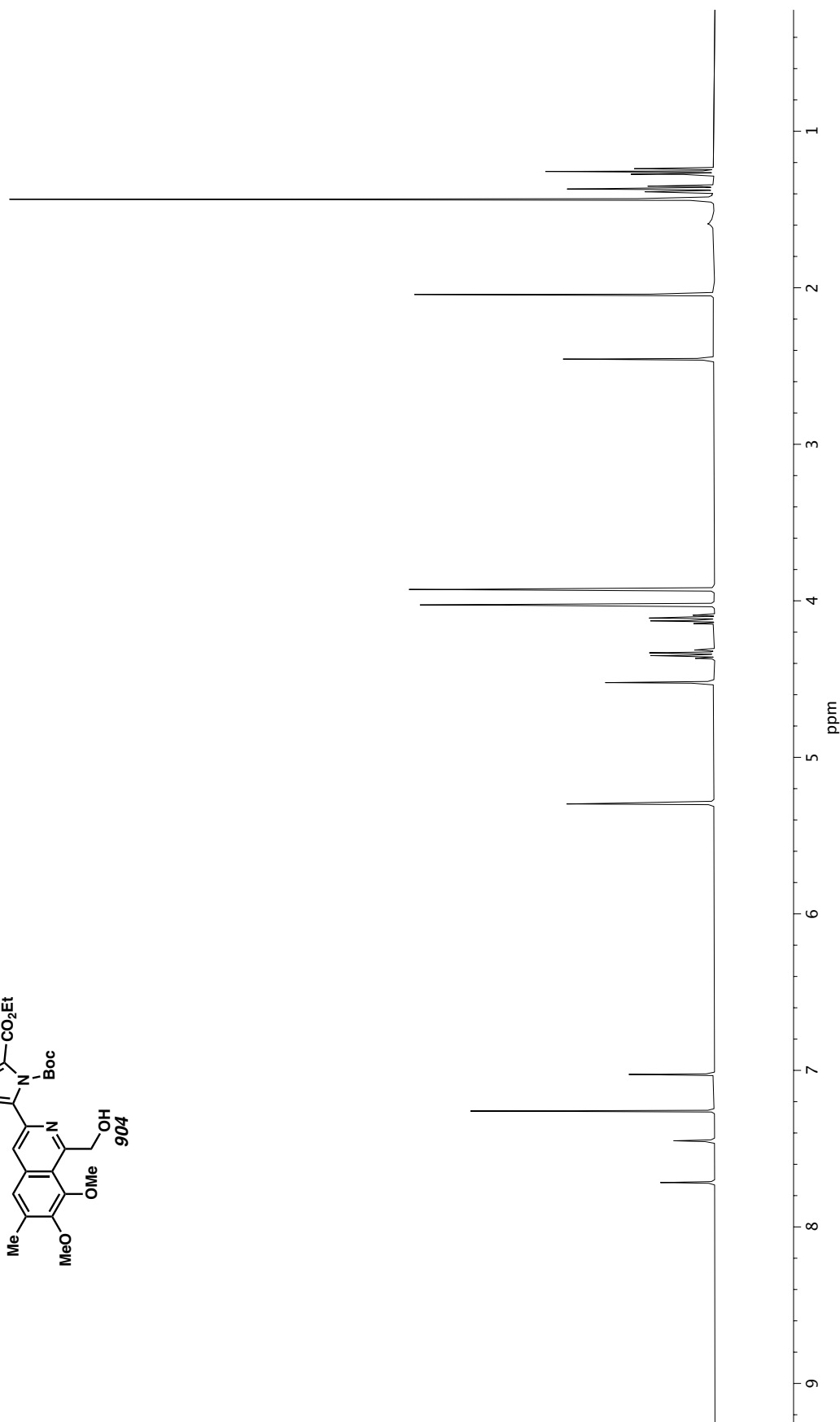
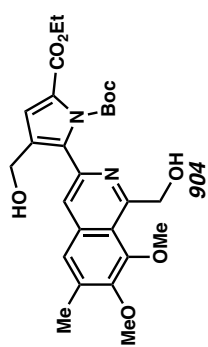
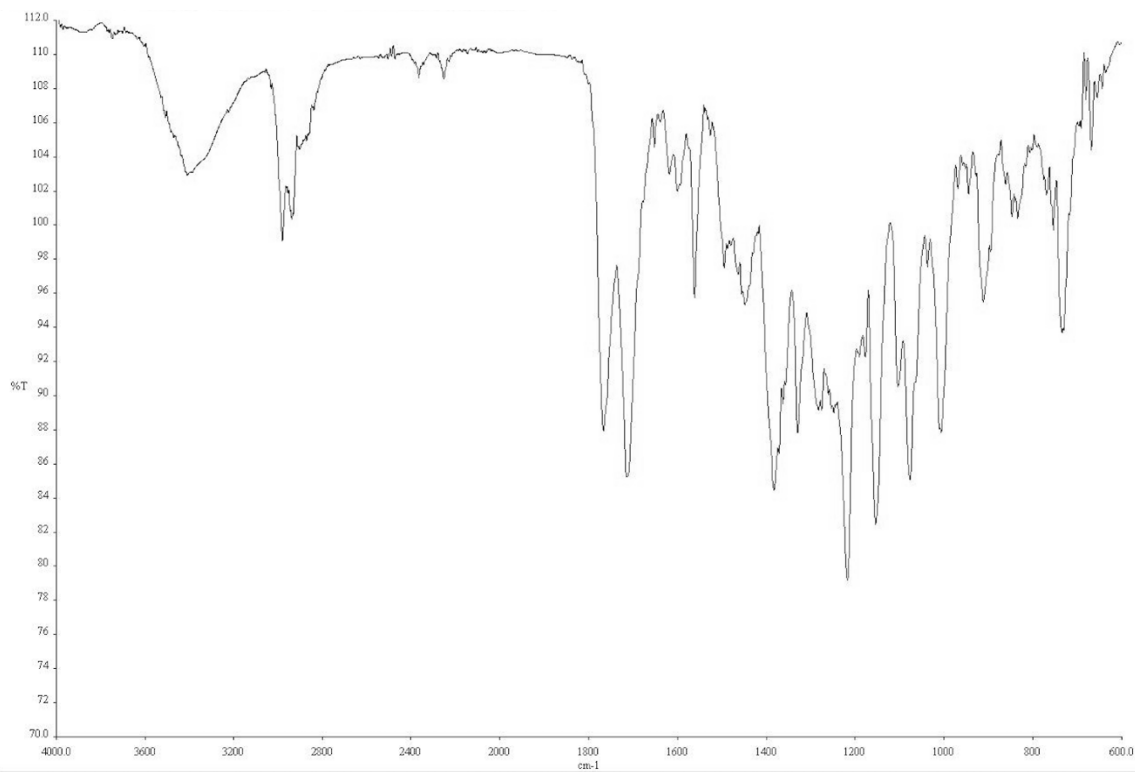
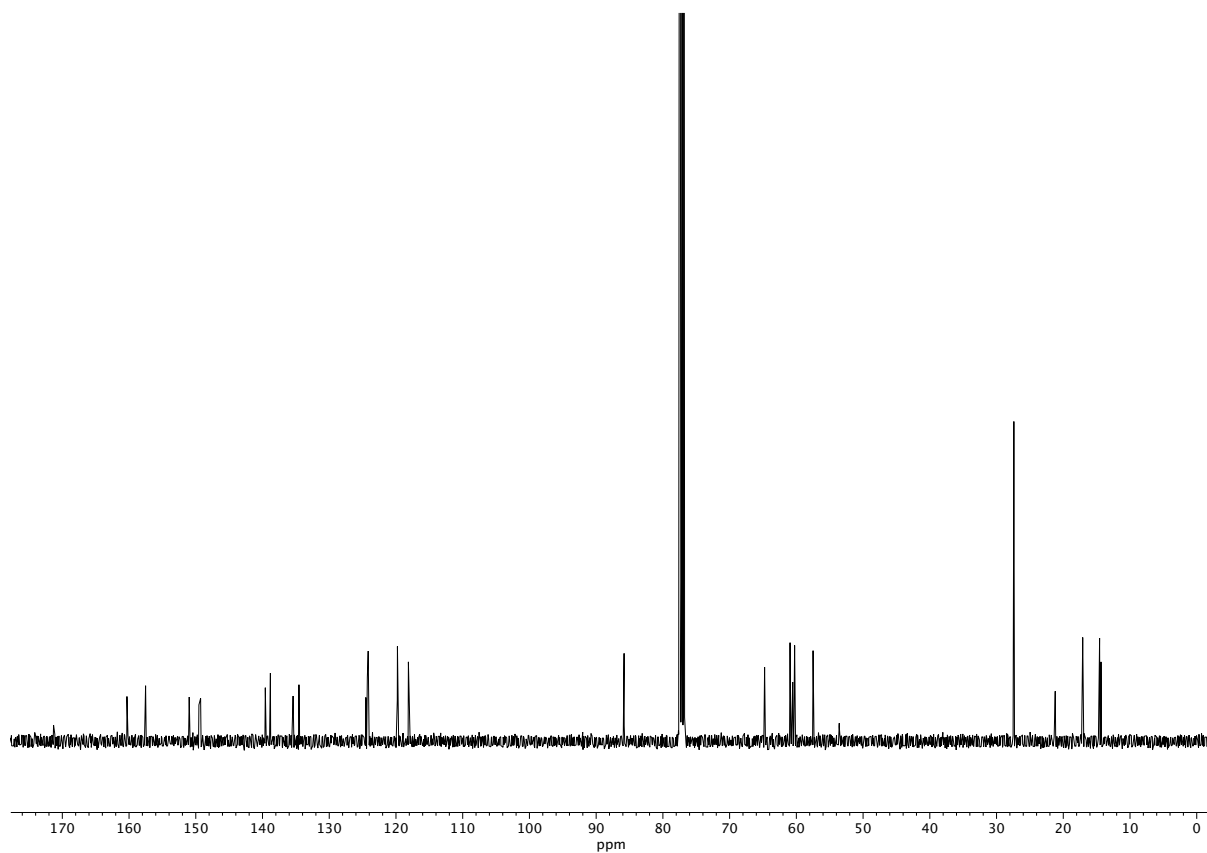


Figure A6.25 <sup>1</sup>H NMR (400 MHz, CDCl<sub>3</sub>) of compound 904.

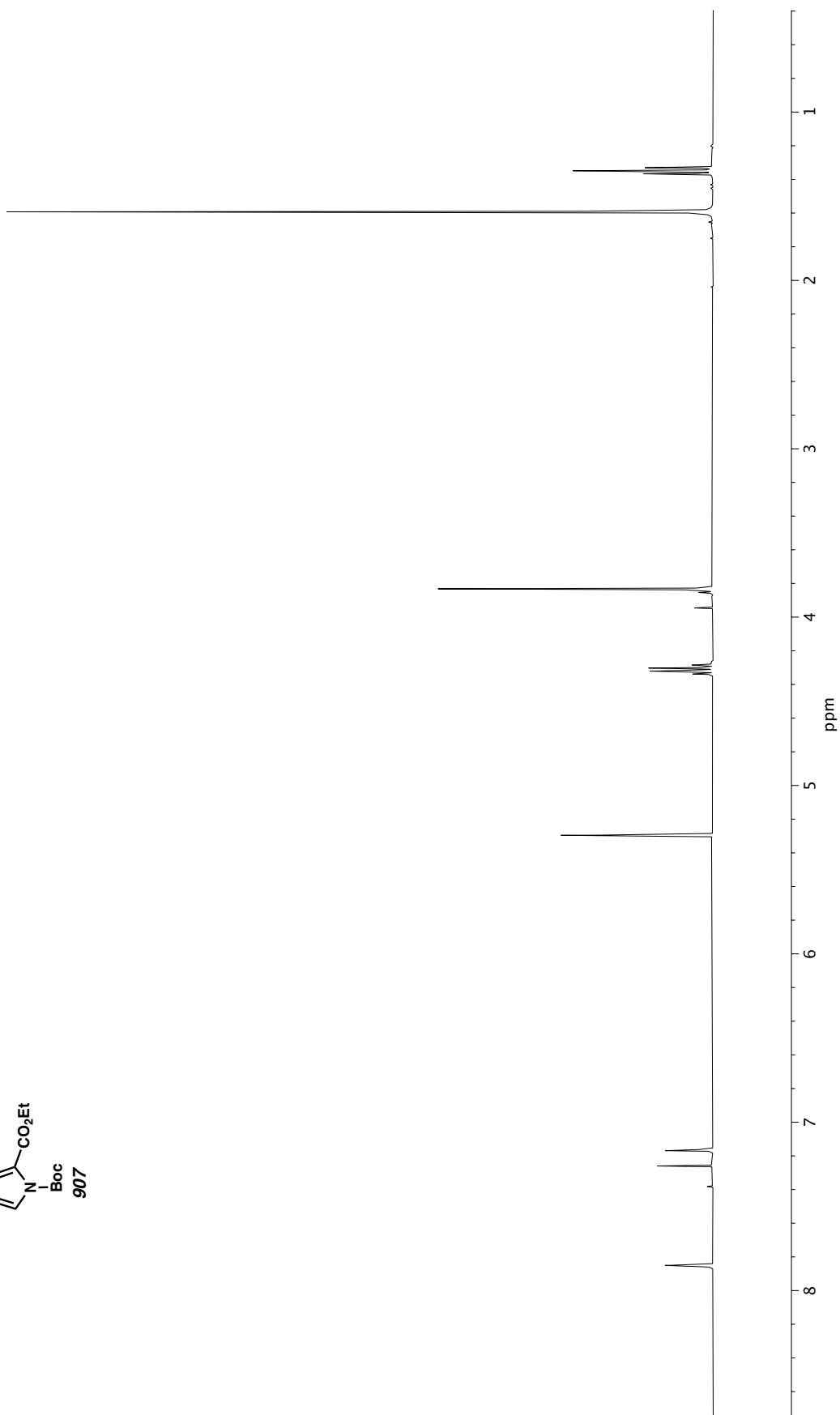
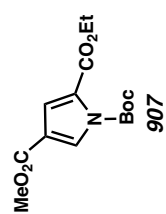


**Figure A6.26** Infrared spectrum (Thin Film, NaCl) of compound **904**.

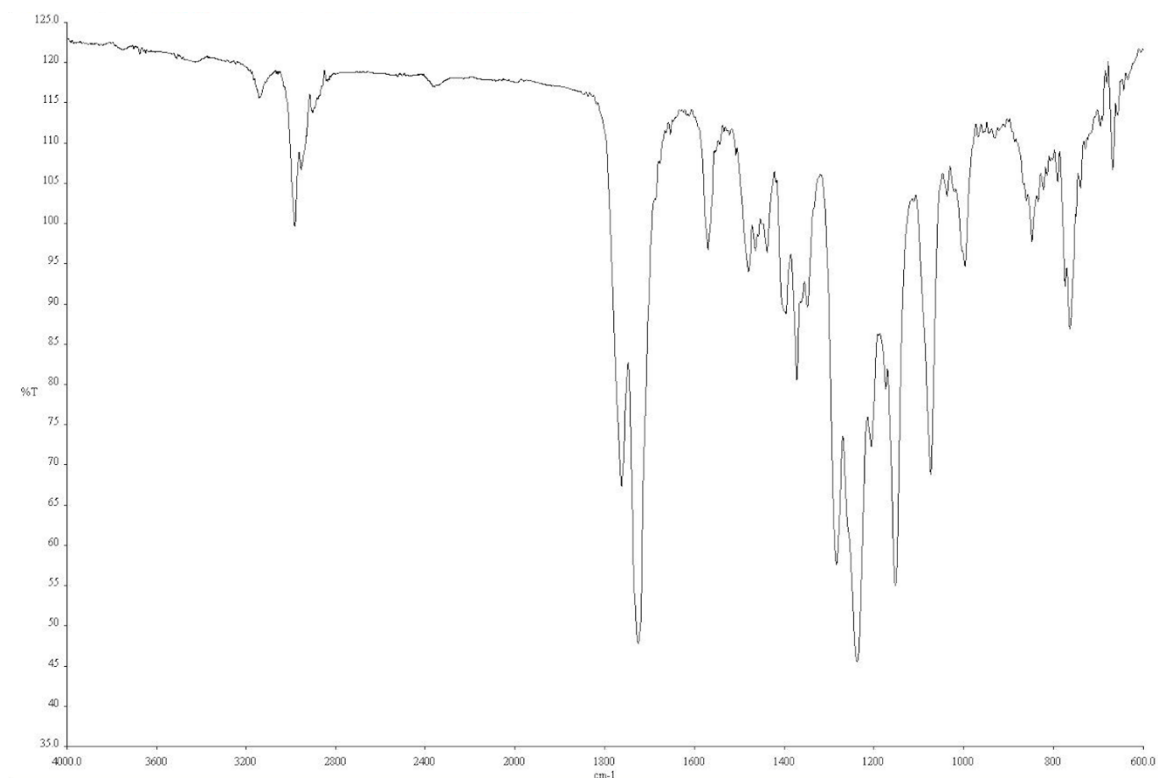


**Figure A6.27** <sup>13</sup>C NMR (100 MHz, CDCl<sub>3</sub>) of compound **904**.

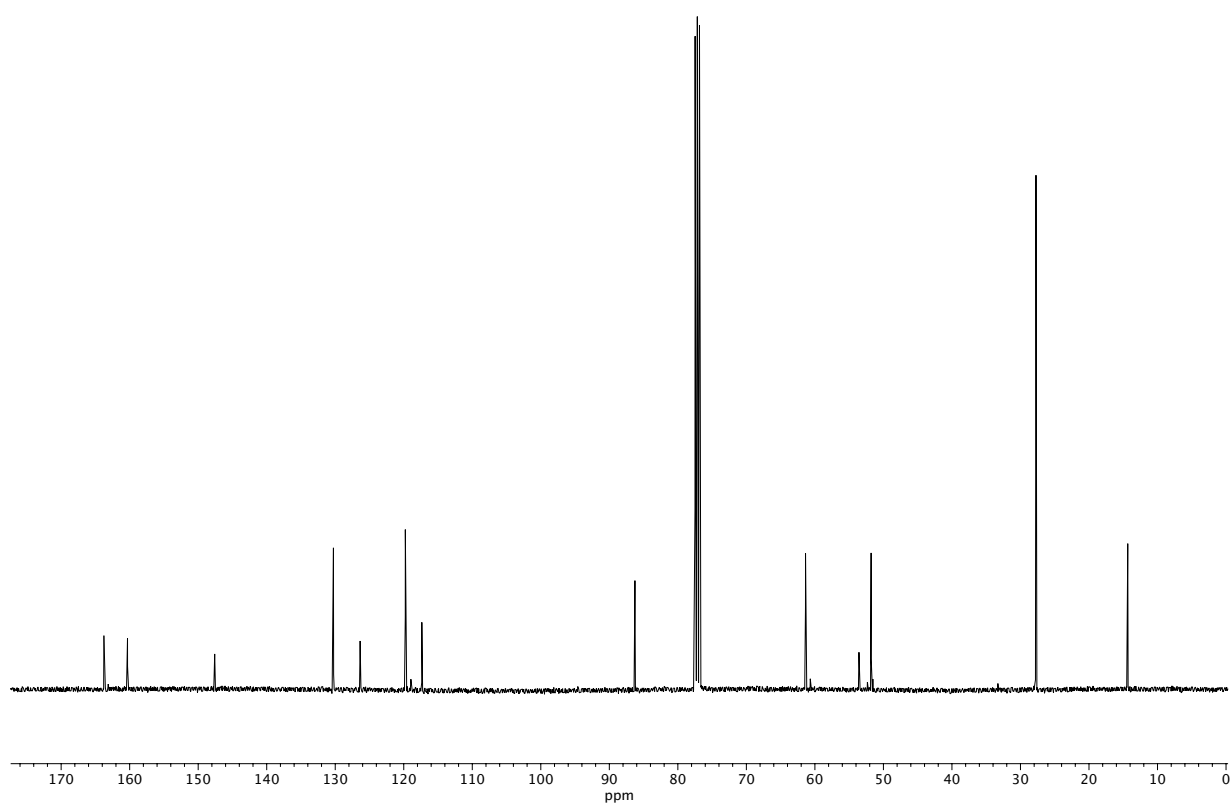




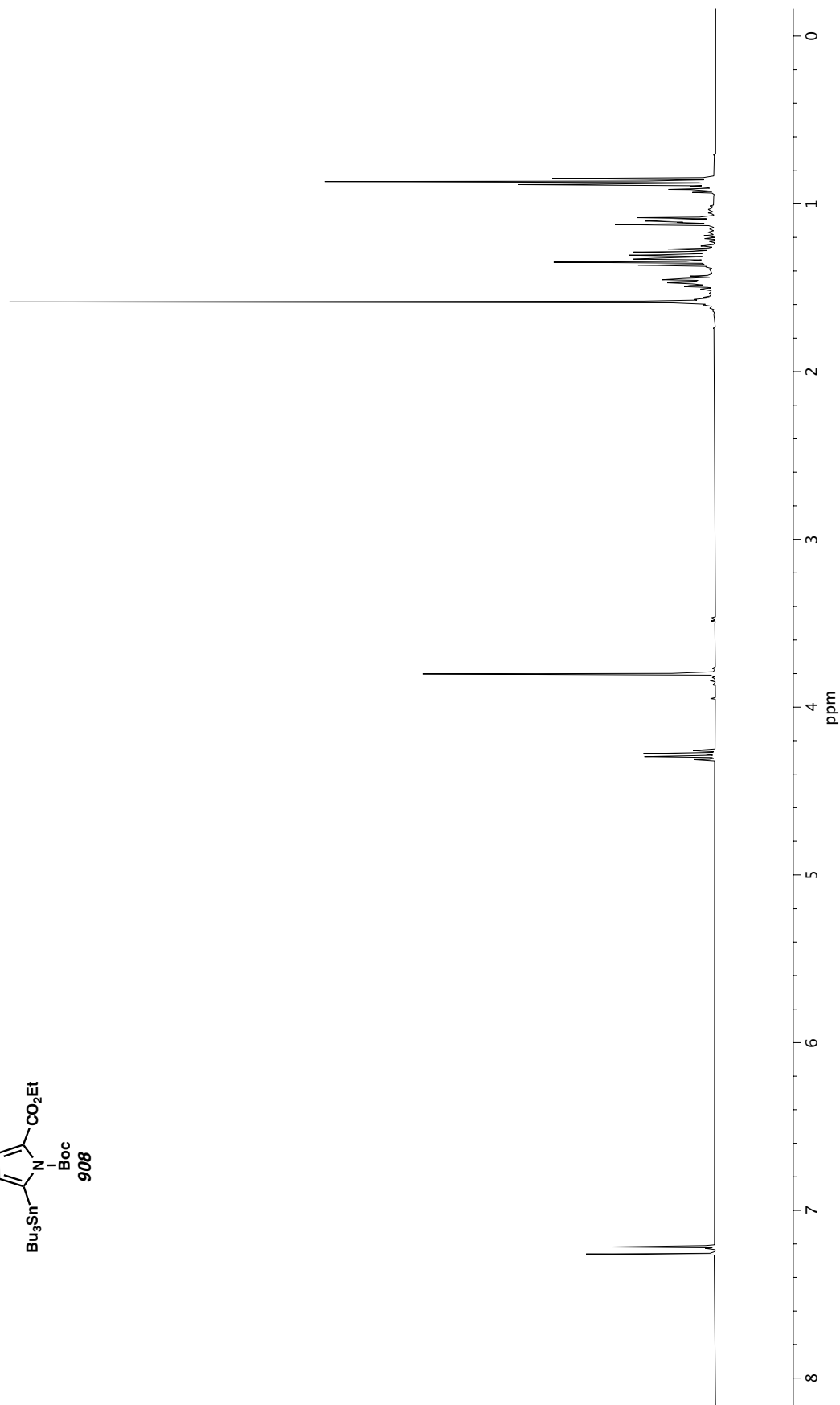
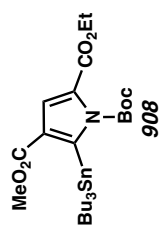
**Figure A6.28**  $^1\text{H}$  NMR (400 MHz,  $\text{CDCl}_3$ ) of compound **907**.



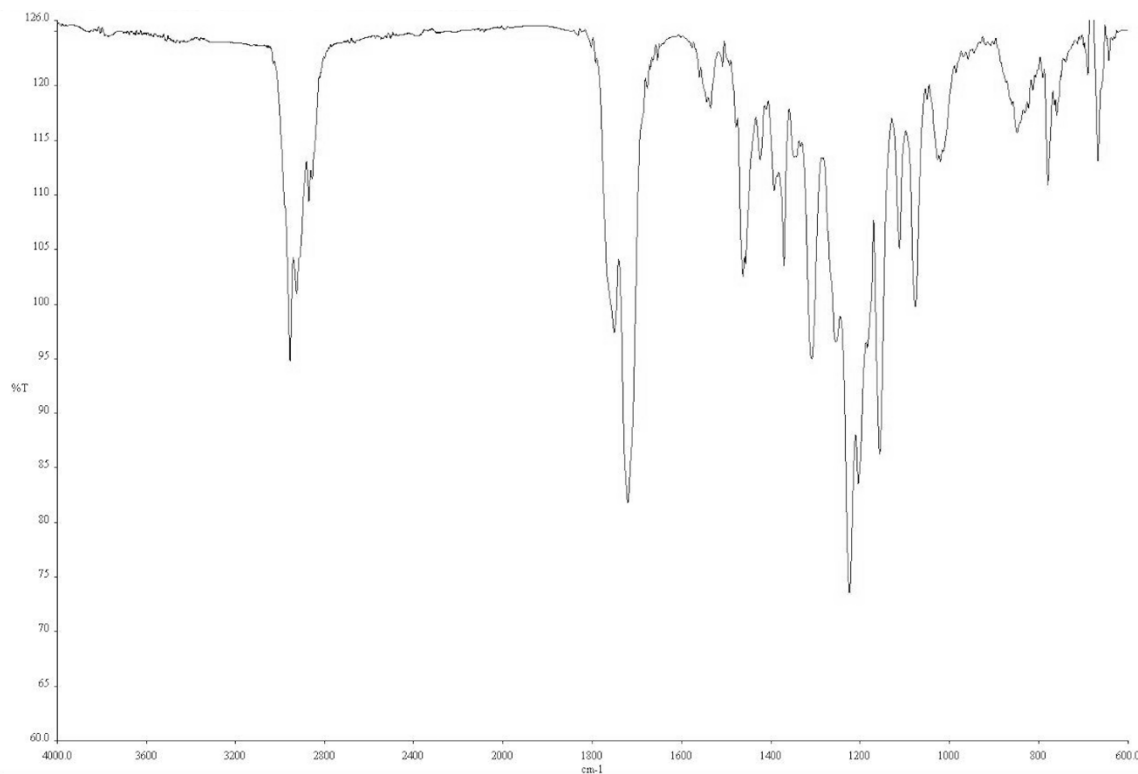
**Figure A6.29** Infrared spectrum (Thin Film, NaCl) of compound **907**.



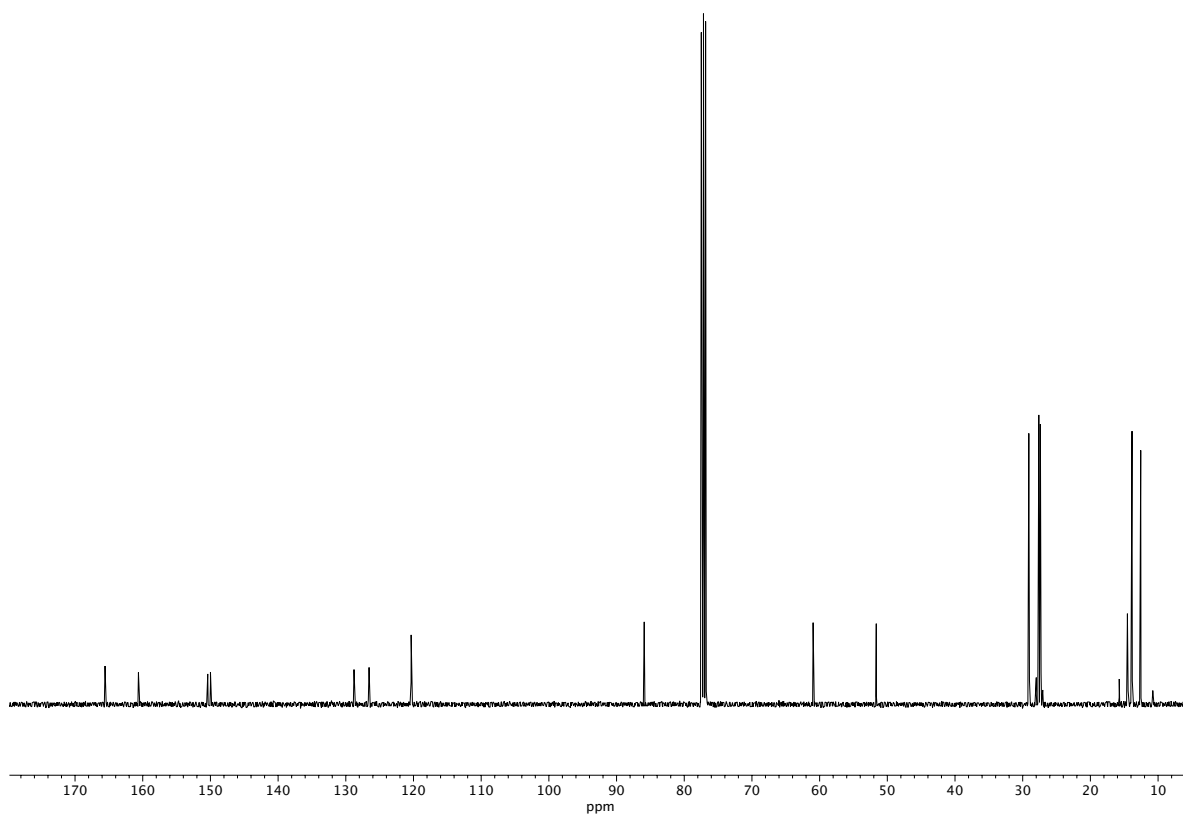
**Figure A6.30** <sup>13</sup>C NMR (100 MHz, CDCl<sub>3</sub>) of compound **907**.



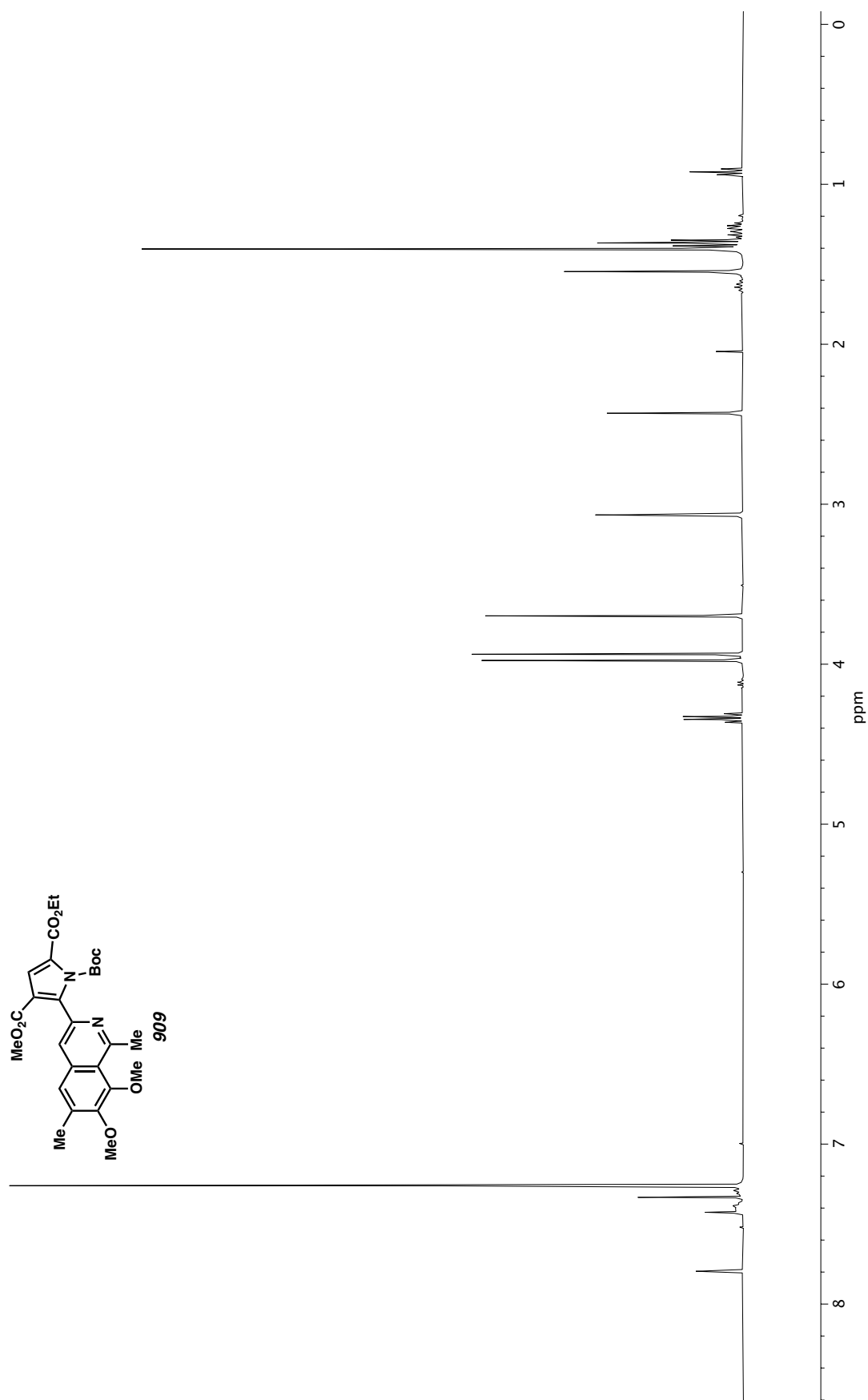
**Figure A6.31**  $^1\text{H}$  NMR (400 MHz,  $\text{CDCl}_3$ ) of compound **908**.



**Figure A6.32** Infrared spectrum (Thin Film, NaCl) of compound **908**.



**Figure A6.33** <sup>13</sup>C NMR (100 MHz, CDCl<sub>3</sub>) of compound **908**.



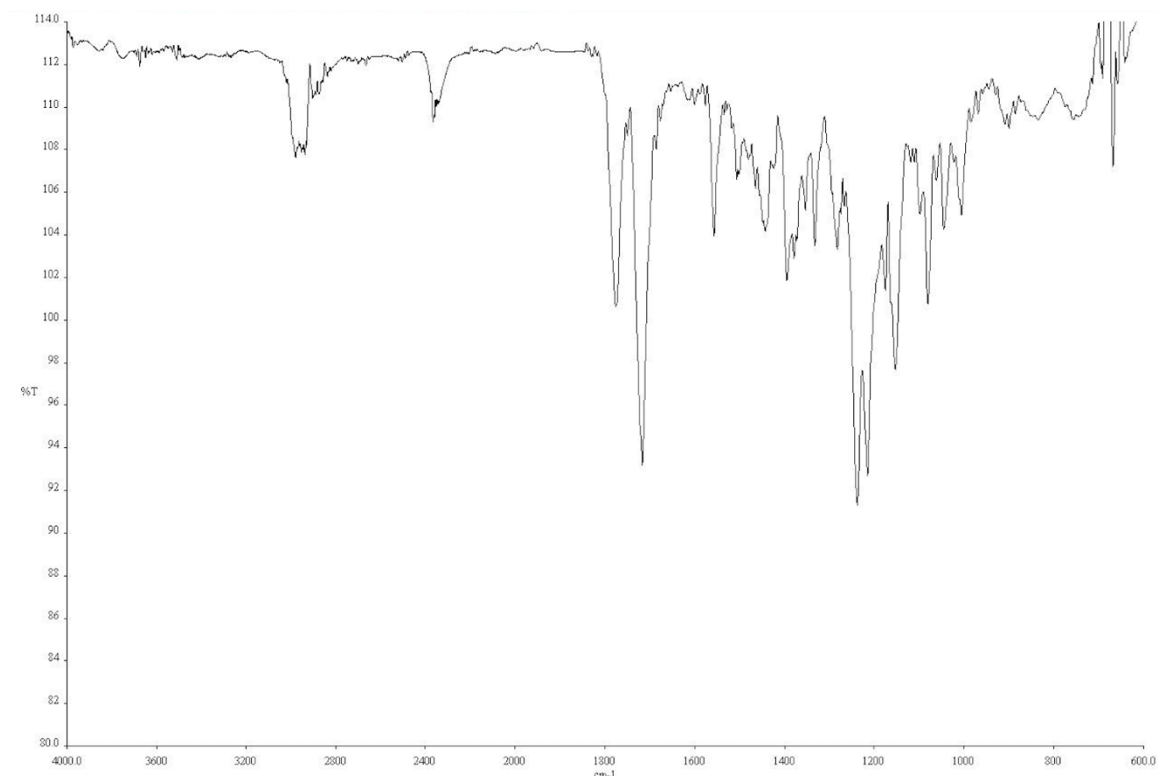


**Figure A6.35** Infrared spectrum (Thin Film, NaCl) of compound **909**.

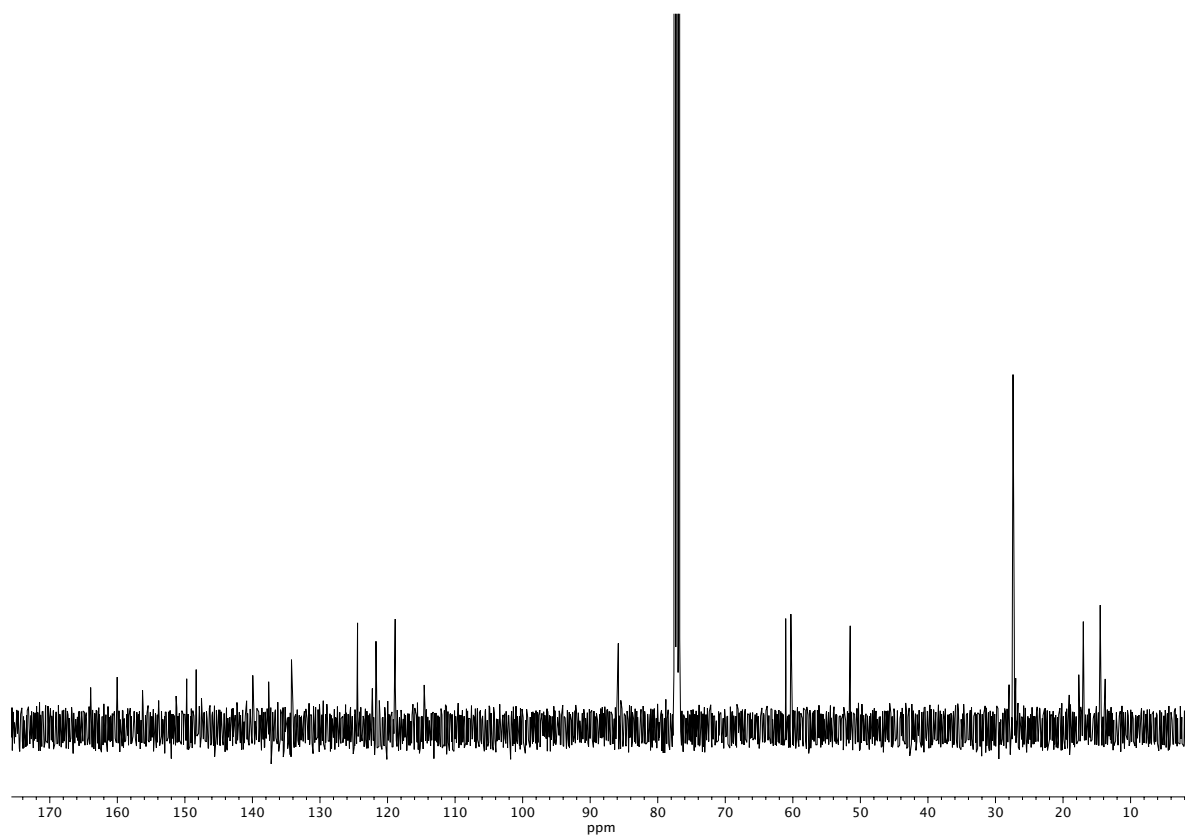


**Figure A6.36** <sup>13</sup>C NMR (100 MHz, CDCl<sub>3</sub>) of compound **909**.

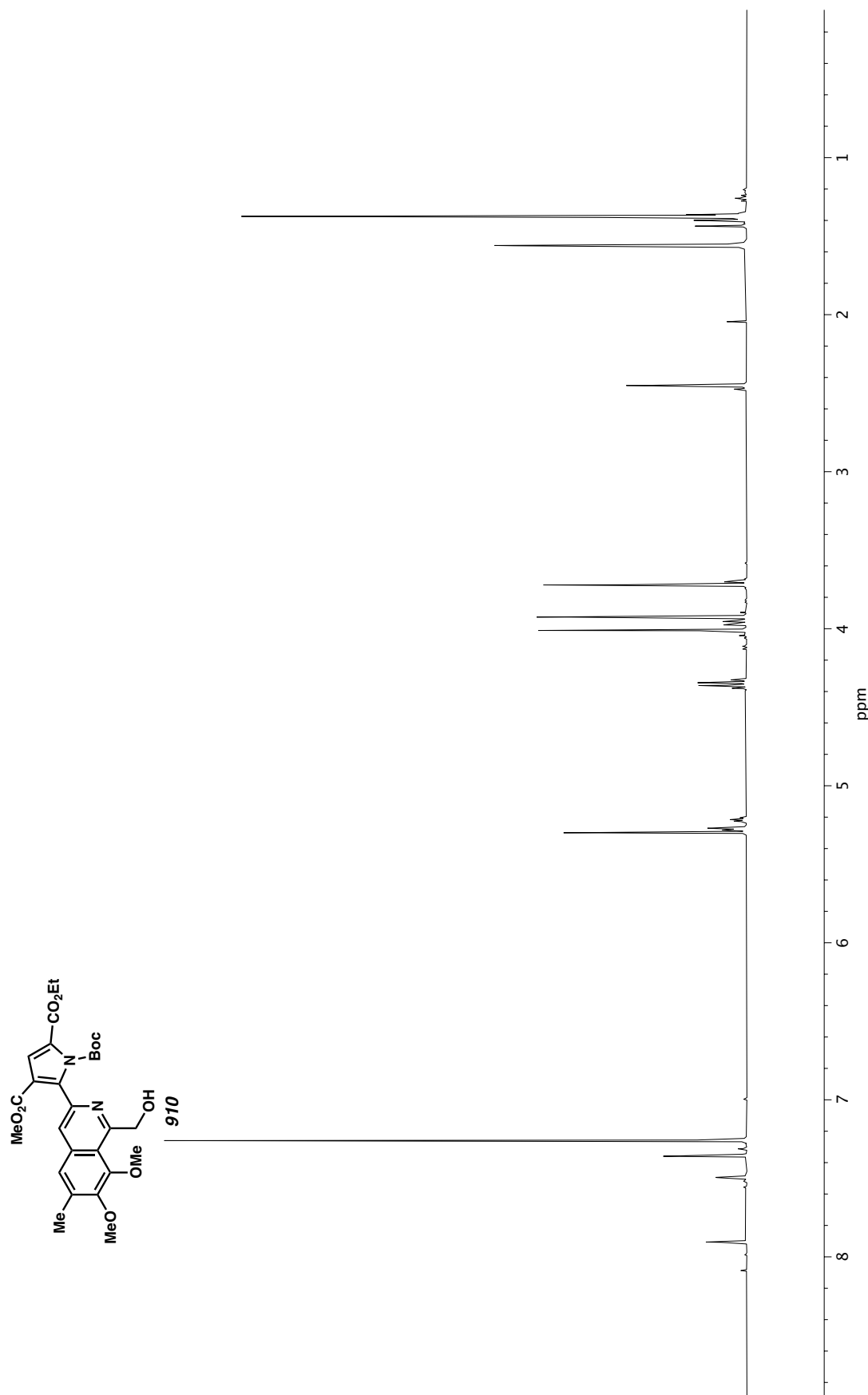


**Figure A6.37** <sup>1</sup>H NMR (400 MHz, CDCl<sub>3</sub>) of compound **910**.

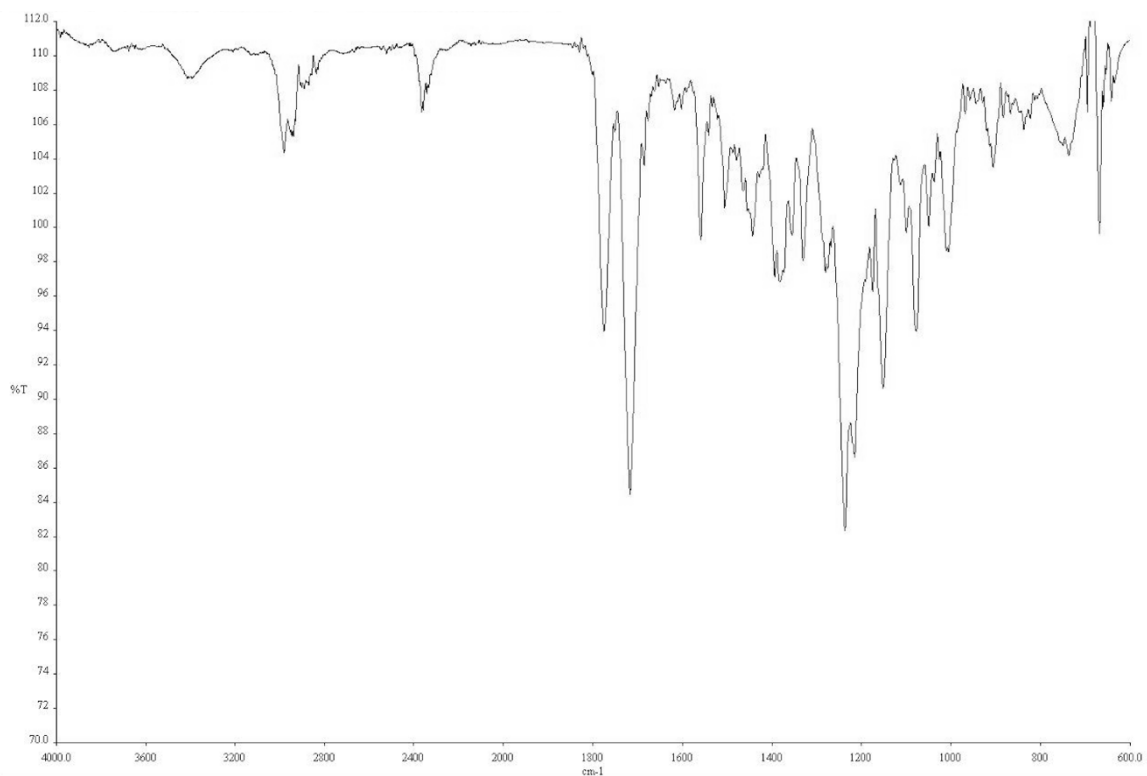


**Figure A6.38** Infrared spectrum (Thin Film, NaCl) of compound **910**.

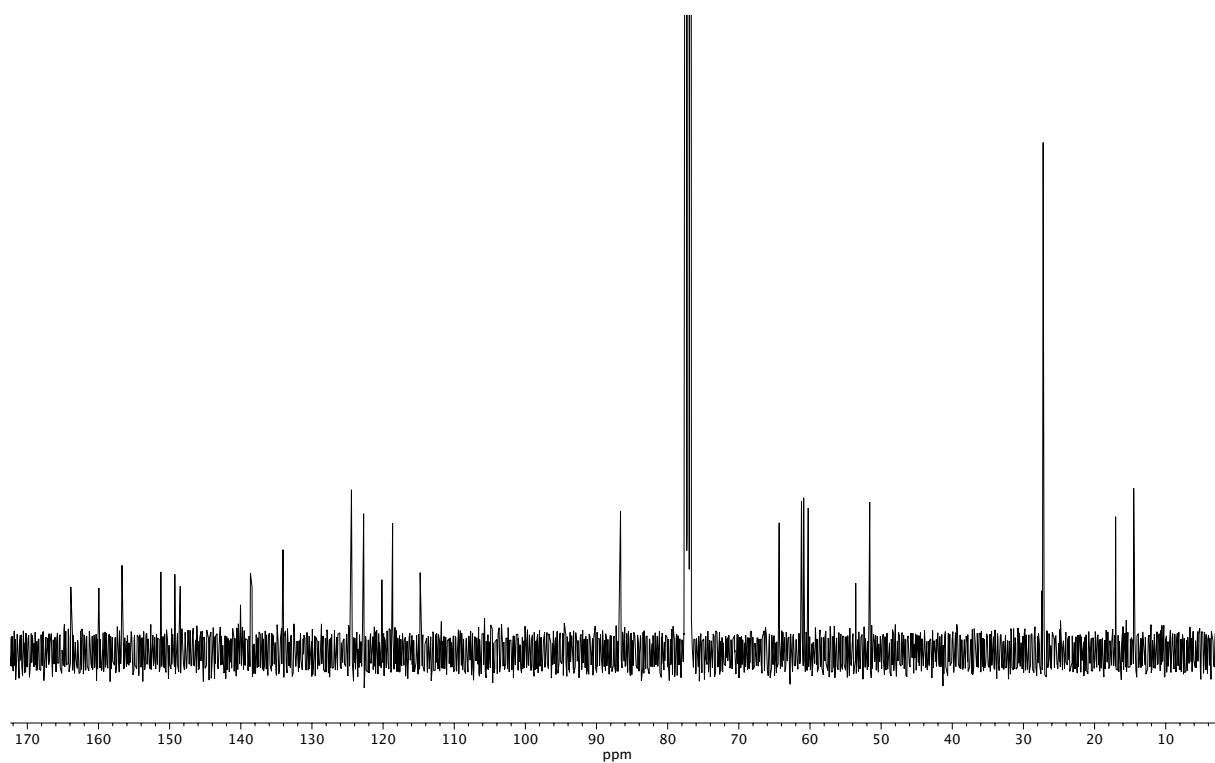


**Figure A6.39**  $^{13}\text{C}$  NMR (100 MHz,  $\text{CDCl}_3$ ) of compound **910**.



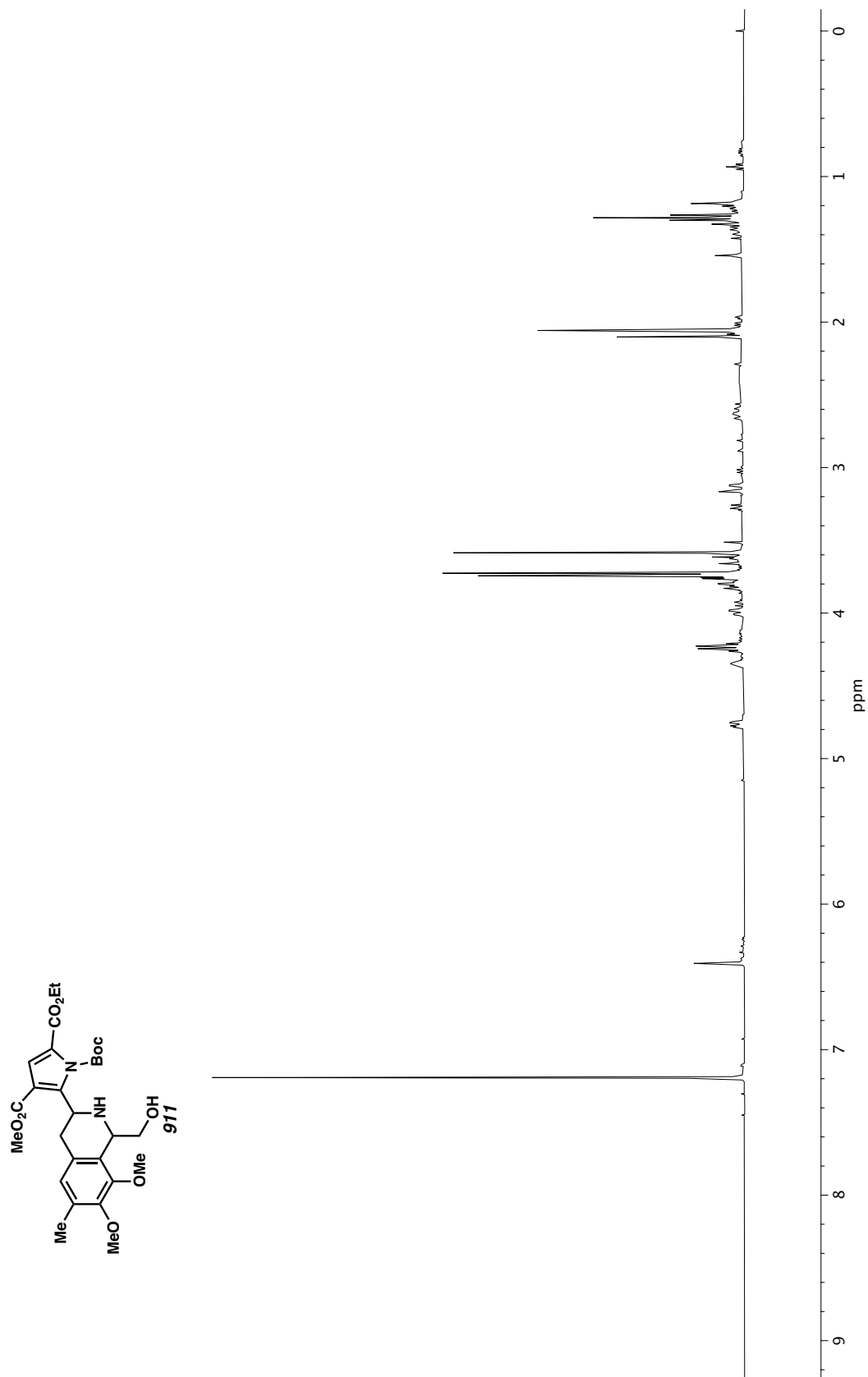


**Figure A6.40**  $^1\text{H}$  NMR (400 MHz,  $\text{CDCl}_3$ ) of compound **911**.

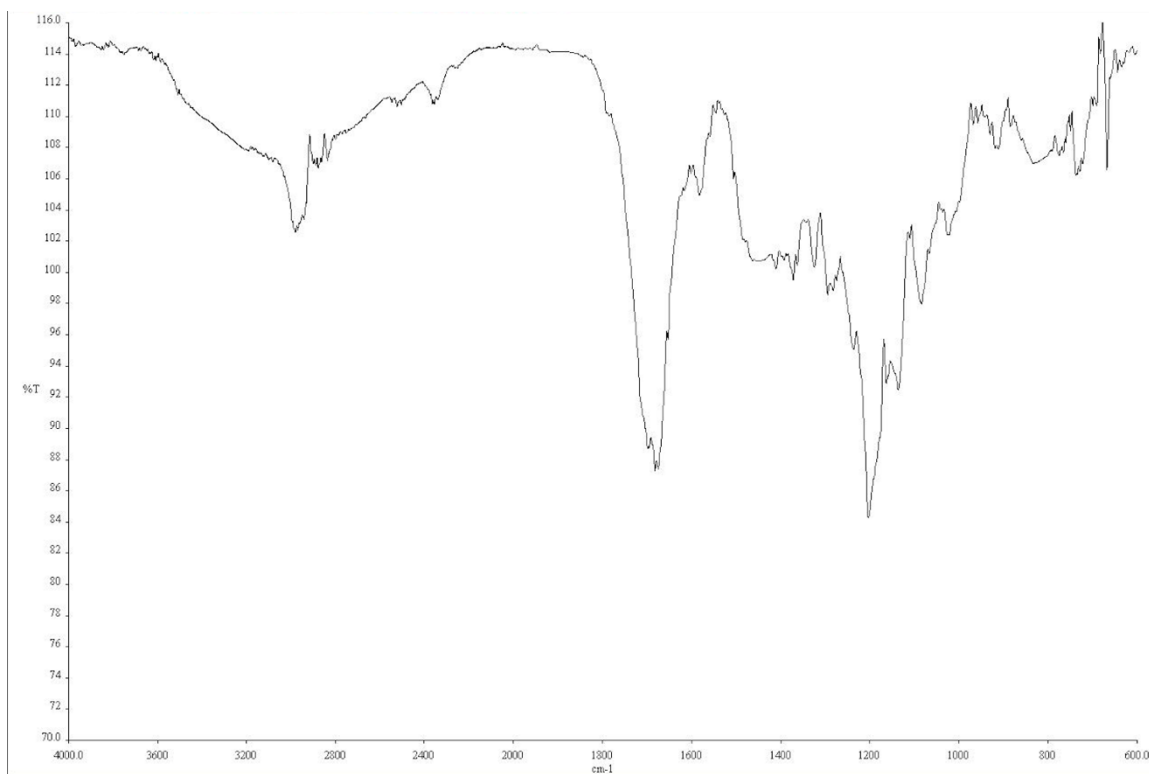


**Figure A6.41** Infrared spectrum (Thin Film, NaCl) of compound **911**.

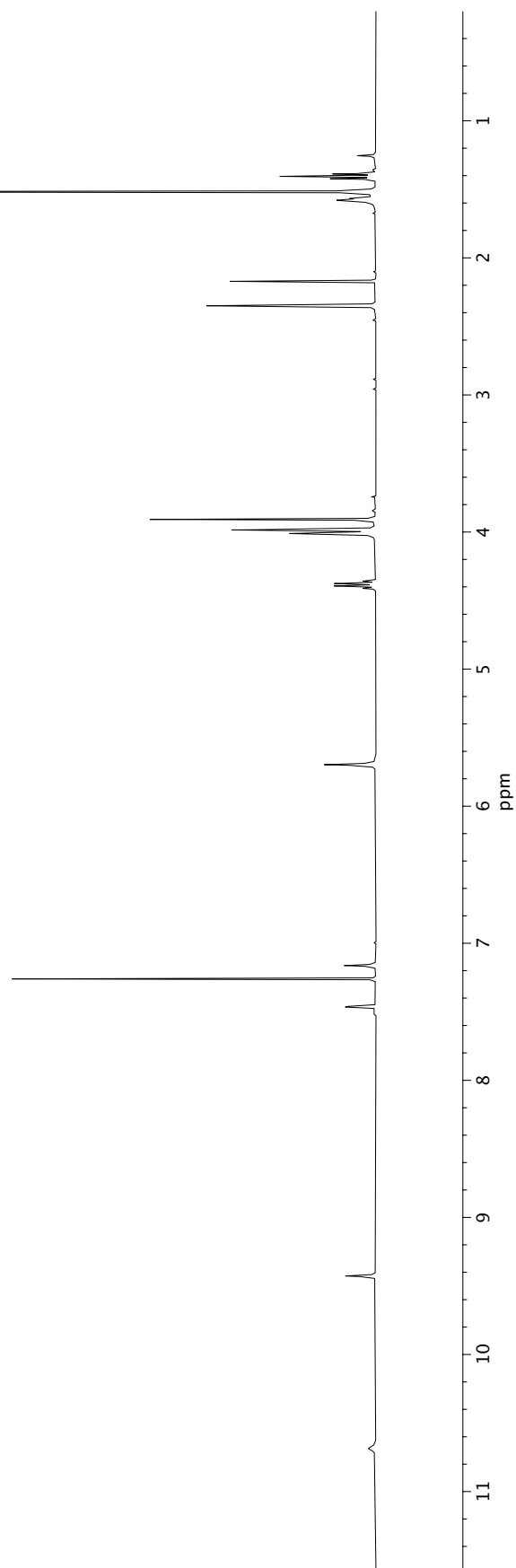
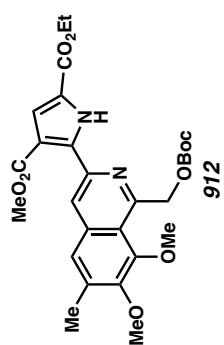
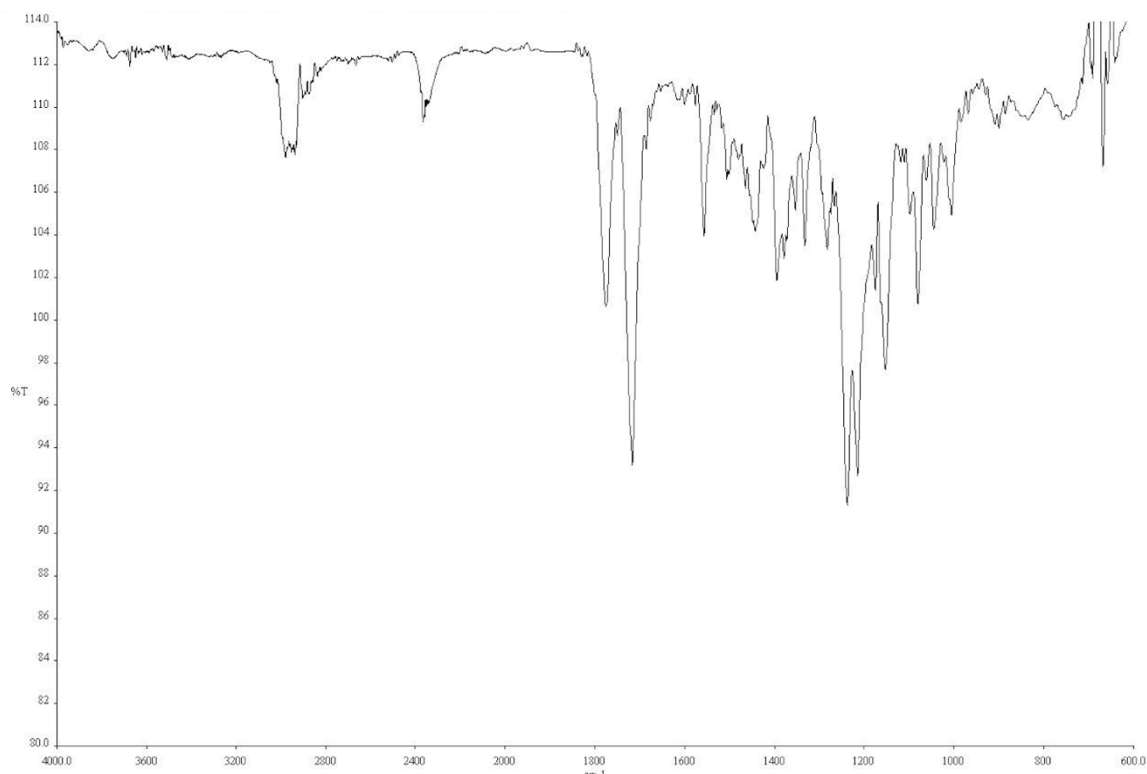
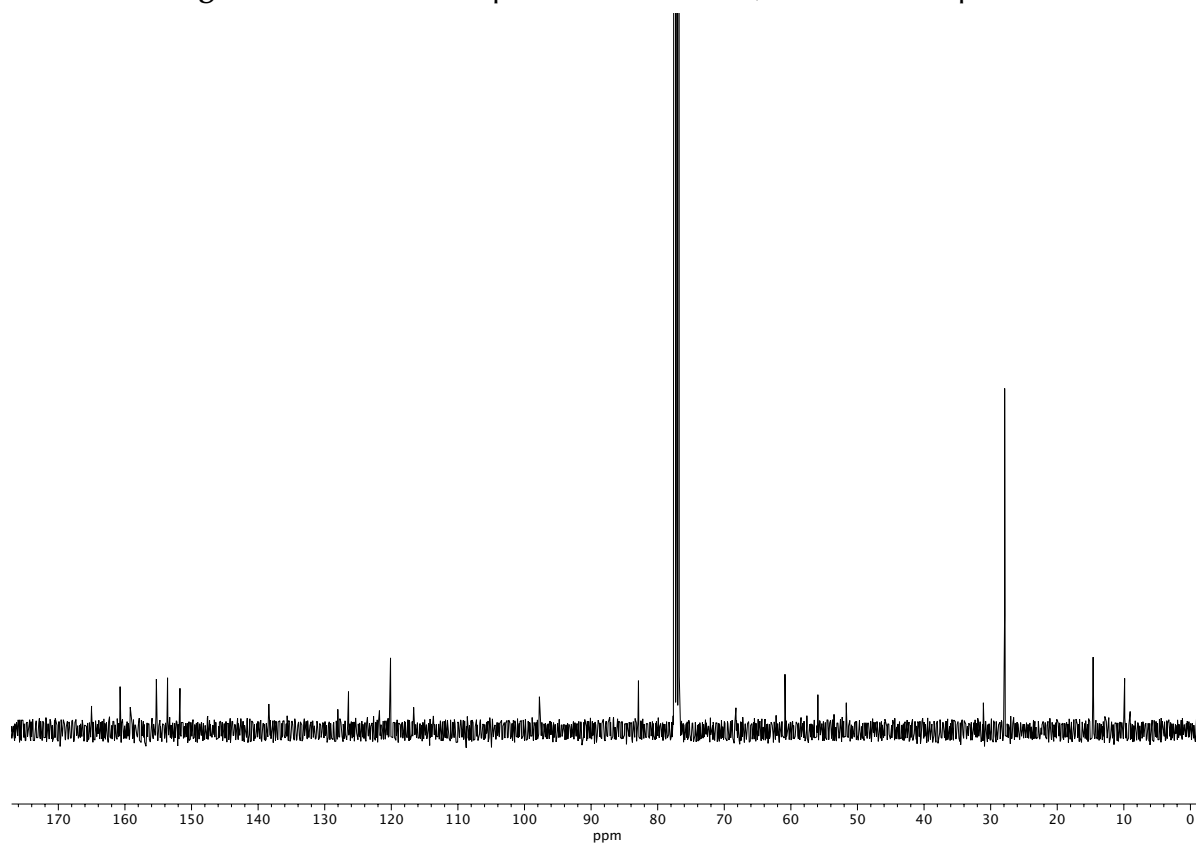


Figure A6.42 <sup>1</sup>H NMR (400 MHz, CDCl<sub>3</sub>) of compound 912.



**Figure A6.43** Infrared spectrum (Thin Film, NaCl) of compound **912**.



**Figure A6.44** <sup>13</sup>C NMR (100 MHz, CDCl<sub>3</sub>) of compound **912**.

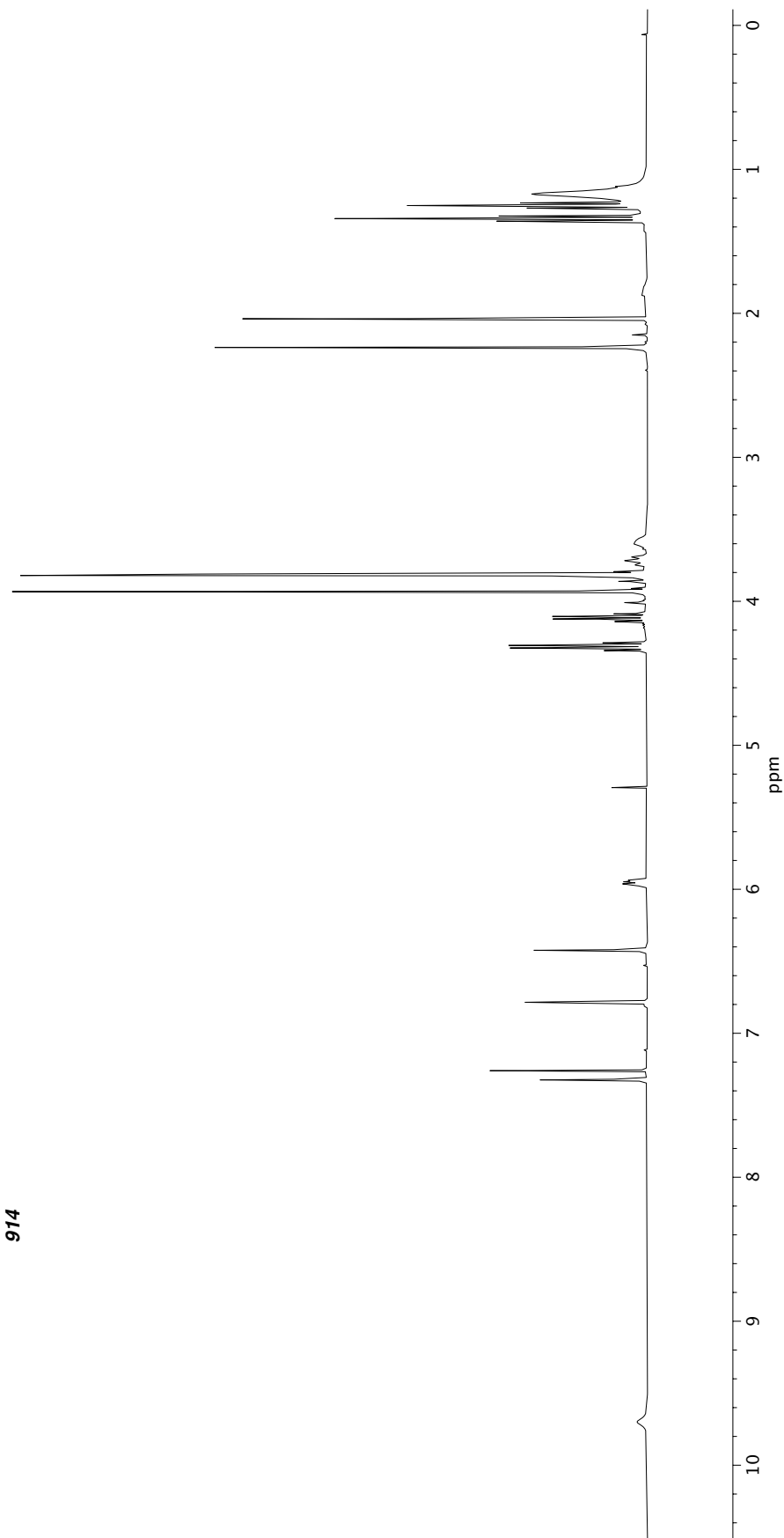
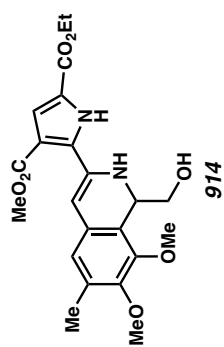
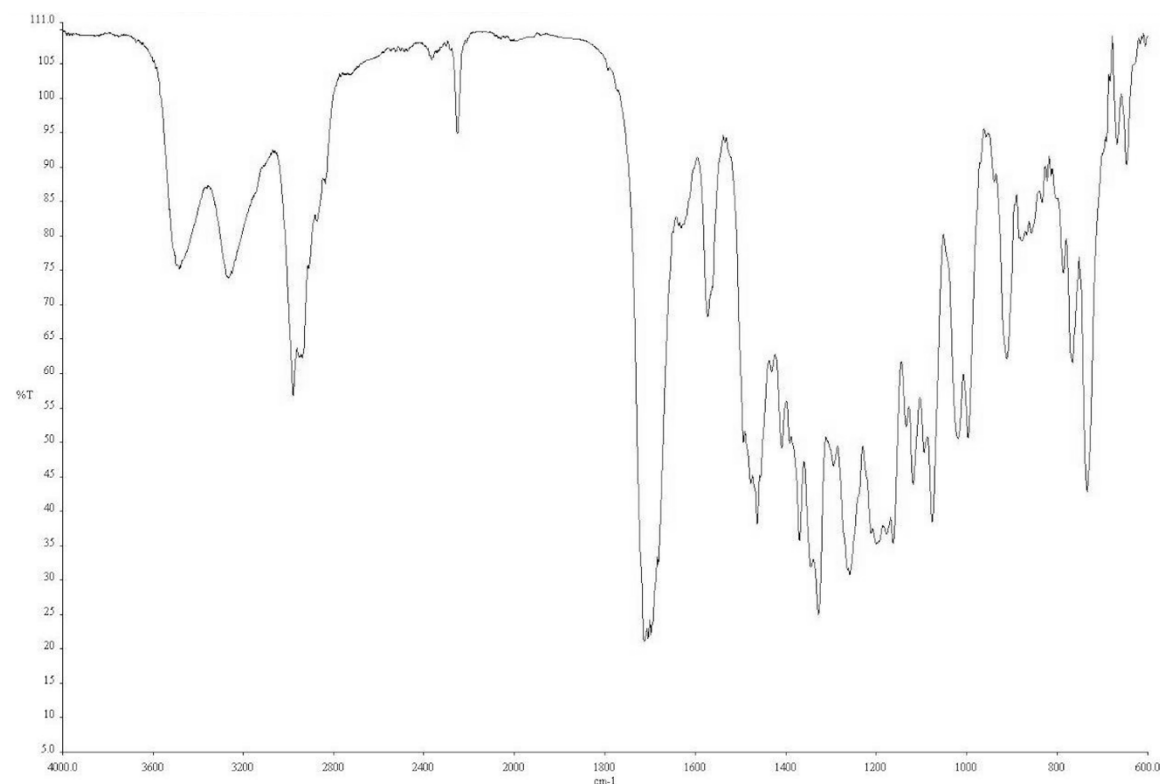
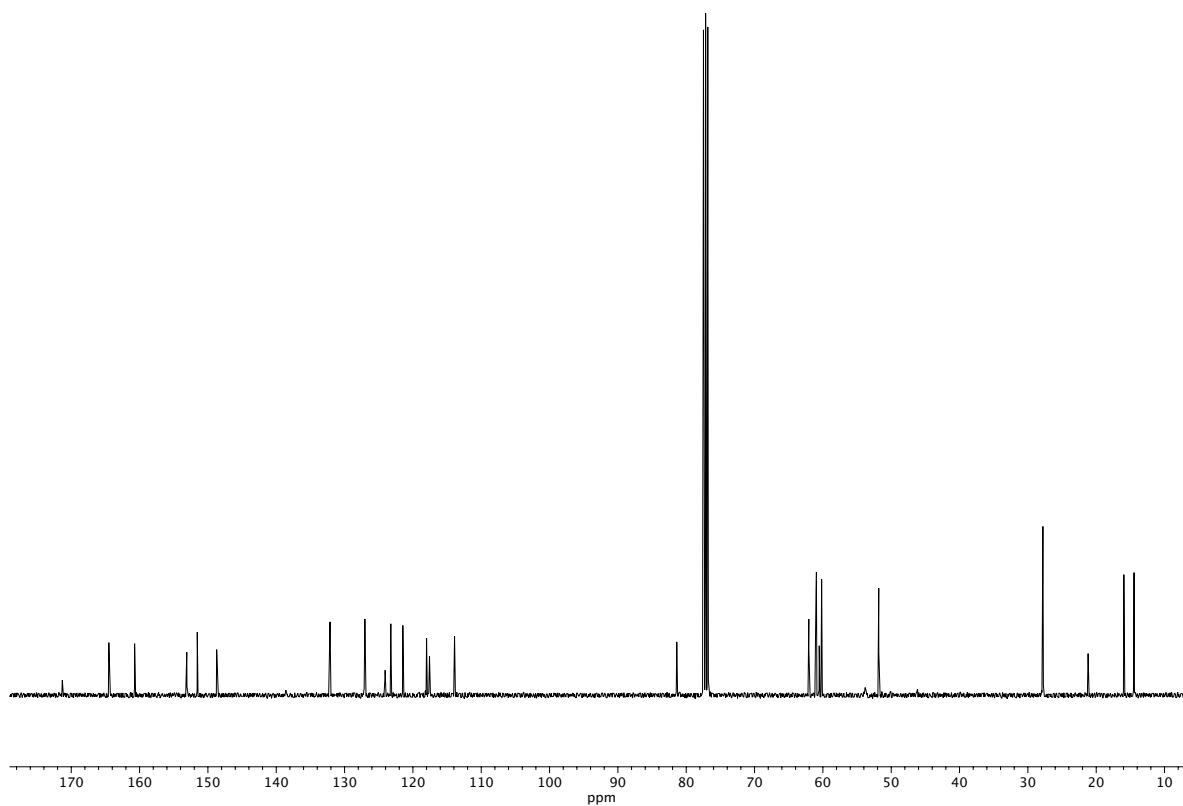


Figure A6.45 <sup>1</sup>H NMR (400 MHz, CDCl<sub>3</sub>) of compound 914.



**Figure A6.46** Infrared spectrum (Thin Film, NaCl) of compound **914**.



**Figure A6.47** <sup>13</sup>C NMR (100 MHz, CDCl<sub>3</sub>) of compound **914**.

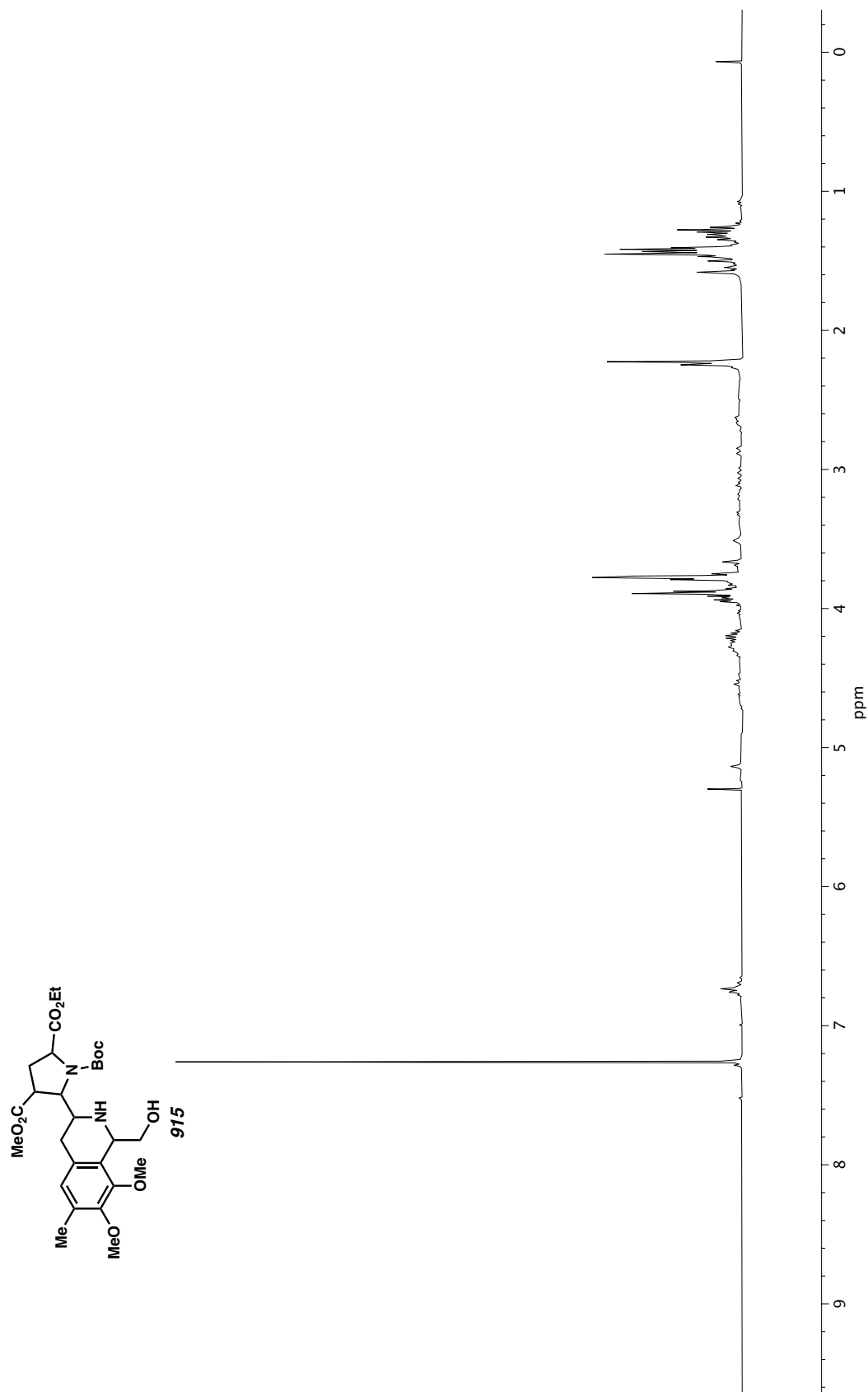


**Figure A6.48**  $^1\text{H}$  NMR (400 MHz,  $\text{CDCl}_3$ ) of compound **915**.

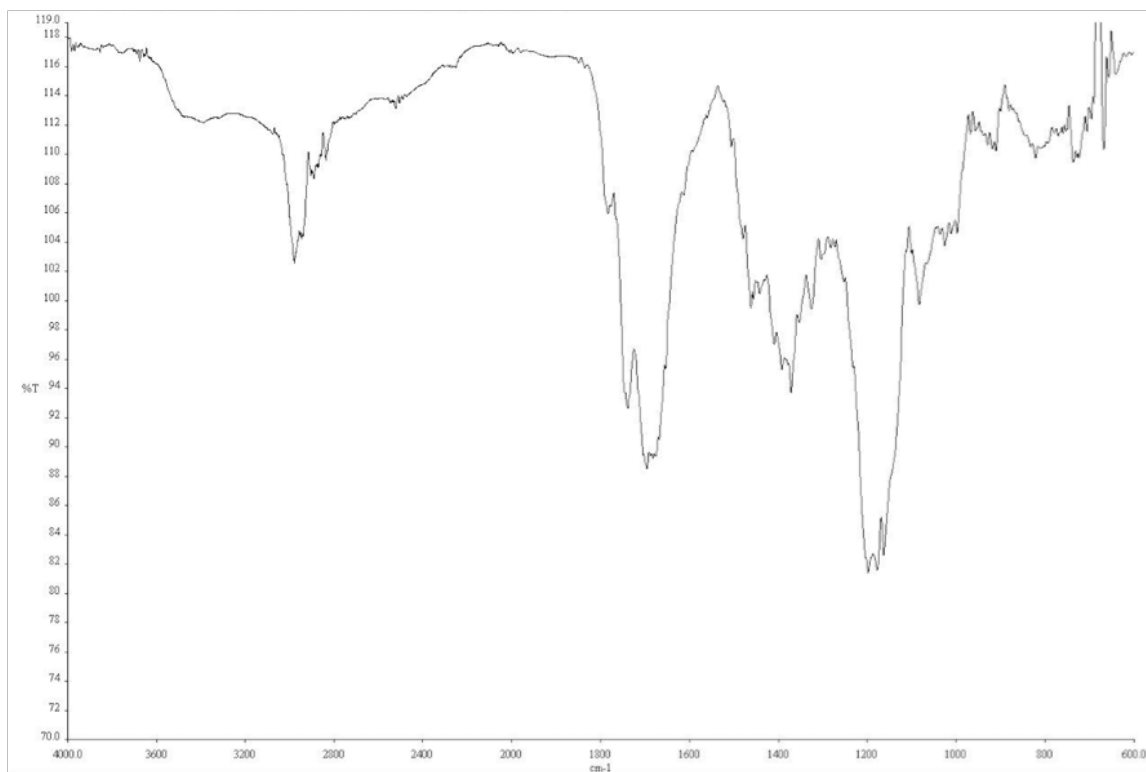


**Figure A6.49** Infrared spectrum (Thin Film, NaCl) of compound **915**.

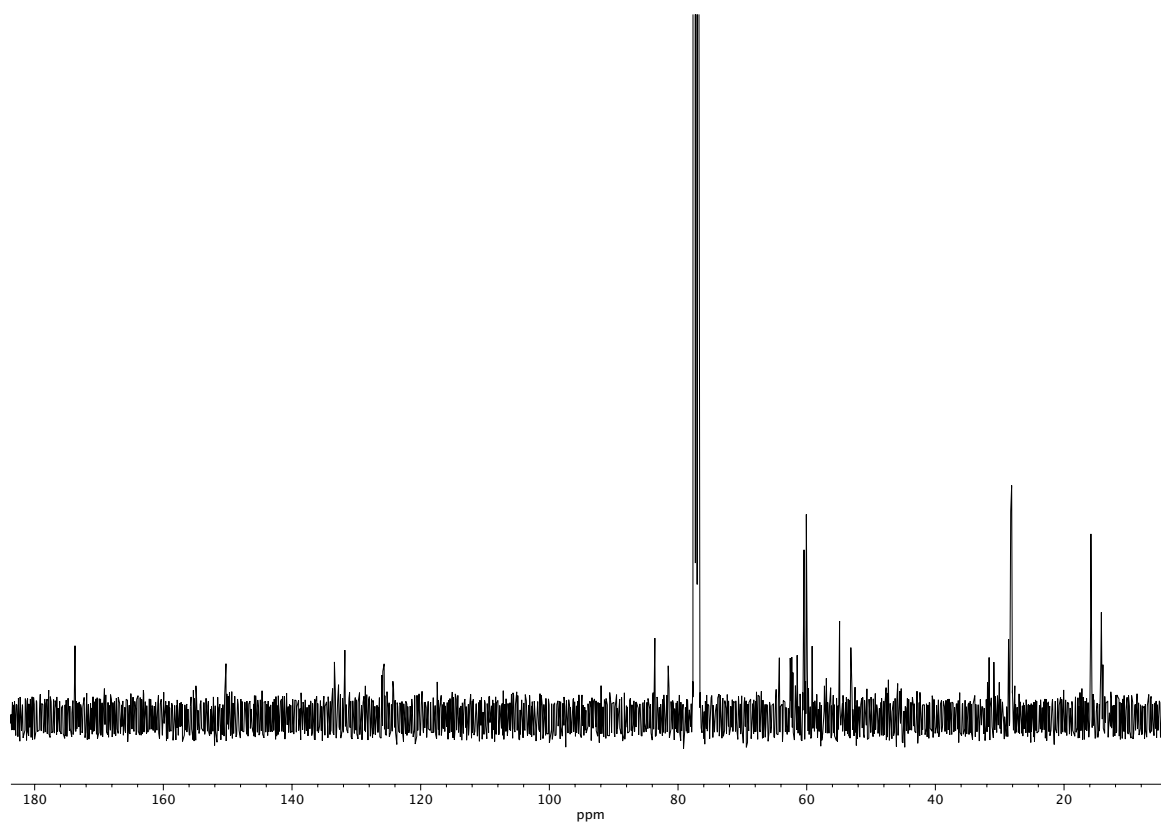


**Figure A6.50** <sup>13</sup>C NMR (100 MHz, CDCl<sub>3</sub>) of compound **915**.



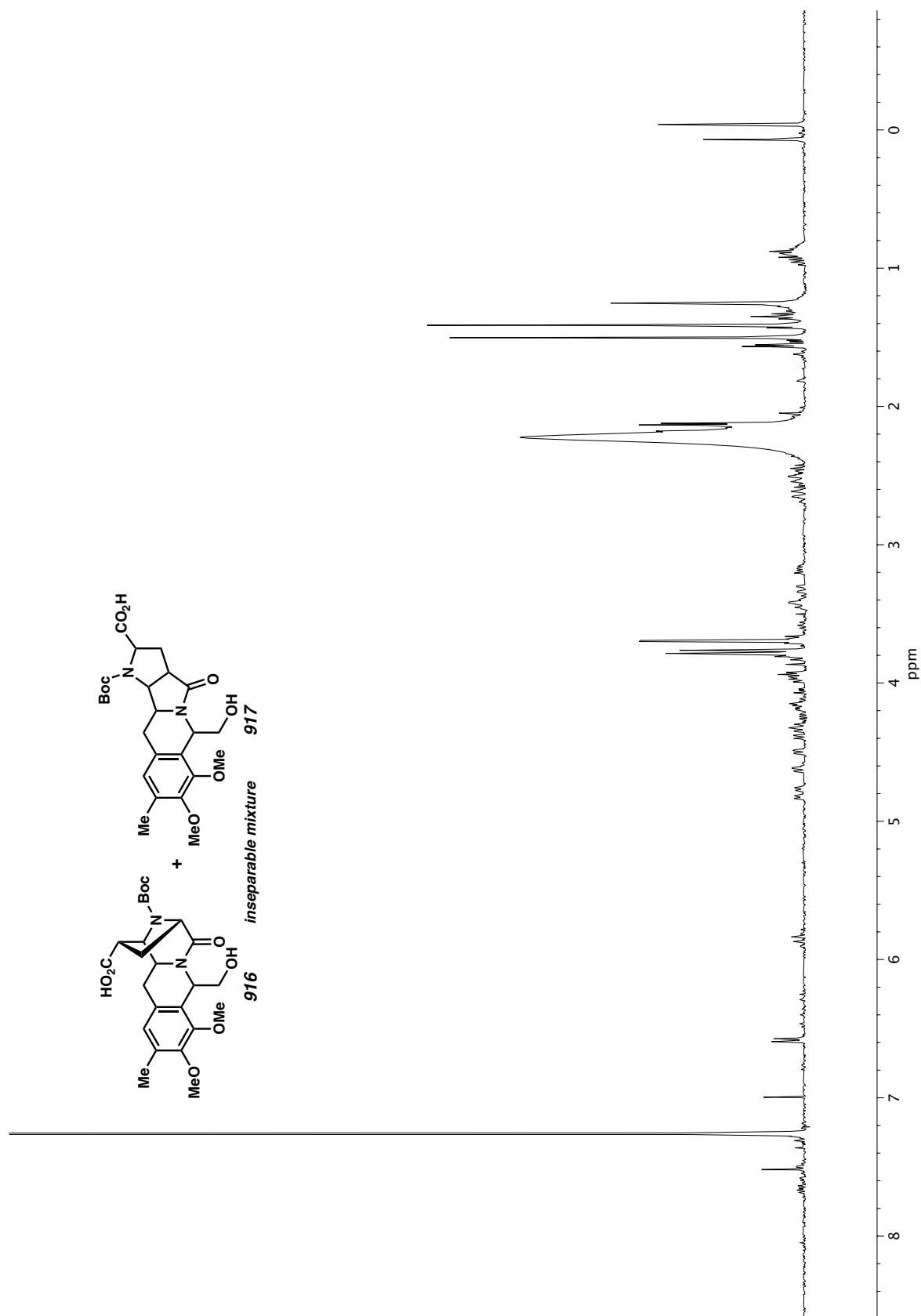


**Figure A6.51**  $^1\text{H}$  NMR (400 MHz,  $\text{CDCl}_3$ ) of compounds **916** + **917**.

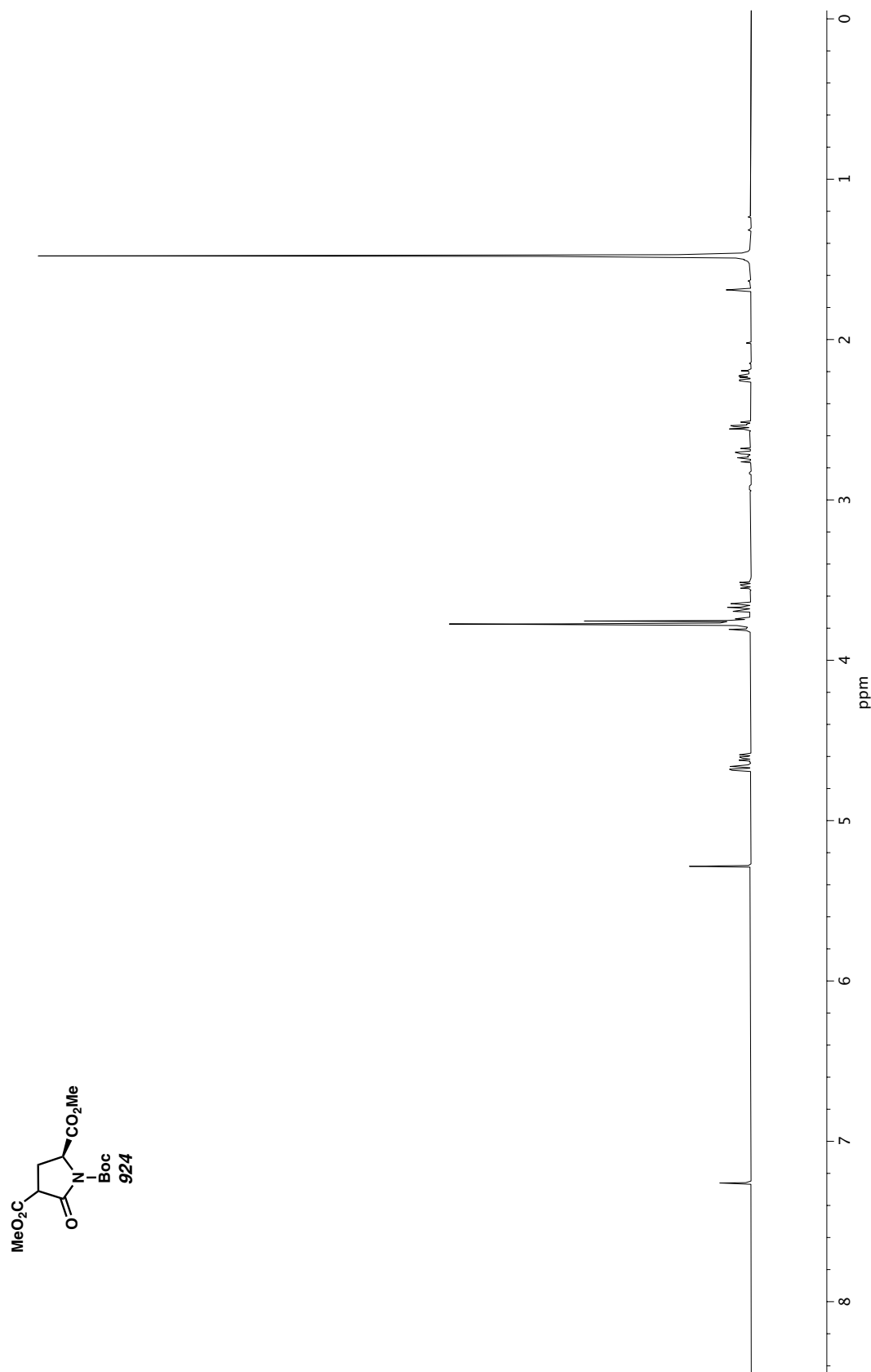


**Figure A6.52** <sup>1</sup>H NMR (400 MHz, CDCl<sub>3</sub>) of compound **924**.

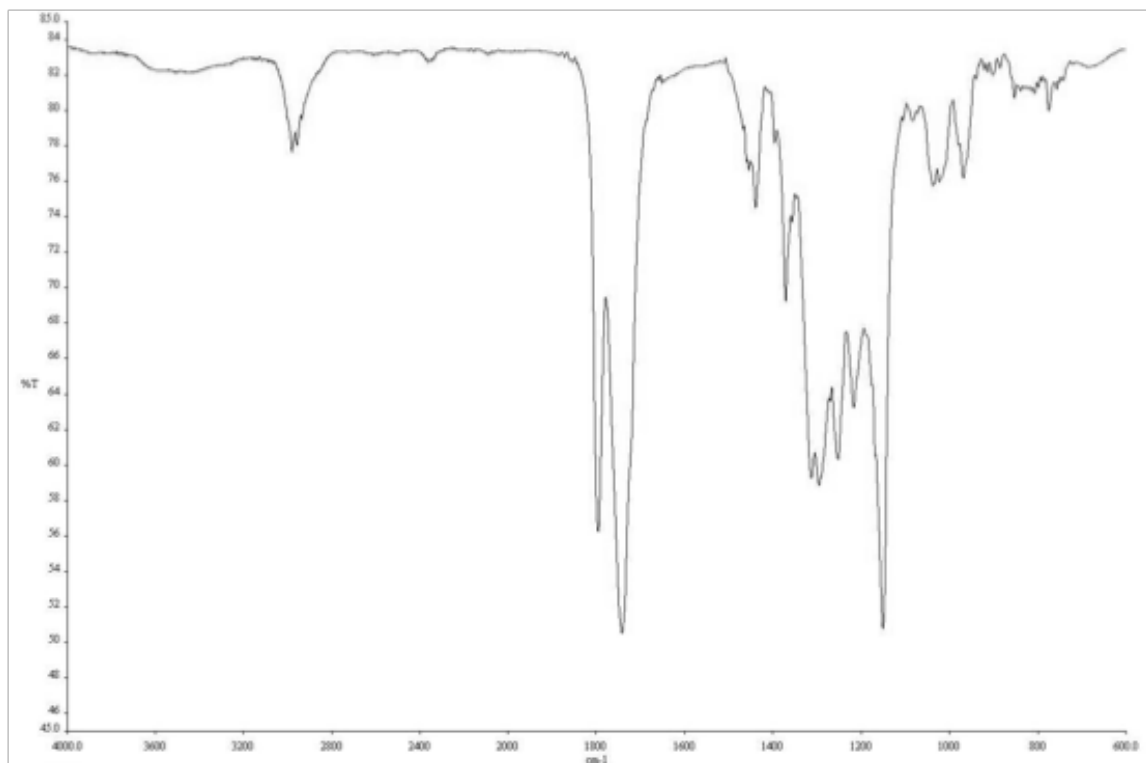


**Figure A6.53** Infrared spectrum (Thin Film, NaCl) of compound **924**.

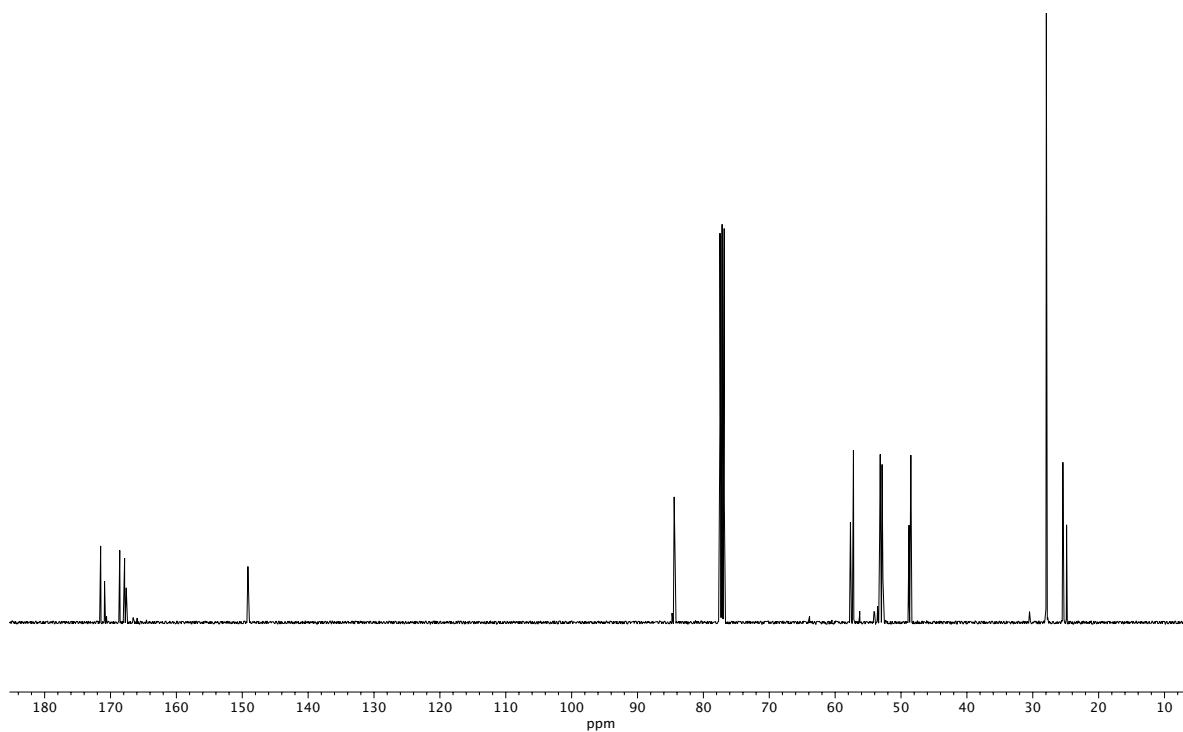


**Figure A6.54** <sup>13</sup>C NMR (100 MHz, CDCl<sub>3</sub>) of compound **924**.

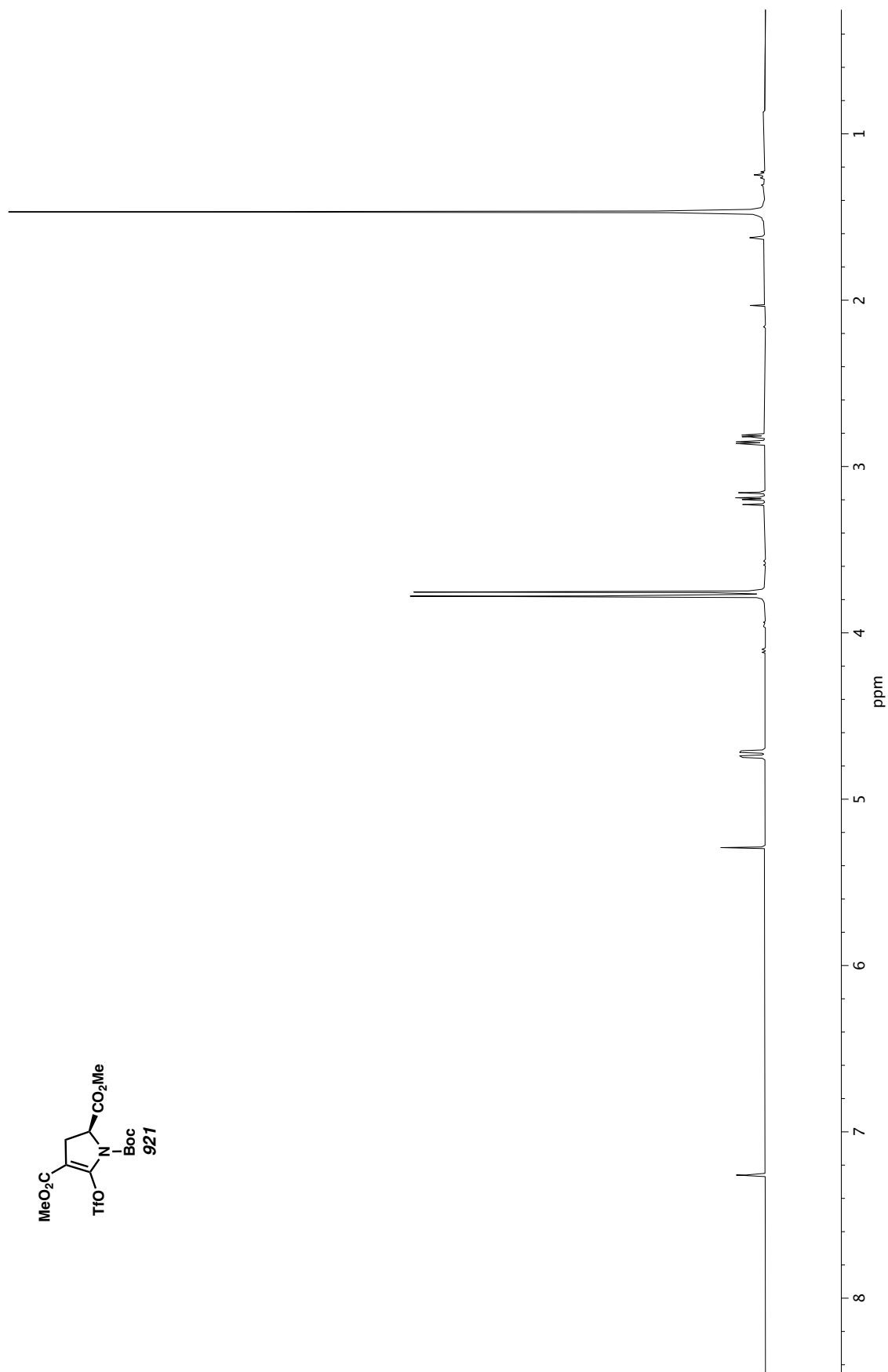


**Figure A6.55**  $^1\text{H}$  NMR (400 MHz, CDCl<sub>3</sub>) of compound **921**.

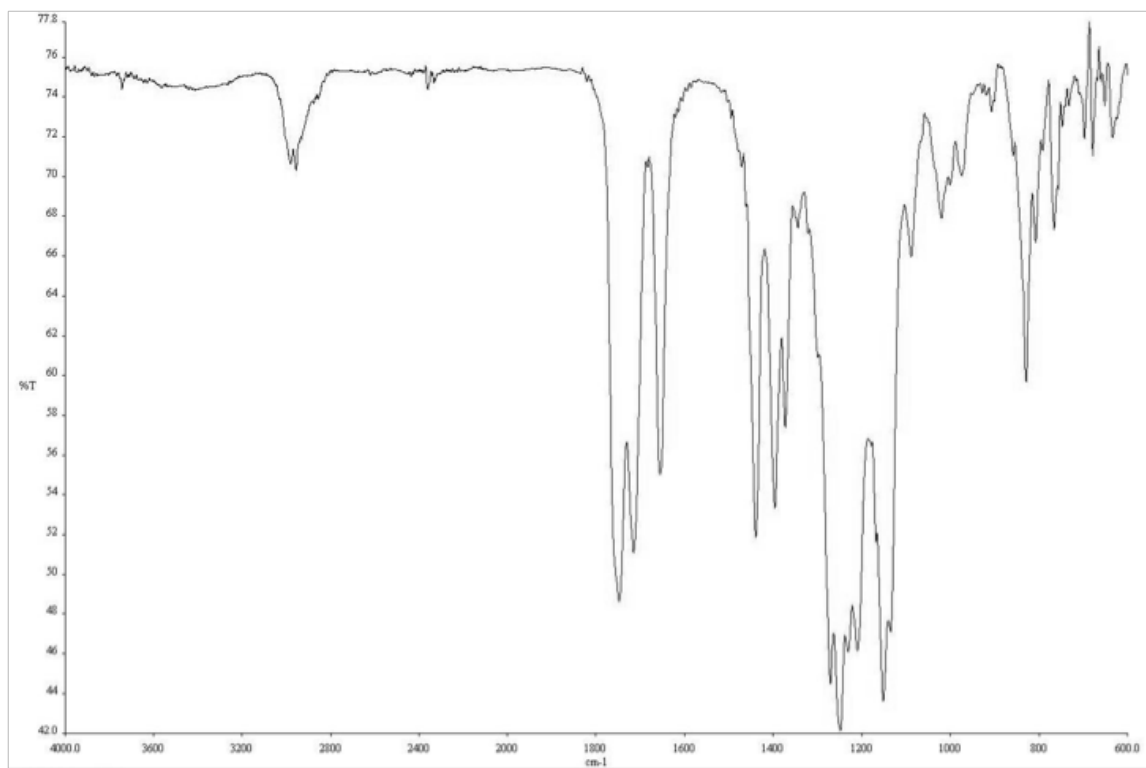


**Figure A6.56** Infrared spectrum (Thin Film, NaCl) of compound **921**.

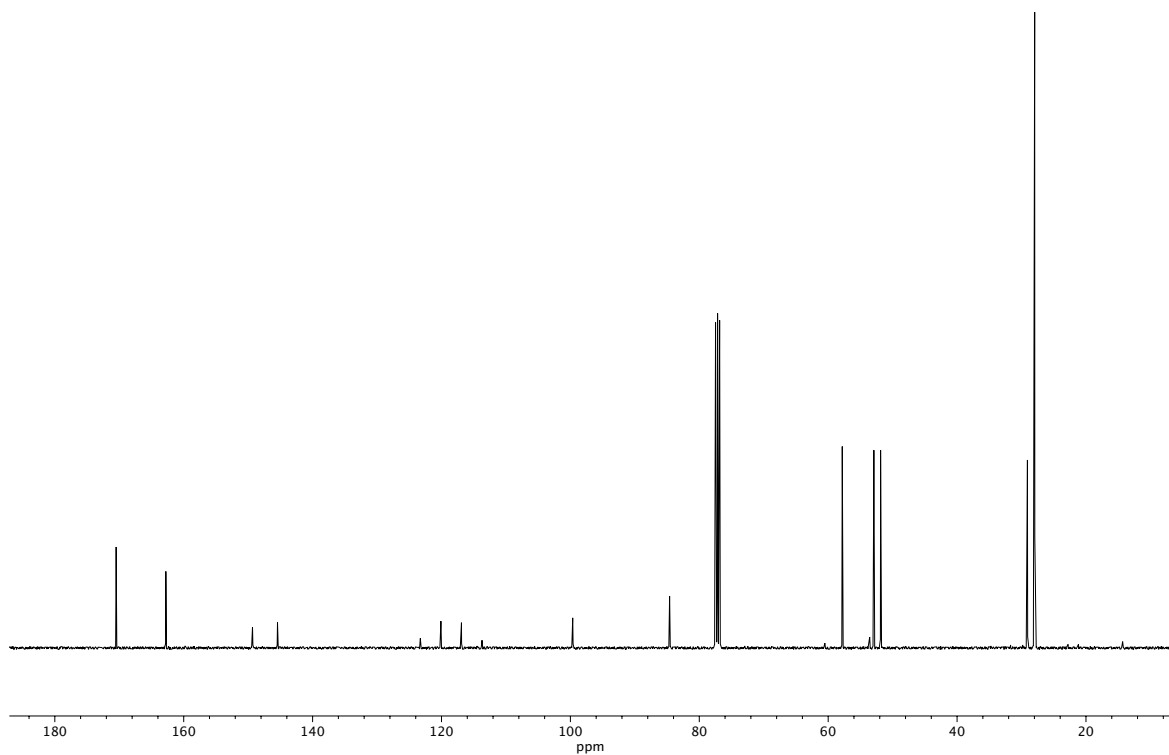


**Figure A6.57** <sup>13</sup>C NMR (100 MHz, CDCl<sub>3</sub>) of compound **921**.

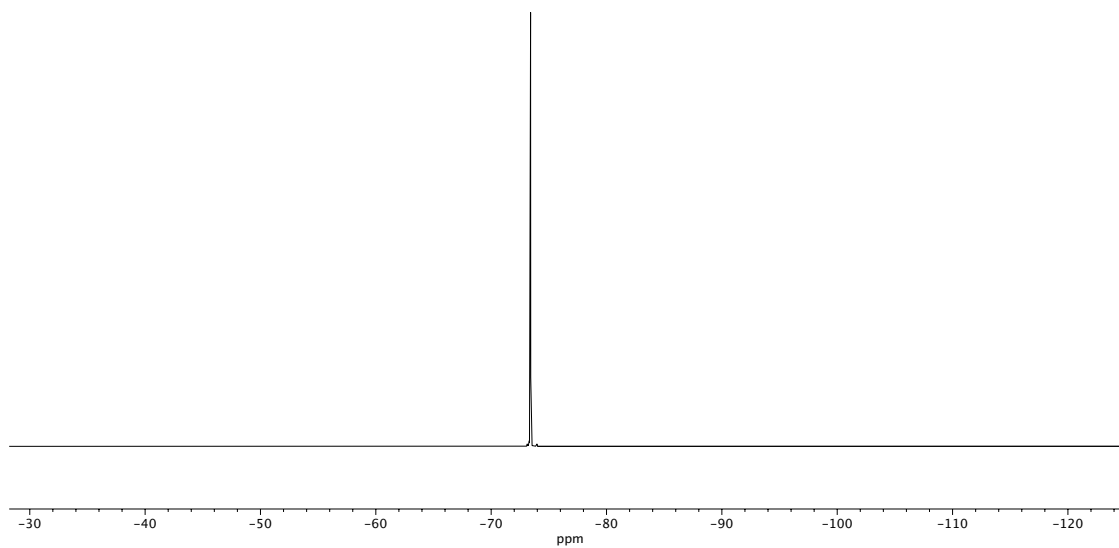


**Figure A6.58**  $^{19}\text{F}$  NMR (282 MHz,  $\text{CDCl}_3$ ) of compound **921**.

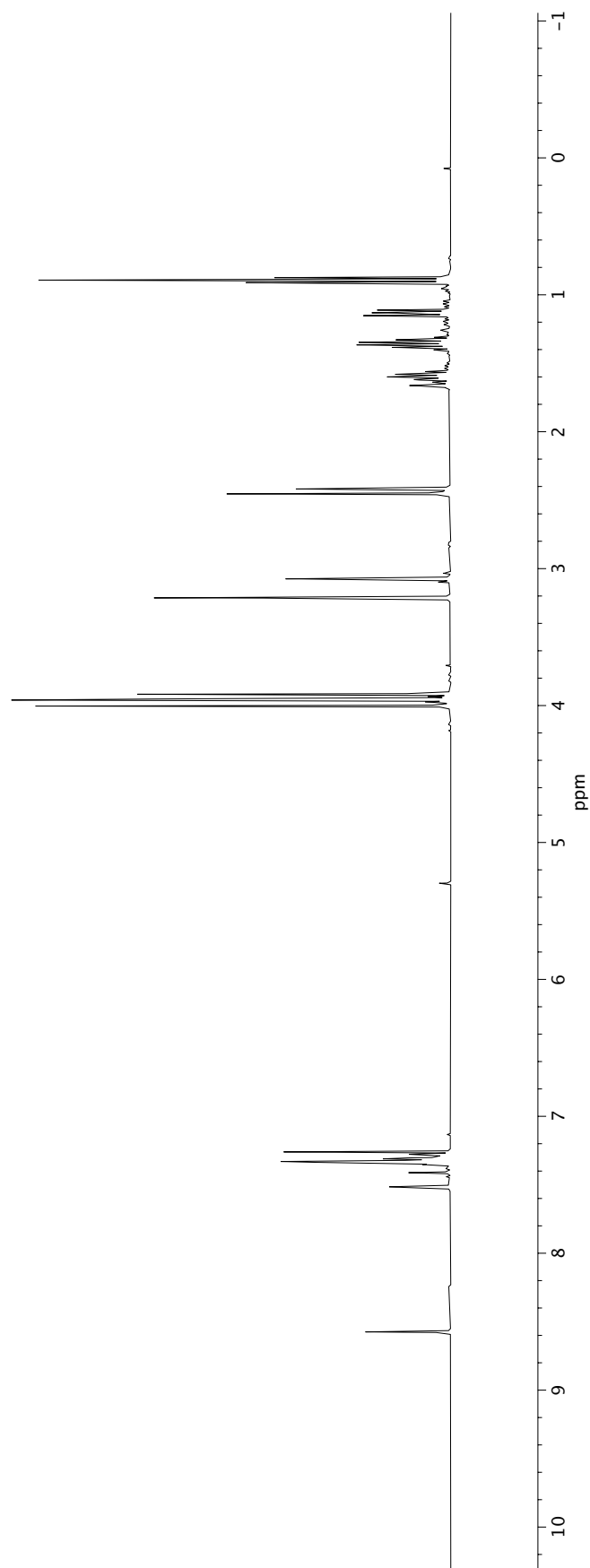
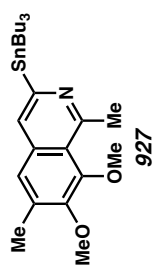
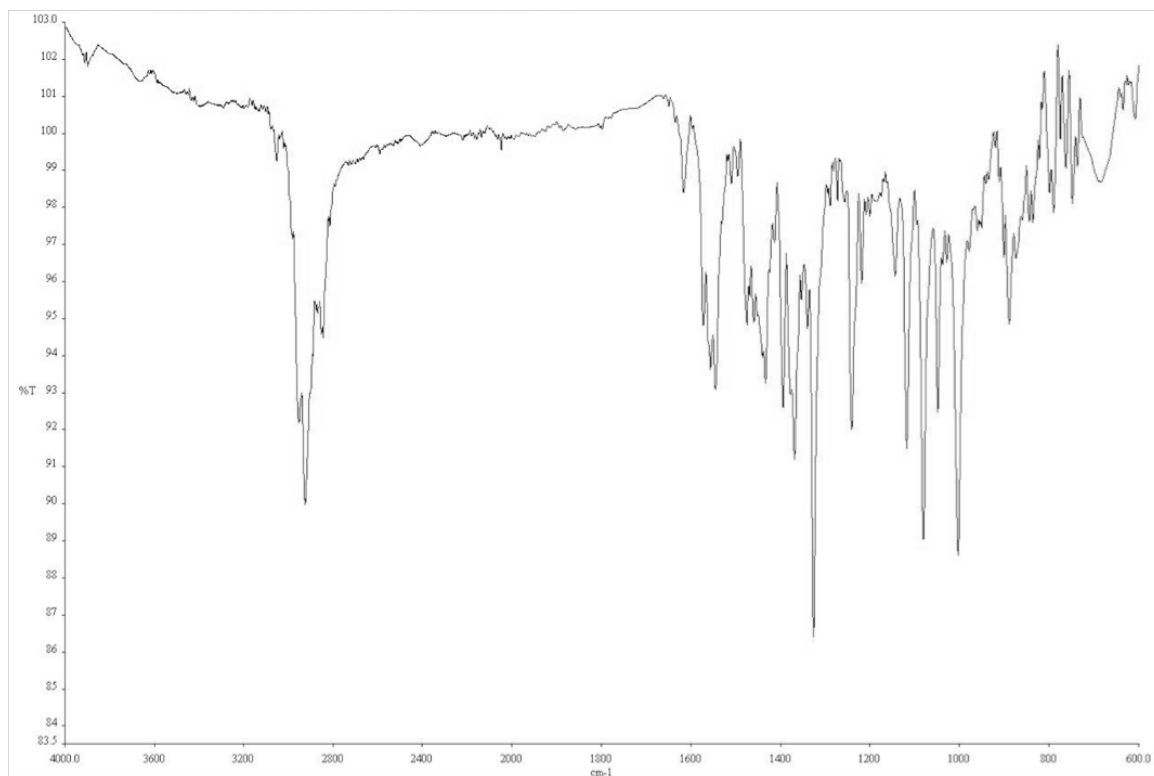
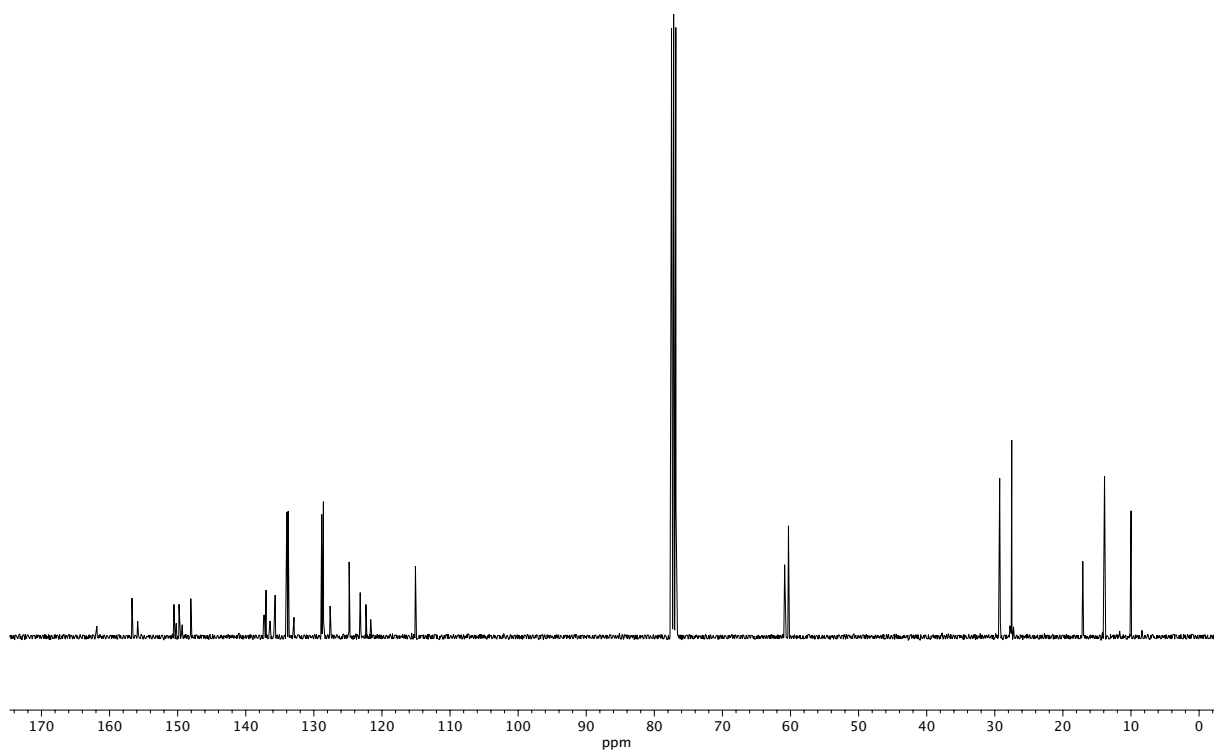


Figure A6.59 <sup>1</sup>H NMR (400 MHz, CDCl<sub>3</sub>) of compound 927.



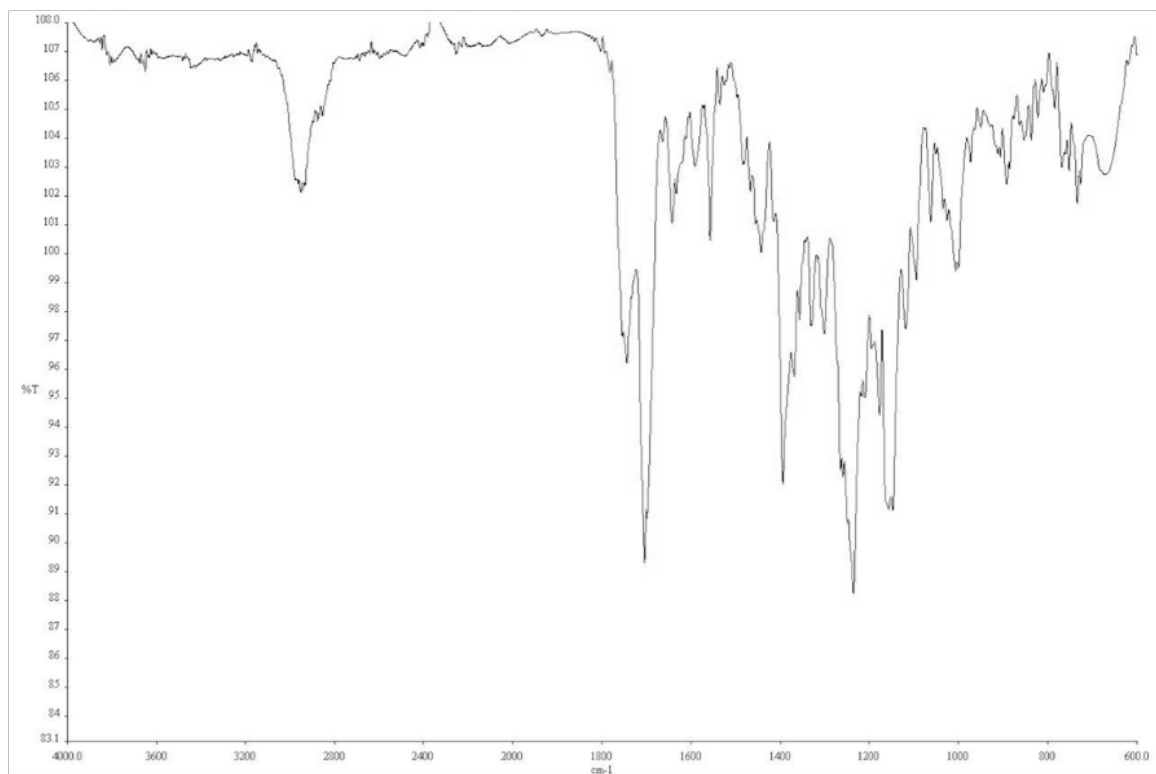
**Figure A6.60** Infrared spectrum (Thin Film, NaCl) of compound **927**.



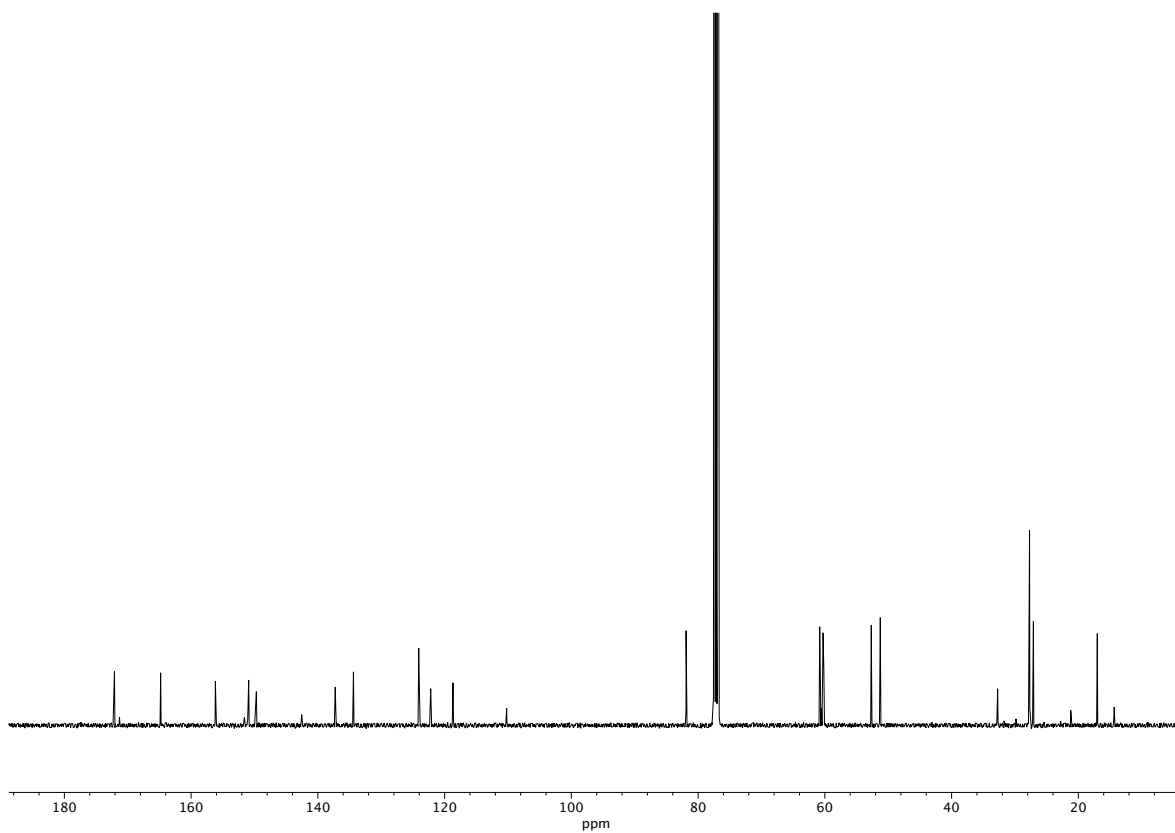
**Figure A6.61** <sup>13</sup>C NMR (100 MHz, CDCl<sub>3</sub>) of compound **927**.



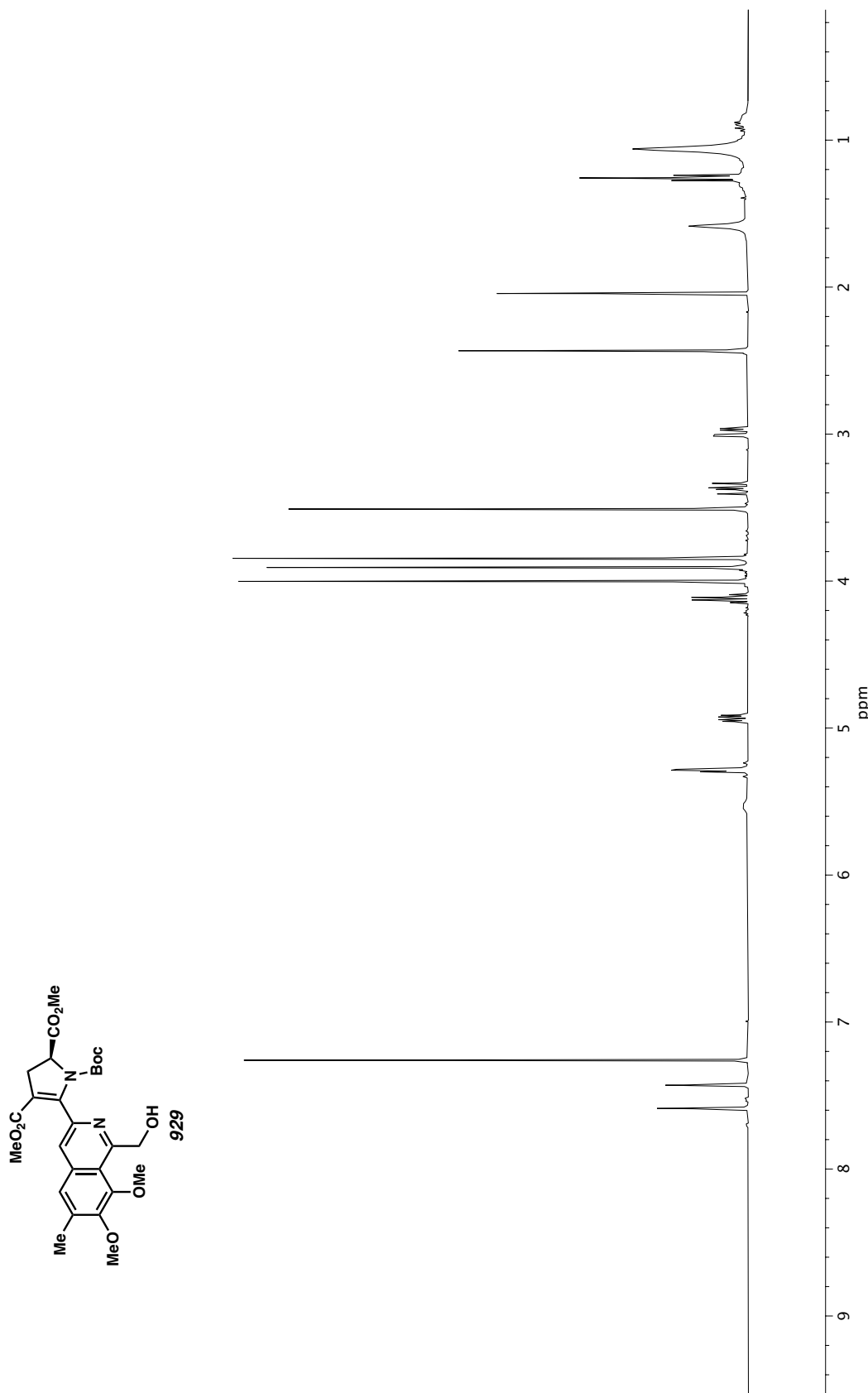




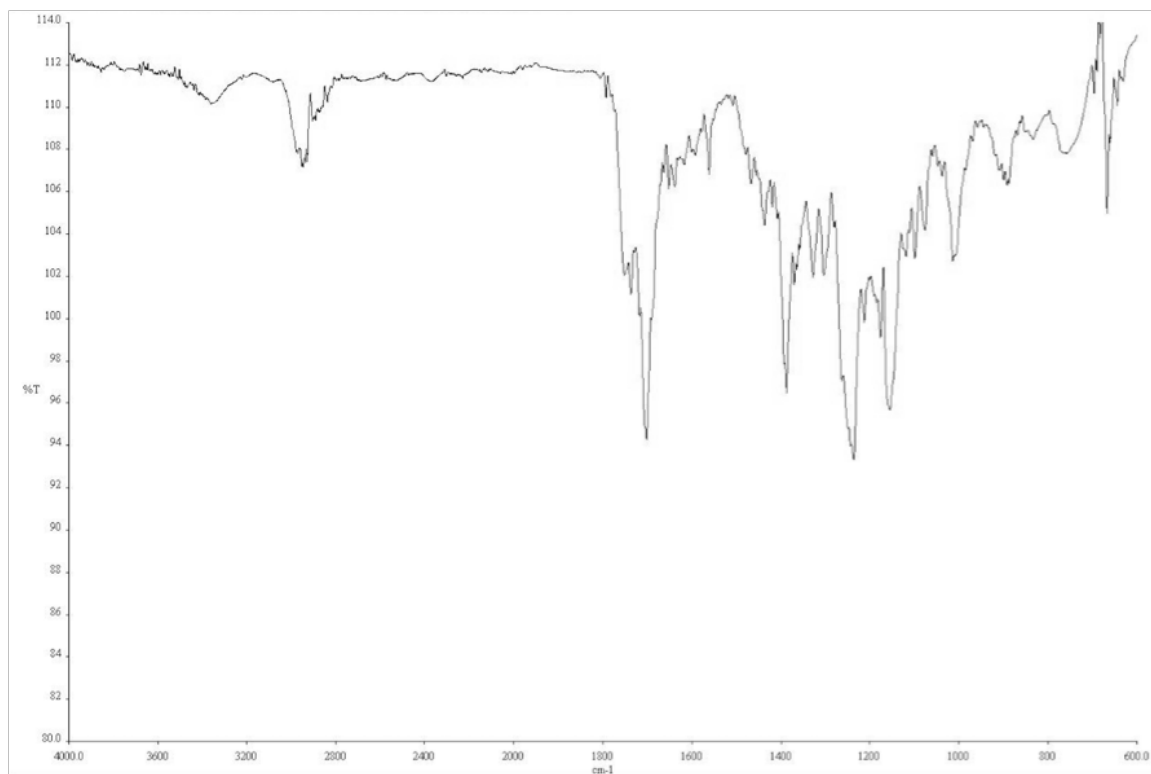
**Figure A6.63** Infrared spectrum (Thin Film, NaCl) of compound **928**.



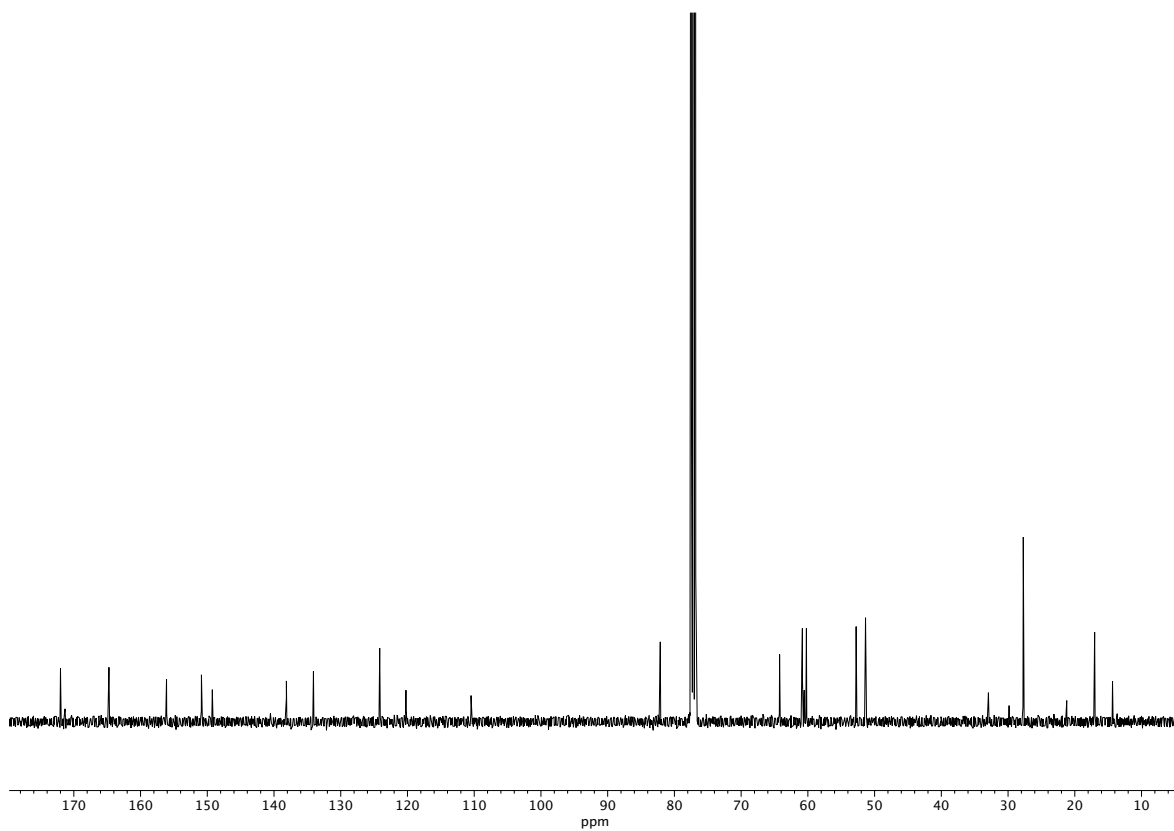
**Figure A6.64**  $^{13}\text{C}$  NMR (100 MHz,  $\text{CDCl}_3$ ) of compound **928**.



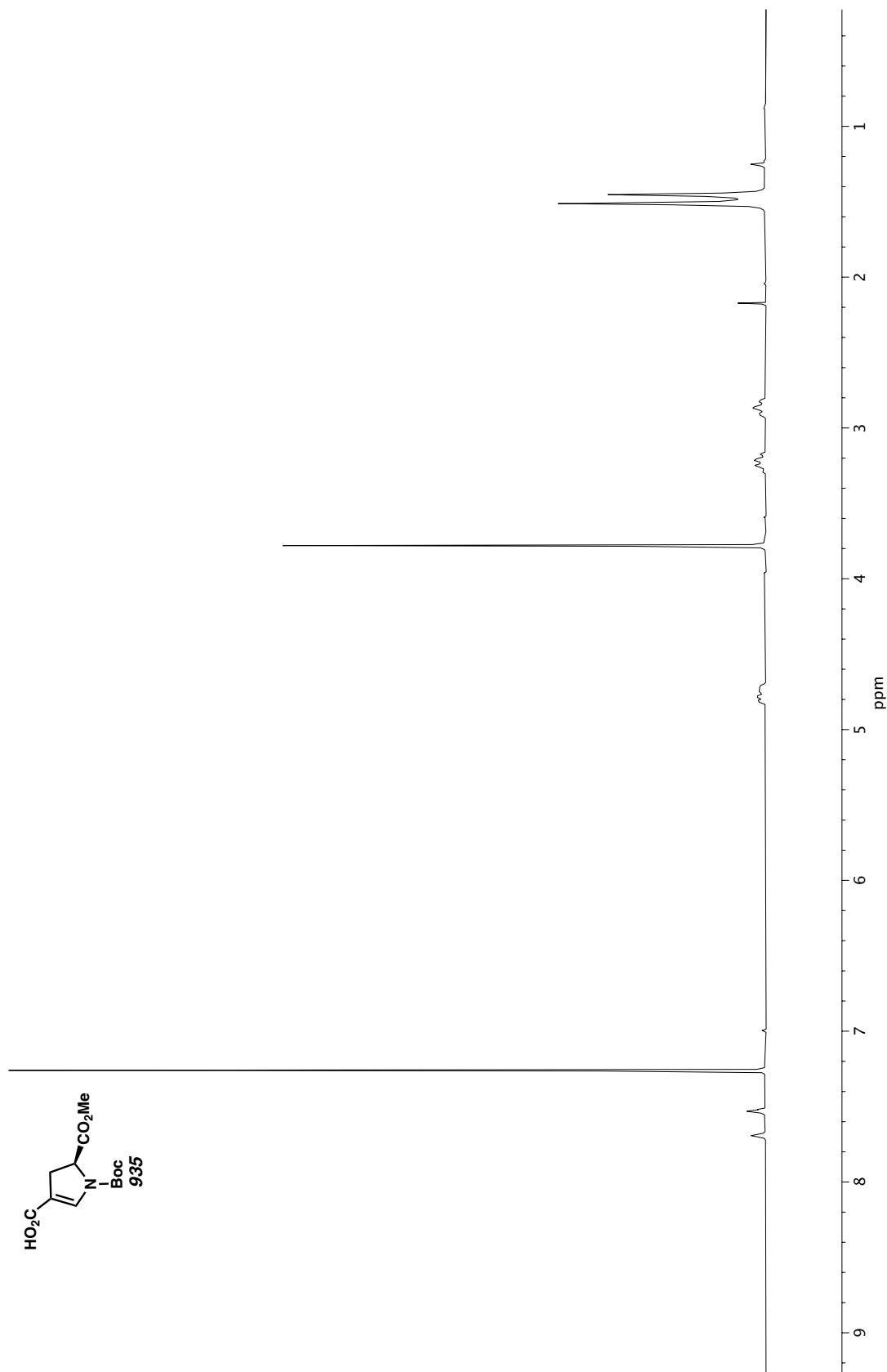
**Figure A6.65** <sup>1</sup>H NMR (400 MHz, CDCl<sub>3</sub>) of compound **929**.



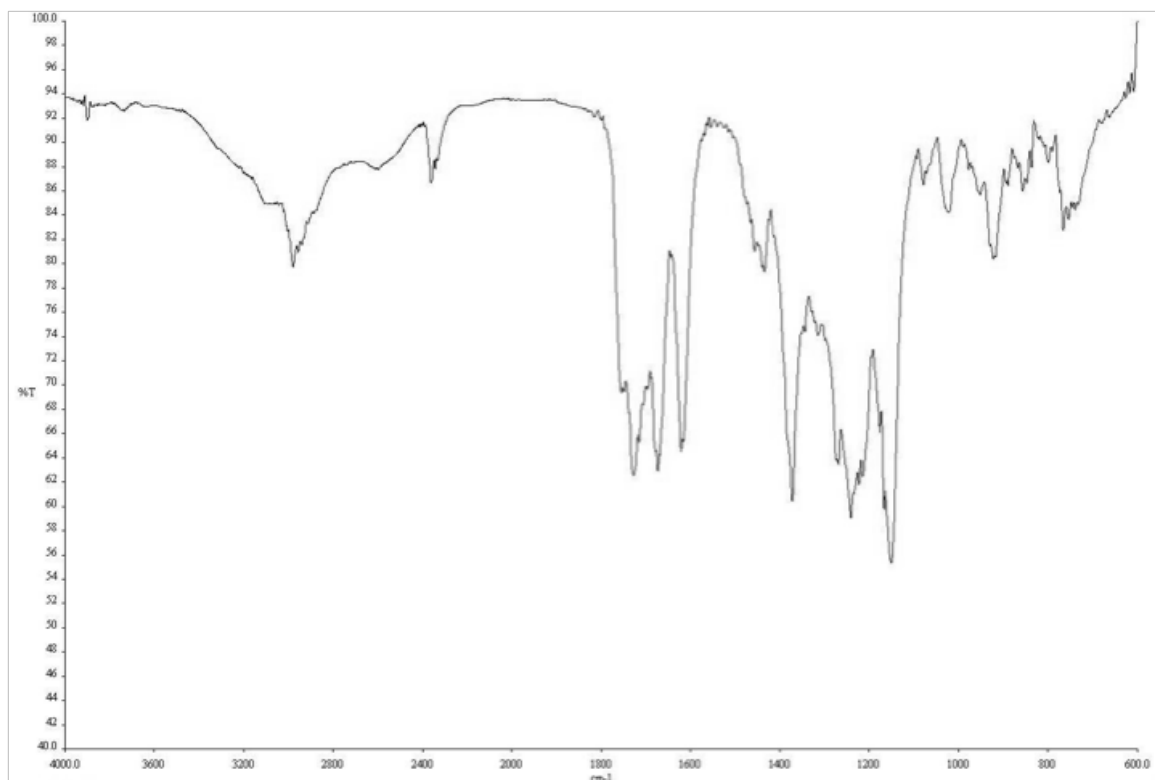
**Figure A6.66** Infrared spectrum (Thin Film, NaCl) of compound **929**.



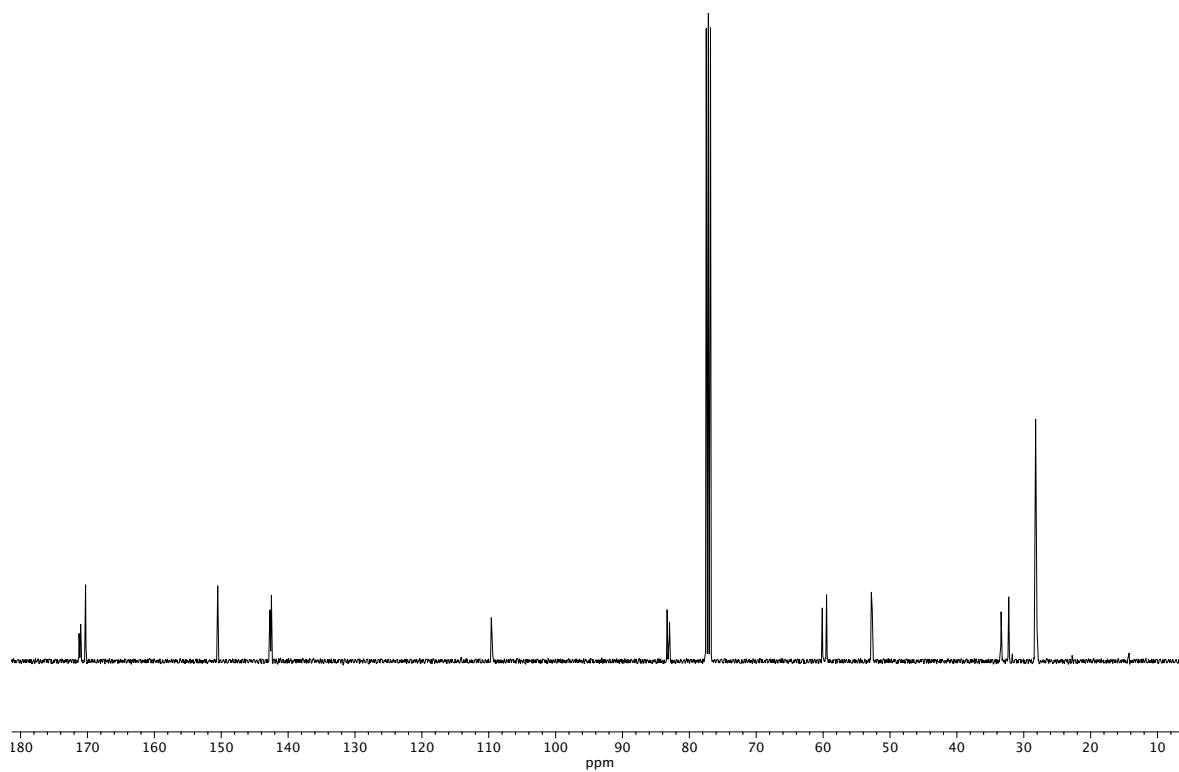
**Figure A6.67** <sup>13</sup>C NMR (100 MHz, CDCl<sub>3</sub>) of compound **929**.



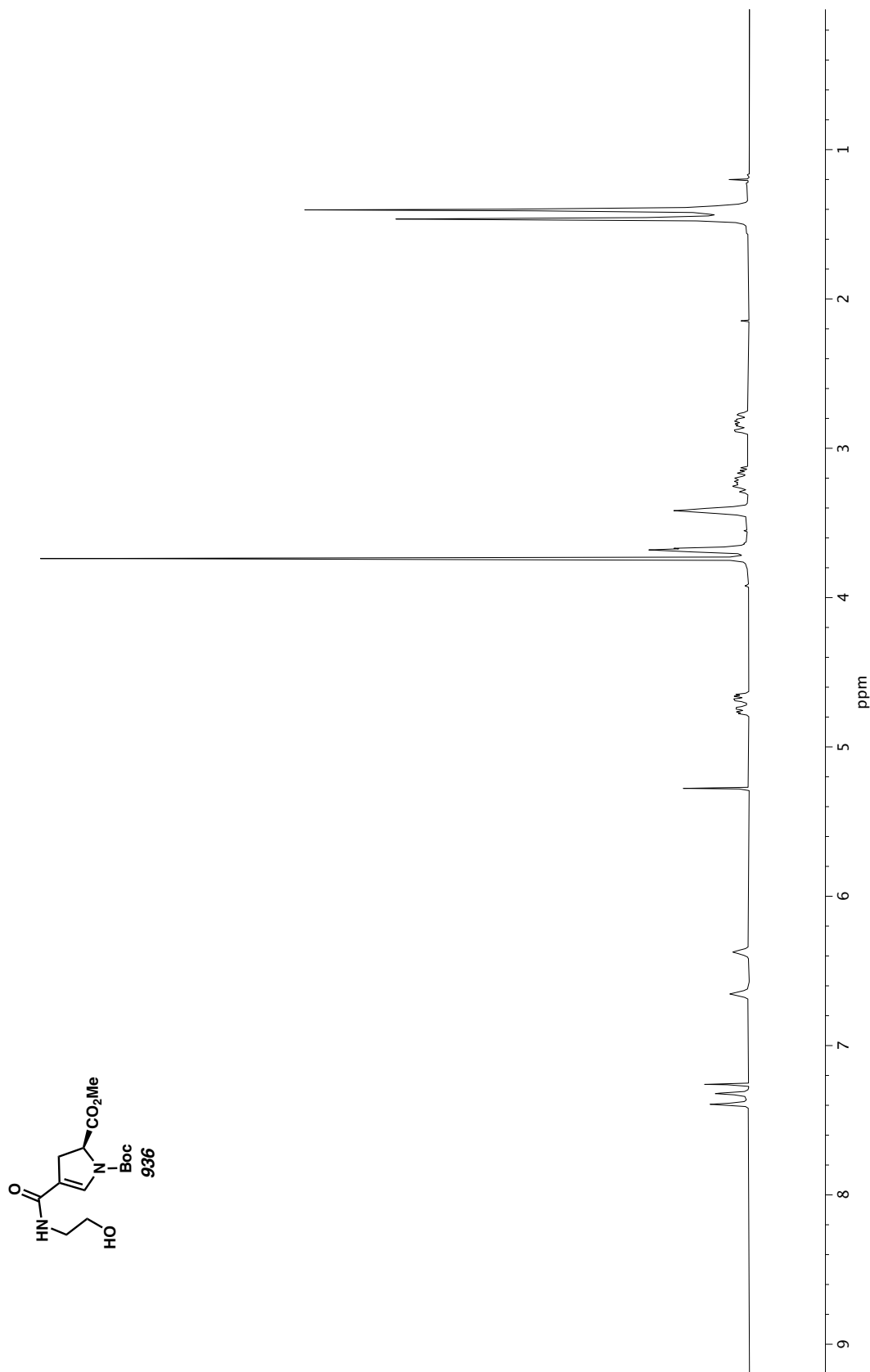
**Figure A6.68**  $^1\text{H}$  NMR (400 MHz,  $\text{CDCl}_3$ ) of compound 935.

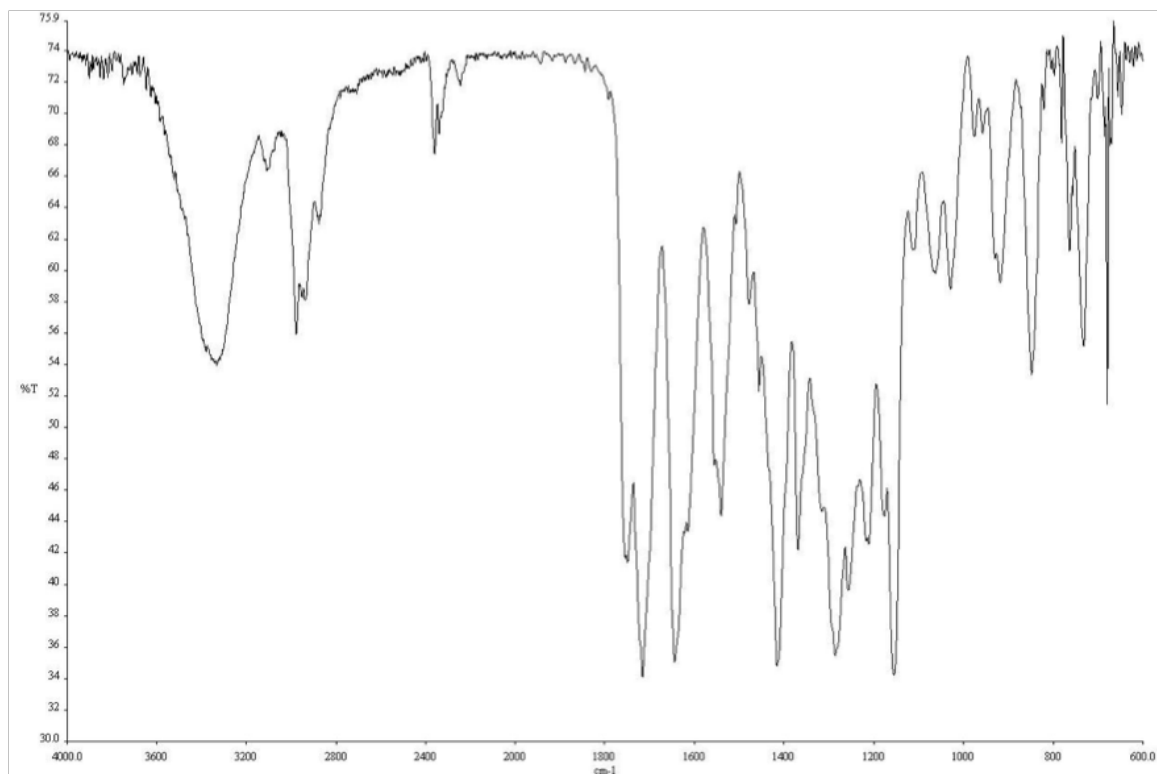


**Figure A6.69** Infrared spectrum (Thin Film, NaCl) of compound **935**.

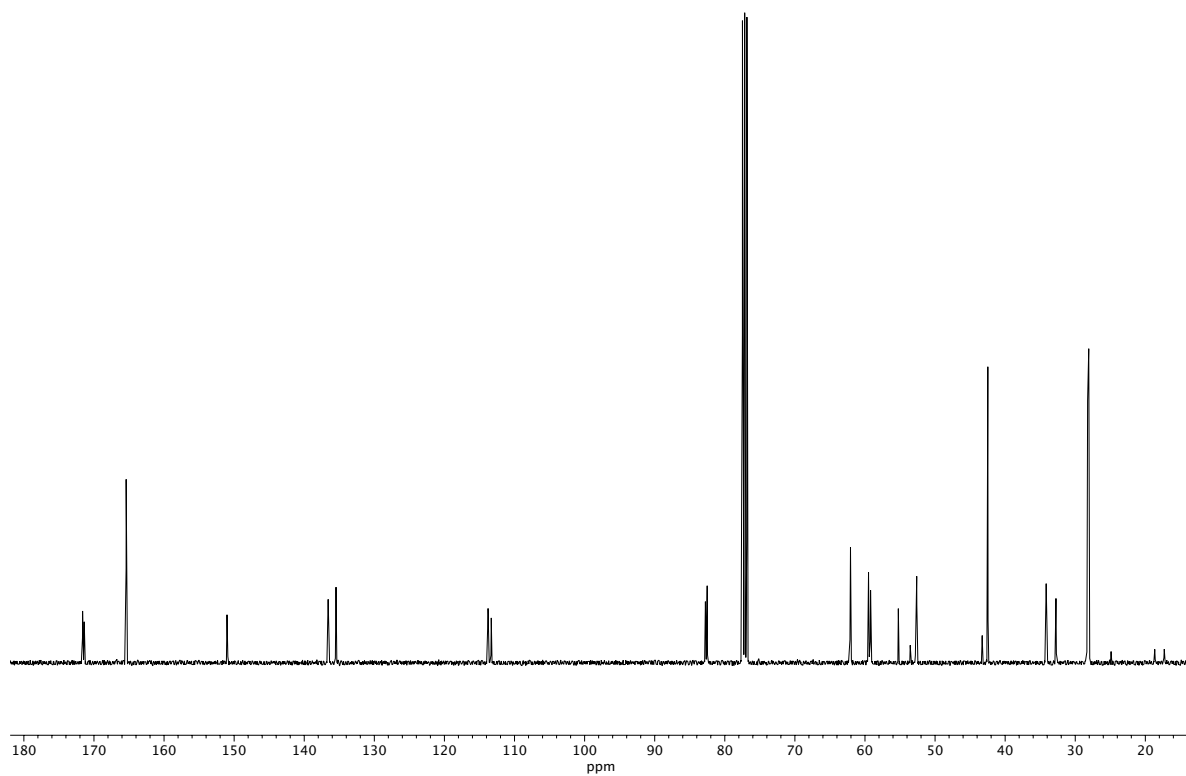


**Figure A6.70** <sup>13</sup>C NMR (100 MHz, CDCl<sub>3</sub>) of compound **935**.



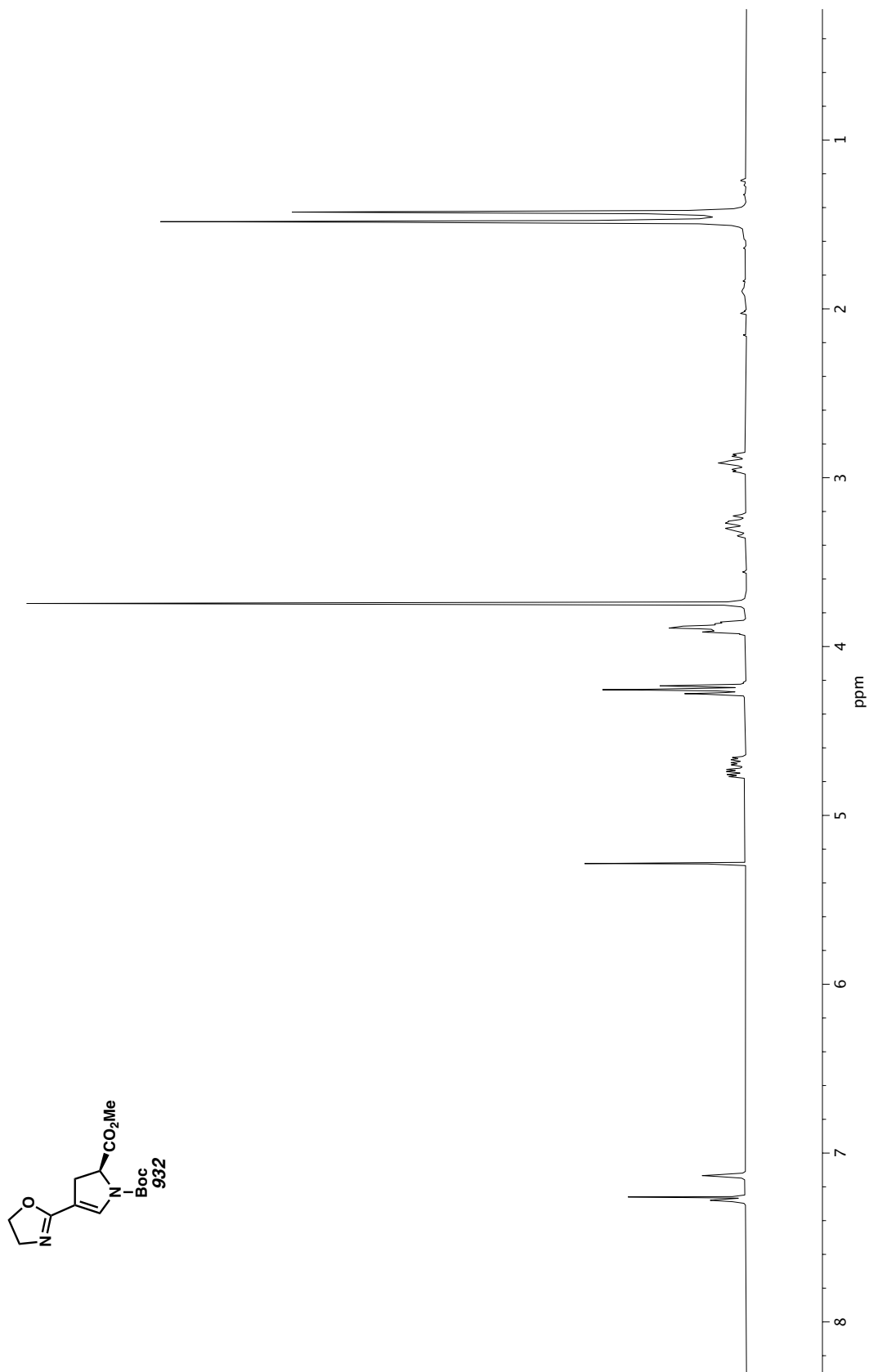


**Figure A6.72** Infrared spectrum (Thin Film, NaCl) of compound **936**.

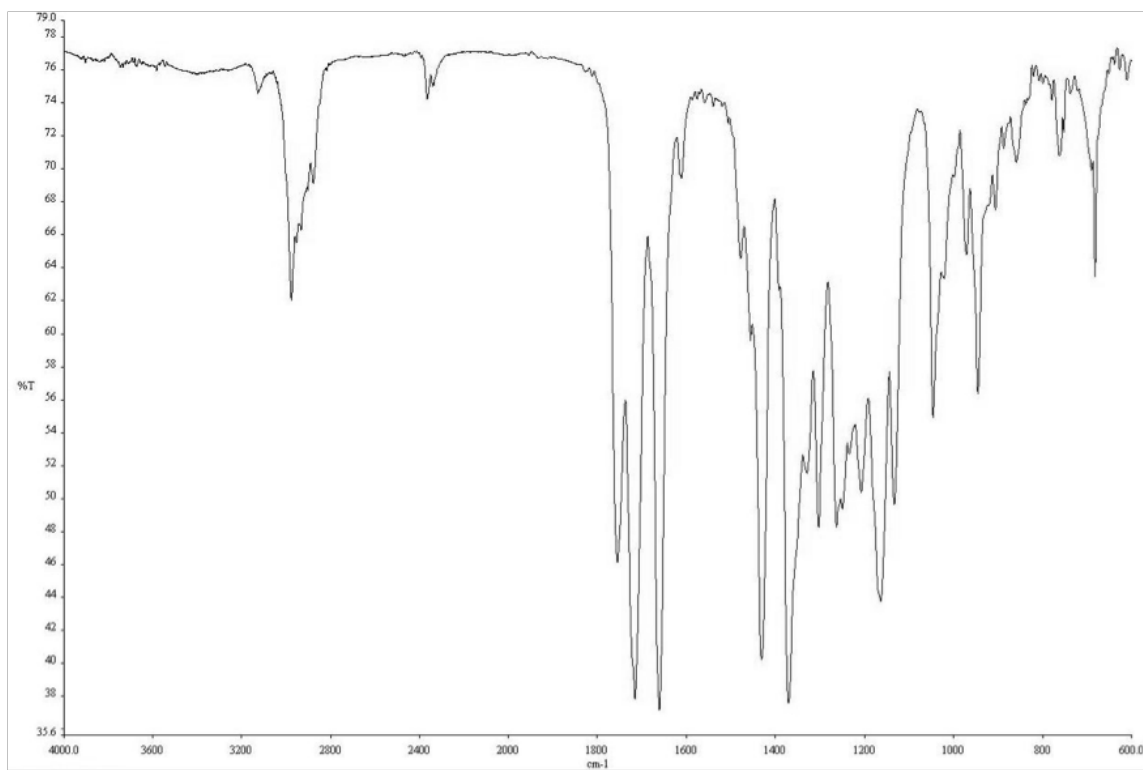


**Figure A6.73**  $^{13}\text{C}$  NMR (100 MHz,  $\text{CDCl}_3$ ) of compound **936**.

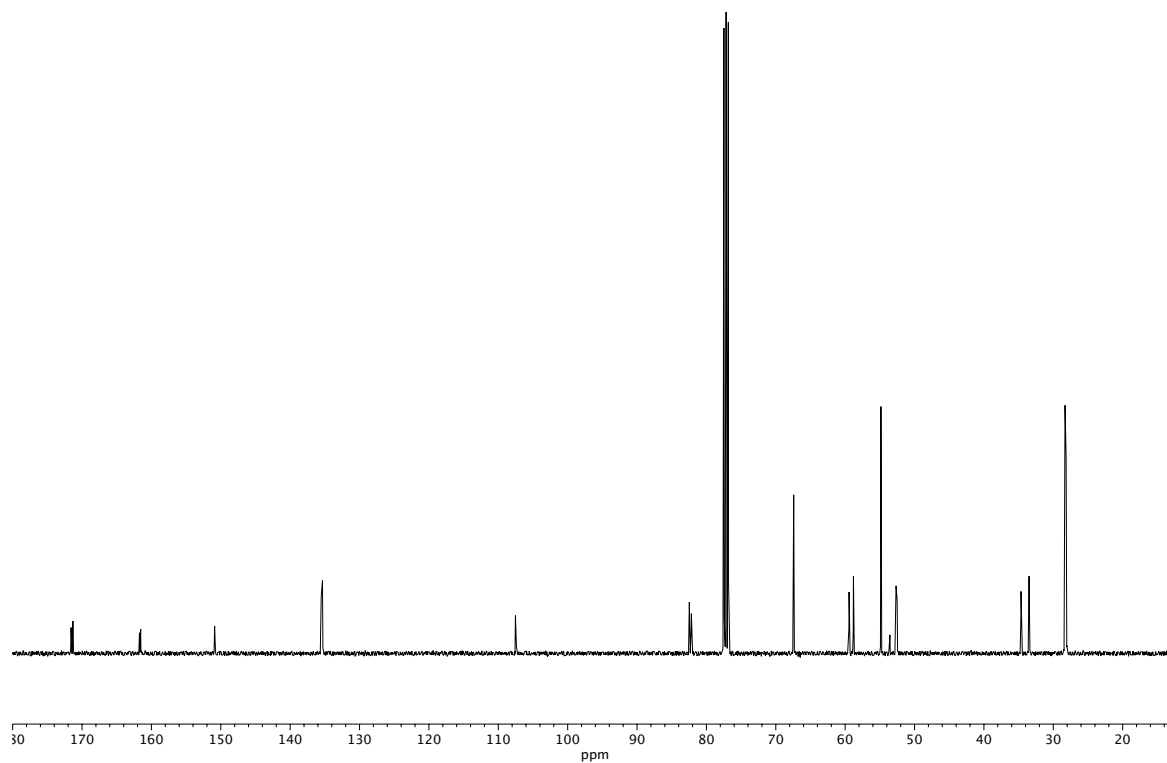




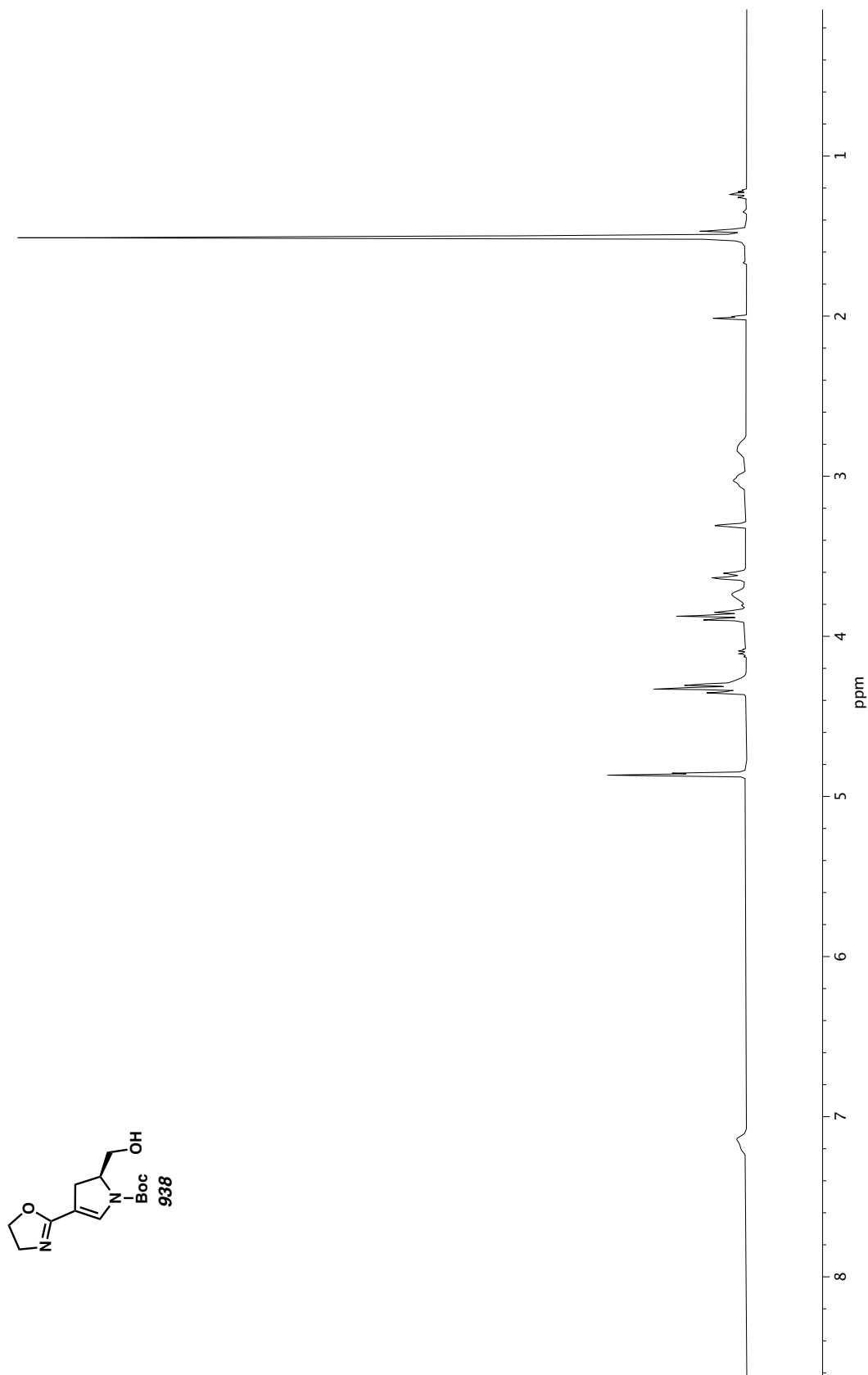
**Figure A6.74**  $^1\text{H}$  NMR (400 MHz,  $\text{CDCl}_3$ ) of compound **932**.



**Figure A6.75** Infrared spectrum (Thin Film, NaCl) of compound **932**.



**Figure A6.76** <sup>13</sup>C NMR (100 MHz, CDCl<sub>3</sub>) of compound **932**.



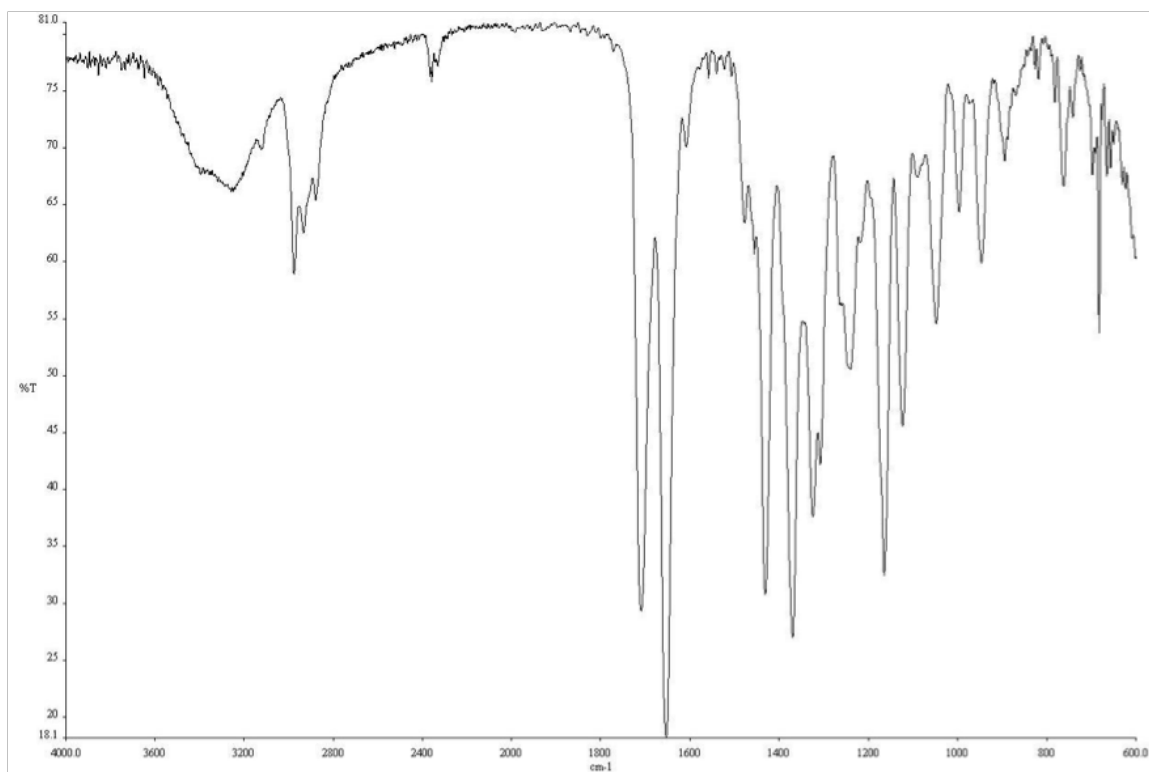


**Figure A6.78** Infrared spectrum (Thin Film, NaCl) of compound **938**.

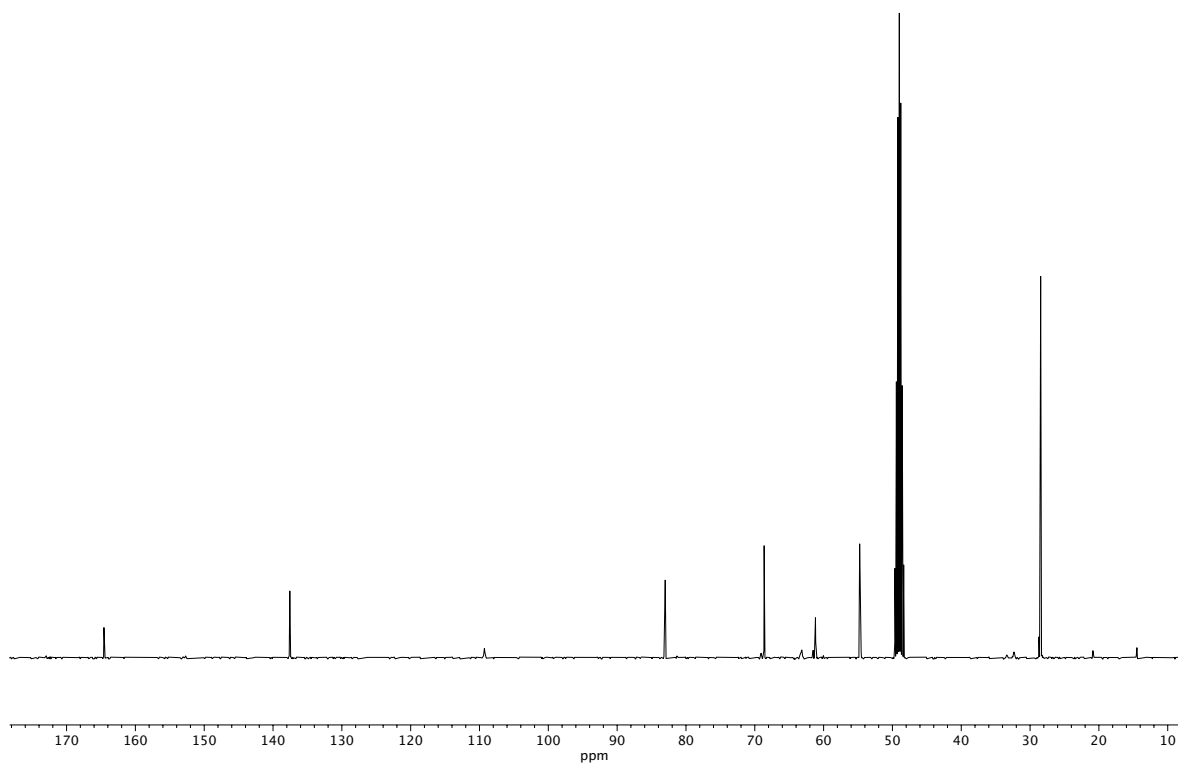


**Figure A6.79** <sup>13</sup>C NMR (100 MHz, CD<sub>3</sub>OD) of compound **938**.

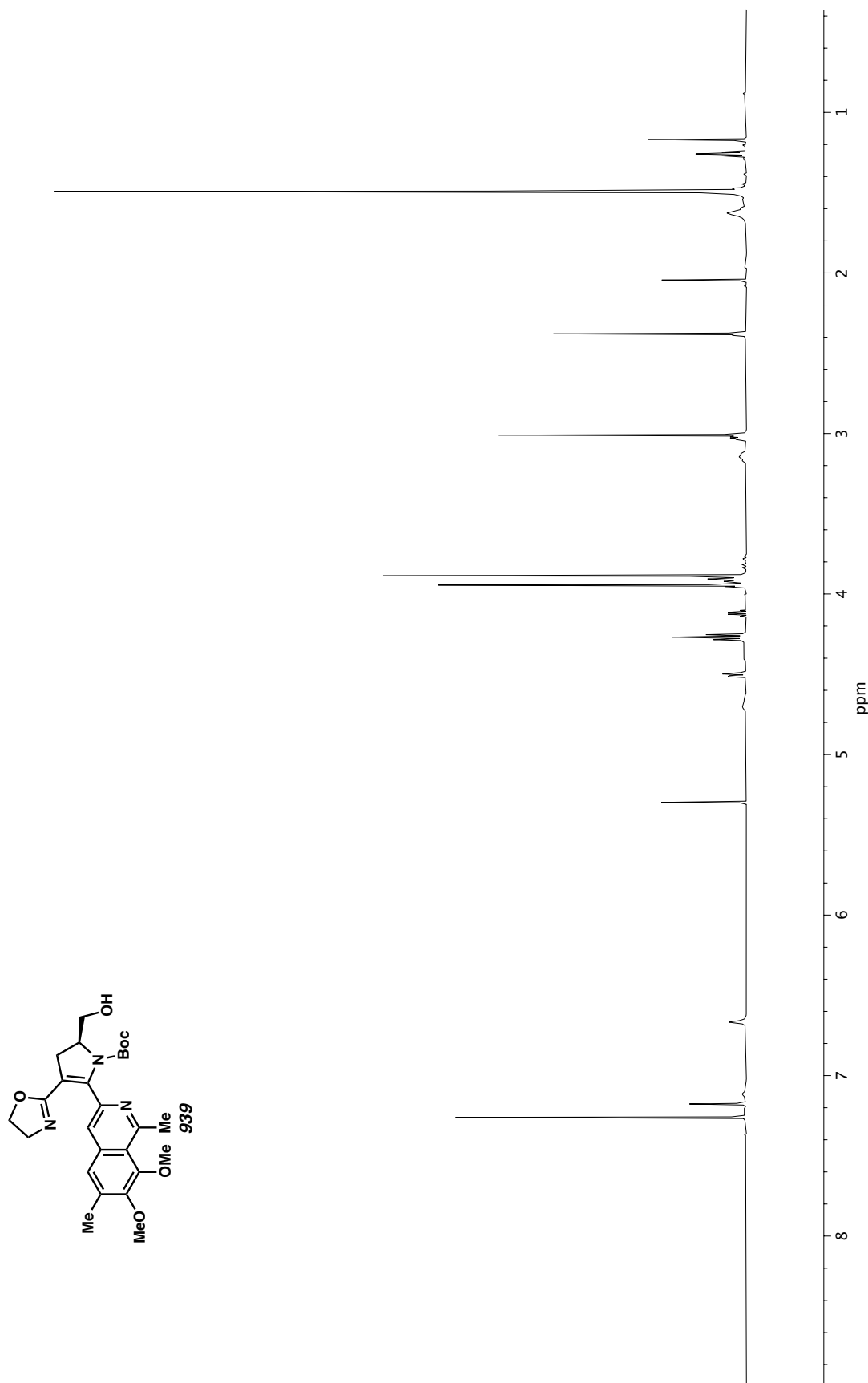


**Figure A6.80**  $^1\text{H}$  NMR (400 MHz, CDCl<sub>3</sub>) of compound **939**.

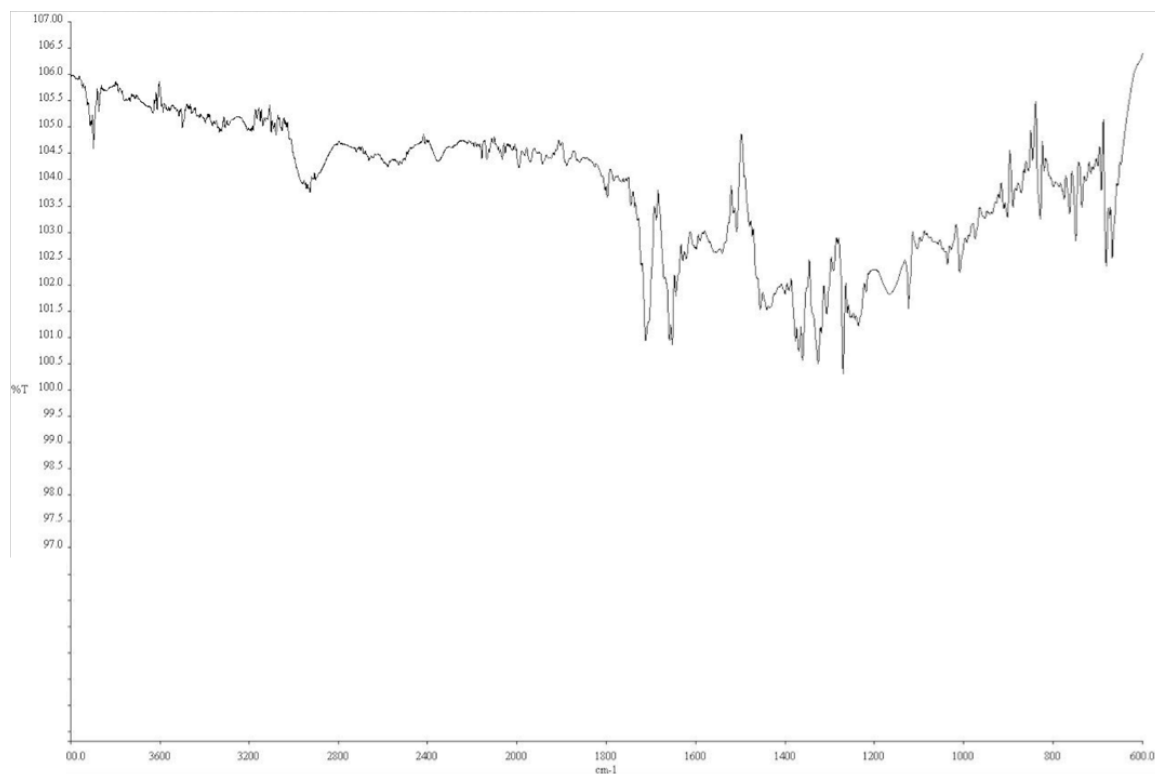


**Figure A6.81** Infrared spectrum (Thin Film, NaCl) of compound **939**.

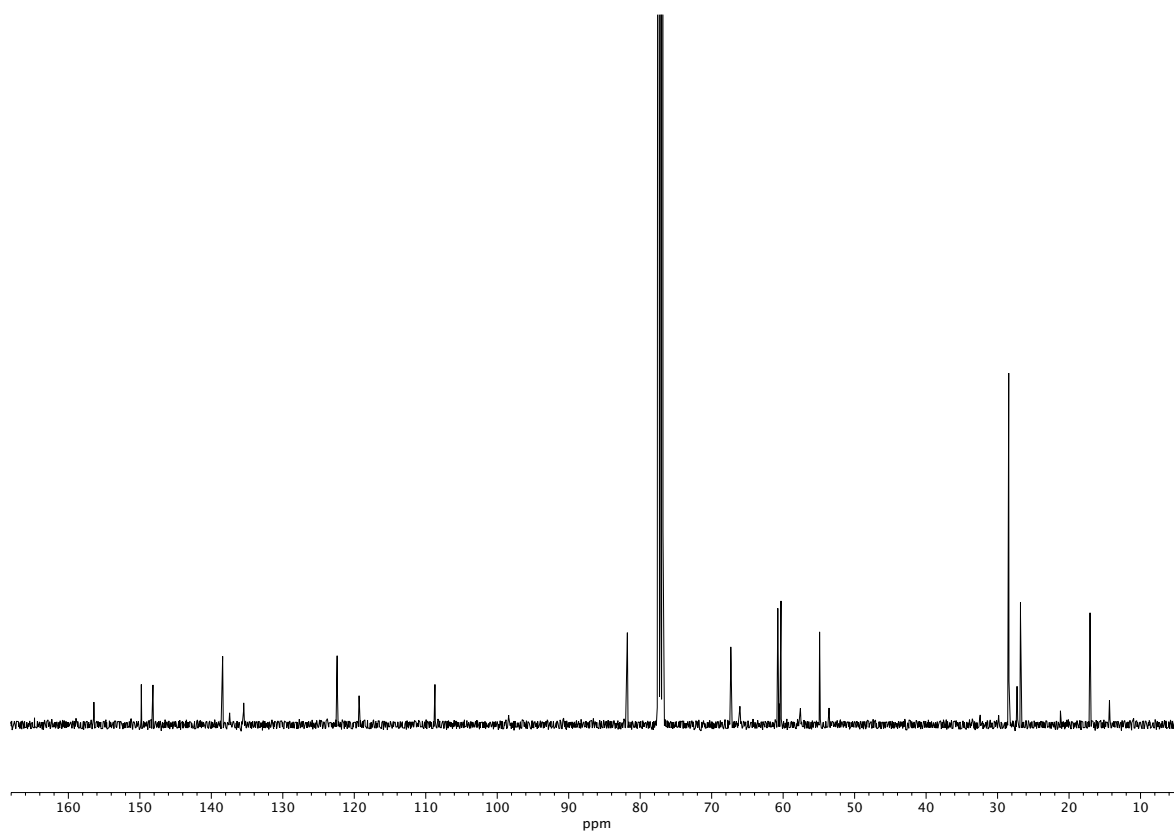


**Figure A6.82** <sup>13</sup>C NMR (100 MHz, CD<sub>3</sub>OD) of compound **939**.

## COMPREHENSIVE BIBLIOGRAPHY

- Abed Ali Abdine, R.; Hedouin, G.; Colobert, F.; Wencel-Delord, J. *ACS Catal.* **2021**, *11*, 215–247.
- Ackermann, L.; Vicente, R.; Kapdi, A. R. *Angew. Chem. Int. Ed.* **2009**, *48*, 9792–9826.
- Allan, K. M.; Hong, B. D.; Stoltz, B. M. *Org. Biomol. Chem.* **2009**, *7*, 4960–4964.
- Allan, K. M.; Stoltz, B. M. *J. Am. Chem. Soc.* **2008**, *130*, 17270–17271.
- Allin, S. M.; Streetley, G. B.; Slater, M.; James, S. L.; Martin, W. P. *Tetrahedron Lett.* **2004**, *45*, 5493–5496.
- Amnuoyopol, S.; Suwanborirux, K.; Pummangura, S.; Kubo, A.; Tanaka, C.; Saito, N. *J. Nat. Prod.* **2004**, *67*, 1023–1028.
- Anakabe, E.; Carrillo, L.; Badía, D.; Vicario, J. L.; Villegas, M. *Synthesis* **2004**, *7*, 1093–1101.
- Arambasic, M.; Hooper, J. F.; Willis, M. C. *Org. Lett.* **2013**, *15*, 5162–5165.
- Ashley, E. R.; Cruz, E. G.; Stoltz, B. M. *J. Am. Chem. Soc.* **2003**, *125*, 15000–15001.
- Barrios-Rivera, J.; Xu, Y.; Wills, M.; Vyas, V. K. *Org. Chem. Front.* **2020**, *7*, 3312–3342.
- Barton, D. H. R.; James, R.; Kirby, G. W.; Widdowson, D. A. *Chem. Commun.* **1967**, 266–268.
- Beng, T. K.; Langevin, S.; Braunstein, H.; Khim, M. *Org. Biomol. Chem.* **2016**, *14*, 830–834.
- Bianchini, C.; Meli, A.; Vizza, F. *Eur. J. Inorg. Chem.* **2001**, *2001*, 43–68.
- Blackham, E. E.; Booker-Milburn, K. I. *Angew. Chem. Int. Ed.* **2017**, *56*, 6613–6616.
- Blakemore, P. R.; White, J. D. *Chem. Commun.* **2002**, 1159–1168.

- Blank, N.; Opatz, T. *J. Org. Chem.* **2011**, *76*, 9777–9784.
- Blum, O.; Milstein, D. *J. Am. Chem. Soc.* **1995**, *117*, 4582–4594.
- Boudou, M.; Enders, D. *J. Org. Chem.* **2005**, *70*, 9486–9494.
- Brown, D. W.; Dyke, S. F.; Hardy, G.; Sainsbury, M. *Tetrahedron Lett.* **1969**, *19*, 1515–1517.
- Bruno, N. C.; Tudge, M. T.; Buchwald, S. L. *Chem. Sci.* **2013**, *4*, 916–920.
- Butora, G.; Hudlicky, T.; Fearnley, S. P.; Gum, A. G.; Stabile, M. R.; Abboud, K. *Tetrahedron Lett.* **1996**, *37*, 8155–8158.
- Cabré, A.; Verdaguer, X.; Riera, A.; *Chem. Rev.* **2022**, *122*, 269–339.
- Cai, X.-F.; Guo, R.-N.; Chen, M.-W.; Shi, L.; Zhou, Y.-G. *Chem. Eur. J.* **2014**, *20*, 7245–7248.
- Cai, X.-F.; Huang, W.-X.; Chen, Z.-P.; Zhou, Y.-G. *Chem. Commun.* **2014**, *50*, 9588–9590.
- Carrillo, L.; Badia, D.; Dominguez, E.; Anakabe, E.; Osante, I.; Tellitu, I.; Vicario, J. L. *J. Org. Chem.* **1999**, *64*, 115–1120.
- Cartigny, D.; Berhal, F.; Nagano, T.; Phansavath, P.; Ayad, T.; Genêt, J.-P.; Ohshima, T.; Mashima, K.; Ratovelomanana-Vidal, V. *J. Org. Chem.* **2012**, *77*, 4544–4556.
- Casado, A. L.; Espinet, P.; Gallego, A. M. *J. Am. Chem. Soc.* **2000**, *122*, 11771–11782.
- Cassels, B. K. *Nat. Prod. Commun.* **2019**, *14*, 85–90.
- Chan, C.; Heid, R.; Zheng, S.; Guo, J.; Zhou, B.; Furuuchi, T.; Danishefsky, S. J. *J. Am. Chem. Soc.* **2005**, *127*, 4596–4598.
- Charupant, K.; Suwanborirux, K.; Amnuoyopol, S.; Saito, E.; Kubo, A.; Saito, N. *Chem. Pharm. Bull.* **2007**, *55*, 81–86.



- Chen, J.; Chen, X.; Bois-Choussy, M.; Zhu, J. *J. Am. Chem. Soc.* **2006**, *128*, 87–89.
- Chen, J.; Chen, X.; Willot, M.; Zhu, J. *Angew. Chem. Int. Ed.* **2006**, *45*, 8028–8032.
- Chen, M.-W.; Deng, Z.; Yang, Q.; Huang, J.; Peng, Y. *Org. Chem. Front.* **2019**, *6*, 746–750.
- Chen, M.-W.; Ji, Y.; Wang, J.; Chen, Q.-A.; Shi, L.; Zhou, Y.-G. *Org. Lett.* **2017**, *19*, 4988–4991.
- Chen, Q.-A.; Gao, K.; Duan, Y.; Ye, Z.-S.; Shi, L.; Yang, Y.; Zhou, Y.-G. *J. Am. Chem. Soc.* **2012**, *134*, 2442–2448.
- Chen, Q.-A.; Wang, D.-S.; Zhou, Y.-G.; Duan, Y.; Fan, H.-J.; Yang, Y.; Zhang, Z. *J. Am. Chem. Soc.* **2011**, *133*, 6126–6129.
- Chen, R.; Liu, H.; Chen, X. *J. Nat. Prod.* **2013**, *76*, 1789–1795.
- Chen, X.; Zhu, J. *Angew. Chem. Int. Ed.* **2007**, *46*, 3962–3965.
- Chen, Y.; He, Y.-M.; Zhang, S.; Miao, T.; Fan, Q.-H. *Angew. Chem. Int. Ed.* **2019**, *58*, 3809–3813.
- Chen, Y.; Pan, Y.; He, Y.-M.; Fan, Q.-H. *Angew. Chem. Int. Ed.* **2019**, *58*, 16831–16834.
- Chen, Z.-P.; Chen, M.-W.; Guo, R.-N.; Zhou, Y.-G. *Org. Lett.* **2014**, *16*, 1406–1409.
- Cheng, J.; Fu, L.; Ling, C.; Yang, Y. *Heterocycles.* **2010**, *81*, 2581–2592.
- Chiba, H.; Oishi, S.; Fujii, N.; Ohno, H. *Angew. Chem. Int. Ed.* **2012**, *51*, 9169–9172.
- Chiba, H.; Sakai, Y.; Ohara, A.; Oishi, S.; Fujii, N.; Ohno, H. *Chem. Eur. J.* **2013**, *19*, 8875–8883.
- Chinnagolla, R. K.; Pimparkar, S.; Jeganmohan, M. *Org. Lett.* **2012**, *14*, 3032–3035.
- Chrzanowska, M. Grajewska, A.; Rozwadowska, M. D. *Chem. Rev.* **2016**, *116*, 12369–12465.

- Chrzanowska, M.; Dreas, A.; Rozwadowska, M. D. *Tetrahedron: Asymmetry* **2004**, *15*, 1113–1120.
- Chu, H.; Sun, S.; Yu, J.-T.; Cheng, J. *Chem. Commun.* **2015**, *51*, 13327.
- Chu, S.; Münster, N.; Balan, T.; Smith, M. D. *Angew. Chem. Int. Ed.* **2016**, *55*, 14306–14309.
- Chuang, K. V.; Navarro, R.; Reisman, S. E. *Chem. Sci.* **2011**, *2*, 1086–1089.
- Corey, E. J.; Gin, D. Y.; Kania, R. S. *J. Am. Chem. Soc.* **1996**, *118*, 9202–9203.
- Cuevas, C.; Francesch, A. *Nat. Prod. Rep.* **2009**, *26*, 322–337.
- Cuevas, C.; Pérez, M.; Martín, M. J.; Chicharro, J. L.; Fernández-Rivas, C.; Flores, M.; Francesch, A.; Gallego, P.; Zarzuelo, M.; de la Calle, F.; García, J.; Polanco, C.; Rodríguez, I.; Manzanares, I. *Org. Lett.* **2000**, *2*, 2545–2548.
- Cuevas, C.; Pérez, M.; Martín, M. J.; Chicharro, J. L.; Fernández-Rivas, C.; Flores, M.; Francesch, A.; Gallego, P.; Zarzuelo, M.; de la Calle, F.; García, J.; Polanco, C.; Rodríguez, I.; Manzanares, I. *Org. Lett.* **2000**, *2*, 2545–2548.
- Cui, C.-X.; Chen, H.; Li, S.-J.; Zhang, T.; Qu, L.-B.; Lan, Y. *Coord. Chem. Rev.* **2020**, *412*, 213251–21327.
- Cuny, G. D. *Tetrahedron Lett.* **2004**, *45*, 5167–5170.
- Daikuhara, N.; Tada, Y.; Yamaki, S.; Charupant, K.; Amnuoypol, S.; Suwanborirux, K.; Saito, N. *Tet. Lett.* **2009**, *50*, 4276–4278.
- Davis, F. A.; Melamed, J. Y.; Sharik, S. S. *J. Org. Chem.* **2006**, *71*, 8761–8766.
- Davis, F. A.; Mohanty, P. K. *J. Org. Chem.* **2002**, *67*, 1290–1296.
- Dewick, P. M. *Medicinal Natural Products: A Biosynthetic Approach*, 2<sup>nd</sup> ed.; John Wiley & Sons, 2002.

- Díaz-Torres, R.; Alvarez, S. *Dalton. Trans.* **2011**, *40*, 10742–10750.
- Ding, K.; Han, Z.; Wang, Z. *Chem. Asian J.* **2009**, *4*, 32–41.
- Ding, Z.-Y.; Wang, T.; He, Y.-M.; Chen, F.; Zhou, H.-F.; Fan, Q.-H.; Guo, Q.; Chan, A. S. C. *Adv. Synth. Catal.* **2013**, *355*, 3727–3735.
- Dobereiner, G. E.; Nova, A.; Schley, N. D.; Hazari, N.; Miller, S. J.; Eisenstein, O.; Crabtree, R. H. *J. Am. Chem. Soc.* **2011**, *133*, 7547–7562.
- Dong, W.; Liu, W.; Liao, X.; Guan, B.; Chen, S.; Liu, Z. *J. Org. Chem.* **2011**, *76*, 5363–5368.
- Dongbang, S.; Pedersen, B.; Ellman, J. A. *Chem. Sci.* **2019**, *10*, 535–541.
- Donohoe, T. J.; Pilgrim, B. S.; Jones, G. R.; Bassuto, J. A. *Proc. Natl. Acad. Sci. U.S.A.* **2012**, *109*, 11605–11608.
- Dorta, R.; Broggini, D.; Kissner, R.; Togni, A. *Chem. Eur. J.* **2004**, *10*, 4546–4555.
- Dorta, R.; Broggini, D.; Stoop, R.; Rüegger, H.; Spindler, F.; Togni, A. *Chem. Eur. J.* **2004**, *10*, 267–278.
- Du, E.; Dong, W.; Guan, B.; Pan, X.; Yan, Z.; Li, L.; Wang, N.; Liu, Z. *Tetrahedron* **2015**, *71*, 4296–4303.
- Duan, Y.; Chen, M.-W.; Chen, Q.-A.; Yu, C.-B.; Zhou, Y.-G. *Org. Biomol. Chem.* **2012**, *10*, 1235–1238.
- Duan, Y.; Li, L.; Chen, M.-W.; Yu, C. B.; Fan, H.-J.; Zhou, Y.-G. *J. Am. Chem. Soc.* **2014**, *136*, 7688–770.
- Dyke, S. F.; Ellis, A. C. *Tetrahedron* **1971**, *27*, 3803–3809.
- Endo, A.; Yanagisawa, A.; Abe, M.; Tohma, S.; Kan, T.; Fukuyama, T. *J. Am. Chem. Soc.* **2002**, *124*, 6552–6554.

- Evans, D. A.; Illig, C. R.; Saddler, J. C. *J. Am. Chem. Soc.* **1986**, *108*, 2478–2479.
- Evans, P.; McCabe, T.; Morgan, B. S.; Reau, S. *Org. Lett.* **2005**, *7*, 43–46.
- Fadhel, A. Z.; Pollet, P.; Liotta, C. L.; Eckert, C. A. *Molecules* **2010**, *15*, 8400–8424.
- Fagnou, K.; Lautens, M. *Angew. Chem. Int. Ed.* **2002**, *41*, 26–47.
- Fahmy, N. M.; Al-Sayed, E.; El-Shazly, M.; Singab, A. N. *Nat. Prod. Res.* **2020**, *34*, 1891–1912.
- Feng, X.; Du, H. *Tetrahedron Lett.* **2014**, *55*, 6959–6964.
- Fishlock, D.; Williams, R. M. *J. Org. Chem.* **2008**, *73*, 9594–9600.
- Fishlock, D.; Williams, R. M. *Org. Lett.* **2006**, *8*, 3299–3301.
- Fleischer, S.; Zhou, S.; Werkmeister, S.; Junge, K.; Beller, M. *Chem. Eur. J.* **2013**, *19*, 4997–5003.
- Fleury-Bregeot, N.; delaFuente, V.; Castilloñ, S.; Claver, C. *ChemCatChem* **2010**, *2*, 1346–1371.
- Fujii, A.; Hashiguchi, S.; Uematsu, N.; Ikariya, T.; Noyori, R. *J. Am. Chem. Soc.* **1996**, *118*, 2521–2522.
- Fukuda, T.; Iwao, M. *Heterocycles* **2007**, *74*, 701–720.
- Fukuyama, T. *Adv. Heterocycl. Nat. Prod. Synth.* **1992**, *2*, 189–249.
- Fukuyama, T.; Li, L.; Laird, A. A.; Keith Frank, R. *J. Am. Chem. Soc.* **1987**, *109*, 1587–1589.
- Fürstner, A.; Funel, J.-A.; Tremblay, M.; Bouchez, L. C.; Nevado, C.; Waser, M.; Ackerstaff, J.; Stimson, C. C. *Chem. Commun.* **2008**, 2783–2875.
- Fürstner, A.; Mamane, V. *Chem. Commun.* **2003**, 2112–2113.

- Gadhiya, S. V.; Giri, R.; Cordone, P.; Karki, A.; Harding, W. W. *Curr. Org. Chem.* **2018**, *22*, 1893–1905.
- Gadhiya, S.; Ponnala, S.; Harding, W. W. *Tetrahedron* **2015**, *71*, 1227–1231.
- Gao, B.; Feng, X.; Meng, W.; Du, H. *Angew. Chem. Int. Ed.* **2020**, *59*, 4498–4504.
- Gao, K.; Yu, C.-B.; Wang, D.-S.; Zhou, Y.-G. *Adv. Synth. Catal.* **2012**, *354*, 483–488.
- Gao, S.; Cheng, J.-J.; Ling, C.-Y.; Chu, W.-J.; Yang, Y.-S. *Tetrahedron Lett.* **2014**, *55*, 4856–4859.
- Garad, D. N.; Mhaske, S. B. *Org. Lett.* **2016**, *18*, 3862–3865.
- Garner, P.; Ümit Kaniskan, H.; Keyari, C. M.; Weerasinghe, L. *J. Org. Chem.* **2011**, *76*, 5283–5294.
- Gates, M.; Tschudi, G. *J. Am. Chem. Soc.* **1952**, *74*, 1109–1110.
- Gatland, A. E.; Pilgrim, B. S.; Procopiou, P. A.; Donohoe, T. J. *Angew. Chem. Int. Ed.* **2014**, *53*, 14555–14558.
- Ge, Y.; Wang, Z.; Han, Z.; Ding, K. *Chem. Eur. J.* **2020**, *26*, 15482–15486.
- Gee, K. R.; Barmettler, P.; Rhodes, M. R.; McBurney, R. N.; Reddy, N. L.; Hu, L.-Y. R.; Cotter, E.; Hamilton, P. N.; Weber, E.; Keana, J. F. W. *J. Med. Chem.* **1993**, *36*, 1938–1946.
- Geffe, M.; Opatz, T. *Org. Lett.* **2014**, *16*, 5282–5285.
- Gelis, C.; Heusler, A.; Nairoukh, Z.; Glorius, F. *Chem. Eur. J.* **2020**, *26*, 14090–14094.
- Gorelsky, S. I.; Lapointe, D.; Fagnou, K. *J. Am. Chem. Soc.* **2008**, *130*, 10848–10849.
- Gözler, B.; Lantz, M. S.; Shamma, M. *J. Nat. Prod.* **1983**, *46*, 293–309.
- Grajewska, A.; Rozwadowska, M. D. *Tetrahedron: Asymmetry* **2007**, *18*, 2910–2914.

- Gribanov, P. S.; Golenko, Y. D.; Topchiy, M. A.; Minaeva, L. I.; Asachenko, A. F.; Nechaev, M. S. *Eur. J. Org. Chem.* **2018**, 2018, 120–125.
- Guo, D.; Li, J.; Lin, H.; Zhou, Y.; Chen, Y.; Sun, H.; Zhang, D.; Li, H.; Shoichet, B. K.; Shan, L.; Xie, X.; Jiang, H.; Liu, H. *J. Med. Chem.* **2016**, 59, 9489–9502.
- Guo, R.-N.; Cai, X.-F.; Shi, L.; Ye, Z.-S.; Chen, M.-W.; Zhou, Y.-G. *Chem. Commun.* **2013**, 49, 8537–8539
- Haftchenary, S.; Nelson, S. D.; Furst, L.; Dandapani, S.; Ferrara, S. J.; Bošković, Z. V.; Lazú, S. F.; Guerrero, A. M.; Serrano, J. C.; Crews, D. K.; Brackeen, C.; Mowat, J.; Brumby, T.; Bauser, M.; Schreiber, S. L.; Phillips, A. J. *ACS. Comb. Sci.* **2016**, 18, 569–574.
- Hagel, J. M.; Facchini, P. J. *Nat. Chem. Biol.* **2010**, 6, 273–275.
- Hashiguchi, S.; Fujii, A.; Takehara, J.; Ikariya, T.; Noyori, R. *J. Am. Chem. Soc.* **1995**, 117, 7562–7563.
- Hayashi, T.; Noto, T.; Nawata, Y.; Okazaki, H.; Sawada, M.; Ando, K. *J. Antibiot.* **1982**, 35, 771–777.
- He, J.; Li, S.; Deng, Y.; Fu, H.; Laforteza, B. N.; Spangler, J. E.; Homs, A.; Yu, J.-Q. *Science* **2014**, 343, 1216–1220.
- He, W.-F.; Li, Y.; Feng, M.-T.; Gavagnin, M.; Mollo, E.; Mao, S.-C.; Guo, Y.-W. *Fitoterapia* **2014**, 96, 109–114.
- He, W.; Zhang, Z.; Ma, D. *Angew. Chem. Int. Ed.* **2019**, 58, 3972–3975.
- Hegedús, L.; Máthé, T. *Appl. Catal., A* **2002**, 226, 319–322.
- Heterocycles in Natural Product Synthesis*; Majumdar, K. C.; Chattopadhyay, S. K., Eds.; John Wiley & Sons: New York, 1991; pp 1–611.

- Hiratsuka, T.; Koketsu, K.; Minami, A.; Kaneko, S.; Yamazaki, C.; Watanabe, K.; Oguri, H.; Oikawa, H. *Chemistry & Biology* **2013**, *20*, 1523–1535.
- Honda, T.; Shigehisa, H. *Org. Lett.* **2006**, *8*, 657–659.
- Hopmann, K. H. *Chem. Eur. J.* **2015**, *21*, 10020–10030.
- Hopmann, K. H.; Bayer, A. *Organometallics*. **2011**, *30*, 2483–2497.
- Horst, B.; Wanner, M. J.; Jørgensen, S. I.; Hiemstra, H.; van Maarseveen, J. H. *J. Org. Chem.* **2018**, *83*, 15110–15117.
- Hu, S.-B.; Zhai, X.-Y.; Shen, H.-Q.; Zhou, Y.-G. *Adv. Synth. Catal.* **2018**, *360*, 1334–1339.
- Hu, X.-H.; Hu, X.-P. *Org. Lett.* **2019**, *21*, 10003–10006.
- Huang, R.-Y.; Chen, W.-T.; Kurtán, T.; Mándi, A.; Ding, J.; Li, J.; Li, X.-W.; Guo, Y.-W. *Future Med. Chem.* **2016**, *8*, 17–27.
- Huang, W.-X.; Liu, L.-J.; Wu, B.; Feng, G.-S.; Wang, B.; Zhou, Y.-G. *Org. Lett.* **2016**, *18*, 3082–3085.
- Huang, W.-X.; Wu, B.; Gao, X.; Chen, M.-W.; Wang, B.; Zhou, Y.-G. *Org. Lett.* **2015**, *17*, 1640–1643.
- Huang, W.-X.; Yu, C.-B.; Shi, L.; Zhou, Y.-G. *Org. Lett.* **2014**, *16*, 3324–3327.
- Huang, Z.; Ji, X.; Lumb, J.-P. *Org. Lett.* **2019**, *21*, 9194–9197.
- Ichiki, M.; Tanimoto, H.; Miwa, S.; Saito, R.; Sato, T.; Chida, N. *Chem. Eur. J.* **2013**, *19*, 264–269.
- Iimuro, A.; Yamaji, K.; Kandula, S.; Nagano, T.; Kita, Y.; Mashima, K. *Angew. Chem. Int. Ed.* **2013**, *52*, 2046–2050.
- Ikeda, Y.; Idemoto, H.; Hirayama, F.; Yamamoto, K.; Iwao, K.; Asao, T.; Munakata, T. *J. Antibiot.* **1983**, *36*, 1279–1283.

- Illig, C. R. Ph.D. Dissertation, Harvard University, Cambridge, MA, 1987.
- Irschik, H.; Trowitzsch-Kienast, W.; Gerth, K.; Hofle, G.; Reichenbach, H. *J. Antibiot.* **1988**, *41*, 993–998.
- J. Kayhan, M. J. Wanner, S. Ingemann, J. H. van Maarseveen and H. Hiemstra, *Eur. J. Org. Chem.* **2016**, 3705–3708.
- Jansat, S.; Picurelli, D.; Pelzer, K.; Philippot, K.; Gómez, M.; Muller, G.; Lecante, P.; Chaudret, B. *New. J. Chem.* **2006**, *30*, 115–122.
- Jayakumar, J.; Cheng, C.-H. *Chem. Eur. J.* **2016**, *22*, 1800–1804.
- Jia, J.; Chen, R.; Liu, H.; Li, X.; Jia, Y.; Chen, X. *Org. Biomol. Chem.* **2016**, *14*, 7334–7344.
- Jiménez, M. V.; Fernández-Tornos, J.; Modrego, F. J.; Pérez-Torrente, J. J.; Oro, L. A. *Chem. Eur. J.* **2015**, *21*, 17877–17889.
- Jin, W.; Metobo, S.; Williams, R. M. *Org. Lett.* **2003**, *5*, 2095–2098.
- Joucla, L.; Djakovitch, L. *Adv. Synth. Catal.* **2009**, *351*, 673–714.
- Kanamaru, R.; Konishi, Y.; Ishioka, C.; Kakuta, H.; Sato, T.; Ishikawa, A.; Asamura, M.; Wakui, A. *Cancer Chemother. Pharmacol.* **1988**, *22*, 197–200.
- Katritzky, A. R. *Chem. Heterocycl. Compd.* **1992**, *28*, 241–259.
- Kawabata, Y.; Naito, Y.; Saitoh, T.; Kawa, K.; Fuchigami, T.; Nishiyama, S. *Eur. J. Org. Chem.* **2014**, 99–104.
- Kawagishi, F.; Toma, T.; Inui, T.; Yokoshima, S.; Fukuyama, T. *J. Am. Chem. Soc.* **2013**, *135*, 13684–13687.
- Kayhan, J.; Wanner, M. J.; Ingemann, S.; van Maarseveen, J. H.; Hiemstra, H. *Eur. J. Org. Chem.* **2016**, 3705–3708.



- Kerr, R. G.; Miranda, N. F. *J. Nat. Prod.* **1995**, *58*, 1618–1621.
- Kim, A. N.; Ngamnithiporn, A.; Bartberger, M. D.; Stoltz, B. M. *Chem. Sci.* **2022**, *13*, 3227–3232.
- Kim, A. N.; Ngamnithiporn, A.; Welin, E. R.; Daiger, M. T.; Grünanger, C. U.; Bartberger, M. D.; Virgil, S. C.; Stoltz, B. M. *ACS Catal.* **2020**, *10*, 3241–3248.
- Kimishima, A.; Umihara, H.; Mizoguchi, A.; Yokoshima, S.; Fukuyama, T. *Org. Lett.* **2014**, *16*, 6244–6247.
- Kimura, S.; Saito, N. *ChemistryOpen* **2018**, *7*, 764–771.
- Kimura, S.; Saito, N. *Tetrahedron* **2018**, *74*, 4504–4514.
- Kita, Y.; Yamaji, K.; Higashida, K.; Sathaiyah, K.; Iimuro, A.; Mashima, K. *Chem. Eur. J.* **2015**, *21*, 1915–1927.
- Klei, S. R.; Golden, J. T.; Tilley, T. D.; Bergman, R. G. *J. Am. Chem. Soc.* **2002**, *124*, 2092–2093.
- Koizumi, H.; Yokoshima, S.; Fukuyama, T. *Chem. Asian. J.* **2010**, *5*, 2192–2198.
- Koketsu, K.; Minami, A.; Watanabe, K.; Oguri, H.; Oikawa, H. *Curr. Opin. Chem. Biol.* **2012**, *16*, 142–149.
- Koketsu, K.; Watanabe, K.; Suda, H.; Oguri, H.; Oikawa, H. *Nat. Chem. Biol.* **2010**, *6*, 408–410.
- Krishnan, S.; Bagdanoff, J. T.; Ebner, D. C.; Ramtohul, Y. K.; Tambar, U. K.; Stoltz, B. M. *J. Am. Chem. Soc.* **2008**, *130*, 13745–13754.
- Ku, A. F.; Cuny, G. D. *J. Org. Chem.* **2016**, *81*, 10062–10070.
- Ku, A. F.; Cuny, G. D. *Org. Lett.* **2015**, *17*, 1134–1137.

- Kubo, A.; Saito, N.; Yamato, H.; Masubuchi, K.; Nakamura, M. *J. Org. Chem.* **1988**, *53*, 4295–4310.
- Kutchan, T. M.; Dittrich, H. *J. Biol. Chem.* **1995**, *270*, 24475–24481.
- Kuwano, R.; Ikeda, R.; Hirasada, K. *Chem. Commun.* **2015**, *51*, 7558–7561.
- Kuwano, R.; Kameyama, N.; Ikeda, R. *J. Am. Chem. Soc.* **2011**, *133*, 7312–7315.
- Kuwano, R.; Kaneda, K.; Ito, T.; Sato, K.; Kurokawa, T.; Ito, Y. *Org. Lett.* **2004**, *6*, 2213–2215.
- Kuwano, R.; Kashiwabara, M. *Org. Lett.* **2006**, *8*, 2653–2655
- Kuwano, R.; Kashiwabara, M.; Ohsumi, M.; Kusano, H. *J. Am. Chem. Soc.* **2008**, *130*, 808–809
- Kuwano, R.; Kashiwabara, M.; Sato, K.; Ito, T.; Kaneda, K.; Ito, Y. *Tetrahedron: Asymmetry* **2006**, *17*, 521–535.
- Kuwano, R.; Morioka, R.; Kashiwabara, M.; Kameyama, N. *Angew. Chem. Int. Ed.* **2012**, *51*, 4136–4139.
- Kuwano, R.; Sato, K.; Kurokawa, T.; Karube, D.; Ito, Y. *J. Am. Chem. Soc.* **2000**, *122*, 7614–7615.
- Kwon, S.; Myers, A. G. *J. Am. Chem. Soc.* **2005**, *127*, 16796–16797.
- Lafrance, M.; Blaquièrre, N.; Fagnou, K. *Chem. Commun.* **2004**, 2874–2875.
- Lafrance, M.; Blaquièrre, N.; Fagnou, K. *Eur. J. Org. Chem.* **2017**, 811–825.
- Lafrance, M.; Fagnou, K. *J. Am. Chem. Soc.* **2006**, *128*, 16496–16497.
- Lahm, G.; Deichmann, J.-G.; Rauen, A. L.; Opatz, T. *J. Org. Chem.* **2015**, *80*, 2010–2016.
- Lane, J. W.; Chen, Y.; Williams, R. M. *J. Am. Chem. Soc.* **2005**, *127*, 12684–12690.
- Lapointe, D.; Fagnou, K. *Chem. Lett.* **2010**, *39*, 1118–1126.

- Legault, C. Y.; Charette, A. B. *J. Am. Chem. Soc.* **2005**, *127*, 8966–8967.
- Lerchen, A.; Knecht, T.; Koy, M.; Daniliuc, C. G.; Glorius, F. *Chem. Eur. J.* **2017**, *23*, 12149–12152.
- Li, B.; Xu, C.; He, Y.-M.; Deng, G.-J.; Fan, Q.-H. *Chin. J. Chem.* **2018**, *36*, 1169–1173.
- Li, C.; Chen, J.; Fu, G.; Liu, D.; Liu, Y.; Zhang, W. *Tetrahedron* **2013**, *69*, 6839–6844.
- Li, H.; Wang, Y.; Lai, Z.; Huang, K.-W. *ACS Catal.* **2017**, *7*, 4446–4450.
- Li, L.; Deng, W.; Song, J.; Ding, W.; Zhao, Q.-F.; Peng, C.; Song, W.-W.; Tang, G.-L.; Liu, W. *J. Bacteriol.* **2008**, *190*, 251–263.
- Li, Q.; Zhang, H. *Chem. Eur. J.* **2015**, *21*, 16379–16382.
- Li, S.; Meng, W.; Du, H. *Org. Lett.* **2017**, *19*, 2604–2606.
- Li, X.; Tian, J.-J.; Liu, N.; Tu, X.-S.; Zeng, N.-N.; Wang, X.-C. *Angew. Chem. Int. Ed.* **2019**, *58*, 4664–4668.
- Li, Z.-W.; Wang, T.-L.; He, Y.-M.; Wang, Z.-J.; Fan, Q.-H.; Pan, J.; Xu, L.-J. *Org. Lett.* **2008**, *10*, 5265–5268.
- Liao, X. W.; Liu, W.; Dong, W. F.; Guan, B. H.; Chen, S. Z.; Liu, Z. Z. *Tetrahedron* **2009**, *65*, 5709–5715.
- Lichman, B. R.; Lamming, E. D.; Pesnot, T.; Smith, J. M.; Hailes, H. C.; Ward, J. M. *Green Chem.* **2015**, *17*, 852–855.
- Lipp, A.; Ferenc, D.; Gütz, C.; Geffe, M.; Vierengel, N.; Schollmeyer, D.; Schäfer, H. J.; Waldvogel, S. R.; Opatz, T. *Angew. Chem. Int. Ed.* **2018**, *57*, 11055–11059.
- Lipp, A.; Selt, M.; Ferenc, D.; Schollmeyer, D.; Waldvogel, S. R.; Opatz, T. *Org. Lett.* **2019**, *21*, 1828–1831.
- Liu, C.-Y.; Angamuthu, V.; Chen, W.-C.; Hou, D.-R. *Org. Lett.* **2020**, *22*, 2246–2250.

- Liu, H.; Wang, W.-H.; Xiong, H.; Nijamudheen, A.; Ertem, M. Z.; Wang, M.; Duan, L. *Inorg. Chem.* **2021**, *60*, 3410–3417.
- Liu, W.; Dong, W.; Liao, X.; Yan, Z.; Guan, B.; Wang, N.; Liu, Z. *Bioorg. Med. Chem. Lett.* **2011**, *21*, 1419–1421.
- Liu, W.; Liao, X.; Dong, W.; Yan, Z.; Wang, N.; Liu, Z. *Tetrahedron* **2012**, *68*, 2759–2764.
- Liu, Y.; Chen, F.; He, Y.-M.; Li, C.; Fan, Q.-H. *Org. Biomol. Chem.* **2019**, *17*, 5099–5105.
- Liu, Y.; Du, H. *J. Am. Chem. Soc.* **2013**, *135*, 6810–6813.
- Liu, Y.; Yue, X.; Luo, C.; Zhang, L.; Lei, M. *Energy Environ. Mater.* **2019**, *2*, 292–312.
- Lovering, F. *MedChemComm* **2013**, *4*, 515–519.
- Lovering, F.; Bikker, J.; Humblet, C. *J. Med. Chem.* **2009**, *52*, 6752–6756.
- Lown, J. W.; Hanstock, C. C.; Joshua, A. V.; Arai, T.; Takahashi, K. *J. Antibiot.* **1983**, *36*, 1184–1194.
- Lown, J. W.; Joshua, A. V.; Lee, J. S. *Biochemistry* **1982**, *21*, 419–428.
- Lu, L.-Q.; Li, Y.; Junge, K.; Beller, M. *J. Am. Chem. Soc.* **2015**, *137*, 2763–2768.
- Lu, S. M.; Wang, Y. Q.; Han, X. W.; Zhou, Y.-G. *Angew. Chem. Int. Ed.* **2006**, *45*, 2260–2263.
- Luo, Y.-E.; He, Y.-M.; Fan, Q.-H. *Chem. Rec.* **2016**, *16*, 2697–2711.
- Luu, H.-T.; Streuff, J. *Eur. J. Org. Chem.* **2019**, 139–149.
- Ma, W.; Chen, F.; Liu, Y.; He, Y.-M.; Fan, Q.-H. *Org. Lett.* **2016**, *18*, 2730–2733
- Ma, W.; Zhang, J.; Xu, C.; Chen, F.; He, Y.-M.; Fan, Q.-H. *Angew. Chem. Int. Ed.* **2016**, *55*, 12891–12894.

- Maegawa, T.; Akashi, A.; Yaguchi, K.; Iwasaki, Y.; Shigetsura, M.; Monguchi, Y.; Sajiki, H. *Chem.-Eur. J.* **2009**, *15*, 6953–6963.
- Magnus, P.; Marks, K. D.; Meis, A. *Tetrahedron* **2015**, *71*, 3872–3877.
- Magnus, P.; Matthews, K. S. *J. Am. Chem. Soc.* **2005**, *127*, 12476–12477.
- Magnus, P.; Matthews, K. S. *Tetrahedron* **2012**, *68*, 6343–6360.
- Maier, U. H.; Rödl, W.; Deus-Neumann, B.; Zenk, M. H. *Phytochemistry* **1999**, *52*, 373–382.
- Maj, A. M.; Suisse, I.; Hardouin, C.; Agbossou-Niedercorn, F. *Tetrahedron* **2013**, *69*, 9322–9328
- Makarova, M.; Endoma-Arias, M. A. A.; Dela Paz, H. E.; Simionescu, R.; Hudlicky, T. *J. Am. Chem. Soc.* **2019**, *141*, 10883–10904.
- Makida, Y.; Saita, M.; Kuramoto, T.; Ishizuka, K.; Kuwano, R. *Angew. Chem. Int. Ed.* **2016**, *55*, 11859–11862
- Manivel, P. Probakaran, K.; Khan, F. N.; Jin, J. S. *Res. Chem. Intermed.* **2012**, *38*, 347–357.
- Marcelli, T.; Hammar, P.; Himo, F. *Chem. Eur. J.* **2008**, *14*, 8562–8571.
- Martinez, E. J.; Corey, E. J. *Org. Lett.* **2000**, *2*, 993–996.
- Mastranzo, V. M.; Yuste, F.; Ortiz, B.; Sánchez-Obregón, R.; Toscano, R. A.; García Ruano, J. L. *J. Org. Chem.* **2011**, *76*, 5036–5041.
- Matsuda, H.; Ninomiya, K.; Shimoda, H.; Nishida, N.; Yoshikawa, M. *Heterocycles* **2001**, *55*, 2043–2050.
- Matsuo, K.; Okumura, M.; Tanaka, K. *Chem. Pharm. Bull.* **1982**, *30*, 4170–4174.
- Meanwell, N. A. *Adv. Heterocycl. Chem.* **2017**, *123*, 245–361.

- Meissner, Z.; Chrzanowksa, M. *Tetrahedron: Asymmetry* **2015**, *26*, 225–229.
- Meng, K.; Xia, J.; Wang, Y.; Zhang, X.; Yang, G.; Zhang, W. *Org. Chem. Front.* **2017**, *4*, 1601–1605.
- Mikami, Y.; Takahashi, K.; Yazawa, K.; Arai, T.; Namikoshi, M.; Iwasaki, S.; Okuda, S. *J. Biol. Chem.* **1985**, *260*, 344–348.
- Mikami, Y.; Takahashi, K.; Yazawa, K.; Hour-Young, C.; Arai, T.; Saito, N.; Kubo, A. *J. Antibiot.* **1988**, *41*, 734–740.
- Miura, Y.; Saito, Y.; Goto, M.; Nakagawa-Goto, K.; *Chem. Pharm. Bull.* **2020**, *68*, 899–902.
- Molander, G. A.; Cavalcanti, L. N.; García-García, C. *J. Org. Chem.* **2013**, *78*, 6427–6439.
- Molander, G. A.; Trice, S. L.; Kennedy, S. M. *J. Org. Chem.* **2012**, *77*, 8678–8688. Hasan, I.; Marinelli, E. R.; Lin, L.-C. C.; Fowler, F. W.; Levy, A. B. *J. Org. Chem.* **1981**, *46*, 157–164.
- Molina Betancourt, R.; Echeverria, P.-G.; Ayad, T.; Phansavath, P.; Ratovelomanana-Vidal, V. *Synthesis* **2021**, *53*, 30–50.
- Moon, J. T.; Jung, J. A.; Ha, S. H.; Song, S. H.; Park, S. J.; Kim, J.; Choo, D. J.; Lee, Y. S.; Lee, J. Y. *Synth. Commun.* **2011**, *41*, 1282–1292.
- More, G. V.; Bhanage, B. M. *Tetrahedron: Asymmetry* **2015**, *26*, 1174–1179.
- Morris, J. S.; Facchini, P. J. *J. Biol. Chem.* **2016**, *291*, 23416–23427.
- Mostowicz, D.; Dygas, M.; Kaluza, Z. *J. Org. Chem.* **2015**, *80*, 1957–1963.
- Mostowicz, D.; Dygas, M.; Kałuza, Z. *J. Org. Chem.* **2015**, *80*, 1957–1963.
- Moulin, S.; Dentel, H.; Pagnoux-Ozherelyeva, A.; Gaillard, S.; Poater, A.; Cavallo, L.; Lohier, J.-F.; Renaud, J.-L. *Chem. Eur. J.* **2013**, *19*, 17881–17890.

- Murata, M.; Oyama, T.; Watanabe, S.; Masuda, Y. *J. Org. Chem.* **2000**, *65*, 164–168.
- Murugesan, K.; Senthamarai, T.; Alshammari, A. S.; Altamimi, R. M.; Kreyenschulte, C.; Pohl, M.-M.; Lund, H.; Jagadeesh, R. V.; Beller, M. *ACS Catal.* **2019**, *9*, 8581–8591.
- Nagano, T.; Iimuro, A.; Schwenk, R.; Ohshima, T.; Kita, Y.; Togni, A.; Mashima, K. *Chem. Eur. J.* **2012**, *18*, 11578–11592
- Naito, Y.; Tanabe, T.; Kawabata, Y.; Ishikawa, Y.; Nishiyama, S. *Tetrahedron Lett.* **2010**, *51*, 4776–4778.
- Nguyen Le, T.; Cho, W.-J. *Bull. Korean Chem. Soc.* **2007**, *28*, 763–766.
- Nimgirawath, S.; Udomputtimekakul, P. *Molecules* **2009**, *14*, 917–924.
- Nimgirawath, S.; Udomputtimekakul, P.; Pongphuttichai, S.; Wanbanjob, A.; Taechowisan, T. *Molecules.* **2008**, *13*, 2935–2947.
- Nishigaichi, Y.; Ohmuro, Y.; Hori, Y.; Ohtani, T. *Chem. Lett.* **2020**, *49*, 118–120.
- Novak, B. H.; Hudlicky, T.; Reed, J. W.; Mulzer, J.; Trauner, D. *Curr. Org. Chem.* **2000**, *4*, 343–362.
- Novak, B. H.; Hudlicky, T.; Reed, J. W.; Mulzer, J.; Trauner, D. *Curr. Org. Chem.* **2000**, *4*, 343–362.
- Núñez-Rico, J. L.; Fernández-Pérez, H.; Benet-Buchholz, J.; Vidal-Ferran, A. *Organometallics* **2010**, *29*, 6627–6631.
- Núñez-Rico, J. L.; Fernández-Pérez, H.; Vidal-Ferran, A. *Green Chem.* **2014**, *16*, 1153–1157.
- Núñez-Rico, J. L.; Vidal-Ferran, A. *Org. Lett.* **2013**, *15*, 2066–2069.
- O'Connor, S. E. Alkaloid Biosynthesis. *Wiley Encycl. Chem. Biol.* **2008**, 1–16.

- Oku, N.; Matsunaga, S.; van Soest, R. W. M.; Fusetani, N. *J. Nat. Prod.* **2003**, *66*, 1136–1139.
- Oliveira, D. F.; Miranda, P. C. M. L.; Correia, C. R. D. *J. Org. Chem.* **1999**, *64*, 6646–6652.
- Ortega, N.; Beiring, B.; Urban, S.; Glorius, F. *Tetrahedron* **2012**, *68*, 5185–5192.
- Ortega, N.; Urban, S.; Beiring, B.; Glorius, F. *Angew. Chem. Int. Ed.* **2012**, *51*, 1710–1713.
- Otto, N.; Ferenc, D.; Opatz, T. *J. Org. Chem.* **2017**, *82*, 1205–1217.
- Pacheco, J. C. O.; Lahm, G.; Opatz, T. *J. Org. Chem.* **2013**, *78*, 4985–4992.
- Padwa, A.; Wang, Q. *J. Org. Chem.* **2006**, *71*, 7391–7402.
- Paladino, M.; Zaifman, J.; Ciufolini, M. A. *Org. Lett.* **2015**, *17*, 3422–3425.
- Pangborn, A. M.; Giardello, M. A.; Grubbs, R. H.; Rosen, R. K.; Timmers, F. J. *Organometallics* **1996**, *15*, 1518–1520.
- Parekh, V.; Ramsden, J. A.; Wills, M. *Tetrahedron: Asymmetry* **2010**, *21*, 1549–1556.
- Park, K.-H.; Chen, D. Y.-K. *Chem. Commun.* **2018**, *54*, 13018–13021.
- Park, K.-H.; Chen, R.; Chen, D. Y.-K. *Chem. Sci.* **2017**, *8*, 7031–7037.
- Pastor, J.; Rezabal, E.; Voituriez, A.; Betzer, J.-F.; Marinetti, A.; Frison, G. *J. Org. Chem.* **2018**, *83*, 2779–2787.
- Paul, D.; Beiring, B.; Plois, M.; Ortega, N.; Kock, S.; Schlüns, D.; Neugebauer, J.; Wolf, R.; Glorius, F. *Organometallics* **2016**, *35*, 3641–3646.
- Pauli, L.; Tannert, R.; Scheil, R.; Pfaltz, A. *Chem. Eur. J.* **2015**, *21*, 1482–1487.
- Payne, J. T.; Valentic, T. R.; Smolke, C. D. *Proc. Natl. Acad. Sci. U.S.A.* **2021**, *118*, 1–12.
- Perecim, G. P.; Deflon, V. M.; Martins, G. R.; Pinto, L. M. C.; Casagrande, G. A.; Oliveira-Silva, D.; Raminelli, C. *Tetrahedron* **2020**, *76*, 131461–131468.



- Perecim, G. P.; Rodrigues, A.; Raminelli, C. A. *Tetrahedron Lett.* **2015**, *56*, 6848–6851.
- Phillipson, J. D.; Roberts, M. F.; Zenk, M. H. *The Chemistry and Biology of Isoquinoline Alkaloids*; Springer, 1985.
- Phipps, R. J.; Grimster, N. P.; Gaunt, M. J. *J. Am. Chem. Soc.* **2008**, *130*, 8172–8174.
- Pieper, P.; McHugh, E.; Amaral, M.; Tempone, A. G.; Anderson, E. A. *Tetrahedron.* **2020**, *76*, 130814–130821.
- Pilgrim, B. S.; Gatland, A. E.; Esteves, C. H. A.; McTernan, C. T.; Jones, G. R.; Tatton, M. R.; Procopiou, P. A.; Donohoe, T. J. *Org. Biomol. Chem.* **2016**, *14*, 1065–1090.
- Pu, J.-Y.; Peng, C.; Tang, M.-C.; Zhang, Y.; Guo, J.-P.; Song, L.-Q.; Hua, Q.; Tang, G.-L. *Org. Lett.* **2013**, *15*, 3674–3677.
- Qin, J.; Chen, F.; He, Y.-M.; Fan, Q.-H. *Org. Chem. Front.* **2014**, *1*, 952–955.
- Qu, B.; Mangunuru, H. P. R.; Tcyrulnikov, S.; Rivalti, D.; Zatochnaya, O. V.; Kurouski, D.; Radomkit, S.; Biswas, S.; Karyakarte, S.; Fandrlick, K. R.; Sieber, J. D.; Rodriguez, S.; Desrosiers, J.-N.; Haddad, N.; McKellop, K.; Pennino, S.; Lee, H.; Yee, N. K.; Song, J. J.; Kozlowski, M. C.; Senanayake, C. H. *Org. Lett.* **2018**, *20*, 1333–1337.
- Rahman, A.; Lin, X. *Org. Biomol. Chem.* **2018**, *16*, 4753–4777.
- Rath, C. M.; Janto, B.; Earl, J.; Ahmed, A.; Hu, F. Z.; Hiller, L.; Dahlgren, M.; Kreft, R.; Yu, F.; Wolff, J. J.; Kweon, H. K.; Christiansen, M. A.; Håkansson, K.; Williams, R. M.; Ehrlich, G. D.; Sherman, D. H. *ACS Chem. Biol.* **2011**, *6*, 1244–1256.
- Rath, C. M.; Janto, B.; Earl, J.; Ahmed, A.; Hu, F. Z.; Hiller, L.; Dahlgren, M.; Kreft, R.; Yu, F.; Wolff, J. J.; Kweon, H. K.; Christiansen, M. A.; Håkansson, K.; Williams, R. M.; Ehrlich, G. D.; Sherman, D. H. *ACS Chem. Biol.* **2011**, *6*, 1244–1256.

Reimann, C. E.; Ngamnithiporn, A.; Hayashida, K.; Saito, D.; Korch, K. M.; Stoltz, B. M.

*Angew. Chem. Int. Ed.* **2021**, *60*, 17957–17962.

Rinner, U.; Hudlicky, T. Synthesis of Morphine Alkaloids and Derivatives In *Alkaloid*

*Synthesis. Topics in Current Chemistry*, Vol. 309; Springer, 2011; pp 33–66.

Rochfort, S. J.; Towerzey, L.; Carroll, A.; King, G.; Michael, A.; Pierens, G.; Rali, T.;

Redburn, J.; Whitmore, J.; Quinn, R. J. *J. Nat. Prod.* **2005**, *68*, 1080–1082.

Rossini, A. F. C.; Muraca, A. C. A.; Casagrande, G. A.; Raminelli, C. *J. Org. Chem.*

**2015**, *80*, 10033–10040.

Roughley, S. D.; Jordan, A. M. *J. Med. Chem.* **2011**, *54*, 3451–3479.

Rueping, M.; Antonchick, A. P. *Angew. Chem. Int. Ed.* **2007**, *46*, 4562–4565.

Rueping, M.; Antonchick, A. P.; Theissmann, T. *Angew. Chem. Int. Ed.* **2006**, *45*, 3683–

3686.

Rueping, M.; Antonchick, A. P.; Theissmann, T. *Angew. Chem. Int. Ed.* **2006**, *45*,

6751–6755.

Rueping, M.; Bootwicha, T.; Sugiono, E. *Beilstein J. Org. Chem.* **2012**, *8*, 300–307.

Rueping, M.; Brinkmann, C.; Antonchick, A. P.; Atodiresei, I. *Org. Lett.* **2010**, *12*,

4604–4607.

Rueping, M.; Theissmann, T.; Stoeckel, M.; Antonchick, A. P. *Org. Biomol. Chem.* **2011**,

*9*, 6844–6850.

Saito, N. *Chem Pharm. Bull.* **2021**, *69*, 155–177.

Saito, N.; Harada, S.; Yamashita, M.; Saito, T.; Yamaguchi, K.; Kubo, A. *Tetrahedron*

**1995**, *51*, 8213–8230.

Saito, N.; Kimura, S.; Kawai, S.; Azuma, M.; Koizumi, Y.; Yokoya, M.; Umehara, Y.

*Heterocycles* **2015**, *90*, 327–343.

Saito, N.; Yoshino, M.; Charupant, K.; Suwanborirux, K. *Heterocycles* **2012**, *84*, 309–314.

Sanemitsu, Y.; Kawamura, S. *J. Pestic. Sci.* **2008**, *33*, 175–177.

Sawamura, M.; Hamashima, H.; Ito, Y. *Tetrahedron: Asymmetry* **1991**, *2*, 593–596.

Schütz, R.; Meixner, M.; Antes, I.; Bracher, F. *Org. Biomol. Chem.* **2020**, *18*, 3047–3068.

Scott, J. D.; Williams, R. M. *Chem. Rev.* **2002**, *102*, 1669–1730.

Scott, J. D.; Williams, R. M. *J. Am. Chem. Soc.* **2002**, *124*, 2951–2956.

Shamma, M.; Slusarchyk, W. A. *Chem. Rev.* **1964**, *64*, 59–79.

Shi, L.; Ye, Z.-S.; Cao, L.-L.; Guo, R.-N.; Hu, Y.; Zhou, Y.-G. *Angew. Chem. Int. Ed.*

**2012**, *51*, 8286–8289.

Siengalewicz, P.; Brecker, L.; Mulzer, J. *Synlett.* **2008**, *16*, 2443–2446.

Siengalewicz, P.; Rinner, U.; Mulzer, J. *Chem. Soc. Rev.* **2008**, *37*, 2676–2690.

Simón, L.; Goodman, J. M. *J. Am. Chem. Soc.* **2008**, *130*, 8741–8747.

Smidt, S. P.; Zimmermann, N.; Studer, M.; Pfaltz, A. *Chem. Eur. J.* **2004**, *10*, 4685–4693.

Song, L.-Q.; Zhang, Y.-Y.; Pu, J.-Y.; Tang, M.-C.; Peng, C.; Tang, G.-L. *Angew. Chem.*

*Int. Ed.* **2017**, *56*, 9116–9120.

Stubba, D.; Lahm, G.; Geffe, M.; Runyon, J. W.; Arduengo III, A. J.; Opatz, T. *Angew.*

*Chem. Int. Ed.* **2015**, *54*, 14187–14189.

Sun, L.; Li, D.; Zhou, X.; Zhang, D.; Wang, J.; He, Z.; Jiang, R.; Chen, W. *J. Org. Chem.*

**2017**, *82*, 12899–12907.

Sun, S.; Nagorny, P. *Chem. Commun.* **2020**, *56*, 8432–8435.

Sunderhaus, J. D.; Dockendorff, C.; Martin, S. F. *Org. Lett.* **2007**, *9*, 4223–4226.

- Suwanborirux, K.; Amnuoypol, S.; Plubrukarn, A.; Pummangura, S.; Kubo, A.; Tanaka, C.; Saito, N. *J. Nat. Prod.* **2003**, *66*, 1441–1446.
- Taber, D. F.; Neubert, T. D.; Schlecht, M. F. in *Strategies and Tactics in Organic Synthesis*; Harnata, M., Ed.; Elsevier: London, 2004, Vol. 5, pp 353–389.
- Takahashi, K.; Kubo, A. *J. Antibiot.* **1977**, *30*, 1015–1018.
- Tambar, U. K.; Ebner, D. C.; Stoltz, B. M. *J. Am. Chem. Soc.* **2006**, *128*, 11752–11753.
- Tanifuji, R.; Koketsu, K.; Takakura, M.; Asano, R.; Minami, A.; Oikawa, H.; Oguri, H. *J. Am. Chem. Soc.* **2018**, *140*, 10705–10709.
- Tatsukawa, M.; Punzalan, L. L. C.; Magpantay, H. D. S.; Villaseñor, I. M.; Concepcion, G. P.; Suwanborirux, K.; Yokoya, M.; Saito, N. *Tetrahedron* **2012**, *68*, 7422–7428.
- Taylor, R. D.; MacCoss, M.; Lawson, A. D. G. *J. Med. Chem.* **2014**, *57*, 5845–5859.
- Thimmaiah, S.; Ningegowda, M.; Shivananju, N. S.; Ningegowda, R.; Siddaraj, R.; Priya, B. S. *Eur. J. Chem.* **2016**, *7*, 391–396.
- Thompson, A. L. S.; Kabalka, G. W.; Akula, M. R.; Huffman, J. W. *Synthesis* **2005**, *4*, 547–550.
- Tianero, M. D.; Balaich, J. N.; Donia, M. S. *Nat. Microbiol.* **2019**, *4*, 1149–1159.
- Tietze, L. F.; Tölle, N.; Kratzert, D.; Stalke, D. *Org. Lett.* **2009**, *11*, 5230–5233.
- Torres, M. A.; Hoffarth, E.; Eugenio, L.; Savtchouk, J.; Chen, X.; Morris, J. S.; Facchini, P. J.; Ng, K. K.-S. *J. Biol. Chem.* **2016**, *291*, 23403–23415.
- Touge, T.; Arai, T. *J. Am. Chem. Soc.* **2016**, *138*, 11299–11305.
- Tu, X.-F.; Gong, L.-Z. *Angew. Chem. Int. Ed.* **2012**, *51*, 11346–11349.
- Tungler, A.; Szabados, E. *Org. Process. Res. Dev.* **2016**, *20*, 1246–1251.
- Uchida, K.; Yokoshima, S.; Kan, T.; Fukuyama, T. *Heterocycles* **2009**, *77*, 1219–1234.

- Uchida, K.; Yokoshima, S.; Kan, T.; Fukuyama, T. *Org. Lett.* **2006**, *8*, 5311–5313.
- Uematsu, N.; Fujii, A.; Hashiguchi, S.; Ikariya, T.; Noyori, R. *J. Am. Chem. Soc.* **1996**, *118*, 4916–4917.
- Uenishi, S.; Kakigi, R.; Hideshima, K.; Miyawaki, A.; Matsuoka, J.; Ogata, T.; Tomioka, K.; Yamamoto, Y. *Tetrahedron* **2021**, *90*, 132165–132176.
- Umihara, H.; Yokoshima, S.; Inoue, M.; Fukuyama, T. *Chem. Eur. J.* **2017**, *23*, 6993–6995.
- Umihara, H.; Yoshino, T.; Shimokawa, J.; Kitamura, M.; Fukuyama, T. *Angew. Chem. Int. Ed.* **2016**, *55*, 6915–6918.
- Ümit Kaniskan, H.; Garner, P. *J. Am. Chem. Soc.* **2007**, *129*, 15460–15461.
- Urban, S.; Ortega, N.; Glorius, F. *Angew. Chem. Int. Ed.* **2011**, *50*, 3803–3806.
- Varin, M.; Barré, E.; Iorga, B.; Guillou, C. *Chem. Eur. J.* **2008**, *14*, 6606–6608.
- Vasconcelos Leitao Da-Cunha, E.; Fehine, I. M.; Guedes, D. N.; Barbosa-Filho, J. M.; Sobral da Silva, M. Protoberberine Alkaloids. In *The Alkaloids: Chemistry and Biology*, Vol. 62; Elsevier Inc., 2005; pp 1–75.
- Velasco, A.; Acebo, P.; Gomez, A.; Schleissner, C.; Rodríguez, P.; Aparicio, T.; Conde, S.; Muñoz, R.; De La Calle, F.; Garcia, J. L.; Sánchez-Puelles, J. M. *Mol. Microbiol.* **2005**, *56*, 144–154.
- Verrier, C.; Lassalas, P.; Théveau, L.; Quéguiner, G.; Trécourt, F.; Marsais, F.; Hoarau, C. *Beilstein J. Org. Chem.* **2011**, *7*, 1584–1601.
- Vincent, G.; Lane, J. W.; Williams, R. M. *Tet. Lett.* **2007**, *48*, 3719–3722.
- Vincent, G.; Williams, R. M. *Angew. Chem. Int. Ed.* **2007**, *46*, 1517–1520.
- Vitaku, E.; Smith, D. T.; Njardarson, J. T. *J. Med. Chem.* **2014**, *57*, 10257–10274.
- von der Höh, A.; Berkessel, A. *ChemCatChem* **2011**, *3*, 861–867.

- Walsh, C. T. *Tetrahedron Lett.* **2015**, *56*, 3075–3081.
- Wang, C.; Li, C.; Wu, X.; Pettman, A.; Xiao, J. *Angew. Chem. Int. Ed.* **2009**, *48*, 6524–6528.
- Wang, D.-S.; Chen, Q.-A.; Li, W.; Yu, C.-B.; Zhou, Y.-G.; Zhang, X. *J. Am. Chem. Soc.* **2010**, *132*, 8909–8911.
- Wang, D.-S.; Chen, Q.-A.; Lu, S.-M.; Zhou, Y.-G. *Chem. Rev.* **2012**, *112*, 2557–2590.
- Wang, D.-S.; Ye, Z.-S.; Chen, Q.-A.; Zhou, Y.-G.; Yu, C.-B.; Fan, H.-J.; Duan, Y. *J. Am. Chem. Soc.* **2011**, *133*, 8866–8869.
- Wang, D.-W.; Wang, X.-B.; Wang, D.-S.; Lu, S.-M.; Zhou, Y.-G.; Li, Y.-X. *J. Org. Chem.* **2009**, *74*, 2780–2787.
- Wang, F.-X.; Zhu, N.; Zhou, F.; Lin, D.-X. *Molecules* **2021**, *26*, 6117–6139.
- Wang, J.; Chen, M.-W.; Ji, Y.; Hu, S.-B.; Zhou, Y.-G. *J. Am. Chem. Soc.* **2016**, *138*, 10413–10416.
- Wang, J.; Zhao, Z.-B.; Zhao, Y.; Luo, G.; Zhu, Z.-H.; Luo, Y.; Zhou, Y.-G. *J. Org. Chem.* **2020**, *85*, 2355–2368.
- Wang, J.; Zhu, Z.-H.; Chen, M.-W.; Chen, Q.-A.; Zhou, Y.-G. *Angew. Chem. Int. Ed.* **2019**, *58*, 1813–1817.
- Wang, L.-R.; Chang, D.; Feng, Y.; He, Y.-M.; Deng, G. J.; Fan, Q.-H. *Org. Lett.* **2020**, *22*, 2251–2255.
- Wang, L.; Carrow, B. P. *ACS Catal.* **2019**, *9*, 6821–6836.
- Wang, T.; Chen, F.; Qin, J.; He, Y.-M.; Fan, Q. H. *Angew. Chem. Int. Ed.* **2013**, *52*, 7172–7176

- Wang, T.; Chen, Y.; Ouyang, G.; He, Y.-M.; Li, Z.; Fan, Q.-H. *Chem. Asian. J.* **2016**, *11*, 2773–2777.
- Wang, T.; Ouyang, G.; He, Y.-M.; Fan, Q.-H. *Synlett* **2011**, *2011*, 939–942.
- Wang, T.; Zhuo, L.-G.; Li, Z.; Chen, F.; Ding, Z.; He, Y.; Fan, Q.-H.; Xiang, J.; Yu, Z. X.; Chan, A. S. C. *J. Am. Chem. Soc.* **2011**, *133*, 9878–9891.
- Wang, W.-B.; Lu, S.-M.; Yang, P.-Y.; Han, X.-W.; Zhou, Y.- G. *J. Am. Chem. Soc.* **2003**, *125*, 10536–10537.
- Wang, Y.-C.; Georghiou, P. E. *Org. Lett.* **2002**, *4*, 2675–2678.
- Wang, Y.; Hennig, A.; Küttler, T.; Hahn, C.; Jäger, A.; Metz, P. *Org. Lett.* **2020**, *22*, 3145–3148.
- Wang, Z.-J.; Zhou, H.-F.; Wang, T.-L.; He, Y.-M.; Fan, Q.-H. *Green Chem.* **2009**, *11*, 767–769.
- Warashina, T.; Matsuura, D.; Sengoku, T.; Takahashi, M.; Yoda, H.; Kimura, Y. *Org. Process Res. Dev.* **2019**, *23*, 614–618.
- Welin, E. R.; Ngamnithiporn, A.; Klätte, M.; Lapointe, G.; Pototschnig, G. M.; McDermott, M. S.; Conklin, D.; Gilmore, C. D.; Tadross, P. M.; Haley, C. K.; Negoro, K.; Glibstrup, E.; Grünanger, C. U.; Allan, K. M.; Virgil, S. C.; Slamon, D. J.; Stoltz, B. M. *Science* **2019**, *363*, 270–275.
- Wen, J.; Fan, X.; Tan, R.; Chien, H.-C.; Zhou, Q.; Chung, L. W.; Zhang, X. *Org. Lett.* **2018**, *20*, 2143–2147.
- Wen, J.; Tan, R.; Liu, S.; Zhao, Q.; Zhang, X. *Chem. Sci.* **2016**, *7*, 3047–3051.
- Wiedner, E. S.; Chambers, M. B.; Pitman, C. L.; Bullock, R. M.; Miller, A. J. M.; Appel, A. M. *Chem. Rev.* **2016**, *116*, 8655–8692.

- Wiesenfeldt, M. P.; Moock, D.; Paul, D.; Glorius, F. *Chem. Sci.* **2021**, *12*, 5611–5615.
- Wiesenfeldt, M. P.; Nairoukh, Z.; Dalton, T.; Glorius, F. *Angew. Chem. Int. Ed.* **2019**, *58*, 10460–10476.
- Willis, N. J.; Bray, C. D. *Chem. Eur. J.* **2012**, *18*, 9160–9173.
- Wollenburg, M.; Heusler, A.; Bergander, K.; Glorius, F. *ACS Catal.* **2020**, *10*, 11365–11370.
- Woo, G. H. C.; Kim, S.-H.; Wipf, P. *Tetrahedron* **2006**, *62*, 10507–10517.
- Wu, Y.-C.; Liron, M.; Zhu, J. *J. Am. Chem. Soc.* **2008**, *130*, 7148–7152.
- Wu, Y.-C.; Zhu, J. *Org. Lett.* **2009**, *11*, 5558–5561.
- Wysocki, J.; Ortega, N.; Glorius, F. *Angew. Chem. Int. Ed.* **2014**, *53*, 8751–8755
- Xu, C.; Feng, Y.; Li, F.; Han, J.; He, Y.-M.; Fan, Q.-H. *Organometallics* **2019**, *38*, 3979–3990.
- Xu, Z.; Xu, X.; O’Laoi, R.; Ma, H.; Zheng, J.; Chen, S.; Luo, L.; Hu, Z.; He, S.; Li, J.; Zhang, H.; Zhang, X. *Bioorg. Med. Chem.* **2016**, *24*, 5861–5872.
- Xue, F.; Silverman, R. B. *Tetrahedron Lett.* **2010**, *51*, 2536–2538.
- Yamakawa, M.; Ito, H.; Noyori, R. *J. Am. Chem. Soc.* **2000**, *122*, 1466–1478.
- Yamakawa, M.; Yamada, I.; Noyori, R. *Angew. Chem. Int. Ed.* **2001**, *40*, 2818–2821.
- Yan, Z.; Xie, H.-P.; Shen, H.-Q.; Zhou, Y.-G. *Org. Lett.* **2018**, *20*, 1094–1097.
- Yang, J.; Song, Y.; Tang, M.-C.; Li, M.; Deng, J.; Wong, N.-K.; Ju, J. *J. Org. Chem.* **2021**, *86*, 11107–11116.
- Yang, Z.; Chen, F.; He, Y.-M.; Yang, N.; Fan, Q.-H. *Catal. Sci. Technol.* **2014**, *4*, 2887–2890.



- Yang, Z.; Chen, F.; He, Y.; Yang, N.; Fan, Q.-H. *Angew. Chem. Int. Ed.* **2016**, *55*, 13863–13866.
- Yang, Z.; Chen, F.; Zhang, S.; He, Y.; Yang, N.; Fan, Q.-H. *Org. Lett.* **2017**, *19*, 1458–1461.
- Yasui, Y.; Koga, Y.; Suzuki, K.; Matsumoto, T. *Synlett.* **2004**, *4*, 615–618.
- Yasui, Y.; Suzuki, K.; Matsumoto, T. *Synlett.* **2004**, *4*, 619–622.
- Yazawa, K.; Takahashi, K.; Mikami, Y.; Arai, T.; Saito, N.; Kubo, A. *J. Antibiot.* **1986**, *39*, 1639–1650.
- Ye, Z.-S.; Guo, R.-N.; Cai, X.-F.; Chen, M.-W.; Shi, L.; Zhou, Y.-G. *Angew. Chem. Int. Ed.* **2013**, *52*, 3685–3689.
- Yokoya, M.; Ito, H.; Saito, N. *Tetrahedron* **2011**, *67*, 9185–9192.
- Yokoya, M.; Kobayashi, K.; Saito, M.; Saito, N. *Marine Drugs* **2015**, *13*, 4915–4933.
- Yokoya, M.; Shinada-Fujino, K.; Saito, N. *Tetrahedron Letters* **2011**, *52*, 2446–2449.
- Yokoya, M.; Shinada-Fujino, K.; Yoshida, S.; Mimura, M.; Takada, H.; Saito, N. *Tetrahedron* **2012**, *68*, 4166–4181.
- Yokoya, M.; Toyoshima, R.; Suzuki, T.; Le, V. H.; Williams, R. M.; Saito, N. *J. Org. Chem.* **2016**, *81*, 4039–4047.
- Yoshida, A.; Akaiwa, M.; Asakawa, T.; Hamashima, Y.; Yokoshima, S.; Fukuyama, T.; Kan, T. *Chem. Eur. J.* **2012**, *18*, 11192–11195.
- Yoshida, K.; Fujino, Y.; Takamatsu, Y.; Matsui, K.; Ogura, A.; Fukami, Y.; Kitagaki, S.; Takao, K. *Org. Lett.* **2018**, *20*, 5044–5047.
- Yoshida, K.; Itatsu, Y.; Fujino, Y.; Inoue, H.; Takao, K. *Angew. Chem. Int. Ed.* **2016**, *55*, 6734–6738.

- Youte, J.-J.; Barbier, D.; Al-Mourabit, A.; Gnecco, D.; Marazano, C. *J. Org. Chem.* **2004**, *69*, 2737–2740.
- Yu, C. B.; Wang, J.; Zhou, Y.-G. *Org. Chem. Front.* **2018**, *5*, 2805–2809.
- Yu, C.-B.; Li, X.; Zhou, Y.-G. *Asian J. Org. Chem.* **2019**, *8*, 1118–1121.
- Yu, J.; Zhang, Z.; Zhou, S.; Zhang, W.; Tong, R. *Org. Chem. Front.* **2018**, *5*, 242–246.
- Zein, A. L.; Dawe, L. N.; Georghiou, P. E. *J. Nat. Prod.* **2010**, *73*, 1427–1430.
- Zeuzala, J.; Hudlicky, T. *Synlett* **2005**, 388–405.
- Zhang, D.-Y.; Wang, D.-S.; Wang, M.-C.; Yu, C.-B.; Gao, K.; Zhou, Y.-G. *Synthesis* **2011**, *2011*, 2796–2802
- Zhang, D.-Y.; Yu, C.-B.; Wang, M.-C.; Gao, K.; Zhou, Y.-G. *Tetrahedron Lett.* **2012**, *53*, 2556–255
- Zhang, F.; Simpkins, N. S.; Blake, A. J. *Org. Biomol. Chem.* **2009**, *7*, 1963–1979.
- Zhang, F.; Simpkins, N. S.; Wilson, C. *Tetrahedron Lett.* **2007**, *48*, 5942–5947.
- Zhang, G.-L.; Chen, C.; Xiong, Y.; Zhang, L.-H.; Ye, J.; Ye, X.-S. *Carbohydrate Research.* **2010**, *345*, 780–786.
- Zhang, J.; Chen, F.; He, Y.-M.; Fan, Q.-H. *Angew. Chem. Int. Ed.* **2015**, *54*, 4622–4625;
- Zhang, Q.; Zhang, F.-M.; Zhang, C.-S.; Liu, S.-Z.; Tian, J.-M.; Wang, S.-H.; Zhang, X.-M.; Tu, Y.-Q. *Nat. Commun.* **2019**, *10*, 2507–2513.
- Zhang, X.-C.; Hu, Y.-H.; Chen, C.-F.; Fang, Q.; Yang, L.-Y.; Lu, Y.-B.; Xie, L. J.; Wu, J.; Li, S.; Fang, W. *Chem. Sci.* **2016**, *7*, 4594–4599.
- Zhang, Y.-Y.; Shao, N.; Wen, W.-H.; Tang, G.-L. *Org. Lett.* **2022**, *24*, 127–131.
- Zhang, Y.; Zhao, R.; Bao, R. L.; Shi, L. *Eur. J. Org. Chem.* **2015**, *2015*, 3344–3351.
- Zhang, Z.-W.; Lin, A.; Yang, J. *J. Org. Chem.* **2014**, *79*, 7041–7050.

- Zhang, Z.; Du, H. *Angew. Chem. Int. Ed.* **2014**, *54*, 623–626.
- Zhang, Z.; Du, H. *Org. Lett.* **2015**, *17*, 2816–2819.
- Zhang, Z.; Du, H. *Org. Lett.* **2015**, *17*, 6266–6269.
- Zhao, D.; Glorius, F. *Angew. Chem. Int. Ed.* **2013**, *52*, 9616–9618.
- Zhao, D.; Lied, F.; Glorius, F. *Chem. Sci.* **2014**, *5*, 2869–2873.
- Zhao, Q.; Li, S.; Huang, K.; Wang, R.; Zhang, X. *Org. Lett.* **2013**, *15*, 4014–4017.
- Zheng, S.; Chan, C.; Furuuchi, T.; Wright, B. J. D.; Zhou, B.; Guo, J.; Danishefsky, S. J. *Angew. Chem. Int. Ed.* **2006**, *45*, 1754–1759.
- Zheng, Y.; Li, X.-D.; Sheng, P.-Z.; Yang, H.-D.; Wei, K.; Yang, Y.-R. *Org. Lett.* **2020**, *22*, 4489–4493.
- Zhong, M.; Jiang, Y.; Chen, Y.; Yan, Q.; Liu, J.; Di, D. *Tetrahedron: Asymmetry.* **2015**, *26*, 1145–1149.
- Zhou, H.; Li, Z.; Wang, Z.; Wang, T.; Xu, L.; He, Y.; Fan, Q.-H.; Pan, J.; Gu, L.; Chan, A. S. C. *Angew. Chem. Int. Ed.* **2008**, *47*, 8464–8467.
- Zhou, S.; Fleischer, S.; Junge, K.; Beller, M. *Angew. Chem. Int. Ed.* **2011**, *50*, 5120–5124.
- Zhou, S.; Tong, R. *Chem. Eur. J.* **2016**, *22*, 7084–7089.
- Zhou, S.; Wang, M.; Wang, L.; Chen, K.; Wang, J.; Song, C.; Zhu, J. *Org. Lett.* **2016**, *18*, 5632–5635.
- Zhou, Y.-G. *Acc. Chem. Res.* **2007**, *40*, 1357–1366.
- Zhu, Z.-H.; Ding, Y.-X.; Wu, B.; Zhou, Y.-G. *Chem. Sci.* **2020**, *11*, 10220–10224.
- Zhu, Z.; Tang, X.; Li, X.; Wu, W.; Deng, G.; Jiang, H. *J. Org. Chem.* **2016**, *81*, 1401–1409.
- Zmijewski, M. J. Jr.; Mikolajczak, M.; Viswanatha, V.; Hruby, V. J. *J. Am. Chem. Soc.* **1982**, *104*, 4969–4971.

Zmijewski, M. J.; Palaniswamy, V. A.; Gould, S. J. *J. Chem. Soc., Chem. Commun.* **1985**,  
*18*, 1261–1262.

## ABOUT THE AUTHOR

Alexia Nahyun Kim was born in Alexandria, VA on July 5<sup>th</sup>, 1995. She is the oldest daughter of two siblings, Branden and Caelan. In 2016, the family also brought in a Havanese dog Daisy, who she considers as her little sister.

Alexia grew up in Fairfax, VA, where she attended Thomas Jefferson High School for Science & Technology that started her passion for chemistry. She then went on to attend Princeton University, where she majored in chemistry and obtained a minor in music performance for flute. Her interest in organic chemistry quickly grew from taking classes taught by Professor Martin Semmelhack, Dr. Paul Reider, and Professor Abby Doyle, and had the pleasure of working in the laboratory of Professor Rob Knowles, focusing on the development of novel photocatalytic methodologies. From her experience in the Knowles group, she decided to pursue graduate school to further develop her academic career as a synthetic chemist. Upon completion of her undergraduate studies, Alexia moved back home to VA to be with family while commuting to Georgetown University as a postbaccalaureate researcher in Professor Tim Warren's lab. At Georgetown, she worked on copper-catalyzed alkylation of unactivated sp<sup>3</sup> C–H bonds, gaining immense experience in organometallic chemistry.

In 2018, Alexia moved to Pasadena, CA to pursue her doctoral education at the California Institute of Technology. Under the guidance of Professor Brian Stoltz, her graduate work focused on asymmetric transition-metal catalysis and the total synthesis of complex alkaloids. Upon completion of her doctoral studies in May 2023, Alexia will stay around the LA area to begin her industrial career as a Process Development Scientist at Amgen in Thousand Oaks, CA.